DEEP-SEA SPONGE ECOSYSTEMS: KNOWLEDGE-BASED APPROACH TOWARDS SUSTAINABLE MANAGEMENT AND CONSERVATION

EDITED BY: Joana R. Xavier, Shirley A. Pomponi and Ellen Kenchington

PUBLISHED IN: Frontiers in Marine Science

frontiers Research Topics

Frontiers eBook Copyright Statement

The copyright in the text of individual articles in this eBook is the property of their respective authors or their respective institutions or funders. The copyright in graphics and images within each article may be subject to copyright of other parties. In both cases this is subject to a license granted to Frontiers.

The compilation of articles constituting this eBook is the property of Frontiers.

Each article within this eBook, and the eBook itself, are published under the most recent version of the Creative Commons CC-BY licence. The version current at the date of publication of this eBook is CC-BY 4.0. If the CC-BY licence is updated, the licence granted by Frontiers is automatically updated to the new version.

When exercising any right under the CC-BY licence, Frontiers must be attributed as the original publisher of the article or eBook, as applicable.

Authors have the responsibility of ensuring that any graphics or other materials which are the property of others may be included in the CC-BY licence, but this should be checked before relying on the CC-BY licence to reproduce those materials. Any copyright notices relating to those materials must be complied with.

Copyright and source acknowledgement notices may not be removed and must be displayed in any copy, derivative work or partial copy which includes the elements in question.

All copyright, and all rights therein, are protected by national and international copyright laws. The above represents a summary only. For further information please read Frontiers' Conditions for Website Use and Copyright Statement, and the applicable CC-BY licence.

ISSN 1664-8714
ISBN 978-2-88976-954-4
DOI 10.3389/978-2-88976-954-4

About Frontiers

Frontiers is more than just an open-access publisher of scholarly articles: it is a pioneering approach to the world of academia, radically improving the way scholarly research is managed. The grand vision of Frontiers is a world where all people have an equal opportunity to seek, share and generate knowledge. Frontiers provides immediate and permanent online open access to all its publications, but this alone is not enough to realize our grand goals.

Frontiers Journal Series

The Frontiers Journal Series is a multi-tier and interdisciplinary set of open-access, online journals, promising a paradigm shift from the current review, selection and dissemination processes in academic publishing. All Frontiers journals are driven by researchers for researchers; therefore, they constitute a service to the scholarly community. At the same time, the Frontiers Journal Series operates on a revolutionary invention, the tiered publishing system, initially addressing specific communities of scholars, and gradually climbing up to broader public understanding, thus serving the interests of the lay society, too.

Dedication to Quality

Each Frontiers article is a landmark of the highest quality, thanks to genuinely collaborative interactions between authors and review editors, who include some of the world's best academicians. Research must be certified by peers before entering a stream of knowledge that may eventually reach the public - and shape society; therefore, Frontiers only applies the most rigorous and unbiased reviews.
Frontiers revolutionizes research publishing by freely delivering the most outstanding research, evaluated with no bias from both the academic and social point of view. By applying the most advanced information technologies, Frontiers is catapulting scholarly publishing into a new generation.

What are Frontiers Research Topics?

Frontiers Research Topics are very popular trademarks of the Frontiers Journals Series: they are collections of at least ten articles, all centered on a particular subject. With their unique mix of varied contributions from Original Research to Review Articles, Frontiers Research Topics unify the most influential researchers, the latest key findings and historical advances in a hot research area! Find out more on how to host your own Frontiers Research Topic or contribute to one as an author by contacting the Frontiers Editorial Office: frontiersin.org/about/contact

DEEP-SEA SPONGE ECOSYSTEMS: KNOWLEDGE-BASED APPROACH TOWARDS SUSTAINABLE MANAGEMENT AND CONSERVATION

Topic Editors:
Joana R. Xavier, University of Porto, Portugal
Shirley A. Pomponi, Florida Atlantic University, United States
Ellen Kenchington, Bedford Institute of Oceanography (BIO), Canada

Citation: Xavier, J. R., Pomponi, S. A., Kenchington, E., eds. (2023). Deep-sea Sponge Ecosystems: Knowledge-based Approach Towards Sustainable Management and Conservation. Lausanne: Frontiers Media SA.
doi: 10.3389/978-2-88976-954-4

Table of Contents

06 ***Editorial: Deep-sea Sponge Ecosystems: Knowledge-based Approach Towards Sustainable Management and Conservation***
Joana R. Xavier, Shirley A. Pomponi and Ellen L. Kenchington

12 ***Sponge Density and Distribution Constrained by Fluid Forcing in the Deep Sea***
Timothy Culwick, Jeremy Phillips, Claire Goodwin, Emily J. Rayfield and Katharine R. Hendry

24 **Chloroflexi *Dominate the Deep-Sea Golf Ball Sponges* Craniella zetlandica *and* Craniella infrequens *Throughout Different Life Stages***
Kathrin Busch, Erik Wurz, Hans Tore Rapp, Kristina Bayer, Andre Franke and Ute Hentschel

36 ***Mortality, Population and Community Dynamics of the Glass Sponge Dominated Community "The Forest of the Weird" From the Ridge Seamount, Johnston Atoll, Pacific Ocean***
Emily G. Mitchell and Simon Harris

57 ***Does Depth Matter? Reproduction Pattern Plasticity in Two Common Sponge Species Found in Both Mesophotic and Shallow Waters***
Tal Idan, Liron Goren, Sigal Shefer, Itzchak Brickner and Micha Ilan

69 ***Sponges in a Changing Climate: Survival of* Agelas oroides *in a Warming Mediterranean Sea***
Tal Idan, Liron Goren, Sigal Shefer and Micha Ilan

80 ***Surface Microornamentation of Demosponge Sterraster Spicules, Phylogenetic and Paleontological Implications***
Paco Cárdenas

107 ***Reproductive Biology of* Geodia *Species (Porifera, Tetractinellida) From Boreo-Arctic North-Atlantic Deep-Sea Sponge Grounds***
Vasiliki Koutsouveli, Paco Cárdenas, Maria Conejero, Hans Tore Rapp and Ana Riesgo

129 ***CRISPR/Cas12a-Mediated Gene Editing in* Geodia barretti *Sponge Cell Culture***
Kylie Hesp, John L. Flores Alvarez, Ana-Maria Alexandru, Jip van der Linden, Dirk E. Martens, Rene H. Wijffels and Shirley A. Pomponi

139 ***The First Cut Is the Deepest: Trawl Effects on a Deep-Sea Sponge Ground Are Pronounced Four Years on***
Katelin M. Morrison, Heidi Kristina Meyer, Emyr Martyn Roberts, Hans Tore Rapp, Ana Colaço and Christopher Kim Pham

152 ***Seasonal Variability in Near-bed Environmental Conditions in the* Vazella pourtalesii *Glass Sponge Grounds of the Scotian Shelf***
Ulrike Hanz, Lindsay Beazley, Ellen Kenchington, Gerard Duineveld, Hans Tore Rapp and Furu Mienis

167 ***Corrigendum: Seasonal Variability in Near-bed Environmental Conditions in the* Vazella pourtalesii *Glass Sponge Grounds of the Scotian Shelf***
Ulrike Hanz, Lindsay Beazley, Ellen Kenchington, Gerard Duineveld, Hans Tore Rapp and Furu Mienis

170 ***Asteroids and Ophiuroids Associated With Sponge Aggregations as a Key to Marine Habitats. A Comparative Analysis Between Avilés Canyons System and El Cachucho, Marine Protected Area***
Maria Eugenia Manjón-Cabeza, Pilar Ríos, Laura María García-Guillén, Aurora Macías-Ramírez, Francisco Sánchez, Augusto Rodríguez-Básalo, Teodoro P. Ibarrola and Javier Cristobo

187 ***Macro and Microstructural Characteristics of North Atlantic Deep-Sea Sponges as Bioinspired Models for Tissue Engineering Scaffolding***
Eva Martins, Hans Tore Rapp, Joana R. Xavier, Gabriela S. Diogo, Rui L. Reis and Tiago H. Silva

205 ***Macrofauna Inhabiting Massive Demosponges From Shallow and Mesophotic Habitats Along the Israeli Mediterranean Coast***
Liron Goren, Tal Idan, Sigal Shefer and Micha Ilan

219 ***An Integrative Model of Carbon and Nitrogen Metabolism in a Common Deep-Sea Sponge (*Geodia barretti*)***
Anna de Kluijver, Martijn C. Bart, Dick van Oevelen, Jasper M. de Goeij, Sally P. Leys, Sandra R. Maier, Manuel Maldonado, Karline Soetaert, Sander Verbiest and Jack J. Middelburg

237 ***Lithistid Demosponges of Deep-Water Origin in Marine Caves of the North-Eastern Mediterranean Sea***
Andrzej Pisera and Vasilis Gerovasileiou

256 **In situ *Growth Rate Assessment of the Hexactinellid Sponge* Asconema setubalense *Using 3D Photogrammetric Reconstruction***
Elena Prado, Javier Cristobo, Augusto Rodríguez-Basalo, Pilar Ríos, Cristina Rodríguez-Cabello and Francisco Sánchez

272 ***Increasing Knowledge of Biodiversity on the Orphan Seamount: A New Species of* Tedania *(*Tedaniopsis*) Dendy, 1924***
Pilar Ríos, Javier Cristobo, Emily Baker, Lindsay Beazley, Timothy Culwick and Ellen Kenchington

286 ***High Resolution Spatial Distribution for the Hexactinellid Sponges* Asconema setubalense *and* Pheronema carpenteri *in the Central Cantabrian Sea***
Augusto Rodríguez-Basalo, Elena Prado, Francisco Sánchez, Pilar Ríos, María Gómez-Ballesteros and Javier Cristobo

301 ***A Microbial Nitrogen Engine Modulated by Bacteriosyncytia in Hexactinellid Sponges: Ecological Implications for Deep-Sea Communities***
Manuel Maldonado, María López-Acosta, Kathrin Busch, Beate M. Slaby, Kristina Bayer, Lindsay Beazley, Ute Hentschel, Ellen Kenchington and Hans Tore Rapp

325 ***A Deep-Sea Sponge Loop? Sponges Transfer Dissolved and Particulate Organic Carbon and Nitrogen to Associated Fauna***
Martijn C. Bart, Meggie Hudspith, Hans Tore Rapp, Piet F. M. Verdonschot and Jasper M. de Goeij

337 ***The Hexactinellid Deep-Water Sponge* Vazella pourtalesii *(Schmidt, 1870) (Rossellidae) Copes With Temporarily Elevated Concentrations of Suspended Natural Sediment***
Erik Wurz, Lindsay Beazley, Barry MacDonald, Ellen Kenchington, Hans Tore Rapp and Ronald Osinga

352 ***Bioactivity of Biosilica Obtained From North Atlantic Deep-Sea Sponges***
Olesia Dudik, Sara Amorim, Joana R. Xavier, Hans Tore Rapp, Tiago H. Silva, Ricardo A. Pires and Rui L. Reis

364 ***Diversity, Distribution and Phylogenetic Relationships of Deep-Sea Lithistids (Porifera, Heteroscleromorpha) of the Azores Archipelago***
Joana R. Xavier, David J. Rees, Raquel Pereira, Ana Colaço, Christopher K. Pham and Francisca C. Carvalho

364 ***Mediterranean Coral Provinces as a Sponge Diversity Reservoir: Is There a Mediterranean Cold-Water Coral Sponge Fauna?***
Andreu Santín, Jordi Grinyó, Maria Jesús Uriz, Claudio Lo Iacono, Josep Maria Gili and Pere Puig

417 ***Life in the Fast Lane: Modeling the Fate of Glass Sponge Larvae in the Gulf Stream***
Shuangqiang Wang, Ellen Kenchington, Zeliang Wang and Andrew J. Davies

441 ***Can Environmental Conditions at North Atlantic Deep-Sea Habitats Be Predicted Several Years Ahead? ——Taking Sponge Habitats as an Example***
Feifei Liu, Ute Daewel, Annette Samuelsen, Sebastian Brune, Ulrike Hanz, Holger Pohlmann, Johanna Baehr and Corinna Schrum

463 ***Environmental Change at Deep-Sea Sponge Habitats Over the Last Half Century: A Model Hindcast Study for the Age of Anthropogenic Climate Change***
Annette Samuelsen, Corinna Schrum, Veli Çağlar Yumruktepe, Ute Daewel and Emyr Martyn Roberts

frontiers | Frontiers in Marine Science

TYPE Editorial
PUBLISHED 20 January 2023
DOI 10.3389/fmars.2023.1132451

Check for updates

OPEN ACCESS

EDITED AND REVIEWED BY
Eva Ramirez-Llodra,
REV Ocean, Norway

*CORRESPONDENCE
Joana R. Xavier
jxavier@ciimar.up.pt

SPECIALTY SECTION
This article was submitted to Deep-Sea Environments and Ecology, a section of the journal Frontiers in Marine Science

RECEIVED 27 December 2022
ACCEPTED 12 January 2023
PUBLISHED 20 January 2023

CITATION
Xavier JR, Pomponi SA and Kenchington EL (2023) Editorial: Deep-sea sponge ecosystems: Knowledge-based approach towards sustainable management and conservation.
Front. Mar. Sci. 10:1132451.
doi: 10.3389/fmars.2023.1132451

COPYRIGHT
© 2023 Xavier, Pomponi and Kenchington. This is an open-access article distributed under the terms of the Creative Commons Attribution License (CC BY). The use, distribution or reproduction in other forums is permitted, provided the original author(s) and the copyright owner(s) are credited and that the original publication in this journal is cited, in accordance with accepted academic practice. No use, distribution or reproduction is permitted which does not comply with these terms.

Editorial: Deep-sea sponge ecosystems: Knowledge-based approach towards sustainable management and conservation

Joana R. Xavier[1,2]*, Shirley A. Pomponi[3] and Ellen L. Kenchington[4]

[1]CIIMAR – Interdisciplinary Centre of Marine and Environmental Research of the University of Porto, Matosinhos, Portugal, [2]Department of Biological Sciences, University of Bergen, Bergen, Norway, [3]Harbor Branch Oceanographic Institute, Florida Atlantic University, Fort Pierce, FL, United States, [4]Department of Fisheries and Oceans, Ocean Ecology Section, Bedford Institute of Oceanography, Dartmouth, NS, Canada

KEYWORDS

Porifera, habitats - conservation, biodiversity and connectivity, ecological function, blue biotechnology, threats and impacts, management tools

Editorial on the Research Topic
Deep-sea sponge ecosystems: Knowledge-based approach towards sustainable management and conservation

Sponge-dominated communities form a variety of habitats – sponge grounds, aggregations, gardens, and reefs – that are widespread throughout the world's oceans (Maldonado et al., 2015). They are especially prevalent in upper bathyal areas within national jurisdictions (e.g. continental shelves and slopes, Klitgaard and Tendal, 2004), but also occur on seamounts, mid-ocean ridges, and canyons in areas beyond national jurisdictions (e.g. Murillo et al., 2012; Xavier et al., 2015). On account of their uniqueness, functional significance (Pham et al., 2019) and vulnerability to direct and indirect impacts from established (e.g. bottom fishing; Murillo et al., 2016) and emerging (e.g. deep-sea mining) anthropogenic activities, these habitats were listed by the Oslo-Paris Convention for the Protection of the Marine Environment of the North-East Atlantic as threatened and/or endangered (OSPAR Commission, 2008), and many are classified as Vulnerable Marine Ecosystems (VMEs – FAO, 2009). Ensuring these habitats' long-term sustainability therefore requires a sound scientific knowledge base to be brought to the highest levels of the political and conservation agendas.

This Research Topic invited the international scientific community to address major knowledge gaps on deep-sea sponge habitats, with a particular focus on those in the North Atlantic and Arctic Ocean, resulting from the H2020 SponGES project[1], but including also studies performed in the Mediterranean Sea and the Pacific Ocean. Collectively, these studies enabled:

1 www.deepseasponges.org

- Strengthening the knowledge on species biology and ecology, for instance on species reproduction, growth rates, and symbioses (Busch et al., 2020; Idan et al., 2020; Koutsouveli et al., 2020; Prado et al., 2021);
- Unraveling biogeographic patterns and connectivity across spatial and temporal scales (Cárdenas, 2020; Pisera and Gerovasileiou, 2021; Ríos et al., 2021; Santín et al., 2021; Wang et al., 2021; Xavier et al., 2021);
- Enlightening the environmental drivers and enhancing the capacity to hind- and forecast changes in distribution using new modeling approaches (Culwick et al., 2020; Mitchell and Harris, 2020; Hanz et al., 2021; Liu et al., 2021; Rodríguez-Basalo et al., 2021; Samuelsen et al., 2022);
- Improving the understanding of ecological functioning and role of these ecosystems on energy transfer and biogeochemical cycling, as well as habitat provision (Bart et al., 2021; deKluijver et al., 2021; Goren et al., 2021; Maldonado et al., 2021; Manjón-Cabeza et al., 2021; Rios et al., 2021);
- Assessing the impact of anthropogenic activities and climate-driven changes, providing a better understanding of resilience and recovery to different stressors (Idan et al., 2020; Morrison et al., 2020; Wurz et al., 2021);
- Unlocking the biotechnological potential of these species and ecosystems particularly towards the development of sponge-derived tissue engineering scaffolds and new model cell systems (Hesp et al.; Dudik et al., 2021; Martins et al., 2021).

The data and knowledge produced in the course of these studies have and will continue to support the development and implementation of strategic policies and instruments towards the achievement of biodiversity and sustainability goals, core principles on the European Union Blue Growth strategy and the United Nations 2030 Agenda for Sustainable Development.

Knowledge base

Fundamental knowledge on species biology and ecology is critical to understand their tolerances to both natural and anthropogenic stressors. Yet, aspects such as reproductive ecology, growth rates, and sponge-microbial symbioses are still poorly documented, especially in the deep sea.

Koutsouveli et al. studied the reproductive cycle and strategy of five *Geodia* species across the boreo-Arctic region. They found all species to be gonochoristic (separate males and females) and oviparous, and to have a similar reproductive season (from late spring to early autumn) during which a large proportion of the population (60–90%) is engaged in reproduction. The relatively large size and high lipid content found in the oocytes of these species suggest an adaptation to deep-sea and cold-water conditions, potentially allowing for a longer planktonic phase duration (and therefore dispersal) of the resulting lecitotrophic larvae. In another study, Idan et al. compared the reproductive strategy in two species - *Chondrosia reniformis* Nardo, 1847 and *Axinella polypoides* Schmidt, 1862 - found both in shallow and mesophotic habitats in the Levantine Sea. The reproductive patterns observed differed in the two habitats with presumably temperature-regulated seasonal sexual reproduction in both species in the shallow-water habitat *vs* year-round high fecundity sexual reproduction in *A. polypoides*, and low fecundity and asexual reproduction in *C. reniformis* in the mesophotic habitat. These observations suggest reproductive plasticity as an adaptation to different environmental conditions.

Using a novel and non-invasive approach, Prado et al. were able to estimate in-situ, the growth rate of the vase-shaped glass sponge *Asconema setubalense* Kent, 1870. Applying a Structure-from-Motion technique to underwater imagery collected in the same area over six years, they estimated an average annual growth rate of 2.2 cm $year^{-1}$ (height) and 2.2 cm $year^{-1}$ (diameter), with higher growth rates in smaller (younger) individuals, and no growth in the largest (older) individual. According to their model, *A. setubalense* reaches maximum size at approximately 98 years of age, thereby confirming the slow growth and high longevity of these deep-sea species.

Busch et al. examined the microbial communities in adults, embryos and recruits of two sponge species – *Craniella zetlandica* (Carter, 1872) and *Craniella infrequens* (Carter, 1876), combining 16S rRNA amplicon sequencing and advanced microscopy techniques such as transmission electron microscopy and Fluorescence *in situ* Hybridization. They found distinct prokaryotic communities associated with the two high microbial abundance species (and control seawater samples), largely dominated by *Chloroflexi* Amplicon Sequence Variants (ASVs), and with most *Chloroflexi* ASVs shared across the three life stages. These results indicate that the microbial consortia are likely to be vertically transmitted from parents to offspring. They also noted that a considerable proportion of core ASVs found belong to the SAR202 clade, a group thought to be involved in the degradation of recalcitrant organic matter, and therefore likely to be playing a nutritional role in these species' holobiont.

Biogeographic patterns and connectivity

Having a good understanding of the biogeographic and connectivity patterns of species and habitats distributions is a fundamental base for the development of area-based management tools.

Many sponge species occur associated with cold-water coral reefs (CWC). Santín et al. examined the sponge diversity in CWC provinces of the Mediterranean Sea. They found 46 species on CWC of the Catalan margin (two new to science), and at least 172 sponge species among all Mediterranean CWC provinces, therefore considered diversity hotspots at a basin scale. The biogeographic patterns observed indicate the presence of a unique Mediterranean CWC sponge fauna, distinct from the Atlantic CWC sponge fauna (despite low endemism), and suggest water masses as key drivers of present-day distribution and diversity within this enclosed basin.

Knowledge of the sponge fauna of the Orphan seamount located off the northeast coast of Newfoundland (Canada) was advanced by Ríos et al. with the description of a new species – *Tedania* (*Tedaniopsis*) *rappi*, and comparison with other congeneric species of the Atlantic Ocean.

Xavier et al. examined the patterns of spatial and bathymetric distribution as well as phylogenetic and biogeographic affinities of deep-sea lithistids of the Azores archipelago. Combining species occurrence data and phylogenetic reconstructions, the authors found this archipelago and its neighboring seamounts to be a lithistid hotspot in the central North Atlantic. This assemblage was characterized by mix of steno- and eurybathic species, with highest diversity in the upper bathyal (200–800 m depth, and greatest similarity and phylogenetic affinities to other areas of the northeast Atlantic and Mediterranean. On another study, Pisera and Gerovasileiou reported the occurrence of three lithistid species in shallow-water caves and upper bathyal habitats in the Aegean Sea. A particularly abundant population of *Neophrissospongia endoumensis* Pisera and Vacelet, 2011 with the largest individual estimated to be up to 900 years in age was found in one of the caves. Their occurrence in these special cryptic habitats is hypothesized to result from colonization from populations in deeper areas after the last glaciation.

Using three-dimensional particle tracking modelling, Wang et al. simulated the dispersal of larvae of the glass sponge *Vazella pourtalesii* (Schmidt, 1870), thereby estimating the connectivity of its populations throughout the northwestern Atlantic. The authors found a clear break around Cape Hatteras, with no larvae exchange between populations to the North and South of it. This suggests that the dense populations of the Canadian Scotian Shelf and those on the east coast of the US are largely isolated and therefore long-term conservation measures require an integrated regional approach.

The vast majority of sponges possess a biosilica-based skeleton, producing highly diverse skeletal structures (spicules) that constitute the basis of sponge taxonomy and systematics, and can be used to reconstruct the evolutionary history of the group. An example of this is the study by Cárdenas that found the patterns micro-ornamentation of sterrasters to match extant and fossil genera within the family Geodiidae. Mapping of these characters onto an updated Geodiidae phylogenetic tree, contested once again the monophyly of the family and suggested this spicule type to have evolved independently multiple times in this group.

Environmental drivers and ecological models

The environmental factors underpinning the distribution of species and habitats in the deep sea are still poorly understood. However, integration of ecological and oceanographic data using modern analytical approaches offer unparalleled opportunities for closer integration across disciplines and enhancing of predictive capacity.

Hanz et al. and Hanz et al. used a benthic lander to investigate the natural near-bottom environmental conditions in Sambro Bank (Scotian Shelf) where a dense aggregation of the glass sponge *Vazella pourtalesii* occurs. With an array of lander-mounted sensors, they were able to record fluctuations in temperature (8.8–12° C), dissolved oxygen (4.9–8.9 mg l^{-1}), current speed (average 0.12 m s^{-1}), and vertical carbon flux (100 ± 72 mg C m^{-2} day^{-1}) of the benthic boundary layer on hourly-seasonal time scales. They found *V. pourtalesii* to be resilient to the effects high levels of sediment resuspension caused by short-term episodical storm events, and to benefit from semi-diurnal tidal currents for food supply. However, high current peaks caused the dislodgement of some sponges from their upright position, potentially impacting their health in the longer term.

Using Maximum Entropy and Generalized Additive modelling techniques, Rodríguez-Basalo et al. developed high-resolution spatial models of two glass sponges – *Pheronema carpenteri* (Thomson, 1869) and *Asconema setubalense* - in a topographically complex area of the Cantabrian Sea. They found substrate type, depth, and current velocity to be the main environmental factors driving the distribution of *A. setubalense*, whereas silicates, eastness, slope, and current velocity where the main factors for *P. carpenteri*'s distribution in the area.

Using 3D reconstructions based on high-resolution imagery collected with a ROV, Mitchell and Harris assessed fine-scale community dynamics of a deep-sea community of the Ridge seamount (Pacific Ocean) dominated by glass sponges and octocorals. Through spatial point process analyses and Bayesian network inference, they found a random distribution of dead individuals amongst the living ones, suggesting density was not an underlying cause of death. They also observed that at different spatial scales there was evidence of competition between taxa sharing the same habitat. On another study area (Labrador Sea, Northwest Atlantic), and coupling field observations with mathematical (fluid flow) modeling, Culwick et al. investigated the patterns of distribution and density of four types of sponge grounds and their linkage to near-bottom flow conditions. By simulating the flow around idealized sponge morphologies (spherical and ellipsoid) and over sponge grounds topographic models, they identified a slowed benthic boundary layer caused by the wake of individual sponges and the community as a whole. This layer is hypothesized to play an important role both on larval recruitment and food uptake, and therefore critical for the maintenance of these habitats.

New modelling approaches, also allowed to both hindcast (Samuelsen et al., 2022) and predict (Liu et al., 2021), at monthly to multi-decadal timescales, the variability of environmental factors underpinning the distribution of these habitats. Combined, the studies by Samuelsen et al., and Liu et al. greatly enhanced our capacity to predict effects of future anthropogenic and climate-driven changes at management-relevant scales.

Ecosystem functions

Sponge habitats are increasingly acknowledged to play key functional roles, delivering various goods and services, from enhancing biodiversity locally to transferring of energy from lower to higher trophic levels, participating in biogeochemical cycling, and provisioning of habitat and nursery areas for many other organisms, from invertebrates to fishes. However, to date, few studies have attempted to quantify such functions and assess their relevance at the ecosystem level.

Using an experimental pulse-chase approach, Bart et al. traced the fate of carbon- and nitrogen-enriched dissolved and particulate organic matter (DOM/POM), and showed the transfer of the organic matter consumed by sponges to brittlestars, demonstrating the occurrence of a sponge-loop pathway. These results corroborate previous findings of the sponge loop in shallow-water (de Goeij et al.,

2013), further highlighting the importance of this taxonomic group on the recycling of major nutrients, and sustaining of food-webs across various marine ecosystems. These findings further supported the development by de Kluijver et al. of a metabolic network model for one of the most common deep-sea habitat-forming species (*Geodia barretti* Bowerbank, 1858) and its microbial symbionts, with quantification of carbon, nitrogen, and oxygen fluxes. Such study found this holobiont to have a complex metabolism, consisting of aerobic and anaerobic processes, with lower (volume-specific) metabolic rates in larger individuals, a pattern characteristic of slow-growing organisms.

In another study, combining *in-situ* and laboratory incubations, Maldonado et al. investigated the nitrogen and phosphorus fluxes in two hexactinellid species - *Vazella pourtalesii* (Schmidt, 1870) and *Schaudinnia rosea* (Fristedt, 1887). The net fluxes of ammonium, nitrite, nitrate, and phosphate upscaled to the level of the habitat that *V. pourtalesii* forms on the Scotian Shelf, showed that 2.6 million kg of ammonium may be taken up annually from the bottom water by this species in the area. Such uptake is hypothesized to limit the bacterioplankton community and consequently the establishment of a more diverse sponge community feeding on it.

The role of sponges as "living hotels" was emphasized in the study by Goren et al., examining the macrofauna associated with massive sponges collected in two habitats (shallow vs mesophotic) on the Israeli Mediterranean Coast. They found over 1000 individuals representing 60 taxa across six major groups, and particularly within Polychaeta, Crustacea and Ophiuroidea, living within the sponge aquiferous system. Distinct sponge-associated communities were found in shallow and mesophotic habitats, with highest richness (and sponge diversity) in the latter, but higher densities (per sponge volume) in the former. In another study, Manjón-Cabeza et al. examined the echinoderm communities found in four types of sponge aggregations occurring in the Cantabrian Sea. They found a diverse assemblage with 42 echinoderm species (28 ophiuroids and 14 starfishes), occurring in the area. However, no evidence of association between the echinoderms and sponges was found, suggesting that other factors such as depth or substrate may be shaping the distribution of species in both groups.

Anthropogenic impacts

To date, only a few studies have addressed the effects of direct and indirect anthropogenic pressures, such as bottom fisheries and climate change, on deep-sea sponge habitats (Murillo et al., 2016; Beazley et al., 2018; Beazley et al., 2020). Morrison et al. investigated the recovery of sponge ground communities of an Arctic seamount (Schulz Bank) four years after physical disturbance by (experimental) bottom trawling. The diversity and abundance of the epibenthic megafauna on the impacted sites were shown to be significantly lower than on control sites, suggesting that recovery to pre-impact conditions is likely to take long timeframes. In addition to physical removal as bycatch, plumes of suspended sediments during fishing operations may have detrimental effects on sponge physiology. Wurz et al. showed, using a mesocosm experiment, that the habitat-forming glass sponge *Vazella pourtalesii* was able to maintain normal physiological performance (respiration and clearing rates) for up to one week of natural sediment exposure (at concentrations up to 57 mg L^{-1}). However, longer-term exposure (i.e., after 14 days) led to a decrease in bacterial clearing rates suggesting an arrest in pumping activity. Such response mechanism is thought to be energetically demanding and to compromise other physiological processes such as growth and reproduction, compromising overall sponge health, and therefore not sustainable for extended periods of time.

Sponge communities, particularly those in shallower waters have been experiencing episodical mass mortality as a result of anomalously-high water temperature events (Garrabou et al., 2009). However, under more gradual changes as those sponges have been considered "winners", when compared to calcifying organisms such as, for instance, scleractinian corals (Bell et al., 2013; Beazley et al., 2018; Beazley et al., 2020). Through an *in-situ* transplantation experiment, Idan et al. showed that individuals of the sponge *Agelas oroides* (Schmidt, 1864) collected at mesophotic depths (100-200 m) and transplanted in a shallow habitat at 10 m depth, experienced overall mortality when water temperature had risen to over 28°C; unlike sponges in the control group that were transplanted at the same mesophotic depths where temperature never rose above 20°C. Taking into account these results they hypothesized that the 3°C increase in water temperature observed in the Israeli coast over the past 60 years to be one of the main factors leading to the disappearance of *A. oroides* from shallow-waters in the area.

Biotechnological potential

Sponges and the sponge holobiont have long been recognized as prolific sources of marine natural products with human health applications (Calado et al., 2022), having attracted great interest from the pharmaceutical industry. In more recent years, there is also an increasing interest on sponge-derived biomaterials such as biosilica and collagen, as these present enormous potential for the development of tissue engineering scaffolds and drug-delivery applications (e.g., Kaya et al., 2021). In their study, Martins et al. characterized the morphological, mechanical, and chemical properties of biosilicas extracted from several deep-sea habitat-forming sponges that are widely distributed across the boreo-Arctic region - *Geodia barretti*, *Geodia atlantica*, *Stelletta normani*, *Phakellia ventilabrum*, and *Axinella infundibuliformis*. The high skeletal interconnectivity and porosity observed revealed these species as interesting biomimetic models for tissue engineering applications. Dudik et al. further explored the bioactivity and osteogenic capacity of the bioceramics of the same species. Their results showed these were non-cytotoxic, and that the biosilica of *Geodia atlantica* in particular promoted the deposition of calcium phosphate, therefore representing a promising avenue for bone tissue regeneration.

The latest development of a sponge cell line (Conkling et al., 2019), and the demonstrated possibility to genetically modify cultured cells using a CRISPR/Cas12a gene editing system as shown by Hesp et al., represents a major scientific breakthrough which further allows the establishment of new models to understand not only evolutionary processes but also upscale the production of bioactive compounds for clinical trials.

Author contributions

Designed the study: JX, SP, EK; edited the contributions: JX, SP, EK; wrote the draft of the manuscript: JX; contributed text and reviewed the manuscript: JX, SP, EK. All authors contributed to the article and approved the submitted version.

Funding

This Research Topic, and much of the research herein reported, has been performed in scope of the SponGES project, which received funding from the European Union's Horizon 2020 research and innovation programme under grant agreement No. 679849. This document reflects only the authors' views and the Executive Agency for Small and Medium-sized Enterprises (EASME) is not responsible for any use that may be made of the information it contains. JX research is further supported by national funds through FCT Foundation for Science and Technology within the scope of UIDB/04423/2020 and UIDP/04423/2020, and CEECIND/00577/2018.

Acknowledgments

We thank all scientists contributing to this Research Topic. A special thanks to the SponGES consortium, from principal investigators, to technicians, early career researchers and undergraduate students for their commitment in producing knowledge on so many aspects of sponge (and deep-sea) biology and ecology. We are greatly indebted to all experts that acted as additional manuscript handling editors (Daniela Zeppilli, Daphne Cuvelier, Chiara Romano, Clara Rodrigues, Cristina Gambi, Lorenzo Angeletti, Jose Angel Alvarez Perez) or as reviewers of the manuscripts herein published. We would also like to thank the editorial staff at Frontiers in Marine Sciences for the invitation and support throughout the development of this volume. We dedicate this Research Topic to our dear friend and coordinator of the SponGES project, Hans Tore Rapp, Professor at the University of Bergen (Norway), who passed away so prematurely, and before this volume was completed. This is both a result of and a tribute to his exceptional contributions to sponge and deep-sea science. You will be missed for many years to come.

Conflict of interest

The authors declare that the research was conducted in the absence of any commercial or financial relationships that could be construed as a potential conflict of interest.

Publisher's note

All claims expressed in this article are solely those of the authors and do not necessarily represent those of their affiliated organizations, or those of the publisher, the editors and the reviewers. Any product that may be evaluated in this article, or claim that may be made by its manufacturer, is not guaranteed or endorsed by the publisher.

References

Beazley, L., Kenchington, E., Murillo, F. J., Brickman, D., Wang, Z., Davies, A. J., et al. (2020). Climate change winner in the deep sea: Predicting the impacts of climate change on the distribution of the glass sponge *Vazella pourtalesii*. *Mar. Ecol. Prog. Ser.* 657, 1–23. doi: 10.3354/meps13566

Beazley, L., Wang, Z., Kenchington, E., Yashayaev, I., Rapp, H. T., Xavier, J. R., et al. (2018). Predicted distribution of the glass sponge *Vazella pourtalesi* on the scotian shelf and its persistence in the face of climatic variability. *PloS One* 13 (10), e0205505. doi: 10.1371/journal.pone.0205505

Bell, J. J., Davy, S. K., Jones, T., Taylor, M. W., and Webster, N. S. (2013). Could some coral reefs become sponge reefs as our climate changes? *Global Change Biol.* 19, 2613–2624. doi: 10.1111/gcb.12212

Bowerbank, J. S. (1858). On the anatomy and physiology of the spongiadae. part i. on the spicula. *Philos. Trans. R. Soc.* 148 (2), 279–332.

Calado, R., Mamede, R., Cruz, S., and Leal, M. C. (2022). Updated trends on the biodiscovery of new marine natural products from invertebrates. *Mar. Drugs* 20, 389. doi: 10.3390/md20060389

Carter, H. J. (1872). On two new sponges from the Antarctic Sea, and on a new species of *Tethya* from shetland; together with observations on the reproduction of sponges commencing from zygosis of the sponge animal. *Ann. Mag. Natural Hist.* 9 (54), 409–435. doi: 10.1080/00222937208696612

Carter, H. J. (1876). Descriptions and figures of deep-Sea sponges and their spicules, from the Atlantic ocean, dredged up on board H.M.S.'Porcupine', chiefly in 1869 (concluded). *Ann. Mag. Natural Hist.* 18 (105), 226–240. (107): 388-410;(108): 458-479.

Conkling, M., Hesp, K., Munroe, S., Sandoval, K., Martens, D. E., Sipkema, D., et al. (2019). Breakthrough in marine invertebrate cell culture: Sponge cells divide rapidly in improved nutrient medium. *Sci. Rep.* 9, 17321. doi: 10.1038/s41598-019-53643-y

Culwick, T., Phillips, J., Goodwin, C., Rayfield, E. J., and Hendry, K. R. (2020). Sponge density and distribution constrained by fluid forcing in the deep Sea. *Front. Mar. Sci.* 7. doi: 10.3389/fmars.2020.00395

de Goeij, J. M., Van Oevelen, D., Vermeij, M. J., Osinga, R., Middelburg, J. J., De Goeij, A. F., et al. (2013). Surviving in a marine desert: the sponge loop retains resources within coral reefs. *Science* 342, 108–110. doi: 10.1126/science.1241981

FAO (2009). *International guidelines for the management of deep-sea fisheries in the high seas. directives internationales sur la gestion de la pêche profonde en haute mer. directrices internacionales para la ordenación de las pesquerías de aguas profundas en alta mar* (Rome: Food and Agriculture Organization of the United Nations), 73.

Fristedt, K. (1887). Sponges from the Atlantic and Arctic oceans and the behring Sea. *Vega-Expeditionens Vetenskap. Iakttagelser (Nordenskiöld)* 4, 401–471.

Garrabou, J., Coma, R., Bensoussan, N., Bally, M., Chevaldonné, P., Cigliano, M., et al. (2009). Mass mortality in northwestern mediterranean rocky benthic communities: effects of the 2003 heat wave. *Global Change Biol.* 15, 1090–1103. doi: 10.1111/j.1365-2486.2008.01823.x

Kaya, M., Bilican, I., Mutjaba, M., Sargin, I., Haskoylu, M. E., Ones, E. T., et al. (2021). Sponge-derived natural bioactive glass microspheres with self-assembled surface channel arrays opening into a hollow core for bone tissue and controlled drug release applications. *Chem. Eng. J.* 407, 126667. doi: 10.1016/j.cej.2020.126667

Kent, W.S. (1870). On the 'Hexactinellidae' or hexradiate spiculed silicious sponges taken in the 'Norna' expedition off the coast of Spain and portugal. with description of new species, and revision of the order. *Mon. Microsc. J.* 4, 241–252.

Klitgaard, A. B., and Tendal, O. S. (2004). Distribution and species composition of mass occurrences of large-sized sponges in the northeast Atlantic. *Prog. Oceanogr.* 61, 57–98. doi: 10.1016/j.pocean.2004.06.002

Maldonado, M., Aguilar, R., Bannister, R. J., Bell, J. J., Conway, K. W., Dayton, P. K., et al. (2015). "Sponge grounds as key marine habitats: A synthetic review of types, structure, functional roles, and conservation concerns," in *Marine animal forests*. Eds. L. Bramanti, A. Gori and C. Orejas Saco del Valle (Cham: Springer). doi: 10.1007/978-3-319-17001-5_24-1

Murillo, F. J., Muñoz, P. D., Cristobo, J., Rios, P., González, C., Kenchington, E., et al. (2012). Deep-sea sponge grounds of the Flemish cap, Flemish pass and the grand banks of Newfoundland (northwest Atlantic ocean): distribution and species composition. *Mar. Biol. Res.* 8, 842–854. doi: 10.1080/17451000.2012.682583

Murillo, F. J., Serrano, A., Kenchington, E., and Mora, J. (2016). Epibenthic assemblages of the tail of the grand bank and Flemish cap (northwest Atlantic) in relation to environmental parameters and trawling intensity. *Deep Sea Res. I* 109, 99–122. doi: 10.1016/j.dsr.2015.08.006

Nardo, G. D. (1847). Osservazioni anatomiche sopra l'animale marino detto volgarmente rognone di mare. atti delle adunanze dell'I. r. *Istituto Veneto di Sci. Lett. ed Arti.* 6, 267–276.

OSPAR Commission (2008). Descriptions of habitats on the OSPAR list of threatened and/or declining species and habitats (Reference Number: 2008-07).

Pham, C. K., Murillo, F. J., Lirette, C., Maldonado, M., Colaco, A., Ottaviani, D., et al. (2019). Removal of deep-sea sponges by bottom trawling in the Flemish cap area: conservation, ecology and economic assessment. *Sci. Rep.* 9, 15843. doi: 10.1038/s41598-019-52250-1

Pisera, A., and Vacelet, J. (2011). Lithistid sponges from submarine caves in the Mediterranean: taxonomy and affinities. *Sci. Marina* 75 (1), 17–40. doi: 10.3989/scsimar.2011.75n1017

Schmidt, O. (1864). Supplement der Spongien des adriatischen Meeres. Enthaltend die Histologie und systematische Ergänzungen. (Wilhelm Engelmann:Leipzig) 1-4, 1–48.

Schmidt, O. (1862). Die spongien des adriatischen meeres. *(Wilhelm Engelmann: Leipzig)* i-viii, 1–88.

Schmidt, O. (1870). *Grundzüge einer spongien-fauna des atlantischen gebietes* Vol. iii-iv (Leipzig: Wilhelm Engelmann), 1–88.

Thomson, C. W. (1869). On *Holtenia*, a genus of vitreous sponges. *Proc. R. Soc. London* 18, 32–35. doi: 10.1111/j.1365-2818.1869.tb01857.x

Xavier, J. R., Tojeira, I., and Van Soest, R. W. M. (2015). On a hexactinellid sponge aggregation at the great meteor seamount (North-east Atlantic). *J. Mar. Biol. Assoc. UK* 95 (7), 1389–1394. doi: 10.1017/S0025315415000685

frontiers in Marine Science

ORIGINAL RESEARCH
published: 04 June 2020
doi: 10.3389/fmars.2020.00395

Sponge Density and Distribution Constrained by Fluid Forcing in the Deep Sea

Timothy Culwick[1], Jeremy Phillips[1], Claire Goodwin[2,3], Emily J. Rayfield[1] and Katharine R. Hendry[1]*

[1] School of Earth Sciences, Faculty of Science, University of Bristol, Bristol, United Kingdom, [2] Huntsman Marine Science Centre, Saint Andrews, NB, Canada, [3] Department of Biological Sciences, University of New Brunswick, Fredericton, NB, Canada

Understanding the distribution and density of sponge grounds in the deep sea is key to appreciating the ecological importance, vulnerability, and role in ocean biogeochemistry of these important habitats. A novel combination of clustering analysis and fluid flow finite element modeling was used to study the distribution of four sponge grounds from the Labrador Sea, which were chosen for their distinct assemblages of sponges. Significant small-scale clustering patterns of sponges were found within each sponge ground, measured using the Ripley K function. A new approach using finite element modeling of fluid flow was then applied to understand the drivers of the observed sponge distribution, with detailed numerical experiments providing insights into the flow patterns that could not be obtained from field measurements. Simulations using idealized sponge shapes suggested that sponge wakes could interact and influence the mean flow conditions at the spacings observed within the sponge grounds. Simulations of flow over topographic models of the sponge grounds showed that these interacting wakes generated a boundary layer of slowed flow, which may be beneficial to sponge development. The boundary layer may be acting as a protective layer, affecting larval recruitment, increasing particle fall out, and increasing the effective radius of pumping. This observation has important implications for the impact of anthropogenic damage on sponge grounds, which changes the sponge distribution and may reduce the boundary layer thickness, affecting potential recovery rates. This study illustrates the power of incorporating mathematical modeling with field observations in the deep sea to increase our understanding of anthropogenic and climate change impacts on sponge ground ecosystem structure and function.

Keywords: Sponges (Porifera), ecological function, finite element analysis, computational fluid dynamics, Labrador Sea, deep-sea ecosystems, sponge grounds

OPEN ACCESS

Edited by:
Shirley A. Pomponi, Florida Atlantic University, United States

Reviewed by:
Ian David Tuck, National Institute of Water and Atmospheric Research (NIWA), New Zealand
Travis William Washburn, University of Hawai'i at Mānoa, United States

****Correspondence:***
Timothy Culwick
timothy.culwick@bristol.ac.uk

Specialty section:
This article was submitted to Deep-Sea Environments and Ecology, a section of the journal Frontiers in Marine Science

Received: *23 February 2020*
Accepted: *07 May 2020*
Published: *04 June 2020*

Citation:
Culwick T, Phillips J, Goodwin C, Rayfield EJ and Hendry KR (2020) Sponge Density and Distribution Constrained by Fluid Forcing in the Deep Sea. Front. Mar. Sci. 7:395. doi: 10.3389/fmars.2020.00395

INTRODUCTION

Sponges (Phylum Porifera) are an often overlooked as important components of benthic marine ecosystems. They are known to perform several functional roles notably as reef building organisms in both the shallow and deep-sea (Miller et al., 2012; Knudby et al., 2013; Roberts et al., 2018). Sponge grounds support areas of high biodiversity (Klitgaard and Tendal, 2004; Murillo et al., 2012;

Hawkes et al., 2019), act as nurseries for many fish species (Klitgaard, 1995; Freese and Wing, 2003), and can influence primary production by controlling nutrient availability (Bell, 2008; Maldonado et al., 2012; Murillo et al., 2012; Kutti et al., 2013; Maldonado, 2016). This ecological importance is complimented by their economic potential from bioengineering (Wu et al., 2019) and novel chemicals for pharmaceutical applications (Koopmans et al., 2009; Anjum et al., 2016). However, despite their ecological and socioeconomic importance, sponges are vulnerable to anthropogenic stressors such as trawl fishing (Kenchington et al., 2014; Pusceddu et al., 2014; Victorero et al., 2018) and oil and gas activities (Vad et al., 2018). Sponge ground locations and densities need to be known, in order to quantify their distribution and function, and—ultimately—protect the critical habitats that they form. In the deep-sea, observational data are very limited due to the difficulties in conducting science at depth, such as the cost and limited field-of-view of remotely operated vehicles (Henry and Roberts, 2014a,b; Howell et al., 2014). Computational models can be used to interpolate and quantitatively predict sponge distribution, helping to circumvent the challenges involved in understanding the factors that control sponge distribution. The large (basin) scale distribution of sponge grounds in the North Atlantic has been studied. However, sponge distribution and density within deep-sea sponge grounds has been understudied and remains poorly constrained (Klitgaard and Tendal, 2004; Cathalot et al., 2015; Kazanidis et al., 2019).

Studies on sponge density and distribution in shallow water environments have been carried out using standard ecology survey techniques, with multiple studies across environments and latitudes (Wilkinson and Evans, 1989; Roberts and Davis, 1996; Xavier and van Soest, 2012). However, the major drivers of these distribution patterns such as wave damage, water opacity, and light levels do not operate in the deep-sea. Empirical analysis of localized distribution in deep-sea sponge grounds is very limited with most data being purely observational or on species occurrence only (Henry and Roberts, 2014a). Studies of sponge density have been carried out in the Faroe-Shetland Channel where fisheries pressure and substrate type (sand, gravel, cobble) were statistically significant factors (Kazanidis et al., 2019). However, a host of other chemical oceanographic variables (silicic acid, temperature, etc.) also exhibited strong controls over sponge density (Kazanidis et al., 2019). The influence of multiple forcing mechanisms results in significant challenges in scaling-up from a small number of observational data points to whole-basin sponge ground densities using oceanographic variables (Howell et al., 2016). Creating mathematical simulations of current conditions in the deep sea allows us to explore whether the observed distribution of sponges is related to prevailing currents. This in turn provides possible explanation of the patterns seen which could be scaled up to infer large-scale distributions. The simulations of the observed sponge grounds also allow a more detailed investigation of the small-scale flow patterns that would not be possible to measure the field, with the potential to increase our understanding of this important and understudied habitat.

Patterns of deep-sea sponge distribution and density have been attributed to several factors in large scale biogeographic studies. The primary drivers of sponge distribution are thought to be silicic acid concentration (Beazley et al., 2015; Howell et al., 2016) temperature, depth (Rice et al., 1990; Bett, 2001; Murillo et al., 2012), and particulate carbon availability (Barthel et al., 1996; Howell et al., 2016), in addition to topography, internal waves, and current speeds which control flow conditions at the seafloor (Klitgaard and Tendal, 2004; Howell et al., 2016). It would be logical to assume these factors would also play a role at the smaller scale and that sponge distribution would potentially be optimized to improve their localized conditions (Kutti et al., 2013). The arrangement of organisms can affect the flow around individuals, either spacing themselves the maximum distance from each other to receive the greatest unprocessed flow potential, or clustering to slow the flow for potentially greater particle dropout or protection from damage. These patterns in distribution are seen abundantly in nature such as in corals (Chindapol et al., 2013; Cresswell et al., 2017) and terrestrially in trees (Holtmeier and Broll, 2017).

Here, we will investigate whether the patterns of density and distribution at small spatial scales in four different sponge grounds in the Labrador Sea are linked to the prevailing flow conditions, and will explore possible explanations for the patterns observed. We discuss the implications and possible explanations of our results, as well as their potential impacts on the greater understanding of the role and sensitivity of sponge grounds in the deep-sea.

MATERIALS AND METHODS

Sponge Ground Imaging

Sponge ground images were recorded on the DY081 RRS *Discovery* cruise summer 2017 at three locations: Orphan Knoll, Nuuk, and Southwest Greenland (SWGL) (**Figure 1**) each chosen due to their differing water mass interactions. High-definition video was recorded via Remotely Operated Vehicle (UK National Marine Facilities ROV *Isis*) using a fixed view Scorpio camera. Images were recorded from a typical height of 1 m above the sea floor, with the field of view varying in width between 1 and 3 m. Lasers were attached to the Scorpio camera at 10 cm spacing so scale could be accurately resolved from images. The study areas were randomly selected within each location. A single study area was chosen for Nuuk (**Figures 1**, **2A**) and SWGL Localities (**Figures 1**, **2B**), which were uniform in depth and have no dominant species. Two study areas were assigned at Orphan Knoll, due to the presence of two distinct sponge grounds at separate depths characterized by different dominant groups. These are (i) a *Geodia* dominated sponge ground (GOK; **Figures 1**, **2C**) and (ii) a hexactinellid dominated sponge ground (HOK; **Figures 1**, **2D**) at greater depth. Still images were the taken from the video at 2 s intervals which was sufficient to ensure that typically 30 individual, overlapping images were available to create a digital surface model of between 3 and 5 m in length.

Digital Surface Model

Surface mesh models were created from sets of images for each study area using photogrammetry. Agisoft PhotoScan

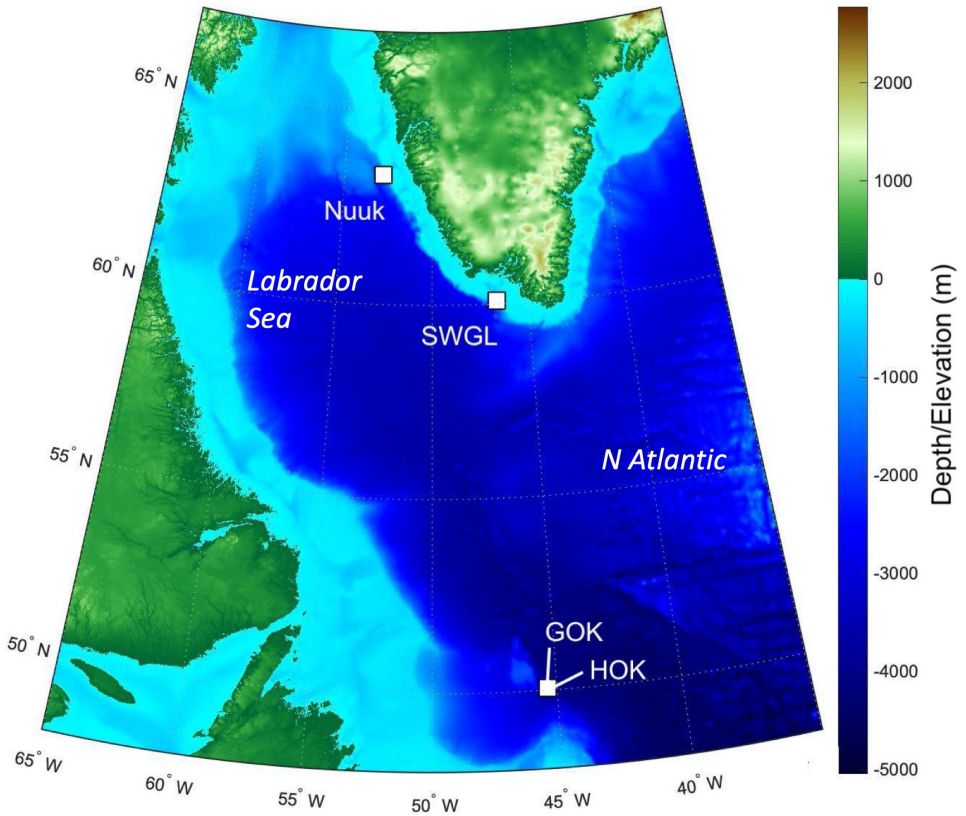

FIGURE 1 | Overview map showing the position and depth of the four localities Nuuk, Southwest Greenland (SWGL), *Geodia* dominated sponge ground at Orphan Knoll (GOK), and hexactinellid dominated sponge ground at Orphan Knoll (HOK) from the DY081 Cruise in the Labrador Sea. Bathymetry used is from ETOPO1 model from https://www.ngdc.noaa.gov/mgg/global/.

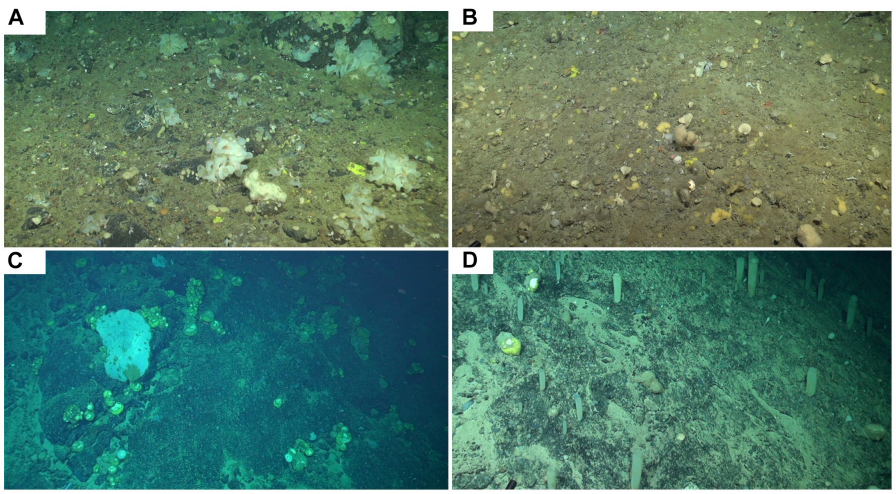

FIGURE 2 | ROV Image of the four study areas from the DY081 Cruise **(A)** Nuuk, **(B)** SWGL, **(C)** GOK, and **(D)** HOK. Red laser scale makers are 10 cm apart.

software was used to align the images and create a 3D surface mesh using structure-form-motion algorithms (Westoby et al., 2012); the SGM algorithm (Hirschmüller, 2005) and scale invariant feature transform (SIFT) operator (Lowe, 2004). A scaled 3D surface mesh was exported as a.stl file and a 2D point cloud map of sponge locations exported as a point pattern dataset. The 3D surface mesh was converted using AutoCAD Software to AutoCAD Drawing format to

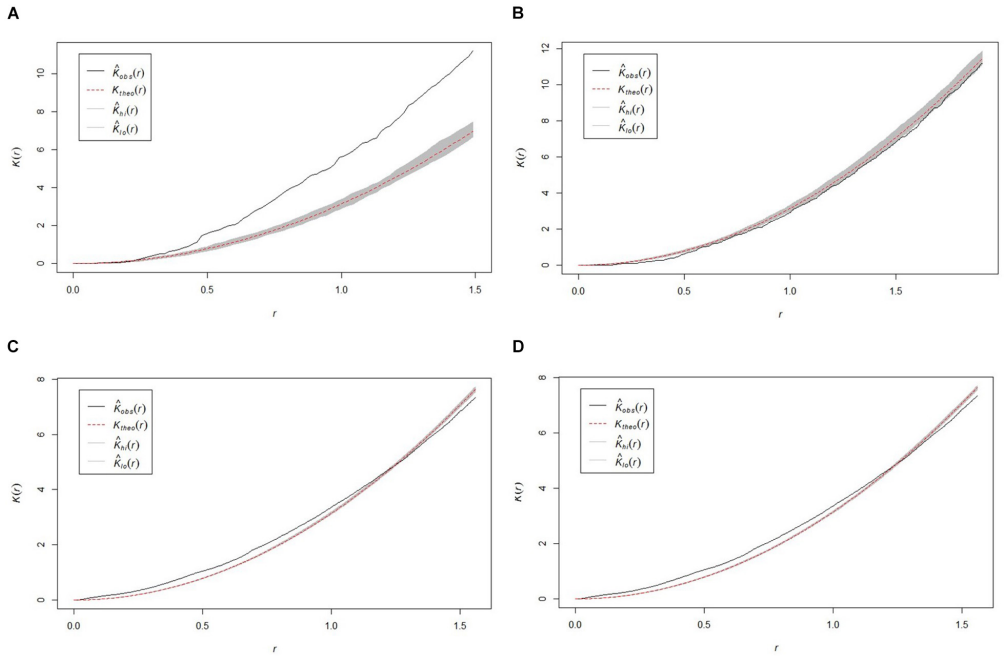

FIGURE 3 | Plots of the Ripley K function clustering analysis (K) for the four study areas **(A)** HOK study area, **(B)** Nuuk study area, **(C)** GOK study area, and **(D)** SWGL study area. Observed value for K [$K_{obs}(r)$] theoretical random distribution value for K [$K_{theo}(r)$] < 95% confidence limit of random distribution between upper confidence bound [$K_{Hi}(r)$] and lower confidence bound [$K_{lo}(r)$].

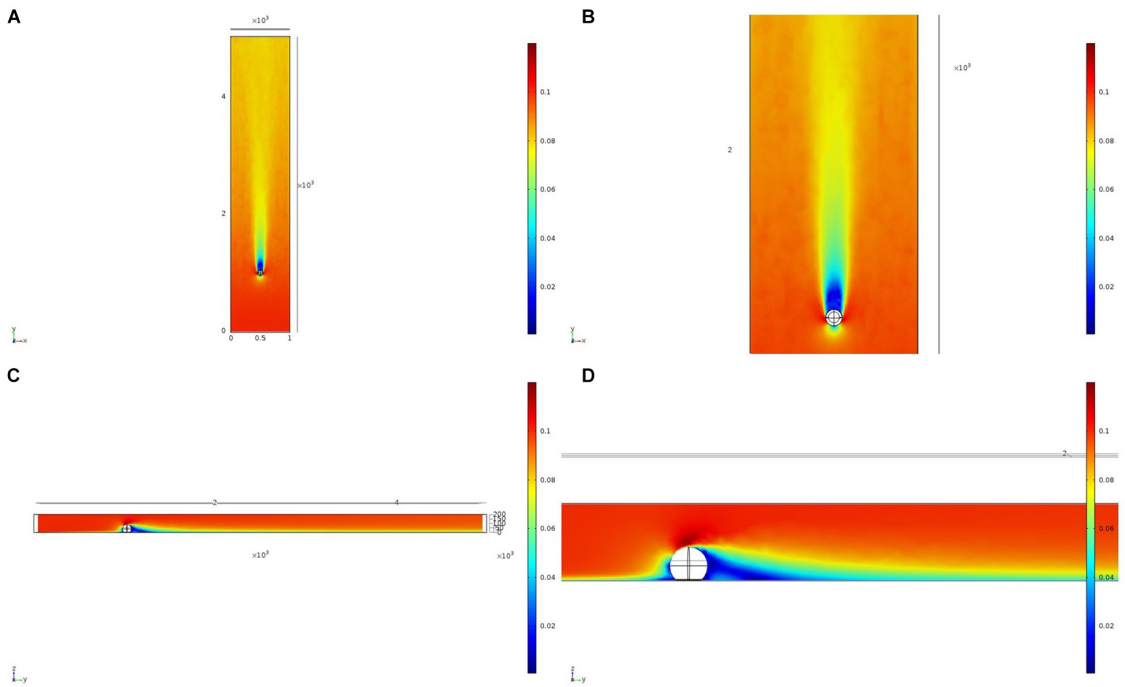

FIGURE 4 | Results of the fluid flow finite element analysis simulation for an idealized sphere, visualized as two-dimensional plots [horizontal **(A,B)** and vertical **(C,D)** cross sections] of flow velocity magnitude (false-color scales m/s). Scale in mm with ambient flow of 0.1 m/s along the *y*-axis. **(B,D)** Zoom in on the wake close to the sphere.

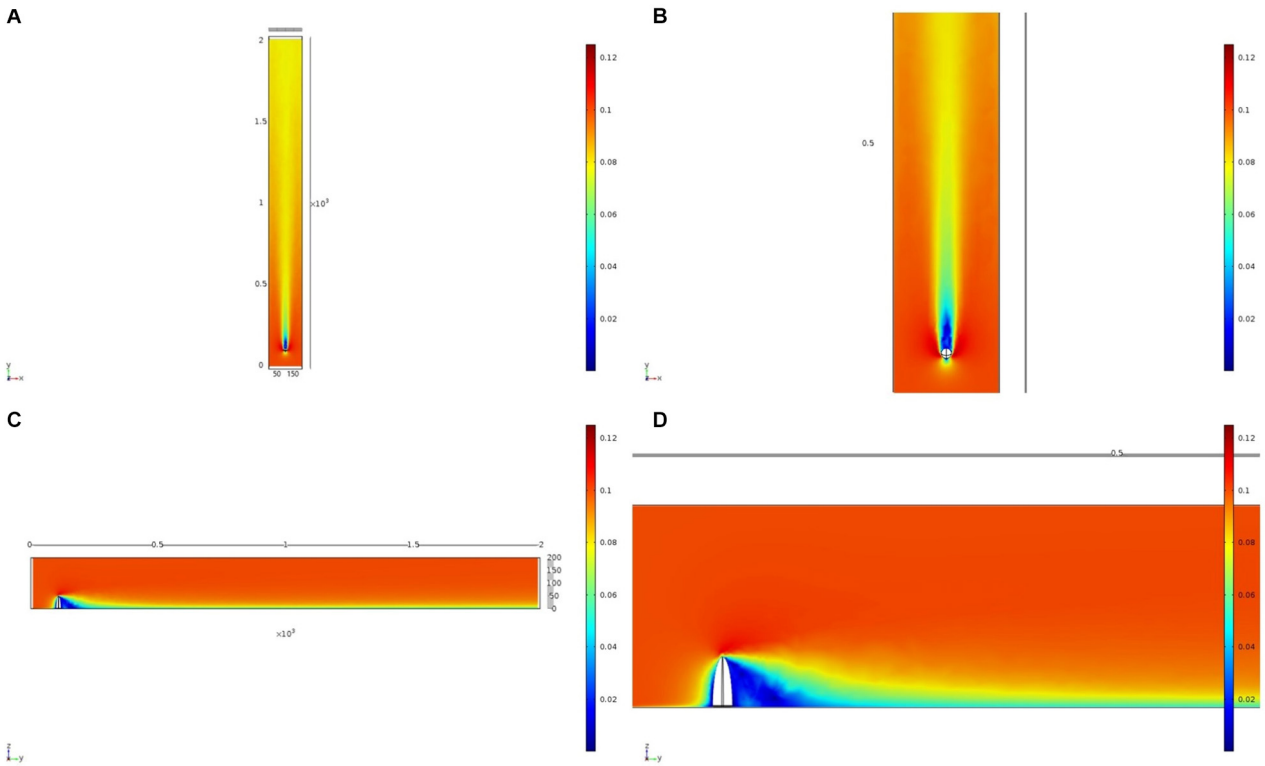

FIGURE 5 | Results of the fluid flow finite element analysis simulation for an idealized ellipsoid, visualized as two-dimensional plots [horizontal **(A,B)** and vertical **(C,D)** cross sections] of flow velocity magnitude (false-color scales m/s). Scale in mm with ambient flow of 0.1 m/s along the *y*-axis. **(B,D)** Zoom in on the wake close to the ellipsoid.

use as a solid boundary in COMSOL Multiphysics flow modeling simulations.

Clustering Analysis

A point pattern map for each locality was input into RStudio, such that each point represents the position of an individual sponge. Multi-distance spatial cluster analysis was carried out using Ripleys K functions (Ripley, 1976, 1977, 1981). The K-function is defined by:

$$\mathrm{K}\left(d\right) = \lambda^{-1} \sum_{i \neq j} \frac{I(d_{ij} < t)}{n}$$

Where d_{ij} is the Euclidean distance between ith and jth points in a dataset of n points, t is the search radius, λ is the average density of points (generally estimated as n/A, where I is the area which contains all the points), and $\pi t^2$is the indicator function (1 if its operand is true, otherwise 0). $\mathrm{K}\left(d\right)$ approximates πt^2 if the points are homogenous with the region. This radial spatial analysis can become unrepresentative when applied close to the edges of the domain, because of the truncation of information at the edge. We used periodic boundary conditions (such that an edge of the domain is joined to its opposite edge and analysis treats this as a continuous surface) to eliminate the edge effect, which may have been significant given the narrow transects. Upper and lower bounds of confidence of statistical significance were produced using Monte Carlo simulations. Monte Carlo simulations randomly generate a distribution of points equal to the number of input points. Multiple simulations were run and used to ensure clustering patterns were not due to random variation (at the 95% confidence level).

Fluid Flow Finite Element Analysis

We modeled the flow around idealized sponge shapes and around the 3D surface models of the sponge ground study areas using the finite-element package Comsol Multiphysics 5.1. The dimensions of the idealized sponge shapes were based on average sponge sizes of *geodia* and *Euplectella* species collected on the DY081 Cruise. The flow field was described using the Reynolds-averaged Navier–Stokes (RANS) equations coupled with the K-epsilon (K-ε) Turbulence model (Hanjaliæ and Launder, 1972). The flow was computed using the 3D surface meshes generated from photogrammetry, with a no-slip basal boundary condition, open boundaries (zero viscous stress condition) for those perpendicular to flow, downstream and upper boundaries, and a uniform inflow velocity at the upstream end. Initial flow conditions within the model area for the simulation calculations were set as a steady flow equal in velocity to that of the inflow. Surface models were orientated so the simulated flow matched the observed current direction over the sea floor recorded at the time of the ROV survey.

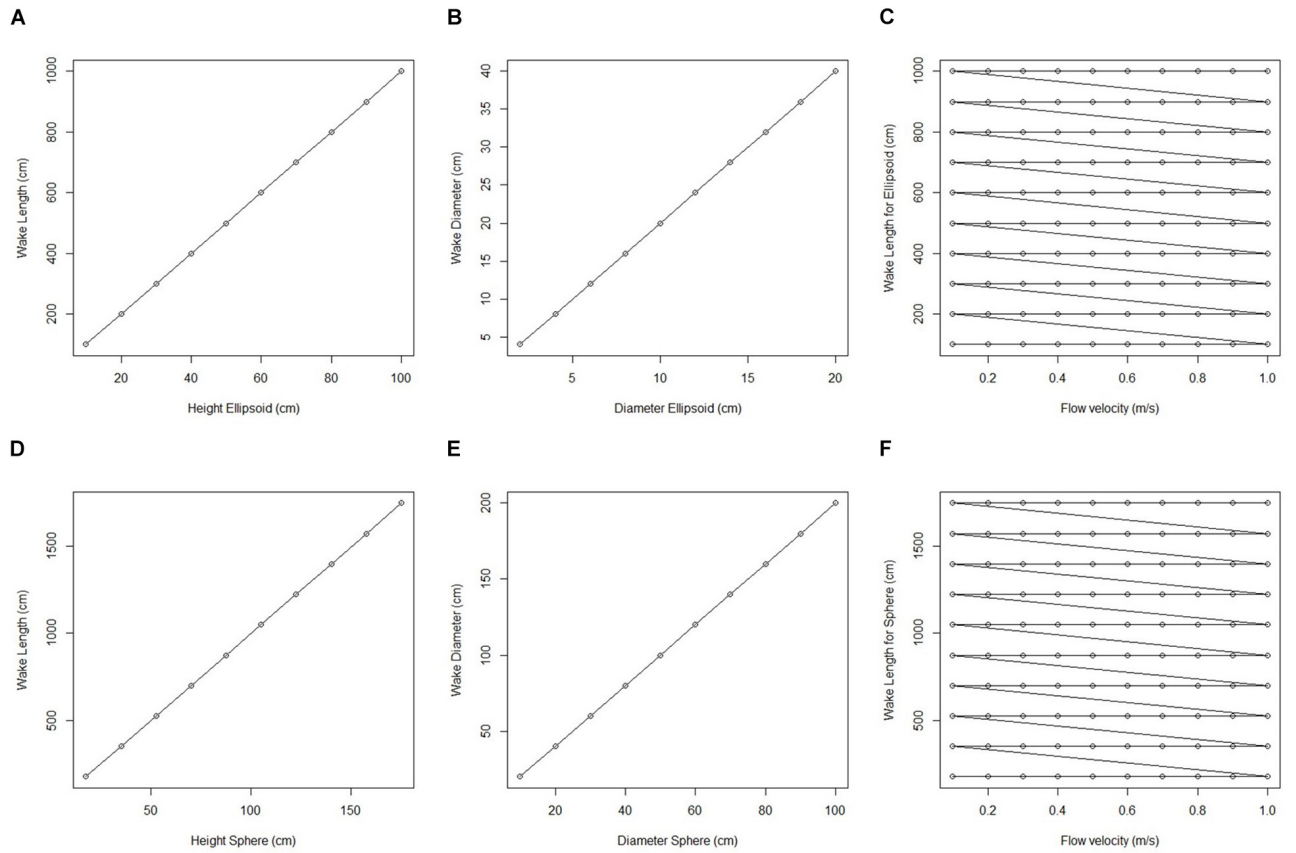

FIGURE 6 | Plots of wake dimension, object dimension and flow speed taken from fluid flow finite element analysis simulation for an idealized sphere and ellipsoid. **(A)** Wake length (cm) plotted against ellipsoid hight (cm). **(B)** Wake diameter (cm) plotted against ellipsoid diameter (cm). **(C)** Wake length for all ellipsoid simulations (cm) plotted against corresponding flow velocity (m/s). **(D)** Wake length (cm) plotted against sphere height (cm). **(E)** Wake diameter (cm) plotted against sphere diameter (cm). **(F)** Wake length for all sphere simulations (cm) plotted against corresponding flow velocity (m/s).

A mesh was created using free tetrahedral elements for the geometries using the finite element mesher by Comsol. A coarse mesh was used to enable an efficient exploration of model parameter space, with some simulations being run at finer mesh resolution to ensure grid scale independence for the simulation results. The inbuilt material properties for water were used with fixed solid geometry for the idealized simulations. In all cases, three-dimensional, incompressible (constant density) flow of water was simulated with idealized structures and sea floor reconstructions were held stationary.

Inlet and initial flow speed were varied between 0.1 and 1 m/s in 0.1 m/s intervals (Reynolds numbers for all simulation fall between approximately 1.53×10^5 and 7.5×10^6). The volumetric flow rate used was matched to the mean bottom flow rates observed using the sonde on the DY081 RRS *Discovery* cruise (Hendry, 2017) and the range based on year-round observations from Orphan Knoll (Greenan et al., 2010). A stationary solver was used to compute the steady-state flow patterns and a Turbulent flow k-ε model was used to solve the RANS equations and conservation of mass.

An initial simulation of three-dimensional flow around a sphere was used to benchmark the main Comsol simulations. The benchmarking method laid out in Nita and Allaire (2017) was used with drag coefficients for the flow around the sphere being in the range of 0.46–0.5 to verify the robustness of the numerical method used. Results were visualized as two-dimensional cross sections of flow velocity magnitude and wake length, and diameters were plotted against height and diameter for the idealized simulations.

RESULTS

Clustering Analysis

All study areas exhibited non-random ($p < 0.05$) sponge distribution patterns, with variation in the presentation of distribution between sites (**Figure 3**). The SWGL (**Figure 3D**) and GOK (**Figure 3C**) sites exhibited similar patterns of distribution. Individual sponges cluster together at distances of 0.1–1.2 m and the distribution becomes more uniform at distances greater than 1.4 m indicating that they form dense, sparse clusters. The HOK (**Figure 3A**) site shows a very strong clustering pattern within the study area, although there is a random distribution at distances less than 0.25 m. The Nuuk

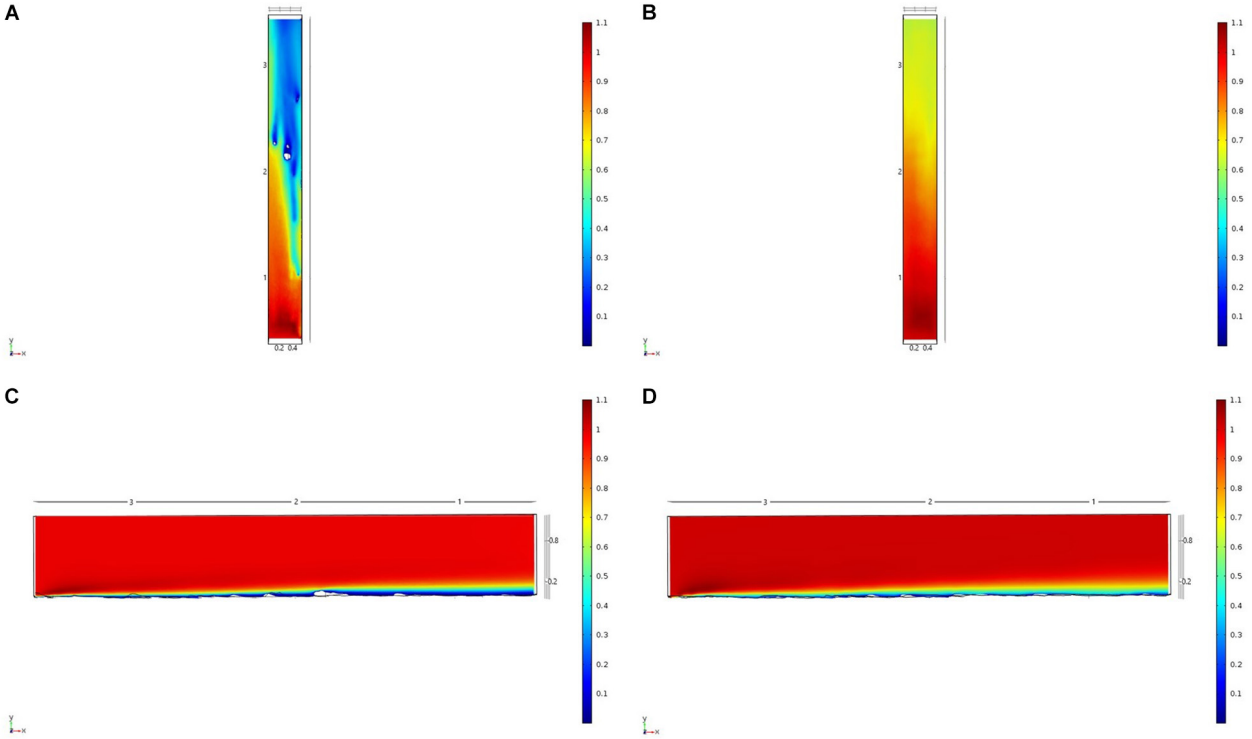

FIGURE 7 | Results of the fluid flow finite element analysis simulation for surface models for Nuuk Study area visualized as two-dimensional plots (horizontal and vertical cross sections) of flow velocity magnitude (false-color scales m/s). **(A,C)** Surface model with sponges present **(B,D)** surface model with sponge structures removed. Scale in m with ambient flow of 1 m/s along the *y*-axis.

(**Figure 3B**) study site in contrast exhibits a consistent non-random but weak dispersion patterning.

Models of Flow Around Idealized Sponge Morphologies

We initially used two simplified shapes to represent sponge morphology: a sphere and an ellipsoid. For both the spherical structure (**Figure 4**) and the ellipsoidal structure (**Figure 5**), the same patterns of wake (downstream regions of reduced flow velocity) are produced. There is a direct correlation between structure height and length of the initial wake, as well as the diameter of the wake and diameter of the structure (**Figure 6**). Wake length and diameter are mostly unaffected by flow speed with the changes of flow speeds within the wake being directly proportional to the changes to the ambient flow speed (**Figure 6**). The length of the effective slowing due to the wake is approximately 10 times the height of the structure, which is similar to wake lengths of submerged hemispherical objects (Shamloo et al., 2001). Beyond this wake region, the near-wall flow velocities are similar to those upstream. A second feature of both models is the presence of an area of lower velocity upstream and around the sides of the sponge structure caused by flow separation, which increases in size at high velocities (**Figures 4**, **5**). These initial tests indicate that, for the sponge spacings (up to 1.4/m^2) and heights (up to 0.5 m) in the four study areas, we expect the wakes of the sponges to be interacting and influencing the flow conditions.

Models of Flow at the Study Area

For each of the study areas, we ran simulations with sponges *in situ* and removed. Individual sponges created wakes that were significantly deeper than the boundary layer resulting from flow over the sea floor topography. The structures in the Nuuk study area (**Figure 7**) produced a boundary layer of similar height to that of the seafloor topography boundary layer but with a significantly slower velocity, which appears reduced by approximately 50% from the same point within the boundary layer. The area of wake influence from each sponge structure extends horizontally in a narrow cone pattern but the distance between each structure is such that a coherent and continuous boundary layer is produced, with properties set by the sponge height and spacing. Both SWGL (**Figure 8**) and HOK (**Figure 9**) sites show similar flow patterns as the Nuuk site but with slightly thinner boundary layers. Both SWGL and HOK have clusters of sponge structures sitting within small depressions causing the sheltering effect of the topography to make a greater contribution to the overall flow pattern. The GOK site (**Figure 10**) differs due to the prominence of a single large sponge $>$ 0.5 m in diameter and height. The flow patterns around the large sponge result in a significantly sheltered area where smaller sponges are clustering. There are other small clusters of medium-sized sponges causing

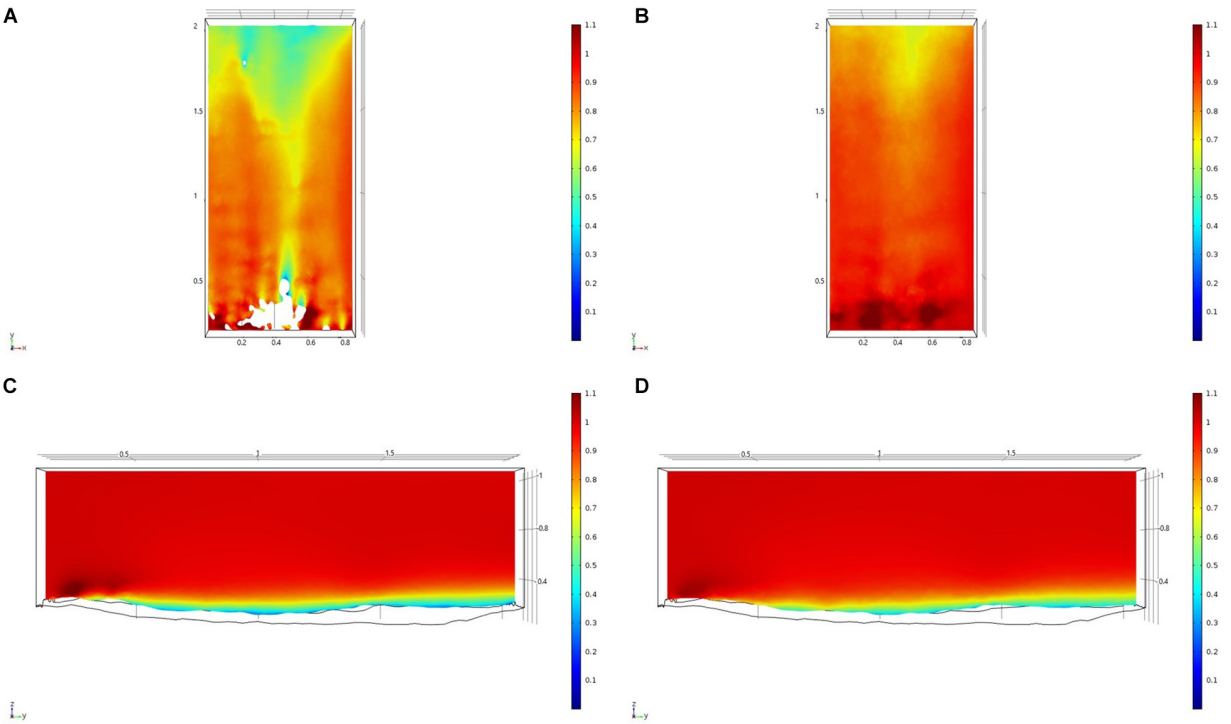

FIGURE 8 | Results of the fluid flow finite element analysis simulation for surface models for SWGL Study area visualized as two-dimensional plots (horizontal and vertical cross sections) of flow velocity magnitude (false-color scales m/s). **(A,C)** Surface model with sponges present. **(B,D)** Surface model with sponge structures removed. Scale in m with ambient flow of 1 m/s along the *y*-axis.

localized areas of low flow. However, an extensive coherent boundary layer is not observed.

DISCUSSION

Do Sponges Cluster?

Patterns of distributions within sponge grounds have been noted before, but there has not been an analysis to date of the clustering patterns themselves (Kutti et al., 2013; McIntyre et al., 2016). Clustering analysis gives a more robust approach to studying these patterns, by removing observational bias and allowing robust statistical tests to be performed to validate observations and hypotheses (Baddeley et al., 2014). As the sponge grounds chosen as study sites are defined by distinct assemblages of sponges, it is interesting but not surprising that different functional groups follow distinct clustering patterns. The ability to scale up the distributions described here are limited due to the small study area. Their size is limited by the diameter of the areas surveyed by the ROV (Hendry, 2017; Hendry et al., 2019). However, our flow-modeling method could be extended to a broader geographical area, and combined with localized environmental data and predictions, to make inferences about environmental driving factors for sponge distribution in sponge grounds on wider spatial and temporal scales. Uniquely, a modeling approach also allows us to simulate a great range of environmental conditions and therefore can be used as a predictive tool for both potential hypotheses and expected optimal conditions.

Why Are Sponges Clustering?

The variability and the driving factors behind these distributions could be wide-ranging, from dispersion of gametes (Abelson and Denny, 1997) to food availability (Robertson et al., 2017). One factor that can be studied within limited geographical areas is localized flow around the sponges. Is this driving distribution patterns in deep-sea sponge grounds? This new application of modeling techniques to localized flow around sponge allows us to address such questions, previously not possible from observational approaches, especially in deep-sea environments.

We need to quantify the pattern of flow around a single structure to understand how fluid flow could be affecting the distribution of individuals within a sponge ground. The creation of both idealized single organism models and study area models give us a better understanding of this flow. The idealized models give us the predicted size and length of the wake given average heights of the sponges. In our study areas, the length of the wake is greater than the spacing between individuals in the sponge grounds, so the wake effect of other sponges is predicted to influence organism structures. The wake length-scales found in this study suggest that sponges that appear isolated may be influenced by the wake of other individuals to a greater extent than previously expected.

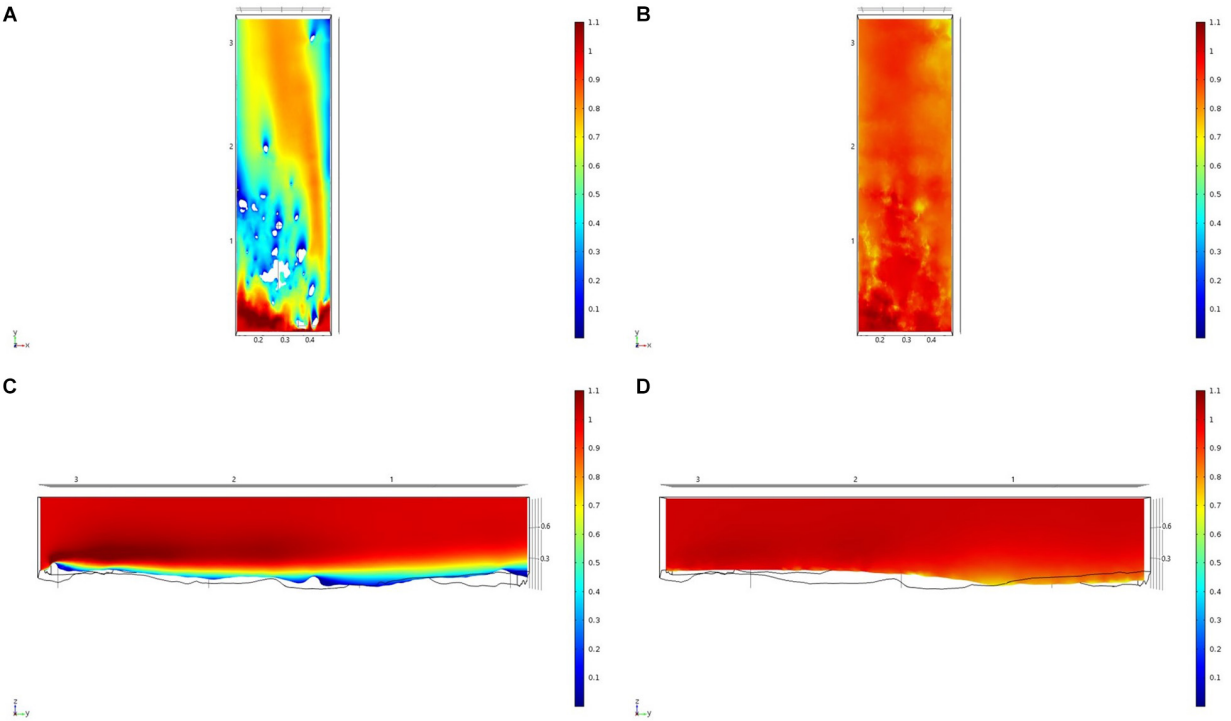

FIGURE 9 | Results of the fluid flow finite element analysis simulation for surface models for HOK Study area visualized as two-dimensional plots (horizontal and vertical cross sections) of flow velocity magnitude (false-color scales m/s). **(A,C)** Surface model with sponges present. **(B,D)** Surface model with sponge structures removed. Scale in m with ambient flow of 1 m/s along the *y*-axis.

When the flow around the sponge structures within each study area is modeled and compared with the same seafloor surface without these structures, a significantly thickened boundary layer is observed as predicted by the idealized models (**Figures 4**, **5**). This slowing effect is due to the overlapping of the wakes of each individual sponge to create a relatively uniform area of slowed flow. Directly linking the slowed boundary layer as the driver behind patterns of distribution is difficult and would require many more and varied study sites. However, the observation of this slowed boundary layer and its potential effect as a factor in sponge distribution is important in its own right. Are the sponges distributing themselves to benefit from the slowed flow in this layer and, if so, what advantage does it provide?

Advantages of Manipulating the Boundary Layer

The effects of flow on an individual sponge organism broadly fall into three categories: gamete dispersion (Abelson and Denny, 1997), nutrient supply (Kahn et al., 2018), and mechanical forcing (Palumbi, 1986). The presence of a slowed boundary layer whose thickness is governed by the velocity of the flow and roughness of the surface has the effect of reducing any mechanical forcing. This lowering in the forces applied to a sponge will reduce the likelihood of damage or attachment failure due to high flow. Average flow velocities in deep sea sponge grounds are low in our study sites (∼0.1 m/s) (Hendry, 2017; Hendry et al., 2019) so this protective effect is likely negligible. However, records of much higher flow velocities during storm events > 1 m/s are recorded the depths of these study areas (Greenan et al., 2010). The high mechanical forcing at these velocities would mean the slowed boundary layer would offer significant protection for both sponges and other organisms associated with sponge grounds (Klitgaard, 1995; Freese and Wing, 2003; Miller et al., 2012).

The most obvious impact of a reduced flow around the sponge on nutrient supply appears to be deleterious: reduced flow would result in a reduced supply of particulate and dissolved organic and inorganic (e.g., dissolved silicon) nutrients to the organism. However, flow speed and nutrient supply may be a more nuanced association due to particulate fallout rate and the active pumping effect of the sponges themselves. The slowing of the boundary layer may result in a greater proportion of the particulates carried by the flow above to be deposited around the sponges. The flow above the boundary layer is not slowed so the vertical supply of particulates to the sponges may increase even if the flow acting on the sponges themselves is reduced. Imposing a sediment flux into the model would be interesting to investigate as a next step in the development of this research.

The reduction in flow speed at the sea floor due to the boundary layer could potentially lead to an increase in larvae deposition and recruitment (Abelson and Denny, 1997). The deposition and retention of larvae in the sponge ground should increase with lower flow speeds, and larvae attachment rates should also increase due to reduced flow stress (Mariani et al.,

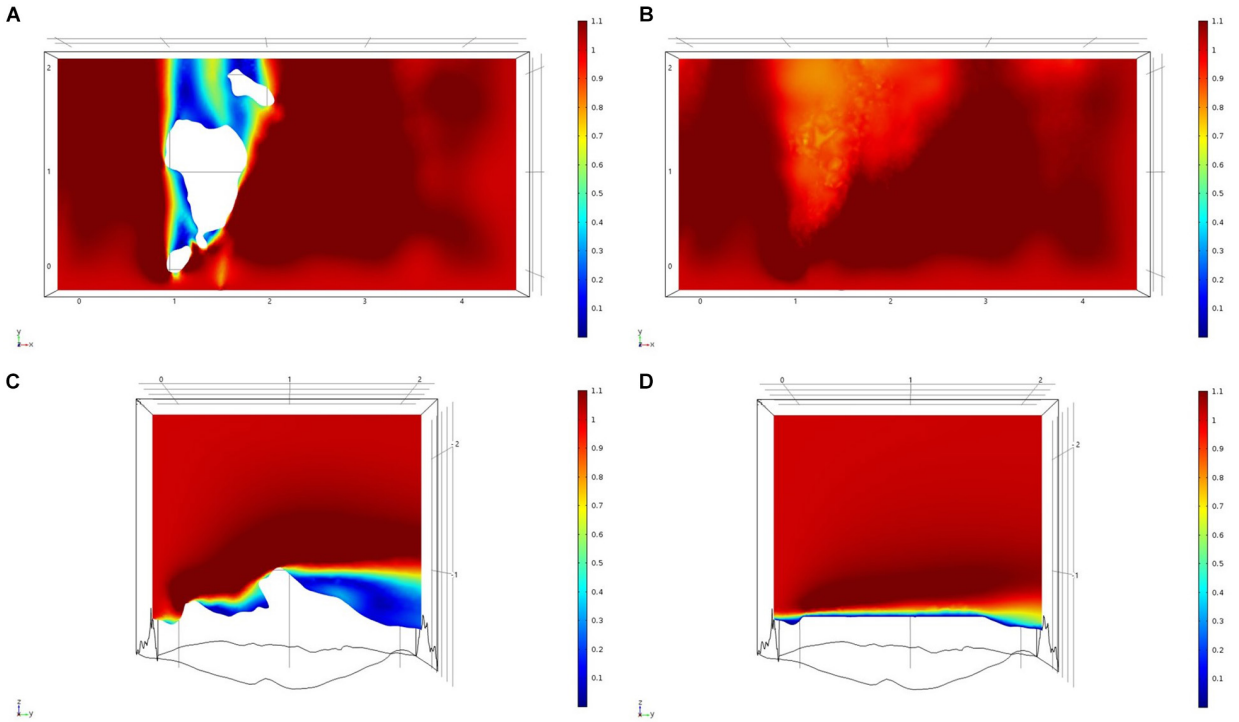

FIGURE 10 | Results of the fluid flow finite element analysis simulation for surface models for GOK Study area visualized as two-dimensional plots (horizontal and vertical cross sections) of flow velocity magnitude (false-color scales m/s). **(A,C)** Surface model with sponges present. **(B,D)** Surface model with sponge structures removed. Scale in m with ambient flow of 1 m/s along the *y*-axis.

2006; Guillas et al., 2019). An increase in larvae deposition and retention impacts the recruitment of new individuals within the sponge grounds and should increase its ability to grow and recover from damage.

The importance of ambient flow rate compared to pumping rates for sponges is challenging to determine (Leys et al., 2011; Ludeman et al., 2017). Sponges appear to stop pumping at higher flows but whether this is to protect the canal system from being clogged and damaged (Ludeman et al., 2017; Strehlow et al., 2017), because it is unnecessary for flow though the sponge (Leys et al., 2011), or due to another underlying mechanism, is currently unclear. Regardless, the presence of a slowed boundary layer is influential for each of these mechanisms. A slowed boundary layer may be advantageous as the sponge may be able to pump for longer before it must shut down for protection, or disadvantageous due to higher energy expenditure.

A noticeable feature of the idealized model is the boundary effect of the structures themselves (**Figures 4**, **5**). A future avenue of exploration would be to investigate how this impacts the potential radius of intake around the sponge due to pumping. At what point does the pumping rate become negligible compared to the dividing flow and increased turbulence around the structure, effectively isolating it from the surrounding flow? Does this result in a slower rate of flow becoming advantageous, as the pumping rate with lower turbulence would be more effective and could draw in particulates that would otherwise be lost to the current? Modeling would be particularly useful in investigating the behavior of particles and turbulent currents around sponges, both of which are challenging to measure or observe *in situ* because of interference from any recording device on the flow.

Regardless of the mechanism by which a slowed boundary layer is created, its presence has additional and important consequences for other organisms associated with sponge grounds (Freese and Wing, 2003; Miller et al., 2012). It also has potential corollaries for conserving sponge grounds under threat of damage by anthropogenic activities. Removal of the sponge structures (e.g., by trawling) would result in the boundary layer velocities not being reduced as much, which—if this feature is beneficial—will have implications for any future recruitment of larvae and recovery of sponges, and so the sponge ground habitat itself.

CONCLUSION

This study shows that there are significant small-scale patterns in distribution of sponges within sponge grounds in the Labrador Sea. Further, we have developed a new approach to studying the drivers of these observed patterns using fluid flow modeling. The models produced allowed detailed quantitative experiments to be conducted, producing data that would be impossible to obtain from field observations alone. By applying these models to sponge structures taken from four study areas in the North Atlantic, we identified a slowed boundary layer caused by sponge aggregations

that may account for some of the distribution patterns. This slowed boundary layer may be acting as a protective layer, increasing larval recruitment or promoting increased particulate organic matter uptake due to increases in both particulate fallout from flow and effective radius of pumping. These observations increase the importance of protecting sponge grounds from anthropogenic damage as the removal of this slowed layer coupled with the relatively slow growth rates of sponges in the deep-sea and decreased larval recruitment could result in the inability of sponge ground to recover once damaged. This study highlights the importance of coupling mathematical modeling with field observations in the deep sea to provide a much greater understanding of anthropogenic and climate change impacts on sponge ground ecosystem structure and function, and biogeochemical cycling by sponges.

DATA AVAILABILITY STATEMENT

The datasets generated for this study are available on request to the corresponding author.

AUTHOR CONTRIBUTIONS

TC, JP, and KH conceived the study. TC carried out the study, wrote the manuscript, and prepared the figures. All authors analyzed the data, revised drafts of the manuscript, and gave final approval for the publication.

FUNDING

Funding was from the European Research Council (ERC Starting Grant 678371 ICY-LAB). JP acknowledges funding through a University of Bristol Research Fellowship.

ACKNOWLEDGMENTS

We would like to thank Mark Woodhouse, Veerle Huvenne, and Kerry-Louise Howell for their discussion and assistance.

REFERENCES

Abelson, A., and Denny, M. (1997). SETTLEMENT OF MARINE ORGANISMS IN FLOW. *Annu. Rev. Ecol. Syst.* 28, 317–339. doi: 10.1146/annurev.ecolsys.28.1.317

Anjum, K., Abbas, S. Q., Shah, S. A. A., Akhter, N., Batool, S., and Hassan, S. S. U. (2016). Marine sponges as a drug treasure. *Biomol. Ther.* 24, 347–362. doi: 10.4062/biomolther.2016.067

Baddeley, A., Diggle, P. J., Hardegen, A., Lawrence, T., Milne, R. K., and Gopalan Nair, A. (2014). On tests of spatial pattern based on simulation envelopes. *Ecol. Monogr.* 84, 477–489. doi: 10.1890/13-2042.1

Barthel, D., Tendal, O. S., and Thiel, H. (1996). A wandering population of the hexactineliid sponge pheronema carpenteri on the continental slope off morocco, Northwest Africa. *Mar. Ecol.* 17, 603–616. doi: 10.1111/j.1439-0485.1996.tb00420.x

Beazley, L., Kenchington, E., Yashayaev, I., and Murillo, F. J. (2015). Drivers of epibenthic megafaunal composition in the sponge grounds of the Sackville Spur, northwest Atlantic. *Deep Sea Res. I Oceanogr. Res. Pap.* 98, 102–114. doi: 10.1016/J.DSR.2014.11.016

Bell, J. J. (2008). The functional roles of marine sponges. *Estuar. Coast. Shelf Sci.* 79, 341–353. doi: 10.1016/J.ECSS.2008.05.002

Bett, B. J. (2001). UK Atlantic Margin Environmental Survey: introduction and overview of bathyal benthic ecology. *Cont. Shelf Res.* 21, 917–956. doi: 10.1016/S0278-4343(00)00119-9

Cathalot, C., Van Oevelen, D., Cox, T. J. S., Kutti, T., Lavaleye, M., Duineveld, G., et al. (2015). Cold-water coral reefs and adjacent sponge grounds: hotspots of benthic respiration and organic carbon cycling in the deep sea. *Front. Mar. Sci.* 2:37. doi: 10.3389/fmars.2015.00037

Chindapol, N., Kaandorp, J. A., Cronemberger, C., Mass, T., and Genin, A. (2013). Modelling growth and form of the scleractinian coral *Pocillopora verrucosa* and the influence of hydrodynamics. *PLoS Comput. Biol.* 9:e1002849. doi: 10.1371/journal.pcbi.1002849

Cresswell, A. K., Thomson, D. P., Trevenen, E. J., and Renton, M. (2017). "A functional-structural coral model," in *Proceedings of the MODSIM2017: 22nd International Congress on Modelling and Simulation*, (Sydney: Modelling and Simulation Society of Australia and New Zealand Inc), 237–243.

Freese, J. L., and Wing, B. L. (2003). Juvenile red rockfish, *Sebastes* sp., associations with sponges in the Gulf of Alaska. *Mar. Fish. Rev.* 65, 38–42.

Greenan, B. J. W., Yashayaev, I., Head, E. J. H., Harrison, W. G., Azetsu-Scott, K., Li, W. K. W., et al. (2010). "Interdisciplinary oceanographic observations of Orphan Knoll," in *Proceedings of the NAFO Sci. Counc. Meet. 10/19*, Dartmouth.

Guillas, K. C., Kahn, A. S., Grant, N., Archer, S. K., Dunham, A., and Leys, S. P. (2019). Settlement of juvenile glass sponges and other invertebrate cryptofauna on the Hecate Strait glass sponge reefs. *Invertebr. Biol.* 138:e12266. doi: 10.1111/ivb.12266

Hanjaliæ, K., and Launder, B. E. (1972). A Reynolds stress model of turbulence and its application to thin shear flows. *J. Fluid Mech.* 52, 609–638. doi: 10.1017/S002211207200268X

Hawkes, N., Korabik, M., Beazley, L., Rapp, H. T., Xavier, J. R., and Kenchington, E. (2019). Glass sponge grounds on the Scotian Shelf and their associated biodiversity. *Mar. Ecol. Prog. Ser.* 614, 91–109. doi: 10.3354/meps12903

Hendry, K. (2017). *RRS Discovery DY081 - Cruise Summary Report*. Available online at: https://www.bodc.ac.uk/resources/inventories/cruise_inventory/report/16378/ (accessed April 9, 2018).

Hendry, K. R., Huvenne, V. A. I., Robinson, L. F., Annett, A., Badger, M., Jacobel, A. W., et al. (2019). The biogeochemical impact of glacial meltwater from Southwest Greenland. *Prog. Oceanogr.* 176:102126. doi: 10.1016/j.pocean.2019.102126

Henry, L.-A., and Roberts, J. M. (2014a). *Applying the OSPAR Habitat Definition of Deep-Sea Sponge Aggregations to Verify Suspected Records of the Habitat in UK Waters*. JNCC Report 508. Peterborough: JNCC.

Henry, L. A., and Roberts, J. M. (2014b). Recommendations for best practice in deep-sea habitat classification: Bullimore et al. as a case study. *ICES J. Mar. Sci.* 71, 895–898. doi: 10.1093/icesjms/fst175

Hirschmüller, H. (2005). "Accurate and efficient stereo processing by semi-global matching and mutua information," in *Proceedings - 2005 IEEE Computer Society Conference on Computer Vision and Pattern Recognition, CVPR 2005*, (Piscataway, NJ: IEEE Computer Society), 807–814.

Holtmeier, F., and Broll, G. (2017). Feedback effects of clonal groups and tree clusters on site conditions at the treeline: implications for treeline dynamics. *Clim. Res.* 73, 85–96. doi: 10.3354/cr01431

Howell, K. L., Bullimore, R. D., and Foster, N. L. (2014). Quality assurance in the identification of deep-sea taxa from video and image analysis: response to Henry and Roberts. *ICES J. Mar. Sci.* 71, 899–906. doi: 10.1093/icesjms/fsu052

Howell, K.-L., Piechaud, N., Downie, A.-L., and Kenny, A. (2016). The distribution of deep-sea sponge aggregations in the North Atlantic and implications for their effective spatial management. *Deep Sea Res. I Oceanogr. Res. Pap.* 115, 309–320. doi: 10.1016/J.DSR.2016.07.005

Kahn, A. S., Chu, J. W. F., and Leys, S. P. (2018). Trophic ecology of glass sponge reefs in the Strait of Georgia, British Columbia. *Sci. Rep.* 8:756. doi: 10.1038/s41598-017-19107-x

Kazanidis, G., Vad, J., Henry, L.-A., Neat, F., Berx, B., Georgoulas, K., et al. (2019). Distribution of deep-sea sponge aggregations in an area of multisectoral activities and changing oceanic conditions. *Front. Mar. Sci.* 6:163. doi: 10.3389/fmars.2019.00163

Kenchington, E., Murillo, F. J., Lirette, C., Sacau, M., Koen-Alonso, M., Kenny, A., et al. (2014). Kernel density surface modelling as a means to identify significant concentrations of vulnerable marine ecosystem indicators. *PLoS One* 9:e109365. doi: 10.1371/journal.pone.0109365

Klitgaard, A. B. (1995). The fauna associated with outer shelf and upper slope sponges (porifera, demospongiae) at the faroe islands, northeastern Atlantic. *Sarsia* 80, 1–22. doi: 10.1080/00364827.1995.10413574

Klitgaard, A. B., and Tendal, O. S. (2004). Distribution and species composition of mass occurrences of large-sized sponges in the northeast Atlantic. *Prog. Oceanogr.* 61, 57–98. doi: 10.1016/j.pocean.2004.06.002

Knudby, A., Kenchington, E., and Murillo, F. J. (2013). Modeling the distribution of geodia sponges and sponge grounds in the Northwest Atlantic. *PLoS One* 8:e82306. doi: 10.1371/journal.pone.0082306

Koopmans, M., Martens, D., and Wijffels, R. H. (2009). Towards commercial production of sponge medicines. *Mar. Drugs* 7, 787–802. doi: 10.3390/md7040787

Kutti, T., Bannister, R. J., and Fosså, J. H. (2013). Community structure and ecological function of deep-water sponge grounds in the Traenadypet MPA—Northern Norwegian continental shelf. *Cont. Shelf Res.* 69, 21–30. doi: 10.1016/J.CSR.2013.09.011

Leys, S. P., Yahel, G., Reidenbach, M. A., Tunnicliffe, V., Shavit, U., and Reiswig, H. M. (2011). The sponge pump: the role of current induced flow in the design of the sponge body plan. *PLoS One* 6:e27787. doi: 10.1371/journal.pone.0027787

Lowe, D. G. (2004). Distinctive image features from scale-invariant keypoints. *Int. J. Comput. Vis.* 60, 91–110. doi: 10.1023/B:VISI.0000029664.99615.94

Ludeman, D. A., Reidenbach, M. A., and Leys, S. P. (2017). The energetic cost of filtration by demosponges and their behavioural response to ambient currents. *J. Exp. Biol.* 220, 995–1007. doi: 10.1242/jeb.146076

Maldonado, M. (2016). Sponge waste that fuels marine oligotrophic food webs: a re-assessment of its origin and nature. *Mar. Ecol.* 37, 477–491. doi: 10.1111/maec.12256

Maldonado, M., Ribes, M., and van Duyl, F. C. (2012). *Nutrient Fluxes Through Sponges. Biology, Budgets, and Ecological Implications*, 1st Edn. Amsterdam: Elsevier Ltd.

Mariani, S., Uriz, M.-J., Turon, X., and Alcoverro, T. (2006). International association for ecology dispersal strategies in sponge larvae: integrating the life history of larvae and the hydrologic component. *Source Oecol.* 149, 174–184. doi: 10.1007/s00442-006-0429-9

McIntyre, F. D., Drewery, J., Eerkes-Medrano, D., and Neat, F. C. (2016). Distribution and diversity of deep-sea sponge grounds on the Rosemary Bank Seamount, NE Atlantic. *Mar. Biol.* 163, 1–11. doi: 10.1007/s00227-016-2913-z

Miller, R. J., Hocevar, J., Stone, R. P., and Fedorov, D. V. (2012). Structure-forming corals and sponges and their use as fish habitat in bering sea submarine canyons. *PLoS One* 7:e33885. doi: 10.1371/journal.pone.0033885

Murillo, F. J., Muñoz, P. D., Cristobo, J., Ríos, P., González, C., Kenchington, E., et al. (2012). Deep-sea sponge grounds of the Flemish Cap, Flemish Pass and the Grand Banks of Newfoundland (Northwest Atlantic Ocean): distribution and species composition. *Mar. Biol. Res.* 8, 842–854. doi: 10.1080/17451000.2012.682583

Nita, B. G., and Allaire, R. (2017). On the three dimensional interaction between flexible fibers and fluid flow. *Fluids* 2:4. doi: 10.3390/FLUIDS2010004

Palumbi, S. R. (1986). How body plans limit acclimation: responses of a demosponge to wave force. *Ecology* 67, 208–214. doi: 10.2307/1938520

Pusceddu, A., Bianchelli, S., Martín, J., Puig, P., Palanques, A., Masqué, P., et al. (2014). Chronic and intensive bottom trawling impairs deep-sea biodiversity and ecosystem functioning. *Proc. Natl. Acad. Sci. U.S.A.* 111, 8861–8866. doi: 10.1073/pnas.1405454111

Rice, A. L., Thurston, M. H., and New, A. L. (1990). Dense aggregations of a hexactinellid sponge, Pheronema carpenteri, in the Porcupine Seabight (northeast Atlantic Ocean), and possible causes. *Prog. Oceanogr.* 24, 179–196. doi: 10.1016/0079-6611(90)90029-2

Ripley, B. D. (1976). The second-order analysis of stationary point processes. *J. Appl. Probab.* 13, 255–266. doi: 10.2307/3212829

Ripley, B. D. (1977). Modelling spatial patterns. *J. R. Stat. Soc. Ser. B* 39, 172–212.

Ripley, B. D. (1981). *Spatial Statistics*. Hoboken, NJ: John Wiley & Sons, Inc.

Roberts, D. E., and Davis, A. R. (1996). Patterns in sponge (Porifera) assemblages on temperate coastal reefs off Sydney, Australia. *Mar. Freshw. Res.* 47, 897–906. doi: 10.1071/MF9960897

Roberts, E. M., Mienis, F., Rapp, H. T., Hanz, U., Meyer, H. K., and Davies, A. J. (2018). Oceanographic setting and short-timescale environmental variability at an Arctic seamount sponge ground. *Deep Sea Res. I Oceanogr. Res. Pap.* 138, 98–113. doi: 10.1016/J.DSR.2018.06.007

Robertson, L. M., Hamel, J.-F., and Mercier, A. (2017). Feeding in deep-sea demosponges: influence of abiotic and biotic factors. *Deep Sea Res. I Oceanogr. Res. Pap.* 127, 49–56. doi: 10.1016/J.DSR.2017.07.006

Shamloo, H., Rajaratnam, N., and Katopodis, C. (2001). Hydraulics of simple habitat structures. *J. Hydraul. Res.* 39, 351–366. doi: 10.1080/00221680109499840

Strehlow, B. W., Pineda, M., Duckworth, A., Kendrick, G. A., Renton, M., Azmi, M., et al. (2017). Sediment tolerance mechanisms identified in sponges using advanced imaging techniques. *PEER J.* 5, 1–26. doi: 10.7717/peerj.3904

Vad, J., Kazanidis, G., Henry, L.-A., Jones, D. O. B., Tendal, O. S., Christiansen, S., et al. (2018). Potential impacts of offshore oil and gas activities on deep-sea sponges and the habitats they form. *Adv. Mar. Biol.* 79, 33–60. doi: 10.1016/bs.amb.2018.01.001

Victorero, L., Watling, L., Deng Palomares, M. L., and Nouvian, C. (2018). Out of sight, but within reach: a global history of bottom-trawled deep-sea fisheries from &gt 400 m depth. *Front. Mar. Sci.* 5:98. doi: 10.3389/fmars.2018.00098

Westoby, M. J., Brasington, J., Glasser, N. F., Hambrey, M. J., and Reynolds, J. M. (2012). "Structure-from-Motion" photogrammetry: a low-cost, effective tool for geoscience applications. *Geomorphology* 179, 300–314. doi: 10.1016/j.geomorph.2012.08.021

Wilkinson, C. R., and Evans, E. (1989). Sponge distribution across Davies Reef, Great Barrier Reef, relative to location, depth, and water movement. *Coral Reefs* 8, 1–7. doi: 10.1007/BF00304685

Wu, C.-S., Wu, D.-Y., and Wang, S.-S. (2019). Bio-based polymer nanofiber with siliceous sponge spicules prepared by electrospinning: preparation, characterisation, and functionalisation. *Mater. Sci. Eng. C* 108:110506. doi: 10.1016/j.msec.2019.110506

Xavier, J. R., and van Soest, R. W. M. (2012). Diversity patterns and zoogeography of the Northeast Atlantic and Mediterranean shallow-water sponge fauna. *Hydrobiologia* 687, 107–125. doi: 10.1007/s10750-011-0880-4

Conflict of Interest: The authors declare that the research was conducted in the absence of any commercial or financial relationships that could be construed as a potential conflict of interest.

Copyright © 2020 Culwick, Phillips, Goodwin, Rayfield and Hendry. This is an open-access article distributed under the terms of the Creative Commons Attribution License (CC BY). The use, distribution or reproduction in other forums is permitted, provided the original author(s) and the copyright owner(s) are credited and that the original publication in this journal is cited, in accordance with accepted academic practice. No use, distribution or reproduction is permitted which does not comply with these terms.

frontiers in Marine Science

ORIGINAL RESEARCH
published: 21 August 2020
doi: 10.3389/fmars.2020.00674

Chloroflexi Dominate the Deep-Sea Golf Ball Sponges *Craniella zetlandica* and *Craniella infrequens* Throughout Different Life Stages

*Kathrin Busch[1], Erik Wurz[2], Hans Tore Rapp[3†], Kristina Bayer[1], Andre Franke[4] and Ute Hentschel[1,5]**

[1] GEOMAR Helmholtz Centre for Ocean Research Kiel, Kiel, Germany, [2] Marine Animal Ecology Group, Wageningen University and Research, Wageningen, Netherlands, [3] Department of Biological Sciences, K.G. Jebsen Centre for Deep Sea Research, University of Bergen, Bergen, Norway, [4] Institute of Clinical Molecular Biology (IKMB), Kiel, Germany, [5] Faculty of Mathematics and Natural Sciences, Christian-Albrechts-Universität zu Kiel, Kiel, Germany

Deep-sea sponge grounds are underexplored ecosystems that provide numerous goods and services to the functioning of the deep-sea. This study assessed the prokaryotic diversity in embryos, recruits, and adults of *Craniella zetlandica* and *Craniella infrequens*, common and abundant representatives of deep-sea sponge grounds in the North Atlantic. Our results reveal that symbiont transmission in the two *Craniella* sponge species likely occurs vertically, as highly similar microbial consortia have been identified in adults, embryos, and recruits. Moreover, transmission electron microscopy revealed high abundances of sponge-associated microorganisms, among which *Chloroflexi* (*SAR202*) were identified as common representatives by amplicon sequencing and fluorescence *in situ* hybridization (FISH). Equal diversity metrices, a similar overall prokaryotic community composition and a distinct dominance of the phylum *Chloroflexi* within all life stages are the key findings of our analyses. Information such as presented here provide understanding on the recruitment of deep-sea sponge holobionts which is needed to develop integrated management tools of such vulnerable marine ecosystems.

Keywords: vulnerable marine ecosystems, sponges, *Craniella*, *Chloroflexi*, symbiosis, early life stages, amplicon sequencing, fluorescence *in situ* hybridization

OPEN ACCESS

Edited by:
Joana R. Xavier, University of Porto, Portugal

Reviewed by:
Cristiane Cassiolato Pires Hardoim, São Paulo State University, Brazil
Lucia Bongiorni, Institute of Marine Science (CNR), Italy

***Correspondence:**
Ute Hentschel
uhentschel@geomar.de

†Deceased March 07, 2020

Specialty section:
This article was submitted to Deep-Sea Environments and Ecology, a section of the journal Frontiers in Marine Science

Received: *23 March 2020*
Accepted: *23 July 2020*
Published: *21 August 2020*

Citation:
Busch K, Wurz E, Rapp HT, Bayer K, Franke A and Hentschel U (2020) Chloroflexi Dominate the Deep-Sea Golf Ball Sponges Craniella zetlandica and Craniella infrequens Throughout Different Life Stages. Front. Mar. Sci. 7:674. doi: 10.3389/fmars.2020.00674

INTRODUCTION

A fundamental process influencing the fitness of many organisms is the establishment of host-microbial colonization during development (Mortzfeld et al., 2016). Microbial consortia enable the respective animal host to expand its range of nutrition (Nicholson et al., 2012), defense (Flórez et al., 2015), immunity (Eberl, 2010), and development (Koropatnick et al., 2004). Host-microbe interactions may be regulated from early developmental stages and transmitted through generations (reviewed in Rosenberg and Zilber-Rosenberg, 2011; McFall-Ngai et al., 2013). In general, beneficial microbial symbionts are expected to be transmitted vertically (from parents to offspring) in order to assure an establishment of a compatible partnership (Björk et al., 2019 and references therein). Further, probability of vertical transmission is expected to increase with increasing dependence of the host on its microbial partners (Ewald, 1987; Bull et al., 1991; Yamamura, 1993; Douglas, 1994; Thompson, 1994; Herre et al., 1999; Wilkinson, 2001;

Sachs et al., 2011). In the marine environment symbioses are common and host-microbe interactions have been assessed at different developmental stages for a variety of model organisms, including cnidarians (Apprill et al., 2009; Mortzfeld et al., 2016), echinoderms (Galac et al., 2016; Carrier et al., 2019), cephalopods (Montgomery and McFall-Ngai, 1994), molluscs (Endow and Ohta, 1990; Wentrup et al., 2014), and annelids (Nussbaumer et al., 2006; Schimak et al., 2015).

Sponges (Porifera) are evolutionarily ancient animals which first appeared between 650 and 700 million years ago (Love et al., 2009; Zumberge et al., 2018). Today, more than 9,000 species (according to the World Porifera Database) are classified into four classes (Demospongiae, Calcarea, Homoscleromorpha, and Hexactinellida) and populate virtually all marine benthic habitats from shallow tropical reefs to the polar seas and the deep ocean (van Soest et al., 2020). Sponges are prominent examples of marine holobionts, consisting of diverse prokaryotic communities with more than 63 prokaryotic phyla detected within sponge hosts (Thomas et al., 2016; Moitinho-Silva et al., 2017a). The prokaryotic communities of sponges are host species-specific and distinct from seawater prokaryotic communities (Hentschel et al., 2002; Thomas et al., 2016). The transmission of microbial sponge symbionts to the next generation occurs vertically or horizontally (De Caralt et al., 2007; Maldonado, 2007; Schmitt et al., 2008; Webster et al., 2010; Gloeckner et al., 2013). Microbial communities have been detected in reproductive stages, such as oocytes, embryos, larvae, and juveniles of various shallow water species (Ereskovsky et al., 2005; Schmitt et al., 2007; Sharp et al., 2007; Gloeckner et al., 2013; Björk et al., 2019) indicating that vertical transmission is an important mechanism for the establishment and maintenance of sponge-microbe associations over evolutionary time scales.

In comparison to sponges from shallow and often warm-water habitats, much less is known about sponges and their microbiomes from deep and cold environments. Sponges are ubiquitous and abundant components of deep-sea benthic communities and can form structurally complex and diverse ecosystems, termed "sponge grounds" (Klitgaard and Tendal, 2004; Xavier et al., 2015; Maldonado et al., 2016). Sponge grounds are known to strongly support biodiversity, either directly by provision of shelter or indirectly via food webs, and further perform a variety of ecosystem functions, among others via participation in bentho-pelagic coupling and biogeochemical cycles (reviewed in Maldonado et al., 2016; Thompson and Fuller, 2020). Deep-sea sponge grounds (syn. "sponge aggregations" or "sponge gardens") have been flagged as vulnerable marine ecosystems (VMEs) that are currently under pressure through fishing and other human activities (Pham et al., 2019; Murillo et al., 2020). The species *Craniella infrequens* and *Craniella zetlandica* are common members of such sponge grounds and have further been recorded in shelf-areas around the globe (**Figure 1**). *Craniella* sponges are spherical in shape and grow up to the size of a golf ball and larger. This study aims to describe the prokaryotic community composition and diversity of two *Craniella* species and their early life stages from the deep North Atlantic Ocean. In particular we sought to address whether prokaryotic community composition, diversity, and dominant microbial phyla differ between different life stages (adults, embryos, and recruits) of the two sponge species. Knowledge about deep-sea sponge holobiont recruitment and plasticity across life stages is crucial to enable, in the long term, an adequate conservation of sponge populations from vulnerable marine ecosystems.

MATERIALS AND METHODS

Sampling

Sponges of different developmental stages (adults, embryos, recruits) were collected during two research cruises onboard the Norwegian research vessel RV G.O.Sars ("GS2017110" and "GS2018108") to the North Atlantic Ocean (Schulz Bank seamount at 73.8°N, 7.5°E; and Stjernsund at 70.3°N, 22.5°E) in July 2017 and August 2018. Samples were collected by remotely operated vehicle (ROV *AEgir*, University of Bergen) or Agassiz trawl at an average depth of 600 m below surface. Tissue chunks of adult sponges and recruits were subsampled onboard ship with sterile scalpels from the mesohyl, rinsed, flash-frozen and stored at −80°C for molecular analyses. Additional pieces of tissue were subsampled with biopsy punches and preserved onboard ship for microscopy. Embryos were carefully picked out of the parent sponges (**Figure 2**) with sterile spring steel forceps using a stereomicroscope. After rinsing, 10 whole embryos were each pooled per adult sponge to account for the small biomass, fixed in RNAlater™ Stabilizing Solution (Thermo Fisher Scientific, Waltham, MA, United States), stored at 4°C overnight, transferred to −20°C on the next day and subsequently to −80°C. In addition, intact embryos were preserved onboard ship for microscopy. In terms of sample numbers, we sampled eight adult *C. infrequens* sponges, of which four were brooding embryos, and nine *C. infrequens* recruits. During the cruise we further sampled eight adult *C. zetlandica* sponges of which one was brooding embryos. In addition to our cruise activities, we sampled nine *C. zetlandica* recruits in September 2018 from an aquarium system (Bergen, Norway). The respective parent sponges had been maintained since summer 2017 in 45 L tanks with sea-water flow through (1 L min^{-1}) pumped from the adjacent fjord at 105 m depth below surface. Seawater was treated with a 20 μm drum filter prior to flowing through the holding tanks. Under these conditions spawning was documented frequently and the new recruits had settled in the tanks. *C. zetlandica* recruits from the aquarium system were smaller (and thus most likely younger) than the *in situ* sampled *C. infrequens* recruits and therefore flash-frozen as a whole. In our case the new sponge recruits had the following sizes: 1 cm mean diameter for *C. infrequens*; and 0.3 cm maximal diameter for *C. zetlandica*. Adult sponges of both sponge species had the size of a fist. In summary, for this study in total 39 sponge individuals of the two sponge species were collected: *C. zetlandica* (eight adults, of which one was brooding embryos, and nine recruits) and *C. infrequens* (eight adults, of which four were brooding embryos, and nine recruits). In addition to the sponge samples, we also sampled 18 seawater microbial communities during the two cruises (at all sponge sampling locations) and

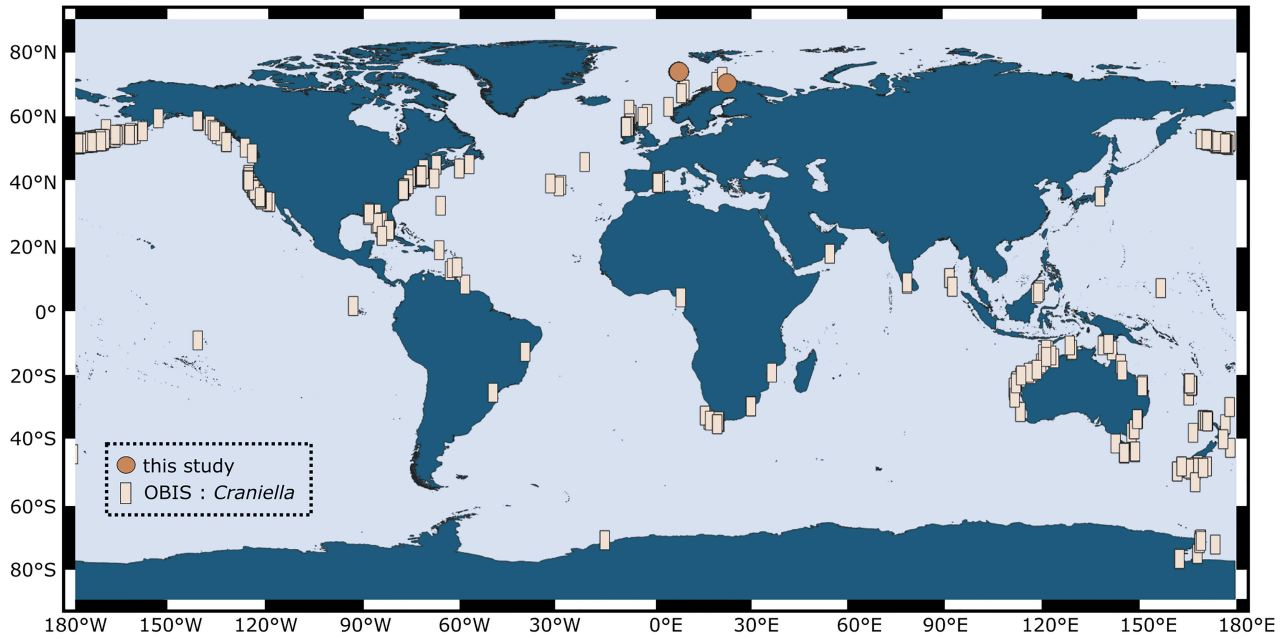

FIGURE 1 | Global distribution of the genus *Craniella*, as compiled from records in the Ocean Biogeographic Information System (OBIS; squares) in March 2020. Sampling locations of individuals from our study are indicated by points.

from the aquarium system as environmental reference samples. Two liters of seawater sample were filtered onto polyvinylidene fluoride (PVDF) filter membranes (with 0.22 μm pore size; Merck Millipore) and stored at −80°C.

16S Amplicon Sequencing

DNA extraction was performed on either ∼ 0.25 g of tissue or bulk of 10 pooled embryos using the DNeasy Power Soil kit (Qiagen, Venlo, Netherlands). For seawater samples DNA was extracted of one half of a PVDF filter membrane. Subsequent DNA quantity and quality controls were performed with a NanoDrop spectrophotometer and by polymerase chain reaction with universal 16S primers (27F-1429R; Weisburg et al., 1991), followed by gel electrophoresis. For amplicon sequencing, the V3-V4 variable regions of the 16S rRNA gene were amplified in a one-step PCR with the primer pair 341F-806R (dual barcoding approach; Kozich et al., 2013). The primer pair has the following nucleotide sequences: 5′-CCTACGGGAGGCAGCAG-3′ (Muyzer et al., 1993) and 5′-GGACTACHVGGGTWTCTAAT-3′ (Caporaso et al., 2011). Verification of PCR-products was performed with gel electrophoresis, followed by normalization and pooling of samples. Sequencing was conducted on a MiSeq platform (MiSeqFGx, Illumina, San Diego, CA, United States) using v3 chemistry. Zero mismatches were allowed in the barcode sequence for demultiplexing.

Raw reads were quality-checked and processed within the QIIME2 environment (version 2018.11; Bolyen et al., 2019). Based on forward reads (truncated to 270 nt), Amplicon Sequence Variants (ASVs) were generated using the DADA2 algorithm (python-based; Callahan et al., 2016). Data were analyzed based on ASVs instead of classical operational taxonomic units (OTUs), in order to resolve fine-scale community patterns and to use a state-of-the-art method which profits from the error correction model conducted by the DADA2 algorithm. Singletons and chimeric sequences were removed during this process.

Phylogenetic trees were calculated based on the resulting ASVs via the FastTree2 plugin. Taxonomic classification of representative ASVs was achieved with the help of a primer-specific trained Naive Bayes taxonomic classifier, based on the Silva 132 99% OTUs 16S database (Quast et al., 2013). Taxonomic filtering was applied on the dataset, meaning that mitochondria, chloroplasts and unassigned sequences were removed. Further, a sampling depth of 3,900 was applied to standardize the number of reads across samples. Diversity metrices were calculated, such as Shannon indices (alpha diversity) and weighted UniFrac distances (beta diversity). Non-metric multidimensional scaling (nMDS) was conducted to evaluate sample separation in ordination space (based on weighted UniFrac distances). We performed PERMANOVAs (999 permutations) on weighted UniFrac distances, and Tukey *Posthoc* tests on Shannon indices following ANOVA type III tests, to assess if the prokaryotic community differed significantly between sample groups. To evaluate further on the differential abundance of microbial phyla present in aquarium sponges (i.e., *C. zetlandica* recruits) in comparison to *in situ* sampled sponges (and in aquarium water vs *in situ* water), we ran the Linear Discriminant Analysis (LDA) Effect Size (LEfSe) algorithm (Segata et al., 2011). Visualizations were created using R (version 3.0.2 with the ggplot2 package loaded; R Development Core Team, 2008; Wickham, 2016) and Inkscape (version 0.92.4; Harrington and the Inkscape Development Team, 2005).

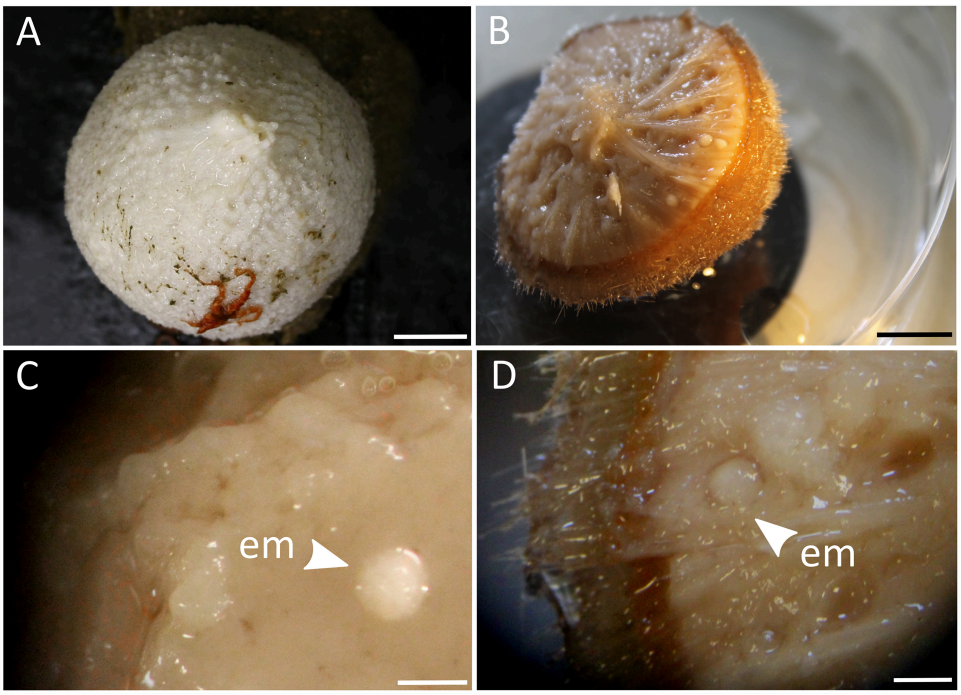

FIGURE 2 | (A) Photograph of an adult *C. zetlandica* individual with an attached red brittle star at the bottom. Scale bar = 1 cm. **(B)** Photograph of an adult *C. infrequens* individual that was cut in half, showing numerous embryos inside the sponge tissue. Scale bar 1 cm. **(C)** Stereomicroscopic magnification of *C. zetlandica* tissue. em, embryo. Scale bar = 1 mm. **(D)** Stereomicroscopic magnification of *C. infrequens* tissue. em, embryo(s) brooding in the mesohyl. Scale bar = 1 mm.

The ternary plot was created using the Ternary plot maker web tool (Blom, 2019[1]).

In order to provide an independent proof-of-concept accompanying our 16S amplicon sequencing results we performed qualitative microscopic analyses. These included light microscopy, transmission electron microscopy (TEM), and fluorescence *in situ* hybridization of the most dominant microbial phylum detected by amplicon sequencing. Especially for the embryo-based DNA libraries we aimed at confirming by microscopy that they contained sequences which were indeed present within the embryos and not merely contaminants.

Light Microscopy and TEM

Tissue samples for light microscopy and TEM were fixed in a cocktail of glutaraldehyde (2.5%) with sodium chloride (0.34 M) and phosphate buffered saline (PBS; 0.4 M). Samples were stored at 4°C. Back on land, samples were washed 3x with buffer (at 4°C; 15 min per washing step), post-fixed in 2% osmiumtetroxide for 2 h and afterward washed three more times with buffer (at 4°C; 15 min per washing step). Subsequently partial dehydration was conducted with an ascending ethanol series, from 30% EtOH (2 × 15 min) to 50% EtOH (1 × 15 min), to 70% EtOH (2 × 15 min, including an overnight storage at 4°C), to 90% EtOH (1 × 15 min) up to 100% EtOH (2 × 15 min). After dehydration, the samples were gradually infiltrated with LR-White resin (at room temperature). The infiltration series covered the following steps: from 1 × 1 h 2:1 EtOH:LR-White, to 1 × 1 h 1:1 EtOH:LR-White, to 1 × 1 h 1:2 EtOH:LR-White, up to 2 × 2 h pure LR-White. Samples were transferred to gelatine embedding capsules filled with fresh LR-White resin and subsequently incubated for polymerization at 57°C for two days. The resulting resin blocks were manually pre-trimmed. Semithin sections (0.5 μm) were cut for light microscopy using an ultramicrotome (Reichert-Jung ULTRACUT E; Leica Camera AG, Wetzlar, Germany) which was equipped with a diamond knife (DIATOME, Biel, Switzerland). After staining with a Richardson solution (after Mulisch and Welsch, 2015), semi-thin sections were mounted onto SuperFrost Ultra Plus® microscopy slides and visualized with the help of an Axio Observer.Z1 microscope (Zeiss, Göttingen, Germany).

For TEM, ultrathin sections (70 nm) were cut with the ultramicrotome, mounted on pioloform coated copper grids (75 mesh) and contrasted with uranyl acetate (20 min incubation and subsequent washing steps) as well as with Reynold's lead citrate (3 min incubation, followed by washing steps). Visualization of the ultra-thin sections was performed on a Tecnai G2 Spirit Bio Twin transmission electron microscope (FEI Company, Hillsboro, United States) at an acceleration voltage of 80 kV.

Fluorescence *in situ* Hybridization

Sponge tissue samples were fixed overnight (at 4°C) onboard with 4% paraformaldehyde (PFA) in 1xPBS (pH was adjusted to approximately 6.9 with the help of NaOH and HCl). For preparation of all FISH solutions, we used filtered

[1]https://www.ternaryplot.com/

(0.22 μm membrane) diethylpyrocarbonate (DEPC)-treated water (Thermo Fisher Scientific, Waltham, United States) to inactivate RNase enzymes, and performed autoclaving for sterilization of buffers and solvents onboard the ship. After fixation with PFA, five washing steps (3 min) were performed with 1xPBS (4°C). Subsequently quenching of free aldehyde groups was conducted by incubation with glycine (50 mM) in 1xPBS for 15 min (room temperature). The quenching step was followed by five additional washing steps (3 min) in DEPC water (at 4°C). Dehydration was performed onboard in a ascending ethanol series (molecular grade, RNase free), covering the following steps: 30% EtOH in 1xPBS (2 × 15 min at 4°C), 50% EtOH in 1xPBS (2 × 30 min). Samples were subsequently stored at −20°C. Back on land, dehydration was continued in following steps: 50% EtOH in MilliQ water (1 × 15 min), 60% EtOH in MilliQ water (2 × 15 min), 70% EtOH in MilliQ water (2 × 15 min), 90% EtOH in MilliQ water (1 × 15 min) up to 100% EtOH (2 × 15 min). The samples were gradually infiltrated with LR-White resin, polymerized, pre-trimmed and cut into semithin sections (0.5 μm) with an ultramicrotome, in the same manner as described in section 2.3. As embryos were embedded in whole, cutting with the microtome was run for a substantial time, until the central part of the embryo was reached. At the area with widest diameter, sections were received and fixed onto two separate SuperFrost Ultra Plus® microscopy slides. While one half of the slides was directly stained with a Richardson solution and mounted using Biomount medium (Plano, Germany; see description in section "Light Microscopy and TEM"). The other half was only fixed onto microscopy slides, without any staining or covering in Biomount medium. Following the procedures described in Bayer et al. (2018), these latter samples were afterward labeled with *Chloroflexi* clade-specific probes. In particular the following probes were used: Cal825 (5′-[Cy3]-ACACCGCCCACACCTCGT-[Cy3]-3′; *E. coli* binding positions 825 to 843) for *Caldilineae*; Ana1005 (5′-[Alexa Fluor 647]-TCCGCTTTCGCTTCCGTA-[Alexa Fluor 647]-3′; *E. coli* binding positions 1005 to 1023) for *Anaerolineae*; and SAR202-104 (5′-[Alexa Fluor 488]-GTTACTCAGCCGTCTGCC-[Alexa Fluor 488]-3′; *E. coli* binding positions 104 to 122) for the *SAR202* group. A double labeling approach at 5′ and 3′ ends was performed for all probes (Sigma-Aldrich, Germany).

Hybridization was performed in Sylgard chambers (GEOMAR in-house production) which were located inside an equilibrated humid chamber (at 46°C for 3 h). The hybridization buffer consisted of 900 mM NaCl, 20 mM Tris-HCl (pH = 7.4), 10% formamide, 0.01% sodium dodecyl sulfate and 20% dextransulfate. All *Chloroflexi* clade-specific probes were co-hybridized, in addition counterstaining of bacterial nucleic acids and sponge cell nuclei was performed with pre-warmed DAPI in hybridization buffer (1 ng/μL), with an incubation time of 20 min at 46°C. After hybridization, the slides were incubated in pre-warmed wash buffer (450 mM NaCl, 20 mM Tris–HCl, 0.01% sodium dodecyl sulfate) at 48°C for 25 min. The washing step was repeated twice. Subsequently, the slides were carefully rinsed with ice cold molecular grade water, dried and mounted in Mowiol medium (Mowiol® 40–88, Kuraray Europe GmbH, Tokyo, Japan). The same procedure was conducted for a negative control for non-specific binding (i.e., hybridization buffer without *Chloroflexi*-specific probes, but with an oligonucleotide complementary to the probe EUB338 (NON-338-probe; Wallner et al., 1993), to prevent falling into the trap of false-positive results. Fluorescence signals at the four specific wavelength ranges were detected using an Axio Observer.Z1 microscope equipped with AxioCam 506 and Zen 2 software (version 2.0.0.0; Zeiss Germany).

RESULTS

In this study, the prokaryotic community composition of 39 *Craniella* sponge individuals was analyzed. A visual overview of the denoising stats is compiled in **Supplementary Figure S1**. The complete dataset after quality filtering consisted of 614,928 reads, which is 82% of the initial input read count. On average each sample had 15,767 reads, but as several samples contained less reads, a sampling depth of 3,900 was applied on the complete dataset for normalization. Four adult *C. infrequens* individuals and one adult *C. zetlandica* individual were found brooding embryos inside their tissue (**Figure 2**). For each of these brooding individuals, ten embryos had been picked and pooled. In *C. infrequens*, the embryos were more numerous compared to *C. zetlandica* and were scattered throughout the mesohyl of the parental sponge. Prokaryotic diversity (as estimated by Shannon index) was similar between the developmental stages within each sponge species (**Figure 3** and **Supplementary Table S1**). Other alpha diversity indices (Pielou's eveness, Faith's PD and number of observed ASVs) led to a similar result (**Supplementary Figure S2**). Average Shannon indices were slighly lower in *C. zetlandica* than in *C. infrequens*, despite not statistically significantly (**Figure 3** and **Supplementary Table S1**). The prokaryotic community compositions of both sponge species were significantly different from seawater (**Figure 4A** and **Supplementary Table S2**). Further, *C. infrequens* and *C. zetlandica* displayed species-specific microbiomes, as shown by their distinct clustering based on weighted UniFrac distances and on PERMANOVA analyses (**Figure 4B**, with some exceptions; **Supplementary Table S2**). Overall *C. zetlandica* samples showed a slightly higher variability than *C. infrequens* samples (please note in this regard that while *C. infrequens* specimens were all sampled at the same geographic

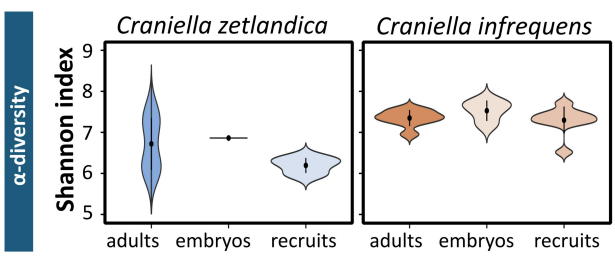

FIGURE 3 | Prokaryotic alpha-diversity for the sampled *Craniella* species. Shannon indices calculated for the different developmental stages of *C. zetlandica* and *C. infrequens*.

location, *C. zetlandica* specimens analyzed in this study originate from different geographic locations).

With respect to the prokaryotic community composition, most bacterial phyla were shared across all life stages, and were not particularly enriched in any specific life stage (**Figure 5A**). *Chloroflexi* were the most abundant prokaryotic phylum in both sponge species and across all life stages and *SAR202* was the most abundant clade, constituting on average 73% of all recorded *Chloroflexi* (**Table 1**). *C. zetlandica* recruits obtained from the aquarium system were a noticeable exception that were dominated by *Proteobacteria* and significantly enriched in this phylum compared to *in situ* sampled sponges (**Figure 5B** and **Supplementary Figure S3A**). *Proteobacteria* were however not significantly enriched in the aquarium water compared to *in situ* sampled seawater (**Supplementary Figures S3B C**).

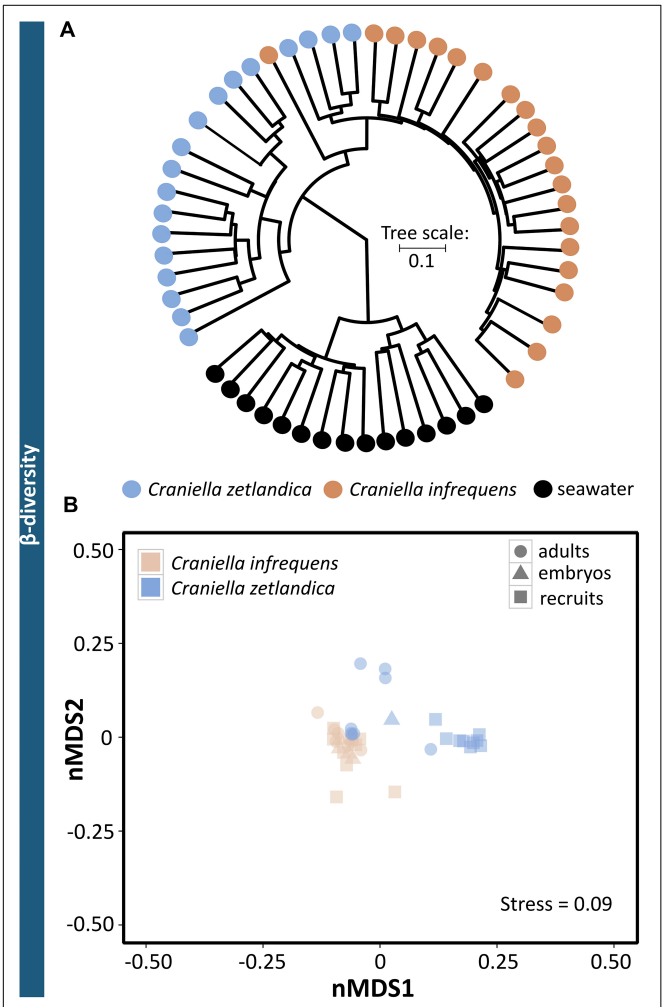

FIGURE 4 | Prokaryotic beta-diversity across the sampled *Craniella* species and reference samples. **(A)** Clustering dendrogram based on weighted UniFrac distances for all samples of seawater and both sponge species. **(B)** Non-metric multidimensional scaling (nMDS) plot based on weighted UniFrac distances. The sponge species *C. zetlandica* and *C. infrequens* are marked by different colors, the different developmental stages (adult, recruit, and embryo) are indicated by different symbols.

Neither were *Chloroflexi* significantly depleted in the aquarium water compared to *in situ* sampled seawater, although *Chloroflexi* were significantly enriched in the *in situ* sampled sponges compared to the aquarium sampled sponges. A total of 390 *Chloroflexi* ASVs were detected in the 39 *Craniella* samples, of which 171 were present in ≥50% of the samples per category (adult, embryo, recruit) (**Figure 6A**). Of these 171 common *Chloroflexi* ASVs, 16 were present in all life stages and both species, while being absent from seawater reference samples. These 16 ASVs are particularly abundant and account for 20–40% of the total *Chloroflexi* prokaryotic community in each sponge sample. Seven ASVs of the 16 ASVs belong to the *SAR202* clade, while the remainder belongs to the classes *JG30-KF-CM66* (4 ASVs), *Anaerolineae* (2 ASVs), *TK17* (2 ASVs), and the order *S085* (1 ASV).

We next explored whether the 171 common *Chloroflexi* ASVs are species-specific or developmental stage-specific (**Figures 6B,C**). We determined 46 ASVs as being *C. zetlandica* specific (absent from *C. infrequens*), and 73 ASVs as being *C. infrequens* specific (absent from *C. zetlandica*). For *C. zetlandica* 26 ASVs were exclusively occurring in adults, 12 in embryos, and 10 in recruits. For *C. infrequens* four ASVs were occurring only in adults, 18 in embryos, and four in recruits. Interestingly, one *Chloroflexi*-ASV, occurred only in embryos of both sponge species. This ASV was affiliated with the *Chloroflexi*-class *TK17*, that could only be classified to class-level. Upon blasting against a sponge microbiome reference database (Moitinho-Silva et al., 2017a), this particular ASV was found in 134 sponges samples, of which 88 samples were identified as *Geodia barretti*. In summary, the major fraction of the detected *Chloroflexi* ASVs were sponge species-specific but not developmental-stage specific. Further information on the relative abundances of the ASV groups is presented in **Supplementary Figure S4**.

Light microscopy revealed that bacterial cells were numerous inside *C. infrequens*. In the embryos, the microbial cells were restricted to a narrow band at the peripheral rim (**Figures 7A,B**), while the interior was devoid of cellular material or bacterial morphotypes. An artifact resulting from cutting through the possibly more fluidic embryo interior can however not be excluded. Fluorescence *in situ* hybridization confirmed high abundances of *Chloroflexi*, in particular *SAR202*, within the "bacterial band" at the embryo rim (**Figure 7C**). The negative control for non-specific binding was negative (**Supplementary Figures S5I–L**). Bacterial cells were further found to be abundant and widely distributed in the mesohyl in adult *C. infrequens* (**Supplementary Figure S6A**). FISH confirmed high abundances of *SAR202* also for adult individuals (**Supplementary Figure S6B**). Microbial cells within the embryos displayed diverse morphologies and were found in dividing stages (see **Figure 7D** for examples).

For *C. zetlandica* we observed an *in situ* (stress-induced) release of ripe propagules, visible by ROV live-footage in August 2018, during the sampling campaign "GS2018108" in Stjernsund (Supplementary Video S1: doi.pangaea.de/10.1594/PANGAEA.918218). We suspect a

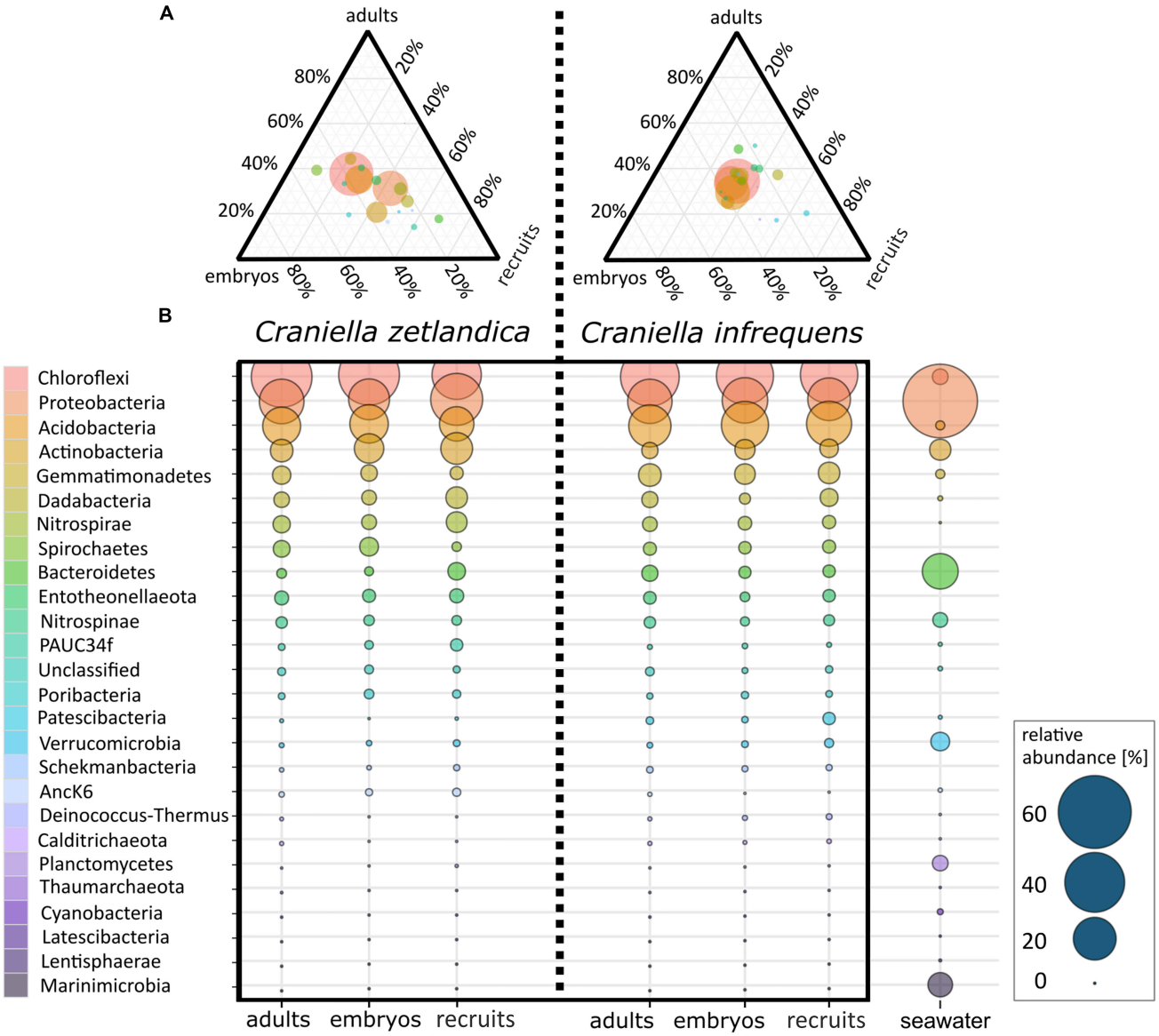

FIGURE 5 | (A) Ternary plot of average prokaryotic phyla distributions for embryos, recruits, and adults of *C. zetlandica* and *C. infrequens*. Colors of phyla are the same in both figures: **(A,B)**. Circle size indicates relative abundance of respective phyla. **(B)** Average prokaryotic community composition of *C. zetlandica* and *C. infrequens* developmental stages as well as seawater. Microbial phyla are sorted in descending order by mean relative abundances. Circle size indicates relative abundances (for exact relative abundance values consider the scale presented at the right bottom).

TABLE 1 | Average relative abundances of *Chloroflexi* (*Anaerolinae*, *Caldilineae*, *SAR202*, others) as determined by 16S amplicon sequencing. mean, and standard deviation per group are indicated.

		Anaerolineales	***Caldilineales***	***SAR202* clade**	**Other *Chloroflexi***
C. zetlandica	Adult	0.1 ± 0.1	6.9 ± 3.4	77.5 ± 8.2	15.5 ± 7.3
	Embryo	0 ± *NA*	7.9 ± *NA*	71.4 ± *NA*	20.7 ± *NA*
	Recruit	0 ± 0	15.6 ± 6.0	52.0 ± 14.2	32.4 ± 9.1
C. infrequens	Adult	0.2 ± 0.1	6.0 ± 4.1	85.2 ± 4.4	8.7 ± 2.0
	Embryo	0.2 ± 0.2	7.1 ± 0.8	78.9 ± 3.7	13.7 ± 3.5
	Recruit	0.5 ± 0.7	11.2 ± 6.1	70.0 ± 11.5	18.2 ± 8.1

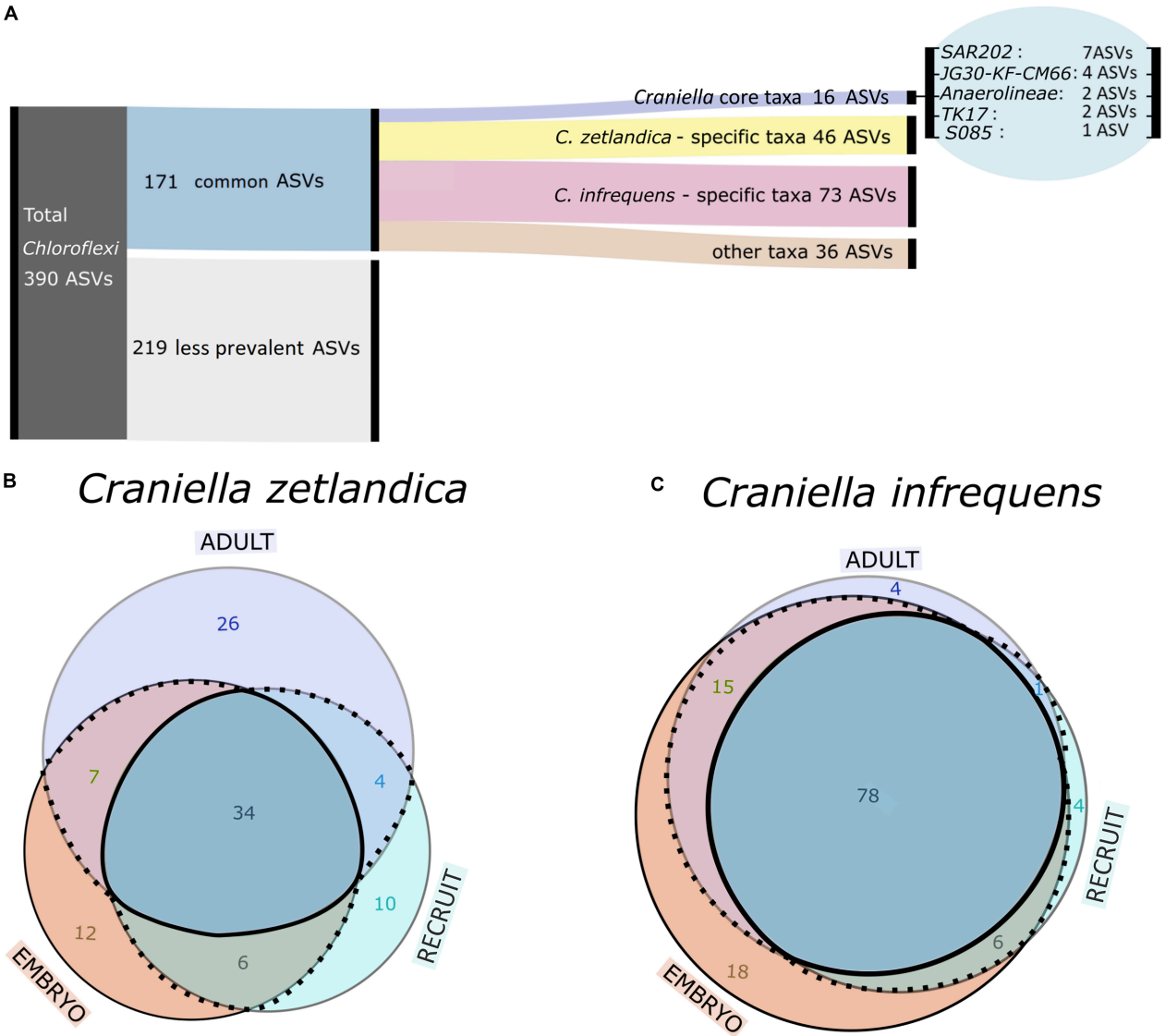

FIGURE 6 | (A) Alluvial diagram showing grouping scheme of *Chloroflexi* ASVs. **(B,C)** Area proportional Venn-diagram showing counts of common *Chloroflexi* ASVs being shared or specific across different life stages for **(B)** *C. zetlandica* and **(C)** *C. infrequens*.

similar timing of spawning in summer for those sponges maintained in the aquarium system in Bergen, as high numbers of settled recruits were found in October 2018 (**Supplementary Figure S7**). These observations point to a synchronized reproductive cycle in aquarium and *in situ* thriving *C. zetlandica* with a spawning in late summer.

DISCUSSION

Deep-sea sponge grounds are underexplored ecosystems that provide numerous goods and services to the functioning of the deep-sea (Maldonado et al., 2016), such as the provision of food, habitat and refugia for commercially relevant fish species. The need to preserve these vulnerable marine ecosystems (VMEs) is thus contradictory to the high demand for socio-economic processes such as fishing in North Atlantic waters. In this study we assessed the prokaryotic diversity of two adult deep-sea sponge species of the genus *Craniella* and their developmental stages. These sponges are prominent although understudied members of deep-sea sponge grounds and have further been recorded in shelf-areas around the globe. While there is one report on the *Proteobacteria*-dominated microbiome of *Craniella australiensis*, which is a shallow water species in the Indo-Pacific and South China Sea (Anbuchezhian and Li, 2014), the microbiome of *C. infrequens* and *C. zetlandica* have—to our knowledge—not been characterized to date.

Our results reveal that *C. zetlandica* and *C. infrequens* are typical high microbial abundance (HMA) sponges

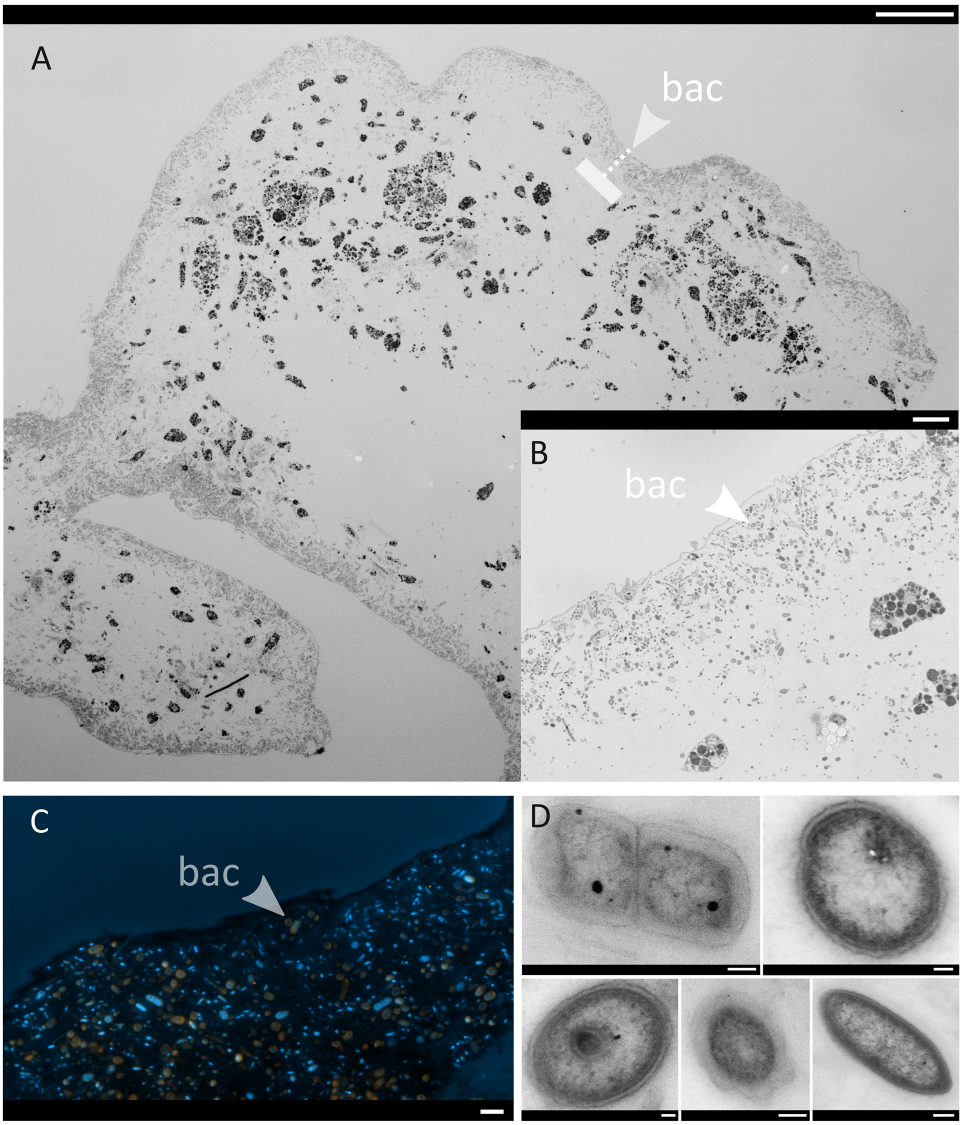

FIGURE 7 | Micrographs of one representative *C. infrequens* embryo (*n* = 3 inspected). Arrows point from the outside to the inside. bac = band of bacterial cells **(A)** A whole *C. infrequens* embryo stained with Richardson solution. Scale bar = 100 μm. The dashed line indicates the band with highest bacterial densities **(B)** Brightfield microscopy of the bacterial band, scale bar = 10 μm. **(C)** Fluorescence *in situ* hybridization of the bacterial band. Merged channels of *SAR202* signals (orange) and the DAPI counter stain (blue) are shown, scale bar = 2 μm. Micrographs of isolated hybridization signals for the specific probes (*Anaerolinae*, *Caldilineae*, and *SAR202*) are included in **Supplementary Figures S5A–D**. **(D)** TEM close-up of microbial cells located within the bacterial band, scale bars = 200 nm.

(Gloeckner et al., 2014; Moitinho-Silva et al., 2017b). We base this statement on our observation that both sponge species harbor diverse and dense microbial communities within their tissues, as observed by TEM. This finding is further supported by the observation that the sponge microbiomes are dominated by *Chloroflexi* (*SAR202*), which are known indicator taxa of HMA sponges (Moitinho-Silva et al., 2017b).

The microbiomes of *C. zetlandica* and *C. infrequens* were host-species specific and distinctly different from seawater which is consistent with previous reports on sponge microbiomes (Easson and Thacker, 2014; Thomas et al., 2016; Steinert et al., 2017). The prokaryotic community composition and alpha diversity were very similar between adults, embryos and recruits within the same sponge species, indicating that entire microbial consortia are very likely vertically transmitted. Vertical transmission has been previously reported for a number of shallow-water HMA sponges (i.e., Schmitt et al., 2007; Björk et al., 2019), but is, to the best of our knowledge, novel in the context of sponge species from sponge grounds. Our results indicate that young deep-sea sponges can already contain a high diversity and density of microorganisms. Despite the observation of very similar prokaryotic community compositions between all examined life stages per species in our study, the recruits of *C. zetlandica* fell somewhat distant from all other samples in

the nMDS plots and were dominated by *Proteobacteria*. It is noteworthy that these samples were collected in an aquarium system and not in the field. Indeed, previous studies have shown that the maintenance of marine organisms in captivity can affect the relative abundances of some associated microbial taxa (Galand et al., 2018). In addition, microbial variability has been observed to be particularly high in recently settled recruits compared to adult individuals (Schmitt et al., 2007; Busch et al., 2020).

The most dominant microbial phylum in all *in situ* sampled sponges of both sponge species and across all developmental stages were *Chloroflexi*. Generally, the probability of vertical symbiont-transmission is assumed to be positively related with the dependence of the host on the microbial partner partners (Ewald, 1987; Bull et al., 1991; Yamamura, 1993; Douglas, 1994; Thompson, 1994; Herre et al., 1999; Wilkinson, 2001; Sachs et al., 2011). Bacteria of the phylum *Chloroflexi* (in particular *SAR202*) are abundant and wide-spread in HMA sponges (Moitinho-Silva et al., 2017b; Bayer et al., 2018) and are suggested to play an important function in the degradation of recalcitrant organic matter (Landry et al., 2017; Bayer et al., 2018). We propose that the 16 *Craniella* core ASVs detected within our study should be considered as sponge symbionts as they were found in high abundances across both species and all developmental stages, while being absent from seawater. Almost half of the 16 *Craniella* core ASVs belong to the *SAR202* clade, making it tempting to speculate about a potential crucial functional role in respect to (recalcitrant) organic matter cycling. Our FISH analyses revealed high abundances of *Chloroflexi* scattered within the bacterial band at the inner periphery of sponge embryos. We conclude that the transmission of *Chloroflexi* through the embryonal stages reflects their tight and evolutionarily long-standing integration in the sponge holobiont. Future research efforts should be geared toward understanding the specific functional roles of *Chloroflexi* symbionts for deep-sea sponges.

DATA AVAILABILITY STATEMENT

The datasets presented in this study can be found in online repositories. The names of the repository/repositories and accession number(s) can be found below: https://www.ncbi.nlm.nih.gov/, PRJNA612549.

AUTHOR CONTRIBUTIONS

KBu and UH designed the study, wrote the manuscript, and were responsible for the microbial pipeline. KBu, HR, and EW conducted sampling. KBa and KBu performed fluorescence *in situ* hybridization. HR led sponge taxonomic analysis. AF was involved in sequencing. KBu performed the data analysis (bioinformatics and visualizations). EW and KBa reviewed and edited the manuscript. All authors contributed to the article and approved the submitted version.

FUNDING

This study was funded by the European Union's Horizon 2020 Research and Innovation Program under Grant Agreement No. 679849 (the SponGES project). This document reflects only the authors' view and the Executive Agency for Small and Medium-sized Enterprises (EASME) is not responsible for any use that may be made of the information it contains.

ACKNOWLEDGMENTS

We express our gratitude to HR, coordinator of the H2020-SponGES project on deep-sea sponge grounds of the North Atlantic, deep-sea sponge taxonomist, explorer, mentor, and friend. We thank the crews and scientific parties of RV G.O.Sars cruises "GS2017110" and "GS2018108". On these cruises the ROV AEgir-team (University of Bergen) enabled sampling of precious samples. Ina Clefsen and Andrea Hethke provided valuable support in the lab back on land. We also thank Heikki Savolainen and Tone Ulvatn for help in aquaria facility management and technical support at the University of Bergen. Heidi Kristina Meyer's support in the acquisition of video material is much appreciated.

SUPPLEMENTARY MATERIAL

The Supplementary Material for this article can be found online at: https://www.frontiersin.org/articles/10.3389/fmars.2020.00674/full#supplementary-material

REFERENCES

Anbuchezhian, R., and Li, Z. (2014). "Marine sponge *Craniella australiensis*-associated bacterial," in *Encyclopedia of Metagenomics*, ed. K. E. Nelson (Berlin: Springer-Verlag), 319–326. doi: 10.1007/978-1-4899-7475-4_604

Apprill, A., Marlow, H. Q., Martindale, M. Q., and Rappé, M. S. (2009). The onset of microbial associations in the coral *Pocillopora meandrina*. *ISME J.* 3, 685–699. doi: 10.1038/ismej.2009.3

Bayer, K., Jahn, M. T., Slaby, B. M., Moitinho-Silva, L., and Hentschel, U. (2018). Marine sponges as *Chloroflexi* hot spots: genomic insights and high-resolution visualization of an abundant and diverse symbiotic clade. *mSystems* 3:e00150-18.

Björk, J. R., Díez-Vives, C., Astudillo-García, C., Archie, E. A., and Montoya, J. M. (2019). Vertical transmission of sponge microbiota is inconsistent and unfaithful. *Nat Ecol Evol.* 3, 1172–1183. doi: 10.1038/s41559-019-0935-x

Blom, J. (2019). *Ternary Plot Maker*. Available online at: https://www.ternaryplot.com/ (accessed March 1, 2020).

Bolyen, E., Rideout, J. R., Dillon, M. R., Bokulich, N. A., Abnet, C., Al Ghalith, G. A., et al. (2019). Reproducible, interactive, scalable, and extensible microbiome data science using QIIME 2. *Nat. Biotechnol.* 37, 852–857.

Bull, J. J., Molineux, I. J., and Rice, W. R. (1991). Selection of benevolence in a host-parasite system. *Evolution* 45, 875–882. doi: 10.1111/j.1558-5646.1991.tb04356.x

Busch, K., Beazley, L., Kenchington, E., Whoriskey, F., Slaby, B., and Hentschel, U. (2020). Microbial diversity of the glass sponge *Vazella pourtalesii* in response to anthropogenic activities. *bioRxiv* [Preprint]. doi: 10.1101/2020.05.19.102806

Callahan, B. J., McMurdie, P. J., Rosen, M. J., Han, A. W., Johnson, A. J. A., and Holmes, S. P. (2016). DADA2: high-resolution sample inference from Illumina amplicon data. *Nat. Methods* 13, 581–583. doi: 10.1038/nmeth.3869

Caporaso, J. G., Lauber, C. L., Walters, W. A., Berg-Lyons, D., Knight, R., Lozupone, C. A., et al. (2011). Global patterns of 16S rRNA diversity at a depth of millions of sequences per sample. *Proc. Natl. Acad. Sci. U.S.A.* 108, 4516–4522. doi: 10.1073/pnas.1000080107

Carrier, T. J., Dupont, S., and Reitzel, A. M. (2019). Geographic location and food availability offer differing levels of influence on the bacterial communities associated with larval sea urchins. *FEMS Microbiol. Ecol.* 95, 1–9.

De Caralt, S., Uriz, M. J., and Wijffels, R. H. (2007). Vertical transmission and successive location of symbiotic bacteria during embryo development and larva formation in *Corticium candelabrum* (*Porifera*: *Demospongiae*). *J. Mar. Biol. Assoc. U. K.* 87, 1693–1699. doi: 10.1017/s0025315407056846

Douglas, A. E. (1994). *Symbiotic Interactions*. Oxford: Oxford University Press.

Easson, C. G., and Thacker, R. W. (2014). Phylogenetic signal in the community structure of host-specific microbiomes of tropical marine sponges. *Front. Microbiol.* 5:532. doi: 10.3389/fmicb.2014.00532

Eberl, G. (2010). A new vision of immunity: homeostasis of the superorganism. *Mucosal. Immunol.* 3, 450–460. doi: 10.1038/mi.2010.20

Endow, K., and Ohta, S. (1990). Occurrence of bacteria in the primary oocytes of vesicomyid clam *Calyptogena soyoae*. *Mar. Ecol. Prog. Ser.* 64, 309–311. doi: 10.3354/meps064309

Ereskovsky, A. V., Gonobobleva, E., and Vishnyakov, A. (2005). Morphological evidence for vertical transmission of symbiotic bacteria in the viviparous sponge *Halisarca dujardini* Johnston (*Porifera*. *Demospongiae*, *Halisarcida*). *Mar. Biol.* 146, 869–875. doi: 10.1007/s00227-004-1489-1

Ewald, P. W. (1987). Transmission modes and evolution of the parasitism-mutualism continuum. *Ann. N. Y. Acad. Sci.* 503, 295–306. doi: 10.1111/j.1749-6632.1987.tb40616.x

Flórez, L. V., Biedermann, P. H. W., Engl, T., and Kaltenpoth, M. (2015). Defensive symbioses of animals with prokaryotic and eukaryotic microorganisms. *Nat. Prod. Rep.* 32, 904–936. doi: 10.1039/c5np00010f

Galac, M. R., Bosch, I., and Janies, D. A. (2016). Bacterial communities of oceanic sea star (*Asteroidea*: *Echinodermata*) larvae. *Mar. Biol.* 163:162.

Galand, P. E., Chapron, L., Meistertzheim, A.-L., Peru, E., and Lartaud, F. (2018). The effect of captivity on the dynamics of active bacterial communities differs between two deep-sea coral species. *Front. Microb.* 9:2565. doi: 10.3389/fmicb.2018.02565

Gloeckner, V., Lindquist, N., Schmitt, S., and Hentschel, U. (2013). *Ectyoplasia ferox*, an experimentally tractable model for vertical microbial transmission in marine sponges. *Microb. Ecol.* 65, 462–474. doi: 10.1007/s00248-012-0142-7

Gloeckner, V., Wehrl, M., Moitinho-silva, L., Schupp, P., Pawlik, J. R., Lindquist, N. L., et al. (2014). The HMA-LMA dichotomy revisited?: an electron microscopical survey of 56 sponge species. *Biol. Bull.* 227, 78–88. doi: 10.1086/bblv227n1p78

Harrington, B., and the Inkscape Development Team (2005). *Inkscape*. Available online at: http://www.inkscape.org/ (accessed February 18, 2019).

Hentschel, U., Hopke, J., Horn, M., Friedrich, A. B., Wagner, M., Hacker, J., et al. (2002). Molecular evidence for a uniform microbial community in sponges from different oceans. *Appl. Environ. Microbiol.* 68, 4431–4440. doi: 10.1128/AEM.68.9.4431-4440.2002

Herre, E. A., Knowlton, N., Mueller, U. G., and Rehner, S. A. (1999). The evolution of mutualisms: exploring the paths between conflict and cooperation. *Trends Ecol. Evol.* 14, 49–53. doi: 10.1016/s0169-5347(98)01529-8

Klitgaard, A. B., and Tendal, O. S. (2004). Distribution and species composition of mass occurrences of large-sized sponges in the northeast Atlantic. *Prog. Oceanogr.* 61, 57–98. doi: 10.1016/j.pocean.2004.06.002

Koropatnick, T. A., Engle, J. T., Apicella, M. A., Stabb, E. V., Goldman, W. E., and Mcfall-ngai, M. J. (2004). Microbial factor-mediated development in a host-bacterial mutualism. *Science* 306, 1186–1189.

Kozich, J. J., Westcott, S. L., Baxter, N. T., Highlander, S. K., and Schloss, P. D. (2013). Development of a dual-index sequencing strategy and curation pipeline for analyzing amplicon sequence data on the Miseq Illumina sequencing platform. *Appl. Environ. Microbiol.* 79, 5112–5120. doi: 10.1128/aem.01043-13

Landry, Z., Swa, B. K., Herndl, G. J., Stepanauskas, R., and Giovannoni, S. J. (2017). *SAR202* genomes from the dark ocean predict pathways for the oxidation of recalcitrant dissolved organic matter. *mBio* 8, e00413-17.

Love, G. D., Grosjean, E., Stalvies, C., Fike, D. A., Grotzinger, J. P., Bradley, A. S., et al. (2009). Fossil steroids record the appearance of Demospongiae during the Cryogenian period. *Nature* 457, 718–721. doi: 10.1038/nature07673

Maldonado, M. (2007). Intergenerational transmission of symbiotic bacteria in oviparous and viviparous demosponges, with emphasis on intracytoplasmically-compartmented bacterial types. *J. Mar. Biol. Assoc. U. K.* 87, 1701–1713. doi: 10.1017/s0025315407058080

Maldonado, M., Aguilar, R., Bannister, R. J., Bell, J. J., Conway, K. W., Dayton, P. K., et al. (2016). "Sponge grounds as key marine habitats: a synthetic review of types, structure, functional roles, and conservation concerns," in *Marine Animal Forests*, eds S. Rossi, L. Bramanti, A. Gori, and C. Orejas (Berlin: Springer-Verlag), 1–39. doi: 10.1007/978-3-319-17001-5_24-1

McFall-Ngai, M., Hadfield, M. G., Bosch, T. C. G., Carey, H. V., Domazet-Lošo, T., and Douglas, A. E. (2013). Animals in a bacterial world, a new imperative for the life sciences. *Proc. Natl. Acad. Sci. U.S.A.* 110, 3229–3236.

Moitinho-Silva, L., Nielsen, S., Amir, A., Gonzalez, A., Ackermann, G. L., Cerrano, C., et al. (2017a). The sponge microbiome project. *Gigascience* 6:gix077.

Moitinho-Silva, L., Steinert, G., Nielsen, S., Hardoim, C. C. P., Wu, Y. C., McCormack, G. P., et al. (2017b). Predicting the HMA-LMA status in marine sponges by machine learning. *Front. Microbiol.* 8:752. doi: 10.3389/fmicb.2017.00752

Montgomery, M. K., and McFall-Ngai, M. (1994). Bacterial symbionts induce host organ morphogenesis during early postembryonic development of the squid *Euprymna scolopes*. *Development* 120, 1719–1729.

Mortzfeld, B. M., Urbanski, S., Reitzel, A. M., Künzel, S., Technau, U., and Fraune, S. (2016). Response of bacterial colonization in *Nematostella vectensis* to development, environment and biogeography. *Environ. Microbiol.* 18, 1764–1781. doi: 10.1111/1462-2920.12926

Mulisch, M., and Welsch, U. (2015). *Romeis Mikroskopische Technik*. Berlin: Springer, 1–603.

Murillo, F. J., Kenchington, E., Koen-Alonso, M., Guijarro, J., Kenchington, T. J., Sacau, M., et al. (2020). Mapping benthic ecological diversity and interactions with bottom-contact fishing on the Flemish Cap (northwest Atlantic). *Ecol. Indic.* 112:106135. doi: 10.1016/j.ecolind.2020.106135

Muyzer, G., Waal, E. C. D. E., and Uitierlinden, A. G. (1993). Profiling of complex microbial populations by denaturing gradient gel electrophoresis analysis of polymerase chain reaction-amplified genes coding for 16S rRNA. *Appl. Environ. Microbiol.* 59, 1–6.

Nicholson, J. K., Holmes, E., Kinross, J., Burcelin, R., Gibson, G., Jia, W., et al. (2012). Metabolic Interactions. *Science* 108, 1262–1268.

Nussbaumer, A. D., Fisher, C. R., and Bright, M. (2006). Horizontal endosymbiont transmission in hydrothermal vent tubeworms. *Nature* 441, 345–348. doi: 10.1038/nature04793

Pham, C. K., Murillo, F. J., Lirette, C., Maldonado, M., Colaço, A., Ottaviani, D., et al. (2019). Removal of deep-sea sponges by bottom trawling in the Flemish Cap area: conservation, ecology and economic assessment. *Sci. Rep.* 9:15843.

Quast, C., Pruesse, E., Yilmaz, P., Gerken, J., Schweer, T., Yarza, P., et al. (2013). The SILVA ribosomal RNA gene database project: improved data processing and web-based tools. *Nucleic Acids Res.* 41, 590–596.

R Development Core Team (2008). *R: A Language and Environment for Statistical Computing*. Vienna: R Foundation for Statistical Computing.

Rosenberg, E., and Zilber-Rosenberg, I. (2011). Symbiosis and development: the hologenome concept. *Birth Defects Res. Part C Embryo Today Rev.* 93, 56–66. doi: 10.1002/bdrc.20196

Sachs, J. L., Skophammer, R. G., and Regus, J. U. (2011). Evolutionary transitions in bacterial symbiosis. *Proc. Natl. Acad. Sci. U.S.A.* 108, 10800–10807. doi: 10.1073/pnas.1100304108

Schimak, M. P., Schoffelen, N. J., Gruhl, A., and Dubilier, N. (2015). *Transmission of Bacterial Symbionts in the Gutless Oligochaete Olavius Algarvensis*. Bremen: University of Bremen, 161–199.

Schmitt, S., Angermeier, H., Schiller, R., Lindquist, N., and Hentschel, U. (2008). Molecular microbial diversity survey of sponge reproductive stages and mechanistic insights into vertical transmission of microbial

symbionts. *Appl. Environ. Microbiol.* 74, 7694–7708. doi: 10.1128/aem.00878-08

Schmitt, S., Weisz, J. B., Lindquist, N., and Hentschel, U. (2007). Vertical transmission of a phylogenetically complex microbial consortium in the viviparous sponge *Ircinia felix*. *Appl. Environ. Microbiol.* 73, 2067–2078. doi: 10.1128/aem.01944-06

Segata, N., Izard, J., Waldron, L., Gevers, D., Miropolsky, L., Garrett, W. S., et al. (2011). Metagenomic biomarker discovery and explanation. *Genome Biol.* 12:R60.

Sharp, K. H., Eam, B., John Faulkner, D., and Haygood, M. G. (2007). Vertical transmission of diverse microbes in the tropical sponge *Corticium* sp. *Appl. Environ. Microbiol.* 73, 622–629. doi: 10.1128/aem.01493-06

Steinert, G., Rohde, S., Janussen, D., Blaurock, C., and Schupp, P. J. (2017). Host-specific assembly of sponge-associated prokaryotes at high taxonomic ranks. *Sci. Rep.* 7, 1–9.

Thomas, T., Moitinho-Silva, L., Lurgi, M., Björk, J. R., Easson, C., Astudillo-García, C., et al. (2016). Diversity, structure and convergent evolution of the global sponge microbiome. *Nat. Commun.* 7:11870.

Thompson, J. N. (1994). *The Coevolutionary Process*. Chicago, IL: The University of Chicago Press, 1–383.

Thompson, T., and Fuller, S. D. (2020). *Technical Measures and Environmental Risk Assessments for Deep-Sea Sponge Conservation*. Rome: FAO, 1–30.

van Soest, R. W. M., Boury-Esnault, N., Hooper, J. N. A., Rützler, K., de Voogd, N. J., Alvarez, B., et al. (2020). *World Porifera Database*. Accessed at: http://www.marinespecies.org/porifera (accessed February 06, 2020).

Wallner, G., Amann, R., and Beisker, W. (1993). Optimizing fluorescent *in situ* hybridization with rRNA-targeted oligonucleotide probes for flow cytometric identification of microorganisms. *Cytometry* 14, 136–143. doi: 10.1002/cyto.990140205

Webster, N. S., Taylor, M. W., Behnam, F., Lücker, S., Rattei, T., Whalan, S., et al. (2010). Deep sequencing reveals exceptional diversity and modes of transmission for bacterial sponge symbionts. *Environ. Microbiol.* 12, 2070–2082.

Weisburg, W. G., Barns, S. M., Pelletier, D. A., and Lane, D. J. (1991). 16S ribosomal DNA amplification for phylogenetic study. *J. Bacteriol.* 173, 697–703. doi: 10.1128/jb.173.2.697-703.1991

Wentrup, C., Wendeberg, A., Schimak, M., Borowski, C., and Dubilier, N. (2014). Forever competent: deep-sea bivalves are colonized by their chemosynthetic symbionts throughout their lifetime. *Environ. Microbiol.* 16, 3699–3713. doi: 10.1111/1462-2920.12597

Wickham, H. (2016). *ggplot2: Elegant graphics for Data Analysis*. New York, NY: Springer-Verlag, 1–213.

Wilkinson, D. M. (2001). Horizontally acquired mutualisms, an unsolved problem in ecology?? *Oikos* 92, 377–384. doi: 10.1034/j.1600-0706.2001.920222.x

Xavier, J. R., Cárdenas, P., Cristobo, J., Van Soest, R., and Rapp, H. T. (2015). Systematics and biodiversity of deep-sea sponges of the Atlanto-Mediterranean region. *J. Mar. Biol. Assoc. U. K.* 95, 1285–1286.

Yamamura, N. (1993). Vertical transmission and evolution of mutualism from parasitism. *Theor. Popul. Biol.* 44, 95–109. doi: 10.1006/tpbi.1993.1020

Zumberge, J. A., Love, G. D., Cárdenas, P., Sperling, E. A., Gunasekera, S., Rohrssen, M., et al. (2018). Demosponge steroid biomarker 26-methylstigmastane provides evidence for Neoproterozoic animals. *Nat. Ecol. Evol.* 2, 1709–1714. doi: 10.1038/s41559-018-0676-2

Conflict of Interest: The authors declare that the research was conducted in the absence of any commercial or financial relationships that could be construed as a potential conflict of interest.

The handling Editor declared a past co-authorship with one of the authors HR.

Copyright © 2020 Busch, Wurz, Rapp, Bayer, Franke and Hentschel. This is an open-access article distributed under the terms of the Creative Commons Attribution License (CC BY). The use, distribution or reproduction in other forums is permitted, provided the original author(s) and the copyright owner(s) are credited and that the original publication in this journal is cited, in accordance with accepted academic practice. No use, distribution or reproduction is permitted which does not comply with these terms.

frontiers in Marine Science

ORIGINAL RESEARCH
published: 20 October 2020
doi: 10.3389/fmars.2020.565171

Mortality, Population and Community Dynamics of the Glass Sponge Dominated Community "The Forest of the Weird" From the Ridge Seamount, Johnston Atoll, Pacific Ocean

Emily G. Mitchell[1]* *and Simon Harris*[2]

[1] Deep-time Ecology Group, Department of Zoology, University of Cambridge, Cambridge, United Kingdom, [2] National Geological Repository Store, British Geological Survey, Nottingham, United Kingdom

OPEN ACCESS

Edited by:
Joana R. Xavier,
University of Porto, Portugal

Reviewed by:
Michael Vecchione,
National Oceanic and Atmospheric Administration (NOAA), United States
Jackson Chu,
University of Victoria, Canada

***Correspondence:**
Emily G. Mitchell
ek338@cam.ac.uk;
emilyghmitchell@gmail.com

Specialty section:
This article was submitted to Deep-Sea Environments and Ecology, a section of the journal Frontiers in Marine Science

Received: 24 May 2020
Accepted: 28 September 2020
Published: 20 October 2020

Citation:
Mitchell EG and Harris S (2020) Mortality, Population and Community Dynamics of the Glass Sponge Dominated Community "The Forest of the Weird" From the Ridge Seamount, Johnston Atoll, Pacific Ocean. Front. Mar. Sci. 7:565171. doi: 10.3389/fmars.2020.565171

The ecosystem dynamics of benthic communities depend on the relative importance of organism reproductive traits, environmental factors, inter-specific interactions, and mortality processes. The fine-scale community ecology of sessile organisms can be investigated using spatial analyses because the position of the specimens on the substrate (their spatial positions) reflects the biological and ecological processes that they were subject to in-life. Consequently, spatial point process analyses (SPPA) and Bayesian network inference (BNI) can be used to reveal key insights into the ecological dynamics of these deep-sea communities. Here we use these analyses to investigate the ecology of deep-sea glass sponge dominated community "The Forest of the Weird" (2,442 m depth, Ridge Seamount, Johnston Atoll, Pacific Ocean). A 3D reconstruction was made of this community using photogrammetry of video stills taken from high-resolution ROV video. The community was dominated by two genera of Hexactinellids: Farreidae *Aspidoscopulia* sp. and Euplectellidae *Advhena magnifica* with octocorals *Narella bowersi*, *Narella macrocalyx,* and *Rhodaniridogorgia* also present in large proportions. SPPA of the dead vs. alive organisms revealed a random distribution of dead amongst the living, showing a non-density dependent cause of death for the majority of taxa. However, in the high-density ridge crest region there was non-random aggregation of dead specimens, revealing density-dependent mortality for *Aspidoscopulia*. SPPA showed that the glass sponges and octocorals were each most strongly influenced by different underlying processes, and reacted to the environmental conditions differently. The octocorals responded to higher density areas with increased intra-specific competition, whilst the glass-sponges seemed impervious to a doubling of specimen density. BNI found that mutual habitat associations between different taxa resulted in inter-specific competition at larger (2–4 m) spatial scales, with instances of competition at small-spatial scales (<0.75 m) in the higher-density ridge crest section. To our knowledge, this study is the first to analyze the mortality, population and community

dynamics of a deep-sea sponge community using SPPA. Our results provide the first insight into the variety of ecological behaviors of these different glass sponges and octocorals, and show how these different organisms have developed diverse responses to the biological and environmental gradients within their habitat.

Keywords: sponges, benthic ecology, deep-sea ecology, Bayesian network inference, community ecology, mortality dynamics, spatial point process analyses, ecological network

INTRODUCTION

Sponge and coral dominated deep-sea communities are complex habitats, providing habitat, and refuge for other benthos creating biodiversity hotspots in the deep ocean (Buhl-Mortensen et al., 2010; Hogg, 2010; Maldonado et al., 2017; Rossi et al., 2017). Deep-sea sponges create these biodiversity hotspots by providing biogenic structures which increase vertical habitat complexity, providing substrate and refugia for macroinvertebrates and demersal fish (Dayton, 1972; Dayton et al., 2013; Kazanidis et al., 2016; Maldonado et al., 2017; Dunham et al., 2018; Meyer et al., 2019; Vieira et al., 2020). Sponges also provide a key link between benthic and pelagic systems, by pumping and filtering large quantities of water (Reiswig, 1974; Bell, 2008), and so increase diversity beyond providing a hard substrate (Mitchell et al., 2020b). Environmental settings have a strong influence on benthic community composition and density across multiple different scales, from global latitudinal and depth gradients to the kilometer and meter scale. Sponge distributions are influenced by different factors such as depth, surface temperature, silicate levels, salinity, sea-floor characteristics and POC over broad scales (Beazley et al., 2015, 2018; Howell et al., 2016; Murillo et al., 2020). Sponges, corals, and other filter feeders often found on elevated features such as seamounts (Genin et al., 1986; Lundsten et al., 2009; Clark et al., 2010), hills (Durden et al., 2015), mounds, and ridges (Chu and Leys, 2010), where raised seabed morphology often induces faster currents providing a richer flow and deposition of organic matter (Lundsten et al., 2009; Howell et al., 2016). Seamounts and other elevated seafloor features often have high species richness and diversity (Richer de Forges et al., 2000; Samadi et al., 2006; Rowden et al., 2010), different community composition and structure (McClain et al., 2009; McClain and Barry, 2010; Mitchell et al., 2020a) with sponges further contributing to this high diversity (Beaulieu, 2001; Kahn et al., 2015; Hawkes et al., 2019).

Ecological analyses of sponge populations and communities have mostly focused on specific ecological processes, such as the importance of episodic recruitment events (Dayton, 1989; Dayton et al., 2013, 2016), distribution patterns (Kenchington et al., 2013; Knudby et al., 2013; Howell et al., 2016; Beazley et al., 2018; Murillo et al., 2020), associations of taxa with the habitat complexity (Robert et al., 2017) or competition and facilitation between sponges (Dayton, 1971; Easson et al., 2014). As such, less is known about the community dynamics in terms of the relative occurrence of multiple different sorts of processes within communities, such as dispersal limitation, habitat associations, facilitation and competition. In this study we infer multiple different types of intra and inter-taxa interactions and associations at the centimeter to meter scale using Spatial Point Process Analyses (SPPA) and Bayesian Network Inference (BNI).

SPPA capitalizes on the spatial position of organisms on the substrate because there are only four different sets of processes which can influence these positions: (1) interactions with environment, (2) dispersal limitation, (3) interactions such as facilitation and competition within and between taxa populations, and (4) density-dependent mortality processes (Illian et al., 2008; Wiegand and Moloney, 2013). Therefore, by analyzing the spatial distributions of the sessile community, the most likely underlying processes for the patterns can be inferred using SPPA. SPPA has been developed extensively for use in forest ecology, but is equally applicable to other sessile organisms such as fungi (Liang et al., 2007) and corals (Muko et al., 2014). Within SPPA each organism is treated as a point and spatial distributions are calculated using distance measures such as pair correlation functions (PCFs) which then describe how the density of points change over different spatial scales (Illian et al., 2008). SPPA has not been widely applied to sessile animal communities, but has been used to investigate coral colony aggregations (Muko et al., 2014), to consider mortality due to adult proximity (Gibbs and Hay, 2015), and has been suggested for quantifying changes over time (Piazza et al., 2020). Most SPPA studies of benthic communities have focused on disease spread through sponge and coral populations (e.g., Jolles et al., 2002; Zvuloni et al., 2009; Muller and van Woesik, 2012; Easson et al., 2013; Deignan and Pawlik, 2015) with limited numbers of analyses using SPPA to investigate population spatial aggregations (Prado et al., 2019). These previous studies on benthic communities mostly focus on describing the spatial patterns found. However, the power of SPPA is the methodological techniques that enable the fitting of multiple different models, which correspond to different underlying processes, to determine the most likely processes within these benthic communities, and thus the driving factors behind their community ecology (cf. Mitchell et al., 2019).

When considering interactions between pairs of taxa, auto-correlation from chains of interactions need to be eliminated to ensure only causal relationships are reported. For example, if taxon A directly interacts with taxon B and B interacts directly with taxon C, we could expect a non-random spatial distribution between A and C. However, this non-random distribution would not be the result of a direct interaction, but would just be a reflection of the two interactions between A and B and B and C. One approach to finding only realized dependencies between taxa is using BI) to reconstruct the ecological network of the community (Heckerman et al., 1995) and then apply bivariate SPPA analyses to these BNI

dependencies (Mitchell and Butterfield, 2018). Bayesian networks are probabilistic models that show causal relationships between variables, whereby different variables are the network nodes; and where a dependency exists between two nodes, this is depicted as an edge (Heckerman et al., 1995). BNIs can infer network structures and non-linear interactions, and have been used extensively to reveal gene regulatory networks (Yu et al., 2002), neural information flow networks and ecological networks (Smith et al., 2006; Milns et al., 2010; Mitchell et al., 2020a), paleontological communities (Mitchell and Butterfield, 2018) and more recently using these networks to infer likely changes for benthic systems (Mitchell et al., 2020b). Note that the Bayesian network found reflects the associations caused by co-localizations rather than a specific association or interaction, which is why SPPA is needed to then infer the most likely underlying process.

As part of the National Oceanic and Atmospheric Administration CAPSTONE field campaign, throughout 2015–2017 a series of expeditions was conducted to collect data from the previously unexplored deep-water habitats within the Pacific Remote Islands Marine National Monument (PRIMNM) region in the Pacific Ocean (Kennedy et al., 2019). The 2017 Laulima O Ka Moana Expedition was focused on increasing the knowledge of deep-sea benthic communities within this Johnston Atoll Unit of PRIMNM, in order to support science, management and conservation efforts (Malik et al., 2018). During Dive 11 of cruise EX17-06, Johnston Atoll, a very high density community which was dominated by medium to large hexactinellids was discovered on top of a ridge, informally named "The Forest of the Weird" (Kelley et al., 2018; Hourigan et al., 2020). We used NOAA video data of the sponge community "The Forest of the Weird" (hereafter FW) to create a 3D reconstruction (Robert et al., 2017) from which we then extracted a community map of the organism taxonomic identifications and positions. We used RLA to investigate mortality processes within this community, and univariate SPPA to consider the relative influences of physical and biological processes on each taxon population. BNI was used to find the direct dependencies between taxa, and then bivariate SPPA was used to infer the most likely underlying processes between the taxa pairs found by BNI. These analyses enable us to describe the mortality processes, population and community ecology of the most abundant taxa of the FW community.

MATERIALS AND METHODS

Study Site

In this study we have focused on the "Forest of the Weird" (FW) community, which was recorded on Dive 11 of Okeanos Explorer expedition EX1706 of the Johnston Atoll Unit in PRIMNM (Kelley et al., 2018, p. 11; **Figure 1**). ROV data places the mapped community between 14°28′24.156″ N, 170°51′18.231″ W and 14°28′24.198″ N, 170°51′17.553″ W at depths of 2,365–2370 m, which corresponds to the ridge running northwest to south east consisting primarily of pillow lava formation of basalt bedrock with manganese crust, with areas of cemented cobble and basalt boulders (Kelley et al., 2018; Malik et al., 2018). The ridge slopes up to the ridge crest at an angle of 24–4.81 m taller than the starting point, then slopes down at a 43° angle (**Figure 2**). The steeper area of the mapped area of the ridge (hereafter named the Ridge Crest area) was notably more dense than the gentler sloped ridge area (hereafter named the Ridge area). The FW community was observed during the dive (Kelley et al., 2018, p. 11) to be dominated by two genera of hexactinellids: Farreidae *Aspidoscopulia* sp. and Euplectellidae *Advhena magnifica* with large proportions of the octocorals *Narella bowersi*, *Narella macrocalyx*, and *Rhodaniridogorgia* (which was confirmed by our analyses, **Table 1**). Other octocorals Coralliidae, Isididae, and Primnoidae were also present, but not in sufficient numbers for the analyses within this study (Kelley et al., 2018; NOAA Office of Ocean Exploration and Research, n.d.).

Video Processing

With the advent of high-resolution ROV cameras and high-powered computers, it is now possible to reconstruct entire benthic communities using photogrammetry to centimeter or millimeter scale (Robert et al., 2017, 2020; Baker et al., 2019; Prado et al., 2019; Price et al., 2019), so providing greater accuracy and resolution than the meter scale of ROV location data alone (Kennedy et al., 2019). These 3D photogrammetric reconstructions avoid the problems of controlling for altitude that often accompany 2D photo-montages because the triangulation of points using photographs from multiple angles limits the possible errors—if there is not enough photographs to accurately reconstruct the area, then the 3D model will not be generated (see Robert et al., 2017 for further details). However, errors can be introduced due to specimen movement, which occurred for this dataset, so size analyses were not performed.

The video recorded from the ROV was 720p five mega-bit per second resolution (Malik et al., 2018). The 3D reconstruction of the FW community was created using photogrammetry in Agisoft Metashape 1.5.4 (formerly Agisoft Photoscan) following a similar procedure to Robert et al. (2017), with the 2D projections of the reconstruction performed in Geomagic Wrap 2015.

1. The start of the FW community was taken to be from the ROV track starting at 14°28′24.156″ N, 170°51′18.231″ W until 14°28′24.198″ N, 170°51′17.553″ W.
2. The edges of the community were taken to be the edges of the ridge. There were organisms outside this region, but the reconstruction did not have sufficient tie point matches to reconstruct the region accurately.
3. This segment of video was sampled at a capture rate of 1 frame/second using ffmpeg—an open source video encoder/decoder.
4. Out of focus and shaky frames were removed, as were frames that were close up of individual specimens and/or had other objects obstructing the view in the frame.
5. The files were then imported into Agisoft Metashape.
6. Chunks of 100 frames were auto-aligned to form a sparse point cloud.
7. These chunks were then aligned into the complete community which was formed from 583 out of a total 600 input frames and 131,322 tie points.

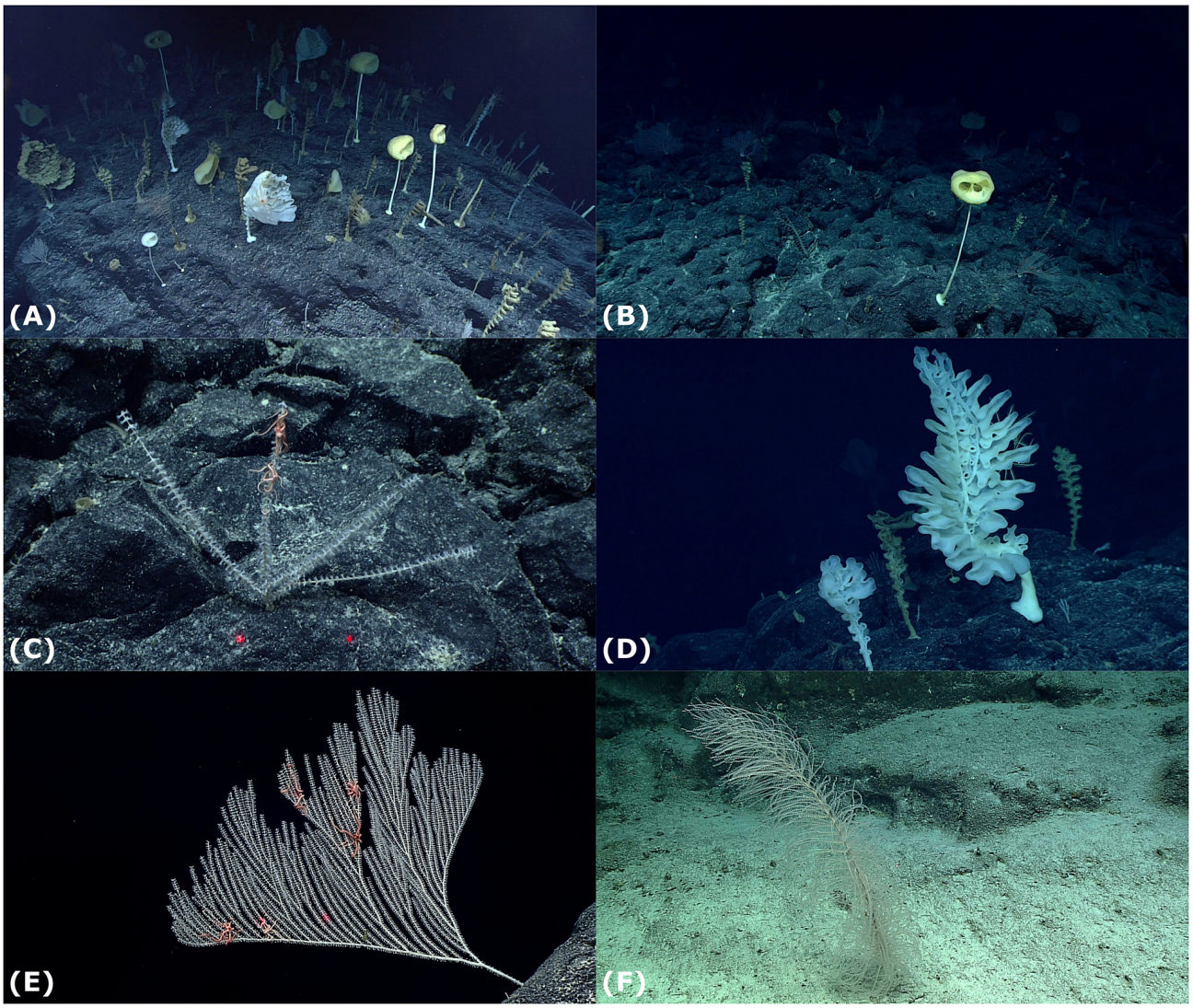

FIGURE 1 | Different taxa identified within this study. Red laser dots are 10 cm apart. **(A)** A photograph of the Ridge Crest Area, **(B)** *Advhena magnifica*, **(C)** *Narella macrocalyx,* **(D)** *Aspidoscopulia,* **(E)** *Narella bowersi*, and **(F)** *Rhodaniridogorgia*.

8. A dense cloud (6 million points) and mesh (4.398 million faces) was created from the combined sparse point cloud.
9. The frames were matched to the ROV GPS tracks by using the epoch timestamp in the GPS log and matching it (using a "join query" in Access) to the image frames, which had been renamed to match. Distances were checked using photographs where 2 red laser dots (10 cm apart) to correctly scale the reconstruction.
10. Individual organisms were marked up and identified on the frames within the 3D reconstruction. Note that the resolution of the videos was less than that of the high-resolution photographs taken which hinders resolution for smaller specimens and also meant that very small (∼<2 cm) specimens may not have been marked.
11. Specimen positions were checked from multiple viewpoints.

Screen shots of the 3D reconstruction show both the strengths and weakness of the reconstruction (**Figure 2**). Generally the substrate and the attachment to the substrate are well resolved. The video footage focused on the ridge so that areas outside the ridge were not well resolved (and thus not included in the analyses). However, the edge of the ridge is clearly visible, and shows a notable decrease in density. The dark blue areas were the deep far-ground which was not sufficiently well resolved to be accurately reconstructed. The organisms' tops often appeared disconnected from their base, probably due to movement, but it was straightforward to infer which holdfast they belonged to.

In order to get the 2D map for our analyses, the 3D reconstruction was exported into Geomagic Wrap, and a best-fit plane was fit to the Ridge and Ridge Crest areas, respectively. The 2D maps for each area were created by rotating the specimen positions to the best-fit planes for each section separately, which

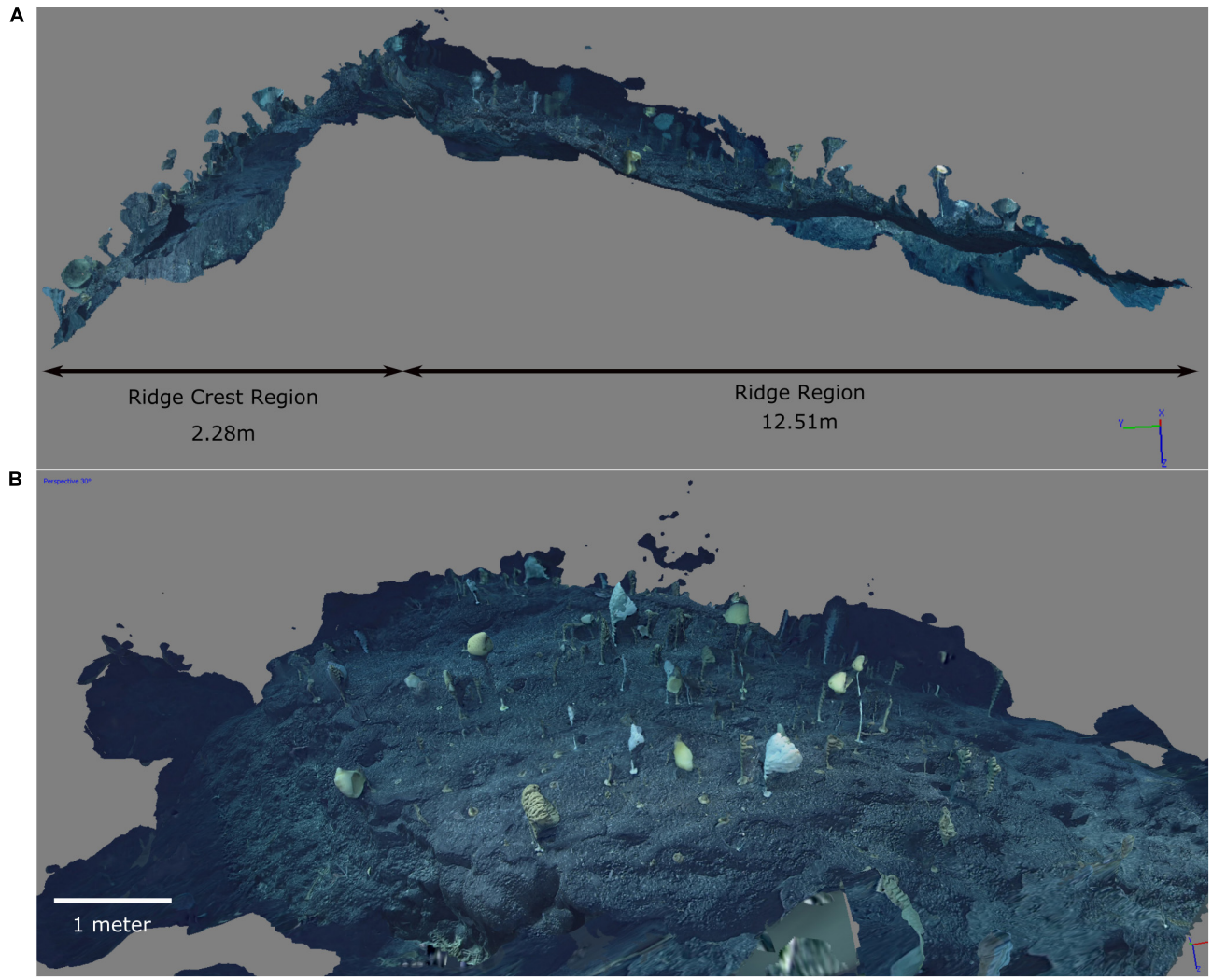

FIGURE 2 | Screenshots of the 3D reconstruction. **(A)** Side view showing the two different areas with the Ridge Crest area on the left and Ridge area on the right. **(B)** A closer view of the Ridge Crest community. The dark blue areas above the community and rising to the left and right are artifacts of the photogrammetry where frames included a lot of the farground. The substrate beyond the edge of the ridge to the right and left has good resolution, and so the edge of the community is clearly resolved. Note the badly resolved section at the bottom of the screenshot, where there wasn't sufficient video coverage to reconstruct the substrate (which was sparsely populated).

were then exported then rejoined as a single 2D projection (see SI for data).

Spatial Analyses

Four different types of spatial analyses were performed on the data: (1) Random labeling analyses were used to investigate the mortality dynamics within the community. (2) Univariate SPPA were used to investigate the population ecology of each taxon. (3) BNI was used to identify primary dependencies between taxa. (4) Bivariate SPPA was used to determine the most likely underlying processes to the primary dependencies found using BNI.

The simplest scenario within SPPA analyses is that all the points (here different organisms) are randomly distributed within the study area. This random distribution is known as complete spatial randomness (CSR), and can be modeled as an homogeneous Poisson model (Illian et al., 2008). Where CSR is found to best describe the spatial distributions observed, there are no biotic and abiotic processes which significantly effect that population at the spatial scales considered. If the spatial distributions are non-CSR, then they can be aggregated, whereby the organisms are closer together than CSR; or segregated, where the organisms are more spaced out than CSR. Non-CSR distributions could also have aggregation and segregation operating at different spatial scales, which is reflecting different processes operating at different scales. Univariate or single population aggregations can be caused by habitat associations, where the taxon has an environmental preference, such as altitudes for alpine tree species (Wang et al., 2012), and these habitat associations are best modeled by heterogeneous Poisson

TABLE 1 | Summary table.

Taxon	All			Ridge Crest			Ridge		
	n	Prop.	Int	n	Prop.	Int	n	Prop.	Int
Aspidoscopulia brown	194	0.33	1.73	102	0.38	3.48	91	0.29	1.27
Aspidoscopulia white	68	0.11	0.61	27	0.10	0.92	41	0.13	0.57
Aspidoscopulia white and brown	7	0.01	0.06	2	0.01	0.07	5	0.02	0.07
Advhena magnifica	17	0.03	0.15	5	0.02	0.17	12	0.04	0.17
Holdfast disc	44	0.07	0.39	15	0.06	0.51	29	0.09	0.41
Holdfast disc with stalk	101	0.17	0.90	47	0.17	1.60	54	0.17	0.76
Narella bowersi	33	0.06	0.29	14	0.05	0.48	19	0.06	0.27
Narella macrocalyx	16	0.03	0.14	8	0.03	0.27	7	0.02	0.10
Other corals	18	0.03	0.16	9	0.03	0.31	10	0.03	0.14
Other sponges	8	0.01	0.07	5	0.02	0.17	3	0.01	0.04
Rhodaniridogorgia	23	0.04	0.21	8	0.03	0.27	15	0.05	0.21
Small undetermined.	63	0.11	0.56	30	0.11	1.02	33	0.10	0.46
All *Aspidoscopulia* (brown, white and mixed)	269	0.45	2.40	131	0.48	4.47	137	0.43	1.92
All *Advhena magnifica* (*Advhena magnifica* and stalked discs)	118	0.20	1.05	52	0.19	1.77	66	0.21	0.92

n is the number of specimens, Prop. is the proportion of the community, and Int. is the density per meter squared of that taxon.

TABLE 2 | Discretized data for BNI.

	Aspidoscopulia	*Advhena magnifica*	*Rhodaniridogorgia*	*Narella macrocalyx*	*Narella bowersi*
Zero	8	10	24	32	20
Low	18	21	13	6	15
High	15	10	4	3	6

Abundant sponge and coral taxa for the area studied. The boundary between the Low and High groups was defined as the median value for each taxa.

models (Wiegand et al., 2007b; Wiegand and Moloney, 2013). Habitat associations can also cause univariate and bivariate segregation when the habitat which the taxon/taxa occupy is itself segregated (Mitchell and Kenchington, 2018). Univariate aggregations can also be caused by dispersal processes, whereby offspring surround their parent (Mitchell et al., 2015), and these are best modeled by Thomas cluster models for a single reproductive event, or double Thomas cluster models for two reproductive events (Wiegand et al., 2007b; Illian et al., 2008). Habitat associations can also result in bivariate (between two taxon) aggregations, which can be best modeled by heterogeneous Poisson models or shared source models (also called shared parent models) where the two sets of taxon aggregate around the same set of mutually exclusive points, i.e., the focus of the taxon clusters are points that are not biological taxa, but some other "environmental" factor (Wiegand et al., 2007b; Wiegand and Moloney, 2013). Bivariate aggregations can also be caused by facilitation whereby one taxon increases another's chance for survival, and is modeled as a linked Thomas cluster model, with aggregations of the facilitated taxon centered on the facilitating taxon (Dickie et al., 2005; Getzin et al., 2006; Dale and Fortin, 2014). Alongside habitat associations, univariate and bivariate segregation also occurs through competition between organisms for resources (Wiegand et al., 2007a; Illian et al., 2008) where it can be modeled by hard-core (where there is no overlap of organisms within a given radius) and soft-core (where organism density is reduced) processes. While untangling processes from these spatial pattern is imprecise (Law et al., 2009; McIntire and Fajardo, 2009), the use of complementary types of SPPA with multiple model fitting and assessment means that the most likely underlying process can be inferred (Levin, 1992; Wiegand and Moloney, 2004, 2013; Illian et al., 2008; Waagepetersen, 2009).

Density-dependent mortality processes are best investigated using a subset of SPPA called Random Labeling Analyses (RLA) (Raventós et al., 2010). While density-dependent mortality processes can be detected through distance measures as described above, RLA is preferable because no assumptions need to be made about the processes underlying the initial spatial distributions, enabling the uncovering of subtle processes that may otherwise be obscured. Instead, the spatial distributions of the dead among the living are investigated in order to investigate whether the dead specimens are aggregated, indicating density-dependent mortality.

Random Labeling Analyses

To investigate mortality processes, we investigated how a state of an organism (dead or alive in this study) changes within organism locations, using RLAs (Pélissier and Goreaud, 2001; Raventós et al., 2010). We followed methods similar to Mitchell et al. (2018). RLAs are a type of SPPA whereby random models are simulated whilst the positions of the specimens remain the same and a given property, such dead or alive, is repeatedly

permutated: the points remain in the same place, but the state allocated to them (representing either dead or alive) is changed. As such, RLAs do not directly measure the aggregation or segregation between two populations, and so do not test the processes that resulted in sponge location, but instead measure the differences in spatial distributions of live/dead state between two populations.

Spatial distributions are commonly described using PCFs which describe how the density of points (i.e., sponge specimens) changes as a function of distance from the average specimen (e.g., Illian et al., 2008). RLAs assess the differences between two characters (dead/alive) of the populations by calculating variations between PCFs by considering the Difference and Quotient tests (Wiegand and Moloney, 2013). The Difference test is the calculation of the distribution of $PCF_{11} - PCF_{22}$, where PCF_{11} is the univariate PCF for group 1 and PCF_{22} is the univariate PCF for group 2. If $PCF_{11} - PCF_{22} = 0$ then both groups are randomly distributed within the locations (i.e., both groups exhibit the same spatial behavior). If $PCF_{11} - PCF_{22} > 0$, then group 1 is more aggregated than group 2; if $PCF_{11} - PCF_{22} < 0$, then group 2 is more aggregated than group 1. To further investigate the differences between the dead and alive populations, the $PCF_{21} - PCF_{22}$ and $PCF_{12} - PCF_{11}$ are calculated. These differences test the relative aggregation (or segregation) of the dead and alive spatial distributions compared to the relative spatial distribution of the dead to alive (and *vice versa*). If $PCF_{12} - PCF_{11} < 0$ then group 1 (alive) are positively correlated with other alive points, and if $PCF_{21} - PCF_{22} < 0$ then group 2 (dead) are positively correlated with other dead specimens. The difference $PCF_{12} - PCF_{21}$ was used to test for edge effects within the study area. If there are excursions outside the Monte Carlo simulations (as is common at larger spatial scales), then edge effects have a significant impact on the analyses, and the scales over which the analyses are done should be reduced.

The Quotient test calculates the bivariate PCF between groups relative to the pattern of both groups taken together (the joined pattern), where PCF_{12} is the bivariate distribution of group 2 relative to group 1 and PCF_{21} is the bivariate distribution of group 1 relative to group 2. For joint patterns, $PCF_{1,1+2}$ is the bivariate distribution of group 1 relative to both groups together, and $PCF_{2,2+1}$ is the bivariate distribution of group 2 relative to the joint pattern. Thus, the Quotient test is the calculation of the distribution: $PCF_{1,1+2}$ - $PCF_{21}/PCF_{2,2+1}$ where $PCF_{12}/PCF_{1,1+2}$ - $PCF_{21}/PCF_{2,2+1} > 0$ indicates that group 2 is mainly located in areas with high density of the joint pattern, and group 1 is in low density areas (i.e., group 2 has more neighbors than group 1). If this quotient is significantly non-zero, then the process underlying the characters is density-dependent; for example, dead specimens occur more commonly in high-density areas, indicating density-dependent mortality.

We test three null hypotheses of mortality spread using RLA of dead/alive state with the organism positions:

(1) H_0^{Comm}: The spatial distribution of dead specimens are randomly distributed within the living community of corals and sponges.
(2) H_0^{Asp}: The spatial distribution of dead specimens of *Aspidoscopulia* are randomly distributed within the living population of *Aspidoscopulia.*
(3) H_0^{Bol}: The spatial distribution of dead specimens dead specimens of within *Advhena magnifica* population are randomly distributed within the living population of *Advhena magnifica.*

Establishing whether the null hypotheses of the Difference and Quotient Tests should be rejected or not is complicated, because there is a lack of independence of the spatial points (organism positions) and a variety of different point pattern distributions (Illian et al., 2008). Two different methods are commonly used to establish acceptance or rejection of the null hypotheses for ecological data (e.g., Wiegand and Moloney, 2013 and references therein): (1) Monte Carlo simulations (Illian et al., 2008), and (2) Diggle's goodness-of-fit test p_d, which represents the total squared deviation between the observed pattern and the simulated pattern across the studied distances (Diggle, 2002; Diggle et al., 2005). The two comparisons are used together because: (1) the Monte Carlo simulation envelopes do not necessarily correspond to confidence intervals, and they run the risk of Type I errors if the observed PCF falls near the edge of the simulation envelope (Illian et al., 2008); (2) the p_d does not strictly test whether a model should be accepted or rejected, but rather whether the test calculation for the observed data are within the range of the stochastic realization of the null hypothesis (Diggle, 2002); and (3) the p_d depends on the range over which it is calculated, meaning that the model may not fit at very small distances due to the physical occupation of that space by the organisms themselves, but may fit well at larger distances (Diggle, 2002; Illian et al., 2008). Thus visual inspection of the PCFs with Monte Carlo simulation envelopes, coupled with p_d, ensures that these errors are minimized. The underlying mathematics is described in detail by Wiegand and Moloney (2004, 2013) and Wiegand et al. (2006).

The following RLAs were conducted using Programita software across three different areas: All mapped area, the Ridge and the Ridge Crest (Wiegand and Moloney, 2004, 2013; Wiegand et al., 2006; Raventós et al., 2010):

(1) To test H_0^{Comm} all living specimens of both coral and sponge taxon were contained in the alive group and, and all brown specimens (including the dead *Aspidoscopulia*, holdfast discs with long stalks and holdfast discs) were grouped as dead. The univariate PCFs of the dead and the alive populations were calculated by creating a distribution map of each dead/alive state according to a 10 cm × 10 cm grid of surface within which the specimen density was calculated. The Difference tests were then performed between the two groups.
(2) To test H_0^{Asp} the white specimens of *Aspidoscopulia* were assumed to be alive, brown specimens dead and those with white and brown patches were excluded from the analyses (7 specimens in total so not sufficient to run separate analyses). Difference and Quotient tests were performed between the dead and alive groups. If the dead

and alive specimens did not have significantly different spatial distributions when compared using the Difference test, they are most likely to be subjected to the same biotic and abiotic processes and so are likely to come from the same single population. If the Difference test finds no significant difference between the dead and alive populations, then the Quotient test was to determine whether the dead specimens are randomly distributed within this population.

(3) To test H_0^{Bol} the holdfast brown discs with long stalks were assumed to be the dead *Advhena magnifica*, and the yellow/white specimens were assumed to be alive. Testing proceeded as for H_0^{Asp}.

Each hypothesis was tested by running 999 Monte Carlo simulations for each group in order to generate simulation envelopes around the random PCF value (i.e., $PCF_{11} - PCF_{22} = 0$). p_d values were calculated using Diggle's goodness-of-fit test (Diggle et al., 2003). A total of 999 simulations were run (instead of 1,000, for example) because the p_d value is calculated using the model simulation data (not the theoretical model), and so by using 999 the p_d simulations could be measured in 0.001 increments. If the observed $PCF_{11} - PCF_{22}$ fell outside the RLA simulation envelopes and had $p_d < 0.1$, then the distributions were found to be significantly different.

Univariate SPPA

Initial data exploration and data visualization were performed in R (R Core Team, 2017) using the package spatstat (Berman, 1986; Baddeley and Turner, 2005; Baddeley et al., 2011). The software Programita (Wiegand et al., 1999, 2006; Wiegand and Moloney, 2004, 2013; Loosmore and Ford, 2006) was used to calculate the PCF and to perform aggregation model fitting (described in detail in Berman, 1986; Wiegand and Moloney, 2004, 2013).

The following analyses were performed on each abundant taxon (*Aspidoscopulia*, *Advhena magnifica*, *Rhodaniridogorgia*, *Narella macrocalyx,* and *Narella bowersi*) across the entire mapped area (All), the shallower section of the ridge (Ridge) and the steeper area of the ridge (Ridge Crest).

To test whether a taxon PCF exhibited CSR, 999 Monte Carlo simulations were run on a homogeneous background and the simulation envelopes chosen to be the 49th highest and lowest values (Wiegand and Moloney, 2013; Mitchell et al., 2018). The models were simulated around CSR, that is PCF = 1. The fit of the observed data to CSR was tested using Diggle's goodness-of-fit test (Diggle et al., 2005) p_d (where $p_d = 1$ corresponds to CSR, and $p_d = 0$ corresponds to non-CSR) with PCF deviations outside the simulation envelope combined with a $p_d << 1$ interpreted to indicate significantly non-CSR distributions.

If a taxon was not randomly distributed on a homogeneous background, and was aggregated, the random model on a heterogeneous background (HP model) was tested by creating a heterogeneous background from the density map of the taxon under consideration, being defined by a circle of radius R over which the density is averaged throughout the sample area. Density maps were formed using estimators in 0.10 m increments over the range of 0.1 m $< R <$ 1 m, and the R corresponding to the best-fit model was used. The radius was increased to account for differing granularity of heterogeneity—the R = 0.1 m will model granular heterogeneities whereas the R = 1 m will be relatively smooth. If excursions outside the simulation envelopes for both homogeneous and heterogeneous Poisson models remained, then Thomas cluster models were fitted to the data as follows:

(1) The PCF and L functions (Levin, 1992) of the observed data were found. Both measures were calculated to ensure that the best-fit model is not optimized toward only one distance measure, and thus encapsulates all spatial characteristics.
(2) Best-fit Thomas cluster processes (Besag, 1974) (TC) were fitted to the two functions where PCF > 1. The best-fit lines were not fitted to fluctuations around the random line of PCF = 1 in order to aid good fit about the actual aggregations, and to limit fitting of the model about random fluctuations. Programita used the minimal contrast method (Diggle, 2002; Diggle et al., 2005; Wiegand et al., 2007b) to find the best-fit model.
(3) If the model did not describe the observed data well, the lines were refitted using just the PCF. If that fit was also poor, then only the L-function was used.
(4) 999 simulations of this model were generated to create the simulation envelope. The 49th highest and lowest simulation values were chosen in line with previous work to be the limits of the simulation envelopes (Wiegand and Moloney, 2013), and the fit was checked using the O-ring statistic (Wiegand and Moloney, 2004).
(5) p_d was calculated over the model range.
(6) If there were no excursions outside the simulation envelope and the p_d -value was high, then a univariate homogeneous Thomas cluster model was interpreted as the best model.
(7) The best-fit TC model was simulated on the best fit HP model following points 4–5 to simulate a Thomas cluster model on a heterogeneous background (ITC).

Bayesian Network Inference

The Bayesian network inference (BNI) algorithm used in this study requires discrete data which ensures data noise is masked and only the relative densities of each taxon are important (Yu et al., 2002; Milns et al., 2010). Previous work has shown that ecological datasets using three different bins provide a good balance between maintaining the amount of information present in the dataset, statistical power, and greater noise masking (Yu, 2005; Milns et al., 2010; Mitchell et al., 2020a). The data were split into three intervals: zero counts, low counts and high counts. Zero was treated as a separate entity because the presence of one individual is very different to a zero presence, in contrast to zero gene expression, for example. Low counts consisted of counts below the median for the species group and high counts were counts over the median. Medians were used rather than means because for some groups the high counts were very high, and would result in a very small number of samples grouped in the highest interval (cf. Milns et al., 2010).

The BNI software used was Banjo v2.0.0, a publicly available Java-based algorithm (Smith et al., 2006). For details of the algorithm please see Smith et al. (2006) and Milns et al. (2010). Pre and post-processing was performed using custom scripts in Haskell (Jones, 2003)[1] and in R (Mitchell, 2011; R Core Team, 2017). The discretized data was input into Banjo which then generated a random network based on the input variables. A "greedy search" was repeated 10 million times for each set of input data and the most probable network was then output. The maximum number of edges leading to a node was set to 3 to limit artefacts (Yu, 2005).

To convert the spatial positions of specimens into discretized data suitable for BNI analyses the following steps were taken (following (Milns et al., 2010):

(1) *Node definition.* The nodes were defined by taxa groups (**Figure 1**).
(2) *Quadrat selection*. Abundance data were calculated in terms of specimen density within quadrats (2 m × 2 m). This size of quadrat was chosen to ensure an even split between the three bins.
(3) *Discretization*. For each quadrat, taxon densities were split into three intervals: zero counts, low counts (under the median) and high counts (above the median) to capture the maximum amount of data information while masking noise.
(4) *Contingency test filtering*. To exclude false positive dependencies between taxa we used contingency filtering (χ^2-tests, $p > 0.25$).

The discretized data for the BNI analyses are given in **Table 2**. To minimize bias from outliers, we bootstrapped at 95% level (Magurran, 2013) by randomly selecting 95% of the total number of grids cells for each subsample and then finding the subsample network using Banjo. For each edge calculated, the probability of occurrence was calculated as the proportion of the bootstrapped samples in which the edge appeared. The resultant distributions analyzed to find the number of Gaussian sub-distributions using normal mixture models (Fraley et al., 2012). This probability distribution was bimodal for each dataset, which suggests that there were two distributions of edges, those with low probability of occurrence, and those highly probable edges. The final network for each area was taken to be those edges which were highly probable. The threshold for being labeled "highly probable" was 55% for this dataset. The magnitude of the occurrence rate is indicated in the network by the width of the line depicting the edge.

The direction of the edge between nodes in the network indicates which node (taxon) has a dependency on the other node (taxon); this direction is indicated in the network by an arrowhead. For each edge, the directionality was taken to be the direction which occurred in the majority of bootstrapped networks. Where there was no majority (directional edges have a probability between 0.35 and 0.65) an edge was said to have bi-directionality, or mutual dependency was indicated; these are shown without arrows.

[1]https://github.com/egmitchell/bootstrap

The influence score (IS) can be used to gauge the type and strength of the interaction between two nodes. Positive dependencies have an IS > 0: that is, a high density of taxon 1 corresponds to a high density of taxon 2, and so the dependency arrow would point from taxon 2 to taxon 1. Negative dependencies have an IS < 0: a high density of taxon 1 corresponds to a low density of taxon 2. Where the dependency is non-monotonic the IS = 0 so that nature of the dependency changes with taxon abundance. The mean IS for each edge was calculated for each site.

Bivariate SPPA

For every dependency found between taxa by BNI, bivariate SPPA were used to infer the most likely underlying processes (cf. Mitchell and Butterfield, 2018).

Bivariate PCFs were calculated from the population density using a grid of 10 cm × 10 cm. To minimize noise, smoothing was applied to the PCF dependent on specimen abundance. The amount of smoothing required depends on the number of points in each taxon's population, with smaller sample sizes requiring more smoothing to ensure that outliers do not overly change the distribution (Illian et al., 2008; Wiegand and Moloney, 2013): A five cell smoothing over this grid was applied to *Aspidoscopulia—N. bowersi*, six cells to *Advhena magnifica—N. bowersi*, and seven cells to *N. macrocalyx—N. bowersi*, across the entire mapped area (All), the shallow section of ridge (Ridge) and the steeper area of the ridge (Ridge Crest) (**Figure 2**).

For each taxon pair which displayed aggregation (bivariate PCF > 1), CSR, HP, Linked clusters (LC) and shared parent (SP) models were fitted to the data. For segregated bivariate distributions (bivariate PCF < 1), CSR, HP, hard and soft core models (HC), and hard/soft core on heterogeneous background (HCHP) models were fitted as follows. The magnitude of the PCF reflects the intensity of underlying biotic and abiotic processes: two taxon populations with a PCF = 4, for example, are four times more aggregated than if they exhibited CSR; thus, the relative magnitudes of the PCFs can be used to compare relative strengths of interactions and associations.

If a taxon was aggregated, the random model on a heterogeneous background (HP model) was tested. Creation of the heterogeneous background was as for the univariate distribution, but instead of a single taxon, the density map of the joint distribution of the two taxon was used.

For each taxon pair, two best-fit Linked cluster models (LC) were found. First, Taxon 1 was kept constant and Taxon 2 was modeled as a Thomas Cluster aggregation around Taxon 1 (following the same procedure as fitting univariate TC models). Then Taxon 2 was kept constant and Taxon 1 was modeled as an aggregation. The shared parents models (SP) modeled both taxa distributions as Thomas Cluster models around randomly distributed shared points, with the respective Thomas Cluster models fitted as per the univariate models.

Segregated distributions were modeled on both homogeneous background and on heterogeneous background. Three different models were determined: Segregation around Taxon 1, around Taxon 2 and around both Taxon 1 and Taxon 2. For each of these the radius was increased from 0.10 m to 1.00 m in 0.10

m increments. The severity of the segregation was modeled in two ways: hard and soft-core. For hard-core models (corresponds to $HC_p = 0.01$), no points are modeled inside the segregation radius while for a soft-core model the density of points within the segregation radius was reduced by a given probability. Where $HC_p = 1$ the probability of placing points is a linear relationship from the point to the radius edge, and is defined by the formula (Wiegand and Moloney, 2013; Getzin et al., 2014): $p_{hc}(r) = d^{1/p}$.

RESULTS

The mapped community consisted of 592 specimens over 100.7 m^2 of substrate. The community was dominated (69.7%) by two genera of Hexactinellids: Farreidae *Aspidoscopulia* sp. and Euplectellidae *Advhena magnifica* with octocorals *Narella bowersi*, *Narella macrocalyx,* and *Rhodaniridogorgia* also present in large proportions (**Table 1**). There was significant increase in organism density between the Ridge and Ridge Crest (4.47 vs. 9.28 specimens/m^2) which were split into two different sub-areas of 71.41 m^2 for the Ridge area and 29.31 m^2 for the Ridge Crest area for further analyses (**Table 1** and **Figure 3**). Community composition remained similar across both areas, with a $< 0.5\%$ mean change in taxa proportions between the two areas (**Table 1**).

Random Labeling Analyses

Analyses to detect edge effects (**Table 3**: $PCF_{12} - PCF_{21}$) found that for the *Aspidoscopulia* population, edge effects occurred over 4.3 m. Therefore, the spatial scale was limited to 0–4.0 m for all plots to enable consistent comparisons.

Within the whole community there was no evidence of significant deviations from zero for any of the RLAs (**Figure 3A**), that is the dead specimens were randomly distributed within the living communities (all $p_d > > 0.1$), so we fail to reject H_0^{Comm}. The *Advhena* population and stalks also did not display significant deviations from zero (all $p_d > > 0.1$; **Figure 3C**). Furthermore, the differences of the univariate distribution of *Advhena* with the univariate distribution of stalks had a very good model fit to zero ($p_d = 0.991$), which provides confirmatory evidence that the stalks are likely to be the dead skeletons of *Advhena*.

The RLAs of the *Aspidoscopulia* population found no significant deviations from zero for the difference between the univariate alive and dead *Aspidoscopulia* populations (all $PCF_{22} - PCF_{11}$ $p_d > > 0.1$, **Figure 3B**) nor the bivariate difference (all $PCF_{12} - PCF_{21}$ $p_d > 0.1$). The difference between the univariate alive *Aspidoscopulia* and the bivariate distributions was also not significantly deviate from zero (all $PCF_{12} - PCF_{11}$ $p_d > 0.1$). There were significant deviations from zero for the Quotient tests (**Figure 3B**) for the population across the whole sample area ($p_d = 0.034$), and in the high density Ridge Crest area ($p_d = 0.043$), but notably not in the Ridge area ($p_d = 0.240$). This pattern is further reflected in the Difference tests ($PCF_{21} - PCF_{22}$) which found that the difference of bivariate distribution with the dead univariate did deviate significantly from zero (**Table 1**) for the whole area ($p_d = 0.033$), and in the high density Ridge Crest area ($p_d = 0.042$) but not the Ridge area ($p_d = 0.221$). The significant deviations in the whole area are likely to reflect the signal from the Ridge Crest sub-section. Within the Ridge Crest section dead specimens of *Aspidoscopulia* were more likely to be found near each other than near living specimens, and these dead specimens occurred in the higher density areas of the joint distribution of alive and dead specimens. In contrast, the dead specimens did not show significant aggregations to each other or to high density areas within the Ridge sub-section of the mapped area.

Univariate SPPA

Rhodaniridogorgia was the only taxon to have a good model-fit to the CSR model ($p_d = 0.704$), although the HP model ($p_d = 0.825$) was a better fit (**Table 4**). The Monte Carlo simulations showed no deviations outside the envelope (**Figure 5E**), so the *Rhodaniridogorgia* spatial distribution should be described as CSR. Of the four of the abundant taxa that exhibited non-CSR best-fit models, *Advhena magnifica* had the same best-fit model (HP) for both the Ridge ($p_d = 0.817$) and Ridge Crest sections of the mapped area ($p_d = 0.562$), with significant segregations occurring over 1.3 m for the Ridge section and over 3 m for the Ridge Crest regions (**Figure 5C** and **Table 4**). The *Aspidoscopulia* (**Figure 5D** and **Table 4**) had a best-fit model of Thomas cluster models for both Ridge ($p_d = 0.727$) and Ridge Crest sections of the mapped area ($p_d = 0.547$) with a segregation in the Ridge area over 1.2 m. In contrast, the *N. macrocalyx* displayed different spatial distributions in the Ridge and Ridge crest area (**Figure 5A** and **Table 4**). The Ridge Crest area was best-modeled by a Thomas Cluster for the aggregations < 1.1m ($p_d = 0.375$), and showed a strong segregation above 1.1 m, whereas the Ridge area was segregated under 0.7 m, and the aggregation above 0.7 m was best-modeled by a heterogeneous Poisson model ($p_d = 0.848$). The *N. bowersi* also exhibited different spatial distributions between areas (**Figure 5B** and **Table 4**), with the Ridge Crest area showing strong aggregation best-modeled by a heterogeneous Poisson model > 1.3 m ($p_d = 0.761$) whereas the Ridge area showed strong segregation < 1.3 m ($p_d = 0.729$).

Bayesian Network Inference

The Bayesian network inference found three significant dependencies between four of the five abundant taxa (**Figure 6**), with *Rhodaniridogorgia* not connected to the network. *Rhodaniridogorgia* also showed a good CSR model fit for the univariate distributions (**Figure 5E** and **Table 4**). All three of the dependencies found were positive with a mean interaction strength of IS = 0.3109. *Narella bowersi* had a dependency upon *Aspidoscopulia* (IS = 0.3454), while both *Advhena* and *N. macrocalyx* had dependencies upon *N. bowersi* (IS = 0.3139 and IS = 0.2735), reflecting similar levels of dependency for all connected taxa.

Bivariate SPPA

The bivariate distribution for *N. bowersi—Aspidoscopulia* was best-modeled by a heterogeneous Poisson process of their joint densities across both Ridge ($p_d = 0.896$) and Ridge Crest sections of the mapped area ($p_d = 0.817$) which were aggregated at distances over 2 m (**Figure 7A** and **Table 5**). There was significant segregation for the Ridge Crest area over 2.8 m but no significant

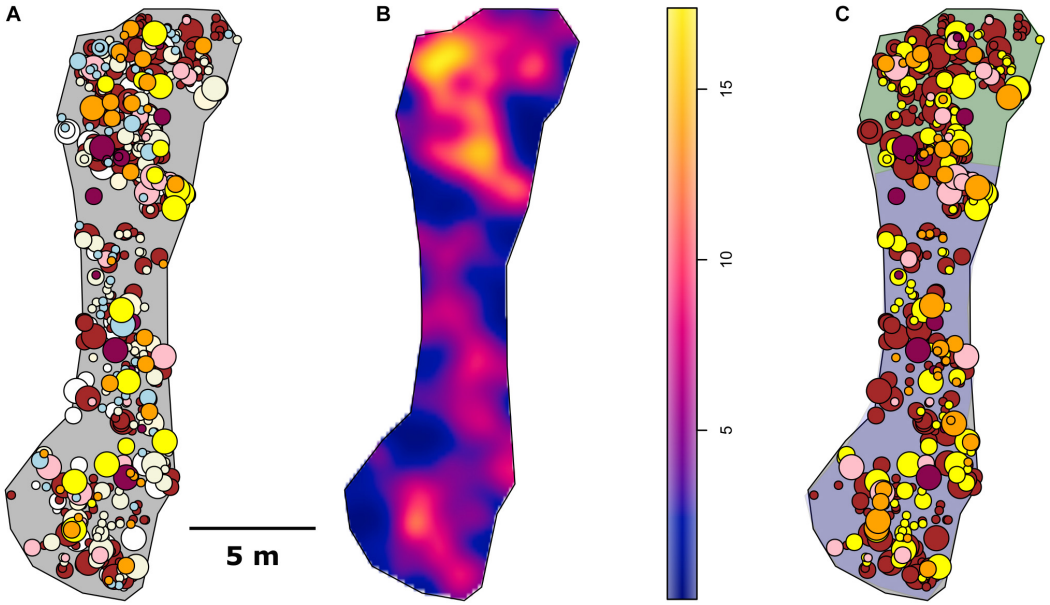

FIGURE 3 | Spatial maps. **(A)** All specimens identified, **(B)** Density map of the 2D project in square meters, and **(C)** the analyzed data. Shaded area of (C) in purple is the Ridge area and green is the Ridge Crest area.

TABLE 3 | Random labeling analyses.

Hypothesis	Dataset	P_d value for difference tests					P_d for quotient test < 2.0 m
		PCF $_{22}$–PCF $_{11}$	PCF $_{12}$–PCF $_{11}$	PCF $_{21}$–PCF $_{22}$	PCF $_{12}$–PCF $_{21}$	PCF $_{12}$–PCF $_{21}$ Excursions	
H_0^{Adv}	All	0.991	0.915	0.911	0.301	None	0.892
H_0^{Adv}	Ridge Crest	0.751	0.811	0.346	0.870	None	0.205
H_0^{Adv}	Ridge	0.265	0.412	0.387	0.278	None	0.260
H_0^{Comm}	All	0.411	0.436	0.672	0.790	None	0.363
H_0^{Comm}	Ridge Crest	0.833	0.617	0.885	0.208	None	0.822
H_0^{Comm}	Ridge	0.498	0.158	0.726	0.982	None	0.192
H_0^{Asp}	All	0.618	0.873	**0.033**	0.429	**> 4.3 m**	**0.034**
H_0^{Asp}	Ridge Crest	0.862	0.997	**0.042**	0.112	**> 4.3 m**	**0.043**
H_0^{Asp}	Ridge	0.546	0.826	0.221	0.755	None	0.240

Each hypothesis was tested using all the area mapped (All), the area leading up to the Ridge Crest (Ridge) and the high density area over the Ridge Crest (Ridge Crest). PCF $_{11}$ describes the spatial distributions of the alive organisms, PCF$_{22}$ the dead organisms, PCF$_{21}$ the bivariate distribution of the dead relative to the alive and PCF$_{12}$ the alive to the dead. p_d indicates the goodness-of-fit of the model (difference or quotient = 0) to the observed values with $p_d = 1$ indicating perfect fit (i.e., no difference) and $p_d = 0$ indicating significant deviations from zero, which is given in bold.

segregation in the Ridge area. For the *N. bowersi—Advhena* distribution, the best-fit model was a linked cluster model (**Figure 7B** and **Table 5**), with the *Advhena* clustering around the *N. bowersi* for both the Ridge (p_d = 0.823) and Ridge Crest areas (p_d = 0.631). The *N. bowersi—N. macrocalyx* displayed aggregation best-modeled as heterogeneous Poisson < 1.0 m for the Ridge area (p_d = 0.912) and segregation < 1.2 m for the Ridge Crest area (p_d = 0.841).

DISCUSSION

This study reconstructed the 592 specimens over 100.7 m^2 of the benthic community of "The Forest of the Weird" from still frames taken from a single stream of video footage using photogrammetry methods (**Figure 3**). There were limitations to the data we could extract from the reconstruction. Our methods accurately reconstructed the sea floor, but the reconstruction of some organisms was more variable due to shadowing or movement. Shadowing occurred where the video footage had not captured all the way around an individual, and so the software needed to approximate the missing data. Movement caused a blurring of specimens and/or stalks to be absent. These issues meant that while the position data was likely to be accurate, size data was less so, and so size-based SPPA was not performed on this data. The lack of size data precludes more detailed analyses of community development. The reconstruction was done using the video data which had a lower resolution than the still

TABLE 4 | Summary table of univariate PCF analyses.

Dataset	Area	Segregation present	CSR	HP	TC	ITC	Hard core	HP radius (cm)	σ	100ρ	Number in clusters	Hard core radius	H_{cp}
Aspidoscopulia	A	No	0.001	0.395	**0.727**	0.23	NA	20	18.694	0.104	37	NA	NA
Aspidoscopulia	RC	No	0.002	0.227	**0.547**	0.25	NA	10	19.048	0.042	38	NA	NA
Aspidoscopulia	R	1.2–2.1 m	0.001	0.505	**0.618**	0.158	NA	10	19.048	0.042	38	NA	NA
Rhodaniridogorgia	A	No	0.704	**0.825**	0.001	0.001	NA	50	2.262	4.798	5	NA	NA
N. macrocalyx	A	No	0.012	0.232	**0.651**	0.211	NA	20	8.737	0.135	17	NA	NA
N. macrocalyx	RC	>1 m	0.004	0.003	**0.375**	0.245	NA	20	8.737	0.135	17	NA	NA
N. macrocalyx	R	No	0.27	**0.848**	0.498	0.249	NA	30	8.737	0.135	17	NA	NA
Advhena magnifica	A	No	0.001	**0.875**	0.253	0.352	NA	20	5.351	0.555	11	NA	NA
Advhena magnifica	RC	>3 m	0.021	**0.562**	0.093	0.102	NA	20	7.174	0.468	14	NA	NA
Advhena magnifica	R	>1.3 m	0.007	**0.817**	0.201	0.154	NA	20	5.351	0.555	11	NA	NA
N. bowersi	A	No	0.032	**0.889**	0.772	0.43	NA	20	5.499	1.097	11	NA	NA
N. bowersi	RC	No	0.001	0.761	0.632	0.316	NA	20	5.499	1.097	11	NA	NA
N. bowersi	R	<1.5 m	0.117	0.117	0.093	0.066	**0.729**	20	5.499	1.097	11	5	0

The sample area is the entire community (A), the Ridge Crest sub-section (RC) or the Ridge sub-section (R). For the inhomogeneous point processes (HP and ITC), the moving window radius is 0.5 m, using the same taxon density as the taxon being modeled. p_d = 1 corresponds to a perfect fit of the model to the data, while p_d = 0 corresponds to no fit. Where observed data did not fall outside CSR Monte Carlo simulation envelopes, no further analyses were performed, which is indicated by NA. σ, cluster radius; ρ, density of specimens; CSR, Complete spatial randomness; HP, Heterogeneous Poisson model; TC, Thomas cluster model; ITC, inhomogeneous Thomas cluster model. Mean number in cluster refers to the mean number of individuals in a cluster estimated as λ/ρ. Note that if the cluster model is not a good fit, the mean number in cluster and number of clusters will not necessarily be appropriate. The extent to which the segregation is hard-core (no points within the given radius) or soft-core (reduced points) is given by H_{cp} where H_{cp} = 0 indicates a hard-core process and H_{cp} = 1 indicates a linear increase in point density between points. CSR models were fitted to the whole spatial scale (0–4 m) and the aggregations and segregations were fitted only to the aggregations (PCF > 1) or the segregations (PCF < 1), depending on the observed distribution. The pd values for the best fit models are given in bold.

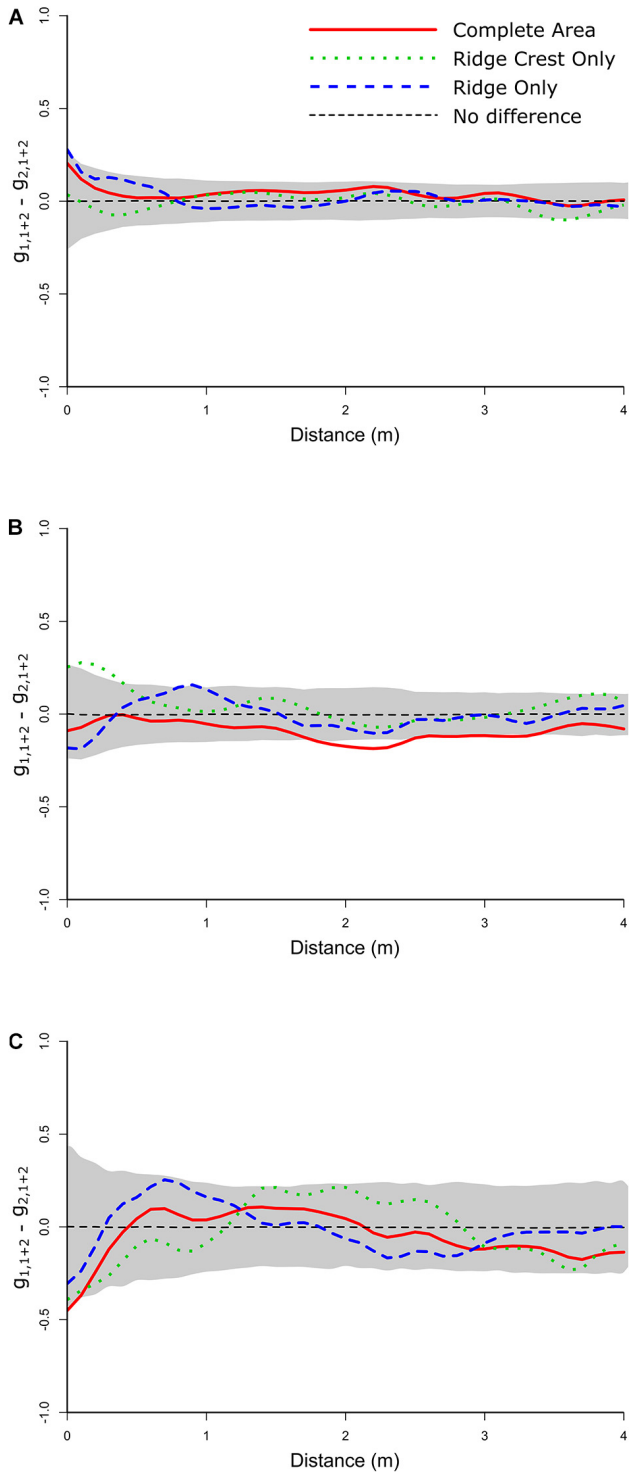

FIGURE 4 | Random labeling analyses plots showing the Quotient test. **(A)** Whole community analyses of the dead population relative to the alive population (including all corals and sponges mapped) showing no significant deviations from zero. **(B)** The *Aspidoscopulia* analyses of dead vs. alive specimens. Note the whole community and the Ridge Crest sub-section both show excursions outside the simulation envelopes. **(C)** The *Advhena magnifica* analyses of dead vs. alive specimens showing no significant deviations from zero.

photographic data and so we were able to use the photographs to compare to the stills extracted from the video. The two consequences of using the lower resolution video were: (1) that small white specimens (<1 cm) may not have been distinguished from the substrate and (2) it was hard to consistently identify different taxonomic groups for smaller specimens. We focused on the most abundant taxa, sponges and those corals which could easily be distinguished by distinct morphologies, which limits more detailed analyses of community composition and diversity. Nonetheless we were able to establish the mortality dynamics and spatial ecology of the five most abundant taxa.

This study has demonstrated how SPPA and BNI provide two new types of insights into the ecology of deep-sea benthic systems. First, SPPA can detect many different types of interactions and associations without any *a priori* knowledge nor expectations of the system. For example, SPPA was able to detect both the competition between *N. bowersi—N. macrocalyx*, the facilitation of the *Advhena magnifica* around the *N. bowersi,* and the habitat associations between *N. bowersi—Aspidoscopulia* (**Figure 7** and **Table 5**). Secondly, SPPA enables the quantification on a continuous scale of interactions and associations from centimeter to meter scale, establishing at what scale the type of interactions may change, such as *N. bowersi—Aspidoscopulia* changing from a mutual habitat association to competition around 3 m (**Figure 7B**).

Mortality Dynamics

A high proportion (37.5%) of the specimens mapped were dead glass sponge skeletons (**Table 1**). The majority of dead specimens within the community were either the stalks of *Advhena* or dead *Aspidoscopulia.* Of the two possible causes of sponge death, age-related mortality or a pathogen, our results suggest that a species-specific pathogen is most likely. The univariate spatial distributions of the dead specimens is not statistically significantly different from the alive specimens (**Table 3**, PCF 22 − PCF 11) for either of the sponge species. *Aspidoscopulia* are best-modeled by a Thomas Cluster model (**Table 4**), which describes reproductive events (Seidler and Plotkin, 2006) so that if these sponges died due to age-related mortality, we would expect the dead specimens to have the spatial distributions corresponding to previous generations (cf. Mitchell et al., 2015). As such, the dead and alive specimens should have different univariate spatial distributions, and because they do not (**Table 3**), it is more likely their death is due to a pathogen. *Advhena* exhibited a non-dispersal spatial pattern so we can't be sure that they were also killed by this pathogen over age-related mortality. However, the unusually high proportion of dead specimens and the presence of a mass-mortality pathogen for the *Aspidoscopulia* suggests that a pathogen cause is likely. While the remains of holdfast discs (12.9% of the dead specimens mapped) were not taxonomically identifiable, they resembled the *Advhena* and *Aspidoscopulia* holdfasts. The lack of density-dependent mortality (non-random RLA) for the *Advhena magnifica* and the Ridge area *Aspidoscopulia* suggests that the pathogen was likely to be water-borne, since transfer via mobile organisms or physical touching of specimens results in mortality clusters (Jolles et al., 2002).

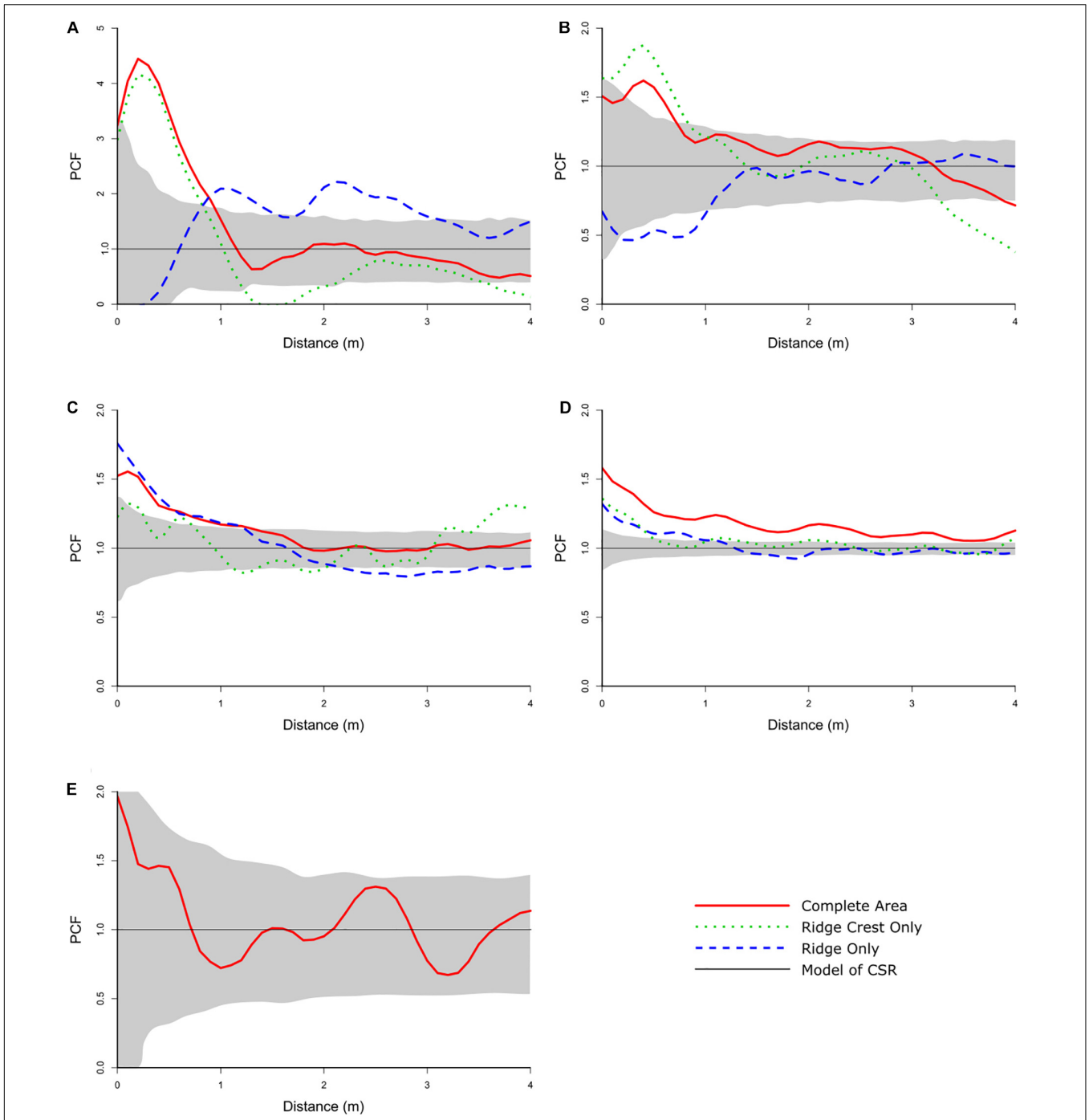

FIGURE 5 | Univariate PCF for the abundant taxa. **(A)** *Narella macrocalyx*, **(B)** *Narella bowersi*, **(C)** *Advhena magnifica,* **(D)** *Aspidoscopulia,* **(E)** *Rhodaniridogorgia*. The gray area is the simulation envelope for 999 Monte Carlo simulations of complete spatial randomness. The *x*-axis is the inter-point distance between organisms in meters. On the *y*-axis PCF = 1 indicates complete spatial randomness (CSR), < 1 indicates segregation, and > 1 indicates aggregation.

The *Advhena* mortality was randomly distributed throughout both the Ridge and Ridge Crest areas of the communities (**Table 3** and **Figure 4**). However, the mortality dynamics were different for the *Aspidoscopulia*, with the Ridge community showing random mortality, but the Ridge Crest community showing significant aggregations of the dead specimens relative to the living ones (**Figure 4** and **Table 3**). A*spidoscopulia* in the Ridge Crest area had a notably higher density than the Ridge area (4.47 vs. 1.92/m^2) and a higher proportion of dead to living specimens (77 vs. 66%), suggesting that the presumed pathogen was spreading faster in these high density areas, but only for the *Aspidoscopulia*. If this difference was due

just to density (i.e., not taxon specific) we would expect the *Advhena* to also have density-dependent mortality, as would the community as a whole, but instead it seems to be *Aspidoscopulia* specific, suggesting a lower resistance to the pathogen in these high density areas.

The Janzen-Cornell hypothesis is an explanation of how high diversity is maintained in tropical forests and coral reefs, whereby species-specific predators or pathogens are attracted to adults and/or high density areas resulting in high mortality surrounding the adults or in the high-density areas (Janzen, 1970; Connell, 1971). Within sponge communities, species-specific disease prevalence has been suggested as a mechanism to help maintain balance in abundance between species (Wulff, 2007). The species-specific mortality then enables different species to occupy these areas. Most studies testing this hypothesis are focused on shallow-water reefs, and have found no density-dependent mortality for giant barrel sponges (Deignan and Pawlik, 2015), Caribbean sponge *Aplysina cauliformis* (Easson et al., 2013) nor Caribbean corals (Muller and van Woesik, 2012), but density-dependent death due to corallivory has been detected in Indo-Pacific corals (Gibbs and Hay, 2015). In our study, we find that species-sensitive density-dependent mortality is likely once a density threshold was reached for *Aspidoscopulia.* The mortality within this community was likely to be a mass-mortality infection rather than a longer-term endemic pathogen because of the high proportion of dead skeletons coupled to relatively few dying specimens (those with brown patches (cf. Luter et al., 2017). In order for the Janzen-Cornell hypothesis to explain this high density community, we would expect episodic infections, so populations build up through time; thus any effects of this species-specific mortality would only become apparent if there were frequent mortality events. At the broad taxonomic levels used in this study, the two areas (Ridge and Ridge Crest) show significantly different densities, but similar community compositions (**Table 1**), suggesting that either this mortality event was rare, or if such events were frequent, then it did not lead to increased diversity (at least in terms of the coarse taxonomic identification used here). Further study of this site and other sites with similar community compositions may be able to elucidate whether such pathogens are likely to contribute to Janzen-Cornell effects.

Mass-mortality events and sponge diseases are on the increase (Webster, 2007) but have been primarily reported from shallow water sponge populations (Luter and Webster, 2017). The underlying causes are suggested to be anthropogenic changes, such as increasing temperature, which increase the susceptibility of benthic organisms such as corals and sponges to diseases through either a weakening of the organisms and/or an increase in pathogen virulence or abundance (Muller and van Woesik, 2012; Luter and Webster, 2017). The death of slow-growth sponges creates unoccupied patches which are often re-populated by faster-growing species (cf. Dayton, 1989; Dayton et al., 2013; Di Camillo and Cerrano, 2015). Sponges provide many ecosystem services, and while some services, such as providing habitat, can be replicated by other taxa (Buhl-Mortensen et al., 2010), sponges are crucial to oceanic mixing and benthic-pelagic coupling (Pile and Young, 2006; Bell, 2008; Coppari et al., 2016) which may be harder to replicate if they are replaced by organisms which do not pump water through their system. As such, there is potential for these deep-sea sponge diseases to impact the extent of benthic-pelagic coupling.

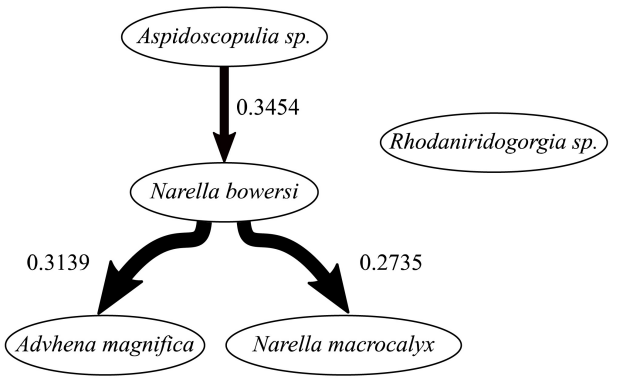

FIGURE 6 | Bayesian networks of associations between abundant sponge and corals. Dependencies between taxa are indicated by the lines connecting the two taxa, the width of which indicates the occurrence rate in the bootstrap analyses (wider lines indicate higher occurrence). Arrows indicate non-mutual dependence between two taxa; A- > B indicates that B depends on A. Mean interaction strengths of the correlations are indicated; positive interaction strengths indicating aggregation, negative interaction strengths indicating segregation. For more details, see section "Materials and Methods."

Population Dynamics

The FW community showed a clear increase in density and change of composition on the Ridge (seen in the 3D reconstruction at the edge of **Figure 2**, and noted on the ROV dive; Kelley et al., 2018). Furthermore, the sharper slope of the area after the Ridge Crest showed a large increase in density (**Table 1**) corresponding to faster water speed, and so probably to greater water-column resources (Malik et al., 2018).

The strength of SPPA lies with describing how the density of different taxa change over the fine scale (here 0–4 m), and then using model fitting to determine the most likely underlying processes. When spatial models such as heterogeneous Poisson models, heterogeneous Thomas cluster models or hard/soft-core models are the best-fit to observed spatial patterns, this suggests that abiotic or habitat heterogeneities are the strongest influence on the studied populations (Illian et al., 2008; Lin et al., 2011; Wiegand and Moloney, 2013; Mitchell et al., 2019). In contrast, random models or Thomas cluster models reflect biological patterns (Illian et al., 2008; Lin et al., 2011; Wiegand and Moloney, 2013; Mitchell et al., 2015), so that by fitting these different models to the observed data we were able to infer for each taxa whether biotic or abiotic effects had the biggest influence. At these fine-spatial scales we found that abiotic influence of habitat heterogeneities were the strongest driver for the majority of the populations studied. Abiotic heterogeneous Poisson models and hard-core models were the best fit for the observed spatial distributions for the populations of *Advhena,*

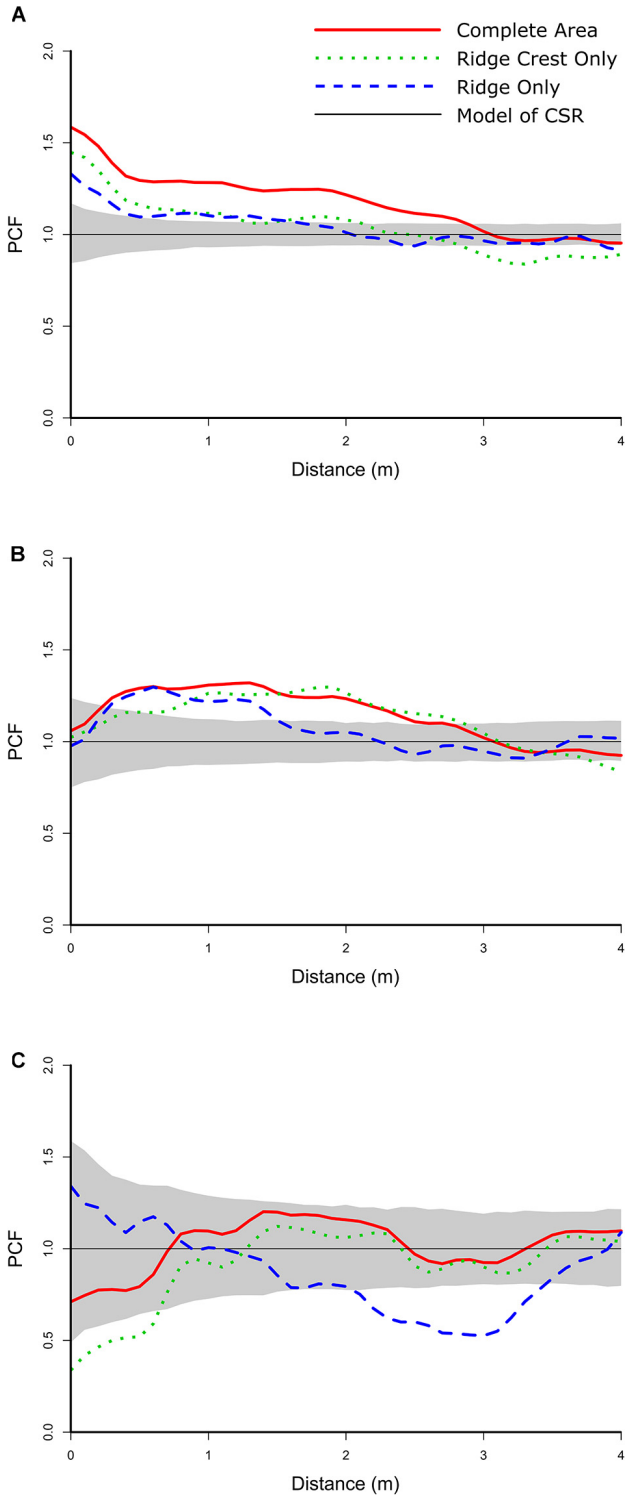

FIGURE 7 | Bivariate PCF analyses for the taxa with non-independent spatial distributions. The gray area is the simulation envelope of complete spatial randomness (CSR) for 999 Monte Carlo simulations. The *x*-axis is the inter-point distance between organisms in meters. On the *y*-axis, PCF = 1 indicates CSR and is indicated by a black line, < 1 indicates segregation, and > 1 indicates aggregation. **(A)** *N. bowersi – Aspidoscopulia.* **(B)** *N. bowersi – Advhena magnifica.* **(C)** *N. bowersi—N. macrocalyx.*

N. bowersi, and *Rhodaniridogorgia* [although the small numbers of specimens, and lack of deviations outside the simulations envelope for *Rhodaniridogorgia*, means that this model was not significantly better than the random (biotic) model (**Table 4** and **Figure 5**)]. For *N. bowersi* the interaction with the local habitat changed between the Ridge and Ridge Crest area, with the Ridge area showing significantly more segregation and thinning of organisms, reflecting a likely resource limitation due to lower water flow. The best-fit heterogeneous Poisson models for the *N. macrocalyx, N. bowersi,* and *Advhena* populations were over the same spatial scales of 20 cm, suggesting the same underlying habitat heterogeneity for all three taxa. While it is not analytically possible to determine what this heterogeneity is using our data, the topological variation of the basalt bedrock is of a similar scale, and so is a likely contender (**Figures 1**, **2**).

In contrast *Aspidoscopulia* showed little sensitivity to these habitat heterogeneities, and instead the population spatial distributions reflected dispersal clusters. *Narella macrocalyx* was unusual in this community because the factors which most influenced its spatial distribution changed between the two community areas. In the Ridge area of the community *N. macrocalyx* was most strongly influenced by abiotic factors (habitat heterogeneity), but in the Ridge Crest area biotic factors (dispersal limitations) dominated. This change in influence is likely to reflect resource limitation in the lower-density Ridge area reducing the survival of juveniles, so that only the ones that settled on the optimal habitat remain. In the Ridge Crest region sufficient resources from increased water-flow result in higher survival rates, and so are a closer reflection of the original dispersal clusters.

The population ecology of the two sponges *Aspidoscopulia* and *Advhena* remained remarkably similar between the Ridge and Ridge Crest areas of the community, despite a doubling of population densities showing a lack of sensitivity to meter-scale variations in ridge topological and water-flow speed. In contrast, the octocorals *N. macrocalyx* and *N. bowersi* both showed significant differences in their spatial distributions, reflecting a higher sensitivity to these abiotic factors. The change for *N. macrocalyx* from an abiotic to biotic influence with increased density demonstrates the interplay between different driving forces and suggests that for at least some populations, different effects drive population under different conditions highlighting the need to record multiple different populations to understand the factors which underlie their dynamics.

Competition Dynamics

Evidence for competition between marine sponges leading to elimination of a species are relatively rare, and most commonly involve outcompeting for a limited substrate, overflowing or chemical mediation (Wulff, 2007). This study has found subtle evidence of both intra and inter-specific competition. The large-scale segregation of the *Aspidoscopulia, Advhena, N. bowersi,* and *N. macrocalyx* suggests that a thinning of the populations is associated with increased competition for limited resources as organisms grow—they do not compete as juveniles but as they increase in size, they need more resources, and when they outcompete their neighbors, this leads to a reduction or

TABLE 5 | Summary table of bivariate PCF analyses.

Taxon 1	Taxon 2	Area	CSR	HP radius (m)	CSR	HP	HCHP	HC	LC1	LC2	SP	σ	100ρ	Number in clusters	Number of clusters	Taxon 1 radius (m)	Taxon 2 radius (m)	H_{cp}^{1}	H_{cp}^{2}	H_{cp}^{12}
Advhena magnifica	*N. bowersi*	A	0.013	0.2	0.026	0.409	NA	NA	0.105	**0.692**	0.164	5.217	0.2951	10	50	NA	NA	NA	NA	NA
Advhena magnifica	*N. bowersi*	R	0.128	0.2	0.001	0.688	NA	NA	0.131	**0.923**	0.319	5.217	0.2951	10	50	NA	NA	NA	NA	NA
Advhena magnifica	*N. bowersi*	RC	0.001	0.2	0.146	0.262	NA	NA	0.244	**0.631**	0.424	5.217	0.2951	10	50	NA	NA	NA	NA	NA
N. bowersi	*Aspidoscopulia*	A	0.011	0.1	0.001	**0.702**	NA	NA	0.15	0.031	0.334	10.55	0.1588	21	17	NA	NA	NA	NA	NA
N. bowersi	*Aspidoscopulia*	R	0.117	0.1	0.001	**0.896**	NA	NA	0.005	0.009	0.206	10.55	0.1588	21	17	NA	NA	NA	NA	NA
N. bowersi	*Aspidoscopulia*	RC	0.001	0.1	0.001	**0.817**	NA	NA	0.221	0.003	0.459	10.55	0.1588	21	17	NA	NA	NA	NA	NA
N. bowersi	*N. macrocalyx*	A	0.032	0.3	0.495	0.604	**0.874**	0.066	NA	NA	NA	NA	NA	NA	NA	NF	0.5	NF	1	1
N. bowersi	*N. macrocalyx*	R	0.146	0.3	0.377	**0.912**	0.426	0.017	NA	NA	NA	NA	NA	NA	NA	NF	0.5	NF	1	1
N. bowersi	*N. macrocalyx*	RC	0.001	0.1	0.274	0.111	0.164	**0.841**	NA	NA	NA	NA	NA	NA	NA	NF	0.3	NF	1	1

The sample area is the entire community (A), the Ridge Crest sub-section (RC) or the Ridge sub-section (R). For the inhomogeneous point processes (HP and HCHP), the moving window radius is given by HP radius, using the joint taxa density. ρ_d = 1 corresponds to a perfect fit of the model to the data, while ρ_d = 0 corresponds to no fit. Where observed data did not fall outside CSR Monte Carlo simulation envelopes, no further analyses were performed, which is indicated by NA. σ, cluster radius; ρ, density of specimens; CSR, Complete spatial randomness; HP, Heterogeneous Poisson model; HC, Hard core segregation model; HPHC, inhomogeneous segregation model; LC1, Linked cluster model of taxon 1 around taxon 2; LC2, Linked cluster model of taxon 2 around taxon 1; SP, Shared parent model. Mean number in cluster refers to the mean number of individuals in a cluster estimated as λ/ρ. Note that if the cluster model is not a good fit, the mean number in cluster will not necessarily be appropriate. The extent to which the segregation is hard-core (no points within the given radius) or soft-core (reduced points) is given by H_{cp} where H_{cp} = 0 indicates a hard-core process and H_{cp} = 1 indicates a linear increase in point density between points. CSR models were fitted to the whole spatial scale (0–4 m) and the aggregations and segregations were fitted only to the aggregations ($PCF > 1$) or the segregations ($PCF < 1$) depending on the observed distribution. Therefore aggregation models will not be fitted to segregated distributions and vice versa (denoted NA). NF refers to not fitted parameters in the best-fit model. The pd values for the best fit models are given in bold.

thinning of the density (Getzin et al., 2006; Lingua et al., 2008). *N. bowersi* also has small-scale segregation reduction of 50%, which is likely to reflect intra-specific competition of juveniles, rather than mature organisms (Getzin et al., 2006, 2014). If the system is stressed, for example through reduction in the nutrients for which the organisms compete, then the strengths of competition are likely to increase, potentially leading to elimination of the weaker taxa.

Community Dynamics

Community composition for deep-sea sponge and coral communities is strongly driven by abiotic factors over broad scales (∼1–100 km) (Murillo et al., 2020). High density and very high density Pacific benthic communities show strong associations with temperature and geography (Hourigan et al., 2020). Despite a dramatic difference in community density between the two sections of the community at FW there remains a remarkable lack of differentiation of community composition (**Table 1**), showing a certain robustness in response to differences in ridge topography. This composition similarity, which is admittedly at a very coarse taxonomic scale, is unlikely to persist over long time scales due to density-dependent death of *Aspidoscopulia* in the Ridge Crest area (in contrast to the Ridge area and the random mortality patterns of *Advhena*). This density-dependent death has resulted in a different distribution of living *Aspidoscopulia*, and has provided a biogenic structure for sponge *Poliopogon* sp. which has grown on the top of the dead specimens (cf. Beazley et al., 2015). The BNI analyses showed that four out of the five abundant taxa were interconnected, with *N. bowersi* the most connected taxon (**Figure 6**). This connectedness means that if one taxon changes abundances, the other abundant taxon will also be affected—the density-dependent mortality of the *Aspidoscopulia* will impact the *N. bowersi*, which will then impact the *Advhena* and the *N. macrocalyx*. As such, we should expect to see a change in composition over time, leading to differentiation between the Ridge and Ridge Crest community compositions due to the linked dependences of the abundant taxa (**Figure 6**).

The nature of these changes depends on the different biotic and abiotic intra and inter-specific interactions. For this community, the strength of the inter-specific interactions (as calculated by the PCF value; **Figure 7**) is of similar magnitude to the intra-specific interactions (**Figure 5**), with the exception of the univariate *N. macrocalyx* distribution which is significantly more aggregated than the other taxa (**Figure 5**). The relative strength of the bivariate interactions suggests that the community will be more sensitive to changes in one taxon's population than a community with only weak bivariate interactions. However, this cascade effect will depend on the nature of each interaction. The habitat association *N. bowersi—Aspidoscopulia* is a mutual correlation to a third factor, the habitat heterogeneity, and so any community effects may be muted via this mutual factor, making the *N. bowersi—Aspidoscopulia* interaction more robust than the other two direct biotic interactions. *Narella bowersi* and *Aspidoscopulia* share a mutual habitat heterogeneity, which in higher density areas leads to spatial segregation over larger spatial scales (**Figure 7A**), suggesting a level of competition or

thinning out between larger specimens (Getzin et al., 2006). Thus, if the density of *Aspidoscopulia* was reduced, the inter-specific competition may also be reduced, potentially leading to less thinning and so higher densities of the *N. bowersi*. Both *Advhena* and *N. macrocalyx* have dependencies on *N. bowersi*, and so these two taxa are likely to be affected by any population changes. The *Advhena*– *N. bowersi* interaction was best-modeled by a linked cluster model (**Table 5**), whereby the *Advhena* were centered around the *N. bowersi.* This facilitation was likely due to the *Advhena* filling the unoccupied space around the *N. bowersi*, seen in the univariate segregation of the *N. bowersi* in the Ridge area (**Table 4** and **Figure 5**), and leading to an aggregation of the *Advhena* around the *N. bowersi* (**Figure 7**). The same best-fit link cluster described the bivariate distribution in the Ridge Crest area but with a lower goodness-of-fit (**Table 5**), suggesting that a weaker version of this effect was occurring there. Therefore, if *N. bowersi* increases in density, such as via a reduction in *Aspidoscopulia,* then the effect on *Advhena* is likely to be positive, due to increased intra-specific *N. bowersi* competition leading to increased segregation. An increase in *N. bowersi* may lead to a decrease of *N. macrocalyx* because an increase in density of *N. macrocalyx* may increase the strength of the competition in the *N. macrocalyx—N. bowersi* interaction. The mix of positive and negative biotic interactions coupled to mutual habitat associations is therefore likely to result in a mixture of positive and negative effects on the community in the event of sudden changes and/or mass-mortality events.

CONCLUSION

To our knowledge, this study is the first to analyze the mortality, population and community dynamics of a deep-sea sponge community using SPPA. Our results provide the first insight into the variety of ecological behaviors within this benthic community, and show how these different organisms have developed diverse responses for the biotic and abiotic gradients within their habitat. We have demonstrated how ecological interactions change with substrate topography, while the community composition remains relatively constant. BNI has demonstrated the connectivity of the abundant taxa, identifying *N. bowersi* as the most connected taxon, and coupled with SPPA analyses has enabled us to speculate on the possible consequences, both positive and negative, of changes to the community. By identifying and quantifying the strength of abiotic and biotic interactions, these analyses have the potential to identify how different taxa are likely to be affected by different environmental changes. Identification of the crucial factors for different taxa have the potential to be used in management and conservation efforts to help mitigate anthropogenic changes.

DATA AVAILABILITY STATEMENT

The datasets presented in this study can be found in online repositories. The names of the repository/repositories and accession number(s) can be found below: https://doi.org/10.6084/m9.figshare.12284249.

AUTHOR CONTRIBUTIONS

EM conceived this study, processed the 3D model to spatial map, analyzed the data, and wrote the manuscript. SH developed the protocol for creating the 3D model from the video data and reconstructed the 3D model. Both authors contributed to the article and approved the submitted version.

FUNDING

The cruise was supported and conducted by the NOAA Office of Ocean Exploration and Research. Data/imagery courtesy of NOAA's Office of Ocean Exploration and Research Archives. The analyses was covered by a Natural Environment Research Council Independent Research Fellowship NE/S014756/1 to EM.

ACKNOWLEDGMENTS

We wish to thank Chris Kelley both as the lead scientist for the cruise and for his help with the data.

REFERENCES

Baddeley, A., Rubak, E., and Møller, J. (2011). Score, pseudo-score and residual diagnostics for spatial point process models. *Stat. Sci.* 26, 613–646. doi: 10.1214/11-STS367

Baddeley, A., and Turner, R. (2005). Spatstat: a R package for analyzing spatial point patterns. *J. Stat. Softw.* 12, 1–42.

Baker, K., Snelgrove, P. V. R., Fifield, D. A., Edinger, E., Wareham, V., Haedrich, R. L., et al. (2019). Small-scale patterns in the distribution and condition of bamboo coral, *Keratoisis grayi*, in Submarine Canyons on the Grand Banks, Newfoundland. *Front. Mar. Sci.* 6:374. doi: 10.3389/fmars.2019.00374

Beaulieu, S. E. (2001). Colonization of habitat islands in the deep sea: recruitment to glass sponge stalks. *Deep Sea Res. Part I Oceanogr. Res. Pap.* 48, 1121–1137. doi: 10.1016/S0967-0637(00)00055-8

Beazley, L., Kenchington, E., Yashayaev, I., and Murillo, F. J. (2015). Drivers of epibenthic megafaunal composition in the sponge grounds of the Sackville Spur, northwest Atlantic. *Deep Sea Res. Part I Oceanogr. Res. Pap.* 98, 102–114. doi: 10.1016/j.dsr.2014.11.016

Beazley, L., Wang, Z., Kenchington, E., Yashayaev, I., Rapp, H. T., Xavier, J. R., et al. (2018). Predicted distribution of the glass sponge Vazella pourtalesi on the Scotian Shelf and its persistence in the face of climatic variability. *PLoS One* 13:e0205505. doi: 10.1371/journal.pone.0205505

Bell, J. J. (2008). The functional roles of marine sponges. *Estuar. Coast. Shelf Sci.* 79, 341–353. doi: 10.1016/j.ecss.2008.05.002

Berman, M. (1986). Testing for spatial association between a point process and another stochastic process. *J. R. Stat. Soc. Ser. C* 35, 54–62. doi: 10.2307/2347865

Besag, J. (1974). Spatial interaction and the statistical analysis of lattice systems. *J. R. Stat. Soc. Ser. B* 36, 192–225. doi: 10.1111/j.2517-6161.1974.tb00999.x

Buhl-Mortensen, L., Vanreusel, A., Gooday, A. J., Levin, L. A., Priede, I. G., Buhl-Mortensen, P., et al. (2010). Biological structures as a source of habitat heterogeneity and biodiversity on the deep ocean margins. *Mar. Ecol.* 31, 21–50. doi: 10.1111/j.1439-0485.2010.00359.x

Chu, J. W. F., and Leys, S. P. (2010). High resolution mapping of community structure in three glass sponge reefs (Porifera. Hexactinellida). *Mar. Ecol. Prog. Ser.* 417, 97–113. doi: 10.3354/meps08794

Clark, M. R., Rowden, A. A., Schlacher, T., Williams, A., Consalvey, M., Stocks, K. I., et al. (2010). The ecology of seamounts: structure, function, and human impacts. *Annu. Rev. Mar. Sci.* 2, 253–278. doi: 10.1146/annurev-marine-120308-081109

Connell, J. H. (1971). "On the role of natural enemies in preventing competitive exclusion in some marine animals and in rain forest trees," in *Dynamics of Populations: Proceedings of the Advanced Study Institute on Dynamics of Numbers in Populations*, eds P. J. den Boer and G. R. Gradwell (Oosterbeek: Wiley), 7–18.

Coppari, M., Gori, A., Viladrich, N., Saponari, L., Canepa, A., Grinyó, J., et al. (2016). The role of Mediterranean sponges in benthic–pelagic coupling processes: *Aplysina aerophoba* and *Axinella polypoides* case studies. *J. Exp. Mar. Biol. Ecol.* 477, 57–68. doi: 10.1016/j.jembe.2016.01.004

Dale, M. R. T., and Fortin, M.-J. (2014). *Spatial Analysis: A Guide For Ecologists*. Cambridge: Cambridge University Press.

Dayton, P., Jarrell, S., Kim, S., Thrush, S., Hammerstrom, K., Slattery, M., et al. (2016). Surprising episodic recruitment and growth of Antarctic sponges: implications for ecological resilience. *J. Exp. Mar. Biol. Ecol.* 482, 38–55. doi: 10.1016/j.jembe.2016.05.001

Dayton, P. K. (1971). Competition, disturbance, and community organization: the provision and subsequent utilization of space in a rocky intertidal community. *Ecol. Monogr.* 41, 351–389. doi: 10.2307/1948498

Dayton, P. K. (1972). "Toward an understanding of community resilience and the potential effects of enrichments to the benthos at McMurdo Sound, Antarctica," in *Proceedings of the Colloquium on Conservation Problems in Antarctica*, Blacksberg, VA, 81–96.

Dayton, P. K. (1989). Interdecadal Variation in an Antarctic Sponge and Its Predators from Oceanographic Climate Shifts. *Science* 245, 1484–1486. doi: 10.1126/science.245.4925.1484

Dayton, P. K., Kim, S., Jarrell, S. C., Oliver, J. S., Hammerstrom, K., Fisher, J. L., et al. (2013). Recruitment, Growth and Mortality of an Antarctic Hexactinellid Sponge, *Anoxycalyx joubini*. *PLoS One* 8:e56939. doi: 10.1371/journal.pone.0056939

Deignan, L. K., and Pawlik, J. R. (2015). Perilous proximity: Does the Janzen–Connell hypothesis explain the distribution of giant barrel sponges on a Florida coral reef? *Coral Reefs* 34, 561–567. doi: 10.1007/s00338-014-1255-x

Di Camillo, C. G., and Cerrano, C. (2015). Mass mortality events in the NW Adriatic Sea: phase Shift from Slow- to Fast-Growing Organisms. *PLoS One* 10:e0126689. doi: 10.1371/journal.pone.0126689

Dickie, I. A., Schnitzer, S. A., Reich, P. B., and Hobbie, S. E. (2005). Spatially disjunct effects of co-occurring competition and facilitation. *Ecol. Lett.* 8, 1191–1200. doi: 10.1111/j.1461-0248.2005.00822.x

Diggle, P. (2002). *Statistical Analysis of Spatial Point Patterns*, 2 Edn. London: Hodder Education.

Diggle, P. J., Ribeiro, P. J., and Christensen, O. F. (2003). "An introduction to model-based geostatistics," in *Spatial statistics and computational methods*, (New York, NY: Springer), 43–86.

Diggle, P., Zheng, P., and Durr, P. (2005). Nonparametric estimation of spatial segregation in a multivariate point process: bovine tuberculosis in Cornwall, UK. *J. R. Stat. Soc. Ser. C* 54, 645–658. doi: 10.1111/j.1467-9876.2005.05373.x

Dunham, A., Archer, S. K., Davies, S. C., Burke, L. A., Mossman, J., Pegg, J. R., et al. (2018). Assessing condition and ecological role of deep-water biogenic habitats: glass sponge reefs in the Salish Sea. *Mar. Environ. Res.* 141, 88–99. doi: 10.1016/j.marenvres.2018.08.002

Durden, J. M., Bett, B. J., and Ruhl, H. A. (2015). The hemisessile lifestyle and feeding strategies of Iosactis vagabunda (Actiniaria, Iosactiidae), a dominant megafaunal species of the Porcupine Abyssal Plain. *Deep Sea Res. Part I Oceanogr. Res. Pap.* 102, 72–77. doi: 10.1016/j.dsr.2015.04.010

Easson, C. G., Slattery, M., Baker, D. M., and Gochfeld, D. J. (2014). Complex ecological associations: competition and facilitation in a sponge–algal interaction. *Mar. Ecol. Prog. Ser.* 507, 153–167. doi: 10.3354/meps10852

Easson, C. G., Slattery, M., Momm, H. G., Olson, J. B., Thacker, R. W., and Gochfeld, D. J. (2013). Exploring individual- to population-level impacts of disease on coral reef sponges: using spatial analysis to assess the fate, dynamics, and Transmission of Aplysina Red Band Syndrome (ARBS). *PLoS One* 8:e79976. doi: 10.1371/journal.pone.0079976

Fraley, C., Raftery, A. E., Murphy, T. B. and Scrucca, L. (2012). mclust version 4 for R: normal mixture modeling for model-based clustering, classification, and density estimation. *Technical Report No. 597*, Department of Statistics, University of Washington.

Genin, A., Dayton, P. K., Lonsdale, P. F., and Spiess, F. N. (1986). Corals on seamount peaks provide evidence of current acceleration over deep-sea topography. *Nature* 322, 59–61. doi: 10.1038/322059a0

Getzin, S., Dean, C., He, F., Trofymow, J. A., Wiegand, K., and Wiegand, T. (2006). Spatial patterns and competition of tree species in a Douglas-fir chronosequence on Vancouver Island. *Ecography* 29, 671–682. doi: 10.1111/j.2006.0906-7590.04675.x

Getzin, S., Nuske, R. S., and Wiegand, K. (2014). Using Unmanned Aerial Vehicles (UAV) to Quantify Spatial Gap Patterns in Forests. *Remote Sens.* 6, 6988–7004. doi: 10.3390/rs6086988

Gibbs, D. A., and Hay, M. E. (2015). Spatial patterns of coral survivorship: impacts of adult proximity versus other drivers of localized mortality. *PeerJ* 3:e1440. doi: 10.7717/peerj.1440

Hawkes, N., Korabik, M., Beazley, L., Rapp, H. T., Xavier, J. R., and Kenchington, E. (2019). Glass sponge grounds on the Scotian Shelf and their associated biodiversity. *Mar. Ecol. Prog. Ser.* 614, 91–109. doi: 10.3354/meps12903

Heckerman, D., Geiger, D., and Chickering, D. M. (1995). Learning Bayesian networks: the combination of knowledge and statistical data. *Mach. Learn.* 20, 197–243. doi: 10.1007/BF00994016

Hogg, M. M. (2010). *Deep-sea Sponge Grounds: Reservoirs of Biodiversity*. Nairobi: UNEP.

Hourigan, T. F., Kelley, C., McGuinn, R., Bingo, S., Moriwake, V. C., Putts, M., et al. (2020). *Forests of the Deep: High-Density Deep-Sea Coral and Sponge Communities in the Central and Western Pacific. Ocean Sciences Meeting 2020*. Washington, DC: American Geophysical Union.

Howell, K.-L., Piechaud, N., Downie, A.-L., and Kenny, A. (2016). The distribution of deep-sea sponge aggregations in the North Atlantic and implications for their effective spatial management. *Deep Sea Res. Part I Oceanogr. Res. Pap.* 115, 309–320. doi: 10.1016/j.dsr.2016.07.005

Illian, J., Penttinen, A., Stoyan, H., and Stoyan, D. (2008). *Statistical Analysis and Modelling of Spatial Point Patterns*. Vol. 70, John Wiley & Sons.

Janzen, D. H. (1970). Herbivores and the Number of Tree Species in Tropical Forests. *Am. Nat.* 104, 501–528. doi: 10.1086/282687

Jolles, A. E., Sullivan, P., Alker, A. P., and Harvell, C. D. (2002). Disease transmission of Aspergillosis in sea fans: inferring process from spatial pattern. *Ecology* 83, 2373–2378.

Jones, S. P. (2003). *Haskell 98 Language and Libraries: The Revised Report*. Cambridge: Cambridge University Press.

Kahn, A. S., Yahel, G., Chu, J. W. F., Tunnicliffe, V., and Leys, S. P. (2015). Benthic grazing and carbon sequestration by deep-water glass sponge reefs. *Limnol. Oceanogr.* 60, 78–88. doi: 10.1002/lno.10002

Kazanidis, G., Henry, L.-A., Roberts, J. M., and Witte, U. F. M. (2016). Biodiversity of Spongosorites coralliophaga (Stephens, 1915) on coral rubble at two contrasting cold-water coral reef settings. *Coral Reefs* 35, 193–208. doi: 10.1007/s00338-015-1355-2

Kelley, C., Elliott, K., and Malik, M. (2018). *Okeanos Explorer ROV Dive Summary Dive 11 [Dive Summary]*. Available online at: https://catalog.data.gov/dataset/ex1706-dive11-ancillary-data-collection-including-reports-kmls-spreadsheets-and-data (accessed September 5, 2020).

Kenchington, E., Power, D., and Koen-Alonso, M. (2013). Associations of demersal fish with sponge grounds on the continental slopes of the northwest Atlantic. *Mar. Ecol. Prog. Ser.* 477, 217–230. doi: 10.3354/meps10127

Kennedy, B. R. C., Cantwell, K., Malik, M., Kelley, C., Potter, J., Elliott, K., et al. (2019). The unknown and the unexplored: insights into the Pacific Deep-Sea Following NOAA CAPSTONE Expeditions. *Front. Mar. Sci.* 6:480. doi: 10.3389/fmars.2019.00480

Knudby, A., Kenchington, E., and Murillo, F. J. (2013). Modeling the distribution of geodia sponges and sponge grounds in the Northwest Atlantic. *PLoS One* 8:e82306. doi: 10.1371/journal.pone.0082306

Law, R., Illian, J., Burslem, D. F. R. P., Gratzer, G., Gunatilleke, C. V. S., and Gunatilleke, I. A. U. N. (2009). Ecological information from spatial patterns

of plants: insights from point process theory. *J. Ecol.* 97, 616–628. doi: 10.1111/j.1365-2745.2009.01510.x

Levin, S. A. (1992). The Problem of Pattern and Scale in Ecology: the Robert H. MacArthur Award Lecture. *Ecology* 73, 1943–1967.

Liang, Y., Guo, L.-D., Du, X.-J., and Ma, K.-P. (2007). Spatial structure and diversity of woody plants and ectomycorrhizal fungus sporocarps in a natural subtropical forest. *Mycorrhiza* 17, 271–278. doi: 10.1007/s00572-006-0096-z

Lin, Y.-C., Chang, L.-W., Yang, K.-C., Wang, H.-H., and Sun, I.-F. (2011). Point patterns of tree distribution determined by habitat heterogeneity and dispersal limitation. *Oecologia* 165, 175–184. doi: 10.1007/s00442-010-1718-x

Lingua, E., Cherubini, P., Motta, R., and Nola, P. (2008). Spatial structure along an altitudinal gradient in the Italian central Alps suggests competition and facilitation among coniferous species. *J. Veg. Sci.* 19, 425–436. doi: 10.3170/2008-8-18391

Loosmore, N. B., and Ford, E. D. (2006). Statistical Inference Using the G or K Point Pattern Spatial Statistics. *Ecology* 87, 1925–1931.

Lundsten, L., Barry, J. P., Cailliet, G. M., Clague, D. A., DeVogelaere, A. P., and Geller, J. B. (2009). Benthic invertebrate communities on three seamounts off southern and central California, USA. *Mar. Ecol. Prog. Ser.* 374, 23–32. doi: 10.3354/meps07745

Luter, H. M., Bannister, R. J., Whalan, S., Kutti, T., Pineda, M.-C., and Webster, N. S. (2017). Microbiome analysis of a disease affecting the deep-sea sponge Geodia barretti. *FEMS Microbiol. Ecol.* 93:fix074. doi: 10.1093/femsec/fix074

Luter, H. M., and Webster, N. S. (2017). "Sponge Disease and Climate Change," in *Climate Change, Ocean Acidification and Sponges: Impacts Across Multiple Levels of Organization*, eds J. L. Carballo and J. J. Bell (Berlin: Springer), 411–428. doi: 10.1007/978-3-319-59008-0_9

Maldonado, M., Aguilar, R., Bannister, R. J., Bell, J. J., Conway, K. W., Dayton, P. K., et al. (2017). "Sponge grounds as key marine habitats: a synthetic review of types, structure, functional roles, and conservation concerns," in *Marine Animal Forests: The Ecology of Benthic Biodiversity Hotspots*, eds S. Rossi, L. Bramanti, A. Gori, and C. Orejas Saco del Valle (Cham: Springer). doi: 10.1007/978-3-319-17001-5_24-1

Magurran, A. E. (2013). *Measuring Biological Diversity*. John Wiley & Sons.

Malik, M., Jerram, K., Wilkins, C., and Baechler, N. (2018). *Mapping Data Acquisition and Processing Summary Report Cruise. EX-17-06: Laulima O Ka Moana Exploring Deep MonumentWaters Around Johnston Atoll (ROV/Mapping)*. Available online at: https://repository.library.noaa.gov/view/noaa/21365 (accessed September 5, 2020).

McClain, C., and Barry, J. P. (2010). Habitat heterogeneity, disturbance, and productivity work in concert to regulate biodiversity in deep submarine canyons. *Ecology* 91, 964–976.

McClain, C. R., Lundsten, L., Ream, M., Barry, J., and DeVogelaere, A. (2009). Endemicity, biogeography, composition, and community structure on a Northeast Pacific Seamount. *PLoS One* 4:e4141. doi: 10.1371/journal.pone.0004141

McIntire, E. J. B., and Fajardo, A. (2009). Beyond description: the active and effective way to infer processes from spatial patterns. *Ecology* 90, 46–56. doi: 10.1890/07-2096.1

Meyer, H. K., Roberts, E. M., Rapp, H. T., and Davies, A. J. (2019). Spatial patterns of arctic sponge ground fauna and demersal fish are detectable in autonomous underwater vehicle (AUV) imagery. *Deep Sea Res. Part I Oceanogr. Res. Pap.* 153:103137. doi: 10.1016/j.dsr.2019.103137

Milns, I., Beale, C. M., and Smith, V. A. (2010). Revealing ecological networks using Bayesian network inference algorithms. *Ecology* 91, 1892–1899. doi: 10.1890/09-0731.1

Mitchell, E. G. (2011). Functional programming through deep time: modeling the first complex ecosystems on earth. *ACM SIGPLAN Notices* 46, 28–31. doi: 10.1145/2034574.2034779

Mitchell, E. G., and Butterfield, N. J. (2018). Spatial analyses of Ediacaran communities at Mistaken Point. *Paleobiology* 44, 40–57. doi: 10.1017/pab.2017.35

Mitchell, E. G., Durden, J. M., and Ruhl, H. A. (2020a). First network analysis of interspecific associations of abyssal benthic megafauna reveals potential vulnerability of abyssal hill community. *Prog. Oceanogr.* 187:102401. doi: 10.1016/j.pocean.2020.102401

Mitchell, E. G., Harris, S., Kenchington, C. G., Vixseboxse, P., Roberts, L., Clark, C., et al. (2019). The importance of neutral over niche processes in structuring Ediacaran early animal communities. *Ecol. Lett.* 22, 2028–2038. doi: 10.1111/ele.13383

Mitchell, E. G., and Kenchington, C. G. (2018). The utility of height for the Ediacaran organisms of Mistaken Point. *Nat. Ecol. Evol.* 2, 1218–1222. doi: 10.1038/s41559-018-0591-6

Mitchell, E. G., Kenchington, C. G., Harris, S., and Wilby, P. R. (2018). Revealing rangeomorph species characters using spatial analyses. *Can. J. Earth Sci.* 55, 1262–1270. doi: 10.1139/cjes-2018-0034

Mitchell, E. G., Kenchington, C. G., Liu, A. G., Matthews, J. J., and Butterfield, N. J. (2015). Reconstructing the reproductive mode of an Ediacaran macro-organism. *Nature* 524, 343–346. doi: 10.1038/nature14646

Mitchell, E. G., Whittle, R., and Huw Griffths (2020b). Investigating benthic ecosystem cascade effects in Antarctica using Bayesian network inference. *Commun. Biol.* doi: 10.1038/s42003-020-01310-8

Muko, S., Shimatani, I. K., and Nozawa, Y. (2014). Spatial analyses for nonoverlapping objects with size variations and their application to coral communities. *J. Anim. Ecol.* 83, 980–990. doi: 10.1111/1365-2656.12193

Muller, E. M., and van Woesik, R. (2012). Caribbean coral diseases: Primary transmission or secondary infection? *Glob. Change Biol.* 18, 3529–3535. doi: 10.1111/gcb.12019

Murillo, F. J., Kenchington, E., Koen-Alonso, M., Guijarro, J., Kenchington, T. J., Sacau, M., et al. (2020). Mapping benthic ecological diversity and interactions with bottom-contact fishing on the Flemish Cap (northwest Atlantic). *Ecol. Indic.* 112:106135. doi: 10.1016/j.ecolind.2020.106135

NOAA Office of Ocean Exploration and Research (n.d.). *NOAA Office of Ocean Exploration and Research Benthic Deepwater Animal Identification Guide*. Available online at: http://oceanexplorer.noaa.gov/okeanos/animal_guide/animal_guide.htm

Pélissier, R., and Goreaud, F. (2001). A practical approach to the study of spatial structure in simple cases of heterogeneous vegetation. *J. Veg. Sci.* 12, 99–108. doi: 10.1111/j.1654-1103.2001.tb02621.x

Piazza, P., Gattone, S. A., Guzzi, A., and Schiaparelli, S. (2020). Towards a robust baseline for long-term monitoring of Antarctic coastal benthos. *Hydrobiologia* 847, 1753–1771. doi: 10.1007/s10750-020-04177-2

Pile, A. J., and Young, C. M. (2006). The natural diet of a hexactinellid sponge: benthic–pelagic coupling in a deep-sea microbial food web. *Deep Sea Res. Part I Oceanogr. Res. Pap.* 53, 1148–1156. doi: 10.1016/j.dsr.2006.03.008

Prado, E., Sánchez, F., Rodríguez-Basalo, A., Altuna, Á., and Cobo, A. (2019). Analysis of the population structure of a gorgonian forest (Placogorgia sp.) *using a photogrammetric* 3D modeling approach at Le Danois Bank, Cantabrian Sea. *Deep Sea Res. Part I Oceanogr. Res. Pap.* 153, 103124. doi: 10.1016/j.dsr.2019.103124

Price, D., Robert, K., Callaway, A., Iacono, C. L., Hall, R., and Huvenne, V. A. I. (2019). Using 3D photogrammetry from ROV video to quantify cold-water coral reef structural complexity and investigate its influence on biodiversity and community assemblage | SpringerLink. *Coral Reefs* 38, 1007–1021.

R Core Team (2017). *R: A Language and Environment for Statistical Computing*. Vienna: R Foundation for Statistical Computing.

Raventós, J., Wiegand, T., and Luis, M. D. (2010). Evidence for the spatial segregation hypothesis: a test with nine-year survivorship data in a Mediterranean shrubland. *Ecology* 91, 2110–2120. doi: 10.1890/09-0385.1

Reiswig, H. M. (1974). Water transport, respiration and energetics of three tropical marine sponges. *J. Exp. Mar. Biol. Ecol.* 14, 231–249. doi: 10.1016/0022-0981(74)90005-7

Richer de Forges, B., Koslow, J. A., and Poore, G. C. B. (2000). Diversity and endemism of the benthic seamount fauna in the southwest Pacific. *Nature* 405, 944–947. doi: 10.1038/35016066

Robert, K., Huvenne, V. A. I., Georgiopoulou, A., Jones, D. O. B., Marsh, L., D. O. Carter, G., et al. (2017). New approaches to high-resolution mapping of marine vertical structures. *Sci. Rep.* 7:9005. doi: 10.1038/s41598-017-09382-z

Robert, K., Jones, D. O. B., Georgiopoulou, A., and Huvenne, V. A. I. (2020). Cold-water coral assemblages on vertical walls from the Northeast Atlantic. *Divers. Distrib.* 26, 284–298. doi: 10.1111/ddi.13011

Rossi, S., Bramanti, L., Gori, A., and Orejas, C. (2017). "An Overview of the Animal Forests of the World," in *Marine Animal Forests*, eds S. Rossi, L. Bramanti, A. Gori, and C. Orejas (Berlin: Springer), 1–26. doi: 10.1007/978-3-319-17001-5_1-1

Rowden, A. A., Schlacher, T. A., Williams, A., Clark, M. R., Stewart, R., Althaus, F., et al. (2010). A test of the seamount oasis hypothesis: seamounts support higher epibenthic megafaunal biomass than adjacent slopes. *Mar. Ecol.* 31, 95–106. doi: 10.1111/j.1439-0485.2010.00369.x

Samadi, S., Bottan, L., Macpherson, E., De Forges, B. R., and Boisselier, M.-C. (2006). Seamount endemism questioned by the geographic distribution and population genetic structure of marine invertebrates. *Mar. Biol.* 149, 1463–1475. doi: 10.1007/s00227-006-0306-4

Seidler, T. G., and Plotkin, J. B. (2006). Seed dispersal and spatial pattern in tropical trees. *PLoS Biol.* 4:e344. doi: 10.1371/journal.pbio.0040344

Smith, V. A., Yu, J., Smulders, T. V., Hartemink, A. J., and Jarvis, E. D. (2006). Computational inference of neural information flow networks. *PLoS Comput. Biol.* 2:e161. doi: 10.1371/journal.pcbi.0020161

Vieira, R. P., Bett, B. J., Jones, D. O. B., Durden, J. M., Morris, K. J., Cunha, M. R., et al. (2020). Deep-sea sponge aggregations (Pheronema carpenteri) in the Porcupine Seabight (NE Atlantic) potentially degraded by demersal fishing. *Prog. Oceanogr.* 183:102189. doi: 10.1016/j.pocean.2019.102189

Waagepetersen. (2009). Two-step estimation for inhomogeneous spatial point processes. *J. R. Stat. Soc. Ser. B* 71, 685–702.

Wang, Y., Camarero, J. J., Luo, T., and Liang, E. (2012). Spatial patterns of Smith fir alpine treelines on the south-eastern Tibetan Plateau support that contingent local conditions drive recent treeline patterns. *Plant Ecol. Divers.* 5, 311–321. doi: 10.1080/17550874.2012.704647

Webster, N. S. (2007). Sponge disease: A global threat? *Environ. Microbiol.* 9, 1363–1375. doi: 10.1111/j.1462-2920.2007.01303.x

Wiegand, T., Gunatilleke, S., and Gunatilleke, N. (2007a). Species Associations in a Heterogeneous Sri Lankan Dipterocarp Forest. *Am. Nat.* 170, E77–E95. doi: 10.1086/521240

Wiegand, T., Kissling, W. D., Cipriotti, P. A., and Aguiar, M. R. (2006). Extending point pattern analysis for objects of finite size and irregular shape. *J. Ecol.* 94, 825–837. doi: 10.1111/j.1365-2745.2006.01113.x

Wiegand, T., and Moloney, K. A. (2004). Rings, circles, and null-models for point pattern analysis in ecology. *Oikos* 104, 209–229. doi: 10.1111/j.0030-1299.2004.12497.x

Wiegand, T., and Moloney, K. A. (2013). *Handbook of Spatial Point-Pattern Analysis in Ecology*. Boca Raton, FL: CRC Press.

Wiegand, T., Moloney, K. A., Naves, J., and Knauer, F. (1999). Finding the missing link between landscape structure and population dynamics: a spatially explicit perspective. *Am. Nat.* 154, 605–627. doi: 10.1086/303272

Wiegand, T., Wiegand, K., and Getzin, S. (2007b). Analyzing the spatial structure of a Sri Lankan tree species with multiple scales of clustering. *Ecology* 88, 3088–3102.

Wulff, J. L. (2007). Disease prevalence and population density over time in three common Caribbean coral reef sponge species. *J. Mar. Biol. Assoc. U.K.* 87, 1715–1720. doi: 10.1017/S002531540705881X

Yu, J. (2005). *Developing Bayesian Network Inference Algorithms to Predict Causal Functional Pathways in Biological Systems*. Ph.D. thesis, Duke University, Durham.

Yu, J., Smith, V. A., Wang, P. P., Hartemink, E. J., and Jarvis, E. D. (2002). "Using bayesian network inference algorithms to recover molecular genetic regulatory networks," in *Proceedings of the 3rd International Conference on System Biology*, Paris.

Zvuloni, A., Artzy-Randrup, Y., Stone, L., Kramarsky-Winter, E., Barkan, R., and Loya, Y. (2009). Spatio-temporal transmission patterns of black-band disease in a coral community. *PLoS One* 4:4993. doi: 10.1371/journal.pone.0004993

Conflict of Interest: The authors declare that the research was conducted in the absence of any commercial or financial relationships that could be construed as a potential conflict of interest.

Copyright © 2020 Mitchell and Harris. This is an open-access article distributed under the terms of the Creative Commons Attribution License (CC BY). The use, distribution or reproduction in other forums is permitted, provided the original author(s) and the copyright owner(s) are credited and that the original publication in this journal is cited, in accordance with accepted academic practice. No use, distribution or reproduction is permitted which does not comply with these terms.

frontiers in Marine Science

ORIGINAL RESEARCH
published: 08 December 2020
doi: 10.3389/fmars.2020.610565

Does Depth Matter? Reproduction Pattern Plasticity in Two Common Sponge Species Found in Both Mesophotic and Shallow Waters

Tal Idan[1], Liron Goren[1,2], Sigal Shefer[1,2], Itzchak Brickner[1] and Micha Ilan[1]*

[1] George S. Wise Faculty of Life Sciences, School of Zoology, Tel Aviv University, Tel Aviv, Israel, [2] The Steinhardt Museum of Natural History, Israel National Center for Biodiversity Studies, Tel Aviv University, Tel Aviv, Israel

Determining demosponge reproductive strategies is essential to understanding their ecology and life history, as well as for the management of benthic marine environments. This is especially important in mesophotic ecosystems, which have been suggested to serve as a refuge for shallow-water populations and for which knowledge is lacking. Here we compared the reproductive strategies of two common Mediterranean demosponges species: *Chondrosia reniformis* and *Axinella polypoides*, which can be found in both shallow and mesophotic habitats along the Israeli coast. Samples were collected over 2 years, via SCUBA diving from the shallow coast (2–32 m) and Remotely Operated Vehicle from the mesophotic sponge grounds (95–120 m). *A. polypoides* and *C. renifornis* differed in oocyte morphology and development, but both demonstrated reproductive plasticity with regard to temperature and depth: temperature appears to regulate their reproduction in the shallow water, as both species exhibited seasonality; whereas, in the mesophotic zone, where the temperature amplitude is much smaller, seasonality was not observed for either species. Furthermore, in the mesophotic zone, *C. reniformis* exhibited low fecundity and probably invests more in asexual reproduction by budding. Mesophotic *A. polypoides*, in contrast, exhibited enhanced and continuous asynchronous sexual reproduction year-round. Our findings suggest that reproduction plasticity may be a general rule for sponge species that inhabit different habitats; such plasticity could allow sponges to thrive in different environmental conditions. These findings further emphasize the importance of protecting the mesophotic sponge grounds, which can serve as a refuge in the face of the adverse impact of anthropogenic disturbances and rising seawater temperatures.

Keywords: ***Chondrosia reniformis*, *Axinella polypoides*, oogenesis, temperature, sexual reproduction, asexual reproduction (budding)**

OPEN ACCESS

Edited by:
Ellen Kenchington, Bedford Institute of Oceanography (BIO), Canada

Reviewed by:
Cecilia Conaco, University of the Philippines Diliman, Philippines
Thierry Perez, UMR 7263 Institut Méditerranéen de Biodiversité et d'Écologie Marine et Continentale (IMBE), France

****Correspondence:***
Tal Idan
talidan@mail.tau.ac.il;
taltul.idan@gmail.com

Specialty section:
This article was submitted to Deep-Sea Environments and Ecology, a section of the journal Frontiers in Marine Science

Received: *26 September 2020*
Accepted: *16 November 2020*
Published: *08 December 2020*

Citation:
Idan T, Goren L, Shefer S, Brickner I and Ilan M (2020) Does Depth Matter? Reproduction Pattern Plasticity in Two Common Sponge Species Found in Both Mesophotic and Shallow Waters. Front. Mar. Sci. 7:610565. doi: 10.3389/fmars.2020.610565

INTRODUCTION

Demosponges comprise the most diverse class in the phylum Porifera (Hooper and Van Soest, 2002; Morrow and Cárdenas, 2015). They play an important role as environmental engineers (Kenchington et al., 2013; Gerovasileiou et al., 2016), especially in temperate and cold seas (Bo et al., 2012; Beazley et al., 2013). This holds particularly true for the Mediterranean Sea, where demosponges often dominate the benthic fauna (Voultsiadou, 2009; Coll et al., 2010). In recent

years mesophotic sponge grounds have been discovered along the Israeli coast of the Mediterranean Sea. In these habitats, sponges grow in high density, accounting for ∼80% of the total live coverage (Idan et al., 2018). They thereby increase structural complexity and provide a settlement substrate for benthic invertebrates, as well as a refuge from predators, in addition to serving as spawning and nursery grounds (Bo et al., 2012; Gerovasileiou et al., 2016).

Due to their distance from land, it was suggested that mesophotic ecosystems are not influenced by anthropogenic activities or natural disturbances (Hinderstein et al., 2010; Locker et al., 2010). Thus, the mesophotic ecosystems have been considered to constitute a refuge for many shallow-water species, as spawning grounds and a source of larvae contributing to species resilience (Hinderstein et al., 2010; Kahng et al., 2010; Smith et al., 2010). Despite the lack of knowledge regarding fundamental aspects of sponge biology and ecology in the mesophotic ecosystems (Maldonado et al., 2017; Cerrano et al., 2019), it has been suggested that mesophotic communities to a great extent represent an extension of the shallow-water ones (Lesser et al., 2009). Such a connection is probably directly dependent on the degree of larval dispersal and gene flow between the two zones, and the reproductive strategies of the relevant sponges (Lesser et al., 2009; Kahng et al., 2010).

Determining the reproductive strategies of sponges is essential to understanding their ecology, life history, and populations and community dynamics, as well as for the management of benthic marine environments. Sexual reproduction in demosponges is diverse, as different species can be either gonochoric, sequential, or simultaneous hermaphrodites, and can also be either brooders (viviparity) or broadcasters (oviparity) (Maldonado, 2006). The majority of the oviparous sponges are gonochoristic (Sará et al., 1992; Ereskovsky, 2010). The onset of gametogenesis, as well as spawning, can be triggered by various stimuli, such as water temperature, lunar phase, photoperiod, and nutrient flux (Elvin, 1976; Simpson, 1984; Witte, 1996; Usher et al., 2004; Riesgo et al., 2007; Riesgo and Maldonado, 2008). Reproduction within a limited time-frame also leads to synchronization in gametogenesis (Usher et al., 2004; Maldonado and Riesgo, 2009b). In Demosponges, male gametes usually derive from choanocytes, whereas the origin of oocytes is more complicated, as in some cases, they can originate from amoebocytes, and in others from choanocytes (Sará et al., 1992; Ereskovsky, 2010). While oogenesis takes several months, studying spermatogenesis is more difficult as it is a quick process that usually occurs within less than a month (Riesgo, 2007; Ereskovsky, 2010).

In the mesophotic zone, many of the above-mentioned stimuli are stable and constant (Kress et al., 2014). Accordingly, we might expect the reproductive patterns of species that inhabit a wide depth range to display a change with depth, as has been demonstrated for some species (Witte, 1996). Other species may follow their regular seasonal cycles, as the shallow-water populations do. Such cycles have been attributed to seasonal changes in food source availability; more precisely—POC flux (Witte, 1996). To the best of our knowledge, only one study to date has compared the reproduction of sponges from different depths. Although that study was limited to the shallow zone (0–30 m), differences in fecundity were found (Meroz-Fine et al., 2005).

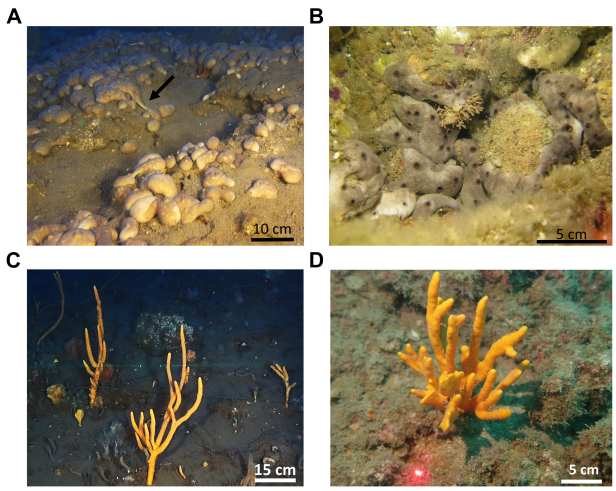

FIGURE 1 | Growth forms of *Chondrosia reniformis* and *Axinella polypoides* in the study sites. **(A)** Extensive open area in the mesophotic habitat (arrow marks a creeping event); **(B)** A small crevice in the shallow water (3 m) inhabited by many specimens. **(C)** Average size specimens in the mesophotic habitat; **(D)**. The largest specimen found in the shallow water (30 m).

Along the Israeli coast, 12 sponge species can be found in both shallow and mesophotic habitats (Idan et al., 2018). This provided us with the opportunity to study and compare the reproduction strategies of two such species: *Chondrosia reniformis* and *Axinella polypoides* (Idan et al., 2018). These species were chosen as they are the only ones that are abundant in both habitats.

C. reniformis is a massive lobate, smooth sponge, common in the Mediterranean and Eastern Atlantic Ocean, found in shallow and mesophotic habitats (**Figures 1A,B**). It is known from shallow habitats in the Mediterranean as a gonochoric broadcaster (Riesgo and Maldonado, 2008; Di Camillo et al., 2012). Its reproductive cycle seems to vary among areas, from seasonal to continuous, with a peak during summer (Riesgo and Maldonado, 2008; Di Camillo et al., 2012; Yaniv, 2013). *A. polypoides,* or the Common Antlers Sponge, is an erect, branching species. It is also a species common throughout the Mediterranean and in the eastern Atlantic Ocean, but in spite of its abundance, its reproductive cycle has not yet been described (**Figures 1C,D**).

MATERIALS AND METHODS

Study Site and Sampling

For a comparison of the reproduction patterns between the mesophotic and shallow populations, samples of *Axinella polypoides* and *Chondrosia reniformis* were collected from both habitats over the course of 2 years (January 2017–January 2019; **Figure 2**). The mesophotic site is located approximately 16 km off the Israeli coast of Herzliya (32.17710°N, 034.63306°E WGS-84) at a depth of 95–120 m; and the shallow-water site is located

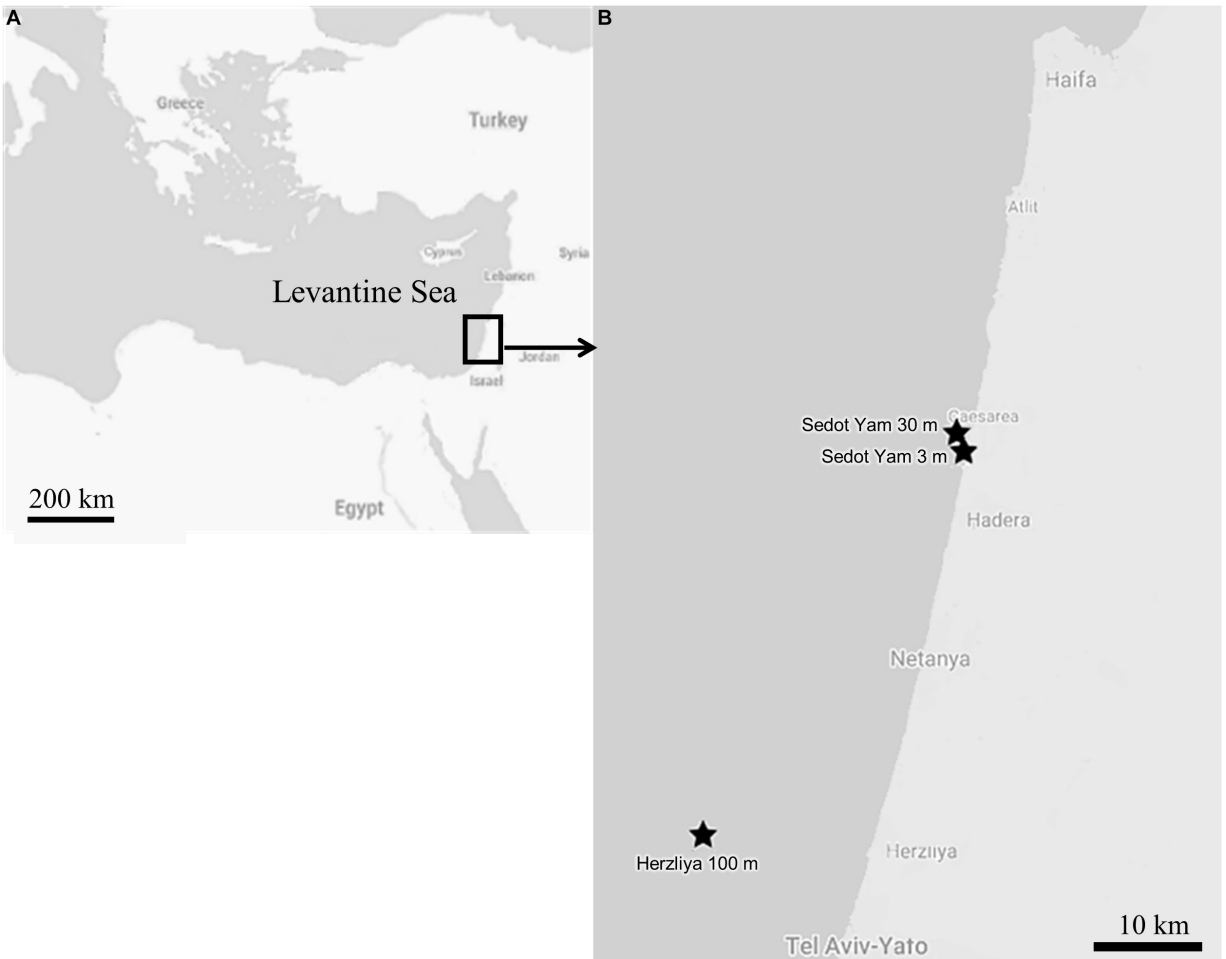

FIGURE 2 | The study area: **(A)** Map of the Levantine Sea. **(B)** Map of the sampling sites along the Israeli coast.

off the coast of Sedot Yam (32.529633°N, 034.858553°E WGS-84). The distance between the shallow and mesophotic sites is ∼40 km (**Figure 2**). In the shallow-water, the sponges were collected monthly by SCUBA diving, *C. reniformis* at a depth of 2–4 m, and *A. polypoides* at a depth of 32–28 m (n = 8–11, per species per month). *C. reniformis* was quite rare in the 28–32 m deep habitat, while *A. polypoides* is rarely found in depths shallower than 27 m in the Israeli coast. Sponge sampling at the mesophotic site was conducted approximately every 3 months (n = 1–6, per species per sampling date), using a remotely operated vehicle (ROV; ECA-Robotics H800 ROV) onboard the R/V Mediterranean Explorer. At the mesophotic site, the temperature was measured using a CTD, and at the shallow site using diving computers. Vouchers of the collected material were deposited at the Steinhardt Museum of Natural History at Tel Aviv University.

Histologic Preparations

The collected specimens were photographed *in situ* (underwater) and in the lab following collection. A 2 cm^3 piece of sponge was cut from the interior part of each sponge. Areas of the collagenous mesohyl were avoided as it had been previously shown that no reproductive elements are present in these sections (Riesgo and Maldonado, 2008). The tissue samples were then fixed in 2.5% glutaraldehyde (in filtered seawater) for at least 24 h, rinsed three times in artificial seawater, followed by dehydration (35, 50, and 70% ethanol), and preserved in 70% ethanol. The rest of the sponge was preserved in absolute ethanol to enable molecular analysis if needed. In *A. polypoides*, skeletal spicules were dissolved by desilicification with 4.8% hydrofluoric acid for 24 h and then rinsed three times in 70% ethanol. The *C. reniformis* samples were not treated with acid because they lack spicules.

The samples were cast in paraffin blocks and cut into 7 μm thick sections using a Shandon Lipshaw M1R microtome. The sections were placed on charged microscope slides, dried, and stained with Hematoxylin and 1% Eosin. The tissue sections were observed (3–5 sections per specimen) with a Zeiss Axioskop microscope equipped with a ZEISS Axiocam 105 color camera (Carl Zeiss, Oberkochen, Germany). Oocyte size was measured and recorded using ZEN lite software to determine gametogenesis (gamete growth) and timing of gamete release.

Data Analysis

The average abundance of oocytes (values ± SD), and their maximal diameter, were calculated monthly for both species for specimens from the shallow site, and approximately every 3 months for those from the mesophotic site. The abundance of oocytes per mm^2 was obtained by counting the number of oocytes in 30 consecutive frames (with no overlap) and dividing this number by the size of a single frame (in mm^2). For maximal diameter, 30 oocytes were measured per sponge. If fewer than 30 oocytes were found, the maximal number found was recorded. Statistical analysis was performed using R (R Core Team, 2020) and RStudio (R Studio Team, 2020) package stats (R Core Team et al., 2018).

All data were found to be normally distributed using the Shapiro-Wilk's test. Linear regression models were used to test the relationship between temperature and oocyte diameter (*C. reniformis*), and the relationship between temperature and oocyte abundance and the proportion of reproducing individuals (*A. polypoides*). The analyzed data included all months in which the sponges reproduced.

A two-tailed Student's *t*-test was performed to compare mean oocyte abundance per specimen and oocyte size at the same developmental stage in *C. reniformis*. In *A. polypoides,* the standard deviations of oocyte diameter per specimen were compared between shallow and mesophotic, for samples collected at the same sampling dates, using a two-tailed Student's *t*-test.

RESULTS

Chondrosia Reniformis

A total of 246 individuals were collected from the mesophotic and shallow habitats. The individuals ranged in length from 2 to 12 cm. No male reproductive elements were recorded

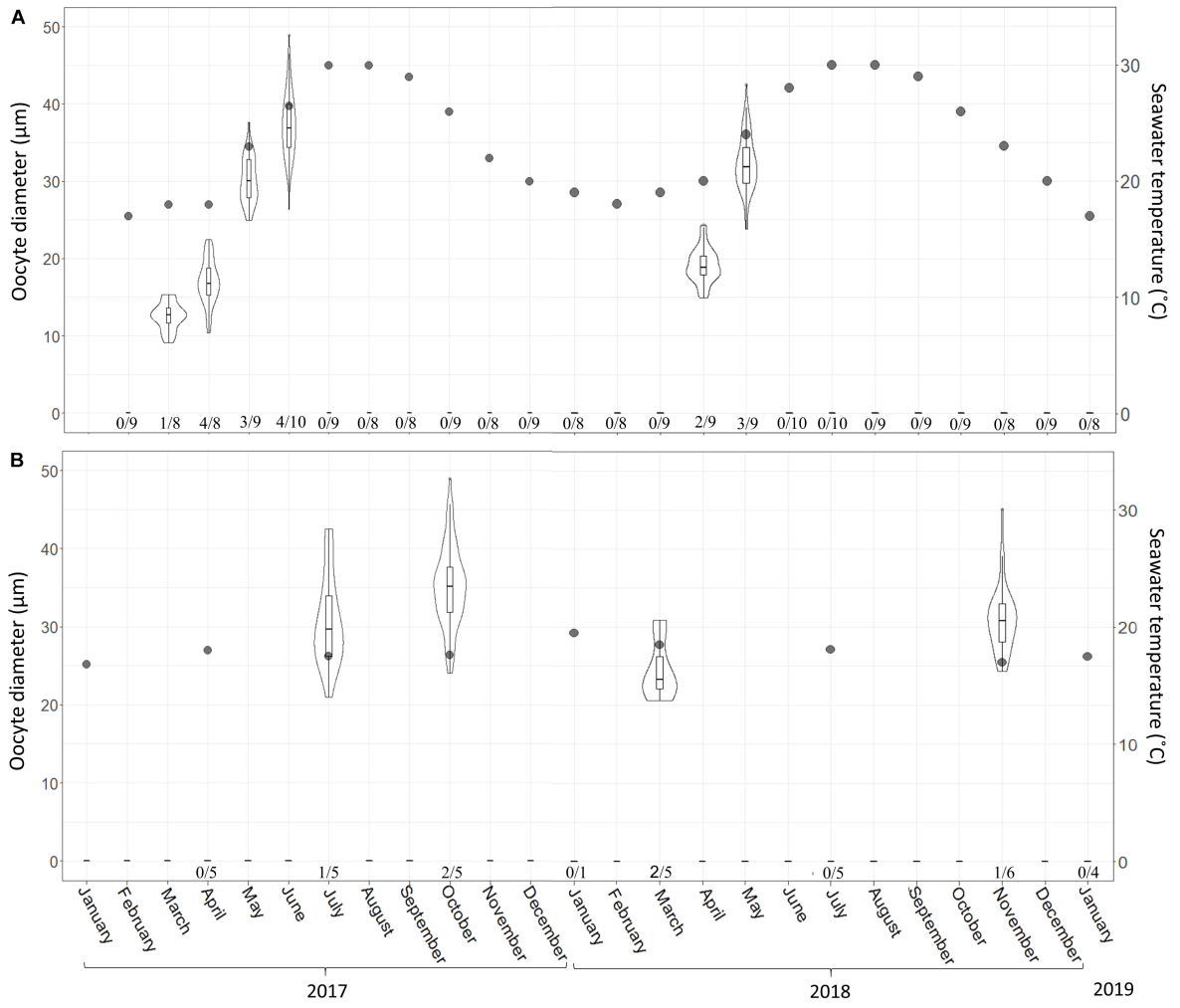

FIGURE 3 | *C. reniformis* oocyte diameter and seawater temperature at 3 m **(A)** and 100 m **(B)** depth between February 2017–January 2019 and January 2017–January 2019, respectively. Shallow-water samples were collected monthly; mesophotic samples were collected seasonally. An arrow marks the month when spermatocytes were found. Number below bars is the number of individuals containing oocytes out of total number of individuals sampled. The violin plot shows size distribution, and the box plot within the violin shows quartiles and median.

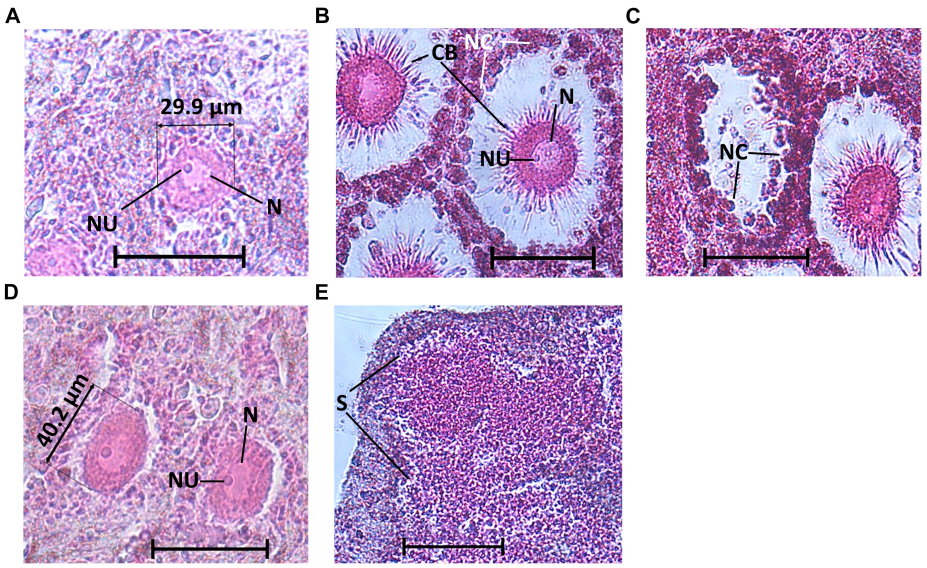

FIGURE 4 | *C. reniformis* oogenesis and spermatogenesis. **(A)** Mid-developed oocytes of a shallow-water *C. reniformis*, **(B)** fully developed oocytes of a shallow-water *C. reniformis* with nurse cells, nucleus, nucleolus, and cytoplasmic bridges, **(C)** a hollow space, from where an oocyte was presumably released, while nurse cells are still visible. **(D)** Mid-developed oocytes of a mesophotic *C. reniformis* with nucleus and nucleolus. **(E)** Spermatocytes. Scale bar is 50 µm. N, nucleus; NU, nucleolus; CB, cytoplasmic bridges; NC, nurse cells; S, spermatocytes.

from the mesophotic zone during this study; while in the shallow zone, only three specimens containing spermatocytes were found in June 2017.

During the reproduction period in the shallow zone, 32% of the individuals (17/53) contained oocytes, and in June 2017 (peak reproduction period), 70% of the individuals contained reproductive elements (three individuals contained spermatocytes and four contained oocytes; **Figure 3A**). In the mesophotic zone, in contrast, over the research period 14% of the individuals (5/36) contained oocytes, with a maximum of 40% of individuals containing oocytes in October 2017 (n = 5, **Figure 3B**). Oocytes were observed throughout the mesohyl, with the exception of the ectosome and areas with a high concentration of collagen. Oocyte shapes ranged from round to oval. Around fully developed oocytes, nurse cells and cytoplasmic bridges (**Figures 4A–C**) were apparent (**Figures 4B,C**). In sponges from the shallow zone, oocyte development seemed to roughly follow the increase in water temperature (**Figure 3A**), while in sponges from the mesophotic zone, only mid-developed oocytes were observed (**Figures 4D**, **3B**). When spermatocytes were observed, they were seen occupying a substantial part of the choanosome, and only a few choanocyte chambers could be observed in these specimens (**Figure 4E**).

In the shallow habitat, the gametogenesis of *C. reniformis* extended from March to June in 2017 and from April to May in 2018. With the increase in temperature, we observed an increase in both oocyte diameter (from a mean ± SD of 12.5 ± 1.8 µm, n = 30 oocytes, to 35.6 ± 4.4 µm, n = 90 oocytes, in 2017 and 19.01 ± 2.17 µm, n = 53 oocytes, to 32.4 ± 3.6 µm, n = 73 oocytes, in 2018; **Figure 3A** and **Supplementary Table 1**), and abundance (from 0.88 ± 0.09 oocytes/mm^2 to 25.45 ± 1.71 in 2017 and from 5.8 ± 0.51 oocytes/mm^2 to 13.07 ± 3.52 in 2018; **Figure 5A** and **Supplementary Table 2**). With the exception of a decrease in abundance in June 2017, when hollow spaces, presumably reflecting where oocytes had been released, appeared in the histological preparations (**Figure 4C**). In contrast, in the mesophotic zone, where the temperature remained stable (16.8–19.5°C, **Supplementary Table 3**), a low abundance of oocytes was observed for all sampling dates (0.11 ± 0.04–6.97 ± 1.1 oocytes/mm^2, similar to the lower values of the shallow zone, **Supplementary Table 4**), and oocyte diameter displayed less variability of size (21–49 µm, **Supplementary Table 5**).

In the shallow zone, a significant relationship was found between oocyte development and temperature. This relationship appears to explain 78% of the variance in oocyte diameter (**Figure 2**; Linear Regression, R^2 = 0.78, F = 62.87, df = 16, p < 0.001) and about a quarter of the variance in oocyte abundance (number of oocytes/mm^2; **Figure 5**; Linear regression, R^2 = 0.23, F = 5.47, df = 14, p = 0.03). In the mesophotic zone, while a significant relationship between oocyte diameter and temperature was found, it explained merely 2% of the variance (**Figure 3**, Linear regression, R^2 = 0.02, F = 4.02, df = 155, p = 0.046). No particular trend was found in regard to the relationship between oocyte abundance (number of oocytes/mm^2) and temperature (**Figure 5**; Linear regression, R^2 = 0.4, F = 4.34, df = 4, p = 0.1). The overall abundance of oocytes was significantly lower than that in the shallow zone (**Figure 5**; Student's t-test: t = 2.813, df = 18.715, p = 0.01122).

Axinella Polypoides

A total of 265 individuals were collected from the shallow and mesophotic populations. The individuals collected from the shallow zone ranged in height from 5 to 15 cm, and in the mesophotic zone, they ranged from 30 to 60 cm in height. No

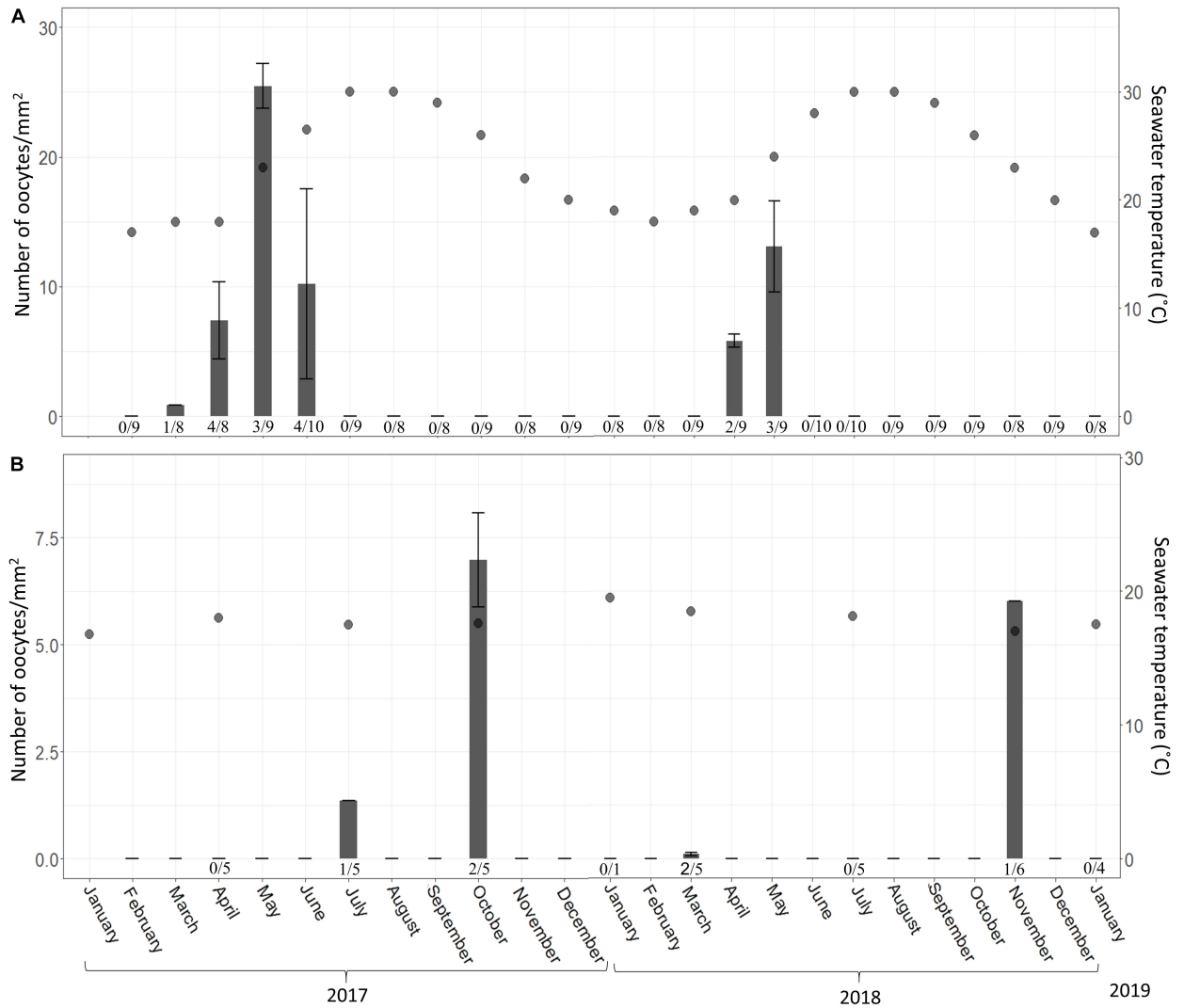

FIGURE 5 | *C. reniformis* oocyte abundance (# oocytes per mm^2 ± SD) at 3 m **(A)** and 100 m **(B)** between February 2017–January 2019 and January 2017–January 2019, respectively. Shallow-water samples were collected monthly; mesophotic samples were collected seasonally. An arrow marks the month when spermatocytes were found. Number below bars is the number of individuals containing oocytes out of total number of individuals collected.

male reproductive elements were recorded during this study from either habitat. In the shallow zone, 21% of the individuals (52\222) contained oocytes, and in the mesophotic zone, ca. 60% (26\43) contained oocytes. Oocytes were observed throughout the mesohyl, with the exception of the sponge axis, which is comprised mainly of dense spongin fibers. Oocyte shape was roughly oval with well-defined borders, but occasionally appeared amorphous, possibly due to physical constraints by other structures in the sponge (i.e., choanocyte chambers, spongin fibers, and canals; **Figure 6**). Oocyte diameter in the shallow-zone sponges ranged from 24 to 112 μm (**Figure 7A** and **Supplementary Table 6**); and in the mesophotic zone from 26 to 120 μm, throughout the study period (**Figure 7B** and **Supplementary Table 7**). Oocyte size variation in each month was high, but in the mesophotic zone the variation was generally significantly higher than in the shallow zone (mean standard deviation 16.9 ± 2 and 12.3 ± 3.8, respectively, Student's *t*-test, $t = 2.55$, $df = 7.55$, $p = 0.035$). This variation is mostly attributed to within-specimen differences. Apart from the differences in size, no other morphological differences could be seen between oocytes from different individuals or dates (**Figure 6**).

In the shallow zone, oocyte abundance followed the temperature pattern: increasing with temperature rise and decreasing when the temperature dropped. For example, the mean number of oocyte per mm^2 increased from 0.28 in May 2017 to 7.04 in July 2017 and then decreased to 0.25 in February 2018 (**Figure 8A** and **Supplementary Table 8**; Linear regression: $R^2 = 0.47$, $F = 19.5$, $p < 0.001$). The abundance of oocytes in the mesophotic zone appeared to be rather constant (0.5–2.5 oocyte per mm^2) along with the constant temperature (**Figure 8B** and **Supplementary Table 9**), with the exception of July 2017, during which a higher abundance was observed. The proportion of reproducing individuals in the shallow zone also varied in accordance with temperature fluctuations (**Figures 7**, **8**). The

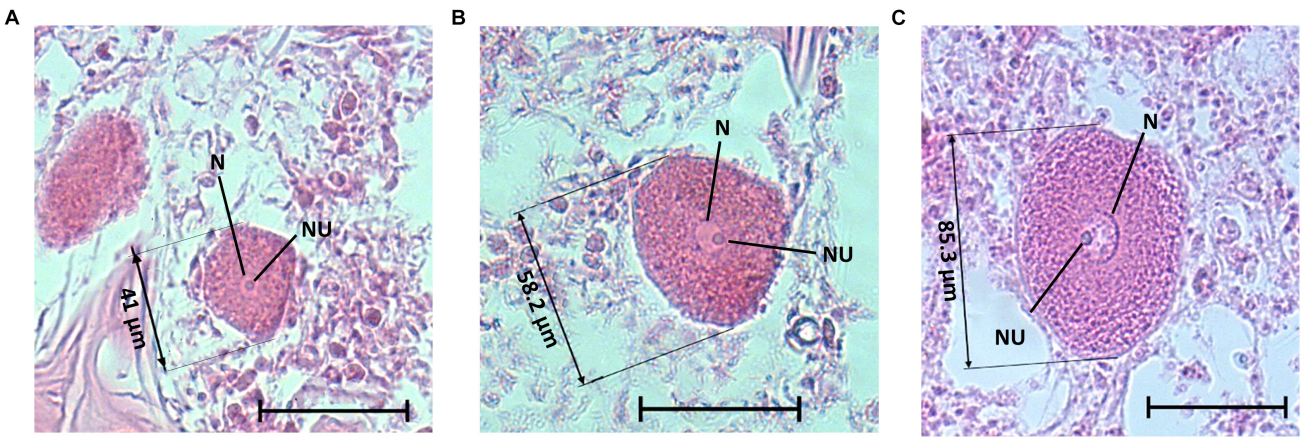

FIGURE 6 | *A. polypoides* oocytes of different sizes from the shallow water, with nucleus, nucleolus, and size of the oocyte. **(A)** Oocyte from *A. polypoides* sampled in June 2017, **(B)** Oocyte from *A. polypoides* sampled in August 2017, **(C)** Oocyte from *A. polypoides* sampled in September 2017. Scale bar is 50 µm. N, nucleus; NU, nucleolus.

strong positive relationship explains approximately 70% of this variance (Linear regression: $R^2 = 0.69$, $F = 49.7$, $p < 0.0001$).

DISCUSSION

A. polypoides and *C. reniformis* are two of the few species that span the entire depth range between 15–130 and 0.5–130 m depth, respectively, along the Israeli coast of the Mediterranean. Here we examined the differences in the reproductive cycles of these two common species, between the mesophotic and the shallow habitats, which have markedly different abiotic conditions (i.e., constant vs. dynamic temperature and light regimes, respectively). Both genera are known to be oviparous (Alvarez and Hooper, 2002; Maldonado and Riesgo, 2009b; Di Camillo et al., 2012), but knowledge regarding the two species' reproductive cycles has been published only for *C. reniformis* in the shallow water (Riesgo and Maldonado, 2008; Di Camillo et al., 2012). This study is the first to report the reproduction patterns of mesophotic populations and compare them with those of shallow-water populations.

Chondrosia Reniformis

The pattern of oocyte development and abundance observed in *C. reniformis* in the shallow habitat revealed seasonality. Oocyte abundance increased with rising seawater temperature, with a peak in May (when the temperature reached 23°C). The decrease in oocyte abundance in June may be related to the release of fully developed oocytes into the environment, in agreement with the pattern reported for this species in other studies in the Mediterranean (Riesgo and Maldonado, 2008; Yaniv, 2013). Spermatogenesis in *C. reniformis* appears to be rapid and has been documented to last less than a month, and it usually coincides with the peak of oogenesis around July and August (Riesgo and Maldonado, 2008; Di Camillo et al., 2012; Yaniv, 2013). In the present study, spermatocytes were observed only in June 2017, probably synchronized with the final developmental stage of the oocytes (**Figure 3A**).

The reproductive cycle in *C. reniformis* is believed to be governed by temperature. Oogenesis starts soon after the water temperature begins to rise, and the oocytes are released before the temperature peak (Riesgo and Maldonado, 2008; Yaniv, 2013). In another study, oocytes were found year-round, with maximum abundance in August, when the temperature was highest (Di Camillo et al., 2012). Thus, in the present study we expected the individuals from the mesophotic habitat, where the temperature is relatively constant and much below summer temperature in the shallow water (16.5–20°C), to exhibit a different pattern of the reproductive cycle. Indeed, the pattern observed in the mesophotic habitat markedly differed from the shallow one. The mean oocyte diameter in the mesophotic zone was larger (32.6 ± 5.8, range 20–49 µm) than in the shallow water (27.1 ± 9.3, range 9–49 µm; current study; Yaniv, 2013), and closer to what is known from the Adriatic Sea (32.6 ± 8.6 µm, range 20–75 µm; Di Camillo et al., 2012) and the Western Mediterranean (average not specified, range 35–65 µm; Riesgo and Maldonado, 2008; Di Camillo et al., 2012). Moreover, maximal oocyte diameter in the mesophotic specimens were similar to those of the fully developed oocytes from the shallow water (49 µm). Still, their morphology differed, indicating that the former were not yet mature, as nurse cells and cytoplasmic bridges were not evident in the mesophotic oocytes (Riesgo and Maldonado, 2008). It stands to reason that a higher sampling effort (i.e., monthly) would have also yielded mature oocytes.

The abundance of mesophotic oocytes was lower than in the shallow habitat's specimens, and similar to what is known from the above-noted studies from the Adriatic and the Western Mediterranean Sea (Riesgo and Maldonado, 2008; Di Camillo et al., 2012).

The intriguing phenomenon of low male ratio (and no males in A. polypoides) was documented in many sponge studies (Ayling, 1980; Corriero et al., 1998; Mercurio et al., 2007;

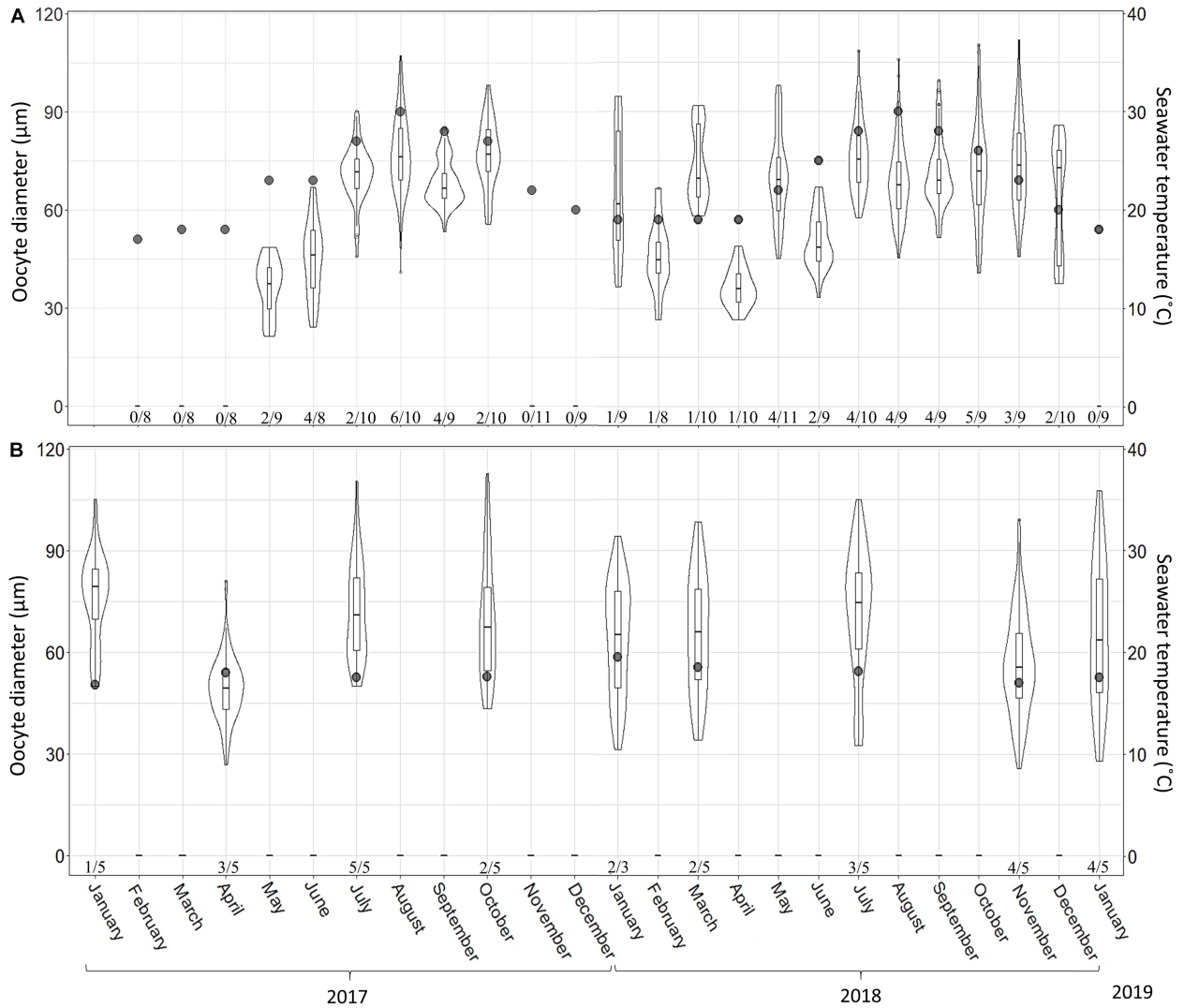

FIGURE 7 | *A. polypoides* oocyte diameter at 30 m **(A)** and 100 m **(B)** depth between February 2017–January 2019 and January 2017–January 2019, respectively. Shallow-water samples were collected monthly; mesophotic samples were collected seasonally. Maximal oocyte diameter was measured (30 oocytes were measured per sponge; if 30 oocytes were not found, the maximal number found was noted). Number below bars is the number of individuals containing oocytes out of total number of individuals collected. Violin plot shows size distribution, and the box plot within the violin shows quartiles and median.

Leong and Pawlik, 2011; Ereskovsky et al., 2017); the absence of males might be due to a very short period of spermatogenesis, as was previously shown for several sponge species (Ayling, 1980; Fromont and Bergquist, 1994; Riesgo and Maldonado, 2008; Maldonado and Riesgo, 2009a; Ereskovsky, 2010).

While in some species asexual reproduction, usually by forming of gemmules, is associated with stressful environmental conditions (Fell, 1992; Ereskovsky, 2010), fragmentation and budding represents an important reproductive strategy for many species (Wulff, 1991; Corriero et al., 1996; Tsurumi and Reiswig, 1997; Maldonado and Uriz, 1999). including *C. reniformis* (Riesgo and Maldonado, 2008).

In *C. reniformis*, asexual reproduction is achieved by creeping and budding (Di Camillo et al., 2012; Fassini et al., 2012). Asexual reproduction may explain how, this is the most abundant sponge species in the mesophotic zone, densely covering large areas, thriving on every surface and even growing over other sponges, despite the lower fecundity (Idan et al., 2018; **Figure 1A**). This may indicate that *C. reniformis* prefers asexual over sexual reproduction in the colder and more stable conditions of the mesophotic zone. The phenomenon of high rates of asexual reproduction in stable environmental conditions was also shown for *Chondrilla* spp. (Zilberberg et al., 2006).

In the shallow habitat, where less favorable conditions exist and *C. reniformis* distribution is limited to semi-dark and patchy areas, such as crevices and overhangs (Wilkinson and Vacelet, 1979; **Figure 1B**), sexual reproduction may be more beneficial as the sponge larva are mobile which allow them to find suitable patches to settle (Leong and Pawlik, 2010). Additionally, the genetic diversity produced by sexual reproduction may elevate its

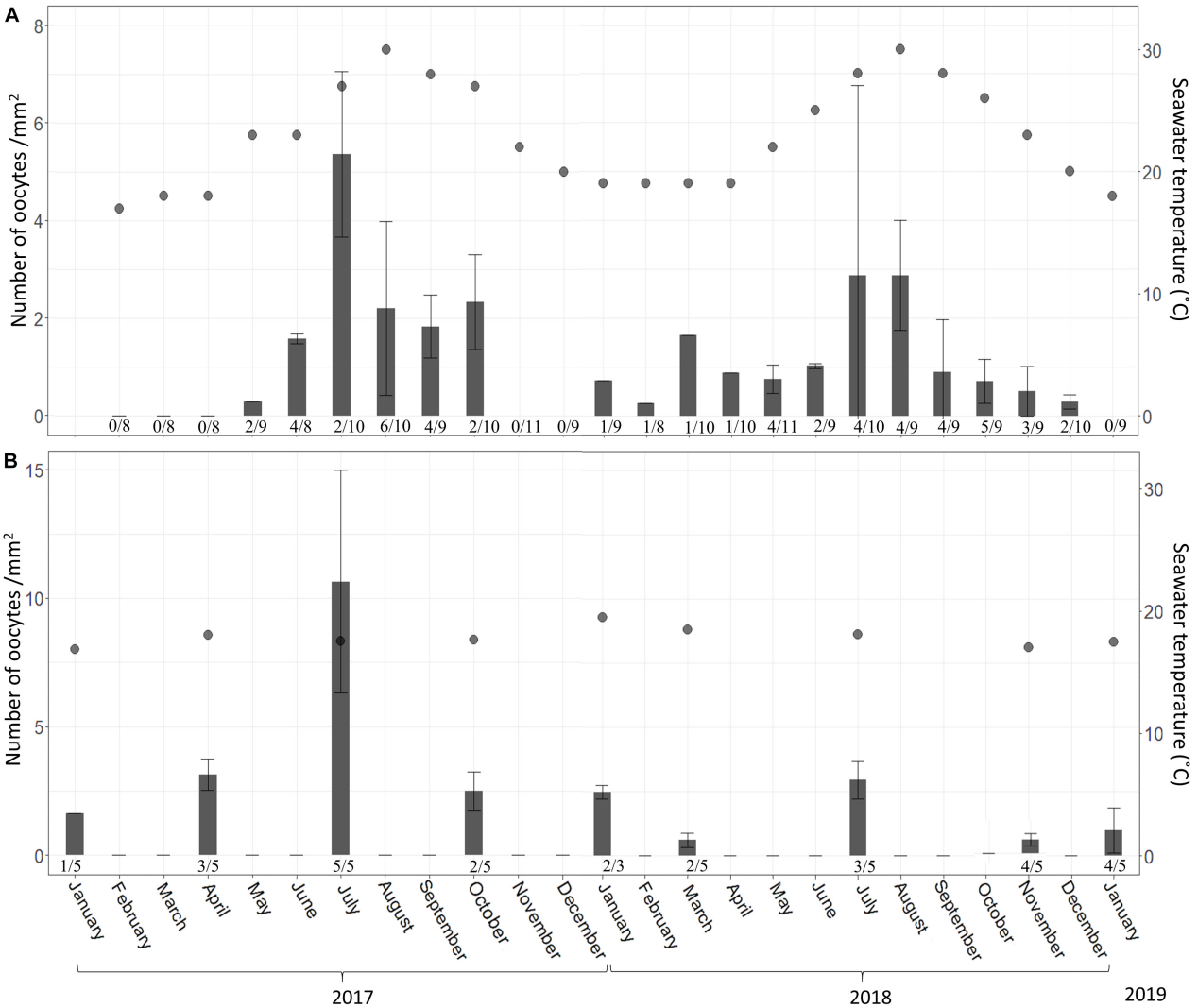

FIGURE 8 | *A. polypoides* oocyte abundance (# oocytes per mm^2 ± SD) at 30 m **(A)** and 100 m **(B)** depth between February 2017–January 2019 and January 2017–January 2019, respectively. Shallow-water samples were collected monthly; mesophotic samples were collected seasonally. Number below bars is the number of individuals containing oocytes out of total number of individuals collected.

fitness allowing C. *reniformis* in the shallow habitat to cope with the harsher and more variable conditions there (Hoekstra, 2005; Leong and Pawlik, 2010).

Axinella Polypoides

This is the first detailed description of a true Axinellid's (Gazave et al., 2010) reproduction cycle.

A. polypoides demonstrated a seasonal pattern of reproduction in the shallow habitat. Both the proportion of reproducing individuals and oocyte abundance increased from early winter to mid-summer, and thereafter decreased, probably due to release of the oocytes. The above-mentioned pattern has been observed in most of the studied sponges in the Mediterranean Sea (Elvin, 1976; Fell, 1976; Meroz-Fine et al., 2005; Riesgo and Maldonado, 2008; Maldonado and Riesgo, 2009a; Di Camillo et al., 2012), with temperature thought to be one of the main factors regulating sponge reproduction (Elvin, 1976; Fell, 1976; Simpson, 1984; Maldonado and Riesgo, 2009a). In contrast, *A. polypoides* from the mesophotic habitat appeared to be reproducing year-round: on every sampling date oocytes were found in at least some of the specimens, including in January and April 2017 and January 2019 when the adjacent shallow-water individuals were not found to be reproducing. Only a few sponge species in the Mediterranean have been reported to reproduce year-round (Riesgo et al., 2007; Maldonado and Riesgo, 2008; Riesgo and Maldonado, 2008; Di Camillo et al., 2012). However, this phenomenon was described only in one locality: the northern Adriatic Sea, whereas in other parts of the Mediterranean, the reproduction of the same species was described as seasonal (Riesgo and Maldonado, 2008; Di Camillo et al., 2012). Our present results indicate that, compared to shallow-water populations, mesophotic *A. polypoides* sponges invest more in sexual reproduction, as

reflected in the higher proportion of reproducing individuals (20–100%) and a more substantial variation in oocyte diameter. Our findings demonstrate that the variance in size of the oocytes in *A. polypoides* is an indicator of their developmental stage, suggesting a greater asynchronization of reproduction both within the population and among individuals in the mesophotic habitat. It has been postulated that the continuous oogenesis found in the northern Adriatic could be due to the high availability of food, which enables sponges to invest their energy surplus in oocyte production (Di Camillo et al., 2012). While the differences in nutrient availability between the Israeli mesophotic and shallow habitats are negligible (Idan, 2020), we suggest that the stability of other environmental conditions in the mesophotic zone could allow *A. polypoides* to invest its energy surplus in reproduction, thus, explaining the higher reproduction effort there. Moreover, it appears that the Israeli shallow habitat represents the edge of distribution of *A. polypoides*, as it is scarcer and individuals are much smaller there than in the mesophotic habitat (**Figures 1C,D**) and other parts of the Mediterranean.

In summary, while the reproduction of *C. reniformis* and *A. polypoides* differed in many aspects, such as oocyte abundance and morphology, both species appear to possess a degree of plasticity in their reproduction strategies with regard to temperature and depth. Temperature would seem to regulate the reproduction of both species in the shallow water, whereas, in the mesophotic zone, the temperature amplitude is much smaller and thus, other factors may be at play. Although both the studied species are oviparous and gonochoristic, they employ different reproductive strategies in the different habitats. *C. reniformis* exhibited low fecundity in the mesophotic zone, and probably invested more in asexual reproduction by budding and fragmentation. Asexual reproduction in *C. reniformis* is considered highly effective, since fragmented individuals quickly regenerate their body wall and attach themselves to the substrate (Parma et al., 2007; Di Camillo et al., 2012; Fassini et al., 2012). While reproduction by means of fragmentations is known to be the primary mode of recruitment in some rope-like and branching sponges (Wulff, 1991, 1995; Tsurumi and Reiswig, 1997), in *A. polypoides*, in contrast, fragments do not seem to re-attach to the substrate, even though they maintain vital signs (i.e., open oscula, and preserved ectosome integrity; Idan unpubl.). Consequently, even though stable conditions favor asexual reproduction by fragmentation, this strategy is not well suited for *A. polypoides*. Instead, it exhibits a shift from seasonal reproduction toward continuous sexual reproduction.

The results of this study, as well as other studies comparing sponge reproduction in different habitats (e.g., Meroz-Fine et al., 2005; Whalan et al., 2007; Maria et al., 2013; Zarrouk et al., 2013), suggest that reproduction plasticity may be a general rule for sponge species that grow in diverse habitats, allowing sponges to thrive along a wide range of environmental conditions.

Globally, shallow reefs (including sponges), are facing the deleterious effects of rising seawater temperatures (Garrabou et al., 2009, 2019; Cerrano et al., 2019; Ereskovsky et al., 2019). The deep reef refuge hypothesis suggests that the upper mesophotic reefs (30–60 m) may serve as a larval source for the adversely impacted shallow reefs (Lesser et al., 2009; Semmler et al., 2017). However, this hypothesis has been rejected for some coral species, as recent studies have demonstrated a reduced fecundity in mesophotic corals (Feldman et al., 2018; Shlesinger et al., 2018; Shlesinger and Loya, 2019) as well as low larval connectivity (Bongaerts et al., 2010, 2017). Although our current knowledge of the reproductive strategies and connectivity of mesophotic sponges, and especially of lower mesophotic communities, is very limited (Maldonado et al., 2017; Cerrano et al., 2019; Pomponi et al., 2019), our findings, along with those of other recent studies, suggest that mesophotic sponge grounds may act as a deep refuge for some sponge species (Meroz-Fine et al., 2005; Idan et al., 2018; Cerrano et al., 2019; Pomponi et al., 2019; Idan, 2020). As different species may exhibit diverse adaptations to environmental conditions that can affect their larval behavior and ability to settle in shallower habitats, the deep refuge hypothesis should be considered with respect to mesophotic sponge communities. Understanding the role of mesophotic sponge grounds as potential source of larvae is especially important, in face of the anthropogenic disturbances and rise in seawater temperatures, that are already affecting sponges in the shallow Israeli coast (Idan et al., 2018; Idan, 2020).

DATA AVAILABILITY STATEMENT

The original contributions presented in the study are included in the article/**Supplementary Material**, further inquiries can be directed to the corresponding author/s.

AUTHOR CONTRIBUTIONS

TI conceived of the study, designed the study, carried out the fieldwork, carried out the data and statistical analyses and drafted the manuscript. LG participated in collection of field data and data analysis and helped draft the manuscript. SS participated in the design of the study, participated in fieldwork, and critically revised the manuscript. IB prepared most of the histological sections and helped with data analysis. MI helped design the study, coordinated the study, and critically revised the manuscript. All authors gave final approval for publication and agreed to be held accountable for the work performed therein.

FUNDING

The study was supported by the Israeli Ministry of Science, Technology, and Space (The Program for the Development of Scientific and Technological Infrastructure, grant no. 3-10343 to MI); the Israeli Ministry of National Infrastructure, Energy and Water (grant no. 217-17-020 to MI); and partially supported by the ISF-NSFC joint research program (grant no. 2577/18 to MI). TI was supported by the Shulamit Aloni fellowship from the Israeli Ministry of Science, Technology, and Space.

ACKNOWLEDGMENTS

The NGO EcoOcean for providing the facility for marine research onboard the R/V Mediterranean Explorer and for the operation of the ROV. Oded Ezra and Itai Katzman who piloted the ROV. The students of MI's group who volunteered for sponge collections during the many dives and cruises on-board the research vessel. Rahaf NGO that provided the boat for the shallow water dives. The undergraduate students, Daniel Raizman, Gal Kaplan, and Erica Manor, for their help preparing the samples. Naomi Paz who edited the manuscript. Collection permit was given by the Israel Nature and Parks Authority.

SUPPLEMENTARY MATERIAL

The Supplementary Material for this article can be found online at: https://www.frontiersin.org/articles/10.3389/fmars.2020.610565/full#supplementary-material

REFERENCES

Alvarez, B., and Hooper, J. N. (2002). "Family axinellidae carter, 1875," in *Systema Porifera*, eds R. W. M. van Soest and J. Hooper (Berlin: Springer), 724–747. doi: 10.1007/978-1-4615-0747-5_80

Ayling, A. L. (1980). Patterns of sexuality, asexual reproduction and recruitment in some subtidal marine Demospongiae. *Biol. Bull.* 158, 271–282. doi: 10.2307/1540854

Beazley, L. I., Kenchington, E. L., Murillo, F. J., and Sacau, M. D. (2013). Deep-sea sponge grounds enhance diversity and abundance of epibenthic megafauna in the Northwest Atlantic. *ICES J. Mar. Sci.* 70, 1471–1490. doi: 10.1093/icesjms/fst124

Bo, M., Bertolino, M., Bavestrello, G., Canese, S., Giusti, M., Angiolillo, M., et al. (2012). Role of deep sponge grounds in the Mediterranean Sea: a case study in southern Italy. *Hydrobiologia* 687, 163–177. doi: 10.1007/978-94-007-4688-6_14

Bongaerts, P., Ridgway, T., Sampayo, E., and Hoegh-Guldberg, O. (2010). Assessing the 'deep reef refugia' hypothesis: focus on Caribbean reefs. *Coral Reefs* 29, 309–327. doi: 10.1007/s00338-009-0581-x

Bongaerts, P., Riginos, C., Brunner, R., Englebert, N., Smith, S. R., and Hoegh-Guldberg, O. (2017). Deep reefs are not universal refuges: reseeding potential varies among coral species. *Sci. Adv.* 3:e1602373. doi: 10.1126/sciadv.1602373

Cerrano, C., Bastari, A., Calcinai, B., Di Camillo, C., Pica, D., Puce, S., et al. (2019). Temperate mesophotic ecosystems: gaps and perspectives of an emerging conservation challenge for the Mediterranean Sea. *Eur. Zool. J.* 86, 370–388. doi: 10.1080/24750263.2019.1677790

Coll, M., Piroddi, C., Steenbeek, J., Kaschner, K., Lasram, F. B., Aguzzi, J., et al. (2010). The biodiversity of the mediterranean sea: estimates, patterns, and threats. *PLoS One* 5:e11842. doi: 10.1371/journal.pone.0011842

Corriero, G., Liaci, L. S., Marzano, C. N., and Gaino, E. (1998). Reproductive strategies of *Mycalecontarenii* (Porifera: Demospongiae). *Mar. Biol.* 131, 319–327. doi: 10.1007/s002270050325

Corriero, G., Sarà, M., and Vaccaro, P. (1996). Sexual and asexual reproduction in two species of Tethya (Porifera: Demospongiae) from a Mediterranean coastal lagoon. *Mar. Biol.* 126, 175–181. doi: 10.1007/bf00347442

Di Camillo, C., Coppari, M., Bartolucci, I., Bo, M., Betti, F., Bertolino, M., et al. (2012). Temporal variations in growth and reproduction of *Tedania anhelans* and *Chondrosia reniformis* in the North Adriatic Sea. *Hydrobiologia* 687, 299–313. doi: 10.1007/978-94-007-4688-6_25

Elvin, D. W. (1976). Seasonal growth and reproduction of an intertidal sponge, *Haliclona permollis* (Bowerbank). *Biol. Bull.* 151, 108–125. doi: 10.2307/1540709

Ereskovsky, A., Ozerov, D. A., Pantyulin, A. N., and Tzetlin, A. B. (2019). Mass mortality event of White Sea sponges as the result of high temperature in summer 2018. *Polar Biol.* 42, 2313–2318. doi: 10.1007/s00300-019-02606-0

Ereskovsky, A. V. (2010). *The Comparative Embryology of Sponges*. Cham: Springer Science & Business Media.

Ereskovsky, A. V., Geronimo, A., and Pérez, T. (2017). Asexual and puzzling sexual reproduction of the Mediterranean sponge Haliclona fulva (Demospongiae): life cycle and cytological structures. *Invertebr. Biol.* 136, 403–421. doi: 10.1111/ivb.12195

Fassini, D., Parma, L., Wilkie, I. C., Bavestrello, G., Bonasoro, F., and Carnevali, M. D. C. (2012). Ecophysiology of mesohyl creep in the demosponge *Chondrosia reniformis* (Porifera: Chondrosida). *J. Exp. Mar. Biol. Ecol.* 428, 24–31. doi: 10.1016/j.jembe.2012.05.025

Feldman, B., Shlesinger, T., and Loya, Y. (2018). Mesophotic coral-reef environments depress the reproduction of the coral *Paramontastraea peresi* in the Red Sea. *Coral Reefs* 37, 201–214. doi: 10.1007/s00338-017-1648-8

Fell, P. E. (1976). The reproduction of *Haliclona loosanoffi* and its apparent relationship to water temperature. *Biol. Bull.* 150, 200–210. doi: 10.2307/1540468

Fell, P. E. (1992). "Porifera," in *Reproductive Biology of Invertebrates*, eds K. G. Adiyodi and R. G. Adiyodi (Oxford: Oxford & IBH publishing co. pvt. ltd), 1–44.

Fromont, J., and Bergquist, P. (1994). Reproductive biology of three sponge species of the genus *Xestospongia* (Porifera: Demospongiae: Petrosida) from the Great Barrier Reef. *Coral Reefs* 13, 119–126. doi: 10.1007/bf00300772

Garrabou, J., Coma, R., Bensoussan, N., Bally, M., Chevaldonné, P., Cigliano, M., et al. (2009). Mass mortality in Northwestern Mediterranean rocky benthic communities: effects of the 2003 heat wave. *Glob. Change Biol.* 15, 1090–1103. doi: 10.1111/j.1365-2486.2008.01823.x

Garrabou, J., Gómez-Gras, D., Ledoux, J.-B., Linares, C., Bensoussan, N., López-Sendino, P., et al. (2019). Collaborative database to track mass mortality events in the Mediterranean Sea. *Front. Mar. Sci.* 6:707. doi: 10.3389/fmars.2019.00707

Gazave, E., Carteron, S., Chenuil, A., Richelle-Maurer, E., Boury-Esnault, N., and Borchiellini, C. (2010). Polyphyly of the genus *Axinella* and of the family Axinellidae (Porifera: Demospongiaep). *Mol. Phylogenet. Evol.* 57, 35–47. doi: 10.1016/j.ympev.2010.05.028

Gerovasileiou, V., Chintiroglou, C. C., Konstantinou, D., and Voultsiadou, E. (2016). Sponges as "living hotels" in Mediterranean marine caves. *Sci. Mar.* 80, 279–289. doi: 10.3989/scimar.04403.14b

Hinderstein, L., Marr, J., Martinez, F., Dowgiallo, M., Puglise, K., Pyle, R., et al. (2010). Theme section on "Mesophotic coral ecosystems: characterization, ecology, and management". *Coral Reefs* 29, 247–251. doi: 10.1007/s00338-010-0614-5

Hoekstra, R. F. (2005). Why sex is good. *Nature* 434, 571–573. doi: 10.1038/434571a

Hooper, J. N., and Van Soest, R. W. (2002). "Class demospongiae sollas, 1885," in *Systema Porifera*, eds R. W. M. van Soest and J. Hooper (Springer), 15–51. doi: 10.1007/978-1-4615-0747-5_3

Idan, T. (2020). *Mesophotic sponge grounds in the Levant basin: Community composition and dynamics*. Ph.D. thesis, Tel Aviv University, Tel Aviv-Yafo.

Idan, T., Shefer, S., Feldstein, T., Yahel, R., Huchon, D., and Ilan, M. (2018). Shedding light on an East-Mediterranean mesophotic sponge ground community and the regional sponge fauna. *Mediterranean Mar. Sci.* 19, 84–106. doi: 10.12681/mms.13853

Kahng, S., Garcia-Sais, J., Spalding, H., Brokovich, E., Wagner, D., Weil, E., et al. (2010). Community ecology of mesophotic coral reef ecosystems. *Coral Reefs* 29, 255–275. doi: 10.1007/s00338-010-0593-6

Kenchington, E., Power, D., and Koen-Alonso, M. (2013). Associations of demersal fish with sponge grounds on the continental slopes of the northwest Atlantic. *Mar. Ecol. Prog. Ser.* 477, 217–230. doi: 10.3354/meps10127

Kress, N., Gertman, I., and Herut, B. (2014). Temporal evolution of physical and chemical characteristics of the water column in the Easternmost Levantine basin (Eastern Mediterranean Sea) from 2002 to 2010. *J. Mar. Syst.* 135, 6–13. doi: 10.1016/j.jmarsys.2013.11.016

Leong, W., and Pawlik, J. R. (2010). Fragments or propagules? Reproductive tradeoffs among *Callyspongia* spp. from Florida coral reefs. *Oikos* 119, 1417–1422. doi: 10.1111/j.1600-0706.2010.18092.x

Leong, W., and Pawlik, J. R. (2011). Comparison of reproductive patterns among 7 Caribbean sponge species does not reveal a resource trade-off with chemical defenses. *J. Exp. Mar. Biol. Ecol.* 401, 80–84. doi: 10.1016/j.jembe.2011.02.043

Lesser, M. P., Slattery, M., and Leichter, J. J. (2009). Ecology of mesophotic coral reefs. *J. Exp. Mar. Biol. Ecol.* 375, 1–8.

Locker, S., Armstrong, R., Battista, T., Rooney, J., Sherman, C., and Zawada, D. (2010). Geomorphology of mesophotic coral ecosystems: current perspectives on morphology, distribution, and mapping strategies. *Coral Reefs* 29, 329–345. doi: 10.1007/s00338-010-0613-6

Maldonado, M. (2006). The ecology of the sponge larva. *Can. J. Zool.* 84, 175–194. doi: 10.1139/z05-177

Maldonado, M., Aguilar, R., Bannister, R. J., Bell, J. J., Conway, K. W., Dayton, P. K., et al. (2017). "Sponge grounds as key marine habitats: a synthetic review of types, structure, functional roles, and conservation concerns," *in Marine Animal Forests: The Ecology of Benthic Biodiversity Hotspots*, eds S. Rossi, L. Bramanti, A. Gori, and C. O. Saco del Valle (Cham: Springer International Publishing), 145–183. doi: 10.1007/978-3-319-21012-4_24

Maldonado, M., and Riesgo, A. (2008). Reproductive output in a Mediterranean population of the homosclerophorid *Corticium candelabrum* (Porifera, Demospongiae), with notes on the ultrastructure and behavior of the larva. *Mar. Ecol.* 29, 298–316. doi: 10.1111/j.1439-0485.2008.00244.x

Maldonado, M., and Riesgo, A. (2009a). Gametogenesis, embryogenesis, and larval features of the oviparous sponge Petrosia ficiformis (Haplosclerida, Demospongiae). *Mar. Biol.* 156, 2181–2197. doi: 10.1007/s00227-009-1248-4

Maldonado, M., and Riesgo, A. (2009b). Reproduction in the phylum Porifera: a synoptic overview. *Treballs de la Societat Catalana de Biologia* 59, 29–49.

Maldonado, M., and Uriz, M. J. (1999). Sexual propagation by sponge fragments. *Nature* 398, 476–476. doi: 10.1038/19007

Maria, M., Giuseppe, C., Miriam, G., Rossella, B., and Gaino, E. (2013). Sexual reproduction in Sarcotragus spinosulus from two different shallow environments. *Mar. Ecol. Evol. Perspect.* 34, 394–408. doi: 10.1111/maec.12039

Mercurio, M., Corriero, G., and Gaino, E. (2007). A 3-year investigation of sexual reproduction in Geodia cydonium (Jameson 1811)(Porifera, Demospongiae) from a semi-enclosed Mediterranean bay. *Mar. Biol.* 151, 1491–1500. doi: 10.1007/s00227-006-0584-x

Meroz-Fine, E., Shefer, S., and Ilan, M. (2005). Changes in morphology and physiology of an East Mediterranean sponge in different habitats. *Mar. Biol.* 147, 243–250. doi: 10.1007/s00227-004-1532-2

Morrow, C., and Cárdenas, P. (2015). Proposal for a revised classification of the Demospongiae (Porifera). *Front. Zool.* 12:7. doi: 10.1186/s12983-015-0099-8

Parma, L., Fassini, D., Bavestrello, G., Wilkie, I. C., Bonasoro, F., and Carnevali, M. C. (2007). "Ecology and physiology of mesohyl creep in Chondrosia reniformis," in *Porifera Research: Biodiversity, Innovation, Sustainability. Proc. 7th International Sponge Symposium*, (Rio de Janeiro: Museu Nacional), 503–508.

Pomponi, S. A., Diaz, M. C., Van Soest, R. W., Bell, L. J., Busutil, L., Gochfeld, D. J., et al. (2019). "Sponges," in *Mesophotic Coral Ecosystems*, eds K. A. Puglise, Y. Loya, and T. C.L. Bridge (Cham: Springer), 563–588.

R Core Team (2020). *R: A Language and Environment for Statistical Computing (Version 4.02)[Software package]*. Vienna: R Foundation for Statistical Computing.

R Core Team, Maintainer, Suggests, M., and Matrix, S. (2018). *Package stats. The R Stats Package*. Vienna: R Foundation for Statistical Computing.

Riesgo, A., and Maldonado, M. (2008). Differences in reproductive timing among sponges sharing habitat and thermal regime. *Invertebr. Biol.* 127, 357–367. doi: 10.1111/j.1744-7410.2008.00128.x

Riesgo, A., Maldonado, M., and Durfort, M. (2007). Dynamics of gametogenesis, embryogenesis, and larval release in a Mediterranean homosclerophorid demosponge. *Mar. Freshw. Res.* 58, 398–417. doi: 10.1071/mf06052

Riesgo, A. G. (2007). *Sexual Reproduction in Demosponges: Ecological and Evolutive Implications/Reproducción sexual en Demosponjas: Implicaciones ecológicas y evolutivas*. Ph.D. thesis, Universidad de Barcelona, Barcelona.

R Studio Team (2020). *R Studio: Integrated Development for R (version 1.1. 463)[Computer Software]*. Boston: RStudio, Inc.

Sará, M., Adiyodi, K., and Adiyodi, R. (1992). Porifera. *Reproduct. Biol. Invertebr.* 5, 1–29.

Semmler, R. F., Hoot, W. C., and Reaka, M. L. (2017). Are mesophotic coral ecosystems distinct communities and can they serve as refugia for shallow reefs? *Coral Reefs* 36, 433–444. doi: 10.1007/s00338-016-1530-0

Shlesinger, T., Grinblat, M., Rapuano, H., Amit, T., and Loya, Y. (2018). Can mesophotic reefs replenish shallow reefs? Reduced coral reproductive performance casts a doubt. *Ecology* 99, 421–437. doi: 10.1002/ecy.2098

Shlesinger, T., and Loya, Y. (2019). "Sexual reproduction of scleractinian corals in mesophotic coral ecosystems vs. shallow reefs," in *Mesophotic Coral Ecosystems*, eds K. A. Puglise, Y. Loya, and T. C.L. Bridge (Cham: Springer), 653–666. doi: 10.1007/978-3-319-92735-0_35

Simpson, T. L. (ed.) (1984). "Gamete, embryo, larval development," in *The Cell Biology of Sponges*, (Cham: Springer), 341–413. doi: 10.1007/978-1-4612-5214-6_7

Smith, T., Blondeau, J., Nemeth, R., Pittman, S., Calnan, J., Kadison, E., et al. (2010). Benthic structure and cryptic mortality in a Caribbean mesophotic coral reef bank system, the Hind Bank Marine Conservation District, US Virgin Islands. *Coral Reefs* 29, 289–308. doi: 10.1007/s00338-009-0575-8

Tsurumi, M., and Reiswig, H. M. (1997). Sexual versus asexual reproduction in an oviparous rope-form sponge, *Aplysina cauliformis* (Porifera; Verongida). *Invertebr. Reproduct. Dev.* 32, 1–9. doi: 10.1080/07924259.1997.9672598

Usher, K. M., Sutton, D. C., Toze, S., Kuo, J., and Fromont, J. (2004). Sexual reproduction in *Chondrilla australiensis* (Porifera: demospongiae). *Mar. Freshw. Res.* 55, 123–134. doi: 10.1071/mf03058

Voultsiadou, E. (2009). Reevaluating sponge diversity and distribution in the Mediterranean Sea. *Hydrobiologia* 628, 1–12. doi: 10.1007/s10750-009-9725-9

Whalan, S., Battershill, C., and De Nys, R. (2007). Variability in reproductive output across a water quality gradient for a tropical marine sponge. *Mar. Biol.* 153, 163–169. doi: 10.1007/s00227-007-0792-z

Wilkinson, C. R., and Vacelet, J. (1979). Transplantation of marine sponges to different conditions of light and current. *J. Exp. Mar. Biol. Ecol.* 37, 91–104. doi: 10.1016/0022-0981(79)90028-5

Witte, U. (1996). Seasonal reproduction in deep-sea sponges-triggered by vertical particle flux? *Mar. Biol.* 124, 571–581. doi: 10.1007/bf00351038

Wulff, J. (1995). Effects of a hurricane on survival and orientation of large erect coral reef sponges. *Coral Reefs* 14, 55–61. doi: 10.1007/bf00304073

Wulff, J. L. (1991). Asexual fragmentation, genotype success, and population dynamics of erect branching sponges. *J. Exp. Mar. Biol. Ecol.* 149, 227–247. doi: 10.1016/0022-0981(91)90047-z

Yaniv, M.-T. (2013). *Life Cycle, Abundance and Distribution of the Mediterranean sponge Chondrosia reniformis*. M.Sc. thesis, Tel Aviv University, Tel Aviv-Yafo.

Zarrouk, S., Ereskovsky, A. V., Mustapha, K. B., Abed, A. E., and Pérez, T. (2013). Sexual reproduction of *Hippospongia communis* (Lamarck, 1814)(Dictyoceratida, Demospongiae): comparison of two populations living under contrasting environmental conditions. *Mar. Ecol.* 34, 432–442. doi: 10.1111/maec.12043

Zilberberg, C., Solé-Cava, A. M., and Klautau, M. (2006). The extent of asexual reproduction in sponges of the genus *Chondrilla* (Demospongiae: Chondrosida) from the Caribbean and the Brazilian coasts. *J. Exp. Mar. Biol. Ecol.* 336, 211–220. doi: 10.1016/j.jembe.2006.05.010

Conflict of Interest: The authors declare that the research was conducted in the absence of any commercial or financial relationships that could be construed as a potential conflict of interest.

Copyright © 2020 Idan, Goren, Shefer, Brickner and Ilan. This is an open-access article distributed under the terms of the Creative Commons Attribution License (CC BY). The use, distribution or reproduction in other forums is permitted, provided the original author(s) and the copyright owner(s) are credited and that the original publication in this journal is cited, in accordance with accepted academic practice. No use, distribution or reproduction is permitted which does not comply with these terms.

frontiers in Marine Science

ORIGINAL RESEARCH
published: 08 December 2020
doi: 10.3389/fmars.2020.603593

Sponges in a Changing Climate: Survival of *Agelas oroides* in a Warming Mediterranean Sea

Tal Idan[1], Liron Goren[1,2], Sigal Shefer[1,2] and Micha Ilan[1]*

[1] School of Zoology, George S. Wise Faculty of Life Sciences, Tel Aviv University, Tel Aviv, Israel, [2] The Steinhardt Museum of Natural History, Israel National Center for Biodiversity Studies, Tel Aviv University, Tel Aviv, Israel

Sponges hold a key role in benthic environments, and specifically in the Mediterranean Sea. Past events of mass mortality in sponge communities have been linked to extended periods of high-temperature anomalies, yet it is unknown how a gradual change, such as the constant rise in global seawater temperatures, will affect biodiversity. Here we present a case study of *Agelas oroides*, a common massive sponge in the Mediterranean Sea, found at a wide depth range of 1–150 m. Last documented in the 1970s, *A. oroides* was considered lost from the Israeli coastal fauna. However, its recent rediscovery in mesophotic depths, where environmental conditions are stable, provided an opportunity to examine whether it can survive the present conditions in the shallow Israeli coast – where temperatures increased by 3°C during the past 60 years, while the nutrients concentration decreased following the damming of the Nile River. To test this hypothesis, *A. oroides* individuals were collected during winter from mesophotic sponge grounds (100–120 m) and transplanted to a shallow rocky habitat (10 m). Control individuals were transplanted back to the mesophotic habitat. Sponge survival, temperature, and nutrient concentrations were measured in both habitats. The shallow-transplanted sponges' survival decreased only when the ambient temperature exceeded 28°C. In contrast, the control group at the mesophotic depth, where the temperature never rose above 20°C, survived the duration of the experiment. Our findings suggest that a prolonged period of high temperatures may constitute a major factor in *A. oroides* survival and disappearance from the Israeli shallow habitats.

Keywords: transplantation, mesophotic, sponge ground, 3D modeling, nutrients, marine ecology, temperature

OPEN ACCESS

Edited by:
Shirley A. Pomponi, Florida Atlantic University, United States

Reviewed by:
Giorgio Bavestrello, University of Genoa, Italy
Sergi Taboada, Autonomous University of Madrid, Spain

****Correspondence:***
Tal Idan
talidan@mail.tau.ac.il;
taltul.idan@gmail.com

Specialty section:
This article was submitted to Deep-Sea Environments and Ecology, a section of the journal Frontiers in Marine Science

Received: *07 September 2020*
Accepted: *13 November 2020*
Published: *08 December 2020*

Citation:
Idan T, Goren L, Shefer S and Ilan M (2020) Sponges in a Changing Climate: Survival of Agelas oroides in a Warming Mediterranean Sea. Front. Mar. Sci. 7:603593. doi: 10.3389/fmars.2020.603593

INTRODUCTION

Porifera (sponges) form the oldest metazoan phylum and have demonstrated resilience and survival under various environmental conditions over different geological eras (Feuda et al., 2017). Nonetheless, environmental conditions are considered a key factor in determining the dynamics of sponge spatial distribution, with temperature playing a central role (Garrabou et al., 2009, 2019; Di Camillo et al., 2013). For example, Mediterranean sponge diversity has been shown to follow an NNW-SSE gradient that correlates with an increase in water temperature and salinity and a decrease in nutrient concentration (Voultsiadou, 2009). In addition, several studies demonstrated that extended periods of high-temperature anomalies during the summer resulted in mass mortality

in sponge communities (Garrabou et al., 2009, 2019; Di Camillo et al., 2013; Ereskovsky et al., 2019). Furthermore, recent studies found that elevated temperatures led to significant physiological responses in several sponge species, such as a decrease in buoyant weight, prevalence of diseases, and an increase in mortality (Webster, 2007; Massaro et al., 2012; Bennett et al., 2017; Laffy et al., 2019; Beepat et al., 2020).

The present case-study species, *Agelas oroides* (Schmidt, 1864), is a sponge common to the Mediterranean Sea, at both shallow (<40 m) and mesophotic (40–150 m) depths (Voultsiadou, 2009; Topaloglu and Evcen, 2014; Costa et al., 2018; Grenier et al., 2018). It inhabits sheltered habitats with low light intensity (i.e., entrances to caves, crevices, or mesophotic habitats) (Tsurnamal, 1968; Gerovasileiou and Voultsiadou, 2012; Gerovasileiou et al., 2017; Grenier et al., 2018). It has an important ecological role, increasing the structural complexity of its surroundings and consequently providing a habitat for the invertebrates and fish that dwell in and on it (Bo et al., 2012; Beazley et al., 2013; Kenchington et al., 2013; Gerovasileiou et al., 2016). *A. oroides* has also proven to be an important source of many new natural products, some with demonstrated bioactivity, e.g., oroidin (Sauleau et al., 2017; Kovalerchik et al., 2020). *A. oroides* is thus of considerable interest in the ecological and biotechnological context and a meaningful study object.

It is therefore of concern that the distribution range of *A. oroides* in the Mediterranean appears to have decreased over time. Historically, *A. oroides* was considered abundant in the shallow water of the Israeli Mediterranean coast. Although few specimens were collected from mesophotic depths in the 1970s, *A. oroides* was last reported from the shallow Israeli coast in the 1960s (Tsurnamal, 1968). Since then, it has been regarded as lost from the Israeli sponge fauna. The reason for its regional disappearance is unclear, but over the past 60 years, seawater temperature along the Israeli Mediterranean coast has risen by over 3°C during the summer, presently surpassing temperatures of 30°C (Lipkin and Safriel, 1971; Shaltout and Omstedt, 2014; Ozer et al., 2017). An alternative explanation may relate to the construction of the Aswan High Dam in 1965 that limited the discharge of the Nile River to the overflow of the dam only (Oren, 1969). This limitation dramatically reduced the primary source of nutrient flow into the south Eastern Mediterranean (Oren, 1969; Azov, 1991), further lowering nutrients concentration and resulting in ultra-oligotrophic conditions in the Levant Basin (Krom et al., 2010; Kress et al., 2014; Ozer et al., 2017). Therefore, these two factors together (temperature and nutrient concentration) are the most likely causes for the disappearance of local *A. oroides* populations. As seawater temperature continues to rise and the ecology of the oceans is changing, it is essential to understand the interaction with other environmental factors and potential effects on biodiversity.

The recent rediscovery of dense populations of *A. oroides* in Israel's mesophotic sponge grounds with environmental conditions markedly different from those along the shallow coast (Idan et al., 2018) has provided the opportunity to test the hypothesis that shallow-water temperature and nutrient levels have adverse effects on *A. oroides* and could limit its distribution along the Israeli coast. To assess the effect of habitat-related environmental factors on the growth and survival of *A. oroides* along the Israeli coast, an experiment was conducted in which sponges from the mesophotic sponge ground were transplanted to a shallow rocky habitat, and others returned to mesophotic depths as controls.

MATERIALS AND METHODS

Study Sites

Mesophotic sponges were collected at a depth of 100–120 m from a site that is part of a submerged sandstone ridge off the coast of Herzliya along the Israeli Mediterranean coast (32.17710°N, 034.63306°E, WGS-84). Sponges were transplanted from this mesophotic site to a rocky, shallow habitat in 10 m depth off the coast of Mikhmoret (32.42854°N, 034.87313°E, WGS-84), where *A. oroides* used to grow in the 1960s both under overhangs and on exposed rocks (Tsurnamal, 1968).

Sponge Collection

Sponges were collected during two expeditions onboard the R/V Mediterranean Explorer (using a Remotely Operated Vehicle (ROV; ECA-Robotics H800). This ROV is equipped with a five-function-manipulator, a full high-definition camera, and two parallel laser beams for scale. The sampled sponges were brought on board in a collection basket and immediately placed in a seawater flow tank, in which they were individually numbered and attached to settlement tiles (environmental cement® 20 cm × 20 cm × 5 cm) using coated electric wire. Twenty *A. oroides* individuals were collected from the mesophotic site between January and March 2018, of which fourteen were transplanted to 10 m depth at Mikhmoret, while six sponges served as a control group and were transplanted back to the mesophotic site.

Transplantation

On the day of collection, the specimens were transferred to running seawater tanks at the Ruppin Academic Center's research facility in Mikhmoret. The following morning the sponges, still maintained unexposed to air, were transferred by SCUBA diving to the transplantation site. Most of the sponge specimens (n = 11) were placed (attached to tiles) in plastic crates (55 cm × 15 cm × 29 cm) that had been bolted to the rocky substrate prior to the translocation (**Figure 1A**). The crates were selected to allow low light and moderate water flow conditions through a mesh-like structure at the top and large holes on the sides. These conditions are naturally favored by *A. oroides* (Tsurnamal, 1968; Gerovasileiou and Voultsiadou, 2012; Gerovasileiou et al., 2017). The crates were cleaned of fouling organisms and algae weekly to ensure the holes stayed open, enabling water flow, and that other filter-feeders are not growing in the crates. Three specimens were attached to the crates' exterior (**Supplementary Table 1**) in order to control for possible effects of the specimens being inside the plastic crates. As a control for handling and translocating the sponges, six individuals were placed with their tiles on two metal trays onboard the R/V and then positioned by ROV back on their

original rocky substrate at the mesophotic site (**Figure 1B**), where *A. oroides* grows abundantly (Idan et al., 2018). The control sponges were not placed inside of crates so that *in situ* visual inspections of them would be possible without bringing them on board and because there was no need to cover them from direct light in the mesophotic zone. The metal trays were chosen in order to provide a sonar signature for easier location in the following visits, and since the sponges were attached to tiles, there was no physical contact between them and the metal. The location of the trays was marked on a high-resolution bathymetric map using the HYPACK® navigational system, which allowed us to return to the trays and monitor the control sponges. The choice of an open tray was made so that we can monitor the appearance of control sponges. All sponges were left to acclimate until April 1st, 2018.

Throughout the experiment (April to August 2018), the transplanted sponges were monitored twice a month for viability and growth. The examined parameters were: ectosome integrity, state of oscula (open or closed); water pumping.

Pumping, which indicates that the sponge is active, was visualized by releasing fluorescein-dyed seawater (fluorescein, 100 mg/L) next to the sponge and documenting if it flowed out of the oscula (Yahel et al., 2005). All parameters were measured at the transplantation site (underwater) with minimal handling of the sponges.

In order to estimate individual growth, sponge volume was assessed using 3D photogrammetry. Six randomly chosen individuals were monitored throughout the experiment. They were photographed from multiple angles twice a month for 3D model reconstruction, beginning on April 12th (Lavy et al., 2015; Olinger et al., 2019). The 3D models were reconstructed using Agisoft PhotoScan v1.4 (Agisoft, 2017) and Metashape v1.5 (Agisoft, 2019) professional edition softwares. Sponges were transferred with their tiles, without direct handling of the sponge and placed on a "Lazy Susan" turntable marked with scale bars and place-markers (**Figure 2A**). The cameras (Canon G16 or G12) were positioned ∼20 cm from the turntable, and the turntables were rotated to capture all possible perspectives of the specimens, rulers, and markers. For each model, 75–160 images were imported to the software and then automatically aligned (high accuracy, key point limit 100,000, tie point limit 20,000). The next step was generating a dense point cloud (high quality, depth filtering mild). Upon completion, a mesh (surface type arbitrary, face count high, calculated vortex colors enabled) was created through interpolation of the points in the dense cloud, and finally, the texture was added (mapping mode generic, blending mode average). Manual proofing was performed for each step to ensure maximal accuracy. To scale the model, markers were placed on at least two scale bars (**Figure 2B**). This stage was performed manually for each image, after which the base and turntable were erased, the remaining gaps were closed, and the volume was assessed.

The growth rate (%) of each individual was calculated using the following formula:

$$\text{Growth rate} = ([(V_t - V_{t-1})/V_{t-1}] \times 100)/n$$

Where V_t is the volume of the sponge measured at time t, V_{t-1} is the volume of the sponge measured in the previous time point, and n is the number of days passed between t and t–1.

Sponges from the control group were monitored every 3 months due to the high cost and technical difficulty of the expeditions. Volume and pumping were not measured for the control group due to the technical incompatibility of the ROV for such tasks.

In all of the specimens, part of the sponge was damaged by the ROV manipulator at the time of collection, and shortly after transplantation, the damaged part became necrotic; sponge #19 is shown as an example (**Figure 3**). In both shallow and mesophotic habitats, all specimens regenerated by creating a new body wall underneath the necrotic area and eventually detaching the necrotic part (**Figure 3**, 14/06/18). The part that was detached was measured and subtracted from the volume estimation, before its detachment, in order to compare the results accurately.

Environmental Parameters

All environmental parameters in both habitats were measured in morning times (7:30–9:00 AM) unless mentioned otherwise.

Nutrients

Water samples were collected from both the mesophotic and shallow habitats in order to compare concentrations of particulate organic carbon (POC), total organic carbon (TOC), and total nitrogen (TN). In the mesophotic habitat, water samples were collected every 3 months using 12 L Niskin bottles placed on a typical rosette sampler (Baetge et al., 2020). The bottles were lowered while open and then closed at approximately one meter above the bottom. For each parameter, at each date, duplicate samples were taken from two separate Niskin bottles. At the shallow site, water was collected during SCUBA dives every 2–4 weeks using a single Niskin bottle, which was closed approximately one meter above the bottom.

TOC and TN Sample Collection

Collection and processing followed a previously established protocol (Morganti et al., 2016; Baetge et al., 2020). Samples were collected directly from the Niskin bottles into pre-combusted 40 mL glass EPA vials with PTFE lined septa. Each vial was washed twice in sample water, then 20 ml of sample water were collected per vial, and 80 μl of HCL 32% were added. These samples were frozen onboard the R/V in dry ice and stored at −80°C (Morganti et al., 2016). Samples were analyzed at the Carlson Microbial Oceanography Lab at the Marine Science Institute, UC, Santa Barbara.

POC Sample Collection and Processing

GF/F filters were pre-combusted at 400°C for 4 h and kept in a dry and clean environment prior to the expedition. Water samples were pre-filtered through 80 μm plankton mesh to avoid large particles that could block the filter and which are not utilized by sponges. Duplicates of ∼4 L from the two Niskin bottles were filtered on each mesophotic expedition, at three consecutive days for each expedition. In the shallow water, duplicates of

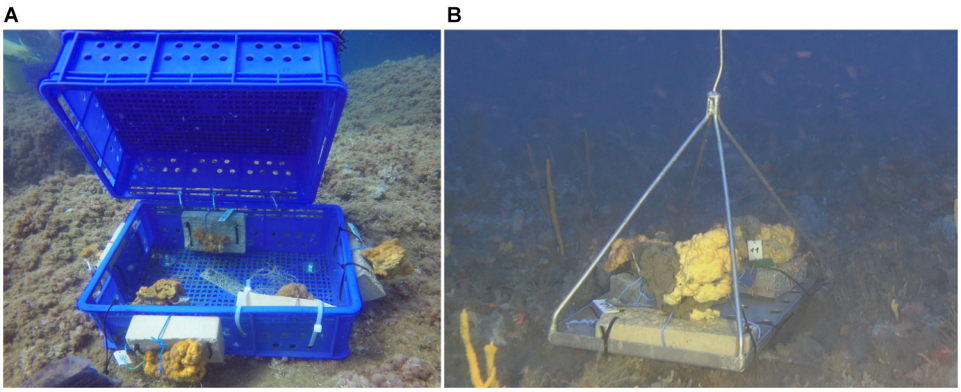

FIGURE 1 | Transplanted *A. oroides*. **(A)** specimens transplanted to the shallow site placed both inside and outside the plastic crates; **(B)** specimens transplanted to the deep site, placed on a metal tray.

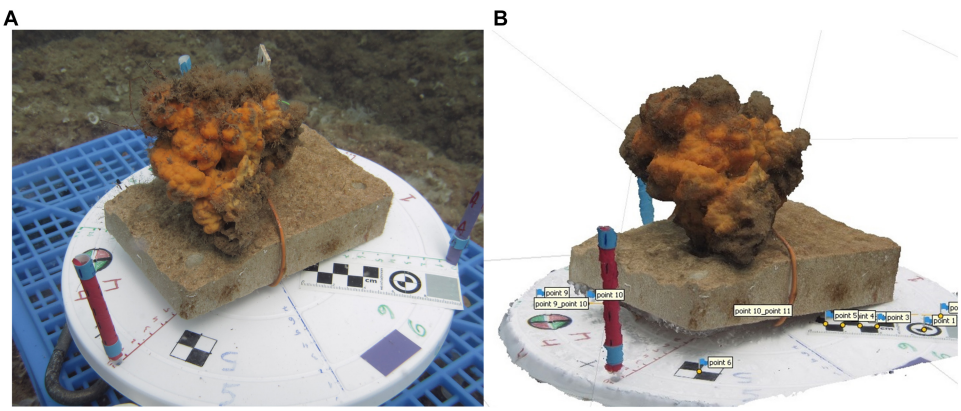

FIGURE 2 | Creating a 3D model of the transplanted *A. oroides*: **(A)** specimen #18 placed on the turntable. Markers and scale bars in the image were used for the alignment stage and later enabled volume assessment. **(B)** 3D model of specimen #18; the blue flags are the manually placed markers.

∼3 L were filtered at least once a month. As GF/F filters can become blocked with particles, the exact amount of water filtered was documented to obtain an accurate estimation of the POC concentration (Morganti et al., 2016). Filters were frozen immediately after filtration, and at least 24 h before analysis, the filters were dried in an oven (60°C). Samples were then analyzed using a TOC analyzer (Shimadzu Instruments), where the Carbon is oxygenized at high temperatures (800–900°C) to create CO_2. The CO_2 creates a signal which is then detected by Infra-Red sensors. The surface of that signal is proportional to the amount of Carbon.

Temperature

Water temperature at the mesophotic sponge ground was measured every three months from January until November 2018, using a CTD mounted on the rosette sampler, creating a temperature profile of the water column. In the shallow habitat, the water temperature was monitored continuously from April to August 2018, using two HOBO Pendant® data loggers (Onset Computer Corporation, Bourne, MA, United States). In order to monitor the temperature and light inside and outside the crates, one of the loggers was placed on the inside of a crate and the other on its exterior.

RESULTS

The experiment lasted four months (April–August 2018) and ended when the last of the specimens transplanted to the shallow site had died. All sponges from the mesophotic control group survived the entire duration of the experiment and beyond.

Environmental Parameters

Water temperature in the shallow habitat increased gradually throughout the experiment (April-August 2018) from 20 to 30.5°C (**Figure 4A**). No difference in temperature was measured between the loggers placed inside the crates and those placed on the crats' exterior (**Supplementary Figure 1**). In contrast, over the same period, the temperature remained relatively stable in the mesophotic habitat below the seasonal thermocline (**Figure 4B**), decreasing by 2.4°C, from 19.5 to 17.1°C (**Figure 4A**).

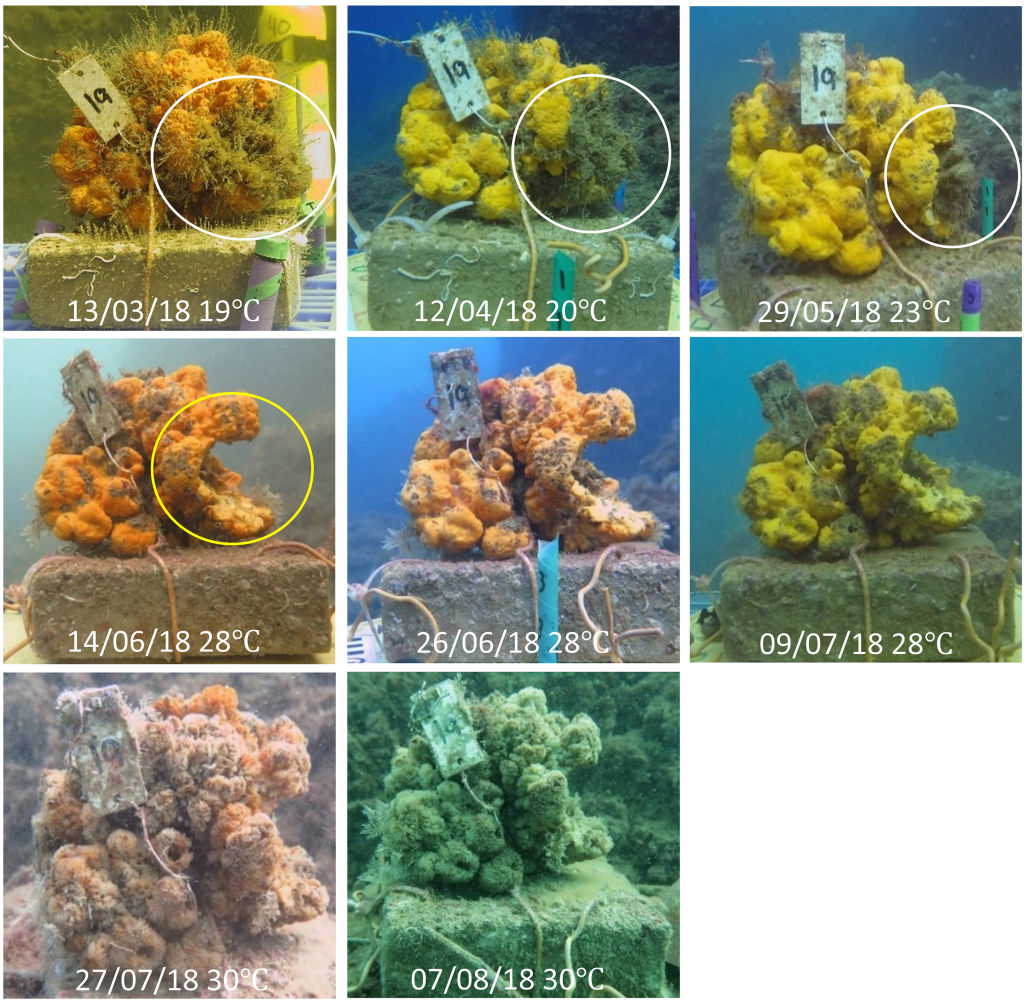

FIGURE 3 | Sponge #19 throughout the experiment: dates and seawater temperatures are noted on each image. The part of the sponge damaged by the ROV during collection became necrotic (circled) on 13/03 – 29/05. Later (14/06), the necrotic part detached, and a new ectosome is visible. On 09/07, the sponge stopped pumping seawater. By 27/07, the sponge was dead, and on the 07/08, only the skeleton remained.

The range of nutrient concentrations (POC, TOC, and TN) in the shallow habitat was 4.3–17.8, 92.0–159.3, and 5.0–8.0 μM, respectively (**Figure 5**). These concentrations were higher and showed greater variability than those in the mesophotic habitat (3.1–7.7, 68.3–101.8, and 3.7–5.8 μM, respectively; **Figure 5**). Differences in TOC and TN concentrations between the mesophotic and shallow water were small, with higher values in the shallow water. POC concentration at the shallow site had a greater variation between sampling dates.

Transplant Survival and Vitality

At the end of June, 3.5 months since the sponges' transplantation, 86% of the sponges at the shallow depth were still alive (i.e., their ectosome was intact and their oscula were open), and 64–86% of them were observed to be pumping at each visit (**Figure 6**). After the temperature at the shallow site had risen to over 28°C in July, the sponges were still alive, but all pumping had ceased (**Figure 6**). Two weeks later (July 27th), only one specimen was still alive while the rest were visibly dead (i.e., their ectosome was completely fragmented). By August, all the sponges at the shallow site had died, and the experiment ended (**Figure 6**). The survival patterns of the sponges that had been mounted inside and outside the crates were similar (**Supplementary Table 1**). In contrast, all the sponges in the mesophotic control group survived until the end of the experiment and were observed alive more than 5 months later (**Figure 7**, **Supplementary Figure 2**).

The growth pattern of the sponges appeared to follow an optimum curve (**Figure 8**). Within 1.5 months, i.e., from 12/04 – 29/05/2018, the shallow site sponges grew on average 0.19% a day, increasing the volume of the sponges by an average of 9.2% ± 2.5 when temperatures reached 24°C. As the temperature continued to rise, we observed a decline in sponges' volume until the end of the experiment, reaching a minimum of −1.7% ± 2.6 of the original volume. The change in sponge volume was not constant: initially, the growth rate was 0.11% a day, and it increased as

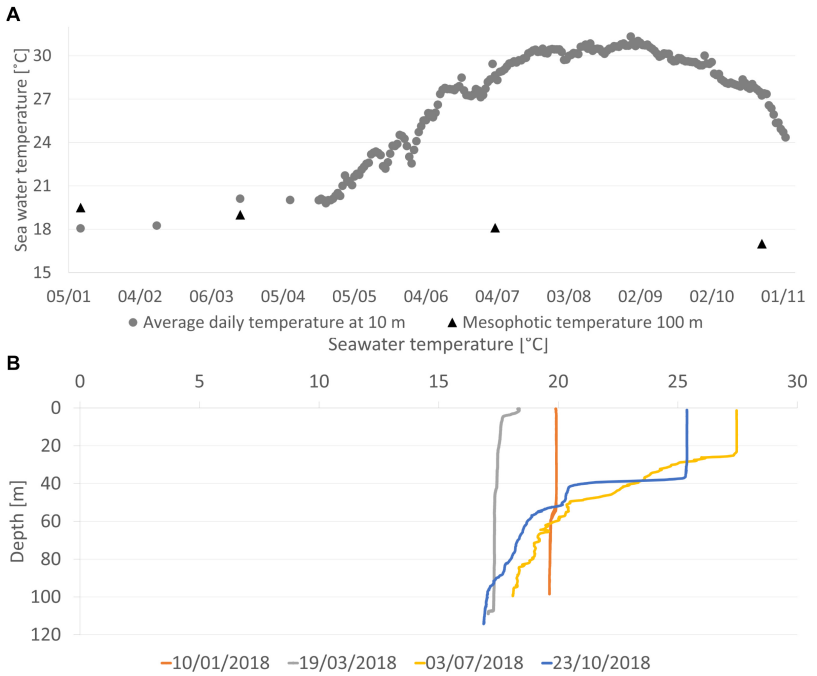

FIGURE 4 | Temperature regime measured from January to November 2018. **(A)** The temperature at the mesophotic sponge ground (100 m depth; black triangles) and at the shallow transplantation site (10 m depth; gray circles). The temperature was measured with CTD in both habitats. In addition, from April to November, the temperature in the shallow water was measured four times a day with a HOBO logger. **(B)** Temperature profile at the mesophotic sponge ground showing seasonal thermocline (measured with CTD).

the temperature rose. Between 15/05 and 29/05, the growth rate reached an average of 0.43% a day. Then the volume decreased at a rather constant rate (0.23–0.26% a day) between 29/05 and 26/06.

DISCUSSION

Agelas oroides is a common sponge in shallow waters throughout the Mediterranean (Carteron, 2002; Voultsiadou, 2005, 2009; Lejeusne et al., 2010; Topaloglu and Evcen, 2014; Costa et al., 2018). In the past, it was recorded as a common species in Israel's coastal water (Tsurnamal, 1968). However, our findings suggest that the current distribution of *A. oroides* might be limited by the increasing water temperatures along the shallow Israeli coast. During the experiment, all *A. oroides* individuals transplanted from mesophotic to shallow water died within 4 months. In contrast, the specimens that were transplanted back to the mesophotic sponge ground survived well past the end of the experiment. The shallow habitat differed from the mesophotic habitat in many aspects that could affect the survival of the transplanted individuals: Differences in concentrations of TOC, TN, and POC were small but higher at the shallow site compared to the mesophotic sponge grounds. These findings are consistent with the results of other studies showing that nutrient levels at the Mediterranean mesophotic depths are usually lower than in the shallow water near the shore because of the run-off of freshwater from land and re-suspension of sediments due to wave action (Santinelli, 2015). While *A. oroides* cannot survive in the shallow local site, it thrives at other shallow locations such as Western Mediterranean, with similar DOC and POC concentrations (Morganti et al., 2017, 2019). Therefore, excess of nutrients, or nutrients limitation, were ruled out as a limiting factor. By placing the sponges inside large crates, we were able to control for other environmental parameters, such as light and water flow regime. Thus, the crates provided the sponges in shallow water conditions closer to their natural habitat, i.e., lower water motion and light intensities (Tsurnamal, 1968; Gerovasileiou et al., 2017). In the current study, the majority of sponges were vital (i.e., ectosome intact, open oscula, and pumping water) throughout the first 2.5 months of the experiment.

Moreover, the sponges seemed to have recovered from the initial damage caused by the ROV collection, rebuilding their body wall and detaching the necrotic parts – indicating that the conditions at the time of the experiment onset were suitable for their survival. In addition, all sponges increased in size during the first part of the experiment. Only when water temperature reached 28°C did the sponges begin to show signs of stress, observed by a decrease in body size and cessation of pumping. Although variations in sponge pumping are well documented as a normal phenomenon (Hoffmann et al., 2008; Lavy et al., 2016; Kumala et al., 2017), the prolonged arrest of pumping is a clear sign of sponge stress, eventually leading to its mortality (Massaro et al., 2012). Many marine organisms, including sponges, are known to be adversely affected by rising

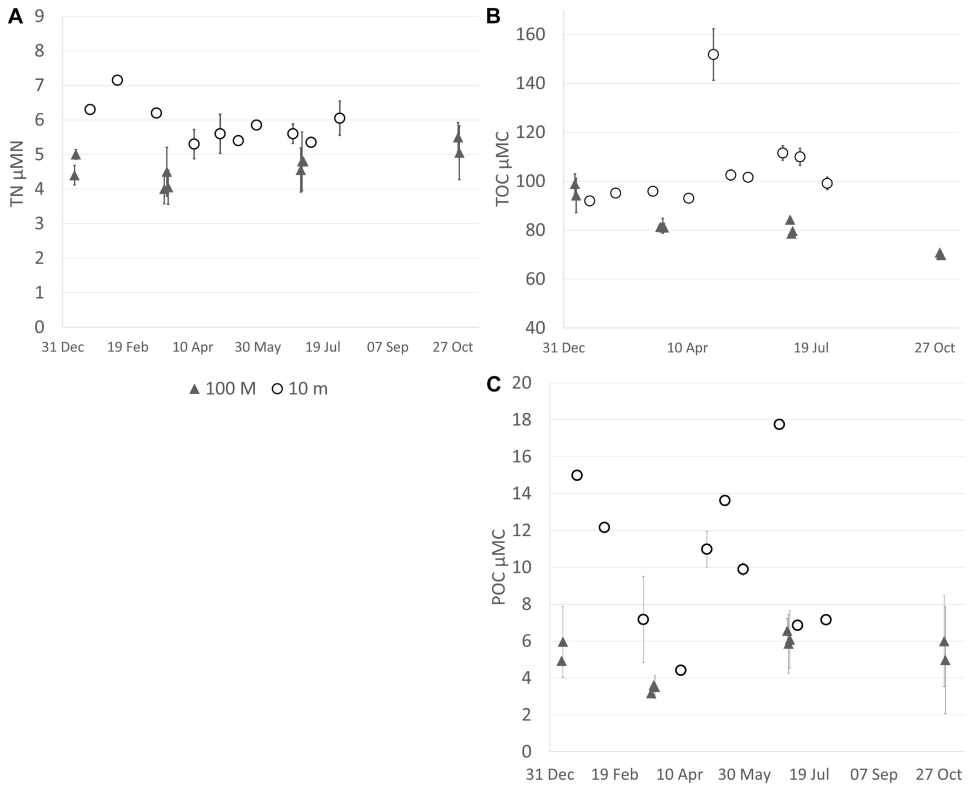

FIGURE 5 | Concentrations of organic carbon and total nitrogen at the mesophotic and transplantation sites over time (01–10/2018). At 10 m, the first three dates have only one sample for TN and TOC, and the same for the first two dates for POC. **(A)** Total nitrogen (TN; µM), **(B)** Total organic carbon (TOC; µM), and **(C)** Particulate organic carbon (POC; µM).

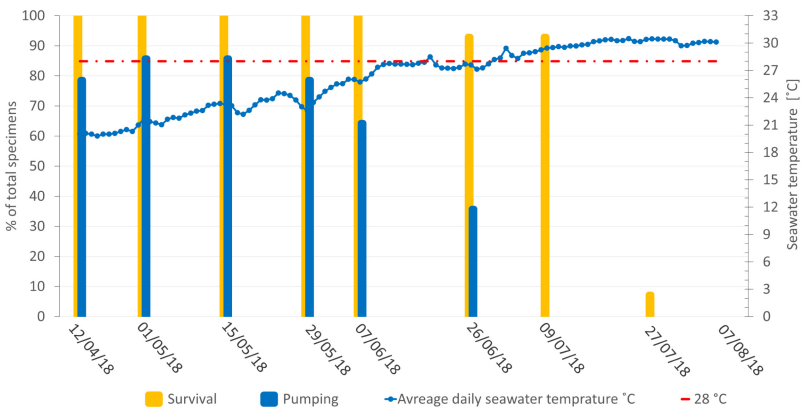

FIGURE 6 | Survival of *Agelas oroides* specimens (%) and water temperature (°C) at the shallow transplantation site. The percentage of survival was calculated as the number of live sponges (not necessarily pumping water) out of the total number of sponges; The percentage of pumping specimens was calculated separately.

temperatures (Webster, 2007; Webster et al., 2008a; Coma et al., 2009; Garrabou et al., 2009, 2019; Cebrian et al., 2011; Pairaud et al., 2014; Laffy et al., 2019), and past events of sponge mass-mortality in the Western Mediterranean have been linked to events of unusually high temperatures (Garrabou et al., 2009, 2019; Lejeusne et al., 2010; Cebrian et al., 2011; Di Camillo et al., 2013; Ledda et al., 2014; Ereskovsky et al., 2019). It has been suggested that sponges in coral reefs are more resilient than corals to the rise in seawater temperatures, and some argue that they may outcompete corals in such cases (Bell et al., 2013, 2018). Others, however, claim that synergistic effects with additional factors (e.g., ocean acidification, reduction in nutrients, and pollution) will adversely affect their populations (Bennett et al., 2017; Lesser and Slattery, 2020). The effect of

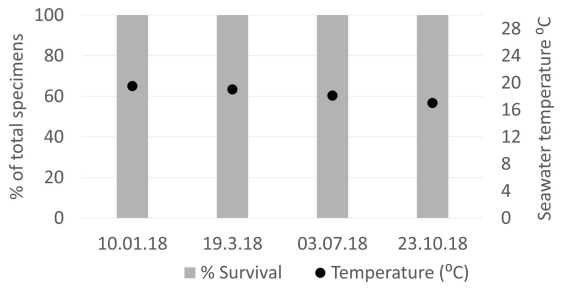

FIGURE 7 | *Agelas oroides* mesophotic control group survival (% specimens) and seawater temperature (°C) at the Herzliya mesophotic sponge ground.

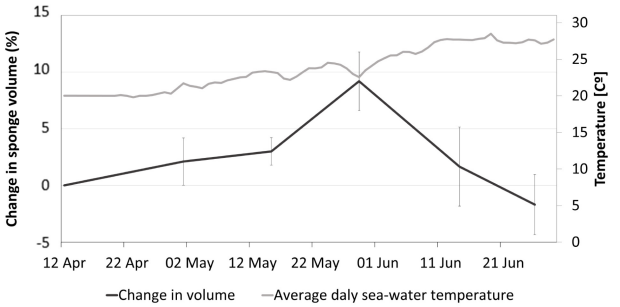

FIGURE 8 | Percentage change in sponge volume throughout the experiment for *A. oroides* specimens transplanted to a shallow site $n = 6$.

rising temperatures may be direct, by causing stress to the sponges themselves – evident by the expression of heat-shock protein (Itskovich et al., 2018), or indirect, by affecting the composition of the microbiota inhabiting the sponges (Webster et al., 2008a,b), in some cases creating favorable conditions for opportunistic or pathogenic microorganisms (Webster et al., 2008a; Laffy et al., 2019). And indeed, with the increase in seawater temperatures worldwide, there were many reports of an increase in sponge diseases and a decline in their populations (Webster et al., 2008a).

Analysis of changes in the hard-bottom community over a period of 25 years at the Ligurian Sea showed that sponges maintained their overall coverage, although this region suffered from severe urbanization of the coastline, pollution, fishing impact, and was exposed to global warming (Bertolino et al., 2016). Specifically, *A. oroides* showed some coverage increase (though the trend was not significant), which might suggest that this species could be resilient to temperature elevation. However, in spite of the reported seawater warming, the temperatures in the Ligurian Sea remained lower than those of the Levantine Sea and probably did not reach the threshold temperature for *A. oroides* survivorship.

A. oroides was last observed at the shallow Israeli coast in 1967 (Tsurnamal, 1968). Since then, the temperature in the shallow waters of the Eastern Mediterranean has risen during the summer by over three degrees, from a maximum of 28.4°C in the 1960s to 31.5°C in present times (Lipkin and Safriel, 1971; Shaltout and Omstedt, 2014; Ozer et al., 2017). In this study, the daily temperature amplitude was around 28°C for 3 weeks (**Figures 4A**, **6**), in which time most of the sponges have stopped pumping. About a week later, the temperature has surpassed 29°C, and no pumping activity was detected. The sponges, however, still appeared alive (by their ectosomes' integrity). The ability of sponges to withstand short-term (several days) thermal stress was also demonstrated for the Mediterranean sponge *Spongia officinalis* (Koutsouveli et al., 2020). That work described the mechanism of genetic expression involved in heat-tolerance and adaptation of *S. officinalis*.

Although we have no specific information about heat-tolerance or intolerance of *A. oroides*, it was shown that a heat-dependent prevalence of disease in different sponges was positively correlated with the duration for which they were exposed to extreme temperature (Erwin et al., 2012; Laffy et al., 2019). Similarly, the heatwave in the year 2003, in which Mediterranean *A. oroides* populations suffered from mass mortality, lasted ∼100 days (Garrabou et al., 2009; Marbà et al., 2015). In 1999, on the other hand, a high-temperature anomaly of 27°C that lasted ∼30 days was reported to cause a decline of some sponge populations in the Mediterranean. *A. oroides* did not appear to be affected (Cerrano et al., 2000; Marbà et al., 2015; Bertolino et al., 2016).

These observations imply that not only high temperature but its duration may affect sponges' survival. At the present study site, seawater temperature in the summer of 2018 remained above 28°C for almost 3 months and reached a maximum of 31.4°C at 10 m depth (**Figures 4**, **5**). This suggests that a prolonged period of time during which the temperature surpasses 28°C may constitute a threshold too high for *A. oroides* survival and that it constitutes one of the main factors affecting the disappearance of *A. oroides* from the Israeli shallow waters. Another support for this hypothesis is the fact that throughout the experiment, the temperature at the mesophotic control site never surpassed 19.5°C, and the control sponges remained alive (**Supplementary Figure 2**). In the past, *A. oroides* did face temperatures surpassing this threshold along the shallow Israeli coast (28.4°C). However, the sponges were only exposed to these conditions for a short time. While sponges may have the capacity to acclimate to such conditions Guzman and Conaco (2016) and Koutsouveli et al. (2020), in long-term exposure, the damage caused by the thermal stress may accumulate and lead to the sponge death.

While other abiotic conditions that were not within the scope of this study (such as the presence of anthropogenic pollutants) may contribute to shaping sponge communities, our findings are in congruence with the notion that low sponge richness in the shallow water of this easternmost part of the Mediterranean Sea, could be attributed to temperature (Voultsiadou, 2005, 2009; Bianchi, 2007). Finally, while sea temperature continues to rise, it is expected that benthic communities in shallow, coastal waters, will likely change and result in a disappearance of temperature-sensitive species (Webster et al., 2013). A loss of habitat-engineering sponge species may have a profound impact on the ecosystem and other organisms that depend on these

sponges [e.g., (Herrnkind et al., 1997; Peterson et al., 2006)]. Our present findings suggest that the mesophotic sponge grounds, in which environmental conditions are much more stable, could provide a refuge for some species like *A. oroides* that may gradually be displaced from shallow water in a warming climate (Webster et al., 2013). Moreover, because the abiotic conditions in the Levantine Sea are changing faster, and the temperature is rising (Marbà et al., 2015), the status of sponge communities there may provide us with a possible prediction for other areas of the Mediterranean Sea as water temperatures continue to increase.

DATA AVAILABILITY STATEMENT

The original contributions presented in the study are included in the article/**Supplementary Material**, further inquiries can be directed to the corresponding author/s.

AUTHOR CONTRIBUTIONS

TI conceived of the study, designed the study, carried out the field work, carried out the data and statistical analyses and drafted the manuscript. LG participated in collection of field data and data analysis and helped draft the manuscript. SS participated in the design of the study, participated in field work, and critically revised the manuscript. MI helped design the study, coordinated the study, and critically revised the manuscript. All authors gave final approval for publication and agreed to be held accountable for the work performed therein.

FUNDING

The study was supported by the following institutions and grants: The Israeli Ministry of Science, Technology, and Space (The Program for the Development of Scientific and Technological Infrastructure, grant 3-10343 to MI); The Israeli Ministry of National Infrastructure, Energy and Water (grant 217-17-020 to MI); and partially supported by the ISF-NSFC joint research program (grant no. 2577/18 to MI). TI was supported by the Shulamit Aloni Fellowship from the Israeli Ministry of Science, Technology, and Space.

ACKNOWLEDGMENTS

The NGO EcoOcean for providing the facility for marine research onboard the R/V Mediterranean Explorer and for the operation of the ROV. Oded Ezra and Itai Katzman, who piloted the ROV. The students of Micha Ilan's group who volunteered for sponge collections during the many dives and cruises onboard the research vessel. Prof. Gitai Yahel helped to plan the experiment, and the students and faculty of the Ruppin Academic Centre who assisted with dives and workspace, and lastly, Reuben Rosenblatt, the diving officer, for his support. Naomi Paz, who edited the manuscript. ECOncrete® for the generous donation of the environmental cement tiles. Collection permit was given by the Israel Nature and Parks Authority.

SUPPLEMENTARY MATERIAL

The Supplementary Material for this article can be found online at: https://www.frontiersin.org/articles/10.3389/fmars.2020.603593/full#supplementary-material

Supplementary Figure 1 | Temperature measured every 6 h by HOBO loggers placed inside and outside the crates at the translocation site off the coast of Mikhmoret at a depth of 10 m.

Supplementary Figure 2 | Control specimens of *A. oroides* in October 2018, sponges seem alive.

Supplementary Table 1 | Sponges in the transplantation experiment. Treatment 2 indicates whether the sponge was attached inside or outside a box. Initially seven sponges were attached outside the crates; two died shortly after transplantation and one was lost in a storm.

REFERENCES

Agisoft, L. (2017). *Agisoft photoscan professional*. St Petersburg, Russia: Agisoft.

Agisoft, L. (2019). *Agisoft metashape user manual, Professional edition, Version 1.5, Agisoft LLC*. St. Petersburg, Russia: Agisoft.

Azov, Y. (1991). Eastern mediterranean—a marine desert? *Mar. Poll. Bull.* 23, 225–232. doi: 10.1016/0025-326x(91)90679-m

Baetge, N., Graff, J. R., Behrenfeld, M. J., and Carlson, C. A. (2020). Net community production, dissolved organic carbon accumulation, and vertical export in the western north atlantic. *Front.Mar. Sci.* 7:227. doi: 10.3389/fmars.2020.00227

Beazley, L. I., Kenchington, E. L., Murillo, F. J., and Sacau, M. D. (2013). Deep-sea sponge grounds enhance diversity and abundance of epibenthic megafauna in the northwest atlantic. *Ices J. Mar. Sci.* 70, 1471–1490. doi: 10.1093/icesjms/fst124

Beepat, S. S., Davy, S. K., Woods, L., and Bell, J. J. (2020). Short-term responses of tropical lagoon sponges to elevated temperature and nitrate. *Mar. Environ. Res.* 157:104922. doi: 10.1016/j.marenvres.2020.104922

Bell, J. J., Bennett, H. M., Rovellini, A., and Webster, N. S. (2018). Sponges to be winners under near-future climate scenarios. *Bioscience* 68, 955–968. doi: 10.1093/biosci/biy142

Bell, J. J., Davy, S. K., Jones, T., Taylor, M. W., and Webster, N. S. (2013). Could some coral reefs become sponge reefs as our climate changes? *Global Change Biol.* 19, 2613–2624. doi: 10.1111/gcb.12212

Bennett, H. M., Altenrath, C., Woods, L., Davy, S. K., Webster, N. S., and Bell, J. J. (2017). Interactive effects of temperature and pCO 2 on sponges: from the cradle to the grave. *Global Change Biol.* 23, 2031–2046. doi: 10.1111/gcb.13474

Bertolino, M., Betti, F., Bo, M., Cattaneo-Vietti, R., Pansini, M., Romero, J., et al. (2016). Changes and stability of a Mediterranean hard bottom benthic community over 25 years. *J. Mar. Biol. Ass. U K.* 96:341. doi: 10.1017/s0025315415001186

Bianchi, C. N. (2007). Biodiversity issues for the forthcoming tropical mediterranean Sea. *Hydrobiologia* 580:7. doi: 10.1007/978-1-4020-6156-1_1

Bo, M., Bertolino, M., Bavestrello, G., Canese, S., Giusti, M., Angiolillo, M., et al. (2012). Role of deep sponge grounds in the mediterranean sea: a case study in southern Italy. *Hydrobiologia* 687, 163–177. doi: 10.1007/978-94-007-4688-6_14

Carteron, S. (2002). *Etude taxonomique des spongiaires du Liban. Stage de Maîtrise*. Marseille, France: Centre d'Océanologie de Marseille.

Cebrian, E., Uriz, M. J., Garrabou, J., and Ballesteros, E. (2011). Sponge mass mortalities in a warming mediterranean sea: are cyanobacteria-harboring species worse off? *PloS One* 6:e20211. doi: 10.1371/journal.pone.0020211

Cerrano, C., Bavestrello, G., Bianchi, C. N., Cattaneo-Vietti, R., Bava, S., Morganti, C., et al. (2000). A catastrophic mass-mortality episode of gorgonians and other organisms in the ligurian sea (north-western mediterranean), summer 1999. *Ecol. Lett.* 3, 284–293. doi: 10.1046/j.1461-0248.2000.00152.x

Coma, R., Ribes, M., Serrano, E., Jiménez, E., Salat, J., and Pascual, J. (2009). Global warming-enhanced stratification and mass mortality events in the mediterranean. *Proc. Nat. Acad. Sci.* 106, 6176–6181. doi: 10.1073/pnas.0805801106

Costa, G., Giussani, V., Kletou, D., Kleitou, P., Pansini, M., Setti, A., et al. (2018). A first preliminary study of the shallow water sponge fauna from cyprus island (eastern mediterranean). *Zootaxa* 4450, 594–596. doi: 10.11646/zootaxa.4450.5.7

Di Camillo, C. G., Bartolucci, I., Cerrano, C., and Bavestrello, G. (2013). Sponge disease in the adriatic sea. *Mar. Ecol.* 34, 62–71. doi: 10.1111/j.1439-0485.2012.00525.x

Ereskovsky, A., Ozerov, D. A., Pantyulin, A. N., and Tzetlin, A. B. (2019). Mass mortality event of white sea sponges as the result of high temperature in summer 2018. *Polar Biol.* 42, 2313–2318. doi: 10.1007/s00300-019-02606-0

Erwin, P. M., Pita, L., López-Legentil, S., and Turon, X. (2012). Stability of sponge-associated bacteria over large seasonal shifts in temperature and irradiance. *Appl. Environ. Microbiol.* 78, 7358–7368. doi: 10.1128/aem.02035-12

Feuda, R., Dohrmann, M., Pett, W., Philippe, H., Rota-Stabelli, O., Lartillot, N., et al. (2017). Improved modeling of compositional heterogeneity supports sponges as sister to all other animals. *Curr. Biol.* 27, 3864–3870. doi: 10.1016/j.cub.2017.11.008

Garrabou, J., Coma, R., Bensoussan, N., Bally, M., Chevaldonné, P., Cigliano, M., et al. (2009). Mass mortality in northwestern mediterranean rocky benthic communities: effects of the 2003 heat wave. *Global Change Biol.* 15, 1090–1103. doi: 10.1111/j.1365-2486.2008.01823.x

Garrabou, J., Gómez-Gras, D., Ledoux, J.-B., Linares, C., Bensoussan, N., López-Sendino, P., et al. (2019). Collaborative database to track mass mortality events in the mediterranean sea. *Front. Mar. Sci.* 6:707. doi: 10.3389/fmars.2019.00707

Gerovasileiou, V., Chintiroglou, C. C., Konstantinou, D., and Voultsiadou, E. (2016). Sponges as "living hotels" in mediterranean marine caves. *Sci. Marina* 80, 279–289. doi: 10.3989/scimar.04403.14b

Gerovasileiou, V., Dimitriadis, C., Arvanitidis, C., and Voultsiadou, E. (2017). Taxonomic and functional surrogates of sessile benthic diversity in mediterranean marine caves. *PloS One* 12:e0183707. doi: 10.1371/journal.pone.0183707

Gerovasileiou, V., and Voultsiadou, E. (2012). Marine caves of the mediterranean Sea: a sponge biodiversity reservoir within a biodiversity hotspot. *PloS One* 7:e39873. doi: 10.1371/journal.pone.0039873

Grenier, M., Ruiz, C., Fourt, M., Santonja, M., Dubois, M., Klautau, M., et al. (2018). Sponge inventory of the french mediterranean waters, with an emphasis on cave-dwelling species. *Zootaxa* 4466, 205–228. doi: 10.11646/zootaxa.4466.1.16

Guzman, C., and Conaco, C. (2016). Gene expression dynamics accompanying the sponge thermal stress response. *PloS One* 11:e0165368. doi: 10.1371/journal.pone.0165368

Herrnkind, W. F., Butler, Iv, M. J., Hunt, J. H., and Childress, M. (1997). Role of physical refugia: implications from a mass sponge die-off in a lobster nursery in florida. *Mar. Freshwater Res.* 48, 759–770. doi: 10.1071/mf97193

Hoffmann, F., Røy, H., Bayer, K., Hentschel, U., Pfannkuchen, M., Brümmer, F., et al. (2008). Oxygen dynamics and transport in the mediterranean sponge aplysina aerophoba. *Mar. Biol.* 153, 1257–1264. doi: 10.1007/s00227-008-0905-3

Idan, T., Shefer, S., Feldstein, T., Yahel, R., Huchon, D., and Ilan, M. (2018). Shedding light on an east-mediterranean mesophotic sponge ground community and the regional sponge fauna. *Mediterr. Mar. Sci.* 19, 84–106. doi: 10.12681/mms.13853

Itskovich, V., Shigarova, A., Glyzina, O., Kaluzhnaya, O., and Borovskii, G. (2018). Heat shock protein 70 (Hsp70) response to elevated temperatures in the endemic baikal sponge lubomirskia baicalensis. *Ecol. Indi.* 88, 1–7. doi: 10.1016/j.ecolind.2017.12.055

Kenchington, E., Power, D., and Koen-Alonso, M. (2013). Associations of demersal fish with sponge grounds on the continental slopes of the northwest atlantic. *Mar. Ecol. Prog. Series* 477, 217–230. doi: 10.3354/meps10127

Koutsouveli, V., Manousaki, T., Riesgo, A., Lagnel, J., Kollias, S., Tsigenopoulos, C. S., et al. (2020). Gearing up for warmer times: transcriptomic response of spongia officinalis to elevated temperatures reveals recruited mechanisms and potential for resilience. *Front. Mar. Sci.* 6:786. doi: 10.3389/fmars.2019.00786

Kovalerchik, D., Singh, R. P., Schlesinger, P., Mahajni, A., Shefer, S., Fridman, M., et al. (2020). Bromopyrrole alkaloids of the sponge agelas oroides collected near the israeli mediterranean coastline. *J. Nat. Prod.* 83, 374–384. doi: 10.1021/acs.jnatprod.9b00863

Kress, N., Gertman, I., and Herut, B. (2014). Temporal evolution of physical and chemical characteristics of the water column in the easternmost levantine basin (eastern mediterranean sea) from 2002 to 2010. *J. Mar. Sys.* 135, 6–13. doi: 10.1016/j.jmarsys.2013.11.016

Krom, M., Emeis, K., and Van Cappellen, P. (2010). Why is the eastern mediterranean phosphorus limited? *Prog. Oceano.* 85, 236–244. doi: 10.1016/j.pocean.2010.03.003

Kumala, L., Riisgård, H. U., and Canfield, D. E. (2017). Osculum dynamics and filtration activity in small single-osculum explants of the demosponge halichondria panicea. *Mar. Ecol. Prog. Series* 572, 117–128. doi: 10.3354/meps12155

Laffy, P. W., Botté, E. S., Wood-Charlson, E. M., Weynberg, K. D., Rattei, T., and Webster, N. S. (2019). Thermal stress modifies the marine sponge virome. *Environ. Microbiol. Rep.* 11, 690–698. doi: 10.1111/1758-2229.12782

Lavy, A., Eyal, G., Neal, B., Keren, R., Loya, Y., and Ilan, M. (2015). A quick, easy and non-intrusive method for underwater volume and surface area evaluation of benthic organisms by 3D computer modelling. *Methods Ecol. Evol.* 6, 521–531. doi: 10.1111/2041-210x.12331

Lavy, A., Keren, R., Yahel, G., and Ilan, M. (2016). Intermittent hypoxia and prolonged suboxia measured in situ in a marine sponge. *Front. Mar. Sci.* 3:263. doi: 10.3389/fmars.2016.00263

Ledda, F. D., Pronzato, R., and Manconi, R. (2014). Mariculture for bacterial and organic waste removal: a field study of sponge filtering activity in experimental farming. *Aquacul. Res.* 45, 1389–1401. doi: 10.1111/are.12084

Lejeusne, C., Chevaldonné, P., Pergent-Martini, C., Boudouresque, C. F., and Perez, T. (2010). Climate change effects on a miniature ocean: the highly diverse, highly impacted mediterranean sea. *Trends Ecol. Evol.* 25, 250–260. doi: 10.1016/j.tree.2009.10.009

Lesser, M. P., and Slattery, M. (2020). Will coral reef sponges be winners in the Anthropocene? *Global Change Biol.* 26, 3202–3211. doi: 10.1111/gcb.15039

Lipkin, Y., and Safriel, U. (1971). Intertidal zonation on rocky shores at mikhmoret (mediterranean, israel). *J. Ecol.* 59, 1–30. doi: 10.2307/2258448

Marbà, N., Jordà, G., Agustí, S., Girard, C., and Duarte, C. M. (2015). Footprints of climate change on mediterranean sea biota. *Front. Marine Sci.* 2:56. doi: 10.3389/fmars.2015.00056

Massaro, A. J., Weisz, J. B., Hill, M. S., and Webster, N. S. (2012). Behavioral and morphological changes caused by thermal stress in the Great Barrier Reef sponge Rhopaloeides odorabile. *J. Exp. Mar. Biol. Ecol.* 416, 55–60. doi: 10.1016/j.jembe.2012.02.008

Morganti, T., Coma, R., Yahel, G., and Ribes, M. (2017). Trophic niche separation that facilitates co-existence of high and low microbial abundance sponges is revealed by in situ study of carbon and nitrogen fluxes. *Limnol. Oceano.* 62, 1963–1983. doi: 10.1002/lno.10546

Morganti, T., Yahel, G., Ribes, M., and Coma, R. V. (2016). VacuSIP, an improved inex method for in situ measurement of particulate and dissolved compounds processed by active suspension feeders. *J. Visual. Exp.: JoVE* 114, 1–14. doi: 10.1007/978-3-319-17001-5_18-1

Morganti, T. M., Ribes, M., Yahel, G., and Coma, R. (2019). Size is the major determinant of pumping rates in marine sponges. *Front. Physiol.*10:1474. doi: 10.3389/fphys.2019.01474

Olinger, L. K., Scott, A. R., Mcmurray, S. E., and Pawlik, J. R. (2019). Growth estimates of caribbean reef sponges on a shipwreck using 3D photogrammetry. *Sci. Rep.* 9, 1–12.

Oren, O. (1969). Oceanographic and biological influence of the suez canal, the nile and the aswan dam on the levant basin. *Prog. Oceano.* 5, 161–167. doi: 10.1016/0079-6611(69)90038-x

Ozer, T., Gertman, I., Kress, N., Silverman, J., and Herut, B. (2017). Interannual thermohaline (1979–2014) and nutrient (2002–2014) dynamics in the levantine surface and intermediate water masses. se mediterranean sea. *Global Planetary Change* 151, 60–67. doi: 10.1016/j.gloplacha.2016.04.001

Pairaud, I. L., Bensoussan, N., Garreau, P., Faure, V., and Garrabou, J. (2014). Impacts of climate change on coastal benthic ecosystems: assessing the current

risk of mortality outbreaks associated with thermal stress in NW mediterranean coastal areas. *Ocean Dyn.* 64, 103–115. doi: 10.1007/s10236-013-0661-x

Peterson, B. J., Chester, C. M., Jochem, F. J., and Fourqurean, J. W. (2006). Potential role of sponge communities in controlling phytoplankton blooms in florida bay. *Mar. Ecol. Prog. Series* 328, 93–103. doi: 10.3354/meps328093

Santinelli, C. (2015). "DOC in the Mediterranean Sea," in *Biogeochemistry of marine dissolved organic matter (second edition)*, eds D. A. Hansell, and C. A. Carlson, (Pisa: Elsevier), 579–608. doi: 10.1016/b978-0-12-405940-5.00013-3

Sauleau, P., Moriou, C., and Al Mourabit, A. (2017). Metabolomics approach to chemical diversity of the mediterranean marine sponge agelas oroides. *Nat. Prod. Res.* 31, 1625–1632. doi: 10.1080/14786419.2017.1285298

Schmidt, O. (1864). *Supplement der Spongien des Adriatischen Meeres: enthaltend die Histologie und systematische Ergänzungen*. Leipzig: Engelmann.

Shaltout, M., and Omstedt, A. (2014). Recent sea surface temperature trends and future scenarios for the mediterranean sea. *Oceanologia* 56, 411–443. doi: 10.5697/oc.56-3.411

Topaloglu, B., and Evcen, A. (2014). Updated checklist of sponges (porifera) along the coasts of Turkey. *Turkish J. Zool.* 38, 665-676.

Tsurnamal, M. (1968). *Studies on the porifera of the mediterranean Littoral of Israel.* Ph.D, Thesis. Jerusalem: The Hebrew University.

Voultsiadou, E. (2005). Demosponge distribution in the eastern mediterranean: a NW-SE gradient. *Helgoland Mar. Res.* 59, 237–251. doi: 10.1007/s10152-005-0224-8

Voultsiadou, E. (2009). Reevaluating sponge diversity and distribution in the mediterranean sea. *Hydrobiologia* 628, 1–12. doi: 10.1007/s10750-009-9725-9

Webster, N., Pantile, R., Botte, E., Abdo, D., Andreakis, N., and Whalan, S. (2013). A complex life cycle in a warming planet: gene expression in thermally stressed sponges. *Mol. Ecol.*22, 1854–1868. doi: 10.1111/mec.12213

Webster, N. S. (2007). Sponge disease: a global threat? *Environ. Microbiol.* 9, 1363–1375. doi: 10.1111/j.1462-2920.2007.01303.x

Webster, N. S., Cobb, R. E., and Negri, A. P. (2008a). Temperature thresholds for bacterial symbiosis with a sponge. *ISME J.* 2, 830–842. doi: 10.1038/ismej.2008.42

Webster, N. S., Xavier, J. R., Freckelton, M., Motti, C. A., and Cobb, R. (2008b). Shifts in microbial and chemical patterns within the marine sponge aplysina aerophoba during a disease outbreak. *Environ. Microbiol.* 10, 3366–3376. doi: 10.1111/j.1462-2920.2008.01734.x

Yahel, G., Marie, D., and Genin, A. (2005). InEx—a direct in situ method to measure filtration rates, nutrition, and metabolism of active suspension feeders. *Limnol. Oceano. Methods* 3, 46–58. doi: 10.4319/lom.2005.3.46

Conflict of Interest: The authors declare that the research was conducted in the absence of any commercial or financial relationships that could be construed as a potential conflict of interest.

Copyright © 2020 Idan, Goren, Shefer and Ilan. This is an open-access article distributed under the terms of the Creative Commons Attribution License (CC BY). The use, distribution or reproduction in other forums is permitted, provided the original author(s) and the copyright owner(s) are credited and that the original publication in this journal is cited, in accordance with accepted academic practice. No use, distribution or reproduction is permitted which does not comply with these terms.

frontiers in Marine Science

ORIGINAL RESEARCH
published: 14 December 2020
doi: 10.3389/fmars.2020.613610

Surface Microornamentation of Demosponge Sterraster Spicules, Phylogenetic and Paleontological Implications

*Paco Cárdenas**

Pharmacognosy, Department of Pharmaceutical Biosciences, Uppsala University, Uppsala, Sweden

Siliceous spicules in demosponges exist in a variety of shapes, some of which look like minute spheres of glass. They are called "sterrasters" when they belong to the Geodiidae family (Tetractinellida order) and "selenasters" when they belong to the Placospongiidae family (Clionaida order). Today, the Geodiidae represent a highly diverse sponge family with more than 340 species, occurring in shallow to deep waters worldwide, except for the Antarctic. The molecular phylogeny of Geodiidae is currently difficult to interpret because we are lacking morphological characters to support most of its clades. To fill this knowledge gap, the surface microornamentations of sterrasters were compared in different genera. Observations with scanning electron microscopy revealed four types of surfaces, which remarkably matched some of the Geodiidae genera: type I characteristic of *Geodia*, type II characteristic of *Pachymatisma, Caminus,* and some *Erylus*; type III characteristic of other *Erylus*; type IV characteristic of *Caminella*. Two subtypes were identified in *Geodia* species: warty vs. smooth rosettes. These different microornamentations were mapped on new Geodiidae *COI* (Folmer fragment) and *28S (C1–D2)* phylogenetic trees. The monophyly of the Geodiidae was once again challenged, thereby suggesting that sterrasters have evolved independently at least three times: in the Geodiinae, in the Erylinae and in *Caminella*. Surface microornamentations were used to review the fossil record of sterrasters and selenasters through the paleontology literature and examination of fossils. It was concluded that "rhaxes" in the literature may represent mixes of sterrasters and selenasters: while *Rhaxella* spicules may belong to the Placospongiidae, *Rhaxelloides* spicules belong to the Geodiidae. The putative Geodiidae fossil genera, *Geoditesia,* and *Geodiopsis*, are reallocated to Tetractinellida *incertae sedis*. Isolated Miocene-Pliocene fossil sterrasters *Hataina* (Huang, 1967), *Silicosphaera* (Hughes, 1985) and *Conciliaspongia* (Robinson and Haslett, 1995) become junior synonyms of *Geodia* (Lamarck, 1815). Overall, the fossil record suggested that Geodiidae was present at least since the Middle Jurassic (163–166 Mya), while *Geodia* sterrasters were present since the Santonian/Campanian boundary, Late Cretaceous (83.6 Mya).

ZooBank Article Registration: urn:lsid:zoobank.org:pub:91B1B3AC-8862-4751-B272-8A3BDF4DEE77.

Keywords: Porifera, systematics, *Geodia*, *Placospongia*, *Rhaxella*, microfossils, sterrasters, selenasters

OPEN ACCESS

Edited by:
Joana R. Xavier,
University of Porto, Portugal

Reviewed by:
Hermann Ehrlich,
Freiberg University of Mining and Technology, Germany
Andrzej Pisera,
Institute of Paleobiology (PAN), Poland

***Correspondence:**
Paco Cárdenas
paco.cardenas@farmbio.uu.se

Specialty section:
This article was submitted to Deep-Sea Environments and Ecology, a section of the journal Frontiers in Marine Science

Received: *02 October 2020*
Accepted: *16 November 2020*
Published: *14 December 2020*

Citation:
Cárdenas P (2020) Surface Microornamentation of Demosponge Sterraster Spicules, Phylogenetic and Paleontological Implications. Front. Mar. Sci. 7:613610. doi: 10.3389/fmars.2020.613610

INTRODUCTION

Siliceous spicules in demosponges exist in a variety of shapes, some of which look like minute spheres of glass. These were first described and illustrated in the literature by Donati (1753), who found them in the species *Geodia cydonium* from the Adriatic Sea: he called these spicules "little balls." They are later called "globular crystalloids," "globate spicules," or "globostellates" by sponge taxonomists, until Sollas (1888, p. lxiv) finally coins the term "sterraster" (from the Greek "sterros" meaning "solid" and "firm"). Meanwhile, similar ball-shaped spicules are observed in another genus, *Placospongia*, and these are at first considered as "sterrasters" (Sollas, 1888) before Hanitsch (1895) coins the term "selenaster" for these different spicules (coming from the Greek word "selene" for "moon," referring to the "half-moon" shape). Finally, an additional term "aspidaster" is created by von Lendenfeld (1910, p. 267), convinced that the flattened sterrasters in the genus *Erylus* are significantly different from those in *Geodia*.

Sterrasters/aspidaster spicules are currently the main synapomorphy of the family Geodiidae (suborder Astrophorina, order Tetractinellida). This family currently includes five genera with sterrasters (*Geodia, Erylus, Pachymatisma, Caminella,* and *Caminus*) and several others that have secondarily lost their sterrasters (*Ecionemia, Stelletinopsis, Rhabdastrella, Melophlus, Penares*), some *Stelletta*, maybe even the Calthropellidae (Cárdenas et al., 2010, 2011). The Geodiidae therefore includes more than 340 species, without the Calthropellidae (Van Soest et al., 2020). They occur in shallow to deep waters worldwide (except for the Antarctic) (**Table 1**). *Geodia* represents the largest group with 163 species (Van Soest et al., 2020), and dozens of undescribed ones (P. Cárdenas, unpublished data). They can be massive animals, more than a meter large (Santucci, 1922; Corriero, 1987 (1989); Cárdenas et al., 2013), and six species of *Geodia* are particularly abundant and therefore important for the North Atlantic deep-sea ecosystems as key boreo-arctic sponge ground forming species (Klitgaard and Tendal, 2004; Cárdenas et al., 2013).

Selenasters are the main synapomorphy of *Placospongia* (family Placospongiidae, order Clionaida), a well-supported monophyletic genus (Becking, 2013) from shallow temperate/tropical waters worldwide. It is not a very diverse genus with only 10 species currently described (WPD) and a handful of undescribed species (Hajdu et al., 2011; Moraes, 2011; Becking, 2013). *Placospongia* species are usually small, encrusting, and never occur in high densities.

Sterrasters/selenasters are big enough to examine in some detail their surfaces with an optical microscope. However, the use of the scanning electron microscope (SEM) enabled a significantly better understanding of the surface microornamentations. A few descriptive terms have also appeared to describe and compare in greater detail the microornamentations of these ball-shaped spicules. Polyaxial spicules such as the sterrasters and aspidasters, are the result of fused "actines" (= branches of asters), later covered with "rosettes" made of different "rays." The "hilum" is a small area without rosettes or any kind of surface pattern. There are no particular terms to describe the surface of selenasters, except for the "hilum," also present. A few authors in the 1990s started to show good quality SEM close-ups of sterraster/selenaster surface and hilum (González-Farías, 1989; Lehnert, 1993; Boury-Esnault et al., 1994) but it is Mothes et al. (1999) and Adams and Hooper (2001) who systematized the SEM observation of the rosettes while revising *Erylus* species. da Silva (2002) continued and surveyed the sterrasters of Western Atlantic and Eastern Pacific *Geodia* species: in particular, she looked at the number of rays in the rosettes and the shape of the hilum in adult-stage sterrasters. This was followed by Cárdenas et al. (2009, 2013) who added measurements of the rosettes and hilum. Although there appears to be no significant variation in the size of the rosettes and hilum between species, Cárdenas et al. (2009, 2013) noticed that rosettes could be smooth or warty and hypothesized that this character could be of phylogenetic value if studied more broadly. Furthermore, the rosette morphology also seemed to be variable between *Geodia*, *Pachymatisma,* and *Caminella* (Cárdenas and Rapp, 2013; Cárdenas et al., 2018) which suggests that a more detailed study of the sterraster/aspidaster surface would potentially bring new characters for Geodiidae genera identification.

The present study proposes to test these two hypotheses: (i) surface microornamentations are different in the Geodiidae genera and (ii) smooth or warty rosette are restricted to certain *Geodia* clades. To this end, new SEM observations were made and mapped on updated molecular *COI* and *28S* phylogenies of the Geodiidae. Results will then be discussed in the light of the spicule microfossil record, especially with respect to the acknowledged and yet recurrent confusion of selenasters with sterrasters, as well as the nature of "rhax" fossils. Indeed, there is a need in sponge paleontology and micropaleontology for more robust loose-spicule markers. Finally, the timing of the emergence of sterrasters and selenasters in the fossil record will be estimated. This data will be essential for future time-calibrated sponge phylogenies, always in great need of robust calibration points.

Abbreviations: CASIZ, California Academy of Sciences Invertebrate Zoology, San Francisco, CA, USA; CNPGG, Colección Nacional del Phylum Porifera "Gerardo Green," Instituto de Ciencias del Mar y Limnología, Universidad Nacional Autónoma de México, Mexico; HBOI, Harbor Branch Oceanographic Institute, Florida Atlantic University, Fort Pierce, FL, USA; MNHN, Muséum National d'Histoire Naturelle, Paris, France; MNRJ, Museu Nacional Rio de Janeiro, Brazil; NHM, Natural History Museum, London, UK; NHMUK PI, Palaeontology collection, Natural History Museum, London, UK; NIWA, National Institute of Water and Atmospheric Research, New Zealand; NTM, Museum and Art Gallery of the Northern Territory, Darwin, Australia; PC, personal collection (P. Cárdenas); RMNH, Rijksmuseum van Natuurlijke Historie, Naturalis Biodiversity Center, Leiden, The Netherlands; SAMA, South Australian Museum, Adelaide, Australia; SME, Station Marine d'Endoume, Marseille, France; UPSZMC, Zoological Museum of Uppsala, Uppsala, Sweden; USNM, Smithsonian National Museum of Natural History, USA; ZMAPOR, Amsterdam Porifera collection, now stored at Naturalis, Leiden, The Netherlands; ZMBN, Bergen Museum, Bergen, Norway.

TABLE 1 | Overview of demosponge groups with ball-shaped spicules.

Family (subfamily) *genus*	Ball-shaped spicule	Number of recent species (WPD)	Habitat	Distribution
Geodiidae (Geodinae)	Sterraster		Shallow to deep-sea (3,100 m)	Worldwide, polar to tropical waters
Geodia		163		
Geodiidae (Erylinae)	Sterraster to aspidaster		Shallow to deep-sea (1,740 m)	Worldwide temperate to tropical waters
Caminus		9		
Caminella		4		
Pachymatisma		6		
Erylus		68		
Placospongiidae	Selenaster		0–67 m	Worldwide, temperate to tropical waters
Placospongia		10		

MATERIALS AND METHODS

Observation of Recent Sterrasters

SEM illustrations of sterrasters from the literature were compiled, especially for species for which molecular data exists, in order to later map these characters on a molecular phylogeny. Additionally, sterraster spicules from several species belonging to all Geodiidae genera (*Geodia, Erylus, Pachymatisma, Caminella,* and *Caminus*) were examined using SEM. Sterrasters were obtained from specimens by digesting a small piece of the cortex (0.5 × 0.2 cm) in chlorine. After several washes with water, 50% ethanol and 100% ethanol, spicules were placed on top of a cover slip glass taped to a stub and coated with a gold/palladium mix, before being observed with a SEM.

To examine the position of sterrasters in the cortex of *Geodia barretti*, two preparations were made. First, a fresh piece including cortex was preserved in 2.5% glutaraldehyde in 0.4 M PBS (with 0.34 M NaCl). The sample was further rinsed using a solution of 0.6 M NaCl and PBS and postfixed in 1% osmium tetroxide-potassium ferrocyanide for 1h at 4°C. Then it was rinsed in PBS and distilled water several times, and dehydrated through an ethanol series. Once in 100% ethanol, the sample was immersed in liquid nitrogen for cryofracture, and hit with a metal hammer to break it in pieces with smooth surfaces. Finally, the sample was critically point-dried, carbon-coated (20 nm), and imaged in a ZEISS Ultra Plus Field Emission SEM. Secondly, a piece was frozen on the field, preserved at −80°C, before being freeze-dried. A thick section cut with a scalpel blade was glued to an SEM stub before being gold/palladium coated and observed in a ZEISS Supra 35VP SEM.

Some Astrophorina subsamples from the U.S. National Cancer Institute's (NCI) collection of sponges and sequenced by the PorToL project (Porifera Tree of Life)[1] were re-examined for this study and their identifications revised. NTM Z005203 (off Darwin, northern Australia, 6 m) was originally identified as *Geodia* sp., "NCI135" in Redmond et al. (2013) but re-examination of the specimen for this study revealed a typical oscule-like cloaca and the presence of characteristic short-shafted triaenes and spherules (albeit irregular) in the ectocortex so it was re-identified as *Caminus* sp. (probably a new species). CASIZ 301086 (South Africa, 27 m) originally identified as *Penares* cf. *alata*, "NCI181" (Redmond et al., 2013; Thacker et al., 2013) was not *Penares alata* and so it was renamed *Penares* sp. CASIZ 300347 (Misima Island, Papua New Guinea, 23 m) originally identified as *Penares nux*, "NCI450" (Redmond et al., 2013; Thacker et al., 2013) was re-identified as *Neamphius* cf. *huxleyi*. HBOI 14-VIII-09-2-004 (Florida, Canaveral bioherms, 492 m) originally identified as *Pachastrella* sp., "JR15" in Thacker et al. (2013) was re-identified as *Characella* sp.

[1] https://poriferatreeoflife.org

Observation of Fossil Material

Slides and specimens from the fossil collection of the NHM were examined, including slides of *Rhaxella perforata* Hinde, 1890 (NHMUK PI S1682, 1683a, 1684) from the type locality, Late Jurassic, Oxfordian (Lower Calcareous Grit Formation, Scarborough, North Yorkshire, England); *R. perforata* spicules were measured using an optical microscope. A thick section from a *Rhaxella* chert (S7502, Oxford, Suffolk, Red Crag Formation, Pliocene-Pleistocene) was also examined. Slides of potential Geodiidae fossils, genera *Geodiopsis* (Schrammen, 1910) and *Geoditesia* Zhuravleva, in Rezvoi et al. (1962) (previously *Geodites*; Carter, 1871), were examined: *Geodiopsis cretacea* (Schrammen, 1899), prepared from holotype (NHMUK PI P6702, P6703, P6704) from the Late Cretaceous, Campanian (Oberg, N. Germany); *Pachymatisma virga* (Hinde, 1885) (NHMUK PI S1070, S1041, S1069, syntypes), *Geodites haldonensis* (Hinde, 1885), *Geodites carteri* (Hinde, 1885), *Geodites gracilis* (Hinde, 1885), *Geodites divergens* (Hinde, 1885) (NHMUK PI S1054, S1073, syntypes), all from the Late Cretaceous, Albian-Cenomanian (Upper Greensand Formation, southern England).

Two specimens (S10–13, S10–18) of *Geoditesia jordanensis* (Ungureanu et al., 2018) (courtesy of F. Ahmad) were examined, they come from the Middle Jurassic, Callovian (Mughanniyya Formation, northwestern Jordan). Specimen S10–13 was sectioned with an ISOMET diamond saw (speed 5) to obtain a 1 mm thick section. After a mild dissolution with 1% acetic acid (7 min), the section was oven-dried (2 h, 60°C) and coated before SEM observation. The surface of half of the specimen S10–18 was directly coated before SEM observation.

Finally, the paleontology literature was surveyed for all records of ball-shaped spicules: sterrasters, selenasters, rhaxes

and spherical/subspherical spicules. The information from 60 articles mentioning ball-shaped fossil spicules was compiled in **Supplementary Table S1**, where the following data was recorded: age, locality/lithostratigraphic unit, morphology of the spicule, abundance, size, siliceous or calcite, paleoenvironment/depth, and taxonomic ID.

Molecular Phylogenetic Study

In order to understand the evolution of sterraster morphology, surface microornamentations were mapped on a molecular phylogeny of the Geodiidae. However, because previous molecular phylogenetic studies challenge the monophyly of the Geodiidae (Cárdenas et al., 2011; Schuster et al., 2015; Kelly et al., 2019) all Astrophorina sequences were included in our analyses; one Thoosina (*Alectona millari*) and the deep-diverging Theneidae were used as outgroups. The Astrophorina *cytochrome c oxidase I* (*COI*) (Folmer fragment) and *28S (C1–D2)* alignments from Kelly et al. (2019) were retrieved and *COI* was sequenced for a few more species for which sterraster SEM detailed observations were available in the literature or examined in this study: *Geodia pocillum* (Van Soest, 2017), holotype RMNH POR 10547; *Geodia garoupa* (Carvalho et al., 2016), holotype MNRJ 7349; *Geodia* cf. *curacaoensis* (Van Soest et al., 2014), HBOI 14-XI-02-1-003 (Bahamas, 439 m), id by PC; *Geodia nodastrella* (Carter, 1876), field# BANGAL 0710-041DR06110810, id by PC (Galicia Bank, 920 m); *Geodia japonica* (Sollas, 1888), field#AB15-0035 (Eastern Gulf of Alaska, United States, 89 m), id by Lehnert and Stone (2016); *Pachymatisma nodosa* (Sim-Smith and Kelly, 2015), holotype NIWA 53817; *Caminella prima* (Sim-Smith and Kelly, 2015), holotype NIWA 51723; *Geodia margarita* (Sim-Smith and Kelly, 2015), holotype NIWA 71189; *Penares euastrum* (Schmidt, 1868), previously called *Erylus euastrum*, PC631 (Capo Rizutto, Italy, 150 m); *Caminus carmabi* (Van Soest et al., 2014), HBOI 11-V-00-1-007 (Curacao, 282 m), id by PC; *Caminus* sp., NTM Z005203, PorToL project, id by PC (Darwin, North Australia, 6 m).

DNA was extracted using the DNeasy Blood and Tissue kit (Qiagen, Hilden, Germany). *COI* (658 bp) amplification was done using universal Folmer primers HCO and LCO with the PCR program: [5 min/94°C; 35 cycles (15 s/94°C, 15 s/46°C, 15 s/ 72°C); 7 min/72°C]. Folmer primers commonly fail to amplify *COI* for most *Erylus/Penares* species so *Penares euastrum COI* was sequenced in two parts: part (1) is the minibarcode (130 bp) obtained with primers LCO/Tetract-minibarR1 (Cárdenas and Moore, 2019) and part (2) obtained with primer jgHCO (Geller et al., 2013) and primer ErylusCOI-F2 (5'-CTCCYGGATCAATGTTGGG-3') (Cárdenas et al., 2018); PCR program was the same for with Folmer primers. *COI* sequences from *Erylus trisphaerus* (de Laubenfels, 1953) (HBOI 12-VIII-95-2-2, Florida, United States, 55 m) could not be amplified so a part of *28S* (the C1–D1–C2 domains, 369 bp) was sequenced instead using primer pair C1'/Ep3 (Chombard et al., 1998) with the same PCR program except for a 50°C annealing temperature. After many failed attempts to amplify *28S (C1–D2)* of *Geodia atlantica* (Stephens, 1915) and *Geodia phlegraei* (Sollas, 1880b) by PCR with primers C1'/D2 (Cárdenas et al., 2011), the shorter C1–C2 fragment was obtained using primers C1'/Ep3. These sequences were used to fish the longer C1–D2 fragment in transcriptomes of these two species (Genbank BioProject ID: PRJNA603347), obtained from specimens from Northeast Atlantic specimens (courtesy of A. Riesgo and V. Koutsouveli); this was done through local Blasts using CLC Genomics Workbench 5.5. All new sequences were submitted to Genbank: 11 *COI* sequences (MT815820–MT815830) and three *28S* sequences (MT835460–MT835462).

The *COI* data matrix included 112 sequences and was 658 bp long; the *28S* data matrix included 110 sequences and was 857 pb long. The *28S* alignment was automatically aligned using MAFFT v.7 (Katoh and Standley, 2013), L-INS-i option, implemented in AliView 1.26 (Larsson, 2014). *COI* and *28S* final alignments can be found in the **Supplementary Material**. Phylogenetic analyses were conducted on the CIPRES science gateway v. 3.3[2] (Miller et al., 2010): RAxML 8.2.12 (Stamatakis, 2014) for maximum likelihood (ML). For RAxML, 1,000 bootstrap iterations were run.

RESULTS AND DISCUSSION

Rosettes of Sterrasters, a Structure for Matrix Attachment

Sterrasters tethered with fibers in the cortex were observed in historical observations with optical microscopes (Donati, 1753; Sollas, 1880c; von Lendenfeld, 1894; **Figures 1A,B**) and much later confirmed with a transmission electron microscope (Müller et al., 2007; **Figures 4G,H**). In this study, these structures are observed for the first time with the SEM. Cryofractured and freeze-dried cortex preparations of *G. barretti* showed that sterrasters were inserted in a dense collagen-type matrix (**Figure 1C**) and linked to each other with fibrils (**Figures 1C,D**). Sollas (1882, p. 142) mentions that a few fusiform cells are intermingled with the collagen fibers but this could not be confirmed. In the cryofractured preparation empty cavities were left after the dissolution of the sterrasters. In the sterraster molds, every rosette had its own mold, giving it a honeycomb-like structure (**Figures 1D,E**); this showed that the rosettes are deeply inserted in the matrix. Moreover, additional holes and thread-like structures were present within each rosette mold (**Figure 1E**), representing the molds of the rosette rays. These observations highlight the role of these rosettes as hook structures on which the collagen matrix is interlocked. On the freeze-dried preparations, where spicules were not dissolved, fibers were clearly seen attached to the sterraster rosettes (**Figure 1F**), enveloping the rosettes rays, thus confirming previous historical observations (Sollas, 1888, p. lxiv). It is reasonable to suggest that the complex microornamentations of rosettes offer a stronger grip for the collagen fibers than if the sterrasters were smooth. This is of importance to fulfill the main function of the sterraster Geodiidae cortex: a solid physical protection of the sponge against predators. Indeed, sterrasters *per se* do not seem to be deterrent to fish spongivores (Chanas and Pawlik, 1995) but when strongly interconnected to each other they form a protective barrier

[2]http://www.phylo.org

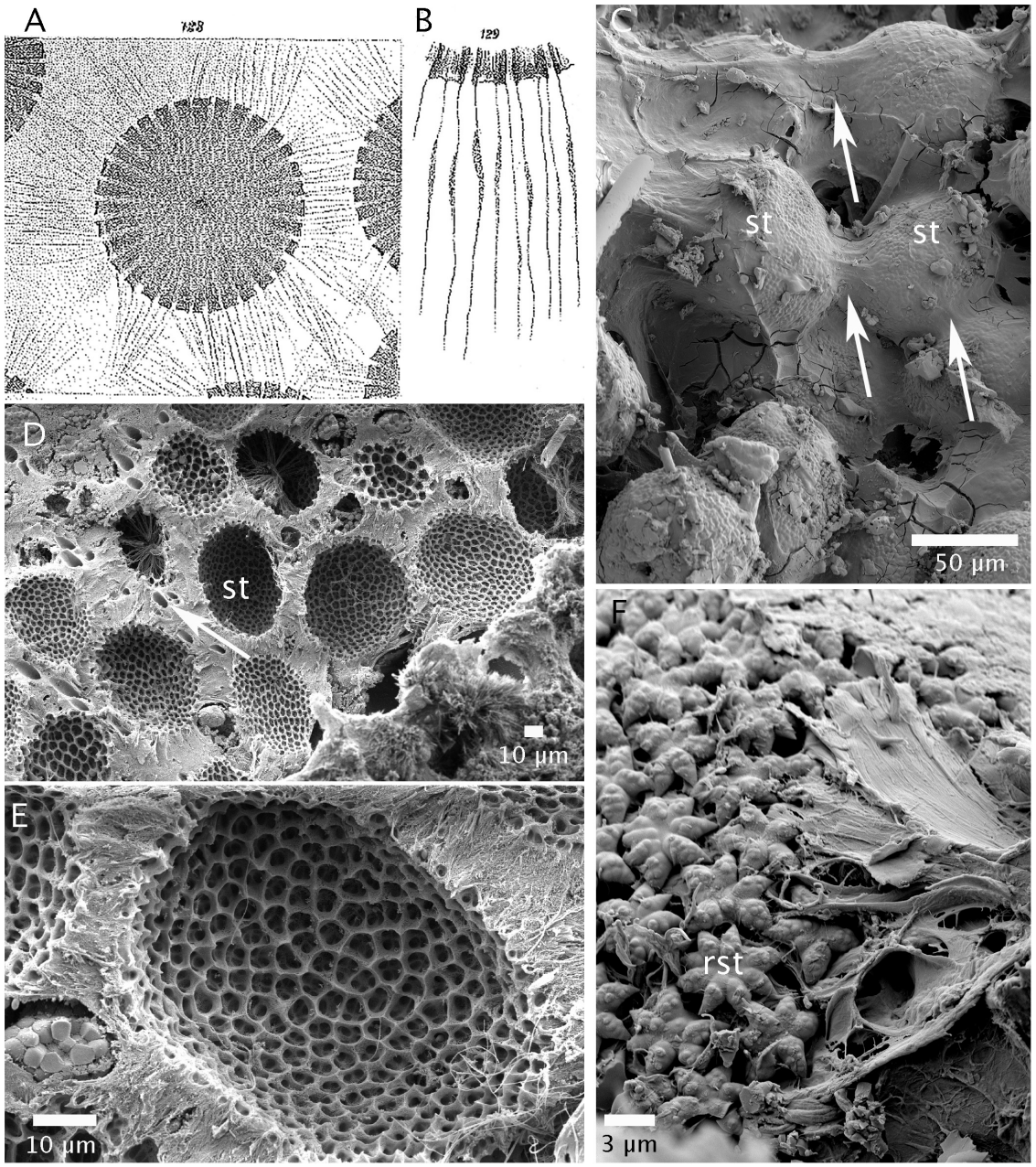

FIGURE 1 | Position of sterrasters in the cortex. **(A)** Sterrasters in the endocortex of *Geodia cydonium*, connected via fibers, drawing is a copy from von Lendenfeld, (1894, plate VIII, 128). A sterraster in this species is 70 μm in diameter. **(B)** Possible fibrous cells attached to sterraster rosettes, drawing is a copy from von Lendenfeld, (1894, plate VIII, 129). A rosette is 5 μm in diameter. **(C)** Freeze-dried cortex of *Geodia barretti* showing fiber bundles (arrows) connecting the sterrasters (st). Scale: 50 μm. **(D)** Cryofracture in the cortex of *G. barretti* with spicules dissolved beforehand. Pockets in which sterrasters (st) are positioned in the endocortex, surrounded by a dense collagen-type matrix. Other holes (white arrow) indicate the position of the microxeas crossing the cortex. Scale: 10 μm. Picture: V. Koutsouveli and A. Riesgo. **(E)** Sterraster mold showing that every rosette is tightly inserted in a pocket, in the matrix. A spherulous cell is visible on the left (just above the scale). Same specimen as in D. Scale: 10 μm. Picture: V. Koutsouveli and A. Riesgo. **(F)** Close-up of a sterraster showing fibrils attached to the warty rosettes (rst), Same specimen as in C. Scale: 3 μm.

against these predators: when *Geodia* species have a damaged cortex, it is common to see fish feed on them (Hill and Hill, 2002; personal observation). The beak of the hawksbill turtle (Meylan, 1988) or the radula of chitons (Todt et al., 2009) are specialized tools that can respectively rupture or dig into the sterraster cortex. And yet, the cortex must be malleable enough to also allow for growth and movement of cells that cross it to reach the surface, e.g., spherulous cells transporting specialized metabolites (**Figure 1E**). The cortex toughness and flexibility is the result of this network of sterrasters, interconnected by fibers hooked to the

rosettes. These silica-collagen composite structures could have biomimetic potential and be a source of inspiration to produce strong and yet flexible structures such as coatings or fasteners.

Differences and Similarities of Sterrasters and Selenasters

Although sterrasters and selenasters are both subspherical spicules, this is the result of convergent evolution as shown by the independent evolutionary history of Geodiidae and Placospongiidae (e.g., Redmond et al., 2013), and by the different ontogeny of these spicules: sterrasters originate from a polyaxial microsclere (euaster) while selenasters originate from a straight to slightly twisted monoaxial microsclere (spiraster-derived), which explains the common bean shape of selenasters (Vosmaer and Vernhout, 1902). **Table 2** summarizes the resulting differences and similarities of both spicules, which will be detailed in this part, based on new SEM observations. These characters will be of importance for the micropaleontology discussions and interpretations that follow.

Both sterrasters and selenasters have a small shallow depression called "hilum" (**Figures 2–8**). In sterrasters, the hilum has been shown to mark the position of the microsclerocyte nucleus during spiculogenesis, taking place in the choanosome (Sollas, 1880c, p. 256). The hilum is usually a smooth depression, with occasional spines in sterrasters (**Figures 2–6**) and occasional ridges in selenasters (**Figure 8**). Therefore, bean-shaped selenasters have a notch marking the bend as well as a hilum (**Figure 7**); selenasters do not always have a notch, but they always have a hilum. In sterrasters, there is always a hilum (**Figures 2–6**), unless the sterraster is too small and it does not compete for space with the nucleus [e.g., no hilum in *Geodia cordata*, the sterrasters are only 25–30 μm (**Figure 2G**) vs. >50 μm in most other *Geodia*].

Hila size is 10–30 μm in diameter in the Geodiidae (Cárdenas and Rapp, 2013; Cárdenas et al., 2013; **Figures 2– 6**) and is 12–15 μm deep (this study) in sterrasters to very shallow in flat aspidasters. Selenaster hilum measurements are absent from the literature except for *Placospongia ruetzleri*, for which a diameter of 10–13 μm is reported (Van Soest, 2017). Selenaster hila measured from a specimen of *Placospongia decorticans* (Pointe Fauconnière, cave near Marseille, France, J. Vacelet collection, Endoume marine station) gave 5–10 μm in diameter and 5 μm deep. Moreover, selenaster hila measured on SEM plates from the literature (Becking, 2013; Rützler et al., 2014) gave dimensions of 4–10 μm. The hilum is therefore smaller and shallower in selenasters than in sterrasters. This incidentally suggests that nuclei in selenaster microsclerocytes are smaller than in sterraster microsclerocytes.

In terms of spicule size, selenasters are 30–100 μm in length (Becking, 2013). *Geodia* sterrasters are usually larger than 50 μm except for shallow water species which can have smaller sterraster sizes (25–50 μm) (da Silva, 2002). Furthermore, many *Geodia* have sterrasters that reach 100 μm in size, and beyond (da Silva, 2002; Cárdenas et al., 2013; Sim-Smith and Kelly, 2015): sterrasters of *Geodia macandrewii* are 124–360 μm in diameter (Cárdenas et al., 2013), *Geodia australis* sterrasters are 266–352 μm (da Silva and Mothes, 2000) while those of *Geodia rex* can reach 565 μm in length (Sim-Smith and Kelly, 2015). Sterrasters in the genus *Erylus* (50–300 μm in length) (Adams and Hooper, 2001; Sim-Smith and Kelly, 2015), *Caminus* (40–210 μm in diameter) (Shim and Sim, 2012; Van Soest et al., 2014), and *Caminella* (35–110 μm in diameter) (Cárdenas et al., 2018) have similar sizes than in *Geodia*. Despite the size overlap, it is noteworthy that sterrasters can be significantly larger than selenasters in some species.

With respect to shape, sterrasters and selenasters can have very similar subspherical shape but can also show differences, depending on the species. Sterrasters are spherical to subspherical (**Figures 2–5**), more rarely lozenge-shape (when viewed from the hilum side); aspidasters are oval to discoid, lemon- or lozenge-shape, to almost cylindrical (**Figures 5**, **6**). Selenasters are never spherical but are commonly subspherical (e.g., in *P. ruetzleri* and *Placospongia caribica*, **Figures 7A–C**). Selenasters of *P. decorticans* are bent and elongate (sausage-like) (**Figure 7F**) while selenasters of *Placospongia mixta*, *Placospongia melobesioides,* and *Placospongia carinata* can have the typical reniform or bean shape (Becking, 2013) although they can also be subspherical without any obvious notch (**Figure 7D**). Finally, one noticeable difference is that selenasters can be colored, and may actually be responsible for the color of the species (Vosmaer and Vernhout, 1902); sterrasters are never colored.

A major difference between sterrasters and selenasters is their surface microornamentations. Selenasters have a polygonal surface, first mentioned by Hanitsch (1895, p. 215) and well illustrated by Lindgren (1898, p. 18). SEM observations of selenasters provided additional details on the surface microornamentations (**Figure 8**). The main knobs are 1 μm in diameter, and 2.5–5 μm away from each other (**Figure 8A**), depending on the species. Each knob was connected to 5–7 radial ridges, which form minor swellings when they meet from opposite sides. The main knobs and its radial ridges formed pentagons, hexagons or heptagons, 3–6 μm wide. Sterrasters from *Geodia* have characteristic surface rosettes, already mentioned by Sollas (1877). However, a comprehensive morphological comparison of these rosettes using the SEM revealed differences between the Geodiidae genera.

Surface Microornamentations, a New Character for Geodiidae Genera Assignation

In this study, only adult-stage sterrasters were considered since early-stage sterrasters are all fairly similar and look like polyaxial asters with no microornamentations. **Figures 2–6** show the diversity of sterrasters within the Geodiidae, and especially the clear differences in surface microornamentations between genera. Four main types of surface microornamentations were singled out and listed in **Table 3**. (1) *Geodia* species have sterrasters with entirely fused actines at the tip of which radial sets of spines form the typical rosettes (**Figures 2**, **3**). (2) *Pachymatisma, Caminus* and some *Erylus* (*E. mamillaris, E. discophorus, E. granularis*) have partly fused actines, the sides and tips of which are covered with numerous spines, often overlaying

TABLE 2 | Morphological comparison of Recent sterrasters and selenaster.

	Shape	Size (length in μm)	Hilum (diameter/depth) in μm	Axial canals	Surface	Color
Sterraster	Spherical to subspherical, and lozenge-shape (more rare)	25–560	10–30/12–15	In actines, rosettes and rays	Rosettes	None
Selenaster	Subspherical to reniform and sausage-like shape	30–100	4–13/5	None	Polygonal pattern around a central knob	None to red

each other, and with no symmetry (i.e., difficult to distinguish clear separated rosettes) (**Figures 4**, **5**). (3) Other *Erylus/Penares* (*E. formosus, E. expletus, E. aleuticus, E. trisphaerus, E. topsenti, Penares euastrum*) have partly or totally fused actines (with often an intermediate stage of entirely smooth aspidaster/sterraster) on which radial sets of spines make up clear single rosettes (**Figure 6**). (4) Finally, *Caminella* actines produce at their tips, small perpendicular bridges that reach toward the other actines, creating a complex fused network (**Figure 4**). These rosette morphology categories might be refined in the future to subdivide these groups even further but more SEM observations and sequenced species are necessary for this, especially amongst the *Erylus* species.

The phylogenetic distributions of these different categories of surface microornamentations match quite well the different Geodiidae clades, except in the Erylinae (**Figure 9** and **Supplementary Figure S1**). *Erylus* is subdivided in at least two groups, with one group (*Erylus discophorus* complex and *E. granularis*) with surface microornamentations similar to those in *Caminus* and *Pachymatisma* than to the other *Erylus*. These *Erylus* species also share with *Pachymatisma* spiny microrhabds (vs. smooth microrhabds in other *Erylus* species). The polyphyly of *Erylus* has already been suggested based on molecular phylogenies and oscule morphology (Cárdenas et al., 2010). As in Cárdenas et al. (2011), the *28S (C1–D2)* marker suggested a sister group relationship of *Pachymatisma* with the *Erylus discophorus/granularis* clade (**Supplementary Figure S1**), albeit unsupported (bootstrap of 48); the *COI* tree does not suggest that relationship (**Figure 9**). Overall, these results suggest that the flattening of sterrasters (aspidasters) happened independently at least twice in the Erylinae.

The *COI* and *28S* phylogenetic results do not recover a monophyletic Geodiidae (**Figure 9** and **Supplementary Figure S1**), although all the intermediate nodes between Geodiinae, Erylinae, and *Caminella* are not supported. Previous molecular trees show a poorly-supported Geodiidae clade (Cárdenas et al., 2011) or even fail to recover the monophyly of the Geodiidae (Redmond et al., 2013; Schuster et al., 2015; Kelly et al., 2019), with *Caminella* somewhat close to the Calthropellidae and the Erylinae (Cárdenas et al., 2018). Knowing how widespread spicule convergent evolution is in sponges (Cárdenas et al., 2011; Vargas et al., 2013; Schuster et al., 2015), the diversity of sterraster surfaces could represent at least three independent evolution of sterrasters—in the Geodiinae, in the Erylinae and in *Caminella*—thereby further questioning the monophyly of the Geodiidae. Each type of sterraster may have evolved from an astrophorin ancestor with euasters. After all, euasters themselves have appeared several times in demosponges: in *Chondrilla*, Tethyida, Stelligeridae, and even in some Poecilosclerida (Vacelet and Cárdenas, 2018).

As a proof of concept of the phylogenetic value of sterraster microornamentations, the phylogenetic position of two Geodiidae with doubtful genera allocations was tested. Cárdenas et al. (2018, p. 193) had already noticed that the sterraster microornamentations of *Caminus primus* (Sim-Smith and Kelly, 2015) from New Zealand suggested its transfer to the genus *Caminella*. Its well-supported phylogenetic position within the *Caminella* clade in our *COI* phylogenetic tree confirms this reallocation under the name *Caminella prima* (**Figure 9**). Likewise, the sterrasters of *Pachymatisma nodosa* (Sim-Smith and Kelly, 2015), from New Zealand have a typical *Geodia* rosette pattern, which hinted to a wrong genera assignment. The *COI* grouping of *P. nodosa* within the *Geodia* clade confirmed this hypothesis (**Figure 9**). Furthermore, after examination of slides made from the holotype (NIWA 53817) "microrhabds" as described by Sim-Smith and Kelly (2015) were observed, thereby confirming their close similarity to *Pachymatisma* microrhabds. However, the *COI* sequence of the holotype was identical to that of a deep-sea *Geodia* sp. (IRD-NC-R1820) from New Caledonia (Stylaster Bank) previously sequenced by Cárdenas et al. (2011), this specimen has mostly irregular strongylasters. Further work is needed to test the conspecificity of *P. nodosa* and our *Geodia* sp. but it revealed that the "microrhabds" of *P. nodosa* are in fact modified strongylasters, thus confirming its reallocation to *Geodia*. The name *Geodia nodosa* comb. nov. is formally proposed for this species. In a similar fashion, sterraster surface microornamentations could be useful to revise further poorly known Geodiidae species with uncertain genus allocations.

With their highly sophisticated morphology and microornamentations, sterrasters and/or selenasters may also be considered for future biotechnological or medical applications, as suggested for other types of biosilica material (Wysokowski et al., 2018). For instance, Kaya et al. (2020) propose to use partially dissolved sterrasters for bone tissue or controlled drug release applications, while Schoeppler et al. (2017) study sterrasters to understand the regularity of silica architecture in spicules.

Warty Rosettes Appearance in *Geodia* Evolution

Cárdenas et al. (2013, p. 50) previously recognized that sterrasters from *Geodia* species had either smooth (**Figure 2**) or warty rosettes (**Figure 3**) and suggested that this could

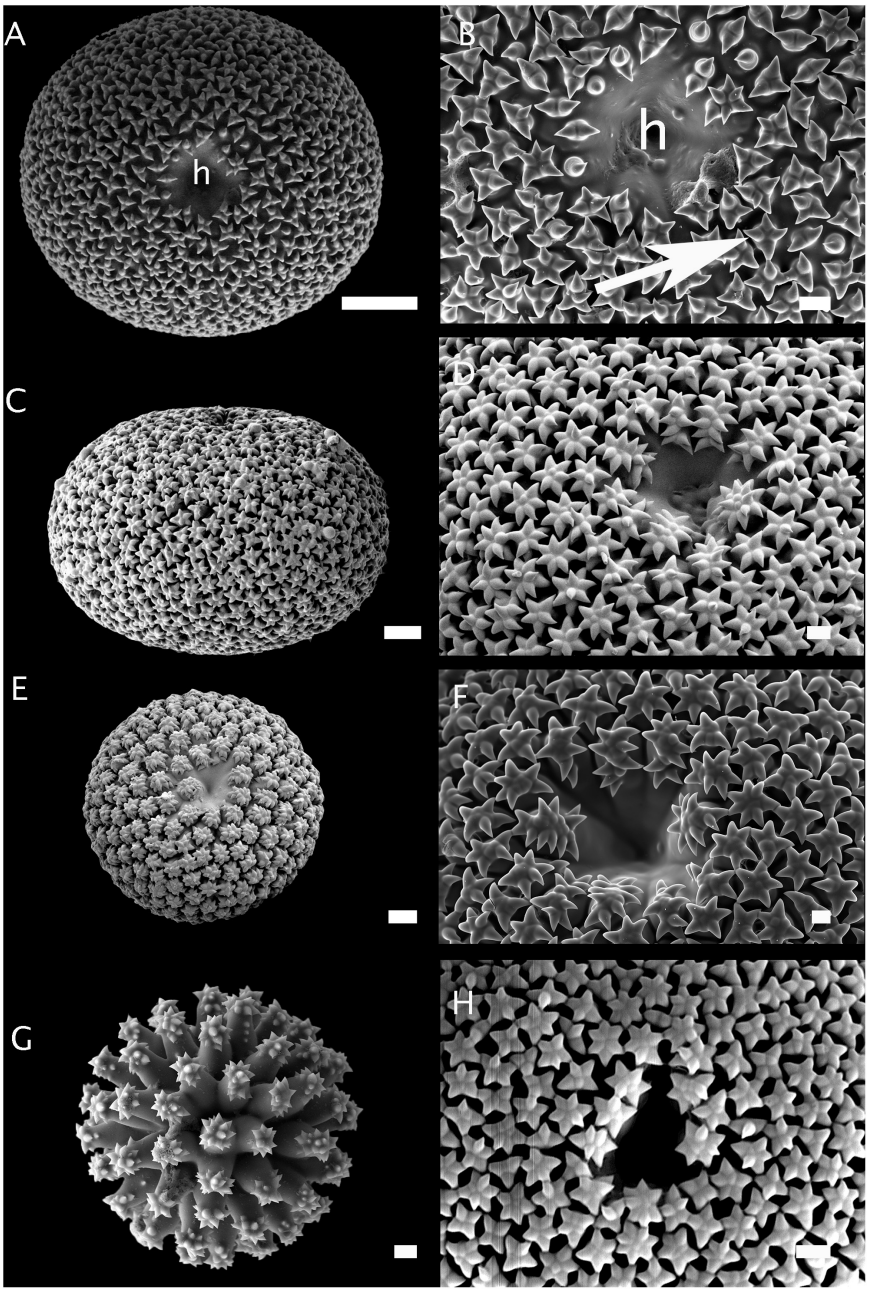

FIGURE 2 | Morphology of sterrasters with smooth rosettes. **(A,B)** Sterraster of *Geodia atlantica* (holotype, S.R.151-27/364-1914); (h) is the hilum; the arrow points to a smooth rosette made up of rays. Scale A: 20 μm. Scale B. 2 μm. **(C,D)** Sterraster of *Geodia phlegraei* (holotype, NHM 1910.1.1.840). Scale C: 10 μm. Scale D. 2 μm. **(E)** Sterraster of *Geodia parva* (holotype, ZMBN 100). Scale: 10 μm. **(F)** Sterraster of *Geodia gibberosa* (holotype, MNHN-DT 608). Scale: 2 μm. **(G)** Sterraster of *Geodia cordata,* previously called *Rhabdastrella cordata* (South Australia, SAMA S1026). Scale: 2 μm. **(H)** Sterraster of *Geodia vaubani* (New Caledonia, MNHN-IP-2015-1667). Scale: 5 μm.

potentially represent an informative phylogenetic character. This character was therefore carefully compiled from the literature and new SEM observations (**Table 3**) and mapped on the *COI* (**Figure 9**) and *28S* trees (**Supplementary Figure S1**). Results showed that warty rosettes are restricted to two sister clades provisionally named *Depressiogeodia*^{p} and *Cydonium*^{p} by Cárdenas et al. (2011), following the rules of the *PhyloCode*[3]. The character of "warty rosettes" would therefore be a morphological synapomorphy for the *Depressiogeodia*^{p}+*Cydonium*^{p} clade, which always appeared monophyletic, albeit with low support (bootstrap of 53 for *28S* and 76 for *COI*).

[3]http://phylonames.org/code/

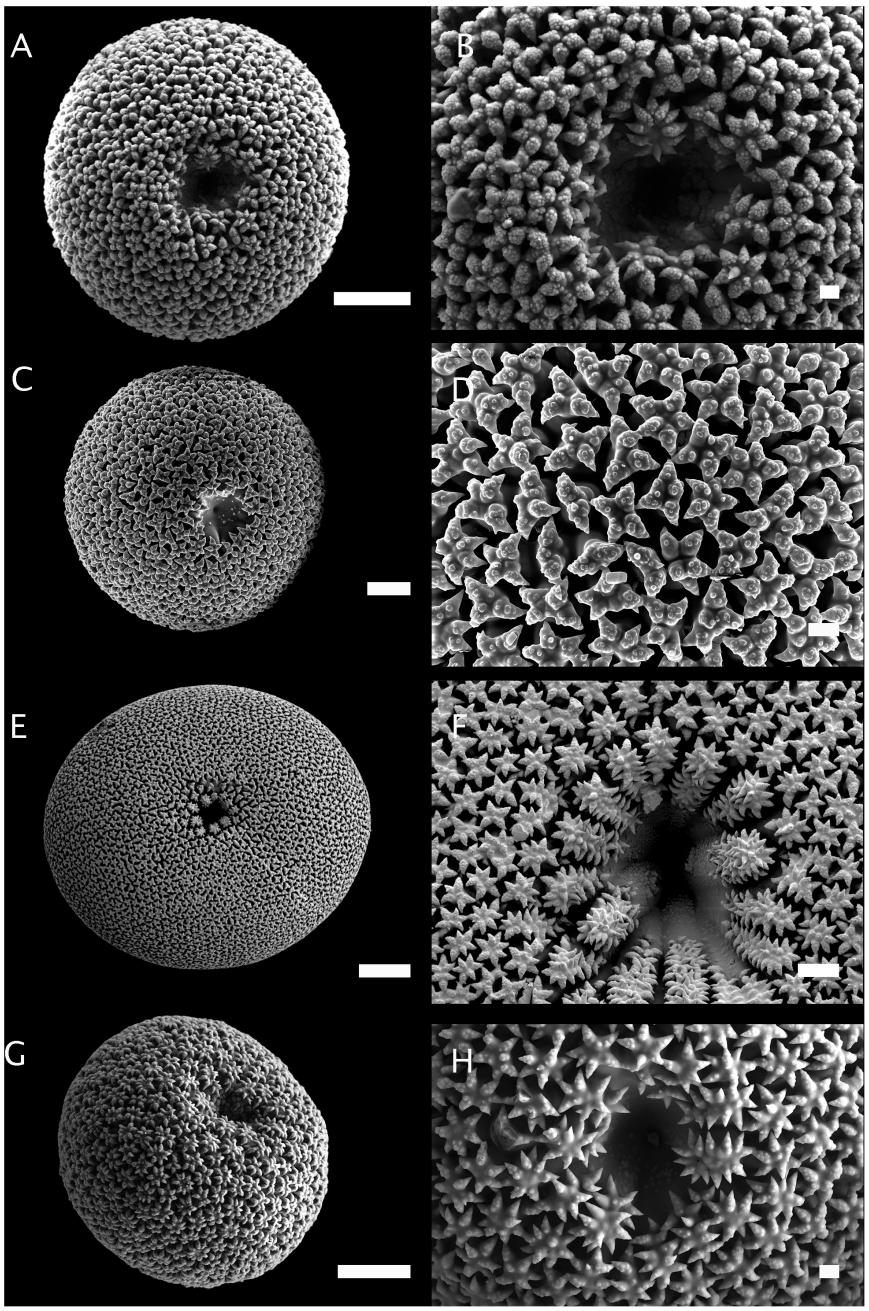

FIGURE 3 | Morphology of sterrasters with warty rosettes. **(A,B)** Sterraster of *Geodia barretti* (Norway, ZMBN 77922). Scale A: 20 μm. Scale B. 2 μm. **(C,D)** Sterraster of *Geodia papyracea* (holotype, YPM 5045). Scale C: 10 μm. Scale D. 2 μm. **(E,F)** Sterraster of *Geodia macandrewii* (Norway, ZMBN 89717). Scale E: 50 μm. Scale F: 2 μm. **(G,H)** Sterraster of *Geodia cydonium* (Croatia, ZMBN 77923). Scale G: 20 μm. Scale H: 2 μm.

Again, as a proof of concept, the *COI* phylogenetic positions of several recently described *Geodia* species with warty rosettes were tested (**Table 3**): *Geodia margarita*, *Geodia japonica*, *Geodia pocillum*, *Geodia garoupa, Geodia curacaoensis,* and *Geodia nodastrella*. These species clustered with *Depressiogeodia*^{p} (*G. garoupa*) or with *Cydonium*^{p} (*Geodia margarita*, *Geodia japonica*, *Geodia pocillum*, *Geodia garoupa*, *Geodia nodastrella,* and *Geodia curacaoensis*) thereby validating the warty rosette as a synapomorphy of the *Depressiogeodia*^{p}+*Cydonium*^{p} clade.

A potential morphological synapomorphy of the *Depressiogeodia*^{p} clade is the deep preoscule (Cárdenas et al., 2011, p. 9). Interestingly, there is no mention of deep preoscules in *G. garoupa* (Carvalho et al., 2016), although its *COI* had only a 2 bp. difference with the NW Atlantic haplotype of *G. barretti* (KC574389). A re-examination of the type material of *G. garoupa*

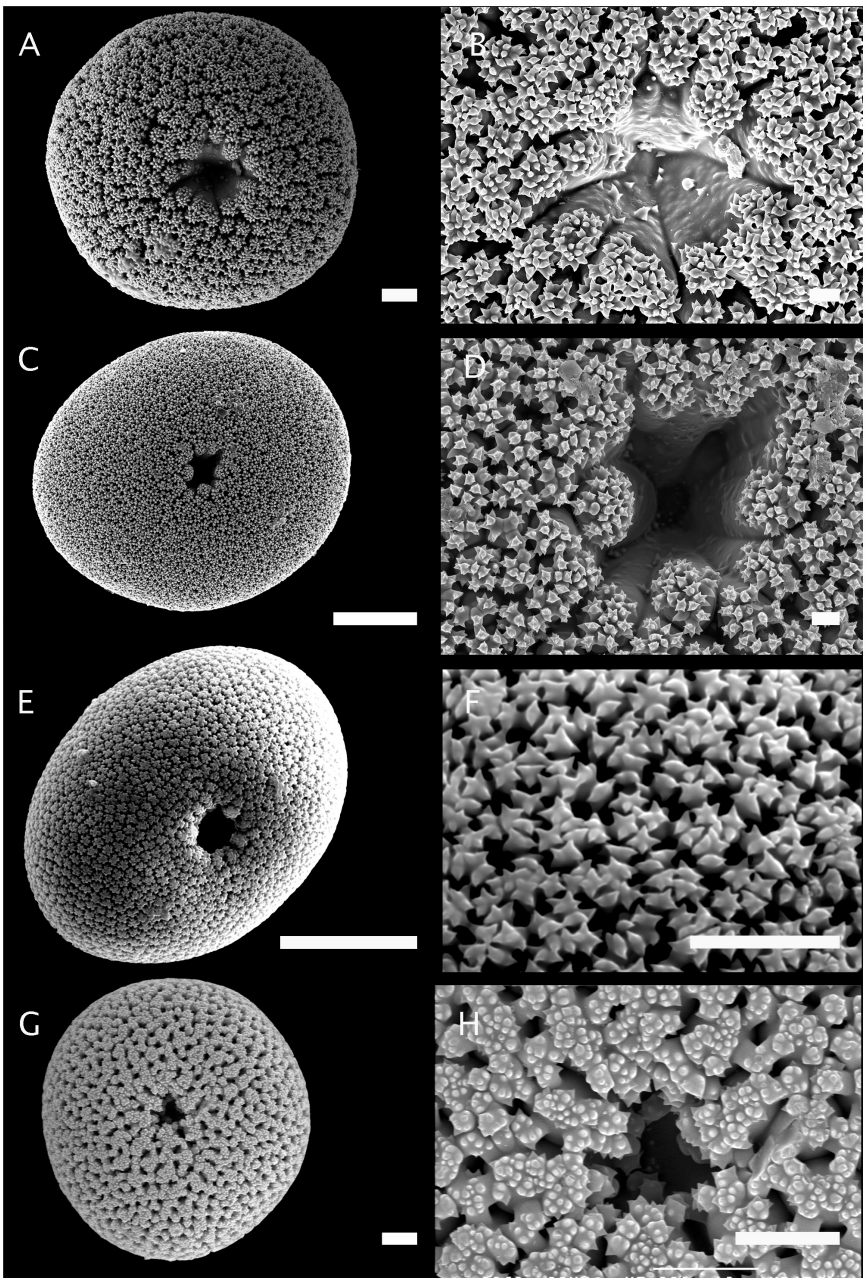

FIGURE 4 | Morphology of sterrasters from *Pachymatisma*, *Caminus,* and *Caminella*. **(A,B)** Sterraster of *Pachymatisma johnstonia* (Roscoff, France, MNHN-DCL 4015). Scale A: 10 μm. Scale B. 3 μm. **(C,D)** Sterraster of *Pachymatisma normani* (Norway, ZMBN 77858). Scale C: 40 μm. Scale D. 2 μm. **(E)** Sterraster of *Caminus chinensis* (holotype, UPSZTY 2102). Scale E: 50 μm. **(F)** Sterraster of *Caminus* sp. (Îles Glorieuses, MNHN-IP-2015-1144). Scale F: 10 μm. **(G,H)** Sterraster of *Caminella pustula* (holotype, MNHN-IP-2008-4). Scale G: 10 μm. Scale H: 10 μm.

should be done to see if the reported small oscules (∼0.5 mm) could be instead small preoscules; similar small preoscules are commonly observed in some *G. barretti* specimens (Cárdenas et al., 2013; Cárdenas and Moore, 2019). There is currently no morphological character supporting the *Cydonium*^{p} clade.

One noticeable exception to the warty/smooth rosette pattern is the specimen *Geodia* sp. (USNM B27, South Reef, Belize) which has clear warty rosettes (this study, data not shown), although it groups within a smooth-rosette *Geodia* group and has an overall morphology fairly close to the *Geodia gibberosa* complex. No explanation for this exception can be put forward at this point and more specimens of that undescribed species are required to confirm this result. It, however, suggests that warty rosettes might have appeared independently in other *Geodia* clades. In the literature *Geodia tenera* (Sim-Smith and Kelly, 2015) also represents a unique case, with microspines

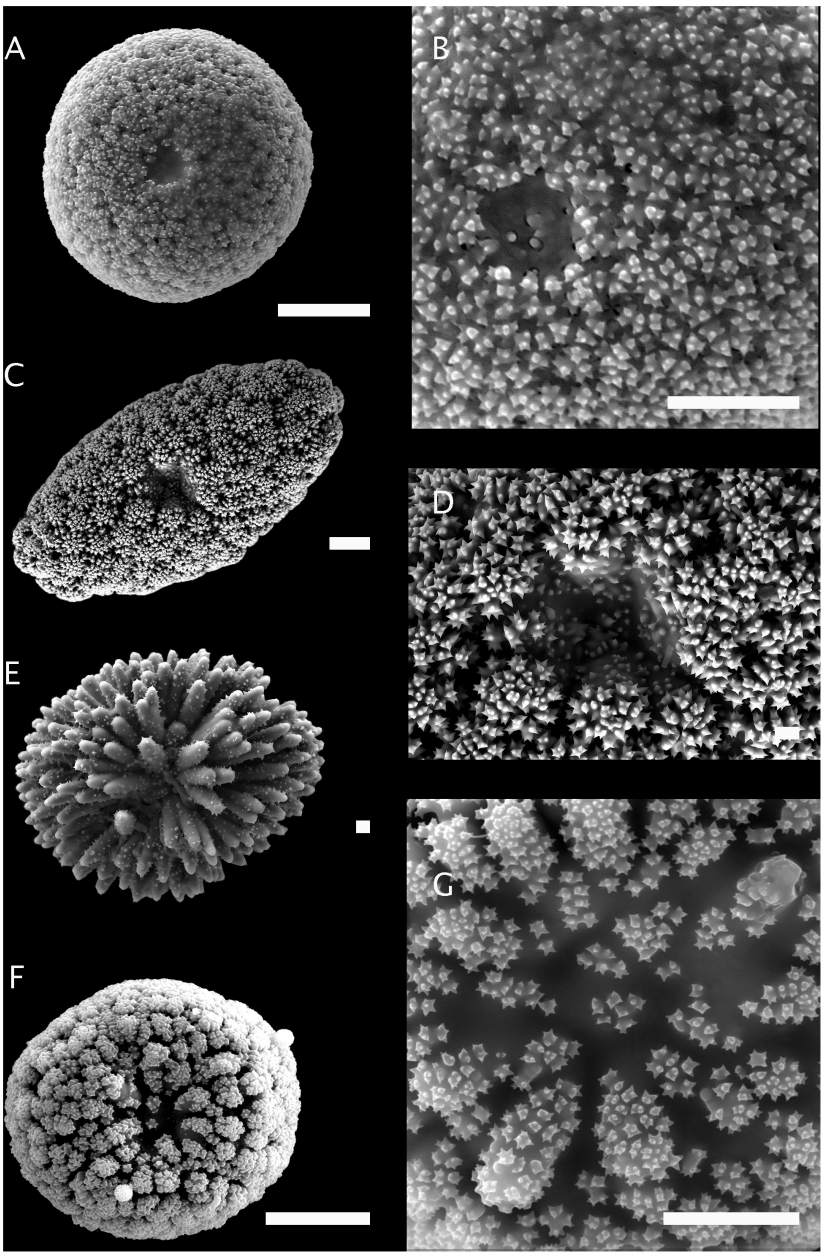

FIGURE 5 | Morphology of sterrasters/aspidasters from *Erylus* and *Caminus*. **(A,B)** Sterraster of *Erylus topsenti* (South of the Azores, ZMAPOR 21657). Scale A: 38 μm. Scale B. 20 μm. **(C,D)** Aspidaster of *Erylus mamillaris* (Azores, ZMAPOR 20421). Scale C: 10 μm. Scale D. 2 μm. **(E)** Aspidaster of *Erylus discophorus* (Portugal, PC81). Scale: 2 μm. **(F,G)** Sterraster of *Caminella vulcani* (Canary Islands, ZMAPOR 20422). Scale F: 30 μm. Scale G: 15 μm.

instead of warts on its rosettes; this species should be further investigated in the future to see if it groups with the warty-rosette clade, as expected.

Fossilization of Sterrasters/Selenasters

The sterraster surface microornamentations could also be used in paleontology, to improve the taxonomic identification of fossil ball-shaped spicules. However, one needs to assess first how these microornamentations are transformed during diagenesis. Unfortunately, ball-shaped spicules (sterrasters and selenasters) tend to loose the surface microornamentations due to typical diagenetic processes of spicules: corrosion (= dissolution), substitution (silica is replaced by calcite, zeolite clinoptilolite, or pyrite) and recrystallization (the original silica, opaline silica, transforms into crystalline silica such as chalcedony) (Bąk et al., 2015). This makes it challenging to discriminate sterrasters from selenasters (**Supplementary Table S1**). As a

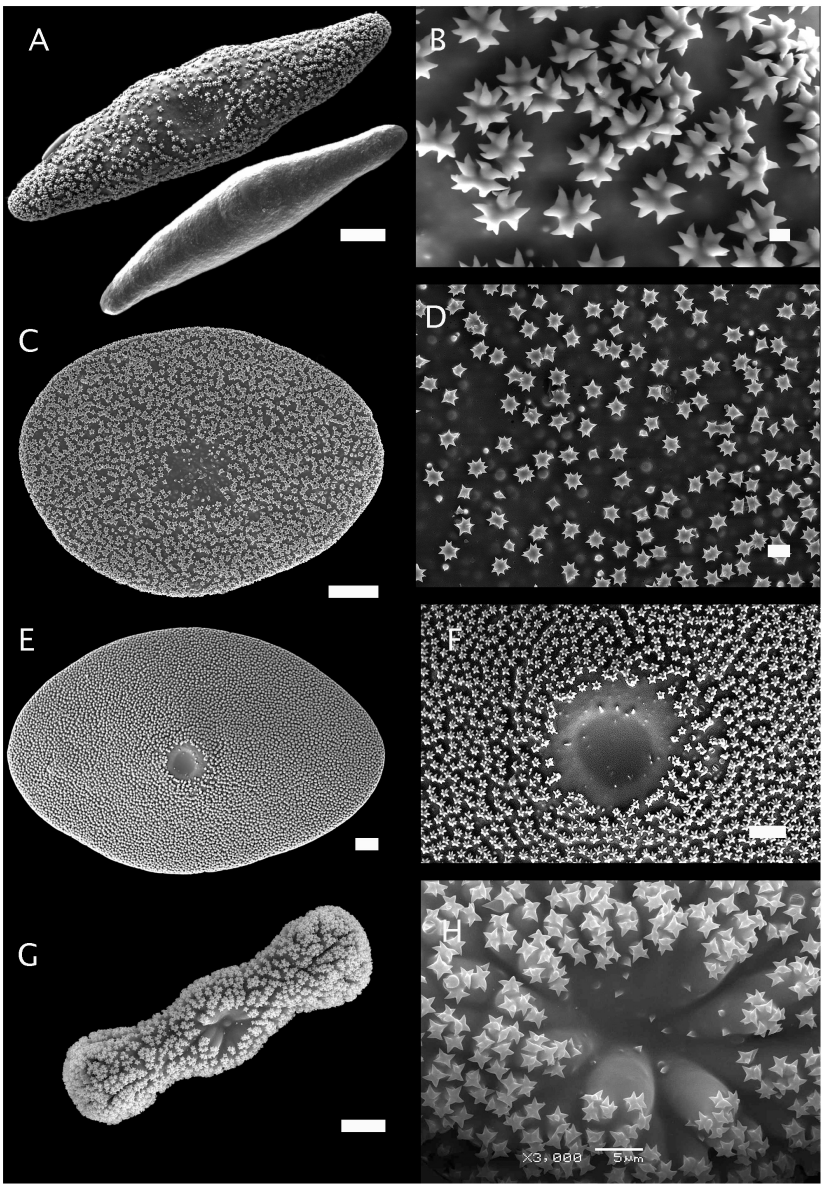

FIGURE 6 | Morphology of aspidasters from *Erylus* and *Penares*. **(A,B)** Aspidaster of *Erylus formosus* (Bocas del Toro, Panama, ZMBN 81644) and its young smooth stage before the growth of rosettes. Scale A: 20 μm. Scale B. 1 μm. **(C,D)** Aspidaster of *Penares euastrum*, previously called *Erylus euastrum* (holotype, MNHN Schmidt collection#76). Scale C: 20 μm. Scale D. 2 μm. **(E,F)** Aspidaster of *Erylus expletus* (Rockall Bank, ZMAPOR 18142). Scale E: 20 μm. Scale F: 10 μm. **(G,H)** Aspidaster of *Erylus trisphaerus* (Campeche Bank, Mexico, CNPGG). Scale G: 20 μm. Scale H: 5 μm. Pictures: P. Gómez and D. Ugalde.

consequence, sterraster/selenaster surface microornamentations are rarely preserved in Cenozoic fossils, very rarely in Cretaceous fossils and never (to this day) in Jurassic fossils (**Supplementary Table S1**). However, when sterrasters fossilize, they sometimes have a regular knobby surface when the rosette rays disappear, with each knob 3–5 μm in diameter (Rigby and Smith, 1992). When the whole rosette and knob disappear, the axial filament canals below each of them is revealed giving a regular porous surface, with pores 1–3 μm in diameter, separated by ∼2 μm, measurements made from SEM pictures (Bonci et al., 1997; Pisera et al., 2006; Vishnevskaya et al., 2009; Łukowiak, 2015). Finally, as the dissolution moves along and widens the axial canals and reaches the center of the sterraster, a central cavity often develops (Říha, 1987; Bonci et al., 1997; Frisone et al., 2014). These processes can happen rather fast, especially in modern tropical reef sediments (Rützler and Macintyre, 1978), typically alkaline and undersaturated in silica. The central cavity makes the sterraster fossils fragile and they can often break open: it is common to find pieces of fossilized sterrasters (e.g., Říha, 1987; Vishnevskaya et al., 2009). Since the actines dissolve or recrystallize more easily

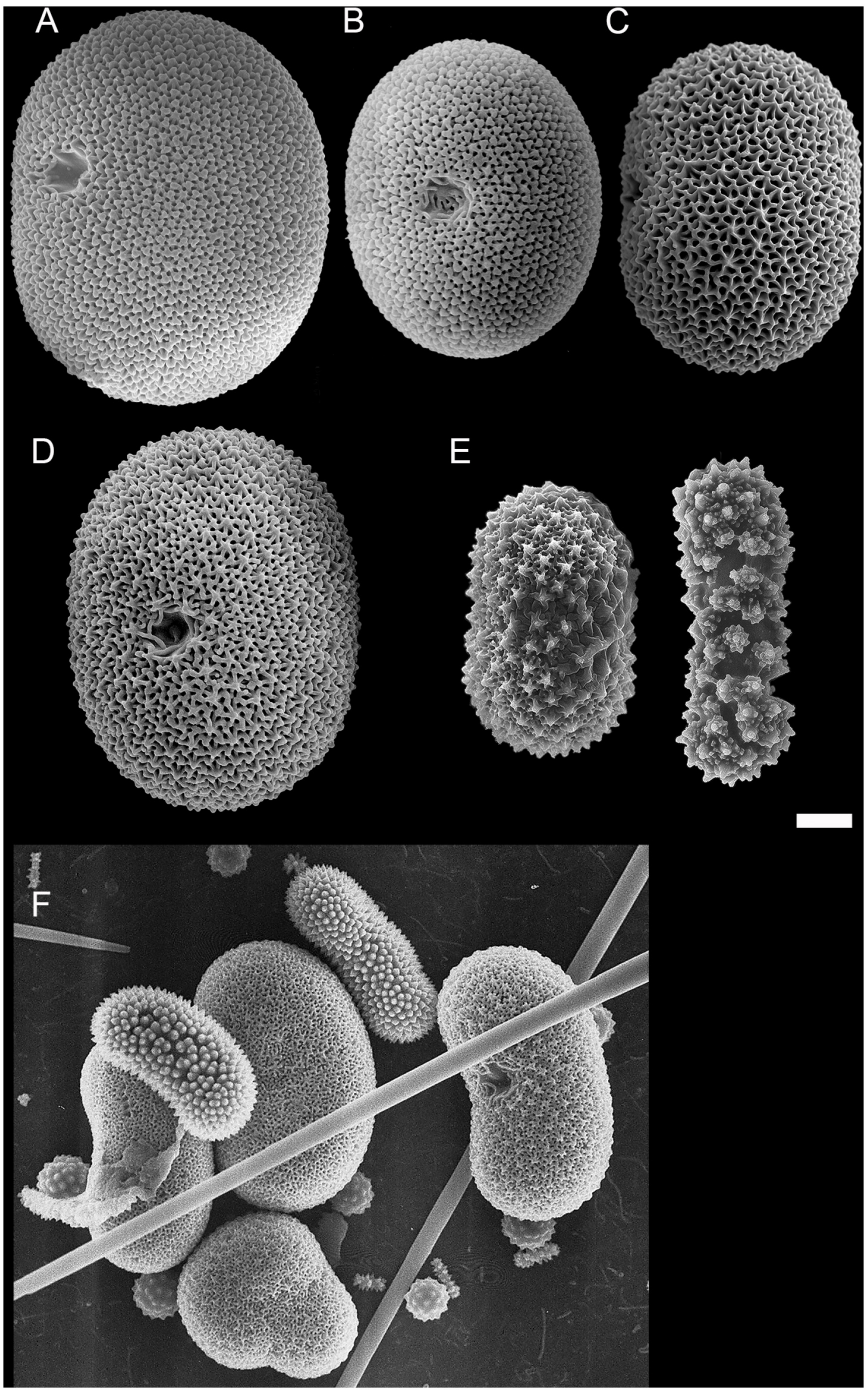

FIGURE 7 | Morphology of selenasters from *Placospongia*. **(A)** Selenaster of *Placospongia ruetzleri* (holotype, RMNH 9872). Picture: R.W.M. van Soest. **(B,C)** Selenasters of *Placospongia caribica* (holotype, USNM 32873). Pictures: K. Rützler. **(D)**. Selenaster of *Placospongia melobesioides* (Florida, USNM 39643). Picture: K. Rützler. **(E)** Selenasters of *Placospongia* sp. (Fernando de Noronha, Brasil, MNRJ 7878). Picture. F. Moraes. **(F)** Selenasters of *Placospongia decorticans* (Ras El Chakaa, cave, Lebanon, Endoume collection). This is a mix of late-stage and early-stage selenasters (smaller). Picture: S. Carteron. Scale A–D, F: 10 μm. Scale E: 50 μm.

than the inter-actine silica (Rigby and Smith, 1992) the radial pattern of fossilized sterrasters is often retained, if the recrystallization is not too coarse. If the surface has been entirely dissolved, sterrasters can appear as spherical/subspherical smooth spicules (Łukowiak and Pisera, 2016) so even in recrystallized sterrasters, the overall spherical/subspherial shape

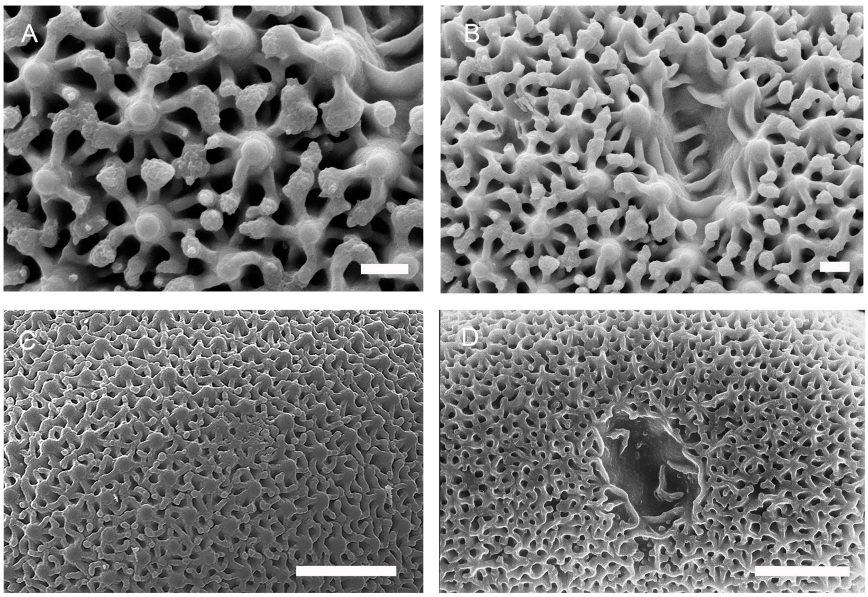

FIGURE 8 | Morphology of selenaster surfaces from *Placospongia*. **(A,B)** Surface and hilum of selenaster, *Placospongia melobesioides* (Florida, USNM 39643). Note the typical polygonal pattern around a central knob. Scale: 2 μm. Picture: K. Rützler. **(C)** Surface of selenaster, *Placospongia ruetzleri* (holotype, RMNH 9872). Scale: 10 μm. Picture: R.W.M. van Soest. **(D)**. Surface and hilum of selenaster, *Placospongia decorticans* (Ras El Chakaa, cave, Lebanon, Endoume collection). Scale: 10 μm. Picture: S. Carteron.

is maintained. Likewise, sterrasters treated with different potassium hydroxide (KOH) (Sollas, 1877) or hydrofluoric acid (HF) treatments (Rützler and Macintyre, 1978; Kaya et al., 2020) show the same patterns as fossil sterrasters: surface covered with pores, 2–3 μm diameter (Kaya et al., 2020), and a central cavity.

When selenasters fossilize and as the pentoradiate surface pattern dissolves, several randomly placed "holes" appear and there is no central cavity or radial pattern, due to the absence of axial canals (Rützler and Macintyre, 1978; Łukowiak, 2015) and therefore, they do not break. Selenasters may also become more or less smooth, and retain their subspherical to bean shape.

This short review on the fossilization shows that the use of surface microornamentations as a taxonomic character is limited essentially to Cenozoic ball-shaped spicules and very rarely to Cretaceous ones. The oldest sterrasters (Vishnevskaya et al., 2009) and selenasters (Gruber and Reitner, 1991) with preserved surfaces both date from the Late Cretaceous (Santonian/Campanian) some 83 Mya. The Cretaceous sterrasters seem to have smooth rosettes but the resolution of the SEM pictures is too low to be entirely certain (Vishnevskaya et al., 2009, Plate II-1a). The smooth/warty rosette character can be observed as long as the rosettes are well preserved: clear warty rosettes are visible in fossilized sterrasters from the Early Miocene, 16 Mya (Říha, 1987).

When the surface microornamentations disappears, one could rely instead on mostly diagenetic structures mentioned earlier: sterrasters would have a regular porous surface, a radial pattern and/or a central cavity; selenasters have an irregular porous pattern without a radial pattern or central cavity. Applying this chain of thought, the paleontological record of ball-shaped spicules (**Supplementary Table S1**) was revised to build a timeline of Geodiidae and *Placospongia* (**Figure 10**), but also to revisit the nature of ball-shaped spicule fossils called rhaxes.

Rhaxes: Sterrasters or Selenasters? Revising the Evidence

Rhaxes are bean-to ball-shaped fossilized spicules, originally described from the Late Jurassic where they are very abundant; they are nearly equally common in the Late Cretaceous (**Figure 10**). After being mistaken for Foraminifera, they were considered as sterrasters, despite some acknowledged common characteristics with *Placospongia* (Hinde, 1890). Based on their bean shape and their presumed higher resistance, Rützler and Macintyre (1978) claim they are without a doubt etched selenasters. Following paleontologists mostly accepted this view (Wiedenmayer, 1994; Pisera, 1997; Łukowiak, 2015). However, taking advantage of this study on sterrasters, this issue is revisited here using illustrations from the literature combined with examination of the fossil *Rhaxella perforata* (now a junior synonym of *R. sorbyana*), type species of the genus *Rhaxella* (**Figure 11**); for a history of the taxonomy of *Rhaxella* see Trejo (1967).

Evidence 1: Size

Hinde (1890) mentions that rhaxes are 110–150 μm in size, the smallest 80 μm. Rhaxes from the NHMUK PI slide S1682 (Late Jurassic, Lower Calcareous Grit, type locality)

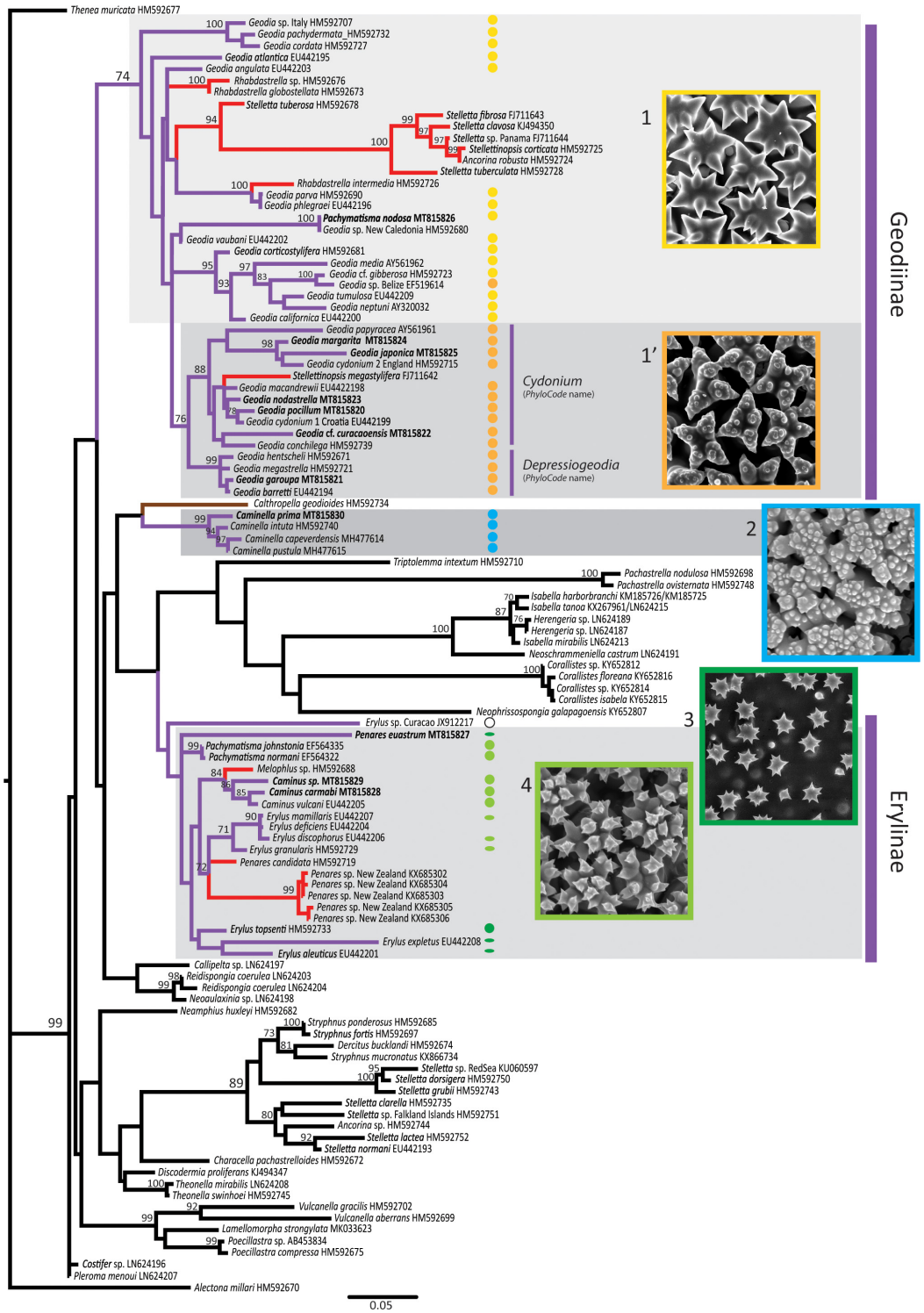

FIGURE 9 | Astrophorina *COI* maximum likelihood (ML) tree reconstructed with RAxML. ML bootstrap supports (1,000 bootstrap replicates) > 70 are indicated. Genbank accession numbers are given after each taxon. In bold are new sequences produced in this study. Geodiidae species have purple branches, Calthropellidae have brown branches. Red branches indicate Geodiidae species which secondarily lost sterrasters (species previously considered to belong to the Ancorinidae). Colored dots indicate sequenced species/specimens for which previous authors or this study have observed the surface of sterrasters with SEM (see **Table 3** for references); round shapes represent sterrasters, flattened shapes represent aspidasters. Image inserts illustrate the five types of sterraster surfaces observed (1. smooth rosettes, in *Geodia atlantica*; 1'. warty rosettes, in *Geodia papyracea*, holotype; 2. complex network, in *Caminella pustula*; 3. clear single rosettes in *Penares euastrum*, holotype; 4. unclear rosettes in *Pachymatisma normani*).

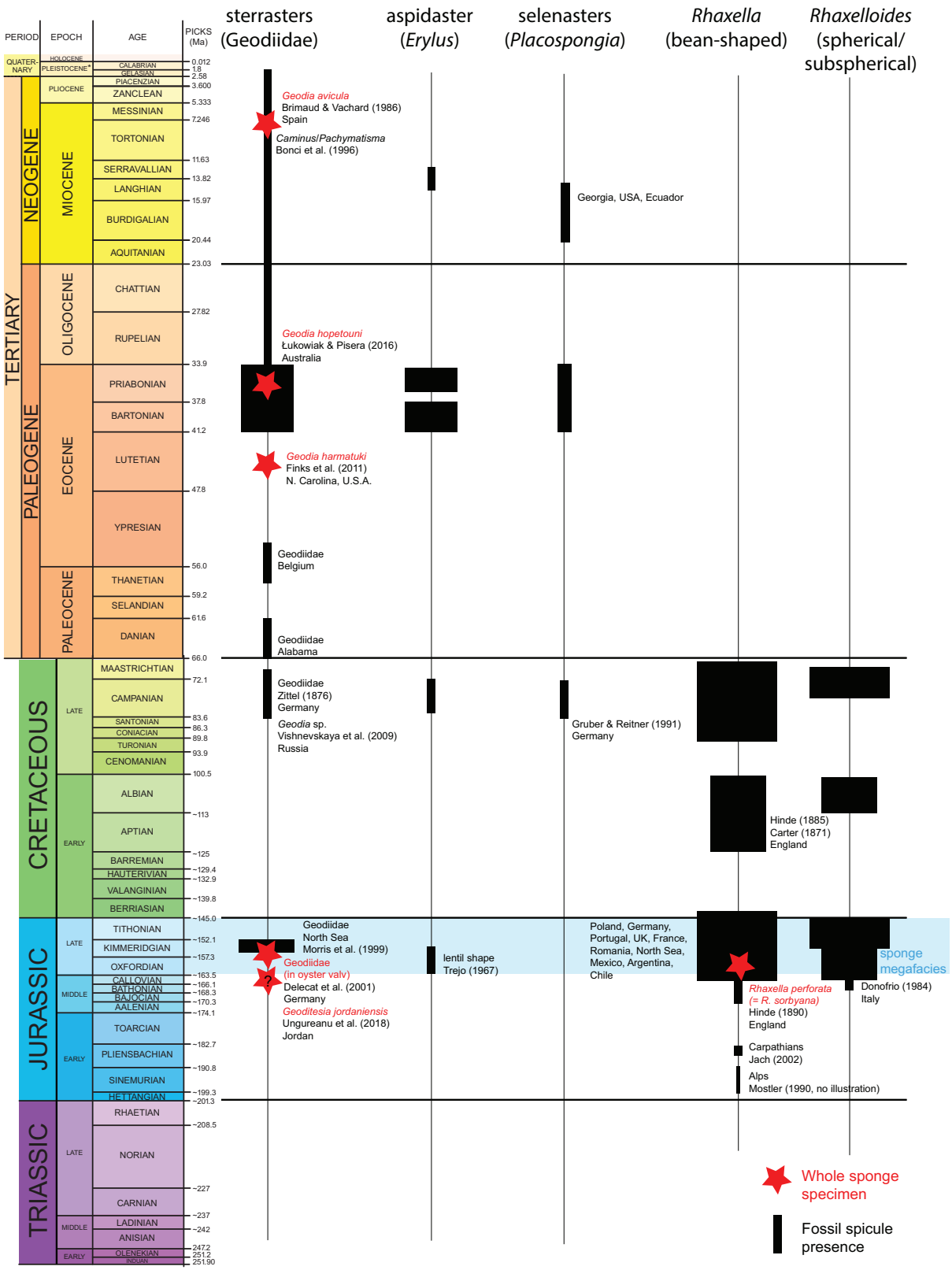

FIGURE 10 | Timeframe of ball-shaped fossil spicules from the Trias to the Holocene. Red stars represent whole body fossils. Black lines represent presence of the respective fossils (sterraster, aspidaster, selenaster, rhax, or smooth sphere); the width of the black lines is indicative of the abundance of these fossils. For literature references used to build this timeframe, see **Supplementary Table S1**.

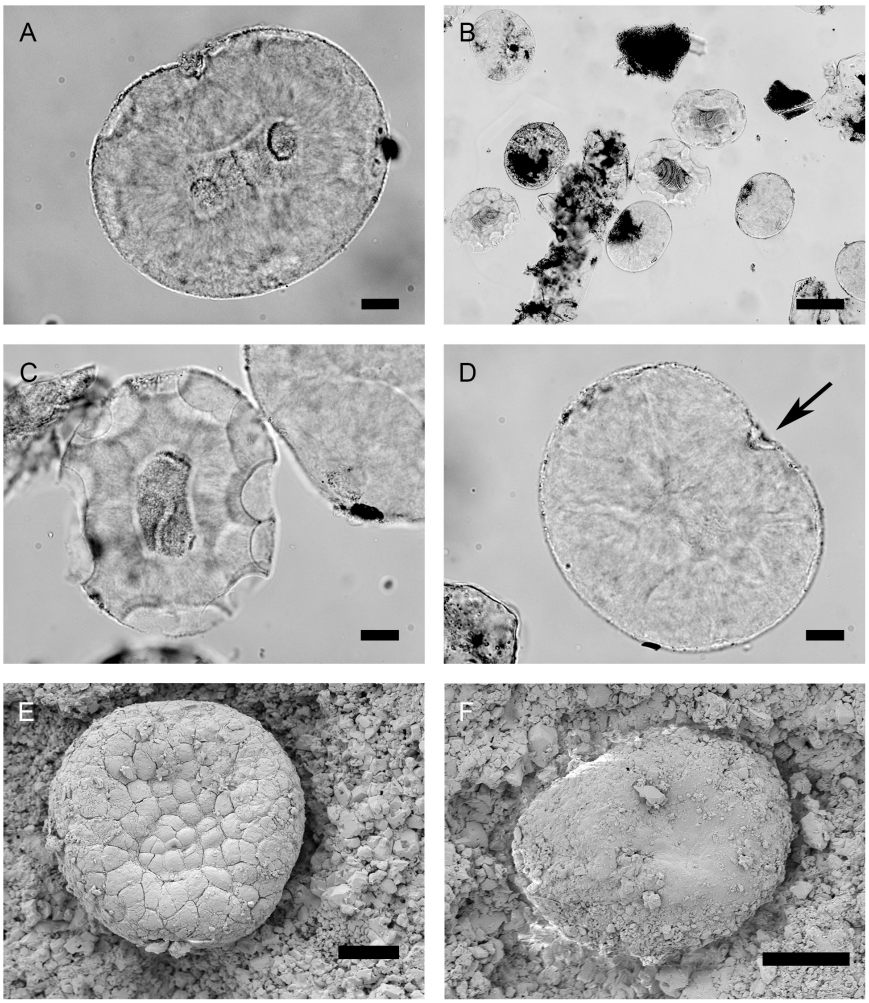

FIGURE 11 | Rhaxes observed with an optical microscope, *Rhaxella perforata* (now a junior synonym of *Rhaxella sorbyana*) (NHMUK PI, slide S1682) from the type locality, Late Jurassic, Oxfordian (Lower Calcareous Grit Formation, Scarborough, North Yorkshire, England). **(A)** Rhax with typical inside double-dot pattern and fibrous chalcedony recrystallization, seen in transparency. Scale: 20 μm. **(B)** Rhaxes with oval to bean shapes. Scale: 100 μm. **(C)** Rhax with typical semicircular etching patterns, fibrous chalcedony forming a dark cavity and a radial pattern. Scale: 20 μm. **(D)** Bean-shaped rhax with a dent (black arrow), and an etching pattern in the dent. Scale: 20 μm. **(E)** Putative subspherical spicule on the surface of *Geoditesia jordanensis* (specimen S10–18), Callovian, Middle Jurassic. The secondary surface polygonal pattern is typical of fibrous chalcedony recrystallization. Scale: 20 μm. **(F)** Putative subspherical spicule on the surface of *G. jordanensis* (specimen S10–18). Scale: 20 μm.

were 129-*147.9*-166 × 107-*120.4*-124 μm (N = 25). In the literature (**Supplementary Table S1**), Jurassic rhaxes have size ranges (80–200 μm), within ranges of sterrasters and selenasters (**Table 2**). However, the upper range (> 120 μm) is more in accordance with that of Recent (25–590 μm) and Eocene (70–350 μm) sterrasters than Recent (30–100 μm) or Eocene (60–120 μm) selenasters (**Supplementary Table S1**). Then again, Jurassic spicules might have been larger than Recent or Eocene sponges. The very few Cretaceous unambiguous sterrasters (122–163 μm) and selenasters (120–150 μm) are within the range of rhaxes (**Supplementary Table S1**) including *R. perforata* measured here; interestingly, Cretaceous selenasters are bigger than any other known Recent selenasters (30–100 μ m).

Evidence 2: Surface and Shape

Hinde (1890) mentions that rhaxes have 2 μm wide spots on the best-preserved specimens. Rhaxes with these spots were not observed on slide S1682 but they have been observed repeatedly by previous studies and explain why *R. sorbyana* was originally described as Foraminifera. Trejo (1967, plate II) confirms that rhaxes have pores about 2 μm wide and 2 μm apart. This pattern and sizes of pores fits with the above mentioned porous pattern observed on some fossilized as well as artificially dissolved sterrasters (∼2 μm spacing between pores). They could also, however, fit with the selenaster knobby pattern: in recent selenasters knobs are spaced 2.5–5 μm from each other, and 2.5–3 μm from each other in Cretaceous ones (our measurements on SEM picture from Gruber and Reitner, 1991). Hinde (1890)

TABLE 3 | Species list for the four types of surface microornamentations (within each type, species are in alphabetical order).

Surface microorna -mentation	Species	References
I	*Geodia angulata* (type) (smooth)	da Silva, 2002
	Geodia atlantica (holotype) (smooth)	Cárdenas et al., 2013
	Geodia barretti (warty)	Cárdenas et al., 2013
	Geodia californica (syntype) (smooth)	da Silva, 2002
	Geodia conchilega (Bonifacio, SME) (warty)	SEM (not shown)
	Geodia cordata (SAMA S1026) (smooth)	**Figure 2G**
	Geodia corticostylifera (holotype) (smooth)	da Silva, 2002
	Geodia cydonium 1 (ZMBN 77923) (warty)	**Figures 3G,H**
	Geodia cydonium 2 (ZMBN 85204) (warty)	SEM (not shown)
	Geodia hentscheli (paratype) (warty)	Cárdenas et al., 2013
	Geodia japonica (AB15-0035) (warty)	Lehnert and Stone, 2016
	Geodia garoupa (holotype) (warty)	Carvalho et al., 2016
	Geodia cf. *gibberosa* (CNPGG-0078) (smooth)	SEM (not shown)
	Geodia gibberosa (holotype) (smooth)	Cárdenas et al., 2009; **Figure 2F**
	Geodia macandrewii (warty)	Cárdenas et al., 2013
	Geodia margarita (holotype) (warty)	Sim-Smith and Kelly, 2015
	Geodia media (smooth)	da Silva, 2002
	Geodia megastrella (warty)	Cárdenas and Rapp, 2015
	Geodia neptuni (smooth)	da Silva, 2002
	Geodia nodastrella (warty)	Boury-Esnault et al., 1994
	Geodia nodosa comb. nov. (holotype) (smooth)	Sim-Smith and Kelly, 2015
	Geodia pachydermata (holotype) (smooth)	da Silva, 2002
	Geodia papyracea (holotype) (warty)	Cárdenas et al., 2009
	Geodia parva (holotype) (smooth)	Cárdenas et al., 2013
	Geodia phlegraei (holotype) (smooth)	Cárdenas et al., 2013
	Geodia pocillum (holotype) (warty)	Van Soest, 2017
	Geodia tumulosa (ZMBN 81780) (smooth)	Cárdenas et al., 2009
	Geodia vaubani (smooth)	Sim-Smith and Kelly, 2015; **Figure 2H**
	Geodia sp. Italy (MNHN-DCL 4075) (smooth)	SEM (not shown)
	Geodia sp. Belize (USNM B27) (warty)	SEM (not shown)
II	*Caminus vulcani* (ZMAPOR 20422)	**Figures 5F,G**
	Caminus chinensis (holotype)	**Figure 4E**
	Caminus sphaeroconia (holotype)	SEM (not shown)
	Caminus sp. (MNHN-IP-2015-1144)	**Figure 4F**
	Caminus carmabi (holotype)	Van Soest et al., 2014
	Erylus deficiens (ZMAPOR 20419)	SEM (not shown)
	Erylus discophorus (PC81, Portugal)	**Figure 5E**
	Erylus granularis (ZMAPOR 21656)	Optical microscope (not shown)
	Erylus mamillaris (ZMAPOR 20421)	**Figures 5C,D**
	Pachymatisma johnstonia (MNHN-DCL 4015)	**Figures 4A,B**
	Pachymatisma normani (ZMBN 77858)	Cárdenas and Rapp, 2013
III	*Erylus aleuticus* (holotype)	Lehnert et al., 2006
	Erylus expletus (ZMAPOR 18142)	**Figures 6E,F**
	Erylus formosus (ZMBN 81644)	**Figures 6A,B**
	Erylus topsenti (ZMAPOR 21657)	**Figures 5A,B**
	Erylus trisphaerus (CNPGG, Campeche Bank)	Ugalde et al., 2015; **Figures 6G,H**
	Penares euastrum (holotype)	**Figures 6C,D**
IV	*Caminella caboverdensis* (holotype)	Cárdenas et al., 2018
	Caminella intuta (paralectotype)	Cárdenas et al., 2018
	Caminella prima (holotype)	Sim-Smith and Kelly, 2015
	Caminella pustula (holotype)	Cárdenas et al., 2018

In the type 1 microornamentation, the "smooth" or "warty" rosette character is also given for each species. When a specific specimen (type or collection specimen) has been observed, it is specified near the species name.

also observes rhaxes which have lost semicircular portions; these etching patterns were fairly common on slide S1682 (**Figure 11C**) but also on Cenozoic *Rhaxella* chert sections (S7502).

One source of confusion on the nature of rhaxes is linked to the nature of the notch in the bean-shaped spicules. Hinde (1890) miscalls the notch a "hilum," which was followed by some subsequent authors (Haslett, 1992; Kozur et al., 1996) while most following authors have considered this notch to derive instead from the bent of selenasters. In that case, one should potentially be able to see a selenaster hilum in the best-preserved rhaxes, but neither previous studies, nor ours were able to find hila on rhaxes, even on the ones with the preserved regular surface spots. This absence of hilum could be due to dissolution of the surface and/or recrystallization, but there is yet another possibility that the spiculogenesis of Jurassic rhaxes took place in larger cells (with no need for the spicule to grow pressed against the nucleus).

Finally, it should be emphasized that the shape of rhaxes also varies from "ellipsoid to subspherical" (Hinde, 1890) so they are not all bean shaped. This is also the case in Recent *Placospongia* species where selenasters can be more or less subspherical and bean-shape (**Figure 7**). Importantly, sterrasters are never bean-shaped, even after erosion or artificial dissolution of spicules (Sollas, 1877; Rützler and Macintyre, 1978).

Evidence 3: Inside Structure

Hinde (1890) mentions that some rhaxes have a central recrystallized cavity with fibrous chalcedony: it appears dark and banded, it can have a slightly bent shape sometimes (**Figures 11A–D**). Usually, a clear radial pattern is visible around this cavity (**Figures 11A,C**), which is probably indicative of fibrous quartz recrystallization, typical in fossilized spicules (Bąk et al., 2015). In the literature, the dark center and clear fibrous corona are recurrent characteristics of rhaxes from the Late Jurassic (e.g., Gramann, 1962; **Supplementary Table S1**). This secondary silicification means that it is unfortunately not possible to know the original inside structure of rhaxes (radial vs. non-radial).

Evidence 4: Associated Megascleres and Whole Sponge Fossils

Hinde (1890) already questioned the total absence of megascleres in the whole sponge *R. perforata*: one would expect associated triaenes if this is a Geodiidae, tylostyles if this is a Placospongiidae. Some argued that megascleres could have been dissolved more easily than the more resistant ball-shaped spicules, others that megascleres were simply absent in *R. perforata* (Hinde, 1890). Only two whole sponge fossils from the Jurassic actually associated triaenes with ball-shaped spicules (**Figure 10**; Delecat et al., 2001; Ungureanu et al., 2018), thereby suggesting they are part of the Geodiidae. Surprisingly, the sterrasters reported are said to be bean-shaped. Delecat et al. (2001) describe a whole sponge fossil from the Late Jurassic, living in reef-building oysters. This sponge associates large calthrops, occasional small triaenes, oxeas and rhaxes; the calthrops and triaenes leave no doubt that this is a Tetractinellida. Furthermore, Delecat et al. (2001) examined the ball-shaped spicules in thin sections so that a sterraster cut transversally in the hilum will appear bean-shaped in section. The "notch" in those rhaxes is 10 μm wide (Delecat et al., 2001) fitting with the hilum size of a sterraster. Therefore, this fossil is a credible Late Jurassic Geodiidae, although no Recent genera has calthrops associated with triaenes; this fossil cannot currently fit into any known genus. Ungureanu et al. (2018) also state that *Geoditesia jordanensis* from the Middle Jurassic has fairly large "reniform sterrasters" (140–330 μm). However, the spicules observed with SEM were not clearly bean shaped (**Figures 11E,F**) and were smaller (∼66–88 μm) than the sizes reported. Their surfaces were smooth, so that it was impossible to decide if they were sterrasters or selenasters (**Figures 11E,F**). The nature of these ball-shaped spicules is uncertain, and so is the nature of this fossil (see section "Discussion").

Evidence 5: Paleogeography and the Abundance of Rhaxes

Late Jurassic rhaxes have a wide distribution, from Argentina, Chile, Mexico, Europe (= Tethys Ocean at the time) to Japan (**Supplementary Table S1**). During the Late Jurassic, all of these locations were in the temperate zone (Argentina, Central Chile, Japan), tropical/temperate zone (Europe) and tropical zone (Mexico) (Paleomap Maker[4], accessed 3rd of September 2020). Late Jurassic rhax records may come from shallow-water paleoenvironments, but also from relatively deep-sea environments, as in the case of the "sponge megafacies" from the Tethys Ocean, considered to be ∼100–600 m depth (Pisera, 1997; **Supplementary Table S1**). At these locations, the large dominance of rhaxes, often representing from 49.7 (Reif, 1967), to 75% (Pisera, 1997) or even 80–90% (Afşar et al., 2014) of all loose spicules is striking. These amounts make rhaxes rock-forming fossils leading to cherts and rhax spiculitic sandstones. Three hypothesis could explain these amounts: either (i) these species were dominant, (ii) these spicules were more resistant than others and accumulated in the sediments or (iii) these spicules were sorted based on size and morphology during transportation.

Selenasters are very numerous in the cortex of *Placospongia*. This genus includes today only a dozen of species, and most are restricted to very shallow tropical waters, in reefs, marine lakes, caves, and anchialine pools (Becking, 2013); only one species, *Placospongia anthosigma* (Tanita and Hoshino, 1989) was recorded from slightly deeper waters (62–67 m), in Sagami Bay, Japan. Recent *Placospongia* species never dominate their habitats or form large aggregations.

Sterrasters are also usually very abundant spicules in Geodiidae, packed in the cortex in the numbers of thousands (Cárdenas et al., 2013). More than 340 species Geodiidae species are found worldwide (except in Antarctica), in shallow and deep waters, up to 3,100 m depth (Cárdenas and Rapp, 2015). Today, large quantities of sterrasters could accumulate in sponge grounds dominated by massive *Geodia* species. Indeed, some North Atlantic *Geodia* species are dominant species in deep-sea boreo-arctic sponge grounds, on continental shelves, slopes, and seamounts (Klitgaard and Tendal, 2004; Murillo et al., 2012; McIntyre et al., 2016). Sterrasters and triaenes from decaying sponges are among the few spicules that remain in deep-sea spicule mats from these boreo-arctic sponge grounds (Wagoner et al., 1989; Murillo et al., 2016). Massive *Geodia cydonium* aggregate in shallow waters of the Western Mediterranean Sea (Mercurio et al., 2006; Grech et al., 2020). Based on modern ecosystems, *Geodia* species are therefore more likely to contribute to large accumulations of ball-shaped spicules. To support this, sterrasters are by far the dominant spicules, over selenasters in the Middle Eocene of NE Italy, a rocky temperate shore at the time (Frisone et al., 2014). In modern tropical shallow-water reef sediments, sterrasters, and selenasters are usually overrepresented: they represent nearly half of all spicules although they represent only a minor portion of the living biomass (Łukowiak et al., 2013). One reason may be that they are

[4]http://portal.gplates.org/map

amongst the most resistant microscleres (Rützler and Macintyre, 1978) and, as mentioned earlier, they are produced in abundance. To sum up, the abundance of rhaxes in the Late Jurassic may indeed reflect the abundance of Geodiidae and/or *Placospongia* (the former being more likely), and a bias of better preservation. Whether sorting of these spicules during transportation could explain their accumulation remains to be proven, in modern shallow-water reef sediments for instance. Modern studies in sediments also raise the possibility that rhaxes could be a mix of ball-shaped spicules.

Rhaxes, a Mix of Sterrasters and Selenasters

Since Recent sterrasters are never bean-shaped, shape alone is a strong argument in favor of rhaxes being connected to selenasters; the surface and inside structure cannot confirm this because of substitutions or recrystallizations. Such a conclusion implies that some *Placospongia* ancestors were common in much deeper waters than today since rhaxes were fairly abundant in the Tethys Ocean at important depths (sponge megafacies, ∼100–600 m depth). In any case, more work on the taphonomy and diagenesis of these spicule fossils is necessary to fully understand their nature.

The recurrent wide range of sizes (80–200 μm) given for rhaxes (**Supplementary Table S1**) as well as the diversity of morphology sometimes described (spherical to subspherical, to bean-shaped) suggest that many of the reported rhaxes or rhax spiculites probably originate from mixes of selenasters and sterrasters, as observed in Recent shallow-water tropical sediments. It is also possible that the terms "rhax" or "bean-shape" have been overused, without a proper definition due to the parataxonomic status of "rhax," as a loose spicule, without being really representative of a species. Some researchers use it for oval shapes (e.g., de Geyter and Willems, 1982) or for just any ball-shaped spicules, especially when only thin sections of rocks were studied, and without realizing that sterrasters could potentially appear bean shape in section, as illustrated in Delecat et al. (2001). Consequently, rhaxes are possibly overrepresented in the literature thus giving the impression that selenasters were more common than they really were in the Late Jurassic, although sterrasters could have been more abundant.

Actually, many studies have shown that one can distinguish in the Late Jurassic different ball-shaped spicules with similar sizes: rhaxes *sensu stricto* (= bean-shaped), spheraster and what some paleontologists call sterrasters (spherical spicule) (**Supplementary Table S1**). Since Recent selenasters are never spherical, spheraster and other spherical spicules are credible sterraster ancestors. In addition to *R. perforata* and its typical bean-shape spicules, Trejo (1967) and Haslett (1992) have actually started to describe different rhax morphologies giving them other parataxonomic names, in order to distinguish different potential species. This is *Rhaxelloides sphaerica* (Trejo, 1967) and *Rhaxelloides cilindricas* (Trejo, 1967), *Rhaxella elongata* (Haslett, 1992) and *Rhaxella winspitensis* (Haslett, 1992). According to the overall shape of selenasters and sterrasters, *R. sphaerica* and *R. cilindricas* would be sterrasters while *R. elongata* and *R. winspitensis* would be selenasters. In accordance, the genus *Rhaxelloides* should be allocated to the Geodiidae, this genus should be used to describe single spherical/subspherical to oval/cylindrical spicules which have lost their surface microornamentations. *Rhaxella* should be used for bean-shaped fossils which have also lost their surface microornamentations (putative selenasters). *R. elongata* looks very much like the selenasters of *P. decorticans* (**Figure 7E**) while *R. winspitensis* cannot be linked to a modern selenaster at this point.

Conversely, some sterraster fossils described under different genera names are not any different from those of modern *Geodia*. *Silicosphaera asteroderma* (Hughes, 1985) (Miocene-Recent) are loose sterrasters from the Sedili River mud (West Malaysia), with clear rosettes. Therefore, *Silicosphaera* (Hughes, 1985) becomes a junior synonym of *Geodia* (Lamarck, 1815). *Conciliaspongia rarus* (Robinson and Haslett, 1995) from the Miocene of Ecuador is clearly a sterraster with rosettes therefore it is formally proposed here that *Conciliaspongia* (Robinson and Haslett, 1995) becomes a junior synonym of *Geodia* (Lamarck, 1815). The Late Miocene-Pliocene *Hataina ovata* (Huang, 1967) from Japan previously described as a radiolarian has been shown to be sterrasters (Inoue and Iwasaki, 1975), with no formal taxonomical act taken. Since the sterraster surface of *H. ovata* clearly has "flower like ornamentation" (Inoue and Iwasaki, 1975), in other words "rosettes," it is formally proposed here that *Hataina* (Huang, 1967) becomes a junior synonym of *Geodia* (Lamarck, 1815). *Silicosphaera asteroderma* and *Hataina ovata* were described under the false premise that these sterrasters could suffice for the description of the total organism. Therefore, the descriptions given are insufficient to differentiate these species from other species of *Geodia*. *Conciliaspongia rarus* was described as a loose spicule but again, its description and its characters alone do not permit an unambiguous identification. A revision of the type material would not help either because in general, the description of a sterraster cannot be enough to describe a new species of *Geodia*, which has several other types of spicules. According to requirement 13.1.1 of the International Code of Zoological Nomenclature (International Commission on Zoological Nomenclature [ICZN], 1999), names published after 1930 must "be accompanied by a description or definition that states in words characters that are purported to differentiate the taxon." Therefore, *S. asteroderma, C. rarus,* and *H. ovata* species become unavailable names.

Geoditesia and *Geodiopsis* Fossils Are Tetractinellida *Incertae sedis*

The Cretaceous genus *Geoditesia* (previously *Geodites*) was founded on arbitrary groupings of loose triaenes and bean-shaped spicules found in the same fine sand layer: Upper Greensand of Albian age in Devon, England (Carter, 1871). Because of this, they have traditionally been placed, albeit with doubt, in the Geodiidae (Rigby, 2004). Slides of type and non-type material of *Geodites* species have been re-examined in this study, including from the type species of the genus (*Geodites haldonensis*), a species defined by an arbitrary association of protriaenes, prodichotriaenes, anatriaenes and ball-shaped spicules. Following authors were more cautious in

their groupings (e.g., *Geodites cretacea* Sollas, 1880a) or took the more reasonable approach of defined the species by only one type of characteristic triaene (Hinde, 1885, 1888; Weller, 1930). As noted previously (Finks et al., 2011, p. 70), *Geodites* triaenes are similar to what can be today observed in several families of Tetractinellida: Geodiidae, Ancorinidae, Tetillidae or even lithistids (Corallistidae, Pleromidae, Phymatellidae, Isoraphiniidae). It makes this genus probably polyphyletic, and used for any loose triaenes; this explains the very wide stratigraphic range of this genus with species described from the Carboniferous (Hinde, 1888; Weller, 1930) to the Late Eocene (Hinde and Holmes, 1892). There is no evidence that the rhaxes included in *G. haldonensis* actually belong to *G. haldonensis*, and according to our previous conclusions they are more probably selenasters. For these reasons, *Geoditesia* should formally leave the Geodiidae and be moved to Tetractinellida *incertae sedis*. Furthermore, since some of these species may be mixes of spicules coming from different species, and to avoid any future confusion a full revision of the genus is necessary to eventually restrict *Geoditesia* species definitions to their main triaene, a task beyond the scope of this study.

The first claimed whole specimen of *Geoditesia* is *Geoditesia jordanensis* from the Middle Jurassic (Callovian), two specimens of which have been examined in the present study. After sectioning of these subspherical 2 cm fossils, the absence of internal structure was confirmed (Ungureanu et al., 2018); just a few oxeas with no particular orientation in a homogeneous matrix; no sterraster cortex could be observed either; at the surface, a disorganized assemblage of oxeas, dichotriaenes and ball-shaped spicules. The absence of internal structure is troubling since this non-lithistid sponge must have been buried quickly to retain its original shape and in that case, some sort of skeleton organization would have been retained. It also contrasts with the preservation of delicate details such as the so-called "osculum," a round structure that was also observed on one of our specimens. This calls into question the whole body nature of these specimens, which would require a full and in-depth revision of the type series to understand their taphonomy. Furthermore, the presence of subspherical spicules on the surface of *G. jordanensis* does not prove their belonging to the fossil either: these microscleres are sometime so abundant that they cover all sponge fossils, and have often confused paleontologists (e.g., Zittel, 1876; Hurcewicz, 1966). Unfortunately, the surface of these ball-shaped spicules had disappeared, and their subspherical shape was also unclear (**Figures 11E,F**). To conclude, the nature and identification of this species remains questionable; its Geodiidae affiliation cannot be confirmed.

Geodiopsis was created for sponge whole fossils from the Campanian (Late Cretaceous) associating oxeas, chubby triaenes and anatriaenes. Although he also finds sterrasters, Schrammen (1910, p. 116) stresses that he cannot associate them with confidence to the *Geodiopsis* specimens. For this reason, the current classification of *Geodiopsis* in the Geodiidae remains doubtful, the combination of triaenes and anatriaenes could also be found in some Ancorinidae genera (*Stelletta, Ancorina, Ecionemia, Stellettinopsis, Stryphnus*) or even Tetillidae. For these reasons, *Geodiopsis* should be transferred from the Geodiidae to the Tetractinellida *incertae sedis*.

As for the Cretaceous *Pachymatisma virga* (Hinde, 1885), it is based only on loose strongyles, which could belong to many different Heteroscleromorpha genera; there is no evidence that this species belongs to *Pachymatisma* and the description is insufficient to identify this species. According to the article 13.1.1. (International Commission on Zoological Nomenclature [ICZN], 1999) cited previously, the species name *P. virga* becomes an unavailable name.

Timing the Emergence of the Geodiidae, *Geodia,* and *Placospongia*

Geodiidae species belong to the Tetractinellida order, defined by the presence of triaene megascleres. The Tetractinellida order is deeply rooted in the Paleozoic with isolated triaene-like fossils already reported from the Middle Cambrian, Georgina Basin, in Australia (van Kempen, 1990; Mehl, 1998) and later sparsely found throughout the Paleozoic periods. Just like the Paleozoic lithistid desmas or microscleres such as toxas and forceps (Mostler, 1996), it is difficult to link these Paleozoic triaenes to the Mesozoic ones which appear only in the Middle Trias (Upper Anisian, ∼242 Mya), and are at this stage already very diverse (Mostler, 1976). According to a time-calibrated molecular phylogeny, the crown-group Tetractinellida would have appeared in the Early Jurassic (Plese et al., 2020). However, (i) the divergence estimate range for this node is between the Early Trias and the Late Jurassic and (ii) Plese et al. (2020) are missing in their calibrated phylogeny deep-diverging groups such as rhizomorine lithistids or *Stupenda* (Kelly and Cárdenas, 2016) which may push back in time this average divergence date. All in all, an emergence of crown-group tetractinellids around the Middle Trias is plausible, and means that Geodiidae must have appeared later. Importantly, the crown-group Clionaida order possibly appeared around Late Trias (Plese et al., 2020) meaning that the Placospongiidae diverged later.

Accordingly, the three Paleozoic reports of sterrasters/rhaxes (**Supplementary Table S1**) are currently not convincing. The Cambrian putative "sterraster" fossils are poorly illustrated and studied (Gruber and Reitner, 1991; Reitner and Mehl, 1995); they are entirely recrystallized so that their original structure/surface is unknown. The report of a single rhax from the Early Ordovician is doubtful since it is more than 1 mm large (Kozur et al., 1996), a size far larger than any of the recent sterrasters/selenasters. As for the two rhaxes found by Hinde (1888) in the Carboniferous, Wiedenmayer (1994, p. 31) suggests they are petrosiid microstrongyles (Haplosclerida order).

Two reports of rhaxes in the Early Jurassic (Mostler, 1990; Jach, 2002) suggest that the Placospongiidae were already present then. In the Middle Jurassic, *Rhaxella* and *Rhaxelloides* are more present: *Rhaxella* have been reported from the Bajocian (Haslett, 1992), *Rhaxella* and spheraster in the Bathonian (Donofrio, 1984), while *Rhaxella* and/or *Rhaxelloides* are already fairly abundant in the Upper Callovian (Trejo, 1967; Block Vagle et al., 1994). In the Late Jurassic (Oxfordian, Kimmeridgian and

Tithonian), *Rhaxella/Rhaxelloides* are abundant and widespread in the sponge megafacies. In this study, the first sterrasters from the Kimmeridgian were formally identified in the North Sea where they were reported as "*Praeconocaryomma* (?) sp.2" radiolarians (Morris et al., 1999, **Figure 9k**); the rosettes are gone but these spicules look very similar to the fossil sterrasters described by Rigby and Smith (1992). Putative aspidasters are reported from the Late Jurassic in Mexico, although not much information is given (Trejo, 1967). The first formally identified *Geodia* sterraster from the Santonian/Campanian boundary, Late Cretaceous were identified in a study by Vishnevskaya et al. (2009, plates II and III) thanks to a clear rosette SEM illustration. Later in the Campanian, sterrasters are fairly common (Zittel, 1876; Schrammen, 1924). At the same time, the first formally identified *Placospongia* selenaster is reported from the Campanian, Late Cretaceous, misidentified as a sterraster in the article (Gruber and Reitner, 1991). To conclude, the fossil record suggests the emergence of Placospongiidae in the Early Jurassic, followed by the emergence of Geodiidae in the Middle Jurassic. The time-calibrated phylogeny suggests a younger emergence since Plese et al. (2020) suggest the Geodiidae stem-group appear in the Albian, Early Cretaceous (112 Mya), although with a divergence estimate range between the Middle Jurassic (174 Mya) and the Paleocene (61 Mya). The appearance of the Geodiidae crown-group would be in the Santonian, Late Cretaceous, around 85 Mya (Plese et al., 2020) with a range from the Barremian, Early Cretaceous (128 Mya) to the Oligocene (24 Mya). This is well in accordance with the first identification of typical *Geodia* sterrasters, from the Santonian/Campanian boundary and their following abundance in the Campanian. No whole specimens are known from this period unfortunately; the Lower Campanian *Geodia* sp. described by Hurcewicz (1966, p. 25) is likely a result of sterraster contamination (Wiedenmayer, 1994, p. 32) and is probably specimens of *Stelletta (Stolleya)* (E. Swierczewska Gladysz, pers. comm.).

While reviewing the paleontological literature, the oldest warty rosettes were observed in fossilized sterrasters from the Early Miocene, 16 Mya (Říha, 1987) so the *Depressiogeodia*^{p}+*Cydonium*^{p} clade had probably diverged by then. Future observations of fossilized sterraster should pay close attention to the morphology of rosettes in order to better determine the timing of divergence of this clade. No *Caminella* sterrasters were found in the paleontological literature, but an SEM picture of a *Pachymatisma* or *Caminus* sterraster was identified, from the Late Miocene in Italy (Bonci et al., 1997, plate 5, **Figure 1**); without other microscleres one cannot discriminate both genera. This is to our knowledge the first fossil ever reported for this group of Geodiidae.

Estimating the origin of the Geodiidae in the Middle Jurassic is relevant with respect to the "sponge biomarker hypothesis" whereby unique unconventional sterols found in some Recent *Geodia* and *Rhabdastrella* species (both part of the Geodiinae), were connected to the sterane biomarker 26-methylstigmastane (26-mes) from a sequence ∼100 My long of Neoproterozoic-Cambrian rocks and oils (Zumberge et al., 2018). The fact that the Geodiidae diverged some 500 My later than the 26-mes records suggests either that (i) these unique sterols appeared independently in the Geodiidae (by convergent evolution) or that (ii) the capacity to make these sterols was inherited from demosponge ancestors since the Neoproterozoic, and secondarily lost in most groups. This second scenario is currently supported by the presence of 26-mes precursors in other demosponge orders than the Tetractinellida (*Geodia/Rhabdastrella*): they are found in large amounts in Haplosclerida [*Petrosia (Strongylophora)* sp.] and in trace amounts in the orders Agelasida (*Cymbaxinella corrugata*) and Verongiida (*Aplysina* spp.) (Bortolotto et al., 1978; Zumberge et al., 2018). Further screening of demosponges for 26-mes precursors in parallel with a revision of their fossil record is required to better evaluate this second scenario.

CONCLUSION

In this study, a new spicule morphological character was explored: the surface microornamentations of sterraster spicules. Collagen fiber-rosette connections may give the cortex its solidity and flexibility, an attachment structure with biomimetic potential deserving to be further studied. Four types of microornamentations were revealed which, for some of them, matched specific Geodiidae clades: type I characteristic of *Geodia*, type II characteristic of *Pachymatisma, Caminus* and some *Erylus*; type III characteristic of other *Erylus*; type IV characteristic of *Caminella*. Within the type I microornamentations of *Geodia*, sterrasters had smooth or warty rosettes; all species with warty rosettes grouped in the "*Depressiogeodia*^{p}+*Cydonium*^{p}" clade. Therefore, the surface microstrucure character alone could be used to identify isolated Recent or fossil sterrasters as belonging to *Geodia* (smooth), *Geodia* (warty), *Caminella*, "*Pachymatisma/Caminus//E. granularis/Erylus discophorus* complex" or the rest of the *Erylus*.

Using this character, this study was able to sort uncertain genus allocations of some modern Geodiidae, and formally identify Geodiidae sterrasters from the Late Jurassic, *Geodia* sterrasters from the Late Cretaceous, as well as for the first time a *Pachymatisma/Caminus* sterraster from the Late Miocene. Evidence from the literature review suggests that the Geodiidae originated in the Middle Jurassic, after the Placospongiidae for which we have some evidence in the Early Jurassic. So-called "rhaxes" probably represent mixes of sterrasters and selenasters: while *Rhaxella* seems to belong to the Placospongiidae, *Rhaxelloides* belongs to the Geodiidae. Miocene-Pliocene fossils sterrasters *Hataina*, *Silicosphaera,* and *Conciliaspongia* become junior synonyms of *Geodia.* Other traditional Geodiidae fossil genera, *Geoditesia,* and *Geodiopsis*, are reallocated to the Tetractinellida *incertae sedis*.

DATA AVAILABILITY STATEMENT

The datasets presented in this study can be found in online repositories. The names of the repository/repositories and accession number(s) can be found in the article/**Supplementary Material**.

AUTHOR CONTRIBUTIONS

PC conceived and designed the study, performed the observations, and the data analyses and literature surveys. PC wrote the manuscript.

FUNDING

PC received support by the European Union's Horizon 2020 Research and Innovation Program under Grant Agreement No. 679849 (the SponGES project). This document reflects only the authors' view and the Executive Agency for Small and Medium-sized Enterprises (EASME) is not responsible for any use that may be made of the information it contains. Visits to the NHM and the HBOI collections were funded by "Inez Johanssons" travel grants to PC (Uppsala University, HT2012, and HT2014).

ACKNOWLEDGMENTS

I am very grateful to Ana Riesgo and Vasiliki Koutsouveli (NHM London) for sharing SEM pictures from a cryofractured *G. barretti* and to A. Riesgo for help with fishing the *28S* sequences of *G. atlantica* and *G. phlegraei* in transcriptomes. I would like to thank Consuelo Sandino for giving access to the NHM paleontology collections. Thanks to Fayez Ahmad (The Hashemite University, Zarqa, Jordan) for sharing two *Geoditesia jordanensis* specimens; thanks to Christian Marshall (Station Marine d'Endoume, Marseille, France) for his help with the preparation of this specimen. Thanks to Marzia Bo (Università degli Studi di Genova, Italy), Sadie Mills, and Michelle Kelly (NIWA, New Zealand), Nicole de Voogd (Naturalis, Leiden, The Netherlands), Shirley Pomponi (HBOI, Fort Pierce, FL, U.S.A.), and Pilar Ríos (IEO, Gijón, Spain) for collecting and/or sharing the material. Thanks to Klaus Rützler, Sophie Carteron, Jean Vacelet, Pilar Ríos, Rob van Soest, Patricia Gómez/Diana Ugalde for sharing SEM pictures of *Geodia, Erylus* or *Placospongia* species which were used for the plates or **Table 3**. Thanks to all the Institutes where I was able to do SEM images throughout these last 12 years: University of Bergen (Norway), MNHN (Paris, France), IMBE (Station Marine d'Endoume, Marseille, France), and Uppsala University (Sweden). Thanks to David Rees (University of Bergen, BIO) for help sequencing the *COI* of some of these species. Thanks to Andrzej Pisera (Institute of Paleobiology, Polish Academy of Sciences, Warsawa, Poland) for discussions on sponge fossils and paleontology literature. Thanks to Karin Steffen (Uppsala University) for helping with the translation of paleontology articles in German. *Caminus* sp. (MNHN-IP-2015-1144) in **Figure 4** originates from the deep-sea cruise BIOMAGLO conducted jointly by French National Museum of Natural History (MNHN) as part of the Tropical Deep-Sea Benthos program, the French Research Institute for Exploitation of the Sea (IFREMER), the French Southern and Antarctic Lands (TAAF), the Departmental Council of Mayotte and the French Development Agency (AFD), with the financial support of the European Union. I am grateful to the crew of R/V Antèa, especially C. Debitus in charge of collecting and documenting sponge specimens, as well as the cruise leaders of BIOMAGLO: L. Corbari, K. Olu-Le Roy, and S. Samadi. *Geodia vaubani* (MNHN-IP-2015-1667) in **Figure 2** originates from the deep-sea cruise KANACONO expedition in New Caledonia (convention MNHN-Province Sud, APA_N_2016_012; PI: N. Puillandre and S. Samadi). KANACONO and KANADEEP2 expeditions operated under the regulations then in force in the country in question and satisfies the conditions set by the Nagoya Protocol for access to genetic resources. NIWA material was provided by the NIWA Invertebrate Collection, Wellington, New Zealand collected on the research programme: "Seamounts: their importance to fisheries and marine ecosystems," undertaken by NIWA and funded by the former New Zealand Foundation for Research, Science and Technology with additional funding from the former NZ Ministry of Fisheries and NOAA Satellite Operations Facility. Research was co-funded under Coasts and Oceans Research Programme 2 Marine Biological Resources: Discovery and definition of the marine biota of New Zealand (2019/2020 SCI). I am grateful to the Porifera Tree of Life (PorToL) project (Dr. Bob Thacker) and Dr. David Newman for providing permission to access the U.S. National Cancer Institute's (NCI) collection of sponges, housed at the U.S. National Museum of Natural History, Smithsonian Institution. These specimens were originally collected under contract to NCI by Dr. Pat Colin and Lori Bell Colin of the Coral Reef Research Foundation (CRRF), Koror, Palau; I thank CRRF for providing access to metadata for these specimens.

SUPPLEMENTARY MATERIAL

The Supplementary Material for this article can be found online at: https://www.frontiersin.org/articles/10.3389/fmars.2020.613610/full#supplementary-material

Supplementary Figure 1 | Astrophorina *28S* (C1–D2) maximum likelihood (ML) tree reconstructed with RAxML. ML bootstrap supports (1,000 bootstrap replicates) > 70 are indicated. Genbank accession numbers are given after each taxon. In bold are new sequences produced in this study. Geodiidae species have purple branches, Calthropellidae have brown branches. Red branches indicate Geodiidae species which secondarily lost sterrasters (species previously considered to belong to the Ancorinidae). Colored dots indicate sequenced species/specimens for which previous authors or this study have observed the surface of sterrasters with SEM (see **Table 3** for references); round shapes represent sterrasters, flattened shapes represent aspidasters.

Supplementary Table 1 | List of paleontological records of ball-shaped spicules (sterrasters, aspidasters, selenasters, rhaxes). Whenever the term "rhax" is used in publications it entails that it is a reniform-shaped spicule. "?" means missing data. Colors stand for periods: blue for Jurassic, green for Cretaceous and yellow/orange for Paleogene. In purple, comments on the identifications given in the papers.

Supplementary Dataset 1 | Astrophorina *COI* alignment in FASTA format.

Supplementary Dataset 2 | Astrophorina *28S (C1–D2)* alignment in FASTA format.

REFERENCES

Adams, C. L., and Hooper, J. N. A. (2001). A revision of Australian *Erylus* (Porifera : Demospongiae : Astrophorida : Geodiidae) with a tabular review of worldwide species. *Invertebr. Syst.* 15, 319–340. doi: 10.1071/IT00028

Afşar, F., Duda, J.-P., Zeller, M., Verwer, K., Westphal, H., and Eberli, G. P. (2014). "First report of sponge rhaxes in the Picuùn Leufuù Formation (Tithonian–Berriasian), Neuqueèn Basin, Argentina," in *"Spongy, slimy, cosy & more.". Commemorative volume in celebration of the 60th birthday of Joachim Reitner*, eds F. Wiese, M. Reich, and G. Arp (Güttingen: Saint Philip Street Press), 49–56.

Bąk, M., Górny, Z., Bąk, K., Wolska, A., and Stożek, B. (2015). Successive stages of calcitization and silicification of Cenomanian spicule-bearing turbidites based on microfacies analysis, Polish Outer Carpathians. *Ann. Soc. Geol. Poloniae* 85, 187–203. doi: 10.14241/asgp.2015.003

Becking, L. (2013). Revision of the genus *Placospongia* (Porifera, Demospongiae, Hadromerida, Placospongiidae) in the Indo-West Pacific. *ZooKeys* 298, 39–76. doi: 10.3897/zookeys.298.1913

Block Vagle, G., Hurst, A., and Dypvik, H. (1994). Origin of quartz cements in some sandstones from the jurassic of the inner moray firth (UK). *Sedimentology* 41, 363–377. doi: 10.1002/9781444304459.ch22

Bonci, M. C., Magnino, G., Radrizzani, C. P., and Pronzato, R. (1997). Finding of *Geodia* (Demospongiae) sterrasters in the Late Miocene of Capella Montei (Alessandria) and comparison with living forms. *Bollettino della Società Paleontol. Ital.* 35, 245–256. doi: 10.1080/00364820410002451

Bortolotto, M., Braeckman, J. C., Daloze, D., and Tursch, B. (1978). Chemical studies of marine invertebrates. XXXVI. Strongylosterol, a novel C-30 sterol from the sponge *Strongylophora durissima* (Dendy). *Bull. Soc. Chimiques Belges* 87, 539–543. doi: 10.1002/bscb.19780870706

Boury-Esnault, N., Pansini, M., and Uriz, M. J. (1994). Spongiaires bathyaux de la mer d'Alboran et du golfe ibéro-marocain. *Mémoires Muséum Natl. d'Histoire Nat.* 160, 1–174.

Cárdenas, P., Menegola, C., Rapp, H. T., and Díaz, M. C. (2009). Morphological description and DNA barcodes of shallow-water *Tetractinellida* (Porifera: Demospongiae) from Bocas del Toro, Panama, with description of a new species. *Zootaxa* 2276, 1–39. doi: 10.11646/zootaxa.2276.1.1

Cárdenas, P., and Moore, J. A. (2019). First records of *Geodia* demosponges from the New England Seamounts, an opportunity to test the use of DNA mini-barcodes on museum specimens. *Mar. Biodivers.* 49, 163–174. doi: 10.1007/s12526-017-0775-3

Cárdenas, P., and Rapp, H. T. (2013). Disrupted spiculogenesis in deep-water Geodiidae (Porifera, Demospongiae) growing in shallow waters. *Invertebr. Biol.* 132, 173–194. doi: 10.1111/ivb.12027

Cárdenas, P., and Rapp, H. T. (2015). Demosponges from the Northern Mid-Atlantic Ridge shed more light on the diversity and biogeography of North Atlantic deep-sea sponges. *J. Mar. Biol. Assoc. U.K.* 95, 1475–1516. doi: 10.1017/S0025315415000983

Cárdenas, P., Rapp, H. T., Klitgaard, A. B., Best, M., Thollesson, M., and Tendal, O. S. (2013). Taxonomy, biogeography and DNA barcodes of *Geodia* species (Porifera, Demospongiae, Tetractinellida) in the Atlantic boreo-arctic region. *Zool. J. Linn. Soc.* 169, 251–311. doi: 10.1111/zoj.12056

Cárdenas, P., Rapp, H. T., Schander, C., and Tendal, O. S. (2010). Molecular taxonomy and phylogeny of the Geodiidae (Porifera, *Demospongiae*, Astrophorida) — combining phylogenetic and Linnaean classification. *Zool. Scripta* 39, 89–106. doi: 10.1111/j.1463-6409.2009.00402.x

Cárdenas, P., Vacelet, J., Chevaldonné, P., Pérez, T., and Xavier, J. R. (2018). From marine caves to the deep sea, a new look at *Caminella* (Demospongiae, Geodiidae) in the Atlanto-Mediterranean region. *Zootaxa* 4466, 174–196. doi: 10.11646/zootaxa.4466.1.14

Cárdenas, P., Xavier, J. R., Reveillaud, J., Schander, C., and Rapp, H. T. (2011). Molecular phylogeny of the Astrophorida (Porifera, *Demospongiae*) reveals an unexpected high level of spicule homoplasy. *PLoS One* 6:e18318. doi: 10.1371/journal.pone.0018318

Carter, H. J. (1871). On fossil sponge-spicules of the Greensand compared with those of existing species. *Ann. Magazine Nat. History* 7, 112–141. doi: 10.1080/00222937108696328

Carter, H. J. (1876). Descriptions and figures of deep-sea sponges and their spicules, from the Atlantic Ocean, dredged up on board H.M.S.'Porcupine', chiefly in 1869 (concluded). *Ann. Magazine Nat. History* 4, 226–240. doi: 10.1080/00222937608682035

Carvalho, M. D. S., Lopes, D. A., Cosme, B., and Hajdu, E. (2016). Seven new species of sponges (Porifera) from deep-sea coral mounds at Campos Basin (SW Atlantic). *Helgoland Mar. Res.* 70:10. doi: 10.1186/s10152-016-0461-z

Chanas, B., and Pawlik, J. R. (1995). Defenses of Caribbean sponges against predatory reef fish. II. Spicules, tissue toughness, and nutritional quality. *Mar. Ecol. Prog. Ser.* 127, 195–211. doi: 10.3354/meps127195

Chombard, C., Boury-Esnault, N., and Tillier, S. (1998). Reassessment of homology of morphological characters in Tetractinellid sponges based on molecular data. *Syst. Biol.* 47, 351–366. doi: 10.1080/106351598260761

Corriero, G. (1987). (1989). The sponge fauna from the Stagnone di Marsala (Sicily): taxonomic and ecological observations. Bollettino dei musei e degli istituti biologici dell'. *Univ. Genova* 53, 101–113.

da Silva, C. M. M. (2002). *Revisão das espécies de Geodia Lamarck, 1815 (Porifera, Astrophorida, Geodiidae) do Atlântico Ocidental e Pacífico Oriental*. Ph.D. thesis, Instituto de Biociências da Universidade de São Paulo, Butantã.

da Silva, C. M. M., and Mothes, B. (2000). Three new species of *Geodia* Lamarck, 1815 (Porifera, Demospongiae) from the bathyal depths off Brazilian coast, Southwestern Atlantic. *Revue Suisse de Zool.* 107, 31–48. doi: 10.5962/bhl.part.80117

de Geyter, G., and Willems, W. (1982). Sponge spicules from the Landen Formation in Belgium. *Tertiary Res.* 3, 153–160.

de Laubenfels, M. W. (1953). Sponges from the Gulf of Mexico. *Bull. Mar. Sci. Gulf Caribbean* 2, 511–557.

Delecat, S., Peckmann, J., and Reitner, J. (2001). Non-rigid cryptic sponges in oyster patch reefs (Lower Kimmeridgian, Langenberg/Oker, Germany). *Facies* 45, 231–254. doi: 10.1007/bf02668115

Donati, V. (1753). *Auszug seiner Natur-Geschichte des Adriatischen Meeres*. Halle: Palala Press.

Donofrio, D. A. (1984). Microfaune triassiche e giurassiche della serie calcareo-silico-marnosa dellaLucania, facies S. Fele (Appennino Campano-Lucano, Italia meridionale). *Geol. Paleont. Mitt. Innsbruck* 13, 177–179.

Finks, R. M., Hollocher, K., and Thies, K. J. (2011). A major Eocene sponge fauna (Castle Hayne Formation, North Carolina). *J. Carolina Acad. Sci.* 127, 39–175. doi: 10.7572/2167-5880-127.2.39

Frisone, V., Pisera, A., Hajdu, E., Preto, N., Zorzi, F., and Zorzin, R. (2014). Isolated spicules of Demospongiae from Mt. Duello (Eocene, Lessini Mts., northern Italy): preservation, taxonomy, and depositional environment. *Facies* 60, 883–904. doi: 10.1007/s10347-014-0407-3

Geller, J., Meyer, C., Parker, M., and Hawk, H. (2013). Redesign of PCR primers for mitochondrial cytochrome c oxidase subunit I for marine invertebrates and application in all-taxa biotic surveys. *Mol. Ecol. Resour.* 13, 851–861. doi: 10.1111/1755-0998.12138

González-Farías, F. (1989). Estudio al microscopio electrónico de barrido de la estructura esquelética de la esponja *Placospongia melobesioides* Gray. *Anales del Instituto de Ciencias del Mar y Limnologia Universidad Nacional Autónoma de México* 16, 81–90.

Gramann, F. (1962). Schwamm-Rhaxen und Schwamm-Gesteine (Spongiolithe, Spiculite) aux dem Oxford NW-Deutschlands. *Geologisches Jahrbuch* 80, 213–220.

Grech, D., van de Poll, B., Bertolino, M., Rosso, A., and Guala, I. (2020). Massive stranding event revealed the occurrence of an overlooked and ecosystem engineer sponge. *Mar. Biodivers.* 50:82. doi: 10.1007/s12526-020-01105-4

Gruber, G., and Reitner, J. (1991). Isolated poriferan micro- and megascleres from the lower Campanian of Höver (northern Germany) and remarks on the phylogeny of the taxon Geodiidae (Demospongiae). *Berliner Geowissenschaftliche Abhandlungen* 134, 107–117.

Hajdu, E., Peixinho, S., and Fernandez, J. C. C. (2011). *Esponjas Marinhas da Bahia - Guia de Campo e Laboratório. Série Livros 45*. Rio de Janeiro: Museu Nacional/UFRJ.

Hanitsch, R. (1895). Notes on a collection of sponges from the West Coast of Portugal. *Trans. Liverpool Biol. Soc.* 9, 205–219.

Haslett, S. K. (1992). Rhaxellid sponge microscleres from the Portlandian of Dorset, UK. *Geol. J.* 27, 339–347. doi: 10.1002/gj.3350270404

Hill, M. S., and Hill, A. L. (2002). Morphological plasticity in the tropical sponge *Anthosigmella varians*: responses to predators and wave energy. *Biol. Bull.* 202, 86–95. doi: 10.2307/1543225

Hinde, G. J. (1885). VII. On beds of sponge-remains in the lower and upper greensand of the South of England. *Philos. Trans. R. Soc. Lond.* 176, 403–453. doi: 10.1098/rstl.1885.0007

Hinde, G. J. (1888). A monograph of the british fossil sponges. Part II. (Pages 93–188; Plate IX.). *Monogr. Palaeontogr. Soc.* 41, 6–188. doi: 10.1080/02693445.1888.12027997

Hinde, G. J. (1890). On a new genus of siliceous sponges from the lower calcareous grit of Yorkshire. *Q. J. Geol. Soc.* 46, 54–61. doi: 10.1144/gsl.jgs.1890.046.01-04.06

Hinde, G. J., and Holmes, W. M. (1892). On the sponge-remains in the lower tertiary strata near oamaru, Otago, New Zealand. *Zool. J. Linn. Soc.* 24, 177–262. doi: 10.1111/j.1096-3642.1892.tb02480.x

Huang, T. (1967). 531. A new radiolaria from the Somachi Formation, Kikai-Jima, Kagoshima perfecture, Japan. *Trans. Proc. Paleontol. Soc. Jpn.* 1967, 177–184. doi: 10.14825/prpsj1951.1967.68_177

Hughes, G. W. (1985). *Silicosphaera asteroderma* (Porifera), a new siliceous microfossil from the South China Sea. *Neues Jahrb Geol. Palaeontol. Monatsh.* 1985, 599–604. doi: 10.1127/njgpm/1985/1985/599

Hurcewicz, H. (1966). Siliceous sponges from the upper cretaceous of Poland. Part I. Tetraxonia. *Acta Palaeontol. Polonica* 11, 1–129.

Inoue, M., and Iwasaki, Y. (1975). A problematic micro-organism similar to the sterraster of sponges. *Proc. Jpn. Acad.* 51, 273–278. doi: 10.2183/pjab1945.51.273

International Commission on Zoological Nomenclature [ICZN] (1999). *International Code of Zoological Nomemclature (ICZN)*, 4th Edn. Available online at: https://www.iczn.org/the-code/the-international-code-of-zoological-nomenclature/the-code-online/ (accessed November 10, 2020).

Jach, R. (2002). Lower Jurassic spiculite series from the Križna Unit in the Western Tatra Mts, Western Carpathians, Poland. *Ann. Soc. Geol. Poloniae* 72, 131–144.

Katoh, K., and Standley, D. M. (2013). MAFFT multiple sequence alignment software version 7: improvements in performance and usability. *Mol. Biol. Evol.* 30, 772–780. doi: 10.1093/molbev/mst010

Kaya, M., Bilican, I., Mujtaba, M., Sargin, I., Erginer Haskoylu, M., Toksoy Oner, E., et al. (2020). Sponge-derived natural bioactive glass microspheres with self-assembled surface channel arrays opening into a hollow core for bone tissue and controlled drug release applications. *Chem. Eng. J.* doi: 10.1016/j.cej.2020.126667 [Epub ahead of print].

Kelly, M., and Cárdenas, P. (2016). An unprecedented new genus and family of Tetractinellida (Porifera, Demospongiae) from New Zealand's Colville Ridge, with a new type of mitochondrial group I intron. *Zool. J. Linn. Soc.* 177, 335–352. doi: 10.1111/zoj.12365

Kelly, M., Cárdenas, P., Rush, N., Sim-Smith, C., McPherson, D., Page, M., et al. (2019). Molecular study supports the position of New Zealand endemic genus *Lamellomorpha* in family Vulcanellidae (Demospongiae, Tetractinellida, Astrophorina), with the description of three new species. *Eur. J. Taxonomy* 506, 1–25. doi: 10.5852/ejt.2019.506

Klitgaard, A. B., and Tendal, O. S. (2004). Distribution and species composition of mass occurrences of large-sized sponges in the northeast Atlantic. *Prog. Oceanogr.* 61, 57–98. doi: 10.1016/j.pocean.2004.06.002

Kozur, H. W., Mostler, H., and Repetski, J. E. (1996). 'Modern' siliceous sponges from the lowermost Ordovician (Early Ibexian - Early Tremadocian) Windfall Formation of the Antelope Range, Eureka County, Nevada, U.S.A. *Geol. Paläeontol. Mitteilungen Innsbruck* 21, 201–221.

Lamarck, J. B. P. (1815). Suite des polypiers empâtés. *Mémoires du Muséum d'Histoire Naturelle* 1, 69–80.

Larsson, A. (2014). AliView: a fast and lightweight alignment viewer and editor for large datasets. *Bioinformatics* 30, 3276–3278. doi: 10.1093/bioinformatics/btu531

Lehnert, H. (1993). The sponges from Cozumel (Mexico). Inventory, critical comparison of taxonomic characters and description of a new species. *Acta Biol. Benrodis* 5, 35–127.

Lehnert, H., Stone, R., and Heimler, W. (2006). *Erylus aleuticus* sp. nov. (Porifera: Demospongiae: Astrophorida: Geodiidae) from the Aleutian Islands, Alaska, USA. *J. Mar. Biol. Assoc. U.K.* 86, 971–975. doi: 10.1017/S0025315406013944

Lehnert, H., and Stone, R. P. (2016). A comprehensive inventory of the Gulf of Alaska sponge fauna with the description of two new species and geographic range extensions. *Zootaxa* 4144:18. doi: 10.11646/zootaxa.4144.3.5

Lindgren, N. G. (1898). Beitrag zur Kenntniss der Spongienfauna des Malayischen Archipels und der chinesischen Meere. *Zool. Jahrbücher* 11, 283–378.

Łukowiak, M. (2015). Late Eocene siliceous sponge fauna of southern Australia: reconstruction based on loose spicules record. *Zootaxa* 3917, 1–65. doi: 10.11646/zootaxa.3917.1.1

Łukowiak, M., and Pisera, A. (2016). Bodily preserved Eocene non-lithistid demosponge fauna from southern Australia: taxonomy and affinities. *J. Syst. Palaeontol.* 15, 473–497. doi: 10.1080/14772019.2016.1197329

Łukowiak, M., Pisera, A., and O'Dea, A. (2013). Do spicules in sediments reflect the living sponge community? A test in a Caribbean shallow-water lagoon. *PALAIOS* 28, 373–385. doi: 10.2110/palo.2012.p12-082r

McIntyre, F. D., Drewery, J., Eerkes-Medrano, D., and Neat, F. C. (2016). Distribution and diversity of deep-sea sponge grounds on the Rosemary Bank Seamount, NE Atlantic. *Mar. Biol.* 163, 1–11. doi: 10.1007/s00227-016-2913-z

Mehl, D. (1998). Porifera and chancelloridae from the middle cambrian of the georgina basin, Australia. *Palaeontology* 41, 1153–1182.

Mercurio, M., Corriero, G., and Gaino, E. (2006). Sessile and non-sessile morphs of *Geodia cydonium* (Jameson) (Porifera, Demospongiae) in two semi-enclosed Mediterranean bays. *Mar. Biol.* 148, 489–501. doi: 10.1007/s00227-005-0092-4

Meylan, A. (1988). Spongivory in hawksbill turtles: a diet of glass. *Science* 239, 393–395. doi: 10.1126/science.239.4838.393

Miller, M. A., Pfeiffer, W., and Schwartz, T. (2010). "Creating the CIPRES Science Gateway for inference of large phylogenetic trees," in *Proceedings of the Gateway Computing Environments Workshop (GCE), 14 Nov. 2010*, (New Orleans, LA), 1–8.

Moraes, F. C. (2011). *Esponjas das Ilhas Oceânicas Brasileiras. Série Livros 44*. Rio de Janeiro: Museu Nacional/UFRJ.

Morris, P. H., Payne, S. N. J., and Richards, D. P. J. (1999). "Micropalaeontological biostratigraphy of the magnus sandstone member (Kimmeridgian-Early Volgian), Magnus Field, UK North Sea," in *Biostratigraphy in Production and Development Geology*, eds R. W. Jones and M. D. Simmons (London: Geological Society), 55–73. doi: 10.1144/gsl.sp.1999.152.01.04

Mostler, H. (1976). Poriferenspiculae der alpinen Trias. *Geol. Paläeontol. Mitteilungen Innsbruck* 6, 1–42.

Mostler, H. (1990). Mikroskleren von Demospongien (Porifera) aus dem basalen Jura der Nördlichen Kalkalpen. *Geol. Paläeontol. Mitteilungen Innsbruck* 17, 119–142.

Mostler, H. (1996). Ein beitrag zur genese Liassischer toxa und forcipes (skelettelemente von demospongien). *Geol. Paläeontol. Mitteilungen Innsbruck* 21, 185–199.

Mothes, B., Lerner, C. B., and da Silva, C. M. M. (1999). Revision of Brazilian *Erylus* (Porifera: Astrophorida: Demospongiae) with description of a new species. *Mem. Queensland Museum* 44, 369–380.

Müller, W. E. G., Schloßmacher, U., Eckert, C., Krasko, A., Boreiko, A., Ushijima, H., et al. (2007). Analysis of the axial filament in spicules of the demosponge *Geodia cydonium*: different silicatein composition in microscleres (asters) and megascleres (oxeas and triaenes). *Eur. J. Cell Biol.* 86, 473–487. doi: 10.1016/j.ejcb.2007.06.002

Murillo, F. J., Kenchington, E., Lawson, J. M., Li, G., and Piper, D. J. W. (2016). Ancient deep-sea sponge grounds on the Flemish Cap and Grand Bank, northwest Atlantic. *Mar. Biol.* 163, 1–11. doi: 10.1007/s00227-016-2839-5

Murillo, F. J., Muñoz, P. D., Cristobo, J., Ríos, P., González, C., Kenchington, E., et al. (2012). Deep-sea sponge grounds of the Flemish Cap, Flemish Pass and the Grand Banks of Newfoundland (Northwest Atlantic Ocean): distribution and species composition. *Mar. Biol. Res.* 8, 842–854. doi: 10.1080/17451000.2012.682583

Pisera, A. (1997). Upper jurassic siliceous sponges from the swabian alb: taxonomy and paleoecology. *Palaeontol. Polonica* 57, 3–216.

Pisera, A., Cachao, M., and Da Silva, C. M. (2006). Siliceous sponge spicules from the Miocene Mem Moniz marls (Portugal) and their environmental significance. *Rivista Italiana Di Paleontologia E Stratigrafia* 112, 287–299. doi: 10.13130/2039-4942/6342

Plese, B., Kenny, N., Rossi, M. E., Cárdenas, P., Schuster, A., Taboada, S., et al. (2020). Mitochondrial evolution in the demospongiae (porifera): phylogeny, divergence time, and genome biology. *Mol. Phylogenet. Evol.* doi: 10.1186/s12862-018-1230-1 [Epub ahead of print].

Redmond, N. E., Morrow, C. C., Thacker, R. W., Diaz, M. C., Boury-Esnault, N., Cárdenas, P., et al. (2013). Phylogeny and systematics of demospongiae in light of new small subunit ribosomal DNA (18S) sequences. *Integr. Compar. Biol.* 53, 388–415. doi: 10.1093/icb/ict078

Reif, W.-E. (1967). Schwammspicula aus dem weissen Jura zeta von Nattheim (Schwäbische Alb). *Palaeontogr. Abteilung A* 127, 85–102.

Reitner, J., and Mehl, D. (1995). Early Paleozoic diversification of sponges: new data and evidences. *Geol. Paläontol. Mitteilungen Innsbruck* 20, 335–347.

Rezvoi, P. D., Zhuravleva, I. T., and Koltun, V. M. (1962). "Phylum Porifera," in *Osnovy Paleontologii [Fundamentals of Paleontology], vol.1, number 2, Porifera, Archaeocyatha, Coelenterata, Vermes*, ed. B. S. Sokolov (Moscow: Izdatel'stvo Akademii Nauk SSSR), 17–74.

Rigby, J. K. (2004). "Part E. Porifera," in *Treatise on Invertebrate Paleontology*, ed. R. L. Kaesler (Boulder, CO: The Geological Society of America and the University of Kansas), 185–192.

Rigby, J. K., and Smith, C. C. (1992). Microscleres of a Paleocene *Geodia* from Western Alabama. *J. Paleontol.* 66, 406–413. doi: 10.1017/S0022336000033965

Říha, J. (1987). Problematicky tvar jehlic hub Sterraster (Rhax) v Miocenu CSSR. Časopis Moravského muzea. *Vědy přírodní* 72, 75–80.

Robinson, P. D., and Haslett, S. K. (1995). A radiolarian dated sponge microsclere assemblage from the Miocene Dos Bocas Formation of Ecuador. *J. S. Am. Earth Sci.* 8, 195–200. doi: 10.1016/0895-9811(95)00005-Z

Rützler, K., and Macintyre, I. G. (1978). Siliceous sponge spicules in coral reef sediments. *Mar. Biol.* 49, 147–159. doi: 10.1007/BF00387114

Rützler, K., Piantoni, C., Van Soest, R. W. M., and Díaz, M. C. (2014). Diversity of sponges (Porifera) from cryptic habitats on the Belize barrier reef near Carrie Bow Cay. *Zootaxa* 3805:129. doi: 10.11646/zootaxa.3805.1.1

Santucci, R. (1922). La *Geodia cydonium* come centro di associazione biologica. *Mem. Comitato Talassografico ltaliano* 103, 5–19.

Schmidt, O. (1868). *Die Spongien der Küste von Algier. Mit Nachträgen zu den Spongien des Adriatischen Meeres (Drittes Supplement)*. Leipzig: Wilhelm Engelmann.

Schoeppler, V., Reich, E., Vacelet, J., Rosenthal, M., Pacureanu, A., Rack, A., et al. (2017). Shaping highly regular glass architectures: a lesson from nature. *Sci. Adv.* 3:eaao2047. doi: 10.1126/sciadv.aao2047

Schrammen, A. (1899). Beitrag zur Kenntnis der obersenonen Tetractinelliden. *Mittheilungen aus dem Roemer-Museum Hildesheim* 10, 1–9.

Schrammen, A. (1910). Die Kieselspongien der oberen Kreide von Nordwestdeutschland. I. Teil. Tetraxonia, Monaxonia und Silicea incertae sedis. *Palaeontographica* 5(Suppl.), 1–175.

Schrammen, A. (1924). Die Kieselspongien der oberen Kreide von Nordwestdeutschland. III. und letzter Teil. *Monogr. Geol. Paläontol.* 1, 1–159.

Schuster, A., Erpenbeck, D., Pisera, A., Hooper, J. N. A., Bryce, M., Fromont, J., et al. (2015). Deceptive desmas: molecular phylogenetics suggests a new classification and uncovers convergent evolution of lithistid demosponges. *PLoS One* 10:e116038. doi: 10.1371/journal.pone.0116038

Shim, E. J., and Sim, C. J. (2012). A new species of the genus *Caminus* (Astroporida: Geodiidae) from Korea. *J. Anim. Syst. Evol. Divers.* 28, 208–211. doi: 10.5635/ASED.2012.28.3.208

Sim-Smith, C., and Kelly, M. (2015). The marine fauna of New Zealand: sponges in the family Geodiidae (Demospongiae: Astrophorina). *NIWA Biodivers. Mem.* 128, 1–102.

Sollas, W. J. (1877). On the changes produced in the siliceous skeletons of certain sponges by the action of caustic potash. *Ann. Magazine Nat. History* 20, 285–300.

Sollas, W. J. (1880a). On the flint nodules of the Trimmingham chalk. *Ann. Magazine Nat. Hist.* 6, 384–395. doi: 10.1080/00222938009458956

Sollas, W. J. (1880b). The sponge-fauna of Norway; a report on the Rev. A.M. Norman's collection of sponges from the Norwegian Coast. *Ann. Magazine Nat. Hist.* 5, 396–409.

Sollas, W. J. (1880c). The sponge-fauna of Norway; a report on the Rev. A.M. Norman's Collection of sponges from the Norwegian Coast. *Ann. Magazine Nat. Hist.* 5, 130–144.

Sollas, W. J. (1882). The sponge-fauna of Norway; a Report on the Rev. A.M. Norman's Collection of Sponges from the Norwegian Coast. *Ann. Magazine Nat. Hist.* 5, 141–165.

Sollas, W. J. (1888). Report on the Tetractinellida collected by H.M.S. Challenger, during the years 1873-1876. Report on the Scientific Results of the Voyage of H.M.S. Challenger, 1873-1876. *Zoology* 25, 1–458.

Stamatakis, A. (2014). RAxML version 8: a tool for phylogenetic analysis and post-analysis of large phylogenies. *Bioinformatics* 30, 1312–1313. doi: 10.1093/bioinformatics/btu033

Stephens, J. (1915). Sponges of the Coasts of Ireland. I.- The Triaxonia and part of the Tetraxonida. *Fish. Ireland Sci. Investig.* 1914, 1–43.

Tanita, S., and Hoshino, T. (1989). *The Demospongiae of Sagami Bay*. Japan: Biological Laboratory, Imperial Household, 1–197.

Thacker, R. W., Hill, A. L., Hill, M. S., Redmond, N. E., Collins, A. G., Morrow, C. C., et al. (2013). Nearly complete 28S rRNA gene sequences confirm new hypotheses of sponge evolution. *Integr. Compar. Biol.* 53, 373–387. doi: 10.1093/icb/ict071

Todt, C., Cárdenas, P., and Rapp, H. T. (2009). The chiton *Hanleya nagelfar* (Polyplacophora, Mollusca) and its association with sponges in the European Northern Atlantic. *Mar. Biol. Res.* 5, 408–411. doi: 10.1080/17451000802572394

Trejo, M. (1967). La esponja fosil *Rhaxella sorbyana* (Blake) y su significacion estratigraphica. *Boletín de la Asociación Mexicana de Geólogos Petroleros* 48, 33–38.

Ugalde, D., Gómez, P., and Simões, N. (2015). Marine sponges (Porifera: Demospongiae) from the Gulf of México, new records and redescription of *Erylus trisphaerus* (de Laubenfels, 1953). *Zootaxa* 3911, 33. doi: 10.11646/zootaxa.3911.2.1

Ungureanu, D., Ahmad, F., and Farouk, S. (2018). A Callovian (Middle Jurassic) poriferan fauna from northwestern Jordan: taxonomy, palaeoecology and palaeobiogeography. *Historical Biol.* 30, 577–592. doi: 10.1080/08912963.2017.1304935

Vacelet, J., and Cárdenas, P. (2018). When is an aster not an aster? A new deep-sea *Discorhabdella* (Demospongiae, Poecilosclerida) with asters, from the Mozambique Channel. *Zootaxa* 4466, 197–204. doi: 10.11646/zootaxa.4466.1.15

van Kempen, T. M. G. (1990). "On the oldest tetraxon megascleres," in *New Perspectives in Sponge Biology. Third International Conference on the Biology of Sponges*, ed. K. Rützler (Washington, D.C: Smithsonian Institution Press), 9–16.

Van Soest, R. W. M. (2017). Sponges of the Guyana Shelf. *Zootaxa* 4217, 1–225. doi: 10.11646/zootaxa.4217.1.1

Van Soest, R. W. M., Boury-Esnault, N., Hooper, J. N. A., Rützler, K., de Voogd, N. J., Alvarez, B., et al. (2020). *World Porifera Database [Online]*. Available online at: http://www.marinespecies.org/porifera (accessed September 29, 2020).

Van Soest, R. W. M., Meesters, E. H., and Becking, L. E. Z. (2014). Deep-water sponges (Porifera) from bonaire and klein curaçao, Southern Caribbean. *Zootaxa* 3878, 401–443. doi: 10.11646/zootaxa.3878.5.1

Vargas, S., Erpenbeck, D., Göcke, C., Hall, K. A., Hooper, J. N. A., Janussen, D., et al. (2013). Molecular phylogeny of *Abyssocladia* (Cladorhizidae: Poecilosclerida) and *Phelloderma* (Phellodermidae: Poecilosclerida) suggests a diversification of chelae microscleres in cladorhizid sponges. *Zool. Scripta* 42, 106–116. doi: 10.1111/j.1463-6409.2012.00560.x

Vishnevskaya, V. S., Dubinina, E. O., and Mokhov, A. V. (2009). Phenomenal structure of some spicule elements of sponge, radiolarians and nanotechnologies [in Russian]. *Collection Sci. Works Instit. Geol. Sci. NAS Ukraine* 2, 78–80. doi: 10.30836/igs.2522-9753.2009.147924

von Lendenfeld, R. (1894). Die Tetractinelliden der Adria. (Mit einem Anhange über die Lithistiden). Denkschriften der Kaiserlichen Akademie der Wissenschaften.Wien. *Math. Naturwissenschaftliche Klasse* 61, 91–204.

von Lendenfeld, R. (1910). The Sponges. 2. The erylidae. in: reports on the scientific results of the expedition to the eastern tropical pacific, in charge of Alexander Agassiz, by the U.S. Fish Commission Steamer 'Albatross', from October, 1904, to March, 1905, Lieut. Commander L.M. Garrett, U.S.N., Commanding, and of other Expeditions of the Albatross, 1888-1904. (21). *Mem. Museum Comp. Zool.* 41, 261–324.

Vosmaer, G. C. J., and Vernhout, J. H. (1902). "The porifera of the siboga-expedition. I. The genus *Placospongia*," in *Siboga-Expeditie. Uitkomsten op zoologisch, botanisch, oceanographisch en geologisch gebied verzameld in Nederlandsch Oost-lndië 1899-1900aan boord H.M. 'Siboga' onder commando van Luitenant ter Zee 1e kl. G.F. Tydeman. 9 (Monographie VIa)*, ed. M. Weber (Leiden: E. J. Brill), 1–17.

Wagoner, N. A. V., Mudie, P. J., Cole, F. E., and Daborn, G. (1989). Siliceous sponge communities, biological zonation, and Recent sea-level change on the Arctic margin: Ice Island results. *Can. J. Earth Sci.* 26, 2341–2355. doi: 10.1139/e89-200

Weller, J. M. (1930). Siliceous sponge spicules of pennsylvanian age from illinois and Indiana. *J. Paleontol.* 4, 233–251.

Wiedenmayer, F. (1994). Contributions to the knowledge of post-Palaeozoic neritic and archibenthal sponges (Porifera). The stratigraphic record, ecology, and global distribution of intermediate and higher taxa. *Schweizerische Paläontol. Abhandlungen* 116, 1–147.

Wysokowski, M., Jesionowski, T., and Ehrlich, H. (2018). Biosilica as a source for inspiration in biological materials science. *Am. Mineral.* 103, 665–691. doi: 10.2138/am-2018-6429

Zittel, K. A. (1876). *Ueber Coeloptychium. Ein Beitrag zur Kenntniss der Organisation fossiler Spongien*. München: Abhandlungen der k. bayr. Akad. der Wissenschaften.

Zumberge, J. A., Love, G. D., Cárdenas, P., Sperling, E. A., Gunasekera, S., Rohrssen, M., et al. (2018). Demosponge steroid biomarker 26-methylstigmastane provides evidence for Neoproterozoic animals. *Nat. Ecol. Evol.* 2, 1709–1714. doi: 10.1038/s41559-018-0676-2

Conflict of Interest: The author declares that the research was conducted in the absence of any commercial or financial relationships that could be construed as a potential conflict of interest.

Copyright © 2020 Cárdenas. This is an open-access article distributed under the terms of the Creative Commons Attribution License (CC BY). The use, distribution or reproduction in other forums is permitted, provided the original author(s) and the copyright owner(s) are credited and that the original publication in this journal is cited, in accordance with accepted academic practice. No use, distribution or reproduction is permitted which does not comply with these terms.

frontiers in Marine Science

ORIGINAL RESEARCH
published: 18 December 2020
doi: 10.3389/fmars.2020.595267

Reproductive Biology of *Geodia* Species (Porifera, Tetractinellida) From Boreo-Arctic North-Atlantic Deep-Sea Sponge Grounds

Vasiliki Koutsouveli[1,2], Paco Cárdenas[2], Maria Conejero[3], Hans Tore Rapp[4] and Ana Riesgo[1,5]**

[1] Department of Life Sciences, The Natural History Museum, London, United Kingdom, [2] Pharmacognosy, Department Pharmaceutical Biosciences, Uppsala University, Uppsala, Sweden, [3] Analytical Methods-Bioimaging Facility, Royal Botanic Gardens, Kew, Richmond, United Kingdom, [4] Department of Biological Sciences, University of Bergen, Bergen, Norway, [5] Departamento de Biodiversidad y Biología Evolutiva, Museo Nacional de Ciencias Naturales, Consejo Superior de Investigaciones Científicas, Museo Nacional de Ciencias Naturales Calle de José Gutiérrez Abascal, Madrid, Spain

OPEN ACCESS

Edited by:
Chiara Romano,
Centre for Advanced Studies of Blanes (CEAB), Spanish National Research Council, Spain

Reviewed by:
Sylvie Marylène Gaudron,
Sorbonne Universités, France
Rhian G. Waller,
University of Gothenburg, Sweden

***Correspondence:**
Vasiliki Koutsouveli
V.Koutsouveli@nhm.ac.uk;
vassiakouts88@gmail.com
Ana Riesgo
A.Riesgo@nhm.ac.uk;
anariesgogil@gmail.com

Specialty section:
This article was submitted to Deep-Sea Environments and Ecology, a section of the journal Frontiers in Marine Science

Received: 15 August 2020
Accepted: 19 November 2020
Published: 18 December 2020

Citation:
Koutsouveli V, Cárdenas P, Conejero M, Rapp HT and Riesgo A (2020) Reproductive Biology of Geodia Species (Porifera, Tetractinellida) From Boreo-Arctic North-Atlantic Deep-Sea Sponge Grounds. Front. Mar. Sci. 7:595267. doi: 10.3389/fmars.2020.595267

Boreo-arctic sponge grounds are essential deep-sea structural habitats that provide important services for the ecosystem. These large sponge aggregations are dominated by demosponges of the genus *Geodia* (order Tetractinellida, family Geodiidae). However, little is known about the basic biological features of these species, such as their life cycle and dispersal capabilities. Here, we surveyed five deep-sea species of *Geodia* from the North-Atlantic Ocean and studied their reproductive cycle and strategy using light and electron microscopy. The five species were oviparous and gonochoristic. Synchronous development was observed at individual and population level in most of the species. Oocytes had diameters ranging from 8 μm in previtellogenic stage to 103 μm in vitellogenic stage. At vitellogenic stages, oocytes had high content of lipid yolk entirely acquired by autosynthesis, with no participation of nurse cells. Intense vertical transmission of bacterial symbionts to the oocytes by phagocytosis through pseudopodia was observed, especially in late stages of oogenesis. The density of oocytes within the sponge tissue was on average 10 oocytes/mm^2 across all species, higher than that of most temperate and tropical oviparous species studied elsewhere. Spermatic cysts were widespread over the tissue during early stages, or fused in larger cysts, around the canals in later stages, and occupying between 1.5 and 12% of the tissue in males. The reproductive season spanned similar periods for all *Geodia* spp.: from late spring to early autumn. During the reproductive peak of each species, between 60 and 90% of the population was engaged in reproduction for most species. Given the present hazards that threaten the boreo-arctic tetractinellid sponge grounds, it becomes crucial to understand the processes behind the maintenance and regeneration

of populations of keystone deep-sea species in order to predict the magnitude of human impacts and estimate their ability to recover. The information provided in this study will be useful for developing adequate conservation strategies for these vulnerable deep-sea habitats.

Keywords: deep sea, sponge grounds, *Geodia*, reproduction, conservation

INTRODUCTION

Deep-sea sponge grounds are marine habitats first described by Klitgaard et al. (1997) in the Faroe Island shelf and slope areas, and later shown to be widespread across the North-Atlantic Ocean (Klitgaard and Tendal, 2004; Murillo et al., 2012; Beazley et al., 2015). These habitats are formed by three-dimensional structures created by the sponges, which provide refuge for other animals, sometimes of high economic value, and enhance biodiversity (e.g., Klitgaard, 1995; Beazley et al., 2013, 2015; Kenchington et al., 2013). Furthermore, because of their high pumping activity (Kutti et al., 2015) and consumption of organic matter (Leys et al., 2018), sponges play a major role in nutrient cycling (Maldonado et al., 2012), specifically in carbon turnover (Pile and Young, 2006; Yahel et al., 2007; Cathalot et al., 2015; Kahn et al., 2015), nitrogen flow (Hoffmann et al., 2009; Rooks et al., 2020) and the silicon cycle (Maldonado et al., 2020). Indeed, recently, studies point to serious impacts on ecosystem function when sponges are removed from the deep sea due to fishing bycatch (Pham et al., 2019).

Despite their importance at functional and ecological level (Kutti et al., 2013; Maldonado et al., 2016), deep-sea sponge grounds have been highly exposed to commercial bottom trawling (e.g., Freese, 2001; Roberts, 2002; Pham et al., 2019). In addition, sediment disturbance caused by equipment deployment at the seafloor from various anthropogenic activities, can lead to the clogging of their aquiferous system and eventually to their death (Kutti et al., 2015). For these reasons, deep-sea sponge grounds in the North Atlantic are now considered as vulnerable marine ecosystems by the OSPAR convention for the protection of the marine environment of the North-East Atlantic (OSPAR, 2008), needing protection according to United Nations General Assembly Resolution 61/105 and Food and Agriculture Organization (UNGA, 2006; FAO, 2009). Up to now, most areas with dense biomass have been protected from bottom trawling in North-West Atlantic by the North-West Atlantic Fisheries Organization (NAFO, 2012, 2014), but there are still areas of deep-sea sponge grounds with high levels of exposure (Thompson and Fuller, 2020). Nowadays, a huge effort is conducted to better understand sponge ground ecosystems' services, to estimate their overall importance, and evaluate the consequences of adverse impacts on these habitats (ICES, 2018; NAFO, 2018).

However, few ecophysiological studies have been conducted on deep-sea sponge species (e.g., Strand et al., 2017) and only two studies regarding their reproductive timing have been published so far. One study focused on the species *Thenea abyssorum* Koltun, 1959 (Koltun, 1959) (order Tetractinellida and suborder Astrophorina), *Tentorium semisuberites* (Schmidt, 1870), and *Radiella sol* Schmidt, 1870 (Schmidt, 1870), previously called *Trichostemma sol* (order Polymastiida) from the Barents Sea (Witte, 1996), which had been described among the most abundant demosponges in abyssal Greenland, Iceland, and Norwegian seas by Barthel and Tendal (1993). The other one focused on the species *Geodia barretti* Bowerbank, 1858 (Bowerbank, 1858; Spetland et al., 2007), which is very abundant in temperate and boreo-arctic grounds of the North-Atlantic Ocean (Klitgaard and Tendal, 2004; Cárdenas et al., 2013). In both publications, researchers found that the studied species were gonochoristic and oviparous with one or two reproductive cycles per year which were dependant on primary production blooms.

Porifera is one of the earliest diverging clades in the phylogeny of the Metazoa (Dohrmann and Wörheide, 2013; Feuda et al., 2017; Zumberge et al., 2018; Laumer et al., 2019). But despite their early origin, sexual reproduction in sponges is not only morphologically similar to that in other Metazoa, but also the molecular toolkit that regulates the gametogenesis is conserved from Porifera to Chordata (Koutsouveli et al., 2020b). Despite the conserved process of reproduction through evolution, even within the phylum Porifera, the reproductive strategy greatly varies among sponge groups in the following traits: e.g., oviparity/viviparity, gonochorism/hermaphrotidism, larval types, number of reproductive cycles per year, and seasonality. These features are mainly constrained by phylogeny (Riesgo et al., 2014), but there is also a high degree of plasticity correlated to the abiotic conditions of their environment. In this sense, sponges lack sensory organs, however, they are able to respond to a variety of abiotic stimuli. One of the main driving factors in latitudes with high seasonal variations is temperature. Many studies reported a correlation of the temperature increase with sex determination, gametogenesis, or induction of spawning, while others have found a triggering of reproductive period after a thermal drop (Chen, 1976; Fromont and Bergquist, 1994; Corriero et al., 1998; Ereskovsky, 2000; Riesgo and Maldonado, 2008). In habitats where temperature is constant all year round, different stimuli have been proposed to play a role, such as photoperiod, wave fluctuation, rainfall, and salinity variations (e.g., Elvin, 1976; Corriero et al., 1998; Calazans and Lanna, 2019). In the deep sea, the reproductive season seems to be dependent on other environmental stimuli such as the primary productivity blooms that occur once or twice over the year (Young and Eckelbarger, 1994; Witte, 1996).

A crucial biological feature for the ecological success of sponges is the larval type and its dispersal potential, which is directly related to the connectivity patterns of these populations and therefore their resilience. All sponge larvae are lecithotrophic since they do not have any digestive tract to process food. So, the major source of energy during larval dispersal is

the yolk previously accumulated during gametogenesis and embryogenesis (Maldonado and Bergquist, 2002), with only few exceptions in which larvae were also observed to phagocytize some nutrients from their environment (Ivanova and Semyonov, 1997). Consequently, the dispersal capabilities of sponge propagules are tightly linked to the quality and quantity of the yolk they acquire even before reaching the larva stage. The origin and type of yolk in the female gametes depends on the reproductive strategy of the species (Riesgo et al., 2015): the yolk can (i) be produced by the oocyte itself, through the Golgi apparatus and the rough endoplasmic reticulum (Fell, 1974; Simpson, 1984), (ii) be acquired by direct phagocytosis from the mesohyl (Fell, 1974; Simpson, 1984), (iii) be provided by nurse cells in the surroundings of the oocytes (Fell, 1974; Simpson, 1984), and (iv) be the product of bacterial phagocytosis by the oocyte (Riesgo and Maldonado, 2009). The yolk in sponges is mainly composed of lipid, protein, and glycogen (Fell, 1969, 1974; Simpson, 1984). The amount and the type of yolk in a given oocyte/embryo can give clues on the duration of the gametogenesis/embryogenesis, and the dispersal time of the released propagules. This knowledge has profound ecological implications for the survival and possible recovery of the populations in case of disturbance, and to a greater extent, of the species in the studied habitat.

Demosponges of the genus *Geodia* (order Tetractinellida, suborder Astrophorina, family Geodiidae) often dominate in terms of abundance and biomass the boreo-arctic sponge grounds (Klitgaard and Tendal, 2004; Cárdenas et al., 2013). A total of six species of *Geodia* form two types of astrophorin sponge grounds, (1) the boreal sponge grounds (Faroe Islands, Norway, Sweden, western Barents Sea and south of Iceland), which are mainly composed of *Geodia phlegraei* (Sollas, 1880), *Geodia macandrewii* Bowerbank, 1858 (Bowerbank, 1858), *Geodia barretti* Bowerbank, 1858 (Bowerbank, 1858) and *Geodia atlantica* (Stephens, 1915) and (2) the arctic sponge grounds (north of Iceland, in most of the Denmark Strait, off East Greenland and north of Spitzbergen) which mainly consist of *Geodia hentscheli* Cárdenas et al., 2010 and *Geodia parva* Hansen, 1885 (Hansen, 1885; Klitgaard and Tendal, 2004; Cárdenas et al., 2010, 2013; Murillo et al., 2012; Knudby et al., 2013). The reproduction of only three species of Geodiidae has been studied to date – *Geodia cydonium, G. barretti*, and *Erylus discophorus* – which are all gonochoristic and oviparous (Liaci and Sciscioli, 1969, 1970; Mercurio et al., 2007; Spetland et al., 2007). While *G. cydonium*, and *E. discophorus* are temperate species, *G. barretti* is the only deep-sea sponge from northern latitudes. Asexual reproduction (budding) has also been reported in the two arctic species, *G. parva* and *G. hentscheli* (Cárdenas et al., 2013). The study of Spetland et al. (2007) mainly focused on describing the reproductive cycle of *G. barretti*, however without providing detailed observations about its reproductive features at the histological/cytological level. All in all, there is very little information about the reproductive biology of *Geodia* species.

In this study, fresh material of five out of the six boreo-arctic North-Atlantic *Geodia* species was collected between 2011 and 2019 in the North-East Atlantic (boreal: *G. phlegraei, G. macandrewii, G. barretti, G. atlantica*; arctic: *G. hentscheli*). The main goal was to study the seasonality and the strategy of gametogenesis of these five species through histological and cytological observations. Knowledge on seasonality and reproductive strategies is crucial for developing appropriate conservation strategies for boreo-arctic sponge grounds; a deeper and wider understanding of the reproduction of key sponge ground species could inform us on the population structure and their dispersion pattern, and the capacity of the population to survive and regenerate in case of disturbance.

MATERIALS AND METHODS

Sample Collection

One hundred and twenty eight specimens were collected from five *Geodia* species: *G. hentscheli*, *G. phlegraei*, *G. barretti*, *G. macandrewii*, and *G. atlantica* during expeditions in the boreo-arctic and North-East Atlantic from the beginning of April to the end of September mainly during the years 2016 and 2017 (**Figure 1**, **Table 1**, and **Supplementary Table S1**). Samples from Hordaland coast, were collected by Agassiz trawl on board the "K. Bonnevie" research vessel (RV), those from the Kosterfjord were collected using an ROV during the expedition of RV "Nereus," and samples from Korsfjord were collected by triangular dredge on board the RV "Hans Brattstrøm." In addition, samples from the Sula reef, Schulz Bank, and Tromsøflaket (western Barents Sea), were collected either by Agassiz trawl, or ROV (AEGIR 6000) on board of the RV "G.O. Sars" (**Table 1** and **Supplementary Table S1**). Finally, samples from Rosemary Bank Seamount were collected by Agassiz trawl on board of MRV "Scotia." All collection details and metadata associated were archived in the PANGAEA data repository[1] (Koutsouveli et al., 2020a). In all expeditions, three cubes of sponge tissue from each specimen were collected (∼5 mm^3 each) and directly fixed in 2.5% glutaraldehyde solution in 0.4M PBS and 0.34M NaCl and stored at 4°C, until their further processing in the laboratory. The identification of all species was performed based on spicule analyses. Regarding the specimens collected by trawl/dredge, we subsampled tissue only from entire or almost entire collected specimens and not from small pieces of sponges in order to avoid to sample tissue from the same specimen several times.

Sample Processing and Histological Sectioning

For further histological processing, samples were then desilicified by immersing the sponge tissue in 5% hydrofluoric acid overnight and then rinsed profusely with distilled water. After that, the tissue was either processed for light microscopy or Transmission Electron Microscopy (TEM). For light microscopy, tissues were dehydrated through an increasing ethanol series and then embedded in paraffin (60°C, melting point) overnight after a brief bath in xylene. For TEM, sponge tissues were postfixed in 2% osmium tetroxide in 0.4M PBS for 1 h at 4°C and then rinsed in distilled water. Similarly, an increasing ethanol series was used

[1] https://doi.pangaea.de/10.1594/PANGAEA.921626

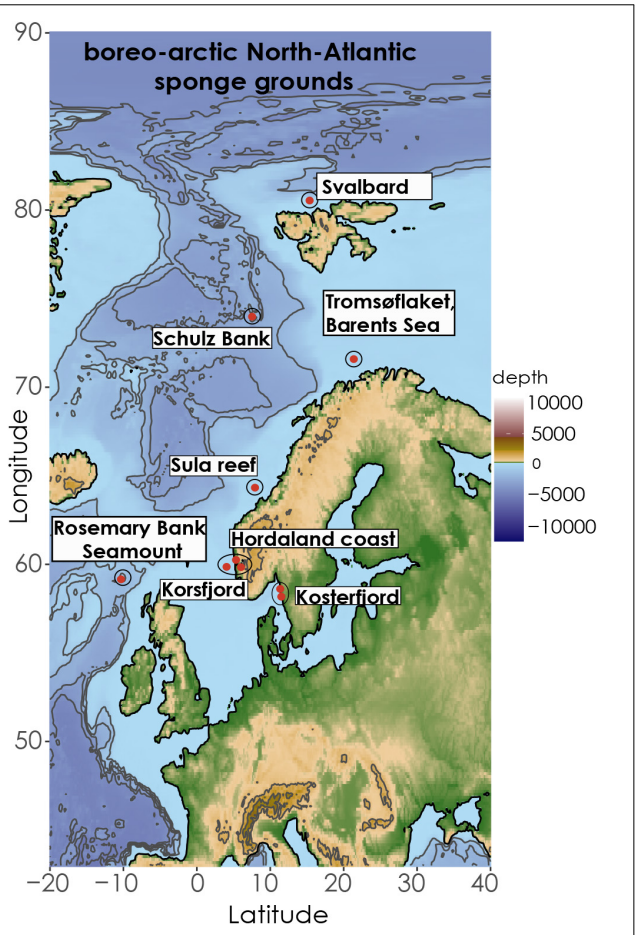

FIGURE 1 | Map of North Atlantic indicating the coordinates of the different sampling areas of the study. The Map was retrieved from the ETOPO1 database from NOAA server (Amante and Eakins, 2009) and illustrated in R.

to dehydrate the tissue, and then it was embedded in LRW resin (preparation according to guidelines of the manufacturer).

The protocol for the preparation of the samples was the same as mentioned in Koutsouveli et al. (2020b). Briefly, for light microscopy preparations, thick sections (5 μm) were obtained with an HM 325 rotary microtome (ThermoFisher Scientific) and stained with a standard Harris' Hematoxylin and Eosin (HandE) and Methylene Blue. For TEM, ultrathin sections (approximately 70 nm) were obtained with an Ultracut ultramicrotome (Reichert-Jung) and then stained with an uranyl acetate/lead citrate staining protocol (Reynolds, 1963). Light microscopy preparations were observed with an Olympus microscope (BX43) with a UC50 camera at the Natural History Museum's imaging facilities, while ultrathin sections on gold coated grids were observed with a Hitachi Transmission Electron Microscope (H-7650) at 80 kV at the imaging facilities in Kew Botanical Gardens.

Measurements on Histological Sections

Several parameters were recorded to understand the life cycle dynamics of all five species of *Geodia*, (i) size, density, and

TABLE 1 | Number of specimens collected in each location and date for the five species of *Geodia*.

Species	April 2019/May 2016	May, 2017	June, 2017	July, 2017	June, 2016	August, 2017	August, 2017	September, 2016	September, 2011-12-16	September, 2011
	Kosterfjord	Hordaland coast	Korsfjord	Sula reef	Schulz bank	Schulz bank	Tromsøflaket, Barents Sea	Korsfjord	Rosemary Bank Seamount	Svalbard
G. phlegraei	–	5 (1 female/3 males)	1 (NR)	3 (1 female/1 male)	–	–	4 (1 female/3 males)	–	–	1 (NR)
G. macandrewii	–	12 (6 females/3 males)	2 (NR)	3 (1 female/1 male)	–	–	8 (NR)	1 (female)	3 (NR)	1 (female)
G. barretti	8 (NR)/3 (NR)	5 (1 female)	5 (1 male)	1 (female)	–	–	17 (1 female/1 male)	7 (NR)	13 (6 males/5 females)	–
G. hentscheli	–	–	–	–	6 (3 females/1 male)	5 (3 females, 1 male)	–	–	–	–
G. atlantica	–	3 (1 male	3 (1 female)	1 (male)	–	–	–	5 (2 females/2 males	10 (4 females)	–

In parenthesis the number of male and female specimens.

fecundity estimations of reproductive features (oocytes and spermatic cysts), (ii) bacteria and yolk abundance within the oocytes, (iii) length of the reproductive period (considering the timing of appearance/disappearance of gametes), and (iv) the percentage of the population engaged in reproduction. In the following sections, specimens with gametes in their tissues were referred as reproductive while specimens without any gamete observed in their tissue sections were called non-reproductive.

Size and Density of Reproductive Features

The measurements of size and density of the reproductive features within the sponge tissue and for the fecundity estimations were obtained from light microscopy images with the Olympus microimaging software CellSens standard, connected to the microscope. Measurements of yolk and bacterial content in the ooplasm were acquired from TEM images with ImageJ (Schneider et al., 2012) on the TEM images.

The size of oocytes and spermatic cysts and density of oocytes were calculated in three different areas (0.58 mm^2 each area) of tissue per specimen at 10x magnification. Size and density of spermatic cells could not be obtained, since that would require their individual measurement and counting, but they were so densely packed within the spermatic cysts that they could not be visually separated and counted. As thus, only the size of spermatic cysts was reported here.

Fecundity Estimations

While female fecundity was estimated based on the total number of oocytes produced per sponge, male fecundity estimations were based on the percentage of the sponge area occupied by spermatic cysts. For the female fecundity estimations, firstly the number of oocytes/mm^3 was extrapolated with the modified Elvin formula (Elvin, 1976), $E = N\left(t/d + t\right)/v$, as used by Di Camillo et al. (2012), where N is the number of the oocytes in a microscopic section; t, the thickness of the section; d, the diameter of the oocytes and v, is the volume of the histological section. Secondly, the area and the volume of each species were calculated. It was considered that almost all the studied sponge species (except for *G. atlantica*) had a spherical shape. The average diameter per species (**Supplementary Table S2**) was based on dimensions previously published (Cárdenas et al., 2013) or observed (personal observations, HTR) for these species, and then the area of the sponge was calculated according to the formula $4 \times \pi \times r^2$ and the volume of the sponge according to the formula, $^4/_3 \times \pi \times r^3$. Regarding *G. atlantica*, its shape was considered more similar to a hollow cone, then using the dimensions (70 cm diameter × 40 cm height) mentioned in Cárdenas et al. (2013) for the maximum volume and using 3 cm as average thickness for the tissue of the sponge, the area of a hollow cone: $\pi \times r \times s$ was calculated, where s, is the slant height, $s = \sqrt{r^2 + h^2}$ and the volume for a hollow cone (outside volume - inside volume; where the volume for the cone is $\pi \times r^2 \times h/3$) (**Supplementary Table S2**). We should report here that although the diameters of *Geodia* spp. might be different in other publications (i.e., Klitgaard and Tendal, 2004; Cárdenas et al., 2013; Kutti et al., 2013) than the mean diameter used here, we mainly used specimens coming from the Arctic region for this analysis and so we extracted the information mainly based on photos of the specimens and personal observations (HTR). Only the dimensions of *G. atlantica* were retrieved by already published data (Cárdenas et al., 2013) as we never collected a whole specimen for this species to estimate dimensions. Consequently, the fecundity rates for the species of this study are a rough estimation and they should be used with caution.

For the fecundity estimations and the oocyte content (bacterial symbionts and yolk content), individuals with the most mature oocytes (maximum diameter of Vi oocytes) were used for *G. phlegraei* (Sula reef, July), *G. atlantica* (Korsfjord, September), and *G. hentscheli* (Schulz Bank, August) while individuals with mature oocytes, but not those with the most mature oocytes, were used for *G. barretti* (Barents sea, August) and *G. macandrewii* (Sula reef, July) because only those specimens had been processed for TEM, having a more complete information. Regarding the male individuals, only some of the *G. phlegraei* and *G. atlantica* individuals were in the latest developmental stages, while specimens of *G. macandrewii*, *G. barretti*, and *G. hentscheli* were in less advanced but similar developmental stages. For each species, the individuals with the most mature SP_II spermatic cysts (i.e., largest average size) were chosen to estimate male fecundity.

RESULTS

Histological Features of *Geodia* Species

General Description of the Mesohyl of *Geodia* spp.

Several common sponge cell types, described previously in sponges, were observed in the mesohyl of all species, including pinacocytes lining the periphery of the canals and collencytes producing collagen in the mesohyl space (**Supplementary Figures S1A-B**). In addition, archeocytes (average size of 5–7 μm) (**Supplementary Figures S1B-D**) and choanocytes (**Supplementary Figures S1B-D**), forming small choanocyte chambers (average 6–10 μm), were observed in the mesohyl (**Supplementary Figures S1C,D**). *G. barretti* and *G. atlantica* had the highest abundance of spherulous cells in their mesohyl, 15–20 μm in the largest diameter (**Supplementary Figures S1E-G**); *G. phlegraei* had spherulous cells of similar size (∼20 μm) but in lower numbers, while *G. macandrewii* and *G. hentscheli* completely lacked spherulous cells. The spherules in the spherulous cells were all electron-dense, but slightly different in size and shape (**Supplementary Figures S1E-G**). All the *Geodia* spp. were High Microbial Abundance (HMA) sponges (**Supplementary Figures S1E-H**). Phagocytosis of bacteria from different types of sponge cells, including archeocytes (**Supplementary Figure S1A**) and choanocytes (**Supplementary Figure S1C**), was observed within the mesohyl of *G. barretti.*

Reproductive Features of *Geodia* spp.

All species of *Geodia* were gonochoristic; not a single specimen of *Geodia* spp. had both female and male reproductive features at the same time. In all species, individuals at the beginning of oogenesis with small previtellogenic (PV) oocytes, and individuals with more developed, vitellogenic (Vi) oocytes were

found (**Supplementary Figure S2A**), although sometimes these two stages were found in the same individual (e.g., *G. atlantica*, Korsfjord June). Similarly, both male individuals with spermatic stage I (SP_I) cysts and more mature, spermatic stage II (SP_II) cysts were identified (**Supplementary Figure S2B**). In all *Geodia* spp., the diameter of PV oocytes measured on average 19 ± 6 μm and that of SP_I spermatic cysts was 30 ± 6 μm (**Supplementary Figure S2**). At a later stage, Vi oocytes had an average diameter of 54 ± 14 μm and SP_II spermatic cysts around 60 ± 25 μm (**Supplementary Figure S2**). *G. hentscheli* had the smallest size of both female and male reproductive features among the *Geodia* species (**Supplementary Figure S2**), when comparing individuals with either early or relatively late developmental stages, while *G. atlantica* had the largest oocytes and mature spermatic cysts found among the species studied here (**Supplementary Figure S2**).

Oogenesis

Oocyte development in most species was synchronous at both individual and population levels. All species showed very similar cytological features which are described together in the following sections. At the beginning of oogenesis (**Figure 2**), ameboid PV oocytes (8-25 μm in max. diameter) (**Supplementary Figure S2A**) with a well distinct nucleus and nucleolus were widespread throughout the mesohyl of the sponges (**Figures 2A,B**). A thin layer of collagen started to form around the PV oocytes (**Figures 2C-E**). PV oocytes were full of electron light vesicles, with few lipid droplets observed in the ooplasm of the oocytes (**Figures 2D-G**). While many bacterial symbionts were present in the mesohyl outside the oocyte (**Figure 2D**), only very few were observed within the oocyte at this stage (**Figures 2E-H**). Phagocytosis of bacteria was achieved with pseudopodia (**Figures 2D,H**). Both the Golgi apparatus and the nuage (among mitochondrial clouds) could be observed at this stage in most species (**Figures 2E,F**).

In a later developmental stage, Vi oocytes were larger in general (>50-60 μm) (**Figure 3** and **Supplementary Figure S2B**) and migrated to the vicinity of the canals (**Figures 3A,C**). Mature oocytes of *G. barretti* (50-60 μm), *G. macandrewii* (40-60 μm) and *G. atlantica* (103 μm in the largest diameter) were ready to get released (**Figures 3B,C** and **Supplementary Figure S2A**). When in the canals, mature oocytes were found in clusters, enveloped by a very thin collagen membrane (**Figure 3B**). A thick collagen layer was formed around the Vi oocytes but no cellular follicle (supportive membrane surrounding the oocyte) was observed in any of the studied species (**Figures 3D-F**). Vi oocytes contained a high amount of yolk, mainly of lipid origin (**Figures 3D-H**, **4**, **5**), and only few protein platelets were observed in the ooplasm (**Figures 3D,E**, **4**, **5**). Nurse cells were not observed in any of the *Geodia* spp. and the yolk was produced by autosynthesis via the rough endoplasmic reticulum and the Golgi apparatus (**Figures 4B,D**). In fact, lipid content was higher than protein content in both PV and Vi stages, increasing from an average of 7.5–17% compared to protein yolk that increased from 2 to 3% (**Figure 5**). Both *G. barretti* and *G. hentscheli* had the highest percentage of lipid content, 20 and 19% respectively, in their small Vi oocytes (35 ± 5 μm and 30 ± 17 μm in diameter respectively) (**Figure 5B**). *G. macandrewii* and *G. atlantica* had 13 and 15% of lipid yolk occupying their mature oocytes (43 ± 3 μm and 95 ± 7 μm in diameter respectively) (**Figure 5B**). Although at the beginning of vitellogenesis, vesicles with heterogenous yolk in oocytes of *G. phlegraei and G. barretti* were observed (**Figure 5A**), at later stages none of the studied species had heterogenous yolk in the ooplasm (**Figures 3D-H**, **4**, **5B**). Unfortunately, no high resolution TEM images of Vi oocytes of *G. phlegraei* could be obtained to investigate the presence of homogeneous and heterogeneous yolk in the later maturation stages.

Extensive vertical transmission of bacterial symbionts from the mother to the descendant at Vi stage in most species was also observed (**Figures 3F-H**, **4A**, **5**). Bacteria were collected by oocyte pseudopods and each bacterium was stored in vesicle in which bacterial division was observed in some cases (**Figure 3G**, insert). No signs of digestion were observed in the stored bacteria in the oocytes (**Figure 3G**). The average bacterial content increased from 1% in PV oocytes to 4% in Vi oocytes across species (**Figure 5**). The Vi oocytes of *G. macandrewii* (diameter ∼43 μm) and *G. atlantica* (with diameter ∼95 μm) had the largest area occupied by bacteria (∼7%) (**Figures 3F**, **4**, **5B**), followed by *G. hentscheli* with 4.4% in Vi oocytes (∼30 μm in diameter) (**Figures 3E**, **5B**). However, Vi oocytes of *G. barretti* of similar size to those of *G. hentscheli* (diameter ∼35 μm), had a very low bacterial content (0.6-0.7%) without a significant increase in bacteria between the PV and Vi stages (**Figures 3D,E**, **5**).

Spermatogenesis

SP_I spermatic cysts were scattered throughout the mesohyl, measuring on average 20-40 μm in all species (**Figure 6A** and **Supplementary Figure S2B**). Very early spermatic cysts contained only a few cells, mainly spermatogonia (**Figures 6A-C**). Bacteria were very abundant in the surroundings of the spermatic cysts, but they were seldomly observed within the lumen of the spermatic cyst. In the SP_I spermatic cysts of *G. hentscheli*, a few bacteria were phagocytosed by the spermatogonia, which were also full of vesicles and stored reserves (**Figures 6C,D**). The spermatogonia did not show a fully functional flagellum, but the axonemal structure could be seen in the cytoplasm of the spermatogonium, probably being resorbed (**Figure 6D**). This indicates that sperm cells, clearly derived from choanocytes, lose the choanocyte flagellum during early spermatogenesis.

At a more mature stage, SP_II spermatic cysts measured on average 40-80 μm (**Figure 6E** and **Supplementary Figure S2B**) and formed clusters around the canals (**Figure 6E**). In some cases, a thin layer of mesohyl between two spermatic cysts seems to disintegrate, inducing the fusion of different spermatic cysts into one (**Figure 6F**). Fused clusters of spermatic cysts reached a maximum length of ∼200 μm (**Figure 6G**). No cellular or collagenous follicle layer surrounding the spermatic cyst was observed at any stage in any of the studied *Geodia* spp. (**Figures 6A,B,H**, **7A**).

Inside SP_II spermatic cysts, there were more than 300 cells in the process of division to be developed into sperm cells (**Figures 6G,H**). Their development within the SP_II spermatic cyst was clearly asynchronous as cells in different developmental stages were observed, the ones dividing at early stages in

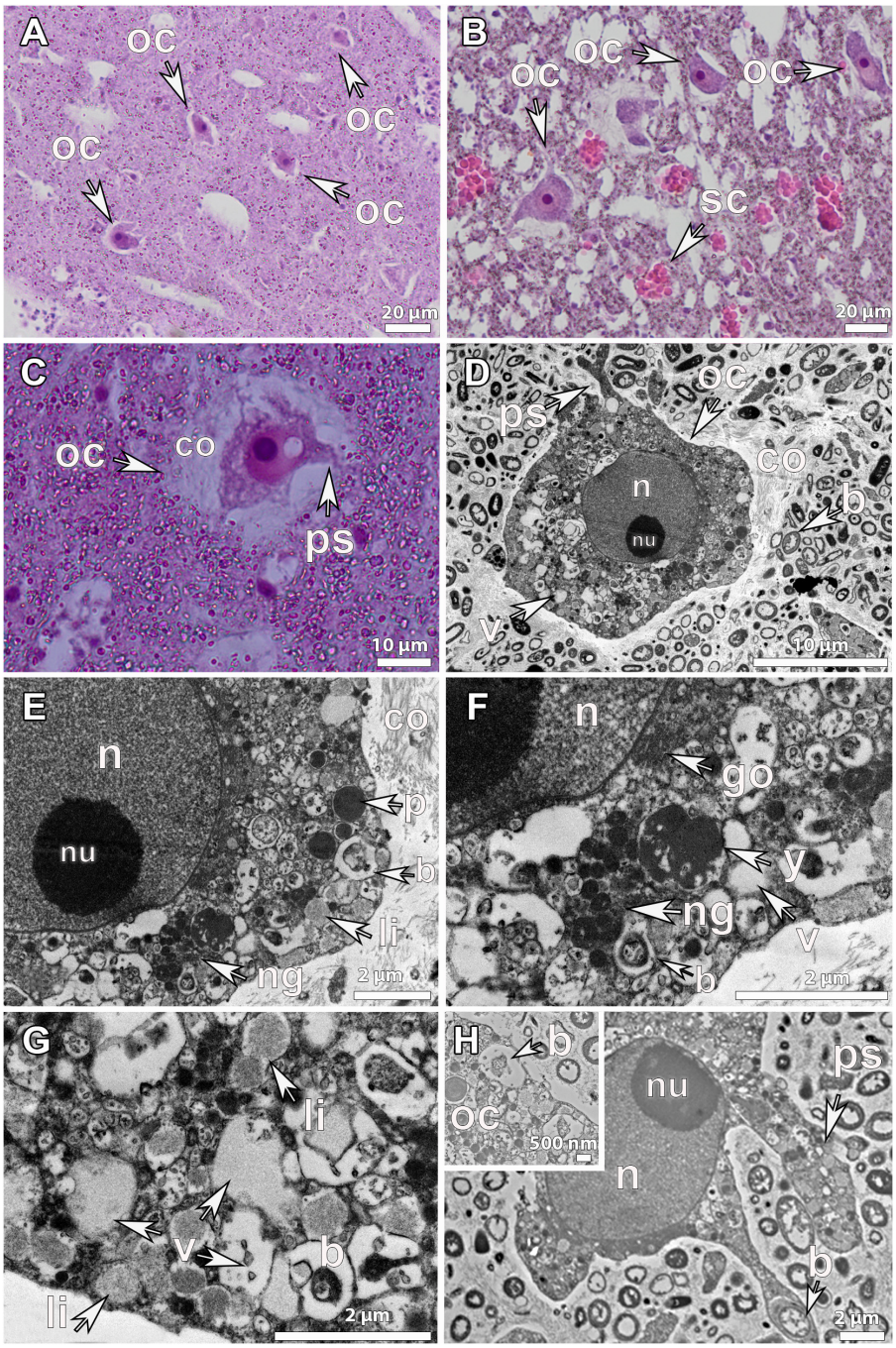

FIGURE 2 | Histological observations and ultrastructure of previtellogenic oocytes from *Geodia* species. **(A)** Previtellogenic oocytes (oc) scattered in the mesohyl of *G. hentscheli* (~12 µm) from the Schulz Bank in June. **(B)** Previtellogenic oocytes (oc) scattered in the mesohyl of *G. barretti* (~23 µm), from Sula reef, end of July. Spherulous cells (sc) (~20 µm) in the mesohyl. **(C)** Previtellogenic oocyte of *G. hentscheli* (oc) (~20 µm) in the mesohyl with pseudopodia (ps) projections and a thin layer of collagen (co) formed around the oocyte. **(D)** Ultrastructure of previtellogenic oocyte of *G. hentscheli,* from the Schulz Bank in June with a nucleus (n) and a well-formed nucleolus (nu) and pseudopodia (ps) in the periphery. Ooplasm full of vesicles (v) and a thin collagen layer (co) around the oocyte. Bacterial symbionts (b) outside the oocyte in the mesohyl. **(E)** Close-up of image 2D, showing the nucleus (n) and the well-formed nucleolus (nu), the nuage granules (ng), small droplets of yolk of protein (p) and lipid origin (li) and one bacterium (b) in the ooplasm of the oocyte. A thin layer of collagen (co) surrounded the oocyte. **(F)** Close-up of image 4E, where the Golgi apparatus (go) around the nucleus, the nuage granules (ng), the lipid yolk droplets (y), the vesicles (v) and the bacteria (b) within the ooplasm were observed. **(G)** Previtellogenic oocyte of *G. hentscheli* from the Schulz Bank in June, with ooplasm full of vesicles (v), some lipid droplets (li), and a bacterium (b) within a vesicle in the ooplasm. **(H)** Ultrastructure of another previtellogenic oocyte of *G. hentscheli*, from the same individual as above with projections of pseudopodia (ps) in the periphery of the oocyte, phagocytizing bacteria (b) from the surrounding mesohyl. Insert: endocytic process with engulfment of symbiotic bacteria (b) from the mesohyl by the oocyte (oc).

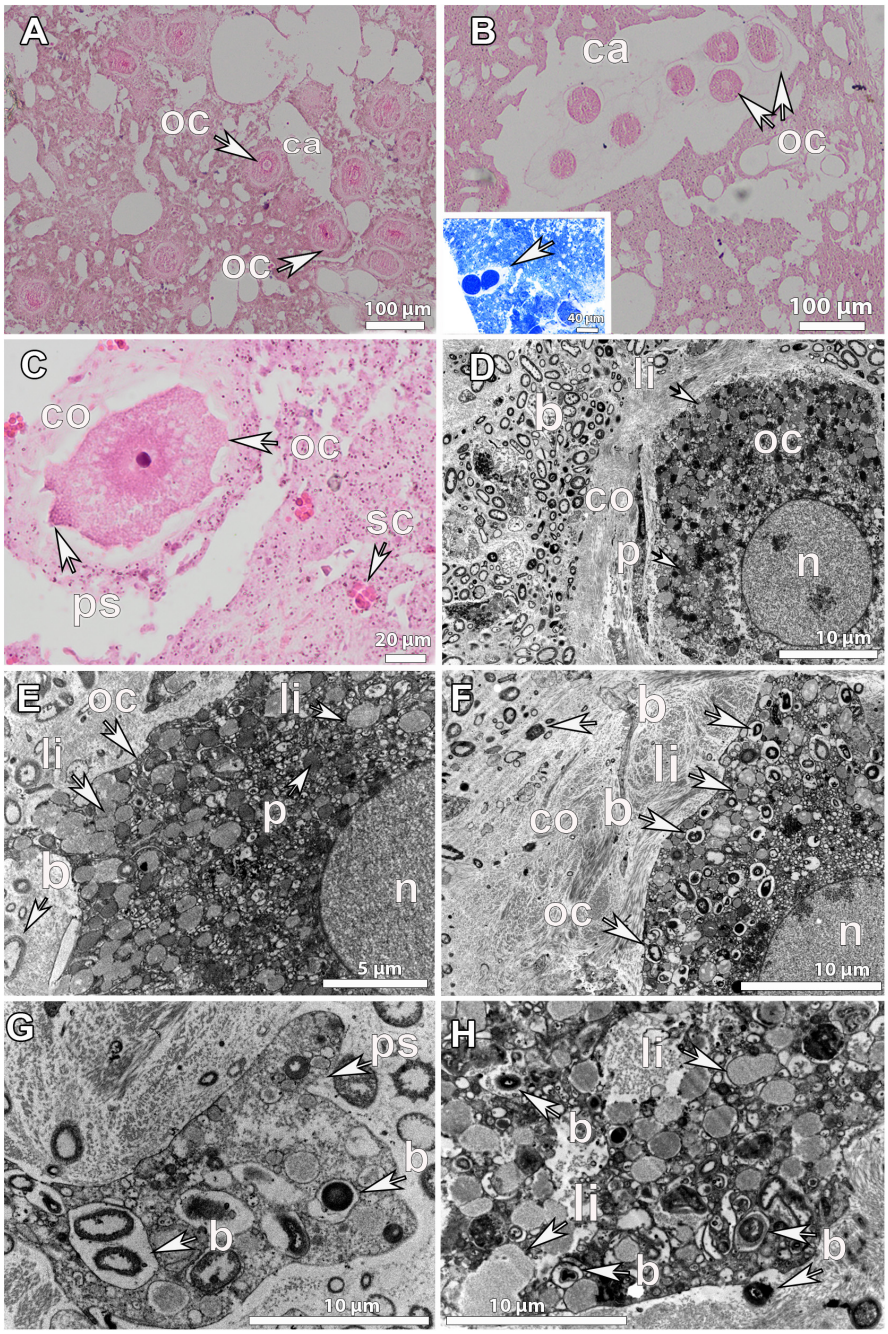

FIGURE 3 | Histological observations and ultrastructure of vitellogenic oocytes from *Geodia* species. **(A)** Vitellogenic oocytes (oc) of *G. atlantica* (~70 µm), from Rosemary Bank Seamount in September, in clusters around the canals (ca). **(B)** Vitellogenic oocytes (oc) of *G. barretti* (50–60 µm), from Rosemary Bank Seamount in September in clusters already released in a canal (ca). Insert: vitellogenic oocytes (oc) of *G. macandrewii* (~40 µm), from the Korsfjord in September, grouped in clusters ready to be released into the canal. **(C)** Vitellogenic oocyte of *G. atlantica* (~80 µm), from the Korsfjord in June, with formed pseudopodia (ps) and a thick collagen layer around it. Spherulous cells (sc) (~20 µm) in the mesohyl. **(D)** Ultrastructure of vitellogenic oocyte of *G. barretti* from Tromsøflaket, western Barents Sea in August, with well-formed lipid yolk droplets (li) and some protein platelets (p). A thick collagen layer (co) surrounding the oocyte separates it from the mesohyl which is full of bacterial symbionts (b), though no bacteria were present within the oocyte. The nucleus (n) has chromatin condensations in two areas but no clear nucleolus. **(E)** Ultrastructure of another vitellogenic oocyte (oc) of *G. barretti* derived from the same individual with well-formed lipid (li) droplets and some protein (p) platelets in the ooplasm. No bacteria were found within the oocyte. The nucleus (n) was without chromatin condensations. **(F)** Vitellogenic oocyte (oc) of *G. macandrewii*, from Sula reef at the end of July, with well-developed lipid droplets (li) and bacterial symbionts (b) within the ooplasm. A thick layer of collagen (co) surrounded the oocyte. **(G)** Vitellogenic oocyte from the same individual of *G. macandrewii* as in 3F, with pseudopodia (ps) phagocytizing the encapsulated bacteria (b) from the mesohyl. **(H)** Close-up of vitellogenic I oocyte of *G. hentscheli*, from Schulz Bank at the beginning of August, with well-developed lipid droplets (li) and bacteria (b) within the ooplasm.

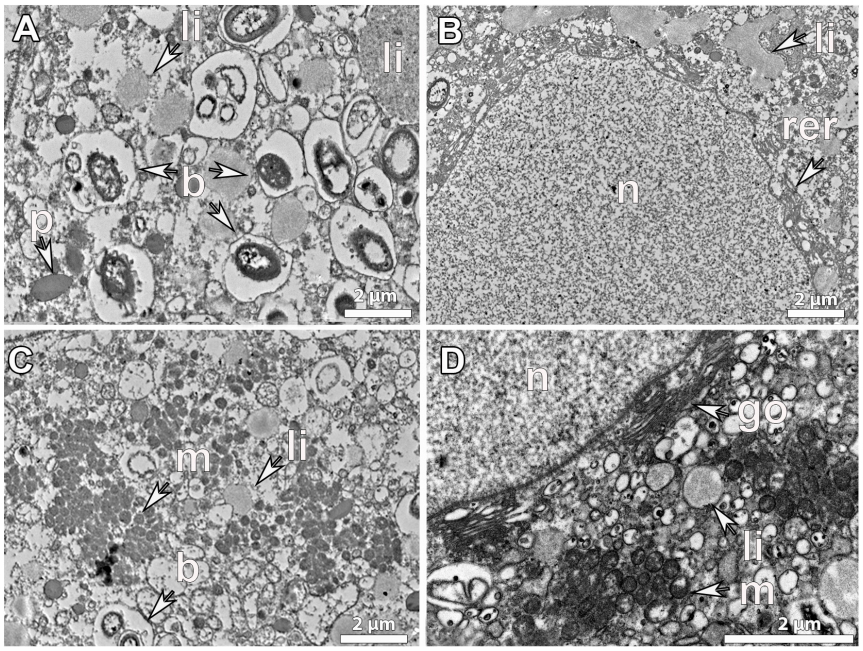

FIGURE 4 | Ultrastructure of mature vitellogenic oocytes. Mature oocyte of *G. atlantica,* from Korsfjord, in September, showing **(A),** a large amount of lipid yolk droplets (li) and bacterial symbionts (b) within its ooplasm; **(B)** a well-developed rough endoplasmic reticulum (rer) close to the nucleus and large lipid droplets probably the result of fusion of several droplets, **(C)** an ooplasm full of mitochondrial clouds (m). **(D)** The structure of nucleus (n), the mitochondria (m) and the Golgi apparatus (go) as well as the formed lipid yolk (li).

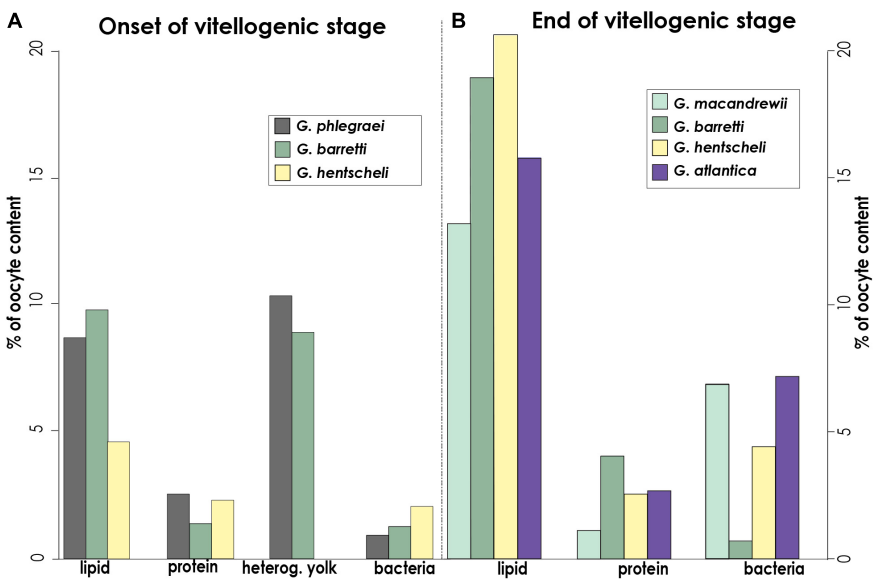

FIGURE 5 | Oocyte content: types of yolk and number of bacteria. Percentage of area occupied by lipid, protein, heterogeneous yolk and bacteria at **(A)**, the onset of the vitellogenenis in oocytes of *G. phlegraei*, *G. barretti*, and *G. hentscheli*, and **(B)**, later vitellogenic stage in oocytes of *G. macandrewii*, *G. barretti*, *G. hentscheli* and *G. atlantica*. No ultrastructural observations were possible for early stages of vitellogenic oocytes of *G. macandrewii* and *G. atlantica* and the mature oocyte of *G. phlegraei*. These measurements were obtained from several oocytes of a selected specimen with oocytes, at the onset of vitellogenesis and another specimen with mature vitellogenic oocytes (*G. barretti* and *G. macandrewii*) or even with the most mature vitellogenic oocytes (*G. atlantica*, *G. hentscheli*) for each species.

the outer parts and the ones in late developmental stages, including spermatids and spermatozoa, toward the lumen of the cyst (**Figure 7A**). Spermatogonia were around 5-10 µm in maximum diameter; they had an amoeboid shape, with a well-developed nucleus and nucleolus (**Figure 7A**), and an internalized flagellum in the cytoplasm (**Figure 7B**). Primary

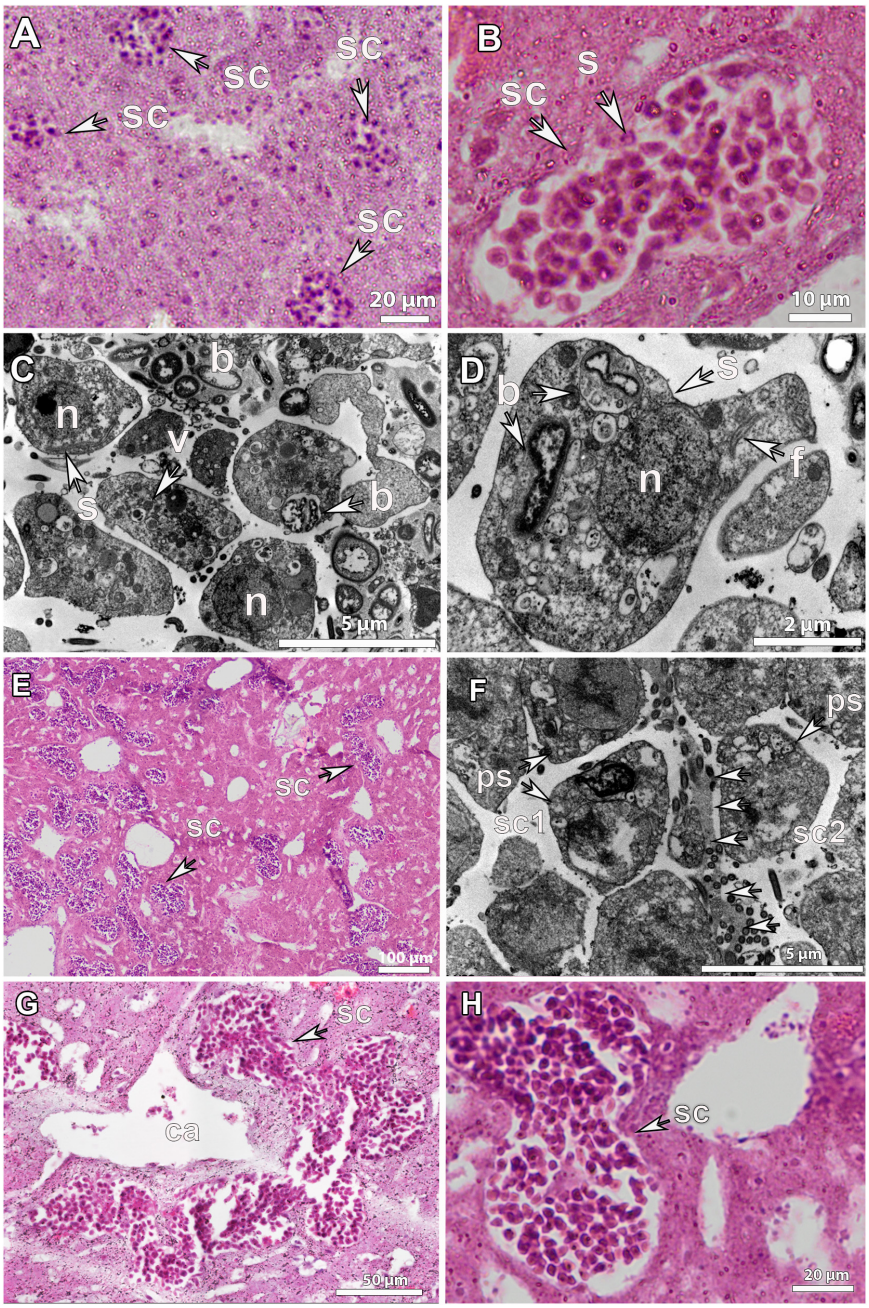

FIGURE 6 | Histological observations and ultrastructure of spermatocytes in *Geodia* spp. **(A)** Spermatic cysts (sc) of early developmental stage (SP_I) scattered in the mesohyl of *G. atlantica,* from Hordaland coast in May. **(B)** SP_I spermatic cyst (sc) in *G. phlegraei* with spermatogonial cells (s) collected in Tromsøflaket, western Barents Sea, in August **(C,D)**, ultrastructure of a SP_I spermatic cyst in *G. hentscheli*, from the Schulz Bank in August. Spermatogonia (s) with a distinct nucleated nucleus (n), vesicles (v), and few bacteria (b). The axonemal structure of the flagellum (f) was in the interior of the spermatogonium (s). **(E)** Spermatic cysts in developmental stage II (SP_II) of *G. phlegraei*, from Tromsøflaket, western Barents Sea in August, accumulated close to the canals. **(F)** Ultrastructure of SP_II spermatic cysts of *G. phlegraei* with primary spermatocytes (ps) in the periphery and thin mesohyl layer (arrows) between the two spermatic cysts (sc1 and sc2). **(G)** Spermatic cysts fused into one large spermatic cyst after mesohyl layer disintegration in *G. phlegraei* and were gathered around the canals (ca). **(H)** Close-up of a SP_II spermatic cyst of *G. phlegraei* with several spermatic cells, smaller than spermatogonial cells in size, compared to those in **Figure 6B**.

spermatocytes were frequently observed dividing, they had a slightly smaller size (∼4-6 µm), no nucleolus, and showed chromatin condensations in the nucleus (**Figures 7C,D**), as well as synaptonemal complexes (**Figures 7D,E**). Secondary spermatocytes had more compacted chromatin and a smaller size (∼4 µm) than the previous developmental stage (**Figures 7E,F**). The internalized flagellum already disappeared at the stage of primary spermatocyte, and in the secondary spermatocyte,

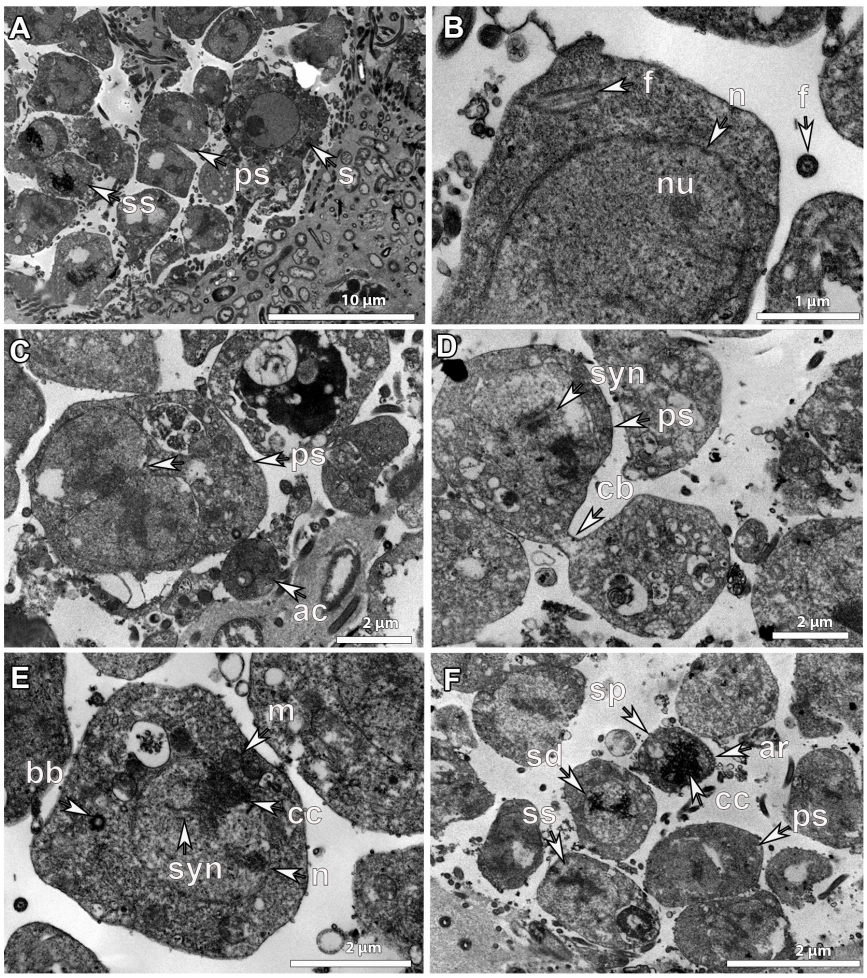

FIGURE 7 | Ultrastructure of developmental stage_II (SP_II) spermatic cysts. SP_II spermatic cysts of *G. phlegraei* from Tromsøflaket, western Barents Sea in August showing **(A),** asynchronous development of sperm cells within the spermatic cyst with spermatogonia (s) in the outer part of the spermatic cyst, primary spermatocytes (ps) and secondary spermatocytes (ss) toward the inner part with increasing chromatin compactions. **(B)** Details of the structure of a spermatogonium with a nucleated (nu) nucleus (n) and the internalized axonemal structure of the flagellum (f). **(C)** Dividing primary spermatocyte with chromatin compaction after nuclear division. In the periphery of the spermatic cyst, ameboid-like cells (ac) are present. **(D)** Dividing primary spermatocytes with a cytoplasmic bridge (cb) before cytokinesis is completed and the synaptonemal complexes (syn) in the nucleus, **(E)** a secondary spermatocyte within a spermatic cyst, with chromatin compaction (cc) within the nucleus (n), synaptonemal complexes (syn), mitochondria (m), and the basal body (bb) before the new flagellum formation. **(F)** SP_II spermatic cyst with primary spermatocytes (ps), secondary spermatocytes (ss), spermatids (sd) and a potential spermatozoon (sp). Chromatin compaction (cc) and the acrosome (ar) of the cone-shaped late spermatid/early spermatozoon.

the basal body was observed indicating that a new flagellum is being formed during late spermatogenesis in *Geodia* spp. (**Figure 7E**). Then, spermatids had an even higher degree of chromatin compaction and a smaller size (∼2 μm) (**Figure 7F**). Finally, although we did not manage to obtain a clear picture of a spermatozoon with a flagellum, a potential spermatozoon (or a mature spermatid) was observed with several acrosomal vesicles in the apical part of the conical cell body (**Figure 7F**). The nucleus at its majority was composed by compacted chromatin and the mitochondria in the cytoplasm could not be observed, probably because of the angle of the image. Putative spermatozoa had the smallest size (∼1.5 μm) within the spermatic cyst, suggesting that this might be indeed the mature sperm cell (**Figure 7F**). Finally, we did not observe bacteria within sperm cells at later developmental stages.

Density and Fecundity Estimations

Density of Oocytes and Female Fecundity (Number of Oocytes Produced per Individual)

The number of oocytes per square millimeter of sponge tissue varied among individuals of the same species and among species (**Figure 8**). In average, *Geodia* spp. produced 7.2 ± 3.6 oocytes/mm^2 of sponge tissue. However, some extreme cases were also identified. For instance, in two specimens of *G. hentscheli* with oocytes in PV stage, one had on average 37 oocytes/mm^2 and the other 1.7 oocytes/mm^2 (**Figure 8**).

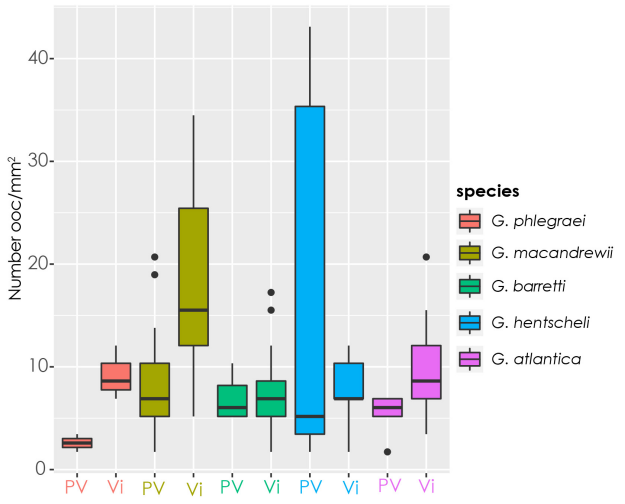

FIGURE 8 | Female gamete density. Number of oocytes per square millimeter of sponge tissue in specimens with previtellogenic (PV) and vitellogenic (Vi) oocytes for each species. Specimens from all the sampling points for each species were included.

Additionally, a specimen of *G. macandrewii* with Vi oocytes, had the second highest value, 27 oocytes/mm^2 on average (**Figure 8**).

According to the calculations based on the modified Elvin's formula and the volume of each species, *G. macandrewii* (which had the second largest body volume among the studied *Geodia* species) contained the maximum number of oocytes within its body (∼116 million oocytes), followed by *G. atlantica* which was estimated to contain ∼78 million oocytes per individual. *G. barretti* and *G. phlegraei* were estimated to potentially release ∼30 and ∼17 million oocytes respectively, and finally, *G. hentscheli* was expected to produce only ∼4 million oocytes per individual (**Table 2**).

Male Fecundity (Area of Tissue Occupied by Spermatic Cysts per Individual)

In *G. phlegraei*, the SP_II spermatic cysts occupied at least 12% of the total area of the sponge, and for *G. atlantica* only 7% of the total area (**Table 2**). For the other three species, *G. macandrewii* and *G. hentscheli* had a similar investment of spermatic cyst production (∼3%) and *G. barretti* had the lowest investment of all species (1.5%) (**Table 2**).

Reproductive Season of *Geodia* Species

From May to September, several individuals from the five *Geodia* spp. were producing gametes (**Figure 9A**, **Table 1**, and **Supplementary Table S1**). An exception was *G. macandrewii*: even though it was reproductive in September (in Svalbard and western Norway), none of the eight specimens collected during August (Tromsøflaket, western Barents Sea) was reproductive (**Figure 9A**, **Table 1**, and **Supplementary Table S1**). For *G. phlegraei,* only one specimen was collected in September (in Svalbard) and it was not engaged in reproduction (**Table 1**). For *G. atlantica,* no samples were collected in August, but otherwise, this species was reproductive throughout the rest of the sampling months and sampling points (**Figure 9A**, **Table 1**, and **Supplementary Table S1**). Finally, some *G. hentscheli* specimens collected in late June and August in Schulz Bank were reproductive (**Figure 9A**, **Table 1**, and **Supplementary Table S1**). Based on the maturation level of the oocytes observed in specimens the specific months and studied areas, the approximate period of spawning for all the *Geodia* spp. was estimated from May to November, depending on the area considered (**Figure 9B**).

In detail, in May and June, almost all the studied species contained reproductive features in early stages of gametogenesis and the size and maturation of gametes increased over the months (**Figure 10** and **Supplementary Figures S3, S4**). During July and August, oocytes of most species were Vi (**Figure 10** and **Supplementary Figure S3**). An exception was *G. barretti*, in which one reproductive individual had already Vi oocytes (56.1 ± 9 μm) in May (in Hordaland coast) when most other individuals had PV oocytes, and another individual had PV oocytes (23.3 ± 6.4 μm) in July (in Sula reef) when all others had Vi oocytes. Other exceptions were an individual of *G. phlegraei* (from Tromsøflaket, western Barents Sea) and another one of *G. hentscheli* (from Schulz Bank) which were also in early developmental stages in August (**Figure 10** and **Supplementary Figure S3**), and surprisingly, one individual of *G. phlegraei* with Vi oocytes obtained in July in Sula reef

TABLE 2 | Estimation of number of oocytes and the area occupied by spermatic cysts in the whole individual, extrapolated by calculations of a theoretical volume and area for each species.

	Theoretical volume of each species (cm^3)	Oocyte diameter (μm) used for fecundity rates	Number of oocytes produced by sponge (million)	Theoretical area of each species (cm^2)	Area occupied by spermatic cysts by sponge (cm^2)	% of area occupied by spermatic cysts
G. phlegraei	1767	67	16	707	84	12
G. macandrewii	4189	43	115	1256	36	3
G. barretti	2153	36	27	806	11	1
G. hentscheli	524	30	4	314	10	3
G. atlantica	8419	95	78	5841	444	8

The calculations were based on the theoretical shape and the mean diameter of each species (based on published dimensions, personal communication with (HTR) and personal observations). The calculations of the volume and area of the sponge per species and the diameter of oocytes used are shown in ***Supplementary Table S2****.*

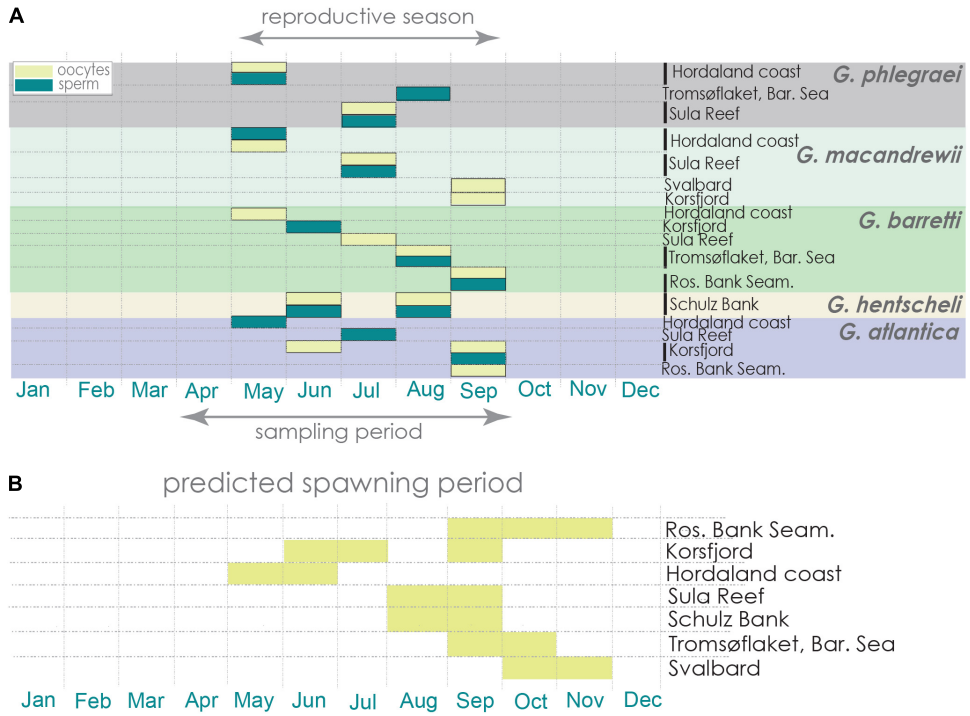

FIGURE 9 | Reproductive period and estimated spawning period. **(A)** Reproductive period of each *Geodia* species across the different locations and dates of sampling. **(B)** Estimation of spawning events for *Geodia* spp. in each sampling area are represented in yellow, based on the maturation level of their oocytes at the time the specimens were collected.

(**Figure 10** and **Supplementary Figure S3**). For *G. macandrewii*, *G. barretti* and *G. atlantica*, their largest Vi oocytes (in the final Vi stage) were observed in September (**Figure 10** and **Supplementary Figure S3**). However, in September in addition to females with mature (Vi) oocytes, there were also females of *G. macandrewii* and *G. atlantica* with PV oocytes in Svalbard (not shown in the graph) and Rosemary Bank Seamount respectively (**Figure 10** and **Supplementary Figure S3**). Regarding the spermatocytes, there was a general tendency of enlargement over the period from May to September (**Supplementary Figures S3, S4**) in all species.

Ratio of Reproductive Individuals (Males/Females) at Population Level

During the reproductive months, a high percentage (65-90%) of *G. phlegraei* individuals participated in reproduction and most of them were male with a sex ratio of 3:1 (**Figure 11A** and **Table 1**). A high percentage (65-75%) of the population of *G. macandrewii* was also engaged in reproduction but with either females predominating (1:2) or with equal proportions of males and females (1:1) (**Figure 11B** and **Table 1**). Regarding *G. barretti* (**Figure 11C** and **Table 1**), although a low percentage of individuals were producing gametes (11.6-20%) in May, June, and August, 80% of the individuals were reproductive in September in the Rosemary Bank, Seamount, while interestingly in the Korsfjord, western Norway, none of the seven individuals were reproducing. For *G. barretti*, the number of male and female individuals was equal (1:1). On the same note, for *G. atlantica*, 30% of the individuals collected were reproducing in May – June. In September, in contrast to *G. barretti*, the latter species had 40% of individuals engaged in reproduction in the Rosemary Bank, Seamount (Rockall Trough, 1034 m) and almost 80% of the individuals reproducing in the Korsfjord (western Norway, continental shelf). The sex ratio for *G. atlantica* was 1:1 (**Figure 11D** and **Table 1**). Finally, *G. hentscheli* recruited between 60 and 80% of its individuals for reproduction in June and August respectively, with more females than males, approximately in a ratio of 1:3 (**Figure 11E** and **Table 1**).

DISCUSSION

Morphological Characteristics of Gametes

The *Geodia* species studied here were all gonochoristic and oviparous, as observed in previous studies on the Geodiidae family (Liaci and Sciscioli, 1969, 1970; Mercurio et al., 2007; Spetland et al., 2007), which belongs to the Astrophorina suborder, one of the three suborders currently recognized in the Tetractinellida order (Astrophorina, Spirophorina and Thoosina). *Thenea abyssorum*, another deep-sea astrophorin (family Theneidae) has also been shown to be gonochoristic and oviparous (Witte, 1996), suggesting that this could be the

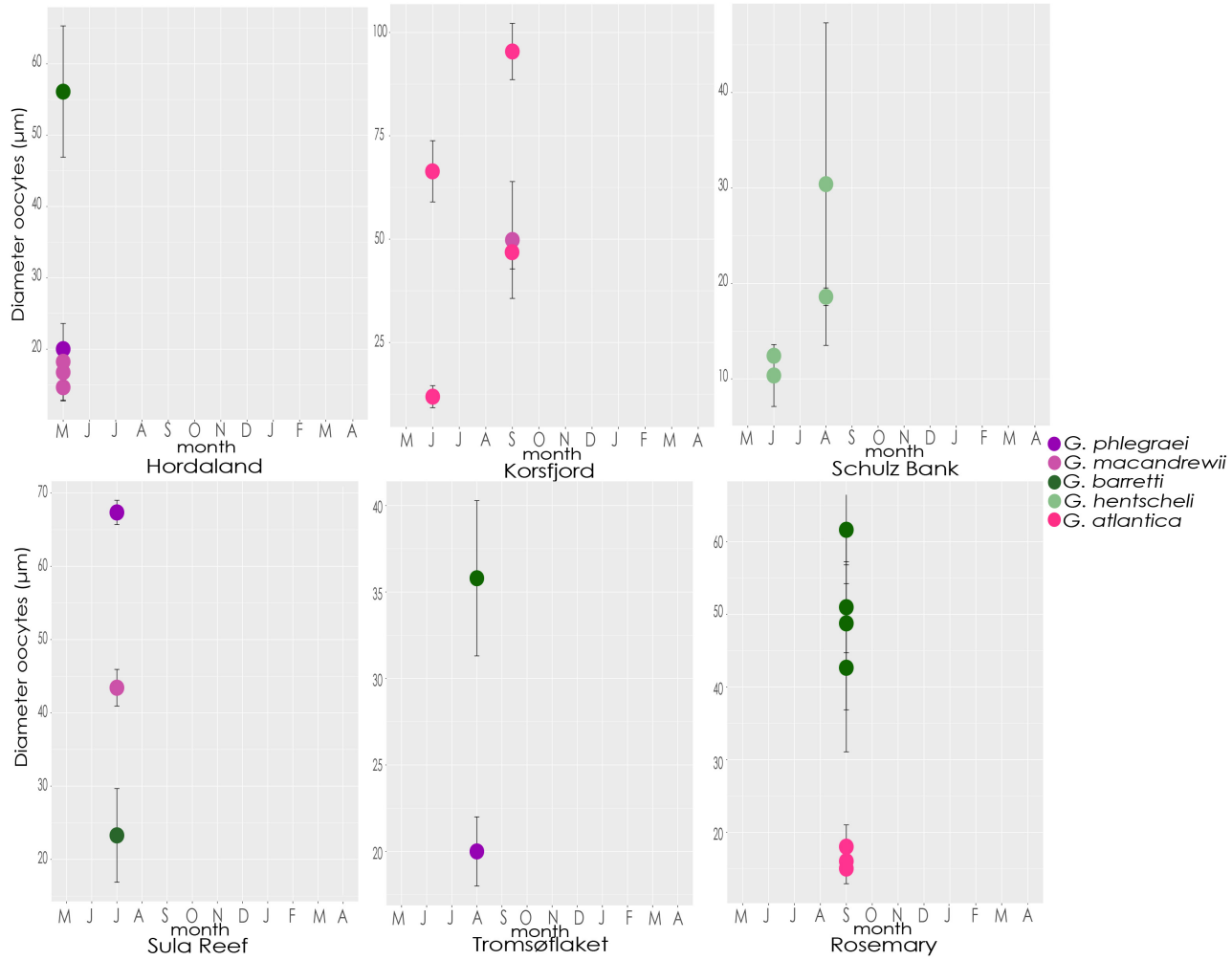

FIGURE 10 | Size of oocytes. Average diameter and standard deviation of oocytes from each specimen of each species collected throughout the different months and locations.

rule for the whole suborder. In the suborder Spirophorina, about half of the Tetillidae studied are also oviparous and gonochoristic (Liaci et al., 1976; Watanabe, 1978; Lepore et al., 2000) while another half, e.g., *Tetilla polyura* (Topsent, 1904) and *Tetilla longipilis* (Topsent, 1904), are viviparous (Topsent, 1904; P. Cárdenas, unpublished data). The suborder Thoosina is entirely hermaphroditic and viviparous (Bautista-Guerrero et al., 2010; Carballo et al., 2018). With the current knowledge of the Tetractinellida phylogenetic tree, and based on previous analyses of ancestral character reconstruction for demosponges (Riesgo et al., 2014), we hypothesize an ancestral gonochoristic and oviparous condition for Tetractinellida which later shifted to hermaphroditism/viviparism in Thoosina, although data are missing on the reproduction of one entire clade of Tetractinellida including the Stupendidae and the Scleritodermidae/Siphonidiidae/Azoricidae (Carballo et al., 2018). Besides the phylogenetic constraints, gonochorism and oviparity seem to be predominant in deep-sea invertebrates as more than 80% of deep-sea corals are also broadcast spawners (oviparous) and gonochoristic, while the most common pattern in shallow-water corals is hermaphroditism and oviparity (Brooke and Young, 2003; Burgess and Babcock, 2005; Waller, 2005; Harrison, 2011; Pires et al., 2014). Whether there is an ecological advantage for gamete release in deep-sea areas, in terms of lower predation over eggs is still unknown, but it would be necessary to investigate it to understand the ecology of deep-sea organisms.

Oogenesis in the studied *Geodia* spp. had very similar characteristics to that described previously for several astrophorins (*Geodia conchilega*, *G. cydonium*, *G. barretti, Stelletta grubii*, *Erylus discophorus*, *T. abyssorum*), including the formation of a collagen layer outside the oocyte, vertical transmission of bacterial symbionts acquired by phagocytosis, absence of nurse cells and autosynthesis of nutrients by the oocyte itself via the Golgi and endoplasmic reticulum apparatus (Liaci and Sciscioli, 1969; Sciscioli et al., 1989, 1991, 1994; Witte, 1996; Mercurio et al., 2007; Spetland et al., 2007). Oocytes in all *Geodia* spp. seemed to derive from archaeocytes, which at

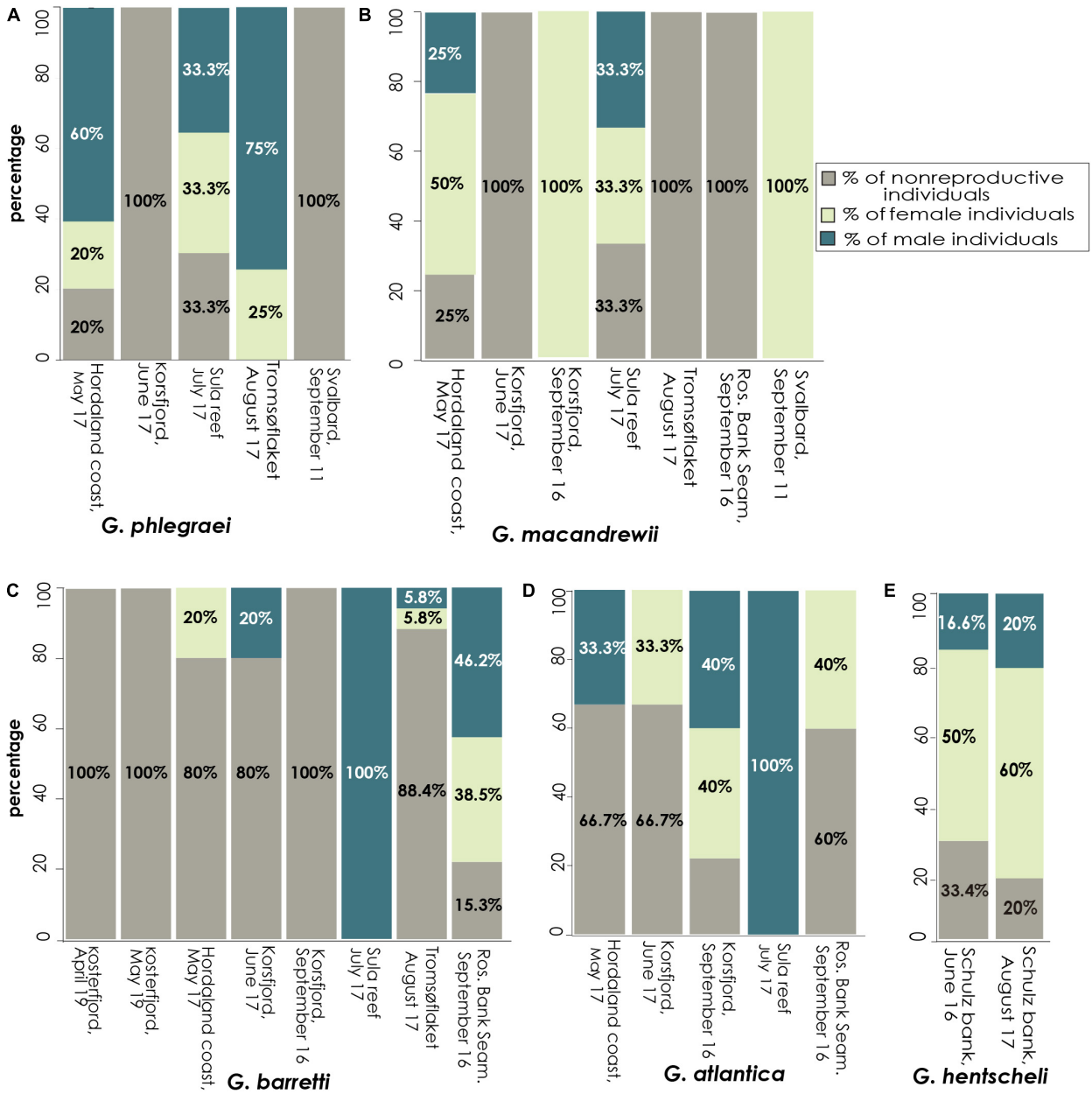

FIGURE 11 | Investment in reproduction at the population level. Percentage of specimens with female and male gametes found per population (separated by location and time of collection) for each species. Data are provided for **(A)** *G. phlegraei,* **(B)** *G. macandrewii,* **(C)** *G. barretti,* **(D)** *G. atlantica,* and **(E),** *G. hentscheli*.

the beginning of the gametogenic cycle have a very similar shape and size (Liaci and Sciscioli, 1969; Sciscioli et al., 1994). On the other hand, spermatic cysts in all the studied species were clearly derived from choanocyte chambers, as previously suggested for other Geodiidae (Liaci and Sciscioli, 1969; Mercurio et al., 2007) but questioned for *G. barretti* (Spetland et al., 2007). These results clearly show a choanocyte origin of spermatic cysts, even for *G. barretti*. Spetland et al. (2007) suggested an alternative origin of the spermatic cysts based on the larger size of cysts than chambers, probably because they did not consider the fusion of several cysts. In this study, there is evidence that the early cysts did show a similar size and morphology to chambers (i.e., no collagen or cellular envelope), and fusion events were observed in later stages across all species.

Reproductive Strategy and Sex Ratio: Commonalities and Differences

Oocytes of deep-sea *Geodia* spp. from this study and of *G. barretti* from Spetland et al. (2007), have overall larger sizes (individuals with oocytes measuring more than 45 μm in diameter were

detected in all species), with some species reaching 100 μm when fully grown, than mature oocytes of the shallower species, *G. cydonium*, that measure 30–40 μm (Sciscioli et al., 1994; Mercurio et al., 2007). Similarly, specimens of the family *Tetillidae* from deeper waters had 30% larger mature female gametes (∼74 μm) than shallow-water specimens (∼57 μm) (Meroz-Fine et al., 2005). The increasing size of eggs with depth had also been observed in deep-sea crustaceans and echinoderms that have larger lecithotrophic eggs than shallow water species (Mauchline, 1973; Corey, 1981; Cameron et al., 1988), indicating a possible general strategy for several marine invertebrates (Thorson, 1950). The size of mature oocytes in marine organisms with lecithotrophic embryonic and larval stages, is indicative of the pelagic larval duration (PLD) as larger oocytes are expected to accumulate a larger content of nutrients. Larger egg size can have profound ecological implications in marine invertebrates, such as longer planktonic phases and PLD and advantages in external fertilization given the larger targets for sperm (Marshall and Keough, 2007).

The planktonic phase duration in lecithotrophic propagules is dictated not only by the amount but also the type of yolk. In their oocytes, all the *Geodia* spp. had far more lipid than protein yolk. Even though lipid yolk in cold-water sponges is not always the rule (Koutsouveli et al., 2018; Koutsouveli et al., unpublished data), it is usually predominant over protein yolk in dispersal propagules of some sponge species from cold environments, while being 30% or less of the nutrient reserves in temperate and tropical species (Riesgo et al., 2015). For example, *Stelletta grubii*, an astrophorin species from temperate shallow waters, produces more protein than lipid yolk (Sciscioli et al., 1991). Furthermore, the temperate species *G. cydonium* also seems to have higher amounts of protein yolk accumulated in their oocytes (Sciscioli et al., 1994) than the *Geodia* spp. of this study. The predominance of fat provides more energy than protein and is metabolized faster, which is important for quick developmental changes in environments that are poor in nutrients, like the deep sea (Giese, 1966; Clarke, 1980). In addition, lipids also provide high buoyancy to the eggs which allows them to float in the water column (Clarke, 1980). The high content of lipids in the released oocytes of the deep-sea *Geodia* spp. could suggest an adaptation to a longer stay in the water column than the propagules of their temperate counterparts, until fertilization and ultimately embryogenesis take place, allowing longer dispersion distances and ensuring population connectivity over larger areas.

The vertical transmission of the bacterial symbionts in *Geodia* spp. was observed in oocytes of late developmental stages. This phenomenon has also been described in *G. cydonium*, as also in other astrophorid species (i.e., *E. discophorus* and *S. grubii*) (Sciscioli et al., 1989, 1991), in which bacteria were acquired by phagocytosis from the mesohyl, and were not digested but rather protected in vesicles within the oocytes, where they divided. As thus, these bacteria are true symbionts and are not consumed for nutritional needs at least during gametogenesis. Vacelet (1975) has suggested that these bacteria can serve as nutrients at a later embryonic stage. A recent study, not yet peer-reviewed, has showed that bacterial symbionts of *Geodia* spp. (including *G. barretti*, *G. hentscheli*, and *G. atlantica*), provide the host with precursor lipid building blocks, contributing to the synthesis of sponge unsaturated long-chain fatty acids (De Kluijver et al., 2020). So, the high content in lipid yolk might be related to the presence of high microbial abundance in these species, and it might be the case that by-products of bacterial symbionts within the oocytes contribute to the "autosynthetic" activity of lipid formation. On the other hand, in spermatogenesis, some bacteria were engulfed by early spermatogonia but disappeared in later spermatogenic stages. So, these sparse phagocytized bacteria are more likely to be used directly as a source of energy. This is a relatively novel observation in sponges, previously found only in the sperm of *Spongia officinalis* (Gaino et al., 1984) and *Petrosia ficiformis* (Maldonado and Riesgo, 2009), and it clearly points to choanocytes as the cells producing sperm.

Although the major reproductive patterns (i.e., oviparity and gonochorism) of the deep-sea *Geodia* spp. are clearly constrained by phylogeny (Riesgo et al., 2014), being the strategy at the genus, and possibly at suborder levels (e.g., Liaci and Sciscioli, 1969, 1970; Witte, 1996; Mercurio et al., 2007; Spetland et al., 2007), there is plasticity in some of the reproductive traits adopted by each species in order to cope with the energetic demands required for gametogenesis in these relatively oligotrophic habitats (Witte, 1996). First of all, slight variations were observed in seasonality among the species. For instance, individuals of *G. barretti* with mature female gametes and those of *G. atlantica* with premature female gametes were found at the same location and year, e.g., in Rosemary Bank Seamount in September 2016. This phenomenon has also been observed in Mediterranean species sharing the same habitat, which have to cope with the same nutrient regimes, staggering in time their resource allocation (Riesgo and Maldonado, 2008; Pérez-Porro et al., 2012; De Caralt et al., 2018). The different timing in gametogenesis and spawning among species could also be a strategy for avoiding cross-fertilization between different species and therefore hybridization. Furthermore, differences in terms of reproductive investment at individual and population levels were observed. Specifically, *G. barretti* seems to be the species with least investment in reproduction as only a small fraction of the population produces gametes and in relatively low numbers compared to the other studied species. This potentially could lead to a fragile situation of *G. barretti* if the environmental conditions or the populations themselves are perturbed. Interestingly, the gametes of *G. barretti* and *G. hentscheli* have smaller sizes compared to *G. phlegraei* or *G. atlantica* (**Figure 10** and **Supplementary Figures S2, S3**) but they contain a higher amount of yolk (even though not the most mature vitellogenic oocytes were measured for *G. barretti*) (**Figure 5**), which can give them all the necessary reserves and buoyancy for longer drifting and thus ensure a higher fertilization success, expecting even higher yolk content in more mature oocytes of *G. barretti*. On the other hand, *G. atlantica*, with relatively lower amounts of yolk (**Figure 5**) will have shorter survival rate and lower buoyancy, so shorter drifting of its oocytes. However, *G. atlantica* produced more oocytes than the rest of species (three times more oocytes per individual, compared to *G. barretti*) (**Figure 8** and **Table 2**), and a high percentage of the population is reproducing each year (**Figure 11D**), which increases the chances for successful

reproduction. These species-specific reproductive traits can be correlated with observations of a most continuous presence of *G. barretti* compared to the patchier distribution of *G. atlantica* for instance, in Northern Norwegian continental shelf, while both showed a high abundance (Kutti et al., 2013). Although phylogenetically distantly related to *G. atlantica* (Cárdenas et al., 2010), *G. macandrewii* seems to follow a fairly similar strategy. Finally, in *G. phlegraei,* a comparatively higher percentage of the population participate in reproduction (**Figure 11A**), producing fewer oocytes (**Figure 8** and **Table 2**) but highly enriched with nutrients (**Figure 5**).

Overall, oocyte densities in *Geodia* spp. (N of oocytes/mm^2) were comparable or even higher to those reported on other oviparous sponges from temperate and tropical habitats. Riesgo and Maldonado (2008) found that the three oviparous and gonochoristic Mediterranean sponge species, *Cymbaxinella damicornis* (called *Axinella damicornis* in the publication), *Raspaciona aculeata,* and *Chondrosia reniformis* reached a maximum of 3–7 oocytes/mm^2, while the coral reef sponge species *Cliona vermifera* had a maximum density of 3.5 oocytes/mm^2 and 60–85% of its population participated in reproduction (Bautista-Guerrero et al., 2014). Two other Mediterranean oviparous, hermaphrodite *Cliona* spp., *C. viridis* and *C. celata*, showed a density of ∼10 oocytes/mm^2 and a 70–90% of the population to participate in reproduction (Piscitelli et al., 2011). An exception was specimens of the family Tetillidae (most possibly the species *Levantiniella levantinensis*) which produced up to 155 oocytes/mm^2 in some Mediterranean deeper habitats (Meroz-Fine et al., 2005). In the *Geodia* spp. of this study, a mean of 10 oocytes/mm^2 was observed across species (**Figure 8**), with some specimens having a much higher number than the average (e.g., 38 ± 4 oocytes/mm^2 in PV individual of *G. hentscheli* and 27 ± 6 oocytes/mm^2 in Vi individual of *G. macandrewii*). In addition, a high percentage of their population participated in reproduction, as also mentioned for *G. cydonium* (Mercurio et al., 2007). So, despite the scarcity of nutrients in these habitats throughout the year, these species seemed to have a high reproductive effort, that together with their interplay with microbial symbionts (Radax et al., 2012; De Kluijver et al., 2020) could explain the dense aggregations of these species in the sponge grounds. This pattern contrasts to the theory that deep-sea benthos has usually a low reproductive effort due to unfavorable abiotic conditions, such as lack of nutrients (e.g., Thorson, 1950).

Even though, a relatively low number of specimens for each species was available, a dominance of females over male individuals (or equal ratios) was still observed in most species of the study, thus confirming previous studies on *Geodia* spp. (Liaci and Sciscioli, 1969; Mercurio et al., 2007; Spetland et al., 2007), as well as in most demosponges (e.g., Wapstra and van Soest, 1987; Tanaka-Ichihara and Watanabe, 1990; Witte et al., 1994, 1996; Corriero et al., 1996, 1998; Lepore et al., 2000; Meroz-Fine et al., 2005; Maldonado and Riesgo, 2008). *G. phlegraei* was the only species where males were three times the females. Also, there was a lower number of oocytes produced by female individuals compared to sperm generation by male individuals (e.g., in *G. phlegraei* ∼16 million oocytes/sponge and ∼30 billion spermatozoa/sponge respectively), which is possibly related to the higher energetic demands of oogenesis. Therefore, more female individuals should be engaged in each reproductive cycle in order to increase the percentage of oocytes released in the water column and a successful fertilization. Male dominance is a rare characteristic for sponges (Simpson, 1984; Sarà, 1993) but the energy requirements and allocation might be behind such a pattern: as the production of yolky female gametes requires higher energetic demands, this implies that the more individuals are involved in female gamete production, the more individuals of a population will be vulnerable at the end of the reproductive cycle due to lack of reserves, and so the whole habitat can be more vulnerable in case of disturbance. An indication that males require less energy to produce their gametes was shown in *Oscarella lobularis,* in which the male to female ratio increased massively (10 male:1 female) during food limitation (Ereskovsky et al., 2013). However, the feature of *G. phlegraei* cannot be directly correlated with abiotic conditions, and further sampling is needed to derive any conclusion.

Seasonality and Adaptations of the Reproductive Strategy to the Deep Sea

Organisms in most deep-sea environments normally face relatively constant abiotic conditions with some very predictable changes along the year, such as nutrient blooms after a seasonal primary production (Southwood, 1977; Clarke, 1980). In these habitats, the phenomenon of seasonality in reproduction is strong, mostly happening during the summer months, after the spring bloom, when the energy reserves have increased due to increased nutrient uptake (George and Menzies, 1967; Clarke, 1980). In general, astrophorin demosponges from the northern hemisphere, both deep-sea (Witte, 1996; Spetland et al., 2007) and shallow ones (Mercurio et al., 2007), reproduce annually, during summer months. In this study, the five boreo-arctic *Geodia* spp. were also reproducing during the summer months (May-September). However, this pattern presented some deviations in the different locations of the study. For example, reproductive specimens of *G. barretti* at Korsfjord (western Norway, 100-400 m) were barely found in June and September, an observation that comes in accordance with Spetland et al. (2007), who detected an annual cycle of *G. barretti* shifted to earlier months of the year (February – June) at this same location. However, reproductive features of *G. barretti* were found at Rosemary Bank Seamount (Rockall Through, 1304 m) in September. On the other hand, Spetland et al. (2007) also found that populations of *G. barretti* in Kosterfjord (Sweden, 80 – 200 m) had two annual cycles, one in February – June (estimated spawning time, May/June) and the other in July - October (estimated spawning time, October). Interestingly, no reproductive activity in specimens collected either in April or May in the same location was observed.

Differences in the reproductive cycle of a species between two locations or even between years in the same location can be explained by variations in environmental factors (Witte et al., 1994; Meroz-Fine et al., 2005). Similar observations have been reported for the deep-sea corals *Primnoa resedaeformis* (Gunnerus, 1763) *and Paramuricea placomus* (Linnaeus, 1758) in

the Gulf of Maine (Fountain et al., 2019), in which populations from different areas showed variations in timing and even in the reproductive potential (e.g., max. size of the gametes, reproductive individuals/population, fecundity ranges). Likewise, populations of the cold-water coral *Lophelia pertusa* (Linnaeus, 1758) in the NE Atlantic and Trondheimfjord populations had variations in timing, maximum size of oocytes, and duration of their reproductive cycle (Waller and Tyler, 2005; Brooke and Järnegren, 2013). Brooke and Järnegren (2013) also attributed those differences likely to regional variations in the food supply. Mercier et al. (2011) found an indirect connection between the increased activity in the spawning of the gametes in six deep-sea species of echinoderms and the new/full moons, suggesting that lunar cycles affect the cyclic currents and the deposition of particular matter to the seafloor, which is then the main factor influencing the reproduction in the deep sea. Nutrient supply determines many aspects of reproduction in deep-sea invertebrates: from initiation of gametogenesis to vitellogenesis and time of spawning, depending on the reproductive strategy of the species (Tyler et al., 1992, 1993; Gooday, 2002; Young, 2003). For instance, deep-sea species tend to generate large eggs and invest a lot of energy on yolk formation of their eggs (even more if they have lecithotrophic larvae), and the stage of maturation/vitellogenesis is synchronized with periods of high food delivery (Eckelbarger and Watling, 1995).

The reproductive cycle of deep-sea sponges, including astrophorins and more specifically *Geodia* spp., was also suggested to be triggered by primary production (Witte, 1996; Spetland et al., 2007). In this analysis, specimens from locations at different depths and geophysical conditions were studied. In the Schulz Bank, only one plankton bloom is observed per year with the peak of carbon flux (input of organic matter) during June (U. Hanz, personal communication). Similarly in the Barents Sea, the peak of particulate organic carbon flux in the seafloor occurs during June – July (von Bodungen et al., 1995), which coincides with the maturation phase of gametes both in species of this study and in another deep-sea astrophorins (Witte, 1996). In Norwegian fjords though, there is an important spring bloom (March – April) and a smaller autumn bloom (August – September) (Wassmann, 1991; Wassmann et al., 1996), and the latter also seems to be synchronized with oocyte maturation for at least some of the studied species here. Deep-sea corals also synchronize their gametogenesis with the influx of nutrients to the seafloor as they take advantage of the spring/summer blooms to initiate their gametogenesis and then they spawn at the beginning of the following year (Maier et al., 2020). In the northern part of the Kosterfjord, very close to the sampling area of this study, spawning of the deep-sea coral *L. pertusa* begins in late January to February (Larsson et al., 2014), though other populations in Trondheimfjord (closer to the Sula reef) spawn from mid-February to late March (Brooke and Järnegren, 2013; Larsson et al., 2014) coinciding with a later summer bloom in this area. As the reproductive activity of many deep-sea invertebrates, which are seasonal reproducers, seems to be dependent on nutrient fluxes coming from the surface, it means that fluctuations in annual primary blooms could slightly displace the reproductive cycle of these species.

Marine Conservation in Boreo-Arctic North-Atlantic Deep-Sea Sponge Grounds

In marine conservation, reproductive timing, larval dispersal, and connectivity are key factors to take into account for developing adequate strategies to protect a variety of marine organisms (e.g., corals, mussels, fish) and habitats (Carson et al., 2010; Treml et al., 2012; Schmiing et al., 2016). In deep-sea sponge grounds, due to lack of essential biological information and to discontinuous monitoring, only prediction models based on generalized approaches are used to assess the potential dispersal of sponge populations and their capacity for regeneration in case of disturbance (e.g., Kenchington et al., 2019). The reproductive timing is a crucial parameter to consider when designing a conservation strategy, not only because it is the period of recruitment, but also because reproductive individuals are more vulnerable to disturbances due to their high energetic investment in gamete production and spawning. In addition, in the case of mechanical disturbance during the reproductive season, organisms may release premature propagules that cannot survive (Henry et al., 2003). For instance, samples of the deep-sea coral *L. pertusa*, from intensively trawled areas on Darwin Mounds, did not produce any gametes, also showing high levels of clonality that indicate a pause of sexual reproduction (Le Goff-Vitry et al., 2004; Waller and Tyler, 2005). In turn, samples of the same species in areas with less exploitation produced larger amounts of gametes during the exact same time (Waller and Tyler, 2005). Shallow-water corals (e.g., *Pocillopora damicornis,* Linnaeus, 1758) and sponges (e.g., *Luffariella variabilis,* Poléjaeff, 1884) reduce their reproductive activity during stress and invest more of their energy in survival (e.g., metabolic maintenance, tissue repair) (Brown and Howard, 1985; Ward, 1995; Ettinger-Epstein et al., 2007). Similar behaviors are then expected for their deep-sea counterparts.

In *Geodia* grounds, the fragmentary information related to lifespan, reproductive activity, reproductive strategy, and population connectivity patterns of the dominant species, has made the development of long-term conservation strategies on these habitats very difficult and in some cases unsupported (Thompson and Fuller, 2020). The species of the genus *Geodia* have one or two annual reproductive cycles. The spawning period for *Geodia* spp. in the studied areas has a broad range (May to November) depending on the area considered. Indeed, the reproductive period of *Geodia* spp. in sponge grounds should be taken into account to implement special protective measures related to fisheries during such times. Estimated spawning periods for *Geodia* spp. are completely different than that observed for deep-sea corals, which in the boreo-arctic areas of the North Atlantic spans from January to March (Brooke and Järnegren, 2013; Larsson et al., 2014). This therefore calls for specific measures of protection for the different habitats in the deep-sea. Such information combined with population genetic studies on these species and oceanographic circulation patterns would give more accurate predictions of dispersal and connectivity patterns of these populations in order

to develop adequate conservation strategies specific to each species and habitat.

DATA AVAILABILITY STATEMENT

The original contributions presented in the study are included in the article/**Supplementary Material** and archived in the PANGAEA data repository (https://doi.pangaea.de/10.1594/PANGAEA.921626). Further inquiries can be directed to the corresponding author/s.

AUTHOR CONTRIBUTIONS

VK, AR, PC, and HR collected the samples. AR and VK contributed to conception and design of the study. VK, AR, and MC processed the samples. VK analyzed the data and drafted the manuscript. AR and PC did essential corrections to the manuscript. All the authors contributed to manuscript revision, read, and approved the submitted version.

FUNDING

This work was supported by the H2020 EU Framework Program for Research and Innovation Project SponGES (deep-sea Sponge Grounds Ecosystems of the North Atlantic: an integrated approach toward their preservation and sustainable exploitation) (Grant Agreement no. 679849). This document reflects only the authors' view and the Executive Agency for Small and Medium-sized Enterprises (EASME) is not responsible for any use that may be made of the information it contains. Funding was also provided by a grant of the Spanish Ministry of Science and Innovation (PID2019-105769GB-I00) to AR.

ACKNOWLEDGMENTS

We are grateful to the scientist Jim Drewery (Marine Scotland Science, Aberdeen, United Kingdom) for the collection of samples in Rosemary Bank Seamount and Dr. Joana Xavier (CIIMAR – University of Porto, Portugal), Ph.D. student Karin Steffen (Department of Pharmaceutical Biosciences, Uppsala University, Sweden) and Dr. Francisca Carvalho (Department of Natural History, University of Bergen, Norway) for their help during fieldwork and sample collection. We are also indebted to Dr. Nadia Santodomingo, Dr. Bruna Plese, Dr. Nathan Kenny and Dr. Sergi Taboada for their help during laboratory processes. Finally, we thank the crew from the research vessels: G.O. Sars, Hans Brattstrøm (UiB), Nereus, Scotia and the research team from Tjärnö Marine Laboratory. This work is dedicated to the memory of HR, who was an esteemed colleague and long champion of sponge grounds of the North Atlantic.

SUPPLEMENTARY MATERIAL

The Supplementary Material for this article can be found online at: https://www.frontiersin.org/articles/10.3389/fmars.2020.595267/full#supplementary-material

REFERENCES

Amante, C., and Eakins, B. W. (2009). *ETOPO1 1 Arc-Minute Global Relief Model: Procedures, Data Sources and Analysis*. NOAA Technical Memorandum NESDIS NGDC-24. Washington, DC: NOAA, 1–19.

Barthel, D., and Tendal, O. S. (1993). The sponge association of the abyssal Norwegian Greenland Sea: species composition, substrate relationships and distribution. *Sarsia* 78, 83–96. doi: 10.1080/00364827.1993.10413524

Bautista-Guerrero, E., Carballo, J. L., and Maldonado, M. (2010). Reproductive cycle of the coral-excavating sponge *Thoosa mismalolli* (Clionaidae) from Mexican Pacific coral reefs. *Invertebr. Biol.* 129, 285–296. doi: 10.1111/j.1744-7410.2010.00209.x

Bautista-Guerrero, E., Carballo, J. L., and Maldonado, M. (2014). Abundance and reproductive patterns of the excavating sponge *Cliona vermifera*: a threat to Pacific coral reefs? *Coral Reefs* 33, 259–266. doi: 10.1007/s00338-013-1094-1

Beazley, L., Kenchington, E., Yashayaev, I., and Murillo, F. (2015). Drivers of epibenthic megafaunal composition in the sponge grounds of the Sackville Spur, northwest Atlantic. *Deep Sea Res. Part I Oceanogr. Res. Pap.* 98, 102–114. doi: 10.1016/j.dsr.2014.11.016

Beazley, L. I., Kenchington, E. L., Murillo, F. J., del Mar, and Sacau, M. (2013). Deep-sea sponge grounds enhance diversity and abundance of epibenthic megafauna in the Northwest Atlantic. *ICES J. Mar. Sci.* 70, 1471–1490. doi: 10.1093/icesjms/fst124

Bowerbank, J. S. (1858). On the anatomy and physiology of the spongiadae. Part I. on the spicula. *Philos. Trans. R. Soc.* 148, 279–332. doi: 10.1098/rstl.1858.0016

Brooke, S., and Järnegren, J. (2013). Reproductive periodicity of the scleractinian coral *Lophelia pertusa* from the Trondheim Fjord, Norway. *Mar. Biol.* 160, 139–153. doi: 10.1007/s00227-012-2071-x

Brooke, S., and Young, C. M. (2003). Reproductive ecology of a deep-water scleractinian coral, *Oculina varicosa*. *Cont. Shelf Res.* 23, 847–858. doi: 10.1016/S0278-4343(03)00080-3

Brown, B. E., and Howard, L. S. (1985). Assessing the effects of 'stress' on reef corals. *Adv. Mar. Biol.* 22, 1–63. doi: 10.1016/S0065-2881(08)60049-8

Burgess, S., and Babcock, R. C. (2005). "Reproductive ecology of three reef-forming, deep-sea corals in the New Zealand region," in *Cold-water corals and ecosystems*, eds A. Freiwald and J. M. Roberts (New York: Springer), 701–7013. doi: 10.1007/3-540-27673-4_36

Calazans, V. P. S. B., and Lanna, E. (2019). Influence of endogenous and exogenous factors on the reproductive output of a cryptogenic calcareous sponge. *Mar. Biodivers.* 49, 2837–2850. doi: 10.1007/s12526-019-01013-2

Cameron, J. L., McEuen, F. S., and Young, C. M. (1988). "Floating lecithotrophic eggs from the bathyal echinothuriid sea urchin *Araeosoma fenestratum*," in *Echinoderm Biology*, eds R. Burke, P. V. Mladenov, P. Lambert, and R. L. Parsley (Rotterdam: A. A. BALKEMA), 23–28.

Carballo, J. L., Bautista-Guerrero, E., Cárdenas, P., Cruz-Barraza, J. A., and Aguilar-Camacho, J. M. (2018). Molecular and morphological data from Thoosidae in favor of the creation of a new suborder of Tetractinellida. *Syst. Biodivers.* 16, 512–521. doi: 10.1080/14772000.2018.1457100

Cárdenas, P., Rapp, H. T., Klitgaard, A. B., Best, M., Thollesson, M., and Tendal, O. S. (2013). Taxonomy, biogeography and DNA barcodes of *Geodia* species (Porifera, Demospongiae, Tetractinellida) in the Atlantic boreo-arctic region. *Zool. J. Linn. Soc.* 169, 251–311. doi: 10.1111/zoj.12056

Cárdenas, P., Rapp, H. T., Schander, C., and Tendal, O. S. (2010). Molecular taxonomy and phylogeny of the *Geodiidae* (Porifera, Demospongiae, Astrophorida) - combining phylogenetic and Linnaean classification. *Zool. Scr.* 39, 89–106. doi: 10.1111/j.1463-6409.2009.00402.x

Carson, H. S., López-Duarte, P. C., Rasmussen, L., Wang, D., and Levin, L. A. (2010). Reproductive timing alters population connectivity in marine metapopulations. *Curr. Biol.* 20, 1926–1931. doi: 10.1016/j.cub.2010.09.057

Cathalot, C., Van Oevelen, D., Cox, T. J. S., Kutti, T., Lavaleye, M., Duineveld, G., et al. (2015). Cold-water coral reefs and adjacent sponge grounds: hotspots of benthic respiration and organic carbon cycling in the deep sea. *Front. Mar. Sci.* 2:37. doi: 10.3389/fmars.2015.00037

Chen, W. (1976). "Reproduction and speciation in *Halisarca*," in *Aspects of Sponge Biology*, ed. C. R. Harrison (New York: Academic Press), 113–139. doi: 10.1016/b978-0-12-327950-7.50014-2

Clarke, A. (1980). A reappraisal of the concept of metabolic cold adaptation in polar marine invertebrates. *Biol. J. Linn. Soc.* 14, 77–92. doi: 10.1111/j.1095-8312.1980.tb00099.x

Corey, S. (1981). Comparative fecundity and reproductive strategies in seventeen species of the *Cumacea* (Crustacea: Peracarida). *Mar. Biol.* 62, 65–72. doi: 10.1007/BF00396952

Corriero, G., Sarà, M., and Vaccaro, P. (1996). Sexual and asexual reproduction in two species of *Tethya* (Porifera: Demospongiae) from a Mediterranean coastal lagoon. *Mar. Biol.* 126, 175–181. doi: 10.1007/BF00347442

Corriero, G., Scalera Liaci, L., Nonnis Marzano, C., and Gaino, E. (1998). Reproductive strategies of *Mycale contarenii* (Porifera: Demospongiae). *Mar. Biol.* 131, 319–327. doi: 10.1007/s002270050325

De Caralt, S., González, J., Turon, X., and Uriz, M. J. (2018). Reproductive strategies of two common sympatric Mediterranean sponges: *Dysidea avara* (Dictyoceratida) and *Phorbas tenacior* (Poecilosclerida). *PeerJ* 6:e5458. doi: 10.7717/peerj.5458

De Kluijver, A., Nierop, K. G. J., Morganti, T. M., Bart, M. C., Beate, M., Hanz, U., et al. (2020). Bacterial precursors and unsaturated long-chain fatty acids are biomarkers of North-Atlantic demosponges. *Biorivx* [Preprint]. doi: 10.1101/2020.10.09.332833

Di Camillo, C. G., Coppari, M., Bartolucci, I., Bo, M., Betti, F., Bertolino, M., et al. (2012). Temporal variations in growth and reproduction of *Tedania anhelans* and *Chondrosia reniformis* in the North Adriatic Sea. *Hydrobiologia* 687, 299–313. doi: 10.1007/s10750-011-0877-z

Dohrmann, M., and Wörheide, G. (2013). Novel scenarios of early animal evolution—is it time to rewrite textbooks? *Integr. Comp. Biol.* 53, 503–511. doi: 10.1093/icb/ict008

Eckelbarger, K. J., and Watling, L. (1995). Role of phylogenetic constraints in determining reproductive patterns in deep-sea invertebrates. *Invertebr. Biol.* 114, 256–269. doi: 10.2307/3226880

Elvin, D. W. (1976). Seasonal Growth and Reproduction of an Intertidal Sponge, *Haliclona permollis* (Bowerbank). *Univ. Chicago Press* 151, 108–125. doi: 10.2307/1540709

Ereskovsky, A. V. (2000). Reproduction cycles and strategies of the cold-water sponges *Halisarca dujardini* (Demospongiae, Halisarcida), *Myxilla incrustans* and *Iophon piceus* (Demospongiae, Poecilosclerida) from the White Sea. *Biol. Bull.* 198, 77–87. doi: 10.2307/1542805

Ereskovsky, A. V., Dubois, M., Ivanišević, J., Gazave, E., Lapebie, P., Tokina, D., et al. (2013). Pluri-annual study of the reproduction of two Mediterranean *Oscarella* species (Porifera, Homoscleromorpha): cycle, sex-ratio, reproductive effort and phenology. *Mar. Biol.* 160, 423–438. doi: 10.1007/s00227-012-2100-9

Ettinger-Epstein, P., Whalan, S. W., Battershill, C. N., and de Nys, R. (2007). Temperature cues gametogenesis and larval release in a tropical sponge. *Mar. Biol.* 153, 171–178. doi: 10.1007/s00227-007-0793-y

FAO (2009). *International Guidelines for the Management of Deep-sea Fisheries in the High Seas*. Rome: FAO.

Fell, P. (1974). "Porifera," in *Reproduction of Marine Invertebrates*, eds A. Giese and P. JS (New York: Academic Press), 51–132.

Fell, P. E. (1969). The involvement of nurse cells in oogenesis and embryonic development in the marine sponge, Haliclona ecbasis. *J. Morphol.* 127, 133–149. doi: 10.1002/jmor.1051270202

Feuda, R., Dohrmann, M., Pett, W., Philippe, H., Rota-Stabelli, O., Lartillot, N., et al. (2017). Improved modeling of compositional heterogeneity supports sponges as sister to all other animals. *Curr. Biol.* 27, 3864.e4–3870.e4. doi: 10.1016/j.cub.2017.11.008

Fountain, C. T., Waller, R. G., and Auster, P. J. (2019). Individual and population level variation in the reproductive potential of deep-sea corals from different regions within the Gulf of Maine. *Front. Mar. Sci.* 6:172. doi: 10.3389/fmars.2019.00172

Freese, J. L. (2001). Trawl-induced damage to sponges observed from a research submersible. *Mar. Fish. Rev.* 63, 7–13.

Fromont, J., and Bergquist, P. R. (1994). Reproductive biology of three sponge species of the genus *Xestospongia* (Porifera: Demospongiae: Petrosida) from the great barrier Reef. *Coral Reefs* 13, 119–126. doi: 10.1007/BF00300772

Gaino, E., Burlando, B., Zunino, L., Pansini, M., and Buffa, P. (1984). Origin of male gametes from choanocytes in *Spongia officinalis* (Porifera, Demospongiae). *Int. J. Invertebr. Reprod. Dev.* 7, 83–93. doi: 10.1080/01688170.1984.10510077

George, R. Y., and Menzies, R. J. (1967). Indication of cyclic reproductive activity in abyssal organisms. *Nature* 215:878. doi: 10.1038/215878a0

Giese, A. C. (1966). Lipids in the economy of marine invertebrates. *Physiol. Rev.* 46, 244–298. doi: 10.1152/physrev.1966.46.2.244

Gooday, A. J. (2002). Biological responses to seasonally varying fluxes of organic matter to the ocean floor: a review. *J. Oceanogr.* 58, 305–332. doi: 10.1023/A:1015865826379

Gunnerus, J. E. (1763). Om en søevext, allevegne ligesom besat med frøehuuse, *Gorgonia resedæformis*. *Det Trondhiemske Selskabs Skrifter* 2, 321–329.

Hansen, G. A. (1885). Spongiadae. The norwegian north-atlantic expedition 1876-1878. *Zoology* 13, 1–26. doi: 10.1080/00364827.1973.10411241

Harrison, P. L. (2011). "Sexual reproduction of scleractinian corals," in *Coral Reefs: An Ecosystem in Transition*, eds Z. Dubinsky and N. Stambler (Dordrecht: Springer), 59–85. doi: 10.1007/978-94-007-0114-4_6

Henry, L. A., Kenchington, E. L. R., and Silvaggio, A. (2003). Effects of mechanical experimental disturbance on aspects of colony responses, reproduction, and regeneration in the cold-water octocoral *Gersemia rubiformis*. *Can. J. Zool.* 81, 1691–1701. doi: 10.1139/z03-161

Hoffmann, F., Radax, R., Woebken, D., Holtappels, M., Lavik, G., Rapp, H. T., et al. (2009). Complex nitrogen cycling in the sponge *Geodia barretti*. *Environ. Microbiol.* 11, 2228–2243. doi: 10.1111/j.1462-2920.2009.01944.x

ICES (2018). *Report of the ICES/NAFO Joint Working Group on Deep-water Ecology (WGDEC)*. Dartmouth: ICES.

Ivanova, L., and Semyonov, V. (1997). Feeding habits of the larvae of sponges, *Berliner geowiss*. *Abh* 20, 93–101.

Kahn, A., Yahel, G., Chu, J., Tunnicliffe, V., and Leys, S. (2015). Benthic grazing and carbon sequestration by deep-water glass sponge reefs. *Limnol. Oceanogr.* 60, 78–88. doi: 10.1002/lno.10002

Kenchington, E., Power, D., and Koen-Alonso, M. (2013). Associations of demersal fish with sponge grounds on the continental slopes of the northwest Atlantic. *Mar. Ecol. Prog. Ser.* 477, 217–230. doi: 10.3354/meps10127

Kenchington, E., Wang, Z., Lirette, C., Murillo, F. J., Guijarro, J., Yashayaev, I., et al. (2019). Connectivity modelling of areas closed to protect vulnerable marine ecosystems in the northwest Atlantic. *Deep Sea Res. Part I Oceanogr. Res. Pap.* 143, 85–103. doi: 10.1016/j.dsr.2018.11.007

Klitgaard, A. (1995). The fauna associated with outer shelf and upper slope sponges (Porifera, Demospongiae) at the Faroe Islands, northeastern Atlantic. *Sarsia* 80, 1–22.

Klitgaard, A. B., and Tendal, O. (2004). Distribution and species composition of mass occurrences of large-sized sponges in the northeast Atlantic. *Prog. Oceanogr.* 61, 57–98. doi: 10.1016/j.pocean.2004.06.002

Klitgaard, A. B., Tendal, O., and Westerberg, H. (1997). "Mass occurrence of large sponges (Porifera) in Faroe Island (NE Atlantic) shelf and slope areas: characteristics, distribution and possible causes," in *The Responses of Marine Organisms to their Environments. Proceedings of the 30th European Marine Biology Symposium*, eds L. E. Hawkins, S. Hutchinson, A. C. Jensen, M. Sheader, and J. A. Williams (Southampton: University of Southampton), 129–142.

Knudby, A., Kenchington, E., and Murillo, F. J. (2013). Modeling the distribution of *Geodia* sponges and sponge grounds in the Northwest Atlantic. *PLoS One* 8:e0082306. doi: 10.1371/journal.pone.0082306

Koltun, V. M. (1959). Donnaia fauna abissalnuich glubin Zhentralnovo Poljarnovo basseina [Fauna from the abyssal of central polar basin]. Dokl. Akad. Nauk SSSR. *Seriya Biol.* 129, 662–665.

Koutsouveli, V., Cárdenas, P., Conejero, M., Rapp, H. T., and Riesgo, A. (2020a). *Collection Information of The Genus Geodia from Boreo-Arctic North-Atlantic Deep-Sea Sponge Grounds*. London: PANGAEA.

Koutsouveli, V., Cárdenas, P., Santodomingo, N., Marina, A., Morato, E., Rapp, H. T., et al. (2020b). The molecular machinery of gametogenesis in *Geodia demosponges* (Porifera): evolutionary origins of a conserved toolkit across animals. *Mol. Biol. Evol.* doi: 10.1093/molbev/msaa183 [Epub ahead of print].

Koutsouveli, V., Taboada, S., Moles, J., Cristobo, J., Ríos, P., Bertran, A., et al. (2018). Insights into the reproduction of some Antarctic dendroceratid, poecilosclerid, and haplosclerid demosponges. *PLoS One* 13:e0192267. doi: 10.1371/journal.pone.0192267

Kutti, T., Bannister, R., Helle, K., Krogness, C., Tjensvoll, I., and Søvik, G. (2015). Metabolic responses of the deep-water sponge *Geodia barretti* to suspended bottom sediment, simulated mine tailings and drill cuttings. *J. Exp. Mar. Bio. Ecol.* 473, 64–72. doi: 10.1016/j.jembe.2015.07.017

Kutti, T., Bannister, R. J., and Fosså, J. H. (2013). Community structure and ecological function of deep-water sponge grounds in the Traenadypet MPA — Northern Norwegian continental shelf. *Cont. Shelf Res.* 69, 21–30. doi: 10.1016/j.csr.2013.09.011

Larsson, A. I., Järnegren, J., Strömberg, S. M., Dahl, M. P., Lundälv, T., and Brooke, S. (2014). Embryogenesis and larval biology of the cold-water coral *Lophelia pertusa*. *PLoS One* 9:e102222. doi: 10.1371/journal.pone.0102222

Laumer, C. E., Fernandez, R., Lemer, S., Combosch, D., Kocot, K. M., Riesgo, A., et al. (2019). Revisiting metazoan phylogeny with genomic sampling of all phyla. *Proc. Biol. Sci.* 286:20190831. doi: 10.1098/rspb.2019.0831

Le Goff-Vitry, M. C., Pybus, O. G., and Rogers, A. D. (2004). Genetic structure of the deep-sea coral *Lophelia pertusa* in the northeast Atlantic revealed by microsatellites and internal transcribed spacer sequences. *Mol. Ecol.* 13, 537–549. doi: 10.1046/j.1365-294X.2004.2079.x

Lepore, E., Scisciolì, M., Liaci, L. S., Santarelli, G., and Gaino, E. (2000). Sexual reproduction of *Cinachyra tarentina* (porifera, demospongiae). *Ital. J. Zool.* 67, 153–158. doi: 10.1080/11250000009356308

Leys, S. P., Kahn, A. S., Fang, J. K. H., Kutti, T., and Bannister, R. J. (2018). Phagocytosis of microbial symbionts balances the carbon and nitrogen budget for the deep-water boreal sponge *Geodia barretti*. *Limnol. Oceanogr.* 63, 187–202. doi: 10.1002/lno.10623

Liaci, L. S, and Scisciolì, M. (1969). La riproduzione sessuale di alcuni tetractinellidi (porifera). *Boll. Zool.* 36, 61–67. doi: 10.1080/11250006909440854

Liaci, L. S, and Scisciolì, M. (1970). The sexual cycle of *Erylus discophorus* (Schmidt) (Porifera, Tetractinellida)]. *Riv. Biol.* 63, 255–270.

Liaci, L. S, Scisciolì, M., and Piscitelli, G. (1976). The sexual reproduction of *Tetilla* sp. *(Tetractinellida-Porifera)*. *Rivista Biol.* 69, 331–342.

Linnaeus, C. (1758). *Systema Naturae per regna tria naturae, secundum classes, ordines, genera, species, cum characteribus, differentiis, synonymis, locis*. doi: 10.5962/bhl.title.542

Maier, S. R., Bannister, R. J., van Oevelen, D., and Kutti, T. (2020). Seasonal controls on the diet, metabolic activity, tissue reserves and growth of the cold-water coral Lophelia pertusa. *Coral Reefs* 39, 173–187. doi: 10.1007/s00338-019-01886-6

Maldonado, M., Aguilar, R., Bannister, R., Bell, J., Conwa, K. W., Dayton, P., et al. (2016). "Sponge grounds as key marine habitats: a synthetic review of types, structure, functional roles, and conservation concerns," in *Marine Animal Forests: Ecology of Benthic Biodiversity*, ed. S. Rossi (Switzerland: Springer International Publishing), 145–183. doi: 10.1007/978-3-319-21012-4_24

Maldonado, M., and Bergquist, P. R. (2002). "Phylum porifera," in *Atlas of Marine Invertebrate Larvae*, eds M. Craig, Young, E. Mary, Rice, A. Mary, and Sewell (London: Academic Press), 21–50.

Maldonado, M., Beazley, L., López-Acosta, M., Kenchington, E., Casault, B., Hanz, U., et al. (2020). Massive silicon utilization facilitated by a benthic-pelagic coupled feedback sustains deep-sea sponge aggregations. *Limnol. Oceanogr.* doi: 10.1002/lno.11610 [Epub ahead of print].

Maldonado, M., Ribes, M., and van Duyl, F. C. (2012). "Chapter three – nutrient fluxes through sponges: biology, budgets, and ecological implications," in *Advances in Sponge Science: Physiology, Chemical and Microbial Diversity, Biotechnology*, eds. M. A. Becerro, M. J. Uriz, M. Maldonado, and M. B. Turon (Academic Press), 113–182. doi: 10.1016/B978-0-12-394283-8.00003-5

Maldonado, M., and Riesgo, A. (2008). Reproduction in the phylum Porifera: a synoptic overview. *Treballs SCB* 59, 29–49. doi: 10.2436/20.1501.02.56

Maldonado, M., and Riesgo, A. (2009). Gametogenesis, embryogenesis, and larval features of the oviparous sponge *Petrosia ficiformis* (Haplosclerida, Demospongiae). *Mar. Biol.* 156, 2181–2197. doi: 10.1007/s00227-009-1248-4

Marshall, D. J., and Keough, M. J. (2007). The evolutionary ecology of offspring size in marine invertebrates. *Adv. Mar. Biol.* 53, 1–60. doi: 10.1016/S0065-2881(07)53001-4

Mauchline, J. (1973). The broods of British mysidacea (Crustacea). *J. Mar. Biol. Assoc. U.K.* 53, 801–817. doi: 10.1017/S0025315400022487

Mercier, A., Sun, Z., Baillon, S., and Hamel, J.-F. (2011). Lunar rhythms in the deep sea: evidence from the reproductive periodicity of several marine invertebrates. *J. Biol. Rhythms* 26, 82–86. doi: 10.1177/0748730410391948

Mercurio, M., Corriero, G., and Gaino, E. (2007). A 3-year investigation of sexual reproduction in *Geodia cydonium* (Jameson 1811) (Porifera, Demospongiae) from a semi-enclosed Mediterranean bay. *Mar. Biol.* 151, 1491–1500. doi: 10.1007/s00227-006-0584-x

Meroz-Fine, E., Shefer, S., and Ilan, M. (2005). Changes in morphology and physiology of an East Mediterranean sponge in different habitats. *Mar. Biol.* 147, 243–250. doi: 10.1007/s00227-004-1532-2

Murillo, F., Muñoz, P., Cristobo, J., Ríos, P., González, C., Kenchington, E., et al. (2012). Deep-sea sponge grounds of the Flemish Cap, Flemish Pass and the Grand Banks of Newfoundland (Northwest Atlantic Ocean): distribution and species composition. *Mar. Biol. Res.* 8, 842–854. doi: 10.1080/17451000.2012.682583

NAFO (2012). Northwest Atlantic Fisheries Organization Conservation and Enforcement Measures. Available online at: https://www.nafo.int/Portals/0/PDFs/fc/2012/fcdoc12-01.pdf

NAFO (2014). *Scientific Council Reports*. Dartmouth: NAFO.

NAFO (2018). *Report of the Scientific Council Meeting*. Dartmouth: NAFO.

OSPAR (2008). *OSPAR List of Threatened and/or Declining Species and Habitats*. London: OSPAR.

Pérez-Porro, A., Gonzalez Ramos, J., and Uriz, M. (2012). Reproductive traits explain contrasting ecological features in sponges: the sympatric poecilosclerids *Hemimycale columella* and *Crella elegans* as examples. *Hydrobiologia* 687, 315–330. doi: 10.1007/s10750-011-0919-6

Pham, C. K., Murillo, F. J., Lirette, C., Maldonado, M., Colaço, A., Ottaviani, D., et al. (2019). Removal of deep-sea sponges by bottom trawling in the Flemish Cap area: conservation, ecology and economic assessment. *Sci. Rep.* 9, 1–13. doi: 10.1038/s41598-019-52250-1

Pile, A., and Young, C. (2006). The natural diet of a hexactinellid sponge: benthic-pelagic coupling in a deep-sea microbial food web. *Deep Sea Res. Part I Oceanogr. Res. Pap.* 53, 1148–1156. doi: 10.1016/j.dsr.2006.03.008

Pires, D. O., Silva, J. C., and Bastos, N. D. (2014). Reproduction of deep-sea reef-building corals from the southwestern Atlantic. *Deep Sea Res. Part II Top. Stud. Oceanogr.* 99, 51–63. doi: 10.1016/j.dsr2.2013.07.008

Piscitelli, M., Corriero, G., Gaino, E., and Uriz, M. J. (2011). Reproductive cycles of the sympatric excavating sponges *Cliona celata* and *Cliona viridis* in the Mediterranean Sea. *Invertebr. Biol.* 130, 1–10. doi: 10.1111/j.1744-7410.2010.00216.x

Poléjaeff, N. (1884). "Report on the Keratosa collected by H.M.S. Challenger during the years 1873-1876," in *Report on the Scientific Results of the Voyage of H.M.S. Challenger During the Years 1873–76*, ed. N. N. Polezhaev (Wyoming: Creative Media Partners).

Radax, R., Rattei, T., Lanzen, A., Bayer, C., Rapp, H. T., Urich, T., et al. (2012). Metatranscriptomics of the marine sponge *Geodia barretti*: tackling phylogeny and function of its microbial community. *Environ. Microbiol.* 14, 1308–1324. doi: 10.1111/j.1462-2920.2012.02714.x

Reynolds, E. S. (1963). The use of lead citrate at high ph as an electron-opaque stain in electron microscopy. *J. Cell Biol.* 17, 208–212. doi: 10.1083/jcb.17.1.208

Riesgo, A., and Maldonado, M. (2008). Differences in reproductive timing among sponges sharing habitat and thermal regime. *Invertebr. Biol.* 127, 357–367. doi: 10.1111/j.1744-7410.2008.00128.x

Riesgo, A., and Maldonado, M. (2009). Ultrastructure of oogenesis of two oviparous demosponges: *Axinella damicornis* and *Raspaciona aculeata* (Porifera). *Tissue Cell* 41, 51–65. doi: 10.1016/j.tice.2008.07.004

Riesgo, A., Novo, M., Sharma, P. P., Peterson, M., Maldonado, M., and Giribet, G. (2014). Inferring the ancestral sexuality and reproductive condition in sponges (Porifera). *Zool. Scr.* 43, 101–117. doi: 10.1111/zsc.12031

Riesgo, A., Taboada, S., Sánchez-Vila, L., Solà, J., Bertran, A., and Avila, C. (2015). Some like it fat: comparative ultrastructure of the embryo in two demosponges of the genus *Mycale* (order Poecilosclerida) from Antarctica

and the Caribbean. *PLoS One* 10:e0118805. doi: 10.1371/journal.pone.0118805

Roberts, C. (2002). Deep impact: the rising toll of fishing in the deep sea. *Trends Ecol. Evol.* 17, 242–245. doi: 10.1016/s0169-5347(02)02492-8

Rooks, C., Fang, J. K.-H., Mørkved, P. T., Zhao, R., Rapp, H. T., Xavier, J. R., et al. (2020). Deep-sea sponge grounds as nutrient sinks: denitrification is common in boreo-Arctic sponges. *Biogeosciences* 17, 1231–1245. doi: 10.5194/bg-17-1231-2020

Sarà, M. (1993). "Porifera," in *Reproductive Biology of Invertebrates, Sexual Differentiation and Behaviour*, eds. K. Adiyodi and R. Adiyodi (Chichester: Wiley), 1–29.

Schmidt, O. (1870). *Grundzüge einer Spongien-Fauna des atlantischen Gebietes*. Leipzig: Lhelm Engelmann.

Schmiing, M., Fontes, J., and Afonso, P. (2016). Predictive mapping of reproductive fish habitats to aid marine conservation planning. *Can. J. Fish. Aquat. Sci.* 74, 1016–1027. doi: 10.1139/cjfas-2015-0538

Schneider, C. A., Rasband, W. S., and Eliceiri, K. W. (2012). NIH Image to ImageJ: 25 years of image analysis. *Nat. Methods* 9, 671–675. doi: 10.1038/nmeth.2089

Sciscioli, M., Lepore, E., Gherardi, M., and Liaci, L. S. (1994). Transfer of symbiotic bacteria in the mature oocyte of *Geodia cydonium* (Porifera, Demosponsgiae): an ultrastructural study. *Cah. Biol. Mar.* 35, 471–478.

Sciscioli, M., Lepore, E., and Scalera-Liaci, L. G. M. (1989). Indagine ultrastrutturale sugli ovociti di *Erylus discophorus* (Schmidt) (Porifera, Tetractinellida). *Oebalia* 15, 939–941.

Sciscioli, M., Liaci, L. S., Lepore, E., Gherardi, M., and Simpson, T. L. (1991). Ultrastructural study of the mature egg of the marine sponge *Stelletta grubii* (porifera demospongiae). *Mol. Reprod. Dev.* 28, 346–350. doi: 10.1002/mrd.1080280406

Simpson, T. (1984). *The Cell Biology of Sponges*. New York: Springer.

Sollas, W. J. (1880). The sponge-fauna of Norway; a Report on the Rev. A.M. Norman's collection of sponges from the Norwegian Coast. *Ann. Mag. Nat. Hist. Zool. Bot. Geol.* 5, 130–144.

Southwood, T. R. E. (1977). Habitat, the templet for ecological strategies? *J. Anim. Ecol.* 46, 336–365. doi: 10.2307/3817

Spetland, F., Rapp, H. T., Hoffmann, F., and Tendal, O. S. (2007). Sexual reproduction of *Geodia barretti* Bowerbank, 1858 (Porifera, Astrophorida) in two *Scandinavian fjords*. *Mus. Nac. Ser. Livros* 1858, 613–620.

Stephens, J. (1915). Sponges of the coasts of Ireland. I. The triaxonia and part of the tetraxonida. *Fish. Irel. Sci. Investig.* 4, 1–43.

Strand, R., Whalan, S., Webster, N. S., Kutti, T., Fang, J. K. H., Luter, H. M., et al. (2017). The response of a boreal deep-sea sponge holobiont to acute thermal stress. *Sci. Rep.* 7, 1–12. doi: 10.1038/s41598-017-01091-x

Tanaka-Ichihara, K., and Watanabe, Y. (1990). "Gametogenic cycle in *Halichondria okadai*," in *New Perspectives in Sponge Biology*, ed. K. Rützler (Washington DC: Smithsonian Institution Press), 170–174.

Thompson, T., and Fuller, S. D. (2020). *Technical Measures and Environmental Risk Assessments for Deep-Sea Sponge Conservation*. Rome: FAO.

Thorson, G. (1950). Reproductive and larval ecology of marine bottom invertebrates. *Biol. Rev.* 25, 1–45. doi: 10.1111/j.1469-185X.1950.tb00585.x

Topsent, E. (1904). Spongiaires des Açores. Résultats des campagnes Sci. Accompl. par le Prince Albert I. *Monaco* 25, 1–280.

Treml, E. A., Roberts, J. J., Chao, Y., Halpin, P. N., Possingham, H. P., and Riginos, C. (2012). Reproductive output and duration of the pelagic larval stage determine seascape-wide connectivity of marine populations. *Integr. Comp. Biol.* 52, 525–537. doi: 10.1093/icb/ics101

Tyler, P. A., Gage, J. D., Paterson, G. J. L., and Rice, A. L. (1993). Dietary constraints on reproductive periodicity in two sympatric deep-sea astropectinid seastars. *Mar. Biol.* 115, 267–277. doi: 10.1007/BF00346344

Tyler, P. A., Harvey, R., Giles, L. A., and Gage, J. D. (1992). Reproductive strategies and diet in deep-sea nuculanid protobranchs (Bivalvia: Nuculoidea) from the rockall trough. *Mar. Biol.* 114, 571–580. doi: 10.1007/BF00357254

UNGA (2006). *The Impacts of Fishing on Vulnerable Marine Ecosystems: Actions taken by States and Regional Fisheries Management Organizations and Arrangements to Give Effect to Paragraphs 66 to 69 of General Assembly Resolution 59/25 on Sustainable Fisheries, Regarding the Impacts of Fishing on Vulnerable Marine Ecosystems*. New York, NY: UNGA.

Vacelet, J. (1975). Étude en microscopie électronique de l'association entre bactéries et Spongiaires du genre *Verongia* (Dictyoceratida). *J. Microsc. Biol. Cell* 23, 271–288.

von Bodungen, B., Antia, A., Bauerfeind, E., Haupt, O., Koeve, W., Machado, E., et al. (1995). Pelagic processes and vertical flux of particles: an overview of a long-term comparative study in the Norwegian Sea and Greenland Sea. *Geol. Rundschau* 84, 11–27. doi: 10.1007/BF00192239

Waller, R. G. (2005). ""Deep-water Scleractinia (Cnidaria: Anthozoa): current knowledge of reproductive processes"," in *Cold-Water Corals And Ecosystems*, eds A. Freiwald and J. M. Roberts (New York: Springer), 691–700. doi: 10.1007/3-540-27673-4_35

Waller, R. G., and Tyler, P. A. (2005). The reproductive biology of two deep-water, reef-building scleractinians from the NE Atlantic Ocean. *Coral Reefs* 24, 594–602. doi: 10.1007/s00338-005-0501-7

Wapstra, M., and van Soest, R. (1987). "Sexual reproduction, larval morphology and behaviour in demosponges from the Southwest of the Netherlands," in *Taxonomy of Porifera. NATO ASI Series (Series G: Ecological Sciences)*, eds J. Vacelet and N. Boury-Esnault (Berlin: Springer), 281–307. doi: 10.1007/978-3-642-70892-3_15

Ward, S. (1995). Two patterns of energy allocation for growth, reproduction and lipid storage in the scleractinian coral Pocillopora damicornis. *Coral Reefs* 14, 87–90. doi: 10.1007/BF00303428

Wassmann, P. (1991). Dynamics of primary production and sedimentation in shallow fjords and polls of western Norway. *Oceanogr. Mar. Biol. an Annu. Rev.* 29, 87–154.

Wassmann, P., Svendsen, H., Keck, A., and Reigstad, M. (1996). Selected aspects of the physical oceanographic and particle fluxes in fjords of northern Norway. *J. Mar. Syst.* 8, 53–71. doi: 10.1016/0924-7963(95)00037-2

Watanabe, Y. (1978). The development of two species of *Tetilla* (Demosponge). *NSR. O. U.* 29, 71–106.

Witte, U. (1996). Seasonal reproduction in deep-sea sponges - triggered by vertical particle flux? *Mar. Biol.* 124, 571–581. doi: 10.1007/BF00351038

Witte, U., Barthel, D., and Tendal, O. (1994). The reproductive cycle of the sponge *Halichondria panicea* Pallas (1766) and its relationship to temperature and salinity. *J. Exp. Mar. Bio. Ecol.* 183, 41–52. doi: 10.1016/0022-0981(94)90155-4

Yahel, G., Whitney, F., Reiswig, H. M., Eerkes-Medrano, D. I., and Leys, S. P. (2007). In situ feeding and metabolism of glass sponges (Hexactinellida, Porifera) studied in a deep temperate fjord with a remotely operated submersible. *Limnol. Oceanogr.* 52, 428–440. doi: 10.4319/lo.2007.52.1.0428

Young, C. M. (2003). "Reproduction, development and life history traits," in *Ecosystems of the Deep Oceans. Ecosystems of the World 28*, ed. P. Tyler (Amsterdam: Elsevier), 381–426.

Young, C. M., and Eckelbarger, K. J. (1994). *Reproduction, Larval Biology, and Recruitment of the Deep-Sea Benthos*. New York, NY: Columbia University Press.

Zumberge, J. A., Love, G. D., Cárdenas, P., Sperling, E. A., Gunasekera, S., Rohrssen, M., et al. (2018). Demosponge steroid biomarker 26-methylstigmastane provides evidence for Neoproterozoic animals. *Nat. Ecol. Evol.* 2, 1709–1714. doi: 10.1038/s41559-018-0676-2

Conflict of Interest: The authors declare that the research was conducted in the absence of any commercial or financial relationships that could be construed as a potential conflict of interest.

Copyright © 2020 Koutsouveli, Cárdenas, Conejero, Rapp and Riesgo. This is an open-access article distributed under the terms of the Creative Commons Attribution License (CC BY). The use, distribution or reproduction in other forums is permitted, provided the original author(s) and the copyright owner(s) are credited and that the original publication in this journal is cited, in accordance with accepted academic practice. No use, distribution or reproduction is permitted which does not comply with these terms.

frontiers in Marine Science

ORIGINAL RESEARCH
published: 23 December 2020
doi: 10.3389/fmars.2020.599825

CRISPR/Cas12a-Mediated Gene Editing in *Geodia barretti* Sponge Cell Culture

Kylie Hesp[1]*, *John L. Flores Alvarez*[1], *Ana-Maria Alexandru*[1], *Jip van der Linden*[1], *Dirk E. Martens*[1], *Rene H. Wijffels*[1,2] *and Shirley A. Pomponi*[1,3]

[1] *Bioprocess Engineering, Wageningen University & Research, Wageningen, Netherlands,* [2] *Faculty of Biosciences and Aquaculture, Nord University, Bodø, Norway,* [3] *Sponge Biotechnology, Marine Biomedical & Biotechnology Research, Harbor Branch Oceanographic Institute, Florida Atlantic University, Fort Pierce, FL, United States*

Sponges and their associated microorganisms are the most prolific source of marine natural products, and many attempts have been made at creating a marine sponge cell line to produce these products efficiently. However, limited knowledge on the nutrients sponge cells require to grow and poor genetic accessibility have hampered progress toward this goal. Recently, a new sponge-specific nutrient medium M1 has been shown to stimulate sponge cells *in vitro* to divide rapidly. In this study, we demonstrate for the first time that sponge cells growing in M1 can be genetically modified using a CRISPR/Cas12a gene editing system. A short sequence of scrambled DNA was inserted using a single-stranded oligodeoxynucleotide donor template to disrupt the 2′,5′-oligoadenylate synthetase gene of cells from the boreal deep-sea sponge *Geodia barretti*. A blue fluorescent marker gene appeared to be inserted in an intron of the same gene and expressed by a small number of *G. barretti* cells. Our results represent an important step toward developing an optimized continuous sponge cell line to produce bioactive compounds.

Keywords: CRISPR/Cas, marine sponge cell culture, genome editing, CRISPRMAX, homologous recombination

OPEN ACCESS

Edited by:
Ellen Kenchington, Bedford Institute of Oceanography (BIO), Canada

Reviewed by:
Bruno Francesco Rodrigues de Oliveira, Federal University of Rio de Janeiro, Brazil
April Hill, Bates College, United States

***Correspondence:**
Kylie Hesp
kylie.hesp@wur.nl

Specialty section:
This article was submitted to Deep-Sea Environments and Ecology, a section of the journal Frontiers in Marine Science

Received: *28 August 2020*
Accepted: *01 December 2020*
Published: *23 December 2020*

Citation:
Hesp K, Flores Alvarez JL, Alexandru A-M, van der Linden J, Martens DE, Wijffels RH and Pomponi SA (2020) CRISPR/Cas12a-Mediated Gene Editing in Geodia barretti Sponge Cell Culture. Front. Mar. Sci. 7:599825. doi: 10.3389/fmars.2020.599825

INTRODUCTION

Developing a marine sponge cell line to produce sponge-derived chemicals *in vitro* has been the holy grail of sponge biotechnology ever since it was discovered that marine sponges host a wide variety of bioactive secondary metabolites in marine sponges (Pomponi, 1999; Rinkevich, 2005; Mayer et al., 2010; Schippers et al., 2011; Newman and Cragg, 2016). Many of these compounds have the potential to be developed into new drugs to combat cancer (Nuijen et al., 2000; Schwartsmann et al., 2003; Jimenez et al., 2018; Khalifa et al., 2019), inflammatory disease (Alcaraz and Paya, 2006) and infections in humans (Laport et al., 2009; Abdelmohsen et al., 2017; Liu et al., 2019a). Others could be used in industrial and commercial applications, for example as anti-fouling agents (Qi and Ma, 2017), cosmetics and nutraceuticals (Balboa et al., 2015). Each of these applications potentially represents a multibillion-dollar market (Thoms and Schupp, 2005; Greco and Cinquegrani, 2016). However, lack of sufficient biomass to produce compounds at the scale required for clinical trials or industrial application has been a major bottleneck (Nuijen et al., 2000; Singh and Thakur, 2016). Harvesting of wild sponges is neither economically nor environmentally sustainable and chemical synthesis of many sponge-derived chemicals is time-consuming and expensive due to their complex nature (Nuijen et al., 2000; Thoms and Schupp, 2005; Montaser and Luesch, 2011; Singh and Thakur, 2016). Underlying metabolic pathways are often equally

complex and poorly understood, making metabolically engineering yeasts or bacteria to produce compounds difficult (Thoms and Schupp, 2005; Montaser and Luesch, 2011). Although mariculture can be suitable in some cases (Brummer and Nickel, 2003; Duckworth and Battershill, 2003; Page et al., 2005), it does not allow to precisely control culture conditions or optimize productivity (Montaser and Luesch, 2011; Santhi et al., 2017). Culturing sponge cells *in vitro* has been proposed as a solution, with sponge cells producing the compound in a controlled environment that can be adapted and optimized. Furthermore, harvesting and downstream processing are simplified compared to mariculture.

Developing such sponge cell cultures has been challenging (Pomponi et al., 1997, Rinkevich, 2005; Schippers et al., 2011). Little was known about the nutrients sponge cells need to proliferate, resulting in short-lived primary cultures (Schippers et al., 2011). Cells in such cultures quickly became less viable and metabolically active, and were often overgrown by bacteria or fungi (Sipkema et al., 2005). Recently, it was shown that cells of the Caribbean sponge *Dysidea etheria* were more metabolically active in sponge-specific cell culture medium, named M1, which contains optimized amino acid concentrations (Munroe et al., 2019). Furthermore, cells of various other sponge species divided rapidly in M1. Cells of 3 species from the genus *Geodia* responded strongly to M1 with limited variation between individuals. Cells could be subcultured 3–5 times and reached a maximum of 7 population doublings (Conkling et al., 2019). One of these was *Geodia barretti*, one of the species that dominates the sponge grounds in the deep waters of the North Atlantic ocean (Klitgaard and Tendal, 2004; Murillo et al., 2012; Knudby et al., 2013). *G. barretti* has been found to produce multiple bioactive compounds, such as barretins, a group of 6-bromoindole derivatives with anti-inflammatory (Lind et al., 2013; Di et al., 2018) and anti-fouling (Sjogren et al., 2004; Hedner et al., 2008) activity, and more recently discovered anti-fouling peptides called barrettides (Carstens et al., 2015).

Having proliferating cells is an important step toward producing compounds in large-scale bioreactors. Moreover, it facilitates developing molecular tools and genetic engineering in particular, as dividing cells are not only more viable, but also more genetically accessible (Wang et al., 2014). Until now, the only molecular technique used successfully in sponge cell culture is transfecting cells with plasmids to transiently express the human telomerase reverse transcriptase oncogene (Pomponi et al., 2007) and green fluorescent protein (Schippers, 2013). No genetic engineering tools that can make permanent changes in sponge cells to create and optimize production strains have been reported. One of the most well-known genetic engineering tools is CRISPR/Cas gene editing. CRISPR (clustered regularly-interspaced palindromic repeat) arrays were discovered as adaptive immune systems in prokaryotes. Short sequences of foreign DNA incorporated into CRISPR arrays in the genome are transcribed and processed into CRISPR RNAs (crRNA), that guide endonucleases to cleave the complementary DNA sequence (Horvath and Barrangou, 2010). These systems use a protospacer-adjacent motif (PAM) to distinguish between foreign DNA and the host genome, since the PAM is present in the foreign DNA but not in the CRISPR array. By altering the crRNA sequence, CRISPR/Cas systems can be used to specifically target any DNA sequence that contains the PAM (**Figure 1**). The endonuclease induces a double-stranded break (DSB) that can be repaired in two ways: the first, non-homologous end joining (NHEJ), often leads to small insertions/deletions causing frameshifts, while the second, homology-directed repair (HDR), can be used to insert DNA sequences by providing a repair template with homology up- and downstream of the target site (Song and Stieger, 2017; Liu et al., 2019a; **Figure 2A**). CRISPR/Cas9 is the most commonly used CRISPR system for gene editing but requires 2 RNA molecules to induce a DSB: the crRNA that matches the target sequence and an additional trans-encoded small crRNA (tracrRNA). The crRNA and tracrRNA can be linked together to create a single guide RNA, but this requires an ∼100 base pair (bp) long RNA molecule for each target sequence (Jinek et al., 2012). Another endonuclease, called Cas12a or Cpf1, was discovered more recently and is an attractive alternative to Cas9, because it does not require a tracrRNA, and instead uses 1 short (∼42 bp) guide RNA (gRNA) molecule (Zetsche et al., 2015; Swarts and Jinek, 2018; **Figure 1**). CRISPR/Cas12a has been used to edit genomes in various cell cultures of plants, animals and humans (Safari et al., 2019).

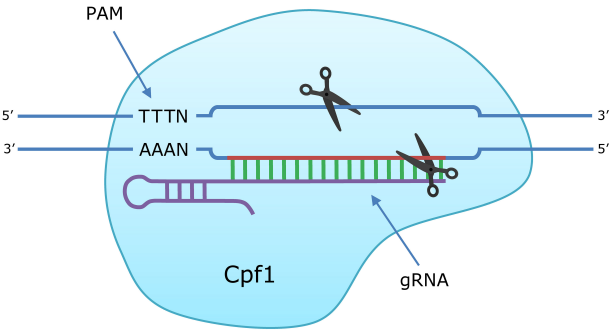

FIGURE 1 | Introduction of a double stranded break (DSB) in DNA by CRISPR/Cas12a (Cpf1). The guide RNA (gRNA) directs the Cas12a endonuclease to the homologous target sequence. When the protospacer-adjacent motif (PAM) is recognized and the crRNA hybridizes with the target sequence, the nuclease domains of Cas12a introduce breaks in each strand: 19 nt (target strand) and 23 nt (complementary strand) downstream from the PAM sequence.

To test whether the highly versatile CRISRP/Cas12a system could also edit the genome of marine sponge cells *in vitro*, we designed a single-stranded oligodeoxynucleotide (ssODN) construct with short homology arms (HA) (30–40 bp). Donor templates provided as ssODN mediate HDR more efficiently than their double-stranded (dsDNA) counterparts (Yoshimi et al., 2016; Ferenczi et al., 2017) and shorter ssODN constructs are more efficient than longer ssODNs (Okamoto et al., 2019). The HAs matched regions upstream (US) and downstream (DS) of the target site in the 3rd OAS1Ab exon and flanked a 108 bp scrambled DNA insert (**Figure 2A**), containing stop codons in all 3 reading frames. To test whether the CRISPR/Cas12a system could be used to overexpress a gene, we designed a construct

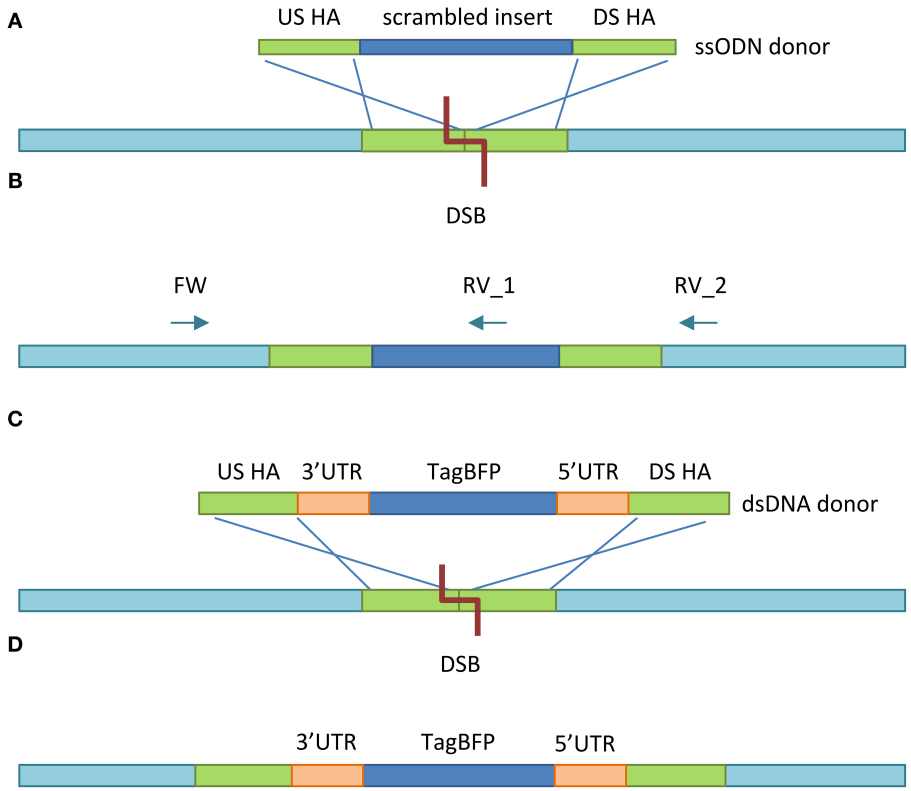

FIGURE 2 | Experimental design. **(A)** After Cas12a introduces the DSB at the target site, HDR takes place between the US HA and DS HA of the ssODN donor template and the homologous regions US and DS from the DSB. **(B)** The insert is incorporated between the US and DS homologous region. Two PCR reactions determine whether mutation was successful: (1) reverse primer 1 (RV_1) anneals inside of the insert, yielding a product of 910 bp, providing HDR took place. (2) Reverse primer 2 (RV_2) anneals to the wild type gene sequence, yielding a 1,025 bp (wild type) or 1,127 (mutant) product. Both reactions use the same forward (FW) primer. **(C)** As with the ssODN donor, the US and DS HA recombine with their homologous regions US and DS of the DSB made by Cas12a. **(D)** The TagBFP gene with 5′ and 3′ UTRs of the *S. domuncula* actin locus is inserted into the genome in reverse orientation.

containing blue fluorescent marker gene TagBFP (Subach et al., 2008). Using the promoter and terminators sequences of a highly expressed gene in the host organism can ensure a heterologous gene can be efficiently recognized by the host cells' transcription machinery. However, no full genome is yet available for *G. barretti*, and no complete sequences of *G. barretti* 5′ and 3′ untranslated regions (UTRs), containing promoters, and terminators, respectively, have been reported. Therefore, we used the 5′ and 3′ UTRs of the *Suberites domuncula* actin locus, which have previously been used to transiently express a fluorescent marker in *S. domuncula* explants (Revilla-I-Domingo et al., 2018; **Figure 2C**). For the same reason, the 2′,5′-oligoadenylate synthetase 1 (OAS1Ab) gene (Accession Number HQ644329.1) was targeted, of which a partial genomic DNA sequence was reported (Vallmann et al., 2011). While the function of OAS1Ab in sponges has not been determined, OAS genes in humans, can induce apoptosis in tumor cells (Mullan et al., 2005). Therefore, OAS1Ab could also be an interesting future target gene to immortalize sponge cells. Heterologous genes would ideally be inserted in non-coding regions between 2 genes, to avoid interfering with the function of host genes. However, since no such intergenic sequences were available, the TagBFP gene would be inserted in the 2nd OAS1Ab intron in reverse orientation (**Figure 2D**), to reduce interfering of the marker gene with the function of the OAS1Ab gene. The ∼2 kilobase (kb) dsDNA construct required longer HAs of 0.5–1 kb each (Zhang et al., 2017; Bier et al., 2018) and our design therefore featured a 533 bp US HA and 601 bp DS HA.

Expressing heterologous genes on plasmids in sponge cells has been a challenge in the past (Schippers, 2013). Therefore, pre-assembled ribonucleoprotein complexes (RNPs) of recombinant Cas12a protein and the guide RNA (gRNA) were used, rather than a plasmid encoding Cas12a and the gRNA. This method has been used to edit genes in mammalian cells (Hur et al., 2016; Liu et al., 2019a), zebrafish (Liu et al., 2019b), mouse embryos (Hur et al., 2016), and plants (Kim et al., 2017). Lipofection was used to deliver the Cas12a-gRNA complexes and donor construct, since this method has been used successfully to transfect sponge cells *in vitro* (Pomponi et al., 2007; Schippers, 2013). We confirmed that the scrambled DNA sequence was inserted by amplifying the region with polymerase chain reaction (PCR) (**Figure 2B**) and Sanger sequencing. Fluorescence microscopy was then used to verify that the TagBFP gene was inserted and expressed.

MATERIALS AND METHODS

Sampling, Dissociation, and Cryopreservation

The *G. barretti* individual used in this study was collected with a triangular dredge at 500 meter depth in the Norwegian fjords (59°58.8′′N 5°22.4′′E) and selected based on size (>15 cm^3) to ensure sufficient cells could be obtained. The sponge was placed in a bucket filled with sea water as swiftly as possible to minimize exposure to air and ice packs were added to the bucket to keep the sponge at low temperature during transport to the laboratory. Sponge cells were dissociated by squeezing small pieces of tissue through a sterile gauze into artificial sea water (ASW) (23.30 g/L NaCl, 10.20 g/L $MgCl_2$, 4.02 g/L Trizma HCl, 2.97 g/L Trizma Base, 1.1 g/L $CaCl_2$, and 1 g/L KCl in dH_2O, sterilized by filtering through a 0.22 μm mesh (Munroe et al., 2018, 2019). The cells were passed through a Falcon® 40 μm cell strainer (Corning, NY, USA), then centrifuged (300 × g, 5 min) and resuspended in ASW twice. The cells were diluted 100x in ASW and counted microscopically using a C-chip™, Neubauer improved disposable hemocytometer (INCYTO, Cheonan, Republic of Korea). Cells were centrifuged once more (300 × g, 5 min) and resuspended in a cryoprotectant solution composed of 10% fetal bovine serum (FBS) and 10% dimethyl sulfoxide (DMSO) in ASW (Pomponi et al., 1997; Mussino et al., 2013; Munroe et al., 2018) at ∼1.00E+08 cells/mL. Aliquots (1 mL) of this cell suspension in cryoprotectant, in Fisherbrand™ 1 mL cryogenic vials (Thermo Fisher Scientific, MA, USA) were cooled at 1°C per min to −80°C in a Mr. Frosty freezing container (Nalgene®, NY, USA).

Medium Preparation

M1 medium was prepared following the original protocol (Munroe et al., 2019). Medium 199 powder (Sigma Aldrich, MO, USA) was dissolved in dH_2O, then salts were added at concentrations like those in seawater, leading to a salinity of 33.5 ppt in M1, which is approximately the salinity of 35 ppt in seawater. The pH of the M1 medium (7.9) was also like that of seawater (8.1). Amino acids were added and the medium was sterilized by filtering through a 0.22 μm mesh. Finally, 30 μg/mL rifampicin (Sigma Aldrich) and 2.50 μg/mL amphotericin B (Sigma Aldrich) were added to control contamination by bacteria and fungi, respectively.

Cell Culture

Before cultures were inoculated, cryopreserved cells were thawed quickly in a water bath set at 50°C to prevent that cells would be damaged by ice crystals. The cells were washed twice with ASW by centrifuging at 300 × g for 5 min, removing the supernatant and resuspending them in 1 mL ASW. Next, cells were counted microscopically using disposable hemocytometers (C-chip™, Neubauer improved) to determine their concentration. M1 medium was inoculated at 3.00E+06 cells/mL in 12-well plates with 1 mL cell suspension per well. To passage the cells, cell concentrations were determined, and the cell suspension was diluted back to 3.00E+06 cells/mL with fresh M1 medium.

gRNA Design and *in vitro* Assay

The online tool CRISPOR® (CRISPOR v4.97, RRID:SCR_015935) (Concordet and Haeussler, 2018) was used to design 3 gRNAs targeting the 3rd exon and 2 gRNAs targeting the 2nd intron (**Supplementary Table 1**) in the genomic *G. barretti* OAS1Ab sequence (Accession Number HQ644329.1) and ordered as synthetic Cas12a gRNA oligonucleotides at Integrated DNA Technologies (Leuven, Belgium). The recombinant Cas12a enzyme (EnGen® Lba Cas12a, derived from *Lachnospiraceae* bacterium ND2006, New England Biolabs, MA, USA) contains a poly-histidine tag and was overexpressed in *Escherichia coli* and purified using immobilized metal affinity chromatography (IMAC) (Loughran and Walls, 2011). All 3 crRNAs were reconstituted with nuclease free water (NFW) to a concentration of 300 nM and then tested *in vitro* for their efficiency in cleaving a 1,025 bp PCR product amplified from *G. barretti* genomic DNA (gDNA) [see "Genomic DNA extraction and PCR" section for DNA extraction, PCR conditions and primers (RV-WT)] in complex with the Cas12a enzyme following the manufacturer's instructions. For each crRNA, 3 μL of 300 nM stock solution (final concentration 30 nM) was mixed with 1 μL of 1 μM stock of Cas12a enzyme (final concentration 33.3 nM) to allow the ribonucleoprotein (RNP) complexes to form. The mixture was incubated for 10 min at 37°C in 3 μL 10x NEBuffer 2.1 Reaction Buffer (New England Biolabs) diluted with 20 μL NFW. Subsequently, 3 μL of 30 nM DNA fragment stock solution (final concentration 3 nM) was added to the reaction mixture and incubated with the RNPs for 10 min at 37°C. The final reaction volume after adding the PCR product was 30 μL. Samples were incubated for 10 min with 20 ng/μL proteinase K (Thermo Fisher Scientific) to stop the reaction. Finally, 10 μL of the reaction mixture was run on a 2% agarose gel at 135 V for 50 min.

ssODN and dsDNA Donor Template Design

Homology-directed repair of DSBs requires a donor template with homology arms up- and downstream of the target site. Synthetic single-stranded oligodeoxynucleotides (ssODNs) were ordered from Integrated DNA Technologies, designed featuring 30–40 bp homology arms flanking a 108 bp scrambled DNA insert containing stop codons in all 3 reading frames (**Supplementary Table 1**). A plasmid containing the dsDNA donor template, consisting of the TagBFP gene with *S. domuncula* actin 5′ and 3′ UTRs in reverse orientation, flanked by the US (533 bp) and DS (601 bp) HA, was ordered from Integrated DNA Technologies (**Supplementary Figure 1**).

Lipofection

Cells of 1 individual of *G. barretti* were cultured in 12-well plates with 1 mL cell suspension/well, starting at a density of 3.00E+06 cells/mL in M1 medium and a temperature of 4°C (Conkling et al., 2019). The ssODNs were transfected together with the RNPs using Lipofectamine™ CRISPRMAX™ (Thermo Fisher Scientific). The TagBFP repair construct plasmid was introduced using Lipofectamine™ 3000 (Thermo Fisher Scientific), 10 min before the RNPs were added using Lipofectamine™ CRISPRMAX™. For each sample, 0.5 μg of

plasmid DNA and 5 μL of P3000™ reagent were added to 50 μL Opti-MEM™ I Reduced Serum Medium (Gibco™, Thermo Fisher Scientific) in a 1.5 mL Eppendorf tube, and 3 μL Lipofectamine™ 3000 in 50 μL Opti-MEM™ in a second tube. The contents of both tubes were mixed and incubated for 15 min at room temperature before the mixture was added dropwise to the sponge cells. RNPs were formed *in vitro* by preparing the following for each sample: 0.5 μg of gRNA E32 or I22, 2.5 μg of Cas12a, and 5 μL of Cas9 Plus™ Reagent in 50 μL Opti-MEM™ in 1 Eppendorf tube, and in another tube 3 μL of Lipofectamine® CRISPRMAX™ transfection reagent in 50 μL Opti-MEM™. The contents of both tubes were combined and incubated for 10 min at room temperature. For transfection with the 108 bp scrambled DNA construct, 0.5 μg ssODN was mixed in at this point, and the solution was then added dropwise to the cells. For TagBFP plasmid transfection, no DNA was added at this stage.

Genomic DNA Extraction and PCR

After 4 days of incubation, gDNA was obtained from transfected and non-transfected cells using the High Pure PCR Template Preparation Kit (Roche Life Science, Penzberg, Germany). Successfully mutated cells were detected using 2 PCR reactions (**Figure 2C**). Both reactions used the same forward primer (FW 5′-ATGGCTAGCCCAGGACTTAGG), while the reverse primer bound either downstream of the target site (RV-wild-type 5′-AACAATGTGGTGCACTCGAA) or inside the scrambled DNA insert (RV-mutant 5′-CTATCCCCACCCCCACATTC). The 1st reaction should always yield a product, either of 1,025 bp in the wild-type, or 1,127 bp in case of mutated cells. The 2nd reaction would only amplify a 910 bp product if some cells in the culture were successfully mutated. The PCR mixture consisted of 25 μL Q5® High-Fidelity 2X Master Mix (New England Biolabs), 2.5 μL of working solution (10 μM) of both primers and ∼20 ng of gDNA brought to a total reaction volume of 50 μL with MilliQ (MQ) water. PCR conditions were as follows: initial denaturation at 98°C for 15 s, followed by 35 cycles of denaturation at 98°C for 10 s, primer annealing at 59°C for 30 s, and extension at 72°C for 45 s, and final extension at 72°C for 10 min. Amplified products were purified using the DNA Clean and Concentrator-5 (capped) kit (Zymo Research, CA, USA) and eluted in a final volume of 10 μL MQ water. Product concentration in the purified samples was measured using NanoDrop™ One (Thermo Fisher Scientific). Approximately 1 μg of purified PCR product per sample was run on a 1% agarose gel at 70 V for 35 min, with 500 ng GeneRuler 1 kb DNA Ladder (Thermo Fisher Scientific) as a marker on both sides.

Mutation Analysis

To verify that the 108 bp scrambled DNA sequence was successfully inserted into the 3rd exon of the OAS1Ab gene, 15 ng purified PCR product per 100 bp length (∼140 ng for WT, ∼155 ng for M products) for each sample was sent to BaseClear for Sanger sequencing as Long run (up to 1,100 nt) Quick Shot Premix samples with 25 pmol primer in a total volume of 20 μL. Sequences were aligned using SnapGene® 4.3 (SnapGene, RRID:SCR_015052) and to compare sequences obtained through Sanger sequencing to the genomic DNA sequence of the *G. barretti* OAS1Ab gene (Accession Number HQ644329.1). The 4′,6-diamidino-2-phenylindole (DAPI) filter on an EVOS™ FL Auto Cell Imaging System (Thermo Fisher Scientific), was used to determine whether TagBFP was successfully inserted into the 2nd intron of the OAS1Ab gene and expressed by the cells.

RESULTS

gRNA Design and *in vitro* Assay

Synthetic gRNAs were designed for both target sites in the *G. barretti* OAS1Ab gene, 3 gRNAs targeted the 3rd exon and 2 gRNAs targeted the 2nd intron, as only 2 suitable target sequences for Cas12a were present in the intron that would leave space for >0.5 kb US and DS HAs (**Figure 3A**). An *in vitro* assay in which RNPs of Cas12a with each of the 5 gRNAs were added to a PCR product of the wild-type OAS1Ab gene was used to test how efficiently each gRNA could induce a DSB (**Figure 2B**, FW + RV primers). The same PCR product incubated with Cas12a but without a gRNA was used as a negative control (C). All 5 tested gRNAs induced cuts at their target sites (**Figure 3B**), but only exon 3 gRNA 2 (gRNA E32), and intron 2 gRNA 2 (gRNA I22) degraded all DNA present. We selected gRNA E32 and I22 to edit the *G. barretti* genome.

Knock-Out OAS1Ab

Geodia barretti cells were transfected with RNPs of Cas12a and gRNA E32 accompanied by the ssODN donor template to insert the 108 bp scrambled DNA sequence and disrupt the OAS1Ab gene. Whether transfected cells were successfully mutated was checked using 2 PCR reactions (**Figure 2B**). The 1st reaction should always yield an either 1,025 bp (wild-type) or 1,127 bp (mutant) product or both, while the 2nd reaction only amplified a 910 bp product if mutated cells were present in the culture. Both the mutant and wild-type PCR reactions amplified their respective products in 2 out of 3 (T1 + T2) transfected cell populations (**Figure 4A**), suggesting the 108 bp scrambled DNA sequence was inserted into the OAS1Ab gene. Only the 1,025 bp wild-type product was detected in PCR 1 of T1 and T2, suggesting that mutated genes were present in small numbers and therefore not amplified due to the majority of wild-type genes in the extracted gDNA. The 3rd transfection (T3) yielded the same results as the negative control of cells transfected with Cas12a and ssODN donor, but without the gRNA (C), where only the wild-type PCR amplified its 1,025 bp product (**Figure 4A**). Sanger sequencing results of the mutant PCR product aligned with the expected sequence (**Figure 4B**), confirming the OAS1Ab gene was successfully edited.

Expression TagBFP Marker Gene

To insert and overexpress the blue fluorescent TagBFP gene, *G. barretti* cells were first transfected with the plasmid containing the TagBFP repair construct (**Figure 2C**), then after 10 min transfected again with the RNPs of Cas12a and gRNA I22. Whether cells were expressing TagBFP was determined by fluorescence microscopy. Sporadic blue fluorescence was observed in cells transfected with RNPs and the TagBFP repair construct (**Figure 5**). No fluorescent sponge cells were

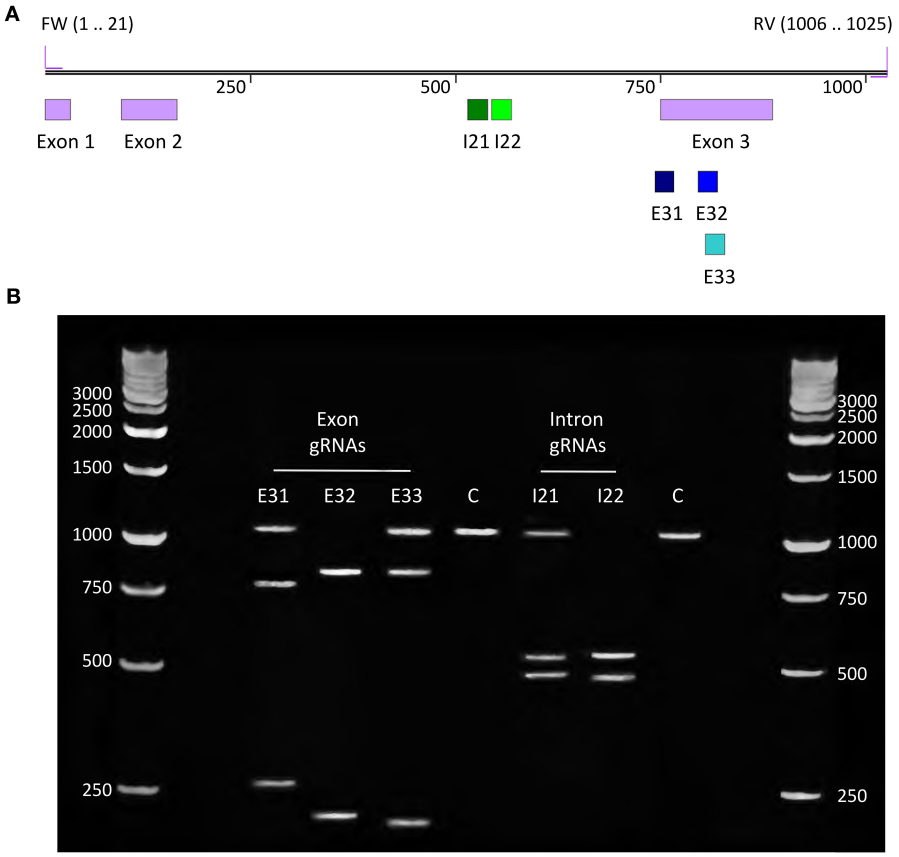

FIGURE 3 | gRNA design & *in vitro* assay. **(A)** Sequence map showing locations of gRNAs on the OAS1Ab wild-type PCR product of 1,025 bp. **(B)** Gel electrophoresis results of the *in vitro* assay to determine how efficiently 5 gRNAs can direct Cas12a to cleave their respective target sites in the 1,025 bp wild-type PCR product. Most gRNAs partially degraded the target DNA, resulting in 3 visible bands (the full-length PCR product and the 2 cleavage products). gRNA E32 and I22 fully degraded the DNA, leaving only their 2 cleavage products as visible bands, and these gRNAs were selected to edit the *G. barretti* OAS1Ab gene.

observed in controls transfected with the repair construct and Cas12a but without the gRNA. No clear PCR results were obtained, likely due to the low number of mutant compared to wild-type genes.

DISCUSSION

We previously reported that cells from several species of marine sponges divided rapidly in M1 medium and could be subcultured for several weeks (Conkling et al., 2019). Considering that proliferating cells are currently available for multiple species, the next step is to improve various characteristics of the cells using molecular tools, to create efficient production strains for sponge-derived biopharmaceuticals. For example, by increasing how many population doublings cells can reach to produce more biomass, activating or optimizing pathways that synthesize potential drug candidates, or improving energy efficiency and other traits. CRISPR/Cas systems are currently the most prominent and promising tools, with new applications being reported in rapid succession (Zhang et al., 2018, 2020; Moon et al., 2019; Li et al., 2020). In this study, we report the first successful use of a CRISPR/Cas system in marine sponges.

We demonstrated that CRISPR/Cas12a (Cpf1) can be used to target and edit sites in the *G. barretti* genome, and that sequences can be inserted at these sites through HDR. We disrupted the OAS1Ab gene in *G. barretti* cells by inserting a 108 bp scrambled DNA sequence with stop codons in all 3 reading frames, ensuring no functional protein could be synthesized. As more genome sequence data from sponges become available, the method presented here could be used to disrupt other targets, like well-known tumor-suppressor genes, but also metabolic genes to direct energy and carbon sources toward producing compounds of interest, or unknown genes to dissect their functions. The role of OAS1Ab in sponges has not yet been determined (Vallmann et al., 2011), but examining how knocking out this gene affects sponge cells in culture would shed light on this question. If OAS1Ab acts as a tumor suppressor in sponges, as OAS1 does in humans, disrupting it could help immortalize sponge cells. In this study, we did not observe increased lifespan in transfected cells. However, cell lines of *G. barretti* in M1 medium have a limited

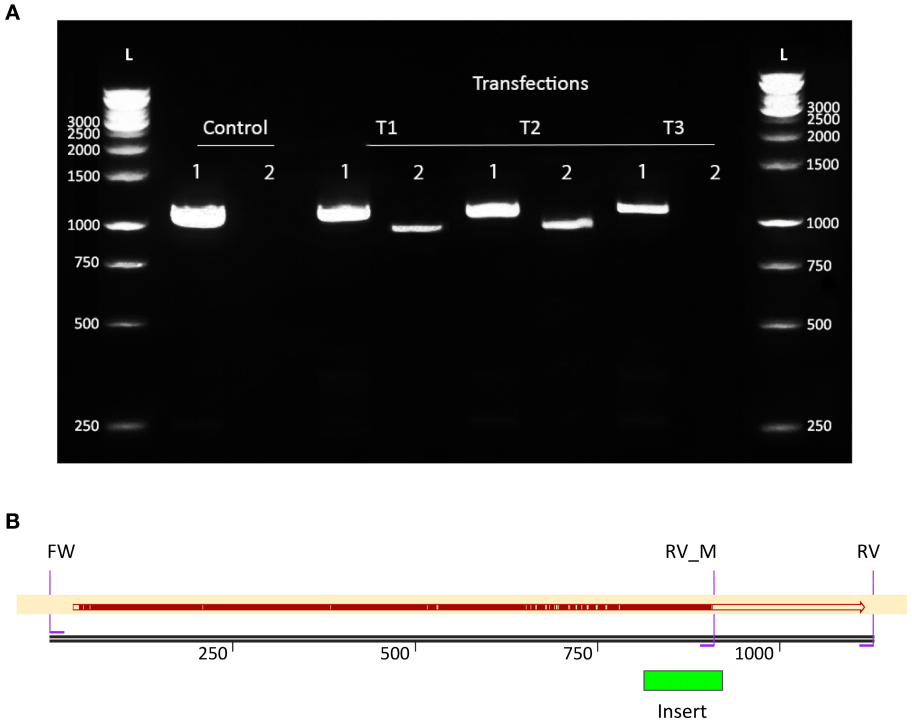

FIGURE 4 | PCR and sequencing results confirm that the scrambled DNA sequence was inserted in populations of transfected cells. **(A)** Results of 2 PCR reactions amplifying part of the OAS1Ab gene in DNA extracted from 3 transfected *G. barretti* cell populations (T1, 2 and 3). Both reactions used the same FW primer. PCR 1 used the wildtype RV primer and should always amplify a 1,025 bp (W) or 1,127 bp (M) product. PCR 2 contained the mutant RV (RV_M) primer and only yields a 910 bp product (M) if the gene was successfully edited. The control (C) contained DNA extracted from cells that were treated the same as T1–3, except that no gRNA was provided in the transfection. T1 and T2 both yielded the M product, indicating the 108 bp scrambled DNA sequence was inserted at the target site in some cells. **(B)** Alignment of the sequencing results of the 910 bp mutant product with the sequence expected if the OAS1Ab gene was successfully edited. Red indicates matching sequences, while yellow indicates gaps. Since the sequenced PCR product was obtained using PCR 2, the sequence between RV_M and RV was not present in the sequence read.

lifespan of maximum 7 population doublings with little variation between individuals (Conkling et al., 2019). As it is unlikely that cells from different individuals are approximately the same number of doublings away from senescence, it seems that M1 medium is not able to support more than 7 doublings, regardless of whether the cells are immortalized. The number of doublings reached by *G. barretti* cells in the further optimized successor of M1 medium (OpM1) that was developed in our group far exceeded 7 doublings (Hesp et al., unpublished). Knocking out OAS1Ab or other potential tumor-suppressor genes in *G. barretti* cells cultured in OpM1 medium could therefore still result in immortalization.

We transfected cells with reporter constructs encoding TagBFP flanked by the promoter and terminator regions of the *S. domuncula* actin locus (Revilla-I-Domingo et al., 2018). TagBFP-transfected cells did sporadically display bright blue fluorescence that was not observed in controls that were transfected with Cas12a and the TagBFP repair construct, but without the gRNA. This excludes the possibility that cells were expressing TagBFP from the donor plasmid and suggests that edited cells could express TagBFP at high levels, but the editing efficiency was extremely low. We attempted to quantify the number of blue fluorescent cells with flow cytometry. However, the number of fluorescent cells was too low, and although the number was higher in transfected cells than controls, the difference was not large enough to draw any conclusions (data

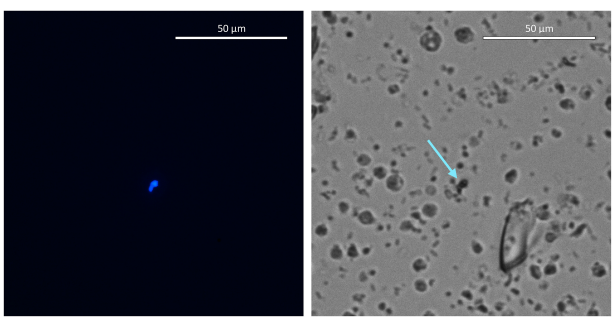

FIGURE 5 | Blue fluorescing cells in images taken with DAPI (Left) and transmitted light (Right) filters at 80x magnification. Arrow indicates the cells that fluoresce blue in the DAPI filter image.

not shown). It is possible that other marker genes would be expressed more efficiently, such as green fluorescent protein (Chalfie et al., 1994) or the deep-red fluorescent mCherry (Merzlyak et al., 2007). Another well-documented method to increase heterologous gene expression is optimizing the use of codons in the gene to match the codon usage bias in the host organism's genome (Angov, 2011). Such bias has been observed in the sponges *S. domuncula* (Perina et al., 2009) and *Geodia cydonium* (Gamulin et al., 2001), and could affect TagBFP expression in *G. barretti*. More efficient gene editing in *G. barretti* could be achieved by optimizing the lipofection protocol or increasing how efficiently cells can perform HDR with the donor template. Varying the length of the homology arms can greatly influence HDR efficiency (Shin et al., 2014; Song and Stieger, 2017), and recently a new promising method was developed, where the dsDNA template is provided on a plasmid, flanked by target sites for the same gRNA as will be used to edit the genome (Zhang et al., 2017; Kanca et al., 2019). Another option would be to select for cells expressing a marker gene that protects them from an otherwise lethal chemical, such as geneticin (G418) or hygromycin B (Santerre et al., 1984). Once larger constructs can be inserted more efficiently, this technique could be used to permanently overexpress oncogenes or genes in pathways synthesizing potential biopharmaceuticals to increase productivity.

Our results represent the first venture into genetically modifying marine sponge cells. We used a CRISPR/Cas12a system to target and accurately disrupt a specific gene in cultured *G. barretti* cells. CRISPR/Cas systems are versatile and have been used in many types of organisms, now including *G. barretti*, which bodes well for using the methods developed in this study in other sponge species. However, because sponge species and individuals often respond differently to certain treatments (Conkling et al., 2019), it is likely that methods will need to be optimized on a case-by-case basis. More research is needed to improve HDR efficiency in sponge cells, in particular for inserting longer constructs needed to express heterologous genes. Nevertheless, we have shown that CRISPR/Cas12a holds promise as a powerful tool in sponge cell culture and that it should be pursued further. Once the method has been fully established and optimized in *G. barretti* and other sponges, it can be used to study gene functions to better understand fundamental aspects of sponge biology, as well as change or improve how genes work in sponge cells for biotechnological applications. for example, to develop promising sponge-derived drug candidates that are either very complex and therefore expensive to chemically synthesize, or present in sponges at concentrations too low for wild harvest or aquaculture (Duckworth and Battershill, 2003; Sipkema et al., 2005; Duckworth, 2009), such as anti-tumor compounds halichondrin B (Hirata and Uemura, 1986) and peloruside A (West et al., 2000). However, since *in vitro* cell cultures are optimizable and scalable, they are an attractive alternative production platform for any sponge-derived compound, even ones produced by symbiotic bacteria, which could be cultured together with sponge cell strains optimized using CRISPR-Cas12a. By demonstrating that CRISPR/Cas12a can be used to edit the genome of *G. barretti* cells *in vitro*, we have taken another important step toward creating and improving sponge cell strains to produce sponge-derived pharmaceuticals in quantities that allow clinical trials and ultimately, treat disease in patients with novel, sponge-derived drugs.

DATA AVAILABILITY STATEMENT

The raw data supporting the conclusions of this article will be made available by the authors, without undue reservation.

AUTHOR CONTRIBUTIONS

KH conceived, designed, and conducted experiments, analyzed data, prepared figures for the paper, and wrote the paper. JF and A-MA conceived, designed, conducted experiments, and reviewed drafts of the paper. JvdL conceived and designed experiments, and reviewed drafts of the paper. DM conceived and designed experiments, analyzed data, contributed reagents, materials, analysis tools, and reviewed drafts of the paper. RW conceived and designed experiments, contributed reagents, materials, analysis tools, and reviewed drafts of the paper. SP conceived and designed experiments, collected the sponges, supervised the research, analyzed data, contributed reagents, materials, analysis tools, field expenses, and reviewed drafts of the paper. All authors contributed to the article and approved the submitted version.

FUNDING

DM, RW, and SP received funding from the European Union Horizon 2020 Project SponGES under Grant Agreement No. 679848.

ACKNOWLEDGMENTS

We gratefully remember Dr. Hans Tore Rapp (University of Bergen) and his unrelenting positivity and willingness to help us and other colleagues, for example by collecting and transporting *Geodia barretti* samples used in this study. May he rest in peace. We thank Mihris Naduthodi (Microbiology Department, Wageningen University & Research) for providing the Cas12a enzyme used in this study.

SUPPLEMENTARY MATERIAL

The Supplementary Material for this article can be found online at: https://www.frontiersin.org/articles/10.3389/fmars.2020.599825/full#supplementary-material

REFERENCES

Abdelmohsen, U. R., Balasubramanian, S., Oelschlaeger, T. A., Grkovic, T., Pham, N. B., Quinn, R. J., et al. (2017). Potential of marine natural products against drug-resistant fungal, viral, and parasitic infections. *Lancet Infect. Dis.* 17, 30–41. doi: 10.1016/S1473-3099(16)30323-1

Alcaraz, M. J., and Paya, M. (2006). Marine sponge metabolites for the control of inflammatory diseases. *Curr. Opin. Invest. Drugs* 7, 974–979.

Angov, E. (2011). Codon usage: nature's roadmap to expression and folding of proteins. *Biotechnol. J.* 6, 650–659. doi: 10.1002/biot.201000332

Balboa, E. M., Conde, E., Soto, M. L., Perez-Armada, L., and Dominguez, H. (2015). "Cosmetics from marine sources," in *Springer Handbook of Marine Biotechnology,* ed S. Kim *(Berlin*: *Springer)*, 1015–1042. doi: 10.1007/978-3-642-53971-8_44

Bier, E., Harrison, M. M., O'Connor-Giles, K. M., and Wildonger, J. (2018). Advances in engineering the fly genome with the CRISPR-cas system. *Genetics* 208, 1–18. doi: 10.1534/genetics.117.1113

Brummer, F., and Nickel, M. (2003). Sustainable use of marine resources: cultivation of sponges. *Prog. Mol. Subcell. Biol.* 37, 143–162. doi: 10.1007/978-3-642-55519-0_6

Carstens, B. B., Rosengren, K. J., Gunasekera, S., Schempp, S., Bohlin, L., Dahlstrom, M., et al. (2015). Isolation, characterization, and synthesis of the barrettides: disulfide-containing peptides from the marine sponge *Geodia barretti*. *J. Nat. Prod.* 78, 1886–1893. doi: 10.1021/acs.jnatprod.5b00210

Chalfie, M., Tu, Y., Euskirchen, G., Ward, W. W., and Prasher, D. C. (1994). Green fluorescent protein as a marker for gene expression. *Science* 263, 802–805. doi: 10.1126/science.8303295

Concordet, J., and Haeussler, M. (2018). CRISPOR: intuitive guide selection for CRISPR/Cas9 genome editing experiments and screens. *Nucleic Acids Res.* 46, 242–245. doi: 10.1093/nar/gky354

Conkling, M., Hesp, K., Munroe, S., Sandoval, K., Martens, D. E., Sipkema, D., et al. (2019). Breakthrough in marine invertebrate cell culture: sponge cells divide rapidly in improved nutrient medium. *Sci. Rep.* 9:17321. doi: 10.1038/s41598-019-53643-y

Di, X., Rouger, C., Hardardottir, I., Freysdottir, J., Molinski, T. F., Tasdemir, D., et al. (2018). 6-Bromoindole derivatives from the icelandic marine sponge *Geodia barretti*: isolation and anti-inflammatory activity. *Mar. Drugs* 16:437. doi: 10.3390/md16110437

Duckworth, A. (2009). Farming sponges to supply bioactive metabolites and bath sponges: a review. *Mar. Biotechnol.* 11, 669–679. doi: 10.1007/s10126-009-9213-2

Duckworth, A. R., and Battershill, C. (2003). Sponge aquaculture for the production of biologically active metabolites: the influence of farming protocols and environment. *Aquaculture* 221, 311–329. doi: 10.1016/S0044-8486(03)00070-X

Ferenczi, A., Pyott, D. E., Xipnitou, A., and Molnar, A. (2017). Efficient targeted DNA editing and replacement in *Chlamydomonas reinhardtii* using Cpf1 ribonucleoproteins and single-stranded DNA. *Proc. Natl. Acad. Sci. U.S.A.* 114, 13567–13572. doi: 10.1073/pnas.1710597114

Gamulin, V., Peden, J. F., Müller, I. M., Müller, W. E. G. (2001). Codon usage in the siliceous sponge *Geodia cydonium*: highly expressed genes in the simplest multicellular animals prefer C- and G-ending codons. *J. Zool. Syst. Evol. Res.* 39, 97–102. doi: 10.1046/j.1439-0469.2001.00163.x

Greco, G. R., and Cinquegrani, M. (2016). Firms plunge into the sea. *Marine biotechnology industry, a first investigation. Front. Mar. Sci.* 2:124. doi: 10.3389/fmars.2015.00124

Hedner, E., Sjögren, M., Hodzic, S., Andersson, R., Göransson, U., Jonsson, P. R., et al. (2008). Antifouling activity of a dibrominated cyclopeptide from the marine sponge *Geodia barretti*. *J. Nat. Prod.* 71, 330–333. doi: 10.1021/np0705209

Hirata, Y., and Uemura, D. (1986). Halichondrins - antitumor polyether macrolides from a marine sponge. *Pure Appl. Chem.* 58, 701–710. doi: 10.1351/pac198658050701

Horvath, P., and Barrangou, R. (2010). CRISPR/Cas, the immune system of bacteria and archaea. *Science* 327, 167–170. doi: 10.1126/science.1179555

Hur, J. K., Kim, K., Been, K. W., Baek, G., Ye, S., Hur, J. W., et al. (2016). Targeted mutagenesis in mice by electroporation of Cpf1 ribonucleoproteins. *Nat. Biotechnol.* 34, 807–808. doi: 10.1038/nbt.3596

Jimenez, P. C., Wilke, D. V., and Costa-Lotufo, L. V. (2018). Marine drugs for cancer: surfacing biotechnological innovations from the oceans. *Clinics* 73:e482s. doi: 10.6061/clinics/2018/e482s

Jinek, M., Chylinski, K., Fonfara, I., Hauer, M., Doudna, J. A., and Charpentier, E. (2012). A programmable dual-RNA-guided DNA endonuclease in adaptive bacterial immunity. *Science* 337, 816–821. doi: 10.1126/science.1225829

Kanca, O., Zirin, J., Garcia-Marques, J., Knight, S. M., Yang-Zhou, D., Amador, G., et al. (2019). An efficient CRISPR-based strategy to insert small and large fragments of DNA using short homology arms. *Elife* 8:e51539. doi: 10.7554/eLife.51539

Khalifa, S. A. M., Elias, N., Farag, M. A., Chen, L., Saeed, A., Hegazy, M. F., et al. (2019). Marine natural products: a source of novel anticancer drugs. *Mar. Drugs* 17:491. doi: 10.3390/md17090491

Kim, H., Kim, S. T., Ryu, J., Kang, B. C., Kim, J. S., and Kim, S. G. (2017). CRISPR/Cpf1-mediated DNA-free plant genome editing. *Nat. Commun.* 8:14406. doi: 10.1038/ncomms14406

Klitgaard, A. B., and Tendal, O. S. (2004). Distribution and species composition of mass occurrences of large-sized sponges in the northeast Atlantic. *Prog. Oceanogr.* 61, 57–98. doi: 10.1016/j.pocean.2004.06.002

Knudby, A., Kenchington, E., and Murillo, F. J. (2013). Modeling the distribution of *Geodia* sponges and sponge grounds in the Northwest Atlantic. *PLoS ONE* 8:e82306. doi: 10.1371/journal.pone.0082306

Laport, M. S., Santos, O. C., and Muricy, G. (2009). Marine sponges: potential sources of new antimicrobial drugs. *Curr. Pharm. Biotechnol.* 10, 86–105. doi: 10.2174/138920109787048625

Li, H., Yang, Y., Hong, W., Huang, M., Wu, M., and Zhao, X. (2020). Applications of genome editing technology in the targeted therapy of human diseases: mechanisms, advances and prospects. *Sig. Transduct. Targeted Ther.* 5:1. doi: 10.1038/s41392-019-0089-y

Lind, F. K., Hansen, E., Østerud, B., Eilertsen, K., Bayer, A., Engqvist, M., et al. (2013). Antioxidant and anti-inflammatory activities of barettin. *Mar. Drugs* 11, 2655–2666. doi: 10.3390/md11072655

Liu, M., El-Hossary, E. M., Oelschlaeger, T. A., Donia, M. S., Quinn, R. J., and Abdelmohsen, U. R. (2019a). Potential of marine natural products against drug-resistant bacterial infections. *Lancet Infect. Dis.* 19, e237–e245. doi: 10.1016/S1473-3099(18)30711-4

Liu, P., Luk, K., Shin, M., Idrizi, F., Kwok, S., Roscoe, B., et al. (2019b). Enhanced Cas12a editing in mammalian cells and zebrafish. *Nucleic Acids Res.* 47, 4169–4180. doi: 10.1093/nar/gkz184

Loughran, S. T., and Walls, D. (2011). Purification of poly-histidine-tagged proteins. *Methods Mol. Biol.* 681, 311–335. doi: 10.1007/978-1-60761-913-0_17

Mayer, A. M., Glaser, K. B., Cuevas, C., Jacobs, R. S., Kem, W., Little, R. D., et al. (2010). The odyssey of marine pharmaceuticals: a current pipeline perspective. *Trends Pharmacol. Sci.* 31, 255–265. doi: 10.1016/j.tips.2010.02.005

Merzlyak, E. M., Goedhart, J., Shcherbo, D., Bulina, M. E., Shcheglov, A. S., Fradkov, A. F., et al. (2007). Bright monomeric red fluorescent protein with an extended fluorescence lifetime. *Nat. Methods* 4, 555–557. doi: 10.1038/nmeth1062

Montaser, R., and Luesch, H. (2011). Marine natural products: a new wave of drugs? *Future Med. Chem.* 3, 1475–1489. doi: 10.4155/fmc.11.118

Moon, S. B., Kim, D. Y., Ko, J. H., and Kim, Y. S. (2019). Recent advances in the CRISPR genome editing tool set. *Exp. Mol. Med.* 51, 1–11. doi: 10.1038/s12276-019-0339-7

Mullan, P. B., Hosey, A. M., Buckley, N. E., Quinn, J. E., Kennedy, R. D., Johnston, P. G., et al. (2005). The 2,5 oligoadenylate synthetase/RNaseL pathway is a novel effector of BRCA1- and interferon-gamma-mediated apoptosis. *Oncogene* 24, 5492–5501. doi: 10.1038/sj.onc.1208698

Munroe, S., Sandoval, K., Martens, D. E., Sipkema, D., and Pomponi, S. A. (2019). Genetic algorithm as an optimization tool for the development of sponge cell culture media. *In vitro cellular & developmental biology. Animal* 55, 149–158. doi: 10.1007/s11626-018-00317-0

Munroe, S., Martens, D. E., Sipkema, D., and Pomponi, S. A. (2018). Comparison of cryopreservation techniques for cells of the marine sponge *Dysidea etheria*. *Cryo Lett.* 39, 269–278.

Murillo, F. J., Muñoz, P. D., Cristobo, J., Ríos, P., González, C., Kenchington, E., et al. (2012). Deep-sea sponge grounds of the flemish cap, flemish pass and the grand banks of newfoundland (Northwest Atlantic Ocean):

distribution and species composition. *Mar. Biol. Res.* 8, 842–854. doi: 10.1080/17451000.2012.682583

Mussino, F., Pozzolini, M., Valisano, L., Cerrano, C., Benatti, U., and Giovine, M. (2013). Primmorphs cryopreservation: a new method for long-time storage of sponge cells. *Mar. Biotechnol.* 15, 357–367. doi: 10.1007/s10126-012-9490-z

Newman, D. J., and Cragg, G. M. (2016). Drugs and drug candidates from marine sources: an assessment of the current "State of Play". *Planta Med.* 82, 775–789. doi: 10.1055/s-0042-101353

Nuijen, B., Bouma, M., Manada, C., Jimeno, J. M., Schellens, J. H., Bult, A., et al. (2000). Pharmaceutical development of anticancer agents derived from marine sources. *Anticancer. Drugs* 11, 793–811. doi: 10.1097/00001813-200011000-00003

Okamoto, S., Amaishi, Y., Maki, I., Enoki, T., and Mineno, J. (2019). Highly efficient genome editing for single-base substitutions using optimized ssODNs with Cas9-RNPs. *Sci. Rep.* 9:4811. doi: 10.1038/s41598-019-41121-4

Page, M. J., Northcote, P. T., Webb, V. L., Mackey, S., and Handley, S. J. (2005). Aquaculture trials for the production of biologically active metabolites in the New Zealand sponge *Mycale hentscheli* (Demospongiae: Poecilosclerida). *Aquaculture* 250, 256–269. doi: 10.1016/j.aquaculture.2005.04.069

Perina, D., Harcet, M., Mikoč, A., Vlahoviček, K., Müller, W. E. G., and Cetković, H. (2009). Highly expressed genes in marine sponge *Suberites domuncula* prefer C- and G-ending codons. *Food Technol. Biotechnol.* 47, 269–274.

Pomponi, S. A. (1999). The bioprocess-technological potential of the sea. *J. Biotechnol.* 70, 5–13. doi: 10.1016/S0079-6352(99)80092-7

Pomponi, S. A., Thompson, J., Bottesch, J., and Sennett, S. (2007). Methods for extending the life span of marine invertebrate cells. *US Patent.* Patent 2007/0254367 A1.

Pomponi, S. A., Willoughby, R., Kaighn, M. E., and Wright, A. E. (1997). "Development of techniques for in vitro production of bioactive natural products from marine sponges," in *Invertebrate Cell Culture: Novel Directions and Biotechnology Applications* (Science Publishers), 231–237.

Qi, S. H., and Ma, X. (2017). Antifouling compounds from marine invertebrates. *Mar. Drugs* 15:263. doi: 10.3390/md15090263

Revilla-I-Domingo, R., Schmidt, C., Zifko, C., and Raible, F. (2018). Establishment of transgenesis in the demosponge *Suberites domuncula*. *Genetics* 210, 435–443. doi: 10.1534/genetics.118.301121

Rinkevich, B. (2005). Marine invertebrate cell cultures: new millennium trends. *Mar. Biotechnol.* 7, 429–439. doi: 10.1007/s10126-004-0108-y

Safari, F., Zare, K., Negahdaripour, M., Barekati-Mowahed, M., and Ghasemi, Y. (2019). CRISPR Cpf1 proteins: structure, function and implications for genome editing. *Cell Biosci.* 9:36. doi: 10.1186/s13578-019-0298-7

Santerre, R. F., Allen, N. E., Hobbs, J. N. Jr., Rao, R. N., and Schmidt, R. J. (1984). Expression of prokaryotic genes for hygromycin B and G418 resistance as dominant-selection markers in mouse L cells. *Gene* 30, 147–156. doi: 10.1016/0378-1119(84)90115-X

Santhi, L. S., Talluri, V. S. S. L., P., and Nagendra, S. Y., Krishna, R.E. (2017). Bioactive compounds from marine sponge associates: antibiotics from bacillus sp. *Nat. Products Chem. Res.* 5, 1–5. doi: 10.4172/2329-6836.1000266

Schippers, K. J., Martens, D. E., Pomponi, S. A., and Wijffels, R. H. (2011). Cell cycle analysis of primary sponge cell cultures. *In vitro cellular* and *developmental biology. Animal* 47, 302–311. doi: 10.1007/s11626-011-9391-x

Schippers, K. J. (2013). *Sponge cell culture* (Ph.D. dissertation), Wageningen: Wageningen University & Research.

Schwartsmann, G., Da Rocha, A. B., Mattei, J., and Lopes, R. (2003). Marine-derived anticancer agents in clinical trials. *Expert Opin. Investig. Drugs* 12, 1367–1383. doi: 10.1517/13543784.12.8.1367

Shin, J., Chen, J., and Solnica-Krezel, L. (2014). Efficient homologous recombination-mediated genome engineering in zebrafish using TALE nucleases. *Development* 141, 3807–3818. doi: 10.1242/dev.108019

Singh, A., and Thakur, N. L. (2016). Significance of investigating allelopathic interactions of marine organisms in the discovery and development of cytotoxic compounds. *Chem. Biol. Interact.* 243, 135–147. doi: 10.1016/j.cbi.2015.09.009

Sipkema, D., Osinga, R., Schatton, W., Mendola, D., Tramper, J., and Wijffels, R. H. (2005). Large-scale production of pharmaceuticals by marine sponges: sea, cell, or synthesis? *Biotechnol. Bioeng.* 90, 201–222. doi: 10.1002/bit.20404

Sjogren, M., Goransson, U., Johnson, A. L., Dahlstrom, M., Andersson, R., Bergman, J., et al. (2004). Antifouling activity of brominated cyclopeptides from the marine sponge *Geodia barretti*. *J. Nat. Prod.* 67, 368–372. doi: 10.1021/np0302403

Song, F., and Stieger, K. (2017). Optimizing the DNA donor template for homology-directed repair of double-strand breaks. *Mol. Ther. Nucleic Acids* 7, 53–60. doi: 10.1016/j.omtn.2017.02.006

Subach, O. M., Gundorov, I. S., Yoshimura, M., Subach, F. V., Zhang, J., Gruenwald, D., et al. (2008). Conversion of red fluorescent protein into a bright blue probe. *Chem. Biol.* 15, 1116–1124. doi: 10.1016/j.chembiol.2008.08.006

Swarts, D. C., and Jinek, M. (2018). Cas9 versus Cas12a/Cpf1: structure-function comparisons and implications for genome editing. *Wiley Interdiscip. Rev. RNA* 9:e1481. doi: 10.1002/wrna.1481

Thoms, C., and Schupp, P. J. (2005). Biotechnological potential of marine sponges and their associated bacteria as producers of new pharmaceuticals (Part II). *J. Int. Biotechnol. Law* 86, 1506–1512. doi: 10.1515/jibl.2005.2.6.257

Vallmann, K., Aas, N., Reintamm, T., Lopp, A., Kuusksalu, A., and Kelve, M. (2011). Expressed 2-5A synthetase genes and pseudogenes in the marine sponge *Geodia barretti*. *Gene* 478, 42–49. doi: 10.1016/j.gene.2011.01.014

Wang, B., Pfeiffer, M. J., Schwarzer, C., Arauzo-Bravo, M. J., and Boiani, M. (2014). DNA replication is an integral part of the mouse oocyte's reprogramming machinery. *PLoS ONE* 9:e97199. doi: 10.1371/journal.pone.0097199

West, L. M., Northcote, P. T., and Battershill, C. N. (2000). Peloruside A: a potent cytotoxic macrolide isolated from the new zealand marine sponge *Mycale* sp. *J. Org. Chem.* 65, 445–449. doi: 10.1021/jo991296y

Yoshimi, K., Kunihiro, Y., Kaneko, T., Nagahora, H., Voigt, B., and Mashimo, T. (2016). ssODN-mediated knock-in with CRISPR-Cas for large genomic regions in zygotes. *Nat. Commun.* 7:10431. doi: 10.1038/ncomms10431

Zetsche, B., Gootenberg, J. S., Abudayyeh, O. O., Slaymaker, I. M., Makarova, K. S., Essletzbichler, P., et al. (2015). Cpf1 is a single RNA-guided endonuclease of a class 2 CRISPR-cas system. *Cell* 163, 759–771. doi: 10.1016/j.cell.2015.09.038

Zhang, C., Quan, R., and Wang, J. (2018). Development and application of CRISPR/Cas9 technologies in genomic editing. *Hum. Mol. Genet.* 27, R79–R88. doi: 10.1093/hmg/ddy120

Zhang, J. P., Li, X. L., Li, G. H., Chen, W., Arakaki, C., Botimer, G. D., et al. (2017). Efficient precise knockin with a double cut HDR donor after CRISPR/Cas9-mediated double-stranded DNA cleavage. *Genome Biol.* 18:35. doi: 10.1186/s13059-017-1164-8

Zhang, Y., Pribil, M., Palmgren, M., and Gao, C. (2020). A CRISPR way for accelerating improvement of food crops. *Nat. Food* 1, 200–205. doi: 10.1038/s43016-020-0051-8

Conflict of Interest: The authors declare that the research was conducted in the absence of any commercial or financial relationships that could be construed as a potential conflict of interest.

Copyright © 2020 Hesp, Flores Alvarez, Alexandru, van der Linden, Martens, Wijffels and Pomponi. This is an open-access article distributed under the terms of the Creative Commons Attribution License (CC BY). The use, distribution or reproduction in other forums is permitted, provided the original author(s) and the copyright owner(s) are credited and that the original publication in this journal is cited, in accordance with accepted academic practice. No use, distribution or reproduction is permitted which does not comply with these terms.

frontiers in Marine Science

ORIGINAL RESEARCH
published: 23 December 2020
doi: 10.3389/fmars.2020.605281

The First Cut Is the Deepest: Trawl Effects on a Deep-Sea Sponge Ground Are Pronounced Four Years on

*Katelin M. Morrison[1], Heidi Kristina Meyer[2], Emyr Martyn Roberts[2], Hans Tore Rapp[2], Ana Colaço[1] and Christopher Kim Pham[1]**

[1] Department of Oceanography and Fisheries, University of the Azores, Horta, Portugal, [2] Department of Biological Sciences and K.G. Jebsen Centre for Deep-Sea Research, University of Bergen, Bergen, Norway

Few studies have described the effects of physical disturbance and post-recovery of deep-sea benthic communities. Here, we explore the status of deep-sea sponge ground communities four years after being impacted by an experimental bottom trawl. The diversity and abundance of epibenthic megafauna of two distinct benthic communities in disturbed versus control areas were surveyed using a remotely operated vehicle on the Schulz Bank, Arctic Ocean. Four years after disturbance, megafaunal densities of the shallow (~600 m depth) and deep (~1,400 m depth) sites were significantly lower on the disturbed patches compared to the control areas. Multivariate analyses revealed a distinct separation between disturbed and control communities for both sites, with trawling causing 29–58% of the variation. Many epibenthic morphotypes were significantly impacted by the trawl, including ascidians, *Geodia parva*, Hexactinellida spp., *Craniella infrequens*, *Lissodendoryx complicata*, *Haliclonia* sp. *Stylocordyla borealis*, *Gersemia rubiformis* and *Actiniaria* sp. However, we found some smaller morphospecies to be equally abundant with control transects, including *Polymastia thielei*, *Geodia hentscheli*, and *Stelletta rhaphidiophora*, reflecting lower trawl impact for these morphotypes. Overall, our results suggest that these are fragile ecosystems that require much more time than four years to recover from physical disturbance typical of trawling activities.

Keywords: recovery, fishing, sponge ground, trawling, seamount, Arctic mid-ocean ridge, deep sea

OPEN ACCESS

Edited by:
Shirley A. Pomponi, Florida Atlantic University, United States

Reviewed by:
Malcolm Ross Clark, National Institute of Water and Atmospheric Research (NIWA), New Zealand
Ian David Tuck, National Institute of Water and Atmospheric Research (NIWA), New Zealand

****Correspondence:***
Christopher Kim Pham
christopher.k.pham@uac.pt

Specialty section:
This article was submitted to Deep-Sea Environments and Ecology, a section of the journal Frontiers in Marine Science

Received: *11 September 2020*
Accepted: *12 November 2020*
Published: *23 December 2020*

Citation:
Morrison KM, Meyer HK, Roberts EM, Rapp HT, Colaço A and Pham CK (2020) The First Cut Is the Deepest: Trawl Effects on a Deep-Sea Sponge Ground Are Pronounced Four Years on. Front. Mar. Sci. 7:605281. doi: 10.3389/fmars.2020.605281

INTRODUCTION

Under favorable environmental conditions, dense aggregations of large sponges form diverse structural habitats known as sponge grounds (Hogg et al., 2010). Sponge grounds are found globally at varying depths and physiographic features, like seamounts, oceanic ridges, continental slopes, and canyons (Howell et al., 2016; Maldonado et al., 2017; Roberts et al., 2018). It is poorly understood what drives the formation of these habitats, but it is known that their distribution relies on moderate water flow to supply nutrients and gases while inhibiting sedimentation (Vogel, 1974).

Sponge grounds serve many functional roles and can influence ecosystem functioning and community composition (Bell, 2008). In addition to being active filter feeders (Vogel, 1977; Yahel et al., 2007) and contributing to benthic-pelagic coupling (Maldonado et al., 2005; Pile and Young, 2006), sponges can alter their habitat and increase

local biodiversity (Kenchington et al., 2013; Hawkes et al., 2019). Sponges with siliceous spicules, especially glass sponges (Hexactinellida spp.) which shed large amounts of spicules, alter the sediment by forming dense spicule mats that can influence the distribution and diversity of epibenthic fauna (Barthel, 1992; Bett and Rice, 1992). As a result, sponge grounds tend to have more abundant and diverse community assemblages than habitats without sponges (Beazley et al., 2013). Many animals are associated with sponge grounds; fishes and invertebrates use them as an indirect food source (Kunzmann, 1996), shelter from predators (Kunzmann, 1996; Cook et al., 2008), spawning, and nursery grounds (Freese and Wing, 2003; Amsler et al., 2009).

Deep-sea sponge aggregations are included in the list of vulnerable marine ecosystems (VMEs) (FAO, 2009) because of their overall low resilience to disturbance and because they are threatened by deep-sea fisheries (OSPAR Commission, 2008). Epibenthic animals known to form complex structures emerging from the seabed including sponges are particularly vulnerable to bottom-contact fishing practices through direct and indirect effects (Clark et al., 2015). Direct effects include the removal of individuals as bycatch but also the damage, dislodgement and crushing caused by the motion of the trawl (Clark et al., 2015). As a result, many studies have observed a reduction in the abundance of epibenthic invertebrates in highly trawled locations (Freese et al., 1999; Fosså et al., 2002; Clark and Rowden, 2009). Furthermore, the removal of habitat forming organisms or structural engineers can lead to long-term changes in community structure and composition (e.g., Sköld et al., 2018). Such shifts have been particularly well documented in shelf communities (Kaiser et al., 2000), whereas in the deep sea, studies are scarcer due to the difficulty in finding comparable untrawled conditions (Goode et al., 2020). In addition to direct physical impacts, sponges can be affected by increased suspended sediments caused by bottom trawlers, even when trawling activity is performed kilometers away (Martín et al., 2014). While certain sponges can tolerate high levels of sedimentation (Bell et al., 2015), some studies found that increased turbidity can reduce the filtering rates (Grant et al., 2019) and compromises the survival of juveniles (Tjensvoll et al., 2013).

The loss of dense sponge aggregations is a detrimental outcome of bottom trawling because it can lead to a loss of ecosystem functioning and decreased biodiversity (Bell, 2008; Pusceddu et al., 2014). The time it takes for a community to recover to its pre-disturbed state depends on the degree of disturbance, the life history characteristics of the fauna, and management practices in place (Lotze et al., 2011; Clark et al., 2019). Most deep-sea organisms have life history characteristics making them particularly vulnerable to anthropogenic disturbances. For example, some cold-water corals have growth rates <1 mm per year with life span exceeding 1,000 years (Roark et al., 2005, 2006, 2009; Carreiro-Silva et al., 2013). Therefore, recovery of deep-water assemblages from external disturbance events occurs extremely slowly and is predicted to take decades to centuries (Leys and Lauzon, 1998; Gatti, 2002; Young, 2003). Williams et al. (2010) studied benthic seamount communities in Australia and New Zealand and found that, due to the slow growth rates and high longevity of deep, structural invertebrates (notably the dominant cold-water corals), it would take decades (at least) for benthic community structure to return to a pre-disturbed state. Clark et al. (2019) also found that deep-sea benthic communities dominated by stony-corals on New Zealand seamounts were unable to recover from bottom trawling after 15 years.

Currently, there are no studies documenting recovery of deep-sea Arctic sponge grounds following disturbance. Information on the recovery of communities living in extreme environments are relevant for understanding the impacts of anthropogenic activities but also to increase our knowledge of the ecological processes of sponge communities. The Schulz Bank, an Arctic seamount, is an ideal case study because it is a pristine sponge-dominated community that remains untouched by direct human activities. Here, we used video surveys collected 4 years after experimental trawls on the summit and on a deeper area of the Schulz Bank to understand the recovery potential of this highly productive seamount after disturbance events. Specifically, we compare the taxonomic composition and abundance of sponges and associated fauna within disturbed areas to nearby control sites.

MATERIALS AND METHODS

Study Area

This study was conducted on the Schulz Bank, a seamount on the Arctic Mid-Ocean Ridge (AMOR) located at the nominal junction between the Mohn and Knipovich Ridges, which separate the Greenland and Lofoten Basins (**Figure 1**). The summit of Schulz Bank is the richest area of the bank with a

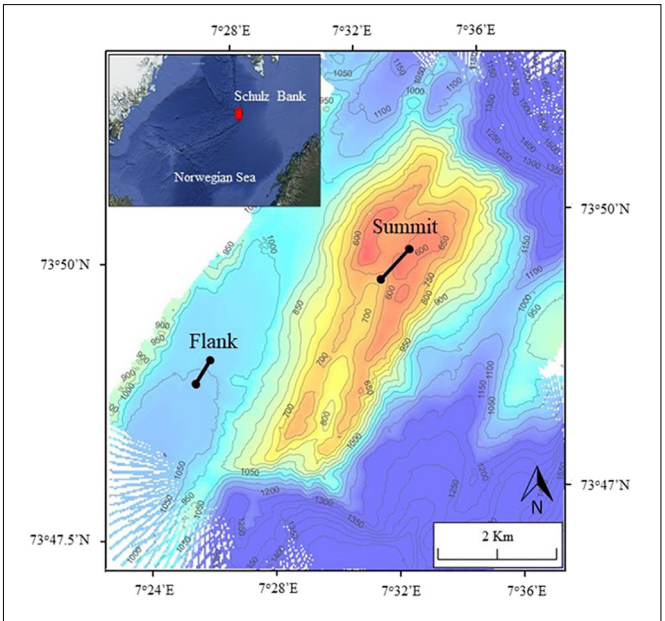

FIGURE 1 | Map of Schulz Bank showing the two Agassiz trawl marks made in 2014. Control transects are located 50 m to the west and east of each trawl mark. The red box in the overview panel highlights the location of Schulz Bank.

diverse and dense benthic community (Roberts et al., 2018; Meyer et al., 2019). As depth increases, species density and richness decreases (Roberts et al., 2018).

Study Design and Data Collection

In 2014, two experimental Agassiz trawls were conducted on the Schulz Bank (**Figure 1**); one at the summit (568–670 m depth) and one on the southwestern flank (1,464 m depth). The 3-m-wide Agassiz trawl, with a 1 cm mesh size in the cod-end (**Figure 2**), was towed along the seafloor for 676 m on the summit and 441 m on the flank, resulting in a disturbed area of 2,028 and 1,323 m^2, for the summit and flank, respectively. Towing speed was maintained at around 2 knots and the initial and final position were recorded.

Although we do not have visual information on the communities inhabiting that specific patch prior to trawling, the densities estimated from the trawl catches suggested that most morphospecies were present in comparable densities compared to neighboring areas (Rapp, H.T, unpublished data). This is further corroborated by the study of Meyer et al. (2019) who found that the distribution of the benthic community in the area is sufficiently homogenous for our purposes.

In August 2018, the two trawl marks and four additional control transects (one on either side of the trawl mark) were surveyed while onboard the *R/V G.O.Sars* (**Table 1**). Video recordings were taken along the trawl marks and control transects with the *ROV AEGIR6000*. Control transects were located 50 m to the east and west of each trawl mark and were performed parallel to the mark. Prior to the collection of video footage, we performed various transects in order to carefully map the trawl marks using the high resolution multibeam mounted on the remotely operated vehicle (ROV). In addition, scrape marks were clearly visible on both sides of the Agassiz trawl transect line, which helped the ROV pilots maintaining the transects.

The ROV was equipped with two high-definition HD video cameras (Imenco Spinner Shark Camera HD-SDI camera,

FIGURE 2 | Agassiz trawl used to create physical disturbance on the Schulz Bank.

TABLE 1 | Details of the 2018 imagery transects recorded on Schulz Bank.

Transect	Start (°N/°E) End (°N/°E)	Avg. depth (m)	Transect area (m^2)	Images used	Sampling units	Avg. sampling unit size (m^2)	Total area covered (m^2)	Transect coverage (%)
Summit (August 1, 2018)								
West	73.8263/7.5376	609 (31)	2082	72	18	16.0 (1.5)	287	13.8%
	73.8304/7.5545							
East	73.8303/7.5555	590 (31)	2043	27	8	14.3 (1.4)	114	5.6%
	73.8261/7.5395							
Trawl	73.8262/7.5384	605 (31)	2040	64	15	14.8 (1.5)	223	10.9%
	73.8303/7.5547							
Flank (August 4, 2018)								
West	73.8159/7.4430	1464 (0.1)	1477	n/a	10	150 (0.2)	1477	100%
	73.8125/7.4340							
East	73.8125/7.4352	1464 (0.1)	1417	n/a	9	150 (0.3)	1417	100%
	73.8157/7.4437							
Trawl	73.8126/7.4349	1464 (0.1)	1323	n/a	9	150 (0.3)	1323	100%
	73.8158/7.4433							

"Images used" shows total numbers of photographs with acceptable quality and covering an area in the 1.5 to 6 m^2 range for the summit. Standard deviations are shown in parentheses.

1080p/720p). Only the downward looking camera was used for quantitative ecological data. Two parallel lasers were used as scale (16 cm apart). The ROV was equipped with both ultra-short baseline navigation to provide absolute global position (accuracy approximately ±10 m), and Doppler velocity log navigation (LINKQUEST Doppler log) to provide very accurate relative position (±0.1 m). During every transect the ROV was run in a straight line, on a set bearing, at a constant speed and at the same set altitude (2–3 m).

Image and Video Analysis

From the summit transects, we extracted 287 randomly selected, non-overlapping images (at least 5 m apart). Seafloor images were excluded if (1) the area of the image was less than 1.5 m^2 or greater than 6 m^2, (2) laser dots were not visible, or (3) the image was obscured by suspended sediment. From the summit, after excluding unusable images, a total of 163 images were used.

All discernable epibenthic megafauna (hereafter referred to as "morphospecies") greater than 1 cm were counted and identified to the lowest possible taxonomic level in each frame. Fauna that could not be identified to genus or species level were grouped by their size. Unidentifiable demosponges smaller than 10 cm were grouped as "small demosponges," those between 10 and 20 cm were grouped as "medium demosponges," and those greater than 20 cm were grouped as "large demosponges." *Schaudinnia rosea*, *Trichasterina borealis*, and *Scyphidium septentrionale* were grouped as "Hexactinellida spp." (Meyer et al., 2019). Hexactinellids smaller than 10 cm were grouped as "small Hexactinellida spp."

For each image, we also measured image area, percent coverage of different substrate types (soft substrate, hard substrate, and spicule mat), and percent coverage of *Lissodendoryx complicata* which could not be distinguished by individuals, using a grid in IMAGEJ software. Substrate types and fauna were counted in each grid cell and divided by the total number of cells and multiplied by 100 to get percent coverage. Percent coverage of *Hexadella dedritifera*, an encrusting sponge, was recorded as part of a subsample.

A subsample of 46 random frames taken from our summit samples was used to count highly abundant fauna (Ascidiacea sp. 1 and *H. dedritifera*), and to assess the sizes (cm^2) of the five largest sponge morphospecies on the summit (*Geodia parva*, *Stelletta rhaphidiophora*, "large demosponges," Hexactinellida spp. and *Hemigellius* sp.).

Single photographs do not represent adequate sampling units because the area of one image is too small to represent benthic communities (Durden et al., 2016). To better represent the community, we chose a desired area based on species accumulation curves (**Figure 3**) using the "Vegan" package in R statistical software (version 4.0.2; R Core Team, 2017). Data from multiple consecutive images were pooled into "sampling units" that covered segments of transect close to the desired area (ranging between 12.23 and 18.54 m^2) (**Table 1**). In our analyses, "sampling units" have been treated as replicates.

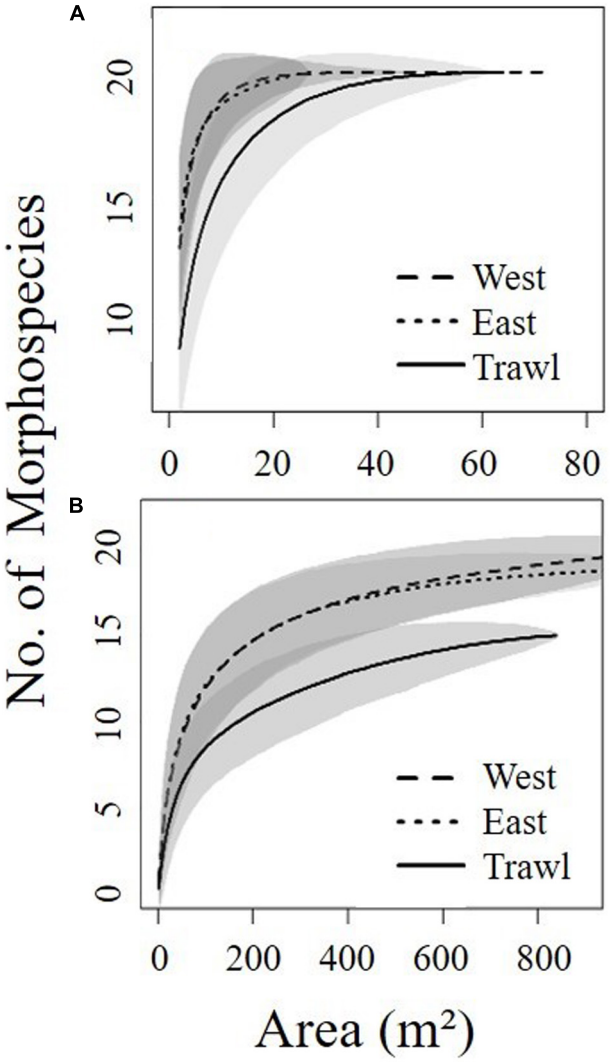

FIGURE 3 | Species accumulation curves for each site determined from seafloor area coverage of the summit **(A)** and the flank **(B)** of Schulz Bank. Shaded areas represent 95% confidence intervals. Curves were made using the species accumulation "random" method in "Vegan" package in R statistical software.

The benthic community found in the deeper area was less dense and patchier, therefore we chose to do continuous annotation of the entire transects to quantify sponges and associated fauna to ensure appropriate coverage. We used OFOP software (Ocean Floor Observation Protocol 3.3.7e) (Huetten and Greinert, 2008) to annotate all observations from the three flank transects. Like the summit, all taxa greater than 1 cm were counted and identified to the lowest possible taxonomic level. Accumulation curves (**Figure 3**) suggested that the observations would be grouped into 28 replicate video segments covering 150 m^2 "sampling units" (**Table 1**). In addition, a subsample of 142 random frames was taken to count ophiuroids, which were highly abundant.

Data Analysis

For each sampling unit, we computed total morphospecies density (individuals m^{-2}) and individual morphospecies densities.

Fishes were excluded from analyses due to their high mobility and, to focus on more abundant and reliably sampled taxa, only data from morphospecies observed at least three times were included in analyses (excluding 20 morphospecies on the summit and 8 on the flank). On the summit 23 morphospecies were used. On the flank 19 morphospecies were used (**Supplementary Table 1**). Sponge morphospecies were designated as "structural" following ICES (2009) and Beazley et al. (2013). Non-structural sponges and other invertebrates were designated as "associated fauna." These included sessile cnidarians, echinoderms, ascidians, and encrusting sponges.

To compare the diversity of morphospecies for each treatment (trawled and control transects), several diversity metrics were computed including number of different morphospecies present (S), Shannon diversity index (H'), Simpson's reciprocal diversity index (1-D), and evenness (J' and E) using the "Vegan" package in R software (Oksanen et al., 2013). We hypothesize that the communities on the trawled areas will have a lower number of morphospecies (S), Shannon diversity index (H') and Simpson's reciprocal diversity index (1-D). However, we expect that both measures of evenness (J' and E) will be higher inside the trawled areas compared to the control transects (**Table 6**).

To evaluate if there were significant differences in morphospecies densities and diversity indices between the different transects, we used either a one-way ANOVA following assumptions of normality or Kruskal–Wallis matched pairs test if normality was not met. Normality was tested using the Anderson–Darling normality test. To identify which treatments differed for each site, *post hoc* tests were performed (Tukey HSD for parametric and Dunn for non-parametric). Significance at the 5% level was reported.

For multivariate community analyses, Bray–Curtis metric was chosen for its capability in handling a large proportion of zeros. Matrices were used in non-metric multidimensional scaling (nMDS) to visualize differences in community composition among transects. The similarity matrices were compared statistically using permutational ANOVA (PERMANOVA, 999 permutations) with pair-wise tests to see statistically significant variations in community composition between treatments. The morphospecies contributing most to dissimilarity between groups were identified using Similarity Percentage (SIMPER) analysis.

Differences in substrate types and in the sizes of the five largest structural sponges between the control and trawled transects

TABLE 2 | Schulz Bank summit mean individuals m^{-2} (SE) of morphospecies and significance of the difference between transects.

	Summit densities (individuals m^{-2})			
Structural sponges	**West**	**East**	**Trawl**	**significance**
Small Hexactinellida spp.	0.16 (0.03)	0.18 (0.07)	0.06 (0.02)	*
Hexactinellida spp.	0.34 (0.06)	0.64 (0.19)	0.07 (0.03)	***
Geodia parva	0.59 (0.04)	0.26 (0.05)	0.12 (0.03)	***
Craniella infrequens	1.82 (0.09)	2.31 (0.37)	0.84 (0.11)	***
Polymastia thielei	0.06 (0.02)	0.04 (0.03)	0.02 (0.01)	•
Stylocordyla borealis	0.07 (0.02)	0.07 (0.04)	0.03 (0.01)	•
Haliclona sp.	0.05 (0.01)	0.09 (0.02)	0.01 (0.01)	***
Hemigellius sp.	0.14 (0.02)	0.13 (0.05)	0.03 (0.01)	**
Stelletta rhaphidiophora	0.45 (0.08)	0.43 (0.09)	0.21 (0.04)	•
Small demosponge	2.19 (0.15)	2.87 (0.32)	3.04 (0.37)	•
Medium demosponge	0.13 (0.03)	0.15 (0.04)	0.57 (0.14)	***
Unidentified demosponge 3	0.14 (0.04)	0.13 (0.03)	0.01 (0.01)	***
Large demosponge	0.17 (0.03)	0.25 (0.07)	0.17 (0.03)	•
Total	**6.25 (0.24)**	**7.54 (0.77)**	**5.18 (0.58)**	*
Associated fauna				
Unidentified demosponge 1	0.58 (0.06)	0.41 (0.06)	0.12 (0.04)	***
Unidentified demosponge 2	0.17 (0.03)	0.04 (0.02)	0.03 (0.02)	***
Gersemia rubiformis	3.52 (0.43)	3.40 (0.44)	1.34 (0.17)	***
Actiniaria sp.	16.74 (0.79)	14.16 (1.50)	6.08 (0.90)	***
Tylaster willei	0.04 (0.01)	0.11 (0.03)	0.02 (0.01)	**
Hymenaster sp.	0.03 (0.01)	0.01 (0.01)	0.02 (0.01)	•
Strongylocentrotus test	0.06 (0.02)	0.15 (0.04)	0.07 (0.01)	•
Ascidiacea sp. 1	6.91 (0.83)	8.24 (0.95)	2.97 (0.64)	***
Total	**28.05 (0.96)**	**26.52 (1.7)**	**10.65 (0.99)**	***

•$p > 0.05$. *$p \leq 0.05$. **$p \leq 0.01$. ***$p \leq 0.001$.

TABLE 3 | Schulz Bank flank mean individuals m^{-2} (SE) of morphospecies and significance of the difference between transects.

	Flank densities (individuals m^{-2})			
Structural sponges	**West**	**East**	**Trawl**	**significance**
Hexactinellida spp.	0.016 (0.006)	0.010 (0.003)	0.002 (0.002)	*
Geodia hentscheli	0.003 (0.002)	0.001 (0.001)	0	•
Craniella infrequens	0.049 (0.012)	0.041 (0.008)	0.024 (0.007)	•
Stylocordyla borealis	0.195 (0.055)	0.181 (0.041)	0.082 (0.016)	*
Lycopodina sp.	0.014 (0.003)	0.045 (0.009)	0.030 (0.006)	**
Haliclona sp.	0.003 (0.001)	0	0	*
Small demosponge	0.022 (0.004)	0.039 (0.007)	0.002 (0.002)	***
Medium demosponge	0.003 (0.002)	0.008 (0.003)	0.004 (0.004)	*
Large demosponge	0.006 (0.002)	0.007 (0.003)	0	*
Total	0.311 (0.058)	0.331 (0.051)	0.144 (0.022)	**
Associated fauna				
Actiniaria sp.	0.105 (0.010)	0.090 (0.011)	0.033 (0.006)	***
Umbellula sp.	0.002 (0.001)	0.001 (0.001)	0.001 (0.001)	•
Bythocaris sp.	0.017 (0.004)	0.010 (0.002)	0.010 (0.003)	•
Scalpellidae indet.	0.012 (0.006)	0.006 (0.003)	0.004 (0.001)	•
Feather star	0.001 (0.001)	0.002 (0.001)	0.001 (0.001)	•
Asteroidea sp.	0.040 (0.005)	0.027 (0.004)	0.047 (0.009)	•
Solaster sp.	0.002 (0.001)	0.002 (0.001)	0	•
Ophiuroid	7.905 (0.265)	9.551 (0.332)	7.352 (0.327)	***
Ascidiacea sp. 1	0.009 (0.003)	0.010 (0.003)	0.002 (0.002)	•
Ascidiacea sp. 2	0.007 (0.004)	0.006 (0.003)	0.001 (0.001)	•
Total	**8.105 (0.265)**	**9.706 (0.344)**	**7.456 (0.337)**	***

*•$p > 0.05$. *$p \leq 0.05$. **$p \leq 0.01$. ***$p \leq 0.001$.*

TABLE 4 | Characteristics of transects on Schulz Bank.

Site	Transect	Total average density (individuals m^{-2})	S mean (SE)	H′ mean (SE)	1-D mean (SE)	J′ mean (SE)	E mean (SE)
Summit	West	34.30	15.39 (0.49)	1.42 (0.03)	0.41 (0.01)	0.52 (0.01)	0.92 (0.03)
	East	34.06	15.88 (0.58)	1.55 (0.07)	0.35 (0.03)	0.56 (0.02)	1.10 (0.09)
	Trawl	15.83	12.20 (0.52)	1.52 (0.04)	0.32 (0.02)	0.61 (0.02)	1.30 (0.06)
Flank	West	8.42	11.70 (0.52)	1.84 (0.04)	0.24 (0.03)	0.75 (0.03)	1.93 (0.21)
	East	10.04	11.67 (0.60)	1.88 (0.08)	0.23 (0.03)	0.77 (0.03)	1.99 (0.18)
	Trawl	7.60	7.78 (0.40)	1.70 (0.04)	0.23 (0.01)	0.83 (0.02)	2.19 (0.10)

For each transect: density of total epibenthic megafauna, number of morphospecies present (S), Shannon Weaver diversity index (H′), Simpson's reciprocal index (1-D), Pielou's evenness (J′), and evenness derived from 1/D (E).

were assessed with one-way Kruskal–Wallis tests. Statistical analyses were performed using the computing environment R (version 4.0.2; R Core Team, 2017).

RESULTS

Epibenthic Megafaunal Density and Composition

The epibenthic megafaunal density and composition on the summit and flank of Schulz Bank were visually different (**Figure 4**). The average densities of morphospecies were significantly different between transects on both the summit and the flank (Summit: Kruskal–Wallis, chi-square = 24.76, df = 2, $p < 0.001$; Flank: Kruskal–Wallis, chi-square = 16.53, df = 2, $p < 0.001$). Pairwise comparisons using Dunn *post hoc* tests showed that the disturbed areas of both sites had significantly lower densities than both control areas (**Figure 5**).

On the summit, the average density of morphospecies (±SE) on the disturbed site was 12.86 ± 1.19 individuals m^{-2}, compared to 26.6 ± 1.27 in the control areas. On average (± SE), control sites had 6.90 ± 0.51 structural sponges m^{-2}, while trawled areas had an average of 5.18 ± 0.58 structural sponges m^{-2}. The most abundant structural sponges on the summit were "small demosponges" (40% of sponges), *Craniella infrequens* (24%), *G. parva* (6%), *S. rhaphidiophora* (5%), and Hexactinellida spp. (5%). Disturbed areas had significantly less Hexactinellida spp., *C. infrequens*, *Lissodendoryx complicata* (**Figure 6**), *Haliclonia* sp., and "unidentified demosponge 3" than both control areas (**Table 2**). For the associated fauna, on average (±SE), control areas had densities of 27.29 ± 1.33 individuals m^{-2}, while trawled areas had an average (±SE) of 10.65 ± 0.99 individuals m^{-2}.

TABLE 5 | Pairwise PERMANOVA and SIMPER results for densities on the Schulz Bank.

PERMANOVA		SIMPER (% contribution)				
Test	**R^2 (*P*-value)**	**#1**	**#2**	**#3**	**#4**	**#5**
Summit						
Trawl vs. West	0.58 (0.002)	*Actiniaria* sp. (27.4%)	*G. rubiformis* (5.5%)	Small demosponge (3.5%)	*C. infrequens* (2.6%)	*Demosponge 1* (1.2%)
Trawl vs. East	0.42 (0.002)	*Actiniaria* sp. (22.2%)	*G. rubiformis* (5.4%)	*C. infrequens* (4.1%)	Small demosponge (3.4%)	Hexactinellida spp. (1.6%)
Flank						
Trawl vs. West	0.29 (0.002)	*S. borealis* (14.3%)	*Actiniaria* sp. (10%)	*C. infrequens* (5%)	Asteroidea sp. (3.2%)	Small demosponge (2.9%)
Trawl vs. East	0.31 (0.002)	*S. borealis* (14.1%)	*Actiniaria* sp. (8.7%)	Small demosponge (5%)	*Lycopodina* sp. (3.6%)	Asteroidea sp. (3.6%)

"SIMPER (% contribution)" are ordered by importance (#1 being the most important morphospecies driving differences between transects).

TABLE 6 | Expected versus observed changes on the Schulz Bank.

		Summit		Flank	
		Expected Change	**Observed Change**	**Expected Change**	**Observed Change**
Density	**West v Trawl**	Decrease	Decrease	Decrease	Decrease
	East v Trawl	Decrease	Decrease	Decrease	Decrease
Taxonomic Richness (S)	**West v Trawl**	Decrease	Decrease	Decrease	Decrease
	East v Trawl	Decrease	Decrease	Decrease	Decrease
Diversity	**West v Trawl**	Decrease	Decrease	Decrease	No change
	East v Trawl	Decrease	No change	Decrease	No change
Evenness	**West v Trawl**	Increase	Increase	Increase	No change
	East v Trawl	Increase	Increase	Increase	No change
PERMANOVA	**West v Trawl**	Strong separation	Strong separation	Strong separation	Strong separation
	East v Trawl	Strong separation	Strong separation	Strong separation	Strong separation
Sizes of large sponges	**West v Trawl**	Smaller size	No change	N/A	N/A
	East v Trawl	Smaller size	No change	N/A	N/A
Substrate cover	**West v Trawl**	Less spicule mat	Less spicule mat	N/A	N/A
	East v Trawl	Less spicule mat	Less spicule mat	N/A	N/A

Changes are what we expected/observed to happen in trawl marks compared to the controls.

Trawled areas had significantly less "unknown demosponge 1," *G. rubiformis*, *Actiniaria* sp., and ascidians than both control areas (**Table 2**). The encrusting sponge *H. dedritifera* covered an average of 2% of the area covered on Control West transect but covered significantly less on Control East and trawled transects (**Figure 6**).

On the flank, the average density of morphospecies (excluding ophiuroids) on the disturbed site was 0.26 ± 0.02 individuals m^{-2} (±SE), compared to 0.52 ± 0.06 individuals m^{-2} (±SE) in the control areas. On average (±SE), control areas contained 0.32 ± 0.05 structural sponges m^{-2}, while trawled areas had an average (±SE) of 0.14 ± 0.02 structural sponges m^{-2}. Trawled areas had significantly less *S. borealis*, "small demosponges," and "large demosponges" than both control areas (**Table 3**). Control areas contained an average (±SE) of 8.91 ± 0.31 associated individuals m^{-2}, while trawled areas had an average (±SE) of 7.46 ± 0.34 associated individuals m^{-2}. The most abundant associated fauna was ophiuroids, which averaged 8.72 ± 0.30 individuals m^{-2} (±SE) in control areas and 7.35 ± 0.33 individuals m^{-2} (±SE) in trawled areas. Ophiuroids comprised 98% of all associated individuals, followed by *Actiniaria* sp. (1%). Trawled areas had significantly less *Actiniaria* sp. than both control areas (**Table 3**).

Taxonomic Richness and Diversity

Summit

The number of different morphospecies present (S) significantly differed between summit transects (Kruska—Wallis; chi-square = 17.01, df = 2, $p < 0.001$). There were significantly less morphospecies in the trawled area. On the summit, the trawled area had an average (±SE) of 12.20 ± 0.52 morphospecies present, while control areas had an average (±SE) of 15.65 ± 0.54 morphospecies present. Simpson's Diversity index (1-D) differed between summit transects

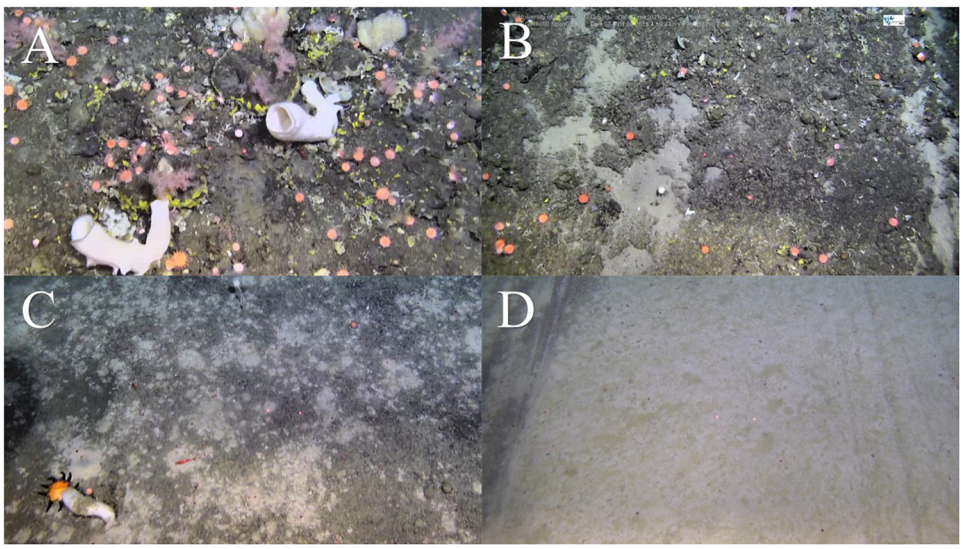

FIGURE 4 | Stills of the epibenthic communities on Schulz Bank; **(A)** summit control, **(B)** summit trawl mark (note the exposed soft sediment), **(C)** flank control, and **(D)** flank trawl mark.

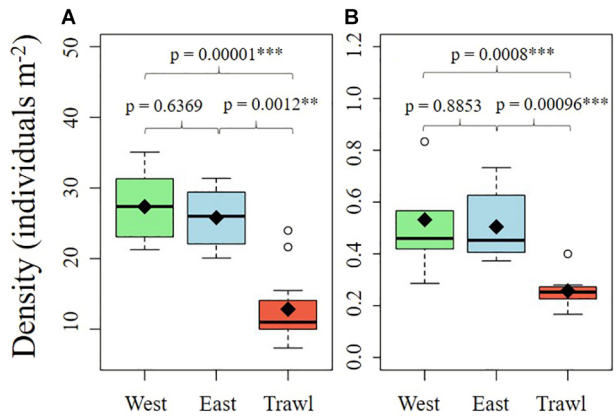

FIGURE 5 | Boxplots of the density of all megafauna found on the summit **(A)** and the flank **(B)** of Schulz Bank. Means are noted by diamond shapes.

(Kruskal–Wallis; chi-square = 12.61, df = 2, $p < 0.01$). In the trawl and Control East areas, there was a lower probability that two random individuals belonged to different morphospecies, indicating lower diversity than in the Control West area. Evenness (E) also differed between transects on the summit (Kruskal–Wallis; chi-square = 18.63, df = 2, $p < 0.001$). Trawling significantly increased the evenness of summit morphospecies (**Table 4**).

Flank

The number of different morphospecies present (S) significantly differed between transects on the flank (Kruskal–Wallis; chi-square = 16.66, df = 2, $p < 0.001$). There were fewer morphospecies within trawled areas. Control transects had an average (±SE) of 11.69 ± 0.56 morphospecies present while the trawled area had an average (±SE) of 7.78 ± 0.40 morphospecies present. Simpson's Diversity index (1-D) did not differ between flank transects (Kruskal–Wallis; chi-square = 1.07, df = 2, $p > 0.5$). Evenness (E) also did not differ between flank transects (Kruskal–Wallis; chi-square = 1.22, df = 2, $p > 0.5$). The morphospecies on the flank were more even than those on the summit (**Table 4**).

Multivariate Community Analyses

Summit

For the summit, the nMDS plot showed strong separation between megafaunal communities in trawled and control areas (**Figure 7**). Pairwise PERMANOVA tests revealed significant differences between the transects, with trawling explaining 42% of the variation between Control East and Trawl transects, and 58% of the variation between Control West and Trawl transects (**Table 5**). SIMPER results revealed that the dissimilarity in community composition between Control and Trawl transects was principally driven by *Actiniaria* sp., *G. rubiformis*, *C. infrequens*, "small demosponges," and Hexactinellida spp. (**Table 5**).

Flank

For the flank, the nMDS plot also showed a strong difference between megafaunal communities in trawled and control areas (**Figure 8**). Pairwise PERMANOVA tests revealed significant differences between transects, with trawling explaining about 30% of the variation between Control and Trawl transects (**Table 5**). On the flank, dissimilarity was driven by *S. borealis*, *Actiniaria* sp., *C. infrequens*, "small demosponges," *Lycopodina* sp., and Asteroidea sp. (**Table 5**).

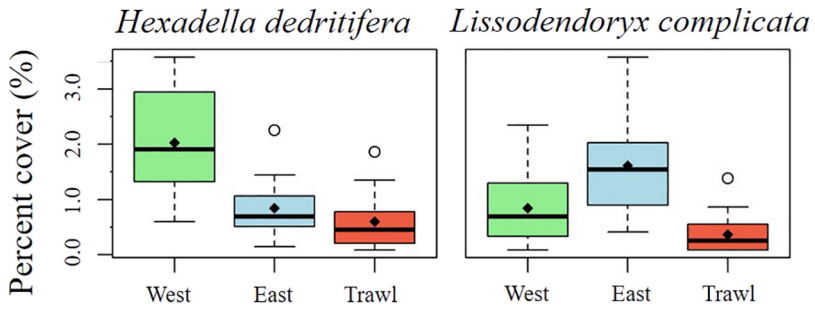

FIGURE 6 | Mean percentage cover of *H. dedritifera* and *L. complicata* on the summit of Schulz Bank.

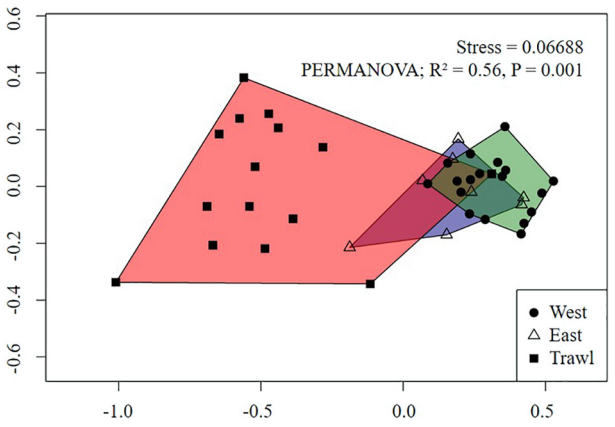

FIGURE 7 | Non-metric Multidimensional Scaling (nMDS) of replicate sampling units for each summit transect on Schulz Bank using Bray-Curtis dissimilarity metric. Each point represents a sampling unit and each polygon represents a transect. Morphospecies abundance values were standardized to individuals m^{-2}.

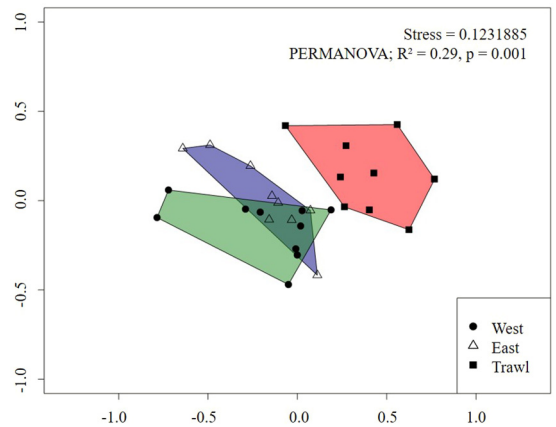

FIGURE 8 | Non-metric Multidimensional Scaling (nMDS) of replicate sampling units for each flank transect on Schulz Bank using Bray-Curtis dissimilarity metric. Each point represents a sampling unit and each polygon represents a transect. Morphospecies abundance values were standardized to individuals m^{-2}.

Size of Large Sponges

Overall, the sizes of the largest sponge morphospecies (*G. parva*, *Hemigellius* sp., Hexactinellida spp., "large demosponges," and *S. rhaphidiophora*) did not differ between control and trawled transects on the summit. However, Dunn *post hoc* tests did reveal that *G. parva* in Control East were significantly larger than those within the trawl mark, and *S. rhaphidiophora* in Control East were larger than those in both Control West and the trawl mark.

Substrate Cover

On the summit, substrate cover was significantly different between control and disturbed transects (Kruskal–Wallis; chi-square = 26.04, df = 2, $p < 0.001$). On the control sites, spicule mat dominated the substrate (99.5 and 100% of substrate), but on the disturbed site, there was significantly higher coverage of soft sediment. On the other hand, the flank had no significant differences in substrate type between the disturbed and control areas, being all exclusively composed of soft sediment.

DISCUSSION

This is the first study looking at recovery of Arctic sponge grounds following physical disturbance. Our results provide useful insight on how the diversity and megafaunal composition of sponge-dominated communities can be affected by anthropogenic activities like trawling. Overall, our results suggest that after four years, benthic communities within trawl marks have not returned to a pre-disturbed state (represented by the control transects) with overall densities of epibenthic morphospecies being significantly lower in the disturbed sites than in nearby control areas. One unavoidable limitation of this study was our lack of true replicates for both trawled areas, implying that are sampling units our essentially pseudo-replicates.

Although many structural sponge morphospecies found on the summit were significantly less abundant within the trawl mark than in control areas, we still observed some large sponges in the disturbed area (**Table 6**). It is likely that these individuals survived the Agassiz trawl in 2014 and are unlikely to be new growth since deep-sea sponges typically have slow growth

rates (Leys and Lauzon, 1998; Fallon et al., 2010). Fallon et al. (2010) found that Antarctic deep-sea hexactinellid sponges have extremely long life expectancies (∼440 years). Similarly, Leys and Lauzon found longevities of another deep-sea hexactinellid (*Rhabdocalyptus dawsoni*, Lamb 1892) to be over 200 years old. Bottom trawls are not 100% selective and occasionally bounce off the seabed, explaining the presence of such large individuals within the trawled area. Moran and Stephenson (2000) studied the effects of otter trawling on macrobenthic invertebrates (>20 cm) and found that a single trawl pass reduced density by only 15.5%. In a similar study, Wassenberg et al. (2002) quantified the direct effects of experimental bottom trawls on sponges and found that selectivity varied based on sponge morphology and size. They found that 30% of large (>500 mm high) globular sponges and 60% of large branched sponges survived trawling. Sainsbury et al. (1992) found that a single trawl pass removed 90% of large sponges. Looking at these studies, the catchability of large sponges by bottom trawls is highly variable, so it is not surprising that we found occasional large sponges in the disturbed area even though Agassiz trawls are among the most efficient types of trawls for sampling benthic communities. Another explanation for the presence of large sponges in the disturbed area comes from video observations obtained from a benthic lander on a Scotian Shelf sponge ground during severe hydrodynamic 'storm' events revealing that large Hexactinellid sponges can be dislodged and transported by currents (Hanz et al., 2020). The Schulz Bank summit is made dynamic by strong internal waves at the water mass boundary (Roberts et al., 2018) perhaps capable of rolling sponges around.

We observed a decrease in the density of many associated fauna in the disturbed area, either due to direct removal (Grassle, 1977; Clarke, 1982) or indirectly by the loss of biogenic habitat provided by the sponges (Klitgaard, 1995; Barrio Froján et al., 2012). Associated fauna have been demonstrated to be more abundant and diverse in and around large and structurally complex sponges compared to nearby areas without sponges (Wendt et al., 1985; Kunzmann, 1996). Sponges serve numerous functional roles which benefit other species (Bell, 2008; Buhl-Mortensen et al., 2010). Sessile invertebrates on the summit, which are abundant in control areas, like anthozoans and ascidians, were found in low abundances four years after disturbance, possibly due to the loss of preferred settlement substrate. On our summit trawl mark, where we found a significant reduction of spicule mat compared to control areas, a full recovery for many associated fauna and sponge species probably relies on sponge growth and formation of a dense spicule mat (Bett and Rice, 1992). Spicule mats likely take generations of sponges to accumulate and are known to influence macrofaunal community structure and diversity (Barrio Froján et al., 2012; Beazley et al., 2013). Roberts et al. (2018) suggested that the summit of Schulz Bank had provided suitable substrate for sponge settlement and, since initial recruitment, a 20 cm thick spicule mat has been deposited, which is also likely to be beneficial to the formation of a diverse benthic community. Because structure-forming sponges create important biogenic habitat, the loss of these large sponge species can lead to a decrease in biodiversity and changes in community structure (Tissot et al., 2006; Buhl-Mortensen et al., 2010; Beazley et al., 2013; Maldonado et al., 2017).

It is important to highlight that the observed differences in spicule mat cover between the disturbed site and control transects should also explain why we found some sponges at a higher or similar abundance inside the trawl mark compared to the control transects. Meyer et al. (2019) noted that demosponges within the spicule mat can appear hidden. Therefore, in such a dense community, it is likely that we were unable to detect all of the demosponges within the spicule mat, thus leading to underestimation of sponges in the control transects.

Overall, the flank has lower megafaunal density than the summit because as depth increases, the benefits brought by the water mass boundary and internal waves near the summit decrease (Roberts et al., 2018), however the effect of trawling was similar. Like the summit, four years after disturbance, epibenthic megafaunal densities on the flank were significantly lower within the trawl mark than in control areas. Compared to the summit, structural sponges on the flank seemed sparse, with only a few large sponges every 100 m^2 of seafloor. A closer look showed that the flank is dotted with many small structural sponges (e.g., *Stylocordyla borealis*, *C. infrequens*, *Lycopodina* sp.). Although this habitat is clearly less diverse and dense, it supports sponge species not seen (or rarely seen) on the summit, like *Lycopodina* sp. and *Geodia hentscheli*. Trawling significantly reduced the overall abundance of structural sponges at this site, where they will likely take decades to recover due to their life history traits (Leys and Lauzon, 1998; Gatti, 2002; Fallon et al., 2010). The most abundant sponge, *S. borealis*, has relatively slow growth rates with average individuals being about 10 years old and the oldest individuals reaching 170 years (Gatti, 2002).

As for associated fauna, the flank was covered with thousands of ophiuroids and, in lower densities, other morphospecies rarely seen on the summit, such as *Umbellula* sp., *Bythocaris* sp., and feather stars. The overall abundance of associated fauna on the deep flank was significantly reduced by trawling. But individually, only *Actiniaria* sp. continued to be affected by trawling four years later. The rest of the associated fauna remained unaffected by the trawl mark, whether this was due to a full recovery or avoidance of the Agassiz trawl is unknown. Mobile epifaunal invertebrates like sea stars and ophiuroids are less affected by trawling, and we did not see any recolonization by organisms taking advantage of the empty space as is sometimes reported for areas once disturbed by bottom contact fishing gear (Engel and Kvitek, 1998; Hixon and Tissot, 2007).

The effect of disturbance on each morphospecies varies depending on their individual selectivity by the gear, their size, resilience, and life history characteristics (Thrush and Dayton, 2002; Williams et al., 2010; Clark et al., 2015). Five years after fishery closures on Tasmanian seamounts, Althaus et al. (2009) saw no recovery in deep coral fauna but found that some resilient species had higher abundances than on actively trawled seamounts. Certain traits, such as small size, flexibility, and mass colonization potentially make some species resilient to physical disturbance (Clark et al., 2010). For example, on the summit, *S. borealis* did not significantly differ between trawl and control transects. *S. borealis* is a relatively small, stalked, and flexible species. Although not every individual morphospecies is

negatively affected in our study, we saw a clear difference between trawled and untrawled communities overall.

Few studies have investigated the recovery of large sponges after trawling. Van Dolah et al. (1987) found that one year after a single experimental trawl pass in a shallow, hard-bottom habitat, large sponges were able to recover greater than their pre-trawl densities. This is not the case in cold, deep-water systems; Malecha and Heifetz (2017) found that a single trawl pass continued to affect large sponges 13 years after disturbance in the Gulf of Alaska (200 m depth). Their trawled sites had 31.7% lower sponge densities and 58.8% higher rates of injury than in reference areas. Another study in Alaska by Rooper et al. (2011) used sponge catch data and logistic population models to estimate growth and recovery rates. They estimated that large deep-sea sponges would take between 13 and 36 years to recover 80% of their original biomass post trawling. These studies provide evidence for slow recovery of deep-sea sponge grounds following physical disturbance.

Our observations and the life history strategies typical of cold water, deep-sea fauna (Grassle and Sanders, 1973; Dayton, 1979; Clarke, 1980; Leys and Lauzon, 1998; Sarà et al., 2002; Young, 2003; Fallon et al., 2010) suggest that four years is not enough for a community on the Schulz Bank to recover from a trawling disturbance. Recovery of disturbed communities in these locations, especially on the summit, will likely take decades to centuries.

The amount and intensity of disturbance is an important factor influencing recovery. Multiple trawls through Schulz Bank sites would have likely caused greater damage to the communities, significantly delaying recovery, as seen in studies where the indirect effects of repeated trawling continue to influence deep benthic communities long after disturbance (Koslow et al., 2001; Althaus et al., 2009; Williams et al., 2010; Clark et al., 2019). In the present study, the small disturbed area benefited from a neighboring healthy benthic community, facilitating re-colonization, which is not the case for large fishing grounds, where pristine populations are located sometimes far away.

Overall, this study provides a quantitative snapshot of the status of a sponge-dominated community of the Arctic four years after being impacted by a bottom trawl and marks the beginning in following its recovery trajectory. This new information, which suggests a slow recovery rate, is important in promoting the conservation of this diverse and sensitive ecosystem. It also provides an evidence-based threat evaluation for a VME, of relevance for other sponge ground ecosystems of the deep sea. We encourage regular monitoring of the area to fully quantify and characterize complete recovery processes of this ecosystem. The remoteness and absence of direct human activities makes the area a perfect case-study for the understanding of recovery dynamics of deep-sea sponge ecosystems following impacts. Future studies would benefit from higher resolution cameras in combination with the collection of physical samples to enable the quantification of small, recently settled sponges.

DATA AVAILABILITY STATEMENT

The original contributions presented in the study are included in the article/**Supplementary Material**, further inquiries can be directed to the corresponding author.

AUTHOR CONTRIBUTIONS

CP and KM conceived and carried out the study. HM, ER, and HR advised on identification of species and analysis methods. KM analyzed the data, wrote the manuscript, and prepared the figures. All authors revised drafts of the manuscript and gave final approval for publication.

FUNDING

The work leading to this publication has received funding from the European Union's Horizon 2020 Research and Innovation Programme through the SponGES project (grant agreement No 679849). This document reflects only the authors' view and the Executive Agency for Small and Medium-sized Enterprises (EASME) is not responsible for any use that may be made of the information it contains.

ACKNOWLEDGMENTS

Thanks are due to the SponGES team for their guidance, advice on our study design, and help with epifaunal morphospecies identification in the image data. Thanks to the IMAR staff for providing office space and resources. And thanks to the G.O.Sars crew, AEGIR6000 crew, and science team that carried out the ROV surveys. Finally, we would like to dedicate this contribution to our friend and colleague Hans Tore Rapp.

SUPPLEMENTARY MATERIAL

The Supplementary Material for this article can be found online at: https://www.frontiersin.org/articles/10.3389/fmars.2020.605281/full#supplementary-material

REFERENCES

Althaus, F., Williams, A., Schlacher, T. A., Kloser, R. J., Green, M. A., Barker, B. A., et al. (2009). Impacts of bottom trawling on deep-coral ecosystems of seamounts are long-lasting. *Mar. Ecol. Prog. Ser.* 397, 279–294. doi: 10.3354/meps08248

Amsler, M. O., Mcclintock, J. B., Amsler, C. D., Angus, R. A., and Baker, B. J. (2009). An evaluation of sponge-associated amphipods from the Antarctic Peninsula. *Antarct. Sci.* 21, 579–589. doi: 10.1017/s0954102009990356

Barrio Froján, C. R., Bolam, S. G., Eggleton, J. D., and Mason, C. (2012). Large-scale faunal characterisation of marine benthic sedimentary habitats around the UK. *J. Sea Res.* 69, 53–65. doi: 10.1016/j.seares.2012.02.005

Barthel, D. (1992). Do hexactinellids structure Antarctic sponge associations? *Ophelia* 36, 111–118. doi: 10.1080/00785326.1992.10430362

Beazley, L. I., Kenchington, E. L., Murillo, F. J., and Sacau, M. D. M. (2013). Deep-sea sponge grounds enhance diversity and abundance of epibenthic megafauna in the Northwest Atlantic. *ICES J. Mar. Sci.* 70, 1471–1490. doi: 10.1093/icesjms/fst124

Bell, J. J. (2008). The functional roles of marine sponges. *Estuar.Coast. Shelf Sci.* 79, 341–353. doi: 10.1016/j.ecss.2008.05.002

Bell, J. J., McGrath, E., Biggerstaff, A., Bates, T., Bennett, H., Marlow, J., et al. (2015). Sediment impacts on marine sponges. *Mar. Pollut. Bull.* 94, 5–13. doi: 10.1016/j.marpolbul.2015.03.030

Bett, B. J., and Rice, A. L. (1992). The influenceof hexactinellid sponge (*Pheronema carpenteri*) spicules on the patchy distribution of macrobenthos in the Porcupine seabight (bathyal ne atlantic). *Ophelia* 36, 217–226. doi: 10.1080/00785326.1992.10430372

Buhl-Mortensen, L., Vanreusel, A., Gooday, A. J., Levin, L. A., Priede, I. G., Buhl-Mortensen, P., et al. (2010). Biological structures as a source of habitat heterogeneity and biodiversity on the deep ocean margins. *Mar. Ecol.* 31, 21–50. doi: 10.1111/j.1439-0485.2010.00359.x

Carreiro-Silva, M., Andrews, A. H., Braga-Henriques, A., De Matos, V., Porteiro, F. M., and Santos, R. S. (2013). Variability in growth rates of long-lived black coral *Leiopathes* sp. from the Azores. *Mar. Ecol. Prog. Ser.* 473, 189–199. doi: 10.3354/meps10052

Clark, M. R., Althaus, F., Schlacher, T. A., Williams, A., Bowden, D. A., and Rowden, A. A. (2015). The impacts of deep-sea fisheries on benthic communities: a review. *ICES J. Mar. Sci.* 73(Suppl._1), i51–i69.

Clark, M. R., Bowden, D. A., Rowden, A. A., and Stewart, R. (2019). Little evidence of benthic community resilience to bottom trawling on seamounts after 15 years. *Front. Mar. Sci.* 6:63. doi: 10.3389/fmars.2019.00063

Clark, M. R., and Rowden, A. A. (2009). Effect of deepwater trawling on the macro-invertebrate assemblages of seamounts on the Chatham Rise, New Zealand. *Deep Sea Res. Part I Oceanogr. Res. Pap.* 56, 1540–1554. doi: 10.1016/j.dsr.2009.04.015

Clark, M. R., Rowden, A. A., Schlacher, T., Williams, A., Consalvey, M., Stocks, K. I., et al. (2010). The ecology of seamounts: structure, function, and human impacts. *Annu. Rev. Mar. Sci.* 2, 253–278. doi: 10.1146/annurev-marine-120308-081109

Clarke, A. (1980). A reappraisal of the concept of metabolic cold adaptation in polar marine invertebrates. *Biol. J. Linn. Soc.* 14, 77–92. doi: 10.1111/j.1095-8312.1980.tb00099.x

Clarke, A. (1982). Temperature and embryonic development in polar marine invertebrates. *Int. J. Invertebr. Reprod.* 5, 71–82. doi: 10.1080/01651269.1982.10553456

Cook, S. E., Conway, K. W., and Burd, B. (2008). Status of the glass sponge reefs in the Georgia Basin. *Mar. Environ. Res.* 66, S80–S86.

Dayton, P. K. (1979). Observations of growth, dispersal and population dynamics of some sponges in McMurdo Sound. Antarctica. *Colloques Internationaux du CNRS* 291, 271–282.

Durden, J. M., Schoening, T., Althaus, F., Friedman, A., Garcia, R., Glover, A. G., et al. (2016). Perspectives in visual imaging for marine biology and ecology: from acquisition to understanding. *Oceanogr. Mar. Biol.* 54, 1–72. doi: 10.1201/9781315368597-2

Engel, J., and Kvitek, R. (1998). Effects of otter trawling on a benthic community in Monterey Bay National Marine Sanctuary. *Conserv. Biol.* 12, 1204–1214. doi: 10.1046/j.1523-1739.1998.0120061204.x

Fallon, S. J., James, K., Norman, R., Kelly, M., and Ellwood, M. J. (2010). A simple radiocarbon dating method for determining the age and growth rate of deep-sea sponges. *Nuclear Instrum. Methods Phys. Res. Sect. B Beam Interact. Mater. Atoms* 268, 1241–1243. doi: 10.1016/j.nimb.2009.10.143

FAO (2009). *International Guidelines for the Management of Deep-Sea Fisheries in the High Seas*. Rome: FAO.

Fosså, J. H., Mortensen, P. B., and Furevik, D. M. (2002). The deep-water coral Lophelia pertusa in Norwegian waters: distribution and fishery impacts. *Hydrobiologia* 471, 1–12.

Freese, J. L., and Wing, B. L. (2003). Juvenile red rockfish. *Sebastes* sp., associations with sponges in the Gulf of Alaska. *Mar. Fish. Rev.* 65, 38–42.

Freese, L., Auster, P. J., Heifetz, J., and Wing, B. L. (1999). Effects of trawling on seafloor habitat and associated invertebrate taxa in the Gulf of Alaska. *Mar. Ecol. Prog. Ser.* 182, 119–126. doi: 10.3354/meps182119

Gatti, S. (2002). The rôle of sponges in high-Antarctic carbon and silicon cycling-a modelling approach= Die Rolle der Schwämme im hochantarktischen Kohlenstoff-und Silikatkreislauf-ein Modellierungsansatz. *Berichte zur Polar Meeresforschung* 434:124.

Goode, S. L., Rowden, A. A., Bowden, D. A., and Clark, M. R. (2020). Resilience of seamount benthic communities to trawling disturbance. *Mar. Environ. Res.* 161:105086. doi: 10.1016/j.marenvres.2020.105086

Grant, N., Matveev, E., Kahn, A. S., Archer, S. K., Dunham, A., Bannister, R. J., et al. (2019). Effect of suspended sediments on the pumping rates of three species of glass sponge in situ. *Mar. Ecol. Prog. Ser.* 615, 79–100. doi: 10.3354/meps12939

Grassle, J. F. (1977). Slow recolonisation of deep-sea sediment. *Nature* 265, 618–619. doi: 10.1038/265618a0

Grassle, J. F., and Sanders, H. L. (1973). Life histories and the role of disturbance. *Deep Sea Res. Oceanogr. Abstracts* 20, 643–659. doi: 10.1016/0011-7471(73)90032-6

Hanz, U., Beazley, L. I., Kenchington, E., Duineveld, G., Rapp, H. T., and Mienis, F. (2020). Seasonal variability in near-bed environmental conditions in the *Vazella pourtalesii* glass sponge grounds of the Scotian Shelf. *Front. Marine Sci.*

Hawkes, N., Korabik, M., Beazley, L., Rapp, H. T., Xavier, J. R., and Kenchington, E. (2019). Glass sponge grounds on the scotian shelf and their associated biodiversity. *Mar. Ecol. Prog. Ser.* 614, 91–109. doi: 10.3354/meps12903

Hixon, M. A., and Tissot, B. N. (2007). Comparison of trawled vs untrawled mud seafloor assemblages of fishes and macroinvertebrates at Coquille Bank, Oregon. *J. Exp. Mar. Biol. Ecol.* 344, 23–34. doi: 10.1016/j.jembe.2006.12.026

Hogg, M. M., Tendal, O. S., Conway, K. W., Pomponi, S. A., van Soest, R. W. M., Gutt, J., et al. (2010). *Deep-sea Sponge Grounds: Reservoirs of Biodiversity*. UNEP-WCMC Biodiversity Series No. 32. Cambridge: UNEP-WCMC.

Howell, K. L., Piechaud, N., Downie, A. L., and Kenny, A. (2016). The distribution of deep-sea sponge aggregations in the North Atlantic and implications for their effective spatial management. *Deep Sea Res. Part I Oceanogr. Res. Pap.* 115, 309–320. doi: 10.1016/j.dsr.2016.07.005

Huetten, E., and Greinert, J. (2008). "Software controlled guidance, recording and postprocessing of seafloor observations by ROV and other towed devices: the software package OFOP," in *Geophysical Research Abstracts*, EGU2008-A-03088, EGU General Assembly 2008 (poster), Vol. 10, Vienna.

ICES (2009). Report of the ICES–NAFO Working Group on Deep-Water Ecology (WGDEC). ICES CM 2009ACOM:23, 94.

Kaiser, M. J., Ramsay, K., Richardson, C. A., Spence, F. E., and Brand, A. R. (2000). Chronic fishing disturbance has changed shelf sea benthic community structure. *J. Anim. Ecol.* 69, 494–503. doi: 10.1046/j.1365-2656.2000.00412.x

Kenchington, E., Power, D., and Koen-Alonso, M. (2013). Associations of demersal fish with sponge grounds on the continental slopes of the northwest Atlantic. *Mar. Ecol. Prog. Ser.* 477, 217–230. doi: 10.3354/meps10127

Klitgaard, A. B. (1995). The fauna associated with outer shelf and upper slope sponges (*Porifera*, *Demospongiae*) at the Faroe Islands, northeastern Atlantic. *Sarsia* 80, 1–22. doi: 10.1080/00364827.1995.10413574

Koslow, J. A., Gowlett-Holmes, K., Lowry, J. K., O'Hara, T., Poore, G. C. B., and Williams, A. (2001). Seamount benthic macrofauna off southern Tasmania: community structure and impacts of trawling. *Mar. Ecol. Prog. Ser.* 213, 111–125. doi: 10.3354/meps213111

Kunzmann, K. (1996). Associated fauna of selected sponges (*Hexactinellida* and *Demospongiae*) from the Weddell Sea, Antarctica. *Ber Polarforsch* 210, 1–93. doi: 10.11646/zootaxa.2136.1.1

Leys, S. P., and Lauzon, N. R. (1998). Hexactinellid sponge ecology: growth rates and seasonality in deep water sponges. *J. Exp. Mar. Biol. Ecol.* 230, 111–129. doi: 10.1016/s0022-0981(98)00088-4

Lotze, H. K., Coll, M., Magera, A. M., Ward-Paige, C., and Airoldi, L. (2011). Recovery of marine animal populations and ecosystems. *Trends Ecol. Evol.* 26, 595–605. doi: 10.1016/j.tree.2011.07.008

Maldonado, M., Aguilar, R., Bannister, R. J., Bell, J. J., Conway, K. W., Dayton, P. K., et al. (2017). "Sponge grounds as key marine habitats: a synthetic review of types, structure, functional roles, and conservation concerns," in *Marine Animal Forests: The Ecology of Benthic Biodiversity Hotspots*, eds L. Bramanti, A. Gori, C. Orejas, and S. Rossi (Berlin: Springer), 145–183. doi: 10.1007/978-3-319-21012-4_24

Maldonado, M., Carmona, M. C., Velásquez, Z., Puig, A., Cruzado, A., López, A., et al. (2005). Siliceous sponges as a silicon sink: an overlooked aspect of benthopelagic coupling in the marine silicon cycle. *Limnol. Oceanogr.* 50, 799–809. doi: 10.4319/lo.2005.50.3.0799

Malecha, P., and Heifetz, J. (2017). Long-term effects of bottom trawling on large sponges in the Gulf of Alaska. *Cont. Shelf Res.* 150, 18–26. doi: 10.1016/j.csr.2017.09.003

Martín, J., Puig, P., Masqué, P., Palanques, A., and Sánchez-Gómez, A. (2014). Impact of bottom trawling on deep-sea sediment properties along the flanks of a submarine canyon. *PLoS One* 9:e104536. doi: 10.1371/journal.pone.0104536

Meyer, H. K., Roberts, E. M., Rapp, H. T., and Davies, A. J. (2019). Spatial patterns of arctic sponge ground fauna and demersal fish are detectable in autonomous underwater vehicle (AUV) imagery. *Deep Sea Res.* 153:103137. doi: 10.1016/j.dsr.2019.103137

Moran, M. J., and Stephenson, P. C. (2000). Effects of otter trawling on macrobenthos and management of demersal scalefish fisheries on the continental shelf of north-western Australia. *ICES J. Mar. Sci.* 57, 510–516. doi: 10.1006/jmsc.2000.0718

Oksanen, J., Blanchet, G. G., Kindt, R., Legendre, P., Minchin, P. R., O'Hara, R. B., et al. (2013). *Package 'vegan'. Cran.Rproject.org.*

OSPAR Commission (2008). "OSPAR list of threatened and/or declining species and habitats (Reference Number: 2008-6)," in *OSPAR Convention For The Protection Of The Marine Environment Of The North-East Atlantic.*

Pile, A. J., and Young, C. M. (2006). The natural diet of a hexactinellid sponge: benthic–pelagic coupling in a deep-sea microbial food web. *Deep Sea Res. Part I Oceanogr. Res. Pap.* 53, 1148–1156. doi: 10.1016/j.dsr.2006.03.008

Pusceddu, A., Bianchelli, S., Martín, J., Puig, P., Palanques, A., Masqué, P., et al. (2014). Chronic and intensive bottom trawling impairs deep-sea biodiversity and ecosystem functioning. *Proc. Natl. Acad. Sci. U.S.A.* 111, 8861–8866. doi: 10.1073/pnas.1405454111

R Core Team (2017). *R: A Language and Environment for Statistical Computing.* Vienna: R Foundation for Statistical Computing.

Roark, E. B., Guilderson, T. P., Dunbar, R. B., Fallon, S. J., and Mucciarone, D. A. (2009). Extreme longevity in proteinaceous deep-sea corals. *Proc. Natl. Acad. Sci. U.S.A.* 106, 5204–5208. doi: 10.1073/pnas.0810875106

Roark, E. B., Guilderson, T. P., Dunbar, R. B., and Ingram, B. L. (2006). Radiocarbon-based ages and growth rates of Hawaiian deep-sea corals. *Mar. Ecol. Prog. Ser.* 327, 1–14. doi: 10.3354/meps327001

Roark, E. B., Guilderson, T. P., Flood-Page, S., Dunbar, R. B., Ingram, B. L., Fallon, S. J., et al. (2005). Radiocarbon-based ages and growth rates of bamboo corals from the Gulf of Alaska. *Geophys. Res. Lett.* 32:L04606.

Roberts, E. M., Mienis, F., Rapp, H. T., Hanz, U., Meyer, H. K., and Davies, A. J. (2018). Oceanographic setting and short-timescale environmental variability at an Arctic seamount sponge ground. *Deep Sea Res. Part I Oceanogr. Res. Pap.* 138, 98–113. doi: 10.1016/j.dsr.2018.06.007

Rooper, C. N., Wilkins, M. E., Rose, C. S., and Coon, C. (2011). Modeling the impacts of bottom trawling and the subsequent recovery rates of sponges and corals in the Aleutian Islands. Alaska. *Cont. Shelf Res.* 31, 1827–1834. doi: 10.1016/j.csr.2011.08.003

Sainsbury, K. J., Campbell, R. A., Whitelaw, W., and Hancock, D. A. (eds) (1992). "Effects of trawling on the marine habitat on the north west shelf of Australia and implications for sustainable fisheries management," in *Sustainable Fisheries Through Sustaining Fish Habitat, Aust. Fish Biol. Soc. Workshop*, (Canberra: Australian Government Publishing Service), 137–145.

Sarà, A., Cerrano, C., and Sarà, M. (2002). Viviparous development in the Antarctic sponge *Stylocordyla borealis* Loven, 1868. *Polar Biol.* 25, 425–431. doi: 10.1007/s00300-002-0360-4

Sköld, M., Göransson, P., Jonsson, P., Bastardie, F., Blomqvist, M., Agrenius, S., et al. (2018). Effects of chronic bottom trawling on soft-seafloor macrofauna in the Kattegat. *Mar. Ecol. Prog. Ser.* 586, 41–55. doi: 10.3354/meps12434

Thrush, S. F., and Dayton, P. K. (2002). Disturbance to marine benthic habitats by trawling and dredging: implications for marine biodiversity. *Annu. Rev. Ecol. Syst.* 33, 449–473. doi: 10.1146/annurev.ecolsys.33.010802.150515

Tissot, B. N., Yoklavich, M. M., Love, M. S., York, K., and Amend, M. (2006). Benthic invertebrates that form habitat on deep banks off southern California, with special reference to deep sea coral. *Fish. Bull.* 104, 167–181.

Tjensvoll, I., Kutti, T., Fosså, J. H., and Bannister, R. J. (2013). Rapid respiratory responses of the deep-water sponge Geodia barretti exposed to suspended sediments. *Aquat. Biol.* 19, 65–73. doi: 10.3354/ab00522

Van Dolah, R. F., Wendt, P. H., and Nicholson, N. (1987). Effects of a research trawl on a hard-bottom assemblage of sponges and corals. *Fish. Res.* 5, 39–54. doi: 10.1016/0165-7836(87)90014-2

Vogel, S. (1974). Current-induced flow through the sponge. Halichondria. *Biol. Bul.* 147, 443–456. doi: 10.2307/1540461

Vogel, S. (1977). Current-induced flow through living sponges in nature. *Proc. Natl. Acad. Sci. U.S.A.* 74, 2069–2071. doi: 10.1073/pnas.74.5.2069

Wassenberg, T. J., Dews, G., and Cook, S. D. (2002). The impact of fish trawls on megabenthos (sponges) on the north-west shelf of Australia. *Fish. Res.* 58, 141–151. doi: 10.1016/s0165-7836(01)00382-4

Wendt, P. H., Van Dolah, R. F., and O'Rourke, C. B. (1985). A comparative study of the invertebrate macrofauna associated with seven sponge and coral species collected from the South Atlantic Bight. *J. Elisha Mitchell Sci. Soc.* 101, 187–203.

Williams, A., Schlacher, T. A., Rowden, A. A., Althaus, F., Clark, M. R., Bowden, D. A., et al. (2010). Seamount megabenthic assemblages fail to recover from trawling impacts. *Mar. Ecol.* 31, 183–199. doi: 10.1111/j.1439-0485.2010.00385.x

Yahel, G., Whitney, F., Reiswig, H. M., Eerkes-Medrano, D. I., and Leys, S. P. (2007). In situ feeding and metabolism of glass sponges (*Hexactinellida*, *Porifera*) studied in a deep temperate fjord with a remotely operated submersible. *Limnol. Oceanogr.* 52, 428–440. doi: 10.4319/lo.2007.52.1.0428

Young, C. M. (2003). "Reproduction, development and life-history traits," in *Ecosystems of the World*, ed. P. A. Tyler (Amsterdam: Elsevier), 381.

Conflict of Interest: The authors declare that the research was conducted in the absence of any commercial or financial relationships that could be construed as a potential conflict of interest.

Copyright © 2020 Morrison, Meyer, Roberts, Rapp, Colaço and Pham. This is an open-access article distributed under the terms of the Creative Commons Attribution License (CC BY). The use, distribution or reproduction in other forums is permitted, provided the original author(s) and the copyright owner(s) are credited and that the original publication in this journal is cited, in accordance with accepted academic practice. No use, distribution or reproduction is permitted which does not comply with these terms.

frontiers in Marine Science

ORIGINAL RESEARCH
published: 08 January 2021
doi: 10.3389/fmars.2020.597682

Seasonal Variability in Near-bed Environmental Conditions in the *Vazella pourtalesii* Glass Sponge Grounds of the Scotian Shelf

Ulrike Hanz[1], Lindsay Beazley[2], Ellen Kenchington[2], Gerard Duineveld[1], Hans Tore Rapp[3†] and Furu Mienis[1]*

[1] Department of Ocean Systems, NIOZ Royal Netherlands Institute for Sea Research, Den Burg, Netherlands, [2] Fisheries and Oceans Canada (DFO), Bedford Institute of Oceanography, Dartmouth, NS, Canada, [3] Department of Biological Sciences and K.G. Jebsen Centre for Deep-sea Research, University of Bergen, Bergen, Norway

OPEN ACCESS

Edited by:
Chiara Romano, Center for Advanced Studies of Blanes (CEAB), Spanish National Research Council, Spain

Reviewed by:
Mar Flexas, California Institute of Technology, United States
Frine Cardone, Stazione Zoologica Anton Dohrn, Italy

***Correspondence:**
Ulrike Hanz
Ulrike.hanz@nioz.nl

† Deceased

Specialty section:
This article was submitted to Deep-Sea Environments and Ecology, a section of the journal Frontiers in Marine Science

Received: *21 August 2020*
Accepted: *10 December 2020*
Published: *08 January 2021*

Citation:
Hanz U, Beazley L, Kenchington E, Duineveld G, Rapp HT and Mienis F (2021) Seasonal Variability in Near-bed Environmental Conditions in the Vazella pourtalesii Glass Sponge Grounds of the Scotian Shelf. Front. Mar. Sci. 7:597682. doi: 10.3389/fmars.2020.597682

The Scotian Shelf harbors unique aggregations of the glass sponge *Vazella pourtalesii* that provides an important habitat for benthic and pelagic fauna. Recent studies have shown that these sponge grounds have persisted in the face of strong inter-annual and multi-decadal variability in temperature and salinity. However, little is known of these environmental characteristics on hourly-seasonal time scales. This study presents the first hydrodynamic observations and associated (food) particle supply mechanisms for the *Vazella* sponge grounds, highlighting the influence of natural variability in environmental conditions on sponge growth and resilience. Near-bottom environmental conditions were characterized by high temporal resolution data collected with a benthic lander, deployed during a period of 10 months in the Sambro Bank Sponge Conservation Area. The lander was equipped with temperature and oxygen sensors, a current meter, a sediment trap and a video camera. In addition, water column profiles of temperature and salinity were collected in an array across the sponge grounds from high to lower sponge presence probability. Over the course of the lander deployment, temperature fluctuated between 8.8–12°C with an average of 10.6 ± 0.4°C. Dissolved oxygen concentration was on average 6.3 mg l^{-1}, and near-bottom current speed was on average 0.12 m s^{-1}, with peaks up to 0.47 m s^{-1}. Semi-diurnal tidal currents promoted constant resuspension of particulate matter in the benthic boundary layer. Surface storm events episodically caused extremely turbid conditions on the seafloor that persisted for several days, with particles being resuspended to more than 13 m above the seabed. The carbon flux in the near-bottom sediment trap peaked during storm events and also after a spring bloom in April, when fresh phytodetritus was observed in the bottom boundary layer. While resuspension events can represent a major stressor for sponges, limiting their filtration capability and remobilizing them, episodes of strong currents and lateral particle transport likely play an

important role in food supply and the replenishment of nutrients and oxygen. Our results contextualize human-induced threats such as bottom fishing and climate change by providing more knowledge of the natural environmental conditions under which sponge grounds persist.

Keywords: *Vazella pourtalesii*, sponge ground, environmental conditions, storm events, particle flux, Scotian Shelf

INTRODUCTION

Sponges are one of the most common megafaunal organisms in the deep sea (Tabachnick et al., 1994). They can have a scattered distribution with low abundances, but under certain environmental conditions may form dense monospecific or mixed sponge aggregations, and even reef-like ecosystems (Maldonado et al., 2017). Sponge aggregations provide ecosystem goods and services by providing shelter from predation, breeding grounds and substrate for many associated species including commercially important fish species (Kutti et al., 2015b), thereby enhancing biodiversity and biomass (Rice et al., 1990; Fuller and Cameron, 1998; Beazley et al., 2013; Beazley et al., 2015; Maldonado et al., 2017; Meyer et al., 2019). Moreover, sponges play a key ecological role in benthic-pelagic coupling by filtering substantial volumes of water (up to 24,000 L per kg^{-1} of sponge day^{-1} in temperate and tropical shallow-water sponge grounds; Leys et al., 2007; Maldonado et al., 2012; Pham et al., 2019). Furthermore, they can release particulate detritus to the associated benthic environment (Reiswig, 1971), a pathway referred to as the sponge loop (Rix et al., 2016). Consequently they transfer energy and nutrients from the pelagic to the benthic environment, and play an important role in carbon, nitrogen, phosphate and silicon cycling (Maldonado et al., 2012; Kutti et al., 2013; Cathalot et al., 2015; Maldonado et al., 2020).

In the North Atlantic, deep-sea aggregations of demosponges (especially Astrophorina) and glass sponges (Hexactinellida) have been found along continental shelves, slopes, seamounts, mid-ocean ridges and canyons, especially at depths between 200 to 3000 m (Tabachnick et al., 1994). These sponge ecosystems either occur as mono-specific or multi-species assemblages. At boreal and boreo-arctic latitudes mixed species assemblages have often been found, like for example on the Arctic Mid-Ocean Ridge (Meyer et al., 2019) and on the northwest Atlantic Canadian margin (Murillo et al., 2012; Murillo et al., 2018). At temperate latitudes monospecific aggregations of glass sponges seem to be a dominant feature, such as for example the *Pheronema carpenteri* grounds in the northeast Atlantic Ocean (Rice et al., 1990), *Geodia* sp. grounds in the western Barents Sea (Klitgaard and Tendal, 2004) and mono-specific *Vazella pourtalesii* grounds in the northwest Atlantic along the Canadian continental shelf (Beazley et al., 2013). The dominant presence of particular sponge species has been related to local environmental conditions such as substrate type, topography, as well as the hydrography (Rice et al., 1990; Chu and Leys, 2010; Murillo et al., 2018; Roberts et al., 2018; Davison et al., 2019). Hexactinellids are most abundant and diverse in the deep ocean on steep rocky substrates with low amounts of suspended sediment in the water column and occur less often on flat shelves (Farrow et al., 1983; Maldonado et al., 2017). Other species, such as *Pheronema carpenteri,* are able to build a basal specular component (comparable to roots) enabling them to anchor in soft substrate (Barthel et al., 1996).

The Scotian Shelf, the continental shelf off Nova Scotia, eastern Canada, harbors unique aggregations of the rosellid glass sponge *V. pourtalesii* (Schmidt 1870), commonly known as "Russian hats" (Fuller and Cameron, 1998). This species is distributed along the continental margin of eastern North America, from the Florida Keys in the southern US, where it occurs in low densities, to the Scotian Shelf, where it forms extensive monospecific aggregations between ∼150 and 240 m depth in The Emerald Basin, reaching average densities of 3.8 ind. m^{-2} (Hawkes et al., 2019; Maldonado et al., 2020). Single individuals were found in an even broader depth range between ∼100 to 498 m depth on the Scotian Shelf (Beazley et al., 2018). High species abundance is likely linked to the high primary productivity on the Scotian Shelf (102 g C m^{-2} $year^{-1}$; Mills and Fournier, 1979), providing an important food source for the sponges and their associated fauna. Accumulations of *V. pourtalesii* harbor an enhanced biodiversity and species abundance of other invertebrates such as shrimp, crabs and anemones. Furthermore, analysis of catch data revealed a significantly different fish community associated with the sponge grounds (Fuller, 2011; Hawkes et al., 2019). In order to protect these sponges from bottom fishing gear Fisheries and Oceans Canada (DFO) established two sponge conservation areas in 2013, the Emerald Basin Sponge Conservation Area (197 km^2) and the Sambro Bank Sponge Conservation Area (62 km^2) (referred to as the 'closure areas' thereafter).

Of 35 environmental predictor layers (representing ocean terrain, fishing effort, and physical oceanographic characteristics) minimum bottom temperature and summer primary production layers were most important in a random forest model used to predict the distribution of *V. pourtalesii* on the Scotian Shelf (Beazley et al., 2018). Variability of environmental factors (e.g., temperature) is defined by the variability of the main water masses entering the Scotian Shelf (McLellan, 1957; Urrego-Blanco and Sheng, 2014), which lies at the confluence of two large ocean gyre currents, the Gulf Stream flowing into a northward direction and the Labrador Current flowing in an equatorward direction (Drinkwater et al., 2003). The contemporary distribution of *V. pourtalesii* is associated with the

Abbreviations: ADCP, Acoustic Doppler current profiler; CTD, Conductivity Temperature Depth; Chl-*a*, Chlorophyll-*a*; DO, dissolved oxygen; mab, meters above bottom; WSW, Warm Slope Water; LSW, Labrador Slope Water; SSW, Shelf Slope Water; *V. pourtalesii, Vazella pourtalesii.*

deep basins and channels on the Scotian Shelf which are bathed by warm and saline slope waters (Smith, 1978; Loder et al., 1997).

In this study we present the first long-term results of near-bed hydrodynamic observations and (food) particle supply mechanisms to highlight the influence of natural fluctuating environmental conditions on sponge growth and resilience. Observational evidence of the hydrodynamic conditions of the *V. pourtalesii* sponge grounds on the Scotian Shelf was collected via a long-term deployment (10-month) of a benthic lander in the framework of the EU-SponGES project. Near-bed environmental conditions (e.g., temperature, current speed, turbidity) were measured at high-resolution to determine hourly to seasonal variability. In addition, the lander was equipped with a sediment trap to determine particle and carbon fluxes, which was used as a measure of food availability. Knowledge on the environmental requirements and natural variability experienced by these sponge grounds may help to improve our understanding of their resilience against environmental stressors and ability to recover after natural and anthropogenic-induced disturbances.

MATERIALS AND METHODS

Topographic and Oceanographic Setting

The Scotian Shelf is a 700 km long and 200 km wide section of the continental shelf off Nova Scotia, Canada, bounded by the Laurentian Channel in the northeast, and the Northeast Channel and Gulf of Maine in the southwest. While the average depth of the shelf is 90 m, it is characterized by a heterogonous topography with several banks, channels, canyons and deeper basins (**Figure 1**; Han et al., 1997). The glass sponge *V. pourtalesii* is distributed in the Northeast Channel at the mouth of the Gulf of Maine in the west, and on the central Scotian Shelf in the Scotian Gulf, an inlet formed by a deeper cross-shelf channel situated between Emerald and LaHave Banks, which opens up to LaHave and Emerald Basins on the inner shelf (Beazley et al., 2018). The densest known concentration of *V. pourtalesii* is located above 200 m depth on a saddle between the two deep basins (>200 m water depth) that comprise Emerald Basin (Beazley et al., 2018), with a second notable concentration occurring on the eastern flank of Sambro Bank, Emerald Basin (**Figure 1**). These two concentrations are mostly encompassed by the Emerald Basin and Sambro Bank closures, respectively.

Two major ocean currents influence the sponge grounds; the Gulf Stream and the equatorward flowing subpolar Labrador Current (Hannah et al., 2001). The variability of the intensity of the Labrador Current influences all water masses on the shelf and results in the highest inter-annual variability of sea surface temperature (Δ 4.6°C) in the North Atlantic (Petrie and Drinkwater, 1993). When the Labrador Current (seasonally) reaches the seafloor it is known to be strong enough to displace organisms and matter, showing the largest volume transport (up to 0.6 Sv) in winter (Drinkwater et al., 1979; Hannah et al., 2001). The water column on the Scotian Shelf has a two-layered structure consisting of surface and slope waters (Drinkwater et al., 2003). The slope waters consist of two components with different signatures: the Warm Slope Water (WSW) and the Labrador Slope Water (LSW). WSW originates from a mixture of Gulf Stream Water, deep North Atlantic Central Water and shelf waters and flows primarily northeastward adjacent to the Gulf Stream. It is characterized by relatively high temperatures (12°C), high salinities (35.4; Gatien, 1976; Mountain, 2012) and high nutrient concentrations (Townsend and Ellis, 2010). The LSW flows in an equatorward direction and is cold (2°C), less saline (32) and low in nutrients (with an exception of relatively high Si; Petrie and Drinkwater, 1993; Petrie and Yeats, 2000; Mountain, 2012). Onshore movement of the warm slope waters through the major channels and gullies fills the basins at the

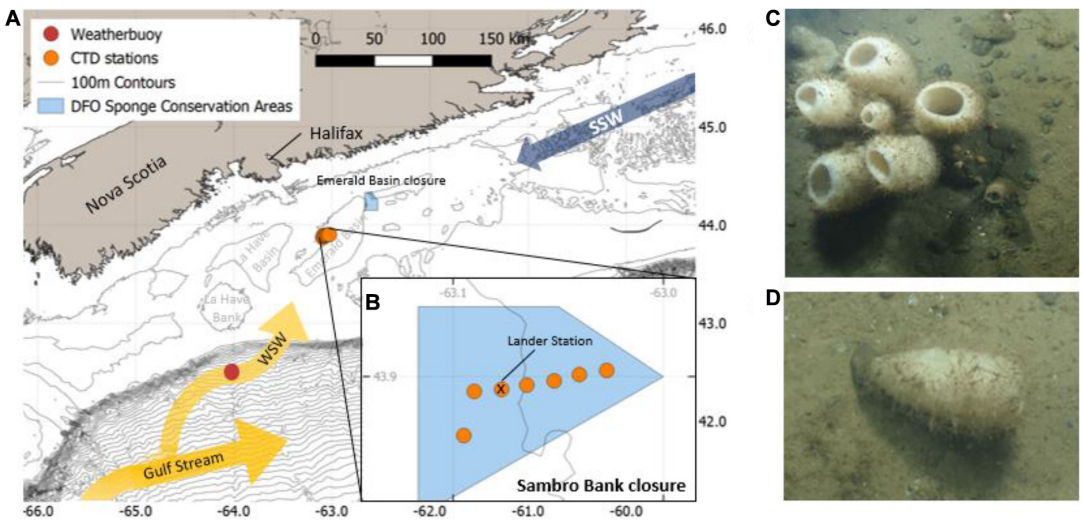

FIGURE 1 | (A) Scotian Shelf with CTD, weather buoy stations and both DFO Sponge conservation areas indicated in light blue. The arrows indicate the flow of the slope waters, WSW (orange arrow) and SSW (dark blue arrow), **(B)** Sambro Bank closure with CTD and lander stations; **(C)** *V. pourtalesii* sponges inside the Sambro Bank closure, **(D)** some sponges were found in a horizontal position.

Scotian Shelf with primarily WSW, resulting in relatively warm waters bathing the sponges year round. The surface water layer (Scotian Shelf Waters, SSW) is mixed by winter winds and contains cold water (2°C) with a relatively fresh signature (32) resulting from terrestrial run-off (McLellan, 1957; Petrie and Drinkwater, 1993). During summer, winter-cooled SSW is sitting in between a warmed up surface layer and the warmer WSW (Drinkwater et al., 2003). The water masses on the Scotian Shelf are influenced by seasonal warming and cooling, whereby the system is usually well stratified in late spring to early autumn, whereas it can be mixed over the shallow banks in winter (Smith et al., 1978). Vertical mixing occurs year round by internal tides, which are generated by the interaction of tidal flow of the stratified water masses over the abrupt bathymetry of the banks and basins (Han and Loder, 2003). This leads to vertical mixing of deep nutrient-rich water into the surface waters (Townsend and Ellis, 2010), but also stirs up sediments and produces intermediate nepheloid layers (Azetsu-Scott et al., 1995). In the Emerald Basin these nepheloid layers have been found at a depth of 140 to 200 m and occur when strong tidal currents flow in a northern direction (Azetsu-Scott et al., 1995). Tidal currents on the Scotian Shelf are dominated by semi-diurnal (M_2) tides (Chen et al., 2011).

Water Column Profiling

During a research cruise onboard the Canadian Coast Guard Ship (CCGS) *Hudson* (HUD2018-021) in June 2018, water column profiles of Conductivity-Temperature-Depth (CTD) were recorded with a Sea-Bird SBE25 V 4.1c system along a transect in the Sambro Bank closure to collect CTD data (each CTD cast was ∼1 km apart) inside and outside of the main sponge grounds (control station in the southwest, **Figure 1B**), which was based on a presence probability model from Beazley et al. (2018).

Lander

A NIOZ-designed ALBEX lander (Duineveld et al., 2004) was deployed at a depth of 154 m (43.898° N, 63.052° E) near the center of the Sambro Bank closure on September 6, 2017 with the CCGS *Martha L. Black*, and retrieved on June 22, 2018 during the CCGS *Hudson* mission (**Figure 1B**). The lander was equipped with a CT sensor (Sea-Bird SBE37SM-RS232, sampling interval = 15 min, accuracy for temperature of 0.002°C and conductivity of 0.003 mS cm^{-1}), ARO-USB oxygen sensor (JFE-Advantech^{TM}, sampling interval = 15 min, accuracy of non-linearity ± 2% of full scale, at 1 atm, 25°C). A 2 point calibration was carried out before deployment to compensate for the time drift and ensure reliable and accurate DO data. An Aquadopp 2 MHz (Nortek^{TM}, sampling interval = 15 min) acoustic doppler current profiler (ADCP) was attached on the lander at a depth of 3 m above bottom (mab). The ADCP measured acoustic backscatter and velocity in 50 cm bins with an accuracy of ±1% of the measured value (0.05 cm s^{-1}). A NIOZ custom-made HD video camera with white lights recorded every 4 h a short video clip of 20 s of the seabed. The lander was also equipped with a Technicap PPS4/3 sediment trap with 12 bottles with the aperture at 3 mab. Sediment trap vials were filled with a pH-buffered mercury chloride ($HgCl_2$) solution in filtered seawater collected from the deployment site and the carousel was programmed to rotate at 30-day intervals.

Sediment Trap Samples

Upon recovery of the lander, sediment trap samples were stored at 4°C until they were split into five subsamples with a WSD10 McLane manual rotor splitter. Four of the subsamples were split and rinsed with MilliQ water and one subsample was washed with filtered seawater for pigment analysis. After splitting, samples were freeze-dried and weighed to calculate mass fluxes, whereby the average weights of two splits was used. It must be stressed that cylindrical traps tend to under-sample when current speed exceeds 15 cm s^{-1} (Gardner et al., 1983). Therefore, trap fluxes presented here, especially during high current conditions, are likely underestimated with regards to the near-bed mass flux (Vangriesheim et al., 2001).

One split of each sample was used for isotope analysis. Half of the sample was used for organic carbon analysis and was first decarbonized by hydrochloric acid (2 M HCl supra) and afterward transferred into pressed tin capsules (Elemental Microanalysis). The other half of the sample was used for nitrogen analysis and was directly transferred into pressed tin capsules. Stable isotopes $\delta^{15}N$, $\delta^{13}C$ and total weight percent of organic carbon and nitrogen were analyzed by a Delta V Advantage isotope ratio MS coupled to a Flash 2000 Elemental Analyzer (EA-IRMS) by a Conflo IV (Thermo Fisher Scientific Inc.). The reference gas was pure N_2. As a standard for $\delta^{13}C$ benzoic acid and acetanilide was used, for $\delta^{15}N$ acetanilide, urea and casein was used. For $\delta^{13}C$ analysis a high signal method was exercised including a 70% dilution. Precision for replicate measurements of $\delta^{13}C$ and $\delta^{15}N$ was ± 0.15 ‰.

The Chlorophyll-*a* (Chl-*a*) concentration of the sediment trap samples was measured by a Fluorescence Spectrometer (F-2500 Hitachi), by comparing the sample absorbance to the absorbance of a known Chl-*a* standard at two wavelengths (431.0/671.0 nm): Chl-*a* was extracted in 90% acetone and fluorescence was measured first on the intact extract and a second time after the extract was acidified with HCl (10%) under dark and cold conditions. HCl was added to the sample to convert Chl-*a* into its degradation products (Phaeopigments). By this the amount of Chl-*a* can be deducted from its degradation products which otherwise interfere with the measurements since they absorb light at the same wavelength (for details Holm-Hansen et al., 1965).

Data Analysis

Daily moving averages of all environmental variables of the long term data were calculated, as well as monthly averages that were related to the sediment trap sampling intervals. Correlations between the measured environmental variables were calculated using Pearson correlations (n = 27,384) in the program R (R Studio 1.2.1335). The pressure data and near-bed horizontal velocity components at 5 mab obtained with the ADCP were analyzed to determine the most important tidal constituents with the "tidem" package in the program R (R Studio 1.2.1335).

Velocity data of the ADCP at 5 mab were used to make a progressive vector diagram. A single passive particle

representing a dissolved or suspended constituent was released and its transport simulated according to the horizontal velocities measured by the current sensor during a period of 30 days; corresponding to the intervals of sediment trap sampling (Duineveld et al., 2007). For this, the velocities per time step were added up in a two-dimensional space simulating the direction of transport. The released particle experiences in any new position the current of the initial position, independently of where the constituent went. Progressive vector diagrams accumulate errors and clearly cannot provide a real estimate of the particle position, but provide an estimate on how far particles or nutrients can disperse after they are released from their original position (Carlson et al., 2010).

RESULTS

Environmental Conditions on the Scotian Shelf

The CTD transect revealed a relatively fresh and solar heated upper layer reaching to a depth of about 20 m below the surface as shown by high temperature (>5°C) and low salinity (<32) (**Figure 2**). Underneath this layer colder winter-cooled SSW water was found from 20 m until a depth of about 75 m (<5°C, **Figure 2B**). Underneath the cold layer WSW was observed, which was characterized by a higher temperature (>6°C) and higher salinity (>33) (**Figure 2A**). Water stratification was very similar at all stations including the control station outside the sponge area, whereas the influence of the cold winter-cooled SSW was decreasing toward the east.

Long-term Environmental Conditions in the Sambro Bank Closure

The lander was deployed at a depth of 154 m and data were recorded during the whole deployment period of ten months (**Figure 3**). Average temperature (T) was 10.6 ± 0.4°C and varied between 8.8 to 12°C (**Figure 3A**). Average salinity was 35.0 ± 0.1 with a range between 34.1 and 35.3 (**Figure 3B**). As shown in **Figures 3A,B**, T and salinity were highly correlated ($r^2 = 0.84$, $p < 0.001$, Pearsons product-moment correlation). The monthly temperature was on average highest in March and April (10.9°C) and lowest in November (average 10.2°C). Salinity was on average highest in April (35.1) and lowest in November (34.8; **Figure 6A**). The average dissolved oxygen (DO) concentration during the whole time period was 6.3 ± 0.5 mg l^{-1} with a range between 4.9 to 8.9 mg l^{-1} (**Figure 3C**), corresponding to an oxygen saturation of on average 57%. The dissolved oxygen (DO) concentration was negatively correlated with density (r^2 = -0.52, $p < 0.001$) and was on average highest in spring from March to June (6.7–7.1 mg l^{-1}), while lowest values were found from September to February (6.0 – 6.2 mg l^{-1}, **Figure 6A**). Currents at 5 mab were on average 0.12 m s^{-1} with peaks in current speed of up to 0.47 m s^{-1} (**Figure 3E**). The direction of the large-scale sub-tidal flow was in a direction of 146°. Tidal flow oscillated between a NW and SE direction with the semi-diurnal tidal cycle (**Figure 3D**). Current direction was not significantly correlated with temperature, salinity or oxygen concentration (**Figure 1** of Supplementary).

The tidal analysis fitted to the pressure data and revealed that the biggest tidal constituent is the principal semi-diurnal lunar constituent (M_2) with an amplitude of 0.596 m, followed by the larger lunar elliptic semidiurnal (N_2) and principal solar

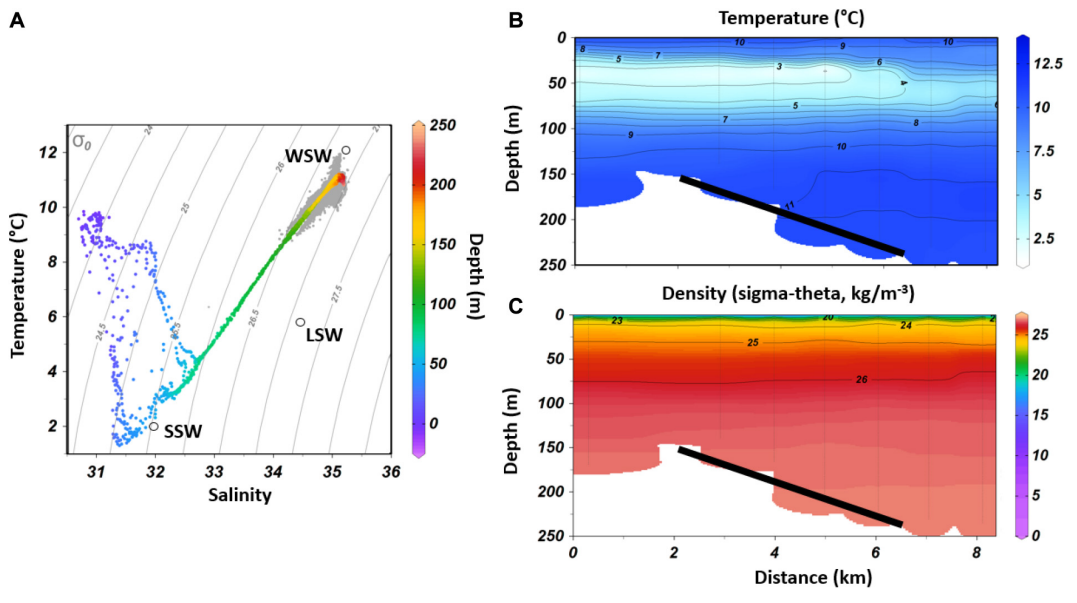

FIGURE 2 | (A) T/S plot of CTD and lander data in gray. The characteristic end members of temperature and salinity for WSW, LSW and SSW are plotted (Mountain, 2012); **(B)** Temperature transect inside the Sambro Bank closure, with the westernmost station (on the left) located outside of the densest sponge area; **(C)** Density along the same transect. The black bars indicate the depth distribution of the sponge ground (150–250 m water depth).

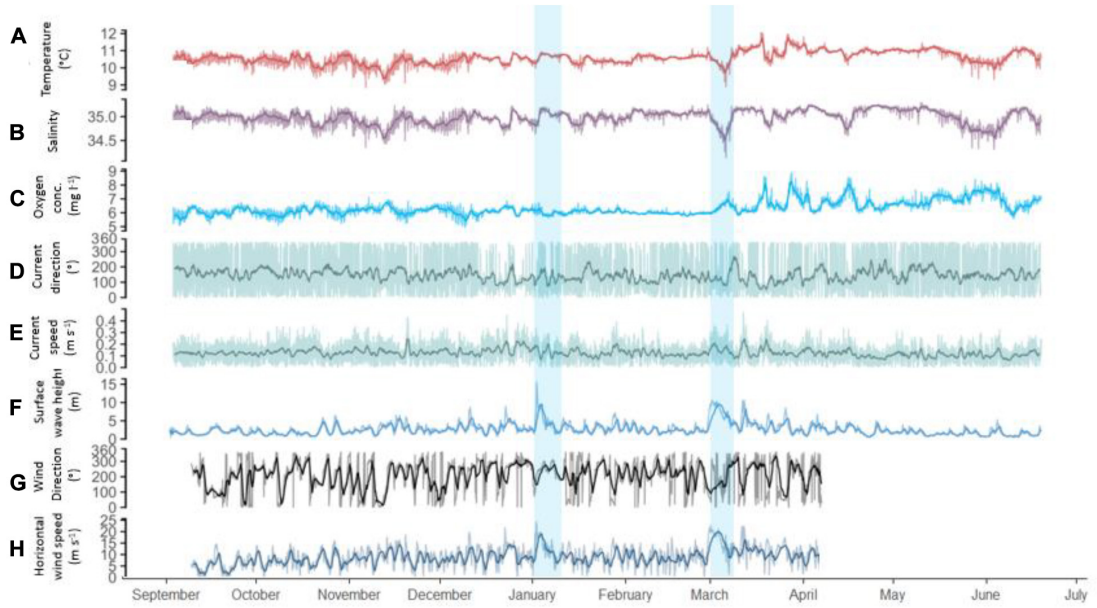

FIGURE 3 | Near-bed hydrodynamic data, recorded by the lander from September 2017 to June 2018, with the daily moving average shown by thick lines. **(A)** Temperature, **(B)** Salinity, **(C)** Dissolved Oxygen concentration, **(D)** Current direction (5 mab), **(E)** Current speed (5 mab). Weather data from buoy: **(F)** Wave height; **(G)** wind direction and **(H)** wind speed (no continuous record) (DFO). Storm events are highlighted in light blue.

semidiurnal constituents (S_2) with an amplitude of in each case of 0.13 m (**Figure 4**, **Table 1**). The tidal analysis fitted to the velocity data revealed that the M_2 tide produces the highest velocity with a current speed of 0.03 m s^{-1}. The second important constituent of the velocity data was the M_4 constituent producing a velocity of 0.01 m s^{-1} (**Table 1**). These tidal signals are evident in the energy spectra in which the largest peaks were found at the above mentioned frequencies (**Figure 4**).

The acoustic backscatter showed a permanently turbid benthic boundary layer up to a height of about 5 mab throughout the deployment period, whereas periodical peaks reached higher up in the water column, up to 13 mab (**Figure 5A**). Lowest backscatter was recorded from May to June 2018. The acoustic backscatter at 5 mab showed the strongest correlation with current speed ($r^2 = 0.25$, $p < 0.001$), temperature and DO concentration (both $r^2 = 0.2$, $p < 0.001$).

Although several high turbidity events were observed throughout the year, two events are highlighted here in more detail, showing an altered daily amplitude of T, salinity, DO concentration (**Figure 3**), and corresponding peak in turbidity (**Figure 5**). Both events were correlated to storm events as observed by weather buoy data, being characterized by peaks in wave height at the 5th of January (max. 15.5 m at 4:20) and the 3th of March (max. 10.6 m at 21:20, **Figure 3**). Wind speed also peaked on these two days, reaching 24.2 m s^{-1} and 21.1 m s^{-1}, respectively, blowing into an eastern direction (DFO, 2020). Based on the acoustic backscatter data, the first extreme event in January resulted in a high load of particles in up to 13 mab for about 24 h (**Figure 5B**). During this event three smaller turbidity peaks were found between the 05th of January and the 06th of January (**Figure 5B**), which were related to a change in current direction due to the semi-diurnal tides. The second storm event in March showed a slightly lower surface wave height, surface wind speed and turbidity than during the winter peak (**Figure 5A**). Additionally, a temporal drop in temperature and salinity was observed during this event, where both parameters fell to a minimum of 8.8°C and 34.1, respectively (**Figure 3**). On the contrary DO increased during the event. Several smaller events with similar characteristics were observed from March to May, showing the same alterations in T, salinity, DO and peaks in acoustic backscatter.

Sediment Trap

The vertical mass flux during the deployment period was on average 3166 ± 3421 mg m^{-2} day^{-1} (**Figure 6F**), while the average carbon flux was 100 ± 72 mg C m^{-2} day^{-1} (**Figure 6G**). Highest vertical mass flux, i.e., 12,390 mg m^{-2} day^{-1}, was observed in the period from December 2017 to January 2018. Highest carbon flux was likewise found in December/January coinciding with the winter storm event (281 mg C m^{-2} day^{-1}, **Figure 6**). The C:N ratio was on average 8.3 ± 0.2, ranging from 7.8 to 8.6 (**Figure 6B**) and the $\delta^{15}N$ was 6.7 ± 0.4‰, ranging from 6.2 to 7.3‰ (**Figure 6C**). The $\delta^{13}C$ ratio ranged from −23.3 to −22.8‰ with an average of −23 ± 0.1‰ (**Figure 6D**). The Chl-*a* concentration was on average 2.1 ± 1.1 mg l^{-1}, with an average Chl-*a*: Phaeo ratio of 0.00069 ± 0.00077 (**Figure 6E**). The largest peak in Chl-*a* (4.05 mg l^{-1}), being two times higher than the average Chl-*a* concentration, was observed in March/April, indicating the arrival of fresh phytodetritus at the seafloor, which occurred after the second storm event in March.

The winter peak (December/January) in mass flux corresponded to a peak in acoustic backscatter (**Figure 5B**), which is likely the result of resuspension of bottom material as indicated by the presence of a large quantity of sponge spicules

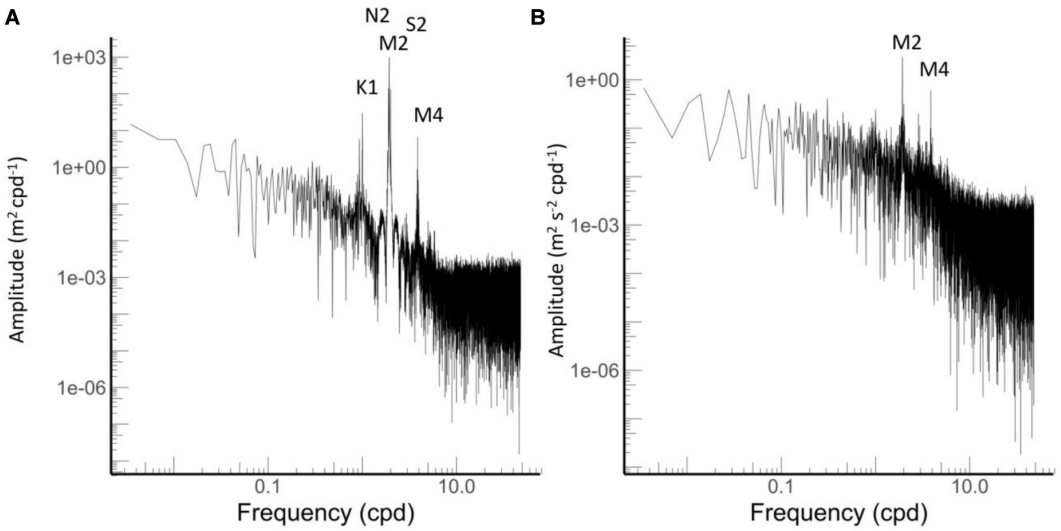

FIGURE 4 | Energy spectra from **(A)** pressure and **(B)** velocity data. Main tidal frequencies are indicated.

in the sediment trap sample. The quality of the organic matter flux in this period was low as indicated by the C:N ratio (8.4), the δ^{15}N (7.3 ‰) and the Chl-*a*: Phaeopigment ratio (0.000009), indicating that high amounts of more degraded organic matter are trapped. This is in contrast to the fresh organic matter observed in March/April with a C:N ratio of 7.9, the δ^{15}N of 6.3 ‰ and the Chl-*a*: Phaeopigment ratio of 0.003 (**Figure 6**).

Particle Displacement

The progressive vector plot showed that particulate suspended matter released at the deployment site was estimated to travel in a mainly southern direction (min. 71 km in June/July to a max. 233 km in December/January) during each 30-day sampling interval (**Figure 7**). SE-NW movements of particles are related to the semi diurnal tidal flow. In autumn, the particles generally traveled in a SSE direction, while after the storm event in January, the residual current direction shifted into a southern direction and showed the longest distance. After the storm event in spring (March/April) particles were transported relatively fast to the southwest. During spring residence time on the shelf was the longest as indicated by the shortest distances. With the shelf edge around 100 km to the south from the lander site, particles would be washed off the shelf in a period between 14 to >30 days.

TABLE 1 | Main tidal components with their frequencys and amplitudes of pressure and velocity data.

Main tidal components	Frequency (cpd)	Amplitude (m)	Amplitude (m s^{-1})
M2	1.932	0.596	0.0294
N2	1.896	0.134	0.0048
S2	1.999	0.103	0.0065
K1	1.003	0.080	0.0061
M4	3.864	0.003	0.0089

The view of the camera showed several upright *V. pourtalesii* individuals as well as many anemones (**Figure 8**, 4th Jan.). Mobile species, such as pollock (*Pollachius virens*) and especially redfish (*Sebastes* spp.) also appeared in the recordings. Pollock were observed to swim relatively quickly through the video frame, mostly in groups of several individuals. Redfish were rather stationary or moving with the currents in a resting stage on the seafloor as single individuals or in small groups. The storm events were clearly captured by the video data. The video observations revealed that during the January storm event an extreme high load of particles was in resuspension for one day, whereas conditions gradually normalized within 2 days (**Figure 8A**), corresponding to the peaks in turbidity. After the water cleared up, sponges and anemones were observed to be dislocated, whereas the lander frame also moved during the storm and another view of the camera was visible. Sponges in the camera view did not appear to be negatively influenced by this dislodgement, since the sponges were white and unaffected in appearance. Nevertheless, some sponges transported in the view of the camera after a high current event, were observed to be dead (**Figure 8B**). Likely they have been ripped off from their initial position and substrate by the high currents. One of the bigger sponge individuals was observed to decompose in a time period of about three weeks (**Figure 8B**).

DISCUSSION

To date the focus of most studies of the *V. pourtalesii* grounds has been on the spatial distribution of the sponge grounds, their associated fauna and biodiversity (Fuller and Cameron, 1998; Beazley et al., 2018; Hawkes et al., 2019). Little is known of the natural environmental characteristics and food supply mechanisms on short to seasonal time scales that influence these habitats. For the first time, we measured the environmental characteristics at high temporal

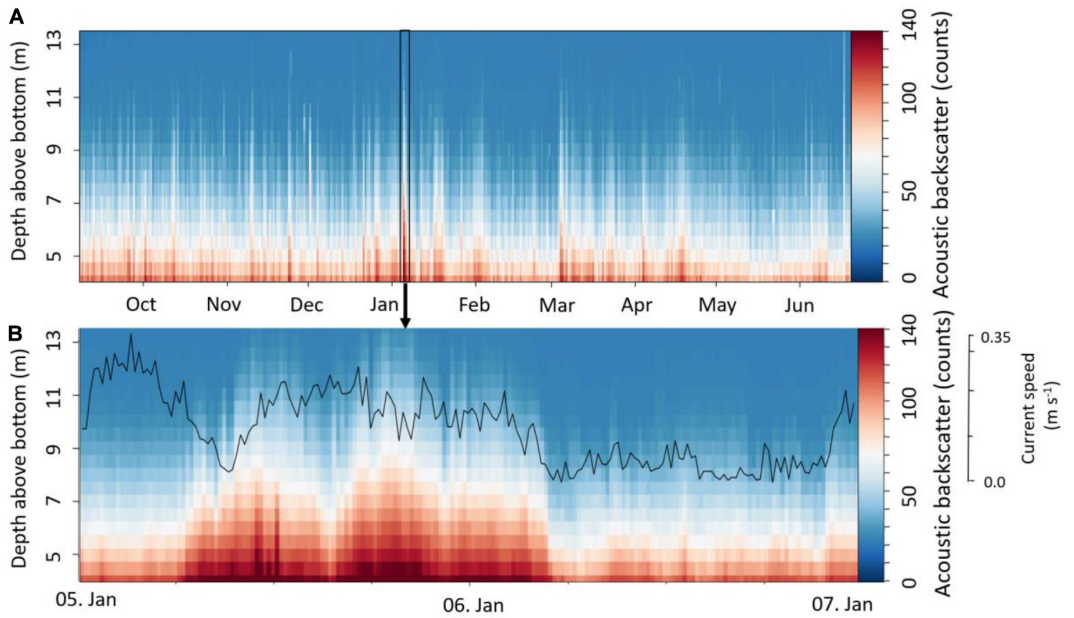

FIGURE 5 | (A) Acoustic backscatter (counts) in 3.5 to 13 m above the sea bottom; **(B)** Resuspension event in January with current speed at 5 mab (bin2).

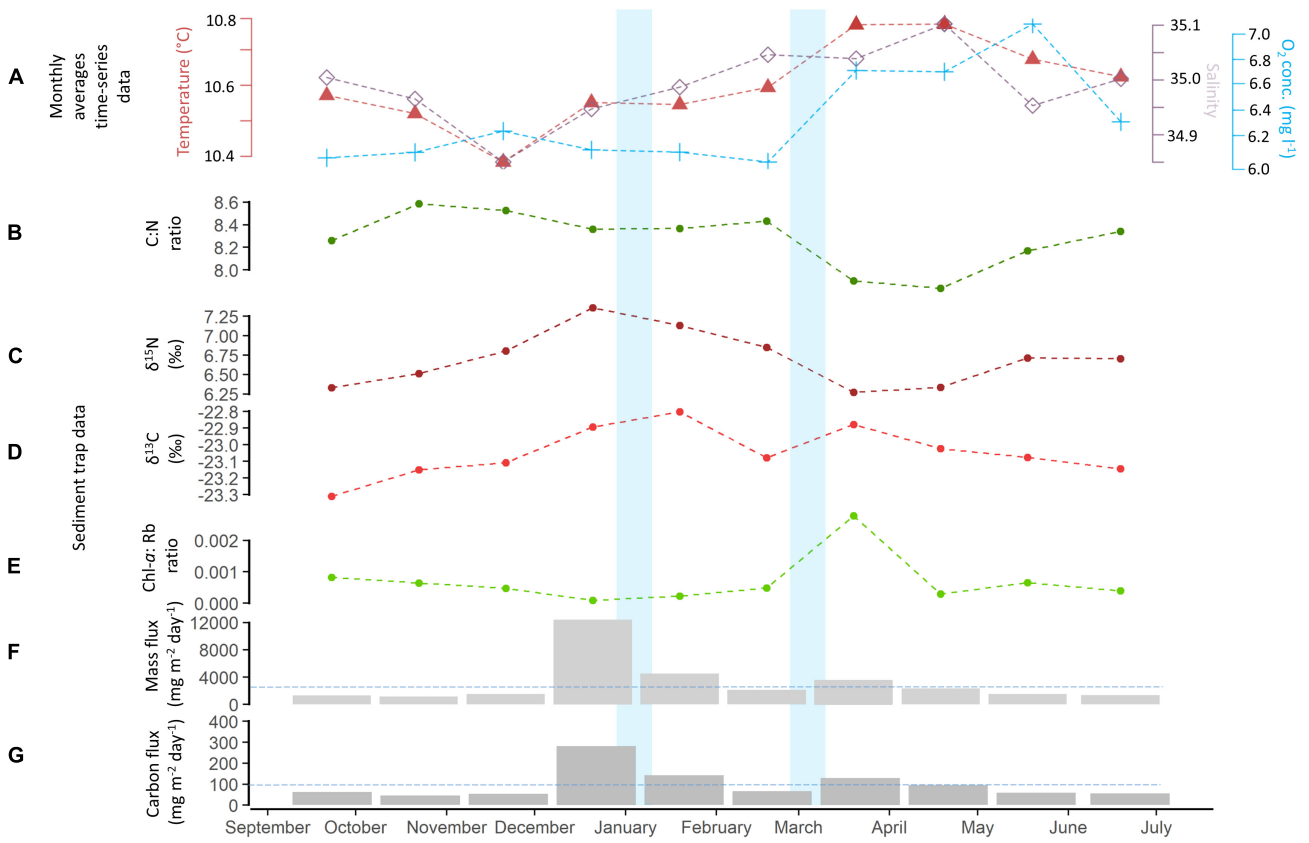

FIGURE 6 | (A) Monthly averages of temperature, salinity and oxygen concentration recorded by the lander, Sediment trap data: **(B)** C:N ratio; **(C)** $\delta^{15}N$; **(D)** $\delta^{13}C$; **(E)** Chlorophyll-a: Phaeopigments ratio of the sediment trap material; **(F)** Mass and **(G)** Carbon flux recorded by the sediment trap. Blue horizontal lines are indicating the average mass and carbon flux. Line charts and histograms represent the average value during the 30 day sediment trap interval. Storm events are highlighted in light blue.

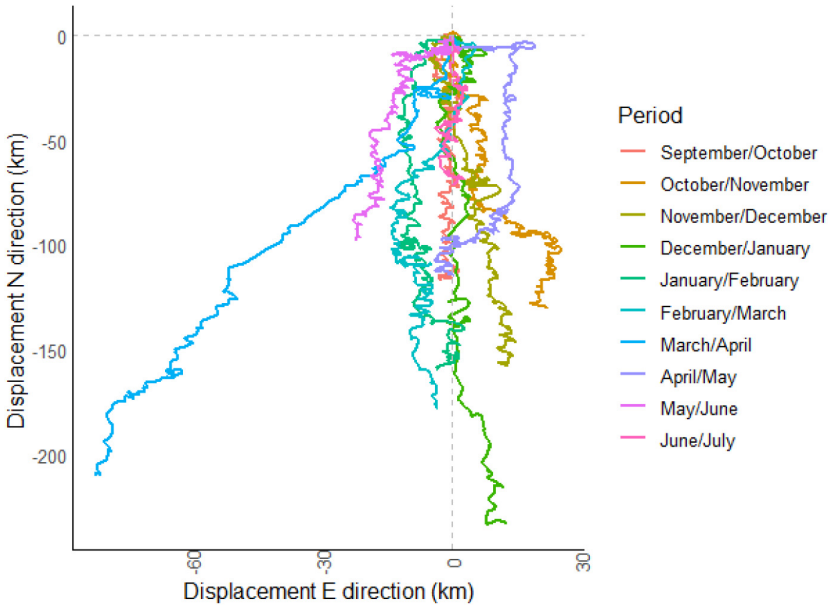

FIGURE 7 | Progressive vector plot of 30-day intervals, corresponding to the sampling interval of the sediment trap. The site where the passive particle was released is the coordinate 0/0, the lander site.

resolution over a 10-month period in the *V. pourtalesii* sponge ground located in the Sambro Bank Sponge Conservation Area.

Environmental Conditions on the Scotian Shelf

Based on the modeling results of Beazley et al. (2018), minimum bottom water temperature is the most important determinant for the distribution of *V. pourtalesii* on the Scotian Shelf, with the highest presence probabilities associated with minimum bottom temperatures of 5°C. In our study, bottom water temperature varied between 8.8 to 12.0°C during the deployment period. The sponge grounds were observed below the boundary of two water masses, mainly bathed in WSW. During most of the year seasonal water column stratification on the Scotian Shelf prevents mixing of the WSW and SSW (McLellan, 1957), and in this study high and relatively stable bottom water temperatures were measured. Short-term daily fluctuations in temperature and salinity were linked to internal tides (M_2) moving stratified waters up and down the sloping topography of the Emerald Basin (Wunsch, 1975; van Haren et al., 1994). Extreme temperature fluctuations during the lander deployment were only observed during some of the storm events in spring, when colder, less saline and oxygen-rich water, typical of winter-cooled surface waters was observed near the bottom (**Figure 3**). These events resulted in abrupt fluctuations in bottom water temperature of up to 3.2°C, which might be related to wind-driven downwelling on the shelf (Greenberg et al., 1997). These fluctuations did not exceed multi-decadal variability (4 to 12°C), which is even higher with bottom temperatures varying by up to 8°C and being as low as ∼4°C (Beazley et al., 2018). That sponges can thrive in a large temperature range was also observed in other studies: glass sponge accumulations in Norway were correlated with temperatures below 12°C (Strand et al., 2017) and even as low as -0.5°C along the arctic mid-Atlantic Ridge (Roberts et al., 2018), whereas *P. carpenteri* were modeled to appear over a temperature range of 2.7 to 20.9°C (Howell et al., 2016). Even though lower and upper temperature ranges of most sponge species are still largely unknown, it seems that they can thrive at larger temperature ranges than other deep-sea species forming hotspots like cold-water coral reefs (4 to 12°C) (Roberts et al., 2006).

The DO concentration of 6.3 ± 0.53 mg l^{-1} measured in this study was about three times higher than the DO concentration (2.05 mg l^{-1}) measured in a sponge reef on the western Canadian margin (Whitney et al., 2005). So far it is not evident which DO concentrations are suitable for sponges. They seem very resilient even at low DO concentrations, as observed at the Namibian margin where DO concentrations were far below 2 mg l^{-1} (Hanz et al., 2019), which seems to be the threshold for growth and survival of many other marine organisms (Gray et al., 2002).

Another important environmental factor for the occurrence and sustenance of sponge grounds is the interaction between hydrography and seafloor topography (van Haren et al., 2017; Davison et al., 2019). Sponge grounds are often associated with areas where the slope angle of the bottom matches the slope of internal tides, producing internal waves. Internal waves, generated by wind or flow over topography are the main causes of strong bottom currents, enhanced turbulence and mixing and resuspension of particulate matter near the seafloor (Garrett and Laurent, 2002; Hosegood and van Haren, 2004), thereby influencing food supply by increasing the vertical and lateral flux (Davison et al., 2019) as has also been observed in cold-water coral ecosystems (Cyr et al., 2016). An example is the *P. carpenteri* belt along the slope of the Porcupine Seabight in the NE

FIGURE 8 | Photographs showing the camera view **(A)** before, during and after the storm event (4. January). Large amounts of suspended matter were observed in the benthic boundary layer from the 4. January to the 7. January; **(B)** Dead sponge in February indicated by a white arrow and its subsequent decomposition until its barely detectable at the 9th of March.

Atlantic (Rice et al., 1990) or the Faroe Shetland channel where sponges were observed in regions with intensified internal wave activity and associated with pronounced changes in temperature (Davison et al., 2019). Such conditions have also been found on seamounts and canyons, where sponge aggregations have been observed in areas of critical slope in the Arctic (Schulz Bank seamount; Busch et al., 2020) and the Azores (Rainbow Basin; van Haren et al., 2017). Based on our data we can only link the environmental fluctuations to the presence of tidal currents. However, other studies have described the presence of internal wave activity in the Emerald Basin (van Haren et al., 1994). Intermediate nepheloid layers were found to coincide with the critical depth for possible generation and amplification of internal waves with semi-diurnal (M2) internal tidal frequency (Azetsu-Scott et al., 1995). The nepheloid layers observed by Azetsu-Scott et al. (1995) in their vertical profiles had an intermittent character that was explained by recurrent resuspension and variable currents. This intermittency was also clearly visible in the near-bed data (current data and video) from this study (**Figures 5**, **8**) showing pulse-like increases of particulate matter concentrations in the benthic boundary layer pointing to local resuspension. These frequent resuspension and subsequent lateral transport

of high near-bed particle concentrations might be an important driver of food supply for *V. pourtalesii* sponge grounds on the Scotian Shelf.

Food Supply

Sponges are very efficient filter feeders and feed on particulate as well as dissolved resources (Reiswig, 1971; Pile and Young, 2006). While the average daily carbon flux in the near-bed sediment trap was 100 ± 72 mg C m^{-2} day^{-1} during the deployment period, carbon flux was highly variable and peaked in December/January (281 mg C m^{-2} day^{-1}) and March/April (130 mg C m^{-2} day^{-1}). During the December peak no major fluctuations in temperature, salinity or DO concentration were observed, likely indicating that the organic matter is not delivered from the surface but rather due to resuspension events inside the bottom boundary layer. Even though this winter event was characterized by a high carbon flux, mainly degraded organic matter was resuspended as shown by the low concentration of Chl-*a* and a high C:N ratio (**Figure 6**), likely related to resuspension and lateral transport of more degraded material from the seafloor. Hill and Bowen (1983) calculated that a current speed of 0.15 m s^{-1} is required to resuspend the coarser sand, whereas fine sand and mud is transported at a speed of 0.11 m s^{-1}. Current speed as measured in this study would be sufficient to resuspend coarse sediment during 31% of the time and 56% for the finer fraction. This was also apparent in the ADCP turbidity data (**Figure 5**) which showed an almost permanent turbid layer close to the bottom. The video recordings showed that during storm-induced resuspension events, particularly the winter event, particles stayed in resuspension for several days, which was however not detected in the acoustic backscatter data of the ADCP, implying that turbidity close to the bottom might be even more persistent. This could possibly be due to the particle size of the particles in resuspension, whereby the finer particles are not resolved by measurements of the ADCP (Bunt et al., 1999).

In March/April the highest amounts of fresh (high concentration of Chl-*a* and lower C:N ratio) organic matter were observed, likely related to a surface algal bloom. The algal bloom period seems indirectly related to the mixing of the water column during the storm event in March (**Figure 6**), when nutrients are stirred up to the surface. Our data on the importance of a mixed water column for the surface productivity was confirmed by an ecosystem model, which predicted highest primary production to appear in the beginning of April (Song et al., 2011).

Taking the estimated carbon demand of a deep-water glass sponge reef (ca. 160 m depth, ∼10°C) at the Canadian coast (1800–4100 mg C m^{-2} day^{-1}, Kahn et al., 2015), the carbon derived from the vertical flux would provide on average approximately <8% of the required carbon demand. *Ex situ* experiments have shown that in the Canadian sponge reefs carbon consumption was much higher (360 mg m^{-2} day^{-1}), compared to the average carbon flux (100 mg m^{-2} day^{-1}), showing that the carbon demand of the *Vazella* grounds will not be satisfied (Bart et al., 2020b). A potential carbon deficit may be alleviated from the resuspended organic-rich sediment itself (Grant et al., 1987), but also from the filtration of bacteria and uptake of DOC from the water column (Bart et al., 2020b). Bacteria are expected to be an even more important food source than suspended particulate matter for some glass sponges and will be assimilated efficiently (Pile and Young, 2006; Kahn et al., 2015; Bart et al., 2020a). On the Scotian Shelf an important source of bacteria can be the resuspended sediments, which are 100–1000 times enriched in heterotrophic bacteria compared to the overlaying water (Kuwae and Hosokawa, 1999). These benthic bacteria are attached to sediment particles with extracellular polymeric substances and can be taken up by the ingestion of sediment particles (Kuwae and Hosokawa, 1999). It was also shown that particles remaining in suspension become more densely packed with bacteria (Wainright, 1987). This was suggested to occur on the Scotian Shelf by Grant et al. (1987), who found a high N content in sand particles, which they hypothesized was due to attachment by bacteria. Considering the fact that several large resuspension episodes were observed during the deployment period, the resuspended sediment with microbes attached and subsequent lateral transport might constitute a major food source for the sponges. The fine carbon- and nitrogen-rich suspended material and even the coarse sandy fraction is constantly resuspended and transported over the shelf (Grant et al., 1987) in a mainly southern direction as was also shown by the progressive vector analysis (**Figure 7**). Even though this type of analysis only provides an estimate, we showed that suspended matter stays on the shelf for 14–>30 days. During the event in March the wind direction was toward the east and the residual current direction changed to the SW in an along slope direction that likely has resulted in downwelling (Greenberg et al., 1997; Li et al., 2014), which was indicated by a decrease in temperature related to the cooler SSW. Due to the occurrence of natural resuspension events throughout the 10-month lander deployment, the question arises if these events and resulting lateral transport of (food) particles are essential for the occurrence of *V. pourtalesii* on the Scotian Shelf.

Events

The extreme events at the seafloor at the 154 m deep lander site were mainly driven by storm events and occurred predominantly in the winter and spring months, influencing the water column structure and particle distribution on the shelf. Only the storm events in spring were observed to introduce colder and less saline water to the sponge ground, which was during the event in March coinciding with a peak in surface wave height as well as an on average more easterly wind direction (**Figure 3**). Water column mixing will result in an increased availability of nutrients from the deeper water masses toward the surface (Townsend et al., 2006), triggering primary productivity and increased benthic-pelagic coupling (Ji et al., 2006). Topography-hydrography interactions can also influence biogeochemistry and microbiology either by mixing or by resuspension as described above, which can result in different sponge associated microbial communities defined by the surrounding near-bed environment (Busch et al., 2020). This mixing will indirectly promote an increased vertical flux and therefore food supply to the sponge grounds and their associated fauna, as was also observed in the Gulf of Mexico and on the Namibian margin (Mienis et al., 2012; Hanz et al., 2019). Wind-induced mixing also can play a major role in the

replenishment of for instance oxygen as was observed during the spring storm events, where colder SSW with a lower salinity and higher DO concentration was observed amidst the sponge ground. Replenishment of nutrients and DO have shown to be vital for the occurrence of sponges as well as other deep-sea ecosystems, like cold-water coral reefs (van Haren et al., 2014; Hanz et al., 2019). However, these events can also act as stressors for the sponge ground. During periods of high current speed sponges and anemones were observed to be dislocated and tipped over into a horizontal position and a dead individual was observed in front of the camera in late winter (February-March). Accumulations of dead individuals have been observed in the Sambro Bank Sponge Conservation Area (Hawkes et al., 2019), caused either by the displacement by high currents or by fishing activities and subsequent transport by the current (trawling and dumping). Our video data showed that large dead individuals were disintegrating in a period of several weeks, which might be important for the silicon cycling on the Scotian Shelf (Maldonado et al., 2020).

Besides the observed events, the Labrador Current which varies seasonally in extent, is in general known for the displacement of biological organisms and materials to the southwest (Hannah et al., 2001). The association of the *V. pourtalesii* with movable hard substrate like stones and pebbles might hence have a benefit for the sponges at the Scotian Shelf. The strong currents during winter and spring storm events might be destructive if sponges would be attached to non-movable hard substrate since they can be ripped off their attachment. Additionally, small stones and pebbles might play a role in helping the sponges to stay upright or regain an upright position after being moved by transferring their mass center to their bottom. That would also explain why only in deeper areas in the Fundian Channel, which are likely less affected by storm activity and high current speeds, sponges are also found on bigger boulders (Fuller and Cameron, 1998; Lacharité and Metaxas, 2017).

High amounts of resuspended material can also be a stressor for *V. pourtalesii* since high amounts of suspended sediment or larger particles can clog the aquiferous system of sponges and could negatively impact their filtering ability and even their survival (Maldonado et al., 2008; Tjensvoll et al., 2013; Kutti et al., 2015a). To avoid complete clogging, sponges exhibit adaptations to high particle loads and can arrest pumping and 'cough' (a clearing response) when exposed to high concentrations of suspended sediment. The exact concentration of suspended particulate matter in the water column during the winter storm events was not measured in this study. However, video observations showed that the extreme conditions in the benthic boundary layer lasted up to several days (**Figure 8**). If *V. pourtalesii* arrest their pumping activity during these periods they would need to do so for a much longer time than has been shown so far in other studies (Tjensvoll et al., 2013; Kutti et al., 2015a; Grant et al., 2019). The Scotian Shelf is subject to severe storms as well as hurricanes on a regular basis, caused by extratropical cyclonic storms that develop along the U.S. east coast and travel northward (Anderson et al., 1989). Modeling studies have indicated that with predicted climate change storm intensity will increase, which likely will have an effect on the sponge grounds situated on the Scotian Shelf (Knutson et al., 2010).

In addition to naturally driven suspension events, sponges on the Scotian Shelf are also influenced by anthropogenic impacts like fishing activities that can also resuspend large amounts of particulate matter. The *Vazella* sponge grounds are situated in traditional fishing grounds for groundfish (Beazley et al., 2018). Bottom-tending fishing gears can directly impact sponge grounds through removal and incidental damage, or through indirect effects such as resuspension of sediment and smothering (Tjensvoll et al., 2013), whereby impacts of plumes were observed kilometers away from the source of the plume (Grant et al., 2019). As mentioned above, resuspension events and lateral transport of particles can positively and negatively influence sponges. Particles suspended by fishing activity are known to decrease the filtering capacity and efficiency in many species which can result in adverse effects on overall metabolism and health of sponges (Bell et al., 2015; Grant et al., 2019). How the concentration of suspended sediment observed during storm events compares to resuspension induced from bottom trawling remains unknown. Nevertheless, *V. pourtalesii* overall does not appear to suffer from the natural resuspension events and showed healthy appearances after the events. Results from this study contextualize the response of sponges to human-induced threats such as bottom fishing and climate change by providing detailed site-specific knowledge of the natural conditions under which these sponges persist and their resilience during changing environmental conditions.

CONCLUSION

Resiliency against environmental and anthropogenic stressors requires that the surrounding environmental conditions, such as temperature, DO concentration and food supply, be within a species' optimal physiological tolerance limits (Odum, 1971; Sokolova et al., 2012). Overall the near-bed environmental conditions in the *Vazella* sponge grounds on the Scotian Shelf fit within the range as described for other glass sponge species. *V. pourtalesii* experienced temperature fluctuations of up to 3.2°C on a seasonal timescale, with maximum temperatures of 12°C in spring and on average lowest temperatures in Autumn (November). Major storm events in winter and spring were additionally observed to cause extreme resuspension events, which were expected to exhibit a stressor but also an important mechanism for food supply. *V. pourtalesii* appeared to withstand these events even for several days, suggesting that sponges are resilient to natural as well as anthropogenic (e.g., fishing) resuspension events of short duration. The vertical flux of organic matter was estimated to not cover the food demand of the sponges as also observed in other sponge grounds, whereas semi-diurnal tidal currents play an important role in the resuspension of sediments, which likely constitute a constant source of particulate food for the sponges. The only directly observed stressor was high currents, which relocated benthic fauna and sometimes caused sponges to dislodge from their

upright position. Our findings show how resilient these sponges are to environmental changes over short time scales, which might be vital for their survival under human-induced threats such as bottom fishing and climate change.

DATA AVAILABILITY STATEMENT

The raw data supporting the conclusions of this article will be made available by the authors, without undue reservation.

AUTHOR CONTRIBUTIONS

UH wrote the main manuscript text, collected the data and is responsible for the analysis and interpretation of the data. FM developed the study concept, sample collection, and helped with interpretation of the data. HR initiated the study. LB and EK organized the fieldwork. All authors, except HR, reviewed the manuscript and contributed to the critical discussion.

FUNDING

This research has been performed in the scope of the SponGES project, which received funding from the European Union's Horizon 2020 Research and Innovation Program under grant agreement no. 679849. Canadian cruises and contributions were funded by Fisheries and Ocean's Canada's International Governance Strategy Science Program through project "Marine Biological Diversity Beyond Areas of National Jurisdiction (BBNJ): 3-Tiers of Diversity (Genes-Species-Communities)" led by EK (2017–2019) and Strategic Program for Ecosystem-Based Research and Advice (SPERA) project "Evaluation of the Effectiveness of Two Sponge Conservation Areas in the Maritimes Region: Identifying Patterns of Dispersal, Connectivity, and Recovery Potential of the Russian Hat Sponge *Vazella pourtalesii*" led by LB and EK. FM was supported financially by the Innovational Research Incentives Scheme of the Netherlands Organisation for Scientific Research (NWO-VIDI grant 016.161.360).

ACKNOWLEDGMENTS

We thank the captain and crew of the CCGS *Martha L. Black* and CCGS *Hudson* for their help with the deployments and recoveries of the research gear. We also thank Barry MacDonald, Francisco Javier Murillo, and the scientific party of both cruises for their help in collecting the samples. Furthermore we thank Ronald van Bommel (NIOZ) for his help with the stable isotope analysis.

SUPPLEMENTARY MATERIAL

The Supplementary Material for this article can be found online at: https://www.frontiersin.org/articles/10.3389/fmars.2020.597682/full#supplementary-material

Supplementary Figure 1 | Pearsons correlations between long-term record data.

Supplementary Figure 2 | u and v components of the current and wind data with the daily moving average shown by thick lines. Main storm events are highlighted in light blue.

REFERENCES

Anderson, C., Dobson, F., Perrie, W., Smith, P., Toulany, B., and Schwing, F. (1989). Storm response in the coastal ocean: the oceanographic component of the Canadian Atlantic Storms Program (CASP). *Eos, Trans. Am. Geophys. Union* 70, 562–572. doi: 10.1029/89eo00142

Azetsu-Scott, K., Johnson, B. D., and Petrie, B. (1995). An intermittent, intermediate nepheloid layer in Emerald Basin, Scotian Shelf. *Continental Shelf Res.* 15, 281–293. doi: 10.1016/0278-4343(93)e0003-q

Bart, M. C., De Kluijver, A., Hoetjes, S., Absalah, S., Mueller, B., Kenchington, E., et al. (2020a). Differential processing of dissolved and particulate organic matter by deep-sea sponges and their microbial symbionts. *Sci. Rep.* 10:17515.

Bart, M. C., Mueller, B., Rombouts, T., Van De Ven, C., Tompkins, G. J., Osinga, R., et al. (2020b). Dissolved organic carbon (DOC) is essential to balance the metabolic demands of North-Atlantic deep-sea sponges. *bioRxiv* [preprint] doi: 10.1101/2020.09.21.305086

Barthel, D., Tendal, O., and Thiel, H. (1996). A wandering population of the hexactineliid sponge pheronema carpenteri on the continental slope off morocco, Northwest Africa. *Mar. Ecol.* 17, 603–616. doi: 10.1111/j.1439-0485.1996.tb00420.x

Beazley, L., Kenchington, E., Yashayaev, I., and Murillo, F. J. (2015). Drivers of epibenthic megafaunal composition in the sponge grounds of the Sackville Spur, northwest Atlantic. *Deep Sea Res. Part I: Oceanographic Res. Papers* 98, 102–114. doi: 10.1016/j.dsr.2014.11.016

Beazley, L., Wang, Z., Kenchington, E., Yashayaev, I., Rapp, H. T., Xavier, J. R., et al. (2018). Predicted distribution of the glass sponge Vazella pourtalesi on the Scotian Shelf and its persistence in the face of climatic variability. *PLoS One* 13:e0205505. doi: 10.1371/journal.pone.0205505

Beazley, L. I., Kenchington, E. L., Murillo, F. J., and Sacau, M. D. M. (2013). Deep-sea sponge grounds enhance diversity and abundance of epibenthic megafauna in the Northwest Atlantic. *ICES J. Mar. Sci.* 70, 1471–1490. doi: 10.1093/icesjms/fst124

Bell, J. J., Mcgrath, E., Biggerstaff, A., Bates, T., Bennett, H., Marlow, J., et al. (2015). Sediment impacts on marine sponges. *Mar. Pollut. Bull.* 94, 5–13. doi: 10.1016/j.marpolbul.2015.03.030

Bunt, J. A., Larcombe, P., and Jago, C. F. (1999). Quantifying the response of optical backscatter devices and transmissometers to variations in suspended particulate matter. *Continental Shelf Res.* 19, 1199–1220. doi: 10.1016/s0278-4343(99)00018-7

Busch, K., Hanz, U., Mienis, F., Mueller, B., Franke, A., Roberts, E. M., et al. (2020). On giant shoulders: how a seamount affects the microbial community composition of seawater and sponges. *Biogeosciences* 17, 3471–3486. doi: 10.5194/bg-17-3471-2020

Carlson, D. F., Muscarella, P. A., Gildor, H., Lipphardt, B. L. Jr., and Fredj, E. (2010). How useful are progressive vector diagrams for studying coastal ocean transport? *Limnol. Oceanography: Methods* 8, 98–106. doi: 10.4319/lom.2010.8.0098

Cathalot, C., Van Oevelen, D., Cox, T. J., Kutti, T., Lavaleye, M., Duineveld, G., et al. (2015). Cold-water coral reefs and adjacent sponge grounds: hotspots of benthic respiration and organic carbon cycling in the deep sea. *Front. Mar. Sci.* 2:37. doi: 10.3389/fmars.2015.00037

Chen, C., Huang, H., Beardsley, R. C., Xu, Q., Limeburner, R., Cowles, G. W., et al. (2011). Tidal dynamics in the Gulf of Maine and New England Shelf: an application of FVCOM. *J. Geophys. Res.: Oceans* 116:12010.

Chu, J. W., and Leys, S. P. (2010). High resolution mapping of community structure in three glass sponge reefs (Porifera, Hexactinellida). *Mar. Ecol. Prog. Ser.* 417, 97–113. doi: 10.3354/meps08794

Cyr, F., Van Haren, H., Mienis, F., Duineveld, G., and Bourgault, D. (2016). On the influence of cold-water coral mound size on flow hydrodynamics, and vice versa. *Geophys. Res. Lett.* 43, 775–783. doi: 10.1002/2015gl067038

Davison, J. J., Van Haren, H., Hosegood, P., Piechaud, N., and Howell, K. L. (2019). The distribution of deep-sea sponge aggregations (Porifera) in relation to oceanographic processes in the Faroe-Shetland Channel. *Deep Sea Res. Part I: Oceanographic Res. Papers* 146, 55–61. doi: 10.1016/j.dsr.2019.03.005

DFO (2020). *Canadian Wave Data ID44150 - La Have Bank", in: 2006/03/01 to 2020/01/14*. Canada: Department of Fisheries and Oceans Canada.

Drinkwater, K., Petrie, B., and Smith, P. (2003). Climate variability on the Scotian Shelf during the 1990s. *ICES Mar. Sci. Symp.* 219, 40–49.

Drinkwater, K., Petrie, B., and Sutcliffe, W. Jr. (1979). Seasonal geostrophic volume transports along the Scotian Shelf. *Estuarine Coastal Mar. Sci.* 9, 17–27. doi: 10.1016/0302-3524(79)90003-3

Duineveld, G., Lavaleye, M., and Berghuis, E. (2004). Particle flux and food supply to a seamount cold-water coral community (Galicia Bank, NW Spain). *Mar. Ecol. Prog. Ser.* 277, 13–23. doi: 10.3354/meps277013

Duineveld, G. C., Lavaleye, M. S., Bergman, M. J., De Stigter, H., and Mienis, F. (2007). Trophic structure of a cold-water coral mound community (Rockall Bank, NE Atlantic) in relation to the near-bottom particle supply and current regime. *Bull. Mar. Sci.* 81, 449–467.

Farrow, G. E., Syvitski, J. P., and Tunnicliffe, V. (1983). Suspended particulate loading on the macrobenthos in a highly turbid fjord: knight Inlet, British Columbia. *Can. J. Fish. Aquatic Sci.* 40, s273–s288.

Fuller, S., and Cameron, P. (1998). *Marine Benthic Seascapes: Fishermen's Perspectives*. Halifax, NS: Ecology Action Centre.

Fuller, S. D. (2011). *Diversity of Marine Sponges in the Northwest Atlantic*. PhD thesis, Dalhousie University: Halifax, NS.

Gardner, W., Richardson, M., Hinga, K., and Biscaye, P. (1983). Resuspension measured with sediment traps in a high-energy environment. *Earth Planetary Sci. Lett.* 66, 262–278. doi: 10.1016/0012-821x(83)90140-1

Garrett, C., and Laurent, L. S. (2002). Aspects of deep ocean mixing. *J. Oceanography* 58, 11–24.

Gatien, M. G. (1976). A study in the slope water region south of Halifax. *J. Fish. Board Canada* 33, 2213–2217. doi: 10.1139/f76-270

Grant, J., Volckaert, F., and Roberts-Regan, D. L. (1987). Resuspendable organic matter in Nova Scotian shelf and slope sediments. *Continental Shelf Res.* 7, 1123–1138. doi: 10.1016/0278-4343(87)90102-6

Grant, N., Matveev, E., Kahn, A., Archer, S., Dunham, A., Bannister, R., et al. (2019). Effect of suspended sediments on the pumping rates of three species of glass sponge in situ. *Mar. Ecol. Prog. Ser.* 615, 79–100. doi: 10.3354/meps12939

Gray, J. S., Wu, R. S.-S., and Or, Y. Y. (2002). Effects of hypoxia and organic enrichment on the coastal marine environment. *Mar. Ecol. Prog. Ser.* 238, 249–279. doi: 10.3354/meps238249

Greenberg, D. A., Loder, J. W., Shen, Y. S., Lynch, D. R., and Naimie, C. E. (1997). Spatial and temporal structure of the barotropic response of the Scotian Shelf and Gulf of Maine to surface wind stress: a model-based study. *J. Geophys. Res.-Oceans* 102, 20897–20915. doi: 10.1029/97jc00442

Han, G., Hannah, C. G., Loder, J. W., and Smith, P. C. (1997). Seasonal variation of the three-dimensional mean circulation over the Scotian Shelf. *J. Geophys. Res.: Oceans* 102, 1011–1025. doi: 10.1029/96jc03285

Han, G., and Loder, J. W. (2003). Three-dimensional seasonal-mean circulation and hydrography on the eastern Scotian Shelf. *J. Geophys. Res.: Oceans* 108. doi: 10.1029/2002JC001463

Hannah, C. G., Shore, J. A., Loder, J. W., and Naimie, C. E. (2001). Seasonal circulation on the western and central Scotian Shelf. *J. Phys. Oceanography* 31, 591–615. doi: 10.1175/1520-0485(2001)031<0591:scotwa>2.0.co;2

Hanz, U., Wienberg, C., Hebbeln, D., Duineveld, G., Lavaleye, M., Juva, K., et al. (2019). Environmental factors influencing benthic communities in the oxygen minimum zones on the Angolan and Namibian margins. *Biogeosciences (BG)* 16, 4337–4356. doi: 10.5194/bg-16-4337-2019

Hawkes, N., Korabik, M., Beazley, L., Rapp, H. T., Xavier, J. R., and Kenchington, E. (2019). Glass sponge grounds on the Scotian Shelf and their associated biodiversity. *Mar. Ecol. Prog. Ser.* 614, 91–109. doi: 10.3354/meps12903

Hill, P. R., and Bowen, A. J. (1983). "Modern Sediment Dynamics at the shelf-slope Boundary off Nova Scotia," in *The Shelfbreak: Critical Interface on Continental Margins*: eds D. J. Stanley, and G. T. Moore (Tulsa: Society Economic Paleontologists Mineralogists Special Publication 33), 265–276. doi: 10.2110/pec.83.06.0265

Holm-Hansen, O., Lorenzen, C. J., Holmes, R. W., and Strickland, J. D. (1965). Fluorometric determination of chlorophyll. *ICES J. Mar. Sci.* 30, 3–15. doi: 10.1093/icesjms/30.1.3

Hosegood, P., and van Haren, H. (2004). Near-bed solibores over the continental slope in the Faeroe-Shetland Channel. *Deep Sea Res. Part II: Top. Stud. Oceanography* 51, 2943–2971. doi: 10.1016/j.dsr2.2004.09.016

Howell, K.-L., Piechaud, N., Downie, A.-L., and Kenny, A. (2016). The distribution of deep-sea sponge aggregations in the North Atlantic and implications for their effective spatial management. *Deep Sea Res. Part I: Oceanographic Res. Papers* 115, 309–320. doi: 10.1016/j.dsr.2016.07.005

Ji, R., Chen, C., Franks, P. J., Townsend, D. W., Durbin, E. G., Beardsley, R. C., et al. (2006). The impact of Scotian Shelf Water "cross-over" on the plankton dynamics on georges bank: a 3-D experiment for the 1999 spring bloom. *Deep Sea Res. Part II: Top. Stud. Oceanography* 53, 2684–2707. doi: 10.1016/j.dsr2.2006.08.007

Kahn, A. S., Yahel, G., Chu, J. W., Tunnicliffe, V., and Leys, S. P. (2015). Benthic grazing and carbon sequestration by deep-water glass sponge reefs. *Limnol. Oceanography* 60, 78–88. doi: 10.1002/lno.10002

Klitgaard, A. B., and Tendal, O. S. (2004). Distribution and species composition of mass occurrences of large-sized sponges in the northeast Atlantic. *Prog. Oceanography* 61, 57–98. doi: 10.1016/j.pocean.2004.06.002

Knutson, T. R., Mcbride, J. L., Chan, J., Emanuel, K., Holland, G., Landsea, C., et al. (2010). Tropical cyclones and climate change. *Nat. Geosci.* 3, 157–163.

Kutti, T., Bannister, R. J., and Fosså, J. H. (2013). Community structure and ecological function of deep-water sponge grounds in the Traenadypet MPA—Northern Norwegian continental shelf. *Continental Shelf Res.* 69, 21–30. doi: 10.1016/j.csr.2013.09.011

Kutti, T., Bannister, R. J., Fosså, J. H., Krogness, C. M., Tjensvoll, I., and Søvik, G. (2015a). Metabolic responses of the deep-water sponge Geodia barretti to suspended bottom sediment, simulated mine tailings and drill cuttings. *J. Exp. Mar. Biol. Ecol.* 473, 64–72. doi: 10.1016/j.jembe.2015.07.017

Kutti, T., Fosså, J. H., and Bergstad, O. A. (2015b). Influence of structurally complex benthic habitats on fish distribution. *Mar. Ecol. Prog. Ser.* 520, 175–190. doi: 10.3354/meps11047

Kuwae, T., and Hosokawa, Y. (1999). Determination of abundance and biovolume of bacteria in sediments by dual staining with 4', 6-diamidino-2-phenylindole and acridine orange: relationship to dispersion treatment and sediment characteristics. *Appl. Environ. Microbiol.* 65, 3407–3412. doi: 10.1128/aem.65.8.3407-3412.1999

Lacharité, M., and Metaxas, A. (2017). Hard substrate in the deep ocean: how sediment features influence epibenthic megafauna on the eastern Canadian margin. *Deep Sea Res. Part I: Oceanographic Res. Papers* 126, 50–61. doi: 10.1016/j.dsr.2017.05.013

Leys, S. P., Mackie, G. O., and Reiswig, H. M. (2007). The biology of glass sponges. *Adv. Mar. Biol.* 52, 1–145. doi: 10.1016/s0065-2881(06)52001-2

Li, Y. Z., He, R. Y., and Mcgillicuddy, D. J. (2014). Seasonal and interannual variability in Gulf of Maine hydrodynamics: 2002-2011. *Deep-Sea Res. Part Ii-Top. Stud. Oceanography* 103, 210–222. doi: 10.1016/j.dsr2.2013.03.001

Loder, J. W., Han, G., Hannah, C. G., Greenberg, D. A., and Smith, P. C. (1997). Hydrography and baroclinic circulation in the Scotian Shelf region: winter versus summer. *Can. J. Fish. Aquatic Sci.* 54, 40–56. doi: 10.1139/f96-153

Maldonado, M., Aguilar, R., Bannister, R. J., Bell, J. J., Conway, K. W., Dayton, P. K., et al. (2017). "Sponge grounds as key marine habitats: a synthetic review of types, structure, functional roles, and conservation concerns," in *Marine Animal Forests: The Ecology of Benthic Biodiversity Hotspots*, eds S. Rossi, L. Bramanti, A. Gori, V. Saco del, and O. Covadonga (Cham: Springer International Publishing), 145–183. doi: 10.1007/978-3-319-21012-4_24

Maldonado, M., Beazley, L., Lopez-Acosta, M., Kenchington, E., Casault, B., Hanz, U., et al. (2020). *Massive Silicate Utilization Facilitated by a Benthic-pelagic Coupled Feedback Sustains Deep-Sea Sponge Aggregations*. Hoboken, NJ: John Wiley & Sons, Inc.

Maldonado, M., Giraud, K., and Carmona, C. (2008). Effects of sediment on the survival of asexually produced sponge recruits. *Mar. Biol.* 154, 631–641. doi: 10.1007/s00227-008-0956-5

Maldonado, M., Ribes, M., and Van Duyl, F. C. (2012). Nutrient fluxes through sponges: biology, budgets, and ecological implications. *Adv. Mar. Biol.* 62, 113–182. doi: 10.1016/b978-0-12-394283-8.00003-5

McLellan, H. (1957). On the distinctness and origin of the slope water off the Scotian Shelf and its easterly flow south of the Grand Banks. *J. Fish. Board Canada* 14, 213–239. doi: 10.1139/f57-011

Meyer, H., Roberts, E., Rapp, H., and Davies, A. (2019). Spatial patterns of arctic sponge ground fauna and demersal fish are detectable in autonomous underwater vehicle (AUV) imagery. *Deep Sea Res. Part I: Oceanographic Res. Papers* 153:103137. doi: 10.1016/j.dsr.2019.103137

Mienis, F., Duineveld, G., Davies, A., Ross, S., Seim, H., Bane, J., et al. (2012). The influence of near-bed hydrodynamic conditions on cold-water corals in the Viosca Knoll area, Gulf of Mexico. *Deep Sea Res. Part I: Oceanographic Res. Papers* 60, 32–45. doi: 10.1016/j.dsr.2011.10.007

Mills, E., and Fournier, R. (1979). Fish production and the marine ecosystems of the Scotian Shelf, eastern Canada. *Mar. Biol.* 54, 101–108. doi: 10.1007/bf00386589

Mountain, D. G. (2012). Labrador slope water entering the Gulf of Maine—response to the North Atlantic Oscillation. *Continental Shelf Res.* 47, 150–155. doi: 10.1016/j.csr.2012.07.008

Murillo, F. J., Kenchington, E., Tompkins, G., Beazley, L., Baker, E., Knudby, A., et al. (2018). Sponge assemblages and predicted archetypes in the eastern Canadian Arctic. *Mar. Ecol. Prog. Ser.* 597, 115–135. doi: 10.3354/meps12589

Murillo, F. J., Muñoz, P. D., Cristobo, J., Ríos, P., González, C., Kenchington, E., et al. (2012). Deep-sea sponge grounds of the Flemish Cap, Flemish Pass and the Grand Banks of Newfoundland (Northwest Atlantic Ocean): distribution and species composition. *Mar. Biol. Res.* 8, 842–854. doi: 10.1080/17451000.2012.682583

Odum, H. T. (1971). *Environment, Power and Society*. New York, NY: Wiley-Interscience.

Petrie, B., and Drinkwater, K. (1993). Temperature and salinity variability on the Scotian Shelf and in the Gulf of Maine 1945–1990. *J. Geophys. Res.: Oceans* 98, 20079–20089. doi: 10.1029/93jc02191

Petrie, B., and Yeats, P. (2000). Annual and interannual variability of nutrients and their estimated fluxes in the Scotian Shelf-Gulf of Maine region. *Can. J. Fish. Aquatic Sci.* 57, 2536–2546. doi: 10.1139/f00-235

Pham, C. K., Murillo, F. J., Lirette, C., Maldonado, M., Colaço, A., Ottaviani, D., et al. (2019). Removal of deep-sea sponges by bottom trawling in the Flemish Cap area: conservation, ecology and economic assessment. *Sci. Rep.* 9:15843.

Pile, A. J., and Young, C. M. (2006). The natural diet of a hexactinellid sponge: benthic–pelagic coupling in a deep-sea microbial food web. *Deep Sea Res. Part I: Oceanographic Res. Papers* 53, 1148–1156. doi: 10.1016/j.dsr.2006.03.008

Reiswig, H. M. (1971). Particle feeding in natural populations of three marine demosponges. *Biol. Bull.* 141, 568–591. doi: 10.2307/1540270

Rice, A., Thurston, M., and New, A. (1990). Dense aggregations of a hexactinellid sponge, Pheronema carpenteri, in the Porcupine Seabight (northeast Atlantic Ocean), and possible causes. *Prog. Oceanography* 24, 179–196. doi: 10.1016/0079-6611(90)90029-2

Rix, L., De Goeij, J. M., Mueller, C. E., Struck, U., Middelburg, J. J., Van Duyl, F. C., et al. (2016). Coral mucus fuels the sponge loop in warm-and cold-water coral reef ecosystems. *Sci. Rep.* 6:18715.

Roberts, E., Mienis, F., Rapp, H., Hanz, U., Meyer, H., and Davies, A. (2018). Oceanographic setting and short-timescale environmental variability at an Arctic seamount sponge ground. *Deep Sea Res. Part I: Oceanographic Res. Papers* 138, 98–113. doi: 10.1016/j.dsr.2018.06.007

Roberts, J. M., Wheeler, A. J., and Freiwald, A. (2006). Reefs of the deep: the biology and geology of cold-water coral ecosystems. *Science* 312, 543–547. doi: 10.1126/science.1119861

Smith, P. C. (1978). Low-frequency fluxes of momentum, heat, salt, and nutrients at the edge of the Scotian Shelf. *J. Geophys. Res.: Oceans* 83, 4079–4096. doi: 10.1029/jc083ic08p04079

Smith, P. C., Petrie, B., and Mann, C. (1978). Circulation, variability, and dynamics of the Scotian Shelf and slope. *J. Fish. Board Canada* 35, 1067–1083. doi: 10.1139/f78-170

Sokolova, I. M., Frederich, M., Bagwe, R., Lannig, G., and Sukhotin, A. A. (2012). Energy homeostasis as an integrative tool for assessing limits of environmental stress tolerance in aquatic invertebrates. *Mar. Environ. Res.* 79, 1–15. doi: 10.1016/j.marenvres.2012.04.003

Song, H., Ji, R., Stock, C., Kearney, K., and Wang, Z. (2011). Interannual variability in phytoplankton blooms and plankton productivity over the Nova Scotian Shelf and in the Gulf of Maine. *Mar. Ecol. Prog. Ser.* 426, 105–118. doi: 10.3354/meps09002

Strand, R., Whalan, S., Webster, N. S., Kutti, T., Fang, J. K.-H., Luter, H. M., et al. (2017). The response of a boreal deep-sea sponge holobiont to acute thermal stress. *Sci. Rep.* 7:1660.

Tabachnick, K., Van Soest, R., Van Kempen, T. M., and Braekamn, J. (1994). *Distribution of Recent Hexactinellida. Sponges in Time and Space*. Rotterdam: Balkema, 225–232.

Tjensvoll, I., Kutti, T., Fosså, J. H., and Bannister, R. (2013). Rapid respiratory responses of the deep-water sponge Geodia barretti exposed to suspended sediments. *Aquatic Biol.* 19, 65–73. doi: 10.3354/ab00522

Townsend, D., and Ellis, W. (2010). "Primary production and nutrient cycling on the Northwest Atlantic continental shelf," in *Carbon and Nutrient Fluxes in Continental Margins: A global synthesis*, eds K.-K. Liu, L. Atkinson, R. Quinones, and L. Talaue-McManus (Berlin: IGBP Book Series. Springer).

Townsend, D. W., Thomas, A. C., Mayer, L. M., Thomas, M. A., and Quinlan, J. A. (2006). Oceanography of the northwest Atlantic continental shelf (1, W). *Sea: Global Coastal Ocean: Interdisciplinary Reg. Stud. Syntheses* 14, 119–168.

Urrego-Blanco, J., and Sheng, J. (2014). Study on subtidal circulation and variability in the Gulf of St. Lawrence, Scotian Shelf, and Gulf of Maine using a nested-grid shelf circulation model. *Ocean Dynamics* 64, 385–412. doi: 10.1007/s10236-013-0688-z

van Haren, H., Hanz, U., De Stigter, H., Mienis, F., and Duineveld, G. (2017). Internal wave turbulence at a biologically rich Mid-Atlantic seamount. *PLoS One* 12:e0189720. doi: 10.1371/journal.pone.0189720

van Haren, H., Mienis, F., Duineveld, G. C., and Lavaleye, M. S. (2014). High-resolution temperature observations of a trapped nonlinear diurnal tide influencing cold-water corals on the Logachev mounds. *Prog. Oceanography* 125, 16–25. doi: 10.1016/j.pocean.2014.04.021

van Haren, H., Oakey, N., and Garrett, C. (1994). Measurements of internal wave band eddy fluxes above a sloping bottom. *J. Mar. Res.* 52, 909–946. doi: 10.1357/0022240943076876

Vangriesheim, A., Springer, B., and Crassous, P. (2001). Temporal variability of near-bottom particle resuspension and dynamics at the Porcupine Abyssal Plain, Northeast Atlantic. *Prog. Oceanography* 50, 123–145. doi: 10.1016/s0079-6611(01)00051-9

Wainright, S. C. (1987). Stimulation of heterotrophic microplankton production by resuspended marine sediments. *Science* 238, 1710–1712. doi: 10.1126/science.238.4834.1710

Whitney, F., Conway, K., Thomson, R., Barrie, V., Krautter, M., and Mungov, G. (2005). Oceanographic habitat of sponge reefs on the Western Canadian Continental Shelf. *Continental Shelf Res.* 25, 211–226. doi: 10.1016/j.csr.2004.09.003

Wunsch, C. (1975). Deep ocean internal waves: what do we really know? *J. Geophys. Res.* 80, 339–343. doi: 10.1029/jc080i003p00339

Conflict of Interest: The authors declare that the research was conducted in the absence of any commercial or financial relationships that could be construed as a potential conflict of interest.

Copyright © 2021 Hanz, Beazley, Kenchington, Duineveld, Rapp and Mienis. This is an open-access article distributed under the terms of the Creative Commons Attribution License (CC BY). The use, distribution or reproduction in other forums is permitted, provided the original author(s) and the copyright owner(s) are credited and that the original publication in this journal is cited, in accordance with accepted academic practice. No use, distribution or reproduction is permitted which does not comply with these terms.

frontiers in Marine Science

CORRECTION
published: 14 May 2021
doi: 10.3389/fmars.2021.696777

Corrigendum: Seasonal Variability in Near-bed Environmental Conditions in the *Vazella pourtalesii* Glass Sponge Grounds of the Scotian Shelf

Ulrike Hanz[1]*, *Lindsay Beazley*[2], *Ellen Kenchington*[2], *Gerard Duineveld*[1], *Hans Tore Rapp*[3†] and *Furu Mienis*[1]

[1] Department of Ocean Systems, NIOZ Royal Netherlands Institute for Sea Research, Den Burg, Netherlands, [2] Fisheries and Oceans Canada (DFO), Bedford Institute of Oceanography, Dartmouth, NS, Canada, [3] Department of Biological Sciences and K.G. Jebsen Centre for Deep-sea Research, University of Bergen, Bergen, Norway

Keywords: ***Vazella pourtalesii*, sponge ground, environmental conditions, storm events, particle flux, Scotian Shelf**

A Corrigendum on

Seasonal Variability in Near-bed Environmental Conditions in the *Vazella pourtalesii* Glass Sponge Grounds of the Scotian Shelf

by Hanz, U., Beazley, L., Kenchington, E., Duineveld, G., Rapp, H. T., and Mienis, F. (2021). Front. Mar. Sci. 7:597682. doi: 10.3389/fmars.2020.597682

OPEN ACCESS

Edited and reviewed by:
Chiara Romano, Spanish National Research Council, Spain

***Correspondence:**
Ulrike Hanz
Ulrike.hanz@nioz.nl

†*Deceased*

Specialty section:
This article was submitted to Deep-Sea Environments and Ecology, a section of the journal Frontiers in Marine Science

Received: *17 April 2021*
Accepted: *22 April 2021*
Published: *14 May 2021*

Citation:
Hanz U, Beazley L, Kenchington E, Duineveld G, Rapp HT and Mienis F (2021) Corrigendum: Seasonal Variability in Near-bed Environmental Conditions in the Vazella pourtalesii Glass Sponge Grounds of the Scotian Shelf. Front. Mar. Sci. 8:696777. doi: 10.3389/fmars.2021.696777

In the original article, there was a mistake in **Figure 6** as published. Due to a database error the flux data shown in **Figures 6F,G** were presented as mg day^{-1} instead of mg day^{-1} m^2. The corrected **Figure 6** appears below.

Because of the database error related to data presented in **Figure 6**, average mass and carbon fluxes also need to be adapted in the text.

A correction has been made to the Results and *Sediment Trap* section:

The vertical mass flux during the deployment period was on average 3166 ± 3421 mg m^{-2} day^{-1} (**Figure 6F**), while the average carbon flux was 100 ± 72 mg C m^{-2} day^{-1} (**Figure 6G**). Highest vertical mass flux, i.e., 12,390 mg m^{-2} day^{-1}, was observed in the period from December 2017 to January 2018. Highest carbon flux was likewise found in December/January coinciding with the winter storm event (281 mg C m^{-2} day^{-1}, **Figure 6**). The C:N ratio was on average 8.3 ± 0.2, ranging from 7.8 to 8.6 (**Figure 6B**) and the δ^{15}N was 6.7 ± 0.4‰, ranging from 6.2 to 7.3‰ (**Figure 6C**). The δ^{13}C ratio ranged from −23.3 to −22.8‰ with an average of −23 ± 0.1‰ (**Figure 6D**). The Chl-*a* concentration was on average 2.1 ± 1.1 mg l^{-1}, with an average Chl-*a*: Phaeo ratio of 0.00069 ± 0.00077 (**Figure 6E**). The largest peak in Chl-*a* (4.05 mg l^{-1}), being two times higher than the average Chl-*a* concentration, was observed in March/April, indicating the arrival of fresh phytodetritus at the seafloor, which occurred after the second storm event in March.

A correction has been made to the Discussion in the *Food Supply* section Paragraph 1:

Sponges are very efficient filter feeders and feed on particulate as well as dissolved resources (Reiswig, 1971; Pile and Young, 2006). While the average daily carbon flux in the near-bed sediment trap was **100 ± 72 mg C m^{-2} day^{-1}** during the deployment period, carbon flux was highly variable and peaked in December/January (**281 mg C m^{-2} day^{-1}**) and March/April (**130 mg C m^{-2} day^{-1}**). During the December peak no major fluctuations in temperature, salinity or DO concentration were observed, likely indicating that the organic matter is not delivered from the surface but rather due to resuspension events inside the bottom boundary layer. Even though this winter event was characterized by a high carbon flux, mainly degraded organic matter was resuspended as shown by

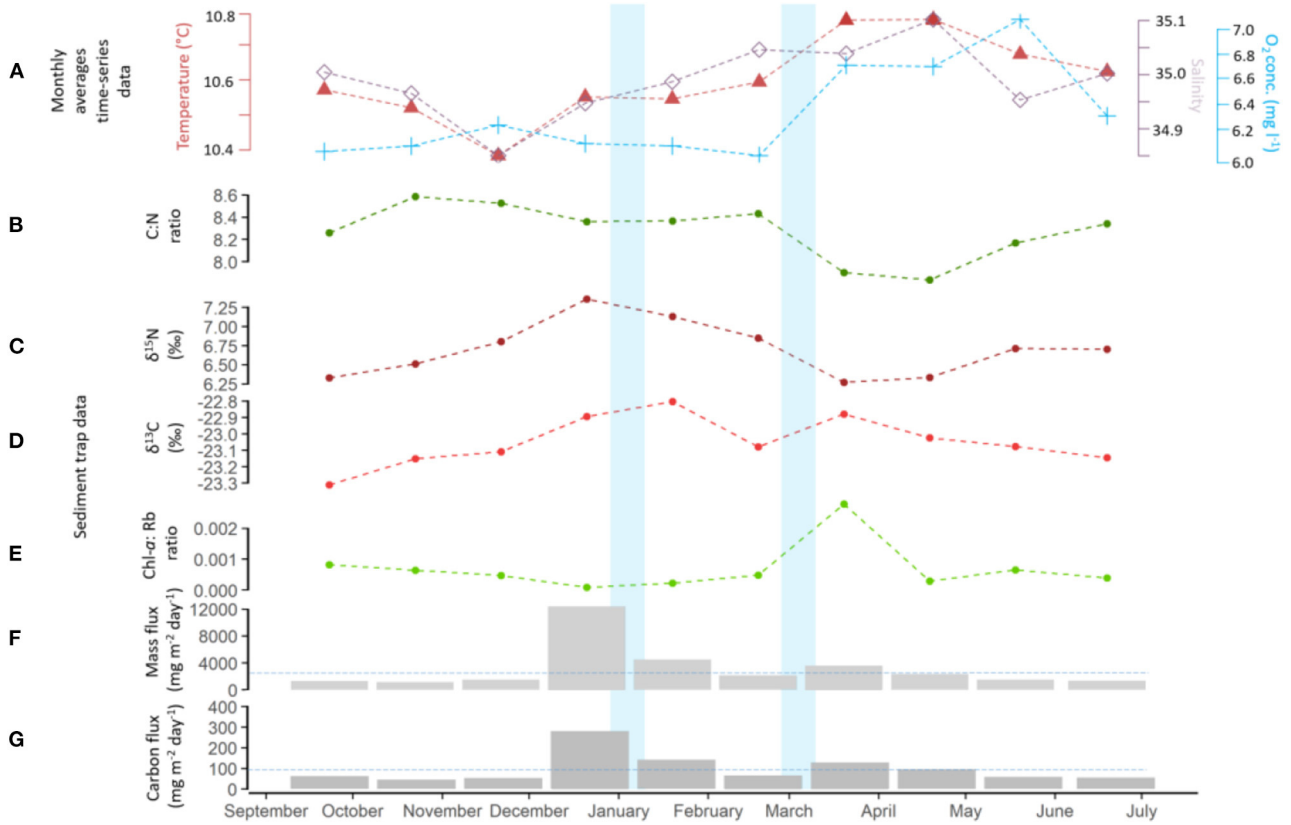

FIGURE 6 | (A) Monthly averages of temperature, salinity and oxygen concentration recorded by the lander, Sediment trap data: **(B)** C:N ratio; **(C)** $\delta^{15}N$; **(D)** $\delta^{13}C$; **(E)** Chlorophyll-a: Phaeopigments ratio of the sediment trap material; **(F)** Mass and **(G)** Carbon flux recorded by the sediment trap. Blue horizontal lines are indicating the average mass and carbon flux. Line charts and histograms represent the average value during the 30 day sediment trap interval. Storm events are highlighted in light blue.

the low concentration of Chl-*a* and a high C:N ratio (**Figure 6**), likely related to resuspension and lateral transport of more degraded material from the seafloor. Hill and Bowen (1983) calculated that a current speed of 0.15 m s^{-1} is required to resuspend the coarser sand, whereas fine sand and mud is transported at a speed of 0.11 m s^{-1}. Current speed as measured in this study would be sufficient to resuspend coarse sediment during 31% of the time and 56% for the finer fraction. This was also apparent in the ADCP turbidity data **(Figure 5)** which showed an almost permanent turbid layer close to the bottom. The video recordings showed that during storm-induced resuspension events, particularly the winter event, particles stayed in resuspension for several days, which was however not detected in the acoustic backscatter data of the ADCP, implying that turbidity close to the bottom might be even more persistent. This could possibly be due to the particle size of the particles in resuspension, whereby the finer particles are not resolved by measurements of the ADCP (Bunt et al., 1999).

A correction has been made to the Discussion in the *Food Supply* section Paragraph 3

Taking the estimated carbon demand of a deep-water glass sponge reef (ca. 160 m depth, ∼10°C) at the Canadian coast (1800–4100 mg C m^{-2} day^{-1}, Kahn et al., 2015), the carbon derived from the vertical flux would provide on average approximately <8% of the required carbon demand. *Ex situ* experiments have shown that in the Canadian sponge reefs carbon consumption was much higher (360 mg m^{-2} day^{-1}), compared to the average carbon flux (100 mg m^{-2} day^{-1}), showing that the carbon demand of the Vazella grounds will not be satisfied (Bart et al., 2020). A potential carbon deficit may be alleviated from the resuspended organic-rich sediment itself (Grant et al., 1987), but also from the filtration of bacteria and uptake of DOC from the water column (Bart et al., 2020).

The authors apologize for this error and state that this does not change the scientific conclusions of the article in any way. The original article has been updated.

REFERENCES

Bart, M. C., Mueller, B., Rombouts, T., Van De Ven, C., Tompkins, G. J., Osinga, R., et al. (2020). Dissolved organic carbon (DOC) is essential to balance the metabolic demands of North-Atlantic deep-sea sponges. *bioRxiv* [preprint] doi: 10.1101/2020.09.21.305086

Bunt, J. A., Larcombe, P., and Jago, C. F. (1999). Quantifying the response of optical backscatter devices and transmissometers to variations in suspended particulate matter. *Continental Shelf Res.* 19, 1199–1220. doi: 10.1016/s0278-4343(99)00018-7

Grant, J., Volckaert, F., and Roberts-Regan, D. L. (1987). Resuspendable organic matter in Nova Scotian shelf and slope sediments. *Continental Shelf Res.* 7, 1123–1138. doi: 10.1016/0278-4343(87)90102-6

Hill, P. R., and Bowen, A. J. (1983). "Modern Sediment Dynamics at the shelf-slope Boundary off Nova Scotia," in *The Shelfbreak: Critical Interface on Continental Margins*: eds D. J. Stanley and G. T. Moore (Tulsa: Society Economic Paleontologists Mineralogists Special Publication 33), 265–276. doi: 10.2110/pec.83.06.0265

Kahn, A. S., Yahel, G., Chu, J. W., Tunnicliffe, V., and Leys, S. P. (2015). Benthic grazing and carbon sequestration by deep-water glass sponge reefs. *Limnol. Oceanography* 60, 78–88. doi: 10.1002/lno.10002

Pile, A. J., and Young, C. M. (2006). The natural diet of a hexactinellid sponge: benthic–pelagic coupling in a deep-sea microbial food web. *Deep Sea Res. Part I: Oceanographic Res. Papers* 53, 1148–1156. doi: 10.1016/j.dsr.2006.03.008

Reiswig, H. M. (1971). Particle feeding in natural populations of three marine demosponges. *Biol. Bull.* 141, 568–591. doi: 10.2307/1540270

Copyright © 2021 Hanz, Beazley, Kenchington, Duineveld, Rapp and Mienis. This is an open-access article distributed under the terms of the Creative Commons Attribution License (CC BY). The use, distribution or reproduction in other forums is permitted, provided the original author(s) and the copyright owner(s) are credited and that the original publication in this journal is cited, in accordance with accepted academic practice. No use, distribution or reproduction is permitted which does not comply with these terms.

frontiers in Marine Science

ORIGINAL RESEARCH
published: 08 January 2021
doi: 10.3389/fmars.2020.606749

Asteroids and Ophiuroids Associated With Sponge Aggregations as a Key to Marine Habitats. A Comparative Analysis Between Avilés Canyons System and El Cachucho, Marine Protected Area

Maria Eugenia Manjón-Cabeza[1], Pilar Ríos[2]*, Laura María García-Guillén[1], Aurora Macías-Ramírez[1], Francisco Sánchez[2], Augusto Rodríguez-Básalo[2], Teodoro P. Ibarrola[3] and Javier Cristobo[3]*

[1] Departamento de Biología Animal, Universidad de Málaga, Málaga, Spain, [2] Centro Oceanográfico de Santander, Instituto Español de Oceanografía, Santander, Spain, [3] Centro Oceanográfico de Gijón, Instituto Español de Oceanografía, Gijón, Spain

OPEN ACCESS

Edited by:
Shirley A. Pomponi, Florida Atlantic University, United States

Reviewed by:
Lorenzo Angeletti, National Research Council (CNR), Italy
Chris Mah, National Museum of Natural History (SI), United States

***Correspondence:**
Maria Eugenia Manjón-Cabeza
mecloute@uma.es
Pilar Ríos
pilar.rios@ieo.es

Specialty section:
This article was submitted to Deep-Sea Environments and Ecology, a section of the journal Frontiers in Marine Science

Received: *15 September 2020*
Accepted: *04 December 2020*
Published: *08 January 2021*

Citation:
Manjón-Cabeza ME, Ríos P, García-Guillén LM, Macías-Ramírez A, Sánchez F, Rodríguez-Básalo A, Ibarrola TP and Cristobo J (2021) Asteroids and Ophiuroids Associated With Sponge Aggregations as a Key to Marine Habitats. A Comparative Analysis Between Avilés Canyons System and El Cachucho, Marine Protected Area. Front. Mar. Sci. 7:606749. doi: 10.3389/fmars.2020.606749

This study analyzes the fauna composition of the community of brittle and sea stars associated with sponge aggregations located in Avilés Canyons System and El Cachucho, Marine Protected Area (MPA). Diverse sampling methods were used depending on bottom morphology, such as rock dredges and specific samplers for sedimentary bottoms, mainly beam trawl models. These banks are made up of sponge and coral species that build a very appropriate substrate for the proliferation of benthic species, which together create Vulnerable Marine Ecosystems that are highly relevant for management and conservation. Among these benthic species, echinoderms are of great interest due to their value as indicators of good habitat. In total, 1261 specimens were collected (934 brittle stars and 327 starfishes), belonging to 42 species (28 ophiuroids and 14 asteroids) from INDEMARES AVILÉS, ECOMARG, and SponGES project surveys. Specimens were distributed among four sponge aggregations (F: fields) that were considered according to the sponge records obtained in the same stations (36). These fields were defined and named based on the five most common sponge species: *Aphrocallistes beatrix* and *Regadrella phoenix* (F1: Avilés Canyon); *Pheronema carpenteri* (F2: Intraslope basin of Le Danois Bank); *Asconema setubalense* (F3: Le Danois Bank); and *Neoschrammeniella* aff. *bowerbankii* (F4: Corbiro Canyon). Faunistic results show that *Ophiactis abyssicola* (55.55% occurrence), *Brisinga endecacnemos, Ophiolycus purpureus,* and *Peltaster placenta* (33.33%) were the most frequently found species in F1; *Psilaster andromeda* (80%), *Pseudarchaster parelii* (60%), and *Nymphaster arenatus* (46.67%) in F2; *Ophiura carnea* (71.43%) and *Ophiacantha smitti* (42.86%) in F3; and *Ophiacantha densa,* and *Henricia caudani* (100%) in F4. The asteroid and ophiuroid species collected seem to be composed of four different communities that fit to areas with particular morphological and biological features, related to the presence of species specialized in the use of the resources they

can find there. In general, the abiotic factor controlling this structure is depth. This assemblage structure, which favors the dissimilarity between the canyons and the bank, is not so clear, since the deepest stations are located on the intraslope basin of El Cachucho, Marine Protected Area (MPA), therefore, using it *a priori* could lead to misunderstandings. Once the structure of the echinoderm community was known, we compared the expected and obtained results to analyze evidence which should prove the existence of any association between echinoderms and sponges, which enabled us to refute the incongruous hypothesis.

Keywords: Asteroidea, asteroids, Ophiuroidea, ophiuroids, environmental control, sponge aggregations, VMEs

INTRODUCTION

The benthic fauna of the Avilés Canyon System and the El Cachucho, Marine Protected Area (MPA) have been studied from a systematic point of view (mostly in Altuna, 2013; Altuna and Ríos, 2014; Manjón-Cabeza et al., 2014b; García-Guillén et al., 2018; Taboada et al., 2019), and under a general ecosystem approach (Sánchez et al., 2008, 2009, 2014a), providing a complete analysis of habitat scene for management and conservation. These studies were very valuable for these areas to be considered a vulnerable ecosystem and, as such, a protected area by the European Union (92/43/CEE) (Sánchez et al., 2014a,b, 2017; Punzón et al., 2016; Rodríguez-Basalo et al., 2019a). However, specific level studies are scarce, from the biological and ecological approach.

Echinoderms, together with sponges and corals, constitute the most important groups, in both biomass and/or abundance (Sánchez et al., 2008, 2009, 2014a, 2017; Manjón-Cabeza et al., 2014b; García-Guillén et al., 2018), as well as specific richness of the deep seabed. The importance of considering the association between these three groups is considerable, and all these previous studies provide us with a unique opportunity to carry out different kinds of analysis. Moreover, many of these bottoms are made up of sponge and coral species that build a very appropriate substrate for the proliferation of other benthic species. Among these benthic species, echinoderms are of high interest, mostly because of their inherent needs in order to survive (Murillo et al., 2012; Manjón-Cabeza et al., 2014a,b; Andrino-Abelaira, 2015; Gómez-Delgado, 2015; Murillo, 2015; Palma-Sevilla, 2015; Hurtado-García, 2016; Moya, 2016; Mah, 2020), or they are found to be associated to specific communities, leading them to be indicators of good habitat.

Recently, Ríos et al. (2020) studied the community composition and characterization of sponge aggregations in the Cantabrian Sea, showing that these aggregations constitute structuring habitats (3D communities) that function as support for different types of benthic communities (Peña-Cantero and Manjón-Cabeza, 2014, among others) and that certain benthic groups seem to have an intrinsic association with these sponge aggregations.

Based on these results, it should be possible to find an echinoderm reliance, preference, or association with these aggregations, but precise studies on the subject were not carried out, which is the main objective of the present study.

For this purpose, four sampling areas were chosen, two in the canyons and two on El Cachucho, Marine Protected Area (MPA), as well as two groups of echinoderms, starfishes, and brittle stars, because these echinoderm taxa tend to be indicators of different morphological and granulometry bottom features and of the assemblage of benthic communities.

According to this objective, to ascertain whether there exists any link between asteroids and ophiuroids and sponge aggregations on sea beds, we proposed the following hypotheses (**Figure 1**):

1 Although sponge aggregations present different specific compositions, there is not enough evidence to consider that the asteroid/ophiuroid community in canyons is different from on El Cachucho, Marine Protected Area (MPA) (**Figures 1A,C**).
2 These echinoderm species distributions will enable us to define four different echinoderm assemblages related to each sponge field (**Figure 1B**).
3 There are two different taxocoenosis, one in the canyons, and another on El Cachucho, Marine Protected Area (MPA) (**Figure 1D**).

MATERIALS AND METHODS

Study Area and Description of Work Fields

The study area is located in the northern continental margin of the Iberian Peninsula in the Cantabrian Sea (**Figure 2A**), specifically the Avilés Canyon Systems (ACS: **Figure 2B**) and

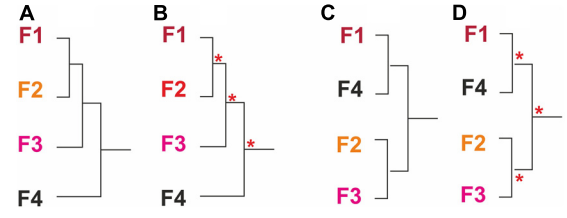

FIGURE 1 | Hypothetical clusters of echinoderm community assemblages **(A–D)**. Asterisks in red illustrates hypothetical strong boundaries segregating significant ($P < 0.001$) clusters (or groups) **(B,D)**.

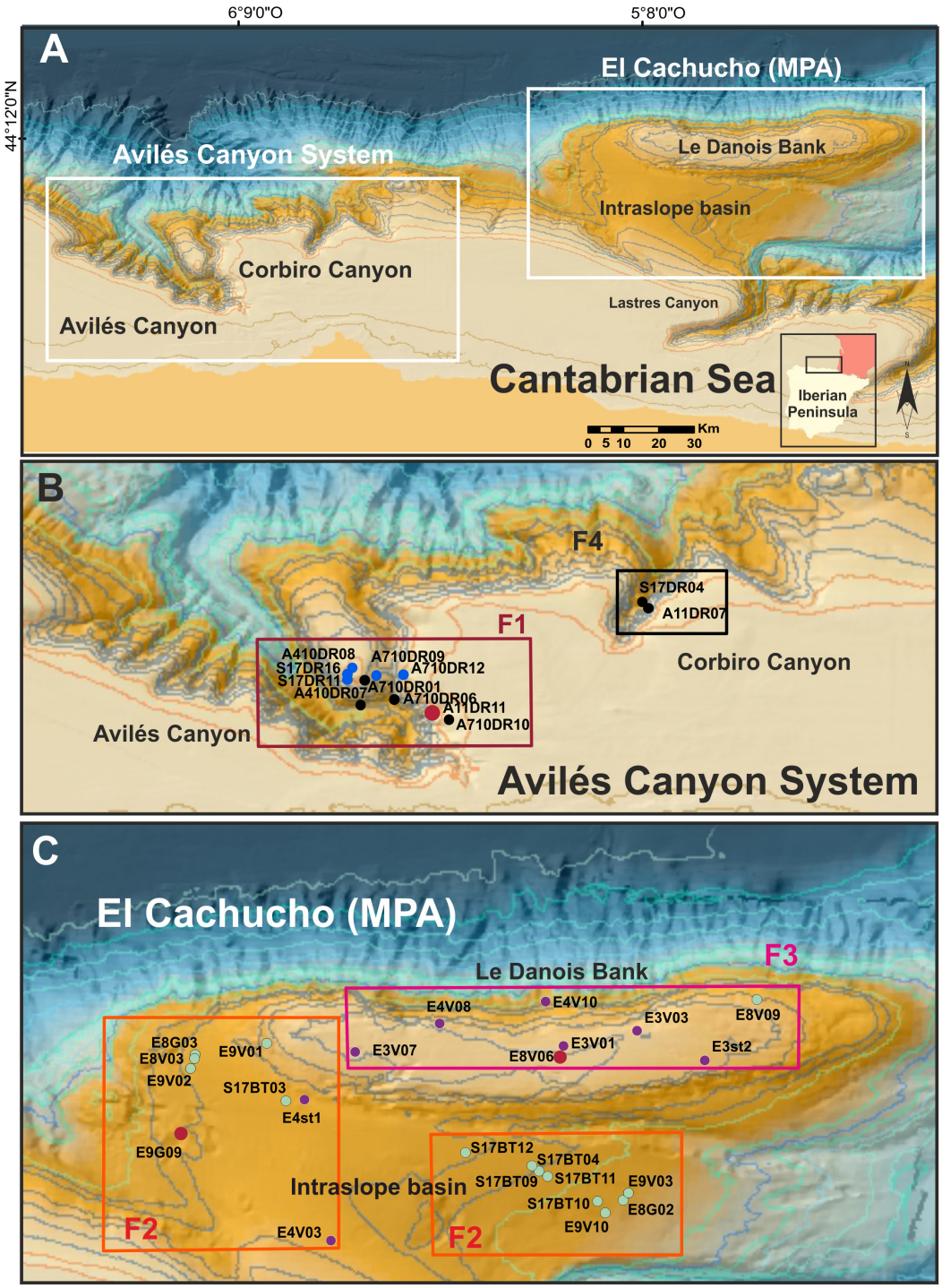

FIGURE 2 | (A) Central Cantabrian Sea, sampling area. **(B)** Avilés Canyon System. Delimited field samling area described as F1: Avilés Canyon field; F4: Corbiro Canyon field**. (C)** El Cachucho, Marine Protected Area (MPA). Field sampling: F2: Intraslope basin and southern Bank Break; F3, Top of the Bank. Rectangle colors define the stations integrated in each sponge field, and dot colors are related to the cluster (Baroni-Urbani similarity coefficient) significant group, G1: purple; G2: black; G3: green; G4: blue (see **Figure 7**).

El Cachucho, Marine Protected Area (MPA) (LDB: **Figure 2C**), which present peculiar geomorphological and habitat features described in several previous papers (Ballesteros et al., 2006; Sánchez et al., 2008, 2009; Van Rooij et al., 2010). These features together with station locations were analyzed and georeferenced by ArcGIS 10.7.

TABLE 1 | Stations positions (DD: decimal degrees), trawl sampling methods, surveys per station included in the present study and depth (m: meters).

Station label	Latitude (DD)	Longitude (DD)	Depth (M)	Species richness (S)	Organic matter (O.M).	Fine sands	Coarse sands	Mud	Trawl type	Survey
A11DR07	43.88	−5.91	551	6	5.08038	78.613029	6.904155	14.482851	Rock dredge	Avilés 0511
A11DR11	43.74	−6.11	560	1	2.780715	73.069511	19.273928	7.657844	Rock dredge	Avilés 0511
A410DR07	43.77	−6.18	1150	1	2.993144	66.57946	13.330684	20.091095	Rock dredge	Avilés 0410
A410DR08	43.78	−6.20	844	10	2.083293	69.159325	19.163313	11.677369	Rock drege	Avilés 0410
A710DR01	43.78	−6.17	810	3	2.821625	74.323586	8.588992	17.087648	Rock drege	Avilés 0710
A710DR06	43.75	−6.15	649	2	4.18501	74.114952	8.779974	17.110119	Rock dredge	Avilés 0710
A710DR09	43.75	−6.19	626	3	6.769381	42.594917	13.366544	44.047024	Rock dredge	Avilés 0710
A710DR10	43.73	−6.10	342	6	2.359874	68.493271	27.756544	3.750027	Rock dredge	Avilés 0710
A710DR12	43.78	−6.14	843	4	3.400344	78.122818	1.736524	20.140703	Rock dredge	Avilés 0710
E3St2	44.08	−4.79	498	2	3.141706	69.795197	2.381698	27.851824	Otter trawlBaca	Ecomarg 03
E3V01	44.07	−4.87	486	3	3.225364	77.87632	6.198897	15.925241	Beam trawl	Ecomarg 03
E3V03	44.10	−4.85	577	8	3.645695	61.037514	3.799862	35.144951	Beam trawl	Ecomarg 03
E3V07	44.06	−5.09	612	1	3.660562	82.994209	1.983048	15.023699	Beam trawl	Ecomarg 03
E4St1	44.01	−5.14	828	3	6.145019	39.749054	0.928039	59.323273	Otter trawl/ Beam trawl	Ecomarg 04
E4V03	43.86	−5.10	636	1	5.6551	38.509182	0.925954	60.564735	Beam trawl	Ecomarg 04
E4V08	44.09	−5.00	458	1	3.484327	85.281425	2.524338	12.194761	Beam trawl	Ecomarg 04
E4V10	44.11	−4.89	819	3	6.150105	57.747826	1.677681	40.583981	Beam trawl	Ecomarg 04
E8G02	43.91	−4.81	1238	4	10.11529	9.439515	0.15593	90.408005	GOC trawl	Ecomarg 08
E8G03	44.06	−5.25	940	2	5.896505	62.467136	2.061242	35.472809	GOC trawl	Ecomarg 08
E8V03	44.05	−5.25	955	3	6.064717	58.448795	2.08347	39.468407	Beam trawl	Ecomarg 08
E8V06	44.05	−4.87	556	1	3.339893	75.221672	7.423264	17.354637	Beam trawl	Ecomarg 08
E8V09	44.11	−4.67	573	2	3.219686	75.022011	2.718862	24.390215	Beam trawl	Ecomarg 08
E9G09	43.97	−5.26	964	1	7.393692	48.521889	1.885192	49.593349	GOC trawl	Ecomarg 09
E9V01	44.07	−5.18	761	6	5.278858	68.415642	2.189937	29.397015	Beam trawl	Ecomarg 09
E9V02	44.04	−5.26	972	6	6.302202	55.234425	2.100391	42.665234	Bou de Vara	Ecomarg 09
E9V03	43.91	−4.80	1205	12	9.854292	9.733132	0.148228	90.120399	Beam trawl	Ecomarg 09
E9V10	43.89	−4.83	1222	11	10.491391	8.616531	0.121215	91.268669	Beam trawl	Ecomarg 09
S17BT03	44.01	−5.16	862	6	6.196742	44.040867	1.274781	54.68409	Beam trawl	Sponges 0617
S17BT09	43.93	−4.89	1100	4	6.421437	18.751524	0.670461	80.56958	Beam trawl	Sponges 0617
S17BT10	43.90	−4.83	1050	4	6.944242	16.984913	0.441254	82.566994	Beam trawl	Sponges 0617
S17BT11	43.90	−4.83	1220	9	9.654444	9.915883	0.123678	89.96283	Beam trawl	Sponges 0617
S17BT12	43.96	−4.97	1225	6	9.730149	9.778616	0.1232	90.100792	Beam trawl	Sponges 0617
S17BT4	43.94	−4.90	890	7	6.117696	47.858704	1.853494	50.285255	Beam trawl	Sponges 0617
S17DR04	43.87	−5.90	695	1	4.790974	79.049644	7.526987	13.423498	Rock dredge	Sponges 0617
S17DR11	43.77	−6.20	1177	1	1.879759	64.495148	21.688709	13.81614	Rock dredge	Sponges 0617
S17DR16	43.78	−6.20	1018	10	1.994119	66.795364	20.510435	12.694198	Rock dredge	Sponges 0617

This work focuses on two canyon heads, Avilés Canyon (AC) and the Corbiro Canyon (CC) (**Figure 2B**), and Le Danois Bank and its intraslope basin (**Figure 2C**), based on sponge aggregation types of settlements described by different authors (Prado et al., 2019; Rodríguez-Basalo et al., 2019b; Ríos et al., 2020). Four sponge fields were established according to sponge species**:** F1 (AC), *Aphrocallistes Beatrix* Gray, 1858, and *Regadrella phoenix* Schmidt, 1880; F2

TABLE 2 | Fauna composition.

Class	Order	Family	Species
Phylum Porifera			
Demospongiae	Verongiida	Ianthellidae	*Hexadella* sp.
	Tetractinellida	Geodiidae	*Geodia barretti* Bowerbank, 1858
			Geodia megastrella Carter, 1876
			Geodia nodastrella Carter, 1876
			Geodia pachydermata (Sollas, 1886)
			Penares sp.
		Corallistidae	*Neoschrammeniella* aff. *bowerbankii* (Johnson, 1863)
		Pachastrellidae	*Characella pachastrelloides* (Carter, 1876)
			Pachastrella nodulosa Cárdenas and Rapp, 2012
			Pachastrella ovisternata Lendenfeld, 1894
	Axinellida	Axinellidae	*Phakellia robusta* Bowerbank, 1866
	Bubarida	Desmanthidae	*Sulcastrella* sp.
	Tetractinellida	Siphonidiidae	*Siphonidium* sp.
		Theneidae	*Thenea schmidti* Sollas, 1886
	Suberitida	Halichondriidae	*Topsentia* sp.
	Poecilosclerida	Cladorhizidae	*Cladorhiza abyssicola* Sars, 1872
		Podospongiidae	*Podospongia lovenii* Barboza du Bocage, 1869
Hexactinellida	Sceptrulophora	Aphrocallistidae	*Aphrocallistes beatrix* Gray, 1858
	Lyssacinosida	Rossellidae	*Asconema setubalense* Kent, 1870
	Amphidiscosida	Pheronematidae	*Pheronema carpenteri* (Thomson, 1869)
	Lyssacinosida	Euplectellidae	*Regadrella phoenix* Schmidt, 1880
Phylum Echinodermata			
Asteroidea	Paxillosida	Astropectinidae	*Plutonaster bifrons* (Wyville Thomson, 1873)
			Psilaster andromeda (Müller & Troschel, 1842)
		Pseudarchasteridae	*Pseudarchaster parelii* (Düben and Koren, 1846)
	Notomyotida	Benthopectinidae	*Pontaster tenuispinus* (Düben and Koren, 1846)
	Valvatida	Goniasteridae	*Ceramaster grenadensis* (Perrier, 1881)
			Peltaster placenta (Müller and Troschel, 1842)
			Nymphaster arenatus (Perrier, 1881)
		Poraniidae	*Poraniomorpha hispida* (M. Sars, 1872)
		Pterasteridae	*Pteraster militaris* (O.F. Müller, 1776)
	Spinulosida	Echinasteridae	*Henricia* sp.
			Henricia caudani (Koehler, 1895)
		Forcipulatida	Zoroasteridae	*Zoroaster fulgens* Wyville Thomson, 1873
		Brisingida	Brisingidae	*Brisinga endecacnemos* Asbjørnsen, 1856
				Novodinia pandina (Sladen, 1889)
		Amphilepidida	Amphiuridae	*Amphiura* sp.
				Amphiura filiformis (O.F. Müller, 1776)
				Amphiura grandisquama Lyman, 1869
				Amphiura griegi Mortensen, 1920
			Ophiactidae	*Ophiactis* sp.
				Ophiactis abyssicola (M. Sars, 1861)
				Ophiactis balli (W. Thompson, 1840)
				Ophiactis nidarosiensis Mortensen, 1920
				Ophiactis virens (M. Sars, 1859)
			Ophiothamnidae	*Ophiothamnus affinis* Ljungman, 1872
Ophiuroidea			Ophiotrichidae	*Ophiothrix* spp.
		Euryalida	Asteronychidae	*Asteronyx loveni* Müller And Troschel, 1842
				Astrodia tenuispina (Verrill, 1884*)*
		Ophiacanthida	Ophiacanthidae	*Ophiacantha abyssicola* G.O. Sars, 1872
				Ophiacantha aristata Koehler, 1895
				Ophiacantha bidentata (Bruzelius, 1805)
				Ophiacantha sp.
				Ophiacantha densa Farran, 1913
				Ophiacantha lineata Koehler, 1896
				Ophiacantha smitti Ljungman, 1872
				Ophiochondrus armatus (Koehler, 1907)
			Ophiotomidae	*Ophiotreta valenciennesi* (Lyman, 1879)
			Ophiobyrsidae	*Ophiophrixus spinosus* (Storm, 1881)
			Ophiomyxidae	*Ophiomyxa serpentaria* Lyman, 1883
		Ophiurida	Ophiopyrgidae	*Ophiopleura inermis* (Lyman, 1878)
			Ophiuridae	*Ophiocten affinis* (Lütken, 1858)
				Ophiura carnea Lütken, 1858
				Ophiura ophiura (Linnaeus, 1758)
		Ophioscolecida	Ophioscolecidae	*Ophiolycus purpureus* (Düben and Koren, 1846)
			Ophiohelidae	*Ophiomyces grandis* Lyman, 1879

Phylum Porifera and Echinodermata species and their classification position.

(intraslope basin of LDB), *Pheronema carpenteri* (Thomson, 1869); F3 (LBD), *Asconema setubalense* Kent, 1870; and F4 (CC), *Neoschrammeniella* aff. *bowerbankii* (Johnson, 1863; **Figures 2B,C**).

These four species were studied based on previous knowledge of the study area (García-Alegre et al., 2014; Sánchez et al., 2014a) and the criteria by which vulnerable marine ecosystems such as sponge grounds are considered (Hogg et al., 2010; Maldonado et al., 2016): they support high biodiversity of other species, are fragile and unlikely to recover from trawl damage, and are limited to discrete areas with suitable environmental conditions.

Sampling was carried out using different trawl gear and surveys, as described in previous studies (Sánchez et al., 2008; Rapp, 2019). A total of 36 stations (**Table 1**) meeting the afore-described criteria requirements were selected.

Material

The biological material consisted of 1261 specimens: 934 ophiuroids and 327 asteroids. Specimens were photographed and conserved in ethanol and identified based on their morphological characteristics using specialized literature (Mortensen, 1927, 1933; Lieberkind, 1935; Paterson, 1985; Clark and Downey, 1992; Southward and Campbell, 2006), and the appropriate protocols for their visualization (light microscopy or SEM).

Data Analysis

Echinoderm and sponge occurrence frequencies were calculated (to analyze the general faunal composition). Echinoderm species were classified into four categories according to their frequency across stations, which is a surrogate for evaluating their importance in the community: the most common species (50% of stations), very common species (between 25 and 50%), common species (between 25 and 10%), and rare or accidental species (<5%) (Mora, 1980; Manjón-Cabeza and García Raso, 1994; Manjón-Cabeza and Ramos, 2003, among others). To investigate the structure of echinoderms, assemblage similarities, related to sponge aggregations, were computed by a hierarchical cluster analysis (classification) using the UPGMA agglomerative algorithm (Sneath and Sokal, 1973; RMACOQUI ver. 1.0 software Olivero et al., 2011; RStudio Ver. 0.99.473) made on the similarity matrix of the Baroni-Urbani coefficients calculated from presence/absence data (Baroni-Urbani and Buser, 1976). The robustness of each cluster was supported by a test of biological significance of the boundaries between echinoderm assemblages. Strong and weak boundaries were defined between assemblages following (McCoy et al., 1986, $P < 0.001$). A strong boundary separates two significantly different clusters (red node number in **Figure 7**). A weak boundary (green asterisk in **Figure 7**) measures the homogeneity of species distribution between stations. When boundaries are not significant, it means that species are randomly distributed. Boundary analysis followed Olivero et al. (1998, 2011).

Stations were identified using Canonical Correspondence Analysis **(CCA)** computed from the presence/absence matrix and based on the eigenvalues of χ^2 distances between all data points (Ter Braak and Prentice, 1988; Hennebert and Lees, 1991; Legendre and Legendre, 1998), using PAST (paleontological statistics, ver. 3.25 computer program (Hammer et al., 2001).

Three analyses were performed**: (CCA1)** only with% sponge occurrence as the biotic variable; **(CCA2)** with all non-correlated abiotic variables, in this case only depth and granulometry (latitude and longitude were discarded) and biotic variable (% sponge occurrence); **(CCA3)** only abiotic variables (granulometry and depth). These were used to define ordination axes on which echinoderm data (with both stations and specimens) were plotted. Environmental variables were plotted as well as correlations with ordination axes.

RESULTS

General Faunal Composition

The faunal composition of the study area presented 42 echinoderm species (28 ophiuroids and 14 starfishes) and 21 sponge species (**Table 2** and **Figures 3–6**). *Ophiolycus purpureus, Ophiophrixus spinosus,* and *Ophiotreta valenciennesi* were new records for the area and as such will be included in the "Echinodermata Spanish Check List" (2020 in press, update of Ministerio de Agricultura y Pesca, Alimentación y Medio Ambiente, 2017).

Two sponge species, *Thenea schmidtii* and *Pachastrella ovisternata,* were the most common, while very common ones were: *Regadrella phoenix*, *Geodia pachydermata, Neoschrammeniella* aff. *bowerbanki, Podospongia loveni, Characella pachastrelloides,* and *Phakellia robusta,* present in more than half of occurrence of the stations (**Figures 3**, **5**). In the case of echinoderm species, occurrence was more evenly spread between them. They were classified as: very common species (between 25 and 50%): *Psilaster andromeda* and *Pseudarchaster parelii;* common species (between 25 and 10%): *Ophiactis abyssicola*, *Henricia caudani*, *Nymphaster arenatus*, *Ophiacantha smitti*, *Ophiothamnus affinis*, *Ophiacantha abyssicola*, *Brisinga endecacnemos*, *Ophiura carnea*, *Zoroaster fulgens*, *Plutonaster bifrons*, *Ophiomyces grandis*, *Ophiopleura inermis*, *Peltaster placenta*, and *Pontaster tenuispinus*; and rare or accidental species (<5%): the rest (**Figures 4**, **6**).

Work Field Faunal Features

Sponge (S) and echinoderm (E) composition of each field are shown in **Figure 3**. **F1** (***Aphrocallistes* and *Regadrella* aggregation**) presented nine sponge species, the most frequent of which were *Aphrocallistes beatrix* (77.78%) followed by *Regadrella phoenix* (22.22%) and *Pachastrella ovisternata* (22.22%) (**Figures 3A–S**). Twenty-three echinoderm species were recorded, 12 of which were exclusive (**Figure 3B**): the most commonly occurring echinoderm species was *Ophiactis abyssicola* (55.5%) (**Figures 4A–E**). **F2** (***Pheronema* aggregation**) was represented by *Pheronema carpenteri* with 92% of sponge species occurrence (**Figure 4A-S**), while the echinoderm community consisted of 24 species, nine of which were only present in F2 (**Figure 3B**). In this case the most common species were *Psilaster andromeda* with 75% and *Pseudarchaster parelii* with 56.25% occurrence, respectively. **F3 (*Asconema* aggregation):** Two sponges, *Asconema setubalense, Podospongia loveni,* established a new field with 40% occurrence. Regarding echinoderms, 12 species were distinguished, three of which

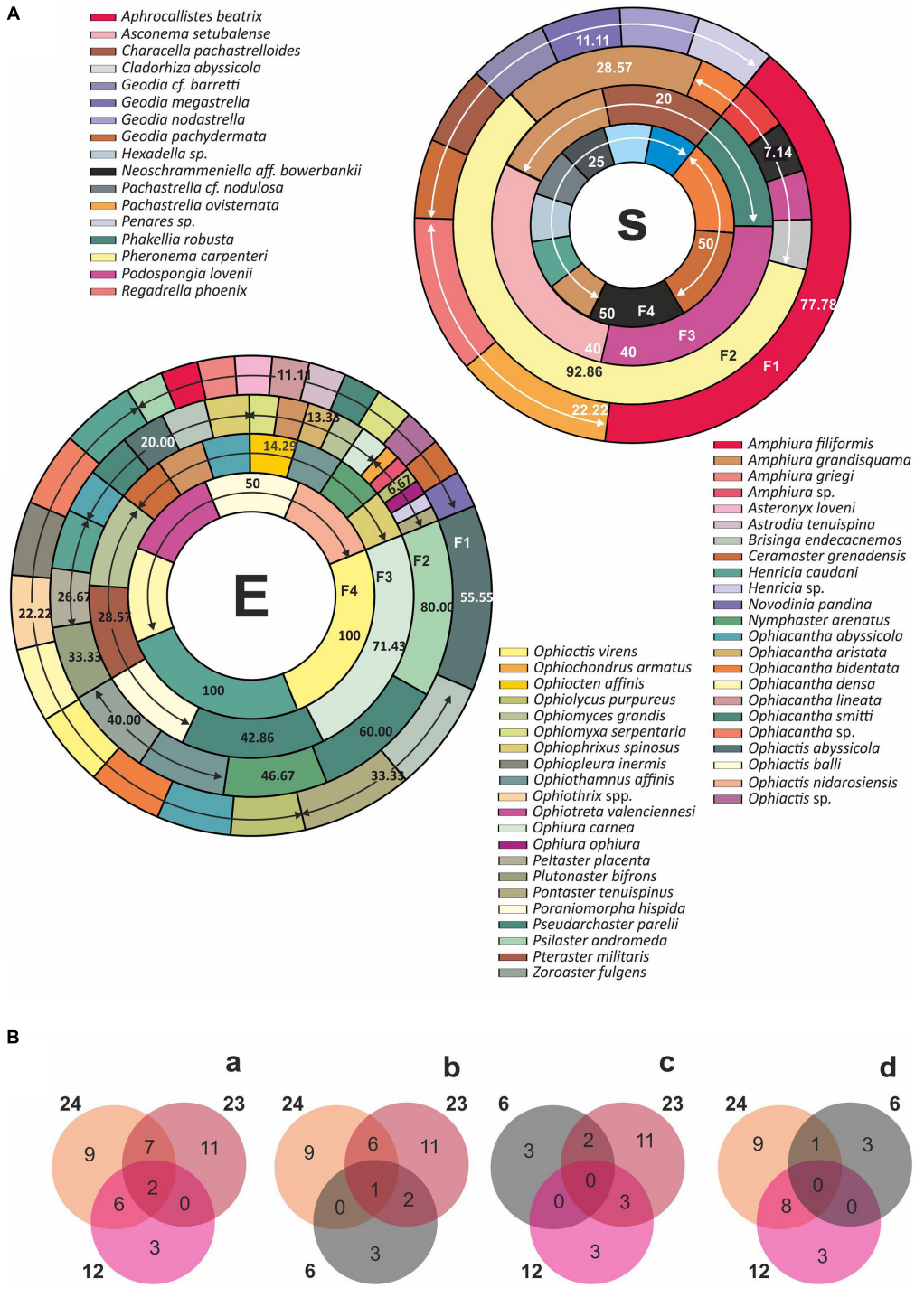

FIGURE 3 | (A) Species richness by field. **(B)** Faunal composition. S: sponges; E: echinoderms, based on occurrence percentages related to the whole area of study.

were exclusive. Echinoderm composition was 14 species, 10 of which were starfish, and four of which were very rare brittle stars (in terms of occurrence). The species featured were *Ophiura carnea* with 55.56% and *Ophiacantha smitti* with 33.33%. **F4 (*Neoschrammeniella* aggregation):** the most frequent sponges (50%) were *Neoschrammeniella* aff. *bowerbankii*, *Pachastrella ovisternata,* and *Geodia pachydermata*. Six echinoderm species made up this field, three of which were exclusive. *Ophiacantha densa* and *Henricia caudani,* were recorded in all stations of this field.

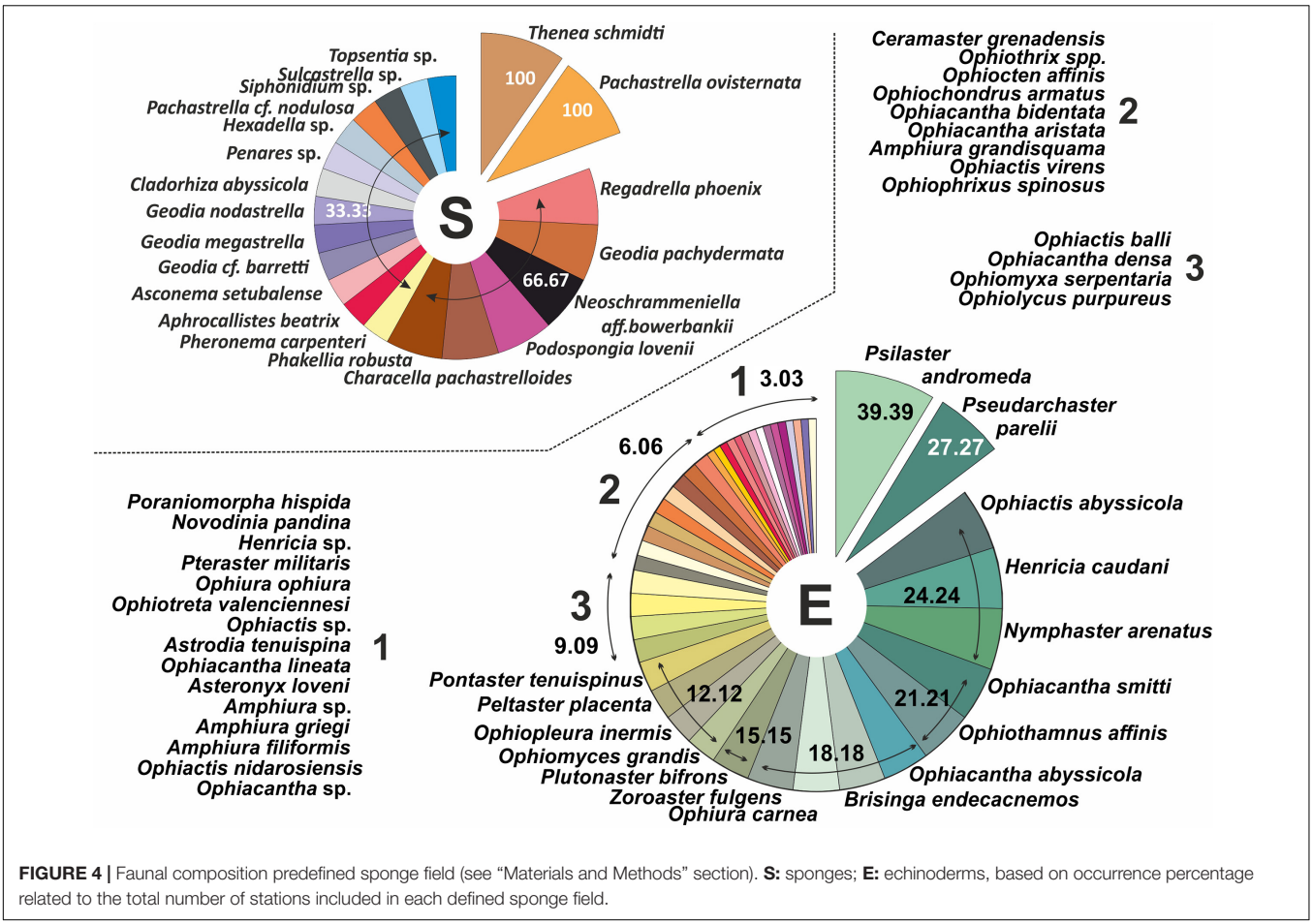

FIGURE 4 | Faunal composition predefined sponge field (see "Materials and Methods" section). **S:** sponges; **E:** echinoderms, based on occurrence percentage related to the total number of stations included in each defined sponge field.

Structure of Echinoderm Assemblages

Classification Analysis

Presence-absence species matrix, and occurrence percentage used for data analysis (**Table 3**). Cluster results display a clear discontinuity between different station groups (**Figure 7**, see dot colors), revealing the existence of four distinctive assemblages (G1, G2, G3, and G4), divided by strong boundaries (red nodes), while three stations did not match up with any other.

However, G3 and G4 represent very homogeneous groups because of the weak boundary found on nodes 22 and 28 (green nodes). **G3** was composed of stations from work field F2, except E8V09 which belongs to F3. The most frequent species in this group were starfishes, such as *Psilaster andromeda* (85.71%), *Pseudarchaster parelii* (64.29%), *Nymphaster arenatus* (50%), *and Zoroaster fulgens* (42.85%). Only one brittle star should be mentioned, *Ophiothamnus affinis* (42.86%). **G4**, on the same cluster branch as G3, consists of stations exclusively from F1. In these cases, the most commonly occurring were *Ophiactis abyssicola*, (100%), followed by *Brisinga endecacnemos*, *Ophiacantha abyssicola*, *Ophiacantha bidentata*, *Ophiochondrus armatus*, *Ophiolycus purpureus,* and *Ophiophrixus spinosus*, present in 40% of stations.

G2 contains four stations from F1 and two stations from F4. In this case there was no evidence of homogeneity, but it was a consolidated group (node 31; $P < 0.00001$) as well as G1. This group was mainly composed of *Henricia caudani* and *Ophiactis balli* (**Figure 6E**) (both 50% occurrence), followed by *Ceramaster grenadensis*, *Ophiacantha densa,* and *Peltaster placenta* (33.33%).

G1 also presents a mix of stations from F2 (2) and F3 (6). It was made up of a group with a high dissimilarity with the rest, consisting exclusively of ophiuroid species. The most frequent species was *Ophiura carnea*.

Reliability of Setting to Preset Fields

Percentage fit of the different cluster groups to the working fields are: **G1**, 75% of **F3** stations; **G2**, 33.33% of **F4** (considering G2 is the only group with F4 stations); **G3,** 94.33% of **F2;** and **G4** representing 100% of **F1**stations.

Ordination Analysis

Results from CCA analysis are shown in **Table 4** (**Figures 8**, **9**). **CCA1** was carried out only with sponge frequency as a biotic variable and echinoderms were ordered according to these, which was not significant (**Table 4**). However, when granulometry was taken into account **(CCA2)** (**Figure 8**), the CCA results became significant despite the very low% explanation. In the case of **CCA3,** only granulometry and depth significance were taken into account, showing the highest significance (**Table 4** and **Figure 9**).

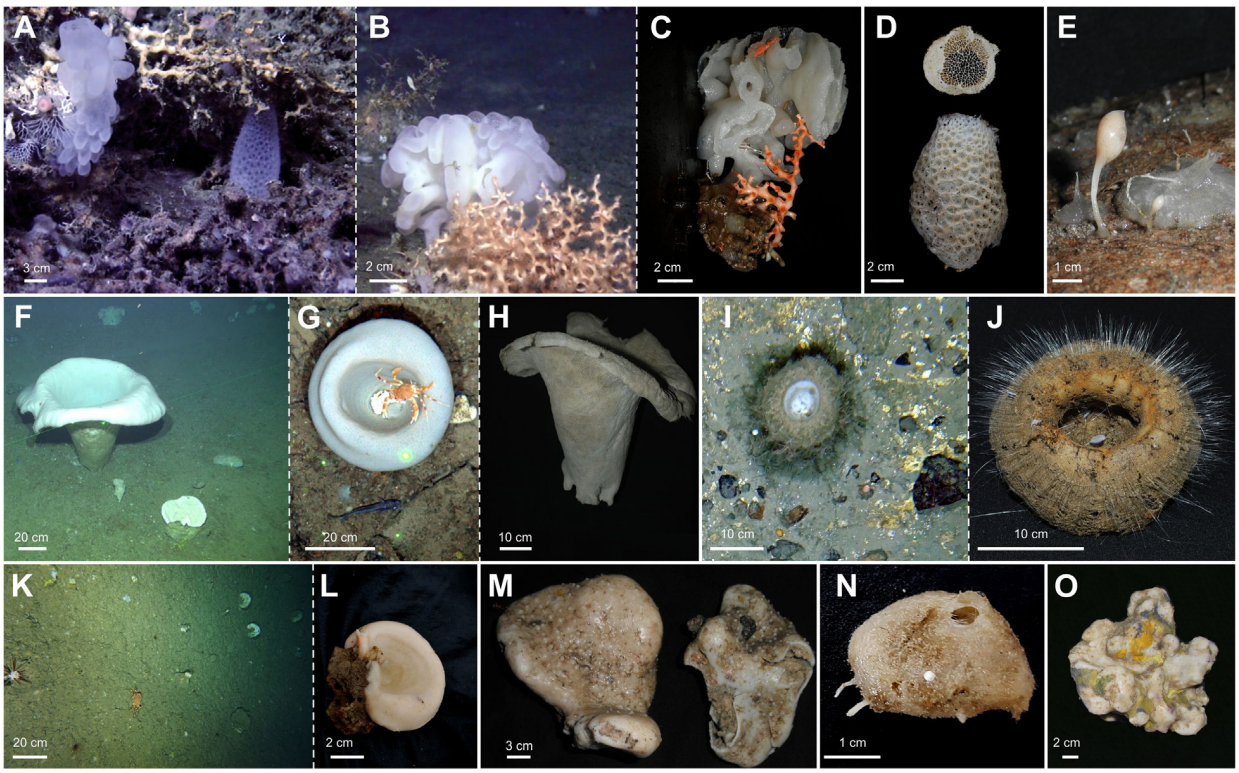

FIGURE 5 | Habitats and species of 3D large sponge aggregations in the Cantabrian sea. **(A)** *Aphrocallistes beatrix* with *Regadrella phoenix* "*in situ*" Avilés Canyon System. Scale bar 3 cm. **(B)** *Aphrocallistes beatrix* "*in situ*" Avilés Canyon System. Scale bar 2 cm. **(C)** *Aphrocallistes beatrix* view of the same specimen. Scale bar 2 cm. **(D)** *Regadrella phoenix.* Scale bar 2 cm. **(E)** *Podospongia lovenii*. Scale bar 1 cm. **(F,G)** *Asconema setubalense "in situ,"* Le Danois Bank. Scale bar 20 cm. **(H)** *Asconema setubalense.* Scale bar 10 cm. **(I)** *Pheronema carpenteri "in situ,"* Le Danois Bank. Scale bar 10 cm. **(J)** *Pheronema carpenteri.* Scale bar 10 cm. **(K)** *Neoschrameniella* aff. *bowerbankii "in situ"* in El Corbiro Canyon.Scale bar 20 cm. **(L)** *Neoschrameniella* aff. *bowerbankii.* Scale bar 2 cm. **(M)** *Geodia pachydermata.*Scale bar 3 cm. **(N)** *Thenea schmidti.* Scale bar 1 cm. **(O)** *Pachastrella ovisternata.* Scale bar 2 cm.

DISCUSSION

Echinoderm Assemblages and Control of Their Environmental Variables

The echinoderm community seems to be composed of four different communities that fit to areas with particular morphological and biological features, related to the presence of species specialized in the use of the resources they can find there (Sánchez et al., 2008; Ríos et al., 2020).

In general, the abiotic factor that mainly controls this community structure is depth. In fact, it is very frequent in echinoderm assemblage studies (Manjón-Cabeza and Ramos, 2003; Moya, 2016). This assemblage structure, which favors the dissimilarity between the canyons and El Cachucho, Marine Protected Area (MPA), is not so clear, since the deepest stations are located on the intraslope basin of the bank, therefore, its use *a priori* could lead to misunderstandings (**Figures 8**, **9**).

Group G4 would represent a community associated to deep, hard bottoms covered by coarse sands. The stations fit perfectly at the head of the Avilés Canyon (**Figures 2**, **7**). The taxa making up this community are suspension feeder species, such as brisingid species like *Brisinga endecacnemos* and *Novodina pandina* (Downey, 1986; Clark and Downey, 1992), which take advantage of the pedestals offered by the rock outcrops, or coral patches of *Madrepora oculata* Linnaeus, 1758; and *Desmophyllum pertusum*; Linnaeus, 1758 (Sánchez et al., 2014b). Coral aggregations are used as support by some ophiacanthids such as *Ophiochondrus armatus*, or species of the Genus *Ophiacantha*. However, *Ophiactis abyssicola,* like the rest of species in the *Ophiactis* genus, lives associated with bottoms that have cavities available, such as oscula sponges (Schejter et al., 2012; Sivadas et al., 2014; Çinar et al., 2019), little holes in stones or associated with dead corals or rest of calcareous algae (rhodoliths), which provides them with shelter (Gofas et al., 2014; Manjón-Cabeza et al., 2014c; Palma-Sevilla, 2015).

The community closest to G4 is G3, which is found on the intraslope basin of the Le Danois bank. This affinity is mainly due to species richness (**Figures 3**, **7**). Depth seems to be the abiotic environmental factor controlling these two communities (**Figures 7**, **8**), although other variables should be taken into account, such as the slope. In fact, steep areas could favor the settlement of structuring species (3D) such as *Pheronema carpenteri,* which would determine the echinoderm community (Cristobo et al., 2010; Sánchez et al., 2010, 2014a). In contrast with the rest of the communities studied, the species making up this one are mainly Asteroids, like *Psilaster*

TABLE 3 | Presence/absence species matrix, and occurrence percentage used for data analysis.

Species	Ocurrence (%)	A11DR07	A11DR11	A410DR07	A410DR08	A710DR01	A710DR06	A710DR09	A710DR10	A710DR12	E3St2	E3V01	E3V03	E3V07	E4St1	E4V03	E4V08	E4V10
Amphiura filiformis	3.03	0	0	0	0	0	0	0	1	0	0	0	0	0	0	0	0	0
Amphiura grandisquama	3.03	0	0	0	0	0	0	0	0	0	0	0	1	0	0	0	0	0
Amphiura griegi	3.03	0	0	0	0	0	0	0	1	0	0	0	0	0	0	0	0	0
Amphiura sp.	3.03	0	0	0	0	0	0	0	0	0	0	0	0	0	0	0	0	0
Asteronyx loveni	3.03	0	0	0	1	0	0	0	0	0	0	0	0	0	0	0	0	0
Astrodia tenuispina	3.03	0	0	0	1	0	0	0	0	0	0	0	0	0	0	0	0	0
Brisinga endecacnemos	18.18	0	0	0	1	0	0	1	0	0	0	0	0	0	0	0	0	0
Ceramaster grenadensis	6.06	0	0	1	0	0	0	0	1	0	0	0	0	0	0	0	0	0
Henricia caudani	24.24	1	0	0	1	0	1	0	0	0	0	0	0	0	0	0	0	0
Henricia sp.	3.03	0	0	0	0	0	0	0	0	0	0	0	0	0	0	0	0	0
Novodinia pandina	3.03	0	0	0	0	0	0	0	0	0	0	0	0	0	0	0	0	0
Nymphaster arenatus	24.24	0	0	0	0	0	0	0	0	0	0	0	0	0	0	0	0	0
Ophiacantha abyssicola	18.18	0	0	0	0	1	0	0	0	0	0	0	0	0	1	0	1	0
Ophiacantha aristata	6.06	0	0	0	0	0	0	0	0	0	0	0	0	0	0	0	0	0
Ophiacantha bidentata	6.06	0	0	0	1	0	0	0	0	1	0	0	0	0	0	0	0	0
Ophiacantha sp.	3.03	0	0	0	0	0	0	0	0	0	0	0	0	0	0	0	0	0
Ophiacantha densa	9.09	1	0	0	0	0	0	1	0	1	0	0	0	0	0	0	0	0
Ophiacantha lineata	3.03	0	0	0	0	0	0	0	0	0	0	0	0	0	0	0	0	0
Ophiacantha smitti	21.21	0	0	0	1	0	0	0	0	0	0	1	1	0	0	0	0	1
Ophiactis abyssicola	24.24	0	0	0	1	1	0	0	0	1	0	0	0	0	0	0	0	0
Ophiactis balli	9.09	1	0	0	0	0	0	1	1	0	0	0	0	0	0	0	0	0
Ophiactis nidarosiensis	3.03	0	1	0	0	0	0	0	0	0	0	0	1	0	0	0	0	0
Ophiactis sp.	3.03	0	0	0	0	0	0	0	0	0	0	0	0	0	0	0	0	0
Ophiactis virens	6.06	0	0	0	0	0	0	0	0	0	0	1	1	0	0	0	0	0
Ophiochondrus armatus	6.06	0	0	0	1	0	0	0	0	0	0	0	0	0	0	0	0	0
Ophiocten affinis	6.06	0	0	0	0	0	0	0	0	0	1	0	1	0	0	0	0	0
Ophiolycus purpureus	9.09	0	0	0	1	0	0	0	0	1	0	0	0	0	0	0	0	0
Ophiomyces grandis	12.12	0	0	0	0	0	0	0	0	0	0	0	1	0	0	1	0	1
Ophiomyxa serpentaria	9.09	0	0	0	0	0	0	0	0	0	0	0	0	0	0	0	0	0
Ophiophrixus spinosus	6.06	0	0	0	1	0	0	0	0	0	0	0	0	0	0	0	0	0
Ophiopleura inermis	12.12	0	0	0	0	0	0	0	0	0	0	0	0	0	0	0	0	0
Ophiothamnus affinis	21.21	0	0	0	0	0	0	0	0	0	0	0	0	0	0	0	0	1
Ophiothrix spp.	6.06	0	0	0	0	0	0	0	1	0	0	0	1	0	0	0	0	0
Ophiotreta valenciennesi	3.03	1	0	0	0	0	0	0	0	0	0	0	0	0	0	0	0	0
Ophiura carnea	18.18	0	0	0	0	0	0	0	0	0	1	0	1	1	1	0	0	0
Ophiura ophiura	3.03	0	0	0	0	0	0	0	0	0	0	1	0	0	1	0	0	0
Peltaster placenta	12.12	0	0	0	0	0	1	0	1	0	0	0	0	0	0	0	0	0
Plutonaster bifrons	15.15	0	0	0	0	0	0	0	0	0	0	0	0	0	0	0	0	0
Pontaster tenuispinus	12.12	0	0	0	0	0	0	0	0	0	0	0	0	0	0	0	0	0
Poraniomorpha hispida	3.03	1	0	0	0	0	0	0	0	0	0	0	0	0	0	0	0	0
Pseudarchaster parelii	27.27	0	0	0	0	0	0	0	0	0	0	0	0	0	0	0	0	0
Psilaster andromeda	39.39	0	0	0	0	1	0	0	0	0	0	0	0	0	0	0	0	0
Pteraster militaris	3.03	1	0	0	0	0	0	0	0	0	0	0	0	0	0	0	0	0
Zoroaster fulgens	18.18	0	0	0	0	0	0	0	0	0	0	0	0	0	0	0	0	0

(Continued)

TABLE 3 | Continued

Species	E8G02	E8G03	E8V03	E8V06	E8V09	E9G09	E9V01	E9V02	E9V03	E9V10	S17BT03	S17BT04	S17BT09	S17BT10	S17BT11	S17BT12	S17DR04	S17DR11	S17DR16
Amphiura filiformis	**0**	**0**	**0**	**0**	**0**	**0**	**0**	**0**	**0**	**0**	**0**	**0**	**0**	**0**	**0**	0	0	0	0
Amphiura grandisquama	**0**	**0**	**0**	**0**	**0**	**0**	**0**	**0**	**1**	**0**	**0**	**0**	**0**	**0**	**0**	0	0	0	0
Amphiura griegi	**0**	**0**	**0**	**0**	**0**	**0**	**0**	**0**	**0**	**0**	**0**	**0**	**0**	**0**	**0**	0	0	0	0
Amphiura sp.	**0**	**0**	**0**	**0**	**0**	**0**	**0**	**0**	**0**	**0**	**0**	**1**	**0**	**0**	**0**	0	0	0	0
Asteronyx loveni	**0**	**0**	**0**	**0**	**0**	**0**	**0**	**0**	**0**	**0**	**0**	**0**	**0**	**0**	**0**	0	0	0	0
Astrodia tenuispina	**0**	**0**	**0**	**0**	**0**	**0**	**0**	**0**	**0**	**0**	**0**	**0**	**0**	**0**	**0**	0	0	0	0
Brisinga endecacnemos	**0**	**0**	**0**	**0**	**0**	**0**	**0**	**0**	**0**	**0**	**1**	**0**	**0**	**1**	**0**	1	0	0	1
Ceramaster grenadensis	**0**	**0**	**0**	**0**	**0**	**0**	**0**	**0**	**0**	**0**	**0**	**0**	**0**	**0**	**0**	0	0	0	0
Henricia caudani	**1**	**0**	**1**	**0**	**0**	**0**	**0**	**0**	**0**	**1**	**0**	**0**	**0**	**0**	**0**	1	1	0	0
Henricia sp.	**0**	**0**	**0**	**0**	**0**	**0**	**0**	**0**	**0**	**1**	**0**	**0**	**0**	**0**	**0**	0	0	0	0
Novodinia pandina	**0**	**0**	**0**	**0**	**0**	**0**	**0**	**0**	**0**	**0**	**0**	**0**	**0**	**0**	**0**	0	0	0	1
Nymphaster arenatus	**0**	**0**	**0**	**0**	**1**	**0**	**0**	**1**	**0**	**0**	**1**	**1**	**1**	**1**	**1**	1	0	0	0
Ophiacantha abyssicola	**0**	**0**	**0**	**0**	**0**	**0**	**0**	**0**	**1**	**0**	**0**	**0**	**0**	**0**	**1**	0	0	0	1
Ophiacantha aristata	**0**	**0**	**0**	**0**	**0**	**0**	**0**	**0**	**1**	**1**	**0**	**0**	**0**	**0**	**0**	0	0	0	0
Ophiacantha bidentata	**0**	**0**	**0**	**0**	**0**	**0**	**0**	**0**	**0**	**0**	**0**	**0**	**0**	**0**	**0**	0	0	0	0
Ophiacantha sp.	**0**	**0**	**0**	**0**	**0**	**1**	**0**	**1**	**0**	**0**	**0**	**0**	**0**	**0**	**0**	0	0	0	0
Ophiacantha densa	**0**	**0**	**0**	**0**	**0**	**0**	**0**	**0**	**0**	**0**	**0**	**0**	**0**	**0**	**0**	0	0	0	0
Ophiacantha lineata	**0**	**0**	**0**	**0**	**0**	**0**	**0**	**0**	**0**	**0**	**0**	**0**	**0**	**0**	**0**	0	0	0	1
Ophiacantha smitti	**0**	**0**	**0**	**0**	**0**	**0**	**0**	**1**	**1**	**1**	**0**	**0**	**0**	**0**	**0**	0	0	0	0
Ophiactis abyssicola	**0**	**0**	**0**	**0**	**0**	**0**	**0**	**0**	**1**	**1**	**0**	**0**	**0**	**1**	**0**	0	0	1	1
Ophiactis balli	**0**	**0**	**0**	**0**	**0**	**0**	**0**	**0**	**0**	**0**	**0**	**0**	**0**	**0**	**0**	0	0	0	0
Ophiactis nidarosiensis	**0**	**0**	**0**	**0**	**0**	**0**	**0**	**0**	**0**	**0**	**0**	**0**	**0**	**0**	**0**	0	0	0	0
Ophiactis sp.	**0**	**0**	**0**	**0**	**0**	**0**	**0**	**0**	**0**	**0**	**0**	**0**	**0**	**0**	**0**	0	0	0	1
Ophiactis virens	**0**	**0**	**0**	**0**	**0**	**0**	**0**	**0**	**0**	**0**	**0**	**0**	**0**	**0**	**0**	0	0	0	0
Ophiochondrus armatus	**0**	**0**	**0**	**0**	**0**	**0**	**0**	**0**	**0**	**0**	**0**	**0**	**0**	**0**	**0**	0	0	0	1
Ophiocten affinis	**0**	**0**	**0**	**0**	**0**	**0**	**0**	**0**	**0**	**0**	**0**	**0**	**0**	**0**	**0**	0	0	0	0
Ophiolycus purpureus	**0**	**0**	**0**	**0**	**0**	**0**	**0**	**0**	**1**	**0**	**0**	**0**	**0**	**0**	**0**	0	0	0	0
Ophiomyces grandis	**0**	**0**	**0**	**0**	**0**	**0**	**1**	**0**	**0**	**0**	**0**	**0**	**0**	**0**	**0**	0	0	0	0
Ophiomyxa serpentaria	**0**	**0**	**0**	**0**	**0**	**0**	**0**	**0**	**1**	**1**	**0**	**0**	**0**	**0**	**0**	0	0	0	1
Ophiophrixus spinosus	**0**	**0**	**0**	**0**	**0**	**0**	**0**	**0**	**0**	**0**	**0**	**0**	**0**	**0**	**0**	0	0	0	1
Ophiopleura inermis	**0**	**0**	**0**	**0**	**0**	**0**	**0**	**0**	**1**	**1**	**0**	**0**	**0**	**1**	**1**	0	0	0	0
Ophiothamnus affinis	**0**	**0**	**0**	**0**	**0**	**0**	**1**	**1**	**1**	**1**	**0**	**0**	**0**	**1**	**1**	0	0	0	0
Ophiothrix spp.	**0**	**0**	**0**	**0**	**0**	**0**	**0**	**0**	**0**	**0**	**0**	**0**	**0**	**0**	**0**	0	0	0	0
Ophiotreta valenciennesi	**0**	**0**	**0**	**0**	**0**	**0**	**0**	**0**	**0**	**0**	**0**	**0**	**0**	**0**	**0**	0	0	0	0
Ophiura carnea	**0**	**0**	**0**	**0**	**0**	**0**	**1**	**0**	**0**	**0**	**0**	**0**	**0**	**0**	**0**	0	0	0	0
Ophiura ophiura	**0**	**0**	**0**	**0**	**0**	**0**	**0**	**0**	**0**	**0**	**0**	**0**	**0**	**0**	**0**	0	0	0	0
Peltaster placenta	**0**	**0**	**0**	**0**	**0**	**0**	**0**	**0**	**0**	**0**	**0**	**0**	**0**	**1**	**0**	0	0	0	1
Plutonaster bifrons	**1**	**0**	**0**	**0**	**0**	**0**	**0**	**0**	**1**	**1**	**0**	**1**	**0**	**1**	**0**	0	0	0	0
Pontaster tenuispinus	**0**	**0**	**0**	**0**	**1**	**0**	**1**	**0**	**0**	**0**	**1**	**0**	**0**	**0**	**0**	1	0	0	0
Poraniomorpha hispida	**0**	**0**	**0**	**0**	**0**	**0**	**0**	**0**	**0**	**0**	**0**	**0**	**0**	**0**	**0**	0	0	0	0
Pseudarchaster parelii	**1**	**1**	**1**	**0**	**0**	**0**	**1**	**1**	**0**	**1**	**1**	**0**	**1**	**0**	**0**	1	0	0	0
Psilaster andromeda	**1**	**1**	**1**	**0**	**0**	**0**	**1**	**1**	**1**	**1**	**1**	**1**	**1**	**1**	**1**	1	0	0	0
Pteraster militaris	**0**	**0**	**0**	**0**	**0**	**0**	**0**	**0**	**0**	**0**	**0**	**0**	**0**	**0**	**0**	0	0	0	0
Zoroaster fulgens	**0**	**0**	**0**	**0**	**0**	**0**	**0**	**0**	**1**	**0**	**1**	**0**	**1**	**1**	**1**	1	0	0	0

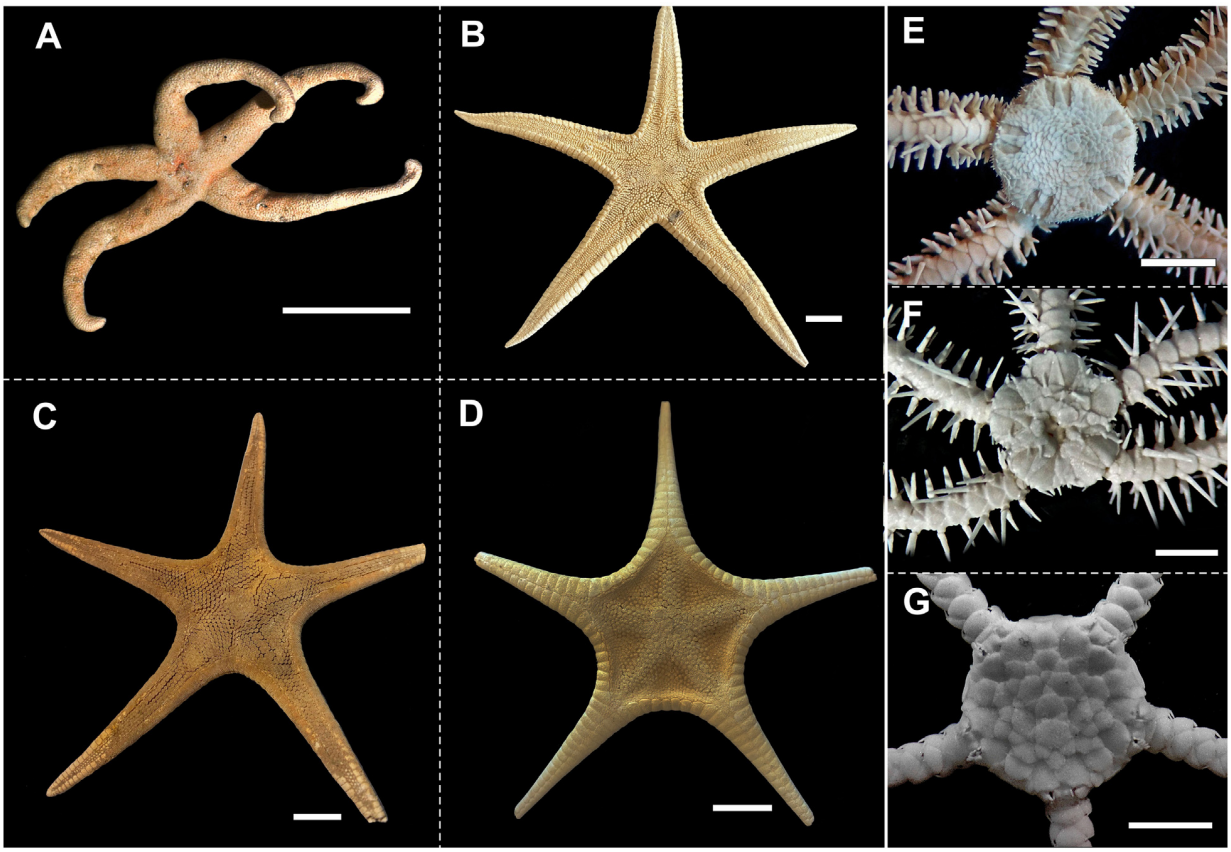

FIGURE 6 | Images of characteristic echinoderm species from each field. **(A)** *Henricia caudani*. Scale bar 2 cm. **(B)** *Psilaster andromeda*. Scale bar 1 cm. **(C)** *Pseudarchaster parelii*. Scale bar 2 cm. **(D)** *Nymphaster arenatus*. Scale bar 2 cm. **(E)** *Ophiactis balli*. Scale bar 0.15 cm. **(F)** *Ophiactis abyssicola*. Scale bar 0.2 cm. **(G)** *Ophiura carnea*. Scale bar 0.2 cm.

andromeda, *Pseudarchaster parelii*, *Nymphaster arenatus*, and *Zoroaster fulgens*, and others of lesser occurrence such as *Plutonaster bifrons* and *Pontaster tenuispinus*. This community is the most homogeneous one, and the one with the greatest specific richness. In this case, the abiotic factor mainly affecting species composition is the presence of fine sands with a high content of organic matter, preferred by sand burrow species such as those belonging to the Genus *Amphiura* (Sánchez et al., 2008).

On the other hand, **G1** is represented by stations located mostly on Le Danois Bank which has fine sand bottoms with *Asconema setubalense*. These features are very well defined in previous publications where the characteristic habitats of the area are described, and a large occurrence of *Callogorgia veticillata* (Pallás, 1766) is attributed to the upper zone of the bank (Sánchez et al., 2008, 2017). These features, indeed, explain the presence of species as diverse as *Ophiura carnea*, *Ophiomyces grandis, Ophiocten affinis,* and *Ophiothamnus affinis*, which live on sandy bottoms; and species of the Genus *Ophiacantha* and *Ophiothrix* (Granja-Fernández et al., 2014) that have a preference for corals, especially gorgonians.

G2 group does not make much biological sense and its stations seem to be a consequence of the scarcity of stations from F4 in the Corbiro Canyon (only two). Another reason that could explain this artifact would be due to stations from F1, associated would have a similar sponge species contents, and *Aphrocallistes beatrix* were not as frequent as in the rest of stations from Avilés Canyon or in the other way round, *Neoschrammeniella* aff. *bowerbankii*, does not represent any echinoderm association. Therefore, the sea star and brittle star community of Corbiro Canyon should be more profusely studied in the near future.

Does There Exist a Real Association of Echinoderms With Sponge Aggregations?

Once the structure of the echinoderm community was known, we were able to compare the expected and obtained results in order to analyze the evidence which should prove the existence of any association between echinoderms and sponges, which enable us to refute the incongruous hypothesis.

In this way, the results obtained do not conform to any of the proposed hypotheses (**Figures 1**, **7**), and the reasons that would explain this issue are developed below.

(1) Although station fit is quite high in G1, G3, and G4 clusters, the G2 cluster has a very low percentage station affiliation.

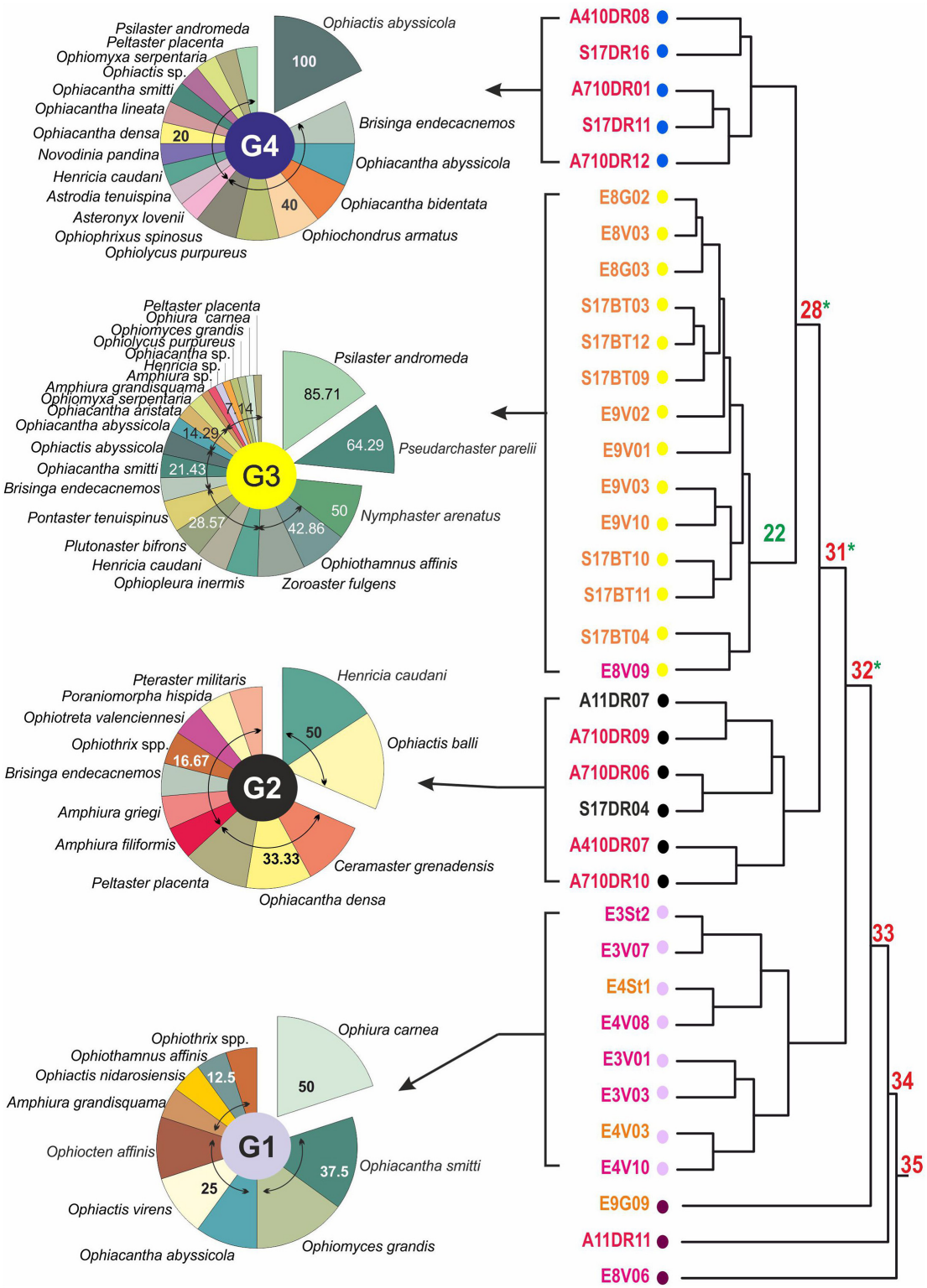

FIGURE 7 | Cluster resulting from Echinoderm species classification (Baroni-Urbani index). Noted group color and dot colors. They are related to the cluster (Baroni-Urbani similarity coefficient) significant group, G1: purple; G2: black; G3: green; G4: blue. Node number in red illustrates strong boundaries segregating significant ($P < 0.001$) clusters (or groups), whereas green asterisks denote where weak boundaries ($P < 0.001$) were found, measuring the homogeneity of species distribution between stations included in these clusters or group. No node number shows non-significant boundaries ($P > 0.001$), in these cases species are randomly distributed (following Olivero et al., 1998, 2011). Sector diagrams show species occurrence percentage related to each significant cluster.

TABLE 4 | Canonical Correspondence analysis values (Eigenvalues, P, Explanation percentage).

	Eigenvalues	*P*	Explanation percentage
CCA1: variables: sponges occurrence %			
Axis I	0.75	$P > 0.1$	18.85%
Axis II	0.67	$P > 0.01$	16.87%
CCA2: variables: sponges occurrence %, depth and granulometry			
Axis I	0.75	$P < 0.05$	19.49%
Axis II	0.66	$P < 0.01$	17.15%
CCA3: variables: sponges occurrence %, depth and granulometry			
Axis I	0.61	$P < 0.001$	32.93%
Axis II	0.57	$P < 0.001$	30.74%

Minimum of significance: P < 0.05. Gray shadow: not significant Axis.

(2) Asteroid/ophiuroid community assemblages do not fit the sponge species composition.

Given the high percentage of adjustment that some of the fields present, it is possible that these small imbalances can be explained, since fields were delimited on the basis of main sponge species, although this occurrence may vary between stations (**Figures 4**, **8**), and then some of them did not fit the field as we expected.

On the other hand, CCA using only an environmental variable set is more significant than using it in combination with occurrence of sponges. There are two ways to address this question: (1) sponges are not a very good biotic factor to control the echinoderm community; (2) echinoderms depend more on other bottom types (for instance related to granulometry, **Figure 9**), so the variable data set should be improved.

Finally, these results enable us to infer that the association of asteroids and ophiuroids with sponge aggregations is conditioned to environmental factors, like granulometry, which control fields such as habitat. Sponge species composition, or the structure they

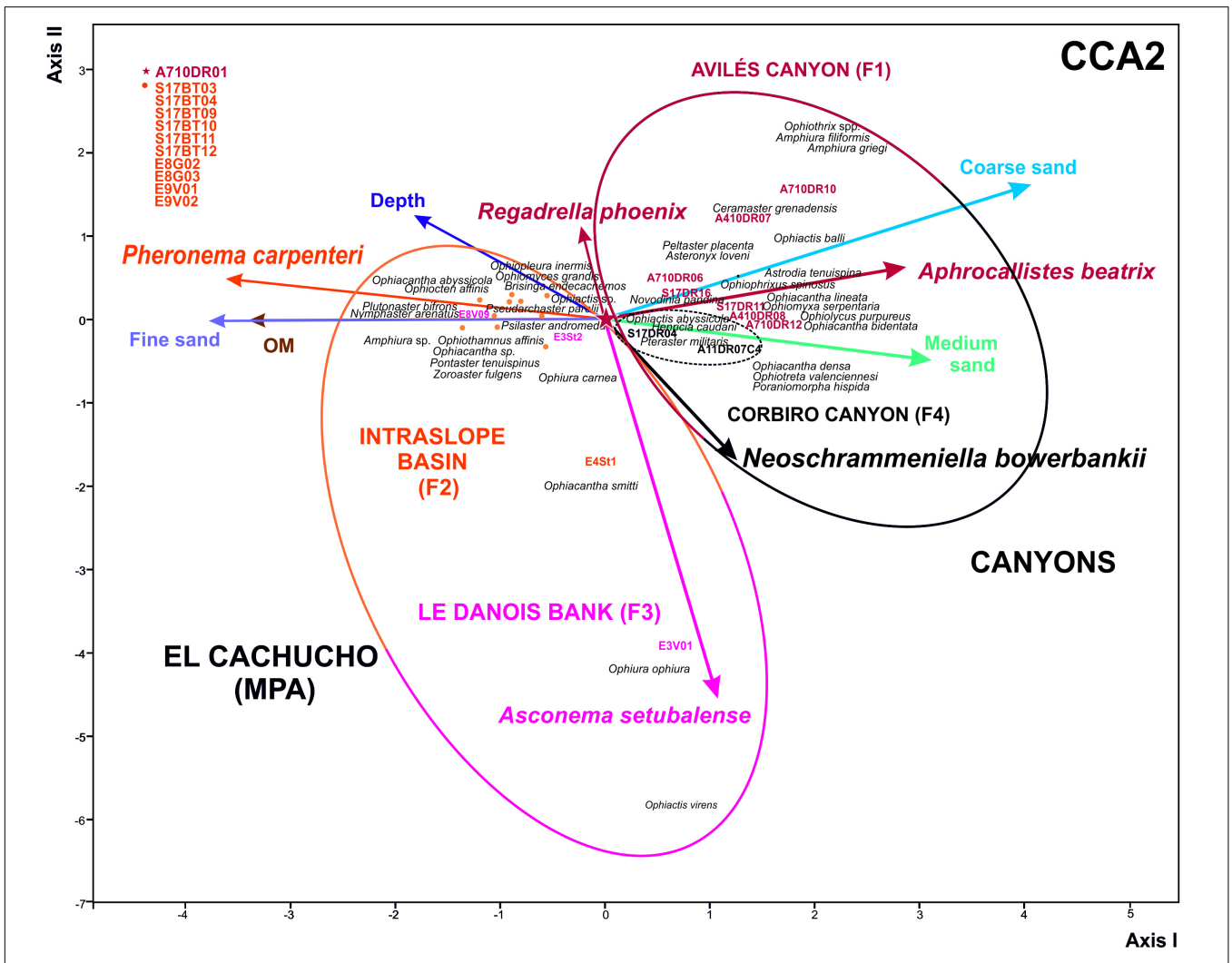

FIGURE 8 | Ordination studies. Canonical Correspondence Analysis **(CCA2).** Physical environmental variables and biotic variable (most relevant sponges): Granulometry characteristics and depth. F1, 2, 3, 4 described in **Figure 2**. Statistical parameters and null hypothesis shown in **Table 4**.

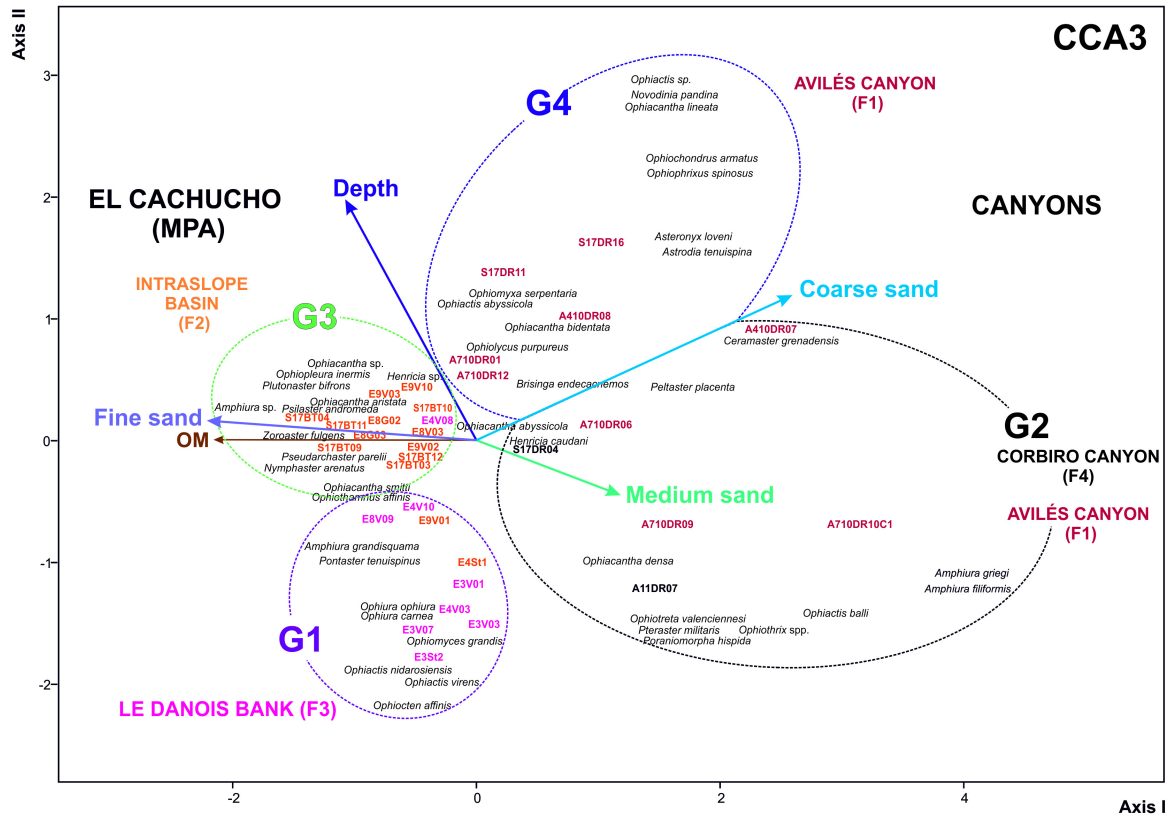

FIGURE 9 | Ordination studies. Canonical Correspondence Analysis **(CCA3).** Physical environmental variables and granulometry characteristics and depth. F1, F2, F3, F4 described in **Figure 2**. CCA3: variables: sponge occurrence%, depth and granulometry. Statistical parameters and null hypothesis shown in **Table 4**.

provide, would not be the main reason for explaining echinoderm assemblage structure.

DATA AVAILABILITY STATEMENT

The raw data supporting the conclusions of this article will be made available by the authors, without undue reservation.

AUTHOR CONTRIBUTIONS

MM-C and PR conceived and designed the study and wrote the manuscript. PR, TI, AR-B, FS, and JC collected the specimens and the pre-identification major taxa. PR and JC identified the sponges. MM-C, PR, AM-R, and LG-G identified the echinoderms, analyzed the data, prepared the figures and tables, reviewed drafts of the manuscript, and helped to writing the manuscript. MM-C, FS, and JC acquired the funding. All authors contributed to the article and approved the submitted version.

FUNDING

This research has been performed in the scope of the SponGES and INTEMARES projects. SponGES received funding from the European Union's Horizon 2020, Research and Innovation Programme under grant agreement no. 679849. The LIFE IP INTEMARES project, is coordinated by the Biodiversity Foundation of the Ministry for the Ecological Transition and the Demographic Challenge. It receives financial support from the European Union's LIFE programme (LIFE15 IPE ES 012). Also, the Spanish Ministry of Environment through a management agreement with the Spanish Institute of Oceanography (IEO) has funded the scientific monitoring of the El Cachucho MPA (ECOMARG Project). This study was partially funded by the Universidad de Málaga/Instituto Español de Oceanografía agreement (contract n°: 2013/0032460 – 80625/47.6006).

ACKNOWLEDGMENTS

This study was made possible thanks to the invaluable work of all the participants in the eight surveys involved and the crews of the R/Vs. Vizconde de Eza (SGPM), Ramón Margalef (IEO), and Ángeles Alvariño (IEO). We would like to thank Shani Jones and Meryl Jones (from Wyn Academy), American native English professional teachers for the revision of the manuscript.

REFERENCES

Altuna, A. (2013). Scleractinia (cnidaria: anthozoa) from ECOMARG 2003, 2008 and 2009 expeditions to bathyal waters off north and northwest spain (northeast atlantic). *Zootaxa* 3641, 101–128. doi: 10.11646/zootaxa.3641.2.1

Altuna, A., and Ríos, P. (2014). Scleractinia (cnidaria: anthozoa) from INDEMARES 2010–2012 expeditions to the avilés canyon system (bay of biscay, spain, northeast atlantic). *Helgol. Mar. Res.* 68, 399–430.

Andrino-Abelaira, J. (2015). *Estructura de la taxocenosis de Holoturoideos de la Plataforma y cañones submarinos de Patagonia*. Spain: Universidad de Málaga, 48.

Ballesteros, M., Acosta, J., Muñoz, A., Rivera, J., and Sánchez, F. (2006). 5^{a} *Asamblea Hispano-Portuguesa de Geodesia y Geofísica, Estudio morfoestructural de "El Cachucho" (Le Danolis Bank) basado en batimetría multihaz. Proyecto ECOMARG*, Spain: Universidad de Málaga.

Baroni-Urbani, C., and Buser, M.W. (1976). Similarity of binary data. *Syst. Zool.* 25, 251–259.

Çinar, M.E., Bakir, K., Doğan, A., Açik, S., Kurt, G., Katağan, T. et al. (2019). Macro-benthic invertebrates associated with the black sponge Sarcotragus foetidus (Porifera) in the levantine and aegean seas, with special emphasis on alien species. *Estuar. Coast. Shelf Sci.* 22:106306. doi: 10.1016/j.ecss.2019.106306

Clark, A.M., and Downey, M.E. (1992). *Starfishes of the Atlantic. Chapman & Hall. Identification Guides, 3*, London: Chapman & Hall, 794.

Cristobo, J., Ríos, P., Sánchez, F., Muñoz, A., Polonio, V., González, D., et al. (2010). Diversity of sponges in bathyal coral reefs of a subsidiary canyon of Aviles Canyon complex (Cantabrian Sea). *VIII World Sponge Conference*, Spain: Instituto Español de Oceanografía.

Downey, M.E. (1986). Revision of the atlantic brisingida (echinodermata: asteroidea), with description of a new genus and family. *Smithson. Contr. Zool.* 435:57.

García-Alegre, A., Sánchez, F., Gómez-Ballesteros, M., Hinz, H., Serrano, A., Parra, S. et al. (2014). Modeling and mapping the local distribution of relevant species on the le danois bank, el cachucho marine protected area (cantabrian sea). *Deep-Sea Res. II* 106, 151–164.

García-Guillén, L.M., Rios, P., and Manjón-Cabeza, M.E. (2018). *Asteroideos del mar Cantábrico. Resultados faunísticos de los proyectos LIFE+INDERMARES del norte de España. I Congreso de jóvenes investigadores del Mar*. Spain: Universidad de Málaga

Gofas, S., Goutayer, J., Luque, A., Salas, C., and Templado, J. (2014). "espacio marino de alborán. proyecto life+ indemares," in *del Ministerio de Agricultura, Alimentación y Medio Ambiente*, ed. Fundación Biodiversidad, Spain: Agricultura, Alimentación y Medio Ambiente en España, 129.

Gómez-Delgado, A. I. (2015). *Ofiuroideos de la Plataforma Patagónica Argentina. Trabajo Fin de Máster*. Spain: Universidad de Málaga, 46.

Granja-Fernández, R., Herrero-Pérezrul, M. D., López-Pérez, R.A., Hernández, L., Rodríguez-Zaragoza, F. A., Jones, R. W., et al. (2014). Ophiuroidea (echinodermata) from coral reefs in the mexican pacific. *ZooKeys* 406, 101–145. doi: 10.3897/zookeys.406.6306

Hammer, Ø., Harper, D.A.T., and Rya, P. D. (2001). PAST: paleontological statistics software package for education and data analysis. *Palaeontol. Electron.* 4, 1–9.

Hennebert, M., and Lees, A. (1991). Environmental gradients in carbonate sediments and rocks detected by correspondence analysis: examples from the recent of norway and the dinantian of southwest england. *Sedimentology* 38, 623–642.

Hogg, M.M., Tendal, O.S., Conway, K.W., Pomponi, S.A., van Soest, R.W.M., Gutt, J. et al. (2010). *Deep-sea Sponge Grounds: Reservoirs of Biodiversity. UNEP-WCMC Biodiversity Series No. 32*, Cambridge, UK: UNEP-WCMC.

Hurtado-García, J. (2016). *Asteroideos (Asteroidea: Echinodermata) de la Plataforma Patagónica Argentina. Trabajo Fin de Máster*, Spain: Universidad de Málaga, 52.

Legendre, P., and Legendre, L. (1998). *Numerical Ecology*.Elsevier: Amsterdam.

Lieberkind, I. (1935). Asteroidea. 1. Porcellanasteridae. *Danish Ingolf Expedit.* 4, 1–37.

Mah, C. (2020). New species, occurrence records and observations of predation by deep-sea asteroidea (echinodermata) from the north atlantic by NOAA ship okeanos explorer. *Zootaxa* 4766, 201–260.

Maldonado, M., Aguilar, R., Bannister, R.J., Bell, J. J., Conway, K.W., Dayton, P.K., et al. (2016). "Sponge grounds as key marine habitats: a synthetic review of types, structure, functional roles, and conservation concerns". In: *Marine Animal Forests: The Ecology of Benthic Biodiversity Hotspots*, eds S. Rossi, L. Bramanti, A. Gori, and C. Orejas, (Berlín: Springer International Publishing). 145–183.

Manjón-Cabeza, M.E., and García Raso, J.E. (1994). Structure and evolution of a decapod crustacean community from the coastal detritic bottoms of barbate (cadiz, southern spain). *J. Nat. Hist.* 32, 1619–1630.

Manjón-Cabeza, M. E., and Ramos, A. (2003). Ophiuroid community structure of the south shetlands islands and antarctic peninsula region. *Polar Biol.* 26, 691–699.

Manjón-Cabeza, M. E., Gómez-Delgado, A. I., and Moya, F. (2014a). *Ofiuroideos Del Mar De Bellingshausen. Xviii Simposio Ibérico De Estudios De Biología Marina*. Spain: Agricultura, Alimentación y Medio Ambiente en España.

Manjón-Cabeza, M. E., Palma-Sevilla, N., Gómez-Delgado, A. I., Andrino-Abelaira, J., and Ríos, P. (2014b). "Echinoderms assemblages of Aviles canyons (preliminary results) (Biscay Bay) (INDEMARES+LIFE Project)," in *XVIII Simposio Ibérico de Estudios de BiologíaMarina. Libro De Resúmenes*. eds P. Ríos, L. A. Suárez, and J. Cristobo, (Gijón: Centro Oceanográfico de Gijón).

Manjón-Cabeza, M.E., Palma-Sevilla, N., and Salas, C. (2014c). *Los Equinodermos De La Isla De Alborán. XVIII Simposio Lbérico de Estudios de Biología Marina*. Spain: Agricultura, Alimentación y Medio Ambiente en España.

McCoy, E.D., Bell, S. S., and Walters, K. (1986). Identifying biotic boundaries along environmental gradients. *Ecology* 68, 749–759.

Ministerio de Agricultura y Pesca, Alimentación y Medio Ambiente, (2017). Boletín Oficial del Estado. 16648–16649. Available Online at: https://www.boe.es/diario_boe/txt.php?id=BOE-A-2017-2401.

Mora, J. (1980). *Poblaciones bénticas de la Ría de Arosa*. Ph.D. Thesis. Spain: Universidad de Santiago de Compostela, 335.

Mortensen, T. (1927). *Handbook of the Echinoderms of the British Isles*. Tomo: Oxford University press, 146-254.

Mortensen, T. (1933). Ophiuroidea. *Danish Ingolf Expedition*. 4, 1–121.

Moya, F. (2016). *Equinodermos del mar de Bellingshausen*. Ph.D. Thesis. Málaga: Universidad de Málaga, 313.

Murillo, F. J., Durán Muñoz, P., Cristobo, J., Ríos, P., González, C., Kenchington, E., et al. (2012). Deep-sea sponge grounds of the flemish cap, flemish pass and the grand banks of newfoundland (northwest atlantic ocean): distribution and species composition. *Mar. Biol. Res.* 8, 842–854. doi: 10.1080/17451000.2012.682583

Murillo, F.J. (2015). *Estudio de los ecosistemas epibentónicos del Atlántico Noroccidental: Gran Banco de Terranova y Flemish CAP*. PhD Thesis. Spain: Universidad de Santiago de Compostela.

Olivero, J., Real, R., and Márquez, A. L. (2011). Fuzzy chorotypes as a conceptual tool to improve insight into biogeographic patterns. *Systematic Biol.* 60, 645–660. doi: 10.1093/sysbio/syr026

Olivero, J., Real, R., and Vargas, J. M. (1998). Distribution of breeding, wintering, and resident waterbirds in europe: biotic regions and the macroclimate. *Ornis Fennica* 75, 153–175.

Palma-Sevilla, N. (2015). *Equinodermos del mar de Alborán. Proyecto LIFE + INDEMARES. Trabajo Fin de Máster*. Málaga: Universidad de Málaga.

Paterson, G. L. J. (1985). The deep-sea ophiuroidea of the north atlantic ocean. *Bull. Br. Mus. Zool.* 49, 1–162.

Peña-Cantero, Á.L., and Manjón-Cabeza, M.E. (2014). Hydroid assemblages from the bellingshausen sea (antarctica): environmental factors behind their spatial distribution. *Polar Biol.* 37, 1733–1740. doi: 10.1007/s00300-014-1557-z

Prado, E., Sánchez, F., Ríos, P., Rodríguez-Basalo, A., and Cristobo, J. (2019). In-situ growth rate assessment of hexactinellid Asconema setubalense using 3D photogrammetric reconstruction in El cachucho marine protected area (le danois bank, cantabrian sea). *Front. Mar. Sci.* 6:163. doi: 10.3389/conf.fmars.2019.08.00163

Punzón, A., Arronte, J.C., Sánchez, F., and García-Alegre, A. (2016). Spatial characterization of the fisheries in the avilés canyon system (cantabrian sea, spain). *Ciencias Mar.* 42, 237–260.

Rapp, H.T. (2019). *Deliverable D1.3 Report On The 2nd Set Of Sampling Cruises. Sponges Project*. Bergan: University of Bergen.

Ríos, P., Prado, E., Carvalho, F. C., Sánchez, F., Rodríguez-Basalo, A., Xavier, J. R., et al. (2020). Community composition and habitat characterization of a rock

sponge aggregation (porifera, corallistidae) in the cantabrian sea. *Front. Mar. Sci.* 7:578. doi: 10.3389/fmars.2020.00578

Rodríguez-Basalo, A., Delgado, F., Ortega, E., Ríos, P., and Sánchez, F. (2019a). High resolution spatial distribution for the hexactinellid sponges Asconema setubalense and Pheronema carpenteri in the central cantabrian sea. *Front. Mar. Sci.* 6:29. doi: 10.3389/conf.fmars.2019.08.00029

Rodríguez-Basalo, A., Sánchez, F., Punzón, A., and Gómez-Ballesteros, M. (2019b). Updating the master management plan for el cachucho mpa (cantabrian sea) using a spatial planning approach. *Cont. Shelf Res.* 19:10. doi: 10.1016/j.csr.2019.06.010

Sánchez, F. M., Serrano, A. G., and Ballesteros, M. G. (2009). Photogrammetric quantitative study of habitat and benthic communities of deep cantabrian sea hard grounds. *Contin. Shelf Res.* 29, 1174–1188. doi: 10.1016/j.csr.2009.01.004

Sánchez, F., Gómez-Ballesteros, M., González-Pola, C., Punzón-Merino, A.M., García-Alegre, A., Druet, M. et al. (2014a). "Sistema de cañones submarinos de Avilés. Proyecto LIFE +INDEMARES," in *del Ministerio de Agricultura, Alimentación y Medio Ambiente*, Ed. Fundación Biodiversidad, (Madrid: Universidad de Málaga), 114.

Sánchez, F., González-Pola, C., Druet, M., García-Alegre, A., Acosta, J., Cristobo, J., et al. (2014b). Habitat characterization of deep-water coral reefs in La gaviera canyon (avilés canyon system, cantabrian sea). *Deep Sea Res. Part II.* 106, 118–140. doi: 10.1016/j.dsr2.2013.12.014

Sánchez, F., Muñoz, A., Cristobo, J., Serrano, A., Druet, M., Parra, S. et al. (2010a). "Caracterización Bionómica Y Geomorfológica De Un Profundo Cañón Submarino Situado En La Zona De Influencia Del Cañón De Avilés (Mar Cantábrico)," in *XVI Simposio Ibérico de Estudios de Biología Marina*. (Málaga: Universidad de Málaga).

Sánchez, F., Rodríguez-Basalo, A., García-Alegre, A., and Gómez-Ballesteros, M. (2017). Hard-bottom bathyal habitats and keystone epibenthic species on Le danois bank (cantabrian sea). *J. Sea Res.* 130, 134–153. doi: 10.1016/j.seares.2017.09.005

Sánchez, F., Serrano, A., Cartes, J.E., Preciado, I., Arronte, J.C., Parra, S. et al. (2010b). "Estimating The Mpa Management Effects On Le Danois Bank Deep-Sea Ecosystem (El Cachucho) Using Trophodynamic Modelization," in *Abstract book of 12 Symposium of Oceanography of the Bay of Biscay*. France: Universidad de Málaga).

Sánchez, F., Serrano, A., Parra, S., Ballesteros, M., and Cartes, J. E. (2008). Habitat characteristics as determinant of the structure and spatial distribution of epibenthic and demersal communities of Le danois bank (cantabrian sea, n. spain). *J. Mar. Syst.* 72, 64–86. doi: 10.1016/j.jmarsys.2007.04.008

Schejter, L., Chiesa, I., Doti, B., and Bremec, C. (2012). Mycale (Aegogropila) magellanica (Porifera, Demospongiae) in the south west atlantic ocean: endobiotic fauna and new distributional information. *Sci. Marina.* 76, 753–761. doi: 10.3989/scimar.03490.21A

Sivadas, S., Redij, A., Sagare, P., Thakur, N., and Ingole, B. (2014). Temporal variation in macroinvertebrates associated with intertidal sponge Ircinia fusca (carter 1880) from ratnagiri, west coast, india. *Indian J. Geo-Mar. Sci.* 43, 921–926.

Sneath, P. H. A., and Sokal, R. R. (1973). *Numerical Taxonomy. The Principles And Practices Of Numerical Classification*. San Francisco: Freeman, 573.

Southward, E.C., and Campbell, A.C., (2006). "Echinoderms. synopses of the british fauna (new series)," in *Linnean Society of London*, ed. Crothers, J.H., & Hayward, P.J, (Avon: The Bath Press), 272.

Taboada, S., Altuna, A., Sánchez, F., and Junoy, J. (2019). A new species of Astacilla (crustacea: isopoda: valvifera) from the le danois bank (n spain, ne atlantic), living on Placogorgia sp. (cnidaria: octocorallia) with notes on the cnidarian host. *Deep Sea Res.* 148, 108–122. doi: 10.1016/j.dsr.2019.04.016

Ter Braak, C.J.F., and Prentice, I. C. (1988). A theory of gradient analysis. *Adv. Ecol. Res.* 18, 271–317.

Van Rooij, D., Iglesias, J., Hernández-Molina, F.J., Ercilla, G., Gomez-Ballesteros, M., Casas, D., et al. (2010). The le danois contourite deposi-tional system: interactions between the mediterranean outflow water and the upper cantabrian slope (north iberian margin). *Mar. Geol.* 274, 1–20.

Conflict of Interest: The authors declare that the research was conducted in the absence of any commercial or financial relationships that could be construed as a potential conflict of interest.

Copyright © 2021 Manjón-Cabeza, Ríos, García-Guillén, Macías-Ramírez, Sánchez, Rodríguez-Básalo, Ibarrola and Cristobo. This is an open-access article distributed under the terms of the Creative Commons Attribution License (CC BY). The use, distribution or reproduction in other forums is permitted, provided the original author(s) and the copyright owner(s) are credited and that the original publication in this journal is cited, in accordance with accepted academic practice. No use, distribution or reproduction is permitted which does not comply with these terms.

frontiers in Marine Science

ORIGINAL RESEARCH
published: 15 January 2021
doi: 10.3389/fmars.2020.613647

Macro and Microstructural Characteristics of North Atlantic Deep-Sea Sponges as Bioinspired Models for Tissue Engineering Scaffolding

Eva Martins[1,2], Hans Tore Rapp[3†], Joana R. Xavier[3,4], Gabriela S. Diogo[1,2], Rui L. Reis[1,2] and Tiago H. Silva[1,2]**

[1] 3B's Research Group, Research Institute on Biomaterials, Biodegradables and Biomimetics, Headquarters of the European Institute of Excellence on Tissue Engineering and Regenerative Medicine, AvePark–Parque de Ciência e Tecnologia, University of Minho, Barco, Portugal, [2] ICVS/3B's–PT Government Associate Laboratory, Guimarães, Portugal, [3] Department of Biological Sciences, K.G. Jebsen Centre for Deep Sea Research, University of Bergen, Bergen, Norway, [4] Interdisciplinary Centre of Marine and Environmental Research, University of Porto, Matosinhos, Portugal

OPEN ACCESS

Edited by:
Shirley A. Pomponi, Florida Atlantic University, United States

Reviewed by:
Hermann Ehrlich, Freiberg University of Mining and Technology, Germany
Lorenzo Angeletti, Istituto di Scienze Marine (ISMAR), Italy

***Correspondence:**
Eva Martins
eva.martins@i3bs.uminho.pt;
eva.biotec@gmail.com
Tiago H. Silva
tiago.silva@i3bs.uminho.pt

†Deceased March 7, 2020

Specialty section:
This article was submitted to Deep-Sea Environments and Ecology, a section of the journal Frontiers in Marine Science

Received: 02 October 2020
Accepted: 04 December 2020
Published: 15 January 2021

Citation:
Martins E, Rapp HT, Xavier JR, Diogo GS, Reis RL and Silva TH (2021) Macro and Microstructural Characteristics of North Atlantic Deep-Sea Sponges as Bioinspired Models for Tissue Engineering Scaffolding. Front. Mar. Sci. 7:613647. doi: 10.3389/fmars.2020.613647

Sponges occur ubiquitously in the marine realm and in some deep-sea areas they dominate the benthic communities forming complex biogenic habitats – sponge grounds, aggregations, gardens and reefs. However, deep-sea sponges and sponge-grounds are still poorly investigated with regards to biotechnological potential in support of a Blue growth strategy. Under the scope of this study, five dominant North Atlantic deep-sea sponges, were characterized to elucidate promising applications in human health, namely for bone tissue engineering approaches. *Geodia barretti* (Gb), *Geodia atlantica* (Ga), *Stelletta normani* (Sn), *Phakellia ventilabrum* (Pv), and *Axinella infundibuliformis* (Ai), were morphologically characterized to assess macro and microstructural features, as well as chemical composition of the skeletons, using optical and scanning electron microscopy, energy dispersive x-ray spectroscopy and microcomputed tomography analyses. Moreover, compress tests were conducted to determine the mechanical properties of the skeletons. Results showed that all studied sponges have porous skeletons with porosity higher than 68%, pore size superior than 149 μm and higher interconnectivity (>96%), thus providing interesting models for the development of scaffolds for tissue engineering. Besides that, EDS analyses revealed that the chemical composition of sponges, pointed that demosponge skeletons are mainly constituted by carbon, silicon, sulfur, and oxygen combined mutually with organic and inorganic elements embedded its internal architecture that can be important features for promoting bone matrix quality and bone mineralization. Finally, the morphological, mechanical, and chemical characteristics here investigated unraveled the potential of deep-sea sponges as a source of biomaterials and biomimetic models envisaging tissue engineering applications for bone regeneration.

Keywords: deep-sea sponges, marine inspired skeletons, biotechnological potential, biomaterials, scaffolds, tissue engineering, biomimetic models, bone regeneration

INTRODUCTION

Sponges (phylum Porifera) are the earliest evolving animal lineage (Simion et al., 2017), which have diversified and adapted to a wide range of aquatic, marine and freshwater habitats (Hooper and Van Soest, 2002). Since early studies on blue biotechnology that marine sponges are associated with their great potential for the production of compounds with biomedical, biopharmaceutical, nutraceutical and ecological importance (Kim and Dewapriya, 2012; Wörheide et al., 2012; Shaala et al., 2019). These compounds have contributed in particular to biomedicine and new therapeutics by providing antiviral, antitumor and antimicrobial bioactives (Belarbi et al., 2003; Wang, 2006), but also biomolecules for tissue engineering (TE). The challenge of TE is to stimulate the regeneration process on human tissues restoring the function previously lost due to the malformation or injuries (Christy et al., 2020) and typically relies on the use of templates for 3D cell culture, acting as scaffold for cell anchoring and proliferation, toward the formation of a new tissue. Sponges are characterized by a structure with unique architectures and a wide range of sizes and shapes, thus exhibiting morphological characteristics matching the requirements of the TE templates, suggesting their use in such context. Interestingly, Porifera species have also extraordinary regenerative capacities of the body wall after substantial damage, studied in North Atlantic species such as *Geodia barretti* (Hoffmann et al., 2003) and *Chondrosia reniformis* (Nickel and Brümmer, 2003; Pozzolini et al., 2019). However, spatial distribution, competition and food availability are factors that affect the rapid regeneration of marine sponges and their tissues (Bell, 2002).

Sponges comprise more than 8600 species distributed in four taxonomic classes: Hexactinellida, Demospongiae, Homoscleromorpha, and Calcarea (Hooper and Van Soest, 2002; Gazave et al., 2012; Horton et al., 2018), with demosponges displaying the highest number of described species. This class is mainly distinguished by the presence of skeletons characterized by the combination of organic and inorganic materials, such as spongins, collagen-like protein or fibrillar collagens – fibers and siliceous spicules, respectively, embedded into a well-organized fibrous network, which retain nutrients and expel metabolic products (Eckert et al., 2006; Maldonado, 2009; Ehrlich et al., 2018b; Aguilar-Camacho et al., 2019). So far, the spongin has been characterized as a collagen-like protein containing halogenated residues, but its chemical characterization is still a scientific challenge (Ehrlich, 2019). Interestingly, spongins (A and B) showed evolutionarily similarities to basement membrane collagens, and type IV collagens (Exposito et al., 2002) and analogous to the human collagen type XIII (Green et al., 2003). Moreover, the skeletal framework of *Chondrosia reniformis* sponge contains collagenous mesohyl supported by spongin fibers, curiously without any mineral elemental (Hooper and Van Soest, 2002; Silva et al., 2016; Martins et al., 2019). Besides, a small group of demosponges has skeletal framework constituted by calcium carbonate, as aragonite or calcite (Uriz, 2006; Gilis et al., 2013; Smith et al., 2013) or the structural polysaccharide chitin, mainly reported on demosponges from Verongiida and Poecilosclerida orders (Ehrlich et al., 2007, 2018a; Żółtowska-Aksamitowska et al., 2018).

Chitin is a natural polymer found in other animals as arthropods, crustacean and fungi and its deacetylation resulting in chitosan, that it is a cationic polymer with biocompatible and biodegradability properties (Younes et al., 2014; Philibert et al., 2017; Santos et al., 2020). Chitin and its derivatives are widely use in wound healing, blood anticoagulants, drug delivery, stem cell technology or on fabrication of nanofibers in biomedicine (Singh and Ray, 2000; Azuma et al., 2014; Chiriboga et al., 2020; Singh and Shrivastava, 2020). Furthermore, sponge-derived chitin scaffolds had been produced maintaining the tube-like chitin skeletal framework in *Aplysina archer* and *Ianthella flabelliformis* demosponges envisaging applications in biomedical field such as drug delivery biomaterials (Klinger et al., 2019; Kovalchuk et al., 2019).

Collagen is also a natural polymer present on marine species, such as sponges and fishes, but also, it is a biopolymer ubiquitously present in the human extracellular matrix and connective tissues of animals (Ramshaw et al., 2009; Silva et al., 2014; Alves et al., 2017; Sousa et al., 2020a) that provides spatial and mechanical support to the cells and tissues, thereby receiving strong attention from the biomedical community, with numerous studies addressing its use as a biocompatible material, based on its biodegradability and low immunogenicity for tissue regeneration (Yannas, 1992; Dong and Lv, 2016; Sorushanova et al., 2019; Sousa et al., 2020b). In addition, collagen provides an available biomimetic material for the development of scaffolds for numerous applications, being highly compatible with human systems (Silva et al., 2012; Chattopadhyay and Raines, 2014; Diogo et al., 2020). Collagens are commonly isolated from mammalian (porcine and bovine) but also from marine origins. The application of marine collagens for the development of biomaterials has been shown as a good alternative related to mammal collagens. Marine collagens have been reported as the safest source for obtaining collagen, showing lower antigenicity properties, free of zoonosis (e.g., bovine spongiform encephalopathy), greater absorption due to low molecular weight, minor constraints due to social/religious reasons and regulatory issues. Each type of collagen displays unique structural features varying according to the species and tissues (i.e., anatomical part) from where it is extracted (Silvipriya et al., 2015; Fassini et al., 2020; Seixas et al., 2020).

Silica by itself is a chemical compound that contains silicon, being this a vital element for the growth and formation of bone and cartilage tissues (Jugdaohsingh, 2007). Moreover, biosilica has been reported to increase mineralization by deposition of calcium phosphates as the formation of hydroxyapatite crystallite, inspiring its utilization for the development of new biomaterials envisioning ultimately the regeneration of human bone tissues (Schröder et al., 2005; Müller et al., 2007). Spicules from marine sponges are mainly constituted by biogenic silica namely phytoliths (Clarke, 2003). Besides the chemical composition, architectural features exhibited by sponges are also striking, with skeletal structures hierarchically arranged from the nano- to the macroscale (Aizenberg et al., 2005), influenced by the environmental conditions of each specific hard-bottom

marine ecosystem and also varying according to the species. Interestingly, sponges have body features similar to anatomic bone structures, in that both are semi-rigid structures with an efficient high interconnected porous architecture composed by inorganic (biosilica or hydroxyapatite) and organic (spongin or collagen) components (Granito et al., 2017). Regarding their morphology, sponges are relatively simple with different cell types specialized in particular biological functions, but not organized into tissues. They are filter-feeding animals with numerous inhalant pores and exhalant oscules, organized water-channels systems, and interconnected architectures that enable the circulation of water, and retention of microorganisms and organic particles due to the highly efficient filtration properties (De Vos et al., 1991).

This anatomical architecture resembles the requirements needed for the manufacturing of biomaterials for tissue engineering applications. Indeed, the high exchange of fluids is a relevant requisite for the fabrication of artificial bone scaffold to enable the transport and delivery of oxygen and nutrients to the cells cultured in this scaffold and of carbon dioxide and metabolic waste in return (Einhorn and Gerstenfeld, 2015). Additionally, skeletons of sponges have great morphological diversity, plasticity in size and shape necessary for growth (Ehrlich and Worch, 2007; Nakayama et al., 2015), which may represent a variability of mechanical properties that can benefit the culture of cells toward human bone tissue engineering (Green et al., 2003), being more biocompatible than synthetic biomaterials due to the natural related properties. Moreover, marine sponges' skeletons can be used as natural inspired templates in the biomedical field related to their chemical composition and wide range of unique properties. Also, the development of biomaterials using biomolecules as collagens, peptides or biogenic silica with marine nature origin can be used for stimulating the biomineralization and consequently enhancement the regeneration process (Fassini et al., 2017; Gabbai-Armelin et al., 2019). Moreover, the remarkable regenerative capacity of sponges has been documented in several demosponges as *Geodia barretti* (Hoffmann et al., 2003), *Halisarca dujardini* (Borisenko et al., 2015), *Hymeniacidon heliophila* (Coutinho et al., 2017) and *Aplysina cavernicola* (Ereskovsky et al., 2019). Interestingly, it has been reported the regenerative signaling proteins (TGF-β and Wnt) in bone therapeutics are also discovered during the early developmental stages of marine sponges (Suga et al., 1999; Green et al., 2013; Pozzolini et al., 2019). The natural organisms have natural frameworks and powerfully regenerative capacity and accessible extraordinary sources of biomolecules, some of which conserved throughout evolution. Given the evidence of the existence of analogous properties between bone and marine sponges, highlighting the use of sponge derived proteins as potentially be used to regenerate living bone or the marine sponges' architectures or in combination with growth factors (IGF-1 and BMP-2), are promising frameworks for bone repair and augmentation (Nandi et al., 2015).

The original form of the sponge architectures has been investigated as potential scaffolds for tissue engineering and regenerative medicine, as in an effort to mimic native extracellular matrix, feasibility biomatrices and prompting the self-sustaining tissues support. This capability of scaffolding properties is mainly inspired firstly in the hierarchical design; one of the natural pre-designed structure adjusting it for a novel purpose addressing specific clinical challenges related to the aspects that promote the natural cycle of regeneration process. Furthermore, biomimetic strategies have led to the study of naturally the marine sponges skeletons envisaging their hierarchical design or complex forms for use as bioscaffolds fabrication with key suitable properties for favorable human implantation (Martins et al., 2019). For instance, *Ianthella labyrinthus* demosponges revealed a naturally 3D pre-structured porous chitin-based skeleton with high biomimetic and biomimesis potential that promote the culture of cardiomyocytes cells demonstrating interesting features for biomedical application for having absorbable hemostats properties (Schubert et al., 2019). Additionally, *Ianthella basta* and *Aplysina aerophoba* demosponges have been used as a promising stem cell-based scaffold, showing high biocompatibility with human mesenchymal stromal cells (Mutsenko et al., 2017b) but also were capable to differentiate into chondrogenic, adipogenic and osteogenic lineages (Mutsenko et al., 2017a). Recently, sophisticated microspheres had developed using the sterrasters spicules of *Geodia macandrewii* showing non-cytotoxicity and osteogenic ability envisaging bone tissue engineering and drug delivery applications (Kaya et al., 2020). Other examples include the use of bioglass-based scaffolds prepared using *Spongia agaricina* and *Spongia lamella* as templates for attaining higher mechanical properties in the scaffolds (Boccardi et al., 2015a) or *S. agaricina* in the development of ceramic bone scaffolds (Cunningham et al., 2010; Clarke et al., 2016).

Geodia barretti (Bowerbank 1858), *Geodia atlantica* (Stephens, 1915), *Stelletta normani* (Sollas, 1880) *Phakellia ventilabrum* (Linnaeus, 1767), and *Axinella infundibuliformis* (Linnaeus, 1759) are five species representative of the deep-sea grounds as part of different taxonomic groups (**Figure 1**), occurring in high density and biomass in the boreal North Atlantic (Klitgaard and Tendal, 2004; Murillo et al., 2012). In this study, the skeletons of these species were characterized, mainly focusing on macro and microstructures and consecutively highlighting the potential of these marine sponges as nature-inspired templates for tissue engineering.

EXPERIMENTAL SECTION

Sponges Collection and Processing

Specimens of *Geodia barretti* (Gb), *Geodia atlantica* (Ga), *Stelletta normani* (Sn), *Phakellia ventilabrum* (Pv), and *Axinella infundibuliformis* (Ai) (**Figure 2**) were collected on September, 2016 at Korsfjord, Norway using a triangular dredge (**Table 1**). Upon collection, specimens of each species were sub-sampled and preserved in absolute ethanol until further analyses.

Macrostructural Analyses

Sponges immersed with absolute ethanol were cut in 1 cm^3 small pieces and dried using a critical point dryer (Tousimis

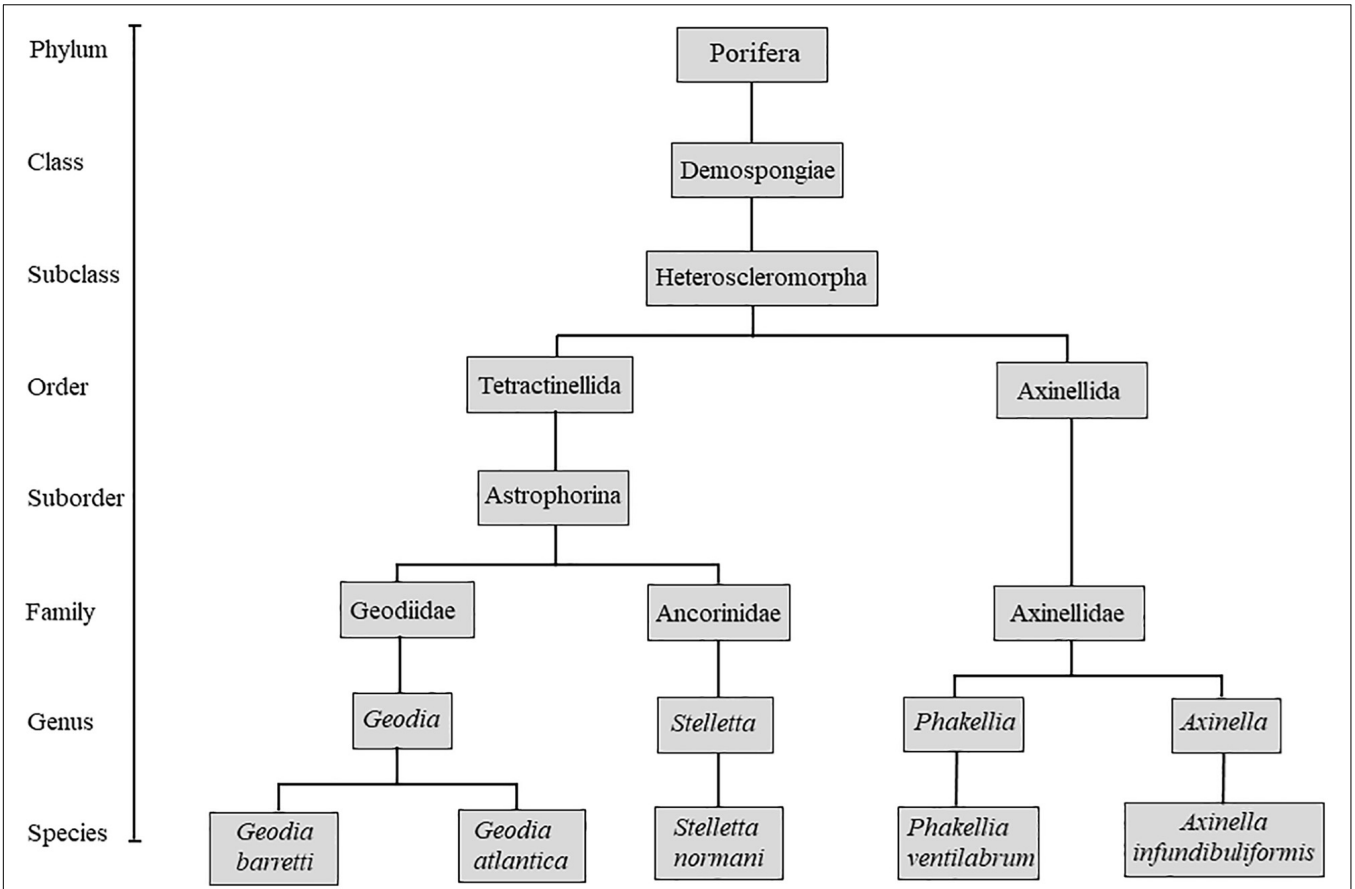

FIGURE 1 | Schematic taxonomic tree of the studied specimens.

Autosamdri 815® series). After this procedure, the acquisition of sponge images was taken using a stereomicroscope (Stemi 1000. ZEISS) equipped with a camera selecting the same photographic parameters (zoom and magnification) for all the specimens (**Figure 3**).

Scanning Electron Microscopy

Scanning electron microscopy (SEM) was used to analyze the surface morphology of the sponges using an analytical scanning electron microscope (JSM-6010 LV, JEOL, Japan), using a beam energy of 10 keV at various levels of magnification. After five sponge species were critical point dried, specimens were sputter-coated with an electrically conducting layer of platinum using the EM Leica ACE600 Sputter coater, before starting the SEM analysis.

Energy Dispersive X-Ray Spectroscopy

Energy dispersive X-ray spectroscopy (EDS) was used to characterize the chemical composition of the sponge architectures, regarding the relative quantity of the chemical elements present their skeletons. EDS analysis was performed in general landscape of the outermost sponge surface and in the spicule elements structures using the INCAx-Act, PentaFET Precision Oxford Instruments at an energy of 10.0 keV coupled to SEM.

Microcomputed Tomography

Microcomputed tomography (μCT) was used for visualization and analyses of the microstructure of marine sponges. The data acquisition was performed on a high-resolution μCT equipment Skycan 1272 (Bruker, Kontich, Belgium) using a series of about 374 projections and a dynamic threshold of 30–255, with a rotation range of 360°, and a resolution of 12 μm after X-ray beam penetrates the samples. The organic and inorganic ratios of sponges were determined considering a threshold of 30–60 for the organic matter represented in red color gradient and 60–255 for the inorganic matter in green color gradient. The X-ray source was set at 50 kV of energy and a current of 200 μA.

Noise was reduced and representative data were reconstructed using nRecon® software, while CT Analyzer® software was used to re-slice all the files of each sample and determine various morphometric parameters such as porosity (%), pore size (μm), the degree of anisotropy (DA) and pore interconnectivity (%). Each of the parameters was determined in triplicates, with data presented as the mean ± standard deviation. CTVox® program was used for the 3D reconstruction of the sponges and video processing.

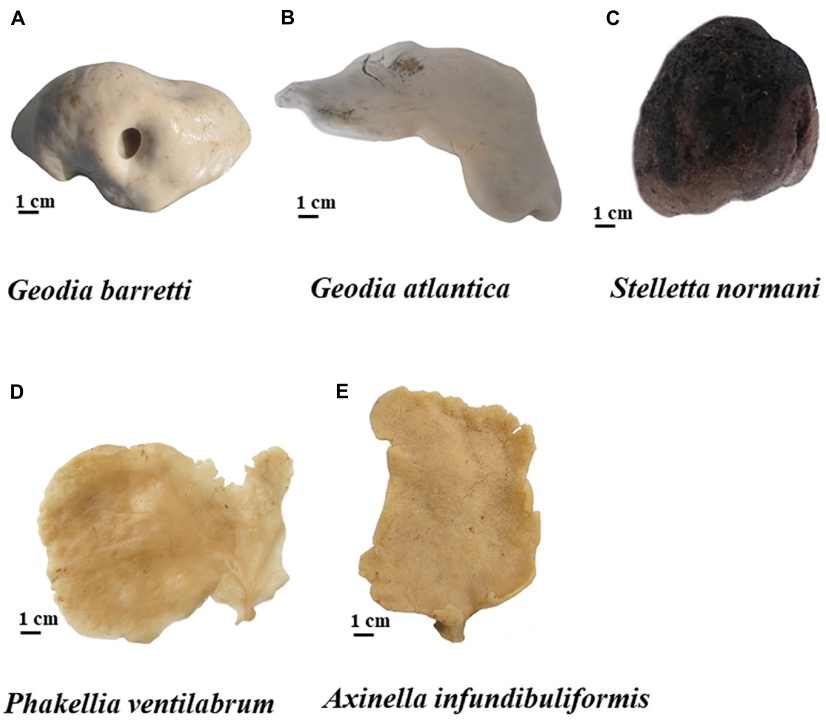

FIGURE 2 | Five marine sponges studied of North Atlantic, namely *G. barretti* **(A)**, *G. atlantica* **(B)** and *S. normani* **(C)**, *P. ventilabrum* **(D)**, and *A. infundibuliformis* **(E)**.

TABLE 1 | Stations and sponge species in which *Geodia barretti* (Gb), *Geodia atlantica* (Ga), *Stelletta normani* (Sn), *Phakellia ventilabrum* (Pv), and *Axinella infundibuliformis* (Ai) were recovered.

Species	Station	Start lat.	Start long.	Start depth (m)	End lat.	End long.	End depth (m)
Gb	2	59° 58.8790′ N	5° 22.4371′ E	332	59° 58.8879′ N	5° 22.7268′ E	97.3
Ga	2	59° 58.8790′ N	5° 22.4371′ E	332	59° 58.8879′ N	5° 22.7268′ E	97.3
Sn	2	59° 58.8790′ N	5° 22.4371′ E	332	59° 58.8879′ N	5° 22.7268′ E	97.3
Pv	2	59° 58.8790′ N	5° 22.4371′ E	332	59° 58.8879′ N	5° 22.7268′ E	97.3
Ai	5	59° 48.8155′ N	5° 36.2325′ E	292	59° 48.9226′ N	5° 35.8771′ E	226

Mechanical Properties

Mechanical properties of the five species were determined using the Instron 5540 universal mechanical testing equipment with a 50N load cell in compressive mode. Eight replicates of each sponges were tested and compressed perpendicularly to the printing plane at a crosshead speed of 1 mm/min up to 30% strain. Compressive modulus was determined from the stress–strain curve specifically the slope of the linear region using Bluehill Universal software.

Statistical Analyses

Statistical analyses were performed using GraphPad Prism 8.0.1 software. Data are presented as the mean ± standard deviation of a least three samples. Non-parametric Kruskal–Wallis tests, following Dunn's multiple comparisons were used for determination of significance level with p-value less than 0.05 ($p < 0.05$) being considered statistically significant.

RESULTS AND DISCUSSION

Macrostructural Characterization

To comprehend the peculiarities in skeletons of these five studied sponge species, the morphology characterization was addressed. For that, Gb, Ga, Sn, Pv, and Ai specimens were photographed and stereomicroscope images are represented in **Figures 2**, **3**, illustrating their macrostructure with visualization of the relevant morphological features. These sponges are constituted by a dense and elastic tissue with highly absorbable capacity due to the presence of pores in their skeletons. The studied species showed differences in terms of their overall morphology and

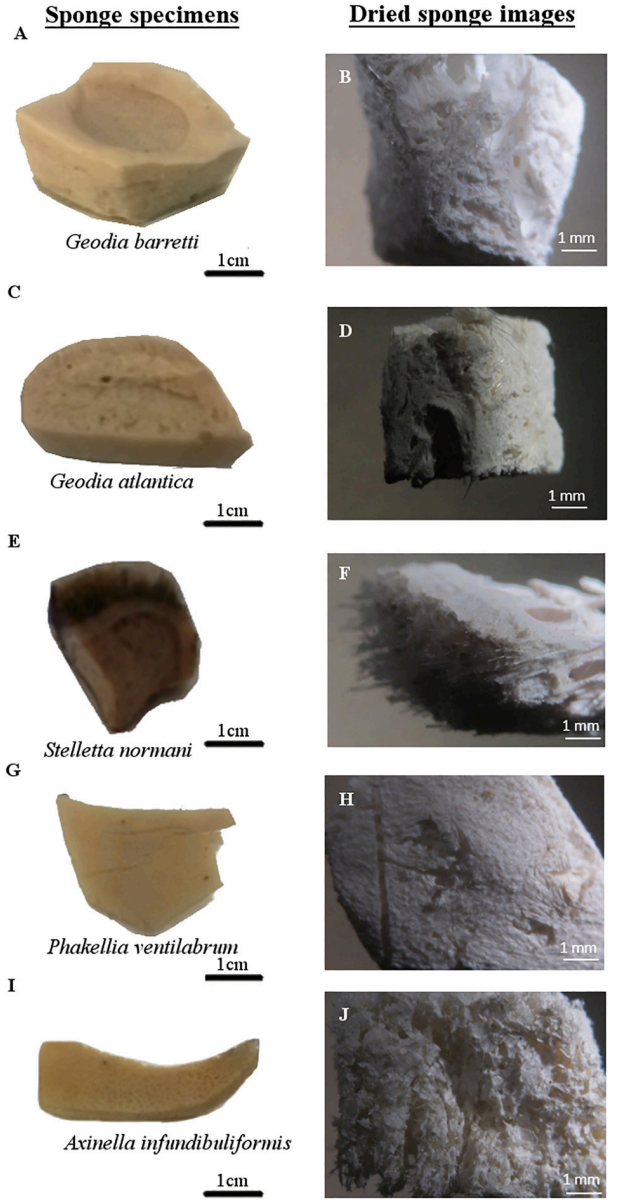

FIGURE 3 | North Atlantic marine sponge macrostructures. Sponge photographs of each specimen took after removal the absolute ethanol **(A,C,E,G,I)** and stereomicroscope images of sponge specimens after critical point drying **(B,D,F,H,J)**.

macrostructure properties. While the tetractinellids Ga, Gb (family Geodiidae), and Sn (family Ancorinidae) exhibit a massive (sub)spherical morphology with a clear distinction of a cortical layer, the axinellids Pv and Ai are typically lamellate or cup-like with a small stalk and lack such a specialized ectosomal layer. Particularly *Geodia* species (Ga and Gb), the cortex essentially composed by a layer of sterraster, a spicule element typical for the family of the Geodiidae. Regarding Pv and Ai specimens exhibit thin walls of fibrous matrix tissues (**Figure 2**); however, Pv showed a more compact and less porous macrostructure (**Figures 3G,H**) than their relative Ai (**Figures 3I,J**).

Microstructural Characterization

The microstructural assessment of sponge (Gb, Ga, Sn, Pv, and Ai) was performed by SEM, aiming to analyze the morphological features of the specimens such as their surface architecture, distribution of morphological elements, as the siliceous spicules and pores structures and EDS analysis was also used to determine the chemical elements present on the sponge skeletons and spicules. Additionally, micro-CT images were obtained to examine the internal architecture of the specimens using a non-destructive and non-invasive method, particularly to evaluate porosity, pore size and interconnectivity, as well as anisotropy properties. The sponge skeletons have the exclusive microscopic features and composition, that the detail of these characterizations can highlight details for use in biomimetic approaches or as inspired models for reproducing both or only organic and inorganic elements, for several biomedical applications.

SEM Analysis

Scanning electron microscopy micrographs of the different Gb, Ga, Sn (**Figure 4**), Pv, and Ai (**Figure 5**) specimens showed outstanding architectures with a variety of organic and inorganic skeletal elements. These SEM images can provide not only the superficial architectural features of sponges but also the pore characteristics, reveal host-microbial associations, reproduction and regeneration mechanisms that remain not completely understood in the marine sponges.

Geodia is distinctively characterized by the presence of unique ball-shaped spicules, the sterrasters that constitute part of the perceptible cortex (Uriz, 2002; Hoffmann et al., 2003; Cárdenas et al., 2013). The type and shape of spicules enable the identification of the *Geodia* species. Gb showed different clad and sterraster shapes in the spicule elements (**Figures 4A–C**). Indeed, Ga has similar general structural features fitted with the skeletal elements and fibrous layer (**Figures 4E,F**) like as the Gb relative, namely the presence of analogous shapes of the spicules. Both *Geodia* showed conservative morphological features, showing the cortex with a layer microscleres supported by radially arranged megascleres (dichotriaenes). Generally, the megascleres are elongated spicules that concoct the main architecture of skeleton and the microscleres have ancillary functions, adopting different sizes and shapes. Sharply, SEM micrographs demonstrated similarities on the morphological characteristics with visible ectossomal specialization between these two species (**Figures 4A,E**), and the presence of the microscleres spicules (sterrasters) (**Figures 4C,G**).

The Sn sponges have mainly siliceous spicules elements with similar needle-like shapes, the megascleres (pro/dichotriaenes and oxeas), hierarchically well-oriented in the ectossomal layer (**Figures 4I–L**). It is possible to observe an outer rigid layer of spicules (**Figure 4G**) which confers support and protection of cells in the marine environment (Burns and Ilan, 2003). In addition, the spicules function as an anchoring structure with robust mechanical properties enabling the fixation of the sponge to the substrate.

Phakellia ventilabrum has thinner walls and a sharp-edged rim to its cup. Internally, Pv sponge showed an architecture formed by a denser mesohyl pierced by megascleres (styles)

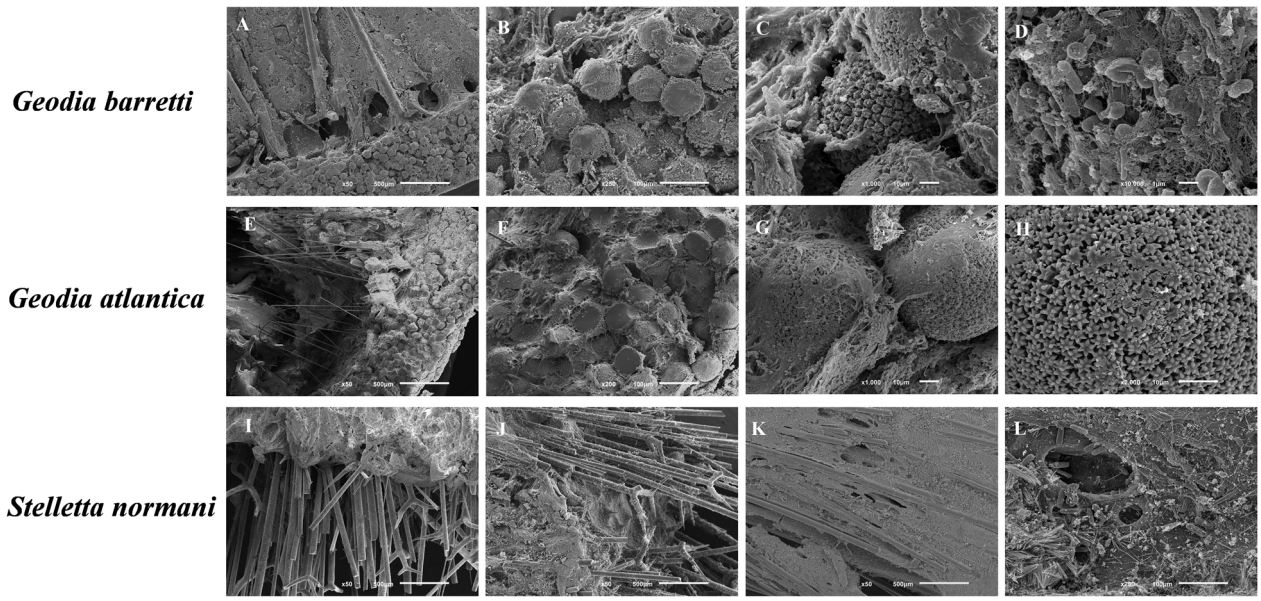

FIGURE 4 | SEM micrographs of the morphological elements and architecture of the massive to (sub)spherical sponge species, namely *G. barretti* **(A–D)**, *G. atlantica* **(E–H)**, and *S. normani* **(I–L)**. **(A)** Cross-section showing the cortex with a layer microscleres (sterrasters), supported by radially arranged megascleres (dichotriaenes). **(B)** Sterrasters embedded in an organic matrix. **(C)** Detail of a sterraster embedded in an organic matrix. **(D)** Cellular and fibrillar organic elements present in the sponge's mesohyl. **(E)** Cross-section showing the cortex with a layer microscleres (sterrasters), supported by radially arranged megascleres (orthotriaenes and oxeas). **(F)** Detail of the cortical layer of sterrasters. **(G)** Two sterrasters embedded in an organic matrix. **(H)** Detailed view of the surface of a sterraster showing its rosettes with smooth rays. **(I)** Cross-section showing megascleres (pro/dichotriaenes and oxeas) protruding the ectosome. **(J)** Trianes spicules **(K)** Radial skeleton arrangement embedded in an organic matrix. **(L)** Choanosome with a rich organic matrix and embedded microscleres (trichodragmata).

and aquiferous system with different pores and inner organic matrix (**Figures 5A–F**). Indeed, the sponge structure may harbor diverse microbiota such as protozoa, bacteria, fungi, microalgae, archaea, being therefore described as a holobiont (Webster and Taylor, 2012), with the ones showing high abundance of microbial communities being associated to a more efficient nutritional capability for feed the dissolved organic matters (Yahel et al., 2003).

The skeletal framework of the Ai has a set of diverse shapes of spicules attached (styles and oxeas) in the collagenous mesohyl layer (**Figures 5G–I**). Interestingly, cellular elements (as sperm cells) had been visualized (**Figures 5J–L**). The high density of globular cells evidences a reproduction mechanism in Ai sponges and the capability of this species produced gemmules probably linked with the high regeneration capability of the marine sponges. The members of Axinellidae, Pv and Ai showed visible differences in their porous architecture, with Pv showing a denser framework structure when compared to the Ai sponges (**Figure 5**).

Succinctly the skeletons of these sponges have unique spicules in a 3D collagenous matrix that facilitates tissue development and transfer water and nutrient mass.

EDS Analysis

Energy dispersive X-ray spectroscopy was performed to determine the different chemical elements present on the surface and particularly on the spicules of the analyzed sponges, as well as their relative ratios, with the obtained results being depicted in **Table 2**. The surface of Gb and Ga revealed higher composition in carbon (53.8 and 61.0%) and oxygen (34.7 and 34.2%), respectively. Additionally, other chemical elements, such as sulfur, silicon, phosphorus, magnesium, and sodium, were also found on the surface of *Geodia* specimens, although in smaller proportion, suggesting that the surface of the deep-sea sponges, although being mostly organic, have a composite nature. According to literature, sulfur element, had been reported in the skeletons of *verongiid* demosponges (Ehrlich et al., 2010; Klinger et al., 2019) and sodium, chlorine, sulfur, calcium, potassium are the major trace elements found in the spicules and siliceous sponge skeletons. These elements are also present in seawater (Sandford, 2003).

Spicules elements of Gb specimen had high content of carbon (23.0%), oxygen (51.4%), and silicon (24.8%), whereas in the spicule of Ga species, oxygen (57.1%) and silicon (39.6%) were the most representative elements. Interesting, results pointed to the differences on the spicule composition between the two *Geodia* species. Results demonstrated that the spicules of *G. atlantica* have a high inorganic nature with a reduce carbon ratio compared to *G. barretti*. The surface of Sn, Pv, and Ai sponges had high contents in carbon (50.2, 57.0, and 56.6%, respectively) and oxygen (38.6, 28.5, and 36.3%, respectively). Similarly, the spicules of these species showed high content of carbon, silicon and oxygen, which seems to be related to the composition in the silicon presenting in nature as silicic acid [$Si(OH)_4$] (Wysokowski et al., 2018).

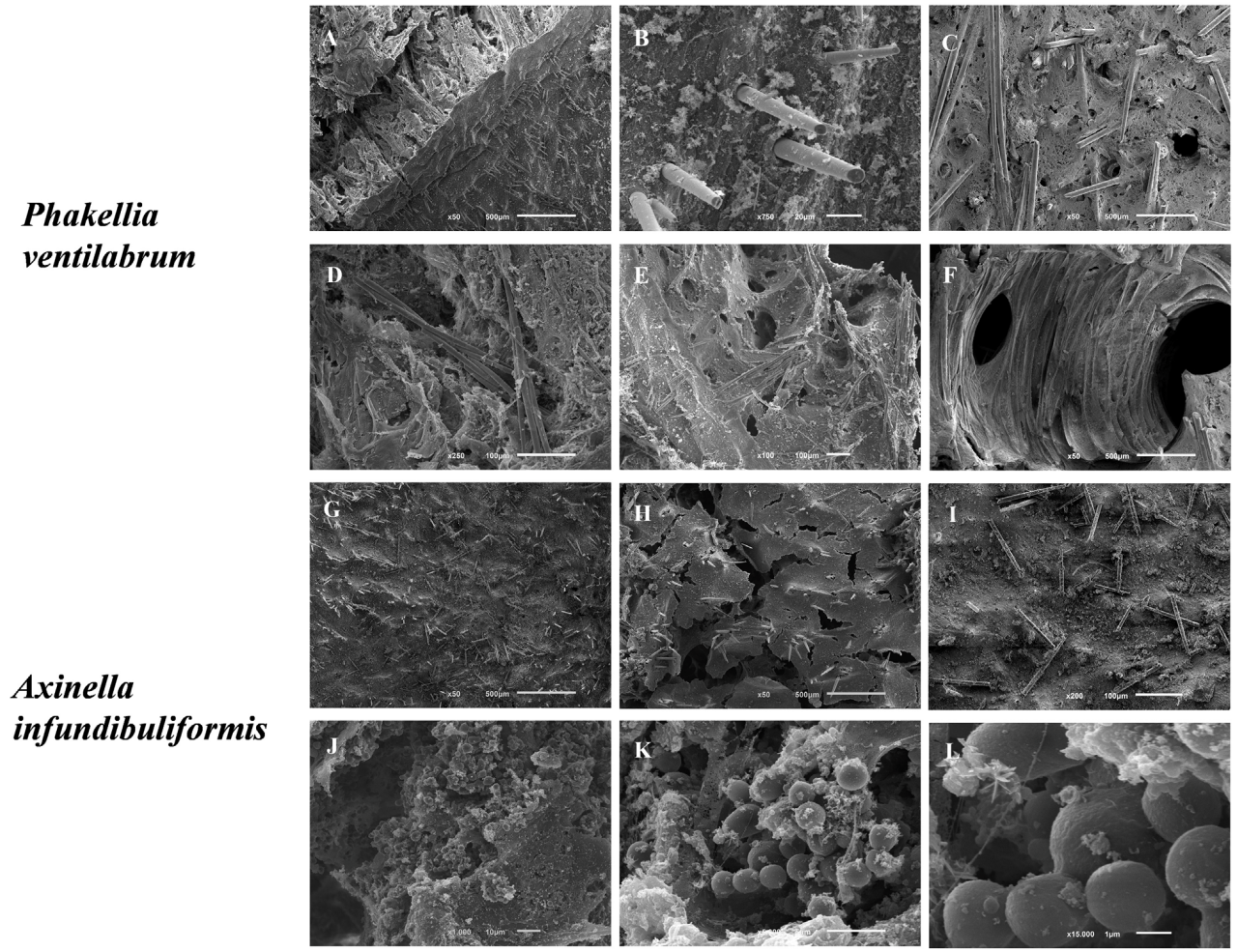

FIGURE 5 | SEM micrographs of the morphological elements and architecture of the flabellate sponge species, namely *P. ventilabrum* **(A–F)** and *A. infundibuliformis* **(G–L)**. **(A)** Cross-section showing megascleres (styles) piercing the sponge surface. **(B)** Detail of the surface with protruding spicules. **(C–E)** Various views of the organic matrix with embedded megascleres (styles and strongyles). **(F)** Aquiferous system with channel interconnected by different pores and inner organic matrix. **(G,H)** Sponge surface with organic matrix and skeletal elements (styles and oxeas). **(J–K)** Cellular elements (likely sperm cells) embedded in the inner organic matrix.

TABLE 2 | Elemental composition weight (%) from the general morphological surface of marine sponge specimens (Gb, Ga, Sn, Pv, and Ai) and from their spicule structures obtained by EDS analysis.

		C	*O*	*S*	*Si*	*P*	*Mg*	*Na*	*Ca*	*Cl*	*K*	*Al*
Gb	Wt (%)	53.8	34.7	3.4	0.6	0.6	1.1	2.6	1.6	1.6	–	–
Gb spicule	Wt (%)	23	51.4	–	24.6	–	–	0.9	–	–	–	–
Ga	Wt (%)	61.0	34.2	1.3	0.9	0.9	0.7	1.0	–	–	–	–
Ga spicule	Wt (%)	3.4	57.1	–	39.6	–	–	–	–	–	–	–
Sn	Wt (%)	50.2	38.6	3.6	3.4	–	0.6	2.1	–	–	–	1.4
Sn spicule	Wt (%)	3.9	57.8	–	37.2	–	–	–	–	–	–	1.1
Pv	Wt (%)	57.0	28.5	5.5	1.0	–	0.5	1.8	4.6	–	1.0	–
Pv spicule	Wt (%)	50.7	32.0	1.8	11.4	–	–	0.9	2.2	–	1.0	–
Ai	Wt (%)	56.6	36.3	2.5	1.9	1.6	1.1	–	–	–	–	–
Ai spicule	Wt (%)	28.9	47.9	–	23.2	–	–	–	–	–	–	–

The main differences of chemical composition among the five studied sponges are the presence of chlorine element in the surface of *G. barretti,* aluminum element in the surface and spicule structure of *S. normani* and the presence of potassium element in the both the analyzed structures of *P. ventilabrum*. On the other hand, the magnesium element is only found

on the surface of the five species and being absent on their spicule structures.

The two *Geodia* species and *A. infundibuliformis* own their surface have the phosphorus, distinctly not found in *S. normani* and *P. ventilabrum* sponges, calcium and chlorine elements are disparately present on the surface structure of *G. barretti* and not in other *Geodia* relative.

The element of sodium is not present either in surface and spicules structures of *A. infundibuliformis*. However, sodium element is found on the surface of the two *G. barretti*, *P. ventilabrum,* and *S. normani* species and also in the spicules of *G. barretti* and *P. ventilabrum*.

The EDS results (**Table 2**) suggested that the design of sponge architecture might be influence by chemical composition among the five studied species. Sponges with skeletal architecture more compact (Gb and Pv) suggested incorporating in their skeletal structure a higher diversity of chemical elements than the Ai sponges.

Microcomputed Tomography

The internal density structure of the five key species was accessed using the Micro-CT analysis, a non-destructive way that preserves the natural sponge skeletons (**Figure 6**). Firstly, sponges were acquired using an X-ray diffraction displaying the following μCT images in **Figures 6A,E,I,M,Q**. The other series of μCT images is the 3D reconstruction of the sponge skeletons and the internal structure. The red or green color μCT images represent the organic and inorganic matter of the marine sponge skeletons, respectively. These images of a longitudinal-sectioned sponge body showed that internal structure formed by a spatial arrangement of the skeleton and inorganic structure, the spicules (**Figure 7**). A video of sponges reconstruction by micro-CT was included as **Supplementary Material**. Also, a quantitative analysis of the microstructural and morphometric parameters of the sponges were analyzed. The porosity (P, %), pore size, interconnectivity (I, %) and degree of anisotropy of each of the sponge species were evaluated by analysis of the respective 3D reconstructed image, defining an appropriate region of interest. Gb, Ga, and Sn have massive (sub)spherical shapes whereas Pv and Ai showed a morphological structure with a flabellate shape. These differences can be confirmed by tomography micrographs (**Figures 6**, **7**). For specimen Gb, P, and I were 84 ± 3 and 99, respectively, whereas for Ga, P, and I were 92 ± 3 and 100, respectively. For Sn specimen, P and I were 82 ± 1 and 99, respectively. For Ai specimen, P and I were 88 ± 1 and 99.8, respectively. The more compact sponge analyzed was Pv, which showed a percentage of P and I 68 ± 7 and 96 ± 2.

Porosity level and interconnectivity

All the sponge samples evaluated by μCT had porosity above 68%, and mostly above 80% that only includes interconnected pores. Moreover, porosity and interconnectivity of Pv and Ga sponges were statistically different with $p = 0.0153$ and $p = 0.0151$, respectively. Moreover, interconnectivity parameter revealed statistical significance between Pv and Ai sponges ($p = 0.0393$). Indeed, sponge samples had a high interconnectivity of pores, with values of about 99% in the Gb, Ga, Sn, and Ai sponges and slightly lower, 96%, for Pv (**Figures 8A,B**). In fact, high values of porosity and pore interconnectivity reflect crucial properties of filter-feeding animals, which feed occurs by sieving suspended food particles from water, typically by passing the water over specialized filtering structures and choanocyte cells, thus taking advantage of a hierarchical and complex system of pores and channels. This is quite interesting from a biomimetic perspective, as in tissue engineering, the panoply of developed scaffold biomaterials are characterized by a variety of requirements, among which the existence of a system capable to support cell migration and the exchange of oxygen, nutrients and waste is of paramount importance (Gao et al., 2017). In this regard, scaffolds with a porosity between 40 and 90% envisaging the engineering of bone tissue have been shown to enable cell adhesion and promote a proper osteointegration (Karageorgiou and Kaplan, 2005).

Pore size and degree of anisotropy

The 3D internal structure of the analyzed sponges showed pore sizes higher than 100 μm more particularly ranging from 149 to 472 μm (**Figure 8C**). Pv sponges showed a denser skeleton characterized by the lowest porosity of the studied species, revealing as well smaller pores, with an average size around 149 μm, comparing to the other sponge species where the average pore size is 300 μm and above. Moreover, the pore size of Ga and Pv showed statistical differences ($p = 0.0162$). The results of the pore sizes of Pv sponges suggested that small pores (**Figures 5C,E,F**) may allow the anchorage of microorganisms, and but also evidencing a strong correlation of a denser mesohyl structure with slower filtration rates, as previously reported (Weisz et al., 2008).

The anisotropy is a property exhibited by the substances and materials showing variations in physical properties dependent on the direction. Conversely, an isotropic structure exhibits the same physical properties independently of direction view (Mitchell and Tojeira, 2013).

Among the studied sponges, the degree of anisotropy of Gb, Ga, and Sn sponges showed values above 0.5, trending to a strategic alignment of fibers and skeletal structures (**Figure 8D**). This alignment of fibers on their skeletons can be an important role in the transport of nutrients along with architecture on the sponges when sponges have a more complex organization. The Pv and Ai members of the Axinellidae family showed an isotropic structure endowed with skeletons organized with the same physical characteristics in all directions. According to the statistical analyses, this property was significant between the Sn and Ai sponges ($p = 0.0148$), where Sn sponge had a degree of anisotropy above 0.5 (the highest value 0.72 DA) comparing with Ai sponges that have isotropy skeleton with a lower value (0.27 DA) below of 0.5 (**Figure 8D**).

Determination of organic and inorganic ratio

For the studied sponges, the organic/inorganic ratio was determined by micro-CT from the characteristic differences in the density between these two classes of materials (**Figure 9**).

All the analyzed demosponges (Gb, Ga, Sn, Pv, and Ai) showed similar ratio of inorganic and organic matter, with a value of around 50% of each component in the matrix (**Figure 9**) obtained

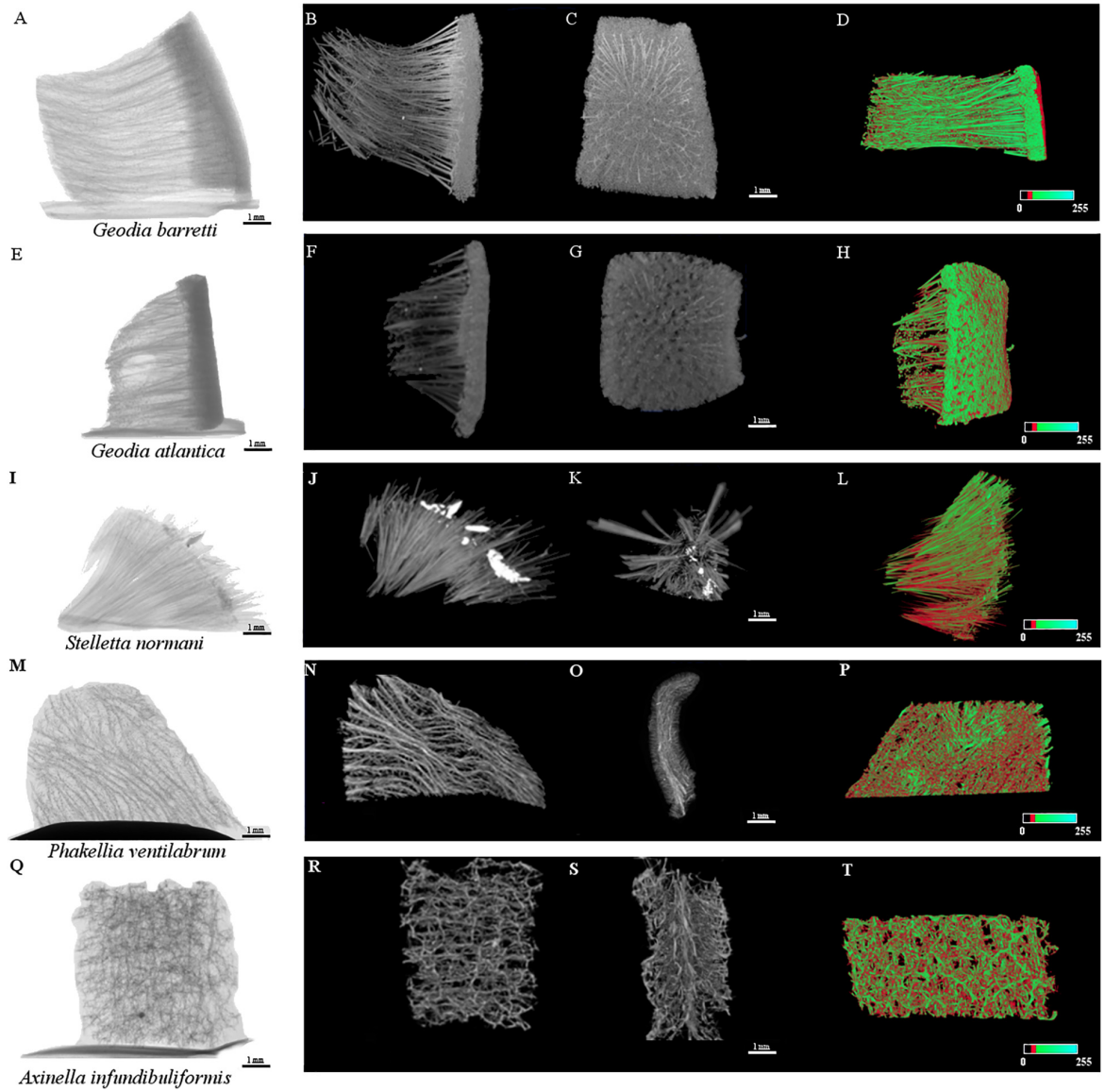

FIGURE 6 | Micro-CT micrographs of the internal microstructure of *Geodia barretti* (Gb), *Geodia atlantica* (Ga), *Stelletta normani* (Sn), *Phakellia ventilabrum* (Pv), and *Axinella infundibuliformis* (Ai). The X-ray diffraction images of the internal microstructure acquired for the five specimens **(A,E,I,M,Q)** respectively, following the order mentioned above. The other series of images represent the three-dimensional (3D) reconstruction. The gray levels micrographs represent two X-ray attenuation in different virtual position **(B,C,F,G,J,K,N,O,R,S)**. The color micrographs represent the distribution of organic (red) and inorganic (green) matter **(D,H,L,P,T)**.

by micro-CT analysis. The skeletons of these marine sponges are fibrous framework composed by organic component rich in a collagenous extracellular matrix that promotes attachment of cells (Green et al., 2003), namely spongin and collagen-like proteins, but also inorganic component as spicules. These elements are combined in a specific spatial arrangement on the healthy sponge skeleton, functioning as the mechanical support of the sponges (Taylor et al., 2007). The results suggested that the inside of the spicules are formed by organic material and outer layer is formed by the inorganic material (**Figure 7**). Statistical analyses showed non-significant differences ($p > 0.05$) in all multiple comparisons between the organic/inorganic content among the five studied sponges.

Mechanical Properties

To understand the particularities of the sponge skeletons is important to determine the mechanical properties present on the sponge porous internal structure. The compressive modulus for

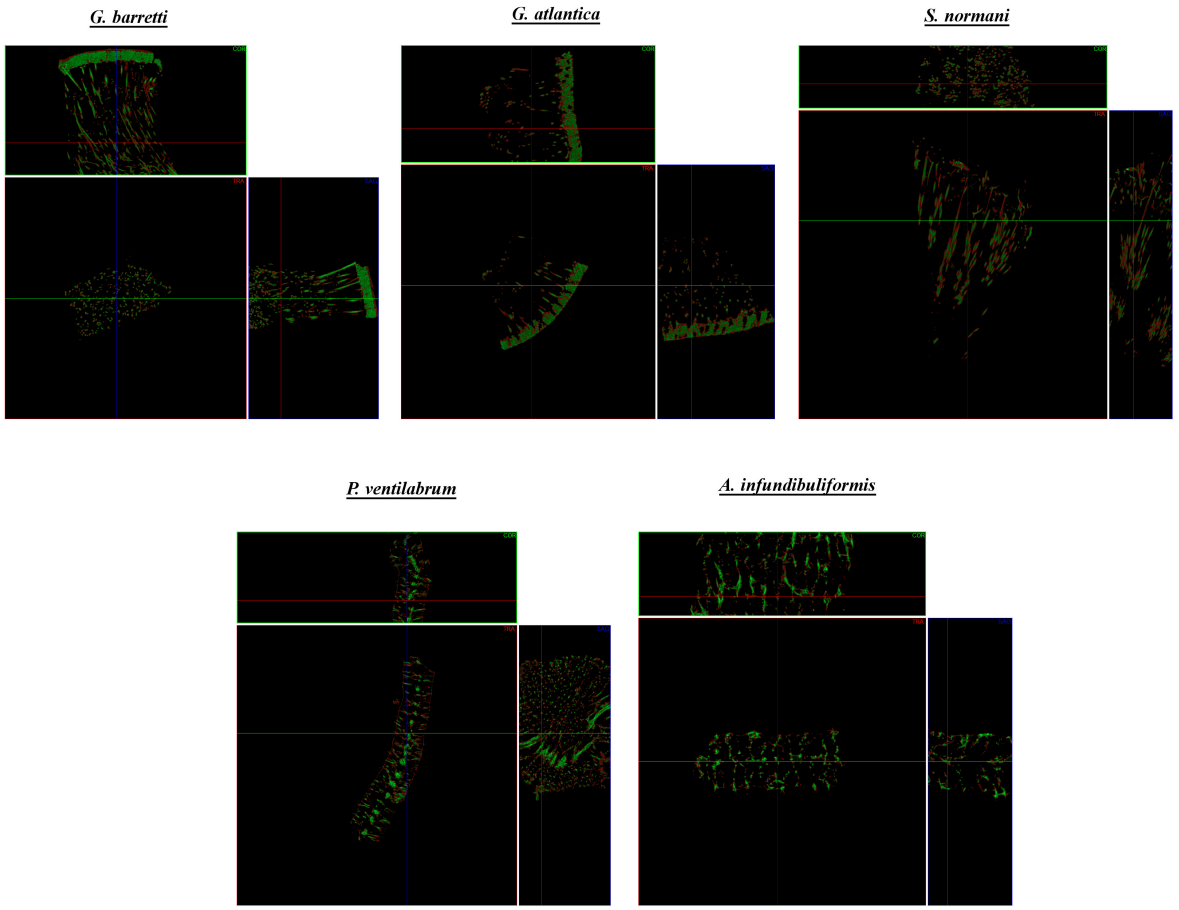

FIGURE 7 | Micro-CT representative coronal (COR), transverse (TRA) and sagittal (SAG) cross-sections of the skeletal of composition of the North Atlantic marine sponges. Each cross-section shows the sponge skeleton composition with the visualization of the organic matter (red) and inorganic matter (green).

each sponge was determined from the linear region of stress–strain curve.

As shown in **Figure 10**, the compressive modulus of Gb, Ga, Sn, Pv, and Ai was 0.022 ± 0.006 vs. 0.021 ± 0.016 vs. 0.032 ± 0.034 vs. 0.142 ± 0.081 vs. 0.046 ± 0.049 (MPa) respectively, assured mechanical values in the range of 0.021–0.142 MPa in the studied sponges. Among these sponge species, Pv showed the highest compressive strength, being statistically significant between Gb (p = 0.036), Ga (p = 0.0022) and Sn (p = 0.0043) sponges (**Figure 10**). Regarding the uniaxial compression testing demonstrated an inverse relationship between the compressive modulus of Pv, and the porosity and pore size. This means that a higher compressive modulus resulting in improvement of the mechanical properties showed the lowest porosity and pore size (**Figures 8A,C**). This phenomenon had been reported in other marine sponges as *Spongia agaricina* and *Spongia lamella*, whereas the reduction of porosity resulting in the enhancement of the mechanical properties (Boccardi et al., 2015b). Furthermore, these sponges provide scaffolds with higher mechanical properties (2–4-MPa). Recently study demonstrated that the skeletal architecture of marine glass sponge (*Euplectella aspergillum*) was used as biomodel for the 3D printing of structures with improved mechanical performance (Fernandes et al., 2020). The analyzed of mechanical behavior materials is relevant for biomimetic the properties of the skeletal tissues such as bone, cartilage, and tendon which present a very organized structure with structural functions (Zadpoor, 2015) also the evaluation of mechanical properties of biological tissue could be useful tool for diagnosis of diseases, as skins problem how collagen fibrils react to mechanical loading test (Nesbitt et al., 2015). However, to develop biomaterials with proper biological and mechanical properties that accurately fit these requirements, representing a gap in tissue engineering. For those reasons, scientist have investigating marine organisms to be used as models for biofabrication of new tissues engineering approaches. The compression strength of the sponges skeletons seems to require the mechanical properties of healthy soft (0.5–70 κPa), and cancerous soft tissues (20–560 κPa) (Hoskins, 2012).

Sponges as Biomimetic Models for Tissue Engineering Application

Marine sponges have a hierarchical architecture with spatial porous arrangement that may be an exceptional source of

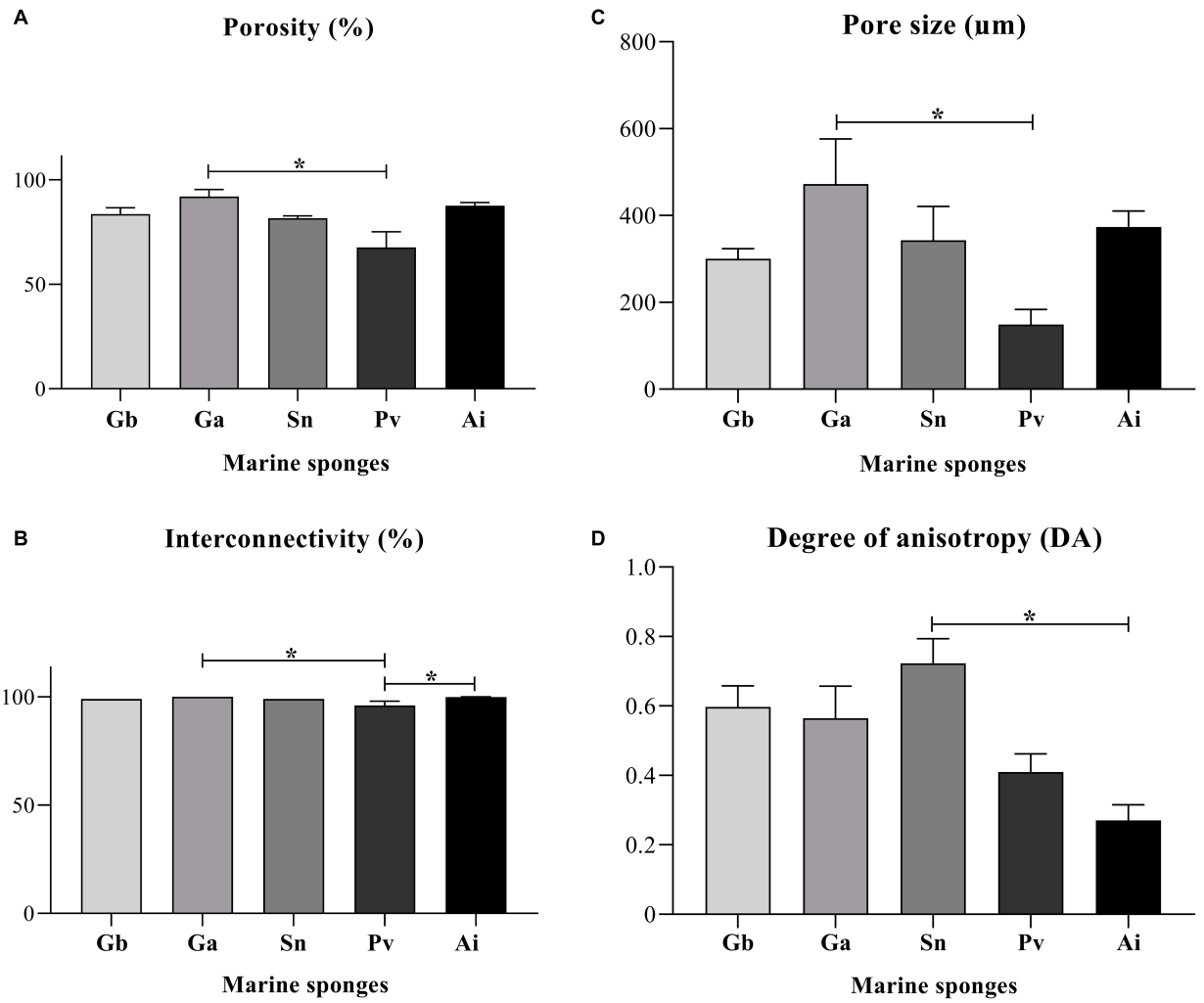

FIGURE 8 | Morphometric parameters of the 3D microstructure of the *Geodia barretti* (Gb), *Geodia atlantica* (Ga), *Stelletta normani* (Sn), *Phakellia ventilabrum* (Pv), and *Axinella infundibuliformis* (Ai). Micro-CT results for porosity (%) **(A)**, interconnectivity (%) **(B)**, pore size (μm) **(C)**, and degree of anisotropy (DA) **(D)**. Data expressed as mean ± SD with three replicates per sponge species and the asterisks (*) indicate statistically significant differences ($p < 0.05$) after Kruskal–Wallis test with Dunn's multiple comparisons.

inspiration for being mimicked in tissue engineering (TE) approaches. These aquatic organisms can be used as models for the isolation of unique molecules or inspired frameworks for development of health applications including controlled drug delivery systems (Langasco et al., 2017), manufacturing of scaffolds (Ehrlich and Worch, 2007; Pallela et al., 2012) and hydrogels (Fassini et al., 2017; Ghosh et al., 2019).

The fabrication of biomaterials has widely been used with the main purpose of successful enhancement the biological properties improving clinical acceptance. These structures maintain adequately high cellular viability for being analogs of the extracellular matrix (ECM), promote the physical cell support and functions accomplished by structure of nature tissues (Mohanty et al., 2015) abundantly constituted by collagen biopolymer. The production of collagen-GAG scaffolds had shown that cell adhesion decreased with increasing mean pore size (O'Brien et al., 2005). However, related phenomena suggest occurring in marine sponges, whereas a lower pore size showed a considerable number of microorganisms. Behind that, the collagenous nature of marine sponge skeletons has been reported to promote attachment of human cells (Green et al., 2003; Murphy et al., 2010; Pozzolini et al., 2018).

The specific architecture of skeletons may influence the regeneration, pointed that sponges internal differentiation in a distinct cortex layer over the choanosome or into stalk and flared portion seems to have a lower regeneration (Wulff, 2010). Indeed, the spontaneous ability of sponge regeneration is affected

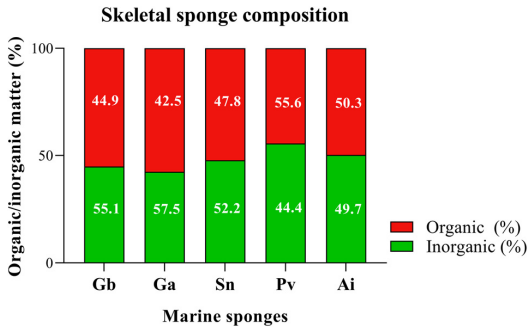

FIGURE 9 | Determination of structural composition of marine sponge of the *Geodia barretti* (Gb), *Geodia atlantica* (Ga), *Stelletta normani* (Sn), *Phakellia ventilabrum* (Pv), and *Axinella infundibuliformis* (Ai). Data expressed as mean of three replicates per sponge species and non-statistically significant differences ($p < 0.05$) after Kruskal–Wallis test with Dunn's multiple comparisons.

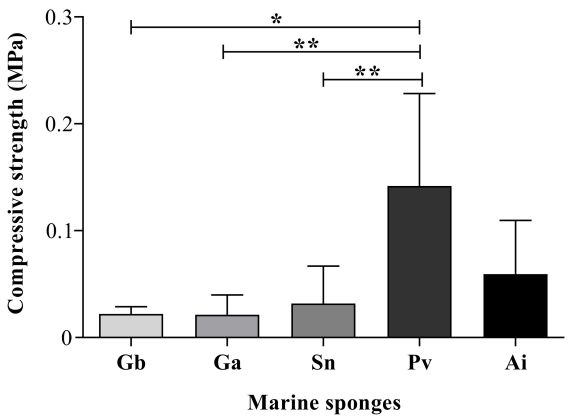

FIGURE 10 | Compressive modulus of the dried sponges. The asterisks indicate statistically significant differences (*$p < 0.05$ or **$p < 0.005$) after Kruskal–Wallis test with Dunn's multiple comparisons.

by different factors, as the dimension of the wound or injured tissue (Osinga et al., 1999), similar to that occurs in human bone. Studies investigated the healing and regeneration process of *G. barretti* during 8 months, as the first effort for the production of sponge tissue (Hoffmann et al., 2003). Recently, it has been reported the regeneration of the body wall of *Aplysina cavernicola* demosponge after the formation of a blastemal mass composed of undifferentiated pluripotent cells involve for the regeneration and ensuring the wound healed within 2 weeks (Ereskovsky et al., 2019). As the sponge tissues, bone has the ability to regenerate and repair itself until at a certain defect size. Large bone defects, caused by degenerative diseases, trauma or tumor resection, are not predictable to regenerate, requiring new approaches to tackle this tissue loss, ideally by promoting its regeneration by inducing the formation of new bone with the purpose of restore the bone form and function (Gómez-Barrena et al., 2015; Fillingham and Jacobs, 2016).

In tissue engineering, mean pore size is a critical aspect for the fabrication of biomaterials. However, it is not consensual which is the optimal range of mean pore sizes required for an ideal tissue engineering approach, probably because it will differ with type of tissue, although a minimum pore size should be around 100 μm to allow cell migration and proliferation to the interior of the scaffold (Karageorgiou and Kaplan, 2005). Nevertheless, it is consistently accepted that too large pores difficult the cell attachment due to the reduction of surface area available and too small pores limit the diffusion flows of gas, nutrients, growth factors as well as the elimination of the residual waste products (Murphy and O'Brien, 2010). Under the scope of different studies, scaffolds with larger pores (300–800 μm) were reported to enhance the formation of new bone and capillaries, while scaffolds with smaller pores (96–150 μm) promote a better attachment of osteoblasts during the osteoconductivity mechanisms (Karageorgiou and Kaplan, 2005; Murphy and O'Brien, 2010). Also, *Callyspongiidae* demosponge in the literature was reported to have a skeleton with a pore dimension between 100 and 300 μm wherein osteoblasts cells demonstrated the ability of anchor onto the surface of collagen fibers, being suitable biomaterial for bone tissue purpose (Lin et al., 2011). Furthermore, the anisotropic microstructure is also present on bone tissue that is constituted by an ordered arrangement of mostly collagen fibers, hydroxyapatite, and calcium phosphates materials (Szabó and Thurner, 2013; Tang et al., 2016; Ozasa et al., 2018). This is an important feature in biological systems, namely regarding cell-material interactions, with specific topographies seeming to positively influence the cell attachment and bioactivity on anisotropic scaffolds (Caliari and Harley, 2011). Also, the organization of cells in tissues are affected by the orientation of fibers in extracellular matrix that have a relevant role in the development and function of the tissue.

The composition of five demosponges studied after characterization of the morphology and chemical component, showed a presence of the organic and inorganic components with possible translation structure as a scaffold for bone tissue application. The skeletons of certain sponges and bone tissues are both composed by organic and inorganic compounds, constituting natural composites. In particular, bone is constituted by 30% of organic components namely collagen, polysaccharides, and other proteins, and 60% of the inorganic component as hydroxyapatite and calcium phosphates and 10% of the water (Feng, 2009). Independently of the composition of scaffolds, the future for regenerative purposes will encompass the manufacturing of nano to macroscopic levels of advanced unconventional biomaterials that mimic the chemical, biological and mechanical properties borrowed from nature in different therapeutic fields including bone, dermal, cardiac, muscle, neural and vascular (Khademhosseini and Langer, 2016; Nguyen and Camci-Unal, 2020).

CONCLUSION

Marine sponges own unique architectures with well spatial arrangement of skeleton components. Also, μCT and SEM analyses of five marine sponges confirmed the presence of highly

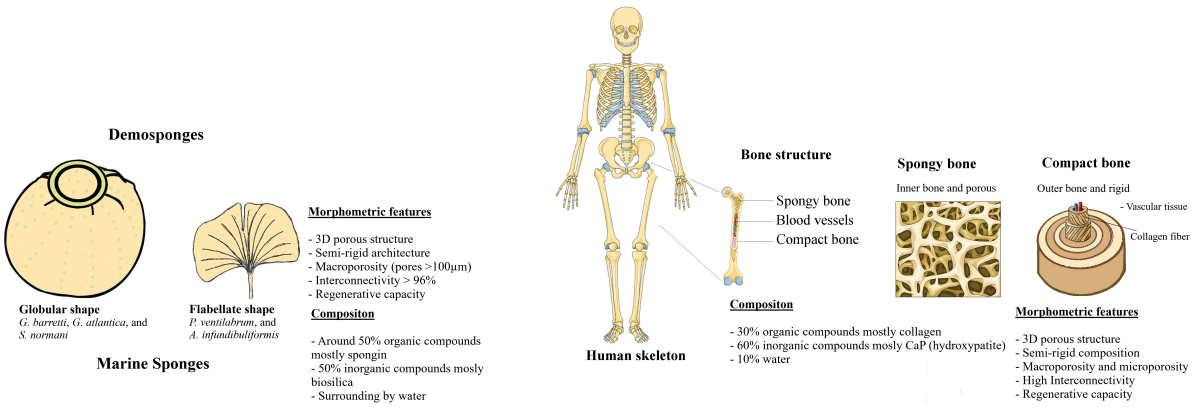

FIGURE 11 | Comparative morphological features of Marine Sponges and Human Bone tissue.

permeated 3D architecture constituted by a microscopic well-organized interconnected channel. The studied demosponges were characterized by a porous 3D structure, in which pores exhibit a mean diameter ranging from 149 to 472 µm, highly interconnected and absorbent with a collagenous matrix skeleton. The skeletons of these marine sponges suggested having the pores in the range suitable for inducing bone ingrowth. The morphological topographical and physical features on the sponges have similarities with bone tissue (**Figure 11**), particularly its extracellular matrix. In this perspective, marine sponges can be strategic models for the development of biomaterials inspired on their porous and interconnected architecture.

Although all sponges shown a combination of organic and inorganic components in approximately equal volumes, their porosities and spatial organization was species dependent, with Pv displaying the denser structure and the members of the Axinellidae family, Pv and Ai, showing an isotropic structure. On the other hand, sponges are animals commonly acquainted by having high and rapid regeneration ratio, while regeneration mechanism of bone is a complex physiological process that occurs constantly along human life by means of remodeling and healing of bone mechanism not yet completely understood. Thus, the further study of marine sponges and the relation between the regenerative capacity and the morphological features may give new clues for the development of tissue engineering scaffolds with improved performance.

This study supports the use of marine sponges as noble candidates for the development of natural matrices, because skeletons of the marine sponges create a microenvironment favorable for the cell adhesion and proliferation. Also, sponge skeletons share structural analogies to the human extracellular matrices regarding the varied chemical composition and also some biologically features that having still few explored in the regeneration of tissues as a bone. Likewise, the architectural design of natural bone is a combination of various mechanical requirements as stiffness, strength, and toughness properties. These properties have been used for reinforcement and biomimetic the architecture of bone in the development of new materials (Gong et al., 2015).

DATA AVAILABILITY STATEMENT

The original contributions presented in the study are included in the article/**Supplementary Material**, further inquiries can be directed to the corresponding author/s.

AUTHOR CONTRIBUTIONS

EM designed and conceived the study, performed the experimental analyses, treated and discussed the results, and wrote the manuscript. HTR sampled the marine sponges' specimens, performed the sponge taxonomic identification, and responsible for funding. JRX contributed to study planning, sampled the marine sponges' specimens, performed the sponge taxonomic identification, discussed the results, and revised the manuscript. GSD supported the µCT analysis and revised the manuscript. RLR conceived the study, revised the manuscript, and responsible for funding. THS conceived and planned the study, discussed the results, and revised the manuscript. All the authors contributed to the work and approved the final version of the article.

FUNDING

The authors would like to acknowledge the funding from the European Union Framework Program for Research and Innovation Horizon 2020 through project SponGES (H2020-BG-01-2015-679849) and from the Northern Portugal Regional Operational Program (NORTE2020), under the Portugal 2020 Partnership Agreement, through the Structured projects for R&D&I NORTE-01-0145-FEDER-000021 and NORTE-01-0145-FEDER-000023. JRX research was further supported by national funds through FCT Foundation for Science and Technology within the scope of UIDB/04423/2020 and UIDP/04423/2020, and CEECIND/00577/2018.

SUPPLEMENTARY MATERIAL

The Supplementary Material for this article can be found online at: https://www.frontiersin.org/articles/10.3389/fmars.2020.613647/full#supplementary-material

Supplementary Material 1 | The determination of the ratios of the organic and inorganic elements present on the North Atlantic Sponges was accessed by micro-CT analyses and recorded in a video. 3D reconstruction of sponges was recorded in video to enable the visualization of the composition of the five demosponges namely, *Geodia barretti*, *Geodia atlantica*, *Stelletta normani*, *Phakellia ventilabrum,* and *Axinella infundibuliformis*.

REFERENCES

Aguilar-Camacho, J. M., Doonan, L., and Mccormack, G. P. (2019). Evolution of the main skeleton-forming genes in sponges (*Phylum porifera*) with special focus on the marine Haplosclerida (class *Demospongiae*). *Mol. Phylogenet. Evol.* 131, 245–253. doi: 10.1016/j.ympev.2018.11.015

Aizenberg, J., Weaver, J. C., Thanawala, M. S., Sundar, V. C., Morse, D. E., and Fratzl, P. J. S. (2005). Skeleton of *Euplectella sp*: structural hierarchy from the nanoscale to the macroscale. *Science* 309, 275–278. doi: 10.1126/science.1112255

Alves, A. L., Marques, A. L., Martins, E., Silva, T. H., and Reis, R. L. (2017). Cosmetic potential of marine fish skin collagen. *Cosmetics* 4:39. doi: 10.3390/cosmetics4040039

Azuma, K., Ifuku, S., Osaki, T., Okamoto, Y., and Minami, S. (2014). Preparation and biomedical applications of chitin and chitosan nanofibers. *J. Biomed. Nanotechnol.* 10, 2891–2920. doi: 10.1166/jbn.2014.1882

Belarbi, E. H., Gomez, A. C., Chisti, Y., Camacho, F. G. A., and Grima, E. M. (2003). Producing drugs from marine sponges. *Biotechnol. Adv.* 21, 585–598. doi: 10.1016/s0734-9750(03)00100-9

Bell, J. J. (2002). Regeneration rates of a sublittoral demosponge. *J. Mar. Biol. Assoc. UK* 82, 169–170. doi: 10.1017/s0025315402005295

Boccardi, E., Belova, I., Murch, G., Boccaccini, A., and Fiedler, T. (2015a). Oxygen diffusion in marine-derived tissue engineering scaffolds. *J. Mater. Sci. Mater. Med.* 26:200.

Boccardi, E., Philippart, A., Juhasz-Bortuzzo, J., Novajra, G., Vitale-Brovarone, C., and Boccaccini, A. R. (2015b). Characterisation of bioglass based foams developed via replication of natural marine sponges. *Adv. Appl. Ceramics* 114, S56–S62.

Borisenko, I. E., Adamska, M., Tokina, D. B., and Ereskovsky, A. V. (2015). Transdifferentiation is a driving force of regeneration in *Halisarca dujardini* (*Demospongiae, Porifera*). *PeerJ* 3:e1211. doi: 10.7717/peerj.1211

Burns, E., and Ilan, M. (2003). Comparison of anti-predatory defenses of red sea and caribbean sponges. II. physical defense. *Mar. Ecol. Prog. Ser.* 252, 115–123. doi: 10.3354/meps252115

Caliari, S. R., and Harley, B. A. (2011). The effect of anisotropic collagen-GAG scaffolds and growth factor supplementation on tendon cell recruitment, alignment, and metabolic activity. *Biomaterials* 32, 5330–5340. doi: 10.1016/j.biomaterials.2011.04.021

Cárdenas, P., Rapp, H. T., Klitgaard, A. B., Best, M., Thollesson, M., and Tendal, O. S. (2013). Taxonomy, biogeography and DNA barcodes of Geodia species (*Porifera, Demospongiae, Tetractinellida*) in the Atlantic boreo-arctic region. *Zool. J. Linn. Soc.* 169, 251–311. doi: 10.1111/zoj.12056

Chattopadhyay, S., and Raines, R. T. (2014). Collagen-based biomaterials for wound healing. *Biopolymers* 101, 821–833. doi: 10.1002/bip.22486

Chiriboga, O. G., Leduff, P., and Rorrer, G. L. (2020). "Extracellular chitin nanofibers from marine diatoms," in *Encyclopedia of Marine Biotechnology*, ed. K. Se-Kwon (Hoboken, NJ: John Wiley).

Christy, P. N., Basha, S. K., Kumari, V. S., Bashir, A., Maaza, M., Kaviyarasu, K., et al. (2020). Biopolymeric nanocomposite scaffolds for bone tissue engineering applications–a review. *J. Drug Deliv. Sci. Technol.* 55:101452. doi: 10.1016/j.jddst.2019.101452

Clarke, J. (2003). The occurrence and significance of biogenic opal in the regolith. *J. Earth-Sci. Rev.* 60, 175–194. doi: 10.1016/s0012-8252(02)00092-2

Clarke, S., Choi, S., Mckechnie, M., Burke, G., Dunne, N., Walker, G., et al. (2016). Osteogenic cell response to 3-D Hydroxyapatite scaffolds developed via replication of natural marine sponges. *J. Mater. Sci. Mater. Med.* 27:22.

Coutinho, C. C., De Andrade Rosa, I., De Oliveira Teixeira, J. D., Andrade, L. R., Costa, M. L., and Mermelstein, C. (2017). Cellular migration, transition and interaction during regeneration of the sponge *Hymeniacidon heliophila*. *PLoS One* 12:e0178350. doi: 10.1371/journal.pone.0178350

Cunningham, E., Dunne, N., Walker, G., Maggs, C., Wilcox, R., and Buchanan, F. (2010). Hydroxyapatite bone substitutes developed via replication of natural marine sponges. *J. Mater. Sci. Mater. Med.* 21, 2255–2261. doi: 10.1007/s10856-009-3961-4

De Vos, L., Rutzler, K., Boury-Esnault, N., Donadey, C., and Vacelet, J. (1991). *Atlas of Sponge Morphology. Atlas de Morphologie Des Éponges*. Washington, DC: Smithsonian Institution Press.

Diogo, G. S., Carneiro, F., Freitas-Ribeiro, S., Sotelo, C. G., Pérez-Martín, R. I., Pirraco, R. P., et al. (2020). *Prionace glauca* skin collagen bioengineered constructs as a promising approach to trigger cartilage regeneration. *J. Mater. Sci. Eng. C* (in press). doi: 10.1016/j.msec.2020.111587

Dong, C., and Lv, Y. (2016). Application of collagen scaffold in tissue engineering: recent advances and new perspectives. *Polymers* 8:42. doi: 10.3390/polym8020042

Eckert, C., Schröder, H. C., Brandt, D., Perovic-Ottstadt, S., and Müller, W. E. (2006). Histochemical and electron microscopic analysis of spiculogenesis in the demosponge suberites domuncula. *J. Histochem. Cytochem.* 54, 1031–1040. doi: 10.1369/jhc.5a6903.2006

Ehrlich, H. (ed.). (2019). "Enigmatic structural protein spongin," in *Marine Biological Materials of Invertebrate Origin. Volume 13 of Biologically-Inspired Systems*, (Berlin: Springer), 161–172. doi: 10.1007/978-3-319-92483-0_11

Ehrlich, H., Maldonado, M., Spindler, K. D., Eckert, C., Hanke, T., Born, R., et al. (2007). First evidence of chitin as a component of the skeletal fibers of marine sponges. part I. verongidae (*Demospongia: Porifera*). *J. Exp. Zool. B Mol. Dev. Evol.* 308, 347–356. doi: 10.1002/jez.b.21156

Ehrlich, H., Shaala, L. A., Youssef, D. T., Żółtowska-Aksamitowska, S., Tsurkan, M., Galli, R., et al. (2018a). Discovery of chitin in skeletons of non-verongiid red sea demosponges. *PLoS One* 13:e0195803. doi: 10.1371/journal.pone.0195803

Ehrlich, H., Simon, P., Carrillo-Cabrera, W., Bazhenov, V. V., Botting, J. P., Ilan, M., et al. (2010). Insights into chemistry of biological materials: newly discovered silica-aragonite-chitin biocomposites in demosponges. *J. Chem. Mater.* 22, 1462–1471. doi: 10.1021/cm9026607

Ehrlich, H., and Worch, H. (2007). "Sponges as natural composites: from biomimetic potential to development of new biomaterials," in *Porifera Research: Biodiversity, Innovation & Sustainability*, eds Márcio Reis, G. Custódio, E. Lobo-Hajdu, G. Hajdu, and Muricy (Brazil: Museu Nacional), 217–223.

Ehrlich, H., Wysokowski, M., Żółtowska-Aksamitowska, S., Petrenko, I., and Jesionowski, T. (2018b). Collagens of poriferan origin. *Mar. Drugs* 16:79. doi: 10.3390/md16030079

Einhorn, T. A., and Gerstenfeld, L. C. (2015). Fracture healing: mechanisms and interventions. *Nat. Rev. Rheumatol.* 11, 45–54. doi: 10.1038/nrrheum.2014.164

Ereskovsky, A. V., Tokina, D. B., Saidov, D. M., Baghdiguian, S., Le Goff, E., and Lavrov, A. I. (2019). Transdifferentiation and mesenchymal-to-epithelial transition during regeneration in Demospongiae (Porifera). *J. Exp. Zool. B Mol. Dev. Evol.* 334, 37–58. doi: 10.1002/jez.b.22919

Exposito, J. Y., Cluzel, C., Garrone, R., and Lethias, C. (2002). Evolution of collagens. *Anat. Rec.* 268, 302–316. doi: 10.1002/ar.10162

Fassini, D., Duarte, A. R., Reis, R., and Silva, T. (2017). Bioinspiring chondrosia reniformis (Nardo, 1847) collagen-based hydrogel: a new extraction method to obtain a sticky and self-healing collagenous material. *Mar. Drugs* 15:380. doi: 10.3390/md15120380

Fassini, D., Oliveira, S. M., Silva, T. H., and Reis, R. L. (2020). "Biotechnological valorization of marine collagens: biomaterials for health applications," in *Encyclopedia of Marine Biotechnology*, ed. S.-K. Kim (Hoboken, NJ: John Wiley).

Feng, X. (2009). Chemical and biochemical basis of cell-bone matrix interaction in health and disease. *Curr. Chem. Biol.* 3, 189–196. doi: 10.2174/187231309788166398

Fernandes, M. C., Aizenberg, J., Weaver, J. C., and Bertoldi, K. (2020). Mechanically robust lattices inspired by deep-sea glass

sponges. *Nat. Mater.* doi: 10.1038/s41563-020-0798-1 Online ahead of print.

Fillingham, Y., and Jacobs, J. (2016). Bone grafts and their substitutes. *Bone Joint J.* 98, 6–9.

Gabbai-Armelin, P., Kido, H., Cruz, M., Prado, J., Avanzi, I., Custódio, M., et al. (2019). Characterization and cytotoxicity evaluation of a marine sponge biosilica. *Mar. Biotechnol.* 21, 65–75. doi: 10.1007/s10126-018-9858-9

Gao, C., Peng, S., Feng, P., and Shuai, C. (2017). Bone biomaterials and interactions with stem cells. *Bone Res.* 5:17059.

Gazave, E., Lapébie, P., Ereskovsky, A. V., Vacelet, J., Renard, E., Cárdenas, P., et al. (2012). No longer Demospongiae: Homoscleromorpha formal nomination as a fourth class of Porifera. *Hydrobiologia* 687, 3–10. doi: 10.1007/s10750-011-0842-x

Ghosh, A., Grosvenor, A. J., and Dyer, J. M. (2019). Marine spongia collagens: protein characterization and evaluation of hydrogel films. *J. Appl. Polym. Sci.* 136:47996. doi: 10.1002/app.47996

Gilis, M., Grauby, O., Willenz, P., Dubois, P., Heresanu, V., and Baronnet, A. (2013). Biomineralization in living *Hypercalcified demosponges*: toward a shared mechanism? *J. Struct. Biol.* 183, 441–454. doi: 10.1016/j.jsb.2013.05.018

Gómez-Barrena, E., Rosset, P., Lozano, D., Stanovici, J., Ermthaller, C., and Gerbhard, F. (2015). Bone fracture healing: cell therapy in delayed unions and nonunions. *Bone* 70, 93–101. doi: 10.1016/j.bone.2014.07.033

Gong, T., Xie, J., Liao, J., Zhang, T., Lin, S., and Lin, Y. (2015). Nanomaterials and bone regeneration. *Bone Res.* 3:15029.

Granito, R. N., Custódio, M. R., and Rennó, A. C. M. (2017). Natural marine sponges for bone tissue engineering: the state of art and future perspectives. *J. Biomed. Mater. Res. B Appl. Biomater.* 105, 1717–1727. doi: 10.1002/jbm.b.33706

Green, D., Howard, D., Yang, X., Kelly, M., and Oreffo, R. (2003). Natural marine sponge fiber skeleton: a biomimetic scaffold for human osteoprogenitor cell attachment, growth, and differentiation. *Tissue Eng.* 9, 1159–1166. doi: 10.1089/10763270360728062

Green, D. W., Padula, M., Santos, J., Chou, J., Milthorpe, B., and Ben-Nissan, B. (2013). A new role for marine skeletal proteins in regenerative orthopaedics. *Key Eng. Mater.* 529, 654–659. doi: 10.4028/www.scientific.net/kem.529-530.654

Hoffmann, F., Rapp, H. T., Zöller, T., and Reitner, J. (2003). Growth and regeneration in cultivated fragments of the boreal deep water sponge *Geodia barretti* bowerbank, 1858 (*Geodiidae, Tetractinellida, Demospongiae*). *J. Biotechnol.* 100, 109–118. doi: 10.1016/s0168-1656(02)00258-4

Hooper, J. N., and Van Soest, R. W. (2002). ""Systema porifera"," in *A guide to the classification of sponges systema porifera*, eds N. A. John Hooper and R. W. M. van Soset (Boston, MA: Springer), 1–7. doi: 10.1007/978-1-4615-0747-5_1

Horton, T., Kroh, A., Ahyong, S., Bailly, N., Boury-Esnault, N., Brandão, S. N., et al. (2018). *World Register of Marine Species*. Available online at: https://www.marinespecies.org at VLIZ (accessed March 24, 2018)

Hoskins, P. R. (2012). Principles of ultrasound elastography. *Ultrasound* 20, 8–15. doi: 10.1258/ult.2011.011005

Jugdaohsingh, R. (2007). Silicon and bone health. *J. Nutr. Health Aging* 11, 99–110.

Karageorgiou, V., and Kaplan, D. (2005). Porosity of 3D biomaterial scaffolds and osteogenesis. *Biomaterials* 26, 5474–5491. doi: 10.1016/j.biomaterials.2005.02.002

Kaya, M., Bilican, I., Mujtaba, M., Sargin, I., Haskoylu, M. E., Oner, E. T., et al. (2020). Sponge-derived natural bioactive glass microspheres with self-assembled surface channel arrays opening into a hollow core for bone tissue and controlled drug release applications. *Chem. Eng. J.* (in press). doi: 10.1016/j.cej.2020.126667

Khademhosseini, A., and Langer, R. (2016). A decade of progress in tissue engineering. *Nat. Protoc.* 11, 1775–1781. doi: 10.1038/nprot.2016.123

Kim, S. K., and Dewapriya, P. (2012). Bioactive compounds from marine sponges and their symbiotic microbes: a potential source of nutraceuticals. *Adv. Food Nutr. Res.* 65, 137–151. doi: 10.1016/b978-0-12-416003-3.00008-1

Klinger, C., Żółtowska-Aksamitowska, S., Wysokowski, M., Tsurkan, M. V., Galli, R., Petrenko, I., et al. (2019). Express method for isolation of ready-to-use 3D chitin scaffolds from *Aplysina archeri* (*Aplysineidae*: *Verongiida*) demosponge. *Mar. Drugs* 17:131. doi: 10.3390/md17020131

Klitgaard, A. B., and Tendal, O. S. (2004). Distribution and species composition of mass occurrences of large-sized sponges in the northeast Atlantic. *Prog. Oceanogr.* 61, 57–98. doi: 10.1016/j.pocean.2004.06.002

Kovalchuk, V., Voronkina, A., Binnewerg, B., Schubert, M., Muzychka, L., Wysokowski, M., et al. (2019). Naturally drug-loaded chitin: isolation and applications. *Mar. Drugs* 17:574. doi: 10.3390/md17100574

Langasco, R., Cadeddu, B., Formato, M., Lepedda, A. J., Cossu, M., Giunchedi, P., et al. (2017). Natural collagenic skeleton of marine sponges in pharmaceutics: innovative biomaterial for topical drug delivery. *Mater. Sci. Eng.* 70, 710–720. doi: 10.1016/j.msec.2016.09.041

Lin, Z., Solomon, K. L., Zhang, X., Pavlos, N. J., Abel, T., Willers, C., et al. (2011). In vitro evaluation of natural marine sponge collagen as a scaffold for bone tissue engineering. *Intl. J. of Biol. Sci.* 7, 968–977. doi: 10.7150/ijbs.7.968

Maldonado, M. (2009). Embryonic development of verongid demosponges supports the independent acquisition of spongin skeletons as an alternative to the siliceous skeleton of sponges. *Biol. J. Linn. Soc.* 97, 427–447. doi: 10.1111/j.1095-8312.2009.01202.x

Martins, E., Rocha, M. S., Silva, T. H., and Reis, R. L. (2019). "Remarkable body architecture of marine sponges as biomimetic structure for application in tissue engineering," in *Marine-Derived Biomaterials for Tissue Engineering Applications. Springer Series in Biomaterials Science and Engineering*, eds A. H. Choi and B. Ben-Nissan (Berlin: Springer), 27–50. doi: 10.1007/978-981-13-8855-2_2

Mitchell, G. R., and Tojeira, A. (2013). Role of anisotropy in tissue engineering. *Procedia Eng.* 59, 117–125. doi: 10.1016/j.proeng.2013.05.100

Mohanty, S., Larsen, L. B., Trifol, J., Szabo, P., Burri, H. V. R., Canali, C., et al. (2015). Fabrication of scalable and structured tissue engineering scaffolds using water dissolvable sacrificial 3D printed moulds. *Mater. Sci. Eng.* 55, 569–578. doi: 10.1016/j.msec.2015.06.002

Müller, W. E., Boreiko, A., Wang, X., Krasko, A., Geurtsen, W., Custódio, M. R., et al. (2007). Morphogenetic activity of silica and bio-silica on the expression of genes controlling biomineralization using SaOS-2 cells. *Calcif. Tissue Int.* 81, 382–393. doi: 10.1007/s00223-007-9075-4

Murillo, F. J., Muñoz, P. D., Cristobo, J., Ríos, P., González, C., Kenchington, E., et al. (2012). Deep-sea sponge grounds of the flemish cap, flemish pass and the grand banks of newfoundland (Northwest Atlantic Ocean): distribution and species composition. *Mar. Biol. Res.* 8, 842–854. doi: 10.1080/17451000.2012.682583

Murphy, C. M., Haugh, M. G., and O'brien, F. J. (2010). The effect of mean pore size on cell attachment, proliferation and migration in collagen–glycosaminoglycan scaffolds for bone tissue engineering. *Biomaterials* 31, 461–466. doi: 10.1016/j.biomaterials.2009.09.063

Murphy, C. M., and O'Brien, F. J. (2010). Understanding the effect of mean pore size on cell activity in collagen-glycosaminoglycan scaffolds. *Cell Adh. Migr.* 4, 377–381. doi: 10.4161/cam.4.3.11747

Mutsenko, V. V., Bazhenov, V. V., Rogulska, O., Tarusin, D. N., Schütz, K., Brüggemeier, S., et al. (2017a). 3D chitinous scaffolds derived from cultivated marine demosponge Aplysina aerophoba for tissue engineering approaches based on human mesenchymal stromal cells. *Int. J. Biol. Macromol.* 104, 1966–1974. doi: 10.1016/j.ijbiomac.2017.03.116

Mutsenko, V. V., Gryshkov, O., Lauterboeck, L., Rogulska, O., Tarusin, D. N., Bazhenov, V. V., et al. (2017b). Novel chitin scaffolds derived from marine sponge Ianthella basta for tissue engineering approaches based on human mesenchymal stromal cells: biocompatibility and cryopreservation. *Int. J. Biol. Macromol.* 104, 1955–1965. doi: 10.1016/j.ijbiomac.2017.03.161

Nakayama, S., Arima, K., Kawai, K., Mohri, K., Inui, C., Sugano, W., et al. (2015). Dynamic transport and cementation of skeletal elements build up the pole-and-beam structured skeleton of sponges. *Curr. Biol.* 25, 2549–2554. doi: 10.1016/j.cub.2015.08.023

Nandi, S. K., Kundu, B., Mahato, A., Thakur, N. L., Joardar, S. N., and Mandal, B. B. (2015). In vitro and in vivo evaluation of the marine sponge skeleton as a bone mimicking biomaterial. *Integr. Biol.* 7, 250–262. doi: 10.1039/c4ib00289j

Nesbitt, S., Scott, W., Macione, J., and Kotha, S. (2015). Collagen fibrils in skin orient in the direction of applied uniaxial load in proportion to stress while exhibiting differential strains around hair follicles. *Materials* 8, 1841–1857. doi: 10.3390/ma8041841

Nguyen, M. A., and Camci-Unal, G. (2020). Unconventional tissue engineering materials in disguise. *Trends Biotechnol.* 38, 178–190. doi: 10.1016/j.tibtech.2019.07.014

Nickel, M., and Brümmer, F. (2003). In vitro sponge fragment culture of Chondrosia reniformis (Nardo, 1847). *J. Biotechnol.* 100, 147–159. doi: 10.1016/s0168-1656(02)00256-0

O'Brien, F. J., Harley, B., Yannas, I. V., and Gibson, L. J. (2005). The effect of pore size on cell adhesion in collagen-GAG scaffolds. *Biomaterials* 26, 433–441. doi: 10.1016/j.biomaterials.2004.02.052

Osinga, R., Tramper, J., and Wijffels, R. H. (1999). Cultivation of marine sponges. *Mar. Biotechnol.* 1, 509–532. doi: 10.1007/pl00011807

Ozasa, R., Matsugaki, A., Isobe, Y., Saku, T., Yun, H. S., and Nakano, T. (2018). Construction of human induced pluripotent stem cell-derived oriented bone matrix microstructure by using in vitro engineered anisotropic culture model. *J. Biomed. Mater. Res. A* 106, 360–369. doi: 10.1002/jbm.a.36238

Pallela, R., Venkatesan, J., Janapala, V. R., and Kim, S. K. (2012). Biophysicochemical evaluation of chitosan-hydroxyapatite-marine sponge collagen composite for bone tissue engineering. *J. Biomed. Mater. Res. A* 100, 486–495. doi: 10.1002/jbm.a.33292

Philibert, T., Lee, B. H., and Fabien, N. J. A. B. (2017). Current status and new perspectives on chitin and chitosan as functional biopolymers. *Appl. Biochem. Biotechnol.* 181, 1314–1337. doi: 10.1007/s12010-016-2286-2

Pozzolini, M., Gallus, L., Ghignone, S., Ferrando, S., Candiani, S., Bozzo, M., et al. (2019). Insights into the evolution of metazoan regenerative mechanisms: roles of TGF superfamily members in tissue regeneration of the marine sponge chondrosia reniformis. *J. Exp. Biol.* 222:jeb207894. doi: 10.1242/jeb.207894

Pozzolini, M., Scarfì, S., Gallus, L., Castellano, M., Vicini, S., Cortese, K., et al. (2018). Production, characterization and biocompatibility evaluation of collagen membranes derived from marine sponge chondrosia reniformis nardo, 1847. *Mar. Drugs* 16:111. doi: 10.3390/md16040111

Ramshaw, J. A., Peng, Y. Y., Glattauer, V., and Werkmeister, J. A. (2009). Collagens as biomaterials. *J. Mater. Sci. Mater. Med.* 20, S3–S8.

Sandford, F. (2003). Physical and chemical analysis of the siliceous skeletons in six sponges of two groups (*Demospongiae* and *Hexactinellida*). *Microsc. Res. Tech.* 62, 336–355. doi: 10.1002/jemt.10400

Santos, V. P., Marques, N. S. S., Maia, P. C. S. V., Lima, M. A. B., Franco, L. O., and Campos-Takaki, G. M. (2020). Seafood waste as attractive source of chitin and chitosan production and their applications. *Intl. J. Mol. Sci.* 21:4290. doi: 10.3390/ijms21124290

Schröder, H. C., Boreiko, O., Krasko, A., Reiber, A., Schwertner, H., and Müller, W. E. (2005). Mineralization of SaOS-2 cells on enzymatically (silicatein) modified bioactive osteoblast-stimulating surfaces. *J. Biomed. Mater. Res. B Appl. Biomater.* 75, 387–392. doi: 10.1002/jbm.b.30322

Schubert, M., Binnewerg, B., Voronkina, A., Muzychka, L., Wysokowski, M., Petrenko, I., et al. (2019). Naturally prefabricated marine biomaterials: isolation and applications of flat chitinous 3D scaffolds from ianthella labyrinthus (*Demospongiae: Verongiida*). *Intl. J. Mol. Sci.* 20:5105. doi: 10.3390/ijms20205105

Seixas, M. J., Martins, E., Reis, R. L., and Silva, T. H. (2020). Extraction and characterization of collagen from elasmobranch byproducts for potential biomaterial use. *Mar. Drugs* 18:E617. doi: 10.3390/md18120617

Shaala, L. A., Asfour, H. Z., Youssef, D. T., Żółtowska-Aksamitowska, S., Wysokowski, M., Tsurkan, M., et al. (2019). New source of 3D chitin scaffolds: the red sea demosponge *Pseudoceratina arabica* (*Pseudoceratinidae, Verongiida*). *Mar. Drugs* 17:92. doi: 10.3390/md17020092

Silva, J. O. C., Barros, A. A., Aroso, I. M., Fassini, D., Silva, T. H., Reis, R. L., et al. (2016). Extraction of collagen/gelatin from the marine demosponge chondrosia reniformis (Nardo, 1847) using water acidified with carbon dioxide–process optimization. *Ind. Eng. Chem. Res.* 55, 6922–6930. doi: 10.1021/acs.iecr.6b00523

Silva, T. H., Alves, A., Ferreira, B., Oliveira, J. M., Reys, L., Ferreira, R., et al. (2012). Materials of marine origin: a review on polymers and ceramics of biomedical interest. *Intl. Mater. Rev.* 57, 276–306. doi: 10.1179/1743280412y.0000000002

Silva, T. H., Moreira-Silva, J., Marques, A. L., Domingues, A., Bayon, Y., and Reis, R. L. (2014). Marine origin collagens and its potential applications. *Mar. Drugs* 12, 5881–5901. doi: 10.3390/md12125881

Silvipriya, K., Kumar, K. K., Bhat, A., Kumar, B. D., John, A., and Lakshmanan, P. (2015). Collagen: animal sources and biomedical application. *J. Appl. Pharm. Sci.* 5, 123–127. doi: 10.7324/japs.2015.50322

Simion, P., Philippe, H., Baurain, D., Jager, M., Richter, D. J., Di Franco, A., et al. (2017). A large and consistent phylogenomic dataset supports sponges as the sister group to all other animals. *Curr. Biol.* 27, 958–967. doi: 10.1016/j.cub.2017.02.031

Singh, D., and Shrivastava, A. K. (2020). "Chitin: promising biopolymer for biomedical application," in *New and Future Developments in Microbial Biotechnology and Bioengineering*, ed. V. K. Gupta (Amsterdam: Elsevier Science), 175–185. doi: 10.1016/b978-0-12-821006-2.00013-3

Singh, D. K., and Ray, A. R. (2000). Biomedical applications of chitin, chitosan, and their derivatives. *J. Macromol. Sci. C. Polym. Rev.* 40, 69–83.

Smith, A. M., Berman, J., Key, M. M. Jr., and Winter, D. J. (2013). Not all sponges will thrive in a high-CO2 ocean: review of the mineralogy of calcifying sponges. *Palaeogeogr. Palaeoclimatol. Palaeoecol.* 392, 463–472. doi: 10.1016/j.palaeo.2013.10.004

Sorushanova, A., Delgado, L. M., Wu, Z., Shologu, N., Kshirsagar, A., Raghunath, R., et al. (2019). The collagen suprafamily: from biosynthesis to advanced biomaterial development. *Adv. Mater.* 31:e1801651.

Sousa, R. O., Alves, A. L., Carvalho, D. N., Martins, E., Oliveira, C., Silva, T. H., et al. (2020a). Acid and enzymatic extraction of collagen from Atlantic cod (*Gadus Morhua*) swim bladders envisaging health-related applications. *J. Biomater. Sci. Polym. Ed.* 31, 20–37. doi: 10.1080/09205063.2019.1669313

Sousa, R. O., Martins, E., Carvalho, D. N., Alves, A. L., Oliveira, C., Duarte, A. R. C., et al. (2020b). Collagen from Atlantic cod (*Gadus morhua*) skins extracted using CO 2 acidified water with potential application in healthcare. *J. Polym. Res.* 27:73.

Suga, H., Ono, K., and Miyata, T. (1999). Multiple TGF-β receptor related genes in sponge and ancient gene duplications before the parazoan–eumetazoan split. *FEBS Lett.* 453, 346–350. doi: 10.1016/s0014-5793(99)00749-8

Szabó, M., and Thurner, P. J. (2013). Anisotropy of bovine cortical bone tissue damage properties. *J. Biomech.* 46, 2–6. doi: 10.1016/j.jbiomech.2012.08.002

Tang, D., Tare, R. S., Yang, L.-Y., Williams, D. F., Ou, K.-L., and Oreffo, R. O. (2016). Biofabrication of bone tissue: approaches, challenges and translation for bone regeneration. *Biomaterials* 83, 363–382. doi: 10.1016/j.biomaterials.2016.01.024

Taylor, M. W., Radax, R., Steger, D., and Wagner, M. (2007). Sponge-associated microorganisms: evolution, ecology, and biotechnological potential. *Microbiol. Mol. Biol. Rev.* 71, 295–347. doi: 10.1128/mmbr.00040-06

Uriz, M. J. (2002). "Family geodiidae gray, 1867," in *Systema Porifera*, eds R. W. M. van Soest and N. A. John Hooper (Boston, MA: Springer), 134–140. doi: 10.1007/978-1-4615-0747-5_14

Uriz, M. J. (2006). Mineral skeletogenesis in sponges. *Can. J. Zool.* 84, 322–356. doi: 10.1139/z06-032

Wang, G. (2006). Diversity and biotechnological potential of the sponge-associated microbial consortia. *J. Ind. Microbiol. Biotechnol.* 33, 545–551. doi: 10.1007/s10295-006-0123-2

Webster, N. S., and Taylor, M. W. (2012). Marine sponges and their microbial symbionts: love and other relationships. *Environ. Microbiol.* 14, 335–346. doi: 10.1111/j.1462-2920.2011.02460.x

Weisz, J. B., Lindquist, N., and Martens, C. S. (2008). Do associated microbial abundances impact marine demosponge pumping rates and tissue densities? *Oecologia* 155, 367–376. doi: 10.1007/s00442-007-0910-0

Wörheide, G., Dohrmann, M., Erpenbeck, D., Larroux, C., Maldonado, M., Voigt, O., et al. (2012). "Deep phylogeny and evolution of sponges (phylum porifera)," in *Advances in Marine Biology*, eds M. A. Becerro, M. J. Uriz, M. Maldonado, and X. Turon (Cambridge, MA: Academic Press), 1–78. doi: 10.1016/b978-0-12-387787-1.00007-6

Wulff, J. (2010). Regeneration of sponges in ecological context: is regeneration an integral part of life history and morphological strategies? *Integr. Comp. Biol.* 50, 494–505. doi: 10.1093/icb/icq100

Wysokowski, M., Jesionowski, T., and Ehrlich, H. (2018). Biosilica as a source for inspiration in biological materials science. *Am. Mineral. J. Earth Planetary Mater.* 103, 665–691. doi: 10.2138/am-2018-6429

Yahel, G., Sharp, J. H., Marie, D., Häse, C., and Genin, A. (2003). In situ feeding and element removal in the symbiont-bearing sponge *Theonella swinhoei*: bulk

DOC is the major source for carbon. *Limnol. Oceanogr.* 48, 141–149. doi: 10.4319/lo.2003.48.1.0141

Yannas, I. (1992). Tissue regeneration by use of collagen-glycosaminoglycan copolymers. *Clin. Mater.* 9, 179–187. doi: 10.1016/0267-6605(92)90098-e

Younes, I., Hajji, S., Frachet, V., Rinaudo, M., Jellouli, K., and Nasri, M. (2014). Chitin extraction from shrimp shell using enzymatic treatment. antitumor, antioxidant and antimicrobial activities of chitosan. *Intl. J. Biol. Macromol.* 69, 489–498. doi: 10.1016/j.ijbiomac.2014.06.013

Zadpoor, A. A. (2015). Mechanics of biological tissues and biomaterials. current trends. *Materials* 21, 4505–4511. doi: 10.3390/ma8074505

Żółtowska-Aksamitowska, S., Shaala, L. A., Youssef, D. T., Elhady, S. S., Tsurkan, M. V., Petrenko, I., et al. (2018). First report on chitin in a non-verongiid marine demosponge: the mycale euplectellioides case. *Mar. Drugs* 16:68. doi: 10.3390/md16020068

Conflict of Interest: The authors declare that the research was conducted in the absence of any commercial or financial relationships that could be construed as a potential conflict of interest.

Copyright © 2021 Martins, Rapp, Xavier, Diogo, Reis and Silva. This is an open-access article distributed under the terms of the Creative Commons Attribution License (CC BY). The use, distribution or reproduction in other forums is permitted, provided the original author(s) and the copyright owner(s) are credited and that the original publication in this journal is cited, in accordance with accepted academic practice. No use, distribution or reproduction is permitted which does not comply with these terms.

frontiers in Marine Science

ORIGINAL RESEARCH
published: 18 January 2021
doi: 10.3389/fmars.2020.612779

Macrofauna Inhabiting Massive Demosponges From Shallow and Mesophotic Habitats Along the Israeli Mediterranean Coast

Liron Goren[1,2], Tal Idan[1], Sigal Shefer[1,2]* and Micha Ilan[1]*

[1] School of Zoology, George S. Wise Faculty of Life Sciences, Tel Aviv University, Tel Aviv, Israel, [2] The Steinhardt Museum of Natural History, Israel National Center for Biodiversity Studies, Tel Aviv University, Tel Aviv, Israel

OPEN ACCESS

Edited by:
Joana R. Xavier, University of Porto, Portugal

Reviewed by:
Carlo Cerrano, Marche Polytechnic University, Italy
Vasilis Gerovasileiou, Hellenic Centre for Marine Research (HCMR), Greece

***Correspondence:**
Liron Goren
goren.liron@gmail.com
Sigal Shefer
shef@tauex.tau.ac.il

Specialty section:
This article was submitted to Deep-Sea Environments and Ecology, a section of the journal Frontiers in Marine Science

Received: *30 September 2020*
Accepted: *24 December 2020*
Published: *18 January 2021*

Citation:
Goren L, Idan T, Shefer S and Ilan M (2021) Macrofauna Inhabiting Massive Demosponges From Shallow and Mesophotic Habitats Along the Israeli Mediterranean Coast. Front. Mar. Sci. 7:612779. doi: 10.3389/fmars.2020.612779

Sponges have long been considered as "living hotels" due to the great diversity and abundance of other taxonomic groups often found in association with them. Sponges are the dominant components of benthic communities in the Levant Sea; and especially in the recently discovered mesophotic sponge grounds off the coast of Israel. However, almost no data exist regarding their associated macrofauna. The current study sought to identify the macrofauna associated with massive sponges along the Israeli Mediterranean coast; and to compare the role of sponges, as ecosystem engineers, or "living hotels," in both the shallow-water and mesophotic habitats. Sixty-four massive sponge specimens, from 10 different species, were collected from shallow and mesophotic habitats by SCUBA diving and Remotely Operated Vehicle, respectively. Sponge volume was estimated, specimens were dissected, and the associated macrofauna were identified. Our results reveal that the sponges supported a diverse assemblage of associated macrofauna. A total of 61 associated taxa were found, including species reported for the first time in Israel. A clear, differentiation existed in the structure of the associated assemblage between the two habitats, which is mainly attributed to four species (two polychaetes, a crustacean, and a brittle star). The trophic composition remained stable across the two habitats. No correlation was found between sponge volume and the associated fauna community parameters. The highest richness of associated fauna was found in the mesophotic habitat, where sponge diversity is also higher. In contrast, a greater endobiont abundance and density were recorded in the shallow habitat, where massive sponges may be a limiting factor due to their lower richness and abundance. Our findings emphasize the importance of sponges as ecosystem engineers, and suggest that sponge diversity may be an important factor that contribute to benthic biodiversity in these regions.

Keywords: sponge grounds, Polychaeta, Ophiuroidea, biodiversity, Crustacea, community ecology, feeding guild

INTRODUCTION

Sponges (phylum Porifera) are essential, often dominant components of benthic communities and interact with a wide range of other organisms (Wulff, 2006; Becerro, 2008). They have long been considered as "living hotels" due to the great diversity and abundance of those other taxonomic groups found in association with them, such as polychaetes, crustaceans, echinoderms, and more (Pearse, 1950; Klitgaard, 1995; Ribeiro et al., 2003). The nature of many of these associations remains unclear, but they can represent a variety of ecological interactions (facultative or obligatory) from mutualism to parasitism (Wulff, 2006). The sponges' bodies, which are composed of a complex network of canals and cavities, provide their associated fauna with a substrate, shelter from predators, food supply, reproduction sites, and nurseries for juveniles (Westinga and Hoetjes, 1981; Çinar et al., 2002; Wulff, 2006; Huang et al., 2008). Various parameters have been thought to affect the composition, diversity, and abundance of sponge-associated fauna. For example, sponge volume is often positively correlated with the diversity of endobionts (Çinar et al., 2002; Özcan and Katağan, 2011), as is the host sponge morphology (Koukouras et al., 1992), geographic location (Klitgaard, 1995), depth (Pearse, 1950), and the surrounding area of the sponges (Westinga and Hoetjes, 1981). In serving as a habitat for a myriad of associated taxa, sponges constitute important reservoirs of marine biodiversity (Cerrano et al., 2006).

Previous studies of sponge-associated fauna have been carried out from the tropics to the poles (Pearse, 1950; Frith, 1976; Peattie and Hoare, 1981; Klitgaard, 1995; Magnino et al., 1999; Abdo, 2007; Schejter et al., 2012; Beepat et al., 2014; Kersken et al., 2014). Although, the sponge-associated fauna of the Mediterranean Sea is considered well-studied (e.g., Rützler, 1976; Koukouras et al., 1985, 1992, 1996; Voultsiadou-Koukoura et al., 1987; Çinar et al., 2002; Gerovasileiou et al., 2016), in the Levantine Sea (Eastern Mediterranean), however, there are only a handful of studies focusing on sponges and their endobiotic community compositions (e.g., Pavloudi et al., 2016; Çinar et al., 2019; Papatheodoulou et al., 2019). Moreover, only one of those studies investigated sponge-associated fauna in the Israeli Mediterranean at a depth of 830 m (Ilan et al., 1994), and examined only three different sponge species (two massive sponges – *Sarcotragus foetidus*, *Ircinia retidermata* and a thickly branched sponge – *Bubaris sarayi*), one specimen of each. The two massive sponges were found to host three species of polychaetes, and one crustacean. No endobionts were recorded inside the branched sponge.

In the last decade, several mesophotic sponge grounds (MSG) were discovered along the Israeli coast of the Mediterranean Sea (Idan et al., 2018). While the Eastern Mediterranean sponge fauna is considered to be impoverished in comparison to the Western Mediterranean (Voultsiadou, 2009), the former are local hotspots for sponge diversity (Idan et al., 2018), and may constitute an oasis of local richness and diversity (Bo et al., 2012). Between the years 2016 and 2020, several expeditions were conducted in order to study the sponge fauna of the Israeli MSGs (Idan et al., 2018; Idan, 2020). These expeditions yielded, among others, dozens of specimens of sponges of several species, which provided us with the opportunity to investigate the macrofauna associated with massive sponges off the Israeli Mediterranean coast. We further compared the role of sponges, as ecosystem engineers, or "living hotels" in both shallow and mesophotic habitats by characterizing the diversity, community composition, and trophic structure of the sponges' endofauna in both habitats.

MATERIALS AND METHODS

Sampling

Sponge species (class Demospongiae) with massive growth forms bearing conspicuous cavities and canals that were collected as part of the ongoing sponge-fauna study (Idan et al., 2018; Idan, 2020), were selected for the study of their associated fauna in the surveyed areas.

The study sites and their depth range are listed in **Table 1**. The species included in this study were *Ircinia oros*, *Ircinia variabilis*, *Sarcotragus foetidus*, *Sacrotragus spinosulus*, *Spongia lamella*, *Spongia nitens*, *Fasciospongia cavernosa, Thymosiopsis conglomerans*, *Stryphnus mucronatus*, and *Agelas oroides*. Details of number of specimens are listed in **Table 2**. The sponges were collected along the Israeli coast of the Mediterranean Sea at five sites (two shallow water, and three from the mesophotic sponge grounds; **Table 2**). Sampling from shallow water sites (<30 m) was done by SCUBA diving. Sponge specimens were covered with plastic bags to avoid loss of motile macrofauna and then detached using a knife. At the mesophotic sites (90–120 m), samples were collected from the R/V Mediterranean Explorer (EcoOcean) using a Remotely Operated Vehicle (ROV; ECA-Robotics H800), equipped with a five-function-manipulator, a full high-definition camera, and two parallel laser beams for scale. Sponge specimens were brought on board in a collection basket and transferred as quickly as possible to a container with seawater.

Specimens from both the shallow and the mesophotic zone were either processed on board or in the laboratory (following preservation in 85% ethanol). To reduce the possibility that the difference in methods of collection between the two habitats might affect our results, six of the shallow habitat sponges (three *I. variabilis* and three *S. spinosulus*) were collected without being covered with a bag and borne along in the water throughout the entire dive before being taken to the surface and preserved.

TABLE 1 | List of the shallow and mesophotic study sites.

Site	Depth (m)	Coordinates
Rosh HaNikra	1–2	33°3′23.7″N 35°6′9.7″E
Sdot Yam	28	32°29′27.4″N 34°53′11.2″E
Haifa –Rosh Carmel	100–130	32°52′31.5″N 34°51′43.1″E
Shefayim	95–123	32°12′51.20″N 34°38′35.62″E
Herzliya	92–127	32°10′34.53″N 34°37′59.60″E

TABLE 2 | Number and mean volume of sponges collected from mesophotic and shallow habitats along the Israeli Mediterranean coast.

Sponge	Mesophotic		Shallow	
	Mean volume (L)	# of specimens	Mean volume (L)	# of specimens
Agelas oroides (Schmidt, 1864)	2.39 ± 3.5	2		
Fasciospongia cavernosa (Schmidt, 1862)	0.35	1	0.18 ± 0.15	4
Ircinia oros (Schmidt, 1864)	1.61 ± 1.63	17		
Ircinia variabilis (Schmidt, 1862)	1. 65 ± 1.6	5	0.33 ± 0.13	8
Sarcotragus foetidus Schmidt, 1862			n/a	2
Sarcotragus spinosulus Schmidt, 1862			0.43 ± 0.11	6
Spongia (Spongia) lamella (Schulze, 1879)	3.63 ± 2.2	2		
Spongia (Spongia) nitens (Schmidt, 1862)	2.5	3		
Stryphnus mucronatus (Schmidt, 1868)	3.8 ± 3.8	12		
Thymosiopsis conglomerans Vacelet, Borchiellini, Perez, Bultel-Poncé, Brouard and Guyot, 2000	2.62	2		

No significant differences were found in richness and abundance of the non-covered specimens of each species, when compared to their covered counterparts (Kruskal Wallis test: $\chi^2 = 0.29$, $p = 0.58$, df = 1). Sponge volume was measured by water displacement. Sponges were then cut into small pieces along their canals and cavities (to minimize endofauna damage), and the associated fauna was removed. The water and the associated macrofauna, which remained in the bags and containers, were washed through a 0.5-mm mesh sieve. Sponge-associated fauna was sorted, counted, and identified to the lowest taxonomic level. Polychaetes were identified mainly according to Fauchald (1977); Fitzhugh (1989), Knight-Jones et al. (1991); Giangrande (1994), Barnich and Fiege (2003); San Martin (2003), Carrera-Parra (2006); Tovar-Hernández and Harris (2010), and Nogueira et al. (2015). The remaining endobionts were identified with the help of experts in the Steinhardt Museum of Natural History or at the Hellenic Centre for Marine Research in Crete, Greece.

Statistical and Faunal Analysis

To compare the endobionts' communities between the mesophotic and shallow sponges, richness per sponge specimen, species density (richness per L sponge), individuals' density (abundance per L sponge), and Shannon-Wiener diversity (H') were calculated. Because statistical analysis was constrained by the un-even availability of sponge specimens of each species, the above-noted parameters were tested only for the six sponge species for which we had more than three replicates: three from the mesophotic habitat (*Ircinia oros, Ircinia variabilis,* and *Stryphnus mucronatus*) and three from the shallow habitat (*Fasciospongia cavernosa*, *Ircinia variabilis,* and *S. spinosulus*). The comparison was made using Kruskal Wallis test, first between the sponge species of each habitat, and then when no differences were found, the data were pooled and compared between the two habitats. Spearman's rank correlation coefficient was used to examine the relationship between sponge volume, number of taxa, and diversity (H') of the endobionts.

Resemblance analysis of the endobionts communities in the six selected sponge species was performed with nMDS based on Bray-Curtis dissimilarity index. ANOSIM was used in order to compare the difference between the composition of endobionts communities in the selected sponges. SIMPER analysis was used to estimate the contribution of each endobiont species to the dissimilarity. For the trophic characterization of the endobionts fauna, all species were assigned to feeding groups based on Fauchald and Jumars (1979); Dauer (1984), Gambi et al. (1995); Chintiroglou (1996), Damianidis and Chintiroglou (1998), Martin et al. (2000); Antoniadou and Chintiroglou (2005), Leclerc et al. (2013a,b), Antoniadou (2014); Faulwetter et al. (2014), Guerra-García et al. (2014); Manousis and Galinou-Mitsoudi (2014), and Gerovasileiou et al. (2016).

Statistical analyses were performed with R version 3.6.1 (R Core Team, 2019), RStudio (RStudio Team, 2020), and the Vegan package (Oksanen et al., 2013).

RESULTS

Host Sponges

A total of 64 massive sponge specimens belonging to 10 sponge species were analyzed (**Table 2** and **Figure 1**). As the shallow coast of Israel contains a lower richness of massive sponges (Idan et al., 2018), only four of these sponge species, *Ircinia variabilis, S. spinosulus, S. foetidus*, and *Fasciospongia cavernosa*, were present and collected from these sites (Achziv, Sdot Yam); while eight species were collected from the mesophotic sites: *Ircinia oros, Ircinia variabilis, Spongia lamella, S. nitens, Fasciospongia cavernosa, Thymosiopsis conglomerans, Stryphnus mucronatus,* and *Agelas oroides*. The size of the specimens varied among species, but, specimens from the shallow habitat were smaller (0.08–0.65 L; **Table 2**) than those from the mesophotic habitat (0.32–11 L; **Table 2**).

Associated Macrofauna

A total of 1099 individuals were identified living within the canals of the 10 sponge species, representing 60 taxa and six major taxonomic groups: Polychaeta, Sipuncula, Crustacea, Insecta, Ophiuroidea, and Mollusca (**Table 3**). The richest group was Polychaeta, accounting for 57% and 79% of the species in the

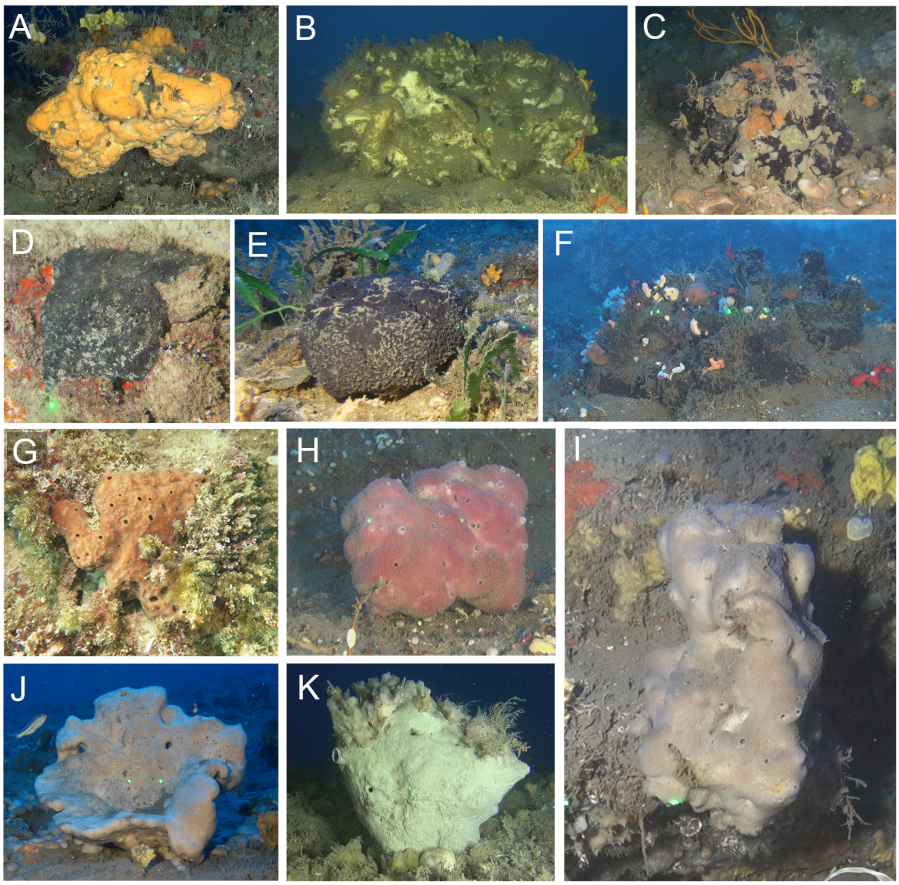

FIGURE 1 | Massive sponge species, collected from the mesophotic sponge grounds and shallow-water habitat along the Mediterranean coast of Israel. **(A)** *Agelas oroides*; **(B)** *Thymosiopsis conglomerans*; **(C)** *Stryphnus mucronatus*; **(D)** *Sarcotragus spinosulus*; **(E)** *Sarcotragus foetidus*; **(F)** *Fasciospongia cavernosa*; **(G)** *Ircinia variabilis* from the shallow zone; **(H)** *Ircinia variabilis* from the MSG; **(I)** *Spongia nitens*; **(J)** *Spongia lamella*; **(K)** *Ircinia oros*.

MSG and shallow zone, respectively, followed by Crustacea (19%) in the MSG and Ophiuroidea (7%) in the shallow zone (**Figures 2A,B**). Seven taxa of Isopods and Amphipods were not included in this analysis, as it was uncertain as to whether they were endobionts or epibionts. Of particular interest was the presence of chironomid larvae (Insecta) in the canals of *S. spinosulus* from the shallow zone. To the best of our knowledge, this is the first time an insect has been recorded inhabiting a marine sponge.

The sponge *S. mucronatus* demonstrated the richest cumulative endobiont fauna (29 species), followed by *I. variabilis* (21 species), while *S. foetidus* and *A. oroides* hosted the poorest fauna (four species; **Figure 3**). The total richness of endobiont species was higher in the MSG (48 species) than in the shallow water (28 species).

Ophiuroidea was the most abundant group in both zones (54% in the MSG and 57% in the shallow zone), with more than half of all 609 specimens belonging to three species. Of these three species, *Ophiactis savignyi* was by far the most abundant in both habitats, with more than 96% and 99% of the ophiurid individuals in the mesophotic habitat and the shallow habitat, respectively. Polychaetes were the second most dominant group, in terms of richness and abundance, in the mesophotic habitat (35% of endobionts), while crustaceans were the second-most dominant group in the shallow habitat (23% of endobionts; **Figures 2C,D**).

The number of individuals in the sponges ranged from 1 to 210, and from 1 to 135 in the mesophotic and shallow habitats, respectively.

In order to compare the endobiont community parameters between the MSG and the shallow habitat, a statistical analysis was conducted on the six selected sponge species for which we had a sufficient number of replicates (more than three replicates each).

No significant differences were found among the endobionts of each habitat in mean richness, species density individuals' density, and Shannon-Wiener diversity (**Table 4**). When data for the three sponge species in each habitat were pooled together, no significant differences were found between the shallow and MSG in mean endobionts richness and Shannon-Wiener diversity index (**Table 4** and **Figure 4A**). This was further supported in the sample-based rarefaction curves (Sanders, 1968; Hurlbert, 1971; **Figure 5**) which did not differ between the two habitats. However, species density, and individual density were significantly higher in the shallow habitat than in the MSG (richness per L sponge:

TABLE 3 | Macrofaunal endobionts found in the canals of massive sponges in the shallow and mesophotic habitats of the Israeli Mediterranean coast.

Taxa	Mesophotic zone	Shallow zone	Feeding guild	No. species
Annelida				38
Polychaeta				38
Amaeana trilobata (Sars, 1863)	X	X	d	
Branchiomma sp.		X	f	
Branchiosyllis exilis (Gravier, 1900)		X	c	
Ceratonereis (Composetia) costae (Grube, 1840)	X	X	o	
Chrysopetalum cf. debile (Grube, 1855)		X	c	
Cirratulidae sp. 1	X		d	
Dodecaceria concharum Örsted, 1843	X		d	
Dorvillea sp.	X		o	
Eunicidae sp.	X	X	c	
Eunoe tuerkayi Barnich and Fiege, 2003 †*	X	X	c	
Exogone sp.		X	o	
Glycera sp.	X		c	
Haplosyllis spongicola (Grube, 1855)	X		c	
Leonnates indicus Kinberg, 1865 §	X	X	o	
Lumbrineris latreilli Audouin and Milne Edwards, 1833	X		c	
Lumbrineris sp.	X		c	
Myxicola infundibulum (Montagu, 1808)	X		f	
Nereis rava Ehlers, 1868		X	o	
Palola siciliensis (Grube, 1840)	X		c	
Parasabella tenuicollaris (Grube, 1861) †	X		f	
Parasabella tommasi (Giangrande, 1994) †*	X		f	
Phyllodocidae sp. 1		X	c	
Polynoidae sp. 1		X	c	
Polyophthalmus pictus (Dujardin, 1839)		X	d	
Pontogenia chrysocoma (Baird, 1865)	X		c	
Prionospio sp. 1		X	d	
Prionospio sp. 2	X		d	
Sabellidae sp. 1	X	X	f	
Sphaerosyllis sp.		X	c	
Subadyte pellucida (Ehlers, 1864) †	X	X	c	
Syllidia armata Quatrefages, 1866	X	X	c	
Syllis gracilis Grube, 1840	X		o	
Syllis sp. 1		X	c	
Syllis sp. 2	X	X	c	
Terebellidae sp. 1	X	X	d	
Terebellidae sp. 2	X		d	
Terebellidae sp. 3	X		d	
Trypanosyllis zebra (Grube, 1860)	X	X	c	
Sipuncula				1
Sipuncula sp.	X	X	d	
Arthropoda				11
Crustacea				10
Alpheus sp.	X		d	
Caridea sp.	X		o	
Caridea sp. 2	X		o	
Eualus cranchii (Leach, 1817 [in Leach, 1815-1875])	X		o	
Eurynome aspera (Pennant, 1777) *	X		o	
Gnathiidae sp.	X		n	
Pilumnus spinifer H. Milne Edwards, 1834	X		o	
Synalpheus gambarelloides (Nardo, 1847)	X	X	o	

(Continued)

TABLE 3 | Continued

Taxa	Mesophotic zone	Shallow zone	Feeding guild	No. species
Thoridae sp.	X		o	
Insecta				1
Chironomidae sp. *		X	d	
Echinodermata				3
Ophiuroidea				3
Amphipholis squamata (Delle Chiaje, 1828)	X	X	d	
Ophiactis savignyi (Müller and Troschel, 1842) §	X	X	d	
Ophiothrix quinquemaculata (Delle Chiaje, 1828)	X		d	
Mollusca				8
Bivalvia				4
Gregariella petagnae (Scacchi, 1832) *	X		f	
Saccella commutata (Philippi, 1844) *	X		f	
Sphenia binghami Turton, 1822	X		f	
Striarca lactea (Linnaeus, 1758)		X	f	
Gastropoda				4
Emarginula adriatica Costa, 1830	X		c	
Mitrella coccinea (Philippi, 1836)	X		c	
Monophorus perversus (Linnaeus, 1758)	X		c	
Muricopsis cristata (Brocchi, 1814)	X		c	
Total	48	28		61

*Feeding guilds: c, carnivore; d, deposit-feeder; f, filter-feeder; n, non-feeder; o, omnivore. * first record in sponges. † first record in Israel. §Non-indigenous species.*

Kruskal Wallis, $\chi^2 = 22.4$, $p < 0.001$, df = 1; density: Kruskal Wallis, $\chi^2 = 26.4$, $p < 0.001$, df = 1; **Table 4** and **Figures 4B,C**).

Relationships Between Sponge Volume and Endobionts' Community Parameters

Five sponge species from which more than three specimens were collected (*Ircinia variabilis, Ircinia oros, Fasciospongia cavernosa, Stryphnus mucronatus*, and *Sarcotragus spinosulus*) were tested for the relationship between their volume and the endobionts' community parameters mentioned above (richness, abundance, diversity H', **Supplementary Table 1**).

In general, no significant correlation was found between the volume of sponges and community parameters in both habitats. A positive correlation between the sponge volume and the abundance of endobionts was found only in one species (*I. variabilis*, $\rho = 1$, $p < 0.003$).

Similarities Among Sponge-Associated Communities

Only 25% of the total endobiont taxa were found in both habitats. A two-dimensional nMDS ordination revealed a clear differentiation between the community composition of the two habitats (stress 0.18; **Figure 6**), which was found to be significant in an ANOSIM test ($R = 0.43$, $P = 0.001$, permutations = 1000). SIMPER analysis indicated that the associated endobiotic species that contributed most to the dissimilarity between the two habitats were the crustacean *Synalpheus gambarelloides* and the nereidid polychaete *Leonnates indicus* which were more common in the shallow habitat; and the brittle star *Ophiactis savignyi* and the nereidid polychaete *Ceratonereis (Composetia) costae* which were more common in the mesophotic habitat. These four species contributed about 67% of the dissimilarity between the two habitats. All four could be found across the entire depth range of the study, but were more common in their respective preferred habitats.

The trophic composition, of the sponge-associated fauna, in terms of richness, did not change significantly across the two habitats ($\chi^2 = 0.95$, df = 3, $p > 0.05$). Carnivores dominated both habitats, followed by deposit feeders, omnivores, and filter feeders (**Figure 7A**). No significant difference was found between the two habitats in term of number of individuals as well ($\chi^2 = 7.42$, df = 3, $p > 0.05$). However, in this case deposit feeders dominated the community, followed by omnivores, and both carnivores and filter feeders comprised only a small portion of the community (about 10%; **Figure 7B**)

DISCUSSION

Endobiont Diversity

The results of this study reveal that massive sponges along the coast of Israel support diverse assemblages of invertebrates (61 species), including six species that are reported for the first time as sponge endobionts, and four species of polychaetes that are new records for Israel. However, a comparison between the endobiont communities of the shallow waters and the mesophotic depth revealed only partial overlap, with merely 15 species being found in both habitats. Moreover, the species richness in the shallow-water habitat was much lower than that in the mesophotic habitat (28 vs. 48 spp., respectively). Other studies in the Eastern Mediterranean have documented

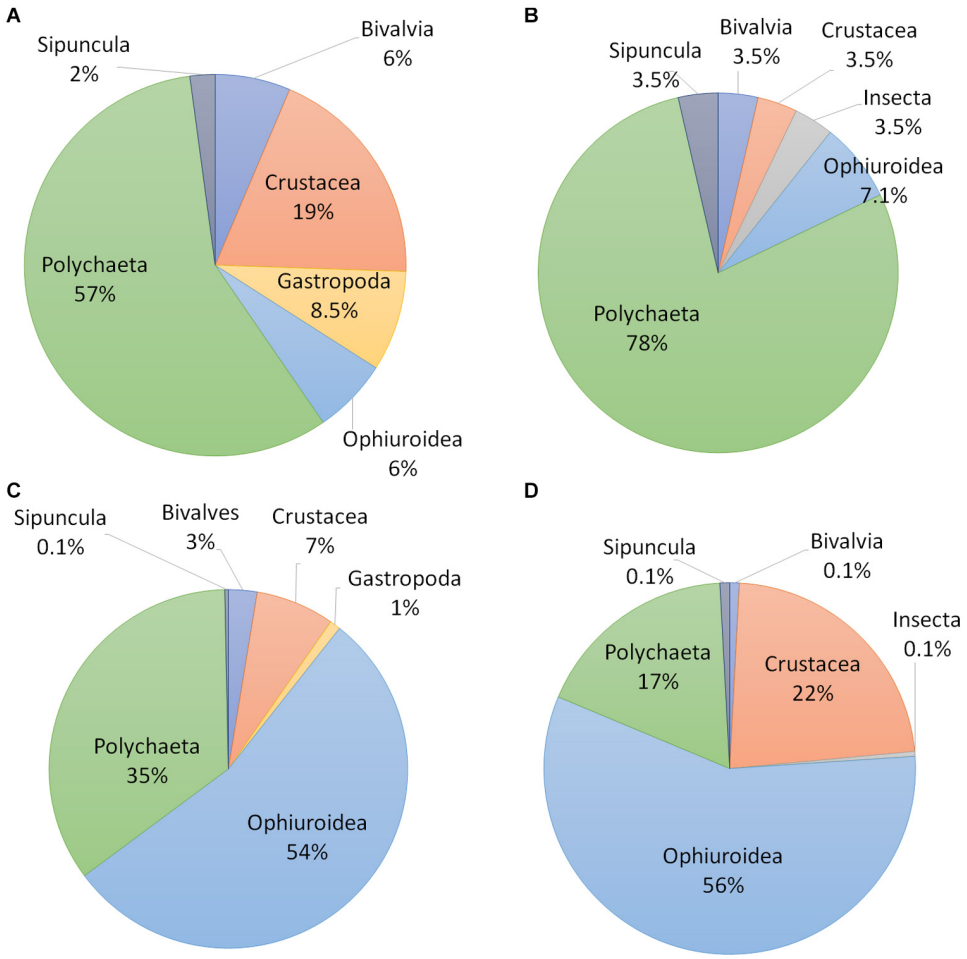

FIGURE 2 | Taxonomic groups inhabiting sponges along the Mediterranean coast of Israel: **(A)** by the number of taxa in the mesophotic habitat; **(B)** by the number of taxa in the shallow habitat; **(C)** by the number of individuals in the mesophotic habitat; **(D)** by the number of individuals in the shallow habitat.

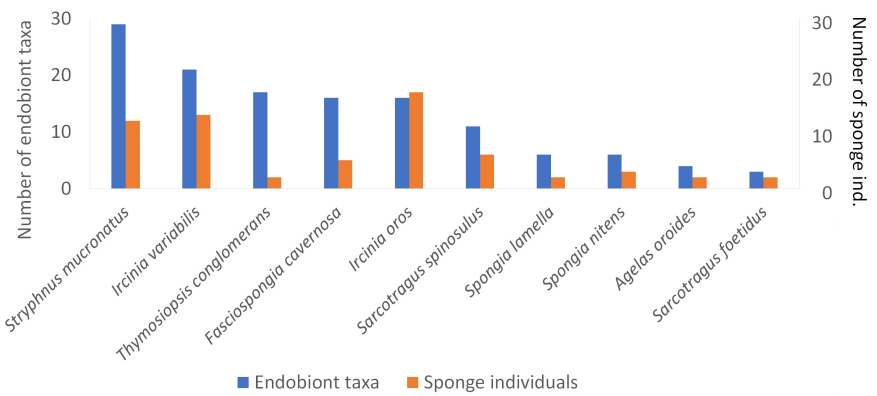

FIGURE 3 | Total richness of sponge endobiont taxa (in orange) found in 10 sponge species (in blue) in the shallow and mesophotic habitats along the Mediterranean coast of Israel.

much higher richness of associated invertebrates within shallow-water sponges, ranging from 86 species around the island of Lesvos to more than 200 along the continental coasts of the northern Aegean Sea (Koukouras et al., 1985, 1996; Voultsiadou-Koukoura et al., 1987; Çinar et al., 2002, 2019; Gerovasileiou et al., 2016). Further east, in Cyprus, the number

TABLE 4 | Results of Kruskal–Wallis tests between community parameters of sponges' endobionts in the shallow water and mesophotic habitats.

Community parameter	Analysis	*p*-value	Chi	df
Mean richness per sponge	among sponge species within sites (shallow, mesophotic)	0.89, 0.09	0.2, 4.7	2, 2
	between sites	0.79	0.07	1
Endobiont species density (per L sponge)	among sponge species within sites (shallow, mesophotic)	0.075, 0.6	5.18, 0.95	2, 2
	between sites	**0.001**	22.403	1
Shannon-Wiener diversity index (per sponge specimen)	among sponge species within sites (shallow, mesophotic)	0.11, 0.21	4.3, 3.04	2, 2
	between sites	>0.05	0	1
Individual density (per L sponge)	among sponge species within sites (shallow, mesophotic)	0.33, 0.6	2.2, 0.99	2, 2
	between sites	**0.001**	26.477	1

Significant results are in bold.

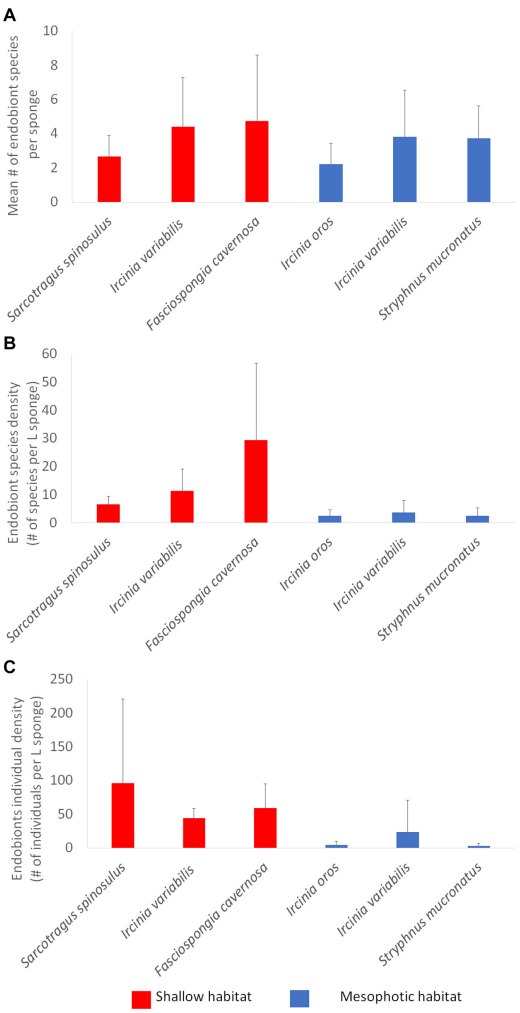

FIGURE 4 | Community parameters of endobionts found in the six sponge species with a sufficient number of specimens ($n \geq 3$). **(A)** Mean number of endobiont taxa per sponge specimen; **(B)** Species density (mean number of endobiont species per L sponge); **(C)** Endobiont density (number of individuals per L sponge). Error bars represent standard deviation.

of species shallow water is lower (44 spp., Pavloudi et al., 2016) but still higher than our findings in the shallow water. The low richness may be in accordance with other studies that documented an NNW-SSE gradual decrease in biodiversity (Voultsiadou, 2009). This decrease is considered to be related to temperature and nutrient concentration differences, which affect both pelagic and benthic communities, with higher temperatures and lower nutrient concentrations associated with lower diversity (Arvanitidis et al., 2002; Coll et al., 2010). The shallow water along the Israeli coast reaches the most extreme summer-temperatures in the Mediterranean (>30°C; Idan et al., 2018; Idan, 2020), thus possibly explaining the lower endobiont richness. In accordance, in the mesophotic habitat, where the temperature is lower and more stable (Idan et al., 2018, 2020), one would expect a higher richness and indeed, the numbers of species found there is higher (**Table 3**), and similar to that found at the same depth in Cyprus (Papatheodoulou et al., 2019).

While the cumulative endobiont richness was higher in the MSG, our quantitative analysis of endobiont community parameters, conducted for the six sponge species with a sufficient number of replicates ($n > 3$), showed contrasting results. In this case mean endobiont richness and Shannon-Wiener diversity per sponge specimen did not differ between the two habitats. Furthermore, the mean endobionts' individual and species densities (# per L sponge) were significantly higher in the shallow habitat than in the MSG. To understand these discrepancies, we should also consider other differences between the two habitats that relate to sponge community parameters:

1. Massive sponge richness in the shallow habitat is lower than in the MSG (4 vs. 16 species, respectively; Idan et al., 2018).
2. Massive sponges in the shallow habitat are scarcer and much smaller than in the MSG (mean 0.7 vs. 2.7 L, respectively). This is probably due to the harsher abiotic conditions in the shallow waters (Burton, 1936; Lévi, 1957; Voultsiadou, 2009; Coll et al., 2010; Idan, 2020; Idan et al., 2020).

We suggest that massive sponge richness, being higher in the MSG, has a positive effect on endobiont richness. Species-specific characteristics of sponges, such as diameter or volume of canals, or chemical composition of the sponge, which were beyond the scope of this study, are known to affect endobiont diversity and richness (Fiore and Jutte, 2010; Ávila and Ortega-Bastida, 2015). Thus, increasing sponge richness may in turn increase endobionts' richness. This is supported by the difference

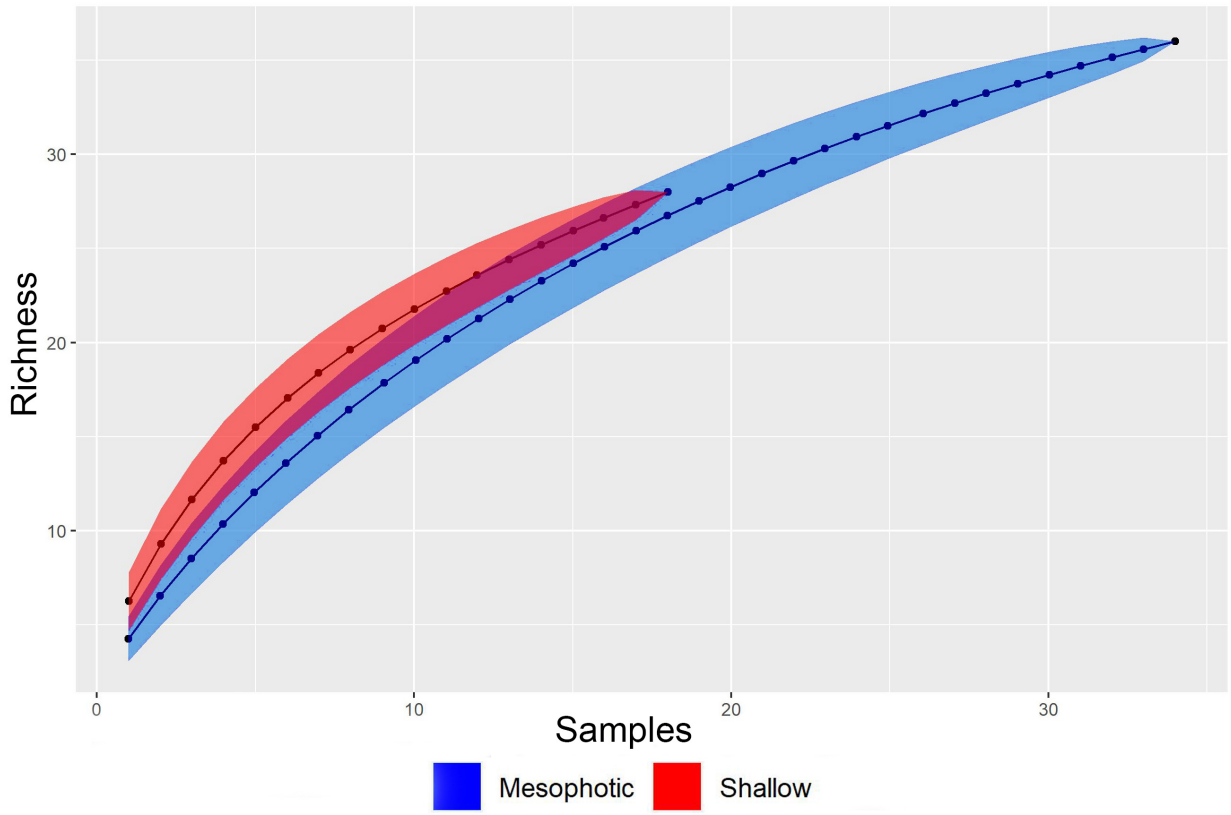

FIGURE 5 | Rarefaction curves from pooled data of sponge-associated taxa found in the six sponge species with more than three replicates in both shallow and mesophotic habitats along the Mediterranean coast of Israel.

in the rarefaction curves constructed for the six sponge species with more than three replicates (**Figure 3**), and for all 10 species collected in the study (**Supplementary Figure 1**). In the former, no significant difference was found between the habitats, while in the latter the MSG curve rises higher and more quickly. Furthermore, massive sponges, being less common in the shallow habitat, in terms of volume and density (Idan et al., 2018; Idan, 2020), may act as a limiting factor, reducing the total endobiont richness, but also forcing the macroinvertebrates to aggregate within them. This may explain their much higher density along the shallow waters of the Israeli coast, and why the well-documented link between sponge volume and their endobiont richness and abundance (Koukouras et al., 1992, 1996; Cinar and Ergen, 1998; Gherardi et al., 2001) is not expressed there (**Supplementary Table 1**).

Nonetheless, the true richness in both habitats is probably higher, as evidenced by the rarefaction curves, which did not approach an asymptotic value, and by the fact that sampling constrains resulted in an un-even number of sponge species collected.

Furthermore, the richness in the mesophotic sponge grounds may be still higher, as some of the endobionts may have been lost during the ascent of the ROV to sea level. However, we believe that this loss was minimal, as no significant difference was found in endobiont richness between the sponges covered at the time of collection and those that were borne along uncovered during the SCUBA dive (see "Materials and Methods").

Endobiont Community Composition

The dominance of Polychaeta in terms of number of taxa is in accordance with other studies (Klitgaard, 1995; Gerovasileiou et al., 2016; Çinar et al., 2019). The numeric dominance of Ophiuroidea in the sponges, however, is uncharacteristic, since in the majority of previous studies, the most important group in terms of abundance, was Crustacea (Koukouras et al., 1996; Gerovasileiou et al., 2016). The result of the community composition analysis in this study showed a clear dissimilarity between the two habitats, which was mainly attributed to four species: *Ophiactis savignyi* (54%), *Ceratonereis (Composetia) costae* (14%), *Synalpheus gambarelloides* (12%), and *Leonnates indicus* (3%), which together comprised 83% of total number of individuals found in the sponges.

Ophiactis savignyi was found to be the most abundant endobiont in both the shallow and mesophotic habitats. It comprised more than 50% of individuals found in the sponges, and it is also the only endobiont that was found in high and equal abundance in both habitats. It is considered to be a Lessepsian migrant, which in the Mediterranean Sea dwells almost exclusively inside sponges (Çinar et al., 2019), unlike in its

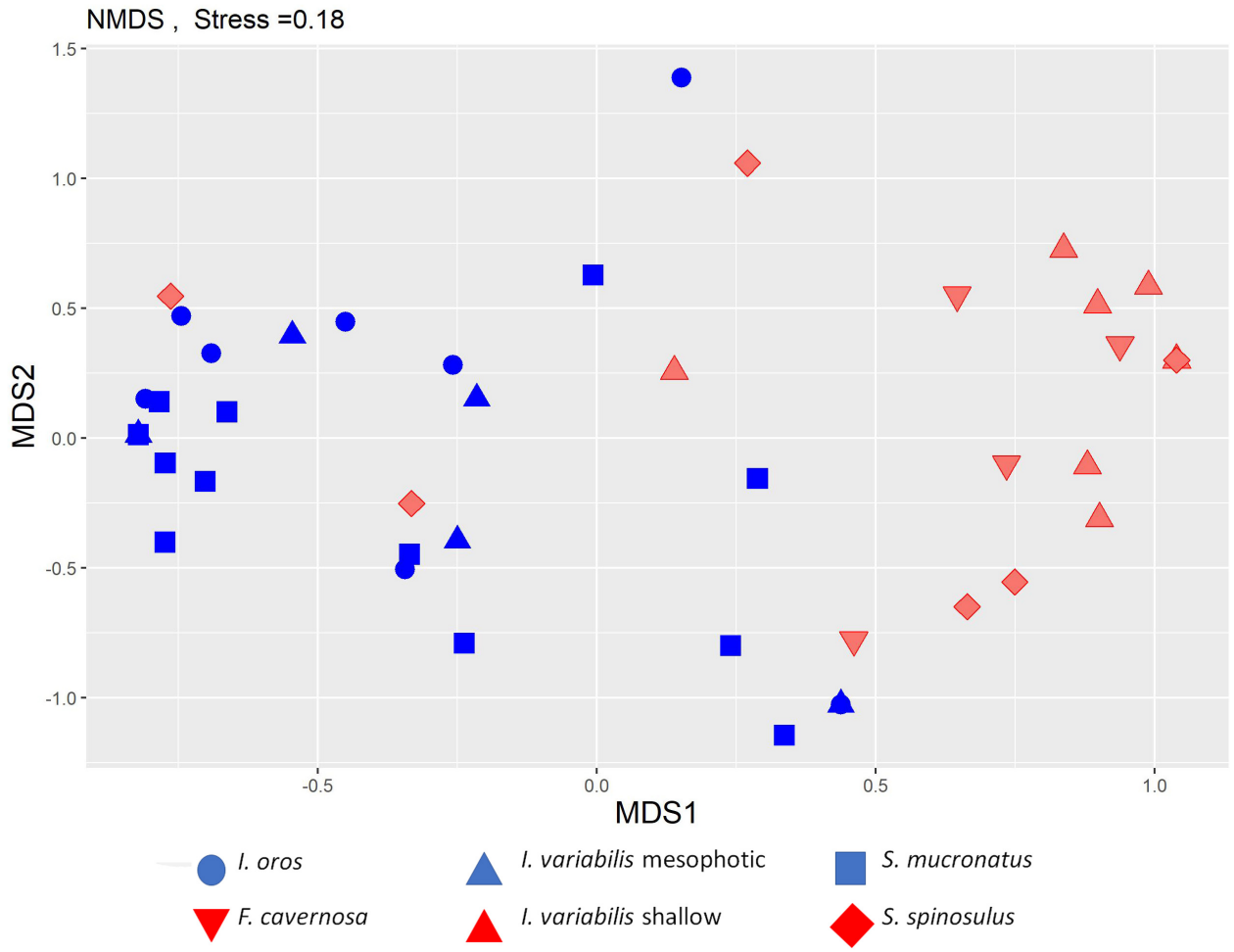

FIGURE 6 | NMDS ordination of the endobiont communities found in the sponges along the Mediterranean coast of Israel. Each symbol represents a community within a sponge. 2D stress: 0.18. Analysis is shown for the six sponge species with sufficient replicates ($n > 3$).

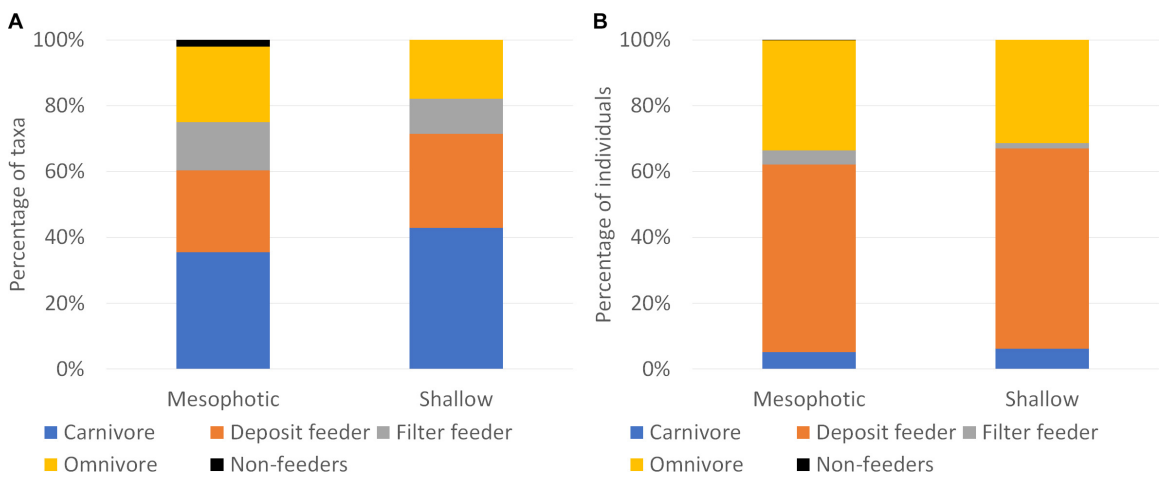

FIGURE 7 | Trophic structure of endobionts found in massive sponges along the Mediterranean coast of Israel, in terms of **(A)** number of taxa (S) and **(B)** abundance (N) of sponge-associated fauna across the surveyed habitats.

native geographic area where it also dwells in other environments such as algae and coral rubble (Mladenov and Emson, 1988).

Ceratonereis costae, the second most abundant organism, and the dominant polychaete in the mesophotic zone, was often reported as an abundant and even dominant species in Mediterranean sponges (Alos et al., 1981; Koukouras et al., 1992; Ilan et al., 1994; Gherardi et al., 2001; Çinar et al., 2002, 2019). In the shallow water *C. costae* is replaced by *L. indicus* as the dominant species. *Leonnates indicus* is another non-indigenous species and a Lessepsian, migrant previously reported from Levantine Sea sponges (Ilan et al., 1994; Çinar et al., 2019). Its dominance in the shallow water suggests that it may competitively exclude *C. costae*. The lower numbers of *L. indicus* in the MSG might reflect this tropical and sub-tropical species preference to shallow (usually warmer) habitats (Ben-Eliahu, 1991; Qiu and Qian, 2000; Çinar, 2009; Çinar et al., 2019).

Synalpheus gambarelloides, is a well-known gregarious crustacean whose adults and juveniles inhabit sponges, and feed off their host (Erdman and Blake, 1987; Ilan et al., 1994). In this study, juveniles and females with eggs were often found.

Other notable organisms that resided in the sponges in both the mesophotic and shallow habitats, were four polychaete species, previously unreported from Israel: *Parasabella tenuicollaris*, *Parasabella tommasi*, *Subadyte pellucida,* and *Eunoe tuerkayi*. All of these are known from other parts of the Mediterranean sea (Giangrande, 1994; Barnich and Fiege, 2003; Tovar-Hernández and Harris, 2010; Gerovasileiou et al., 2016). *P. tenuicollaris* and *S. pellucida* are also recognized as sponge inhabitants (Cinar and Ergen, 1998; Gerovasileiou et al., 2016). Three individuals of Chironomidae were found in two sponge specimens from the shallow water. This is the first record of insects inhabiting sponges in the Mediterranean Sea. While, chironomids are known to inhabit demosponges in freshwater habitats (Gugel, 2001; Roque et al., 2004) and are also known from algae and submerged wood panels in marine environments (Olander and Palmén, 1968; Santhakumaran et al., 1984), to the best of our knowledge this is the first record of an insect inhabiting sponges in a marine environment. Of the Mollusca, *Sphenia binghami* was the most common. It is known to inhabit crevices as well as habitats previously inhabited by the bivalve *Hiatella arctica*. Both *S. binghami*, and *H. arctica* are outwardly similar, and can be easily misidentified. The latter is often reported from sponges in the Levant (Pavloudi et al., 2016; Çinar et al., 2019). Other molluscs found in the sponges included bivalves such as *Saccella commutata* and *Gregariella petagnae,* which have never previously been recorded from sponges, and gastropods (*Muricopsis cristata*, *Mitrella coccinea, Emarginula adriatica*, and *Monophorus perversus*). The last three are known, or thought to, feed off sponges (Taylor, 1987; Kantor and Medinsakaya, 1991; Manousis and Galinou-Mitsoudi, 2014).

Trophic Structure of the Shallow and Mesophotic Habitats

The trophic structure of the endobiont assemblages was similar between the two habitats. with carnivores being the most prevalent group in both, followed by deposit feeders. Gerovasileiou et al. (2016) also found carnivores and deposit-feeders to be the most speciose groups in cave-dwelling *A. oroides* and *Aplysina aerophoba*. In regards to abundance, the dominance of deposit feeders in both habitats, is attributed to the extremely high numbers of *O. savignyi*. The second most prevalent group was the omnivores, mainly represented by *S. gambarelloides,* which was the most dominant species in the shallow water and *C. costae* in the MSGs. Other studies have usually found carnivorous endobionts to be the most prevalent group, mainly due to the abundance of amphipods (Gerovasileiou et al., 2016; Navarro-Barranco et al., 2016). In the present study, however, amphipods were not prevalent and nor were they considered in the analysis, as they were usually found on only the external parts of the sponge.

Summary

The present study has shown that sponges along the Israeli coast provide a habitat for a diverse community of endobionts. The highest richness of endobionts was found in the MSGs, where sponge diversity is higher; while, in contrast, the highest endobiont density and mean abundance was found in the shallow zone, where massive sponges may be a limiting factor. This emphasizes the importance of sponges as ecosystem engineers and indicating that their role as habitat builders is an important factor affecting benthic biodiversity in this region. This role of sponges may also promote the establishment of non-indigenous species that use them as (primary) habitat, with the sponges essentially acting as stepping stones for their dispersion. While many studies have explained endobiont diversity according to factors such as volume, morphology and surroundings habitat and biota of the sponges, the results of the present study suggest that sponge diversity and density too, constitute variables that should be considered in relation to endobiont diversity.

DATA AVAILABILITY STATEMENT

The original contributions presented in the study are included in the article/**Supplementary Material**, further inquiries can be directed to the corresponding authors.

AUTHOR CONTRIBUTIONS

LG, SS, and MI contributed to conception and design of the study. LG, SS, and TI performed the field and laboratory work. LG organized the database and wrote the first draft of the manuscript. LG and TI performed the statistical analysis. TI wrote sections of the manuscript. All authors contributed to manuscript revision, read, and approved the submitted version.

FUNDING

This research was partially funded by grants from the Israel Ministry of Energy and Infrastructures (#217-17-020 to MI) and the Nature and Parks Authority (#01023182 to MI). LG was supported by a VATAT fellowship.

ACKNOWLEDGMENTS

We would like to acknowledge and thank the members of Ilan's group, who participated and assisted in sponge and endobionts collections during the many dives and expeditions on board the research vessel. We thank the environmental NGO EcoOcean personnel and the many volunteers on board the R/V Mediterranean Explorer and Oded Ezra, Itay Katzman and Asi Gil'adi for the operation of the Remotely Operated Vehicle. The many species that were collected were identified with the help of experts from The Steinhardt Museum of Natural History at Tel Aviv University: Dr. Henk Mienis (Mollusca), Dr. Omri Bronstein (Echinodermata), Dr. Bella Galil, and Ya'arit Levitt-Barmats (Crustacea). Some of the polychaetes were identified with the help of Dr. Christos Arvanitidis from the Hellenic Centre for Marine Research in Crete, Greece.

SUPPLEMENTARY MATERIAL

The Supplementary Material for this article can be found online at: https://www.frontiersin.org/articles/10.3389/fmars.2020.612779/full#supplementary-material

REFERENCES

Abdo, D. A. (2007). Endofauna differences between two temperate marine sponges (Demospongiae; Haplosclerida; Chalinidae) from southwest Australia. *Mar. Biol.* 152, 845–854. doi: 10.1007/s00227-007-0736-7

Alos, C., Campoy, A., and Pereira, F. (1981). *Contribución al estudio de los anélidos poliquetos endobiontes de esponjas. Actas do II Simposio Iberico de Estudos do Benthos Marino*. 3, 139–157.

Antoniadou, C. (2014). Succession patterns of polychaetes on algal-dominated rocky cliffs (Aegean Sea, Eastern Mediterranean). *Mar. Ecol.* 35, 281–291. doi: 10.1111/maec.12079

Antoniadou, C., and Chintiroglou, C. (2005). Response of Polychaete populations to distrubance: an evaluation of methods in hard substratum. *Fresenius Environ. Bull.* 14, 1066–1073.

Arvanitidis, C., Bellan, G., Drakopoulos, P., Valavanis, V., Dounas, C., Koukouras, A., et al. (2002). Seascape biodiversity patterns along the Mediterranean and the Black Sea: lessons from the biogeography of benthic polychaetes. *Mar. Ecol. Prog. Ser.* 244, 139–152. doi: 10.3354/meps244139

Ávila, E., and Ortega-Bastida, A. L. (2015). Influence of habitat and host morphology on macrofaunal assemblages associated with the sponge Halichondria melanadocia in an estuarine system of the southern Gulf of Mexico. *Mar. Ecol.* 36, 1345–1353. doi: 10.1111/maec.12233

Barnich, R., and Fiege, D. (2003). The Aphroditoidea (Annelida: Polychaeta) of the Mediterranean Sea. *Abhandlungen der Senckenbergischen Naturforschenden Gesellschaft* 559, 1–167.

Becerro, M. A. (2008). Quantitative trends in sponge ecology research. *Mar. Ecol.* 29, 167–177. doi: 10.1111/j.1439-0485.2008.00234.x

Beepat, S. S., Appadoo, C., Marie, D. E. P., and Paula, J. P. M. (2014). Macrofauna associated with the sponge Neopetrosia exigua (Kirkpatrick, 1900) from Mauritius. *West. Indian Ocean J. Mar. Sci.* 13, 133–142.

Ben-Eliahu, M. N. (1991). Nereididae of the Suez Canal—potential lessepsian migrants? *Bull. Mar. Sci.* 48, 318–329.

Bo, M., Bertolino, M., Bavestrello, G., Canese, S., Giusti, M., Angiolillo, M., et al. (2012). Role of deep sponge grounds in the Mediterranean Sea: a case study in southern Italy. *Hydrobiologia* 687, 163–177. doi: 10.1007/s10750-011-0964-1

Burton, M. (1936). The fishery grounds near Alexandria. IX. Sponges. *Notes Mem. Fish Res. Cairo* 17, 1–28.

Carrera-Parra, L. F. (2006). Revision of Lumbrineris de Blainville, 1828 (Polychaeta: Lumbrineridae). *Zootaxa* 1336, 1–64.

Cerrano, C., Calcinai, B., Pinca, S., and Bavestrello, G. (2006). "Reef sponges as hosts of biodiversity: cases from North Sulawesi," in *Proceedings of the 10th International. Coral Reef Symposym. Okinawa 2006*, Okinawa.

Chintiroglou, C. C. (1996). Feeding guilds of polychaetes associated with Cladocora Caespitosa (L.) (anthozoa, cnidaria) in the North Aegean Sea. *Isr. J. Ecol. Evol.* 42, 261–274. doi: 10.1080/00212210.1996.10688847

Çinar, M. E. (2009). Alien polychaete species (Annelida: Polychaeta) on the southern coast of Turkey (Levantine Sea, eastern Mediterranean), with 13 new records for the Mediterranean Sea. *J. Nat. Hist.* 43, 2283–2328. doi: 10.1080/00222930903094654

Çinar, M. E., Bakir, K., Doğan, A., Açik, S., Kurt, G., Katağan, T., et al. (2019). Macro-benthic invertebrates associated with the black sponge *Sarcotragus foetidus* (Porifera) in the Levantine and Aegean Seas, with special emphasis on alien species. *Estuar. Coast. Shelf Sci.* 227:106306. doi: 10.1016/j.ecss.2019.106306

Cinar, M. E., and Ergen, Z. (1998). Polychaetes associated with the sponge sarcotragus muscarum schmidt, 1864 from the turkish aegean coast. *Ophelia* 48, 167–183. doi: 10.1080/00785236.1998.10426964

Çinar, M. E., Katağan, T., Ergen, Z., and Sezgin, M. (2002). Zoobenthos-inhabiting *Sarcotragus muscarum* (Porifera: Demospongiae) from the Aegean Sea. *Hydrobiologia* 482, 107–117. doi: 10.1023/A:1021260314414

Coll, M., Piroddi, C., Steenbeek, J., Kaschner, K., Lasram, F. B. R., Aguzzi, J., et al. (2010). The biodiversity of the Mediterranean Sea: estimates, patterns, and threats. *PLoS One* 5:e11842. doi: 10.1371/journal.pone.0011842

Damianidis, P., and Chintiroglou, C. C. (1998). Feeding guilds of polychaetes associated with Mytilus Galloprovincialis (Lam .) Assemblage in the North Aegean Sea. *Rapp. Comm. Int. Mer. Médit.* 35, 416–417.

Dauer, D. M. (1984). The use of polychaete feeding guilds as biological variables. *Mar. Pollut. Bull.* 15, 301–305. doi: 10.1016/0025-326X(84)90199-1

Erdman, R. B., and Blake, N. J. (1987). Population dynamics of the sponge-Dwelling Alpheid Synalpheus longicarpus, with Observations on *S. brooksi* and *S. pectiniger*, in Shallow-Water assemblages of the Eastern Gulf of Mexico. *J. Crustac. Biol.* 7, 328–337. doi: 10.2307/1548613

Fauchald, K. (1977). The Polychaete Worms. Definitions and keys to the Orders, Families and Genera. *Nat. Hist. Museum Los Angeles County. Sci. Ser.* 28:188. doi: 10.3354/dao063107

Fauchald, K., and Jumars, P. A. (1979). The diet of worms: a study of polychaete feeding guilds. *Oceanogr. Mar. Biol. Annu. Rev.* 17, 193–284. doi: 10.12691/marine-1-1-6

Faulwetter, S., Markantonatou, V., Pavloudi, C., Papageorgiou, N., Keklikoglou, K., Chatzinikolaou, E., et al. (2014). Polytraits: a database on biological traits of marine polychaetes. *Biodivers. Data J.* 2:e1024. doi: 10.3897/BDJ.2.e1024

Fiore, C. L., and Jutte, P. C. (2010). Characterization of macrofaunal assemblages associated with sponges and tunicates collected off the southeastern United States. *Invertebr. Biol.* 129, 105–120. doi: 10.1111/j.1744-7410.2010.00184.x

Fitzhugh, K. (1989). A systematic revision of the sabellidae-caobangiidae-sabellongidae complex (Annelida: Polychaeta). *Bull. Am. Museum Nat. Hist.* 192, 1–104.

Frith, D. W. (1976). Animals associated with sponges at North Hayling, Hampshire. *Zool. J. Linn. Soc.* 58, 353–362. doi: 10.1111/j.1096-3642.1976.tb01005.x

Gambi, M., Giangrande, A., Martinelli, M., and Chessa, L. (1995). Polychaetes of a *Posidonia oceanica* bed off Sardinia (Italy): spatio-temporal distribution and feeding guild analysis. *Sci. Mar.* 59, 129–141.

Gerovasileiou, V., Chintiroglou, C. C., Konstantinou, D., and Voultsiadou, E. (2016). Sponges as "living hotels" in Mediterranean marine caves. *Sci. Mar.* 80, 279–289. doi: 10.3989/scimar.04403.14B

Gherardi, M., Giangrande, A., and Corriero, G. (2001). Epibiontic and endobiontic polychaetes of Geodia cydonium (Porifera, Demospongiae) from the Mediterranean Sea. *Hydrobiologia* 443, 87–101. doi: 10.1023/A:1017500321330

Giangrande, A. (1994). The genus demonax (Polychaeta, sabellidae) in the mediterranean sea, with description of d. tommasi n.sp. *Bolletino di Zool.* 61, 229–233. doi: 10.1080/11250009409355890

Guerra-García, J. M., Tierno de Figueroa, J. M., Navarro-Barranco, C., Ros, M., Sánchez-Moyano, J. E., and Moreira, J. (2014). Dietary analysis of the marine Amphipoda (Crustacea: Peracarida) from the Iberian Peninsula. *J. Sea Res.* 85, 508–517. doi: 10.1016/j.seares.2013.08.006

Gugel, J. (2001). Life cycles and ecological interactions of freshwater sponges (Porifera, Spongillidae) in the River Rhine in Germany. *Limnologica* 31, 185–198. doi: 10.1016/S0075-9511(01)80020-7

Huang, J. P., McClintock, J. B., Amsler, C. D., and Huang, Y. M. (2008). Mesofauna associated with the marine sponge Amphimedon viridis. Do its physical or chemical attributes provide a prospective refuge from fish predation? *J. Exp. Mar. Bio. Ecol.* 362, 95–100. doi: 10.1016/j.jembe.2008.06.007

Hurlbert, S. H. (1971). The nonconcept of species diversity: a critique and alternative parameters. *Ecology* 52, 577–586.

Idan, T. (2020). *Mesophotic Sponge Grounds in the Levant basin: Community Composition and Dynamics*. Ph.D. thesis, Tel Aviv University, Tel Aviv.

Idan, T., Goren, L., Shefer, S., and Ilan, M. (2020). Sponges in a changing climate: survival of *Agelas oroides* in a warming Mediterranean Sea. *Front. Mar. Sci.* 7:1064.

Idan, T., Shefer, S., Feldstein, T., Huchon, D., and Ilan, M. (2018). Shedding light on an East-Mediterranean mesophotic sponge ground community and the regional sponge fauna. *Mediterr. Mar. Sci.* 19, 84–106. doi: 10.12681/mms.13853

Ilan, M., Ben-Eliahu, M. N., and Galil, B. S. (1994). Three deep water sponges from the eastern mediterranean and their associated fauna. *Ophelia* 39, 45–54. doi: 10.1080/00785326.1994.10429901

Kantor, Y. I., and Medinsakaya, A. I. (1991). Morphology and feeding of *Mitrella burchardi* (Gastropoda: Columbellidae). *Asian Mar. Biol.* 8, 25–33.

Kersken, D., Göcke, C., Brandt, A., Lejzerowicz, F., Schwabe, E., Anna Seefeldt, M., et al. (2014). The infauna of three widely distributed sponge species (Hexactinellida and Demospongiae) from the deep Ekström Shelf in the Weddell Sea, Antarctica. *Deep. Res. Part II Top. Stud. Oceanogr.* 108, 101–112. doi: 10.1016/j.dsr2.2014.06.005

Klitgaard, A. B. (1995). The fauna associated with outer shelf and upper slope sponges (porifera, demospongiae) at the faroe islands, northeastern Atlantic. *Sarsia* 80, 1–22. doi: 10.1080/00364827.1995.10413574

Knight-Jones, P., Knight-Jones, W., and Ergen, Z. (1991). Sabelliform polychaetes, mostly from turkey's aegean coast. *J. Nat. Hist.* 25, 837–858. doi: 10.1080/00222939100770561

Koukouras, A., Russo, A., Voultsiadou-Koukoura, E., Arvanitidis, C., and Stefanidou, D. (1996). Macrofauna associated with sponge species of different morphology. *Mar. Ecol.* 17, 569–582. doi: 10.1111/j.1439-0485.1996.tb00418.x

Koukouras, A., Russo, A., Voultsiadou-Koukoura, E., Dounas, C., and Chintiroglou, C. (1992). Relationship of sponge macrofauna with the morphology of their hosts in the North Aegean Sea. *Int. Rev. der gesamten Hydrobiol. Hydrogr.* 77, 609–619. doi: 10.1002/iroh.19920770406

Koukouras, A., Voultsiadou-Koukoura, E., Chintiroglou, H., and Dounas, C. (1985). Benthic bionomy of the North Aegean sea. III: a comparison of the macrobenthic animal assemblages associated with seven sponge species. *Cah. Biol. Mar.* 26, 300–319.

Leclerc, J. C., Riera, P., Leroux, C., Lévêque, L., and Davoult, D. (2013a). Temporal variation in organic matter supply in kelp forests: linking structure to trophic functioning. *Mar. Ecol. Prog. Ser.* 494, 87–105. doi: 10.3354/meps10564

Leclerc, J. C., Riera, P., Leroux, C., Lévêque, L., Laurans, M., Schaal, G., et al. (2013b). Trophic significance of kelps in kelp communities in Brittany (France) inferred from isotopic comparisons. *Mar. Biol.* 160, 3249–3258. doi: 10.1007/s00227-013-2306-5

Lévi, C. (1957). Spongiaires des côtes d'Israel. *Bull. Res. Counc. Isr.* 6, 201–212.

Magnino, G., Sara, A., Lancioni, T., and Gaino, E. (1999). Endobionts of the Coral Reef Sponge Theonella swinhoei (Porifera, Demospongiae). *Invertebr. Biol.* 118:213. doi: 10.2307/3226993

Manousis, T., and Galinou-Mitsoudi, S. (2014). New gastropod records for the Eastern mediterranean sea and one new alien (Emarginula decorata deshayes, 1863) for the mediterranean sea from NW Aegean sea, Greece. *J. Biol. Res.* 21:20. doi: 10.1186/2241-5793-21-20

Martin, D., Pinedo, S., and Sardá, R. (2000). Distribution patterns and trophic structure of soft-bottom polychaete assemblages in a North-Western Mediterranean shallow-water bay. *Ophelia* 53, 1–17. doi: 10.1080/00785326.2000.10409431

Mladenov, P., and Emson, R. (1988). Density, size structure and reproductive characteristics of fissiparous brittle stars in algae and sponges: evidence for interpopulational variation in levels of sexual and asexual reproduction. *Mar. Ecol. Prog. Ser.* 42, 181–194. doi: 10.3354/meps042181

Navarro-Barranco, C., Guerra-García, J. M., Sánchez-Tocino, L., Florido, M., and García-Gómez, J. C. (2016). Amphipod community associated with invertebrate hosts in a Mediterranean marine cave. *Mar. Biodivers.* 46, 105–112. doi: 10.1007/s12526-015-0328-6

Nogueira, J. M. D. M., Carrerette, O., and Hutchings, P. (2015). Review of Amaeana Hartman, 1959 (Annelida, Terebelliformia, Polycirridae), with descriptions of seven new species. *Zootaxa* 3994, 1–52. doi: 10.11646/zootaxa.3994.1.1

Oksanen, J., Blanchet, F. G., Kindt, R., Legendre, P., Minchin, P. R., and O'Hara, R. B. (2013). *Package Vegan. R Package Version 2.5–7*. Available online at: https://CRAN.R-project.org/package=vegan

Olander, R., and Palmén, E. (1968). Taxonomy, ecology and behaviour of the northern Baltic Clunio marinus Halid . (Dipt ., Chironomidae). *Ann. Zool. Fennici* 5, 97–110.

Özcan, T., and Katağan, T. (2011). Decapod Crustaceans associated with the sponge Sarcotragus muscarum Schmidt, 1864 (Porifera: Demospongiae) from the Levantine coasts of Turkey. *Iran. J. Fish. Sci.* 10, 286–293.

Papatheodoulou, M., Jimenez, C., Petrou, A., and Thasitis, I. (2019). Endobiotic communities of Marine Sponges in Cyprus (Levantine Sea). *Heliyon* 5:e01392. doi: 10.1016/j.heliyon.2019.e01392

Pavloudi, C., Christodoulou, M., and Mavidis, M. (2016). Macrofaunal assemblages associated with the sponge Sarcotragus foetidus Schmidt, 1862 (Porifera: Demospongiae) at the coasts of Cyprus and Greece. *Biodivers. Data J.* 30:e8210. doi: 10.3897/BDJ.4.e8210

Pearse, A. A. S. (1950). *Notes on the Inhabitants of Certain Sponges at Bimini*. Hoboken, NJ: Wiley, 149–151.

Peattie, M. E., and Hoare, R. (1981). The sublittoral ecology of the Menai Strait. II. The sponge *Halichondria panicea* (Pallas) and its associated fauna. *Estuar. Coast. Shelf Sci.* 13, 621–635. doi: 10.1016/S0302-3524(81)80044-8

Qiu, J., and Qian, P. (2000). Revision of the genus Leonnates Kinberg, 1866 (Polychaeta: Nereididae), with descriptions and comments on other species described in Leonnates. *Proc. Biol. Soc. Washingt.* 113, 1111–1146.

R Core Team (2019). *R: A Language and Environment for Statistical Computing. Industrial and Commercial Training*. Vienna: R Core Team. doi: 10.1108/eb003648

Ribeiro, S. M., Omena, E. P., and Muricy, G. (2003). Macrofauna associated to Mycale microsigmatosa (Porifera, Demospongiae) in Rio de Janeiro State, SE Brazil. *Estuar. Coast. Shelf Sci.* 57, 951–959. doi: 10.1016/S0272-7714(02)00425-0

Roque, F., de, O., Trivinho-Strixino, S., Couceiro, S. R. M., Hamada, N., Volkmer-Ribeiro, C., et al. (2004). Species of Oukuriella Epler (Diptera, Chironomidae) inside freshwater sponges in Brazil. *Rev. Bras. Entomol.* 48, 291–292. doi: 10.1590/s0085-56262004000200020

RStudio Team (2020). *RStudio: Integrated Development for R*. Boston, MA: Rstudio Team. doi: 10.1145/3132847.3132886

Rützler, K. (1976). Ecology of Tunisian commercial sponges. *Tethys* 7, 249–264.

San Martin, G. (2003). *Fauna Iberica Annelida Polychaeta II: Syllidae*, Vol. 21. Madrid: Museo National de Ciencias Natureles.

Sanders, H. L. (1968). Marine benthic diversity: a comparative study. *Am. Nat.* 102, 243–282. doi: 10.1086/282541

Santhakumaran, L. N., Sneli, J. A., and Sundnes, G. (1984). The larvae of halocladius (halocladius) variabilis (diptera: Chironomidae) from the fouling assemblages on wooden test panels submerged in Trondheims-Fjorden, Norway. *Sarsia* 69, 155–158. doi: 10.1080/00364827.1984.10420601

Schejter, L., Chiesa, I. L., Doti, B. L., and Bremec, C. (2012). Mycale (aegogropila) Magellanica (Porifera: Demospongiae) en el Atlántico suroeste: Fauna endobiótica y nuevos datos de su distribución. *Sci. Mar.* 76, 753–761. doi: 10.3989/scimar.03490.21A

Taylor, J. D. (1987). Feeding ecology of some common intertidal neogastropods at Djerba, Tunisia. *Vie Milieu* 37, 13–20.

Tovar-Hernández, M. A., and Harris, L. H. (2010). Parasabella Bush, 1905, replacement name for the polychaete genus Demonax Kinberg, 1867 (Annelida, Polychaeta, Sabellidae). *Zookeys* 60, 13–19. doi: 10.3897/zookeys.60.547

Voultsiadou, E. (2009). Reevaluating sponge diversity and distribution in the Mediterranean Sea. *Hydrobiologia* 628, 1–12. doi: 10.1007/s10750-009-9725-9

Voultsiadou-Koukoura, H. E., Koukouras, A., and Eleftheriou, A. (1987). Macrofauna associated with the sponge *Verongia aerophoba* in the north Aegean Sea. *Estuar. Coast. Shelf Sci.* 24, 265–278. doi: 10.1016/0272-7714(87)90069-2

Westinga, E., and Hoetjes, P. C. (1981). The intrasponge fauna of Spheciospongia vesparia (Porifera, Demospongiae) at Curaçao and bonaire. *Mar. Biol.* 62, 139–150. doi: 10.1007/BF00388176

Wulff, J. L. (2006). Ecological interactions of marine sponges. *Can. J. Zool.* 84, 146–166. doi: 10.1139/z06-019

Conflict of Interest: The authors declare that the research was conducted in the absence of any commercial or financial relationships that could be construed as a potential conflict of interest.

Copyright © 2021 Goren, Idan, Shefer and Ilan. This is an open-access article distributed under the terms of the Creative Commons Attribution License (CC BY). The use, distribution or reproduction in other forums is permitted, provided the original author(s) and the copyright owner(s) are credited and that the original publication in this journal is cited, in accordance with accepted academic practice. No use, distribution or reproduction is permitted which does not comply with these terms.

frontiers in Marine Science

ORIGINAL RESEARCH
published: 18 January 2021
doi: 10.3389/fmars.2020.596251

An Integrative Model of Carbon and Nitrogen Metabolism in a Common Deep-Sea Sponge (*Geodia barretti*)

Anna de Kluijver[1], Martijn C. Bart[2], Dick van Oevelen[3], Jasper M. de Goeij[2], Sally P. Leys[4], Sandra R. Maier[3], Manuel Maldonado[5], Karline Soetaert[1,3], Sander Verbiest[1] and Jack J. Middelburg[1]*

[1] Department of Earth Sciences, Faculty of Geosciences, Utrecht University, Utrecht, Netherlands, [2] Department of Freshwater and Marine Ecology, Institute for Biodiversity and Ecosystem Dynamics, University of Amsterdam, Amsterdam, Netherlands, [3] Department of Estuarine and Delta Systems, Royal Netherlands Institute for Sea Research (NIOZ) and Utrecht University, Yerseke, Netherlands, [4] Department of Biological Sciences, University of Alberta, Edmonton, AB, Canada, [5] Center for Advanced Studies of Blanes (CEAB), Spanish National Research Council (CSIC), Girona, Spain

Deep-sea sponges and their microbial symbionts transform various forms of carbon (C) and nitrogen (N) *via* several metabolic pathways, which, for a large part, are poorly quantified. Previous flux studies on the common deep-sea sponge *Geodia barretti* consistently revealed net consumption of dissolved organic carbon (DOC) and oxygen (O_2) and net release of nitrate (NO_3^-). Here we present a biogeochemical metabolic network model that, for the first time, quantifies C and N fluxes within the sponge holobiont in a consistent manner, including many poorly constrained metabolic conversions. Using two datasets covering a range of individual *G. barretti* sizes (10–3,500 ml), we found that the variability in metabolic rates partially resulted from body size as O_2 uptake allometrically scales with sponge volume. Our model analysis confirmed that dissolved organic matter (DOM), with an estimated C:N ratio of 7.7 ± 1.4, is the main energy source of *G. barretti.* DOM is primarily used for aerobic respiration, then for dissimilatory NO_3^- reduction to ammonium (NH_4^+) (DNRA), and, lastly, for denitrification. Dissolved organic carbon (DOC) production efficiencies (production/assimilation) were estimated as 24 ± 8% (larger individuals) and 31 ± 9% (smaller individuals), so most DOC was respired to carbon dioxide (CO_2), which was released in a net ratio of 0.77–0.81 to O_2 consumption. Internally produced NH_4^+ from cellular excretion and DNRA fueled nitrification. Nitrification-associated chemoautotrophic production contributed 5.1–6.7 ± 3.0% to total sponge production. While overall metabolic patterns were rather independent of sponge size, (volume-)specific rates were lower in larger sponges compared to smaller individuals. Specific biomass production rates were 0.16% day^{-1} in smaller compared to 0.067% day^{-1} in larger *G. barretti* as expected for slow-growing deep-sea organisms. Collectively, our approach shows that metabolic modeling of hard-to-reach, deep-water sponges can be used to predict community-based biogeochemical fluxes and sponge production that will facilitate further investigations on the functional integration and the ecological significance of sponge aggregations in deep-sea ecosystems.

Keywords: allometry, metabolic network model, sponge holobiont metabolism, production, biogeochemistry, chemoautotrophy, sponge ground, LIM

OPEN ACCESS

Edited by:
Daniela Zeppilli, Institut Français de Recherche pour l'Exploitation de la Mer (IFREMER), France

Reviewed by:
Christopher Freeman, College of Charleston, United States
Clara F. Rodrigues, University of Aveiro, Portugal

****Correspondence:***
Anna de Kluijver
a.dekluijver@uu.nl;
anna.dekluijver@rvo.nl

Specialty section:
This article was submitted to Deep-Sea Environments and Ecology, a section of the journal Frontiers in Marine Science

Received: *18 August 2020*
Accepted: *30 November 2020*
Published: *18 January 2021*

Citation:
de Kluijver A, Bart MC, van Oevelen D, de Goeij JM, Leys SP, Maier SR, Maldonado M, Soetaert K, Verbiest S and Middelburg JJ (2021) An Integrative Model of Carbon and Nitrogen Metabolism in a Common Deep-Sea Sponge (Geodia barretti). Front. Mar. Sci. 7:596251. doi: 10.3389/fmars.2020.596251

INTRODUCTION

Sponges are abundant and key ecosystem engineers of the deep sea that occur scattered on soft- and hard-bottomed surfaces and in multi- or mono-specific aggregations (Maldonado et al., 2017). These so-called sponge grounds create complex habitats and thereby support high local biodiversity (Klitgaard, 1995; Hogg et al., 2010; Beazley et al., 2013). As deep-sea sponges process large amounts of water for filter feeding, they are implicated to have an important role in the biogeochemical cycling and benthic–pelagic coupling of carbon (C), nitrogen (N), and silicon (Si) (Maldonado et al., 2012, 2019; Kutti et al., 2013; Kahn et al., 2015).

Deep-sea sponges efficiently filter (preferably nano- and pico-) plankton (Pile and Young, 2006; Yahel et al., 2007; Kahn et al., 2015) and, similar to their shallow counter parts (de Goeij et al., 2013), consume dissolved organic carbon (DOC), constituting most of their diet (Bart et al., 2020b). The efficiency at which sponges process (*e.g.*, assimilate, respire, release) organic and inorganic nutrients (*e.g.*, C, N) is termed production efficiency, which is an important ecological and metabolic parameter to determine energy (re)cycling in organisms (also referred to as growth efficiency) (Thomassen and Riisgard, 1995; Sterner and Elser, 2002; Maldonado et al., 2012; de Goeij et al., 2017) and ecosystems (Keesing et al., 2013; Kahn et al., 2015; Porada et al., 2018). Despite its potential relevance, the C and N production efficiency of deep-sea sponges and most other deep-sea benthos are largely unknown—especially *in situ* assessments of metabolic rates and conversions—because of the technical constraints of conducting (properly controlled) experiments in the deep sea. Recent advances in technology and accessibility of remotely operated vehicle have increased the ability to collect live deep-sea sponges for *ex situ*-controlled laboratory experiments (*e.g.*, Kutti et al., 2015; Leys et al., 2018; Bart et al., 2020a,b) and even *in situ* metabolic rate measurements (Yahel et al., 2007; Kahn et al., 2015; Maldonado et al., 2020a).

Geodia barretti (Porifera, Demospongiae) is one of the best studied deep-sea sponge species. In the North-Atlantic Ocean, along the continental shelf and in fjords, the massive, ball-shaped *G. barretti* can be present in large densities of up to 0.4–5 individuals per square meter, known as "*Geodia* grounds" (Murillo et al., 2012; Kutti et al., 2013; Beazley et al., 2015). It is considered to be a slow-growing sponge species that, if undisturbed, can reach a meter in diameter, although most specimens have a diameter of 20–30 cm (Klitgaard and Tendal, 2004; Kutti et al., 2013). Oxygen (O_2) consumption by *G. barretti* individuals, combined with biomass estimates from video imaging, indicated that *Geodia* sponge grounds have high metabolic activity and C demand (*ex situ,* Kutti et al., 2013; eddy correlation, Cathalot et al., 2015). To date, the metabolic C demands of *G. barretti* have been derived from O_2 consumption measurements and a supposed respiratory quotient (RQ) for organic matter (OM) mineralization (O_2:CO_2). Despite the importance of RQ in estimating the C demand from O_2 measurements, its value has never been empirically determined for *G. barretti*. The RQ values for *G. barretti* might deviate from values for canonical organic matter mineralization because of the various metabolic pathways conducted by the endosymbionts.

G. barretti is considered as a high microbial abundance (HMA) species, containing a dense and diverse community of microbial symbionts ($\sim 10^{11}$ microbes per cubic centimeter) (Hoffmann et al., 2009; Leys et al., 2018). Microbial symbionts (*i.e.*, the microbiome) and sponge host are a metabolically integrated functional unit, known as a "holobiont." This, generally considered mutualistic, symbiosis is known to benefit in a variety of ways, which include nutrition, development, defense, and immunity (Pita et al., 2018). In *G. barretti*, the microbiome is actively involved in the (re)cycling of C and N compounds and, therefore impacts the holobiont nutrition (Hoffmann et al., 2009; Leys et al., 2018; Bart et al., 2020a). As for many sponge species, anaerobic and aerobic N-transforming processes occur in *G. barretti*, thereby expanding its metabolic capacity (Hoffmann et al., 2009; Rooks et al., 2020). It has been hypothesized that *G. barretti* actively controls the oxygenation level of its tissue to maintain aerobic and anaerobic micro-environments that facilitate the co-existence of aerobic and anaerobic symbionts (Hoffmann et al., 2005). The nitrifying and denitrifying potential of the microbial populations within the tissue of *G. barretti* has been demonstrated by cutting sponges in small fragments (0.3–0.4 cm^3) and incubating those pieces under labeled substrates (Hoffmann et al., 2009; Rooks et al., 2020). However, N transformations within intact, pumping *G. barretti* individuals have yet to be resolved and quantified.

Two studies have examined the C, N, and O_2 exchange rates of intact *G. barretti* individuals. Leys et al. (2018) studied larger specimens (∼1-L volume) using the "in–ex" methodology, *i.e.*, sponge filtration rates are combined with the composition of inhalant and exhalant water to obtain release/uptake fluxes. Bart et al. (2020b) used incubation flow chambers to quantify fluxes for smaller (∼100-ml volume) specimens. Both studies found that *G. barretti* effectively removed organic C and concluded that the observed organic matter consumption was sufficient to sustain the minimal metabolic needs. Bart et al. (2020b) found a relatively higher net organic C intake compared to Leys et al. (2018). This difference can be attributed to the smaller size of the individuals tested by Bart et al. (2020b), as volume-specific pumping rates may be related to sponge size (Morganti et al., 2019). Regarding N, intact *G. barretti* was found to release nitrate (NO_3^-) rather than ammonium (NH_4^+), indicative of net nitrification (Leys et al., 2018), yet the metabolic conversions of O_2, C, and N within and exchanges among sponge and symbionts can be complex, and it is not straightforward to derive those from net fluxes obtained by the in–ex and chamber incubation techniques.

To integrate existing experimental metabolic flux data, we constructed a metabolic network model for the holobiont. Metabolic (or stoichiometric) network models are common tools to quantify and predict the intracellular metabolism of, for example, eukaryotic cells and microbes (Palsson and Varma, 1994; Edwards and Covert, 2002) based on net resource (*e.g.*, C, N) fluxes. Such models are underexplored to quantify sponge–symbiont metabolism, despite their potential to elucidate

the intricacies of the sponge physiology and their ecological significance. To date, only one study that employs a genome-scale metabolic network model to reconstruct biochemical conversions in the sponge–symbiont system of the tropical sponge *Amphimedon queenslandica* exists (Watson, 2017). In our study, we applied the metabolic network model to quantify internal and unconstrained C, N, and O_2 fluxes of the common and abundant deep-sea *G. barretti* holobiont. To assess the size dependency of *G. barretti* metabolism, we compared and separately analyzed the metabolic datasets of Leys et al. (2018) and Bart et al. (2020b) because they assessed different size classes. The size dependency of metabolism is particularly relevant when estimating the metabolic fluxes and metabolic demands of sponge grounds from video images. The outcome of the model advances the understanding on *G. barretti* metabolism and its potential role in biogeochemical cycling within the vast, benthic deep-sea ecosystems where it abounds.

MATERIALS AND METHODS

Datasets

The experimental data of Leys et al. (2018) and Bart et al. (2020b) were used to develop and constrain the metabolic network model for larger and smaller *G. barretti*, respectively, since they cover different size ranges. We refer to their publications (Leys et al., 2018; Bart et al., 2020b) for a full description of sponge collection, experimental procedures, data analyses, and data presentation and only briefly recap some relevant aspects here.

In short, Leys et al. (2018) maintained *G. barretti* individuals in *ex situ* (running seawater) conditions in the Institute of Marine Research aquarium facilities at Austevoll (Norway) and measured exchange fluxes using the "in–ex" method. The flow rates and O_2 uptake of *G. barretti* were collected simultaneously in 2012 (n = 17, sponge volume = 150–3,500 ml) (**Table 1**). Dissolved inorganic N [DIN, consisting of NH_4^+, nitrite (NO_2^-), and NO_3^-] exchange rates and bacterial cell removal were measured in 2011 (n = 53, sponge volume = 125–3,400 ml), and DIN exchange rates and total OC (TOC = DOC + POC) removal were measured in 2014 (n = 29, sponge volumes unknown) (**Table 1**). Leys et al. (2018) converted bacterial cell removal to bacterial C uptake using standard conversion factors and defined DOC uptake as TOC uptake minus bacterial C uptake (**Table 1**). Bart et al. (2020b) measured exchange fluxes in *G. barretti* individuals (n = 12, sponge volume = 9–210 ml) (**Table 1**) using incubation flow chambers under *ex situ* (running seawater) conditions in aquarium facilities in Bergen (Norway) in 2017 (n = 9) and 2018 (n = 3). O_2, DOC, and living POC (LPOC, consisting of bacteria and phytoplankton C) removal rates were calculated from changes in incubation water and used to calculate a C budget (**Table 1**; Bart et al., 2020b). For both studies, the incubation water was collected from 160-m depth (Leys et al., 2018) and 200-m depth (Bart et al., 2020b) from nearby fjords, thus representing deep water. This corresponds with the depth range of 200–300 m where *G. barretti* grounds are typically found (Klitgaard and Tendal, 2004).

DIN Exchange Rates From Incubation Chambers

Changes in DIN (NH_4^+, NO_2^-, and NO_3^-) were also measured by Bart et al. (2020b), but as these data were not presented before, the procedures and the results are presented in this paper. DIN fluxes were determined as follows: duplicate samples for DIN (NH_4^+, NO_2^-, and NO_3^-) were collected at t = 0, 1, 2, 3, and 4 h in 2017 and t = 0, 2, 4, 6, and 8 h in 2018 from the incubation chambers with acid-washed 100-ml polycarbonate syringes. The samples were subsequently filtered over sterile 0.2-μm polyethersulfone syringe filters (Whatman Puradisc), collected in 10-ml high-density polyethylene vials, and stored at −20°C until further analysis. Nutrients were analyzed in the laboratory with a QuAAtro Gas Segmented Continuous Flow Analyzer. Measurements were made simultaneously for NH_4^+ (Helder and de Vries, 1979), NO_2^-, and NO_3^- combined with NO_2^- (Grasshoff et al., 2009). All measurements were calibrated with standards diluted in low-nutrient seawater. DIN exchange rates were calculated from a linear regression slope and incubation volume and corrected with changes in control (*i.e.*, no sponge) incubations. Fluxes were normalized to sponge volume to obtain fluxes in μmol N cm^{-3} (sponge) day^{-1} (**Table 1**, **Supplementary Figure 1**).

Linear Inverse Modeling Concepts

Metabolic network models are a type of linear inverse modeling (LIM), which are based on mass balances under steady-state conditions. This implies that the internal changes of a substance due to chemical reactions are balanced by the inflow and outflow into a system and that the system can be solved by a set of linear equations (Edwards and Covert, 2002). The steady-state metabolic situation is justified by the rationale that chemical reactions take place on shorter timescales than transport (exchange) fluxes (Edwards and Covert, 2002). As detailed through subsequent sections, LIM of stoichiometric (metabolic) networks requires the following: (1) selection of relevant substances and (chemical) processes and conceptualization of the metabolic network, (2) stoichiometrically balancing of all chemical reactions and construction of mass balances for each substance, (3) constraining model solutions with actual flux measurements or fluxes derived from literature (although LIM can solve for or constrain missing flux data), and (4) mathematically solving the model, including variability and uncertainty analysis (Edwards and Covert, 2002; Soetaert and van Oevelen, 2009; van Oevelen et al., 2010).

Sponge Metabolic Network Model Concept

The metabolic network model integrates the C, N, and O_2 metabolism of *G. barretti* and consists of both net holobiont metabolism and host *versus* symbiont-driven metabolism (**Figure 1** and **Table 2**). In detail, sponges rely largely on heterotrophy as they filter the water column for LPOC, consisting predominantly of bacterioplankton in the deep sea (Bart et al., 2020b; **Table 1**) (r1), and consume dissolved organic matter (DOM) (r11). Sponges aerobically respire assimilated organic matter to obtain energy for basal metabolism (r1–r2).

TABLE 1 | Experimental metabolic datasets of intact *Geodia barretti* sponges (Leys et al., 2018; Bart et al., 2020b) which were analyzed with the metabolic network model.

Dataset	Smaller—incubation chambers (Bart et al., 2020b)	Larger—in–ex (Leys et al., 2018)
Volume (cm^3)	9–210	150–3,500
C-content (mmol cm^{-3})	4.1	3.2
Fluxes (μmol cm^{-3} day^{-1})	Mean ± SD (*n* = 12)	Mean ± SD (*n* = 17 to *n* = 53)
Bacteria-C (r1)	0.15 ± 0.15	0.30 ± 0.11
Phytoplankton-C	0.0010 ± 0.0013[a]	n.d.
Dissolved organic carbon, DOC (r11)	25.7 ± 12.3[b]	5.2 ± 2.1
O_2 (r12)	11.2 ± 8.1	7.7 ± 5.8
NH_4^+ (r13)	−0.061 ± 0.47[c]	0.0096 ± 0.0032
NO_3^- (r14)	−0.95 ± 0.79[c]	−0.82 ± 0.53
NO_2^- (r15)	−0.023 ± 0.046[c]	0.018 ± 0.013

Positive fluxes indicate uptake, and negative fluxes indicate release. [a]*Phytoplankton-C assimilation was not included in the model because of its small contribution to organic C uptake.* [b]*The DOC range is larger than the range reported by Bart et al. (2020b) to match the variation in O_2 uptake rates.* [c]*Dissolved inorganic N flux data are analyzed as part of this study.*

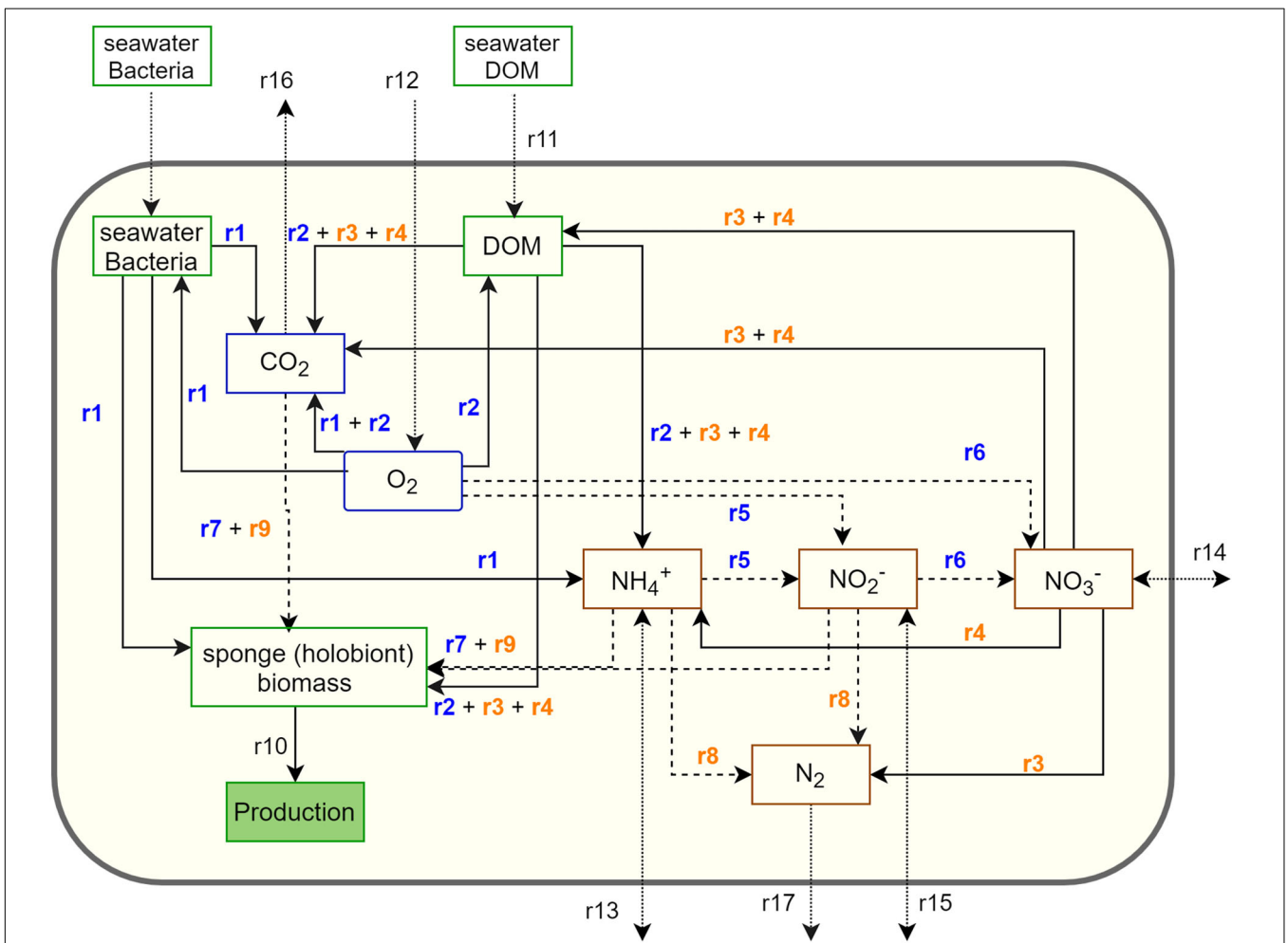

FIGURE 1 | Schematic representation of the metabolic network model for a sponge holobiont (large yellow box) containing nitrogen species (brown boxes), organic substances (green boxes), and O_2/CO_2 (blue boxes). Production (filled green) is not a standing stock, but a closure term for production of sponge biomass. The arrows indicate metabolic transformations: solid arrows refer to heterotrophic processes, dashed arrows refer to chemoautotrophy, and dotted arrows indicate exchange with the environment. Reaction numbers correspond with those in **Table 2**: blue numbers indicate aerobic processes, and orange numbers indicate anaerobic processes.

TABLE 2 | Reactions and coefficients involved in C, N, and O metabolism as implemented in the metabolic network model.

r	Description	Reactions	Coefficients and ranges (no units)
Aerobic consumption			
1	Bacteria consumption	$Bac_w + f_{r_C_{bac}} \cdot RQ \cdot C:N_{bac} \cdot O_2 \rightarrow f_{p_N_{bac}} \cdot Spo + f_{r_C_{bac}} \cdot C:N_{bac} \cdot CO_2 + (1 - f_{p_N_{bac}}) \cdot NH_4^+$	$f_{p_N_{bac}}$ 0.2–0.8 $f_{r_C_{bac}}$ $1 \frac{f_{p_N_{bac}} \cdot C:N_{spo}}{C:N_{bac}}$ RQ (O_2:CO_2) 1-1.16 (Del Giorgio and Williams, 2005) C:N_{spo} = 3.9–4.5 (measured) C:N_{bac} = 4–6 (Zimmerman et al., 2014; White et al., 2019)
2	DOM consumption	$DOM + f_{r_C_{DOM}} \cdot RQ \cdot C:N_{DOM} \cdot O_2 \rightarrow f_{p_N_{DOM}} \cdot Spo + f_{r_C_{DOM}} \cdot C:N_{DOM} \cdot CO_2 + (1 - f_{p_N_{DOM}}) \cdot NH_4^+$	$f_{p_N_{DOM}}$ 0.2–0.8 $f_{r_C_{DOM}}$ $1 - \frac{f_{p_N_{DOM}} \cdot C:N_{spo}}{C:N_{DOM}}$ C:N_{DOM} = 6–11 RQ and C:N_{spo} as in equation 1
Microbial processes			
Anaerobic consumption			
3	Denitrification	$DOM + f_{r_C_{denit}} \cdot C:N_{DOM} \cdot \varphi_{denit} \cdot NO_3^- \rightarrow f_{p_N_{denit}} \cdot Spo + f_{r_C_{denit}} \cdot C:N_{DOM} \cdot CO_2 + (1 - f_{p_N_{denit}}) \cdot NH_4^+ + 0.5 \cdot f_{r_C_{denit}} \cdot C:N_{DOM} \cdot \varphi_{denit} \cdot N_2$	φ_{denit} 0.8 (Soetaert et al., 1996) $f_{p_N_{denit}}$ 0.3–0.6 $f_{r_C_{denit}}$ $1 \frac{f_{p_N_{denit}} \cdot C:N_{spo}}{C:N_{DOM}}$
4	DNRA	$DOM + f_{r_C_{DNRA}} \cdot C:N_{DOM} \cdot \varphi_{DNRA} \cdot NO_3^- \rightarrow f_{p_N_{DNRA}} \cdot Spo + f_{r_C_{DNRA}} \cdot C:N_{DOM} \cdot CO_2 + (1 - f_{p_N_{DNRA}}) \cdot NH_4^+ + f_{r_C_{DNRA}} \cdot C:N_{DOM} \cdot \varphi_{DNRA} \cdot NH_4^+$	φ_{DNRA} 0.56 (Koeve and Kähler, 2010) $f_{p_N_{DNRA}}$ 0.3–0.6 $f_{r_C_{DNRA}}$ $1 \frac{f_{p_N_{DNRA}} \cdot C:N_{spo}}{C:N_{DOM}}$
Chemoautotrophy			
5	NH_4^+ oxidation	$NH_4^+ + 1.5 \cdot O_2 \rightarrow NO_2^-$	
6	NO_2^- oxidation	$NO_2^- + 0.5 \cdot O_2 \rightarrow NO_3^-$	
7	Production from nitrification	$NH_4^+ + C:N_{spo} \cdot CO_2 \rightarrow Spo$	
8	Anammox	$NO_2^- + NH_4^+ \rightarrow N_2$	
9	Production from anammox	$19.4 \cdot NO_2^- + C:N_{spo} \cdot CO_2 \rightarrow Spo + 16.1 \cdot NO_3^- + 1.2 \cdot N_2$	Adjusted from Prosser (2005)
(Biomass) Production (closure term)			
10	Production	$Spo \rightarrow$ production	
Stoichiometric coupling			
-	Production from nitrification	$r7 = C_{fix_ao} \cdot N:C_{spo} \cdot r5 + C_{fix_{no}} \cdot N:C_{spo} \cdot r6$	C_{fix_ao} 0.073 (Zhang et al., 2020) range 0.04–0.11 C_{fix_no} 0.022 (Zhang et al., 2020), range 0.01–0.03
-	Production from anammox	$r9 = C_{fix_am} \cdot N:C_{spo} \cdot r8$	C_{fix_am} 0.066 (Prosser, 2005), range 0.03–0.1

The details are explained in the Section "Sponge Metabolic Network Model Concept". The consumption processes of bacteria (Bac_w) [reaction (r) 1] and dissolved organic matter (r2–4) include the production of sponge biomass (Spo) with a source- and process-dependent production efficiency that is explicit for N ($f_{p_N_{bac}}$ in r1, $f_{p_N_{DOM}}$ in r2, $f_{p_N_{denit}}$ in r3, and $f_{p_N_{DNRA}}$ in r4) and implicit for C. The fraction not used for production (1 − production efficiency) is respired. The respired C fractions are $f_{r_C_{bac}}$ in r1, $f_{r_C_{DOM}}$ in r2, $f_{r_C_{denit}}$ in r3, and $f_{r_C_{DNRA}}$ in r4 and are dependent on the stoichiometry (C:N) of the sponge (C:N_{spo}) relative to the source (C:N_{bac} and C:N_{DOM}). The ratios of electron acceptor per C respired are RQ for O_2 and φ_{denit} and φ_{DNRA} for NO_3 (r1-r4). Chemoautotrophic processes (r5–6, r8) include the production of sponge biomass (Spo) (r7, r9) with a stoichiometric coupling (C fixation efficiency) that is process dependent (C_{fix_ao} for r5–r7, C_{fix_no} for r6–r7, and C_{fix_am} for r8–r9). The reaction numbers (r) correspond to those in ***Figure 1****.*

The metabolic waste of N is mineralized to NH_4^+ (r1–r2). The assimilated organic matter that is not required for basal metabolism is allocated to biomass production (r10). The C (or N) balance for sponges applied in the network model is: assimilation = production + respiration (mineralization in case of N) (Thomassen and Riisgard, 1995; Maldonado et al., 2012).

Microbial symbionts expand the metabolic capacity of the sponge host by exploiting metabolic pathways additional to mere aerobic respiration, such as heterotrophy coupled to denitrification (r3) (Hoffmann et al., 2005; Rooks et al., 2020) and dissimilatory NO_3^- reduction to NH_4^+ (DNRA) (r4) in anoxic parts of the sponge. The latter process has not been measured, but the accompanying genes (*napA*, *nrfA*) were found in *G. barretti* (Gavriilidou, personal communication). The included chemoautotrophic processes are nitrification in oxic (r5, r6) and anaerobic NH_4^+ oxidation (anammox) (r8) in anoxic parts of the sponge holobiont (Hoffmann et al., 2005; Rooks et al., 2020). N_2 fixation is not considered in the model since, at present, no genetic evidence exists for *G. barretti* (Rooks et al., 2020). All considered microbial processes yield production (growth) of symbionts, either *via* anaerobic heterotrophy (denitrification and DNRA) or chemoautotrophy (nitrification and anammox) (r7, r9; **Table 2**). The production of symbiont biomass is considered an integrative part of sponge holobiont production, as the sponge host can phagocyte and ingest (in an undetermined amount) microbial symbionts that may continuously grow within the sponge tissue, including chemoautotrophic bacteria. The process of NH_4^+ assimilation by symbionts (for which

genetic evidence exists; Gavriilidou, personal communication) is considered implicit in organic matter consumption (r1–r2), where it functions as an internal feedback loop (from NH_4^+ to production). Because of the steady-state approach, production of sponge (holobiont) biomass is treated as a closure term (r10).

Finally, all remaining mass-balanced substances, *i.e.*, DOM (r11), O_2 (r12), NH_4^+ (r13), NO_3^- (r14), NO_2^- (r15), CO_2 (r16), and N_2 (r17), have an exchange with the environment (**Figure 1**).

Reactions and Coefficients

All reactions are stoichiometrically coupled for N and C, with N as base and C derived from the stoichiometry of the substrates. For example, in reaction 2, assimilated DOM is converted to sponge (holobiont) biomass ("Spo") with a N production efficiency ($f_{p_N_{DOM}}$), while the remaining fraction is excreted as NH_4^+ ($1-f_{p_N_{DOM}}$). The C production efficiency ($f_{p_C_{DOM}}$) and the fraction that is respired to CO_2 ($f_{r_C_{DOM}} = 1-f_{p_C_{DOM}}$) depends on the stoichiometry (molar C:N ratio) of DOM and sponge biomass: $f_{p_C_{DOM}} = f_{p_N_{DOM}} \cdot C{:}N_{spo} / C{:}N_{DOM}$ (**Table 2**). Reactions 1, 3, and 4 have a similar structure as reaction 2 (**Table 2**). The measured (molar) stoichiometry of *G. barretti* biomass "Spo" ($C{:}N_{spo}$) is 4.2 ± 0.29 [$n = 20$ specimens collected by Bart et al. (2020b) and Maier et al. (2020)]. The C:N ratios of assimilated food sources (bacteria and DOM) are unconstrained, but experimental studies indicated that *G. barretti* preferentially assimilates N-rich DOM, with C:N ratios close to or below Redfield (C:N < 6.6) (Maier et al., 2020; Bart et al., 2020a). The C:N ratios of marine bacteria ($C{:}N_{bac}$) are typically 4 to 6, thus below the Redfield ratio (Sterner and Elser, 2002; Zimmerman et al., 2014; White et al., 2019). The C:N ratios of seawater DOM ($C{:}N_{DOM}$) are generally higher, with average C:N ratios of labile DOM of 10.7 (Hopkinson and Vallino, 2005). The C production efficiencies of metazoans typically range from ∼20 to 30%, which would correspond to $f_{p_N_{DOM}}$ of 32–48% on Redfield DOM ($C{:}N_{DOM}$ = 6.6). However, *G. barretti* might have a higher $f_{p_N_{DOM}}$ as heterotrophic symbionts can assimilate NH_4^+ into organic N (Hentschel et al., 2012; Gavriilidou pers. communication). The C production efficiency for denitrification ($f_{p_C_{denit}}$) is ∼25% (Koike and Hattori, 1975; van den Berg et al., 2016), and DNRA has a comparable production efficiency ($f_{p_C_{DNRA}}$) (Strohm et al., 2007; van den Berg et al., 2016). Depending on the stoichiometry of DOM, the N production efficiencies ($f_{p_N_{denit}}$) and ($f_{p_N_{DNRA}}$) are expected to range from 30 to 60%. The variability and uncertainty in C:N of the assimilated substrates and production efficiencies were considered in model solutions (**Table 2**, "Section Model Implementation and Solutions").

Oxygen is used as electron acceptor in r1 and r2, and the respiratory quotient (RQ; O_2 consumed to CO_2 produced) depends on the elemental composition of the substrate and the fraction of substrate that is respired (**Table 2** and **Figure 1**). RQ ranges from 1 for oxidation of glucose to 1.16 for complete mineralization of plankton Redfield OM (C:N = 6.6) to NH_4^+ (Del Giorgio and Williams, 2005; Middelburg, 2019). In anoxic parts of the sponge tissue, NO_3^- may be used as an electron acceptor and is reduced to N_2 in denitrification (r3, **Table 2**) and to NH_4^+ in DNRA (r4, **Table 2**). NO_3^- consumption per CO_2 produced for Redfield OM in denitrification (φ_{denit}) is 0.8 (r3; Soetaert et al., 1996; Strohm et al., 2007). In DNRA, this ratio (φ_{DNRA}) is determined as 0.56 (r4; Koeve and Kähler, 2010). In the oxic compartments of the sponge holobiont, NH_4^+ is oxidized to NO_2^- (r5) and NO_2^- is oxidized to NO_3^- (r6). NH_4^+ oxidation in *G. barretti* is primarily conducted by archaea, while NO_2^- oxidizers are primarily *Nitrospira* bacteria (Radax et al., 2012). The energy and the corresponding chemoautotrophic yields are higher for NH_4^+ oxidation than for NO_2^- oxidation, with an average reported molar $C_{fix}{:}N_{oxidized}$ ratios of 0.073 for NH_4^+-oxidizing archaea (Zhang et al., 2020) and 0.022 for NO_2^--oxidizing bacteria (Zhang et al., 2020). These chemoautotrophic yields were used to constrain the production of sponge holobiont "Spo" (r7) as a function of r5 and r6 (**Table 2** and **Figure 1**). In the anoxic compartments of the sponge holobiont, anammox takes place (Hoffmann et al., 2009), in which N_2 is produced from NO_2^- and NH_4^+ by anammox bacteria (r8). The growth and the energy yields of anammox bacteria are well studied; anammox bacteria fix inorganic C coupled to NO_2^- oxidation (r9), with ∼0.07 $C_{fix}{:}NH_4^+$ oxidized (Prosser, 2005; Thamdrup, 2012), which was used to constrain r9 as a function of r8 (**Table 2** and **Figure 1**).

Model Constraints

The metabolic network model is generic and can be applied to any sponge volume, depending on data availability. Since two almost complete metabolic flux datasets were available for *G. barretti* that covered distinct volumes [9–210 ml (Bart et al., 2020b) *versus* 150–3,500 ml (Leys et al., 2018)] and are based on different methods, we quantified metabolism of "smaller" (from incubation chambers) and "larger" (by in–ex) *G. barretti* individuals separately (**Table 1**). This not only allowed us to evaluate the potential size dependence of metabolic activities but also provided an independent assessment of the eventual metabolic patterns inferred.

The measured metabolic exchange fluxes ($\mu mol\ cm^{-3}\ day^{-1}$) were used to constrain the exchange fluxes of O_2 (r12), NH_4^+ (r13), NO_3^- (r14), and NO_2^- (r15) for smaller (incubation chambers) and larger (in–ex) specimens (**Table 1**). For external bacteria uptake (r1) and DOM uptake (r11), the measured bacteria C and DOC uptake fluxes combined with $C{:}N_{bac}$ and $C{:}N_{DOM}$ constrained the model.

In addition, the model was constrained with 13 inequalities (soft constraints), of which 10 stated that all metabolic reactions (r1–r10) must be positive. Furthermore, two inequalities limited DOM consumption in denitrification and DNRA (r3, r4) to be lower than aerobic DOM consumption (r2). Lastly, the anammox rates (r8) were constrained to be limited to a maximum of 20% of denitrification rates (r3) (Hoffmann et al., 2009; Rooks et al., 2020).

Model Implementation and Solutions

The metabolic network model of *G. barretti* was implemented and solved in the modeling environment R (R Core Team, 2018) with R-package LIM (van Oevelen et al., 2010). With 17 unknowns (reactions) and 16 knowns (eight mass balances

and eight constraints), the model was almost even determined, resulting in small ranges of possible solutions for each reaction. The (small) ranges in reaction rates were assessed by Bayesian sampling of the solution space with 500 iterations using the function "xsample" (Van den Meersche et al., 2009). This resulted in reaction rate values with standard deviations < 4% of average. The variation in reaction rates is mostly depending on model input parameters, which comprises reaction coefficients (*e.g.*, C:N_{DOM} and $f_{p_N_{DOM}}$) (**Table 2**) and constraints (*e.g.*, measured O_2 uptake and NO_3^- release; **Table 1**). However, the linear setup allows only single-parameter values rather than ranges. Inclusion of uncertainty and variability in parameters was achieved by creating one million model input files with values that were randomly sampled from parameter ranges. The ranges for reaction coefficients are as explained in "Section "Reactions and Coefficients"" (**Table 2**), and the ranges for constraints are mean ± standard deviation (SD) for larger and smaller sponges (**Table 1**). Only ∼0.2–1.0% of parameter combinations resulted in a feasible model solution, corresponding to 10,088 and 2,228 feasible model solutions for smaller and larger sponges, respectively. The feasibility of parameters to produce successful results gives an indication on the likelihood of these parameter values. A successful input file is available in the **Supporting Information**. The R code to run the model is available at Zenodo (doi: 10.5281/zenodo.4139792). The model results from all feasible model solutions, and the likelihood of parameter values in smaller and larger sponges was analyzed for mean, SD, and min and max based on 5 and 95% confidence intervals (CI).

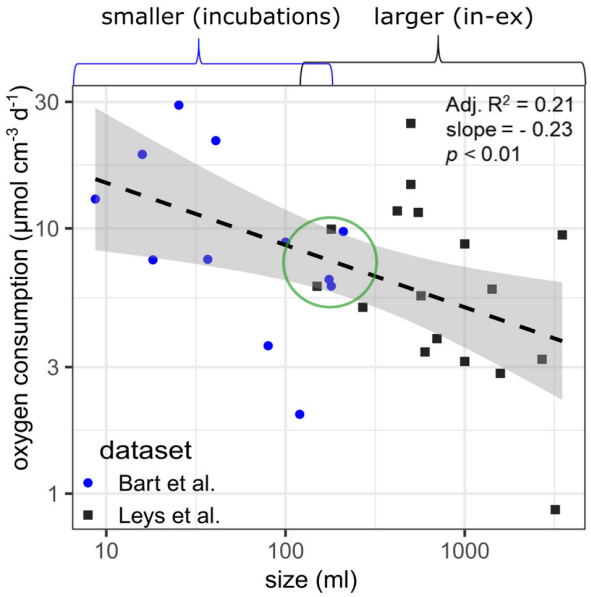

FIGURE 2 | Regression between sponge volume (cm^{-3}) and measured volume-specific oxygen consumption (µmol O_2 cm^{-3} day^{-1}) in *Geodia barretti* by Bart et al. (2020b) (blue circles) and Leys et al. (2018) (dark gray squares). Log-log linear models were used to fit all data (dashed black line). The gray zones indicate the 95% confidence interval. The green circle indicates that the two methods (incubation chambers and in–ex) can produce consistent results (despite the large variability).

RESULTS

Analysis of Measured Flux Data

DIN Exchange in Incubation Chambers

All *G. barretti* showed a net release of NO_3^-, corrected to control incubations in which NO_3^- concentrations remained constant (**Supporting Figure 1**), of, on average, 0.95 ± 0.79 µmol N cm^{-3} day^{-1} (mean ± SD, used throughout text, n = 12, **Table 1**). NO_3^- release was positively correlated to O_2 consumption (r = 0.82, p < 0.01, n = 12). The NO_2^- and NH_4^+ concentrations in the chambers did not significantly change (*i.e.*, the regression slope was not significant) during incubations with sponges and neither in control incubations without sponges (**Supporting Figure 1**). Although the concentration changes were insignificant, we calculated control-corrected NO_2^- and NH_4^+ fluxes to obtain feasible ranges for the metabolic network model analysis. The average (control-corrected) NO_2^- release and NH_4^+ release rates by *G. barretti* in incubation chambers were 0.023 ± 0.069 and 0.061 ± 0.47 µmol N cm^{-3} day^{-1}, respectively (n = 12, **Table 1**).

Size Relationships

The datasets of smaller *G. barretti* individuals (9–210 ml in incubation chambers) and larger *G. barretti* individuals (150–3,500 ml with in–ex) were analyzed together to explore for allometric relationships in data. A statistically significant allometric relationship was found between sponge volume and O_2 consumption rates, although only 21% of the variation could be explained with this regression (**Figure 2**). The allometric equation for volume-specific O_2 consumption rates (vOcr, µmol cm^{-3} day^{-1}) as a function of volume (V, cm^{-3}) for *G. barretti* is: $vOcr = 25.5 \cdot V^{-0.23}$ ($p < 0.01$, $R^2 = 0.21$, $n = 29$, **Figure 2**). No temperature correction was needed since all data were collected at a similar temperature of 8–9°C. At overlapping sizes, O_2 consumption rates are comparable between the two datasets (green circle, **Figure 2**). No allometric relations were found for DIN net exchange data (data not shown).

Model Results

The equalities (hard constraints) and inequalities (soft constraints) were internally consistent, as the model was able to resolve an internal metabolic flux network for smaller and larger *G. barretti* sponges (**Table 3**). As imposed with measured metabolic flux data (**Table 1**), almost all model-produced metabolic rates (µmol cm^{-3} day^{-1}) were higher in smaller compared to larger specimens (**Table 3**), except the assimilation of bacteria (r1), which was higher in larger sponges (**Tables 1**, **3**). However, the overall relative partitioning of internal C- and N-transforming processes was similar for smaller and larger sponge individuals (**Figures 3**, **4**).

Sponge Host Metabolism

G. barretti metabolism was dominated by heterotrophy, with DOM as primary food source (**Table 3** and **Figure 3**). DOM assimilation and aerobic respiration by the sponge (holobiont) (r2) were the main heterotrophic processes in *G. barretti*, independent of size (**Table 3** and **Figure 3**). Because this process dominated sponge metabolism, it was also most sensitive to

TABLE 3 | Metabolic network model results for smaller and larger *Geodia barretti* for C/O_2 and N.

	Smaller sponges—incubations				Larger sponges—in–ex			
	C/O_2		N		C/O_2		N	
	Mean	SD	Mean	SD	Mean	SD	Mean	SD
Fluxes (μmol cm^{-3} day^{-1})								
Bacteria assimilation (r1)	0.15	0.090	0.031	0.019	0.30	0.064	0.062	0.015
Dissolved organic matter (DOM) assimilation (r2)	14.0	4.5	1.9	0.74	4.4	1.1	0.60	0.17
Denitrification (r3) (DOC-NO_3^-)	0.81	0.62	0.47	0.35	0.19	0.16	0.11	0.09
DNRA (r4) (DOC-NO_3^-)	4.5	2.7	1.9	1.1	1.5	0.90	0.62	0.39
NH_4^+ oxidation (r5)			3.0	1.2			1.1	0.39
NO_2^- oxidation (r6)			2.9	1.2			1.1	0.39
Production - nitrification (r7)	0.28	0.13	0.067	0.032	0.10	0.043	0.025	0.010
Anammox (r8)			0.011	0.0094			0.0051	0.0050
Production (r10)	6.5	2.9	1.5	0.68	1.7	0.59	0.40	0.14
Total DOM uptake (r11)	19.3	4.0	2.6	0.79	6.1	0.93	0.82	0.17
Oxygen uptake (r12)	15.8	2.5			6.1	1.0		
NH_4^+ exchange (r13)			0.017	0.26			0.010	0.0019
NO_3^- release (r14)			−0.59	0.32			−0.40	0.10
NO_2^- exchange (r15)			−0.022	0.027			0.019	0.0073
CO_2 release (r16)	−12.9	2.1			−4.7	0.83		
N_2 release (r17)			−0.49	0.37			−0.12	0.10
Fractions and efficiencies (%) and ratios (-)								
Production efficiency on DOM	31	9	55	14	24	8	42	12
Production efficiency (total)	31	14	57	12	24	8	45	11
Fraction microbial production to total production	28	16	28	16	32	16	32	16
Fraction chemoautotrophy to total production	5.1	3.0	5.1	3.0	6.7	2.9	6.7	2.9
RQ	1.23	0.065			1.30	0.055		
Fraction denitrification to nitrification			18	15			11	10
Fraction DNRA of nitrification			58	21			50	20

Release is indicated with a negative sign.

input parameters. Lower values of $C:N_{DOM}$ input range (**Table 2**) resulted in more feasible model solutions (**Figure 5**). Feasible $C:N_{DOM}$ values averaged 7.6 ± 1.4 in both smaller and larger sponges (**Figure 5**). Higher values of $f_{p_N_{DOM}}$ from the rather wide input range (20–80%, **Table 2**) resulted in more feasible model solutions in smaller sponges, while the opposite was found in larger sponges (**Figure 5**). The averages of feasible $f_{p_N_{DOM}}$ values were 58 ± 18% in smaller sponges compared to 41 ± 17% in larger sponges (**Figures 5**, **6**). The corresponding average C production efficiency ($f_{p_C_{DOM}}$) was 33 ± 12% in smaller sponges and 24 ± 11% in larger sponges (**Figures 5**, **6**). The associated C (biomass) production rate was 4.8 ± 2.8 and 1.0 ± 0.55 μmol C cm^{-3} day^{-1} in smaller and larger sponges, respectively (**Figures 3**, **6**). The majority of assimilated DOC, *i.e.*, 67 ± 12% in smaller sponges and 76 ± 11% in larger sponges, was aerobically respired to CO_2 (**Figure 6**).

Microbial N-Transforming Processes

Oxic N-transforming processes dominated over anoxic N-transforming processes necessary to create a net NO_3^- release (**Table 3** and **Figures 4**, **6**). The dominant microbial N-transforming processes were nitrification (r5–r6) and DNRA (r4) (**Table 3**, **Figure 4**). The nitrification rates in smaller sponges ranged from 1.1 to 5.1 μmol N cm^{-3} day^{-1} (5–95% confidence interval), with an average of 3.0 ± 1.2 μmol N cm^{-3} day^{-1} (**Table 3** and **Figures 4**, **6**). The nitrification rates in larger sponges ranged from 0.51 to 1.8 μmol N cm^{-3} day^{-1} (1.1 ± 0.39 μmol N cm^{-3} day^{-1}; **Table 3** and **Figures 4**, **6**). Nitrification was responsible for 38 ± 14% of the O_2 consumption, independent of sponge size. Nitrification (r5–r6) and DNRA (r4) are positively related: nitrification uses the produced substrate of DNRA (NH_4^+) and *vice versa*. The model results indicate that N cycling from coupled NH_4^+ / NO_3^- conversion in DNRA and nitrification is 58 ± 21% of nitrification in smaller sponges and 50 ± 20% in larger sponges (**Table 3** and **Figure 6**). The remaining part of NH_4^+ comes from the mineralization of organic N (r1–r4) (**Figure 6**). The modeled DNRA and nitrification rates were sensitive to the imposed maximum ratio DNRA *vs.* aerobic respiration (r4 *vs.* r2) because more O_2 is available to nitrification if OM is mineralized anaerobically (*via* DNRA) compared to aerobic mineralization (r2) (**Supplementary Figure 2**). Denitrification rates (r3) were consistently below DNRA rates (r4) in both sponges (**Table 3** and **Figure 4**). The anammox rates, which were constrained to be below denitrification rates, were the lowest of all nitrogen-transforming rates (**Table 3** and **Figure 4**). N_2 loss *via* denitrification was 18 ± 15% of

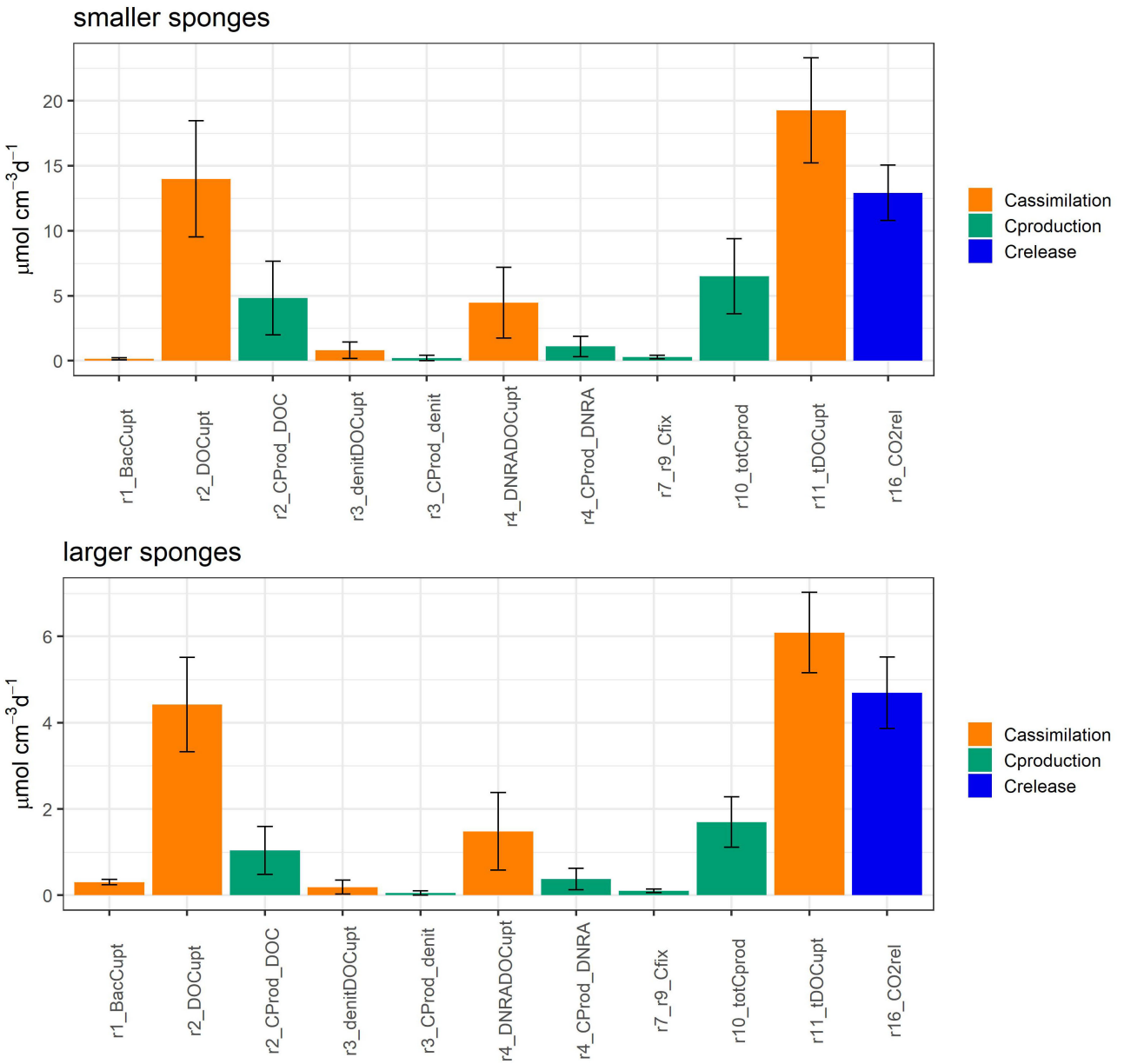

FIGURE 3 | Model-calculated average C fluxes ± SD (µmol C cm^{-3} day^{-1}) in smaller *Geodia barretti* specimens (top) and larger *G. barretti* specimens (bottom). *G. barretti* assimilates bacteria (r1_BacCupt) and mainly dissolved organic carbon (r11_tDOCupt), which is used for aerobic respiration (r2_DOCupt), denitrification (r3_denitDOCupt), and DNRA (r4_DNRA_DOCupt). Production processes are shown in green, where r10_totCprod is the total C (biomass) production by the holobiont. r16_CO2rel (blue) is the net CO_2 release rate. The reaction numbers correspond to **Figure 1** and **Table 2**.

nitrification in smaller sponges and 11 ± 10% in larger sponges (**Table 3** and **Figures 4**, **6**). The N_2 release rates were 0.49 ± 0.37 and 0.12 ± 0.10 µmol N cm^{-3} day^{-1} in smaller and larger sponges, respectively (**Table 3** and **Figure 6**).

Microbial symbiont C (biomass) production was 1.6 ± 1.1 µmol C cm^{-3} day^{-1} in smaller sponges, from which 1.3 ± 0.98 µmol C cm^{-3} day^{-1} came from heterotrophy (denitrification, DNRA) and 0.28 ± 0.13 µmol C cm^{-3} day^{-1} came from chemoautotrophy (nitrification, anammox) (**Figures 3**, **6** and **Table 3**). In larger sponges, symbiont C (biomass) production was 0.53 ± 0.34 µmol C cm^{-3} day^{-1}, from which 0.43 ± 0.30 µmol C cm^{-3} day^{-1} came from heterotrophy and 0.10 ± 0.043 µmol C cm^{-3} day^{-1} came from chemoautotrophy (**Figures 3**, **6** and **Table 3**).

Integrated Holobiont Metabolism and Net Exchange

Integrated *G. baretti* holobiont metabolism comprises biomass production rates and efficiencies of sponge and microbial symbionts. The holobiont production (r10) rates in smaller sponges were 6.5 ± 2.9 µmol C cm^{-3} day^{-1} and 1.5 ± 0.68 µmol

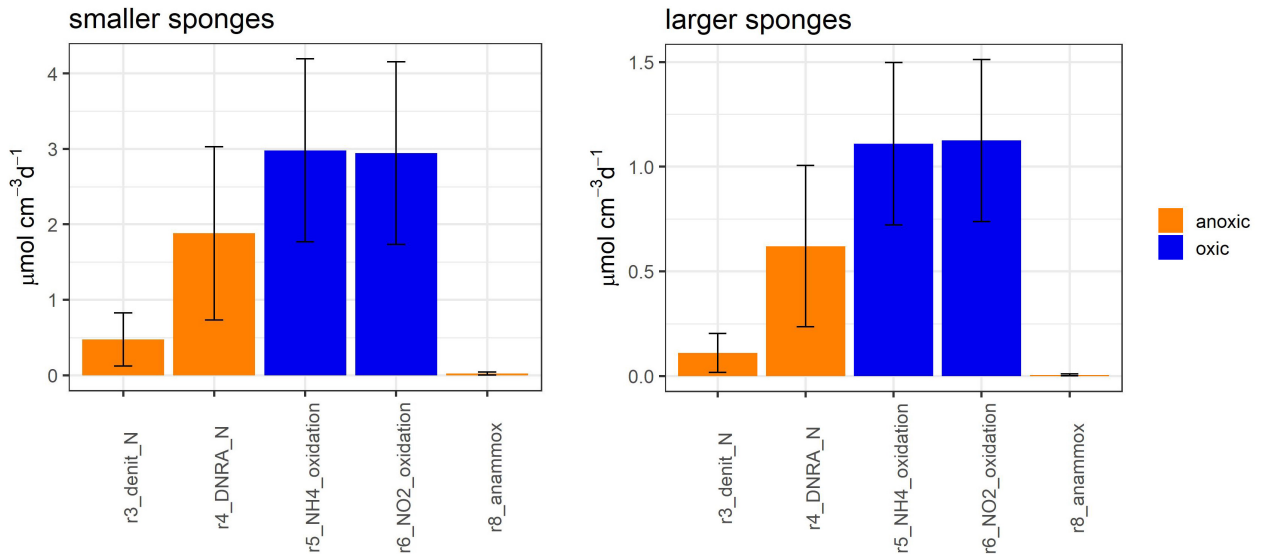

FIGURE 4 | Model-calculated metabolic aerobic (blue) and anaerobic (orange) nitrogen-transforming fluxes in smaller *Geodia barretti* individuals (left) and larger *G. barretti* individuals (right). The reaction numbers refer to **Figure 2** and **Table 2**.

N cm^{-3} day^{-1} (C:N = 4.2) (**Table 3** and **Figures 3**, **6**), with an estimated contribution of 28 ± 16% by nitrogen-transforming symbionts, comprising 5.1 ± 3.0% of total production from chemoautotrophy. The holobiont production (r10) in larger sponges was 1.7 ± 0.59 µmol C cm^{-3} day^{-1} and 0.40 ± 0.14 µmol N cm^{-3} day^{-1} (C:N = 4.2) (**Table 3** and **Figures 3**, **6**), with a contribution of 32 ± 16% by nitrogen-transforming symbionts, comprising 6.7 ± 2.9% of total production from chemoautotrophy. Overall production efficiencies for all assimilated OM, including bacterial uptake [production / assimilated OM, r10/(r11 + r1)], were 31 ± 14% for C and 57 ± 12% for N in smaller sponges compared to 24 ± 8% for C and 45 ± 11% for N in larger sponges (**Table 3**). The CO_2 release rates were 13 ± 2.1 µmol C cm^{-3} day^{-1} in smaller *G. barretti* and 4.7 ± 0. 83 µmol C cm^{-3} day^{-1} in larger *G. barretti* (**Table 3** and **Figures 3**, **6**). The overall RQ (O_2: CO_2) was 1.23 ± 0.065 in smaller *G. barretti* and 1.30 ± 0.056 in larger *G. barretti* (**Table 3**).

The model-calculated exchange rates of O_2 and NO_3^- comprised a smaller range compared to the measured rates (compare **Tables 1**, **3**) because not all combinations of flux measurements resulted in feasible model solutions. The average model-based NO_3^- release rates were lower compared to the averages of the measured rates because more feasible solutions were obtained at the low end of measured NO_3^- release rates (compare **Tables 1**, **3**). Higher O_2 uptake values from the measured range resulted in more feasible solutions in smaller sponges, while the opposite occurred in large sponges (compare **Tables 1**, **3**).

Specific Rates

Specific rates (day^{-1}) are derived from C-based reaction rates (µmol C cm^{-3} day^{-1}) (**Table 3**) relative to C content (M, µmol cm^{-3}; **Table 1**). The specific assimilation rates derived from total organic matter consumption (r1 + r11) were 4.7 10^{-3} and 2.0 × 10^{-3} day^{-1} for smaller and larger sponges, respectively (**Table 4**). Daily production rates (r10) were 1.6 × 10^{-3} (0.16%) and 0.67 × 10^{-3} (0.067%) day^{-1} for smaller and larger sponges, respectively (**Table 4**), indicative of allometric scaling.

DISCUSSION

The aim of this study was to infer internal C and N metabolic conversions in a deep-sea sponge holobiont system. To this end, a metabolic network model integrating C and N metabolism of the sponge *G. barretti* and its microbial symbionts was developed. The presented model can serve as a valuable data analysis tool to quantify internal and intermediate routes in sponge metabolism given any metabolic dataset. In this study, we used two independent metabolic datasets to constrain internal *G. barretti* metabolism that encompassed a range of sponge volumes. The model results indicate that *G. barretti* has complex but flexible metabolism consisting of aerobic and anaerobic processes. The measured fluxes and model metabolic results suggest that specific metabolic rates decline with increasing *G. barretti* size, while the ratios between oxic and anoxic processes and between sponge host and microbial metabolism seem rather independent of size.

Organic Matter Assimilation by *G. barretti*

The measured DOC assimilation rates (Bart et al., 2020b) as well as the estimated DOC assimilation rates (*i.e.*, not directly measured but derived from TOC; Leys et al., 2018) show that DOC is the dominant C source (> 90%) that fuels

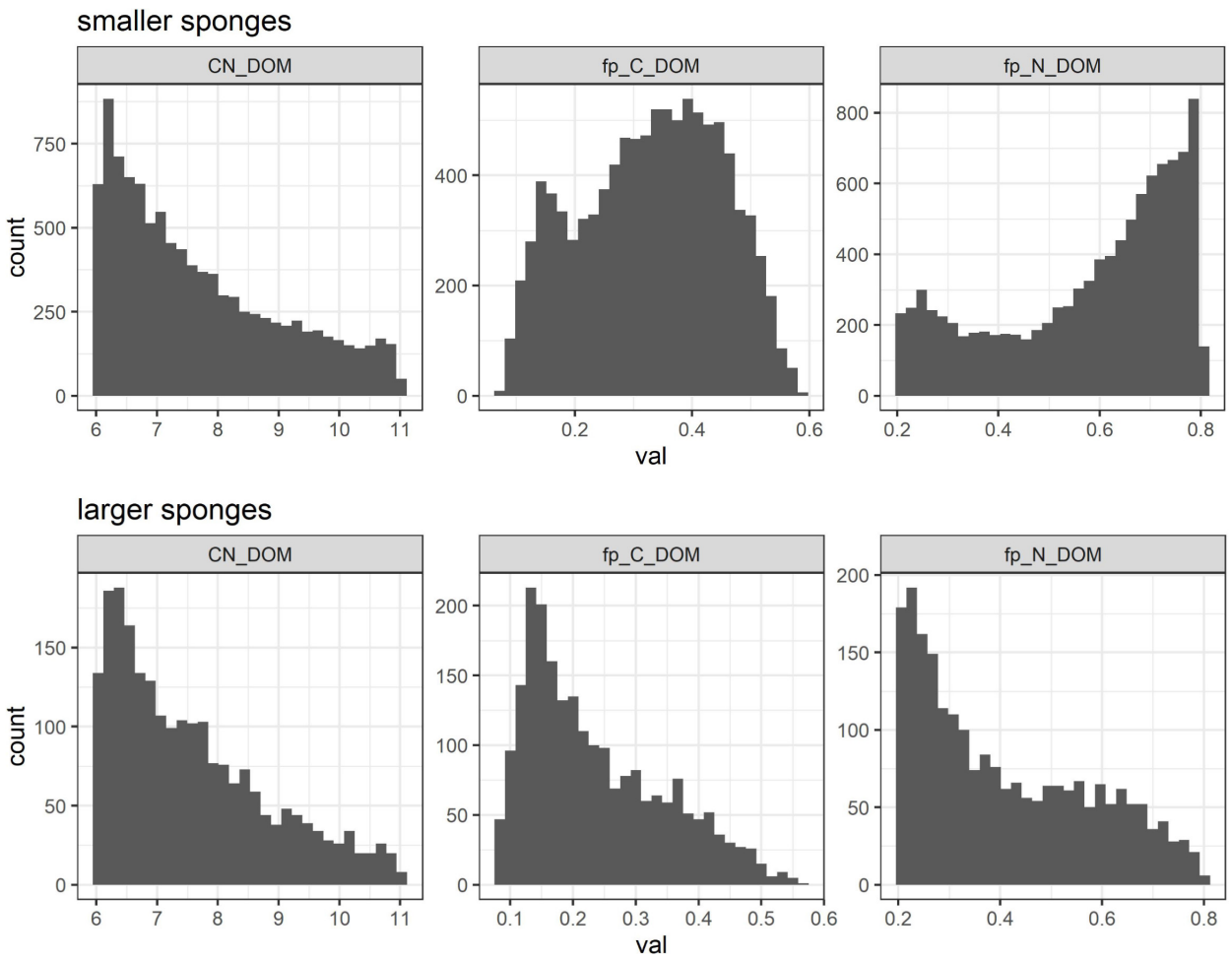

FIGURE 5 | Distribution of coefficients in reaction 2 [(DOM) assimilation and aerobic respiration] to produce feasible model solutions: stoichiometry (C:N) of DOM (left) and C (middle) and N (right) production efficiencies in smaller (top) and larger (bottom) *Geodia barretti*.

G. barretti metabolism. Our metabolic network analysis showed that assimilated DOM serves multiple purposes, since it is used as energy source for aerobic and anaerobic respiration and as a substrate to produce sponge (holobiont) biomass (**Table 3** and **Figures 3**, **6**). While the DOC assimilation rates were available to constrain the model, the stoichiometry (molar C:N ratio) of assimilated DOM was not known *a priori* and was inferred by uncertainty analysis (**Figure 5**). DOM assimilation was feasible when DOM had a C:N < 9 (**Figure 5**). This indicates a preference for N-rich DOM because the reported bulk C:N ratios for DOM range from 9 for fresh (labile) to 17 for more refractory material (Hopkinson and Vallino, 2005). Sponges are recently shown to be more selective feeders than traditionally assumed on both particulate (*e.g.*, plankton) (Maldonado et al., 2010; McMurray et al., 2016) and dissolved organic food (Fiore et al., 2017). Selective assimilation (and retention) of N-rich organic matter by *G. barretti* and other deep-sea sponges has been demonstrated in tracer assimilation studies using dual-isotope-labeled substrates (Kazanidis et al., 2018; Bart et al., 2020a). Most marine heterotrophs preferentially assimilate N, as they have C:N ratios which are lower than the C:N ratios of available food sources (Steinberg and Landry, 2017). The average C:N ratio of 4.2 for *G. barretti* tissue matches well with the C:N ratios of sponges and other deep-sea North Atlantic benthos that had an average C:N of 3.9 (Parzanini et al., 2018) and with those of marine bacteria (C:N = 4–6; **Table 2**). Whether the preferential assimilation of N-rich DOM is opportunity driven or an actual metabolic requirement of *G. barretti* metabolism remains to be determined. Because sponges filter water for DOM, they will increase the C:N ratio of surrounding seawater DOM as they selectively retain N, which might influence its bioavailability for surrounding seawater bacteria.

As the C and N production efficiencies for *G. barretti* and other deep-sea sponges were largely unknown, they were inferred by sensitivity analysis (**Figure 5**). Our estimated C production efficiency values of 24 ± 8% in larger individuals and 31 ± 14% in smaller individuals (**Table 3** and **Figures 3**, **5**, **6**) are within the reported range of 20–30% for metazoans (Sterner and Elser, 2002) and ∼30% in pelagic marine

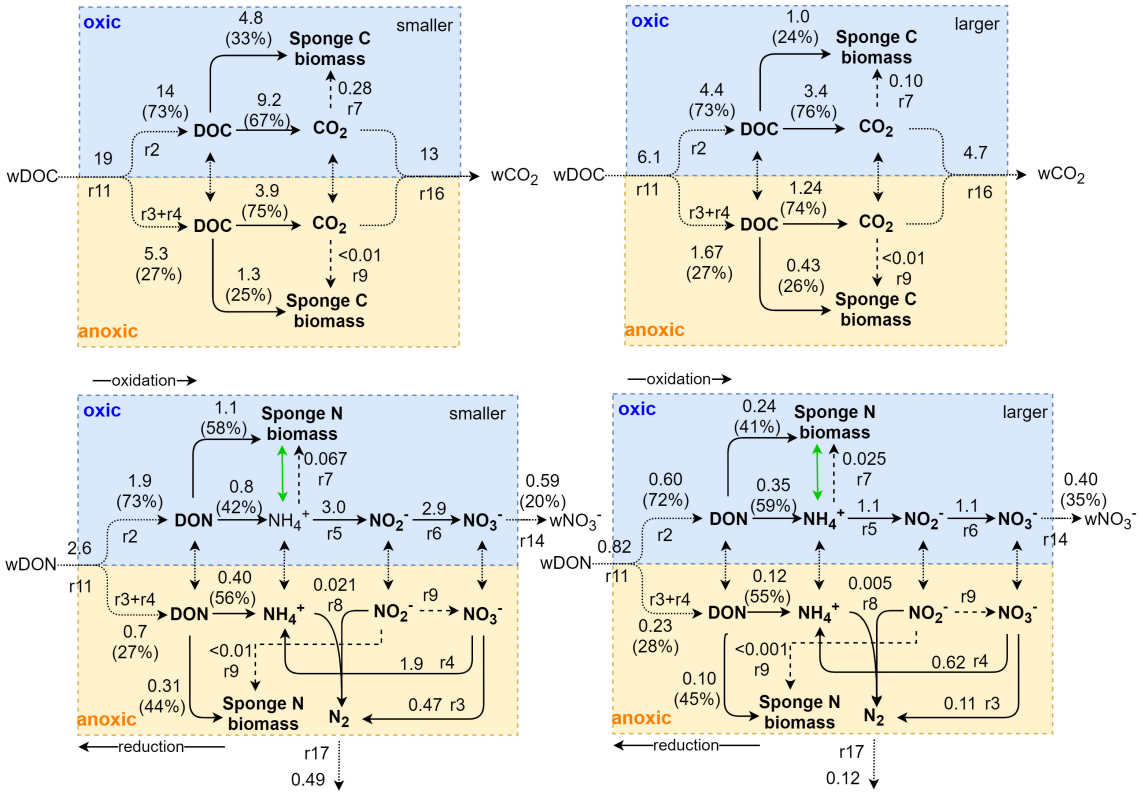

FIGURE 6 | Schematic representation of internal C and N metabolism in *Geodia barretti*. Metabolic processes are indicated with solid arrows with reaction (r) numbers corresponding to those of **Figure 2** and **Table 2**. Aerobic and anaerobic processes are separated in the blue and yellow part, respectively. Exchange fluxes are shown with dotted arrows. Model-calculated average metabolic rates in μmol C cm^{-3} day^{-1} or μmol N cm^{-3} day^{-1}, shown adjacent to arrows, differ between smaller and larger *G. barretti* (right). The partition of dissolved organic matter to oxic and anoxic processes and to (C and N) sponge biomass production and respiration are shown with percentages. Dashed arrows indicate chemoautotrophic processes. Internal NH_4^+ excretion and re-assimilation, shown by the green arrow, is expected to take place but is not explicitly modeled. Bacteria uptake (r1) and NO_2^- (r15) and NH_4^+ (r13) exchange are not shown for simplicity.

microbes in the same temperature range (Rivkin and Legendre, 2001). High production efficiencies for *G. barretti* (∼80%) have been reported in isotope tracer studies with labeled diatom DOM and marine bacteria (Maier et al., 2020; Bart et al., 2020b). In contrast, the encrusting deep-sea sponge *Hymedesmia coricea* had a maximum production efficiency of 10% when fed with stable-isotope-labeled algae and bacteria for 10 days (van Oevelen et al., 2018). Although isotope tracer experiments are advantageous to identify and quantify certain metabolic routes, the obtained values might depend on the incubation time and are representative for the added isotopically labeled substrates only, making it hard to compare the uptake efficiencies to natural diet C and N processing rates. Compared to C production efficiencies, very little information is available on N production efficiencies, especially in sponges. Our estimated N production efficiencies (57 ± 14% in smaller *G. barretti* and 45 ± 11% in larger *G. barretti*) (**Table 3** and **Figures 5**, **6**) are comparable to (larger sponges) or above (smaller sponges) those of 40–50% reported for marine zooplankton and bacteria (Touratier et al., 1999). The presence of genes for NH_4^+ assimilation through glutamine metabolism in *G. barretti* (Gavriilidou, personal communication) and several other sponges (Hentschel et al., 2012) is a possible explanation for the slightly higher N production efficiencies in *G. barretti* compared to those in other organisms. Overall, our estimated values for the C:N ratio of assimilated DOM and the C and N production efficiencies agree with previous estimates for marine organisms, indicating that our model produces reasonable results and might serve as a valuable tool to estimate the efficiencies by which assimilated food is turned into production.

Most of the assimilated DOC (76 ± 8% in larger sponges and 69 ± 9% in smaller sponges) was respired to CO_2 (**Figures 3**, **6**). Model quantification of net CO_2 release rate (respiration minus fixation) relative to O_2 consumption allowed us to estimate an integrated RQ. The estimated RQ values (O_2:CO_2) were very similar between the two datasets, 1.25–1.30 ± 0.06 (**Table 3**; 0.77–0.80 for CO_2:O_2), a value in between complete mineralization of Redfield DOM to NH_4^+ (1.16) and NO_3^- (1.43) (Del Giorgio and Williams, 2005; Middelburg, 2019). These values can be used to translate measured O_2 consumption into C respiration as has been done previously using RQ values of 1 (Kutti et al., 2013; Maier et al., 2020; Bart et al., 2020b), 1.30 (Cathalot et al., 2015, closest to our estimates), and 1.4 (Leys et al., 2018).

Microbial Nitrogen-Transforming Processes

In contrast to most marine animals, several sponge species (in particular, HMA demosponges) release NO_3^- rather than NH_4^+ (Jiménez and Ribes, 2007; Keesing et al., 2013). NO_3^- release also seems a consistent feature of *G. barretti* as observed in incubation studies with intact *G. barretti* (Bart et al., 2020b; also presented in this study), explants (Strand et al., 2017; Fang et al., 2018), and tissue fragments (Hoffmann et al., 2009) and by direct in–ex measurements in intact *G. barretti* (Leys et al., 2018). The average measured NO_3^- release by intact *G. barretti* in incubation chambers (0.95 ± 0.79 μmol N cm^{-3} day^{-1}; **Table 1**) was at the high end compared to average values of 0.20–0.65 μmol N cm^{-3} day^{-1} in explants and fragments (Radax et al., 2012; Strand et al., 2017; Fang et al., 2018). A plausible explanation for the higher NO_3^- release in intact sponges is that the functional integration between the host sponge and the microbiome has not been disrupted and that active pumping (not possible within tissue fragments) results in better tissue oxygenation. Indeed a positive relation between O_2 consumption and NO_3^- release in incubation chambers was found to be in agreement with Fang et al. (2018). The NH_4^+ and NO_2^- exchange rates were much smaller compared to the NO_3^- release rates as observed by direct in–ex measurements and incubation experiments with *G. barretti* (this study; Fang et al., 2018) (**Table 1**). This implies that most substrate for nitrification is produced internally either *via* sponge cell excretion of NH_4^+ as metabolic waste or *via* microbial DNRA (**Figures 2**, **6**).

All model-based internal N-transforming process rates were higher compared to previous estimates from isotope tracer incubations with *G. barretti* tissue fragments (volume 0.30–0.45 cm^{-3}) (Hoffmann et al., 2009; Rooks et al., 2020). Especially model-inferred nitrification rates in intact sponges were twice (1.1 ± 0.39 μmol cm^{-3} day^{-1} in larger *G. barretti*) to five times (3.0 ± 1.2 μmol cm^{-3} day^{-1} in smaller *G. barretti*) higher compared to rates (0.57 μmol cm^{-3} day^{-1}) that were experimentally obtained by isotope tracer incubations with sponge tissue fragments (Hoffmann et al., 2009; **Table 3** and **Figures 4**, **6**). Furthermore, the model-based denitrification rates (0.18–0.81 μmol cm^{-3} day^{-1}) were high compared to the measured rates of 0.010 μmol cm^{-3} day^{-1} in oxic conditions and 0.16 μmol cm^{-3} day^{-1} in anoxic conditions as obtained by isotope tracer experiments with *G. barretti* tissue fragments (Hoffmann et al., 2009; Rooks et al., 2020; **Table 3** and **Figures 4**, **6**). It might therefore well be that the model-inferred rates from intact (pumping) sponges are more representative from the natural holobiont condition than the rates obtained from just tissue fragments. Anammox genes accompanied with low anammox rates (∼0.003 μmol cm^{-3} day^{-1}) were found in *G. barretti* by Hoffmann et al. (2009) but were absent in *G. barretti* in the study by Rooks et al. (2020). Model-based anammox rates (0.005–0.011 μmol cm^{-3} day^{-1}) imposed to be below denitrification also hardly contributed to nitrogen cycling in *G. barretti* (**Figures 4**, **6**).

Genes (*napA*, *nrfA*) involved in all steps of DNRA have been found in metagenomes of *G. barretti* (Gavriilidou, personal communication) and other deep-sea sponges (Li et al., 2014), but the DNRA process rates in *Geodia* (or other sponges) have not been quantified yet. The model-based DNRA rates were higher than the model-based denitrification rates (**Table 3** and **Figures 4**, **6**). The high organic C concentrations compared to NO_3^- concentrations would indeed favor DNRA (van den Berg et al., 2016), but whether these conditions are found in *G. barretti* remains to be validated. Studies on DNRA and denitrification gene expression might help to understand the relative role of each process, and that information can be used to constrain the rates in the model. It is however likely that DNRA is an important nitrogen-transforming process in *G. barretti*. In an earlier version of the model without DNRA, more NH_4^+ had to be produced by excretion, which was balanced by the assimilation of DOM with an even lower C:N, lower nitrification rates, and NO_3^- release.

Dark carbon fixation rates in *G. barretti* (or other Geodiidae spp.) associated with nitrification and anammox have not yet been experimentally quantified. The first model-based estimates of dark carbon fixation rates for *G. barretti* are presented here (**Table 3** and **Figure 3**), acknowledging the different energy yields from each nitrogen-transforming process (*e.g.*, NH_4^+ oxidation, NO_2^- oxidation, anammox). CO_2 fixation rates contributed only a small fraction of 5.1–6.5% of *G. barretti* production and ∼1.5% of total C assimilation. These contributions are very similar to the range of 0.2–2.1% fixation relative to assimilation for the deep-sea encrusting sponge *Hymedesmia coriacea* (van Duyl et al., 2020). The benefit of hosting nitrifiers by the sponge holobiont is hypothesized to decrease or rapidly inactivate the internal concentration of NH_4^+ produced as metabolic waste, which is possibly toxic to the host cells. In addition, it provides the substrate (NO_3^-) for heterotrophic symbiont production in anoxic parts of the sponges. Combined with the production of DNRA and denitrification, N-transforming processes enhance the metabolic capacity of *G. barretti* and contribute significantly to *G. barretti* production [28 ± 16% (smaller individuals) and 32 ± 16% (larger individuals) of total production] (**Table 3** and **Figure 3**). The substantial production by endosymbionts supports the idea that *G. barretti*, which is a HMA sponge, uses "microbial farming" and phagocytes and digests part of the microbiome as part of heterotrophic feeding.

The model covers N-based metabolism but not sulfur-based metabolism because sulfur data were not available. Both genes for sulfate reduction (heterotrophy) and sulfur oxidation (chemoautotrophy) are found in *G. barretti* (Jensen et al., 2017). The contribution of microbial production to *G. barretti* might become even higher if these processes would be included in the metabolic network model.

TABLE 4 | Model-based specific rates (day^{-1}) for small and larger *Geodia barretti*.

Specific rates (day^{-1})	Smaller	Larger
Assimilation (r1 + r11)	0.0047	0.0020
Respiration (r16)	0.0031	0.0015
Production (r10)	0.0016	0.00067

These rates are derived from model results (μmol C cm^{-3} day^{-1}) per carbon biomass (mmol cm^{-3} day^{-1}).

Size Dependency of Metabolism

Based on the metabolic datasets of Leys et al. (2018) and Bart et al. (2020b), all measured and modeled volume-specific rates, except the assimilation of external bacteria, were lower in larger than smaller sponges (**Tables 1**, **3**). The measured O_2 consumption by *G. barretti* showed large variability within and across the two metabolic datasets, which can be partly attributed (21% based on R^2) to sponge volume (**Figure 2**; Leys et al., 2018; Bart et al., 2020b). The large variability within each metabolic dataset (**Figure 2**) might be linked to the intrinsic variability between individuals, *e.g.*, the physiological and metabolic state of the holobiont (and analytical uncertainty), rather than external conditions as individuals were measured under the same experimental conditions. We cannot exclude that differences across the two metabolic datasets are partially caused by methodology [non-invasive in–ex, but snapshot (minutes) sampling *vs.* incubations, longer time integration (hours), but more prone to incubation effects]. However, comparable estimates of O_2 consumption rates were obtained in sponges of similar size (green circle, **Figure 2**), indicating that the two complementary methods give consistent results.

O_2 consumption in *G. barretti* is directly linked to pumping since pumping supplies sponge tissue with O_2 and *G. barretti* that reduce their pumping activity rapidly become anoxic (Hoffmann et al., 2005; Leys et al., 2018). Lower specific pumping and clearance rates in larger individuals have been shown for some massive (*i.e.*, non-encrusting) sponge species (Reiswig, 1974; Morganti et al., 2019), including *G. barretti* (Leys et al., 2018). Reduced pumping and O_2 uptake in larger-sized ball-shaped sponges might be an effect of longer flow paths in larger individuals, resulting in increasing constraints to oxygenate the whole tissue. Lower O_2 consumption in larger individuals did not result in a shift from aerobic to anaerobic processes. This is surprising because we had presumed that larger sponges would run easily into anoxic conditions at the deepest and less water-irrigated portions of their mesohyl. In contrast, the results suggest that all mesohyl regions are similarly, well irrigated by the network of aquiferous canals. However, it could be that any metabolic differences were masked by the large uncertainty associated with aerobic and anaerobic N-transforming processes (**Figure 4**). It will be interesting to compare microbial community structure between smaller- and larger-sized *G. barretti* to see how that changes with size.

The lower production efficiencies (24 ± 8% for C, 45 ± 11% for N; **Table 3** and **Figure 5**) and production rates (0.067% day^{-1}; **Table 4**) in larger *G. barretti* compared to smaller *G. barretti* (31 ± 14% for C, 57 ± 12% for N; **Table 3** and **Figure 5**; 0.19% day^{-1}, **Table 4**) fit with theoretical predictions that production efficiencies decrease with size (Banse, 1979; Sterner and Elser, 2002) because organisms cannot grow infinitely. Larger individuals will relatively use more energy for maintenance, while smaller individuals will allocate more energy to growth. Reiswig (1973) measured oscula growth in tubular sponge populations and observed that smaller individuals grow faster than larger individuals of the same sponge species and that a sharp decline in growth rate occurred when sponges reached maturity and started reproducing, thus allocating energy to gametes.

Sponge (Biomass) Production

Production by the sponge holobiont is allocated to various processes, which are mainly growth, reproduction, and renewal. The magnitudes and portions of each flow are largely unquantified for *Geodia* (and other deep-sea sponges). Therefore, we did not go any further with our model beyond estimating production by the sponge holobiont. Our production rates for *G. barretti* of 0.16% day^{-1} in smaller sponges and 0.067% day^{-1} in larger sponges (**Table 4**) seem low compared to modeled estimates for deep-sea sponges (0.23% day^{-1}; Gontikaki et al., 2011), but not unrealistic as Geodiidae are generally considered to be slow growing. The yearly production would be 0.15 $year^{-1}$ for larger sponges and 0.57 $year^{-1}$ for smaller sponges, although temporal upscaling comes with large uncertainty as sponge metabolism, related to environmental conditions, might vary seasonally (Koopmans and Wijffels, 2008; Morley et al., 2016). Several sponge species (*e.g.*, de Goeij et al., 2013; Alexander et al., 2014; Maldonado, 2016), including deep-sea species (Witte et al., 1997; Rix et al., 2016), release a substantial (up to 10% day^{-1}) part of biomass as sponge detritus, but other studies show no or only limited production by (mostly non-encrusting) species (*e.g.*, Yahel et al., 2007; Maldonado, 2016; McMurray et al., 2018; Pawlik and McMurray, 2020). Sponge detritus production by *G. barretti* was found to be low (Leys et al., 2018; Maier et al., 2020). Maier et al. (2020) estimated detritus release by *G. barretti* from tracer experiments as 0.03% day^{-1}, which would still be 19–44% of our estimated sponge production. However, because of their efficiency in turning metabolic waste into new products, it could also be that any organic waste gets recycled within the holobiont rather than excreted. The low production rates, from which only an unconstrained fraction will be used for net growth, can explain why this sponge species is typically considered slow growing.

Ecosystem Context Using Model Estimations

The metabolic activity of *G. barretti* influences local C and N cycling at the benthic boundary layer, given the enormous abundance of this species over the extensive deep-sea area of the boreal region, forming the so-called *Geodia* grounds (Pham et al., 2019). *G. barretti* and other Geodiidae can make up > 90% of total benthic biomass (Klitgaard and Tendal, 2004; Murillo et al., 2012) in these regions at up to 6 kg WW m^{-2} (Klitgaard and Tendal, 2004; Kutti et al., 2013), although their distribution is patchy (Pham et al., 2019). Our sponge metabolic model results may aid in the first estimates of biogeochemical fluxes of C and N in these areas, specifically when only a subset of fluxes or environmental settings is known (*e.g.*, only O_2 fluxes, no C or N). For example, *Geodia* grounds have been identified as hotspots of metabolic activity compared to bare sediments (Kutti et al., 2013; Cathalot et al., 2015), showing one order of magnitude higher O_2 consumption at high-abundance sponge grounds than for bare sediments (54 *versus* 6 mmol O_2 m^{-2} day^{-1}; based on 3 kg *G. barretti* WW m^{-2}; Cathalot et al., 2015). Using our model-estimated RQ and C:N conversions, future studies can now approximate C and N fluxes based on *in situ*-assessed O_2 fluxes

alone. For example, *G. barretti* enhances nutrient recycling *via* DIN (NO_3^-) release (0.4–1.1 mmol N m^{-2} day^{-1} for a biomass of 1–3 kg WW m^{-2}), which is comparable to or in excess of values typical for marine sediments [0.06 mmol N m^{-2} day^{-1} in the north Norwegian coast (Glud et al., 1998) to 0.64 mmol N m^{-2} day^{-1} in Logachev mound province, North-Atlantic (de Froe et al., 2019)]. However, sponge grounds are also a sink for N, as they release N_2 at rates of 0.1–0.3 mmol N m^{-2} day^{-1}, comparable to fluxes found in shelf sediments (0.1–1.0 mmol N m^{-2} day^{-1}; Middelburg et al., 1996; Seitzinger and Giblin, 1996).

Care must be taken, however, since, on a larger ecosystem scale, the average *G. barretti* biomass in the south-west Barents Sea region (*i.e.*, Trømso Plateau, North Cap bank, and areas in between; approximately 125,000 km^2) is ∼50 g WW m^{-2} (Anisimova et al., 2010; Kêdra et al., 2017) and is even lower within the entire Barents Sea (∼15 g WW sponge m^{-2}, 1.5 million km^2; Wassmann et al., 2006). This points to orders-of-magnitude differences in local (see above) *versus* ecosystem-scale biogeochemical fluxes driven by sponges, including many species other than *G. barretti* from different phyla. In addition to (largely unknown) variations in metabolic rates between sponge species, the effect of metabolic rates under varying environmental conditions, including seasonality or hydrodynamics, is not yet well understood, considering the two available datasets that we used for our model.

Another important aspect of our model that can improve the ecological context of deep-sea sponges and sponge grounds is the size dependence on metabolic rates. Currently, benthic biomass estimations in deep-sea ecosystems, such as the Barents Sea, are largely based on trawl catch data (*e.g.*, Wassmann et al., 2006; Jørgensen et al., 2014). Trawling is an invasive and only semi-quantitative (but cost-effective) method to assess benthic biomass and is generally skewed to larger individuals. The abundance and size distributions of deep-sea sponges can be better quantified on a larger scale by the non-invasive method of video transects (*e.g.*, Kutti et al., 2013; Kêdra et al., 2017; Kazanidis et al., 2019; Maldonado et al., 2020b). Those data, combined with our modeled biogeochemical rates and efficiencies for different size classes of sponges, will further allow (first estimates of) quantifications of biogeochemical fluxes in sponge grounds of the NorthAtlantic Ocean and assess the functional integration of these sponge-dominated communities into deep-sea ecosystems.

DATA AVAILABILITY STATEMENT

The dataset of Leys et al. (2018) is available at University of Alberta Education and Research Archive: doi: 10.7939/R3057D48V. The dataset of Bart et al. (2020b) will be made available at Pangaea. The model input files and R scripts are available on Zenodo: doi: 10.5281/zenodo.4139792.

AUTHOR CONTRIBUTIONS

AK developed the model, performed the data analyses and model analyses, prepared the figures, and wrote the manuscript. MB and JG designed and conducted the incubation experiments, performed nutrient analyses, and contributed to the writing of the manuscript. SV contributed to model conceptualization and development. JM acquired funding and contributed to the conceptualization of the model, interpretation, and writing of the manuscript. MM contributed to the conceptualization of the model, interpretation, and writing. SL and SM contributed data for model development. KS contributed technically with model implementation and analyses. DO designed the model, contributed to model development and interpretation, and writing of the manuscript. All authors contributed to the article and approved the submitted version.

FUNDING

This research has been performed in the scope of the EU SponGES project, which received funding from the European Union's Horizon 2020 Research and Innovation Program under grant agreement no. 679849. Further support included ERC starting grant agreement no. 715513 to JG and the Netherlands Earth System Science Center to JM. This document reflects only the authors' views, and the Executive Agency for Small and Medium-sized Enterprises (EASME) is not responsible for any use that may be made of the information it contains.

ACKNOWLEDGMENTS

Titus Rombouts and Pieter Slot (UvA) and Sharyn Ossebaar (NIOZ) are acknowledged for their analytical assistance with the nutrient measurements of the incubation experiments. We thank Asimenia Gavriilidou and Detmer Sipkema (WUR, SponGES) for their input on the microbial genome in *G. barretti*. We thank last Hans Tore Rapp (UiB) for the excellent project coordination. We would like to thank CF and CR for their valuable and constructive reviews.

SUPPLEMENTARY MATERIAL

The Supplementary Material for this article can be found online at: https://www.frontiersin.org/articles/10.3389/fmars.2020.596251/full#supplementary-material

REFERENCES

Alexander, B. E., Liebrand, K., Osinga, R., Geest, H. G., Van Der, Admiraal, W., et al. (2014). Cell turnover and detritus production in marine sponges from tropical and temperate benthic ecosystems. *PLoS One* 9:e0109486. doi: 10.1371/journal.pone.0109486

Anisimova, N. A., Jørgensen, L. L., Lyubin, P. A., and Manushin, I. E. (2010). *Mapping and Monitoring of Benthos in the Barents Sea and Svalbard waters:*

Results From the Joint Russian - Norwegian Benthic Programme 2006-2008. IMR-PINRO Joint Report Series 1-2010. ISSN 1502-8828. 114 pp.

Banse, K. (1979). On weight dependence of net growth efficiency and specific respiration rates among field populations of invertebrates. *Oecologia* 38, 111–126. doi: 10.1007/bf00346558

Bart, M. C., de Kluijver, A., Hoetjes, S., Absalah, S., Mueller, B., Kenchington, E. L., et al. (2020a). Differential processing of dissolved and particulate organic matter by deep-sea sponges and their microbial symbionts. *Sci. Rep.* 10:17515. doi: 10.1038/s41598-020-74670-0

Bart, M. C., Mueller, B., Rombouts, T., van de Ven, C., Tompkins, G., Osinga, R., et al. (2020b). Dissolved organic carbon (DOC) is essential to balance the metabolic demands of North-Atlantic deep-sea sponges. *Limnol. Oceanogr.* 1–14. doi: 10.1002/lno.11652

Beazley, L., Kenchington, E., Yashayaev, I., and Murillo, F. J. (2015). Drivers of epibenthic megafaunal composition in the sponge grounds of the Sackville Spur, northwest Atlantic. *Deep. Res. Part I Oceanogr. Res. Pap.* 98, 102–114. doi: 10.1016/j.dsr.2014.11.016

Beazley, L. I., Kenchington, E. L., Murillo, F. J., and Sacau, M. (2013). Deep-sea sponge grounds enhance diversity and abundance of epibenthic megafauna in the Northwest Atlantic. *ICES J. Mar. Sci.* 70, 1471–1490. doi: 10.1093/icesjms/fst124

Cathalot, C., Van Oevelen, D., Cox, T. J. S., Kutti, T., Lavaleye, M., Duineveld, G., et al. (2015). Cold-water coral reefs and adjacent sponge grounds: hotspots of benthic respiration and organic carbon cycling in the deep sea. *Front. Mar. Sci.* 2:37. doi: 10.3389/fmars.2015.00037

de Froe, E., Rovelli, L., Glud, R. N., Maier, S. R., Duineveld, G., Mienis, F., et al. (2019). Benthic oxygen and nitrogen exchange on a cold-water coral reef in the north-east Atlantic ocean. *Front. Mar. Sci.* 6:665. doi: 10.3389/fmars.2019.00665

de Goeij, J. M., Lesser, M. P., and Pawlik, J. R. (2017). "Nutrient fluxes and ecological functions of coral reef sponges in a changing ocean," in *Climate Change, Ocean Acidification and Sponges: Impacts Across Multiple Levels of Organization*, eds J. L. Carballo and J. J. Bell (Berlin: Springer), 373–410. doi: 10.1007/978-3-319-59008-0

de Goeij, J. M., van Oevelen, D., Vermeij, M. J. A. A., Osinga, R., Middelburg, J. J., de Goeij, A. F. P. M., et al. (2013). Surviving in a marine desert: the sponge loop retains resources within coral reefs. *Science* 342, 108–110. doi: 10.1126/science.1241981

Del Giorgio, P., and Williams, P. (2005). *Respiration in Aquatic Ecosystems*. Oxford: OUP, doi: 10.1093/acprof:oso/9780198527084.001.0001

Edwards, J. S., and Covert, M. (2002). Metabolic modelling of microbes: the flux-balance approach. *Environ. Microbiol.* 4, 133–140. doi: 10.1046/j.1462-2920.2002.00282.x

Fang, J. K. H., Rooks, C. A., Krogness, C. M., Kutti, T., Hoffmann, F., and Bannister, R. J. (2018). Impact of particulate sediment, bentonite and barite (oil-drilling waste) on net fluxes of oxygen and nitrogen in Arctic-boreal sponges. *Environ. Pollut.* 238, 948–958. doi: 10.1016/j.envpol.2017.11.092

Fiore, C. L., Freeman, C. J., and Kujawinski, E. B. (2017). Sponge exhalent seawater contains a unique chemical profile of dissolved organic matter. *PeerJ* 5:e2870. doi: 10.7717/peerj.2870

Glud, R., Holby, O., Hoffmann, F., and Canfield, D. E. (1998). Benthic mineralization and exchange in Arctic sediments (Svalbard, Norway). *Mar. Ecol. Prog. Ser.* 173, 237–251. doi: 10.3354/meps173237

Gontikaki, E., van Oevelen, D., Soetaert, K., and Witte, U. (2011). Food web flows through a sub-arctic deep-sea benthic community. *Prog. Oceanogr.* 91, 245–259. doi: 10.1016/j.pocean.2010.12.014

Grasshoff, K., Kremling, K., and Ehrhardt, M. (eds) (2009). *Methods of Seawater Analysis*. Weinheim: John Wiley and Sons.

Helder, W., and de Vries, R. T. P. (1979). An automatic phenol-hypochlorite method for the determination of ammonia in sea-and brackish waters. *Neth. J. Sea Res.* 13, 154–160. doi: 10.1016/0077-7579(79)90038-3

Hentschel, U., Piel, J., Degnan, S. M., and Taylor, M. W. (2012). Genomic insights into the marine sponge microbiome. *Nat. Rev. Microbiol.* 10, 641–654. doi: 10.1038/nrmicro2839

Hoffmann, F., Larsen, O., Thiel, V., Rapp, H. T., Pape, T., Michaelis, W., et al. (2005). An Anaerobic World in Sponges. *Geomicrobiol. J.* 22, 1–10. doi: 10.1080/01490450590922505

Hoffmann, F., Radax, R., Woebken, D., Holtappels, M., Lavik, G., Rapp, H. T., et al. (2009). Complex nitrogen cycling in the sponge *Geodia barretti*. *Environ. Microbiol.* 11, 2228–2243. doi: 10.1111/j.1462-2920.2009.01944.x

Hogg, M. M., Tendal, O. S., Conway, K. W., Pomponi, S. A., Van Soest, R. W. M., Gutt, J., et al. (2010). *Deep-Sea Sponge Grounds: Reservoirs of Biodiversity*. Cambridge: UNEP-WCMC. UNEP-WCMC Biodiversity Series No. 32.

Hopkinson, C. S., and Vallino, J. J. (2005). Efficient export of carbon to the deep ocean through dissolved organic matter. *Nature* 433, 142–145. doi: 10.1038/nature03191

Jensen, S., Fortunato, S. A. V., Hoffmann, F., Hoem, S., Rapp, H. T., Øvreås, L., et al. (2017). The relative abundance and transcriptional activity of marine sponge-associated microorganisms emphasizing groups involved in sulfur cycle. *Microb. Ecol.* 73, 668–676. doi: 10.1007/s00248-016-0836-3

Jiménez, E., and Ribes, M. (2007). Sponges as a source of dissolved inorganic nitrogen: nitrification mediated by temperate sponges. *Limnol. Oceanogr.* 52, 948–958. doi: 10.4319/lo.2007.52.3.0948

Jørgensen, L. L., Ljubin, P., Skjoldal, H. R., Ingvaldsen, R. B., Anisimova, N. A., and Manushin, I. (2014). Distribution of benthic megafauna in the Barents Sea: Baseline for an ecosystem approach to management. *ICES J. Mar. Sci.* 72, 595–613. doi: 10.1093/icesjms/fsu106

Kahn, A. S., Yahel, G., Chu, J. W. F., Tunnicliffe, V., and Leys, S. P. (2015). Benthic grazing and carbon sequestration by deep-water glass sponge reefs. *Limnol. Oceanogr.* 60, 78–88. doi: 10.1002/lno.10002

Kazanidis, G., Vad, J., Henry, L. A., Neat, F., Berx, B., Georgoulas, K., et al. (2019). Distribution of deep-sea sponge aggregations in an area of multisectoral activities and changing oceanic conditions. *Front. Mar. Sci.* 6:163. doi: 10.3389/fmars.2019.00163

Kazanidis, G., van Oevelen, D., Veuger, B., and Witte, U. F. M. (2018). Unravelling the versatile feeding and metabolic strategies of the cold-water ecosystem engineer *Spongosorites coralliophaga* (Stephens, 1915). *Deep. Res. Part I Oceanogr. Res. Pap.* 141, 71–82. doi: 10.1016/j.dsr.2018.07.009

Kêdra, M., Renaud, P. E., and Andrade, H. (2017). Epibenthic diversity and productivity on a heavily trawled Barents Sea bank (Tromsøflaket). *Oceanologia* 59, 93–101. doi: 10.1016/j.oceano.2016.12.001

Keesing, J. K., Strzelecki, J., Fromont, J., and Thomson, D. (2013). Sponges as important sources of nitrate on an oligotrophic continental shelf. *Limnol. Oceanogr.* 58, 1947–1958. doi: 10.4319/lo.2013.58.6.1947

Klitgaard, A. B. (1995). The fauna associated with the outer shelf and upper slope sponges (Porifera, Demospongiae) at the Faroe Isands, Northeastern Atlantic. *Sarsia* 80, 1–22. doi: 10.1530/EJE-11-0663

Klitgaard, A. B., and Tendal, O. S. (2004). Distribution and species composition of mass occurrences of large-sized sponges in the northeast Atlantic. *Prog. Oceanogr.* 61, 57–98. doi: 10.1016/j.pocean.2004.06.002

Koeve, W., and Kähler, P. (2010). Heterotrophic denitrification vs. autotrophic anammox-quantifying collateral effects on the oceanic carbon cycle. *Biogeosciences* 7, 2327–2337. doi: 10.5194/bg-7-2327-2010

Koike, I., and Hattori, A. (1975). Energy yield of denitrification: an estimate from growth yield in continuous cultures of *Pseudomonas denitrijicans* under nitrate-, nitrite- and nitrous oxide-limited conditions. *J. Gen. Microbiol.* 88, 11–19. doi: 10.1099/00221287-88-1-11

Koopmans, M., and Wijffels, R. H. (2008). Seasonal growth rate of the sponge *Haliclona oculata* (*Demospongiae*: *Haplosclerida*). *Mar. Biotechnol.* 10, 502–510. doi: 10.1007/s10126-008-9086-9

Kutti, T., Bannister, R. J., and Fosså, J. H. (2013). Community structure and ecological function of deep-water sponge grounds in the Traenadypet MPA-Northern Norwegian continental shelf. *Cont. Shelf Res.* 69, 21–30. doi: 10.1016/j.csr.2013.09.011

Kutti, T., Bannister, R. J., and Fosså, J. H., Krogness, C. M., Tjensvoll, I., and Søvik, G. (2015). Metabolic responses of the deep-water sponge Geodia barretti to suspended bottom sediment, simulated mine tailings and drill cuttings. *J. Exp. Mar. Bio. Ecol.* 473, 64–72. doi: 10.1016/j.jembe.2015.07.017

Leys, S. P., Kahn, A. S., Fang, J. K. H., Kutti, T., and Bannister, R. J. (2018). Phagocytosis of microbial symbionts balances the carbon and nitrogen budget for the deep-water boreal sponge *Geodia barretti*. *Limnol. Oceanogr.* 63, 187–202. doi: 10.1002/lno.10623

Li, Z. Y., Wang, Y. Z., He, L. M., and Zheng, H. J. (2014). Metabolic profiles of prokaryotic and eukaryotic communities in deep-sea sponge *Neamphius huxleyi* indicated by metagenomics. *Sci. Rep.* 4, 1–12. doi: 10.1038/srep03895

Maier, S., Kutti, T., Bannister, R., Fang, J., van Breugel, P., van Rijswijk, P., et al. (2020). Recycling pathways in cold-water coral reefs: use of dissolved organic matter and bacteria by key reef suspension feeders. *Sci. Rep* 10:9942. doi: 10.1038/s41598-020-66463-2

Maldonado, M. (2016). Sponge waste that fuels marine oligotrophic food webs: a re-assessment of its origin and nature. *Mar. Ecol.* 37, 477–491. doi: 10.1111/maec.12256

Maldonado, M., Aguilar, R., Bannister, R. J., Bell, J. J., Conway, K. W., Dayton, P. K., et al. (2017). "Sponge grounds as key marine habitats: a synthetic review of types, structure, functional roles, and conservation concerns," in *Marine Animal Forests the Ecology of Benthic Biodiversity Hotspots*, eds S. Rossi, L. Bramanti, A. Gori, and C. Orejas (Berlin: Springer), 145–183. doi: 10.1007/978-3-319-17001-5

Maldonado, M., Beazley, L., Kenchington, E., Koutsouveli, V., and Riesgo, A. (2020a). Cooperation between passive and active silicon transporters clarifies the ecophysiology and evolution of biosilicification in sponges. *Sci. Adv.* 6:eaba9322. doi: 10.1126/sciadv.aba9322

Maldonado, M., Beazley, L., López-Acosta, M., Kenchington, E., Casault, B., Hanz, U., et al. (2020b). Massive silicon utilization facilitated by a benthic-pelagic coupled feedback sustains deep-sea sponge aggregations. *Limnol. Oceanogr.* 1–26. doi: 10.1002/lno.11610

Maldonado, M., López-Acosta, M., Sitjà, C., García-Puig, M., Galobart, C., Ercilla, G., et al. (2019). Sponge skeletons as an important sink of silicon in the global oceans. *Nat. Geosci.* 12, 815–822. doi: 10.1038/s41561-019-0430-7

Maldonado, M., Ribes, M., and van Duyl, F. C. (2012). Nutrient fluxes through sponges. biology, budgets, and ecological implications. *Adv. Mar. biol.* 62, 113–182. doi: 10.1016/B978-0-12-394283-8.00003-5

Maldonado, M., Zhang, X., Cao, X., Xue, L., Cao, H., and Zhang, W. (2010). Selective feeding by sponges on pathogenic microbes: a reassessment of potential for abatement of microbial pollution. *Mar. Ecol. Prog. Ser.* 403, 75–89. doi: 10.3354/meps08411

McMurray, S. E., Johnson, Z. I., Hunt, D. E., Pawlik, J. R., and Finelli, C. M. (2016). Selective feeding by the giant barrel sponge enhances foraging efficiency. *Limnol. Oceanogr.* 61, 1271–1286. doi: 10.1002/lno.10287

McMurray, S. E., Stubler, A. D., Erwin, P. M., Finelli, C. M., and Pawlik, J. R. (2018). A test of the sponge-loop hypothesis for emergent Caribbean reef sponges. *Mar. Ecol. Prog. Ser.* 588, 1–14. doi: 10.3354/meps12466/

Middelburg, J. J. (2019). *Marine Carbon Biogeochemistry, A Primer for Earth System Scientist*. Cham: Springer Nature, doi: 10.1007/978-3-030-10822-9

Middelburg, J. J., Soetaert, K., Herman, P. M. J., and Heip, C. H. R. (1996). Denitrification in marine sediments: a model study. *Global Biogeochem. Cy.* 10, 661–673. doi: 10.1029/96gb02562

Morganti, T. M., Ribes, M., Yahel, G., and Coma, R. (2019). Size is the major determinant of pumping rates in marine sponges. *Front. Physiol.* 10:1417. doi: 10.3389/fphys.2019.01474

Morley, S. A., Berman, J., Barnes, D. K. A., Carbonell, C., de, J., Downey, R. V., et al. (2016). Extreme phenotypic plasticity in metabolic physiology of Antarctic demosponges. *Front. Ecol. Evol.* 3:157. doi: 10.3389/fevo.2015.00157

Murillo, F. J., Muñoz, P. D., Cristobo, J., Ríos, P., González, C., Kenchington, E., et al. (2012). Deep-sea sponge grounds of the flemish cap, flemish pass and the grand banks of newfoundland (Northwest Atlantic Ocean): distribution and species composition. *Mar. Biol. Res.* 8, 842–854. doi: 10.1080/17451000.2012.682583

Palsson, B. Ø, and Varma, A. (1994). Metabolic flux balancing: basic concepts, scientific and practical use. *Biotechnology* 12, 994–998. doi: 10.1038/nbt1094-994

Parzanini, C., Parrish, C. C., Hamel, J., and Mercier, A. (2018). Trophic relationships of deep-sea benthic invertebrates on a continental margin in the NW Atlantic inferred by stable isotope, elemental, and fatty acid composition. *Prog. Oceanogr.* 168, 279–295. doi: 10.1016/j.pocean.2018.10.007

Pawlik, J. R., and McMurray, S. E. (2020). The emerging ecological and biogeochemical importance of sponges on coral reefs. *Annu. Rev. Mar. Sci.* 12, 3.1–3.23.

Pham, C. K., Murillo, F. J., Lirette, C., Maldonado, M., Colaço, A., Ottaviani, D., et al. (2019). Removal of deep-sea sponges by bottom trawling in the Flemish Cap area: conservation, ecology and economic assessment. *Sci. Rep.* 9, 1–13. doi: 10.1038/s41598-019-52250-1

Pile, A. J., and Young, C. M. (2006). The natural diet of a hexactinellid sponge: benthic-pelagic coupling in a deep-sea microbial food web. *Deep. Res. Part I Oceanogr. Res. Pap.* 53, 1148–1156. doi: 10.1016/j.dsr.2006.03.008

Pita, L., Rix, L., Slaby, B. M., Franke, A., and Hentschel, U. (2018). The sponge holobiont in a changing ocean: from microbes to ecosystems. *Microbiome* 6:46. doi: 10.1186/s40168-018-0428-1

Porada, P., Thurner, M., Winterdahl, M., Beer, C., Vico, G., and Way, D. (2018). Reviews and syntheses: carbon use efficiency from organisms to ecosystems – definitions, theories, and empirical evidence. *Biogeosciences* 15, 5929–5949. doi: 10.5194/bg-15-5929-2018

Prosser, J. I. (2005). ""Nitrification," in *Encyclopedia of Soils in the Environment*, eds D. Hillel and J. L. Hatfield (Amsterdam: Elsevier Inc), 31–39. doi: 10.1016/B0-12-348530-4/00512-9

R Core Team (2018). *R: A Language and Environment for Statistical Computing. R Foundation for Statistical Computing*. Vienna: R Core team.

Radax, R., Hoffmann, F., Rapp, H. T., Leininger, S., and Schleper, C. (2012). Ammonia-oxidizing archaea as main drivers of nitrification in cold-water sponges. *Environ. Microbiol.* 14, 909–923. doi: 10.1111/j.1462-2920.2011.02661.x

Reiswig, H. M. (1973). Coral reef project - papers in memory of Dr. Thomas F. Goreau. 8. population dynamics of three jamaican *Demospongiae*. *Bull. Mar. Sci.* 23, 191–226.

Reiswig, H. M. (1974). Water transport, respiration and energetics of three tropical marine sponges. *J. Exp. Mar. Bio. Ecol.* 14, 231–249. doi: 10.1016/0022-0981(74)90005-7

Rivkin, R. B., and Legendre, L. (2001). Biogenic carbon cycling in the upper ocean: effects of microbial respiration. *Science* 291, 2398–2400. doi: 10.1126/science.291.5512.2398

Rix, L., de Goeij, J. M., Mueller, C. E., Struck, U., Middelburg, J. J., van Duyl, F. C., et al. (2016). Coral mucus fuels the sponge loop in warm- and cold-water coral reef ecosystems. *Sci. Rep.* 6:18715. doi: 10.1038/srep18715

Rooks, C., Fang, J. K.-H., Mørkved, P. T., Zhao, R., Rapp, H. T., Xavier, J. R., et al. (2020). Deep-sea sponge grounds as nutrient sinks: high denitrification rates in boreo-arctic sponges. *Biogeosciences* 17, 1231–1245. doi: 10.5194/bg-17-1231-2020

Seitzinger, S. P., and Giblin, A. E. (1996). Estimating denitrification in North Atlantic continental shelf sediments. *Biogeochemistry* 35, 235–260. doi: 10.1007/bf02179829

Soetaert, K., Herman, P. M. J., and Middelburg, J. J. (1996). A model of early diagenetic processes from the shelf to abyssal depths. *Geochim. Cosmochim. Acta* 60, 1019–1040. doi: 10.1016/0016-7037(96)00013-0

Soetaert, K., and van Oevelen, D. (2009). Modeling food web interactions in benthic deep-sea ecosystems: a practical guide. *Oceanography* 22, 128–143. doi: 10.5670/oceanog.2009.13

Steinberg, D. K., and Landry, M. R. (2017). Zooplankton and the Ocean Carbon Cycle. *Ann. Rev. Mar. Sci.* 9, 413–444. doi: 10.1146/annurev-marine-010814-015924

Sterner, R., and Elser, J. (2002). *Ecological Stoichiometry: The Biology of Elements from Molecules to the Biosphere*. Princeton: Princeton university press.

Strand, R., Whalan, S., Webster, N. S., Kutti, T., Fang, J. K. H., Luter, H. M., et al. (2017). The response of a boreal deep-sea sponge holobiont to acute thermal stress. *Sci. Rep.* 7:1660. doi: 10.1038/s41598-017-01091-x

Strohm, T. O., Griffin, B., Zumft, W. G., and Schink, B. (2007). Growth yields in bacterial denitrification and nitrate ammonification. *Appl. Environ. Microbiol.* 73, 1420–1424. doi: 10.1128/AEM.02508-06

Thamdrup, B. (2012). New pathways and processes in the global nitrogen cycle. *Annu. Rev. Ecol. Evol. Syst. Annu. Rev.* 43, 407–428. doi: 10.1146/annurev-ecolsys-102710-145048

Thomassen, S., and Riisgard, H. U. (1995). Growth and energetics of the sponge *Halichondria panicea*. *Mar. Ecol. Prog. Ser.* 128, 239–246. doi: 10.3354/meps128239

Touratier, F., Legendre, L., and Vézina, A. (1999). Model of bacterial growth influenced by substrate C:N ratio and concentration. *Aquat. Microb. Ecol.* 19, 105–118. doi: 10.3354/ame019105

van den Berg, E. M., Boleij, M., Kuenen, J. G., Kleerebezem, R., and van Loosdrecht, M. C. M. (2016). DNRA and denitrification coexist over a broad range of acetate/N-NO_3^- ratios, in a chemostat enrichment culture. *Front. Microbiol.* 7:1841. doi: 10.3389/fmicb.2016.01842

Van den Meersche, K., Soetaert, K., and van Oevelen, D. (2009). xsample (): an R function for sampling linear inverse problems. *J. Stat. Softw.* 30, 1–15. doi: 10.1002/wics.10

van Duyl, F. C., Lengger, S. K., Schouten, S., Lundälv, T., van Oevelen, D., and Müller, C. E. (2020). Dark CO_2 fixation into phospholipid-derived fatty acids by the cold-water coral associated sponge *Hymedesmia (Stylopus) coriacea* (Tisler Reef, NE Skagerrak). *Mar. Biol. Res.* 16, 1–17. doi: 10.1080/17451000.2019.1704019

van Oevelen, D., Mueller, C. E., Lundälv, T., van Duyl, F. C., de Goeij, J. M., and Middelburg, J. J. (2018). Niche overlap between a cold-water coral and an associated sponge for isotopically-enriched particulate food sources. *PLoS One* 13:e0194659. doi: 10.1371/journal.pone.0194659

van Oevelen, D., van den Meersche, K., Meysman, F. J. R., Soetaert, K., Middelburg, J. J., and Vézina, A. F. (2010). Quantifying food web flows using linear inverse models. *Ecosystems* 13, 32–45. doi: 10.1007/s10021-009-9297-6

Wassmann, P., Reigstad, M., Haug, T., Rudels, B., Carroll, M. L., Hop, H., et al. (2006). Food webs and carbon flux in the Barents Sea. *Prog. Oceanogr.* 71, 232–287. doi: 10.1016/j.pocean.2006.10.003

Watson, J. R. (2017). *Modelling Sponge-Symbiont Metabolism.* Dissertation, The University of Queensland, Brisbane, QLD, doi: 10.14264/uql.2017.180

White, A. E., Giovannoni, S. J., Zhao, Y., Vergin, K., and Carlson, C. A. (2019). Elemental content and stoichiometry of SAR11 chemoheterotrophic marine bacteria. *Limnol. Oceanogr. Lett* 4, 44–51. doi: 10.1002/lol2.10103

Witte, U., Brattegard, T., Graf, G., and Springer, B. (1997). Particle capture and deposition by deep-sea sponges from the Norwegian-Greenland Sea. *Mar. Ecol. Prog. Ser.* 154, 241–252. doi: 10.3354/meps154241

Yahel, G., Whitney, F., Reiswig, H. M., Eerkes-Medrano, D. I., and Leys, S. P. (2007). In situ feeding and metabolism of glass sponges (Hexactinellida, Porifera) studied in a deep temperate fjord with a remotely operated submersible. *Limnol. Oceanogr.* 52, 428–440. doi: 10.4319/lo.2007.52.1.0428

Zhang, Y., Qin, W., Hou, L., Zakem, E. J., Wan, X., Zhao, Z., et al. (2020). Nitrifier adaptation to low energy flux controls inventory of reduced nitrogen in the dark ocean. *Proc. Natl. Acad. Sci. U.S.A.* 117:201912367. doi: 10.1073/pnas.1912367117

Zimmerman, A. E., Allison, S. D., and Martiny, A. C. (2014). Phylogenetic constraints on elemental stoichiometry and resource allocation in heterotrophic marine bacteria. *Environ. Microbiol.* 16, 1398–1410. doi: 10.1111/1462-2920.12329

Conflict of Interest: The authors declare that the research was conducted in the absence of any commercial or financial relationships that could be construed as a potential conflict of interest.

Copyright © 2021 de Kluijver, Bart, van Oevelen, de Goeij, Leys, Maier, Maldonado, Soetaert, Verbiest and Middelburg. This is an open-access article distributed under the terms of the Creative Commons Attribution License (CC BY). The use, distribution or reproduction in other forums is permitted, provided the original author(s) and the copyright owner(s) are credited and that the original publication in this journal is cited, in accordance with accepted academic practice. No use, distribution or reproduction is permitted which does not comply with these terms.

frontiers in Marine Science

ORIGINAL RESEARCH
published: 04 February 2021
doi: 10.3389/fmars.2021.630900

Lithistid Demosponges of Deep-Water Origin in Marine Caves of the North-Eastern Mediterranean Sea

Andrzej Pisera[1]* *and Vasilis Gerovasileiou*[2]

[1] *Institute of Paleobiology, Polish Academy of Sciences, Warsaw, Poland,* [2] *Hellenic Centre for Marine Research (HCMR), Institute of Marine Biology, Biotechnology and Aquaculture (IMBBC), Heraklion, Greece*

Desmas-bearing demosponges known as lithistids have heavily silicified skeleton and occur typically in bathyal environments of warm and tropical areas but may be found in certain shallow marine caves. Here we report, for the first time two lithistid species, i.e., *Neophrissospongia endoumensis*, and *N*. cf. *nana*, that were earlier known from Western Mediterranean marine caves, from four marine caves in the north-eastern Mediterranean, and their congener *Neophrissospongia nolitangere* from deep waters (ca. 300 m) of the Aegean Sea. All marine caves, and sections within these caves, where lithistids occur, have freshwater springs. We interpret this surprising association between lithistids and freshwater input by elevated concentration of silica in water in cave sections where such springs occur, being 8–11 times higher in comparison with shallow water outside caves, and comparable to that of deep waters, that promoted lithistids' development. One of the studied caves harbored an abundant population of *N. endoumensis* which formed large masses. The age estimation of these lithistids, based on known growth rate of related deep-water sponges, suggest that they could be approximately 769–909 years old in the case of the largest specimen observed, about 100 cm large. These sponges could have colonized the caves from adjacent deep-water areas not earlier than 7,000–3,000 years ago, after the last glaciation, because earlier they were emerged. High variability of spicules, especially microscleres, and underdevelopment of megascleres may be related to silicic acid concentration.

Keywords: Porifera, demosponges, lithistids, marine caves, deep sea, Mediterranean Sea, silicate

OPEN ACCESS

Edited by:
Joana R. Xavier, University of Porto, Portugal

Reviewed by:
John Hooper, Queensland Museum, Australia
Vacelet Jean, UMR 7263 Institut Méditerranéen de Biodiversité et d'Ecologie Marine et Continentale (IMBE), France

***Correspondence:**
Andrzej Pisera
apis@twarda.pan.pl

Specialty section:
This article was submitted to Deep-Sea Environments and Ecology, a section of the journal Frontiers in Marine Science

Received: *18 November 2020*
Accepted: *07 January 2021*
Published: *04 February 2021*

Citation:
Pisera A and Gerovasileiou V (2021) Lithistid Demosponges of Deep-Water Origin in Marine Caves of the North-Eastern Mediterranean Sea. Front. Mar. Sci. 8:630900. doi: 10.3389/fmars.2021.630900

INTRODUCTION

Lithistids are those demosponges of various systematic position with "rocky" choanosomal skeleton [hence their name derives from the Greek word "λίθος" (lithos) meaning stone], that consist of articulated, more or less regular and usually strongly sculptured spicules called desmas. They inhabit mostly waters deeper than 100 m to about 2000 m, but some species occur also in shallow-water settings (Zea, 1987), including coral reefs (Vacelet and Vasseur, 1965; Hall et al., 2014), and marine caves (Pisera and Vacelet, 2011; Gerovasileiou and Voultsiadou, 2012).

The Mediterranean lithistid fauna includes 13 species of which 10 have been recorded in marine caves. These are *Aciculites mediterranea* Manconi et al., 2006, *Desmanthus incrustans*

(Topsent, 1889), *Discodermia polymorpha* Pisera and Vacelet, 2011, *Gastrophanella phoeniciensis* Perez et al., 2004, *Microscleroderma lamina* Perez et al., 2004, *Neophrissospongia endoumensis* Pisera and Vacelet, 2011, *N. nana* Manconi and Serusi, 2008, *Neophrissospongia nolitangere* (Schmidt, 1870), *Neophrissospongia radjae* Pisera and Vacelet, 2011, and *Neoschrammeniella bowerbankii* (Johnson, 1863). The remaining three species that have not been reported from marine caves, but mostly from deep waters, are: *Leiodermatium lynceus* Schmidt, 1870, *Leiodermatium pfeifferae* (Carter, 1873), and *Siphonidium ramosum* (Schmidt, 1870). Therefore, the marine cave environment seems to be particularly favorable for lithistids, harboring 77% of the Mediterranean lithistid diversity, including six endemic species which are known only from a single marine cave but not from other habitats – at least so far – and could be considered cave-exclusive *sensu lato* (Gerovasileiou and Voultsiadou, 2012).

The problem with specific attribution of many lithistid sponges is the fact that numerous species are known only from a single, or two specimens and no systematic studies of intraspecific variability or/and environmental variability in their morphology exist. Even more it concerns their spiculation, that, in the case when more specimens are known, good SEM photos are available only for one specimen. Atop of these problems is the fact that particular regions in the same specimen, that differ in structure and function, differ also in details of desma morphology and ectosomal spicules types (see for example *Theonella wrightae* in Pisera and Pomponi, 2015; A. Pisera unpublished observations). Thus, one may suspect that some lithistid species may in fact be only environmental variants of earlier described species. Another problem is that only well oriented samples showing the surface of desma skeleton can be compared, and random cut surface of choanosomal skeleton shows apparently chaotic desma articulation (what is not true). A separate question concerns microscleres which often exhibit high variability that should be assessed independently.

Mediterranean lithistid records are generally few and geographically scattered (Van Soest et al., 2020), mostly from the northern section of the basin, with some exceptions (e.g., Perez et al., 2004). Although the sponge fauna of the Aegean Sea (north-eastern Mediterranean), and particularly its Greek waters, is the most comprehensively studied in the eastern Mediterranean basin (Voultsiadou, 2005a,b, 2009; Voultsiadou et al., 2016), only two lithistids have been recorded in this area. These are *Discodermia polymorpha*, reported as *Discodermia polydiscus* (Bowerbank, 1869) from several locations, at a depth range of 10–360 m, including marine caves (Voultsiadou, 2005a,b; Pisera and Vacelet, 2011), and *Leiodermatium lynceus*, collected at 207 m depth, off Epidaurus (Peloponnese, southern Aegean Sea) by Vamvakas (1970). More recently, another lithistid, belonging to the genus *Neophrissospongia* was reported from a semi-submerged marine cave in Agios Efstratios Island, northern Aegean Sea (Dimarchopoulou et al., 2018).

During the last decade, numerous marine caves have been studied in the north-eastern Mediterranean Sea, shedding light on new records and new sponge species (Gerovasileiou et al., 2015; Lage et al., 2018, 2019). The discovery of lithistids from marine caves with freshwater input coupled with the acquisition of material from deep waters constitute the basis of this work. This study aims at (a) describing for the first time lithistid demosponges collected from shallow marine caves of the north-eastern Mediterranean Sea; (b) investigating environmental factors that potentially control their distribution and occurrence; and (c) comparing congeneric lithistids from marine caves and deep waters of the north-eastern Mediterranean Sea.

MATERIALS AND METHODS

During the last decade, approximately 40 marine caves and cave groups (i.e., sites with several caves and tunnels, sometimes connected) have been surveyed in the north-eastern Mediterranean Sea, and mostly in the island-dominated Aegean Archipelago, within different expeditions (Gerovasileiou et al., 2015; Sini et al., 2017; Galani et al., 2019). Lithistid sponges were found and collected from three marine caves (**Figure 1**) located on both northern and southern coasts of Crete (Aegean Sea: Blue Cave; Libyan Sea: Lithistid and Italian caves) and one cave (Trypia Spilia) in the isolated Agios Efstratios Island, northern Aegean Sea. The fact that the common feature between these marine caves was the presence of internal freshwater springs led us to collect water samples from the entrance zone and the internal freshwater springs in two of these caves (three replicates from each zone) in order to measure silicate concentration. In addition, the acquisition of a lithistid sample collected by the MEDITS Survey from deep waters of the south-eastern Aegean Sea, provided additional material allowing for comparisons between congeneric lithistids from marine caves and deep waters in the same ecoregion. Descriptions for each sampling site and event are provided below.

Two caves are located on the south coast of Crete (Libyan Sea), close to each other (ca. 80 m away), within the marine area of the National Park of Samaria, in Sfakia area: the "Lithistid Cave" (named after this work) and the Italian Cave. The Lithistid Cave (35.2008°N, 24.1191°E) is a large, semi-submerged tunnel cave (0–6 m deep). Lithistids develop in the semi-dark and dark zones of the cave, where freshwater springs are present, at a distance of 15–40 m from the main semi-submerged entrance and 5 m from the second submerged entrance of the tunnel. The highest lithistid abundance and biggest specimens were observed in areas with freshwater mixing and close to freshwater springs. Mean silicate concentration at the internal cave zone was 7.170 μM ± 1.244 (SD) versus 0.663 μM ± 0.042 (SD) at the cave entrance. The cave harbors a rich sessile benthic community (high sponge abundance and cover) that is highly diversified from other marine caves of the north-eastern Mediterranean, possibly due to the influence of freshwater influx (Galani et al., 2019). The Italian Cave (35.2013°N, 24.1198°E) is a large, submerged cave with an internal air pocket. Its entrance is located at 8–12 m depth and leads to a narrow corridor, descending to 18 m depth, which separates the entrance zone from the internal cave chamber that is filled with cool fresh water. While this chamber is seemingly azoic, the cave entrance hosts rich benthic fauna, with a few small-sized lithistids developing on the overhanging

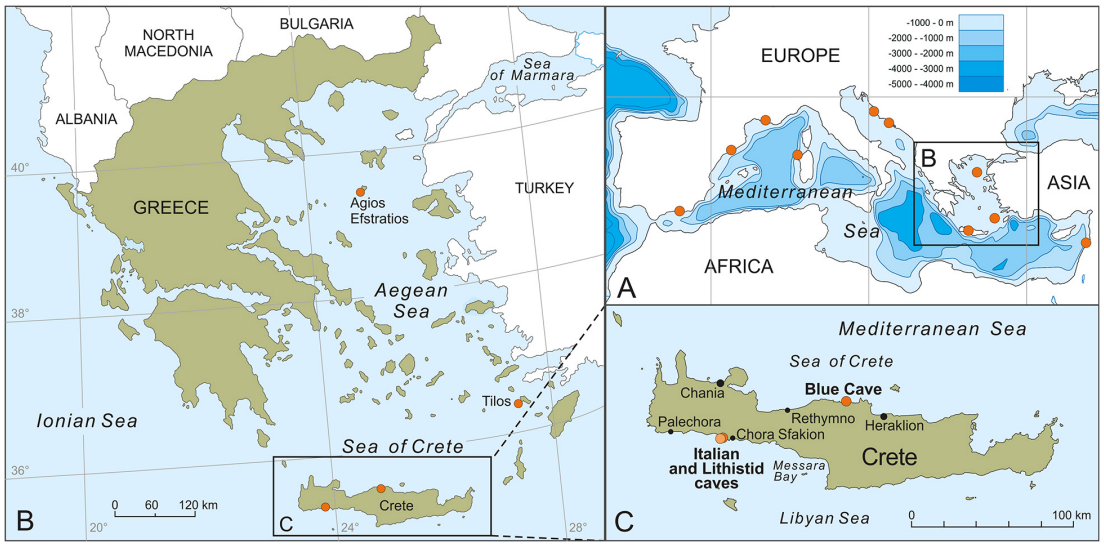

FIGURE 1 | Locations of the studied specimens in the north-eastern Mediterranean Sea **(A–C)** and other discussed occurrences of lithistid demosponges in Mediterranean marine caves **(A)**.

walls and ceiling of the entrance, in proximity to small crevices of freshwater influx. No silicate measurements were made due to the small size of crevices and rapid water mixing. The water temperature in both Italian and Lithistid caves was 25–26°C (measured with a SUUNTO dive computer in July 2016 and August 2017) while it was ten degrees lower (16°C) in the internal freshwater chamber of the Italian Cave.

The Blue Cave is a large semi-submerged cave (0–17 m) located at Agia Pelagia area (35.4198°N, 24.9794°E), on the north coast of Crete (**Figure 1**). The cave hosts a rich sessile benthic community, including one new homoscleromorph sponge species that was recently described by Lage et al. (2018) from a dark sub-vertical tunnel descending from the cave bed. Few lithistids developed in a narrow crevice with freshwater influx, in the terminal section of the cave, at a depth of 3–4 m (**Figure 2A**). Mean silicate concentration at the opening to this crevice was 3.280 μM ± 1.365 (SD) versus 0.427 μM ± 0.137 (SD) at the cave entrance. Water temperature inside the cave was 25°C (measured with a SUUNTO dive computer in July 2017).

Trypia Spilia (meaning hollow cave in Greek) is a large semi-submerged tunnel on the western coasts of Agios Efstratios Island (39.5349°N, 24.9777°E), northern Aegean Sea. The cave is characterized by a complex geomorphology and hosts a rich sessile benthic community that have been described in detail by Dimarchopoulou et al. (2018). The presence of freshwater input dropping from the emerged ceiling and influx from springs in the shallow cave bed (1–2 m deep) was observed during sampling in July 2011, but not in earlier expeditions (August 2009), indicating a sporadic and ephemeral character (V. Gerovasileiou, personal observation). Lithistids were found on the walls and floor of the semi-dark cave zone (10–30 m from the two entrances of the tunnel), where freshwater influx was observed. They had a mean surface cover of 0.4% throughout the cave and a maximum cover of 5.5%, count in 25 cm × 25 cm photoquadrats (Dimarchopoulou et al., 2018). The water temperature in the marine cave was 22–24°C (measured with a HOBO data logger in August 2009 and a SUUNTO dive computer in July 2011).

A deep-water lithistid was trawled during the 2018 MEDITS Survey in the frame of the Greek National Data Collection Project from a depth range of 313–352 m, off Tilos Island, in the Dodecanese Islands' marine region, south-eastern Aegean Sea (Trawl start: 36.3534°N, 27.1804°E, depth: 313 m, Temp: 14.76°C; Trawl end: 36.3375°N, 27.1976°E, depth: 352 m, Temp: 14.72°C).

The sampled material was investigated morphologically under the binocular microscope, as well as under SEM. Preparation of samples followed that described by Pisera and Pomponi (2015). Samples for SEM analyses were sputter-coated with platinum and observed at 25 kV using a Philips XL-20 scanning electron microscope (Institute of Paleobiology, Warsaw). The investigated material is housed in the Institute of Paleobiology, Warszawa, under the collection number ZPAL Pf. 30.

RESULTS

Systematic Description

Order TETRACTINELLIDA Marshall, 1876
Suborder ASTROPHORINA Sollas, 1887
Family CORALLISTIDAE Sollas, 1888
Genus *Neophrissospongia* Pisera and Lévi, 2002

Type species

Corallistes nolitangere Schmidt, 1870

Remarks

There are four *Neophrissospongia* species reported from the Mediterranean Sea: *N. nolitangere* (Schmidt, 1870), *N. endoumensis* Pisera and Vacelet, 2011, *N. radjae*

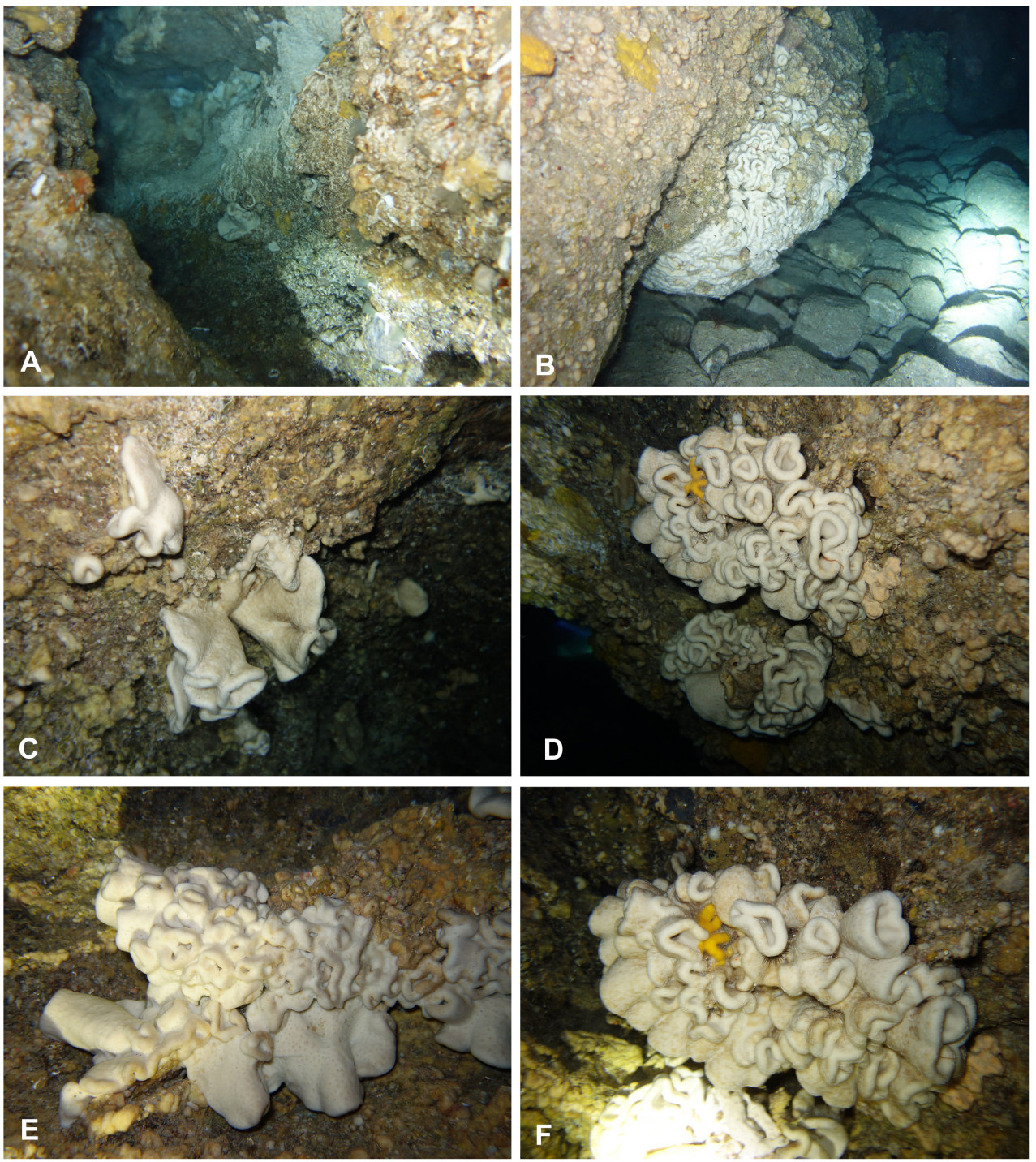

FIGURE 2 | *In situ* underwater photos of *Neophrissospongia endoumensis* Pisera and Vacelet, 2011. **(A)** Blue Cave, northern Crete; **(B–F)** Lithistid Cave, southern Crete. Photos by V. Gerovasileiou.

Pisera and Vacelet, 2011, and *N. nana* Manconi and Serusi, 2008. Other two known species, i.e., *Neophrissospongia microstylifera* Lévi and Lévi 1983 and *Neophrissospongia galapagoensis* Schuster et al., 2018, are reported from the Pacific. The species *N. nolitangere* was earlier reported from marine caves in the western Mediterranean but occurs also in the northern Atlantic Ocean (Azores, Madeira, Selvagens, and Canary Islands) (Cruz, 2002; Pisera and Vacelet, 2011; Carvalho et al., 2020). The report of *N.* cf. *nolitangere* form the Caribbean Sea (Pomponi et al., 2001) concerns most probably a new, yet undescribed

species (A. Pisera, unpublished data). On the other hand, *Neophrissospongia tubulata* (van Soest and Stentoft, 1988) does not belong to *Neophrissospongia* (it represents a new undescribed genus – A. Pisera, unpublished).

The species *N. endoumensis* is known from a single marine cave in the western Mediterranean Sea (Pisera and Vacelet, 2011); *N. nana* occurs in a single marine cave in Sardinia, western Mediterranean (Manconi and Serusi, 2008) while *N. radjae* is known from a single marine cave in the Adriatic Sea (Pisera and Vacelet, 2011). Among those known from the Mediterranean and the Atlantic, two species (*N. radjae* and *N. nana*) have different habitus, i.e., either massive club shaped (*N. radjae*) or encrusting (*N. nana*); thus they are clearly different from our material from the north-eastern Mediterranean Sea. *N. nolitangere* may be ear-shaped to forming large folded masses (exactly like to studied specimens) while *N. endoumensis*, when small (only such specimen is known), is cup-shaped and can be developed to folded masses when large (this study). Also, the characters of exhalant and inhalant surfaces are similar in those two species not allowing for easy differentiation. The situation is not simpler in the case of skeletal characters: all these species have very similar dicranoclone desmas, streptaster-spiraster ectosomal microscleres, and microtylostyle choanosomal microscleres; differences between these two species are in small details.

Neophrissospongia endoumensis Pisera and Vacelet, 2011, Figures 2, 3A–G, 4–9.

N. endoumensis Pisera and Vacelet, 2011: 27, Figures 2H–J, 13–15 and Table 1.

Material Examined

Blue Cave, Agia Pelagia area, north coast of Crete (one specimen – collected on 11 July 2017 by Vasilis Gerovasileiou and Guilherme Muricy); Italian Cave, Sfakia, south coast of Crete (one specimen – collected on 19 August 2017 by Vasilis Gerovasileiou); Lithistid Cave, south coast of Crete (three fragmentary specimens – collected on 11 July 2016 by Vasilis Gerovasileiou and Thanos Dailianis).

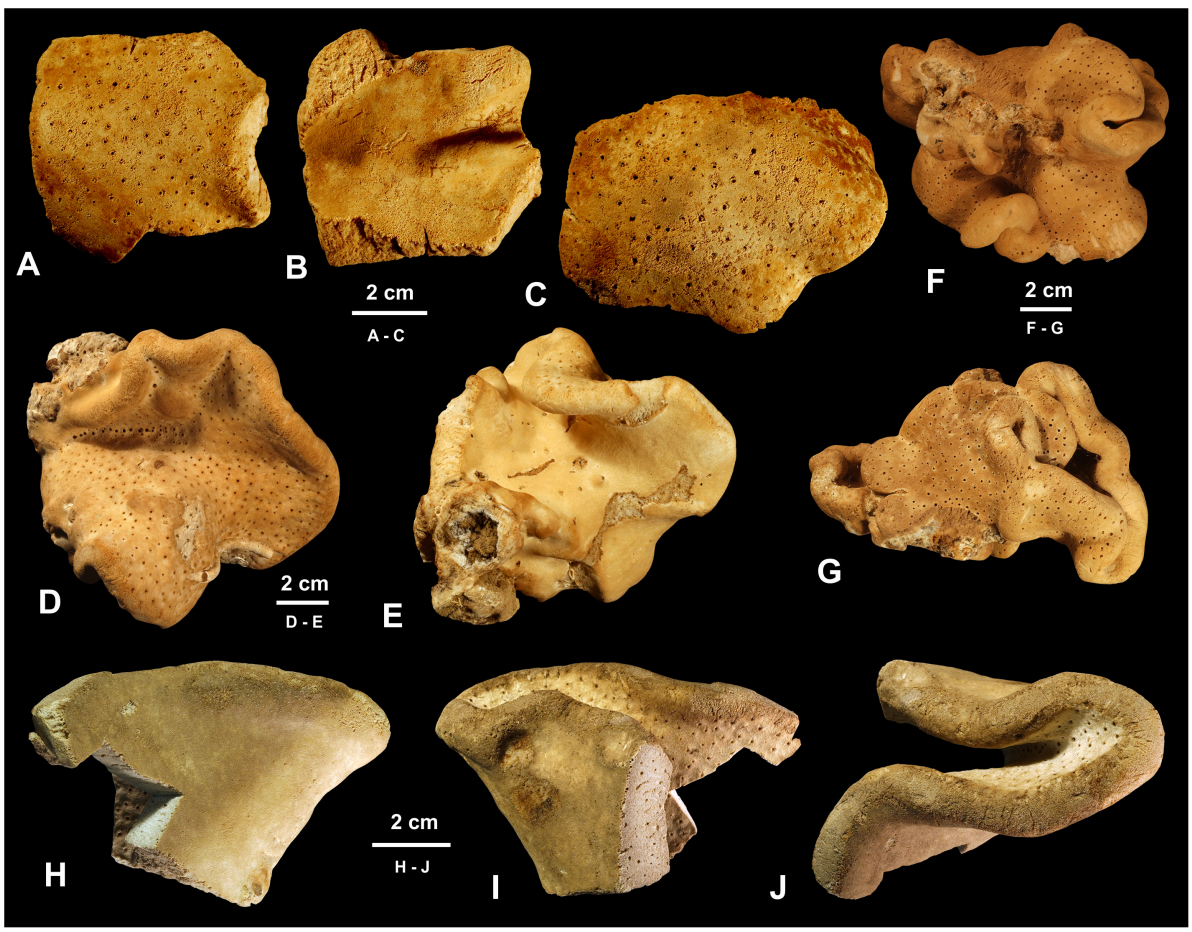

FIGURE 3 | Morphology of studied specimens. **(A–G)** *Neophrissospongia endoumensis* Pisera and Vacelet, 2011. **(A–C)** Specimen ZPAL Pf. 30/1, fragments, Lithistid Cave, southern Crete. **(A,C)** Exhalant surface view; **(B)** Inhalant surface view; **(D,E)** Specimen ZPAL Pf. 30/2, Blue Cave, northern Crete; **(D)** Exhalant surface view; **(E)** Inhalant surface view; **(F,G)** Specimen ZPAL Pf. 30/3, Italian Cave, southern Crete complete contorted specimen in different views. **(H–J)** *Neophrissospongia nolitangere* (Schmidt, 1870), fragmentary specimen ZPAL Pf. 30/4, deep Aegean Sea, off Tilos Island [**(H–J)** inhalant surface views; **(J)** top view of a folded fragment].

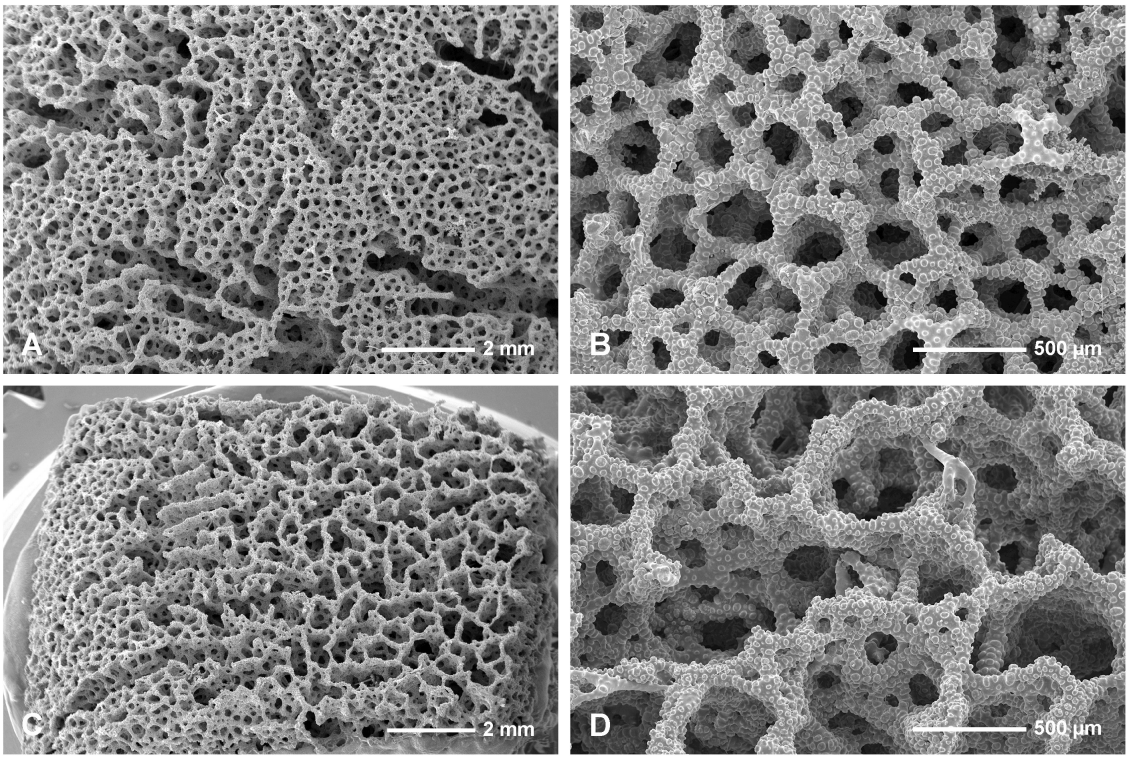

FIGURE 4 | *Neophrissospongia endoumensis*, Pisera and Vacelet, 2011, Blue Cave, northern Crete. **(A,B)** Exhalant surface of the choanosomal skeleton of dicranoclone desmas, with system of canals corresponding to oscular openings **(A)**; **(C,D)** Inhalant surface of the choanosomal skeleton of dicranoclone desmas; **(C)** General view showing net-like structure; **(B)** Details of articulated dicranoclones.

Description

In habitus all investigated specimens are very similar (observed *in situ* in the caves mostly) being cup- to ear-shaped when small (**Figure 2C**), later they form large (up to 100 cm × 40 cm) folded masses with some cup-trumpet-tubular elements (**Figures 2B,D–F**). The investigated specimen from the Blue Cave is a complete slightly folded plate about 12 cm × 10 cm; it has wall with rounded margins and is about 1.2 cm (**Figures 3D,E**). The other specimen from the Italian Cave, southern Crete, measuring 11 cm × 9 cm, is more irregularly folded and complex (**Figures 3F,G**). There are three fragmentary specimens (fragments of larger folded sponges) investigated from the nearby Lithistid Cave that measure about 6 cm × 5 cm, and 1.4 cm thick wall; 8 cm × 6 cm large and 1.5 cm thick wall and 5 cm × 5 cm large and 1.5 cm thick wall (**Figures 3A–C**). In all specimens one side (inhalant) is smooth (**Figures 3A,E,F**), except faint growth lines, and display small 30–50 μm in diameter ostia that are densely distributed over most of the surface. They are vaguely grouped above underlying meshes of choanosomal skeleton. The other surface (upper one) displays round, about 0.5–1 mm large openings (oscula) that are at the level with sponge surface or in some regions slightly raised (**Figures 3A,C,D**). In furrows of the folds these openings are slightly larger, up to 2 mm in size and much more densely located.

In all studied specimens choanosomal skeleton consists of strongly tuberculated and arched dicranoclones that are approximately (it is difficult to measure articulated spicules) (285 μm minimum) 333–446 μm on average in size (see **Table 1** for differences in specimens from particular caves). Dicranoclones form dense irregular choanosomal skeleton on the exhalant side (**Figures 4A,B**, **7A,B**) and less dense, in the form of less regular net, on the inhalant one (**Figures 4C,D**, **7C,D**). On exhalant surface of choanosomal skeleton openings (about 1 mm in size) corresponding to oscula are visible; often they are surrounded by irregularly radial furrows in the surface of the skeleton (**Figures 4A**, **7A**). Dicranoclones densely covered (especially on exhalant side) by large, mushroom shaped tubercles that may bear smaller low tubercles (**Figure 5**). Ectosomal dichotriaenes with massive clades, and strongly tuberculated upper surface of the cladome; they are covered with numerous densely packed, vertically pointed, tubercles that bear (are divided into) several spines on their top. Cladomes are between 181 and 349 μm in diameter (it varies between particular caves: see **Table 1**). Rhabdomes are 434–766 μm long (see **Table 1**) and 30.8–55.0 μm thick at the top and with rounded lower tip.

Microscleres are of two types: choanosomal spinose microtylostyles, and massive streptasters/spirasters with short and thick arms covered with triangular low spines, concentrated in the ectosome. Microtylostyles are from 64.4 to 99.2 μm long and 1.21 to 2.89 thick, while streptasters/spirasters size varies between 10.3–17.5 × 9.8–14.2 μm (see **Table 1**).

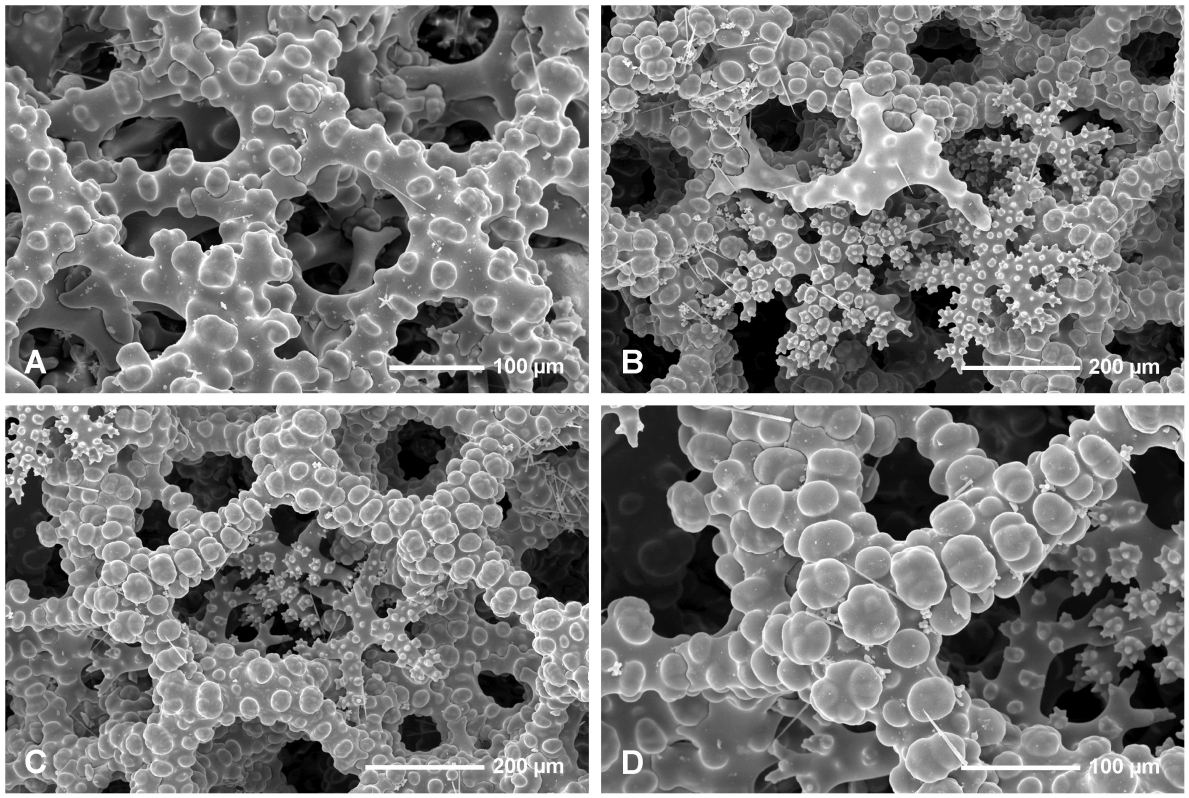

FIGURE 5 | *Neophrissospongia endoumensis* Pisera and Vacelet, 2011, Blue Cave, northern Crete. **(A)** Sculpture of dicranoclone desmas of the inhalant surface; **(B)** Young dicranoclone and ectosomal dichotriaenes inserted among desmas of choanosomal skeleton, exhalant surface; **(C,D)** Sculpture of dicranoclone desmas of the exhalant surface.

Remarks

The investigated specimens differ from the holotype, the only one earlier known specimen that is cup-shaped, by forming large folded masses. This difference follows, most probably, from the fact that the holotype is much smaller/younger. Otherwise, all characters of the specimens from Crete are the same as in the holotype. Dichotriaenes in our material have slightly larger cladomes and longer rhabdomes; on the contrary microtylostyles may be longer in the holotype, and slightly larger are streptasters, but in all cases their size overlaps in part with our material. In all the studied caves several motile invertebrates (e.g., crinoids, sea urchins, and gastropods) were sheltering in the cavities of the lithistids' folded plates while small-sized sessile taxa (e.g., brachiopods attached to exposed dead fragments of choanosomal skeleton, and thinly encrusting sponges) developed on the lithistids' hard surface. Therefore, *Neophrissospongia* seems to have an important ecosystem engineering role in the marine cave ecosystem, providing micro-habitats to various taxa.

This species is very similar to *N. nolitangere*, being identical with it in habitus. The difference is in details of spiculation, mostly character of streptasters/spirasters and ectosomal dichotriaenes. Streptasters are more massive, regular and with shorter arms and larger in *N. endoumensis* than in *N. nolitangere*. Dichotriaenes in *N. endoumensis* have more complex and massive cladomes while its desmas are more massive, often with swollen central part, while in *N. nolitangere* they are rather linear. Anyway, these differences are small and great intraspecific variability, as shown by specimens from different caves (**Table 1**), allows to raise the question if these two nominal species are not only ecophenotypic variants (cave versus deep-water) of the same species (see section "Discussion"). These aspects should be investigated in detail, especially by systematic study of spicules variability contrasted with silica contents of sea water, and by molecular methods. Finally, it is worth to mention that similar problems to interpret variations in morphology have been encountered in case of different populations (especially bathyal and shallow water cave populations) of the sphinctozoan sponge *Vaceletia* having calcareous skeleton (Vacelet et al., 1992; Wörheide and Reitner, 1996; Vacelet, 2002).

Neophrissospongia nolitangere (Schmidt, 1870), Figures 3H–J, 10–12 and Table 1.

Neophrissospongia nolitangere (Schmidt, 1870); Pisera and Vacelet, 2011: 26 cum syn., Figures 2C–G, 10–12 and Table 1; Carvalho et al., 2015: Figure 2B.

Material Examined

Aegean Sea; deep-water specimen from a depth of 313 to 352 m, off Tilos Island (Dodecanese Islands, southern Aegean Sea) (**Figure 1**). Collected on 12 July 2018 by Panagiota Peristeraki.

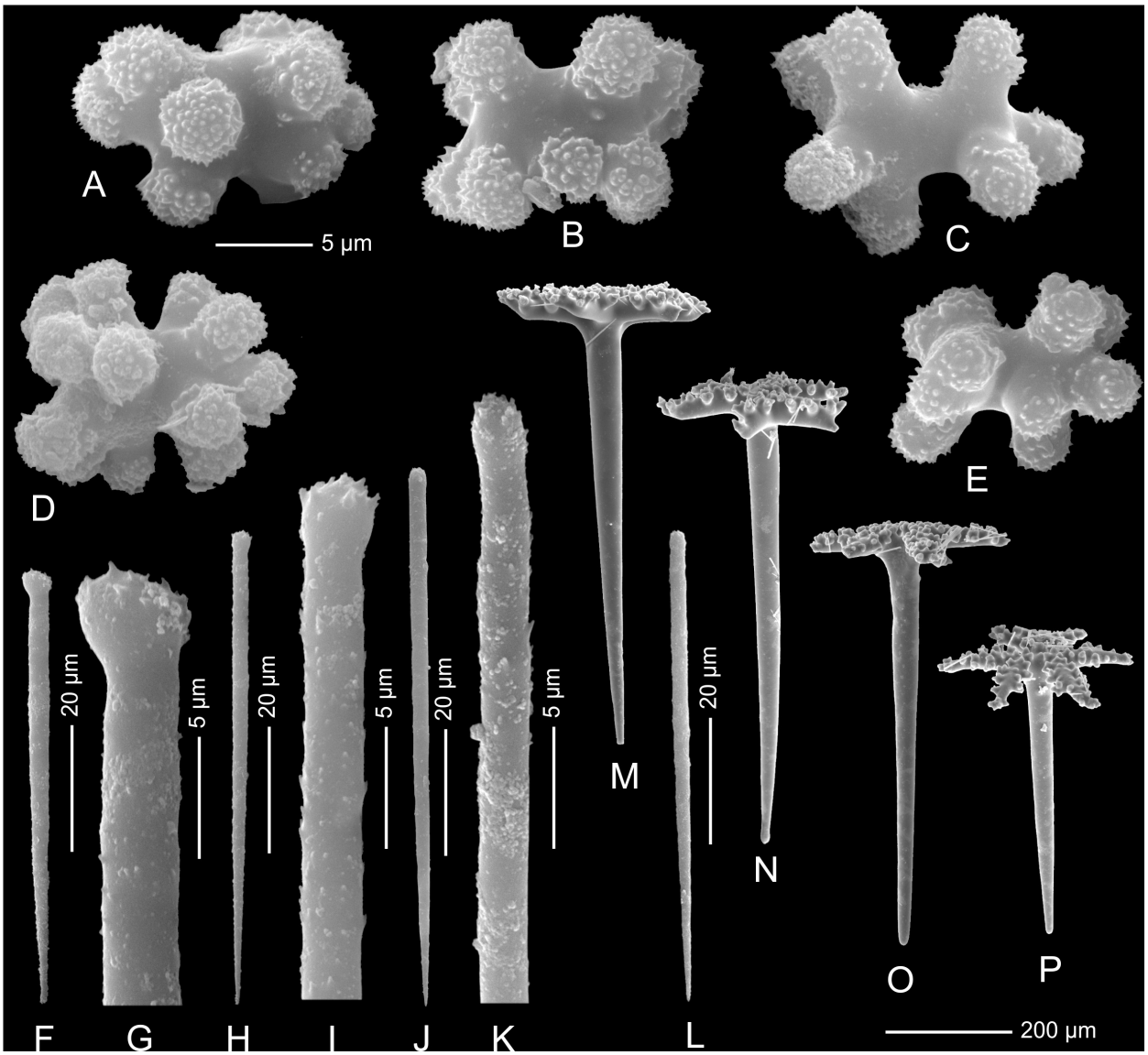

FIGURE 6 | *Neophrissospongia endoumensis* Pisera and Vacelet, 2011, Blue Cave, northern Crete; **(A–E)** Streptasters-spirasters microscleres; **(F–L)** Choanosomal microtylostyles, general view **(F,H,J,L)**, heads **(G,I,K)**; Ectosomal dichotriaenes in side view **(M,N,O)** and oblique view **(P)**.

Description

The fragmentary specimen is about 9 cm × 6 cm large and represents a folded/contorted plate-like sponge with rounded margins; thickness of the wall is about 1.2 cm. One side smooth, with ostia, that are about 3–40 µm in diameters and organized in a vague field above underlying meshes of choanosomal skeleton. The opposite (exhalant) side with numerous oscula, about 0.7–1 mm in diameter, with slightly raised margins; they are evenly distributed over the entire surface.

Choanosomal desmas are strongly tuberculated dicranoclones (tubercles are mushroom-shaped, may be divided into low smaller tubercles) and arched, rather linear, and are 296–360 µm in size. They form irregular and dense net with small meshes on the exhalant surface, and irregular net with larger, 0.5–0.6 mm wide meshes on the inhalant surface.

Ectosomal dichotriaenes with regular and not branched (except slightly on tips) clades that bear on the upper surface numerous tubercles and spines (toward the tips) that may be divided into smaller spines. Cladomes are 299–411 µm in diameter, while rhabdomes are 543–904 µm long.

Microscleres are of two types: choanosomal spinose microtylostyles, and massive streptasters/spirasters with short and thick arms covered with triangular low spines, concentrated in the ectosome. Microtylostyles are from 90.8 to 116 µm long and 1.3–1.6 µm thick, while streptasters/spirasters size varies between 8–9 µm × 13–14 µm (see **Table 1**).

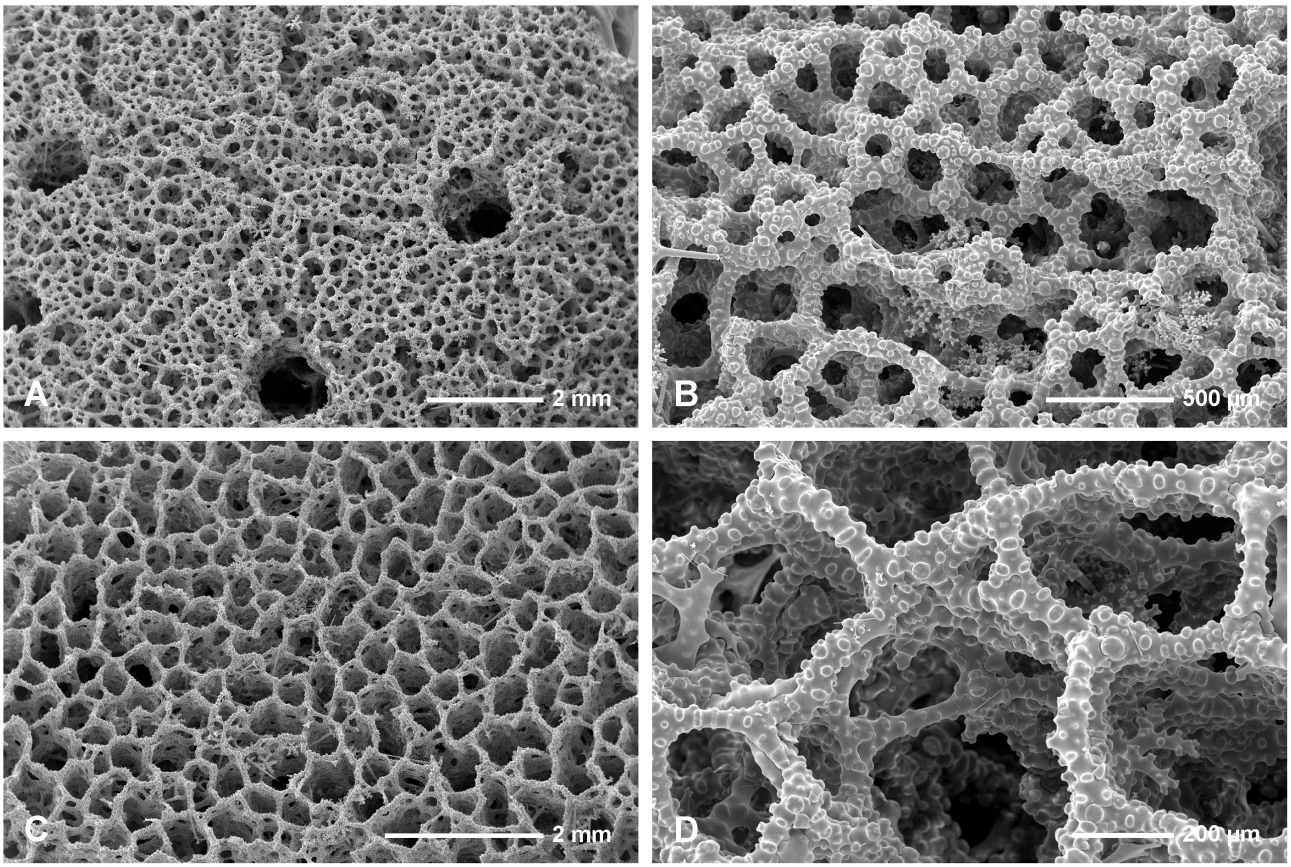

FIGURE 7 | *Neophrissospongia endoumensis* Pisera and Vacelet, 2011, Lithistid Cave, southern Crete. **(A,B)** Choanosomal skeleton on the exhalant surface. **(A)** General view of choanosomal desma skeleton with canal openings corresponding to oscula. **(B)** Details of dicranoclones desmas articulation and sculpture on the surface; **(C,D)** Choanosomal skeleton of dicranoclone desmas on inhalant surface; **(C)** Net-like organization of dicranoclone desmas and **(D)** details of dicranoclone desmas.

Remarks

This species is very similar in habitus to *N. endoumensis* described above. It differs from the investigated here specimens of *N. endoumensis* from Crete in details of spiculation. It has less massive clades/cladomes of the dichotriaenes that are more strongly tuberculated. Rhabdomes of the dichotriaenes are slightly longer in *N. nolitangere*. Meshes of choanosomal skeleton on the inhalant surface is less regular in *N. nolitangere* than in *N. endoumensis*; streptasters are smaller and less regularly developed, while microtylostyles are slightly longer and thinner than in *N. endoumensis* from Crete. See also remarks for *N. endoumensis* above.

Neophrissospongia cf. *nana* Manconi and Serusi, 2008, Figure 13.

cf. *Neophrissospongia nana* Manconi and Serusi, nov. sp.: p. 73–76, Figures 1–4 and Table 1.

Material Examined

Trypia Spilia Cave, Agios Efstratios Island, north Aegean Sea (fragmentary specimen ZPAL Pf. 30/5 – collected on 5 July 2011 by Vasilis Gerovasileiou and Elena Akritopoulou).

Description

The studied material consists of small fragments of a small encrusting sponge found in one cave (Trypia Spilia) in Agios Efstratios Island. An original sponge is about 6 cm in max diameter, low domical and rounded in shape (**Figures 13A,B**). Choanosomal skeleton consists of very irregular tuberculated desmas (dicranoclones) that form very irregular (confused) choanosomal skeleton. Desmas are so irregular that they can be interpreted as pathologic/not fully developed. No microscleres were observed. Only one young (not fully developed) dichotriaene with axial canals, still not closed, has been found.

Remarks

The investigated specimens lack important characters, i.e., microscleres, and well developed dichotriaenes that are either underdeveloped or pathologic, making precise determination impossible. In habitus and irregularity of the skeleton it resembles mostly the specimens from Sardinia described as *N. nana* (Manconi and Serusi, 2008). We are inclined to interpret our specimen as

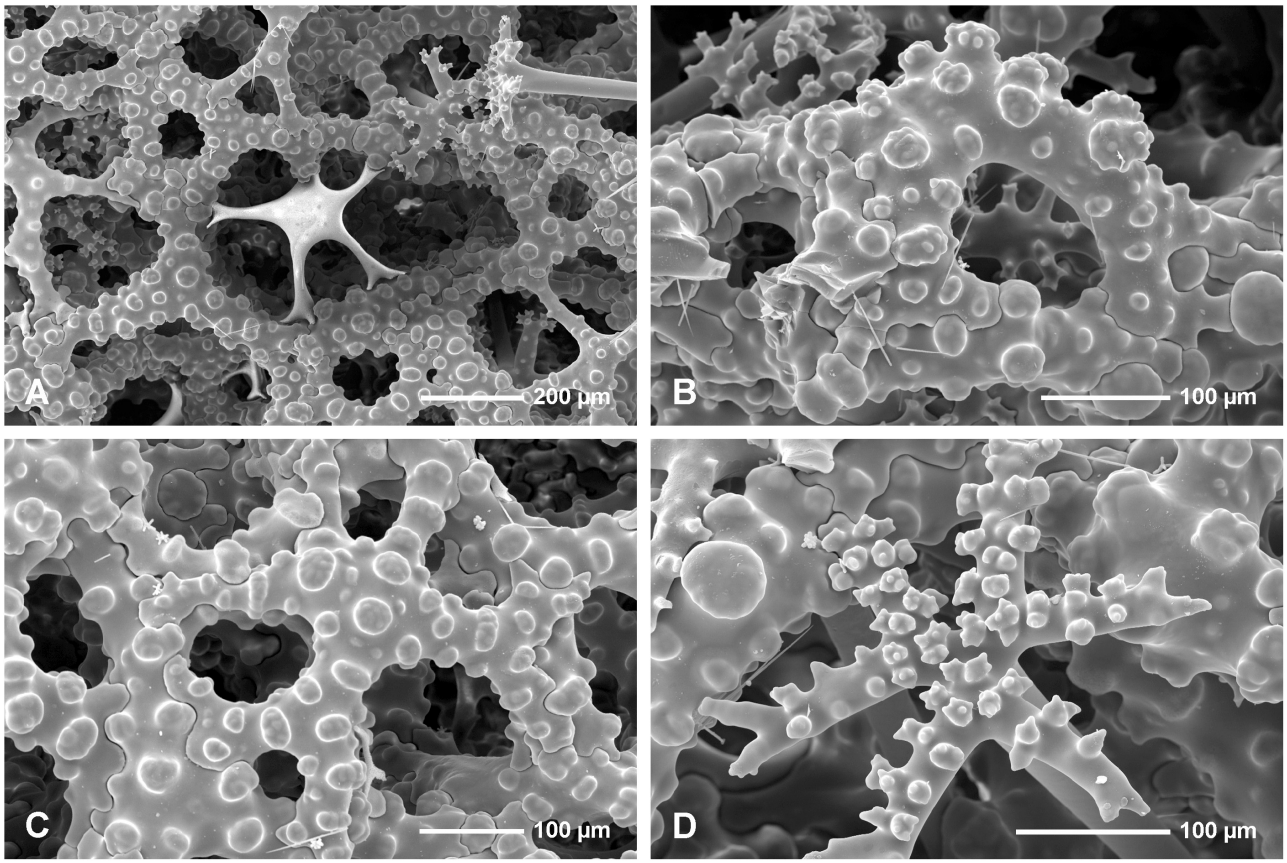

FIGURE 8 | *Neophrissospongia endoumensis* Pisera and Vacelet, 2011, Lithistid Cave, southern Crete; Exhalant surface of the choanosomal skeleton. **(A)** Young desma inserted in a large mesh formed by fully developed desma; **(B)** Strongly arched and sculptured dicranoclone desma as seen in oblique view; **(C)** Strongly sculptured dicranoclone desmas as seen from the top; **(D)** Top surface of the cladome of the dichotriaene *in situ*; note that one arm is partly articulated with choanosomal skeleton of dicranoclones.

pathologic (possibly due to low silicate content of water). The same might concern species *N. nana* described by Manconi and Serusi (2008).

DISCUSSION

The Provenance of the Lithistid Cave Fauna

A number of lithistid demosponges are known only from a single marine cave: *Aciculites mediterranea* from Grotta dei Laghi, Sardinia, Italy (Manconi et al., 2006), *Gastrophanella phoeniciensis* and *Microscleroderma lamina* from Lithistid Cave, Chak El Hatab, Lebanon (Perez et al., 2004), *Neophrissospongia nana* from Grotta delle Terrazze, Sardinia, Italy (Manconi and Serusi, 2008), *N. endoumensis* from Grotte d'Endoume, Marseille, France (Pisera and Vacelet, 2011), *N. radjae* from a cave in Korčula Island, Croatia (Pisera and Vacelet, 2011), and also some undescribed species from the Canary Islands (A. Pisera, unpublished data). In the context that cave lithistids fauna consist of species often not known outside particular caves, a question arises if these species are really restricted to this habitat and evolved within the cave system, representing cave-exclusive fauna, or are just vestiges of unrecognized deep-sea populations whose larvae just colonized suitable shallow caves from some yet unknown deep-water populations. The hypothesis of cave-exclusive (stygobiotic) fauna for lithistids should be rather rejected due to the fact that some of these species occur in geographically distant and fragmented marine caves; *N. radjae* in a single Adriatic cave and also in Spanish (Alboran Sea) caves (A. Pisera, unpublished data), and *N. endoumensis* in Marseille and now in caves of Crete. Thus, exchange of their propagules between these caves seems impossible, especially if we consider time available since cave colonization (see below).

A similar hypothesis has been suggested for the demosponge *Lycopodina hypogea* (Vacelet and Boury-Esnault, 1996), belonging to the carnivorous deep-sea family Cladorhizidae, that was first described from a submarine cave with deep-sea affinities in Marseille (Trois Pépés Cave), then was recorded in two other caves in Marseille and the Adriatic Sea (Bakran-Petricioli et al., 2007) and was recently observed to thrive in several deep-water areas in the Mediterranean Sea (e.g., Aguilar et al., 2011; Bo et al., 2020) and in the

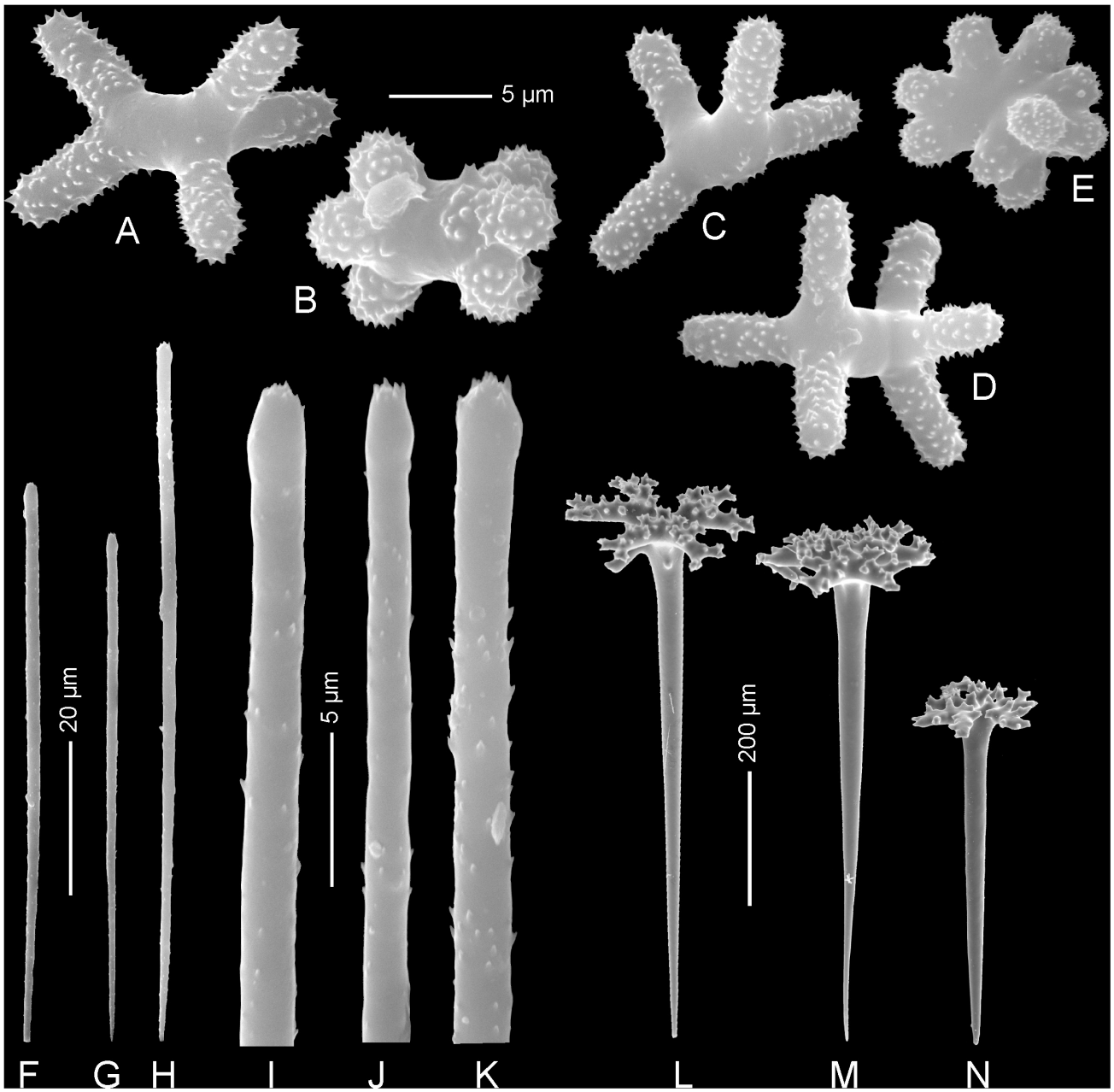

FIGURE 9 | *Neophrissospongia endoumensis* Pisera and Vacelet, 2011, Lithistid cave, southern Crete. **(A–E)** Streptasters-spirasters microscleres; **(F–K)** Choanosomal microtylostyles, general view **(F,G,H)**, and their heads **(I,J,K)**; **(L–N)** Ectosomal dichotriaenes in slightly oblique view.

north-eastern Atlantic (Chevaldonné et al., 2015). Another typical example of deep-sea sponges known from submarine caves is the hexactinellid *Oopsacas minuta* Topsent, 1927 that was known from the deep western Mediterranean Sea and Trois Pépés Cave in Marseille (Vacelet et al., 1994) and was later found in caves of the Adriatic Sea and several deep-water sites in the western and central Mediterranean basins (Bakran-Petricioli et al., 2007). The usual occurrence of several deep-water or "cryptobiotic" (i.e., preferring cryptic habitats) species in caves, which originate from external marine environments but become characteristic of this particular habitat only secondarily, has been also described as "secondary stygobiosis" (Gerovasileiou and Bianchi, in press, and references therein).

Dark marine caves present several analogies with deep-sea ecosystems and have been characterized as natural "mesocosms" of the bathyo-abyssal zone, providing an easily accessible model for the study of deep marine ecosystems (Vacelet, 1996;

TABLE 1 | Spicules size of the studied sponges and other conspecific known material.

Species/specimen	Desma	Dichotriaenes	Microtylostyles	Streptasters
Neophrissospongia nolitangere (Topsent, 1904; Azores)	350–500 μm	rhabdome 450–1200 μm long / cladome 230–310 μm in diameter		10–13 μm × 8–10 μm
Neophrissospongia nolitangere (from Pisera and Vacelet, 2011)	289–382 μm	rhabdome 313–800 μm long / cladome 160–313 μm in diameter	74–137 μm long / 1.4–2.1 μm thick	8.4–15.4 μm × 6.1–12.9 μm
Neophrissospongia nolitangere (ZPAL Pf. 30/4; Aegean Sea)	296–368 μm	rhabdome 543–904 μm long / cladome 299–411 μm in diameter	90.8–116 μm long / 1.3–1.6 μm thick	8–9 μm × 13–14 μm
Neophrissospongia endoumensis (from Pisera and Vacelet, 2011)	318–490 μm	rhabdome 320–615 μm long / cladome 248–283 μm in diameter	68.8–123 μm long / 1.6–1.7 μm thick	12.7–20.1 μm × 11.4–16.6 μm
Neophrissospongia endoumensis (ZPAL Pf. 30/2; Blue Cave)	333–446 μm	rhabdome 434–696 μm long / cladome 265–337 in diameter	69.2–84.8 μm long / 2.25–2.89 μm thick	13.0–15.8 μm × 10.0–13.1 μm
Neophrissospongia endoumensis (ZPAL Pf. 30/3; Italian Cave)	346–438 μm	rhabdome 464 –624 μm long / cladome 249–349 μm in diameter	84.1–99.2 μm long / 1.21–2.04 μm thick	11.7–17.5 μm × 9.8–14.2 μm
Neophrissospongia endoumensis (specimen ZPAL Pf. 30/1; Lithistid Cave)	285–436 μm	rhabdome 487–766 μm long / cladome 181–295 μm in diameter	64.4–89.6 μm long / 1.5–1.9 μm thick	10.3–17.3 μm × 9.86–13.1 μm

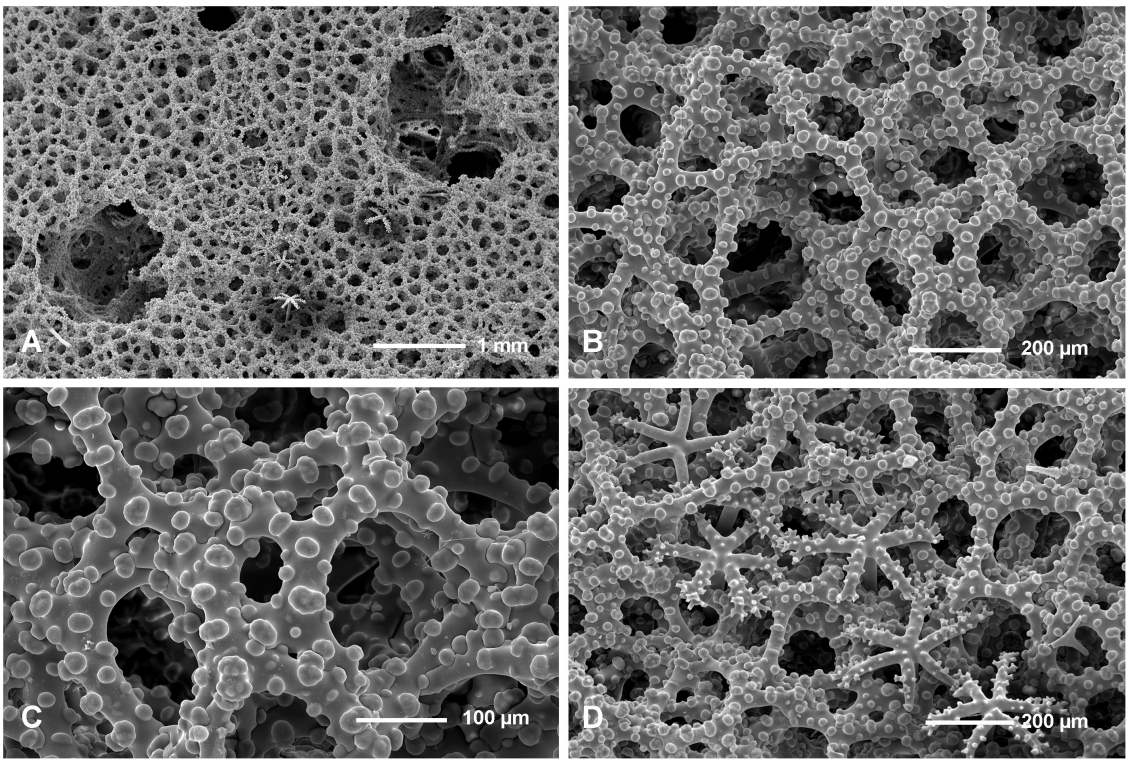

FIGURE 10 | *Neophrissospongia nolitangere* (Schmidt, 1870), south-eastern Aegean Sea (deep-water), off Tilos Island; Exhalant surface of the choanosomal skeleton. **(A)** General view of choanosomal desma skeleton with canal openings corresponding to oscula; **(B,C)** Details of dicranoclone desmas articulation and sculpture; **(D)** Ectosomal dichotriaenes *in situ*.

Harmelin and Vacelet, 1997). The main ecological features shared between marine caves and deep-sea ecosystems include the lack of light (and primary production), oligotrophy and, in some cases, density-trapped seawater which remains cold and at a nearly constant temperature all year round (Vacelet et al., 1994; Harmelin, 1997), among others. Such conditions allow for the colonization of propagules of deep-sea species which are upwelled from adjacent deep-waters; for instance, this is the case for many bathyal species in Trois Pépés Cave, whose likely source of propagules is the nearby Cassidaigne Canyon (Vacelet et al., 1994; Vacelet, 1996; Harmelin and Vacelet, 1997). Large populations of lithistid sponges have been recently described in the deep Mediterranean Sea, specifically aggregated clumps of *Leiodermatium pfeifferae* on the top of seamounts

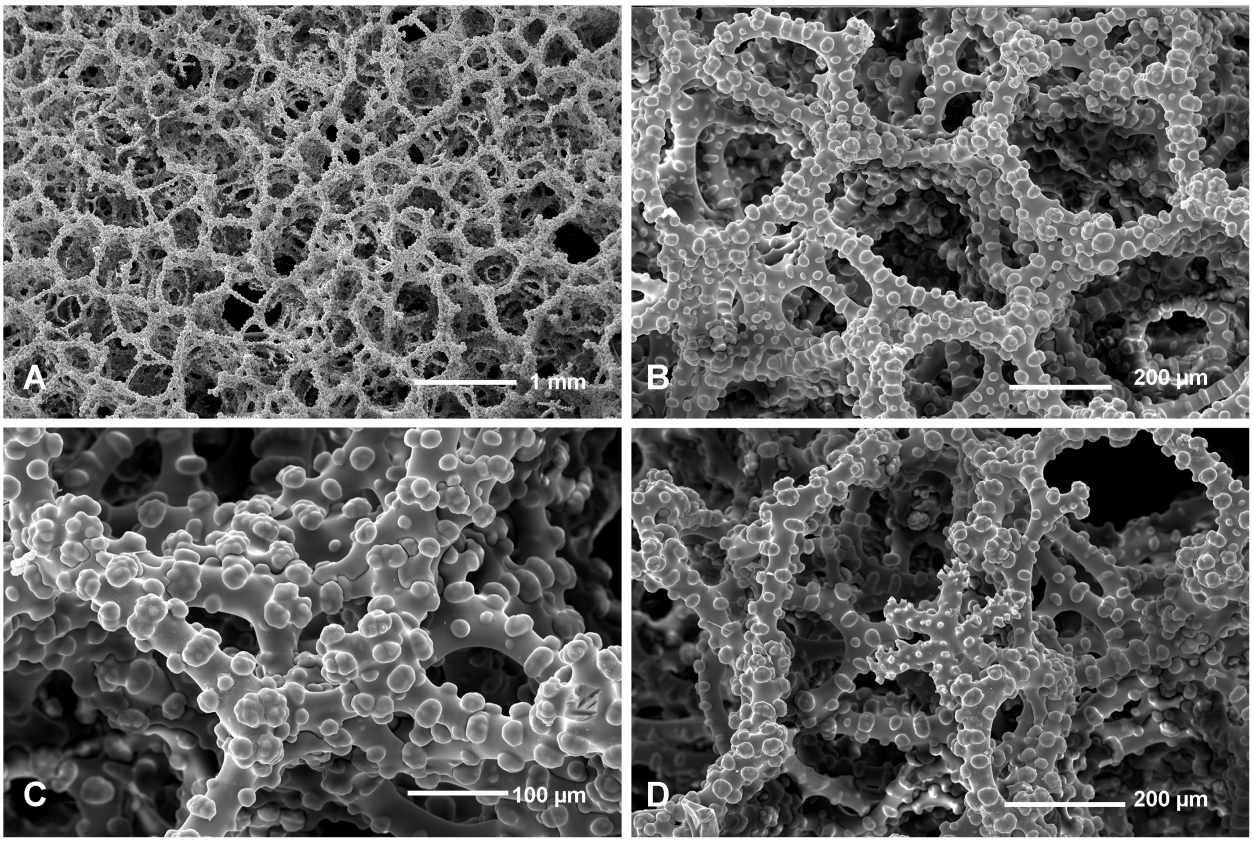

FIGURE 11 | *Neophrissospongia nolitangere* (Schmidt, 1870), south-eastern Aegean Sea (deep-water), off Tilos Island. Inhalant surface of the choanosomal skeleton; **(A)** General view of choanosomal skeleton to show irregular net; **(B,C)** Details of dicranoclone desmas articulation and sculpture; **(D)** Ectosomal dichotriaene *in situ*, among desmas.

off the Balearic Islands (Maldonado et al., 2015). Indications that such unrecognized deep-water populations of lithistid sponges, which may be a source of propagules for shallow marine caves, exist in the deep north-eastern Mediterranean Sea, include the here described occurrence of *N. nolitangere* from the south-eastern Aegean Sea (313–352 m) and photos of tetractinellids on low outcropping reefs (473 m depth), possibly *Neophrissospongia*, taken by a Remotely Operated Vehicle in the central Aegean Sea (Figure 15A in Bo et al., 2020 and unpublished sources of V. Gerovasileiou). It is also worth noting that the steep southern margin of Crete, and specifically the marine area off Samaria, where two of the surveyed caves are located (Italian and Lithistid caves), is incised by numerous gullies and deep canyons. The occurrence of *N. endoumensis* in caves on both southern and northern coasts of Crete indicates that populations should exist in intermediate areas as well, which encompass extensive carbonate rocky coasts, with a high number of still unstudied marine caves, some of which have internal freshwater influx (V. Gerovasileiou unpublished data), but also deep waters. More specifically, the 200 m isobath is only ca. 2 km away from the Italian and Lithistid caves and ca. 3.5 km from the Blue Cave, while it is much closer to the coasts in intermediate locations between these caves (based on data from the EMODnet Bathymetry portal[1]). Agios Efstratios is one of the most isolated islands in the Aegean Archipelago, being approximately 30 km away from the nearest island (Lemnos), and is surrounded by waters deeper than 200 m (ca. 11 km from Trypia Spilia), standing in the center of the northern Aegean Sea (Dimarchopoulou et al., 2018).

It was also suggested that some submarine cave organisms may be "very old [even Mesozoic] elements" of relictual character and that "marine caves served as faunal refuges over very long periods of time" (HartJr., Manning and Iliffe, 1985). Lithistids from Lebanese caves have been characterized as "palaeoendemic" remnants of the subtropical/tropical assemblages, which thrived in the Mediterranean during warm periods of its history and survived only in the warmer south-eastern section of the basin during the subsequent cooling episodes (Perez et al., 2004). This hypothesis cannot be maintained in the case of the studied lithistids from submarine caves of Crete in particular, and the Mediterranean in general (but in fact it concerns any shallow water marine caves) because it is ahistorical, i.e., not accounting for

[1]http://www.emodnet-bathymetry.eu

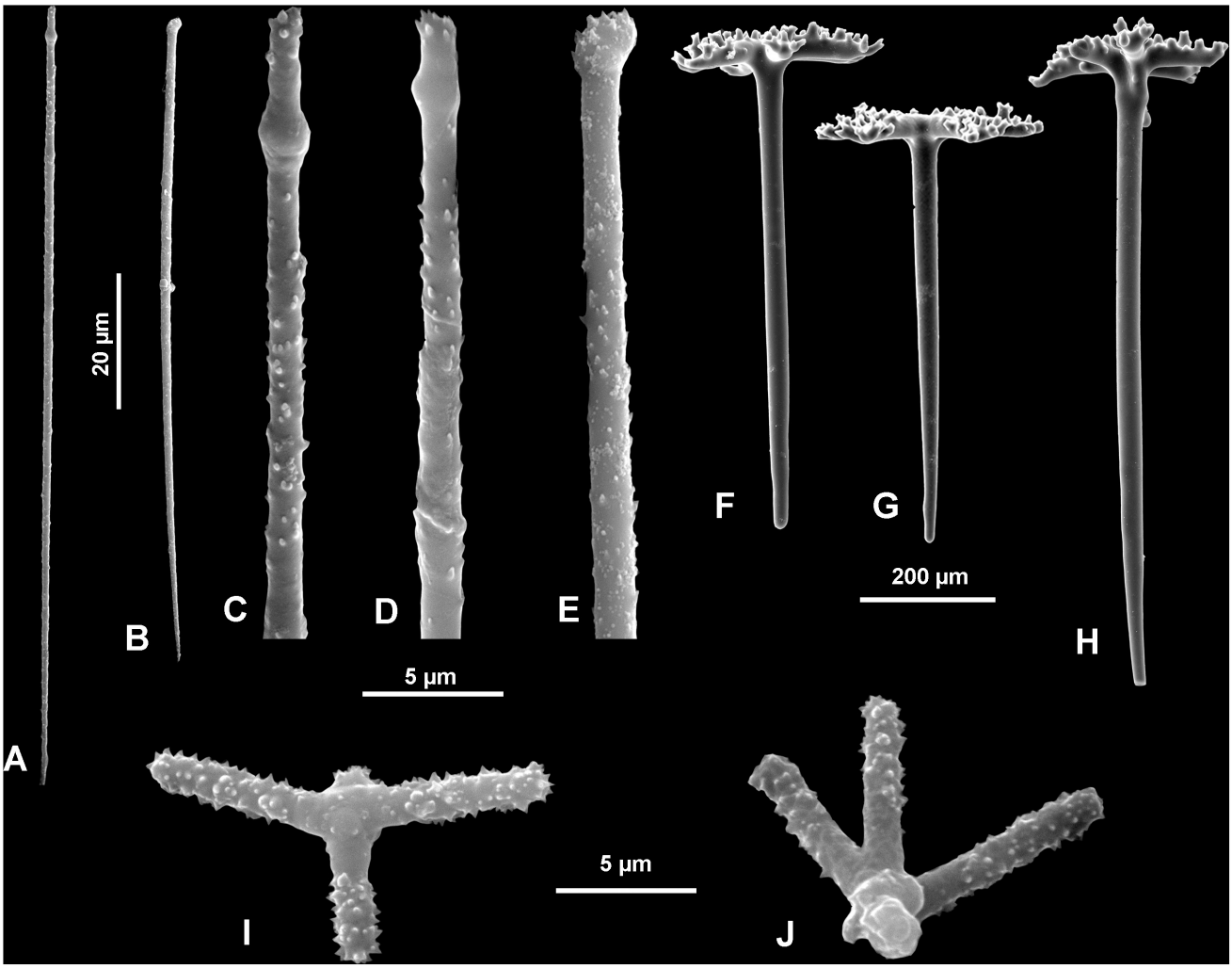

FIGURE 12 | *Neophrissospongia nolitangere* (Schmidt, 1870), south-eastern Aegean Sea (deep-water), off Tilos Island. **(A–E)** Choanosomal microtylostyles, general view **(A,B)** and their heads **(C–E)**; **(F–H)** Ectosomal dichotriaenes in lateral view; **(I,J)** Streptasters.

physiographic changes leading to formation and appearance of caves, palaeogeography and sea level changes during long periods of time. In the Mediterranean case such events and sea level changes include, for example, Messinian salinity crisis (about 5.6 My ago) (Bianchi et al., 2012), and more recently last glaciation that is global and lasted between 115,000 and 11,700 years ago, causing sea level drop of about 145 m in the region of Crete about 20,000 years ago (Lambeck and Purcell, 2005).

Caves themselves cannot be of Mesozoic or even Paleogene in age. Most of the karstic caves in the Mediterranean region originated subaerially, most probably during glaciations (especially last glaciation, i.e., during the period between 115,000 to 11,700 years ago) and were submerged after (Arko-Pijevac et al., 2001). Thus, cave invertebrates, including the studied here lithistid demosponges must have colonized the surveyed caves rather recently, after the last glaciation. During the last glaciation sea level around Crete was about 145 m lower than today, similarly as in the rest of the Mediterranean, and still about 10 m below the present sea level about 7,000 years ago and about 2 m lower about 3,000 years ago (Lambeck and Purcell, 2005). One has to remember that during Holocene relative sea level stands in western-central and eastern parts of Crete were considerably different due to tectonic movements (Mourtzas et al., 2016). Having in mind those values, the colonization of the studied caves that are 3–12 m deep could occur between about 7,000 and 3,000 years ago, but not earlier (depending on the cave).

The only relictual sponges known to date are fossilized lithistids ("mummies" – sponges preserved as complete specimens by early precipitation of calcium carbonate, see Matyja, 1978; Pisera, 1997) from Trois Pépés Cave (Pisera and Vacelet, 2011). They may be interpreted as relicts from previous submergence of the cave, about 8,000 years ago, or during earlier warm interglacial periods. Similar fossilized

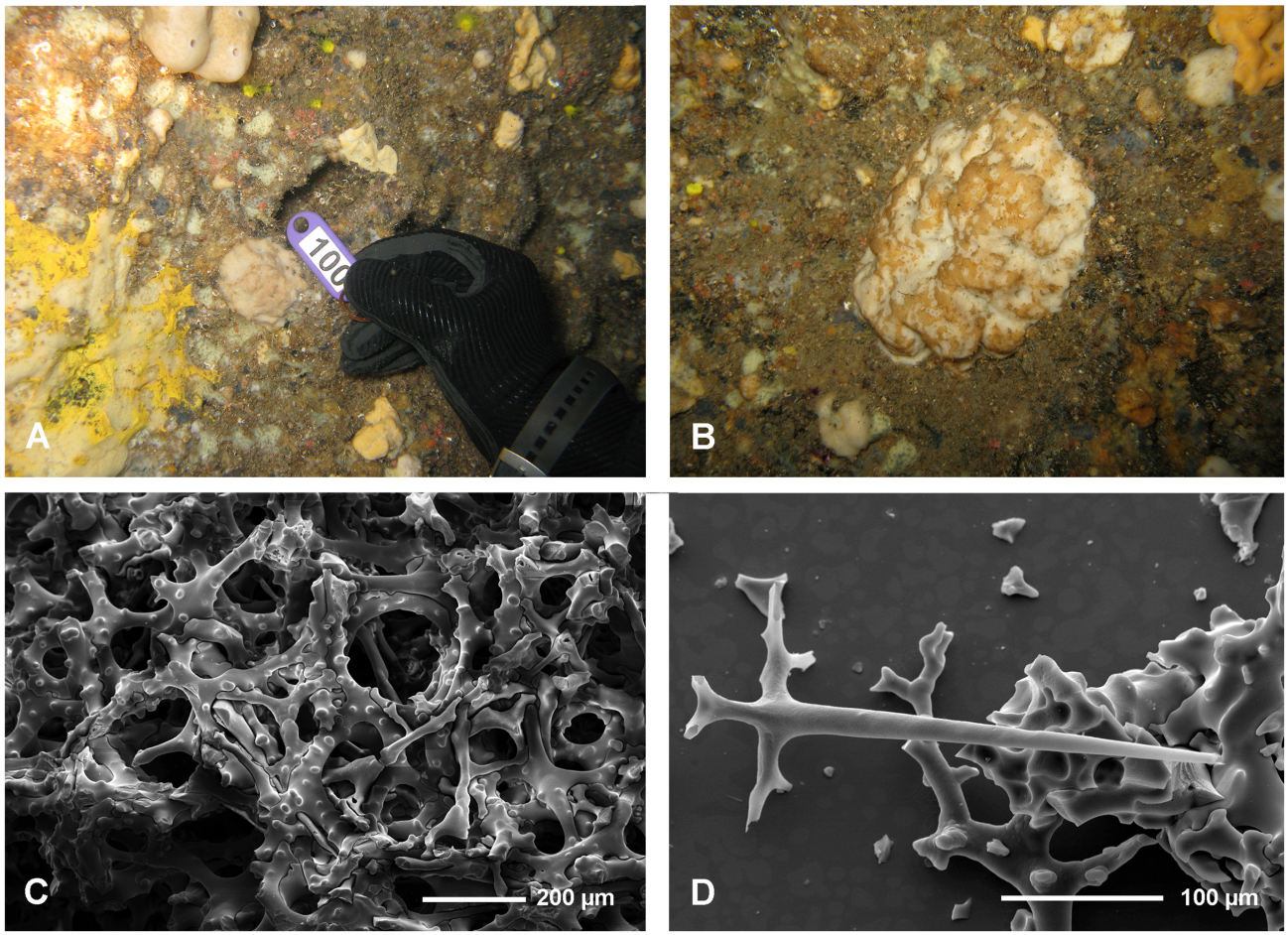

FIGURE 13 | *Neophrissospongia* cf. *nana* Manconi and Serusi, 2008, **(A,B)** Habitus; underwater photo of sponges *in situ*; **(C)** Choanosomal skeleton of confused and malformed dicranoclone desmas; **(D)** Young (not completely formed; note open axial canals) dichotriaene. Photos **(A,B)** by V. Gerovasileiou.

relictual sponges were observed in Sardinian caves (A. Pisera, unpublished) but were described also from deep Mediterranean waters (Allouc, 1987).

In the case of very old, relictual character of lithistid sponges, one should expect either much larger sponges to occur, or numerous fossilized (dead) sponges that should accumulate in a cave (lithistids due to their articulated skeleton preserve well after death). None of these is observed in all known to us caves (not only here reported). Very little is known about growth rate of lithistid demosponges. The only systematic study is the report by Ellwood et al. (2007) on growth rate of *Corallistes undulatus* Lévi and Lévi, 1983 (closely related genus to *Neophrissospongia*) from deep waters off New Caledonia, that was about 20 × 30 cm large, and revealed values between 1.1 and 1.3 mm/year, giving 135–160 years old. Should we apply these values to the largest specimen observed in the Lithistid Cave, that was 100 cm × 40 cm in size (**Figure 2B**), the estimated age of this specimen is between 769 and 909 years, if longer dimension is used. Although this is only a first approximate estimation, in the absence of other data for comparison, it equally indicates relatively new (in accordance with known geological history and sea level changes) colonization of the caves.

Silica Content of Sea Water and Occurrence of Lithistid Demosponges

Lithistid demosponges with their dense choanosomal skeleton consisting of articulated desmas are heavily silicified, being even called "hypersilicified" sponges. They occur mostly in deep waters below 100 m, being very common at several hundreds of meters, where silica concentration is much higher than in shallow water. Numerous species of lithistid demosponges, including *Neophrissospongia*, are known from Mediterranean marine caves (Pisera and Vacelet, 2011; Gerovasileiou and Voultsiadou, 2012), as well as from the Atlantic and Pacific oceans (A. Pisera, unpublished data). This is usually explained by the fact that the dark zones of marine caves are characterized by conditions similar to bathyal depths (see previous section) by being dark, oligotrophic and often with low temperature. Nevertheless, in the studied marine caves lithistids were not found exclusively in dark

zones, but also close to entrances and in semi-dark zones, while water temperatures reached 22–26°C in summer versus 14.7°C in the deep Aegean Sea (313–352 m), where *N. nolitangere* was trawled.

Lithistid demosponges are found in some, but not all dark submarine caves. Their absence from some caves and presence in others may be caused by chance: lack/presence of deep-water sources of propagules, unfavorable/favorable physiographic conditions of the sea floor near the caves, and similar factors. We have identified, however, an interesting coincidence between the occurrence of lithistid sponges (in case of the Lithistid Cave of large masses of these sponges) in different marine caves of the oligotrophic eastern Mediterranean Sea; all caves – and sections within these caves – where lithistids were found have freshwater springs. In addition to our observations from the north-eastern Mediterranean, Perez et al. (2004) found dense populations of lithistids in a shallow (2–5 m deep) cave of Lebanon, Levantine Sea, including areas with freshwater mixing. Publications reporting lithistids from other Mediterranean marine caves do not provide specific information on freshwater input, except for caves with freshwater infiltrations in their inner and upper portions (Pouliquen, 1972). Such infiltrations (e.g., through cracks and percolations of rocks) are very common in Mediterranean marine caves but are usually sporadic and/or seasonal (Gerovasileiou and Bianchi, in press).

This association between caves with freshwater springs and lithistids is surprising and difficult to understand at the first moment due to the fact that lithistid demosponges are typical marine invertebrates. This situation is easier to understand if we consider that silicic acid concentration of water in such parts of the caves are 8–11 times higher (and comparable to deep seawater at several hundred meters) than its concentration in water near the cave entrance (and average of surface water in the area). In the case of Blue Cave silicic acid concentration is 3.280 μM ± 1.365 (SD) in the zone where lithistid sponges occur (similar values of about 2–3 μM characterized seawater at a depth of 200–300 m in the Cretan Sea, Souvermezoglou and Krasakopoulou, 2000) versus 0.427 μM ± 0.137 (SD) at the cave entrance. In the Lithistid Cave silicate concentration is 7.170 μM ± 1.244 (SD) in the zone where lithistid sponges thrive (6–11 μM for several hundred meters deep in the eastern Mediterranean Sea, Krom et al., 2014) versus 0.663 μM ± 0.042 (SD) at the cave entrance. In addition to the lithistid populations, other "hypersilicified" sponges (geodiids) also occur in high abundances and/or size in the Lithistid cave, but are uncommon in external environments of Crete, except for rocky areas with freshwater springs (V. Gerovasileiou, personal observations). The specimens of *N. nolitangere* found off Tilos Island, at about 300 m depth, occurred in waters characterized by values of 2.5–3 μM (Souvermezoglou and Krasakopoulou, 2000) that are still lower than those observed in the studied caves. Such differences may be significant for lithistids, with their heavily silicified skeleton as proven by desma-less theonellids occurring in shallow water (thus very low in silicic acid) of the Great Barrier Reef (Hall et al., 2014). Higher siliceous acid concentration, resulting from hydrothermal vents, is recalled as a factor promoting sponge growth in shallow waters of Indonesia (Bertolino et al., 2017). The importance of silicic acid concentration (however, much more extreme and under experimental conditions) for spiculogenesis in demosponges was demonstrated by Maldonado et al. (1999), while correlation between this concentration and disruption of spiculogenesis in natural conditions in other heavily silicified demosponges, i.e., geodiids was discussed by Cardenas and Rapp (2013). They have demonstrated that some spicules in shallower water characterized by lower silica concentration may become irregular and underdeveloped as it is the case of our *N.* cf. *nana*, for example. Also, high variability of spicules in other species described here may be of similar origin. Specifically, the difference between microscleres (that are the first to react to lower silica concentration – Cardenas and Rapp, 2013) between *N. endoumensis* and *N. nolitangere* could be the result of such dependence, and we should check if these two nominal species could be just ecomorphological variants. One has to remember that such correlation is not a simple one and not associated with particular level of silicic acid concentration alone, and probably depends on other associated factors such as food availability and temperature (Cardenas and Rapp, 2013). This possibility must be investigated more systematically in case of other marine caves with lithistid sponges with quantitative approaches and molecular methods.

Conclusions

All the three *Neophrissospongia* species described in this study are reported for the first time from the eastern Mediterranean Sea, revealing a broad geographic distribution, and are also new elements for the sponge fauna of Greece. The species *N. endoumensis*, previously known from only a single cave in Marseille (France), was described from three shallow marine caves on both southern and northern coasts of Crete. One of these caves harbored an abundant population of this lithistid that may reach large size (100 cm × 40 cm) and old age (approximate estimation between 769 and 909 years). Another species, i.e., *N. nolitangere* was described from deep waters (ca. 300 m) off Tilos Island (south-eastern Aegean Sea) and *N.* cf. *nana* from a shallow marine cave in Agios Efstratios Island (northern Aegean Sea). The studied caves in Crete had to be colonized by these sponges relatively recently, i.e., not earlier than 7 ky, and most probably 2–3 ky ago from yet unknown deep-water sources, as proven by the presence of *N. nolitangere* and other lithistids in the deep north-eastern Mediterranean Sea. To our opinion they are not relictual forms from the past that survived in marine caves from long time ago as sometime suggested.

Here we hypothesize that the presence of these lithistid sponges in specific marine caves of this marine area, out of the several tens of explored caves, was controlled not only, as postulated earlier, by the fact that dark zones of the studied caves resemble deep-water environment by lack of light and oligotrophy, but also because these parts are characterized by relatively high (as for the Mediterranean) concentration of silicic acid, delivered to the caves by freshwater sources occurring in these sections. This conclusion is also supported by the presence of other "hypersilicified" sponges in high abundances and size in these marine caves, which are uncommon in other

habitats, and also from observations in other marine caves with freshwater springs.

We also hypothesize that high intraspecific variability of spiculation, as well as underdevelopment of spicules and/or pathologic development of the skeleton (our *N.* cf. *nana*) may be caused by great differences in, and/or low silicic acid concentration. If this is true then conspecificity of *N. nolitangere* and *N. endoumensis* must be seriously considered and investigated in a more rigorous way, as well as a possibility that *N.* cf. *nana* (and *N. nana* itself) is just an underdeveloped ecomorph of some other known species.

The occurrence of such slow-growing and ecosystem-engineering invertebrates of deep-water origin in shallow marine caves with particular characteristics, within an oligotrophic marine basin, highlight an urgent need for further study, appropriate management, and conservation actions.

DATA AVAILABILITY STATEMENT

The original contributions presented in the study are included in the article. Further inquiries can be directed to the corresponding author.

AUTHOR CONTRIBUTIONS

AP and VG conceived and wrote the manuscript, and acquired funding sources. AP examined the specimens and performed morphological lab work and taxonomic analysis. VG conducted sampling and provided collection data and underwater images. Both authors approved the submitted version of the manuscript.

FUNDING

This study was in part supported by the NSC Poland, grant no. 2016/21/B/ST10/02332 to AP who was also supported by statuary funds of the Institute of Paleobiology, Polish Academy of Sciences. Additional funds were provided to VG by the project "Centre for the study and sustainable exploitation of Marine Biological Resources (CMBR)" (MIS 5002670), which is implemented under the Action "Reinforcement of the Research and Innovation Infrastructure," funded by the Operational Programme "Competitiveness, Entrepreneurship and Innovation" (NSRF 2014–2020) and co-financed by Greece and the EU (European Regional Development Fund). The studied deep-water sponge specimen was collected during the 2018 MEDITS Survey in the frame of the Greek National Data Collection Project.

ACKNOWLEDGMENTS

We acknowledge Snezana Zivanović, Eleni Dafnomili, and Manolis Tsapakis from the Hellenic Centre for Marine Research for measuring silicate concentration in water samples from the studied marine caves. We are grateful to Guilherme Muricy, Thanos Dailianis, and Elena Akritopoulou for their valuable help during fieldwork and Panagiota Peristeraki for providing the deep-water lithistid sample.

REFERENCES

Aguilar, R., López Correa, M., Calcinai, B., Pastor, X., De La Torriente, A., and Garcia, S. (2011). First records of *Asbestopluma hypogea* Vacelet and Boury-Esnault, 1996 (Porifera, Demospongiae Cladorhizidae) on seamounts and in bathyal settings of the Mediterranean Sea. *Zootaxa* 2925, 33–40. doi: 10.11646/zootaxa.2925.1.3

Allouc, J. (1987). Les paléocommunautés profondes sur fond rocheux du Pléistocène méditerranéen. Description et essai d'interprétation paléoécologique. *Geobios* 20, 241–263. doi: 10.1016/S0016-6995(87)80036-0

Arko-Pijevac, M., Benac, Č, Kovačič, M., and Kirinčić, M. (2001). A submarine cave at the Island of Krk (North Adriatic Sea). *Nat. Croat.* 10, 163–184.

Bakran-Petricioli, T., Vacelet, J., Zibrowius, H., Petricioli, D., Chevaldonné, P., and Rađa, T. (2007). New data on the distribution of the 'deep-sea' sponges *Asbestopluma hypogea* and *Oopsacas minuta* in the Mediterranean Sea. *Mar. Ecol.* 28, 10–23. doi: 10.1111/j.1439-0485.2007.00179.x

Bertolino, M., Oprandi, A., Santini, C., Castellano, M., Pansini, M., Boyer, M., et al. (2017). Hydrothermal waters enriched in silica promote the development of a sponge community in North Sulawesi (Indonesia). *Eur. Zool. J.* 84, 128–135. doi: 10.1080/11250003.2016.1278475

Bianchi, C. N., Morri, C., Chiantore, M., Montefalcone, M., Parravicini, V., and Rovere, A. (2012). "Mediterranean Sea biodiversity between the legacy from the past and a future change," in *Life in the Mediterranean Sea: A Look at Habitat Changes*, Chap. 1, ed. N. Stambler (New York, NY: Vova Science Publishers), 1–55.

Bo, M., Al Mabruk, S. A. A., Balistreri, P., Bariche, M., Batjakas, I. E., Betti, F., et al. (2020). New records of rare species in the Mediterranean Sea (October 2020). *Mediterr. Mar. Sci.* 21, 608–630. doi: 10.12681/mms.23674

Cardenas, P., and Rapp, T. T. (2013). Disrupted spiculogenesis in deep-water Geodiidae (Porifera, Demospongiae) growing in shallow waters. *Invertebr. Biol.* 132, 173–194. doi: 10.1111/ivb.12027

Carvalho, F. C., Cárdenas, P., Ríos, P., Cristobo, J., Rapp, H. T., and Xavier, J. R. (2020). Rock sponges (lithistid Demospongiae) of the Northeast Atlantic seamounts, with the description of ten new species. *PeerJ* 8:e8703. doi: 10.7717/peerj.8703

Carvalho, F. C., Pomponi, S. A., and Xavier, J. R. (2015). Lithistid sponges of the upper bathyal of Madeira, Selvagens and Canary Islands, with description of a new species of *Isabella*. *J. Mar. Biol. Assoc. U. K.* 95, 1287–1296. doi: 10.1017/s0025315414001179

Chevaldonné, P., Pérez, T., Crouzet, J.-M., Bay-Nouailhat, W., Bay-Nouailhat, A., Fourt, M., et al. (2015). Unexpected records of 'deep-sea' carnivorous sponges *Asbestopluma hypogea* in the shallow NE Atlantic shed light on new conservation issues. *Mar. Ecol.* 36, 475–484. doi: 10.1111/maec.12155

Cruz, T. (2002). *Esponjas Marinas de Canarias*. S/C Tenerife: Consejería de Política Territorial y Medio Ambiente del Gobierno de Canarias. doi: 10.1111/maec.12155

Dimarchopoulou, D., Gerovasileiou, V., and Voultsiadou, E. (2018). Spatial variability of sessile benthos in a semi-submerged marine cave of a remote Aegean Island (eastern Mediterranean Sea). *Reg. Stud. Mar. Sci.* 17, 102–111. doi: 10.1016/j.rsma.2017.11.015

Ellwood, M. J., Kelly, M., and Richer de Forges, B. (2007). Silica banding in the deep-sea lithistid sponge *Corallistes undulatus*: investigating the potential influence of diet and environment on growth. *Limnol. Oceanogr.* 52, 1865–1873. doi: 10.4319/lo.2007.52.5.1865

Galani, A., Dailianis, T., Sini, M., Katsanevakis, S., and Gerovasileiou, V. (2019). "Characterization of benthic communities in marine caves of the island-dominated Aegean ecoregion (Eastern Mediterranean Sea)," in *Proceedings of the 2nd Mediterranean Symposium on the Conservation of Dark Habitats*, eds H. Langar and A. Ouerghi (Tunis: SPA/RAC publi), 67–68.

Gerovasileiou, V., Chintiroglou, C., Vafidis, D., Koutsoubas, D., Sini, M., Dailianis, T., et al. (2015). Census of biodiversity in marine caves of the Eastern Mediterranean Sea. *Mediterr. Mar. Sci.* 16, 245–265. doi: 10.12681/mms.1069

Gerovasileiou, V., and Voultsiadou, E. (2012). Marine caves of the Mediterranean Sea: a sponge biodiversity reservoir within a biodiversity hotspot. *PLoS One* 7:e39873. doi: 10.1371/journal.pone.0039873

Gerovasileiou, V., and Bianchi, C. N. (in press). Mediterranean marine caves: a synthesis of current knowledge. *Oceanogr. Mar. Biol. Annu. Rev.* 59.

Hall, K. A., Ekins, M. G., and Hooper, J. N. A. (2014). Two new desma-less species of *Theonella* Gray, 1868 (Demospongiae: Astrophorida: Theonellidae), from the Great Barrier Reef, Australia, and a re-evaluation of one species assigned previously to Dercitus Gray, 1867. *Zootaxa* 3814, 451–477. doi: 10.11646/zootaxa.3814.4.1

Harmelin, J.-G. (1997). Diversity of bryozoans in a Mediterranean sublittoral cave with bathyal like conditions: role of dispersal processes and local factors. *Mar. Ecol. Prog. Ser.* 153, 139–152. doi: 10.3354/meps153139

Harmelin, J.-G., and Vacelet, J. (1997). Clues to deep-sea biodiversity in a nearshore cave. *Vie Milieu* 47, 351–354.

Hart, C. W. Jr., Manning, R. B., and Iliffe, T. M. (1985). The fauna of Atlantic marine caves: evidence of dispersal by sea floor spreading while maintaining ties to deep waters. *P. Biol. Soc. Wash.* 98, 288–292.

Krom, M. D., Kress, N., and Fanning, K. (2014). Silica cycling in the ultra-oligotrophic eastern mediterranean sea. *Biogeosciences* 11, 4211–4223. doi: 10.5194/bg-11-4211-2014

Lage, A., Araújo, H. P. M., Gerovasileiou, V., and Muricy, G. (2018). A new cave-dwelling species of *Plakina* (Porifera: Homoscleromorpha) from Crete. Greece (Aegean Sea). *Zootaxa* 4466, 39–48. doi: 10.11646/zootaxa.4466.1.5

Lage, A., Gerovasileiou, V., Voultsiadou, E., and Muricy, G. (2019). Taxonomy of *Plakina* (Porifera: Homoscleromorpha) from Aegean submarine caves, with description of three new species and new characters for the genus. *Mar. Biodivers.* 49, 727–747. doi: 10.1007/s12526-018-0847-z

Lambeck, K., and Purcell, A. (2005). Sea-level change in the Mediterranean Sea since the LGM: model predictions for tectonically stable areas. *Quat. Sci. Rev.* 24, 1969–1988. doi: 10.1016/j.quascirev.2004.06.025

Maldonado, M., Aguilar, R., Blanco, J., García, S., Serrano, A., and Punzón, A. (2015). Aggregated clumps of lithistid sponges: a singular, reef-like bathyal habitat with relevant paleontological connections. *PLoS One* 10:e0125378. doi: 10.1371/journal.pone.0125378

Maldonado, M., Carmona, M. C., Uriz, M. J., and Cruzado, A. (1999). Decline in Mesozoic reef-building sponges explained by silicon limitation. *Nature* 401, 785–788. doi: 10.1038/44560

Manconi, R., and Serusi, A. (2008). Rare sponges from marine caves: discovery of *Neophrissospongia nana* nov. sp. (Demospongiae, Corallistidae) from Sardinia with an annotated checklist of Mediterranean lithistids. *ZooKeys* 4, 71–87. doi: 10.3897/zookeys.4.39

Manconi, R., Serusi, A., and Pisera, A. (2006).). A new Mediterranean 'lithistid' sponge, *Aciculites mediterranea* sp. nov. (Porifera: Demospongiae) from a dark marine cave in Sardinia. *J. Mar. Biol. Assoc. U. K.* 86, 691–698. doi: 10.1017/S0025315406013580

Matyja, B. A. (1978). Struktury wczesnodiagenetyczne w wapiennych utworach oksfordu. *Przegląd Geol.* 3, 156–158.

Mourtzas, N., Kolaiti, E., and Anzidei, M. (2016). Vertical land movements and sea level changes along the coast of Crete (Greece) since Late Holocene. *Quat. Int.* 401, 43–70. doi: 10.1016/j.quaint.2015.08.008

Perez, T., Vacelet, J., Bitar, G., and Zibrowius, H. (2004). Two new lithistids (Porifera: Demospongiae) from a shallow eastern Mediterranean cave (Lebanon). *J. Mar. Biol. Ass. U. K.* 84, 15–24. doi: 10.1017/S0025315404008859h

Pisera, A. (1997). Upper Jurassic siliceous sponge from the Swabian Alb: taxonomy and paleoecology. *Palaeontol. Pol.* 57, 1–216.

Pisera, A., and Lévi, C. (2002). "Family Corallistidae Sollas, 1888," in *Systema Porifera. A Guide to the Classification of Sponges*, eds J. N. A. Hooper and R. W. M. Van Soest (New York, NY: Kluwer Academic/Plenum Publishers), 312–320. doi: 10.1007/978-1-4615-0747-5_35

Pisera, A., and Pomponi, S. A. (2015). New data on lithistid sponges from the deep Florida shelf with description of a new species of *Theonella*. *J. Mar. Biol. Assoc. U. K.* 95, 1297–1309. doi: 10.1017/S0025315414001477

Pisera, A., and Vacelet, J. (2011). Lithistid sponges from submarine caves in the Mediterranean: taxonomy and affinities. *Sci. Mar.* 75, 17–40. doi: 10.3989/scsimar.2011.75n1017

Pomponi, S. A., Kelly, M., Reed, J. K., and Wright, A. E. (2001). Diversity and bathymetric distribution of lithistid sponges in the tropical western Atlantic. *Bull. Biol. Soc. Wash.* 10, 344–353.

Pouliquen, L. (1972). Les spongiaires des grottes sous-marines de la région de Marseille. Ecologie et systématique. *Téthys* 3, 717–758.

Schmidt, O. (1870). *Grundzüge einer Spongien-Fauna des Atlantischen Gebietes*. Leipzig: Wilhelm Engelmann.

Schuster, A., Cárdenas, P., Pisera, A., Pomponi, S. A., Kelly, M., Wörheide, G., et al. (2018). Seven new deep-water Tetractinellida (Porifera: Demospongiae) from the Galápagos Islands – morphological descriptions and DNA barcodes. *Zool. J. Linn. Soc. Lond.* 184, 273–303. doi: 10.1093/zoolinnean/zlx110

Sini, M., Katsanevakis, S., Koukourouvli, N., Gerovasileiou, V., Dailianis, T., Buhl-Mortensen, L., et al. (2017). Assembling ecological pieces to reconstruct the conservation puzzle of the aegean sea. *Front. Mar. Sci.* 4:347. doi: 10.3389/fmars.2017.00347

Souvermezoglou, E., and Krasakopoulou, E. (2000). Chemical oceanography in the Cretan Sea: changes associated to the transient. *Mediterr. Mar. Sci.* 1, 91–103. doi: 10.12681/mms.292

Topsent, E. (1904). Spongiaires des Açores. Résultats des campagnes scientifiques accomplies par le Prince Albert I. Monaco. *Résultats des campagnes scientifiques accomplies sur son yacht* 25, 1–280.

Vacelet, J. (1996). Deep-sea sponges in a Mediterranean cave. *Biosystem. Ecol. Ser.* 11, 299–312.

Vacelet, J. (2002). "Recent 'Sphinctozoa', order verticillitida, family Verticillitidae Steinmann, 1882," in *Systema Porifera. A Guide to the Classification of Sponges*, eds J. N. A. Hooper and R. W. M. Van Soest (New York, NY: Kluwer Academic/Plenum Publishers), 1097–1098. doi: 10.1007/978-1-4615-0747-5_113

Vacelet, J., and Boury-Esnault, N. (1996). A new species of carnivorous sponge (Demospongiae: Cladorhizidae) from a Mediterranean cave. *Bull. Inst. R. Sci. Nat. Belg.* 66, 109–115.

Vacelet, J., Boury-Esnault, N., and Harmelin, J.-G. (1994). Hexactinellid cave, a unique deep-sea habitat in the scuba zone. *Deep Sea Res. Pt I* 41, 965–973. doi: 10.1016/0967-0637(94)90013-2

Vacelet, J., Cuif, J.-P., Gautret, P., Massot, M., Richer de Forges, B., and Zibrowius, H. (1992). Un Spongiaire Sphinctozoaire colonial apparenté aux constructeurs de récifs triasiques survivant dans le bathyal de Nouvelle-Calédonie. *C. R. Hebd. Séances Acad. sci.* 314, 379–385.

Vacelet, J., and Vasseur, P. (1965). Spongiaires des grottes et surplombs des récifs de Tuléar. *Recl. Trav. Stn. Mar. Endoume Marseille* 4, 71–123.

Vamvakas, C. E. (1970). Peuplements Benthiques des Substrats Meubles du Sud de la Mer Egée. *Tethys* 2, 89–130.

Van Soest, R. W. M., Boury-Esnault, N., Hooper, J. N. A., Rützler, K., de Voogd, N. J., Alvarez, B., et al. (2020). *World Porifera Database*. Available online at: http://www.marinespecies.org/porifera (accessed 18 October, 2020).

Voultsiadou, E. (2005a). Demosponge distribution in the eastern Mediterranean: a NW–SE gradient. *Helgoland Mar. Res.* 59, 237–251. doi: 10.1007/s10152-005-0224-8

Voultsiadou, E. (2005b). Sponge diversity in the Aegean Sea: check list and new information. *Ital. J. Zool.* 72, 53–64. doi: 10.1080/11250000509356653

Voultsiadou, E. (2009). Reevaluating sponge diversity and distribution in the Mediterranean Sea. *Hydrobiologia* 628, 1–12. doi: 10.1007/s10750-009-9725-9

Voultsiadou, E., Gerovasileiou, V., and Bailly, N. (2016). Porifera of Greece: an updated checklist. *BDJ* 4:e7984. doi: 10.3897/BDJ.4.e7984

Wörheide, G., and Reitner, J. (1996). "'Living fossil' sphinctozoan coralline sponge colonies in shallow water caves of the Osprey Reef (Coral Sea) and the Astrolabe Reefs (Fiji Islands)," in *Global and Regional Controls on Biogenic Sedimentation. I. Reef Evolution. Research Reports*, eds J. Reitner, F. Neuweiler, and F. Gunkel (Göttinger Arb: Geol. Paläont), 145–148.

Zea, S. (1987). *Esponjas del Caribe Colombiano*. Bogota: Catalogo Cientifico.

Conflict of Interest: The authors declare that the research was conducted in the absence of any commercial or financial relationships that could be construed as a potential conflict of interest.

Copyright © 2021 Pisera and Gerovasileiou. This is an open-access article distributed under the terms of the Creative Commons Attribution License (CC BY). The use, distribution or reproduction in other forums is permitted, provided the original author(s) and the copyright owner(s) are credited and that the original publication in this journal is cited, in accordance with accepted academic practice. No use, distribution or reproduction is permitted which does not comply with these terms.

frontiers in Marine Science

ORIGINAL RESEARCH
published: 05 February 2021
doi: 10.3389/fmars.2021.612613

In situ Growth Rate Assessment of the Hexactinellid Sponge *Asconema setubalense* Using 3D Photogrammetric Reconstruction

Elena Prado[1], Javier Cristobo[2], Augusto Rodríguez-Basalo[1], Pilar Ríos[1], Cristina Rodríguez-Cabello[1] and Francisco Sánchez[1]*

[1] Centro Oceanográfico de Santander, Instituto Español de Oceanografía (IEO), Santander, Spain, [2] Centro Oceanográfico de Gijón, Instituto Español de Oceanografía (IEO), Gijón, Spain

OPEN ACCESS

Edited by:
Shirley A. Pomponi, Florida Atlantic University, United States

Reviewed by:
Dorte Janussen, Senckenberg Museum, Germany
Ian David Tuck, National Institute of Water and Atmospheric Research (NIWA), New Zealand
Martin Dohrmann, Bayerische Staatssammlung Für Paläontologie und Geologie, Germany

***Correspondence:**
Elena Prado
elena.prado@ieo.es

Specialty section:
This article was submitted to Deep-Sea Environments and Ecology, a section of the journal Frontiers in Marine Science

Received: *30 September 2020*
Accepted: *08 January 2021*
Published: *05 February 2021*

Citation:
Prado E, Cristobo J, Rodríguez-Basalo A, Ríos P, Rodríguez-Cabello C and Sánchez F (2021) In situ Growth Rate Assessment of the Hexactinellid Sponge Asconema setubalense Using 3D Photogrammetric Reconstruction. Front. Mar. Sci. 8:612613. doi: 10.3389/fmars.2021.612613

We describe the first application of a non-invasive and novel approach to estimate the growth rate of *Asconema setubalense* (Porifera, Hexactinellida) through the use of 3D photogrammetric methodology. Structure-from-Motion techniques (SfM) were applied to videos acquired with the *Politolana* ROTV in the El Cachucho Marine Protected Area (MPA) (Cantabrian Sea) on three different dates (2014, 2017, and 2019) over six years. With these data, a multi-temporal study was conducted within the framework of MPA monitoring. A complete 3D reconstruction of the deep-sea floor was achieved with Pix4D Mapper Pro software for each date. Having 3D point clouds of the study area enabled a series of measurements that were impossible to obtain in 2D images. In 3D space, the sizes (height, diameter, cup-perimeter, and cup-surface area) of several *A. setubalense* specimens were measured each year. The annual growth rates recorded ranged from zero ("no growth") for a large size specimen, to an average of 2.2 cm year^{-1} in cup-diameter, and 2.5 cm year^{-1} in height for developing specimens. Von Bertalanffy growth parameters were estimated. Taking into account the size indicators used in this study and based on the von Bertalanffy growth model, this sponge reaches 95% maximum size at 98 years of age. During the MPA monitoring program, a high number of specimens disappeared. This raised suspicions of a phenomenon affecting the survival of this species in the area. This type of image-based methodology does not cause damage or alterations to benthic communities and should be employed in vulnerable ecosystem studies and MPA monitoring.

Keywords: underwater photogrammetry, *Asconema setubalense*, Marine Protected Area (MPA), Le Danois Bank, deep-sea sponges, sponges growth rate

INTRODUCTION

There are gaps in knowledge with regard to growth rates of many benthic organisms, but is especially prevalent in deep-sea sponges, in which basic biological aspects are still unknown today. However, it is evident that sponges play a fundamental role in seabed communities, one of the principal of which is linked to their filtration capacity, removing up to 95% of bacteria and particles from the water and 90% of dissolved organic carbon, thereby converting suspended particles and

dissolved matter into food for other animals. Sponges also seem to play a role in the recirculation of carbon, silicon, and nitrogen; and are also rich in chemical components, some of which are emerging as innovative pharmaceutical products and new drugs (e.g., Maldonado et al., 2012, 2020; Kahn et al., 2015; Ercolano et al., 2019).

Deep-sea coral and sponge habitats are considered exceptional ecosystems from a biodiversity perspective. Sponges and their aggregations provide refuge for other animals, adding complexity and three-dimensionality to deep habitats, therefore favoring biodiversity in their environment. These three-dimensional complex habitats have become a focus of conservation efforts in the deep sea.

Very few studies have been conducted on the biology of hexactinellid sponges because they usually inhabit deep areas, far beyond the limits of diving, complicating access to the places where they are found. Many aspects of their biology remain unknown, related to reproduction, feeding habits, and growth. These aspects of the deep-habitat hexactinellid *Rhabdocalyptus dawsoni* (Lambe, 1893) were studied previously, but only in an area accessible to diving (Leys and Lauzon, 1998).

Hexactinellid sponges are very vulnerable due to their nature, size, and fragility. Fishing gear and other anthropogenic impacts can damage and destroy them, endangering these habitats. Therefore, in recent years, numerous protected areas have been established based on the presence of these vulnerable (or essential) habitats. Follow-up surveys are being performed to monitor their conservation in compliance with the EU Habitats Directive. These efforts for the protection and conservation of vulnerable habitats have been linked to some objectives of ECOMARG, INDEMARES, INTEMARES, and also SponGES projects. SponGES (H2020 grant agreement No. 679849) is a research and innovation project with the goal of developing an integrated ecosystem-based approach to preserve and sustainably use deep-sea sponge ecosystems in the North Atlantic.

The existence of these marine protected areas (MPA) entails the regulation and control of anthropogenic activities. This regulation must be based on thorough scientific research focusing primarily on the conservation and sustainability of vulnerable habitats and species. Quantifying growth rates is an important aspect of establishing the recovery times of ecosystems in the event of possible impact or damage. Establishing practical strategies and guidelines for low-impact monitoring and research of deep-water sponge-ground habitats *in situ* is recommended (Hogg et al., 2010). It is clearly necessary to establish non-destructive and minimally invasive sampling in order to establish time series without affecting vulnerable habitats.

Growth rates of sponges have been studied using different approaches. Some studies constantly monitored growth under controlled laboratory conditions (De Caralt et al., 2003; Duckworth and Pomponi, 2005; Sipkema et al., 2005), but numerous species (especially in the deep-sea) do not survive cultivation in captivity and must be studied *in situ*. Some methods used for measuring growth are destructive, such as recording underwater weight, wet weight, and ash-free dry weight, or radiocarbon dating method (Fallon et al., 2010). Photographing and determination of sponge surface area, however, is non-destructive and provides good results for encrusting sponges (Ayling, 1983; Turón et al., 1998; Garrabou and Zabala, 2001), but three-dimensional shaped sponges (massive, branching, and others) need different approaches because the 2D surface area does not represent a sponge's growth. It is, therefore, necessary to use other non-destructive methods to measure 3D shapes and volume of sessile benthic organisms (Abdo et al., 2006; Koopmans and Wijffels, 2008). These types of studies have usually been conducted for sponge species that inhabit shallow depths, because they are accessible by diving techniques (Hermans et al., 2010). Nonetheless, species that inhabit deep areas remain, in many cases, inaccessible for studies of biological aspects such as reproduction or growth.

In recent decades, technological advances in underwater vehicles and image acquisition and processing techniques have increased the possibilities of accessing these deep areas and expanding the range of species studied. 3D photogrammetry has also been a breakthrough, enabling morphometric parameters to be very precisely measured from images. The use of Structure-from-Motion (SfM) techniques in the marine environment is increasingly widespread and has been applied in studies on the structural complexity of reefs (Leon et al., 2015; Ferrari et al., 2016; Burns et al., 2019), and to investigate the influence of structural complexity on biodiversity and community assemblage (Price et al., 2019), as well as in deep-sea studies to achieve population structure of gorgonian forests using 3D size of colonies (Palma et al., 2018; Prado et al., 2019). Using 3D photogrammetry, it was possible to observe growth and external erosion of coral colonies of tabular *Acropora* spp. (Ferrari et al., 2017), growth rates of total length of *Paragorgia arborea* (Linnaeus, 1758) and *Primnoa resedaeformis* (Gunnerus, 1763) (Bennecke et al., 2016), and growth of nine coral species (branching, massive, and encrusting corals) in the Chagos Archipelago, the Indian Ocean (Lange and Perry, 2020). However, all these studies focused on coralline, and it is more difficult to find this type of methodologies applied to sponges (Ríos et al., 2020). Olinger et al. (2019) used these technologies to measure the volume, surface area, and age estimation of 16 sponge species on the Tibbetts shipwreck off Cayman Brac, in the Caribbean Sea.

The presence of gorgonian forests and deep-sea sponge aggregations on the Le Danois Bank caused its declaration as the "El Cachucho" MPA by the Spanish Ministry of the Environment, and its inclusion in the Natura 2000 network. Although there are no dense populations of *A. setubalense* on Le Danois Bank, their presence has been confirmed by numerous ROV records in this MPA. Numerous studies are being carried out in El Cachucho MPA with the aim of monitoring the populations of *A. setubalense* at the top of the bank in order to describe its geographic distribution in an area of exclusion of bottom fisheries (Sánchez et al., 2017; Rodríguez-Basalo et al., 2021), as well as conducting connectivity studies, and others that analyze the presence of species associated with these populations (Manjón-Cabeza et al., 2021).

Growth rates of deep-sea sponges provide valuable information on their biology and their ability to recover from possible impacts, such as physical damage from fishing activity.

Only a few studies have been published on Hexactinellids (Dayton, 1979; Leys and Lauzon, 1998; Dayton et al., 2013; Fillinger et al., 2013; Marliave, 2015), but no previous growth studies about *Asconema setubalense* in the Cantabrian Sea have been carried out.

Asconema setubalense Kent, 1870, is a cup- or vase-shaped hexactinellid sponge that can reach large sizes. Previously, this species had only been reported at greater depths (93–4,270 m) in the North Atlantic Ocean (Tabachnick and Menshenina, 2007), but more recently it was reported in the Mediterranean during the ROV exploration (>250 m) of the Alboran Sea, the "Seco de los Olivos" (Pardo et al., 2011), and on the shelf of the Alboran Island (Sitjà and Maldonado, 2014). It is sometimes reported forming aggregations or sponge grounds with a high density of specimens. Densities of occurrence are hard to quantify, but sponges in the class Hexactinellida have been reported at densities of 4–5 per m^2 (OSPAR Commission, 2010).

In this study, we present (1) a time series of 3D photogrammetric reconstructions of *Asconema setubalense* sponge specimens recorded at a depth of about 550 m and, based on these 3D models, (2) estimate growth rates through measurements recorded *in situ* at high spatial resolution.

MATERIALS AND METHODS

Study Area

The Le Danois Bank (also known as El Cachucho fishing ground by local fishermen) is an extensive offshore bank and seamount surrounded by slopes and a complex system of channels and canyons (**Figure 1A**). The topographic anomaly formed by Le Danois Bank on the continental slope of the Cantabrian Sea seems to favor the mixing of water masses through isopycnals (Fiuza et al., 1998; Van Aken, 2000; González-Pola et al., 2012), thereby affecting the general current dynamics of the Cantabrian Sea, predominantly in a W–E direction, and playing a very important role in sedimentation processes and ecosystem productivity. The bank and its intraslope basin, declared as El Cachucho MPA (Heredia et al., 2008), covers 234,000 ha. Depths within the area vary from 425 to 4,000 m, and several studies confirm it as a biodiversity hotspot in the Cantabrian Sea (Sánchez et al., 2008, 2017). The management plan for the area includes specific measures for fishing activities, oil exploration, minerals, and military activity (BOE, 2011).

Within this MPA, two small areas with numerous *Asconema setubalense* were selected for our study, located on hard substrate in the north-west and north-east of the bank (**Figure 1A**). Their bathymetric range covers from 540 to 575 m of depth. In these areas, *A. Setubalense* grows accompanied mainly by other sponges such as *Geodia* cf. *barretti*, and *Phakellia robusta,* and also cnidaria, such as *Callogorgia verticillata*. The two selected areas have different population characteristics: Zone 1 (**Figure 1B**): large *A. setubalense* specimens, no small specimens were recorded; Zone 2 (**Figure 1C**): specimens of small and medium size, no large specimens were recorded. Both zones have a rocky substratum with little terrain roughness.

Sampling

The presence of *A. setubalense* had been verified through numerous oceanographic surveys carried out in the area. The May 2014 survey was part of the work carried out to study this area of interest and its declaration as a Marine Protected Area. The July 2017 and 2019 surveys were part of the monitoring program of the MPA. In June 2017, a survey was also carried out in this area within the framework of the H2020 SponGES Project. The images analyzed in this study were obtained during the ESMAREC_0514, ECOMARG_0717, and ECOMARG_0719 surveys, using the Remotely Operated Towed Vehicle (ROTV), *Politolana*. This vehicle can be operated up to a maximum of 2,000 m in depth and transects were carried out at a speed of 0.6–0.8 knots, between 1 and 3 m above the sea floor. This ROTV simultaneously acquires still pictures and HD video, and synchronizes these with environmental variables (pressure, temperature, and salinity). The *Politolana* uses telemetry to send and receive data in real-time from the equipment comprising the monitoring system: altimeter, CTD, positioning system, and cameras (Sánchez and Rodríguez, 2013).

The acoustic positioning system, Kongsberg HIPAP 502, was used to obtain the absolute position of the underwater vehicle. It is based on the Super (Ultra) Short Base Line (SSBL) principle that establishes a three-dimensional position of the transponder. An SSBL system measured the horizontal and vertical angles together with the range to the ROTV. Then, OFOP (Ocean Floor Observation Protocol) software (Huetten and Greinert, 2008) processed the coordinate observation files and merged them with additional sensor data. Finally, a complete data set for each ROTV trajectory deployment was obtained, enabling geo-referencing of image data.

Sampling and video-transect planning were carried out with the aim of monitoring the conservation status of this vulnerable habitat structuring species within this MPA. Given the high quality of the image sampling system described above, it was possible to repeat the observation of the same specimens of *A. setubalense* sponges. This repeat observation of the same individuals is central to our approach, and is generally very challenging, because it is very difficult, at depths greater than 500 m, to locate specific individual species and specimens that often do not exceed 50 cm in size. These video-transects acquired in different years (**Figures 2**, **3**) were used to generate 3D models. The camera was a full-HD video-camera (Sony HD-700-CX) with two LED lights (12,600 lumens/6,000 Kelvin) attached to the image system. Two parallel laser beams spaced 20 cm apart provided scale for videos and constant distances so as to validate results.

Photogrammetric Reconstructions

First, specific zones with specimens of *A. setubalense* observed on different dates were selected. 3D models of these areas were created from the 2014, 2017, and 2019 footage via photogrammetric reconstruction approaches using the software Pix4D Mapper Pro (Pix4D SA, Switzerland). The workflow used a sequence of images taken from single video-camera frames. Pix4D uses the Structure-from-Motion approach (the process

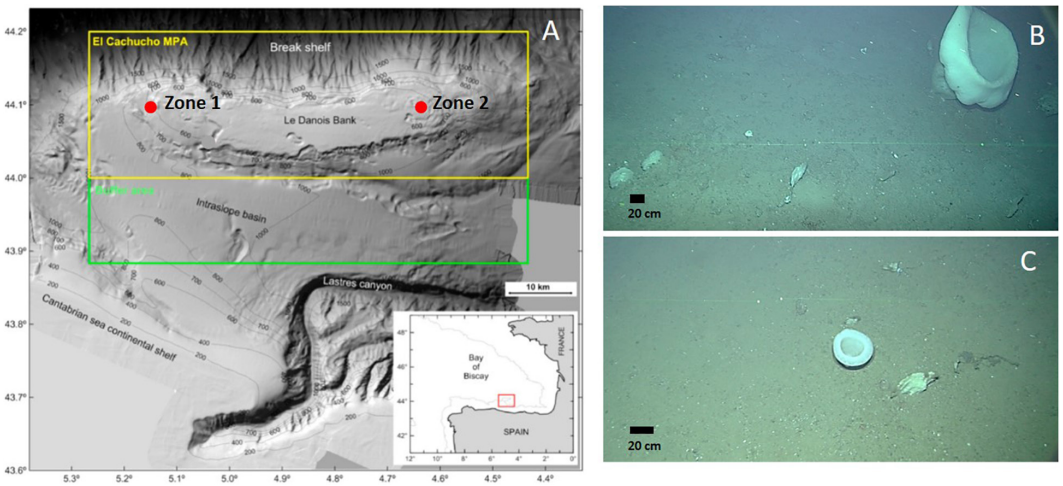

FIGURE 1 | (A) Location of "El Cachucho" MPA on the Bay of Biscay, and some topographic features that characterize the area. Red dots show the location of study zones with specimens of *A. setubalense* analyzed in this study. **(B)** Example of *A. setubalense* specimen in study zone 1: large *A. setubalense* specimens, no small specimens were recorded; **(C)** zone 2, specimens of small and medium size, no large specimens were recorded. Scales of the images were calculated from the constant spacing of the laser beams (20 cm).

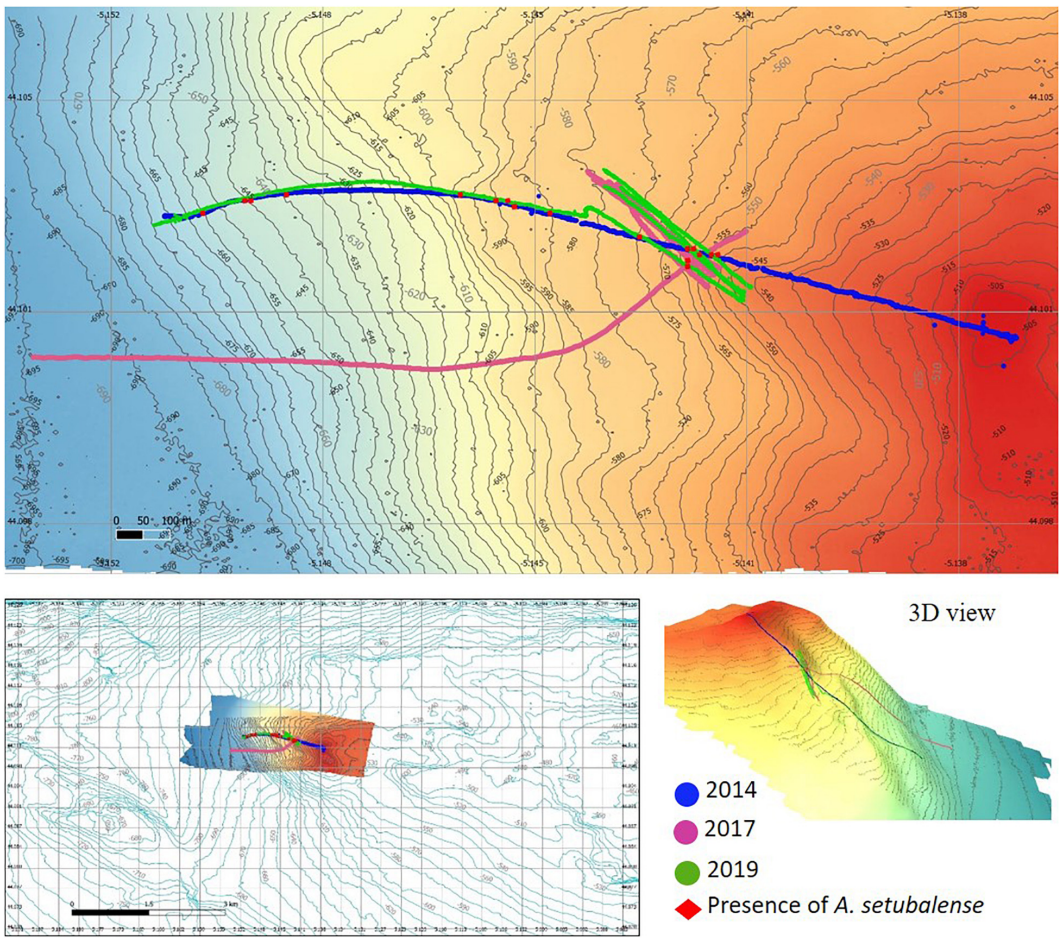

FIGURE 2 | Study zone 1: bathymetric characteristics, temporal image sampling series and presence of *A. setubalense* specimens.

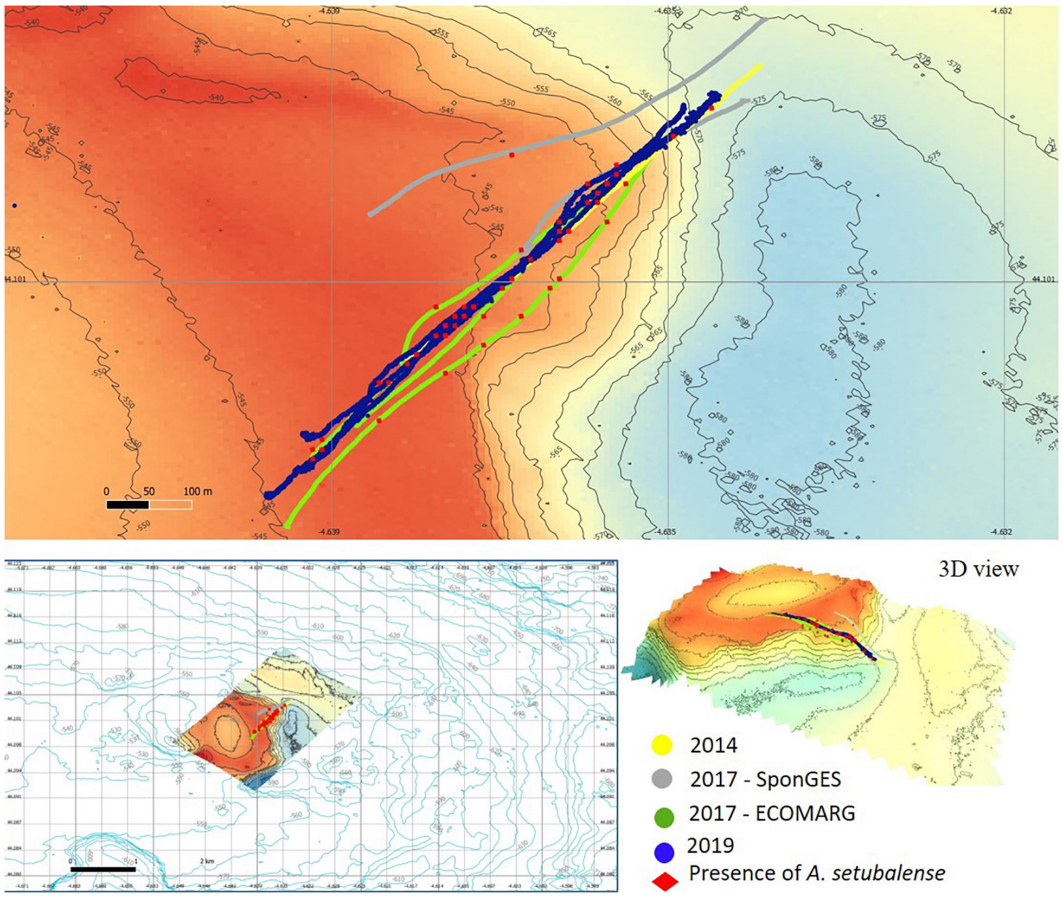

FIGURE 3 | Study zone 2: bathymetric characteristics, temporal image sampling series and presence of *A. setubalense* specimens.

of estimating the 3D structure of a scene from a set of 2D images). It requires point correspondence between images and finds corresponding points by matching features. The software generates 3D dense point clouds (**Figure 4**), Digital Surface Models (DSM), and orthomosaics through integration of the point measurements, camera calibration, and camera position data. Parallel lasers projected onto the ocean floor were used to fine rescale the 3D models. All information was geo-referenced in a cartographic system (UTM-WGS84).

Assessment of Errors in Model Reconstruction

The use of camera location coordinates enables SfM techniques to scale and geo-reference 3D models in a cartographic reference system. However, to improve this scaling and also to be able to evaluate the uncertainty of measurements made in the models, other reference scales are used. These scales are known distances between two points and in this study two types of scales were used. The first type were scales formed by the parallel lasers included in the camera system. These lasers are spaced 20 cm apart and when they are visible in images on a flat surface, they are used to fine rescale the 3D blocks. The second type were distances taken between points on the seabed that are considered fixed in time, such as features in seafloor rocks (**Figure 5**). These distances were taken as a reference in 1 year and transferred as scales to the second year of the series, thus proceeding to rescale the models among themselves. These scales were selected to be as close as possible to each of the *A. setubalense* specimens evaluated in this study.

Reprojection errors calculated for the 3D models were also evaluated. Once the 3D coordinates of the point were computed, the 3D point was re-projected on all images where it appeared. Distance between the marked and re-projected point in each image was the reprojection error. This parameter could be used to validate the internal consistency of the model.

Size Measurements and Age of *A. setubelense*

Size of *A. setubalense* sponges was measured in 3D models, i.e., 3D point clouds. As parameters to define specimen sizes, diameter, height, length, maximum cup-surface area, and external perimeter were selected (**Figure 6A**). The average of four crossed diameters was measured from the highest points forming the specimen's cup. Perimeter and surface area were the perimeter of the outermost edge of the cup and the area it encloses. Height of specimens was the distance from the base to the top (upper

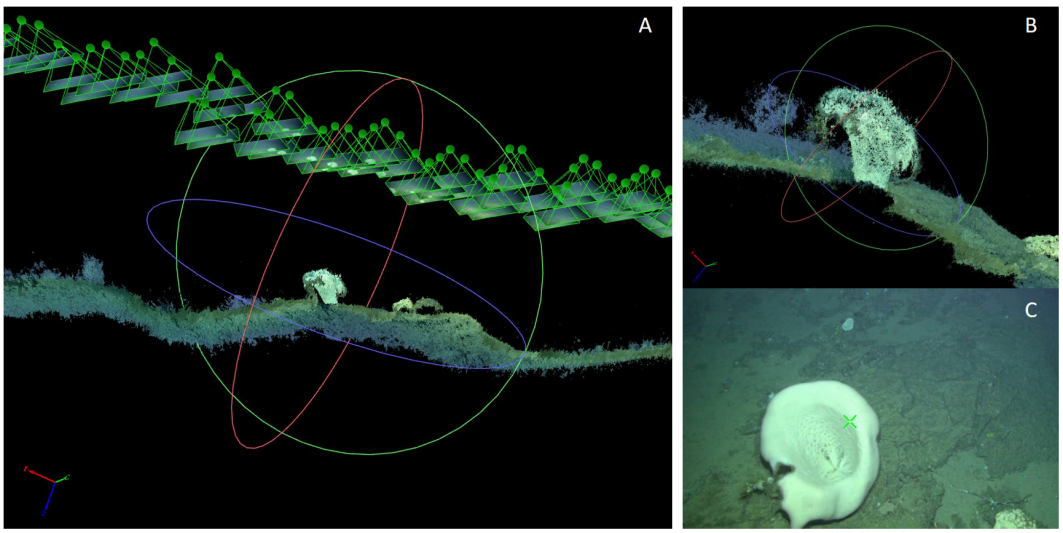

FIGURE 4 | Example of one of the 3D point clouds of an *A. setubalense* sponge used in this study. **(A)** View of the 3D point cloud. **(B)** Detail of *A. setubelense* in the 3D point cloud. **(C)** Original video-frame.

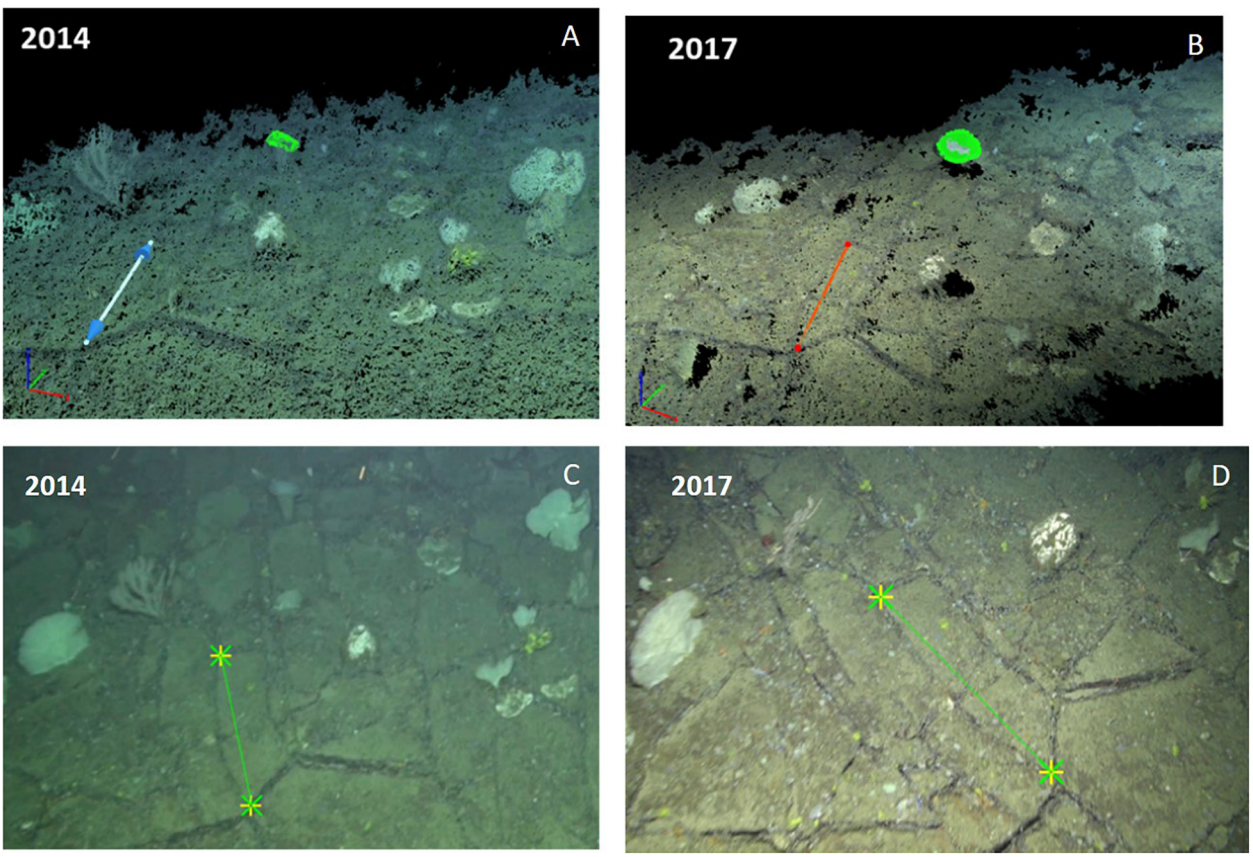

FIGURE 5 | Constant distance used for fine scaling between 3D blocks on different dates (0.88 m). **(A)** Distance marked in 2014 in 3D point cloud. **(B)** Distance marked in 2017 in 3D point cloud. **(C)** Distance in a 2014 video-frame where the vertices can be adjusted. **(D)** Distance in a 2017 video-frame where the vertices can be adjusted.

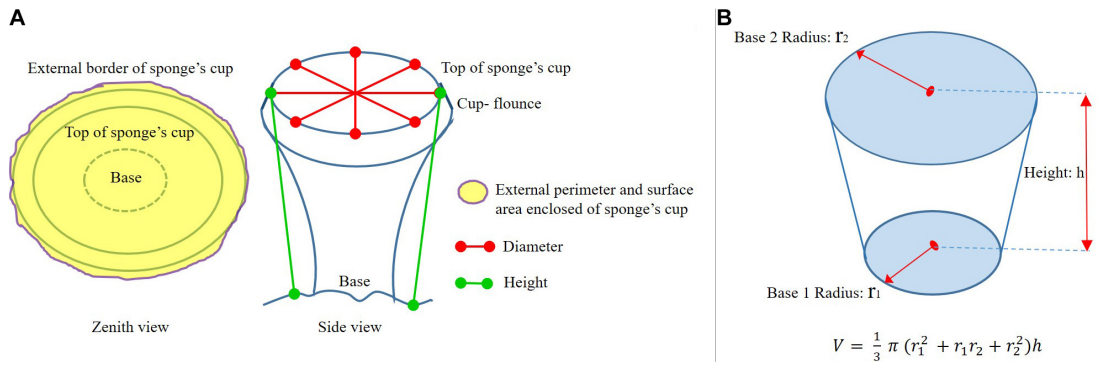

FIGURE 6 | (A) Diagram of the parameters measured to define the size of the *A. setubalense* specimens in this study. **(B)** Diagram of truncated cone geometric shape used for the calculation of volume of *A. setubalense*.

external surface or crown). If the base was not visible, a point on the substrate where it was settled was taken.

Two specimens were measured in Zone 1 and 15 in Zone 2 in the different years. In most cases the point clouds did not completely reconstruct specimens, and gaps or shadow areas appeared. Furthermore, in some cases the point cloud was not dense enough to reconstruct the morphometric complexity of some specimens. Hence, the volume of the sponges could not be measured directly on the 3D point cloud.

However, cup-shape is usually completely built in 3D models. Although in the largest specimens the base is hidden by its own cup, due to the presence of a frill or corbel, points on the seafloor adjacent to the base can always be used as base points for measuring length or height. All measurements were made with the utilities offered by the Pix4D software (**Figure 7**). To complete the drawing and add higher accuracy to the shapes, Pix4D enables geometrical objects (polyline or surface) to be selected in the 3D view, and the position of the vertices to be corrected, marking them in a least two 2D images, which have a higher resolution than 3D point clouds. Differences in average diameter, height (length), cup perimeter, and cup surface area of the same sponges from models from data collected on the different dates were used to calculate growth rates.

Since volume could not be measured directly, in order to approximate this very important parameter in sponges, an approximation to a truncated cone (**Figure 6B**) was made. This regular geometric figure is quite similar to the development of *A. setubalense*. The volume of the giant barrel sponge *Xestospongia muta* in Caribbean coral reef communities was calculated in a similar approach (McMurray et al., 2008). Directly measured parameters were used to calculate the volume of the truncated cone. The only parameter that was not directly measured in this study was the radius of the base, which was estimated from the images to be 1/5 of the cup size in the large specimens in Zone 1, and 1/3 in the smallest specimens in study area 2. Since the volume parameter was not measured in the 3D models, it is considered only an approximation to be used in a descriptive way for the specimens. These volume data were not used for subsequent calculations of the growth model or for calculating sponge age.

To estimate the age of specimens and obtain a growth curve model for *A. setubalense* specimens in the study areas, increments in growth between observations were fitted to the Von Bertalanffy (1938), a mathematical model for individual growth which has been shown to be adjustable to the growth observed in most species of fish. This and similar models consider body size as a function of age.

$$L(t) = L_\infty * \left[1 - exp\,(-K * (t - t_0))\right]$$

Where $L\,(t)$ is the size as a function of age; $L\infty$ is the maximum size to be reached by the species or the asymptotic size; K is the curvature parameter which determines how fast specimens grow. K is obtained from the slope of the line equation that adjusts the relationship between size parameter increment and time. Finally, $(t - t0)$ is the time increment for which the equation is calculated. To estimate growth parameters $(t0,\ K\ and\ L\infty)$ the methodology of Gulland and Holt (1959) was used.

RESULTS

Photogrammetry

Three models from 2014, 4 models from 2017, and 1 model from 2019 (**Table 1**) were reconstructed, covering different surfaces of seafloor, from 80 to 1,000 m^2, and including several specimens of *A. setubalense*. The models had an average Ground Sampling Distance (GSD) of 0.28 cm.

Accuracy Evaluation

All models were geolocated, oriented, and scaled within bundle adjustment processing using geographic coordinates of the camera positions. The 3D blocks that also had lasers projected on the seabed and were visible in the images were fine scaled with these scales. In addition, in order to ensure the adjustment between 3D models on different dates, constant distances were taken as scales, measured between seafloor features in a model on one date and used as a scale in a model on another date so as to fine rescale the data.

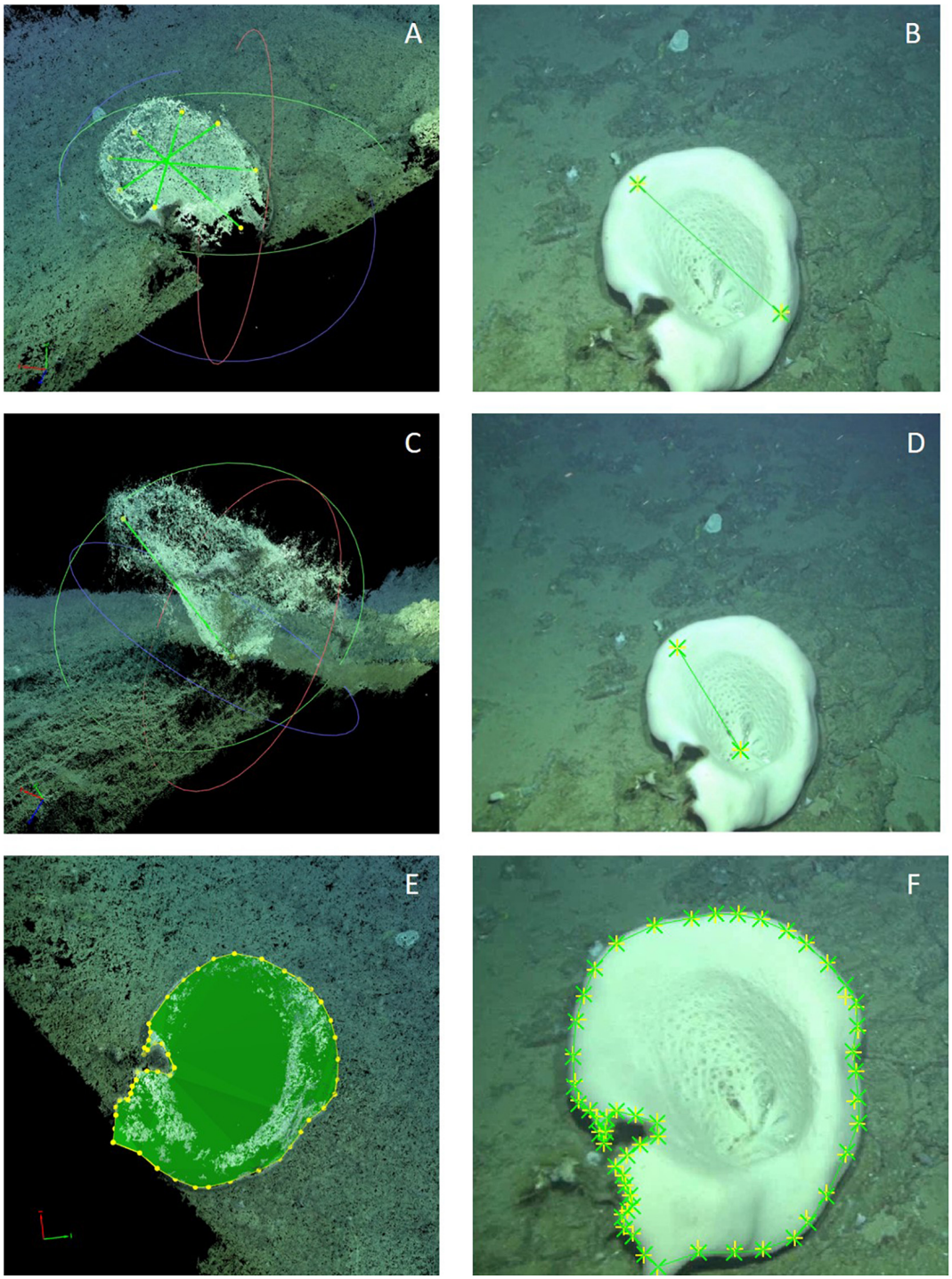

FIGURE 7 | Measurements taken to characterize the sizes of *A. setubalense* specimens: **(A,B)** Diameter; **(C,D)** Height; **(E,F)** External cup-perimeter and enclosed cup-surface area. All measurements were made on a 3D point cloud **(A,C,E)**; and by correcting the position of the vertices marking them on 2D images with higher resolution **(B,D,F)**.

E0514_TV30_f1790_f1890 (2014): calibrated with 2 scales, natural features of seafloor from E0719_TV04_045 (2019). E0514_TV30_f1900_f2000 (2014) calibrated with 3 scales, natural features of seafloor from E0717_TV51_20 (2017). E0514_TV28_f520_f925 (2014) calibrated with 4 scales, natural features of seafloor from E0717_TV23_f1015_f1205 (2017). E0717_TV51_20 calibrated with 4 scales, laser beams; and 1 scale, natural features of seafloor from

TABLE 1 | Summary of 3D models characteristics and specimens ID located in them.

Year	Study zone	3D model name	Specimen ID located	Calibrated images	Median of keypoints per image	Average GSD (cm)	Area covered (m^2)	3D points for bundle block adjustment	Average point density (per m^3)	Mean reprojection error (pixels)
2014	1	E0514_TV30_f1790_f1890	A01	101	11,680	0.28	82	94,215	774,822	0.266
	1	E0514_TV30_f1900_f2000	A02	101	11,766	0.34	99	81,916	428,233	0.27
	2	E0514_TV28_f520_f925	A03, A04, A05, A07, A08, A09	391	11,583	0.33	920	342,147	111,574	0.253
2017	1	E0717_TV51_20	A02	904	7,298	0.26	1,156	739,317	1.77e+06	0.165
	2	E0717_TV23_f580_f990	A05, A12	411	9,622	0.26	1,050	352,929	1.06e+06	0.223
	2	E0717_TV23_f1015_f1205	A06, A08, A09, A10	191	10,492	0.23	348	253,194	863,739	0.206
	2	E0717_TV23_f1245_f1390	A13, A14, A15, A16, A17	116	10,405	0.29	275	148,271	296,894	0.201
2019	1	E0719_TV04_045	A01	631	85,40	0.21	498	749,214	3.23e+06	0.155

E0514_TV30_f1900_f2000 (2014). E0717_TV23_f580_f990 (2017) and E0717_TV23_f1015_f1205 (2017) oriented and scaled models from coordinates of input camera poses. E0717_TV23_f1245_f1390 (2017) calibrated with 2 scales, laser beams. E0719_TV04_045 (2019) calibrated with 4 scales, laser beams.

Mean reprojection errors expressed in pixels are shown in **Table 1**. All values were below 0.5 pixels.

Some independent measurements (not used for fine rescaling) were used to indicate geometric matching uncertainty between 3D models (**Table 2**). All differences between constant measurements made in different years were under 10 mm. If these same distances were constant between models, it was assumed that differences in size of *A. setubalense* specimens were due to growth in the specimens.

This accuracy evaluation was not carried out for E0717_TV23_f1245_f1390 (2017), since all the specimens measured in this transect had disappeared in 2019, therefore no comparative measurements were made between years.

A. setubalense Growth Rates and Ages

The sizes of 2 specimens (A01, A02) of *A. setubalense* in Zone 1, and 5 specimens (A05, A06, A08, A09, and A10) in Zone 2 were measured in the 3D models from different dates. Measurements from different dates are provided in **Table 3** and presented in **Figure 8**.

Minimum growth rate was zero (or no growth) recorded for specimen A02 (zone 1). This specimen was the largest observed, reaching just over 1 m in height and almost 1 m in diameter. Maximum growth increment was 11 cm in diameter and was recorded for specimens A08 and A09 between 2014 and 2017; 14 cm in height for A10 between 2014 and 2017; 65 cm of cup-perimeter for specimen A05 between years 2014 and2017; and 0.11 m^2 of cup-surface area for A01 between 2014 and 2019. The largest variation in volume was 27 l for specimen A01. Average annual growth rates recorded for specimens were 2.2 cm $year^{-1}$ in diameter, 2.5 cm $year^{-1}$ in height, 11.9 cm $year^{-1}$ in external cup-perimeter, and 121.8 cm^2 $year^{-1}$ in cup-surface area.

Higher growth rates corresponded to smaller specimens, in both diameter and height, following an exponential trend with very high R^2 (**Figure 9**). However, *A. setubalense* external cup-perimeter and cup-surface area revealed a different relationship. Smaller specimens did not have high increments in cup-development (no frill or flounce) (**Figure 10**), rather, this cup-flounce development occurred in medium-sized specimens and stabilized again in large specimens (**Figure 9**). Development of the cup-flounce did not imply a clear relationship with the specimen's size and consequently with its age. Therefore, for the study of the growth and age curve, two parameters—diameter and height—were used.

To estimate growth parameters, two assumptions were made for L_∞ and t_0. The specimen A02 from study zone 1 in which no growth in diameter or height was detected between dates was used as L_∞ (or infinite L). Since there was one specimen that did not appear on the first date, its size on the first date was considered to be zero. This implies an uncertainty since the method does not allow the exact time when the larvae fixed to be determined. Furthermore, the first months of development were neglected, as the small size of the specimen did not allow it to be detected or measured with the images used in this study.

With these input data a growth model was estimated for *A. setubalense* in Le Danois Bank (**Figure 11**). The results show a growth curve in which the growth rate decreases the larger the individual sizes.

Taking into account the size indicators used in this study and based on von Bertalanffy growth model, the largest specimen (A02) or L∞ reaches 95% of the size of maximum size at 98 years of age. However this sponges recorder a very low growth rate from 60 years of age, with a very low variation from there ($<$0.5 cm $year^{-1}$). The ages calculated from the height of the

TABLE 2 | Independent measurements between 3D models to get the uncertainty of the data.

Cte. distances	**E0514_TV30_f1790_f1890 (2014)**	**E0719_TV04_045 (2019)**	**Difference (mm)**
D1 (m)	0.3421	0.3392	2.97
D2 (m)	0.5476	0.5455	2.09
	E0514_TV30_f1900_f2000 (2014)	**E0717_TV51_20 (2017)**	**Difference (mm)**
D4 (m)	0.6172	0.6157	1.55
D5 (m)	0.9475	0.9448	2.69
	E0514_TV28_f520_f925 (2014)	**E0717_TV23_f580_f990 (2017)**	**Difference (mm)**
D6 (m)	0.4511	0.4425	8.85
D7 (m)	0.7527	0.7449	7.86
	E0514_TV28_f520_f925 (2014)	**E0717_TV23_f1015_f1205 (2017)**	**Difference (mm)**
D8 (m)	0.5379	0.5462	−8.28
D9 (m)	0.7833	0.7737	9.66

TABLE 3 | Size measurements made for the specimens in zone 1 and zone 2 (2014, 2017, and 2019) and growth ratios found for each of the measured parameters.

	Diameter (m)	**Height (m)**	**Perimeter (m)**	**Área (m^2)**	**Volume (m^3)**	**Year**
Total growth rate/growth rate per year	***(m)/(m year^{-1})***	***(m)/(m year^{-1})***	***(m)/(m year^{-1})***	***(m^2)/(m^2 year^{-1})***	***(m^3)/(m^3 year^{-1})***	***Days between samples***
A01	0.580	0.485	2.925	0.420	0.0530	2014
	0.641	0.598	3.333	0.530	0.0800	2019
	0.060/0.012	*0.114/0.022*	*0.408/0.080*	*0.110/0.022*	*0.027/0.0053*	*1,858*
A02	0.954	1.107	4.120	1.241	0.3250	2014
	0.955	1.108	4.466	1.245	0.3250	2017
	0.001/0.000	*0.001/0.000*	*0.347/0.114*	*0.004/0.001*	*0.0/0.0*	*1,112*
A05	0.171	0.254	0.681	0.033	0.003	2014
	0.255	0.345	1.329	0.110	0.008	2017
	0.084/0.027	*0.091/0.030*	*0.647/0.211*	*0.077/0.025*	*0.005/0.0016*	*1,119*
A06	0.020	0.046	0.100	0.001	0.0	2014
	0.086	0.121	0.329	0.008	0.0003	2017
	0.066/0.021	*0.075/0.024*	*0.229/0.075*	*0.007/0.002*	*0.0003/0.0001*	*1,119*
A08	0.159	0.170	0.589	0.021	0.0015	2014
	0.271	0.248	0.939	0.067	0.0047	2017
	0.112/0.027	*0.077/0.025*	*0.350/0.114*	*0.046/0.015*	*0.0032/0.001*	*1,119*
A09	0.158	0.175	0.716	0.034	0.0018	2014
	0.271	0.263	1.111	0.087	0.0073	2017
	0.113/0.036	*0.088/0.029*	*0.395/0.129*	*0.053/0.017*	*0.0055/0.0018*	*1,119*
A10	0	0	0	0	0.0	2014
	0.084	0.139	0.339	0.008	0.0006	2017
	0.084/0.027	*0.139/0.045*	*0.339/0.110*	*0.008/0.003*	*0.0006/0.0002*	*1,119*

Days between samples.

specimens measured in this study were: A01, 19 years; A05, 9 years; A06, 4 years; A08 and A09, 7 years; and A10, 3 years.

DISCUSSION

Unfortunately, annual growth rates of many benthic marine organisms remain unknown. Growth indicators of benthic species contribute to the knowledge of their biology and these growth rates can be used to determine ages. In addition, the growth rate is a fundamental parameter for recovery studies in the event of possible impacts. This is especially relevant in species that structure vulnerable habitats or Essential Fish Habitats (EFH) for other groups.

3D Photogrammetry

The studies carried out to date that base their methodology on 2D image measurements have limitations, since many sessile benthic species have three-dimensional developments (e.g., branching corals and massive emergent sponges). Obtaining a 3D representation of the ocean floor at very high spatial resolution enabled us to go beyond 2D methodologies. 3D models are able to resolve the evaluation of complex three-dimensional habitats. In addition, 3D measurements can be correlated in a simple way with the biomass of the specimens in different species (Palma et al., 2018; Ríos et al., 2020).

The accuracy of the reconstructed models (average uncertainty < 10 mm in constant distances between years) shows very low values of geometric uncertainty, which validate the

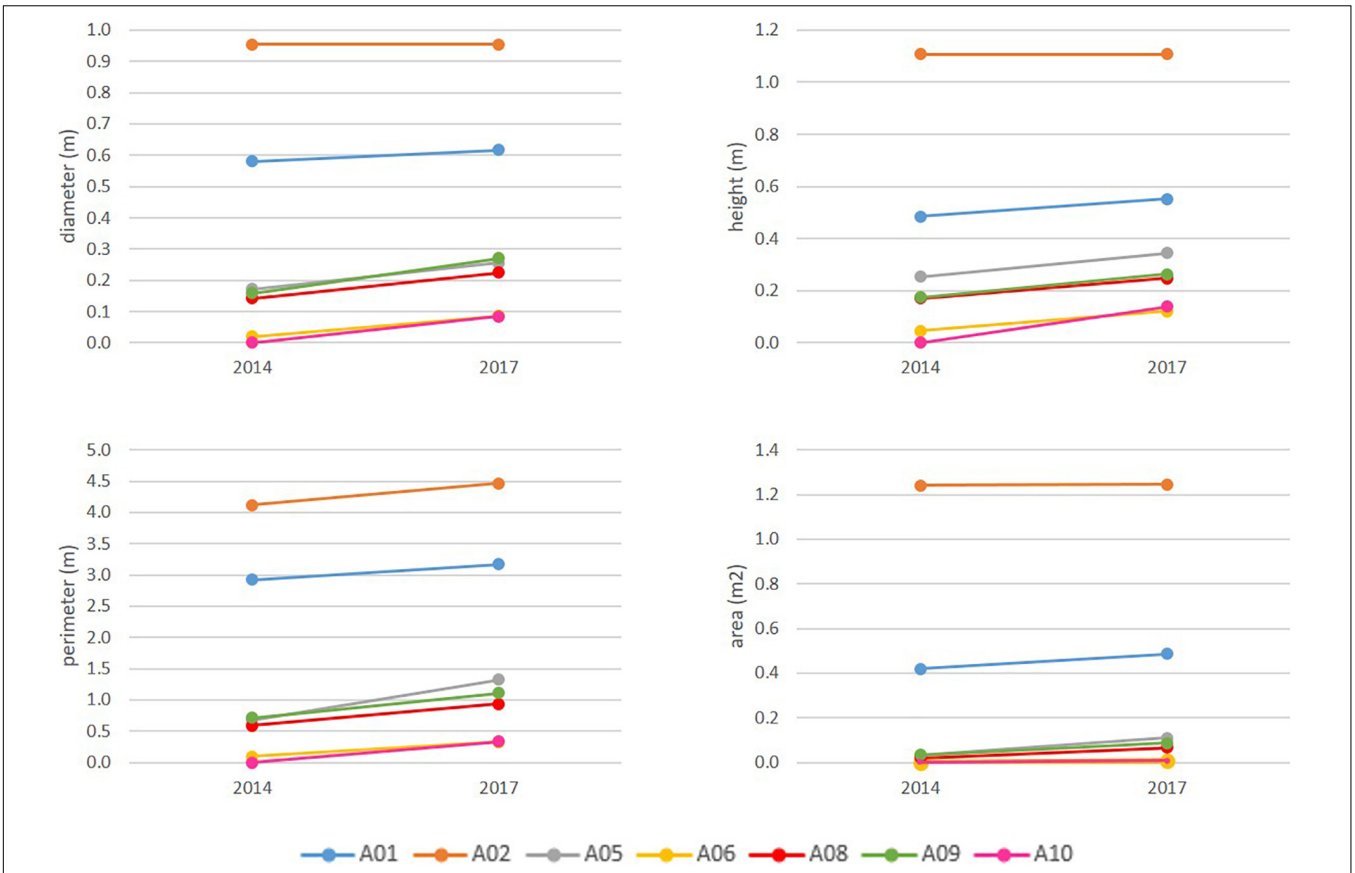

FIGURE 8 | Size reached by the *A. setubalense* specimens in 2014 and 2017 according to the parameters that define their size. For the A01 size recorded in 2014 and 2019, a linear interpolation was made to calculate its size in 2017.

application of this approach for sponge growth rate evaluation. Mean reprojection error values were always below 0.3 pixels, with less than 2-pixels assumed to be indicators of the effectiveness of SfM programs for creating highly accurate 3D reconstructions of underwater habitats (Burns and Delparte, 2017).

Video resolution, track coordinates, direction, and view angles determine the quality of the 3D point clouds. The medium density of points and the presence of gaps limit the use of these point clouds for 3D measurements such as volume. In the deep-sea using underwater vehicles it is very difficult to obtain images that surround the target species. This is easier to achieve through diving surveys as divers can access the specimens more easily and therefore obtain higher quality images (Olinger et al., 2019). However, the quality of the 3D models obtained with ROTV are suitable for conducting measurements in 3D space that can be used to precisely define the size of sponges and their variation over time. 3D models generated by photogrammetry from ROV videos can be used to obtain growth rates of corals and can be applied to videos collected for monitoring purposes (Bennecke et al., 2016; Ferrari et al., 2017).

Growth Rates

The sponges measured in this 6-year study cover the entire size range of individuals, from a new specimen (recruit) recorded to maximum size in this study zone. The average annual growth rate of sponges measured from 2014 to 2019 using a 3D photogrammetric approach was 2.2 cm year^{-1} (diameter), 2.5 cm year^{-1} (height), 11.91 cm year^{-1} (external cup-perimeter), and 121.8 cm^2 year^{-1} (cup-surface area). The minimum growth rate recorded was 0 (no-growth) for the largest specimen in diameter and height. And the maximum annual growth rates recorded were 3.64 cm year^{-1} (diameter) and 4.54 cm year^{-1} (height), which correspond to small specimens, indicating that for *A. setubalense,* growth rate decreases with increasing size of animals, as observed by Leys and Lauzon (1998).

Results obtained for *Asconema setubalense* are quite similar to growth rates of the hexactinellid sponge *Rhabdocalyptus dawsoni* achieved in the fjords of British Columbia (Leys and Lauzon, 1998). The average growth rate of *R. dawsoni* measured over the course of 3 years was 1.98 cm year^{-1} (min. −0.76 cm year^{-1}, max. 5.7 cm year^{-1}). Regarding volume, the variation detected for *A. setubalense* was on average 1,438 ml year^{-1} (min. 0 ml year^{-1}, max. 5,300 ml year^{-1}), differing from the hexactinellid *R. dawsoni* (average of 167 ml year^{-1}). However, using a radiocarbon dating method, the linear growth rate of the hexactinellid sponge *Rossella racovitzaeracovitzae* (Topsent, 1901) was calculated to be around 2.9 mm year^{-1}

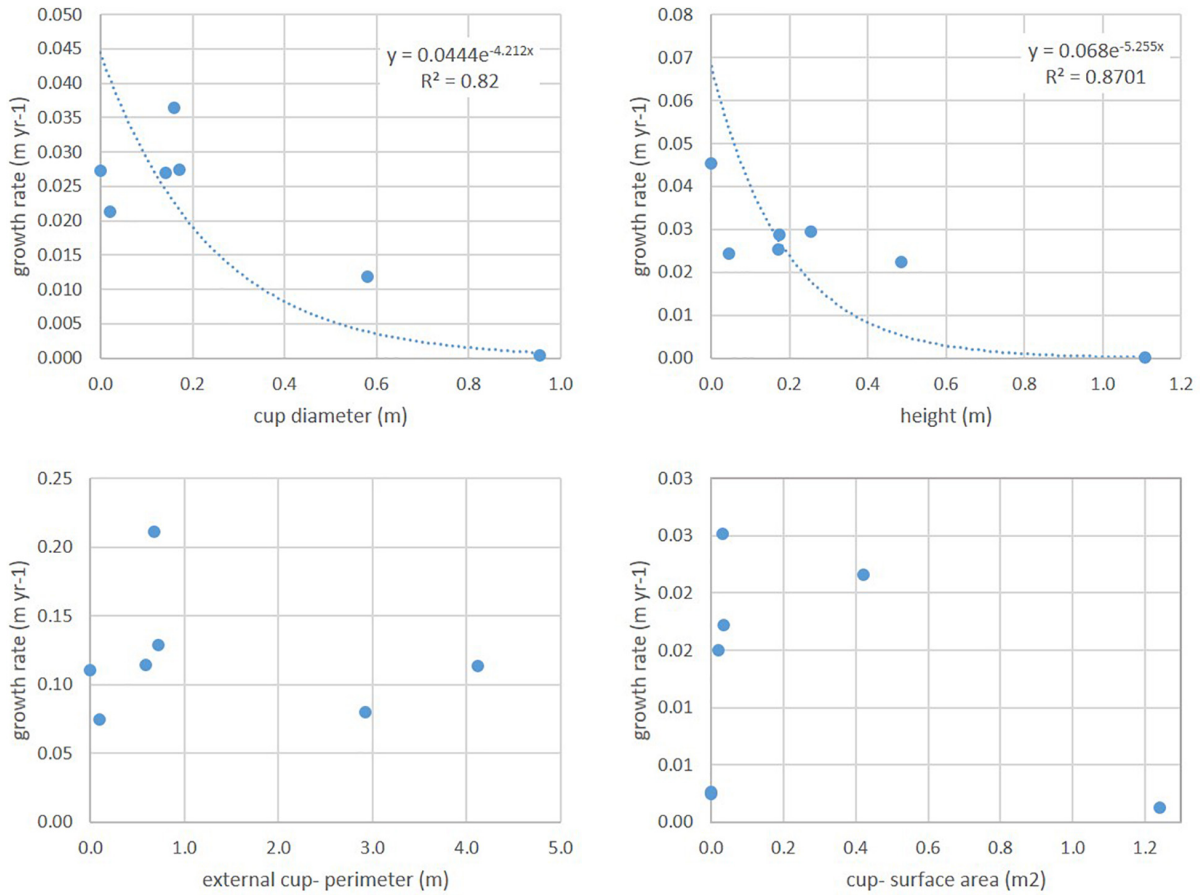

FIGURE 9 | Relationship between annual growth ratios and *A. setubalense* specimen sizes defined by the four parameters chosen (diameter, height, external cup-perimeter, and cup-surface area).

FIGURE 10 | Specimens of *A. setubalense* with different sizes. Different degree of flounce development can be observed. **(A,B)** Two small specimens without a flounce. **(B)** Medium size of *A. setubalense* where the development of the flounce can be seen. **(C)** Large size specimen with a notable cup-flounce.

(Fallon et al., 2010). This growth rate is approximately 10 times lower than that calculated for *A. setubalense*.

Populations of the hexactinellid sponge *Anoxycalyx* (*Scolymastra*) joubini (Topsent, 1916) have been monitored for nearly 50 years (Dayton et al., 2013). This is the largest Antarctic sponge, with individuals growing over two meters tall. Over a 22-years period from 1967 to 1989, no growth was recorded for *A. (S.) joubini*; however, in 2004 and 2010, *A. (S.) joubini* was observed to have grown almost 30%, demonstrating the potential for fast growth rates. The present study reveals the existence of possible variations in growth rates of sponges depending on environmental conditions, food availability (Ellwood et al., 2007), and other factors.

Age Estimation

Age estimation was undertaken using the general von Bertallanfy growth function model, which is commonly used for the analysis

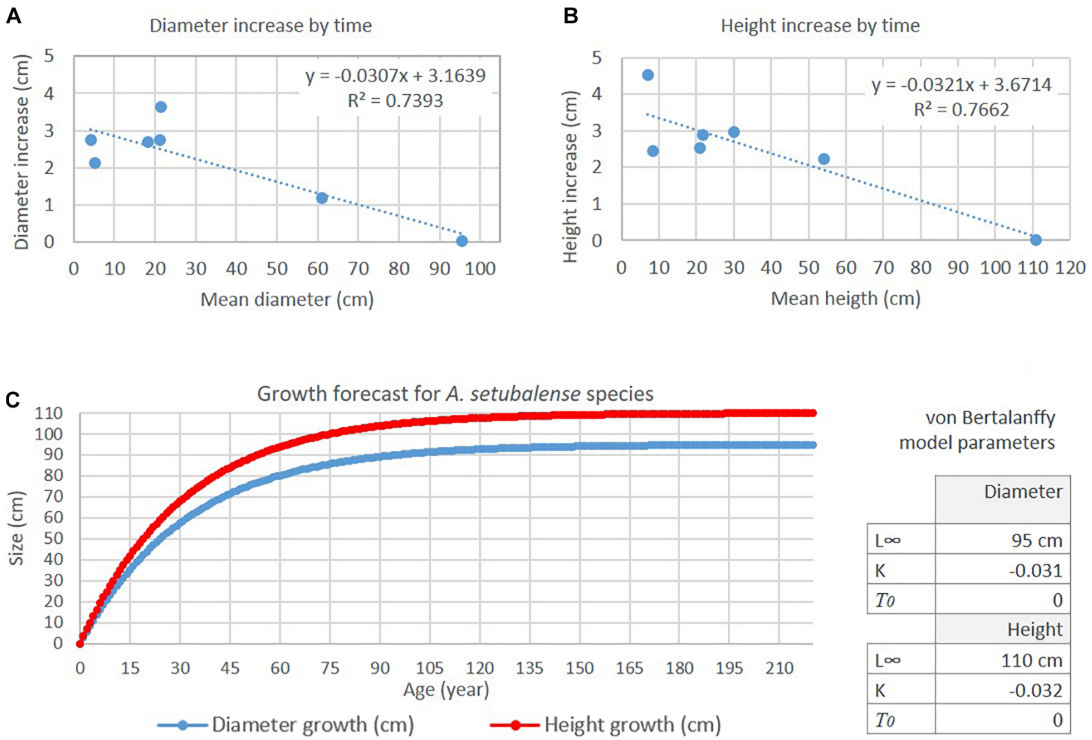

FIGURE 11 | (A,B) K (curvature parameter) is obtained from the slope of the line equation that adjusts the relationship between size parameter increment (diameter and height) and time, and determines how fast specimens grow. **(C)** Growth model curve for *A. setubalense* according to von Bertanaffy function.

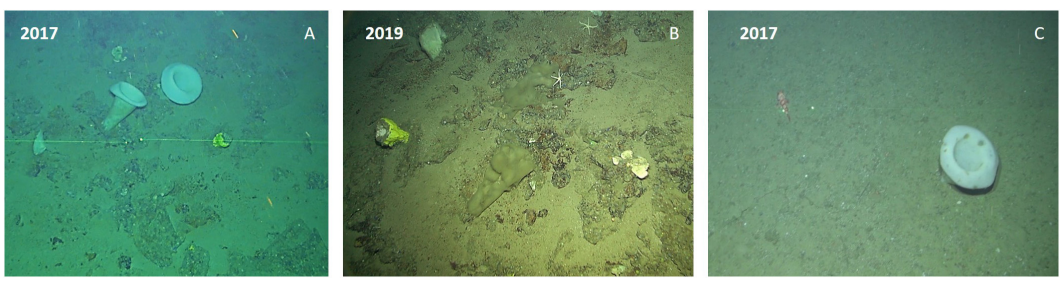

FIGURE 12 | (A) Two *A. setubalense* specimens recorded in 2017. **(B)** These specimens appeared dead in 2019. Their biological remains can be observed in the 2019 image. **(C)** *A. setubalense* recorded in study zone 2 with brown spots on its surface.

of vertebrates. However, it has also been used in sponge age determination studies (McMurray et al., 2008). There is currently no specific growth model function for hexactinellid sponges. On the basis of the growth increments recorded, specimens of *A. setubalense* practically reach their maximum size at approximately 60 years of age. From there on, the specimens vary in a very slow way (<0.5 cm year^{-1}). The largest specimen considered in this study of approximately 1 meter in height (95 cm in diameter) could well be over 120 years old, although it is very difficult through images to estimate age once an animal has stopped growing. Comparable results were reported for another hexactinellid sponge *Rhabdocalyptus dawsoni* (Leys and Lauzon, 1998). These authors estimated 220 years of age for large specimens (1 m in length) based on the assumption of constant growth rate. Considering that growth rate is not constant but decreases as sponges get larger, these are quite possibly conservative estimates of the ages of large *R. dawsoni* (Leys and Lauzon, 1998). Using a different approach with radiocarbon dating methodology, the hexactinellid *Rossella racovitzae racovitzae* was estimated to be ∼440 years old (Fallon et al., 2010).

It is evident that the specimens recorded in these 6 years are too few in number to obtain a curve that can be extended to the entire species, although it is true that the different sizes are fairly well represented, including a recruit within the period of time to a large specimen in which no size variation was recorded over the past 6 years. Nonetheless, it is necessary to continue researching, increasing the number of specimens, studying whether there are

changes in seasonal growth within the same area, and whether there are differences in growth rates of *A. setubalense* between different geographical areas.

Mortality

Fourteen *A. setubalense* observed in study zone 2 were dead by 2017 and 2019. The size of the specimens when last recorded alive varied from 10 to 40 cm in diameter and 10–50 cm in height. As mentioned, the smaller-sized specimens appeared in Zone 2 of the study area. In some cases, the biological remains could still be recorded on the seafloor (**Figures 12A,B**). This could indicate that in these cases not much time had elapsed between the taking of the image and the death of the specimens.

The disappearance of specimens makes one suspect that for some unknown cause a mortality event is taking place in this species in study zone 2. It was checked that only the *Asconema* were affected, so this indeed indicates a species-specific stress factor. In addition, some specimens were recorded to have brown spots on their surface (**Figure 12C**), leading us to suspect that this may be related to the death of these specimens, which might be a bacterial infection.

This detection was possible owing to the methodology of fixed sampling stations set up in this MPA monitoring framework. In order to verify this hypothesis, more data are necessary as well as the collection of samples that can help us to identify possible pathogens that affect this species. A similar event, but over a longer time period (40 years), occurred with 35 large Antarctic Hexactinellid *A. (S.) joubini*. In 1974, 35 specimens were recorded, six of which were dead by 1977, and none of which were alive in 2010, possibly from infestations of the amphipod *S. antarctica* (Dayton et al., 2013).

CONCLUSION

This study forms part of the surveys designed to monitor the El Cachucho Marine Protected Area. The non-invasive methodology and comparable data collected between dates is crucial to assess *in situ* growth rates from the photogrammetric approach. Further, within the Marine Strategy Framework Directive (Directive, 2008/56/EC; Borja et al., 2011), it provides a useful indicator that could help to assess the environmental status of deep-sea benthic habitats. Monitoring programs, acquiring precise samples that reflect the population of benthic species, are essential for MPAs (Addison, 2011). This study contributes not only to the improvement of the knowledge of this species but is useful for the help of the implementation of monitoring plans of Marine Protected Areas, or the implementation of directives such as Marine Strategies.

Using a novel approach for photogrammetric reconstructions from ROV or ROTV video (Kwasnitschka et al., 2013; Prado et al., 2019), the *in situ* growth rate of *A. setubalense* was estimated. This is the first time that this biological parameter has been estimated for *A. setubalense* in the Cantabrian Sea.

DATA AVAILABILITY STATEMENT

The raw data supporting the conclusions of this article will be made available by the authors, without undue reservation.

AUTHOR CONTRIBUTIONS

EP applied photogrammetry and structure from motion techniques. EP, AR-B, and PR processed the video and image material. EP and CR-C analyzed growth rate data. FS and JC led the ship surveys. FS and JC acquired the funding. All authors conceived and designed the study, helped to collect process and map field data, prepared the figures and tables, reviewed drafts of the manuscript, and helped to writing the manuscript.

FUNDING

This research has been performed in the scope of the SponGES project, which received funding from the European Union's Horizon 2020 Research and Innovation Programme under grant agreement No. 679849. The three oceanographic cruises were made in the framework of two agreements with Spain Ministry MITECO (Ministerio para la Transición Ecológica y el Reto Demográfico): "Scientific and technical assistance for the declaration, management and protection of protected marine areas of state competence and for the evaluation and monitoring of the Network of Marine Protected Areas of Spain." This study was partially funded by the European Commission LIFE+ "Nature and Biodiversity" call, and included in the INDEMARES Project (07/NAT/E/000732). The Biodiversity Foundation, of the Ministry of the Environment, was the institution responsible for coordinating this project.

ACKNOWLEDGMENTS

This study was made possible thanks to the invaluable work of all the participants in the surveys involved and the crews of the R.Vs. ÁngelesAlvariño (IEO) and Ramón Margalef (IEO). We also appreciate the helpful assistance of the technicians of the ROTV Politolana.

REFERENCES

Abdo, D. A., Seager, J. W., Harvey, E. S., McDonald, J. I., Kendrick, G. A., and Shortis, M. R. (2006). Efficiently measuring complex sessile epibenthic organisms using a novel photogrammetric technique. *J. Exp. Mar. Biol. Ecol.* 399, 120–133. doi: 10.1016/j.jembe.2006.07.015

Addison, P. (2011). "A global review of long-term marine protected area monitoring programmes: the application of a good framework to marine biological monitoring," in *Affiliation: A Report Prepared for JNCC by Prue*

Addison, School of Botany. JNCC Report No. 455. (Melbourne, VC: University of Melbourne).

Ayling, A. L. (1983). Growth and regeneration rates in thinly encrusting demospongiae from temperate waters. *Biol. Bull.* 165, 343–352. doi: 10.2307/1541200

Bennecke, S., Kwasnitschka, T., Metaxas, A., and Dullo, W. C. (2016). In situ growth rates of deep-water octocorals determined from 3d photogrammetric reconstructions. *Coral Reefs* 35, 1227–1239. doi: 10.1007/s00338-016-1471-7

BOE (2011). *Real Decreto 1629/2011, de 14 de noviembre, por el que se declara como Área Marina Protegida y como Zona Especial de Conservación el espacio marino de El Cachucho, y se aprueban las correspondientes medidas de conservación*. BOE núm Report No. 295. China: BOE.

Borja, A., Galparsoro, I., Irigoien, X., Iriondo, A., Menchaca, I., Muxika, I., et al. (2011). Implementation of the european marine strategy framework directive: a methodological approach for the assessment of environmental status, from the basque country (Bay of Biscay). *Mar. Poll. Bull.* 62, 889–904. doi: 10.1016/j.marpolbul.2011.03.031

Burns, J. H. R., and Delparte, D. (2017). Comparison of commercial structure-from-motion photogrammety software used for underwater three-dimensional modeling of coral reef environments. *Int. Arch. Photogrammetry Remote Sens. Spatial Inform. Sci.* 42, 127–131. doi: 10.5194/isprs-archives-xlii-2-w3-127-2017

Burns, J. H. R., Fukunaga, A., Pascoe, K. H., Runyan, A., Craig, B. K., Talbot, J., et al. (2019). 3D habitat complexity of coral reefs in the northwestern Hawaiian Islands is driven by corals assemblage structure. *Int. Arch. Photogramm. Remote Sens. Spatial Inf. Sci.* XLII-2/W10, 61–67. doi: 10.5194/isprs-archives-xlii-2-w10-61-2019

Dayton, P. K. (1979). "Observations of growth, dispersal and population dynamics of some sponges in McMurdo Sound, Antarctica," in *Colloques Internationaux du Centre National de la Recherché Scientifique*, eds C. Lèvi and N. Boury–Esnault (Paris: Biologie des Spongiaires (Sponge Biology)), 271–282.

Dayton, P. K., Kim, S., Jarrell, S. C., Oliver, J. S., Hammerstrom, K., Fisher, J. L., et al. (2013). Recruitment, growth and mortality of an Antarctic hexactinellid sponge, Anoxycalyx joubini. *PLoS One* 8:e56939. doi: 10.1371/journal.pone.0056939

De Caralt, S., Agell, G., and Uriz, M. J. (2003). Long-term culture of sponge explants: conditions enhancing survival and growth, and assessment of bioactivity. *Biomol. Eng.* 20, 339–347. doi: 10.1016/s1389-0344(03)00045-5

Directive (2008/56/EC). The European Parliament and of the Council of 17 June 2008 establishing a framework for community action in the field of marine environmental policy (Marine Strategy Framework Directive).

Duckworth, A. R., and Pomponi, S. A. (2005). Relative importance of bacteria, microalgae and yeast for growth of the demospongiae *Halichondria melanadocia*. *J. Exp. Mar. Biol. Ecol.* 323, 151–159. doi: 10.1016/j.jembe.2005.03.007

Ellwood, M. J., Kelly, M., and de Forges, B. R. (2007). Silica banding in the deep-sea lithistid sponge Corallistes undulatus: investigating the potential influence of diet and environment on growth. *Limnol. Oceanogr.* 52, 1865–1873. doi: 10.4319/lo.2007.52.5.1865

Ercolano, G., De Cicco, P., and Ianaro, A. (2019). New drugs from the sea: pro-apoptotic activity of sponges and algae derived compounds. *Mar. Drugs* 17:31. doi: 10.3390/md17010031

Fallon, S. J., James, K., Norman, R., Kelly, M., and Ellwood, M. J. (2010). A simple radiocarbon dating method for determining the age and growth rate of deep-sea sponges. *Nuclear Instruments Methods Phys. Res. Sec B, Beam Interact. Materials Atoms* 268, 1241–1243. doi: 10.1016/j.nimb.2009.10.143

Ferrari, R., Figueira, W. F., Pratchett, M. S., Boube, T., Adam, A., Kobelkowsky-Vidrio, T., et al. (2017). 3D photogrammetry quantifies growth and external erosion of individual coral colonies and skeletons. *Sci. Rep.* 7:16737.

Ferrari, R., McKinnon, D., He, H., Smith, R. N., Corke, P., González-Rivero, M., et al. (2016). Quantifying multiscale habitat structural complexity: a cost-effective framework for underwater 3D modelling. *Remote Sens.* 8:113. doi: 10.3390/rs8020113

Fillinger, L., Janussen, D., Lundälv, T., and Richter, C. (2013). Rapid glass sponge expansion after climate-induced Antarctic ice shelf collapse. *Curr. Biol.* 23, 1330–1334. doi: 10.1016/j.cub.2013.05.051

Fiuza, A., Hamann, M., Ambar, I., Díaz, del Rio, G., González, N., et al. (1998). Water masses and their circulation off western Iberia during May 1993. *Deep-Sea Res. Part I Oceanogr. Res. Pap.* 45, 1127–1160. doi: 10.1016/s0967-0637(98)00008-9

Garrabou, J., and Zabala, M. (2001). Growth dynamics in four Mediterranean demosponges. *Estuarine Coastal Shelf Sci.* 52, 293–303. doi: 10.1006/ecss.2000.0699

Gunnerus, J. E. (1763). Om en søevext, allevegne ligesom besat med frøehuuse, Gorgonia resedæformis. *Det Trondhiemske Selskabs Skrifter* 2, 321–329.

González-Pola, C., Díaz, del Río, G., Ruiz-Villarreal, M., Sánchez, R. F., Mohn, et al. (2012). Circulation patterns at Le Danois Bank, an elongated shelf-adjacent seamount in the Bay of Biscay. *Deep-Sea Res. Part I Oceanogr. Res. Pap.* 60, 7–21. doi: 10.1016/j.dsr.2011.10.001

Gulland, J. A., and Holt, S. J. (1959). Estimation of growth parameters for data at unequal time intervals. *J. Cons. CIEM.* 25, 47–49. doi: 10.1093/icesjms/25.1.47

Heredia, B., Pantoja, J., Tejedor, A., and Sánchez, F. (2008). El Cachucho, un oasis de vida en el Cantábrico. *Ambienta* 76, 10–17.

Hermans, J., Dubois, P., Andre, L., Vacelet, J., and Willenz, P. (2010). Growth rate and chemical features of the massive calcium carbonate skeleton of *Petrobiona massiliana* (Baeriida: Calcaronea: Calcispongiae). *J. Mar. Biol. Assoc. U K.* 90:749754.

Hogg, M. M., Tendal, O. S., Pomponi, S. A., van Soest, R. W. M., Gutt, J., et al. (2010). *Deep-sea Sponge Grounds: Reservoirs of Biodiversity*. Cambridge: UNEP-WCMC. UNEP-WCMC Biodiversity Series No.32.

Huetten, E., and Greinert, J. (2008). Software controlled guidance, recording and postprocessing of seafloor observations by ROV and other towed devices: the software package OFOP. *Geophys. Res. Abstr.* 10:EGU2008-A-03088.

Kahn, A. S., Yahel, G., Chu, J. W. F., Tunnicliffe, V., and Leys, S. P. (2015). Benthic grazing and carbon sequestration by deep-water glass sponge reefs. *Limnol. Oceanography* 60, 78–88. doi: 10.1002/lno.10002

Kent, W. S. (1870). On the 'Hexactinellidae' or Hexradiate Spiculed Silicious Sponges taken in the 'Norna' Expedition off the coast of Spain and Portugal. with description of new species, and revision of the order. *Monthly Microscop. J.* 4, 241–252. doi: 10.1111/j.1365-2818.1870.tb01123.x

Koopmans, M., and Wijffels, R. H. (2008). Seasonal growth rate of the sponge *Haliclona oculata* (Demospongiae: Haplosclerida). *Mar. Biotechnol.* 10, 502–510. doi: 10.1007/s10126-008-9086-9

Kwasnitschka, T., Hansteen, T. H., Devey, C. W., and Kutterolf, S. (2013). Doing fieldwork on the seafloor: photogrammetric techniques to yield 3D visual models from ROV video. *Comput. Geosci.* 52, 218–226. doi: 10.1016/j.cageo.2012.10.008

Lambe, L. M. (1893). On some sponges from the pacific coast of Canada and Behring Sea. *Trans. Royal Soc. Canada* 10, 67–78.

Lange, I. D., and Perry, C. T. (2020). A quick, easy and non-invasive method to quantify coral growth rates using photogrammetry and 3D model comparisons. *Methods Ecol. Evol.* 2020, 714–726. doi: 10.1111/2041-210x.13388

Leon, J. X., Roelfsema, C. M., Saunders, M. I., and Phinn, S. R. (2015). Measuring coral reef terrain roughness using 'Structure-from-Motion' close-range photogrammetry. *Geomorphology* 242, 21–28. doi: 10.1016/j.geomorph.2015.01.030

Leys, S. P., and Lauzon, N. R. J. (1998). Hexactinellid sponge ecology: growth rates and seasonality in deep water sponges. *J. Exp. Mar. Biol. Ecol.* 230, 111–129. doi: 10.1016/s0022-0981(98)00088-4

Linnaeus, C. (1758). *Systema Naturae per regna tria naturae, secundum classes, ordines, genera, species, cum characteribus, differentiis, synonymis, locis.* Editio decima, reformata [10th revised edition], Vol. 1. Laurentius Salvius: Holmiae, 824.

Maldonado, M., López-Acosta, M., Beazley, L., Kenchington, E., Koutsouveli, V., and Riesgo, A. (2020). Cooperation between passive and active silicon transporters clarifies the ecophysiology and evolution of biosilicification in sponges. *Science Advance* 6:eaba9322. doi: 10.1126/sciadv.aba9322

Maldonado, M., Ribes, M., and Van Duyl, F. C. (2012). Nutrient fluxes through sponges: biology, budgets, and ecological implications. *Adv. Mar. Biol.* 62, 114–182.

Manjón-Cabeza, M. E., Ríos, P., García-Guillén, L. M., Macías-Ramírez, A., Sánchez, F., Rodríguez-Básalo, A., et al. (2021). Asteroids and ophiuroids associated with sponge aggregations as a key to marine habitats. A Comparative

Analysis Between Avilés Canyons System and El Cachucho, Marine Protected Area. *Front. Mar. Sci.* 7:606749. doi: 10.3389/fmars.2020.606749

Marliave, J. (2015). Cloud sponge, *Aphrocallistes vastus* (Porifera: Hexactinellida), fragment healing and reattachment. *Can. Field-Nat.* 129, 399–402. doi: 10.22621/cfn.v129i4.1763

McMurray, S. E., Blum, J. E., and Pawlik, J. R. (2008). Redwood of the reef: growth and age of the giant barrel sponge Xestospongia muta in the Florida Keys. *Mar. Biol.* 155, 159–171. doi: 10.1007/s00227-008-1014-z

Olinger, L. K., Scott, A. R., Mcmurray, S. E., and Pawlik, J. R. (2019). Growth estimates of caribbean reef sponges on a shipwreck using 3D photogrammetry. *Sci. Rep.* 9:18398.

OSPAR Commission (2010). *Background Document for Deep-sea Sponge Aggregations*. London: OSPAR Commission.

Palma, M., Rivas-Casado, M., Pantaleo, U., Pavoni, G., Pica, D., and Cerrano, C. (2018). SfM-Based method to assess gorgonian forests (*Paramuricea clavata* (Cnidaria. Octocorallia)). *Remote Sens.* 10:1154. doi: 10.3390/rs10071154

Pardo, E., Aguilar, R., García, S., de la Torriente, A., and Ubero, J. (2011). Documentación de arrecifes de corales de agua fría en el Mediterráneo occidental (Mar de Alborán). *Chronica Naturae* 1, 20–34.

Prado, E., Sánchez, F., Rodríguez-Basalo, A., Altuna, A., and Cobo, A. (2019). Analysis of the population structure of a gorgonian forest (Placogorgia sp.) using a photogrammetric 3D modeling approach at Le Danois Bank, Cantabrian Sea. *Deep-Sea Res. Part I Oceanogr. Res. Pap.* 153: 3124.

Price, D. M., Robert, K., Callaway, A., Lacono, C. L., Hall, R. A., and Huvenne, V. A. I (2019). Using 3D photogrammetry from ROV video to quantify cold- water coral reef structural complexity and investigate its influence on biodiversity and community assemblage. *Coral Reefs* 38, 1007–1021. doi: 10.1007/s00338-019-01827-3

Ríos, P., Prado, E., Carvalho, F. C., Sánchez, F., Rodríguez-Basalo, A., Xavier, J. R., et al. (2020). Community composition and habitat characterization of a rock sponge aggregation (Porifera, Corallistidae) in the Cantabrian Sea. *Front. Mar. Sci.* 7:578. doi: 10.3389/fmars.2020.00578

Rodríguez-Basalo, A., Prado, E., Sánchez, F., Ríos, P., Gómez-Ballesteros, M., and Cristobo, J. (2021). High resolution spatial distribution for the hexactinellid sponges *Asconema setubalense* and *Pheronema carpenteri* in the Central Cantabrian Sea. *Front. Mar. Sci.* doi: 10.3389/fmars.2021.612761

Sánchez, F., and Rodríguez, J. M. (2013). POLITOLANA, a new low cost towed vehicle designed for the characterization of the deep-sea floor. *Instrum. Viewpoint* 15:69.

Sánchez, F., Rodríguez-Basalo, A., García-Alegre, A., and Gómez-Ballesteros, M. (2017). Hard bottom bathyal habitats and keystone epibenthic species on Le Danois bank (Cantabrian sea). *J. Sea Res.* 130, 134–153. doi: 10.1016/j.seares.2017.09.005

Sánchez, F., Serrano, A., Parra, S., Ballesteros, M., and Cartes, J. E. (2008). Habitat characteristics as determinant of the structure and spatial distribution of epibenthic and demersal communities of Le Danois Bank (Cantabrian Sea, N. Spain). *J. Mar. Syst.* 72, 64–86. doi: 10.1016/j.jmarsys.2007.04.008

Sipkema, D., Osinga, R., Schatton, W., Mendola, D., Tramper, J., and Wijffels, R. H. (2005). Large-scale production of pharmaceuticals by marine sponges: Sea, cell, or synthesis? *Biotechnol. Bioeng.* 90, 201–222. oi/pdf/10.1002/bit.20404

Sitjà, C., and Maldonado, M. (2014). New and rare sponges from the deep shelf of the Alboran Island (Alboran Sea, Western Mediterranean). *Zootaxa* 3760, 141–179. doi: 10.11646/zootaxa.3760.2.2

Tabachnick, K. R., and Menshenina, L. L. (2007). Revision of the genus Asconema (Porifera: Hexactinellida: Rossellidae). *J. Mar. Biol. Assoc. U K.* 87, 1403–1429. doi: 10.1017/s0025315407058158

Topsent, E. (1901). Spongiaires. Résultats du voyage du S.Y. 'Belgica'en 1897–99 sous le commandement de A. de Gerlache de Gomery. Expédition antarctique belge. *Zoologie* 4, 1–54.

Topsent, E. (1916). Diagnoses d'éponges recueillies dans l'Antarctique par le Pourquoi-Pas?. *Bulletin du Muséum national d'histoire naturelle, Paris* 22, 163–172.

Turón, X., Tarjuelo, I., and Uriz, M. J. (1998). Growth dynamics and mortality of the encrusting sponge *Crambe crambe* (Poecilosclerida) in contrasting habitats: correlation with population structure and investment in defence. *Funct. Ecol.* 12, 631–639. doi: 10.1046/j.1365-2435.1998.00225.x

Van Aken, H. M. (2000). The hydrography of the mid-latitude Northeast Atlantic Ocean. II: the intermediate water masses. *Deep-Sea Res. Part I Oceanogr. Res. Pap.* 47, 789–824. doi: 10.1016/s0967-0637(99)00112-0

Von Bertalanffy, L. (1938). A quantitative theory of organic growth (Inquires on growth laws. II). *Hum. Biol.* 10, 181–213.

Conflict of Interest: The authors declare that the research was conducted in the absence of any commercial or financial relationships that could be construed as a potential conflict of interest.

Copyright © 2021 Prado, Cristobo, Rodríguez-Basalo, Ríos, Rodríguez-Cabello and Sánchez. This is an open-access article distributed under the terms of the Creative Commons Attribution License (CC BY). The use, distribution or reproduction in other forums is permitted, provided the original author(s) and the copyright owner(s) are credited and that the original publication in this journal is cited, in accordance with accepted academic practice. No use, distribution or reproduction is permitted which does not comply with these terms.

frontiers in Marine Science

ORIGINAL RESEARCH
published: 16 February 2021
doi: 10.3389/fmars.2021.612857

Increasing Knowledge of Biodiversity on the Orphan Seamount: A New Species of *Tedania* (*Tedaniopsis*) Dendy, 1924

Pilar Ríos[1], Javier Cristobo[1], Emily Baker[2], Lindsay Beazley[2], Timothy Culwick[3] and Ellen Kenchington[2]*

[1] Centro Oceanográfico de Gijón, Instituto Español de Oceanografía, Madrid, Spain, [2] Department of Fisheries and Oceans, Bedford Institute of Oceanography, Dartmouth, NS, Canada, [3] School of Earth Science, University of Bristol, Bristol, United Kingdom

A new *Tedania* species (Porifera) was collect using remotely operated vehicles during the Canadian mission HUD2010-029 and the British RRS Discovery Cruise DY081, on the Orphan Seamount near the Orphan Knoll, northwest Atlantic, between 2999.88 and 3450.4 m depth. Orphan Knoll is an isolated, drowned continental fragment 550 km northeast Newfoundland in the Labrador Sea. This region is biologically rich and complex and in 2007, the regional fisheries management organization operating in the area regulated that no vessel shall engage in bottom-contact fishing activities until reviewed in 2020 with a review slated at the end of this year. Members of the genus *Tedania* are uncommon in the temperate northern hemisphere with only six species known previously: *Tedania* (*Tedania*) *anhelans*; *Tedania* (*Tedania*) *pilarriosae*; *Tedania* (*Tedania*) *suctoria*; *Tedania* (*Tedania*) *urgorrii*; *Tedania* (*Tedaniopsis*) *gurjanovae*; and *Tedania* (*Tedaniopsis*) *phacellina*. The particular features of the new sponge we describe are the very peculiar external morphology which is tree-like with dichotomous branching—a morphology not previously described in this subgenus; and the combination of spicules found: long styles, the typical tornotes of the subgenus and two sizes of onychaetes. Additional information is provided on other species of *Tedaniopsis* described from the Atlantic Ocean. Based on the characteristics reported, we propose a new species, *Tedania* (*Tedaniopsis*) *rappi* sp. nov. in honor of Prof. Hans Tore Rapp (1972–2020), University of Bergen, Norway, a renowned sponge taxonomist and coordinator of the Horizon 2020 SponGES project. The holotype of *T.* (*T.*) *phacellina* Topsent, 1912 from the Azores, the only other northern Atlantic species in the subgenus *Tedaniopsis*, was reviewed for comparison.

Keywords: sponges, VMEs, taxonomy, new species, *Tedania (Tedaniopsis) rappi*

OPEN ACCESS

Edited by:
Daphne Cuvelier, Center for Marine and Environmental Sciences (MARE), Portugal

Reviewed by:
Merrick Ekins, Queensland Museum, Australia
Jose Cruz-Barraza, National Autonomous University of Mexico, Mexico

****Correspondence:***
Pilar Ríos
pilar.rios.lopez@gmail.com;
pilar.rios@ieo.es

Specialty section:
This article was submitted to Deep-Sea Environments and Ecology, a section of the journal Frontiers in Marine Science

Received: *30 September 2020*
Accepted: *14 January 2021*
Published: *16 February 2021*

Citation:
Ríos P, Cristobo J, Baker E, Beazley L, Culwick T and Kenchington E (2021) Increasing Knowledge of Biodiversity on the Orphan Seamount: A New Species of Tedania (Tedaniopsis) Dendy, 1924. Front. Mar. Sci. 8:612857. doi: 10.3389/fmars.2021.612857

INTRODUCTION

Orphan Knoll is an isolated, drowned continental fragment 550 km northeast of Newfoundland in the Labrador Sea (NW Atlantic) (Meredyk et al., 2020). The top of Orphan Knoll stands at 1,800–2,000 m and is marked by a series of protruding mounds at depths of between 1,800 and 2,300 m. The Orphan Seamount is located 9 km northeast of the southern-most extension of Orphan Knoll and is a volcanic seamount (Meredyk, 2017). Physical properties indicate that

mid-depth waters above Orphan Knoll are in a boundary region between outflow from the Labrador Sea (subpolar gyre) and northward flow of the North Atlantic Current (subtropical gyre). Near-bottom current measurements provide evidence for anti-cyclonic (clockwise) circulation around the knoll (Greenan et al., 2010) that could have impacts on the benthic communities. The Orphan Basin-Orphan Knoll region is biologically rich and complex (Wudrick et al., 2020), and strongly influenced by local processes and advection.

By the Northwest Atlantic Fisheries Organization (NAFO) to protect coral, sponges and other vulnerable marine ecosystems from impact by bottom contact fishing gear. Orphan Knoll is also considered an Ecologically or Biologically Significant Area (EBSA) by the Convention on Biological Diversity (2015).

In 2010, Fisheries and Oceans Canada (DFO) in collaboration with academic partners conducted a multidisciplinary oceanographic survey of Flemish Cap and Orphan Knoll onboard the CCGS *Hudson* in support of the identification and characterization of vulnerable marine ecosystems as part of Canada's contribution to the NEREIDA program (NAFO, 2016).

On Orphan Knoll and its associated seamount (Orphan Seamount), the remotely operated vehicle (ROV) ROPOS was used to collect high-resolution continuous video and digital still images of Orphan Knoll's diverse benthic communities and geological landscape. Specimen samples were collected using the manipulator arm of ROPOS to serve as taxonomic voucher specimens. We augment data collected during this survey with samples collected during the Isotope CYcling in the LABrador Sea (ICY-LAB) mission onboard RRS *Discovery* in 2017. The overall aim of that mission was to understand nutrient and isotope cycling regions of the Labrador Sea and Greenland fjords (Hendry et al., 2019).

During dive number 1340 by ROV ROPOS at Orphan Seamount, the holotype of the new species was collected. The transect took place between depths of 1,862 and 3,004 m, with an average of 2,455 m and a distance traveled of 11,515 m (Wudrick et al., 2020). This new species of the genus *Tedania* Gray, 1867, was collected close to 3,000 m in depth, inside the NAFO closed area and CBD EBSA, where the substrate were rocks of volcanic origin (Meredyk et al., 2020).

The genus *Tedania* is cosmopolitan and comprises 83 species, with 29 of them distributed in the northern hemisphere (Van Soest et al., 2021). *Tedania* is characterized by having diactinal ectosomal tornotes, or tylotes, usually provided with spines on the tyles, or smooth oxea-like spicules with mucronate apices. Choanosomal megascleres are styles with smooth or microspined bases and the microscleres are onychaetes that characterize the Family Tedaniidae Ridley and Dendy, 1886. The choanosomal megascleres (styles) are arranged in plumose, reticulate, plumo-reticulate or dendritic columns in the genus *Tedania* and the ectosomal skeleton is tangential or paratangential.

The genus *Tedania* had been subdivided into different subgenera. Desqueyroux-Faúndez and Van Soest (1996) followed by Van Soest (2002) created a subgeneric classification of *Tedania* with three subgenera: *Tedania*, *Tedaniopsis*, and *Trachytedania*. The last one is considered currently to be a valid genus (Cristobo and Urgorri, 2001; Van Soest, 2017) and is characterized by species having acanthostyles as choanosomal megascleres. Recently, a third subgenus was recognized, *Stylotedania* Van Soest, 2017 and nowadays the World Porifera Database (Van Soest et al., 2021) consider again three valid subgenera: *Tedania* Gray, 1867, *Tedaniopsis* Dendy, 1924, and *Stylotedania* Van Soest, 2017. The first one, differentiates those species of genus *Tedania* with ectosomal diactinal spicules with smooth or microspined heads, choanosomal monactinal or diactinal spicules and onychaetes. The second differentiates those where the ectosomal diactinal spicules have smooth heads, the choanosomal spicules are monactinal or diactinal and the typical onychaetes are present. The third differentiates those in which the ectosomal and choanosomal spicules are monactinal, diactinal spicules being absent and also have onychaetes (Van Soest, 2017; Aguilar-Camacho et al., 2018).

MATERIALS AND METHODS

Sampling was carried out on board the CCGS *Hudson* using the remotely operated vehicle ROPOS, in July 2010 during mission HUD2010-029 and on the RRS *Discovery* Cruise DY081 with the ROV *ISIS*, in July 2017. During the Hudson mission, a single specimen was collected using the manipulator arm of ROPOS at 2999.88 m depth from Orphan Seamount (**Figure 1**) and stored in its "biobox" until the ROV surfaced. A Seabird 49 CTD attached to this ROV provided temperature (2.1°C) and salinity (34.89‰) data at the time of collection. During the RRS *Discovery* cruise, sponges were collected either using the manipulator arms, or using a suction system. Upon recovery of the ROV to the surface, samples were transferred to buckets and taken into a wet lab for processing. Then, each sponge sample was labeled, measured and photographed.

The specimen from ROPOS was immediately preserved in 70% ethanol upon surfacing. The sample from ROV ISIS was carried in pre-chilled seawater into the cold room (4°C) to commence sampling triage and was preserved in 95% ethanol.

Details of the specimens examined are deposited in PANGAEA® Data Publisher[1] under the digital object identifier (DOI): https://doi.pangaea.de/10.1594/PANGAEA.924814

For the study of dissociated spicules, the organic matter was digested in sodium hypochlorite following the methods of Rapp (2006) and Cárdenas and Rapp (2012) and digested in nitric acid for SEM, following methods described in Cristobo et al. (1993). Spicules and skeleton were coated with gold-palladium using an Emscope Sputter coater SC 500 and examined with a Hitachi S570 SME at Station Marine d'Endoume (France) and a JEOL-JSM-6610 LV of the Oviedo University. The data for spicule sizes are based on 25 measurements for each spicule category, comprising minimum, maximum and average lengths in micrometers (μm). A light microscope (Nikon Eclipse 50i with a Nikon DS-Fi1 camera) was used. The skeleton was also photographed with the same camera system and stacking performed using the Helicon Focus program (129 images).

[1] www.pangaea.de

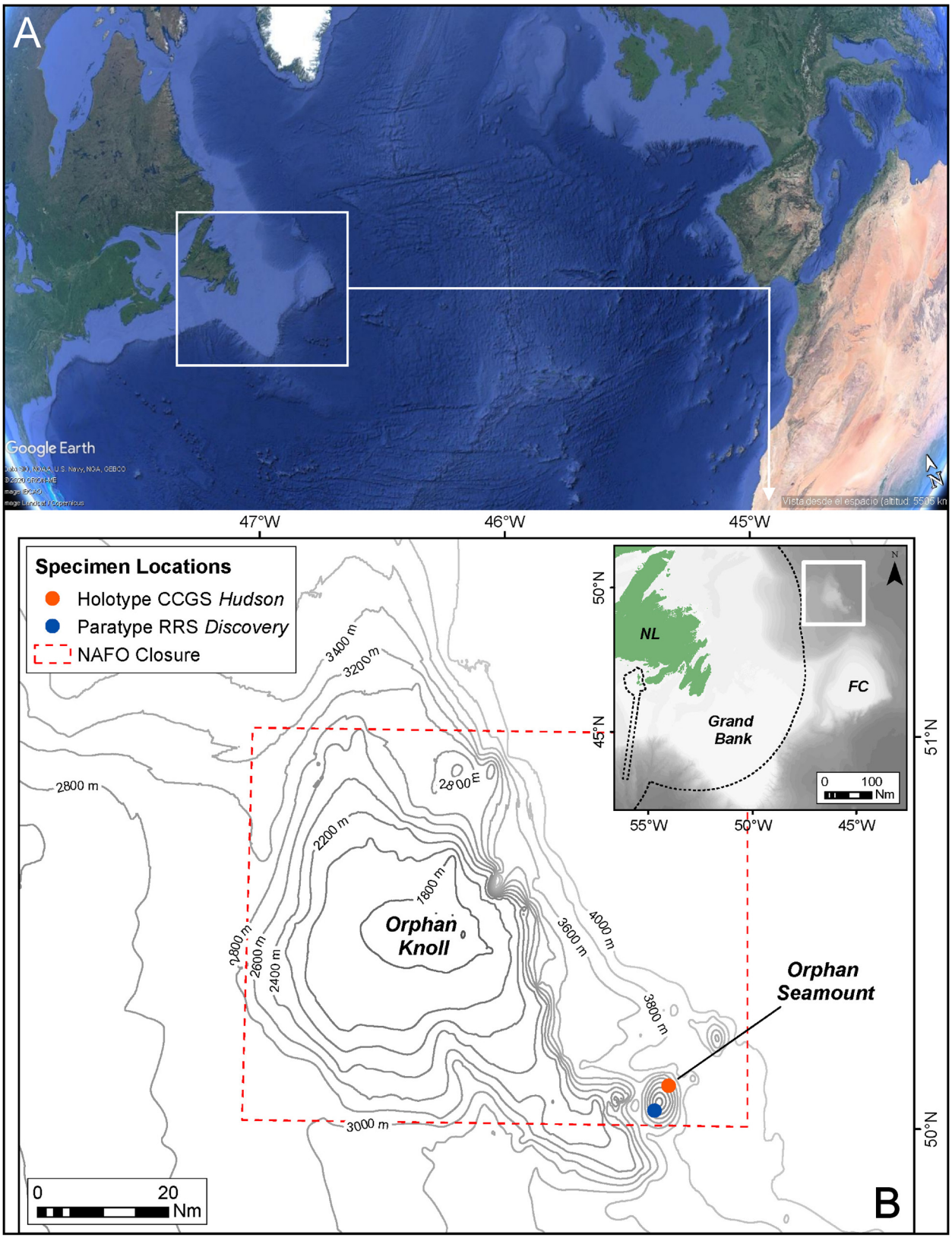

FIGURE 1 | Location of sampling sites of new species. **(A)** Situation of Orphan Knoll in the North Atlantic (from Google Earth). **(B)** Positions of specimens locations (Holotype and Paratype) on Orphan Seamount.

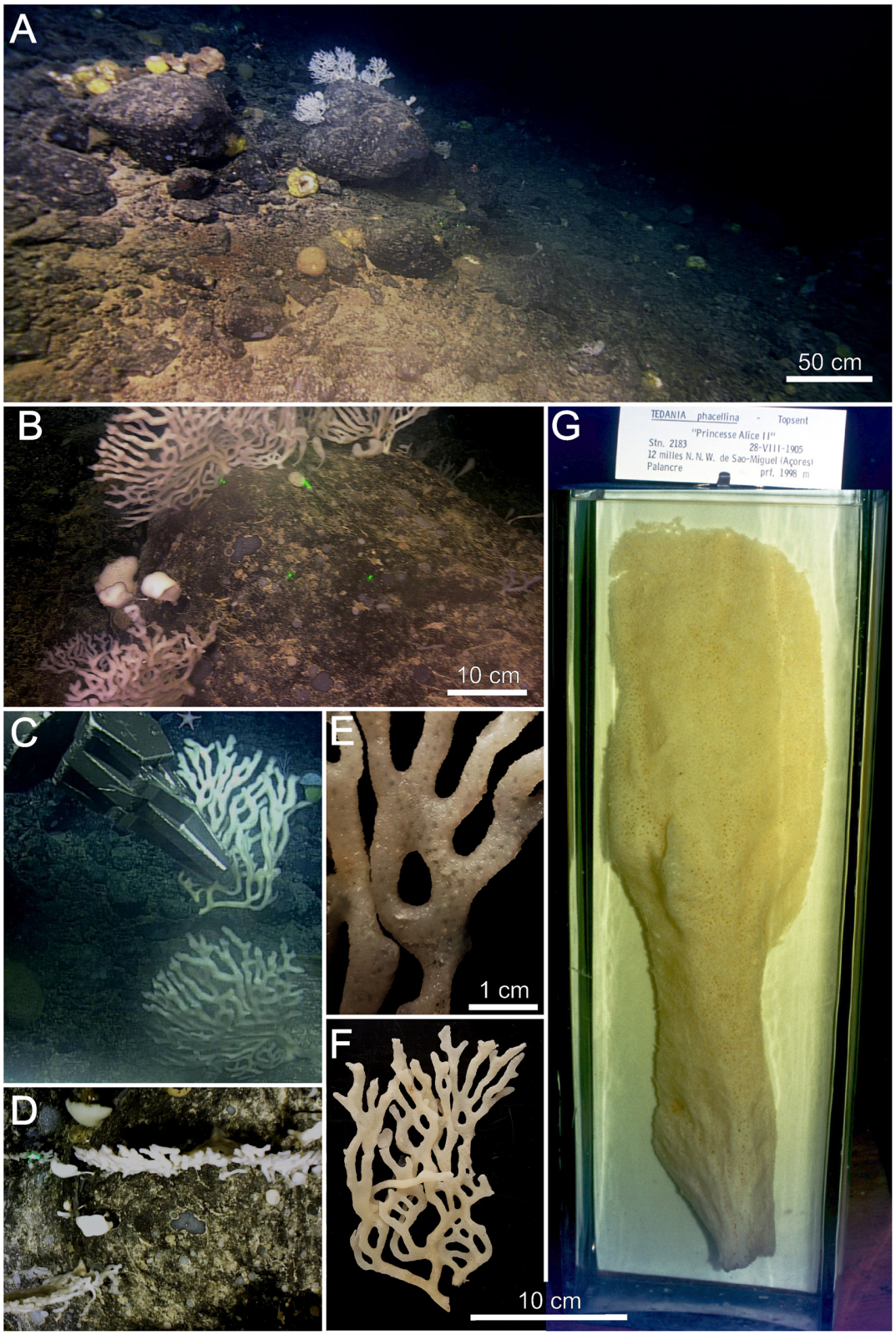

FIGURE 2 | *Tedania* (*Tedaniopsis*) *rappi* sp. nov. **(A,B)** Environment of holotype. **(C)** *In situ* collection of holotype. **(D)** View of two specimens from the downward facing camera. **(E)** Detail of the surface of the holotype on which the oscula are seen. **(F)** Holotype. **(G)** *Tedania* (*Tedaniopsis*) *phacellina*, Topsent's holotype located in the display cases of the Oceanographic Museum of Monaco. Note that figures **(F,G)** are on the same scale to compare the proportions and shapes of both species.

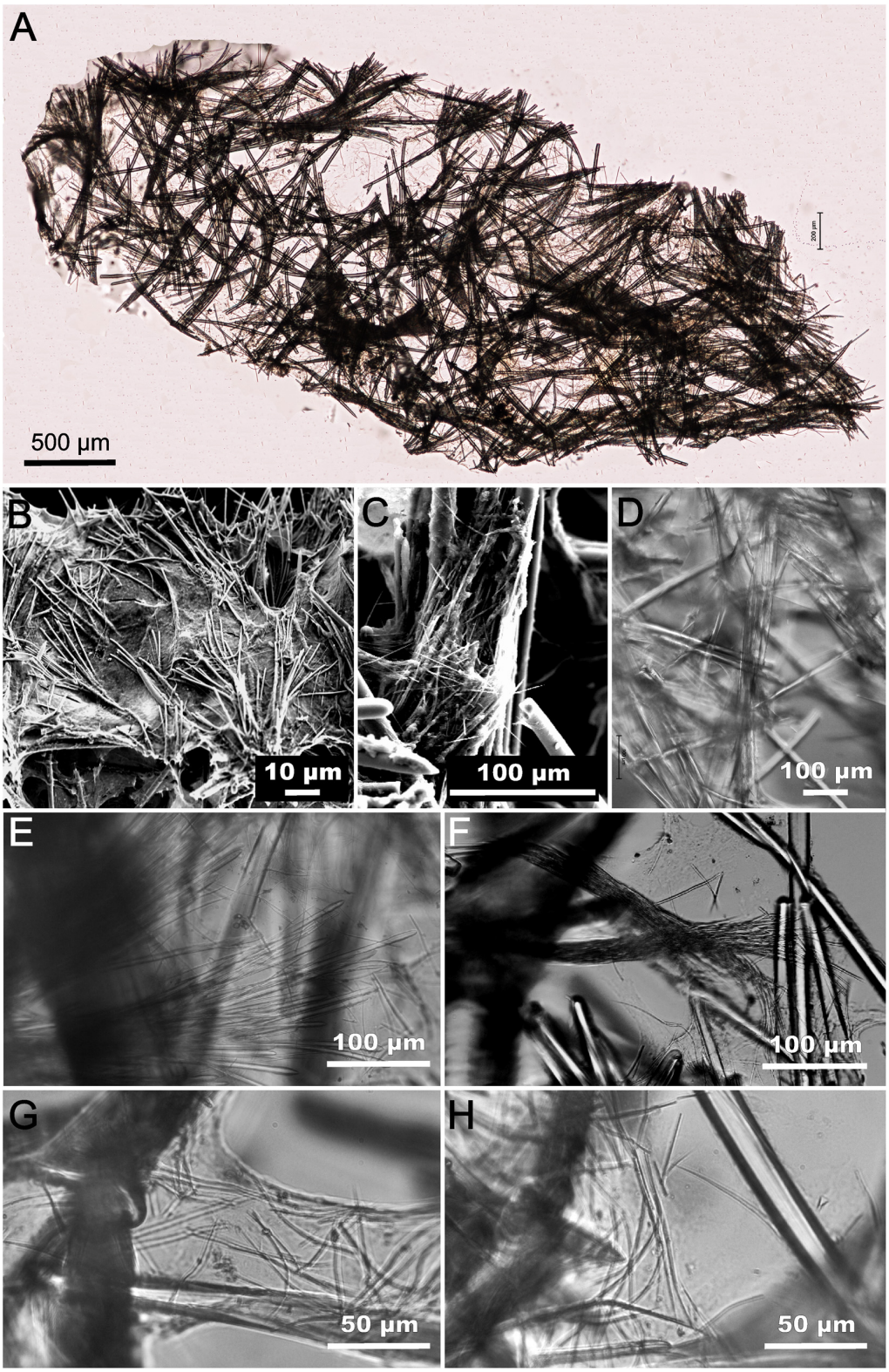

FIGURE 3 | *Tedania* (*Tedaniopsis*) *rappi* sp. nov. **(A)** Transversal section of a branch of holotype (light microscope, LM). **(B)** Scanning Electron Microscope (SEM) picture of the surface of sponge ectosomal tornotes protruding. **(C)** Detailed picture of group of onychaetes in choanosome (SEM). **(D)** Bundle of styles in choanosome (LM). **(E)** Bundles of tornotes projected in bouquets in the ectosome (LM). **(F)** Two trichodragmata in the ectosome (LM). **(G)** Onychaetes within a spongin fiber (LM). **(H)** Onychaetes in the choanosome (LM).

DNA was extracted from the holotype using a Qiagen DNeasy Blood and Tissue Kit (QIAgen) following an adapted version of the protocol provided by the manufacturer (overnight incubation in lysis buffer and proteinase K). We selected two molecular markers to amplify, *18S rDNA* (*18S*) and *28S rDNA* (*28S*). The complete 18S (1,766 bp) was amplified in three legs using the primers 1F-5R, 4F-7R, and a.20-9R (Giribet and Wheeler, 2001), and a fragment of 589 bp of 28S (D6 – D8 region) was amplified using the primers CMPOR1490F and CMPOR2170R (Morrow et al., 2012). D6 – D8 region was selected because these where the most successful PCRs regarding 28S. All 18S fragments were amplified using the PCR protocol 94°C, 5 min; (94°C, 1 min, 52°C, 1 min, 72°C, 1 min) × 38 cycles; 72°C, 10 min. We used a different protocol for 28S of 94°C, 5 min; (94°C, 1 min, 55°C, 1 min, 72°C, 1 min) × 38 cycles; 72°C, 10 min. All DNA markers were amplified in 12.5 μL reactions using 10.5 μL of VWR Red Taq DNA Polymerase 1.1× Master Mix (VWR International bvba/sprl, Belgium), 0.5 μL of the forward and reverse primers, and 1 μL of DNA template. PCR products, stained with GelRed® (Biotium, United States), were visualized in a 2.5% agarose gel electrophoresis, run at 90 V for 30 min. Sequencing was conducted on an ABI 3730XL DNA Analyser (Applied Biosystems, United States) at the Molecular Core Labs (Sequencing Facility) of the NHMUK, using the forward and reverse primers mentioned above. The DNA was degraded and the results were negative, probably because the genomic DNA loses quality in depth water samples (Kersken et al., 2018).

The electronic version of this article in PorTable Document Format (PDF) will represent a published work according to the International Commission on Zoological Nomenclature (ICZN), and hence the new names contained in the electronic version are effectively published under that Code from the electronic edition alone. This published work and the nomenclatural acts it contains have been registered in ZooBank, the online registration system for the ICZN. The ZooBank Life Science Identifiers (LSIDs) can be resolved and the associated information viewed through any standard web browser by appending the LSID to the prefix http://zoobank.org/. The LSID for this

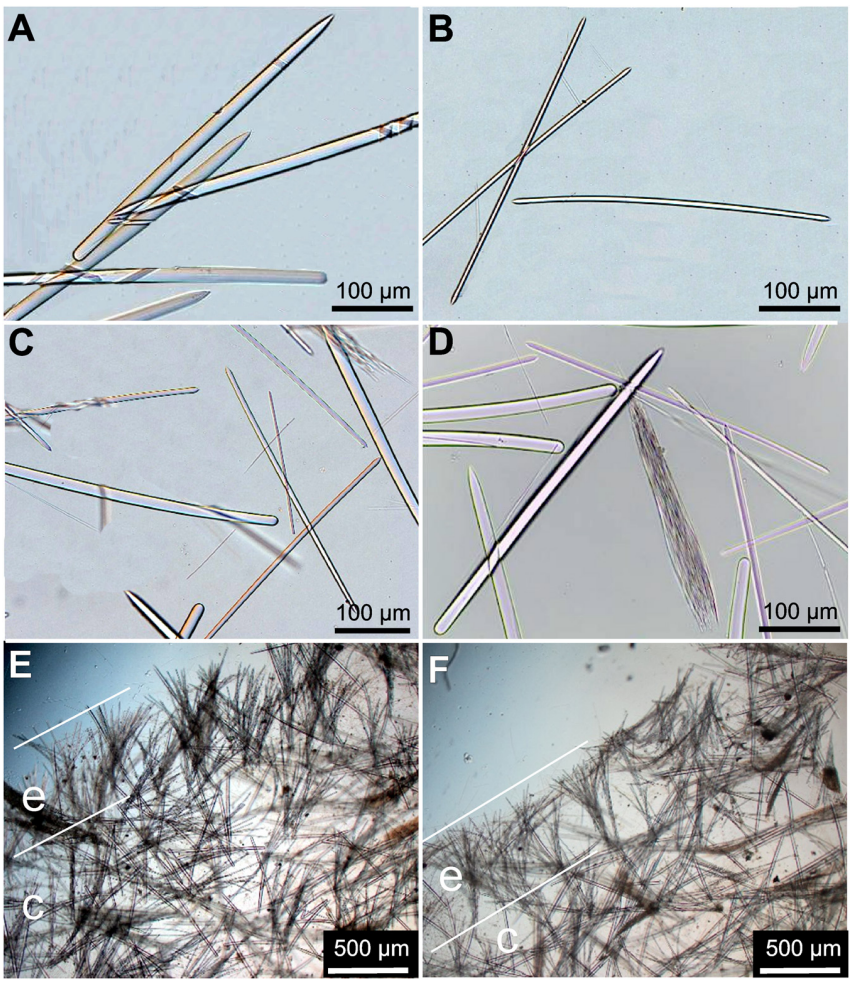

FIGURE 4 | Spicules of *Tedania* (*Tedaniopsis*) *rappi* sp. nov. (Paratype) as seen with a light microscope. **(A)** Styles. **(B)** Tornotes. **(C)** Different kinds of spicules. **(D)** Group of onychaetes in tricodragmata formation. **(E,F)** Skeleton with marked differentiation between ectosome (e) and choanosome (c).

publication is: urn:lsid:zoobank.org:pub:687D7886-46D4-461A-8799-2B76BB446D0C.

Global subgenus maps were derived from data provided by the World Porifera Database (Van Soest et al., 2021).

RESULTS

In this study we analyzed a new species of the *Tedaniopsis* subgenus collected in Orphan Seamount and re-examined *Tedania* (*Tedaniopsis*) *phacellina* Topsent, 1912 from Azores for comparison. This material is described and illustrated. The new species described here has the taxonomic authority restricted to Ríos, Cristobo, and Kenchington.

Systematics follow the SystemaPorifera (Hooper and Van Soest, 2002) chapter on Family Tedaniidae (Van Soest, 2002) and Morrow and Cárdenas (2015).

Phylum PORIFERA Grant, 1836

Class DEMOSPONGIAE Sollas, 1885

SubClass HETEROSCLEROMORPHA Cárdenas et al., 2012

Order POECILOSCLERIDA Topsent, 1928

Family TEDANIIDAE Ridley and Dendy, 1886

Genus *Tedania* Gray, 1867

Definition: Tedaniidae with differentiated ectosomal and choanosomal megascleres Van Soest (2002).

Subgenus *Tedaniopsis* Dendy, 1924

Diagnosis: *Tedania* with relatively long thick, smooth styles, occasionally modified to anisostrongyles or anisoxeas, as structural megascleres. Ectosomal megascleres are mucronate or tylostrongylote tornotes occasionally with one or more vestigial spines (Desqueyroux-Faúndez and Van Soest, 1996).

Tedania (*Tedaniopsis*) *rappi* Ríos, Cristobo and Kenchington sp. nov.

Type material: Holotype: TBD Orphan Seamount (NW Atlantic), 50.1119; −45.3199. Depth 2999.88 m, Coll. CCGS *Hudson*, 19.07.2010, 1 specimen. Rock substrate. In 70% Ethanol Canadian Museum of Nature number CMNI 2020-0004. Paratype: Atlantic Reference Centre (ARC) Museum (ARC 81604) Orphan Seamount (NW Atlantic), 50.0484; -45.3757, 3,450 m depth, Coll. RRS *Discovery*, 08.07.2017, 1 specimen. Rock substrate. In 100% Ethanol.

Holotype of *Tedania (Tedaniopsis) phacellina* Topsent, 1912, was revised. Museé Oceanographique Monaco; Collection of S.A.S. Le Prince de Monaco Station 2183, 28th August 1905, 1,998 m in depth. A small fragment (Schizotype) was analyzed by SEM.

Derivatio nominis: In honor of Prof. Hans Tore Rapp (1972–2020), University of Bergen, Norway, a renowned sponge taxonomist and dear colleague, who described 50 new species of sponges for science. Prof. Rapp was also coordinator and leader of the EU Horizon 2020 SponGES project which focused much needed attention on deep-sea sponges and their habitats.

Description

The *habitus* of the new species is arborescent, erect, branching, tree-like in appearance, flat, fan-shaped, it grows in one plane (bidimensional structure, **Figure 2D**). Size: 25 cm (width) × 15 cm (height). Attached to the substrate by a short and single peduncle [1 cm (width) × 2 cm height] from which it branches mainly in dichotomous arrangement; often, the branches anastomose between them (**Figures 2B,E**). The ends of each branch are rounded (**Figure 2**). The holotype (half of the whole specimen) measures 19 cm long and 12 cm wide (Paratype 6.5 × 6 cm). Each branch is elliptical in section from 5 to 9 mm. Slightly velvety surface with pores (oscules <1 mm diameter) arranged in regular distribution along branches. Consistency flexible and elastic. Color in life and in preservation white.

Skeleton

The choanosomal skeleton is a loose reticulation of bundles of 2–5 styles (paucispicular) with weaker interconnections of 1–2 spicules cemented with spongin (**Figures 3A,B,D**). The ectosomal skeleton consists of bundles of tornotes that are projected in bouquets to the surface (**Figure 3E**). Onychaetes, of two sizes, are scattered in the choanosome and within spongin fibers (**Figures 3G,H**). Both size classes of onychaetes can be placed among the tornotes of the ectosomal skeleton and frequently in tricodragmata (**Figure 3F**).

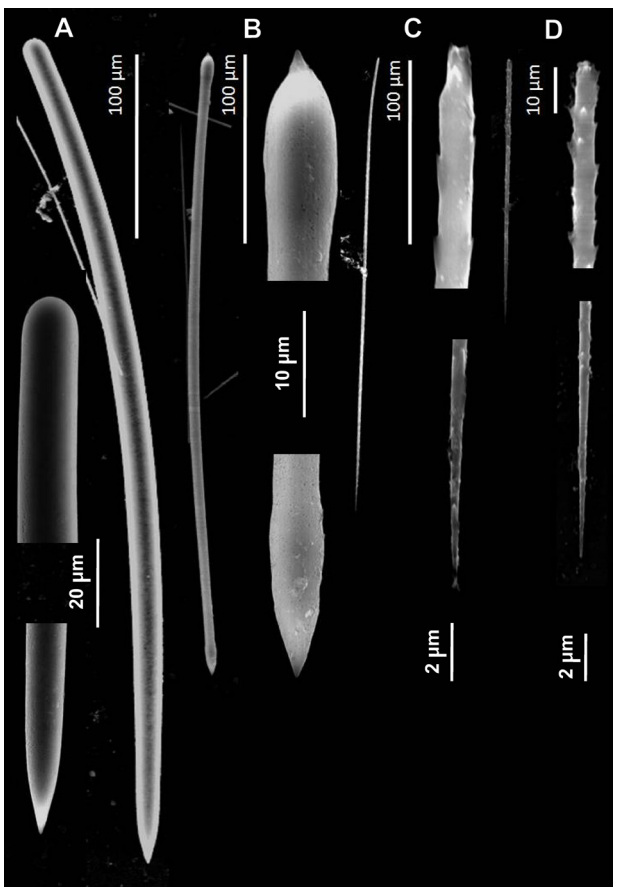

FIGURE 5 | Spicules of *Tedania* (*Tedaniopsis*) *rappi* sp. nov. (Holotype) as seen with a Scanning Electron Microscope. **(A)** Styles. **(B)** Tornotes. **(C)** Onychaetes I. **(D)** Onychaetes II.

Spicules Styles, Tornotes, and Onychaetes

Styles (**Figures 4A,B**, **5A**). Straight or slightly curved near the basal end with a sharp point in the apical end. Uniform in length and thickness: 457.94 (505) 554.64 × 11.41 (14.05) 17.41 μm (Holotype). 406 (459) 504 × 14 (15.3) 17 μm (Paratype).

Tornotes (**Figures 4A–C**, **5B**) Anisotornotes, with slightly inflated and lanceolate ends one of them more mucronate than the other. Measurements: 363.13 (408.68) 440.400 × 5.79 (6.58) 7.42 μm (Holotype). 379 (399.8) 422 × 6 (7.2) 8.6 μm (Paratype).

Onychaetes of two sizes. The largest (I) are 203.3 (234.40) 268.02 μm long (Holotype) 240 (268.3) 307 μm long (Paratype) (**Figures 4C**, **5C**). The smallest (II) are 67.85 (76.19) 86.28 μm long (Holotype) 68 (79.8) 82 μm long (Paratype) (**Figures 3F–H**, **4C,D**, **5C,D**). The largest have uneven ends, one pointed and the other more or less rounded. The smaller ones have one end pointed and the other straight with 3–4 spines. We have observed the largest onychaetes grouped in trichodragmata (**Figures 3**, **4**).

Distribution and Ecology

Orphan Seamount, where this new species was collected, is in a transition area between the Arctic and the Temperate Northern Atlantic ecoregions (Spalding et al., 2007). Specimens of the new species were seen in the slopes NE and SW of Orphan Seamount (Labrador Sea, NW Atlantic) attached to rocks of volcanic origin at 2,999–3,450 m; the mean bottom temperature was of 2.39 ± 0.03°C.

On the rock where the holotype specimen was sampled, there were at least 10 specimens of the same species and 39 in the whole transect (ROV dive number 1340, 11,515 m in total distance on bottom). The most characteristic fauna associated with the habitat are other Porifera mainly belonging to genus *Geodia* which represents the highest biomass and the highest number of specimens of the sponge grounds, mainly due to *G. phlegraei* (Sollas, 1880), and also *G. megastrella* Carter, 1876, *G. barretti* Bowerbank, 1858, *G. atlantica* (Stephens, 1915), *G. macandrewii* Bowerbank, 1858, and *G. hentscheli* Cárdenas et al., 2010. Other frequent Porifera are *Lissodendoryx (Lissodendoryx) complicata* (Hansen, 1885), *Hexadella detritifera* Topsent, 1913, *Stryphnus fortis* (Vosmaer, 1885), and *Polymastia corticata* Ridley and Dendy, 1886. Also hexactinellids such as *Farrea herdendorfi* Duplessis and Reiswig, 2004, cup-like species such as *Asconema fristedti* Tabachnick and Menshenina, 2007, *Chenolasma* sp. and cylindrical species such as *Dictyaulus romani* Murillo et al., 2013 or representatives of the families Euplectellidae or Rosellidae were present. Other invertebrates included Cnidarians such as *Bathypathes* sp., representatives of the family Clavulariidae, Chrysogorgiidae, several species of Scleractinia, *Anthomastus* sp., Echinoderms and fishes. The total number of individuals of each taxon/morphotype, abundance by transect and a pictorial guide of megafauna can be seen in Wudrick et al. (2020).

Remarks

The most notable difference from other species of subgenus *Tedaniopsis* is the erect, tree-like appearance of this species, which has never been recorded before in this subgenus. Goodwin et al. (2012) and Aguilar-Camacho et al. (2018) compiled the data from the majority of species of this subgenus from the Antarctic and South Atlantic and worldwide respectively, and none have any features like the new species, being mostly massives, such as *Tedania* (*Tedaniopsis*) *charcoti* Topsent, 1907; *T.* (*T.*) *armata*

TABLE 1 | Spicule characteristics of *Tedania* (*Tedaniopsis*) species from the northern hemisphere.

Specie	Megascleres (μm)		Microscleres (μm)		Habitus	Depth (m)	Distribution
	Choanosomal	Ectosomal	Onychaetas				
T. (*T.*) *phacellina*	Style	Tornote	Largest (I)	Smaller (II)			
Topsent, 1912	515–550 × 20–23	440–470 × 7	290–330 × 1.7	70–80	Erect blade	1,998	Azores
Topsent, 1912 re-measured (this study)	Styles I: 384.64 (471.65) 519.53 × 9.55 (16.78) 26.67 *N* = 25 Styles II: 438 (467.90) 511.04 × 5.7 (7.55) 11.58 *N* = 7	348.61 (379.23) 408 × 5.79 (7.20) 9.27 *N* = 25	180.08 (252.15) 285.26 *N* = 25	49.48 (64.93) 85.89 *N* = 25	Erect blade	1,998	Azores
T. (*T.*) *gujarnovae*							
Koltun, 1958	260–343 × 8–14	202–280 × 4–8	197–312 × 2	77–157 × 3–4	Cushion-shaped	60–100	E Tatar Strait, off Sakhalin, USSR
Bakus, 1964	296–373 × 9–13	204–252 × 4–7	142–265 × 1.5–1.6	40–91 × 2.2–3.5	Amorphous encrusting sponge	73–198	President Channel and San Juan Channel, San Juan Archipelago
T. (*T.*) *rappi* sp. nov.							
Holotype	457.94 (505) 554.64 × 11.41 (14.05) 17.41 *N* = 25	363.13 (408.68) 440.44 × 5.79 (6.58) 7.42 *N* = 25	229.93 (257.49) 277.22 *N* = 25	67.85 (76.19) 86.28 *N* = 25	Tree-like	2,999	Orphan Seamount
Paratype	406 (459) 504 × 14(15.3)17 *N* = 25	379 (399.8) 422 × 6(7.2)8.6 *N* = 25	240 (268.3) 307 × 1(1.2)2 *N* = 25	68 (79.8) 82 *N* = 20	Tree-like	3,450	Orphan Seamount

Sarà, 1978; *T.* (*T.*) *corticata* Sarà, 1978; *T.* (*T.*) *laminariae* Sarà, 1978; *T.* (*T.*) *cristagalli* Dendy, 1924; *T.* (*T.*) *gracilis* Hentschel, 1914; *T.* (*T.*) *massa* Ridley and Dendy, 1886; *T.* (*T.*) *sarai* Bertolino et al., 2007; *T.* (*T.*) *tenuicapitata* Ridley, 1881; *T.* (*T.*) *vanhoeffeni* Hentschel, 1914; globular such as *T.* (*T.*) *gracilis* Hentschel, 1914; *T.* (*T.*) *lanceta* Koltun, 1964; cup shaped such as *T.* (*T.*) *turbinata* (Dendy, 1924); *T.* (*T.*) *infundibuliformis* Ridley and Dendy, 1886; *T.* (*T.*) *tantula* (Kirkpatrick, 1907) or crust such as *T.* (*T.*) *aurantiaca* Goodwin et al., 2012 and *T.* (*T.*) *wellsae* Goodwin et al., 2012. The differences with respect to the two species from the northern hemisphere are also *habitus*, the spicule morphology and their ecology (**Table 1**). Topsent (1912) described *Tedania* (*Tedaniopsis*) *phacellina* from the NW São Miguel Island, in the Azores at 1,998 m in depth. Only one specimen was found and it has not been seen since, but it is a shallower species than the new one. Its shape is clearly different: *T. (T.) phacellina*, above its attachment, first rolls up into a cone, then, almost immediately, reopens to take the form of a vertical blade, flat and without branches. The blade is divided into two parts: the lower, narrow, in a fairly deep gutter; the upper one, longer, wider and slightly concave. It has the appearance of an oar paddle. *T. (T.) rappi*, as described above is branched, arborescent, and tree-like in appearance. Regarding the size, *T. (T.) phacellina*, is a large and robust sponge (47 cm high) (**Figure 2**).

Table 1 presents a comparison of the *Tedania* (*Tedaniopsis*) species from the northern hemisphere. *Habitus* is very different among them: Arborescent in the new species, cushion-shaped in *T.* (*T.*) *gujarnovae* and lamellate or cup-shaped in *T.* (*T.*) *phacellina.* Although they present a similar composition of the spicular types, differences between the three species can be appreciated. The styles of *T.* (*T.*) *gujarnovae* are clearly shorter (260–373 μm) than in the new species (406–554.6 μm). Those of *T.* (*T.*) *phacellina*, (384–550 × 9.5–26 μm) similar in length to *T.* (*T.*) *rappi*, however, they are much thicker (11.4–17.4 μm in the new) This is a remarkable difference. Also a second category of styles was found in the analysis of the holotype (**Figures 6**, **7**); these are slightly thinner (5.7–11.5 μm) and scarce. The ectosomal tornotes are shorter in *T.* (*T.*) *gujarnovae* (202–280 μm) than in *T.* (*T.*) *phacellina* (348.6–470 μm) and in *T.* (*T.*) *rappi* (363–440.4 μm). In *T (T.) rappi* tornotes are mucronate in one end while *T.* (*T.*) *phacellina* have a short end (conical). In *T.* (*T.*) *phacellina* the ends are slightly more swollen than in *T.* (*T.*) *rappi*; tornotes do not have lanceolate ends in *T. (T.) gujarnovae*. The largest onychaetes in *T. (T.) gujarnovae* (142–312 μm) are also slightly smaller than in the other two species: *T.* (*T.*) *rappi* (229.9–307 μm), *T.* (*T.*) *phacellina* (180–330 μm). However, the small onychaetes (40–157 μm) are larger than in the other two species: *T.* (*T.*) *rappi* (67.8–86.2 μm), *T.* (*T.*) *phacellina* (49.4–85.8 μm).

In the three species, the bathymetric distribution is quite different: in shallower waters from the South Sakhalin and the South Kurile Island region, *T. (T.) gujarnovae* (60–190 m), *T. (T.) phacellina* from the Azores (1998 m) and the one that has been found deeper is *T. (T.) rappi* (2999–3450 m) from Orphan Seamount, in the North Western Atlantic.

A comparative table of all *Tedania* (*Tedaniopsis*) described species worldwide can be seen in Goodwin et al. (2012) and Aguilar-Camacho et al. (2018). Therefore, the new species is characterized by the external appearance as tree-like with dichotomous branching, long styles, the typical tornotes of the subgenus with lanceolated ends and two sizes of onychaetes.

DISCUSSION

The principal reviews of the *Tedania* genus have been carried out by Bergquist and Fromont (1988); Desqueyroux-Faúndez and Van Soest (1996), Van Soest (2002), and Aguilar-Camacho et al. (2018). The genus *Tedania* actually contain 83 species (Van Soest et al., 2021), 60 of them are included in the *Tedania* subgenus, 21 in *Tedaniopsis,* 1 in *Stylotedania* and one more without a description—*Tedania rubra* Von Lendenfeld, 1888 synonymized with *Tedania anhelans* by Hooper and Wiedenmayer (1994) but it remains *incertae sedis* as the description of Lendenfeld is inadequate (added by Van Soest, 2010 in Van Soest et al., 2021).

Most species of the genus *Tedania* have been reported from the southern hemisphere (54). The subgenus

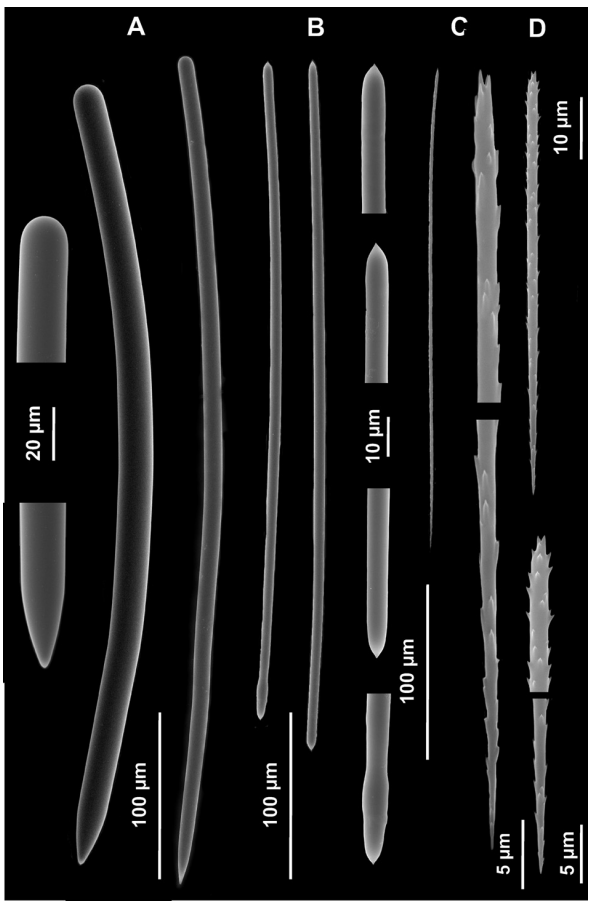

FIGURE 6 | Spicules of *Tedania* (*Tedaniopsis*) *phacellina*, Topsent, 1912. (Holotype) as seen with a Scanning Electron Microscope. **(A)** Styles. **(B)** Tornotes. **(C)** Onychaetes I. **(D)** Onychaetes II.

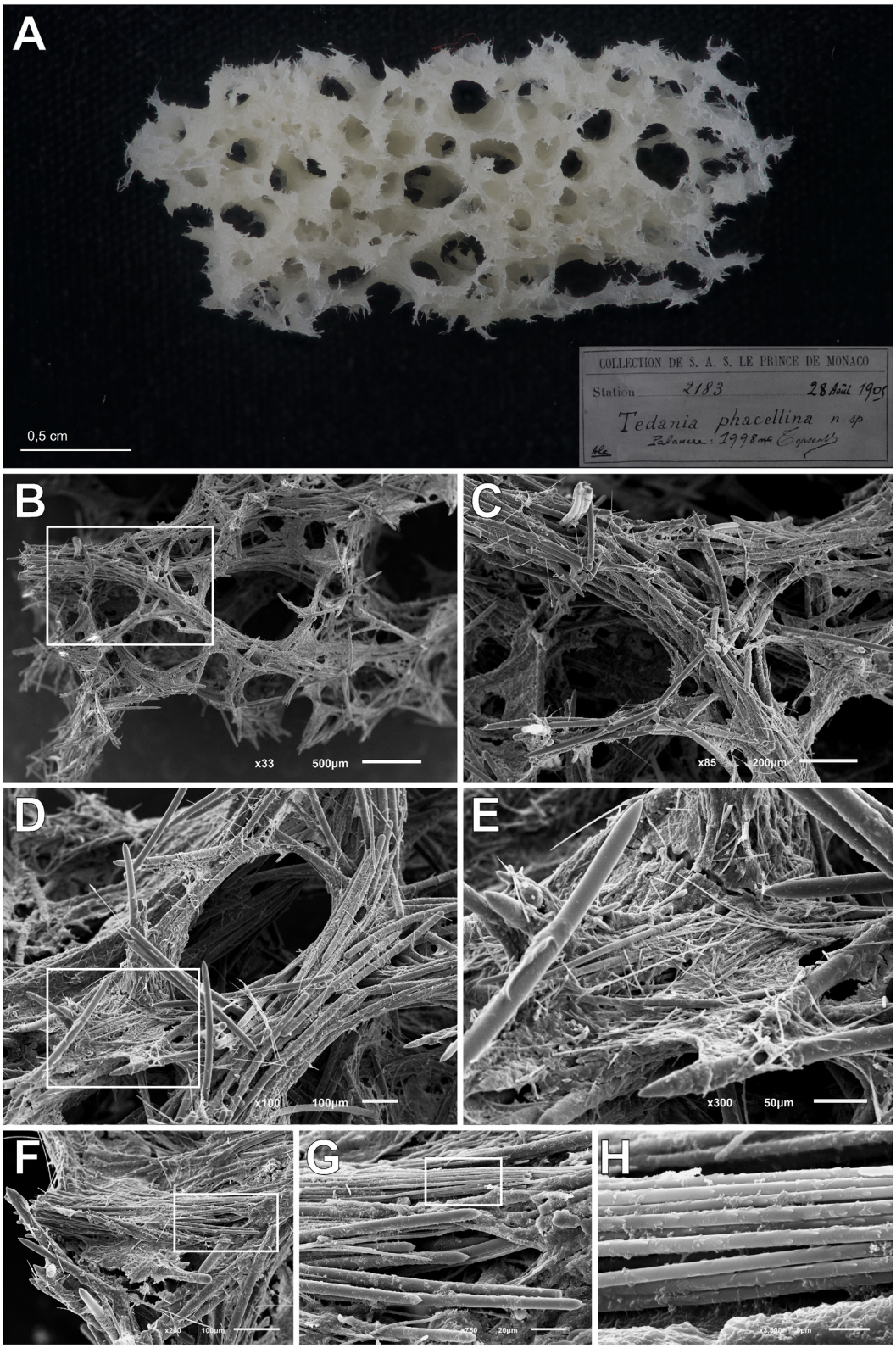

FIGURE 7 | *Tedania* (*Tedaniopsis*) *phacellina*, Topsent, 1912. **(A)** Schyzotype, the small fragment extract from the holotype used in this paper. **(B,C)** Section of choanosomal skeleton where the bundles of styles can be seen. **(D,E)** Skeleton around the aquiferous system composed of multispicular tracts and styles; onychaetes covering the tracts and imbibed in the spongin can be seen. **(F,G)** Bundles of ectosomal tornotes. **(H)** Onychaetes in trichodragmata.

Tedania is present in all oceans except Antarctica where the subgenus that predominates is *Tedaniopsis* (19 spp.). The distribution of *Tedania* (*Stylotedania*) *folium* Van Soest, 2017 is the tropical-Atlantic Guyana shelf (**Figures 8**, **9**).

With respect to the northern hemisphere, the subgenus *Tedania* is represented by 26 species. The most abundant is *Tedania* (*Tedania*) *ignis* (Duchassaing de Fonbressin and Michelotti, 1864) frequent in both hemispheres, from the Bermudas in the north to Santa Catarina, southeast Brazil, Belize

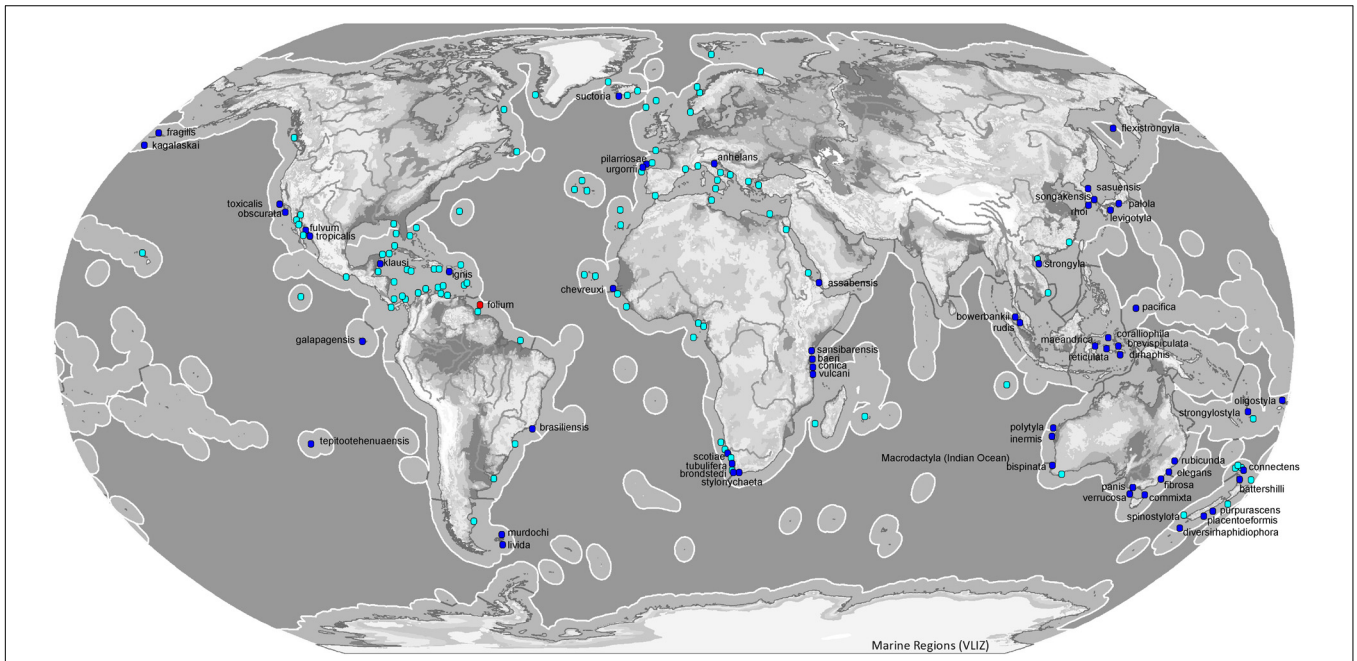

FIGURE 8 | Map of ecoregions (Spalding et al., 2007) showing the global diversity and distribution of the subgenus *Tedania* (blue marine dots for holotypes, light blue dots other records) and *Stylotedania* (red dot holotype) based on data derived from the World Porifera Database 2020.

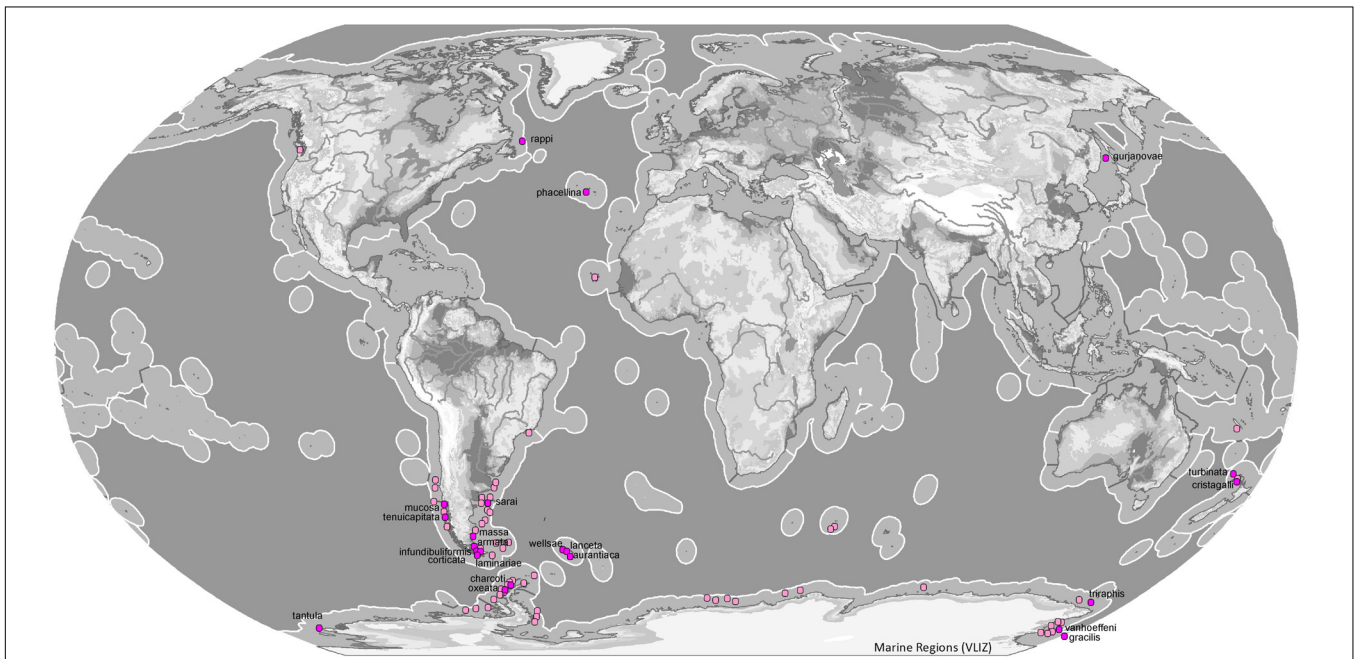

FIGURE 9 | Map of ecoregions (Spalding et al., 2007) showing the global diversity and distribution of the subgenus *Tedaniopsis* (purple dots for holotypes, pinks dots for other records) based on data derived from the World Porifera Database 2020 combined with the new data from the present study.

in the west and Fernando de Noronha, northeast of Brazil. The species was first noted in Hawaii in 1950 (Núñez-Pons et al., 2017). The occurrence of this species includes the Tropical Atlantic, Temperate South America and Eastern Indo-Pacific ecoregions (Spalding et al., 2007). *Tedania (Tedania) suctoria* Schmidt, 1870, has a wide distribution in both ecoregions and one more. From the Kola Fiord (Breitfuss, 1912) and Davis Strait (Murillo et al., 2018)in the Arctic to Cape Vert in the Tropical Atlantic ecoregion (Topsent, 1928) and the Azores (Topsent, 1904, 1928) in the Temperate North Atlantic ecoregion. *Tedania* (*Tedania*) *anhelans* (Vio G in Olivi,, 1792) is one of the most common species, distributed from the Celtic Seas in the north to the Gulf of Guinea in the south, the Azores in the west and the Levantine Sea in the east. Other species that live in the Temperate Northern Atlantic waters are *Tedania (Tedania) pilarriosae* Cristobo, 2002 and *Tedania (Tedania) urgorrii* Cristobo, 2002.

In the northern hemisphere the subgenus *Tedaniopsis* has been represented until now by two species: *Tedania (Tedaniopsis) phacellina* Topsent, 1912 in the Azores (Temperate Northern Atlantic) and *Tedania (Tedaniopsis) gurjanovae* Koltun, 1958 in Tatar Strait (Koltun, 1959) and San Juan Archipelago (Bakus, 1964) in the Temperate Northern Pacific ecoregion.

In summary, the main differences found between *T. (T.) rappi* (Tr) and *T. (T.) phacellina* (Tp) are the very different *habitus* –arborescent (Tr)/massive (Tp)—(**Figure 2**), coanosomal skeletal arrangement –paucispicular (Tr)/multispicular tracts (Tp)—(**Figures 3**, **4**, **7**); styles thickness –double in Tp–. Head terminations of tornotes –mucronate (Tr)/conical (Tp) with the ends somewhat swallowed in Tr–. The onychaetes have short spines (Tr) and the base is blunt (**Figures 5**, **6**).

In fact, the new *Tedania* (*Tedaniopsis*) *rappi* is the first species of this subgenus in the Arctic ecoregion as defined by Spalding et al. (2007). It was found not infrequently in an area closed to protect vulnerable marine ecosystems from the impacts of bottom contact fishing and in a CBD EBSA, the latter conferring enhanced motivation to identify and adopt appropriate measures for conservation and sustainable use by all industrial sectors. The identification of this unique species may warrant including the area in networks of marine protected areas in accordance with international law.

DATA AVAILABILITY STATEMENT

The datasets generated for this study can be found in the online repositories. The names of the repository/repositories and accession number(s) can be found below: ZooBank (urn:lsid:zoobank.org:act:4535FF69-E29C-4C2B-B47F-EC78117C8F2C).

AUTHOR CONTRIBUTIONS

EK and JC acquired the funding. LB and TC conducted the sampling. PR, EB, TC, and JC identified the fauna. JC and PR made the figures and tables with help from LB for **Figure 1**. All authors conceived and designed the study, reviewed drafts of the manuscript, and helped to write the manuscript.

FUNDING

This research has been performed in the scope of the SponGES project, which received funding from the European Union's Horizon 2020 Research and Innovation Programme under Grant Agreement No. 679849 and the European Research project ICY-LAB (ERC-2015-STG Grant Agreement No. 678371). Canadian field work was supported through Fisheries and Oceans Canada (DFO) International Governance Strategy (IGS) funded by EK and with DFO ship time allocated to EK.

ACKNOWLEDGMENTS

We would like to thank the captain and crew of CCGS Hudson and the Canadian Scientific Submersible Facility (CSSF) ROV team, for support during the Hudson 2010-029 mission. We would also like to thank the Principal Investigator Kate Hendry and Claire Goodwin, together with the captain, crew, and scientific party of the ICY-LAB expedition DY081. Also Camille Lirette (DFO, Canada) for send photos and frame grabs from ROPOS 2010 cruise dive 1340 and to Marieve Bouchard Marmen (DFO, Canada) for arranging the shipment of the holotype of *T.* (*T.*) *rappi* to be sent to the Canadian Museum of Nature (CMN) in Otawa. We thank J. M. Gagnon, CMN for his acceptance and rapid cataloging of that holotype. Technical assistance was obtained from our IEO colleagues Alejandra Calvo, from Marseille colleagues, Sandrine Chenesseau, and Jean Vacelet and Sergio Taboada from the Natural History Museum of London, who has worked in the DNA extraction and amplification of the holotype. We thank to Victor Vega (Universidad Oviedo) for his technical assistance during SEM image acquisition. Our most sincere thanks also, to Michelle Bruni of the Monaco Oceanographic Museum for her agile efforts and response for the revision of the holotype of *T. phacelina*. We are also grateful to the two reviewers for their valuable and constructive comments to previous version of this manuscript.

REFERENCES

Aguilar-Camacho, J. M., Carballo, J. L., and Cruz-Barraza, J. A. (2018). *Tedania* (*Porifera*: *Demospongiae*: *Poecilosclerida*) from the Mexican Pacific with the description of two new species. *J. Nat. Hist.* 52, 1311–1332.

Bakus, G. J. (1964). Morphogenesis of *Tedania gurjanovae* Koltun(*Porifera*). *Pacif. Sci.* 18, 58–63.

Bergquist, P. R., and Fromont, P. J. (1988). The marine fauna of New Zealand: *Porifera*, *Demospongiae*, Part 4 *Poecilosclerida*. New Zealand Ocean. *Inst. Mem.* 96, 1–197. doi: 10.1007/978-3-319-23534-9_1

Bertolino, M., Schejter, L., Calcinai, B., Cerrano, C., and Bremec, C. (2007). "Sponges from a submarine canyon of the Argentine sea," in *Porifera Research. Biodiversity, Innovation and Sustainability. Livros de Museu Nacional 28*, eds

M. R. Custódio, G. Lôbo-Hajdu, E. Hajdu, and G. Muricy (Rio de Janeiro), 189–201.

Bowerbank, J. S. (1858). On the anatomy and physiology of the spongiadae. part i. on the Spicula. *Philos. T. Roy. Soc.* 148, 279–332. doi: 10.1098/rstl.1858.0016

Breitfuss, L. L. (1912). Zur Kenntniss der Spongio-Fauna des Kola Fjords. *Trav. Soc. Imp. Nat. St. Pet. Sec. Zool.* 41I–II, 61–80.

Cárdenas, P., Pérez, T., and Boury-Esnault, N. (2012). "Sponge systematics facing new challenges," in *Advances in Sponge Science: Phylogeny, Systematics, Ecology. Advances in Marine Biology*, Vol. 61, eds M. A. Becerro, M. J. Uriz, M. Maldonado, X. Turon. 79–209. doi: 10.1016/b978-0-12-387787-1.00010-6

Cárdenas, P., and Rapp, H. T. (2012). A review of Norwegian streptaster-bearing Astrophorida (*Porifera*: *Demospongiae*: *Tetractinellida*), new records and a new species. *Zootaxa* 52, 1–52. doi: 10.11646/zootaxa.3253.1.1

Cárdenas, P., Rapp, H. T., Schander, C., and Tendal, O. S. (2010). Molecular taxonomy and phylogeny of the Geodiidae (Porifera, Demospongiae, Astrophorida) - combining phylogenetic and Linnaean classification. *Zool. Scr.* 39, 89–106. doi: 10.1111/j.1463-6409.2009.00402.x

Carter, H. J. (1876). Descriptions and figures of deep-sea sponges and their spicules, from the atlantic ocean, dredged up on board H.M.S.'Porcupine', chiefly in 1869 (concluded). *Ann. Mag. Nat. Hist.* 18, 226–240. doi: 10.1080/00222937608682035

Convention on Biological Diversity (2015). *Ecologically or Biologically Significant Areas (EBSAs) Orphan Knoll*. Avaliable at: https://chm.cbd.int/database/record?documentID=204103 (accessed September 15, 2020).

Cristobo, F. J. (2002). The Genus *Tedania* (*Porifera*, *Demospongiae*, *Poecilosclerida*) in the waters of the iberian peninsula (Northeast Atlantic) with a description of two new Species. *Sarsia* 87, 362–377. doi: 10.1080/00364820210001558 15

Cristobo, F. J., and Urgorri, V. (2001). Revision of the genus Trachytedania (*Porifera*: *Poecilosclerida*) with a description of *Trachytedania ferrolensis* sp. nov. from the north-east Atlantic. *J. Mar. Biol. Ass.* 81, 569–579. doi: 10.1017/s0025315401004258

Cristobo, J., Urgorri, V., Solorzano, M. R., and Ríos, P. (1993). Métodos de recogida, estudio y conservación de las colecciones de poríferos. *Int. Symp. First World Cong. Preserv.Conserv. Nat. Hist. Coll.* 2, 277–287.

Dendy, A. (1924). Porifera. Part I. non-antarctic sponges. natural history report. british antarctic (Terra Nova) Expedition, 1910. *Zoology* 6, 269–392.

Desqueyroux-Faúndez, R., and Van Soest, R. W. M. (1996). A review of Iophonidae, *Myxillidae* and Tedaniidae occurring in the South East Pacific (*Porifera*: *Poecilosclerida*). *Rev. Suisse. Zool.* 103, 3–79. doi: 10.5962/bhl.part.79938

Duchassaing de Fonbressin, P., and Michelotti, G. (1864). Spongiaires de la mer Caraibe. Natuurkundige verhandelingen van de Hollandsche maatschappij der wetenschappen te Haarlem. *Natuurkundige verhandelingen van de Hollandsche maatschappij der wetenschappen te Haarlem* 21, 1–124.

Duplessis, K., and Reiswig, H. M. (2004). Three new species and a new genus of Farreidae (*Porifera*: *Hexasterophora*: *Hexactinosida*). *Proc. Biol. Soc. Wash.* 117, 199–212.

Giribet, G., and Wheeler, W. C. (2001). Some unusual small-subunit ribosomal RNA sequences of metazoans. *Am. Museum Novit.* 3337, 1–16. doi: 10.1206/0003-00822001337<0001:SUSSRR<2.0.CO;2

Grant, R.E. (1836). "Animal kingdom," in *The Cyclopaedia of Anatomy and Physiology*, Vol. 1, ed. R. B. Todd (London: Sherwood, Gilbert, and Piper), 1–813.

Goodwin, C., Brewin, P. E., and Brickle, P. (2012). Sponge biodiversity of South Georgia island with descriptions of fifteen new species. *Zootaxa* 3542, 1–48. doi: 10.11646/zootaxa.3542.1.1

Gray, J. E. (1867). Notes on the arrangement of sponges, with the descriptions of some New Genera. *Proc. Zool. Soc. Lond.* 1867, 492–558.

Greenan, B. J. W., Yashayaev, I., Head, E. J. H., Harrison, W. G., Azetsu-Scott, K., Li, W. K. W., et al. (2010). *Interdisciplinary Oceanographic Observations of Orphan Knoll. NAFO SCR Doc. 10/19. Serial No. N5774*. Avaliable at: https://www.nafo.int/Portals/0/PDFs/sc/2010/scr10-019.pdf (accessed August 15, 2018).

Hansen, G. A. (1885). Spongiadae. the norwegian north-atlantic expedition 1876-1878. *Zoology* 13, 1–26. doi: 10.1080/00364827.1973.10411241

Hendry, K. R., Cassarino, L., Bates, S. L., Culwick, T., Frost, M., Goodwin, C., et al. (2019). Silicon isotopic systematics of deep-sea sponge grounds in the North Atlantic. *Quaternary Sci. Rev.* 210, 1–14. doi: 10.1016/j.quascirev.2019.02.017

Hentschel, E. (1914). Monaxone Kiesel schwämme und Hornschwämme der Deutschen Südpolar-Expedition 1901-1903. *Deutsche Südpolar-Expedition* 15, 35–141.

Hooper, J. N. A., and Van Soest, R. W. M. (eds) (2002). *Systema Porifera. A Guide to the Classification of Sponges*. New York, NY: Kluwer Academic, xix–xlviii. doi: 10.1007/978-1-4615-0747-5

Hooper, J. N. A., and Wiedenmayer, F. (1994). "*Porifera*," in *Zoological Catalogue of Australia*, ed. A. Wells (Melbourne: CSIRO), 12.

Kersken, D., Kocot, K., Janussen, D., Schell, T., Pfenninger, M., and Martínez Arbizu, P. (2018). First insights into the phylogeny of deep-sea glass sponges (*Hexactinellida*) from polymetallic nodule fields in the Clarion-Clipperton Fracture Zone (CCFZ), northeastern Pacific. *Hydrobiologia* 811, 283–293. doi: 10.1007/s10750-017-3498-3

Kirkpatrick, R. (1907). preliminary report on the monaxonellida of the national antarctic expedition. *Ann. Mag. Nat. Hist.* 7, 271–291. doi: 10.1080/00222930709487333

Koltun, V. M. (1958). [Cornacuspongia of sea waters washing the South Sakhalin and the South Kurile Island region.]. *Issledovaniya dal'nevostochnÿkh morei SSR SSR.* 5, 42–77.

Koltun, V. M. (1959). [Siliceous horny sponges of the northern and fareastern seas of the U.S.S.R.] [In Russian]. *Opredeliteli po faune SSR, izdavaemye Zoologicheskim muzeem Akademii nauk*. 67, 1–236.

Koltun, V. M. (1964). "Sponges of the Antarctic. 1Tetraxonida and Cornacuspongida," in *Biological Reports of the Soviet Antarctic Expedition (1955-1958). Akademya Nauk SSSR [English translation,1966, Israel Program for Scientific Translation]*, eds E. P. Pavlovskii, A. P. Andriyashev, and P. V. Ushakov 6–133,443–448.

Meredyk, S. P. (2017). *Physical Characterization and Benthic Megafauna Distribution and Species Composition on Orphan Knoll and Orphan Seamount, NW Atlantic*. Masters thesis, Memorial University of Newfoundland, St. John's, NL.

Meredyk, S. P., Edinger, E., Piper, D. J. W., Huvenne, V. A. I., Hoy, S., and Ruffman, A. (2020). Enigmatic deep-water mounds on the orphan knoll. Labrador Sea. *Front. Mar. Sci.* 6:744. doi: 10.3389/fmars.2019.00744

Morrow, C., and Cárdenas, P. (2015). Proposal for a revised classification of the *Demospongiae* (*Porifera*). *Front. Zool.* 12:7. doi: 10.1186/s12983-015-0099-8

Morrow, C. C., Picton, B. E., Erpenbeck, D., Boury-Esnault, N., Maggs, C. A., and Allcock, A. L. (2012). Congruence between nuclear and mitochondrial genes in *Demospongiae*: a new hypothesis for relationships within the G4 clade (*Porifera*: *Demospongiae*). *Mol. Phylogen. Evol.* 62, 174–190. doi: 10.1016/j.ympev.2011.09.016

Murillo, F. J., Kenchington, E., Tompkins, G., Beazley, L., Baker, E., Knudby, A., et al. (2018). Sponge assemblages and predicted archetypes in the eastern Canadian Arctic. *Mar. Ecol. Prog. Ser.* 597, 115–135. doi: 10.3354/meps12589

Murillo, F. J., Tabachnick, K. R., and Menshenina, L. L. (2013). Glass Sponges off the Newfoundland (Northwest Atlantic): Description of a New Species of *Dictyaulus* (Porifera: Hexactinellida: Euplectellidae). J. Mar. Biol. 2013:438485. doi: 10.1155/2013/438485

NAFO (2016). *Potential Vulnerable Marine Ecosystems Impacts of Deep-Sea Fisheries*. Avaliable at: https://www.nafo.int/Portals/0/PDFs/NEREIDA/diptico-nereida.pdf?ver=2016-08-09-104633-013 (accessed January 7, 2021).

Núñez-Pons, L., Calcinai, B., and Gates, R. D. (2017). Who's there? - First morphological and DNA barcoding catalogue of the shallow Hawaiian sponge fauna. *PLoS One* 12:e0189357. doi: 10.1371/journal.pone.0189357

Rapp, H. T. (2006). Calcareous sponges of the genera *Clathrina* and Guancha (*Calcinea*, *Calcarea*, *Porifera*) of Norway (north-east Atlantic) with the description of five new species. *Zool. J. Linn. Soc. Lon.* 147, 331–365. doi: 10.1111/j.1096-3642.2006.00221.x

Ridley, S. O., and Dendy, A. (1886). Preliminary report on the Monaxonida collected by H.M.S. *Challenger. Part I. Ann. Mag. Nat. Hist.* 18, 325–351. doi: 10.1080/00222938609459982

Ridley, S. O. (1881). "XI. Spongida. Horny and Siliceous Sponges of Magellan Straits, S.W. Chili, and Atlantic off SW Brazil," in *Account of the Zoological Collections made during the Survey of H.M.S. 'Alert' in the Straits of Magellan and on the Coast of Patagonia,* ed. A. Gunther (Proceedings of the Zoological Society of London), 107–141.

Sarà, M. (1978). Demospongie di acquesuperficialidella Terra del Fuoco (Spedizioni AMF Mares-GRSTS e SAI). *Boll. Mus. Ist. Biol. Univ. Genova.* 46, 7–117.

Schmidt, O. (1870). *Grundzüge Einer Spongien-Fauna des atlantischen Gebietes*, Vol. iii–iv. Leipzig: Wilhelm Engelmann, 1–88.

Sollas, W. J. (1880). The sponge-fauna of Norway; a report on the Rev. A.M. Norman's collection of sponges from the norwegian coast. *Ann. Mag. Nat. Hist.* 5, 130–144.

Sollas, W. J. (1885). A Classification of the Sponges. *Ann. Mag. Nat. His.* 16:395.

Spalding, M. D., Fox, H. E., Allen, G. R., Davidson, N., Ferdaña, Z. A., Finlayson, M., et al. (2007). Marine ecoregions of the world: a bioregionalization of coastal and shelf areas. *BioScience* 57, 573–583. doi: 10.1641/b570707

Stephens, J. (1915). Sponges of the coasts of Ireland. I.-the triaxonia and part of the Tetraxonida. *Fis. Ireland Sci. Invest.* 1914, 1–43.

Tabachnick, K. R., and Menshenina, L. L. (2007). Revision of the genus *Asconema* (Porifera: Hexactinellida: Rossellidae). *J. Mar. Biolog. Assoc. U.K.* 87, 1403–1429. doi: 10.1017/S0025315407058158

Topsent, E. (1904). Spongiaires des Açores. Résultats des campagnes scientifiques accomplies par le Prince Albert I. *Monaco* 25, 1–280.

Topsent, E. (1907). Poecilosclérides nouvelles recueillies par le Français dans l'Antarctique. *B. Mus. Natl. Hist. Nat. Paris* 13, 69–76.

Topsent, E. (1912). Sur une grande *Tedania* abyssale des Açores (*Tedania phacellina*, n. sp.). *Bulletin de l'Institut océanographique, Monaco.* 252, 1–7. doi: 10.1007/978-3-319-23534-9_1

Topsent, E. (1913). Spongiaires provenant des campagnes scientifiques de la 'Princesse Alice' dans les Mers du Nord (1898-1899 - 1906-1907). *Résultats des Campagnes Scientifiques Accomplies par le Prince Albert I de Monaco.* 45, 1–67.

Topsent, E. (1928). Spongiaires de l'Atlantique et de la Méditerranée provenant des croisières du Prince Albert ler de Monaco. *Résultats des campagnes scientifiques accomplies par le Prince Albert I. Monaco* 74, 1–376.

Van Soest, R. W. M. (2002). "Family Tedaniidae Ridley & Dendy, 1886," in *Systema Porifera. A Guide to the Classification of Sponges. 1*, eds J. N. A. Hooper and R. W. M. Van Soest (New York, NY: Kluwer Academic), 625–632. doi: 10.1007/978-1-4615-0747-5_66

Van Soest, R. W. M. (2017). Sponges of the Guyana Shelf. *Zootaxa* 4217, 1–225. doi: 10.11646/zootaxa.4217.1.1

Van Soest, R. W. M., Boury-Esnault, N., Hooper, J. N. A., Rützler, K., de Voogd, N. J., Alvarez, B., et al. (2021). *World Porifera Database*. Accessed at http://www.marinespecies.org/porifera (accessed January 8, 2021).

Vio G in Olivi, , G. (1792). *Letter on sponges From the Gulf of Smyrna*, Chap. Bassano. Zoologia Adriatica, xi–xxxi.

Von Lendenfeld, R. (1888). *Descriptive Catalogue of the Sponges in the Australian Museum, Sidney*, Vol. i–xiv. London: Taylor & Francis, 1–260.

Vosmaer, G. C. J. (1885). The sponges of the 'willem Barents' expedition 1880 and 1881. *Bijdragen tot de Dierkunde* 12, 1–47.

Wudrick, A., Beazley, L., Culwick, T., Goodwin, C., Cárdenas, P., Xavier, J., et al. (2020). A pictorial guide to the epibenthic megafauna of orphan knoll (northwest Atlantic) identified from in situ benthic video footage. *Can. Tech. Rep. Fish. Aquat. Sci.* 3375:154.

Conflict of Interest: The authors declare that the research was conducted in the absence of any commercial or financial relationships that could be construed as a potential conflict of interest.

Copyright © 2021 Ríos, Cristobo, Baker, Beazley, Culwick and Kenchington. This is an open-access article distributed under the terms of the Creative Commons Attribution License (CC BY). The use, distribution or reproduction in other forums is permitted, provided the original author(s) and the copyright owner(s) are credited and that the original publication in this journal is cited, in accordance with accepted academic practice. No use, distribution or reproduction is permitted which does not comply with these terms.

frontiers in Marine Science

ORIGINAL RESEARCH
published: 23 February 2021
doi: 10.3389/fmars.2021.612761

High Resolution Spatial Distribution for the Hexactinellid Sponges *Asconema setubalense* and *Pheronema carpenteri* in the Central Cantabrian Sea

Augusto Rodríguez-Basalo[1], Elena Prado[1], Francisco Sánchez[1], Pilar Ríos[1], María Gómez-Ballesteros[2] and Javier Cristobo[3]*

[1] Centro Oceanográfico de Santander, Instituto Español de Oceanografía (IEO), Santander, Spain, [2] Centro Oceanográfico de Madrid, Instituto Español de Oceanografía (IEO), Madrid, Spain, [3] Centro Oceanográfico de Gijón, Instituto Español de Oceanografía (IEO), Gijón, Spain

OPEN ACCESS

Edited by:
Shirley A. Pomponi, Florida Atlantic University, United States

Reviewed by:
Eduardo Carlos Meduna Hajdu, Federal University of Rio de Janeiro, Brazil
Frine Cardone, Anton Dohrn Zoological Station, Italy

***Correspondence:**
Augusto Rodríguez-Basalo
augusto.rodriguez@ieo.es

Specialty section:
This article was submitted to Deep-Sea Environments and Ecology, a section of the journal Frontiers in Marine Science

Received: *30 September 2020*
Accepted: *02 February 2021*
Published: *23 February 2021*

Citation:
Rodríguez-Basalo A, Prado E, Sánchez F, Ríos P, Gómez-Ballesteros M and Cristobo J (2021) High Resolution Spatial Distribution for the Hexactinellid Sponges Asconema setubalense and Pheronema carpenteri in the Central Cantabrian Sea. Front. Mar. Sci. 8:612761. doi: 10.3389/fmars.2021.612761

In the present work we focus on the distribution of two species of sponges. One of these is *Asconema setubalense*, a sponge found in rocky substrate that was sampled with a photogrammetric vehicle through georeferenced images. The other is *Pheronema carpenteri*, which inhabits soft bottoms and was sampled by beam trawl. For the spatial distribution modeling of both sponges, the geomorphological variables of depth, slope, broad and fine scale bathymetric position index (BPI), aspect, and types of bottoms were used, all with a resolution of 32 m. Additionally, layers of silicates and currents near the bottom were extracted from Copernicus Marine Environment Monitoring Service (CMEMS), with a resolution of ∼4 and ∼9 km, respectively. Due to the low resolution of the layers, it was considered necessary to validate their use by model comparison, where those that included these variables turned out to be more explanatory than the others. The models were developed in a complex continental break of the Central Cantabrian Sea, which comprises several submarine canyons and a seamount (Le Danois Bank). On the one hand, a very high resolution (32 m) spatial distribution model based on *A. setubalense* presence was developed using the MaxEnt maximum entropy model. On the other, depending on the availability of density data, generalized additive models (GAMs) were developed for *P. carpenteri* distribution, although in this case the sampler only allowed a maximum resolution of almost 1 Km. For the *A. setubalense*, the variables that best explained their distribution were ground types and depth, and for *P. carpenteri*, silicates, slope, northness, and eastward seawater velocity. The final model scores obtained were an AUC of 0.98 for the MaxEnt model, and an R squared of 0.87 for the GAM model.

Keywords: VME, Porifera, Cachucho, Cantabrian Sea, sponges distribution modeling

INTRODUCTION

The great majority of sponges are sessile filter feeders whose importance lies in that, along with corals, they are essential for characterizing a multitude of specific deep-sea habitats. In many deep-sea areas, sponges may be the dominant organism, forming structurally complex and often highly diverse ecosystems known as sponge grounds (Hogg et al., 2010; Beazley et al., 2013; Maldonado et al., 2017). Further, due to their vulnerability, mainly to trawl fisheries, their need for protection has been the object of great concern since the beginning of the present century. Thus, the designation of vulnerable marine ecosystems (VME) has relied to a great extent on the presence of sponges and sponge grounds, as remarked in the United Nations General Assembly Resolution 61/105 (UN General Assembly, 2007; Rogers and Gianni, 2010). Therefore, the need to create a coherent network of marine protected areas (MPAs) that preserves the most vulnerable benthic habitats has, in many cases, consumed a great deal of time and resources, which have served to increase knowledge of the biology and distribution of the large structuring species that support these benthic habitats.

Hence, given that the preservation of VMEs will be the first step toward achieving a good environmental status (GES) of the marine environment, and that the preservation of sponges will be one of the main contributions to establish the necessary environmental objectives and associated indicators, their protection will be a good starting point for developing the maritime spatial planning (MSP) required in the Marine Strategy Framework Directive (MSFD) as it relates to MSP Community action (European Union, 2014).

The aforementioned objectives can be carried out as long as we draw from a good knowledge of the deep bottoms, or at least good enough to be able to delimit the area occupied by the habitat-forming sponges in the most reliable way possible. Thus, given the difficulties generated by the study of deep-sea, both due to inaccessibility and the high economic cost, this scarce knowledge should be optimized with the most reliable possible species distribution models (SDMs). This modeling approach has been used widely to map vulnerable habitats and species on a broad scale, especially in corals and sponges (Knudby et al., 2013), but the number of fine scale studies are scarce.

In this study we have worked in two well-defined areas of the central Cantabrian Sea. The first area is one of the first MPAs declared in Spain, El Cachucho (Le Danois Bank and its intraslope basin), which in December 2008 received preventive protection measures and was proposed as a site of community importance (SCI), mainly due to the presence of sponges and other habitat forming species, such as black corals and gorgonians, the main representation of the 1170 reef habitat. In 2009 it was included in the OSPAR network of MPAs and finally declared a special area of conservation (SAC) in the Natura 2000 network in November 2011. Throughout this process, numerous studies were carried out, beginning with the necessary knowledge of its morphology (Van Rooij et al., 2010; Gómez-Ballesteros et al., 2015) and water dynamics (González-Pola et al., 2012), going through others focused on benthos and demersal species (Cartes et al., 2007; Cristobo et al., 2009; Preciado et al., 2009; Sánchez et al., 2009a; García-Alegre et al., 2014), analyses of the influence of seamounts on pelagic species fisheries (Rodríguez-Cabello et al., 2009), and ending with the necessary studies of vulnerable habitats (Sánchez et al., 2008, 2009b, 2017). Further, the need to protect the area was highlighted by constituting an integrated trophodynamic system (Sánchez et al., 2010) and its management plan has been recently reviewed after the development of new surveys (Rodríguez-Basalo et al., 2019).

The other area under study, located west of Le Danois Bank, called Avilés Canyon System (ACS), is a very complex geomorphologic zone made up of three different canyons, Avilés, El Corbiro, and La Gaviera, and is currently an SCI of Natura 2000 network. It is characterized by a high hydrodynamic activity that produces strong sediment transport from the head of the canyons to the abyssal plain (Gómez-Ballesteros et al., 2014). Besides, enhanced near-bed currents are believed to cause high sediment re-suspension, providing an increased food supply for benthic filter feeder species (Sánchez et al., 2014), which, together with the presence of rocky outcrops, make it home to numerous vulnerable species and habitats (Sánchez et al., 2014; Ríos et al., 2017, 2019).

When a particular area is of interest to form part of the Natura 2000 network, knowledge of the status and distribution of the characteristic species of benthic habitats is key to providing the necessary tools that the different actors will need in the decision-making process, and one of the most direct tools are the maps of vulnerable habitats and species that are supplied by SDMs. Consequently, given the impossibility of direct knowledge of the deep-sea, SDMs have become an indispensable tool for the declaration of protected natural areas and the review of their monitoring plans. However, for a good development of the SDM, there are a series of concepts that will be key for the subsequent development of the modeling, such as the selection of the resolution at which the works will be developed, the choice of algorithm or algorithms and thresholds, or the variables to be used in the process (Guisan and Thuiller, 2005; Benito et al., 2013).

In the present study, spatial distribution modeling of two very different hexactinellid species, *Asconema setubalense* and *Pheronema carpenteri*, was carried out. *A. setubalense* is a large sponge with a big osculum and an everted marginal part when it reaches a large size (Tabachnick and Menshenina, 2007), while *P. carpenteri*, the nest sponge, is a spherical sponge with spicules that fix it to the ground, and is usually covered with mud (**Figure 1**). Since *A. setubalense* lives on rocky bottoms with more or less sedimentary cover and *P. carpenteri* needs bottoms of fine sediment or mud, the methods used to sample these species are different, as the resolution of the models, which complicates the selection of the environmental variables available and studies on the adequacy of their inclusion in the models. Therefore, in this study we focused on:

- A comparative analysis of the samplers used for each of the sponge species from the point of view of their implications in the different processes developed in the SDM.
- Obtaining and calibrating a layer that accurately reproduces the different ground types by combining sampling

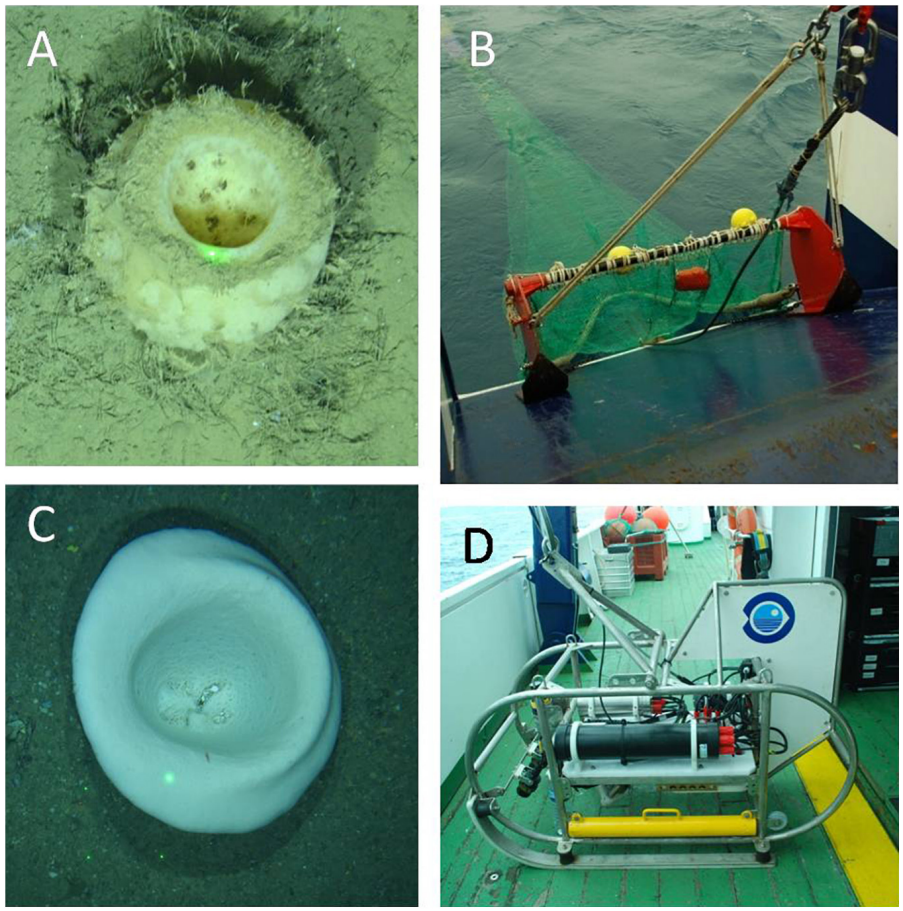

FIGURE 1 | Sponges images and their samplers: **(A)** Pheronema carpenteri specimen, and **(B)** beam trawl, the sampler used for its quantification; **(C)** *Asconema setubalense* specimen, and **(D)** ROTV, the sampler used for its study.

based on ground truthing, box corer, and multibeam echosounder backscatter.

- Assessing the convenience of combining variables of very different resolutions in a single model.
- Analyzing the contribution of the most important variables available to characterize the distribution of these species from a geomorphological and physicochemical approach.
- Studying the need for high resolution spatial models and their importance for the analysis of the interactions between VMEs and the uses and activities carried out in Natura 2000 areas.

MATERIALS AND METHODS

Study Area

The central Cantabrian Sea is an area of complex morpho-structural characteristics dominated by an intricate canyon system and a seamount partially isolated from the continental shelf. This complexity led to the study and characterization of two important areas with different protection figures. One of these is the SCI ACS, which is a complex, structurally controlled canyon and valley system consisting of three different canyons, Avilés, El Corbiro, and La Gaviera, each with specific morpho-structural characteristics (**Figure 2**). This system starts from the continental shelf, at 140 m depth, and ends in the Biscay Abyssal Plain, at 4,700 m depth. Strong continental margin water dynamics in the ACS avoids thicker sediment deposition, with the littoral sedimentary dynamics being responsible for transport to the canyons' heads and finally conducting sediments to the Biscay Abyssal Plain (Gómez-Ballesteros et al., 2014).

The second one is El Cachucho marine protected area. This MPA comprises a seamount, the Le Danois Bank, and its intraslope basin, and is separated from the continental shelf by the Lastres Canyon (**Figure 2**). The Le Danois Bank has an elongated convex southward shape of about 72 km long and 15 km wide. Its top is flat, representing a large W-E platform between 425 and 600 m water depth, with rocky bottoms and scarce sedimentary coverage (Van Rooij et al., 2010). The presence of Le Danois Bank creates the W-E intraslope basin, which is 17–25 km wide and approximately 50 km long. This sedimentary basin is the so-called Le Danois contourite depositional system (CDS) and is characterized by high-thickness muddy bottoms. This geological complexity, along with current

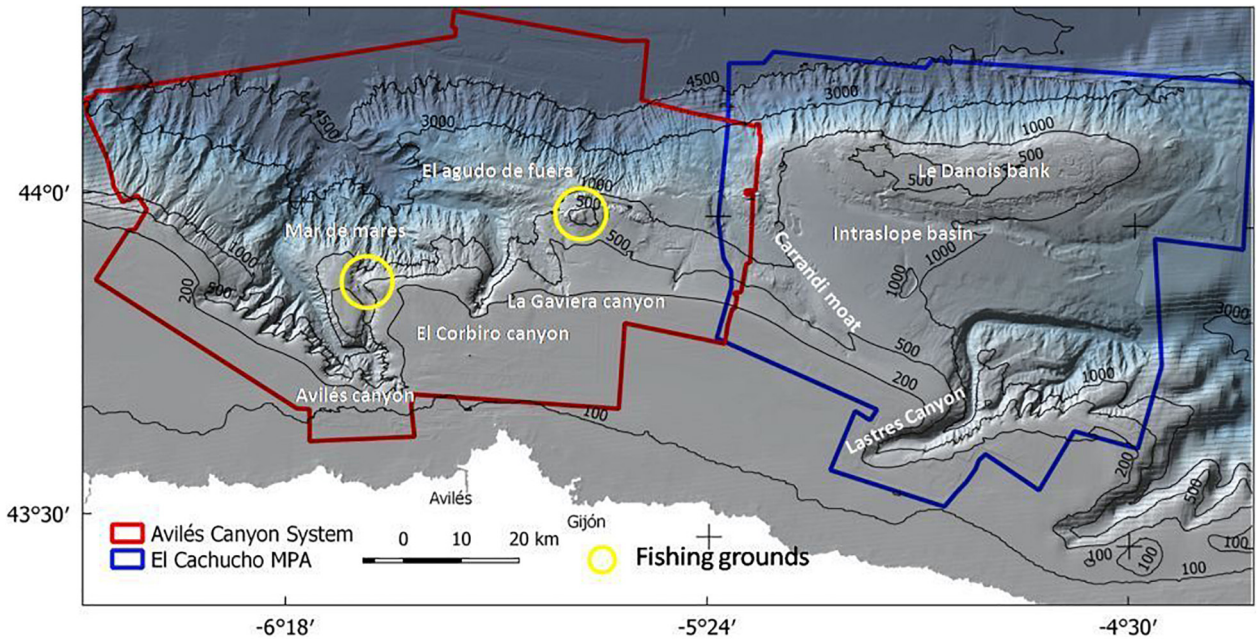

FIGURE 2 | Map of the study area comprising the Avilés Canyon System and the El Cachucho MPA.

circulation patterns and anticyclonic flow at the seamount summit (González-Pola et al., 2012), make these areas a very important diversity hotspot (Sánchez et al., 2008).

Samplers and Species Data Acquisition

Due to the different characteristics of the two species studied, which are especially relevant given the substrates they inhabit, two different types of samplers were used, one based on images and the other on beam trawl collection and classification (**Figure 1**). Sampling effort is shown in **Figure 3**. For the identification and localization of the species requiring bedrock, *A. setubalense*, we used the *in situ* analysis of the video images captured during three different surveys: ECOMARG 0717, ECOMARG 0719, and SponGES 0617. These images come from the photogrammetric ROTV (Remote Operated Towed Vehicle) Politolana (Sánchez and Rodríguez, 2013). During transects, Ocean Floor Observation Protocol (OFOP) software (Huetten and Greinert, 2008) was used to capture the position of each specimen through the transponder located in the towed vehicle. In total, 85 transects were accomplished in the whole area to obtain the species data. Total recording time was almost 50 h during which an area of around 16 ha was covered. Visual transects were divided into 30-m sections, which became the sample unit, since this is the resolution of our digital elevation model (DEM).

In the case of *P. carpenteri*, the surveys were carried out during seven bottom trawl surveys: INDEMARES-AVILES (2010 and 2011), ECOMARG (2003, 2004, 2008, and 2009), and SponGES 0617. There were also images captured by the photogrammetric towed vehicle, but these were finally decided not to be combined with the ones obtained with the beam trawl and were discarded because of the difficulties that merging different resolution samples generates to the SDM process. During the surveys, several trawls were carried out, each covering a length of almost 1 km, wherefore, for this model, the resolution of the DEM and its derivatives had to be increased. The sampling unit in this case was the 15′ haul at a speed of 2.0 knots transect, which covers an area of about 0.35 ha or 0.18 ha, depending on the survey, so throughout the 23 hauls, a surface of 6 ha was covered.

Obtaining Geomorphological Layers

The original resolution of the DEM for the entire area was 32 m (**Figure 2**) and was carried out by joining three bathymetries of different resolutions taken with a multibeam echo sounder: the top of Le Danois bank (32 m resolution), the ACS, and the rest of El Cachucho MPA (75 m resolution). Before joining the layers, they were previously interpolated to a resolution of 32 m to avoid loss of information. Afterward, a set of bathymetric derivatives were extracted from the complete DEM: slope in degrees, broad and fine scale bathymetric position index (BPI), and aspect, which is a two-dimensional vector representing the orientation that a slope faces (0–360° from north). In order to avoid problems derived from dealing with circular data, it was divided into two components: northness, obtained as the sin(aspect), and eastness, obtained as the cos(aspect) (**Figure 4**). Slope and aspect were selected due to the influence they have on both sediment transport and exposure to dominant currents. Regarding the BPI, the relative position of an area with respect to the surrounding zone, was previously revealed to be decisive in benthos studies at both broad and fine resolution (Sánchez et al., 2017).

To obtain the hardness of the bottom, the reflectivity of the two areas was used. Unfortunately, the reflectivity of the

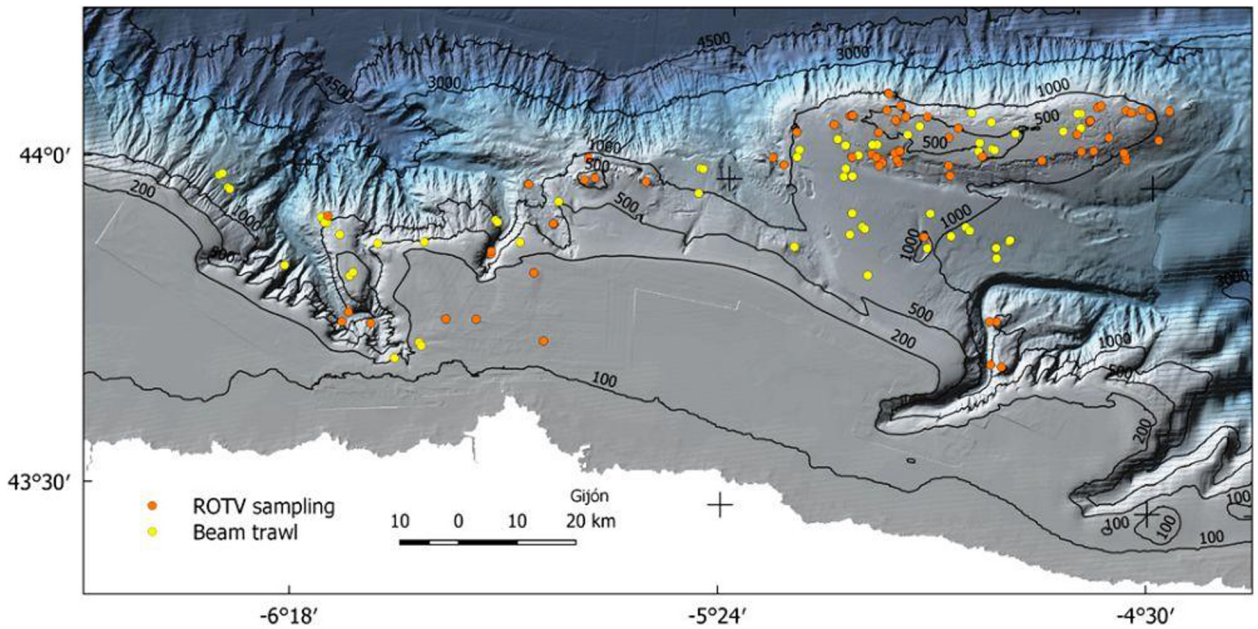

FIGURE 3 | Sampling effort in the study area for beam trawl and ROTV.

ACS could not be used directly since, due to problems with the multibeam calibration and filtering, it was not suitable for high resolution modeling. In addition, the reflectivity of the compacted mud, and that of canyon bottoms and steep slopes can be misleading, so it was preferred to use a categorized layer of bottom types. Thus, with the analysis of the sediment samples (from box corer stations) and review of the images (ground truthing), the reflectivity values were calibrated, turning them into a layer of the entire area with 7 different categories (**Figure 5**).

Physicochemical Layers

Additionally, a biogeochemical and physical approach was used. As siliceous species of hexactinellid need Si (dissolved silica) to form spicules, which provides support to the sponge, a layer containing silicate in depth was processed with the highest possible resolution. To assess dissolved silicate concentration in bottom waters (i.e., seafloor), a forecast raster product from CMEMS (Copernicus Marine Environment Monitoring Service) was downloaded. This product covers the IBI region (Iberia-Biscay-Ireland region) with a resolution of 4 km × 4 km. An application of the biogeochemical model PISCES (Aumont et al., 2015), running simultaneously with the NEMO ocean model, was used to generate the IBI ocean forecasts in order to obtain the main biogeochemical variables. Thus, the mole concentration of silicate (mmol m^{-3}) in sea water next to the bottom was obtained by extracting the deepest valid value on each pixel for every month of a complete year. With these data, four layers were obtained with the range, maximum, minimum, and average values.

Finally, to take into account deep-sea dynamics, high energy dynamics also based on CMEMS were used. The original layer was downloaded from the IBI Ocean Reanalysis system (Sotillo et al., 2015), providing information on oceanic hydrodynamic variables at 50 different depth levels at a resolution of 9 km × 9 km. In this study we selected, for each pixel of the area, the bottom values in ms^{-1} of the eastward sea water velocity (uo) and the northward sea water velocity (vo). The same four layers of each sea water current component were obtained.

Asconema setubalense Spatial Distribution Models

In order to avoid the redundancy of information in the variables, a correlation analysis was carried out between them using Spearman's rank correlation coefficient, eliminating variables with a redundancy greater than 70%. In the case of silicates and currents, and according to similar studies (Knudby et al., 2013), we started by eliminating the range and mean variables, leaving the maximum and minimum values for the end, since they are the ones that can mark the tolerance limits of the species. The variables used are those shown in **Table 1**. Roughness was also eliminated due to it being highly correlated with slope.

In the model carried out for *A. setubalense*, we did not have sufficient data on absences in sedimentary substrate because sampling with the photogrammetric ROTV was directed to the rocky substrate. To counter this shortcoming, the MaxEnt model, based on a machine-learning technique called maximum entropy modeling (Phillips et al., 2006), was run. This model is based on pseudo-absences and distributes the absences randomly, so those types of substrate which were not sampled because they hardly had the possibility of harboring hard bottom habitats, would also be represented. Thus, a total of 10 replicates were reproduced, selecting the average of all of them for the final

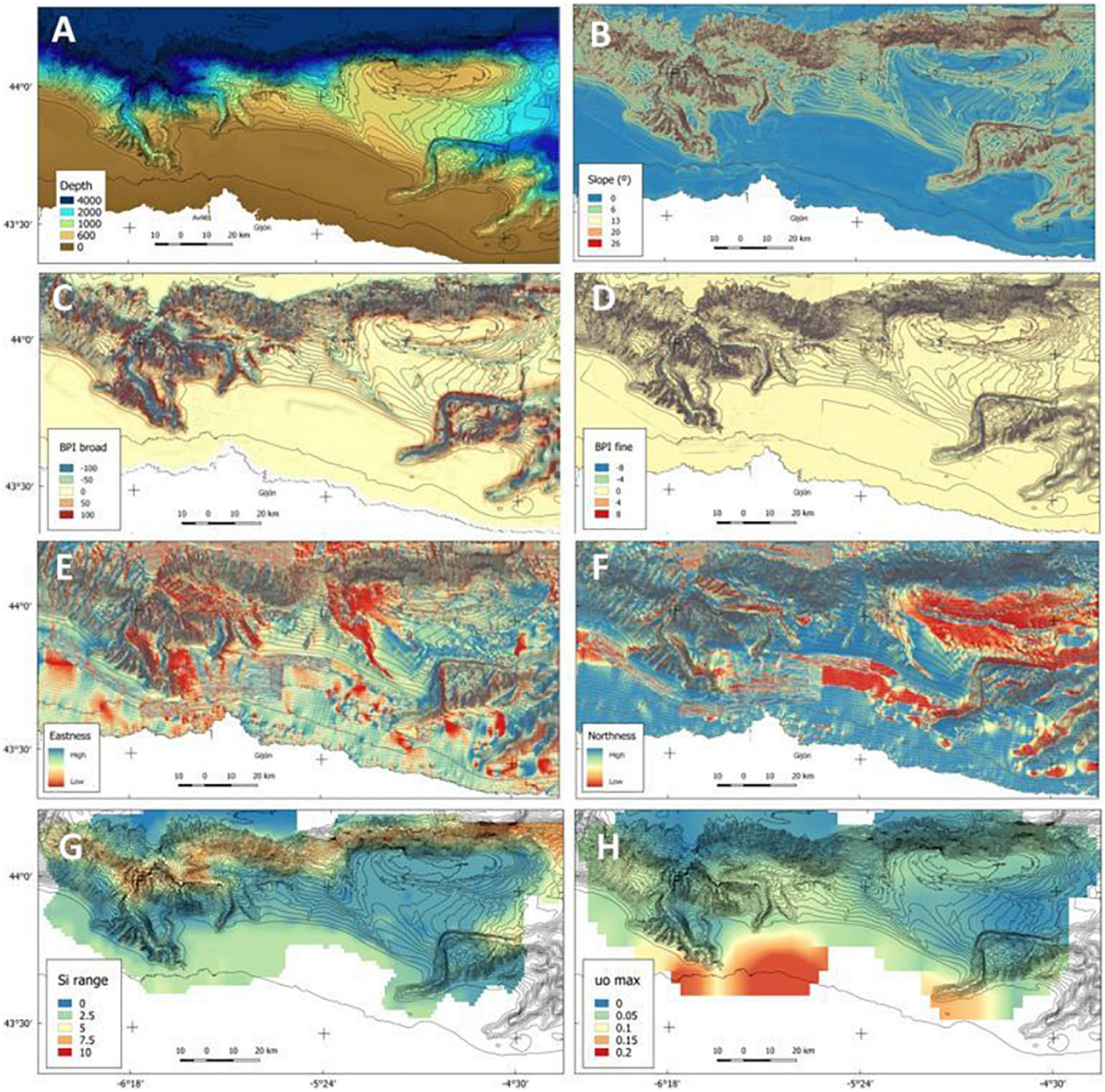

FIGURE 4 | DEM of the study area and layers used for the models: the geomorphological predictors depth **(A)**, slope **(B)**, BPI broad **(C)** and fine **(D)** scale, eastness **(E)** and northness **(F)**, and two of the physicochemical layers: silicates range **(G)**, and eastwards bottom current component **(H)**.

model. Validation of the model was accomplished by randomly reserving a total of 30% of the presences to be used for test data. Finally, in order to compare the importance of physicochemical predictors with geomorphological ones, two different models were developed, one with only ground types and bathymetry derivatives (Model 1) and another adding the silicates and currents (Model 2) (**Table 1**).

As for the use of physicochemical variables, it was considered necessary to check whether they provided relevant information to the study, as long as they had a resolution of at least 30 times coarser than the geomorphological layers. Therefore, since this species has three very localized populations, three different scenarios were considered: the presences of each population was removed to develop three different models, using the presences removed as test data for their validation. The models were run without (Model 1) and with physicochemical variables (Model 2) for the model comparison of each scenario. It has been done this way because using random presences as test data would not have given much reliability because they are localized in these three populations and the test data would greatly coincide with the rest of the presences. The AUC (Area Under the Curve) was used to compare models. The AUC is the area under the ROC

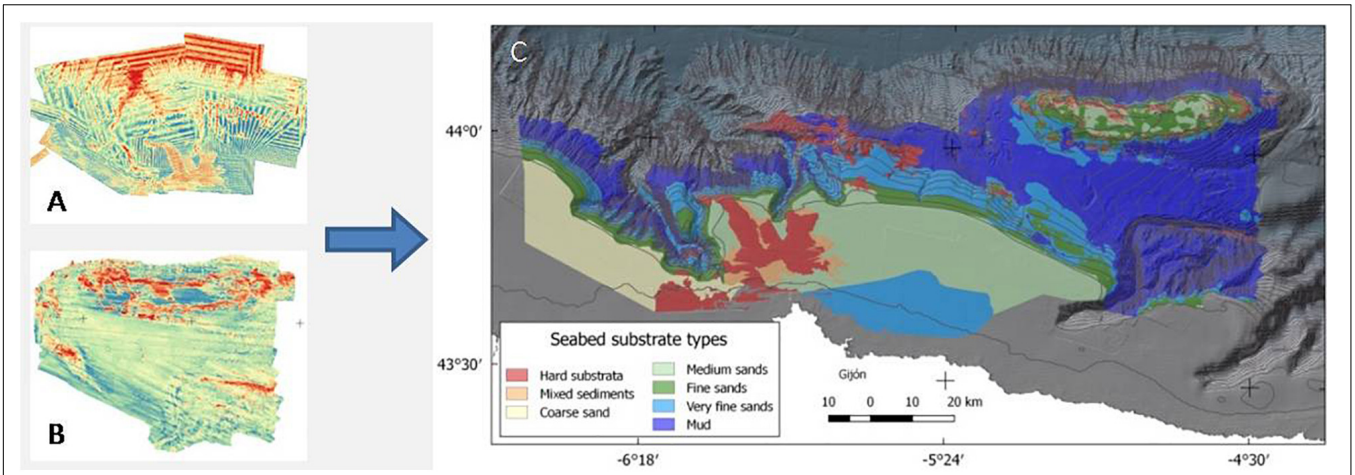

FIGURE 5 | Backscatter of ACS **(A)** and El Cachucho MPA **(B)**, and Ground types layer **(C)** extracted by backscatter values validated by images ground truthing and sediment studies.

TABLE 1 | MaxEnt univariate models AUC and contribution of each variable for two models: Model 1, constructed only with geomorphological variables; and Model 2, which includes the physicochemical variables of currents and silicates.

		Model 1 (*A. setubalense*)		Model 2 (*A. setubalense*)	
	Resolution	AUC (Univariant)	Contribution (%)	AUC (Univariant)	Contribution (%)
Depth	32 m	0.88	23.3	0.88	20.8
BPI fine		0.69	1	0.69	0.72
BPI broad		0.89	1.3	0.89	0.52
Slope (°)		0.72	0.1	0.72	0.08
North		0.63	1.4	0.63	1.27
East		0.59	0.9	0.59	0.42
Ground types		0.92	72	0.92	68.4
Si Range	4,000 m		N/A	0.88	1.94
Si min			N/A	0.91	0
uo max	9,000 m		N/A	0.88	1.65
uo min			N/A	0.81	0.63
vo max			N/A	0.9	3.59
vo min			N/A	0.89	0.02
Full model		0.97		0.98	

curve (Receiver Operating Characteristics), which is a graphical representation of sensitivity versus specificity (**Table 2**). It is very reliable for model comparison and provided information as to whether these coarse layers could improve the model or not.

TABLE 2 | Comparative study of the AUC test data of two different models, one taking into account only the geomorphological variables (Model 1), and the other that also includes the physicochemical variables of currents and silicates (Model 2).

	AUC test 1	AUC test 2	AUC test 3	AUC average
Model 1	0.56	0.93	0.94	0.81
Model 2	0.8	0.97	0.93	0.9

Each case is validated with a set of presences that corresponds to each of the populations of A. setubalense: Avilés (Test 1), west Cachucho (Test 2), and East Cachucho (Test 3).

Pheronema carpenteri Spatial Distribution Models

The model developed for *P. carpenteri,* based on densities and physicochemical variables, was also tested. For the layer preparation, the resolution of the geomorphological predictors was reduced, and that of the silicate and current layers was increased to a pixel size of 960 m × 960 m. This resolution of almost 1 km was based on the average distance traveled by the beam trawl. Given that it is not possible to know the exact point where the sample was collected, it was the finest resolution that could be reached. The model developed for the distribution of this species was the Generalized Additive Model (GAM), which enabled us to work with densities. The first step was the development of univariate models in order to obtain the most important predictors for the distribution of each species. Then, the most important variables were selected according

to the variance explained, without losing the significance (p-value < 0.05) of those chosen in the final model. As in the case of *A. setubalense*, two different models were developed, one with only geomorphological predictors (Model 1) and another adding the physicochemical ones (Model 2) (**Table 3**).

RESULTS

For the full model (Model 2) developed for *A. setubalense*, the predictor that contributed the most to the final model was ground types (68.4%), followed by depth (20.8%) and maximum northward sea current velocity (3.6%). The remaining 7% was distributed among the rest of the variables, whose contribution in explaining the distribution of the species was very low. In total, 500 iterations were reproduced, giving a final AUC value of 0.98 for the test data (**Table 1**). As for the univariate models, ground types, depth, and broad BPI were the most important variables with AUC values above 0.85. Physicochemical predictors also had high AUC univariate values, but their contribution to the final model was scarce. Otherwise, for *P. carpenteri*, the univariate GAM models (**Table 3**) showed that the most important predictors are silicates, eastness, slope and seawater current velocity. In the trend curves of the final model (**Figure 6**), the variables with the clearest trend were eastness, with a negative trend, and the minimum value of silicates, with a clearly positive trend for the range considered.

The results of the different scenarios developed for *A. setubalense* by excluding the presence of the different populations and using them in the validation, are shown in **Table 2**. Test 1 was validated with the population located in ST01 (**Figure 7A**), and it shows a value of 0.56 for the model constructed with only geomorphological variables, which means that it has no discrimination capacity to distinguish between positive and negative class. The value increased to 0.8 after including physicochemical variables. For the models validated using the presences located in ST02 and ST03, west and east of the seamount, values were similar for both models although Model 2 was still quite a lot better in Test 2.

Species distribution maps are shown in **Figure 7**. **Figures 7A,B** are the *A. setubalense* habitat suitability (HS) for Models 1 and 2, respectively. Four areas were marked according to the populations displayed by the model. The westernmost one (ST01) is the so-called "Mar de mares" fishing ground, which is characterized by a high concentration of longline fisheries. In fact, several specimens are surrounded and damaged by longlines in our images (**Figure 8**). ST02 and ST03 are located at the top of the Le Danois Bank and are protected from deep-sea fisheries by the MPA management plan, although with no remarkable bottom fisheries during the last decades. In ST04, a fishing ground called "El Agudo de Fuera" by fishermen, also had many longlines hooked to the floor, but no specimens were found in the three transects made. According to Model 1, which takes into account only the geomorphological variables, there was a high likelihood of finding this species, but this probability disappeared as physicochemical variables were included (Model 2), with wider ranges of silicates and higher rates of eastward current velocity (**Figure 4**).

Regarding *P. carpenteri*, **Figures 7C,D** display the predictive maps of Models 1 and 2. The predictors that finally best fitted Model 1 were ground types, depth, and both BPIs; whereas for Model 2 they were minimum silicate value, maximum value of eastward sea current velocity, slope, and eastness. The distribution map of Model 1 was more irregular than the one originated by Model 2, which showed clearer suitability areas, due to the complicated orography of the terrain and because the variations in the layers of currents and silicates are more uniform. Both models were consistent, with R^2 values of 0.77 and 0.87 for Models 1 and 2, respectively. Otherwise, this species reflected a much wider distribution area, since samples were collected in areas of mud and very fine sand, which occupy a wide portion of the study area. Thus, the area covered by mud and very fine sand is 13,770 ha, while the area occupied by rock is less than 2,500 ha.

TABLE 3 | Variance, R^2, and significance for GAM univariate models.

	Univariate GAM (*P. carpenteri*)			Predictors selected	
	Variance (%)	R^2	p-value	Model 1 (p-value)	Model 2 (p-value)
Depth	4.88	0	0.4		
Fine BPI	0.9	0.04	0.67	0.0003***	
Broad BPI	19.3	0.12	0.2	0.0003***	
Slope (°)	62.7	0.46	0.04*		0.09.
North	2.7	0.03	0.8		
East	31.5	0.28	0.006**	0.006**	0.002**
Ground types	1.2	0.03	0.08.	0.09.	
Si range	53.2	0.49	0.001***	N/A	
Si min	41.4	0.32	0.03*	N/A	0.006***
uo max	35.1	0.26	0.09.	N/A	0.048**
uo min	0.7	0.04	0.7	N/A	
vo max	1.9	0.02	0.5	N/A	
vo min	31.8	0.28	0.006**	N/A	
Model 1	87	0.77			
Model 2	94.3	0.87			

For the full models, Models 1 and 2 represent the comparative study that was developed taking into account only geomorphologic variables (Model 1), or including the physicochemical variables of currents and silicates (Model 2). ($P < 0.1$, $P \leq 0.05$, $P \leq 0.01$**, $P \leq 0.001$***).*

DISCUSSION

The need of comprehensive knowledge of the seabed is increasingly urgent, especially in regard to VMEs. Besides, this is particularly difficult in the deep-sea, where, due to its remoteness, the sampling is too often very scarce, or focused on a particular aspect, or does not have the quality of data that would be desirable. This is why it is so necessary to optimize the data yield while achieving consistent spatial resolution that is in accordance with the objectives of the study. Therefore, it is highly recommended to gather accurate data on nutrients and oceanic dynamics near the bottom and highlight the information they can provide, as these variables are important limiting factors for

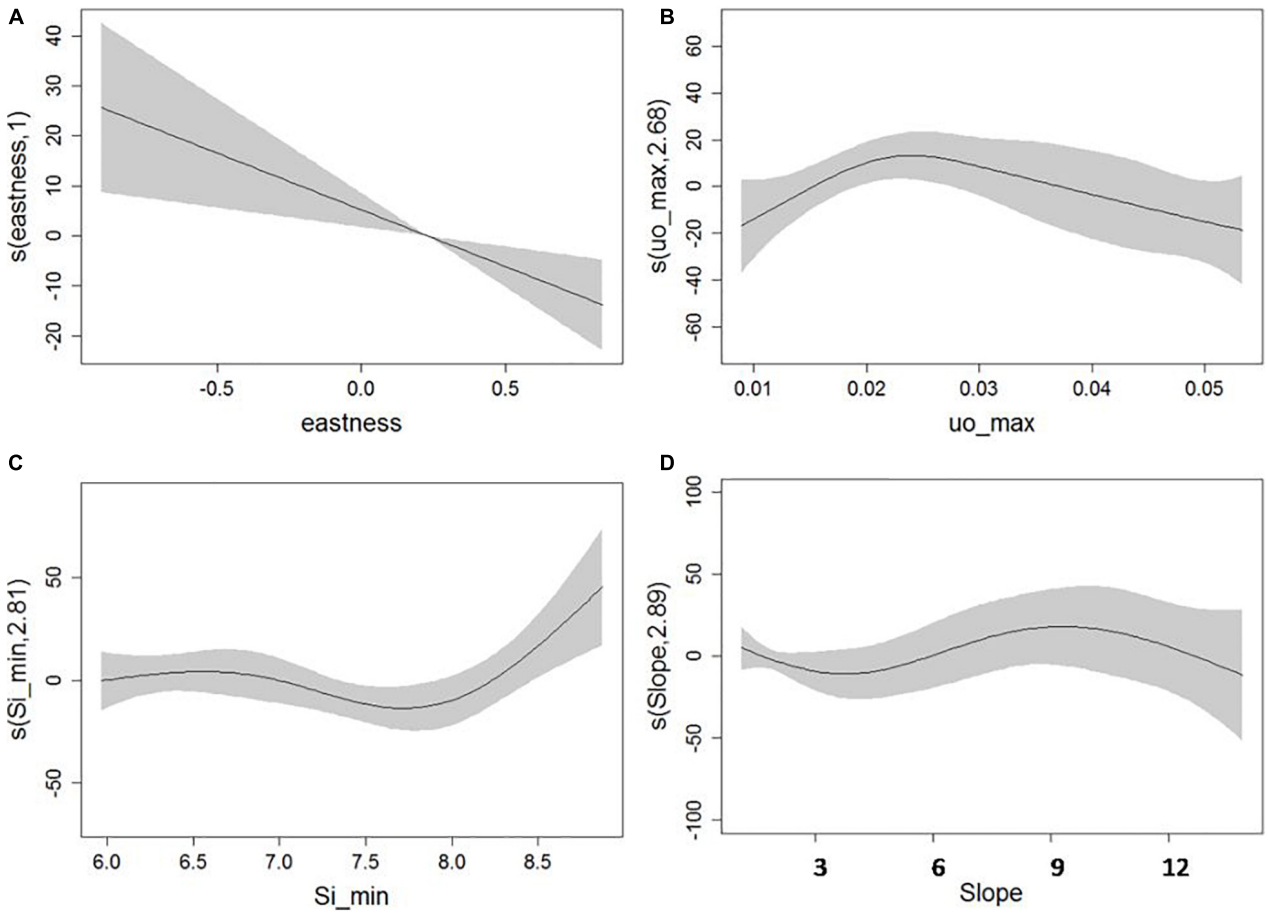

FIGURE 6 | Generalized additive models response curves for eastness **(A)**, bottom current u component **(B)**, minimum value of silicates during 1 year **(C)**, and slope **(D)**.

vulnerable species such as sponges and corals. This will supply more accurate data when providing relevant information on VME to the discussion forums of the declaration processes of MPAs, as well as those included in the more global framework of marine spatial planning.

The morpho-structural characteristics of our study area are very complex, since it encompasses an intricate system of canyons and a seamount, as well as an extensive circalittoral rocky platform at the head of the Avilés canyon and an internal mud basin that separates the Seamount from the continental shelf. This great complexity means that the need of a complete picture of oceanographic dynamics, which has been shown to greatly affect the VME of canyons and seamounts, cannot be ignored. Thus, numerous studies of spatial modeling in seamounts have demonstrated the great importance of currents near the bottom in the spatial distribution of various hexactinellid sponges (Howell et al., 2016; Roberts et al., 2018; Ramiro-Sánchez et al., 2019), while others have focused on the continental shelf, highlighting that near-bed currents at the shelf canyons can increase particle residency times, thereby favoring the presence of hexactinellid sponges (Whitney et al., 2005). On the other hand, some studies on silicic acid have revealed that this can be a strong limiting factor for some siliceous sponges (Maldonado et al., 2011), which can play an important role in the benthopelagic coupling of the silicon cycle (Maldonado et al., 2005); thus, in our opinion, an accurate layer of silicates should be taken into account in studies on the spatial distribution of siliceous sponges.

Spatial Resolution of the Layers and Data Availability

One of the most important issues when conducting a study of SDMs is the choice of appropriate spatial resolution (Vierod et al., 2014; Lecours et al., 2015; Ross et al., 2015). If the optimum in any work is the possibility of choosing spatial resolution depending on the species or habitat to be studied and the work area, too often there is no such possibility, since there are multiple factors influencing the approach of the SDM (Braunisch and Suchant, 2010). The use of multibeam results together with box corer stations for mapping substratum types in the study of the distribution of benthic species is already well recognized, but its accuracy in structurally complex deep-sea sites is limited. On the other hand, visual transects provide high resolution of spatial presence of long-lived and large

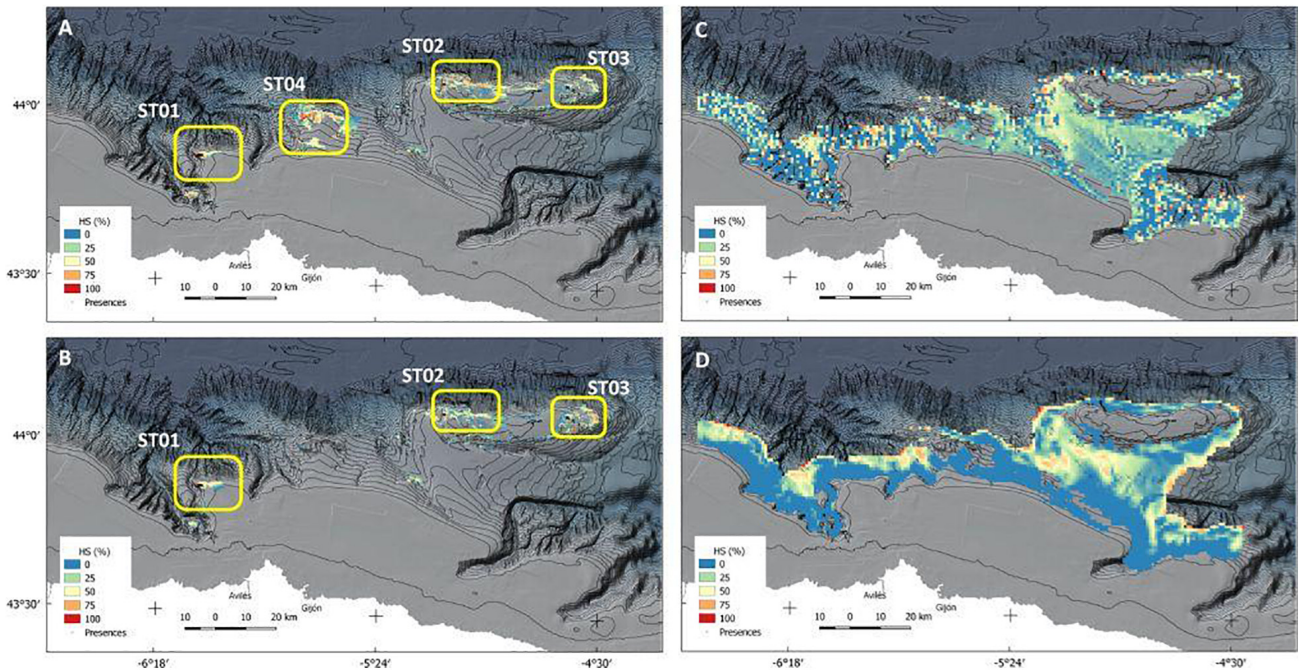

FIGURE 7 | Habitat suitability (HS) predictive maps for each of the species: part labels **(A,B)** corresponds to *A. setubalense* models 1 and 2, and **(C,D)** to the *P. carpenteri* Models 1 and 2 respectively. Model 1 has been constructed only with geomorphologic predictors, and model 2 includes physicochemical predictors for both species.

benthic organisms (Sánchez et al., 2009a; Davies et al., 2014; Buhl-Mortensen et al., 2015). Modeling approaches combining both methods have the potential to contribute significantly to spatial management of deep-sea ecosystems, particularly for sponge grounds (Kostylev et al., 2001; Conway et al., 2005; Harris and Baker, 2012; Neves et al., 2014).

In our case, two factors influenced the spatial resolution of the models. The first was the type of sampler. In the case of *P. carpenteri* it was carried out with the beam trawl in 15′ hauls of almost 1 km long, so it does not make sense to use a lower resolution. The second factor was multibeam resolution, which enabled a very high resolution for the large study area that we had. This advises maintaining the maximum possible resolution when using a high-resolution sampler, as is the case of the georeferenced images from ROTV, which has been proved to be a very useful tool for microhabitat characterization in the circalittoral area of the ACS (Prado et al., 2020).

Understanding what occurs in the Benthic Boundary Layer (BBL), both at the level of oceanographic dynamics and physicochemical properties, is essential for the knowledge of the biology and distribution of benthic species (Lecours et al., 2015). Thus, it is important to consider bottom currents and limiting nutrients as key factors for the distribution of these species, as is reflected in the increasingly growing number of SDM works (Howell et al., 2016; Beazley et al., 2018; Ramiro-Sánchez et al., 2019). However, there are two important limitations to the application of SDMs to benthic species or habitats: spatial resolution, and the specific characteristics of the BBL, because the information available refers to water column models. Consequently, the role of the layers of physicochemical variables used should be interpreted with great caution as they do not take into account topographical effects on currents or sediment re-suspension on the availability of silicates (Sánchez et al., 2014).

Asconema setubalense Spatial Distribution

The vase-shaped *A. setubalense* has been found on seamounts and bathyal depths of several areas of the North Atlantic. Details of its extension, biomass, and densities have not been obtained, but clumps of up to 5 individuals m^{-2} have been recorded (Maldonado et al., 2017). In our study area, the densities found are well below this, with maximum values close to 0.013 individuals m^{-2}, which could mean either that the environmental characteristics are not so suitable for the development of its populations, or that fishing pressure has seriously endangered its resilience. Besides, relatively close regions, such as the Alboran Sea (Mediterranean) and around the Canary Islands, have much denser sponge grounds of this species (González-Porto et al., 2014; de la Torriente et al., 2019).

In the MaxEnt model generated for *A. setubalense*, an excellent AUC score cross-validation result was obtained, with values of training and test data located between the range 0.9–1, very close to 1. This may be due to various factors; one of them seems to be that this sponge, although scarce and not forming aggregations, is well represented within the scanty rock coverage, in contrast to the sedimentary zone. Another is because the random selection chosen by the model for its validation selects presences from

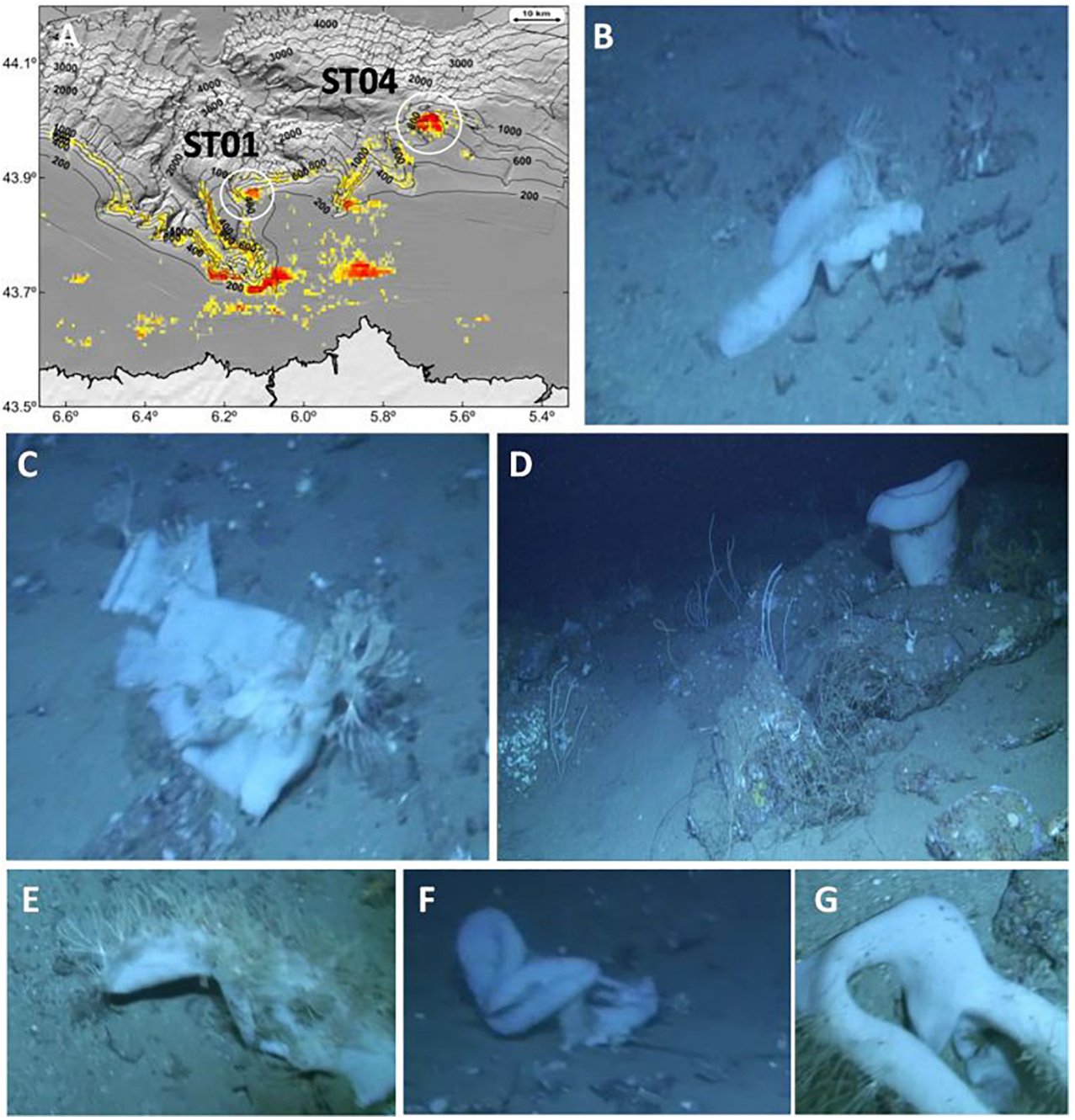

FIGURE 8 | Fishing effort of longliners **(A)** and some of the specimens of *A. setubalense* damaged by longlines and gillnets in the area ST01 **(B–G)**.

within the same populations, which makes it inconsistent. That is why a more accurate study was conducted by removing entire populations (**Table 2**), revealing an average AUC of 0.81 and 0.9 for Models 1 and 2, respectively, which still seems good enough, especially including silicates and currents. However, the inclusion of physicochemical variables shows two different scenarios in area ST04, as can be seen in **Figures 7A,B**. This area was sampled in three different transects using the photogrammetric vehicle but no presence of *A. setubalense* was found. Rather than a sign of this species, a large number of longlines and fishing gears appeared. This leads us to think that either the presence of *A. setubalense* was affected by fishing pressure, or the physicochemical conditions have not allowed its settlement. Additional studies must be carried out if we want to gain more comprehensive knowledge of the role of these predictors.

Further, station ST01 is located in an important fishing ground for gillnetters and longliners (Punzón et al., 2016) and this can be verified in the transects carried out in the area. ST01 study images

had many sponges that were damaged or had longlines tangled around them (**Figure 8**), so it would be advisable to take this into account for future management plans.

Finally, if seabed substrate types are important, depth is also decisive, probably due to its correlation to many different environmental factors, such as general currents. Thus, the shallowest current in the area is found in Eastern North Atlantic Central Water (ENACW), which exerts its influence to a depth of 650 m; from 650 m deep to 1,300, Mediterranean Water (MW) prevails; ending where Labrador Sea Water (LSW) begins (González-Pola et al., 2012). Taking into account the depth range of the species, which in station ST01 is 327–333 m while in ST02 and ST03 it is 540–730 m, this indicates that the lower limit of the species on the seamount is MW, although in the Avilés canyon it is ENACW, suggesting that the *A. setubalense* distribution cannot have been driven by either of them, with it probably being more affected by tidal-controlled currents shaped by the characteristic geomorphology of submarine canyons and seamounts.

Pheronema carpenteri Spatial Distribution

The hexactinellid nest sponge *P. carpenteri* probably forms the most extensive sponge aggregation at temperate latitudes. These appear in the East Atlantic from southern Iceland to Morocco at 800–1,350 m depth. It fixes to the muddy substrate through a large number of spicules often forming mats. The peak abundances are up to 6 individuals m^{-2} (Maldonado et al., 2017), although in our study area the densities found are well below this data, with highs close to 0.072 individuals m^{-2}.

The use of physicochemical layers is highly recommendable in the case of *P. carpenteri*, as long as the sampling method does not allow the resolution that geographical variables would. The good results of the model seem to confirm the great influence that the layer of the minimum value of silicates has for the distribution of the sponge, achieving very highly explained variance and R squared. It also reveals that this could be a valid approach in order to obtain the influence that the processes in the BBL may have in the spatial distribution of species. Thus, although information on the demand for dissolved silicon by sponge populations is extremely scarce because of the technical complexity of the approaches for its quantification, different studies have shown the great importance for sponges of silicate buried in the marine sediments from the rain of diatoms, largely concentrated on continental margins (Maldonado et al., 2011, 2012). In the Porcupine Seabight, Rice et al. (1990) suggested that *P. carpenteri* aggregations occur close to, but not within regions of the upper continental slope where the bottom topography enhances the near-bottom current velocities, but may nevertheless be dependent upon the re-suspended or undeposited organic matter carried there from these regions. The results of our studies show a strong spatial correlation between the availability of silicates (**Figure 4G**) and the presence of *P. carpenteri* (**Figure 7D**), as they generally appear on the muddy bottoms of the continental margin on 400–1,200 m depth. In the Cantabrian Sea, the importance of near-bottom currents at each tidal cycle has been described on the break shelf and canyons (Sánchez et al., 2014). Enhanced near-bed currents are believed to cause high re-suspension, providing an increased food supply and silicate availability for sponges.

The results obtained in this study area are consistent with the one carried out for this species in the El Cachucho MPA by García-Alegre et al. (2014), where the importance of the BPI was revealed by showing similarities to the low positive values of broad-scale BPI and values close to 0 for the fine-scale BPI of our Model 1. Furthermore, in that work, the presence of this species was related to that of the MOW current and its speed (between 0.02 and 0.03 ms^{-1}). This influence has been corroborated in our study, as can be seen in **Figure 6**, where it is observed that the probability of occurrence of the species reaches its maximum when the eastward current velocity value is slightly above 0.02 ms^{-1}, values that agree with the study developed by Ramiro-Sánchez et al. (2019). Above this value, it decreases uniformly, although from 0.03 ms^{-1}, the uncertainty is greater.

Implications for MPA Monitoring

This study indicates the locations with the highest probabilities of the two main vulnerable sponge grounds in the Cantabrian Sea, which may guide future management in the Natura 2000 network. In the case of El Cachucho MPA, the most likely zones to find both species are already protected from the most impactful anthropic activities (bottom fisheries and gas extraction) by the new management plan governing the area (Rodríguez-Basalo et al., 2019). These results highlight the need to keep MPA protection active, and to continue monitoring the effects of management measures on the distribution range of the two species as well as their health status.

Numerous studies are being carried out in El Cachucho MPA with the aim of monitoring the populations of *A. setubalense* at the top of the bank in order to trace its evolution in an area of exclusion of bottom fisheries (Prado et al., 2021), as well as conducting connectivity studies, and others that analyze the presence of species associated with these populations (Manjón-Cabeza et al., 2021). The results obtained here, along with the spatial distribution of these sponges in the ACS, may influence decision-making on the limitations imposed over particular fishing techniques affecting each species. The known spatial distribution of certain artisanal fisheries (Punzón et al., 2016), such as gillnets and longlines, has significant overlaps with the suitable habitat of *A. setubalense*. This will involve designing management measures that somehow limit the use of these fishing techniques or mitigate the impact that fishing gears can have on VME in the areas identified as ST01 and ST02.

Trawling, mainly targeting blue whiting with pair trawls (Punzón et al., 2016), is likely to limit the potential spatial distribution of *P. carpenteri* when its suitable habitat is considered. This overlap of vulnerable habitat and anthropic socio-economic activities will require collaborative study with stakeholders in order to find an agreement on the necessary management measures that reach the participation and acceptance of the main sectors affected. One of the main

objectives of the LIFE + INTEMARES project is to train Natura 2000 network managers and other relevant stakeholders and create networks to promote cooperation and information exchange, and to improve the required knowledge for protected areas management. In this sense, the type of approaches presented in this study is necessary in order to be able to make the right decisions and create a coherent network of MPAs in the context of the Natura 2000 network.

DATA AVAILABILITY STATEMENT

The datasets presented in this article are not readily available because some studies depend on them. Requests to access the datasets should be directed to augusto.rodriguez@ieo.es.

AUTHOR CONTRIBUTIONS

AR-B, FS, and EP conceived and designed the study, and wrote the manuscript. FS and JC led the surveys, sampling strategies, and acquired the funding. PR and JC collected and identified the specimens collected by the beam trawl. All authors analyzed the data, prepared the figures and tables, reviewed drafts of the manuscript, and helped writing the manuscript.

FUNDING

This research has been performed in the scope of the SponGES and INTEMARES projects. SponGES received funding from the European Union's Horizon 2020, Research and Innovation Programme under grant agreement no. 679849. The LIFE IP INTEMARES project is coordinated by the Biodiversity Foundation of the Ministry for the Ecological Transition and the Demographic Challenge. It receives financial support from the European Union's LIFE Programme (LIFE15 IPE ES 012). Also, the Spanish Ministry of Environment through a management agreement with the Spanish Institute of Oceanography (IEO) has funded the scientific monitoring of the El Cachucho MPA (ECOMARG Project).

ACKNOWLEDGMENTS

This study was made possible thanks to the invaluable work of all the participants in the five surveys involved and the crews of the R/Vs. Vizconde de Eza (SGPM), Angeles Alvariño and Ramón Margalef (IEO). The authors also appreciate the helpful assistance of the technicians of the ROTV Politolana, for their skill in executing the dangerous visual transects very close to the rough bottoms of the study area.

REFERENCES

Aumont, O., Éthé, C., Tagliabue, A., Bopp, L., and Gehlen, M. (2015). PISCES-v2: an ocean biogeochemical model for carbon and ecosystem studies. *Geosci. Model Dev.* 8, 2465–2513. doi: 10.5194/gmd-8-2465-2015

Beazley, L., Wang, Z., Kenchington, E., Yashayaev, I., Rapp, H. T., Xavier, J. R., et al. (2018). Predicted distribution of the glass sponge Vazella pourtalesi on the Scotian shelf and its persistence in the face of climatic variability. *PLoS One* 13:e0205505. doi: 10.1371/journal.pone.0205505

Beazley, L. I., Kenchington, E. L., Murillo, F. J., and Sacau, M. D. M. (2013). Deep-sea sponge grounds enhance diversity and abundance of epibenthic megafauna in the Northwest Atlantic. *ICES J. Mar. Sci.* 70, 1471–1490. doi: 10.1093/icesjms/fst124

Benito, B. M., Cayuela, L., and Albuquerque, F. S. (2013). The impact of modelling choices in the predictive performance of richness maps derived from species-distribution models: guidelines to build better diversity models. *Methods Ecol. Evol.* 4, 327–335. doi: 10.1111/2041-210x.12022

Braunisch, V., and Suchant, R. (2010). Predicting species distributions based on incomplete survey data: the trade-off between precision and scale. *Ecography* 33, 826–840. doi: 10.1111/j.1600-0587.2009.05891.x

Buhl-Mortensen, L., Buhl-Mortensen, P., Dolan, M. J. F., and Gonzalez-Mirelis, G. (2015). Habitat mapping as a tool for conservation and sustainable use ofmarine resources: some perspectives from the MAREANO Programme, Norway. *J. Sea Res.* 100, 46–61. doi: 10.1016/j.seares.2014.10.014

Cartes, J. E., Huguet, C., Parra, S., and Sanchez, F. (2007). Trophic relationships in deep-water decapods of Le Danois bank (Cantabrian Sea, NE Atlantic): trends related with depth and seasonal changes in food quality and availability. *Deep Sea Res. I Oceanogr. Res. Pap.* 54, 1091–1110. doi: 10.1016/j.dsr.2007.04.012

Conway, K. W., Barrie, J. V., and Krautter, M. (2005). Geomorphology of unique reefs on the western Canadian shelf: sponge reefs mapped by multibeam bathymetry. *Geo Mar. Lett.* 25, 205–213. doi: 10.1007/s00367-004-0204-z

Cristobo, J., Ríos, P., Sánchez, F., and Anadón, N. (2009). Redescription of the rare species Podospongia loveni (Porifera) from the Cantabrian Sea. *Cont. Shelf Res.* 29, 1157–1164. doi: 10.1016/j.csr.2008.11.021

Davies, J. S., Howell, K. L., Stewart, H. A., Guinan, J., and Golding, N. (2014). Defining biological assemblages (biotopes) of conservation interest in the submarine canyons of the South West approaches (offshore United Kingdom) for use in marine habitat mapping. *Deep Sea Res. II Top. Stud. Oceanogr.* 104, 208–229. doi: 10.1016/j.dsr2.2014.02.001

de la Torriente, A., González-Irusta, J. M., Aguilar, R., Fernández-Salas, L. M., Punzón, A., and Serrano, A. (2019). Benthic habitat modelling and mapping as a conservation tool for marine protected areas: a seamount in the western Mediterranean. *Aquat. Conserv.* 29, 732–750. doi: 10.1002/aqc.3075

European Union (2014). Directive 2014/89/EU of the European parliment and of the council of 23 July 2014 establishing a framework for maritime spatial planning. *Off. J. Eur. Union* 257, 135–145.

García-Alegre, A., Sánchez, F., Gómez-Ballesteros, M., Hinz, H., Serrano, A., and Parra, S. (2014). Modelling and mapping the local distribution of representative species on the Le Danois Bank, El Cachucho Marine Protected Area (Cantabrian Sea). *Deep Sea Res. II Top. Stud. Oceanogr.* 106, 151–164. doi: 10.1016/j.dsr2.2013.12.012

Gómez-Ballesteros, M., Druet, M., Muñoz, A., Arrese, B., Rivera, J., Sánchez, F., et al. (2014). Geomorphology of the Avilés Canyon System, Cantabrian Sea (Bay of Biscay). *Deep Sea Res. II Top. Stud. Oceanogr.* 106, 99–117. doi: 10.1016/j.dsr2.2013.09.031

Gómez-Ballesteros, M., Sánchez, F., García-Alegre, A., González-Pola, C., Hernández- Molina, J., Ercilla, G., et al. (2015). "Morphosedimentary characterization of Le Danois Bank (El Cachucho MPA, Cantabrian sea)," in *Abstract Book. VIII Simposio sobre el Margen Ibérico Atlántico MIA15 Málaga* (Marbella: Centro Oceanográfico de Málaga).

González-Pola, C., Díaz del Río, G., Ruiz-Villarreal, M., Sánchez, R. F., and Mohn, C. (2012). Circulation patterns at Le Danois Bank, an elongated shelf-adjacent seamount in the Bay of Biscay. *Deep Sea Res. I Oceanogr. Res. Pap.* 60, 7–21. doi: 10.1016/j.dsr.2011.10.001

González-Porto, M., Almón-Pazos, B., Falcón, J. M., González-Irusta, J. M., González-Jiménez, J., Barreiro-Jueguen, S., et al. (2014). "XVIII Simposio Ibérico de Estudios de Biología Marina," in *Banco de La Concepción (Canary Islands): Vunerable Marine Ecosystems (VMEs) Spatial Distribution*, eds P. Ríos, L. A. Suárez and J. Cristobo Libro de resúmenes. (Gijón: Centro Oceanográfico de Gijón), 252.

Guisan, A., and Thuiller, W. (2005). Predicting species distribution: offering more than simple habitat models. *Ecol. Lett.* 8, 993–1009.

Harris, P. T., and Baker, E. K. (eds) (2012). "Why map Benthic habitats?," in *Seafloor Geomorphology as Benthic Habitat*. Amsterdam: Elsevier, 3–22. doi: 10.1016/b978-0-12-814960-7.00001-4

Hogg, M. M., Tendal, O. S., Conway, K. W., Pomponi, S. A., Van Soest, R. W. M., Gutt, J., et al. (2010). *Deep-Seas Sponge Grounds: Reservoirs of Biodiversity*. Nairobi: United Nations Envir Programme.

Howell, K. L., Piechaud, N., Downie, A. L., and Kenny, A. (2016). The distribution of deep-sea sponge aggregations in the North Atlantic and implications for their effective spatial management. *Deep Sea Res. I Oceanogr. Res. Pap.* 115, 309–320. doi: 10.1016/j.dsr.2016.07.005

Huetten, E., and Greinert, J. (2008). Software controlled guidance, recording and post-processing of seafloor observations by ROV and other towed devices: the software package OFOP. *Geophys. Res. Abstr.* 10:3088.

Knudby, A., Kenchington, E., and Murillo, F. J. (2013). Modeling the distribution of *Geodia* sponges and sponge grounds in the Northwest Atlantic. *PLoS One* 8:e82306. doi: 10.1371/journal.pone.0082306

Kostylev, V., Todd, B., Fader, G., Courtney, R., Cameron, G., and Pickrill, R. (2001). Benthic habitat mapping on the Scotian shelf based on multibeam bathymetry, surficial geology andseafloor photographs. *Mar. Ecol. Prog. Ser.* 219, 121–137. doi: 10.3354/meps219121

Lecours, V., Devillers, R., Schneider, D. C., Lucieer, V. L., Brown, C. J., and Edinger, E. N. (2015). Spatial scale and geographic context in benthic habitat mapping: review and future directions. *Mar. Ecol. Prog. Ser.* 535, 259–284. doi: 10.3354/meps11378

Maldonado, M., Aguilar, R., Bannister, R. J., Bell, J. J., Conway, K. W., Dayton, P. K., et al. (2017). "Sponge grounds as key marine habitats: a synthetic review of types, structure, functional roles, and conservation concerns," in *Marine Animal Forests*, eds S. Rossi, L. Bramanti, A. Gori, C. O. S. del Valle (Berlin: Springer).

Maldonado, M., Carmona, M. C., Velásquez, Z., Puig, A., Cruzado, A., López, A., et al. (2005). Siliceous sponges as a silicon sink: an overlooked aspect of benthopelagic coupling in the marine silicon cycle. *Limnol. Oceanogr.* 50, 799–809. doi: 10.4319/lo.2005.50.3.0799

Maldonado, M., Navarro, L., Grasa, A., Gonzalez, A., and Vaquerizo, I. (2011). Silicon uptake by sponges: a twist to understanding nutrient cycling on continental margins. *Sci. Rep.* 1:30.

Maldonado, M., Ribes, M., and van Duyl, F. C. (2012). Nutrient fluxes through sponges: biology, budgets, and ecological implications. *Adv. Mar. Biol.* 62, 113–182. doi: 10.1016/b978-0-12-394283-8.00003-5

Manjón-Cabeza, M. E., Ríos, P., García-Guillén, L. M., Macías-Ramírez, A., Sánchez, F., Rodríguez-Básalo, A., et al. (2021). Asteroids and ophiuroids associated with sponge aggregations as a key to marine habitats. a comparative analysis between avilés canyons system and El cachucho, marine protected area. *Front. Mar. Sci.* 7:606749. doi: 10.3389/fmars.2020.606749

Neves, B. M., Preez, C. D., and Edinger, E. (2014). Mapping coral and sponge habitats on a shelf-depth environment using multibeam sonar and ROV video observations: Learmonth Bank, northern British Columbia, Canada. *Deep Sea Res. II Top. Stud. Oceanogr.* 99, 169–183. doi: 10.1016/j.dsr2.2013.05.026

Phillips, S. J., Anderson, R. P., and Schapire, R. E. (2006). Maximum entropy modeling of species geographic distributions. *Ecol. Modell.* 190, 231–259. doi: 10.1016/j.ecolmodel.2005.03.026

Prado, E., Cristobo, J., Rodríguez-Basalo, A, Ríos, P., Rodríguez-Cabello, C. and Sánchez, F. (2021). In situ growth rate assessment of the hexactinellid sponge asconema setubalense using 3D photogrammetric reconstruction. *Front. Mar. Sci.* 8:612613. doi: 10.3389/fmars.2021.612613

Prado, E., Rodríguez-Basalo, A., Cobo, A., Ríos, P., and Sánchez, F. (2020). 3D Fine-scale terrain variables from underwater photogrammetry: a new approach to benthic microhabitat modeling in a circalittoral rocky shelf. *Remote Sens.* 12:2466. doi: 10.3390/rs12152466

Preciado, I., Cartes, J. E., Serrano, A., Velasco, F., and Olaso, I. (2009). Resource utilization by deep-sea sharks at the Le Danois Bank. Cantabrian Sea, north-east Atlantic Ocean. *J. Fish Biol.* 75, 1331–1355. doi: 10.1111/j.1095-8649.2009.02367.x

Punzón, A., Arronte, J. C., Sánchez, F., and García-Alegre, A. (2016). Spatial characterization of the fisheries in the Avilés Canyon System (Cantabrian Sea. Spain). *Cienc. Mar.* 42, 237–260. doi: 10.7773/cm.v42i4.2628

Ramiro-Sánchez, B., González-Irusta, J. M., Henry, L. A., Cleland, J., Yeo, I., Xavier, J. R., et al. (2019). Characterization and mapping of a deep-sea sponge ground on the Tropic Seamount (Northeast Tropical Atlantic): implications for spatial management in the high seas. *Front. Mar. Sci.* 6:278. doi: 10.3389/fmars.2019.00278

Rice, A. L., Thurston, M. H., and New, A. L. (1990). Dense aggregations of a hexactinellid sponge, Pheronema carpenteri, in the Porcupine Seabight (northeast Atlantic Ocean), and possible causes. *Prog. Oceanogr.* 24, 179–196. doi: 10.1016/0079-6611(90)90029-2

Ríos, P., Cristobo, J., and Sánchez, F. (2017). Porifera del cañón de la Gaviera (Sistema de Cañones de Avilés, mar Cantábrico). *Avances En Estudios de Biología Marina: Contribuciones del XVIII SIEBM GIJÓN. Temas de Oceanografía* (Madrid: Instituto Español de Oceanografía), 10, 123–134.

Ríos, P., Prado, E., Carvalho, F. C., Sánchez, F., Rodríguez-Basalo, A., Xavier, J. R., et al. (2019). Community composition and habitat characterization of a rock sponge aggregation (Porifera. Corallistidae) in the Cantabrian Sea. *Front. Mar. Sci.* 7:578. doi: 10.3389/fmars.2020.00578

Roberts, E. M., Mienis, F., Rapp, H. T., Hanz, U., Meyer, H. K., and Davies, A. J. (2018). Oceanographic setting and short-timescale environmental variability at an Arctic seamount sponge ground. *Deep Sea Res. I Oceanogr. Res. Pap.* 138, 98–113. doi: 10.1016/j.dsr.2018.06.007

Rodríguez-Basalo, A., Sánchez, F., Punzón, A., and Gómez-Ballesteros, M. (2019). Updating the Master Management Plan for El Cachucho MPA (Cantabrian Sea) using a spatial planning approach. *Cont. Shelf Res.* 184, 54–65. doi: 10.1016/j.csr.2019.06.010

Rodríguez-Cabello, C., Sánchez, F., Ortiz de Zárate, V., and Barreiro, S. (2009). Does Le Danois Bank (El Cachucho) influence albacore catches in the Cantabrian Sea? *Cont. Shelf Res.* 29, 1205–1212. doi: 10.1016/j.csr.2008.12.018

Rogers, A. D., and Gianni, M. (2010). The Implementation of UNGA Resolutions 61/105 and 64/72 in the Management of Deep-Sea Fisheries on the High Seas. Report prepared for the Deep-Sea Conservation Coalition. International Programme on the State of the Ocean London: Dscc. 97. Available online at: http://www.savethehighseas.org/publicdocs/61105-Implemention-ExecSummary.pdf.

Ross, L., Ross, R. E., Stewart, H. A., and Howell, K. L. (2015). The influence of data resolution on predicted distribution and estimates of extent of current protection of three 'Listed' deep-sea habitats. *PLoS One* 10:e0140061. doi: 10.1371/journal.pone.0140061

Sánchez, F., Cartes, J. E., Parra, S., Gómez-Ballesteros, M., Preciado, I., Frutos, I., et al. (2009b). "Vulnerable habitats and threatened species distribution of El Cachucho deep sea MPA," in *Proceedings of the ICES International Symposium" Issues Confronting the Deep Oceans", Session E-Fisheries and Ecosystem Sustainability and Conservation* (Burnaby, BC:ICES) doi: 10.1590/S0074-02762003000300003

Sánchez, F., González-Pola, C., Druet, M., García-Alegre, A., Acosta, J., Cristobo, J., et al. (2014). Habitat characterization of deep-water coral reefs in La Gaviera Canyon (Avilés Canyon System, Cantabrian Sea). *Deep Sea Res. Top. Stud. Oceanogr.* 106, 118–140. doi: 10.1016/j.dsr2.2013.12.014

Sánchez, F., and Rodríguez, J. M. (2013). Politolana, a new low cost towed vehicle designed for the characterization of the deep-sea habitats and benthic communities. *Instrum. Viewp.* 15:69.

Sánchez, F., Rodríguez Basalo, A., García-Alegre, A., and Gómez-Ballesteros, M. (2017). Hard-bottom bathyal habitats and keystone epibenthic species on Le Danois Bank (Cantabrian Sea). *J. Sea Res.* 130, 134–153. doi: 10.1016/j.seares.2017.09.005

Sánchez, F., Serrano, A., and Ballesteros, M. G. (2009a). Photogrammetric quantitative study of habitat and benthic communities of deep Cantabrian Sea hard grounds. *Cont. Shelf Res.* 29, 1174–1188. doi: 10.1016/j.csr.2009.01.004

Sánchez, F., Serrano, A., Cartes, J., Preciado, I., Arronte, J. C., Parra, S., et al. (2010). "Estimating the MPA management effects on Le Danois Bank deep-sea ecosystem (El Cachucho) using trophodynamic modelization," in *Abstract book of 12 Symposium of Oceanography of the Bay of Biscay* (France: Universidad de Málaga), doi: 10.13140/RG.2.1.4115.2400.

Sánchez, F., Serrano, A., Parra, S., Ballesteros, M., and Cartes, J. E. (2008). Habitat characteristics as determinant of the structure and spatial distribution of epibenthic and demersal communities of Le Danois Bank (Cantabrian Sea, N. Spain). *J. Mar. Syst.* 72, 64–86. doi: 10.1016/j.jmarsys.2007.04.008

Sotillo, M. G., Cailleau, S., Lorente, P., Levier, B., Aznar, R., Reffray, G., et al. (2015). The MyOcean IBI ocean forecast and reanalysis systems: operational products and roadmap to the future Copernicus service. *J. Oper. Oceanogr.* 8, 63–79. doi: 10.1080/1755876x.2015.1014663

Tabachnick, K. R., and Menshenina, L. L. (2007). Revision of the genus Asconema (Porifera: Hexactinellida: Rossellidae). *J. Mar. Biolog. Assoc. UK.* 87, 1403–1429. doi: 10.1017/S0025315407058158

UN General Assembly (2007). *Resolution 61/105 Sustainable Fisheries, Including Through the 1995 Agreement for the Implementation of the Provisions of the United Nations Convention on the Law of the Sea of 10 December 1982*. New York, NY: UN General Assembly.

Van Rooij, D., Iglesias, J., Hernández-Molina, F. J., Ercilla, G., Gomez-Ballesteros, M., Casas, D., et al. (2010). The Le Danois Contourite depositional system: interactions between the mediterranean outflow water and the upper Cantabrian slope (North Iberian margin). *Mar. Geol.* 274, 1–20. doi: 10.1016/j.margeo.2010.03.001

Vierod, A. D., Guinotte, J. M., and Davies, A. J. (2014). Predicting the distribution of vulnerable marine ecosystems in the deep sea using presence-background models. *Deep Sea Res. Top. Stud. Oceanogr.* 99, 6–18. doi: 10.1016/j.dsr2.2013.06.010

Whitney, F., Conway, K., Thomson, R., Barrie, V., Krautter, M., and Mungov, G. (2005). Oceanographic habitat of sponge reefs on the Western Canadian Continental Shelf. *Cont. Shelf Res.* 25, 211–226. doi: 10.1016/j.csr.2004.09.003

Conflict of Interest: The authors declare that the research was conducted in the absence of any commercial or financial relationships that could be construed as a potential conflict of interest.

Copyright © 2021 Rodríguez-Basalo, Prado, Sánchez, Ríos, Gómez-Ballesteros and Cristobo. This is an open-access article distributed under the terms of the Creative Commons Attribution License (CC BY). The use, distribution or reproduction in other forums is permitted, provided the original author(s) and the copyright owner(s) are credited and that the original publication in this journal is cited, in accordance with accepted academic practice. No use, distribution or reproduction is permitted which does not comply with these terms.

frontiers in Marine Science

ORIGINAL RESEARCH
published: 17 March 2021
doi: 10.3389/fmars.2021.638505

A Microbial Nitrogen Engine Modulated by Bacteriosyncytia in Hexactinellid Sponges: Ecological Implications for Deep-Sea Communities

Manuel Maldonado[1]*, *María López-Acosta*[1], *Kathrin Busch*[2], *Beate M. Slaby*[2], *Kristina Bayer*[2], *Lindsay Beazley*[3], *Ute Hentschel*[2,4], *Ellen Kenchington*[3] and *Hans Tore Rapp*[5†]

[1] Department of Marine Ecology, Center for Advanced Studies of Blanes (CEAB-CSIC), Girona, Spain, [2] GEOMAR Helmholtz Centre for Ocean Research Kiel, Kiel, Germany, [3] Department of Fisheries and Oceans, Bedford Institute of Oceanography, Dartmouth, NS, Canada, [4] Unit of Marine Symbioses, Christian-Albrechts University of Kiel, Kiel, Germany, [5] Department of Biological Sciences, University of Bergen, Bergen, Norway

OPEN ACCESS

Edited by:
Lorenzo Angeletti,
Institute of Marine Science (CNR), Italy

Reviewed by:
Robert W. Thacker,
Stony Brook University, United States
Cole G. Easson,
Middle Tennessee State University, United States
Fengli Zhang,
Shanghai Jiao Tong University, China
Giorgio Bavestrello,
University of Genoa, Italy

***Correspondence:**
Manuel Maldonado
maldonado@ceab.csic.es

†Deceased

Specialty section:
This article was submitted to Deep-Sea Environments and Ecology, a section of the journal Frontiers in Marine Science

Received: 06 December 2020
Accepted: 16 February 2021
Published: 17 March 2021

Citation:
Maldonado M, López-Acosta M, Busch K, Slaby BM, Bayer K, Beazley L, Hentschel U, Kenchington E and Rapp HT (2021) A Microbial Nitrogen Engine Modulated by Bacteriosyncytia in Hexactinellid Sponges: Ecological Implications for Deep-Sea Communities. Front. Mar. Sci. 8:638505. doi: 10.3389/fmars.2021.638505

Hexactinellid sponges are common in the deep sea, but their functional integration into those ecosystems remains poorly understood. The phylogenetically related species *Schaudinnia rosea* and *Vazella pourtalesii* were herein incubated for nitrogen and phosphorous, returning markedly different nutrient fluxes. Transmission electron microscopy (TEM) revealed *S. rosea* to host a low abundance of extracellular microbes, while *Vazella pourtalesii* showed higher microbial abundance and hosted most microbes within bacteriosyncytia, a novel feature for Hexactinellida. Amplicon sequences of the microbiome corroborated large between-species differences, also between the sponges and the seawater of their habitats. Metagenome-assembled genome of the *V. pourtalesii* microbiota revealed genes coding for enzymes operating in nitrification, denitrification, dissimilatory nitrate reduction to ammonium, nitrogen fixation, and ammonia/ammonium assimilation. In the nitrification and denitrification pathways some enzymes were missing, but alternative bridging routes allow the microbiota to close a N cycle in the holobiont. Interconnections between aerobic and anaerobic pathways may facilitate the sponges to withstand the low-oxygen conditions of deep-sea habitats. Importantly, various N pathways coupled to generate ammonium, which, through assimilation, fosters the growth of the sponge microbiota. TEM showed that the farmed microbiota is digested by the sponge cells, becoming an internal food source. This microbial farming demands more ammonium that can be provided internally by the host sponges and some 2.6 million kg of ammonium from the seawater become annually consumed by the aggregations of *V. pourtalesii*. Such ammonium removal is likely impairing the development of the free-living bacterioplankton and the survival chances of other sponge species that feed on bacterioplankton. Such nutritional competitive exclusion would favor the monospecific character of the *V. pourtalesii* aggregations. These aggregations also affect the surrounding environment through an annual release of 27.3 million kg of nitrite and, in smaller quantities, of nitrate and phosphate. The complex metabolic integration

among the microbiota and the sponge suggests that the holobiont depends critically on the correct functioning of its N-driven microbial engine. The metabolic intertwining is so delicate that it changed after moving the sponges out of their habitat for a few days, a serious warning on the conservation needs of these sponge aggregations.

Keywords: sponge physiology, sponge microbiota, nitrogen cycling, phosphorous cycling, functional deep-sea ecology, benthic-pelagic coupling, sponge aggregations, nutritional competitive exclusion

INTRODUCTION

Glass sponges (phylum Porifera, class Hexactinellida) are marine organisms markedly restricted to the deep sea (Tabachnick, 1994), with only a handful of species that can be found at SCUBA-diving depths (Mackie and Singla, 1983; Vacelet et al., 1994; Cook et al., 2008). Such bathymetric confinement has hindered empirical investigations on this large sponge lineage, the physiology and functional ecology of which remains poorly understood. During the last two decades, the advent of high-capacity remote operated vehicles (ROVs) has opened deep-sea communities to experimental and manipulative research, making it possible to approach the physiology of the organisms and their functional integration into the deep-water ecosystems.

At bathyal depths, hexactinellid sponges can occur forming dense and extensive aggregations (reviewed in Maldonado et al., 2017). While the physical presence of the sponges increases the 3D-complexity of the habitats (Beazley et al., 2013; Dunham et al., 2018; Hawkes et al., 2019), their physiological activity also carries an exchange of organic and inorganic nutrients with the surrounding environment (Pile and Young, 2006; Yahel et al., 2007; Kahn et al., 2018). Such nutrient exchange is foreseen to affect the surrounding deep-sea system in a multiplicity of ways, but the exact mechanisms behind it, as well as the magnitude of the net fluxes, remain poorly investigated, at least in comparison with the information available for shallow-water demosponges (reviewed in Maldonado et al., 2012 and Zhang et al., 2019). The implications of the hexactinellid aggregations on the cycling of silicon have been demonstrated at regional oceanographic levels (Chu et al., 2011; Maldonado et al., 2021), but their role in respect to the flux of nitrogen (N) and phosphorous (P) nutrients remains less understood. Traditionally, hexactinellid sponges have been interpreted as long-lived organisms with low rates of physiological activity, so that the net flux rates of nutrient exchange with the environment were *a priori* expected to be modest. However, while the rates of silicon utilization depend directly on the metabolic activity of the sponge cells, the net flux of N and P inorganic nutrients of the sponges depend on the metabolic activity not only of the sponge cells but also of the microbial populations (the microbiota) that the sponges host. From studies on shallow-water demosponges, it is well-known that the "holobiont" constituted by a sponge and its microbiota is able to either incorporate or release a variety of dissolved inorganic nutrients such as ammonium, nitrate, nitrite, and phosphate, depending on the sponge species (Diaz and Ward, 1997; Maldonado et al., 2012; Ribes et al., 2012; Fiore et al., 2013; Keesing et al., 2013; Hoer et al., 2018; Pita et al., 2018; López-Acosta et al., 2019; Zhang et al., 2019). Often the microbial communities hosted by demosponges are complex and may include simultaneously archaea and bacteria, including cyanobacteria. Demosponges with high abundance of microbes in their tissues (i.e., HMA sponges) often —but not always (Bayer et al., 2008)— take up ammonium from seawater, which is a N source for chemo- and phototrophic bacteria and an energy source for ammonia-oxidizing bacteria (AOB) and archaea (AOA). In contrast, the HMA demosponges typically release nitrate and nitrite, as the probable result of the metabolic activity of nitrifying symbiotic bacteria (Corredor et al., 1988). The demosponges with low abundance of associated microbes (LMA sponges) are typically net sources of both nitrate and nitrite as well, and, in many cases, also release ammonium (Jiménez and Ribes, 2007; Southwell et al., 2008a,b; Morganti et al., 2017). Most investigated demosponges —but not all— are net sources of phosphate, which is released at very low rates (Maldonado et al., 2012; Ribes et al., 2012; López-Acosta et al., 2019).

In this regard, there is no comprehensive information for hexactinellids about the sign and magnitude of the net flux of ammonium, nitrite, nitrate and phosphate. Given the idiosyncrasy of the syncytial tissues of hexactinellids, it is not even clear whether these sponges can be objectively identified as belonging to either the HMA or LMA models established for demosponges and, if so, it remains to be described where the abundance of microbes would be located within their body, typically consisting of large internal aquiferous spaces and only very thin threads of tissue (i.e., epithelia + mesohyl) attached to the siliceous skeleton. A recent study of South Pacific deep-sea sponges, including demosponges and hexactinellids, has reported microbial communities in hexactinellids that appear to show patterns equivalent to the LMA-HMA dichotomy known for shallow-water demosponges (Steinert et al., 2020). Likewise, a recent pioneering study (Tian et al., 2016) on the hexactinellid *Lophophysema eversa* has reported the microbial community to be dominated by chemoautotrophic bacteria, mostly ammonia-oxidizing archaea (AOA), nitrite-oxidizing bacteria (NOB), and sulfur-oxidizing bacteria (SOB). These three functional groups of microbes were interpreted as playing roles in the cycling of carbon, nitrogen and sulfur in the micro-environment inside the sponge body, being scavengers of toxic ammonia, nitrite and sulfide waste produced by the metabolism of the sponge cells in the conditions of the deep-sea environment. The NOB groups also appear to participate in pathways that lead to production of vitamin B12 (Tian et al., 2016). In a recent study on the hexactinellid *Vazella pourtalesii*, the microbiome has been well-characterized through genomic approach, as well as the functional traits that allow the microbes to survive and

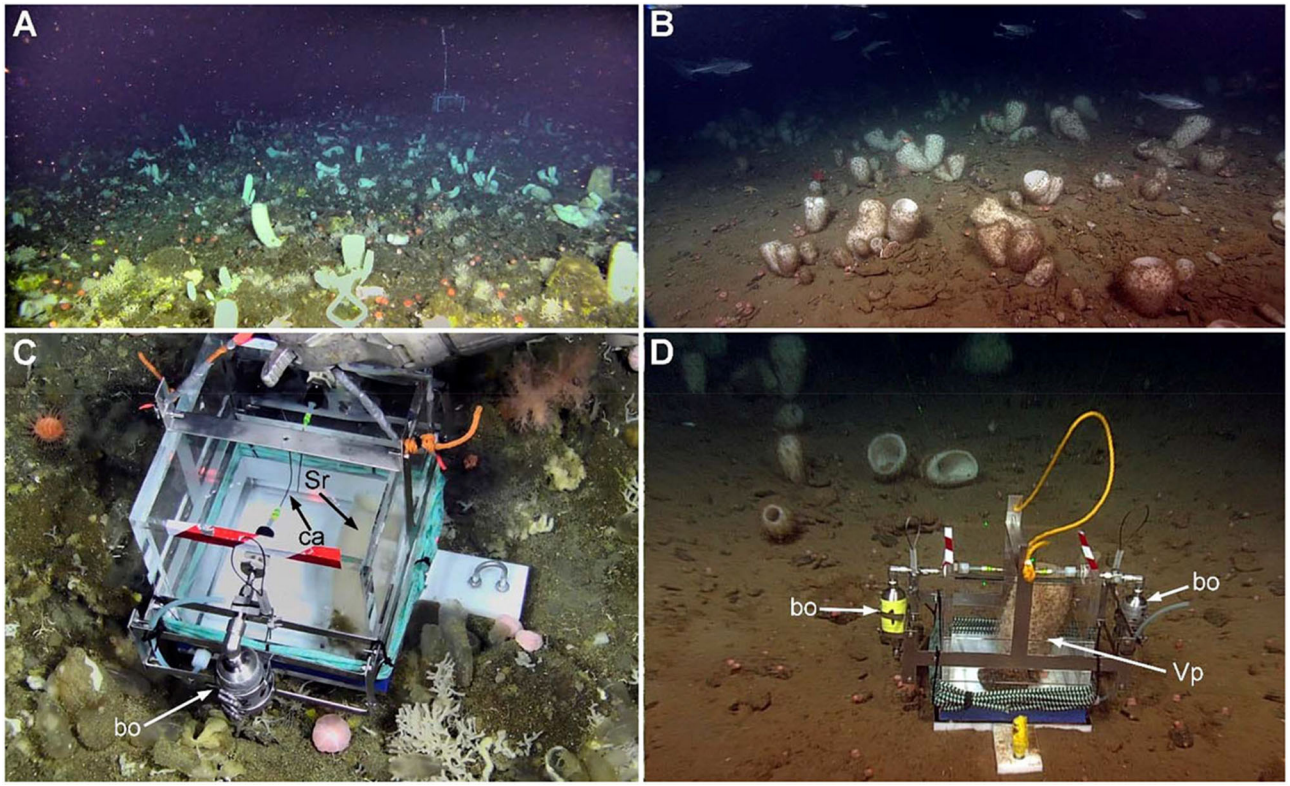

FIGURE 1 | (A) View of a multi-species sponge community at the Schulz Bank seamount (located between the Greenland and Norwegian Seas; 73.8 °N; 7.5 °E), where the whitish tubes of the hexactinellid *Schaudinnia rosea* co-dominate in abundance along with a variety of demosponges and small cnidarians. **(B)** View of the monospecific aggregations of the hexactinellid *Vazella pourtalesii* that extend on the deep region of the continental shelf in Nova Scotia (Canada). **(C,D)** *In-situ* incubation of an individual of *Schaudinnia rosea* (Sr) and a *Vazella pourtalesii* (Vp) in their respective natural communities at depths of 580 and 180 m, respectively. Note that the incubation chambers incorporate two external steel bottles (bo) for water sampling within the camera by means of capillaries (cp) that pierce the chamber wall.

proliferate within the sponge tissue (Bayer et al., 2020). In the current study, we attempt to integrate the genomic microbial information in a physiological and ecological context to better understand the nitrogen and phosphorus fluxes of the sponges, what sponge capabilities may rely on the metabolic integration with their microbes, and what the implications are for the deep-sea ecosystem where aggregations of these hexactinellid sponges occur.

To this aim, in the frame of the EU H2020 project "SponGES," we have investigated two ecologically important deep-sea hexactinellid sponge species, *Schaudinnia rosea* (Fristedt, 1887) and *Vazella pourtalesii* (Schmidt, 1870). In both cases, the sponges form dense aggregations, representing relevant community components at both the physical and the functional levels. We have quantified *in situ* the net flux rates of ammonium, nitrate, nitrite, and phosphate, using benthic incubation chambers manipulated by high-capacity ROVs. By collecting live animals, net flux rates were also measured in laboratory experiments for one of the species, namely *V. pourtalesii*. Through metagenomic analysis, the main microbial lineages occurring within the sponges have been revealed along with their functional implication in a variety of relevant biochemical routes in the N and P metabolism. Through ultrastructural research, the particular locations of the microbes within the sponge body have also been unveiled. Therefore, this study seeks to contribute to a better understanding of (1) the mechanisms behind the nutrient flux rates of hexactinellid sponges and (2) the ecological significance of those fluxes to the deep-sea ecosystems.

MATERIALS AND METHODS

Sponge Species

The studied hexactinellid sponges, *S. rosea* and *V. pourtalesii*, are phylogenetically closely related, both belonging to the subfamily Rossellinae in the family Rossellidae. The species *S. rosea* is distributed along the Arctic Ocean from 90 to 3110 m depth. This species becomes co-dominant in abundance at the Schulz Bank, a seamount located on the Arctic Mid-Ocean Ridge (73.8 °N; 7.5 °E) between the Greenland and Norwegian Seas. There it forms, along with several demosponges, a sponge-dominated benthic community that extends over the top of the seamount at depths of 550–600 m (**Figure 1A**, **Supplementary Video 1**). The species *V. pourtalesii* occurs in the northwest Atlantic, from 100 to 935 m depth. This species is mostly known from dense, monospecific aggregations (**Figure 1B**, **Supplementary Video 2**) extending on the deep continental shelf of Nova Scotia (Canada) at 150–200 m deep (Beazley et al., 2018; Maldonado et al., 2021). At those depths, the areas of the Scotian continental

shelf where the sponge aggregations occur are an aphotic environment with bottom water temperatures below the 10°C permanent thermocline, features favored by the high latitude. Those conditions, according to a functional definition of the deep-sea (Gage and Tyler, 1991), qualify the *Vazella* grounds as a deep-sea habitat despite being topographically located on the continental shelf.

Field Incubations of Sponges

We built 6 benthic incubation chambers in methyl methacrylate and inox steel, with an incubation volume of either 17.3 or 13.3 L (as described in Maldonado et al., 2020). Chambers incorporated a floor piece of Delrin acetal resin, which allowed for the incubation of sponges in isolation from the external environment. This approach avoided interference by nutrient fluxes from the resuspended sediments that occurred during deployments and ROV activity on the sea bottom. The chambers incorporated two external sampling bottles (120 mL) made of steel and internally folded with polytetrafluoroethylene (**Figures 1C,D**). Through a steel capillary (20 cm long and 0.6 mm wide) that pierced the wall of the chamber, each bottle was designed to collect a water sample (under negative pressure conditions) from inside the incubation chamber while it was opened for 5 min and then closed using the ROV manipulator arms (**Figures 1C,D**).

In-situ incubations were conducted during two oceanographic cruises. In August 2018, on board of R/V GO Sars and using the ROV ÆGIR 6000, we incubated seven individuals of *S. rosea* (**Supplementary Video 3**) and a control on the Schultz Massif seamount, at depths of 577–580 m. In September 2017, on board of CCGS Martha L Black and using the ROV ROPOS, a total of four individuals of *V. pourtalesii* and a control (see below) were incubated *in situ* on the Scotian Shelf at depths of 160–180 m (**Supplementary Video 4**), as described in Maldonado et al. (2020). The number of incubations was limited by inclement weather in the area during the entire cruise. For the incubations, each sponge was grabbed by the manipulator arm from the small rock on which it was attached, then placed on the floor piece of the incubation chamber, and covered with the methyl methacrylate box, which rested into a groove in the floor piece designed to prevent leakages from the incubation unit. Once the sponge was inside the chamber and the chamber properly sealed, one of the sampling bottles was opened to collect water for 5 min and then closed again to avoid water exchange with the surrounding seawater. As a control, we used a rock selected from the sponge grounds but without an attached sponge. After an incubation period of 19–28 h (incubation time varied due to weather and the logistics of the cruises), the ROV returned to the chamber position and triggered the second sampling bottle. After this second water collection, the sponge and its attachment rock were collected to estimate volume and biomass, needed to normalize N and P flux rates by sponge volume (mL); sponges were later combusted for flux rates to be also normalized by ash-free dry weight (AFDW; g). Seawater samples were processed for determination of nutrient concentrations to further derive net flux rates of ammonium, nitrate, nitrite, and phosphate (see method section on "Nutrient analyses").

Laboratory Incubations of Sponges

To examine whether differences occur in the magnitude and/or the sign between *in-situ* and laboratory sponge incubations, we collected individuals of *V. pourtalesii* (at Sambro Bank Sponge Conservation Area and LaHave Basin), took them to the aquarium room of the Bedford Institute of Oceanography (Dartmouth, Canada) and conducted seven laboratory incubations during a period of 2 weeks, as detailed in Maldonado et al. (2020). The enormous distance from Schulz Bank to any land laboratory made it logistically impossible to repeat the laboratory experiments with the species *S. rosea*.

In short, 11 individuals of *V. pourtalesii* were collected along with the small rock on which it was attached. Sponges were maintained alive on board for 5 days in a 700 L tank filled with seawater refrigerated to 9 ± 1°C. Upon arrival to the laboratory, sponges were transferred to a 360 L tank and left there 2 days for acclimation to a refrigerated (9 ± 0.5°C) seawater system with recirculation, fed with seawater from the Bedford Basin at the head of Halifax Bay. The seawater was filtered on a 1 μm mesh, a pore size preventing phytoplankton but allowing in part of the natural sponge food (i.e., most of the bacterioplankton). After acclimation, each sponge was incubated separately in a polypropylene 16 L container for 24 h and then transferred, along with all other incubated individuals, to a common 300 L water tank for resting during the following 24 h, until starting a new 24 h period of individual incubations in the 16 L containers. The sponges were subjected to a total of seven successive incubations intercalated with their corresponding 24 h resting periods. The idea for this design was to examine whether a midterm exposure to the coastal water in laboratory conditions would induce detectable changes in the sign and magnitude of the net flux of the various nutrients and relative to the field incubations. From each individual incubating container, seawater was sampled at the beginning and at the end of each incubation period to determine the magnitude and the sign of the change in the respective nutrient concentrations (i.e., ammonium, nitrate, nitrite, and phosphate), following the methods explained in the below section of "Nutrient analyses."

Nutrient Analyses

Immediately after recovering the sampling bottles from deployment, seawater samples were passed through 0.22 μm-pore, syringe filters (Millex-GS Millipore) and frozen at −20°C, until they were analyzed using an Auto-Analyzer AA3 (Bran+Luebbe) following the standard colorimetric method (Strickland and Parsons, 1972), with a determination accuracy of 1%. The nutrient flux was finally calculated as the value of its concentration at the beginning of the incubation minus that at the end of incubation, being normalized by duration of incubation (h), sponge size (mL), and seawater volume in the incubation unit (L) after discounting sponge and rock volume. Flux rates were also corrected by the control flux. Therefore, negative flux values represent nutrient release by the sponges and positive values incorporation. We preferentially expressed data normalized to sponge volume because it facilitates their future applicability to field sponge populations using ROV images without the need of collecting individuals. However, we have also

expressed data as AFDW-normalized, for more correct between-species physiological comparisons. Finally, we examined the potential relationships between flux rates by nutrient pairs and between the flux rate of a nutrient and its ambient concentration at the beginning of the incubation, using linear and non-linear regression analysis.

Diversity and Functional Gene Analysis of Associated Microbiota

Microbial Diversity From Amplicon Sequencing

In order to examine the microbial diversity in the studied sponges, 13 individuals of *V. pourtalesii* were collected from Sambro Bank and 13 of *S. rosea* from Schulz Bank. The sample processing procedure is described in detail elsewhere (Busch et al., 2020, 2021; see also these references for data availability). Briefly, from each sponge individual chunks of tissue were subsampled, rinsed and frozen at −80°C until DNA extraction. Seawater reference samples were also collected from each of the two sponge habitats. At Sambro Bank, three samples of bottoms seawater (3 m from bottom) were collected with a Niskin bottle deployed on the ROV. At Schulz Bank, six seawater samples were collected, three of which by Niskin bottles deployed on the ROV (3 m from bottom) and three by a CTD rosette water sampler. All seawater samples (2 L) were filtered onto PVDF filter membranes (Merck Millipore) with a pore size of 0.22 μm and a diameter of 47 mm. Until DNA extraction the filters were stored at −80°C.

Approximately, 0.25 g of sponge tissue and half of a seawater filter were used for DNA extraction with the DNeasy Power Soil Kit (Qiagen). Quality and quantity of extracted DNA was checked and a one-step PCR conducted to amplify the V3 and V4 variable regions of the 16S rRNA gene (primer pair 341F-806R). Afterwards, PCR-products were examined by gel electrophoresis, normalized and pooled. Sequencing was performed on a MiSeq platform (MiSeqFGx, Ilumina) using v3 chemistry (producing 2 × 300 bp).

Adapters were removed and raw sequences (forward reads) were truncated to a length of 270 nt. Quality of sequences was evaluated in QIIME2 version 2018.11 (Bolyen et al., 2019) before applying the DADA2 algorithm (Callahan et al., 2016); one million reads were used to train the error model. Several denoising steps were conducted to remove chimeras, chloroplasts, unassigned and mitochondrial sequences. A minimum sequencing depth of 13000 was applied. Taxonomic classification of Amplicon Sequence Variants (ASVs) was performed using a Bayes classifier (Bokulich et al., 2018) trained on the Silva 132.99% OTUs 16S database (Quast et al., 2013). Between-sample Weighted UniFrac distances (Lozupone et al., 2011) were calculated based on a phylogeny produced with FastTree2 (Price et al., 2010). To assess the effect on Weighted UniFrac distances on the spatial distribution of samples in an ordination space, a non-metric multidimensional scaling (nMDS) was performed, followed by PERMANOVA tests to examine the statistical significance of the between-group differences identified by the nMDS.

Microbial Functional Gene Repertoire in *V. pourtalesii*

To assess the involvement of microbial symbionts in nitrogen and phosphorous cycling, we focused on the *V. pourtalesii* holobiont. The functional gene repertoire of metagenome-assembled genomes (MAGs) that were used for this objective has been published recently (Bayer et al., 2020) and is available on NCBI under BioProject PRJNA613976. Briefly, metagenomes were sequenced from seven sponge samples and five seawater controls by Illumina Next Generation Sequencing (HiSeq 4000, 2 × 150 bp paired-end) at the Institute of Clinical Molecular Biology (IKMB) of Kiel University. The raw reads were trimmed with Trimmomatic v0.36 and co-assembled with Megahit v1.1.3 (Li et al., 2016). The metagenomic assembly was binned with the metaWRAP pipeline v1.0.2 (Uritskiy et al., 2018), and functionally annotated by Interproscan v5.30-69.0 including GO term and pathway annotations (Jones et al., 2014; Sangrador-Vegas et al., 2016). Interpro annotations are available *via* DOI 10.6084/m9.figshare.12280313. Taxonomy was determined with GTDB-Tk (Chaumeil et al., 2019). *V. pourtalesii*-enriched MAGs were identified by linear discriminant analysis (LDA) scores using LEfSe v1.0 (Segata et al., 2011). For enzymes or functions of specific pathways whose genes were not found in MAGs of identified microbial lineages, we still searched the unbinned metagenomic data (i.e., all contigs not assigned to a specific MAG) to determine whether the genes for the missing metabolic step could be present somehow within the sponge microbial community.

Histology and Ultrastructure of Deep-Sea Hexactinellids

To understand and document where the various microbes may physically occur within the sponge body, we conducted both light microscopy and transmission electron microscopy (TEM) on *V. pourtalesii* and *S. rosea*.

For light microscopy, tissue pieces of 0.5 cm^3 were fixed in 4% formalin in saline dibasic phosphate buffer for 3 weeks, until arriving to the laboratory. Samples were then rinsed in distilled water, desilicified in 5% hydrofluoric acid for 5 h, rinsed in distilled water, dehydrated through an ethanol series of increasing concentration (50–100%) and finally xylene, embedded in paraffin, and sectioned in a Leica RM2125 RTS manual microtome. The obtained 5 μm-thick sections were extended on glass slides, stained with hematoxylin and eosin, and a cover-slide attached using DPX mounting medium for observation through an IX50 Olympus microscope connected to a ProgRes C7 digital camera.

For TEM, tissue pieces of about 2 mm^3 were immersed for 3 h in a fixative cocktail consisting of 2% glutaraldehyde, 2% osmium tetroxide, 65% sodium acetate buffer, 11% sucrose, and 20% distilled water (Maldonado, 2015). Initial dehydration steps took place in 50% ethanol and then 70% ethanol, in which samples were preserved for 1 month, until their arrival to the laboratory. Some of these samples were then rehydrated and desilicified in hydrofluoric acid for 5h prior to dehydration; the rest of the samples were subjected to dehydration without desilicification. Dehydration was then resumed in 70% (10 min), 80% (10 min),

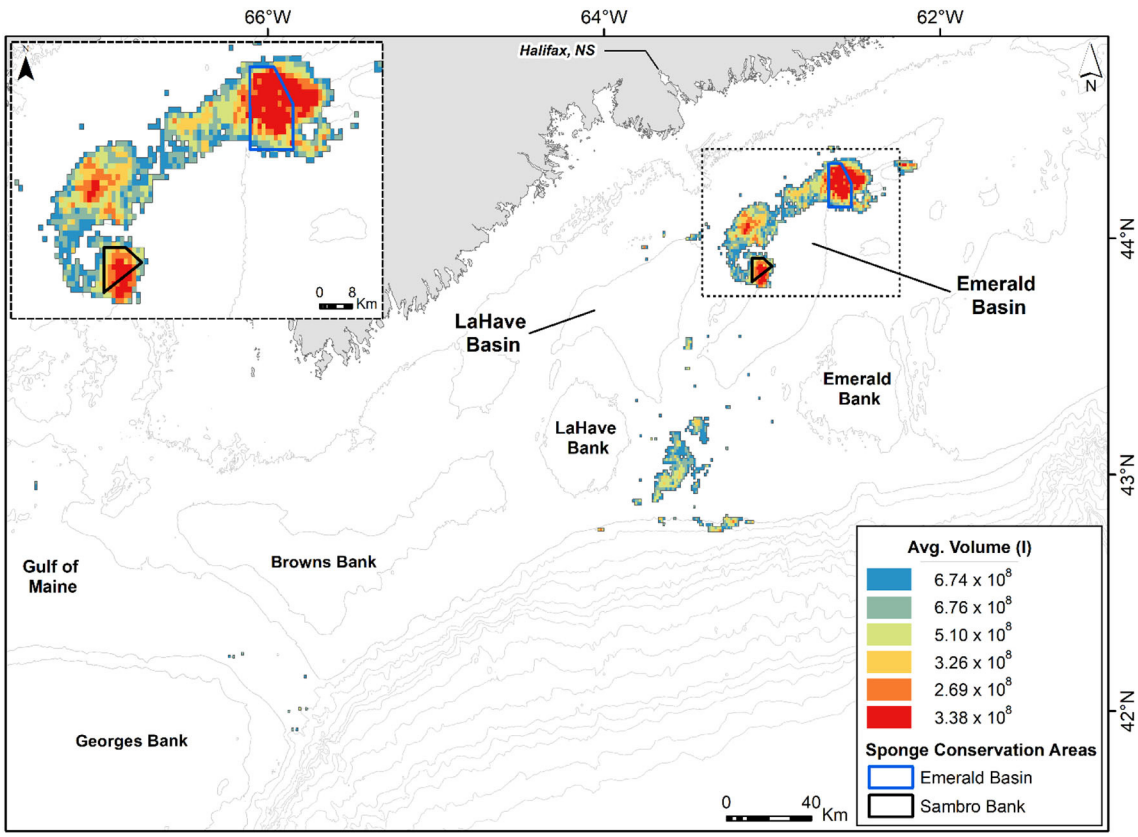

FIGURE 2 | Spatial distribution of *Vazella pourtalesii* biomass (by volume in liters) across the Central Scotian Shelf, as calculated in Maldonado et al. (2021). The sponge grounds correspond to areas predicted to have > 70% presence probability of the species, according to Beazley et al. (2018). The areas of densest sponge aggregation are protected from any bottom fishing activity through the creation of two Sponge Conservation Areas (SCA): Emerald Basin SCA and Sambro Bank SCA.

90% (3 × 10 min), 96% (3 × 10 min), and 100% ethanol (3 × 10 min), followed by propylene oxide (2 × 10 min). Embedding in Spur resin required five immersion steps with gentle shaking during each one: 6 h in a 3:1 propylene-oxide/resin solution, 12 h in 2:2 propylene-oxide/resin solution, 7 h in a 1:3 propylene-oxide/resin solution and two 6-h steps in pure resin. Resin was hardened at 60°C for 2 days. Ultrathin sections were obtained with an Ultracut Reichert-Jung ultramicrotome, mounted on gold grids and stained with 2% uranyl acetate for 30 min, then with lead citrate for 10 min. Observations were conducted with a JEOL 1010 TEM operating at 80 kv and provided with an external Gatan module for acquisition of digital images.

Nutrient Fluxes at the Deep-Sea Community Level

The nutrient utilization rates measured during the *in-situ* and laboratory incubations were used to estimate the net annual flux of ammonium, nitrite, nitrate, and phosphate at the aggregation of *V. pourtalesii*, which is well-characterized in terms of the spatial distribution of the sponge biomass. The area occupied by the *Vazella* sponge grounds on the Scotian Shelf was estimated by applying a threshold criterion (70%) to the modeled presence probability outputs for this species, as indicated in Beazley et al. (2018). The presence probability surface was generated from random forest modeling using presence/absence data. Using ArcMap version 10.6.1., the 1 × 1 km raster grid containing all predicted presence probabilities of *V. pourtalesii* from > 70 to 100% and displayed in 5% equal presence probability intervals in Beazley et al. (2018), was converted to a polygon layer of 1 × 1 km cells, each representing a given presence probability. The total area encompassed by all cells with probability values within each 5% probability interval (six intervals from > 70 to 100%) was calculated at 2,105 km^2 (**Figure 2**). The two densest areas of the sponge aggregation were closed by Fisheries and Oceans Canada to all bottom fishing activities, creating in 2013 the Emerald Basin Sponge Conservation Area (195 km^2) and the Sambro Bank Sponge Conservation Area (62 km^2), as indicated in **Figure 2**. ROV-driven, transect and quadrat surveys in the two Sponge Conservation Areas additionally characterized the spatial distribution of both the individuals (i.e., density) and the individual biomass (in volume) in cells of highest presence probability, as detailed in Maldonado et al. (2021). It was found that, at the densest areas of the aggregations (cells of 0.975 presence probability), the sponge density was 3.78 ± 3.22 individuals m^{-2}, with a biomass of 1.6 ± 2.8 L of sponge tissue

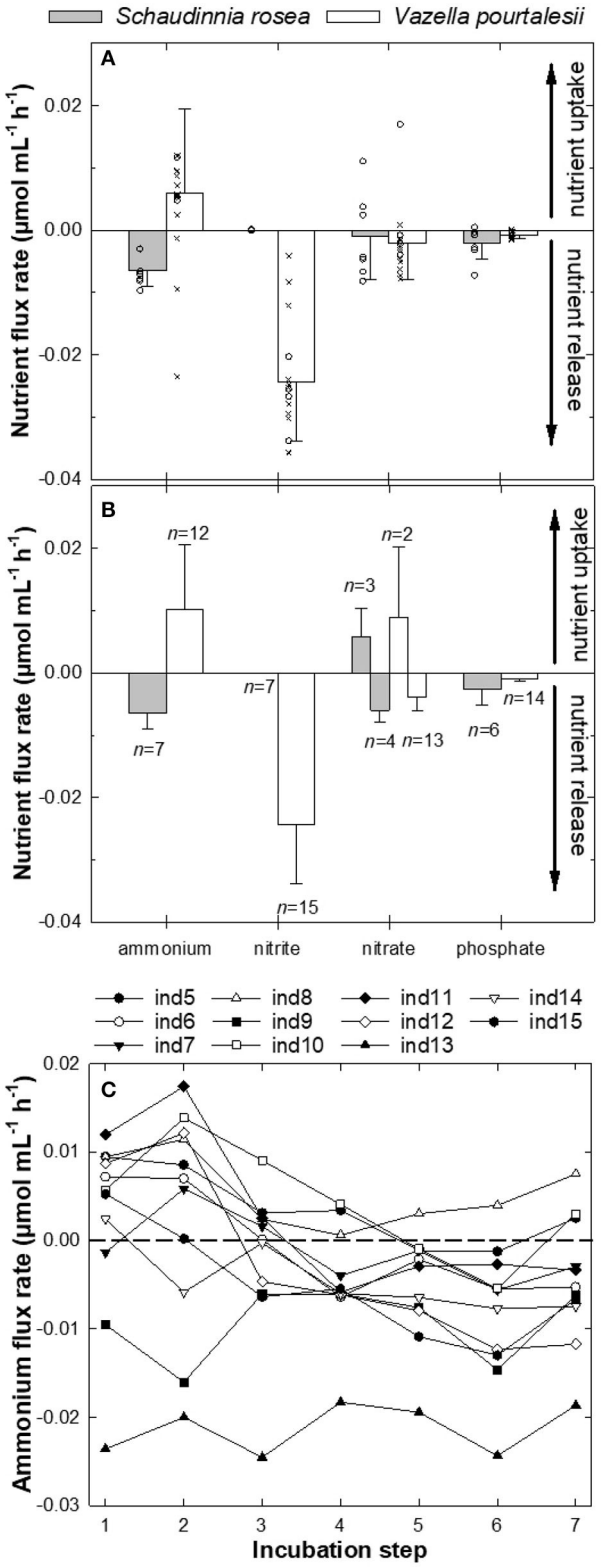

FIGURE 3 | (A,B) Magnitude (average ±SD) and sign of the flux (µmol mL^{-1} h^{-1}) of ammonium (NH_4^+), nitrite (NO_2^-), nitrate (NO_3^-), and phosphate (PO_4^{3-}) measured for individuals of the hexactinellid sponges *Schaudinnia rosea* and *Vazella pourtalesii*. Note that positive values indicate incorporation of a nutrient from the seawater into the sponge, while negative values indicate nutrient release from the sponge. **(A)** Global average (±SD) flux rate (µmol mL^{-1} h^{-1}) for each nutrient and sponge species when all assayed individuals are considered in the calculations (*S. rosea, n* = 7; *V. pourtalesii, n* = 15). Note that individual measurements for *in-situ* incubations (crosses) and the first laboratory incubation of *V. pourtalesii* (open circles) are also plotted to show between individual variability. **(B)** Average (±SD) flux rates (µmol mL^{-1} h^{-1}) considering only individuals with the same flux sign in the averaging process. The number of individuals (*n*) considered in these averages by flux sign for each nutrient and species are indicated in the graph. **(C)** Ammonium flux rate in the *V. pourtalesii* individuals over the seven successive laboratory incubations. See **Supplementary Table 2** for ammonium concentration at the onset of incubations.

(Continued)

m^{-2}. Finally, in order to convert presence probability into density of sponges and sponge biomass, as required for successively estimating the flux rate of the respective dissolved inorganic nutrient across the *Vazella* grounds, the average sponge density and volume of sponge tissue were respectively multiplied by the mid-point of each 5% presence probability bin. This procedure revealed that the aggregation consists of some 6,479 ± 5,518 million sponges, with a total sponge biomass (in volume) of 2,791 ± 3,832 million L (Maldonado et al., 2021). The biomass is known to be spatially distributed on the Nova Scotia Central Shelf, as it is indicated in **Figure 2**. The resulting spatial cells of sponge biomass were then multiplied by the global average value of the net flux rate obtained for each nutrient after combining all individuals from *in-situ* and laboratory incubations. For the laboratory net flux, the average values considered only the first incubation of the individuals. By considering only the first laboratory incubation, we had more chances of avoiding the effects that the coastal seawater feeding the laboratory could have on the microbiota of *V. pourtalesii,* minimizing physiological artifacts in the sponge response. Indeed, to test whether the results of "*in-situ*" and "first-day laboratory" incubations could be pooled safely, we examined potential differences in the net flux rate between *in-situ* incubations and the first-day laboratory incubations for each nutrient, using either the *t*-test or its non-parametric equivalent Mann-Whitney *U*-test, whenever required to deal with non-normal and/or heteroscedastic data sets. In all cases, there were no statistically significant differences between *in-situ* and laboratory flux rates (see **Supplementary Table 1**) and, consequently, data were suitable for pooling. The result of the subsequent calculations provided a mean (± SD) estimate of the annual net flux rate of each nutrient through the *V. pourtalesii* aggregations on the Nova Scotia Continental Shelf.

It must be noted that the large standard deviations associated to the average values of number of sponges per square meter, volume of sponge per square meter, and total number of individuals in the aggregation obtained from Maldonado et al. (2021), when propagated through the scaling up of data to the aggregation level, will lead to a large SD value associated to the average of the global fluxes. As explained in Maldonado et al. (2021), the large SD values of sponge density and volume initially derive from the largest individuals of *V. pourtalesii* being often connected by their bases, forming small clumps of individuals. As a result, even within the most densely populated areas of the

aggregation, some square meters of bottom are devoid of sponges while others contain many. Such spatial pattern, aggregated at a scale <1 m^2, does not affect the accuracy and reliability of the average values derived for the entire extension of the sponge aggregation despite increasing their SD.

RESULTS

Nutrient Flux Rates of Sponges

The two assayed species showed different patterns in the sign of ammonium flux, despite the fact that they were exposed to nearly identical ambient concentrations of this nutrient during the incubations (1.18 ± 1.13 μM for *S. rosea* and 1.23 ± 0.66 μM for *V. pourtalesii*). All assayed individuals of *S. rosea* were net sources of ammonium in their natural habitat. Individual efflux rate ranged from -3.0 to -9.7×10^{-3} μmol mL^{-1} h^{-1}, with an average rate of $-6.5 \pm 2.6 \times 10^{-3}$ μmol mL^{-1} h^{-1} (**Figures 3A,B**, **Table 1**). In contrast, all *V. pourtalesii* incubated *in situ* (**Figure 3A**, **Table 2**: individuals 1–4) were net ammonium sinks ($15.8 \pm 17.4 \times 10^{-3}$ μmol mL^{-1} h^{-1}). During the first laboratory incubation, most of the 11 assayed individuals of *V. pourtalesii* were also net ammonium sinks, except for individuals #7, #9, and #13, which released this nutrient at a rate of -1.4, -9.5, and -23.6×10^{-3} μmol mL^{-1} h^{-1}, respectively (**Figures 3A,B**, **Table 2**, **Supplementary Table 2**). Pairwise tests revealed no statistically significant difference in the average flux rate of ammonium (neither in the rest of nutrients) when measured *in situ* or during the 1st day of laboratory incubations (**Supplementary Table 1**). Therefore, flux rates from *in-situ* and laboratory incubation were pooled, yielding an average rate of ammonium consumption by *V. pourtalesii* of $5.9 \pm 13.5 \times 10^{-3}$ μmol mL^{-1} h^{-1} (**Figure 3A**, **Table 2**). However, it was surprising that after the first laboratory incubation, the ammonium flux started changing in most individuals, which shifted toward net ammonium sources after the third day of incubation and persisted in that condition for the following 4 incubations, to the end of the experiment (**Figure 3C**, **Table 2**, **Supplementary Table 2**). This shift suggests that changes in the population of associated microbes responsible for the ammonium are happening, even if only a few days after the sponges were moved from their natural habitats (see Discussion). Similar shifts in the flux rate of nitrite, nitrate, and phosphate did not occur.

Regarding nitrite, the assayed individuals of *S. rosea* showed insignificant flux rates close to zero that fell below the detection limits of the analysis and, therefore, these sponges cannot be defined as either sinks or sources of nitrite from our incubation approach (**Figure 3**, **Table 1**). In contrast, all *V. pourtalesii* released nitrite during both *in-situ* and laboratory incubations. The nitrite concentration in the sponge habitat was 0.12 ± 0.06 μM and the nitrite release rate during the *in-situ* incubations averaged $-26.6 \pm 5.6 \times 10^{-3}$ μmol mL^{-1} h^{-1} (**Table 2**). The nitrite concentration in the laboratory water was higher (2.22 ± 0.07 μM) than in the natural sponge habitat and the average rate of nitrite release in the laboratory incubation was only slightly smaller than that in field conditions, $-23.4 \pm 10.7 \times 10^{-3}$ μmol mL^{-1} h^{-1} (**Table 2**).

The nitrate flux reflected marked inter-individual differences in both its magnitude and sign, obscuring the identification of a consistent pattern in any of the two assayed species (**Figure 3**). In the natural habitat of *S. rosea*, nitrate concentration was 14.55 ± 0.94 μM. In those conditions, four of the *in-situ* incubated individuals released nitrate at an average rate of $-6.0 \pm 1.8 \times 10^{-3}$ μmol mL^{-1} h^{-1} and three others consumed nitrate at a similar average rate, $5.7 \pm 4.7 \times 10^{-3}$ μmol mL^{-1} h^{-1} (**Figure 3**, **Table 1**). In the case of *V. pourtalesii*, 3 of the 4 *in-situ* incubated individuals, at natural nitrate concentrations of 17.21 ± 1.56 μM, were net sources of nitrate, with a rate of $-3.8 \pm 2.3 \times 10^{-3}$ μmol mL^{-1} h^{-1}. Likewise, most individuals incubated in the laboratory —at the nitrate concentration 7.86 ± 0.15 μM characterizing the laboratory seawater— were also net nitrate sources, rendering a collective average efflux rate of $-3.8 \pm 2.3 \times 10^{-3}$ μmol mL^{-1} h^{-1}. Among the net nitrate consumers there was individual #2, which consumed nitrate during the *in-situ* incubation at a rate

TABLE 1 | Flux of nutrients measured through *in-situ* incubations of *Schaudinnia rosea*.

Code	*Size* (*mL*)	Initial nutrient concentration (μM)				Nutrient flux rate (10^{-3} μmol mL^{-1} h^{-1})			
		NH_4^+	NO_2^-	NO_3^-	PO_4^{3-}	NH_4^+	NO_2^-	NO_3^-	PO_4^{3-}
1	114.8	1.75	0.04	14.15	0.91	−8.2	0.0	−6.7	−7.3
2	287.5	3.29	0.05	14.50	0.67	−3.0	0.0	11.0	0.5
3	143.6	1.61	0.06	14.06	0.79	−9.7	0.1	−4.3	−2.8
4	168.8	0.18	0.06	13.80	0.90	−7.1	0.0	−4.7	−0.8
5	258.7	0.23	0.03	14.04	0.87	−3.0	0.0	−8.2	−0.8
6	120.0	0.72	0.04	14.73	0.91	−6.6	0.0	3.7	−0.4
7	270.0	0.47	0.04	16.57	0.99	−7.8	−0.1	2.4	−3.2
AVG	194.8	1.18	0.05	14.55	0.86	−6.5	0.0	−1.0	−2.1
SD	74.8	1.13	0.01	0.94	0.10	2.6	0.1	6.9	2.6

Seven individuals were incubated (code), their size (mL) determined, and the initial concentration of nutrients (ammonium: NH_4^+; nitrite: NO_2^-; nitrate: NO_3^-; phosphate: PO_4^{3-}) in the chamber measured, along with the detected nutrient flux rate (10^{-3} μmol per hour and mL of sponge tissue). Nutrient flux rates were corrected by the control effect. The average (AVG) and standard deviation (SD) of the set of individual measurements are given in the bottom rows.

TABLE 2 | Summary of nutrient fluxes and associated parameters in the incubations of *Vazella pourtalesii*.

Code	Size (mL)	Initial nutrient concentration (μM)						Nutrient flux rate (10^{-3} μmol mL^{-1} h^{-1})					
		NH_4^+			NO_2^-	NO_3^-	PO_4^{3-}	NH_4^+			NO_2^-	NO_3^-	PO_4^{3-}
		1st	1st-3th	4–7th				1st	1st-3th	4–7th			
1	492.4	0.04	–	–	0.14	15.66	1.08	5.3	–	–	−25.5	−4.0	−0.9
2	64.5	0.12	–	–	0.05	17.35	1.14	41.6	–	–	−33.8	17.0	−0.4
3	126.4	0.08	–	–	0.09	16.51	1.11	11.7	–	–	−20.3	−0.8	−0.5
4	323.4	0.56	–	–	0.19	19.31	1.26	4.7	–	–	−26.7	−2.2	−1.0
5	65.2	1.52	1.71	0.68	2.13	7.91	0.96	9.4	7.0	0.9	−30.2	−2.8	−0.3
6	144.3	1.57	1.73	0.81	2.25	7.84	0.97	7.2	4.7	−4.8	−29.5	−4.6	−0.3
7	104.8	1.62	1.84	0.74	2.20	7.72	0.95	−1.4	2.0	−3.4	−24.8	−7.9	−1.5
8	108.4	1.55	1.58	0.64	2.22	7.73	0.96	9.4	7.7	3.8	−35.8	−6.3	−1.4
9	50.8	1.64	1.76	0.74	2.14	8.01	0.95	−9.5	−10.5	−8.6	−12.1	−3.1	−1.3
10	58.0	1.78	1.76	0.69	2.21	7.89	0.91	5.7	9.5	0.2	−28.0	0.8	0.1
11	86.8	1.56	1.69	0.75	2.40	8.19	0.97	11.9	10.6	−3.7	−35.7	−7.3	−1.3
12	65.2	1.58	1.70	0.72	2.20	7.85	0.96	8.7	5.4	−9.6	−24.0	−5.1	−0.9
13	36.5	1.58	1.80	0.70	2.19	7.88	0.99	−23.6	−22.7	−20.2	−4.1	−1.4	−0.2
14	65.2	1.66	1.77	0.68	2.21	7.81	0.95	2.4	−1.2	−6.9	−25.3	−2.4	−1.6
15	43.6	1.59	1.80	0.76	2.22	7.64	0.99	5.2	−0.3	−9.0	−8.4	−1.7	−1.0
AVG	122.4	1.23	1.74	0.72	1.66	10.35	1.01	5.9	1.1	−5.6	−24.3	−2.1	−0.8
SD	124.1	0.66	0.07	0.05	0.96	4.34	0.09	13.5	9.9	6.5	9.5	5.8	0.5

The table contains reference labels for the 15 incubated individuals, with individuals #1 to #4 corresponding to in-situ incubations and individuals #5 to #15 corresponding to laboratory incubations. It is also given the size of the incubated sponges, the initial concentration (μM) of the dissolved inorganic nutrients (ammonium: $NH4^+$; nitrate: $NO3^-$; nitrite: $NO2^-$; phosphate—PO_4^{3-}) at each incubation event, and the nutrient flux rate (10^{-3} μmol mL^{-1} h^{-1}) detected during the incubation and normalized by incubation duration and sponge biomass. Nutrient flux rates have also been corrected for the control effect. Note that for the laboratory ammonium flux rate, data are presented for only the 1st day of laboratory incubations (1st), then as the individual responses averaged across the first three laboratory incubations (1st–3th), then as the individual responses averaged across the last four laboratory incubations (4th–7th). See also ***Supplementary Table 2*** *for raw data on ammonium flux rate across all laboratory incubations. The global average (AVG) and standard deviation (SD) of the various parameters for the entire set of assayed individuals are summarized at the two bottom rows of the table.*

of 17.0 × 10^{-3} μmol mL^{-1} h^{-1}; individual #10 also consumed nitrate during the laboratory incubations, but at much smaller rate of 0.8 × 10^{-3} μmol mL^{-1} h^{-1} (**Table 2**).

Regarding phosphate, both species were predominantly net sources, but with low rates. Natural phosphate concentration during the *in-situ* incubations of *S. rosea* was 0.86 ± 0.10 μM (**Table 1**). At that nutrient concentration, 6 of the 7 assayed individuals released phosphate, with an average rate of −2.5 ± 2.6 × 10^{-3} μmol mL^{-1} h^{-1} (**Figure 3**). In contrast, individual #2 consumed phosphate at a low rate of 0.5 × 10^{-3} μmol mL^{-1} h^{-1} (**Table 1**). All four individuals of *V. pourtalesii* incubated *in situ* under a natural phosphate concentration of 1.15 ± 0.08 μM released phosphate at an average rate of −0.7 ± 0.3 x 10^{-3} μmol mL^{-1} h^{-1}. Ten of the 11 individuals incubated in the laboratory at a phosphate concentration of 0.96 ± 0.02, that is, similar to the one in the natural habitat, also released phosphate consistently, with an average rate of −1.0 ± 0.5 × 10^{-3} μmol mL^{-1} h^{-1} (**Figure 3**). Individual #10 consumed phosphate at a rate as low as 0.1 × 10^{-3} μmol mL^{-1} h^{-1} (**Table 2**), so that it cannot be discarded that it was indeed inactive in terms of release and that the sign of the flux is an artifact derived from the flux rates being at the limit of the methodological detection.

When the relationship between flux rates was examined by pairs of nutrients using both linear and non-linear regression analyses, no statistically significant relationships were found for *S. rosea* in any case ($n = 7$, $p > 0.05$). In contrast, statistically significant relationships, although of only moderate intensity, were found in *V. pourtalesii* (**Figure 4**). It was detected that the increase in the release rate of nitrite is linearly coupled to an increase in the ammonium consumption ($n = 15$, $R^2 = 0.474$, $p = 0.005$; **Figure 4A**). Another detected relationship was that the rate of nitrate consumption decreased linearly with the increase of phosphate release ($n = 14$, $R^2 = 0.379$, $p = 0.019$; **Figure 4B**).

When the relationship between the flux rate of a nutrient and its ambient concentration was examined by linear regression, no statistical significance was found for any of the nutrients in any of the two sponge species (**Supplementary Figure 1**).

Microbial Insights Into the Sponge Nitrogen Flux

The analysis of amplicon sequences sampled from *V. pourtalesii* and *S. rosea* showed that each species harbors a distinct microbiome (**Figure 5**, **Supplementary Table 3**, **Supplementary Data File 1**). In each case, there are also statistically significant differences between the sponge microbiome and that of the surrounding seawater. Microbiome differences between *V. pourtalesii* and *S. rosea* may be responsible for some of the between-species differences detected in the sign

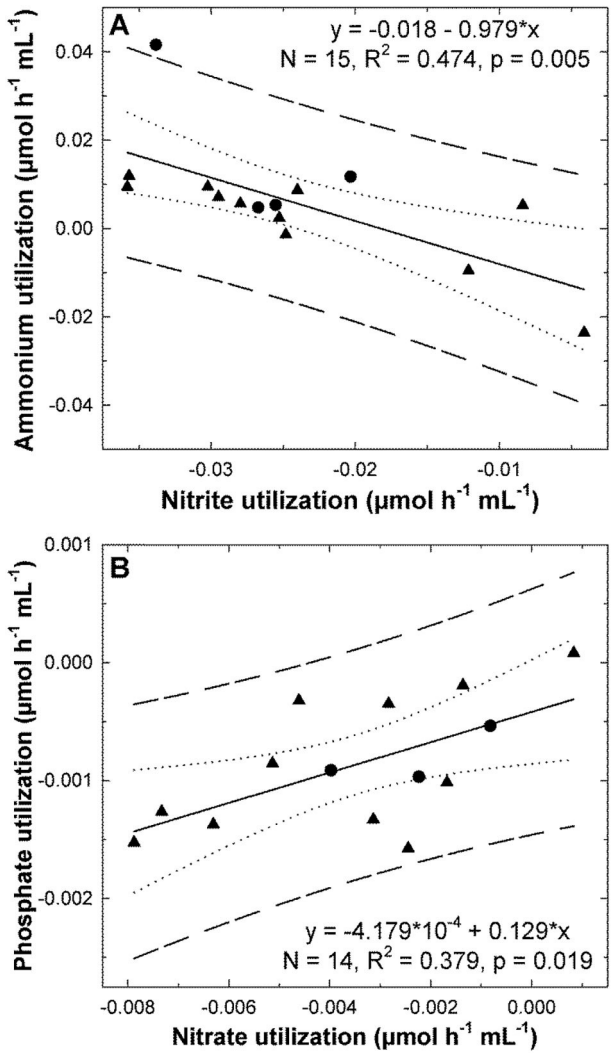

FIGURE 4 | Significant relationships between nutrient fluxes in *Vazella pourtalesii*. **(A)** The lower the rate of nitrite release, the higher the ammonium consumption. **(B)** When individual #2, an atypical outlier consuming nitrate at the abnormally high rate of 17 nmol mL^{-1} h^{-1} —rather than releasing it–, was excluded from the analysis, a linear significant relationship was revealed between the release rates of nitrate and phosphate. The rest of possible pairwise combinations among the flux rates of all four nutrients were also examined, but none had statistically significant support.

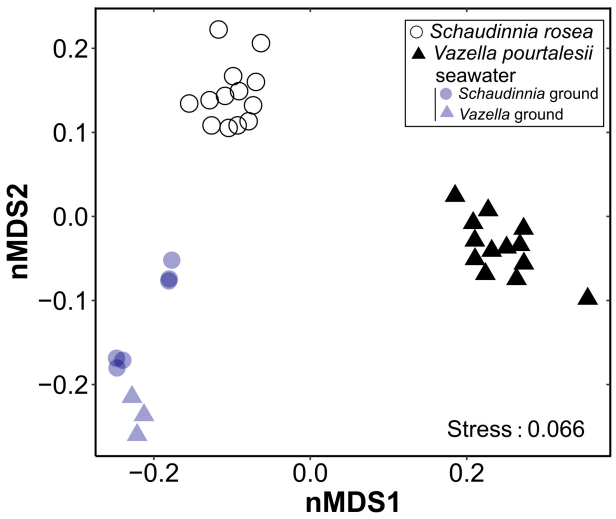

FIGURE 5 | Non-metric dimensional scaling (nMDS; $k = 2$, maxit = 100) plot on weighted UniFrac distances for each of the assayed sponge species, *Vazella pourtalesii* and *Schaudinnia rosea*, and the seawater of their respective habitats. The results of the PERMANOVA tests that gives statistical support to the between-group differences is given in **Supplementary Table 3**.

and magnitude of the flux of the various nutrients (**Figures 3A,B**, **Tables 1**, **2**).

Microbes of the Nitrogen Cycle in *V. pourtalesii*

We evaluated the potential metabolic functions of *V. pourtalesii*-associated microbes involved in the nitrogen cycle by searching for key enzymes in the MAGs, which allows the assignment of function to members of the microbiome. For enzymes or functions encoded on contigs that were not sorted into specific MAGs, we assumed that the function might be present in the microbial community (**Supplementary Table 4**). Genes involved in nitrification, denitrification, dissimilatory nitrate reduction, nitrogen fixation and ammonia assimilation were identified. Genes encoding for anammox or assimilatory nitrate reduction were found neither in MAGs nor in the unbinned metagenomic data.

Nitrification

The enzyme ammonia-monooxygenase (AMO), responsible for the first reaction in the first step of nitrification (i.e., oxidation of ammonia to hydroxylamine), was detected in the Nitrosopumilaceae (Crenarchaeota, MAGs 74, 90, 131, 143) and in the Nitrosomonadaceae (Proteobacteria, MAG 46). This microbial metabolism may contribute to explain why most individuals of *V. pourtalesii* were essentially net consumers of ammonium. After 3 incubation steps in the laboratory using coastal water, all *V. pourtalesii* individuals became net sources of ammonium. Thus, we cannot discard the possibility that the Nitrosopumilaceae and Nitrosomonadaceae populations decayed in laboratory seawater because being highly dependent on the seawater/holobiont conditions of the natural habitat (see Discussion). Interestingly, the MAGs enriched in *V. pourtalesii* compared to seawater (**Supplementary Table 4**, **Supplementary Data File 2**) include the genus *Cenarchaeum* (MAGs 74, 90, 143), which is a common sponge-specific AOA symbiont. MAG 131 was found in equal abundances in both habitats and represents the genus *Nitrosopumilus*, a common sea-water AOA. The hydroxylamine-oxidoreductase (HAO), responsible for the second reaction in the first step of nitrification converting hydroxylamine to nitric oxide that is subsequently converted to nitrite by a not yet identified enzyme (Caranto and Lancaster, 2017), was not detected in

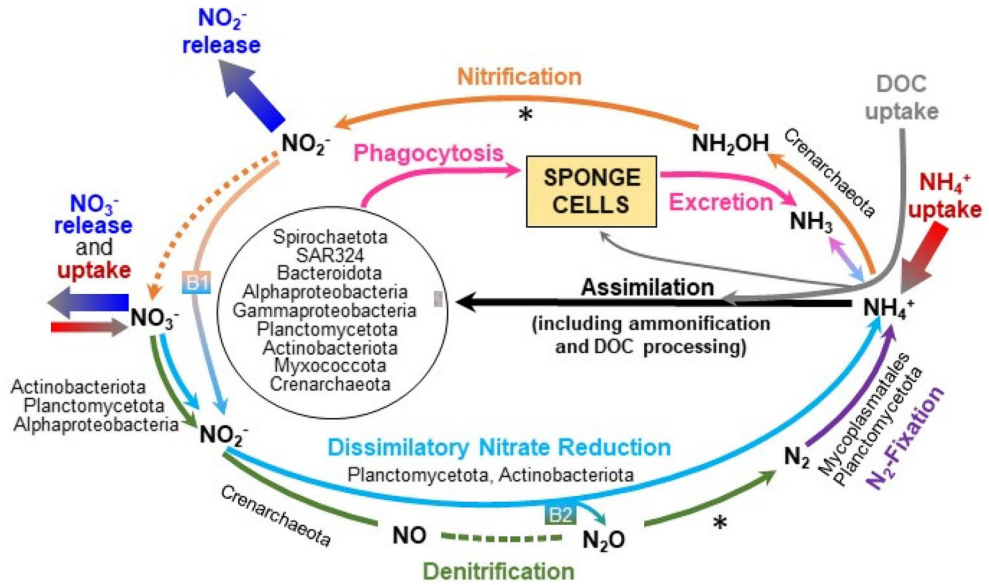

FIGURE 6 | Graphical summary of the microbiome-driven nitrogen cycle in *Vazella pourtalesii,* as it has been deduced through the metagenomic study and the incubation experiments. Note that only those N pathways for which MAGs were found to be enriched in the sponge are named in the graph. The dashed lines indicate enzymatic pathways for which genes were not detected and the asterisk (*) indicates genes that were present only in the unbinned data. "B1" and "B2" refer to putative bridges between major biochemical pathways, which provide alternative routes to palliate the effects of some missing enzymes, also allowing an efficient closing of the N cycle in the holobiont. The N microbial engine of *V. pourtalesii* appears to revolve around the incorporation of ammonium from the seawater and its internal recycling. This nutrient fosters N assimilation by the sponge microbiota, which also benefits from the important amounts of DOC taken up by the sponge. All available evidence suggests that the nourishment of *V. pourtalesii* does not appear to be based on filter feeding of the free-living bacterioplankton but rather on the phagocytosis of its internal microbiota, which is mostly farmed in the bacteriosyncytia through the supply of ammonium and DOC.

the MAGs. However, *haoB*-related genes were found in the unbinned metagenome data, suggesting that this enzyme may be present in at least some of the microbial lineages and that nitrite is produced out of ammonia/ammonium. Genes responsible for nitrite oxidation, the second step of nitrification, were found neither in MAGs nor in the unbinned metagenomic data. The lack of those enzymes would explain why nitrite, which appears not to be further processed in the nitrification pathway (**Figure 6**), is released at high rate by *V. pourtalesii* (**Figure 3**, **Table 2**, **Supplementary Tables 1, 2**). The occurrence of ammonia oxidation activity in the absence of nitrite oxidation was in agreement with the finding that ammonium consumption and nitrite release are activities associated with statistical significance in *V. pourtalesii* (**Figure 4A**).

Denitrification

Genes encoding enzymes involved in two of the four reactions of the denitrification pathway were found in the microbiome of *V. pourtalesii.* Genes annotated as nitrate reductase, which catalyze the reduction of nitrate to nitrite, were found in three MAGs (**Supplementary Table 4**) assigned to Alphaproteobacteria (MAG 70), Actinobacteria (MAG 64), and Planctomycetota (MAG 52). All three MAGs were enriched in the sponge compared to seawater. Yet, the sources of nitrate to initially feed denitrification remain unclear, since nitrification cannot be completed in *V. pourtalesii* and external nitrate was not consistently incorporated from seawater by all assayed individuals, only a minority of them being net nitrate consumers (**Figures 3**, **6**, **Table 2**). The genes *nirS and nirK* encoding the nitrite reductase that catalyzes the conversion of nitrite into nitric oxide were detected in five MAGs belonging to Crenarchaeota (MAGs 36, 90, 101, 131, 143) and in the acidobacterial MAG 86. The MAGs 90 and 143 were enriched in *V. pourtalesii* over seawater. Regarding the last two reactions of denitrification that lead to production of molecular N_2 gas, we could not detect the genes encoding for the nitric oxide reductase and nitrous-oxide reductase enzymes in the MAGs, but the gene for the latter was present in the unbinned data (**Figure 6**). Given that nitrite is accumulated by an incomplete nitrification and released by the sponges at relatively high rates (**Figure 3**), it cannot be discarded that part of the accumulated nitrite can be used to feed the denitrification pathway at its intermediate step (**Figure 6**) and also the pathway of dissimilatory nitrate reduction to ammonium, as it is explained in the section below.

Dissimilatory Nitrate Reduction to Ammonium (DNRA)

We detected genes involved in DNRA, which is an important intermediate process in the N cycling, linking N-compound oxidation and reduction processes, that is, operating at the oxic-anoxic interface. Genes coding for nitrate reductase —which may operate not only in the DNRA pathway but also in the previously described denitrification pathway— were found in three MAGs (**Supplementary Table 4**) of Alphaproteobacteria (MAG 70), Actinobacteria (MAG 64), and Planctomycetota

(MAG 52). All three MAGs were enriched in the sponge compared to seawater. The second step in the dissimilatory reduction to ammonium is mediated by two enzymes. One is a respiratory cytochrome c nitrite reductase, encoded by genes *nrfA/ H,* which was detected only in the unbinned metagenomic data (**Supplementary Table 4**). The other is a NADH depended nitrite reductase encoded by the genes *nirB/ D*, detected in four MAGs affiliated with Planctomycetota (MAGs 52, 99), Actinobacteria (MAG 64), and Gammaproteobacteria (MAG 89), although the latter was not significantly enriched in *V. pourtalesii* over seawater. These features agree with the idea that the holobiont metabolism of *V. pourtalesii,* in its natural habitat, tends to produce internally ammonia/ammonium, which appears to be subsequently used as a preferred substrate to sustain the populations of archaea and bacteria of the microbiota (**Figure 6**). Note that only some of the assayed individuals of *V. pourtalesii* incorporated nitrate from seawater (**Figures 3**, **6**). Therefore, it is assumed that the DNRA pathway is mostly fed with nitrite at an intermediate step, using for that purpose part of the nitrate accumulated after the incomplete nitrification (**Figure 6,** B1 arrow). This bridging mechanism is relevant because it connects the aerobic process of nitrification to the anaerobic process of DNRA and it would provide an explanation of the withstanding of *V. pourtalesii* to low oxygen conditions.

Nitrogen Fixation

Genes for nitrogenase enzymes involved in N fixation through reduction of N_2 gas to NH_4^+ were detected in several MAGs (**Figure 6**, **Supplementary Table 4**) affiliated with Firmicutes (MAGs 77, 88, 127), Planctomycetota (MAG 91), Bacteroidota (MAG 24), and Alphaproteobacteria (MAG 135). The MAGs 88 and 91 were enriched in *V. pourtalesii* over seawater. Note that if the incomplete denitrification process previously identified in *V. pourtalesii* can be completed somehow by the sponge microbiome (see Discussion from bridging between DNRA and denitrification), the resulting N_2 could well provide substratum for this N-fixation pathway (**Figure 6**).

Ammonia Assimilation

The enzymes glutamine synthetase (*glnA, GLUL*) and glutamate dehydrogenase (*gudB, rocG*) were found in the MAGs of several members of the *V. pourtalesii*-microbiota (**Supplementary Table 4**), indicating that amino acids can be formed from ammonia. MAGs enriched in *V. pourtalesii* were affiliated with the phyla Alpha- and Gammaproteobacteria, Spirochaetota, Crenarchaeota, Planctomycetota, SAR324, Actinobacteriota, and Verrucomicrobiota (**Figure 6**; **Supplementary Table 4**, **Supplementary Data File 2**). Again, these findings support the notion that the pool of ammonium within the sponge, which consists of the ammonium excreted by the sponge cells (i.e., ammonia that undergoes molecular auto-ionization to ammonium and amide ions) plus that produced by the denitrification and DNRA pathways and that taken up from seawater, serves as a preferred substratum to sustain the growth of the bulk of the microbiota in *V. pourtalesii*.

Identification of Genes and Microorganisms of the Phosphorus Cycle

We searched for enzymes involved in the phosphorous cycle in the annotation data derived from the *V. pourtalesii* microbiome to elucidate which members might be responsible for the low but consistent release of phosphate detected in the sponges (**Figure 3**, **Table 1**). Components of the C–P lyase multienzyme complex were found (**Supplementary Table 4**, **Supplementary Data File 2**). This complex is encoded by 14 genes (*phnCDE, phnF, phnGHIJKLM*) and catalyzes the dephosphonation reaction in a range of structurally diverse phosphonates, that is, organophosphorus compounds containing C-PO(OX)$_2$ groups, where "*X*" is either H or an alkyl or aryl radical. Phosphonates are one of the sources of phosphate intake into cells. The dephosphonation reaction by biological vias (i.e., enzymatically) is physiologically relevant because the C-P bond is extremely stable and its cleavage by chemical vies requires very aggressive conditions. Enzyme subunits of the C–P lyase complex were found only in MAG 124 belonging to Alphaproteobacteria, but the detection in the unbinned data suggests that more members in the microbiome may be using this enzyme for phosphonate utilization. This assumption is supported by the detection of subunits of the ABC transporter in several MAGs representing different phylogenetic groups (**Supplementary Table 4**). The predominant biogenic orthophosphate in nature is 2-Aminoethylphosphonate (2AEP) and its utilization is a two-step process. The first step is the transamination of 2AEP (+ pyruvic acid) to 2-phosphoacetaldehyde (PAA) and L-alanine (Ternan et al., 1998). This enzyme was found in several MAGs (**Supplementary Table 4**) of which members of Planctomycetota (MAGs 52, 94, 116, 119), Crenarchaeota (MAGs 74, 90, 143), Alphaproteobacteria (MAG 75), and Gammaproteobacteria (MAG 10) were enriched in the sponge. The second step is the hydrolytic cleavage of PAA in phosphate and acetaldehyde mediated by the enzyme phosphonoacetaldehyde hydrolase. This was found only in two *V. pourtalesii*-enriched MAGs (52, 119) representing Planctomycetota.

The enzyme phosphonoacetate hydrolase is a alkaline phosphatase, cleaving C-P bounds of a given substrate to form acetate and phosphate (reviewed in Villarreal-Chiu et al., 2012). This was found in one *V. pourtalesii*-enriched member of Planctomycetota (MAG 121) and in several MAGs of different phylogenetic groups (**Supplementary Table 4**). Collectively, the results suggest that part of the sponge microbiota use phosphonates as a source of phosphorous to grow and, through this activity, the sponge gets help in the hard task of degrading phosphonates. The level at which this process explains the net phosphate efflux from the sponges remain unclear from our approach and more research is needed to better understand the P circuit in the holobiont.

Ultrastructural Observations

The histological study of *S. rosea* and *V. pourtalesii* indicated that the tissue in these hexactinellids is a delicate network of thin strands through which the large silica pieces of the skeleton and

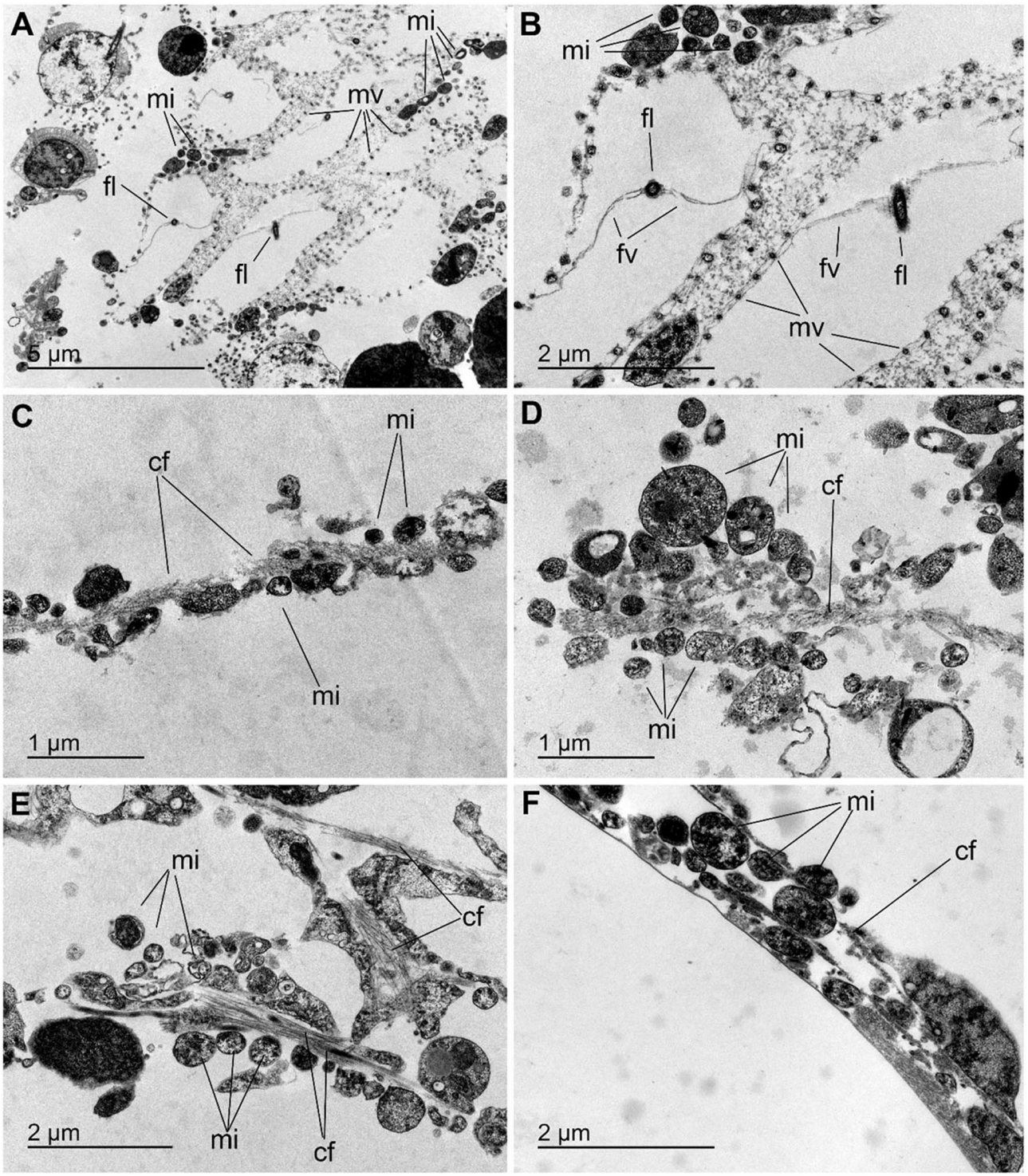

FIGURE 7 | Microbes in *Schaudinnia rosea.* **(A,B)** View of flagellated chambers showing the collar bodies with their microvilli (mv) and a flagellum (fl) provided with flagellar vanes (fv). Small groups of prokaryotic microorganisms (mi) occur intracellularly associated to the thin cytoplasmic zones sandwiched between the microvilli of adjacent collar bodies. **(C–F)** Views of small groups of microbes (mi) that gather around the packs of collagen fibrils (cf) that run across the thin mesohyl bands located within the trabecular strands of the sponge body.

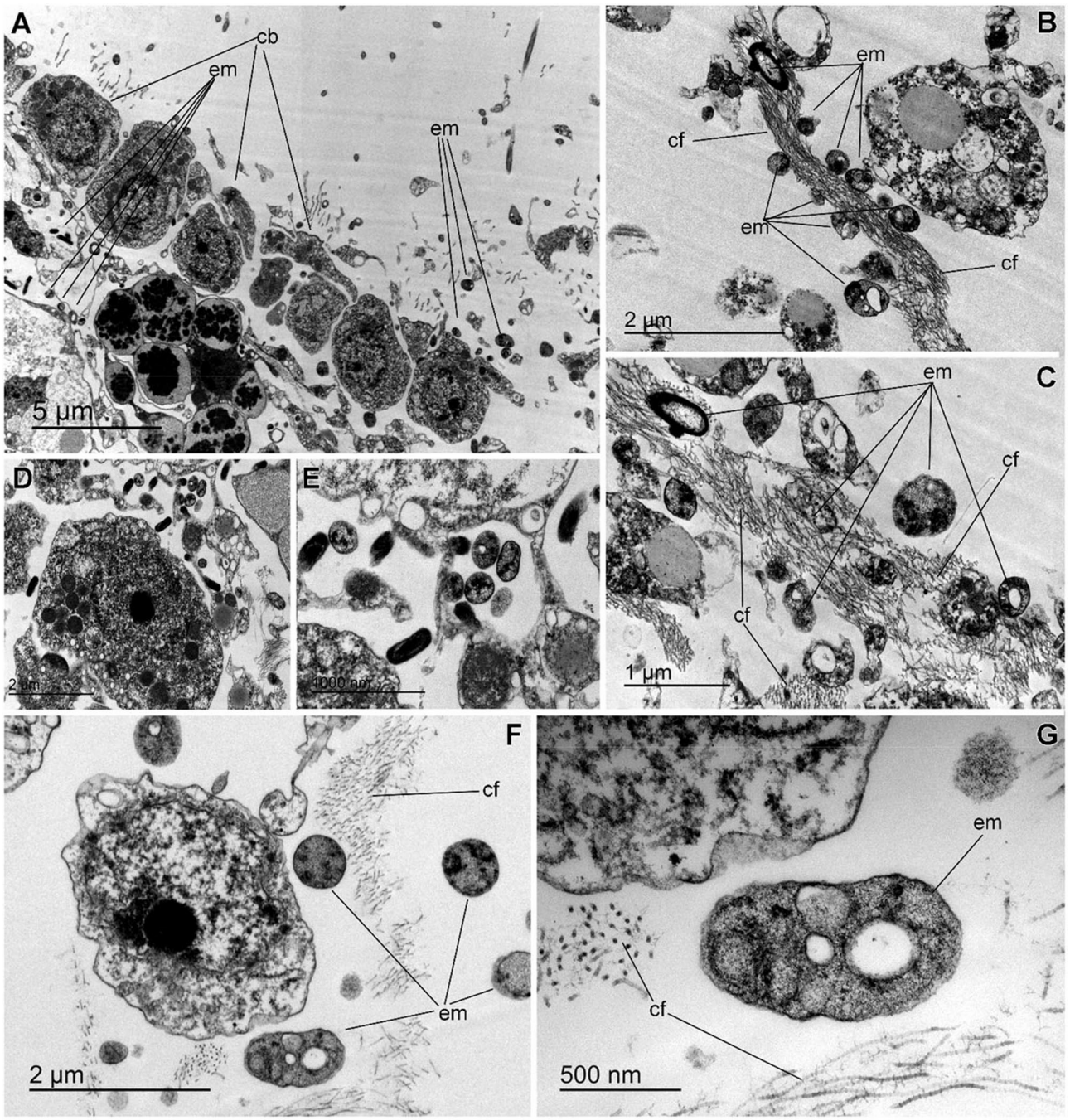

FIGURE 8 | Extracellular microbes in *Vazella pourtalesii.* **(A)** Partial view of flagellated chamber, showing the collar bodies (cb) and the underlying trabecular tissue, which is relatively poor in extracellular microbes (em). **(B,C)** Images showing that, in the mesohyl, the extracellular microbes (em) often proliferate in close association to accumulations of collagen fibrils (cf). **(D,E)** Two enlargements of a zone of the trabecular tissue where electron-dense rod-like microbes occur adjacent to coccoid microbes contained intracellularly into a cytoplasmic vesicle of a sponge cell. **(F)** Comparative view of different microbial morphologies, typically characterized by a variety of electron-clear and/or electron-dense granules and cell sizes smaller than 1 µm. **(G)** Detail of an unidentified extracellular microbial cell (em) showing a variety of intracytoplasmic granules. Note the collagen fibrils (cf) around the microbe.

ample aquiferous spaces run. The ultrastructural TEM approach revealed that extracellular microbes of both coccoid and rod-like shape are scattered in both species, but at low density (**Figures 7**, **8**). In *S. rosea*, small groups of microbes were also found intracellularly in the thin cytoplasmic bands that separate the microvilli of adjacent collar bodies (**Figures 7A,B**). However,

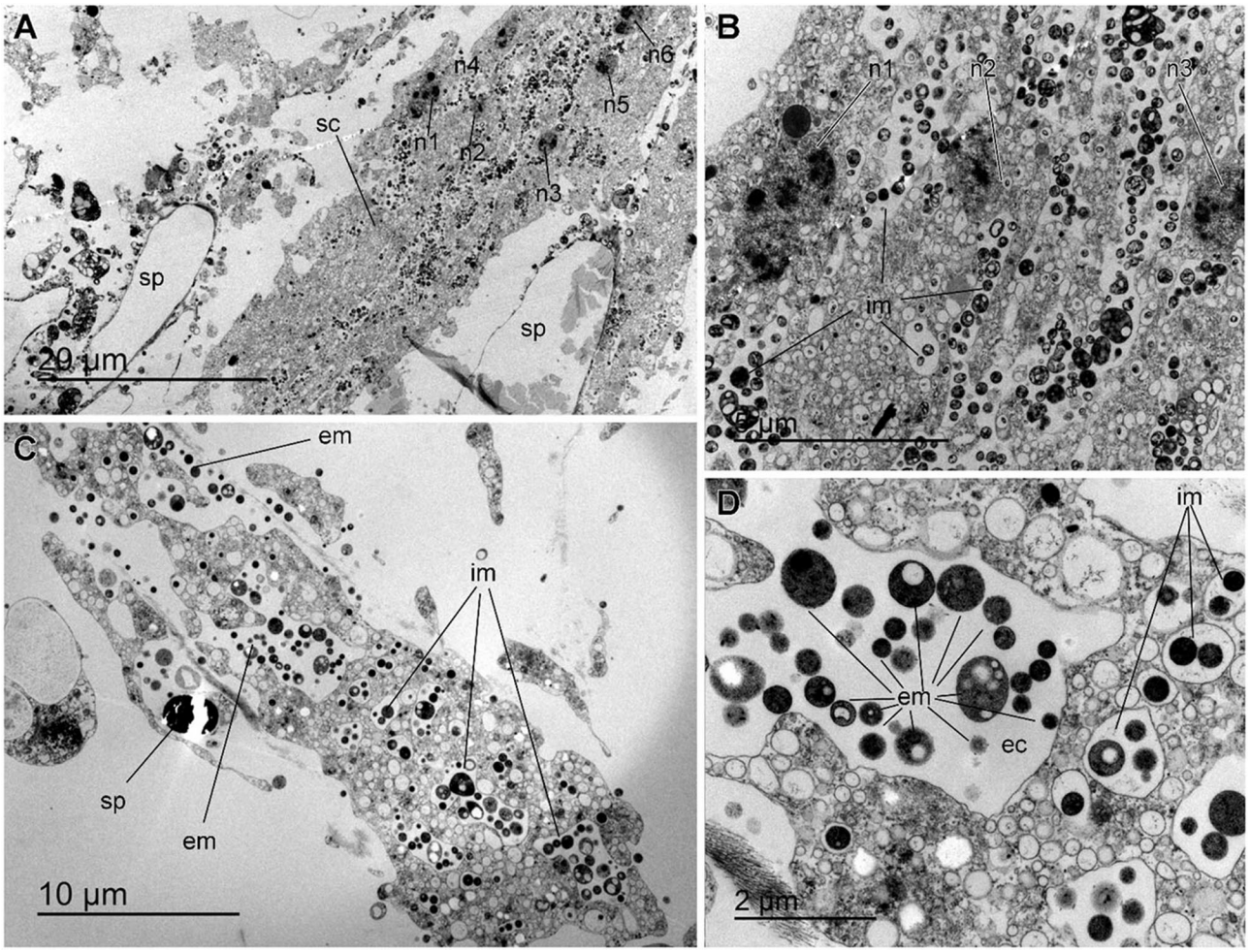

FIGURE 9 | Bacteriosyncytia in *Vazella pourtalesii*. **(A)** Partial general view of a bacteriosyncytium (sc) in which six nuclei (n1 to n6) can be seen, along with many intracellular microbes (im). The cell is in a tissue zone where the whole of two large spicules (sp) occurred before we desilicified them for tissue sectioning. **(B)** Enlargement of a zone of the **Figure 8A** in which nuclei n1 to n3 can be seen along with large abundance of intracellular microbes within membrane-bound vesicles. **(C)** Partial general view of bacteriosyncytium, showing abundant intracellular microbes (im), along with abundance of extracellular microbes (em), which proliferate around the syncytium and particularly in the valleys formed by the pseudopodia of the bacteriosyncytium. Because this tissue was not desilicified for sectioning, remains of a silica spicule (sp) can be seen by the side of the bacteriosyncytium. **(D)** Enlargement of **Figure 8C** detailing the variety of sizes and ultrastructure of intracellular microbes (im) within membrane bound vesicles in the cytoplasm of the bacteriosyncytium. Note the presence of extracellular microbes (em) in a large extracellular cavity (ec) formed among the pseudopodia of the bacteriosyncytium.

most of the small groups of microbes occurred extracellularly, associated to the collagen fibrils of the mesohyl matrix in the thin trabecular strands (**Figures 7C–F**, **8**). The relative paucity of extracellular microbes across most of the studied tissue in both sponge species suggested that the extracellular microbial populations are too poor as for being entirely responsible by themselves for the important N fluxes detected in the sponges, particularly in *V. pourtalesii*. In this regard, we discovered large (>70 µm) amoeboid, multinucleate syncytia in *V. pourtalesii*, which are charged with high density of microbes (i.e., archaea and bacteria) in a variety of morphological types. Most of them were coccoid forms smaller than 0.8 microns in their largest diameter (**Figures 9**, **10**). To our knowledge, this is the first description in hexactinellid sponges of a cytological system specialized in holding microbes. These hexactinellid cytological system is herein referred to as bacteriosyncytia, being the cytological analogous of the non-syncytial bacteriocytes known from demosponges (e.g., Maldonado, 2007). It is worth noting that the microbes were not in direct contact with the cytoplasmic environment of the bacteriosyncytia but they were included in a membrane-bound vesicle. Each vesicle contained one or few bacteria from either identical or different morphological types. Most bacteria contained one to several intracytoplasmic granules and compartments. At the present moment, a correspondence between the microbial morphotypes and the genome-defined groups remains uncertain. Importantly, many of the microbes in the vesicles appeared to be partially degraded or digested, suggesting that the sponge

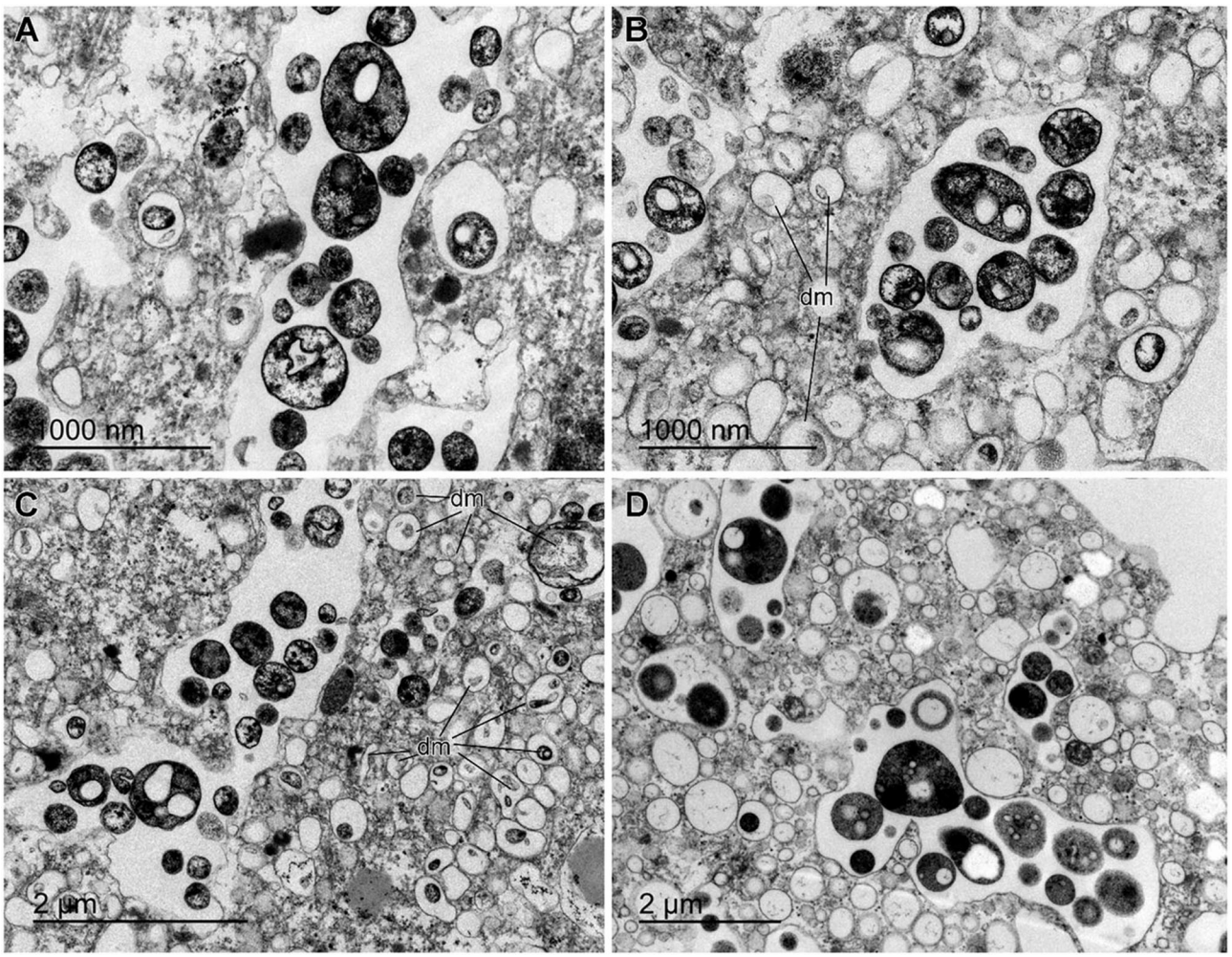

FIGURE 10 | Details of bacteria in the bacteriosyncytia of *Vazella pourtalesii*. **(A–D)** Diversity of intracellular microbes hosted in either individualized or collective membrane-bound vesicles. Coccoid cell shapes predominate, typically characterized by one or several granules and inclusions. Documented microbial sizes rarely exceed 0.8 µm in the largest diameter. Some of the microbes appear to be degraded or digested within the vesicles (dm).

is feeding at some point on the microbes farmed into the bacteriosyncytia (see Discussion). It was also documented that the microbes proliferated in abundance extracellularly but only in the close periphery of the bacteriosyncytia (**Figures 9C,D**: em), and particularly in the valleys formed by the large pseudopodia emitted by the bacteriosyncytia. Bacteriosyncytia were not detected in *S. rosea*, but a more extensive body sampling would be required to definitively discard their occurrence.

Nutrient Utilization Throughout the Hexactinellid Grounds

Annual flux rates for the several studied nutrients through the aggregations of *V. pourtalesii* on the Scotian Shelf were estimated (**Supplementary Data File 2**) from the average flux rates depicted in **Figure 3A**. It was calculated that the sponge grounds consume annually 144.8 ± 334.2 × 10^6 mole of ammonium, while simultaneously releasing 594.2 ± 232.2 × 10^6 mole of nitrite, 93.2 ± 66.1 × 10^6 mol of nitrate, and 20.5 ± 12.8 × 10^6 mole of phosphate (**Figure 11**).

DISCUSSION

Net Flux of Nutrients and Ecological Implications

The analysis of the net flux of nutrients reveals several patterns: (1) the processing of ammonium and nitrite appears to be markedly different between the two investigated hexactinellid species, despite *V. pourtalesii* and *S. rosea* being phylogenetically related as members of the family Rossellidae; (2) both species are consistently small sources of phosphate, a pattern also in agreement with nearly all studies on demosponges; and (3) both species have strong inter-individual differences in the magnitude and sign of the nitrate flux, with some individuals being net sources and others being net sinks.

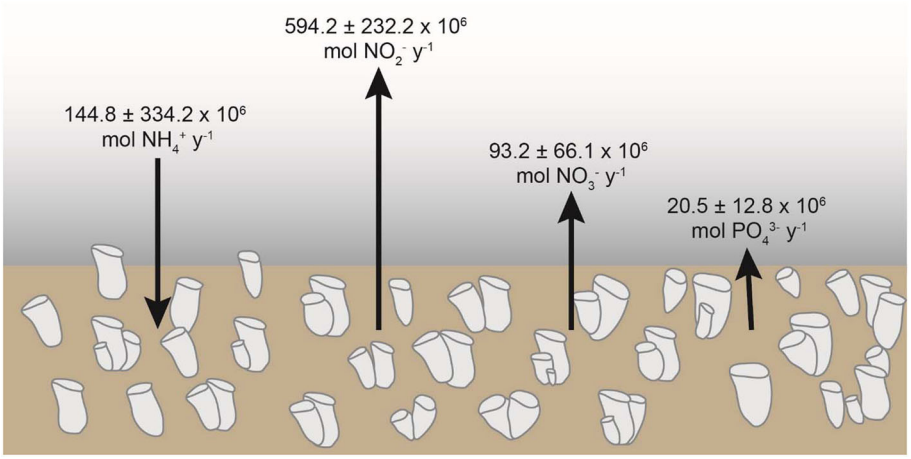

FIGURE 11 | Summary of the annual net flux of ammonium (NH_4^+), nitrite (NO_2^-), nitrate (NO_3^-), and phosphate (PO_4^{3-}) across the aggregations of *Vazella pourtalesii* at the Scotian Shelf (Canada).

Another interesting feature is that most individuals of *V. pourtalesii* shifted from being net consumers of ammonium to being net releasers after a few days exposed to the laboratory conditions (**Figure 3C**). Those conditions included the use of coastal seawater with similar temperature and ammonium concentration than those in the natural habitat of the sponges but twice nitrite concentration and half of nitrate (**Supplementary Table 2**). This coastal water, close to the big city of Halifax, is also assumed to be characterized by different populations of microbes in suspension and higher quantities of total organic matter than available in the natural offshore habitat. Unfortunately, neither the microbial populations in the laboratory seawater nor in the tissue of the laboratory-maintained sponges were investigated after the experiments. Therefore, because of several uncontrolled factors, the exact reasons of the shift in the ammonium flux remain unclear. One of the most plausible hypotheses is that the original composition of the sponge microbiota associated to the processing of ammonium experienced a progressive detrimental shift after being exposed for to laboratory water. A mechanism for that process would be a much higher level of oxygenation of the seawater (95% in laboratory water versus <43% in the sponge habitat), which may favor the colonization of the sponge tissue by lineages of coastal microbes, which would displace part of the original microbiota. If this is so, it means that the functional integration between the sponge and the microbes involved in the ammonium routes is more delicate and habitat-dependent than that involved in the phosphate metabolism. In line with this view, a recent study revealed significant differences in the microbiota between individuals of *V. pourtalesii* grown on natural substrata and individuals grown on adjacent artificial substrata that raised a mere couple of meters from the sea bottom (Busch et al., 2021). The individuals growing on the artificial substratum were significantly enriched in Bacteroidetes, Verrucomicrobia and Cyanobacteria compared to those growing on natural substrata. In the only two other hexactinellid sponges where nutrient fluxes have been investigated so far, *Aphrocallistes vastus* (Fam. Aphrocallistidae) and *Rhabdocalyptus dawsoni* (Fam. Rossellidae), ammonium was released by both species (Yahel et al., 2007). The flux determination in both species was conducted by the in-ex methods, which yielded instant flux rates of 0.201 ± 0.128 μmol L^{-1} and −0.388 ± 0.068 μmol L^{-1}, respectively. Those nutrient instant rates can be neither compared to those measured in our incubations nor scaled up to the entire sponge populations.

When the net flux rate of ammonium consumption by *V. pourtalesii* was scaled up through the extension of the sponge aggregations on the Scotian Shelf, an annual ammonium demand of 144.8 ± 334.2 $\times 10^6$ mole (some 2.6 million kg; **Figure 11**) was estimated. The significance of this figure emerges more clearly when the hourly rate of ammonium consumption by *V. pourtalesii* (5.9 μmol L^{-1} of sponge tissue h^{-1}) is compared to the ammonium consumption (47 × 10^{-3} μmol L^{-1} of seawater h^{-1}) measured for the marine plankton community (bacterioplankton + phytoplankton) of a coastal area in the eutrophic Baltic Sea (Klawonn et al., 2019). The comparison reflects that a *V. pourtalesii* individual of 1 liter in body volume consumes about three orders of magnitude more ammonium than the entire plankton community in a liter of eutrophic coastal seawater, which, in turn, is known to have higher rates than those of the plankton community in worldwide oceanic and estuarine systems (Klawonn et al., 2019). This incorporation of external ammonium by the sponges to fuel the internal microbiota is not ecologically inconsequential, since it may decrease the ammonium availability for the free-living microbial populations in the seawater of the sponge habitat. Indeed, the ammonium concentration at the sponge habitat is abnormally low, ranging from 0.04 to 0.56 μM (**Table 2**). Ammonium being one of the main N nutrient of the bacterioplankton, its depletion through the sponge uptake is assumed to have negative effects on the development of the bacterioplankton community. A poor free-living bacterioplankton community in the demersal water mass around the aggregations of *V. pourtalesii* would decrease the feeding chances for those sponge species that do

not farm their bacteria internally but that rather rely on the filter feeding of external bacterioplankton and picophytoplankton. In line with this view, it has recently being found (Bart et al., 2020) that the bulk energy for the aerobic metabolism of *V. pourtalesii* is not provided by the filter-feeding of the free-living bacterioplankton (only about 10%). Rather, the sponge appears to largely rely on the uptake of dissolved organic matter (about 90%), a carbon source that can be likely processed by both the internal microbiota and the sponge cells (**Figure 6**), as also demonstrated for demosponges (Rix et al., 2020). Therefore, most of the available evidence suggests that the remarkable incorporation of ammonium by *V. pourtalesii* may result in a nutritional competitive exclusion of other sponge species and this may be one of the reasons why the aggregations of *V. pourtalesii* are markedly monospecific. This view is also supported by indirect evidence on other hexactinellid species. For instance, *Schaudinnia rosea,* characterized by low microbial abundance, and *Aphrocallistes vastus*, which apparently lacks an associated microbiota, both release ammonium and both form multispecies sponge assemblages rather than monospecific aggregations. It has already been corroborated that *A. vastus* heavily relies on filter-feeding of external bacteria and other picoplankton, with negligible energetic contribution by incorporation of dissolved organic matter (Yahel et al., 2007; Kahn et al., 2018). Certain groups of filter-feeding organisms, such as bivalves, are known to have large filtration ability (up to 100 m^3 m^{-2} d^{-1}) for phytoplankton, an activity that has been shown to regulate directly primary production in the local systems where bivalves thrive (Kimmerer et al., 1994). The energy requirements estimated for several species of shallow-water sponges have revealed that some of them must process particles at the same order of magnitude as some bivalves (reviewed in Gili and Coma, 1998). The ecological effects of such sponge activity have seldom been quantified in terms of food limitation, but there is indirect evidence of their ecological relevance. For instance, picoplankton is frequently depleted in the water layer overlying coral reefs and the filter-feeding activity of sponges has been suggested to be one of the main drivers (de Goeij and Van Duyl, 2007; Nelson et al., 2011). In summary, despite growing suspicion that competition by particulate food may be a relevant factor in the sponge aggregations, the process has not yet being properly quantified in any aggregation and its role remains poorly understood (Maldonado et al., 2017).

Regarding nitrite, the notable release rate by *V. pourtalesii* (i.e., 24.3 μmol per liter of sponge tissue and hour, and some 27.3 million kg at the sponge ground level annually) is also thought to be of some ecological significance. The nitrite is an intermediate product used as a source of nitrogen by the phytoplankton and, in a more important way, by the bacterioplankton. Because in seawater the nitrite concentration is typically low, the important nitrite release by the sponges is expected to favor the co-existence of different populations of nitrifiers, avoiding the typical competitive exclusions driven by low nitrite + low ammonium availability (Zakem et al., 2018). A majority of HMA demosponges consume ammonium and release nitrite (Scheffers et al., 2004; Jiménez and Ribes, 2007; Morganti et al., 2017), just as *V. pourtalesii* does. From this perspective, and given that the bacteriosyncytia contain large amounts of microorganisms, *V. pourtalesii* would be functionally closer to HMA demosponges and *S. rosea* to LMA demosponges, but without actually fitting in such categories. Although bacteriosyncytia have not been detected in our TEM exploration of *S. rosea*, additional studies involving sampling of more individuals and more body regions would be required to discard their occurrence definitively.

The nitrate released by the *V. pourtalesii* ground (93.2×10^6 mol or some 5.8 million kg) is of far lower magnitude than the nitrite release, with most of its further consumption being expected to be due to the phytoplankton community once the nitrate rich demersal water of the sponge ground is uplifted to the photic zone by any of the advective processes contributing to water mixing on continental shelves.

The phosphate release in the two hexactinellid species herein investigated agrees with the only other measurement available for Hexactinellida, which reported in *Aphrocallistes vastus* a low release of phosphate at instantaneous rates of $35 \pm 80 \times 10^{-3}$ μmol L^{-1} (Yahel et al., 2007). Low rates of phosphate release have also been detected in most investigated demosponges (Maldonado et al., 2012; Ribes et al., 2012; López-Acosta et al., 2019). Through the entire sponge ground of *V. pourtalesii*, we have estimated an annual release of 20.5×10^6 mol of phosphate, which represent some 1.9 million kg of phosphate. Because phosphate is known to be a limiting nutrient in many bacterioplankton and phytoplankton communities (Smith, 1984; Brembu et al., 2017), the low but continuous release of phosphate by sponges is expected to have positive effects on the development of microplankton communities at the regional scale.

In our study, we found no significant relationship between nutrient flux rate and ambient concentration for any nutrient in any of the two species (**Supplementary Figure 1**). One of the reasons is that, at the time of our sampling, the between-site variation in the ambient concentration of the investigated nutrients in the bottom seawater of the sponge grounds was minimal (**Tables 1**, **2**). However, changes in concentration may occur between summer and winter conditions (Petrie et al., 1999; Maldonado et al., 2021). Future studies would be advisable to evaluate how episodic and/or seasonal changes in the biogeochemistry of the sponge habitat may affect the net nutrient fluxes of the sponges and the composition of their microbiome. Investigations of nutrient flux rates in different populations and/or subpopulations of the HMA, Caribbean demosponges *Xetospongia muta* and *Ircinia felix* revealed between-site differences in the ambient concentration of inorganic nutrients and also in the magnitude and sign of the flux rate for some of those nutrients (Fiore et al., 2013; Archer et al., 2017). Despite the absence of information on the plausible between-site differences in the microbiome of those sponges, the studies concluded that functioning as sink or source was mostly a direct response of the sponges to the differences in the ambient concentration of the nutrients. Nevertheless, our findings on the metabolic intricacies of the sponge microbiome suggest that the underlying mechanism behind the sponge holobionts shifting from being sources to sinks or vice versa for a N nutrient must involve more complex

processes than a mere modest change in the ambient nutrient concentration. The idea that nutrient flux rates in HMA sponges can somehow be predicted from ambient nutrient concentrations neglects the metabolic and physiological complexity behind such flux rates: there will always be biological confounding factors seriously interfering the mathematical relationship between the two parameters of the regression. For instance, in the case of the ammonium flux rate in *V. pourtalesii*, the important incorporation of external ammonium by the sponges suggested, *a priori*, a negative correlation between consumption rate and ambient concentration, but no significant correlation was detected (**Supplementary Figure 1**). The reason may be that the ammonia excretion of the sponge cells supplies ammonium internally, obscuring the expected mathematical relationship between the ambient concentration of ammonium and the rate of ammonium incorporation by the sponges. Yet, in this particular example, more interferences overlap, because ammonium is also internally generated by dissimilatory nitrate reduction and by the "denitrification+fixation" pathways. Therefore, the intertwining of processes generating ammonium internally advises against the idea of interpreting the rate of ammonium incorporation as a mere function of its ambient concentration, since it is not straightforward relationship and may lead to report spurious (i.e., biologically meaningless) correlations. This situation may applies to all other inorganic nutrients with high microbial involvement.

Another uncertainty relative to the determination of sponge flux rates is the methodological approach: sampling the inhalant and exhalant water flows of the sponges (in-ex method) versus incubating the sponges for a given period of time. Both methods have pros and cons. Although it is always difficult to predict how the confinement of a sponge in an incubation chamber may affect its physiology, we have indirect evidence that the assayed sponges remained healthy and physiologically active through the 24 h incubations. We sequenced the transcriptome of six individuals of *V. pourtalesii* subjected to successive laboratory incubations for 24 h in 16L of seawater to examine their silicon consumption. The analysis of differential gene expression revealed no sign of anoxia, stress, starvation or apoptosis in the incubated sponges, compared to wild control sponges (Maldonado et al., 2020). Rather, the sponges were actively incorporating silicon for skeletal and body growth. Additionally, there was not a single casualty during either the *in-situ* incubations or the 2 weeks of laboratory experiments.

Integrating the Nitrogen Pathways of the Microbiome

Nitrification is a key process in oceanic N cycling as it oxidizes ammonia *via* nitrite to nitrate, which is the main source of nitrogen for many marine primary producers. There are two functionally distinct groups of aerobic microbes involved in the nitrification process: (1) bacteria and archaea that oxidize ammonia to nitrite (i.e., ammonia-oxidizing bacteria and archaea, previously referred to as AOB and AOA); (2) bacteria that oxidize the resulting nitrite to nitrate (i.e., nitrite-oxidizing bacteria, referred to as NOB) and that are often named with the prefix "Nitro," such as *Nitrospinae*, *Nitrospirae*, *Nitrococcus*, etc. To date, no organism is known to carry out both oxidation steps.

Oxidation of ammonia/ammonium to nitrite has been studied quite intensively in marine shallow-water demosponges (Diaz and Ward, 1997; Jiménez and Ribes, 2007; Bayer et al., 2008; Southwell et al., 2008a; Hoffmann et al., 2009; Schläppy et al., 2010; Ribes et al., 2012; Morganti et al., 2017; Subina et al., 2018), with the abundance of AOA being more important than that of AOB both in marine sponges (Radax et al., 2012; Steinert et al., 2020) and, in general, also in the seawater (Francis et al., 2005; Wuchter et al., 2006). In this regard, Van Duyl et al. (2008) reported nitrite release by individuals of *Nodastrella nodastrella*, another rossellid hexactinellid. Those results are in full agreement with our findings on *V. pourtalesii*, a sponge releasing important amounts of nitrite, because its further oxidation is not possible or it happens at very low rates. However, this was not the case of *S. rosea*, which showed nitrite flux rates to be around zero. These two different physiological responses involve that nitrite oxidizing bacteria (NOB) are absent in the tissue of *V. pourtalesii* but not in that of *S. rosea*. The metagenome analysis corroborated such an interpretation, since genes responsible for nitrite oxidation to nitrate were not found in *V. pourtalesii*, neither in MAGs nor in the unbinned metagenomic contigs.

The nitrite oxidizing bacteria, although less investigated in sponges than the ammonium oxidizing microbes, have also been found recurrently as part of the microbiota of demosponges (Thomas et al., 2016; Moitinho-Silva et al., 2017). Their functional role has been made evident through both a consistent excretion of nitrate by the sponges (Jiménez and Ribes, 2007; Bayer et al., 2008; Ribes et al., 2012; Leys et al., 2017; Subina et al., 2018) and metagenomic studies (Bayer et al., 2014). The absence of these genes in the microbiota of *V. pourtalesii* and probably in that of *N. nodastrella* (Van Duyl et al., 2008) opens new questions about its significance for the sponge physiology and ecology. The fact that most individuals of *V. pourtalesii* shifted their initial condition of ammonium consumers toward net ammonium releasers after being exposed to laboratory conditions different from those in the sponge habitat strongly suggests that the sponge microbiota involved in the nitrification is markedly habitat-dependent in at least this sponge species. The noticed shift in the nitrification likely derived from the AOA and AOB populations being negatively affected or even largely replaced by new microbial populations favored by the conditions of the coastal seawater that fed the laboratory.

The negative relationship between ammonium consumption and nitrite release by *V. pourtalesii* (**Figure 4A**) suggests that most released nitrite derives from a first step in nitrification, which cannot be processed further in the sponge through nitrification (**Figure 6**). Yet, we suggest that part of the nitrite produced by the nitrification is not released but rather diverted toward the aerobic process of denitrification and the anaerobic DNRA pathway, so that those three major pathways become bridged through their intermediate steps (**Figure 6**: bridge B1) rather than through the more conventional production of nitrate by nitrification (**Supplementary Table 4**). While the DNRA pathway yields as final product ammonium to close a N cycle in the holobiont (**Figure 6**), denitrification yields as final product inert nitrogen gas (N_2) that needs to enter the N-fixation pathway to become ammonium through the nitrogenase of Mycoplasmatales and Plantomycetota (**Figure 6**).

Nitrogen fixation has also been reported in shallow-water sponges (Wilkinson and Fay, 1979; Wilkinson et al., 1999; Mohamed et al., 2008; Ribes et al., 2015), reducing biologically inaccessible N_2 gas to ammonium and representing a source of dissolved inorganic nitrogen (DIN) additional to that available by sponge feeding.

The coupling/bridging among these four pathways to close a N cycle in *V. pourtalesii* (**Figure 6**) is not trivial, as the aerobic metabolism of the holobiont becomes connected to anaerobic and facultative chains of reactions, what helps to explain how these sponges are able to deal with the low oxygen conditions (<60%) that often characterize deep-sea benthic habitats. The oxygen concentration in the bottom water of the *V. pourtalesii* grounds is only 2.8 ml L^{-1} (Beazley et al., 2018), a mere 42.4% relative to the maximum oxygen values occurring in the superficial waters of that area. In the absence of NOB within the sponges, the main source of nitrate to fuel the denitrification pathway remains intriguing (**Figure 6**), as some individuals of *V. pourtalesii* consumed nitrate from seawater while others released it (**Figure 4B**, **Table 2**). The nitrate concentration in the deep-water habitat of *V. pourtalesii* is relatively high (17.2 μM) compared to that in the coastal water (7.9 μM) and could well cover the sponge's demands. From our current approach, it also remains unclear whether a full microbial denitrification from nitrate to N_2 gas can be accomplished in *V. pourtalesii*. On the one side, the genes coding for nitrate and nitrite reductases have been identified reliably. On the other side, the occurrence of the genes coding for the enzymes involved in the last two denitrification reactions (nitric oxide reductase and nitrous oxide reductase) was not as certain (**Figure 6**). The nitrous oxide reductase was not found in MAGs, but it was detected in the unbinned data, making it impossible to assign a microbial lineage for this activity. More importantly, the nitric oxide reductase, which converts nitric oxide (NO) into nitrous oxide (N_2O) was detected in neither the MAGs nor the unbinned data. This would mean that the produced nitric oxide —a highly toxic intermediate compound with a lifetime of just seconds but able to diffuse freely across membranes with relevant roles as signaling molecule (Hancock, 2017)— could not be further processed to complete denitrification. Yet, we suggest that denitrification can be completed in *V. pourtalesii* because nitrous oxide is available as an intermediate product from the DNRA pathway (**Figure 6**: bridge B2). Because our findings leave some unanswered questions and unresolved aspects regarding denitrification, disentangling the metabolic integration of the denitrifying microbes in *V. pourtalesii* will require further research. Some sponge grounds consisting essentially of an assemblage of deep-water astrophorid demosponges have shown high denitrification activity (i.e., similar in rate values to those of marine sediments). Denitrification in those astrophorid grounds was so intense that the sponges were estimated to incorporate a large part of the nitrate available in the seawater of their habitat (Rooks et al., 2020). From the available results in *V. pourtalesii*, the conventional coupling of nitrification to denitrification through nitrate does not appear to happen (**Figure 6**): the nitrifying enzymes for the conversion of nitrite into nitrate are missing. Likewise, the coupling of denitrification to nitrification through the process of N_2 fixation is not happening through the common pathways, since the enzymes responsible for converting nitric oxide (NO) into nitrous oxide (N_2O) are not yet found in this sponge species (**Figure 6**), but nitrous oxide diverted from the DNRA pathway allows to produce the final N_2 product of denitrification that feeds the nitrogen fixation. Therefore, two bridges among major nitrogen pathways —which would be mediated through intermediate N by-products— are required for the microbiome to close efficiently the N cycle in the sponge.

We have found little evidence of anaerobic ammonium oxidation (anammox), in which ammonium and nitrite are converted into N_2 and water. In contrast, some studies on demosponges have found nitrification to be coupled with denitrification and anammox (Hoffmann et al., 2009; Schläppy et al., 2010; Fiore et al., 2013). Genes involved in the production of urea or its hydrolysis have not been found either.

By combining the functional roles of the detected N-involved enzymes in the microbiome of *V. pourtalesii* (**Supplementary Table 4**), most of the nutrient fluxes that we measured in the living sponges (**Figure 3**, **Table 2**) become explained by the microbial metabolic pathways (**Figure 6**). Nitrite and nitrate are often products of nitrification processes and, if not used in other microbial processes, excreted. In some demosponges, nitrite release was not detected (as it is also the case of *S. rosea*) and only the final product, nitrate, was released (Bayer et al., 2008). In the present study, nitrite excretion in *V. pourtalesii* may be explained by a higher abundance of ammonia-oxidizing microbes (Radax et al., 2012; Steinert et al., 2020) and the absence or low abundance of nitrite-oxidizing bacteria (NOB) and microbes relying on nitrogen reduction pathways (denitrification, nitrate and/ or nitrite reduction). Indeed, genes responsible for nitrite oxidation, which are typical of NOB, were neither found in MAGs nor in the unbinned metagenomic data. NOBs appear to have a high mortality rate (Kitzinger et al., 2020), probably resulting in underestimation of their abundance, which might be the reason why we could not detect the functional genes in the metagenome data. Variable nitrate fluxes (excretion and/or uptake), depending on the individuals, might be a result of unbalanced nitrification-nitrate reduction (DNRA, denitrification) coupling due to transient changes in physiological rhythms (e.g., pumping activity) that may change oxygen availability and the effectiveness sensitivity of some of the involved enzymes.

A large proportion of microbes in *V. pourtalesii* appear able to assimilate ammonia/ammonium (**Figure 6**), which could explain the incorporation of ammonium from seawater detected during the sponge incubations. Collectively, the identified pathways of the microbial N metabolism support the notion that the ammonium incorporated from seawater, along with the ammonia excreted by the sponge cells (which undergoes molecular auto-ionization to form ammonium and amide ions), and along with the ammonia/ammonium resulting from the DNRA and the denitrification+N fixation pathways, supply the microbiota of *V. pourtalesii* with this crucial substratum that, through N assimilation, fuels its growth (**Figure 6**). The detection of prokaryotic glutamine synthetase and glutamate dehydrogenase in the MAGs (**Supplementary Table 4A**) suggests

that a large part of the microbiota N assimilation occurs through ammonification of ammonia to produce basic amino acids, as already concluded for the SAR3254 symbiont in a previous study of *V. pourtalesii* (Bayer et al., 2020). The recent finding that *V. pourtalesii* covers its energetic demands mostly (90%) through uptake of dissolved organic carbon (DOC) rather than through filter feeding (10%) of bacterioplankton and other particulate carbon (Bart et al., 2020) also suggests that a substantial part of the DOC taken up by the sponges could indeed not be used by the sponge cells themselves but running through the assimilation pathway of the microbiota (**Figure 6**), as it has also been shown for some HMA demosponges (Rix et al., 2020).

The finding that most of the sponge-associated microbes in *V. pourtalesii* appear to live within large, amoeboid syncytia (**Figures 7–10**) has also important functional implications: (1) the proliferation of microbes may be under a better control by the sponges; (2) the microbes can be potentially transported readily toward the required tissue areas for dealing with waste and/or to ensure the optimal redox conditions for the needed metabolic routes; (3) the microbes, farmed by the sponge out of both its waste and the incorporation of ammonium and DOC, can be readily digested within the syncytia, potentially becoming an internal food source that is independent from the availability of external particulate food (**Figure 6**). Therefore, the complex N microbial engine that internally provides food to the sponges may constitute an important adaptive advantage for these sponges to cope with starvation during periods of limited food supply to the deep-sea habitat. Collectively, our physiological, ultrastructural, and genetic findings support the idea of a N biochemical network entailing not only the various microbial lineages but also the cell metabolism of the sponge, so that the correct metabolic functioning of the *V. pourtalesii* holobiont will depend substantially on the correct functioning of its N microbial engine.

Phosphate Release

Phosphate (or orthophosphate ion, PO_4^{-3}) is the most bioavailable form of phosphorus in the biosphere. Its availability has long been identified as a key determinant of marine productivity and its cycling is closely linked to carbon and nitrogen dynamics in the oceans (Villarreal-Chiu et al., 2012). Dissolved organic phosphorus (DOP) accounts for up to 80% of total soluble P and is rapidly utilized by the microbial fraction in oligotrophic waters (Björkman and Karl, 2003), playing a pivotal role in driving growth, community composition and population dynamics of free-living marine microorganisms (Dyhrma et al., 2007). Phosphonates are widespread in nature in a range of biogenic molecules, representing an important component of marine DOP. Unlike the more common C–O–P bond characterizing most biological compounds containing phosphate, phosphonates are characterized by a highly stable —and apparently ancient— direct carbon–phosphorus (C–P) bond (Ternan et al., 1998; White and Metcalf, 2007), which resists biochemical, thermal, and photochemical decomposition. Phosphonates are produced by many primitive life forms, including a wide range of marine invertebrates in which the phosphate bound in phosphonates may comprise as much as 50% of the total P content (Quin, 2000). Such natural-product phosphonates are 2-aminoethylphosphonic acid (2-AEP; ciliatine) or 2-amino-3-phosphonopropionic acid (phosphonoalanine), which are found as side groups on exopolysaccharides or glycoproteins, or in the polar head groups of membrane phosphonolipids. There are quite some enzymes found to be responsible for degradation/utilization of such substances (for reviews see Ternan et al., 1998; Villarreal-Chiu et al., 2012).

Our results suggest that at least some microorganisms in the *V. pourtalesii* microbiome are able to utilize host-derived organo-phosphonates, such as representatives of Planctomycetota, Crenarcheota, Gamma- and Alphaproteobacteria. We did not look for biosynthesis pathways of phosphonates. Even if phosphate is either re-used by sponge-associated microbes or the host itself, the final outcome is a low rate of phosphate release from the sponges, as it was measured in the incubations of *V. pourtalesii* and *S. rosea* (**Figure 3**, **Tables 1**, **2**). However, there are many remaining gaps in the current understanding of the utilization of P by sponge-associated microbes, as well as on their functional integration in the sponge metabolism.

CONCLUSIONS

Our study reveals that important physiological differences occur between the hexactinellid sponges *Schaudinnia rosea* and *Vazella pourtalesii*, despite them being phylogenetically closely related as members of the family Rossellidae. Differences were particularly important regarding the net flux of ammonium and nitrite. The MAG study of the *V. pourtalesii* microbiome revealed a rich community of archaea and bacteria driving nitrification, denitrification, DNRA, nitrogen fixation, and ammonia assimilation. The various biochemical microbial pathways are partially coupled and/or bridged to each other closing a N cycle in the sponge and internally generating ammonium, which, through assimilation, appears to sustain the bulk of the sponge microbiome. The ammonium needs of the sponges to fuel their internal microbiota are so large that they cannot be fulfilled by the internal N cycle and ammonium has to be incorporated from seawater. It is here estimated that about 2.6 million kg of ammonium are taken up annually from the bottom water by the aggregations of *V. pourtalesii* established at the deep zone of the Nova Scotia continental shelf. It is herein postulated that such an important ammonium removal has a negative impact on the development of the free-living bacterioplankton around the sponge aggregations. An impoverished bacterioplankton community may reduce the feeding chances of the many sponge species that rely on filter feeding free-living bacteria. Such a nutritional competitive exclusion would explain, along with other factors, why the aggregations of *V. pourtalesii* are markedly monospecific. This sponge species appears to nourish out of the digestion of its microbiota, which is mostly farmed within its bacteriosyncytia through a network of nitrogen-based biochemical reactions revolving around the processing of ammonia/ammonium. Beside the ammonium intake, the sponges also affect the deep-sea

ecosystem through an important annual release of nitrite (some 27.3 million kg) and, in smaller quantities, of nitrate and phosphate. The finely tuned metabolic integration among various N-depending microbial lineages and between these and the sponge *V. pourtalesii* suggest that the metabolism of the holobiont depends substantially on the correct functioning of its microbial engine. However, the sponge-microbe functional equilibrium appears to be delicate and can easily be altered just by moving the sponges out of their natural habitat for a few days. Such a susceptibility raises concerns about the need of preserving the habitat conditions in these deep-sea systems. This study also brings in the novel perspective that hexactinellid sponges are not always the slow-metabolism organisms we have traditionally assumed. Some species that grow in dense aggregations may carry intense nutrient exchanges with the surrounding deep-sea environment through a complex metabolic integration with their microbiota and the resulting intense physiological activity has implications of ecological scale for the deep-sea communities.

DATA AVAILABILITY STATEMENT

The original contributions presented in the study are included in the article and **Supplementary Material**. Detailed sample metadata were deposited in the PANGAEA database: https://doi.pangaea.de/10.1594/PANGAEA.917599, following Bayer et al. (2020). Amplicon and metagenomic raw data including reads and assembled MAGs were deposited in the NCBI database under BioProject PRJNA613976. Individual accession numbers for assembled MAGs are listed in **Supplementary Table 2** of Bayer et al. (2020). Interpro annotation output is available on figshare under https://doi.org/10.6084/m9.figshare.12280313. Further inquiries can be directed to the corresponding authors.

AUTHOR CONTRIBUTIONS

This study was initially conceived by MM. The first draft was assembled by MM, ML-A, KBa, and KBu, being further refined through input from all co-authors. EK, LB, and HR provided logistic field support for field and laboratory work. EK, LB, MM, and ML-A were responsible for mapping and sponge biomass determination in the *Vazella* grounds. MM and ML-A conducted field and laboratory sponge incubations and scaled up net fluxes. UH, KBa, KBu, and BS were responsible for the amplicon sequencing of the microbiomes of *S. rosea* and *V. pourtalesii*, for sequencing and annotating the metagenome, and metagenome-assembled genomes (MAGs) of the *Vazella* microbial community. MM conducted the histological and TEM study. All authors contributed to the manuscript elaboration at different steps and approved the submitted version.

FUNDING

This research was funded mostly by the SponGES H2020 grant (BG-01-2015.2, agreement number 679849-2) awarded to HR (coordinator) and the associated international partner consortium. Much of the logistics was also funded by the Fisheries and Oceans Canada International Governance Strategy (IGS) projects awarded to EK and HR. Manuscript elaboration benefited from funding by the Dark-Si grant (MICIU-PID2019-108627RB-I00) to MM.

ACKNOWLEDGMENTS

The authors thank C. Sitjà and M. García for help with the embedding and sectioning of light microscopy samples. This study is in memory of HR, our co-author, friend, and main coordinator of the H2020 SponGES project, who made this research possible and passed away on 7 March 2020.

SUPPLEMENTARY MATERIAL

The Supplementary Material for this article can be found online at: https://www.frontiersin.org/articles/10.3389/fmars.2021.638505/full#supplementary-material

REFERENCES

Archer, S. K., Stevens, J. L., Rossi, R. E., Matterson, K. O., and Layman, C. A. (2017). Abiotic conditions drive significant variability in nutrient processing by a common Caribbean sponge, *Ircinia felix*. *Limnol. Oceanogr.* 62, 1783–1793. doi: 10.1002/lno.10533

Bart, M. C., Mueller, B., Rombouts, T., van de Ven, C., Tompkins, G. J., Osinga, R., et al. (2020). Dissolved organic carbon (DOC) is essential to balance the metabolic demands of four dominant North-Atlantic deep-sea sponges. *Limnol. Oceanogr.* 11652. doi: 10.1002/lno.11652

Bayer, K., Busch, K., Kenchington, E., Beazley, L., Franzenburg, S., Michels, J., et al. (2020). Microbial strategies for survival in the glass sponge *Vazella pourtalesii*. *mSystems* 5, e00473–e00420. doi: 10.1128/mSystems.00473-20

Bayer, K., Moitinho-Silva, L., Brümmer, F., Cannistraci, C. V., Ravasi, T., and Hentschel, U. (2014). GeoChip-based insights into the microbial functional gene repertoire of marine sponges (high microbial abundance, low microbial abundance) and seawater. *FEMS Microbiol. Ecol.* 90, 832–843. doi: 10.1111/1574-6941.12441

Bayer, K., Schmitt, S., and Hentschel, U. (2008). Physiology, phylogeny and *in situ* evidence for bacterial and archaeal nitrifiers in the marine sponge *Aplysina aerophoba*. *Environ. Microbiol.* 10, 2942–2955. doi: 10.1111/j.1462-2920.2008.01582.x

Beazley, L., Wang, Z., Kenchington, E., Yashayaev, I., Rapp, H. T., Xavier, J. R., et al. (2018). Predicted distribution of the glass sponge *Vazella pourtalesi* on the Scotian Shelf and its persistence in the face of climatic variability. *PLoS ONE* 13:e0205505. doi: 10.1371/journal.pone.0205505

Beazley, L. I., Kenchington, E. L., Murillo, F. J., and Sacau, M., del M. (2013). Deep-sea sponge grounds enhance diversity and abundance of epibenthic megafauna in the Northwest Atlantic. *ICES J. Mar. Sci. J. du Cons.* 70, 1471–1490. doi: 10.1093/icesjms/fst124

Björkman, K. M., and Karl, D. M. (2003). Bioavailability of dissolved organic phosphorus in the euphotic zone at Station ALOHA, North Pacific Subtropical Gyre. *Limnol. Oceanogr.* 48, 1049–1057. doi: 10.4319/lo.2003.48.3.1049

Bokulich, N. A., Kaehler, B. D., Rideout, J. R., Dillon, M., Bolyen, E., Knight, R., et al. (2018). Optimizing taxonomic classification of marker-gene amplicon sequences with QIIME 2's q2-feature-classifier plugin. *Microbiome* 6:90. doi: 10.1186/s40168-018-0470-z

Bolyen, E., Rideout, J. R., Dillon, M. R., Bokulich, N. A., Abnet, C. C., Al-Ghalith, G. A., et al. (2019). Reproducible, interactive, scalable and extensible microbiome data science using QIIME 2. *Nat. Biotechnol.* 37, 852–857. doi: 10.1038/s41587-019-0209-9

Brembu, T., Mühlroth, A., Alipanah, L., and Bones, A. M. (2017). The effects of phosphorus limitation on carbon metabolism in diatoms. *Philos. Trans. R. Soc. B Biol. Sci.* 372:20160406. doi: 10.1098/rstb.2016.0406

Busch, K., Beazley, L., Kenchington, E., Whoriskey, F., Slaby, B. M., and Hentschel, U. (2021). Microbial diversity of the glass sponge *Vazella pourtalesii* in response to anthropogenic activities. *Conserv. Genet.* 21, 1001–1010. doi: 10.1007/s10592-020-01305-2

Busch, K., Hanz, U., Mienis, F., Mueller, B., Franke, A., Martyn Roberts, E., et al. (2020). On giant shoulders: How a seamount affects the microbial community composition of seawater and sponges. *Biogeosciences* 17, 3471–3486. doi: 10.5194/bg-17-3471-2020

Callahan, B. J., McMurdie, P. J., Rosen, M. J., Han, A. W., Johnson, A. J. A., and Holmes, S. P. (2016). DADA2: High-resolution sample inference from Illumina amplicon data. *Nat. Methods* 13, 581–583. doi: 10.1038/nmeth.3869

Caranto, J. D., and Lancaster, K. M. (2017). Nitric oxide is an obligate bacterial nitrification intermediate produced by hydroxylamine oxidoreductase. *Proc. Natl. Acad. Sci. U. S. A.* 114, 8217–8222. doi: 10.1073/pnas.1704504114

Chaumeil, P.-A., Mussig, A. J., Hugenholtz, P., and Parks, D. H. (2019). GTDB-Tk: a toolkit to classify genomes with the Genome Taxonomy Database. *Bioinformatics* 36, 1925–1927. doi: 10.1093/bioinformatics/btz848

Chu, J. W. F., Maldonado, M., Yahel, G., and Leys, S. P. (2011). Glass sponge reefs as a silicon sink. *Mar. Ecol. Prog. Ser.* 441, 1–14. doi: 10.3354/meps09381

Cook, S. E., Conway, K. W., and Burd, B. (2008). Status of the glass sponge reefs in the Georgia Basin. *Mar. Environ. Res.* 66(Suppl.), S80–S86. doi: 10.1016/j.marenvres.2008.09.002

Corredor, J. E., Wilkinson, C. R., Vicente, V. P., Morell, J. M., and Otero, E. (1988). Nitrate release by Caribbeaan reef sponges. *Limnol. Oceanogr.* 33, 114–120. doi: 10.4319/lo.1988.33.1.0114

de Goeij, J. M., and Van Duyl, F. C. (2007). Coral cavities are sinks of dissolved organic carbon (DOC). *Limnol. Oceanogr.* 52, 2608–2617. doi: 10.4319/lo.2007.52.6.2608

Diaz, M., and Ward, B. (1997). Sponge-mediated nitrification in tropical benthic communities. *Mar. Ecol. Prog. Ser.* 156, 97–107. doi: 10.3354/meps156097

Dunham, A., Archer, S. K., Davies, S. C., Burke, L. A., Mossman, J., Pegg, J. R., et al. (2018). Assessing condition and ecological role of deep-water biogenic habitats: glass sponge reefs in the Salish Sea. *Mar. Environ. Res.* 141, 88–99. doi: 10.1016/j.marenvres.2018.08.002

Dyhrma, S. T., Ammerman, J. W., and Van Mooy, B. A. S. (2007). Microbes and the marine phosphorus cycle. *Oceanography* 20, 110–116. doi: 10.5670/oceanog.2007.54

Fiore, C. L., Baker, D. M., and Lesser, M. P. (2013). Nitrogen biogeochemistry in the caribbean sponge, *Xestospongia muta*: a source or sink of dissolved inorganic nitrogen? *PLoS ONE* 8:72961. doi: 10.1371/journal.pone.0072961

Francis, C. A., Roberts, K. J., Beman, J. M., Santoro, A. E., and Oakley, B. B. (2005). Ubiquity and diversity of ammonia-oxidizing archaea in water columns and sediments of the ocean. *Proc. Natl. Acad. Sci. U. S. A.* 102, 14683–14688. doi: 10.1073/pnas.0506625102

Fristedt, K. (1887). Sponges from the Atlantic and Arctic Oceans and the Behring Sea. Vega-Expeditionens Vetenskap. *Iakttag.* 4, 401–471.

Gage, J. D., and Tyler, P. A. (1991). *Deep-Sea Biology: A Natural History of Organisms at the Deep-Sea Floor*. Cambridge: Cambridge University Press. doi: 10.1017/CBO9781139163637

Gili, J.-M., and Coma, R. (1998). Benthic suspension feeders: their paramount role in littoral marine food webs. *Trends Ecol. Evol.* 13, 316–321. doi: 10.1016/S0169-5347(98)01365-2

Hancock, J. T. (2017). *Cell Signalling, 4th Edn*. Oxford: Oxford University Press.

Hawkes, N., Korabik, M., Beazley, L., Rapp, H. T., Xavier, J. R., and Kenchington, E. (2019). Glass sponge grounds on the Scotian Shelf and their associated biodiversity. *Mar. Ecol. Prog. Ser.* 614, 91–109. doi: 10.3354/meps12903

Hoer, D. R., Tommerdahl, J. P., Lindquist, N. L., and Martens, C. S. (2018). Dissolved inorganic nitrogen fluxes from common Florida Bay (U.S.A.) sponges. *Limnol. Oceanogr.* 63, 2563–2578. doi: 10.1002/lno.10960

Hoffmann, F., Radax, R., Woebken, D., Holtappels, M., Lavik, G., Rapp, H. T., et al. (2009). Complex nitrogen cycling in the sponge *Geodia barretti*. *Environ. Microbiol.* 11, 2228–2243. doi: 10.1111/j.1462-2920.2009.01944.x

Jiménez, E., and Ribes, M. (2007). Sponges as a source of dissolved inorganic nitrogen: nitrification mediated by temperate sponges. *Limnol. Oceanogr.* 52, 948–958. doi: 10.4319/lo.2007.52.3.0948

Jones, P., Binns, D., Chang, H. Y., Fraser, M., Li, W., McAnulla, C., et al. (2014). InterProScan 5: genome-scale protein function classification. *Bioinformatics* 30, 1236–1240. doi: 10.1093/bioinformatics/btu031

Kahn, A. S., Chu, J. W. F., and Leys, S. P. (2018). Trophic ecology of glass sponge reefs in the Strait of Georgia, British Columbia. *Sci. Rep.* 8:756. doi: 10.1038/s41598-017-19107-x

Keesing, J. K., Strzelecki, J., Fromont, J., and Thomson, D. (2013). Sponges as important sources of nitrate on an oligotrophic continental shelf. *Limnol. Oceanogr.* 58, 1947–1958. doi: 10.4319/lo.2013.58.6.1947

Kimmerer, W. J., Gartside, E., and Orsi, J. (1994). Predation by an introduced clam as the likely cause of substantial declines in zooplankton of San Francisco Bay. *Mar. Ecol. Prog. Ser.* 1113, 81–93. doi: 10.3354/meps113081

Kitzinger, K., Marchant, H. K., Bristow, L. A., Herbold, C. W., Padilla, C. C., Kidane, A. T., et al. (2020). Single cell analyses reveal contrasting life strategies of the two main nitrifiers in the ocean. *Nat. Commun.* 11:3. doi: 10.1038/s41467-020-14542-3

Klawonn, I., Bonaglia, S., Whitehouse, M. J., Littmann, S., Tienken, D., Kuypers, M. M. M., et al. (2019). Untangling hidden nutrient dynamics: rapid ammonium cycling and single-cell ammonium assimilation in marine plankton communities. *ISME J.* 13, 1960–1974. doi: 10.1038/s41396-019-0386-z

Leys, S. P., Kahn, A. S., Fang, J. K. H., Kutti, T., and Bannister, R. J. (2017). Phagocytosis of microbial symbionts balances the carbon and nitrogen budget for the deep-water boreal sponge *Geodia barretti*. *Limnol. Oceanogr.* 63, 187–202. doi: 10.1002/lno.10623

Li, D., Luo, R., Liu, C. M., Leung, C. M., Ting, H. F., Sadakane, K., et al. (2016). MEGAHIT v1.0: a fast and scalable metagenome assembler driven by advanced methodologies and community practices. *Methods* 102, 3–11. doi: 10.1016/j.ymeth.2016.02.020

López-Acosta, M., Leynaert, A., Chavaud, L., Amice, E., Bihannic, I., Le Bec, T., et al. (2019). In situ determination of Si, N, and P utilization by the demosponge *Tethya citrina*: a benthic-chamber approach. *PLoS ONE* 14:218787. doi: 10.1371/journal.pone.0218787

Lozupone, C., Lladser, M. E., Knights, D., Stombaugh, J., and Knight, R. (2011). UniFrac: an effective distance metric for microbial community comparison. *ISME J.* 5, 169–172. doi: 10.1038/ismej.2010.133

Mackie, G. O., and Singla, C. L. (1983). Studies on hexactinellid sponges. I. Histology of *Rhabdocalyptus dawsoni* (Lambe, 1873). *Philos. Trans. R. Soc. London* 301, 365–400. doi: 10.1098/rstb.1983.0028

Maldonado, M. (2007). Intergenerational transmission of symbiotic bacteria in oviparous and viviparous demosponges, with emphasis on intracytoplasmically-compartmented bacterial types. *J. Mar. Biol. Assoc. United Kingdom* 87, 1701–1713. doi: 10.1017/S0025315407058080

Maldonado, M. (2015). Sponge waste that fuels marine oligotrophic food webs: a re-assessment of its origin and nature. *Mar. Ecol.* 37, 1–15. doi: 10.1111/maec.12256

Maldonado, M., Aguilar, R., Bannister, R. J., Bell, J. J., Conway, K. W., Dayton, P. K., et al. (2017). "Sponge grounds as key marine habitats: a synthetic review of types, structure, functional roles, and conservation concerns," in *Marine Animal Forests: The Ecology of Benthic Biodiversity Hotspots*, eds L. Sergio Rossi, A. Bramanti, A. Gori, and C. Orejas (Cham, Switzerland: Springer International Publishing), 145–183.

Maldonado, M., Beazley, L., López-Acosta, M., Kenchington, E., Casault, B., Hanz, U., et al. (2021). Massive silicon utilization facilitated by a benthic-pelagic coupled feedback sustains deep-sea sponge aggregations. *Limnol. Oceanogr.* 66, 366–391. doi: 10.1002/lno.11610

Maldonado, M., López-Acosta, M., Beazley, L., Kenchington, E., Koutsouveli, V., and Riesgo, A. (2020). Cooperation between passive and active silicon transporters clarifies the ecophysiology and evolution of biosilicification in sponges. *Sci. Adv.* 6:eaba9322. doi: 10.1126/sciadv.aba9322

Maldonado, M., Ribes, M., and van Duyl, F. C. (2012). Nutrient fluxes through sponges. Biology, budgets, and ecological implications. *Adv. Mar. Biol.* 62, 113–182. doi: 10.1016/B978-0-12-394283-8.00003-5

Mohamed, N. M., Tal, Y., and Hill, R. T. (2008). Diversity and expression of nitrogen fixation genes in bacterial symbionts of marine sponges. *Environ. Microbiol.* 10, 2910–2921. doi: 10.1111/j.1462-2920.2008.01704.x

Moitinho-Silva, L., Nielsen, S., Amir, A., Gonzalez, A., Ackermann, G. L., Cerrano, C., et al. (2017). The sponge microbiome project. *Gigascience* 6, 1–7. doi: 10.1093/gigascience/gix077

Morganti, T., Coma, R., Yahel, G., and Ribes, M. (2017). Trophic niche separation that facilitates co-existence of high and low microbial abundance sponges is revealed by *in situ* study of carbon and

nitrogen fluxes. *Limnol. Oceanogr.* 62, 1963–1983. doi: 10.1002/lno.10546

Nelson, C. E., Alldredge, A. L., McCliment, E. A., Amaral-Zettler, L. A., and Carlson, C. A. (2011). Depleted dissolved organic carbon and distinct bacterial communities in the water column of a rapid-flushing coral reef ecosystem. *ISME J.* 5, 1374–1387. doi: 10.1038/ismej.2011.12

Petrie, B., Yeats, P., Strain, P., and Services, M., of S. and (1999). *Nitrate, silicate and phosphate atlas for the Scotian shelf and the gulf of Maine*. Dartmouth, NS: Fisheries and Oceans Canada.

Pile, A. J., and Young, C. M. (2006). The natural diet of a hexactinellid sponge: benthic-pelagic coupling in a deep-sea microbial food web. *Deep. Res. Part I Oceanogr. Res. Pap.* 53, 1148–1156. doi: 10.1016/j.dsr.2006.03.008

Pita, L., Rix, L., Slaby, B. M., Franke, A., and Hentschel, U. (2018). The sponge holobiont in a changing ocean: from microbes to ecosystems. *Microbiome* 6:46. doi: 10.1186/s40168-018-0428-1

Price, M. N., Dehal, P. S., and Arkin, A. P. (2010). FastTree 2 - approximately maximum-likelihood trees for large alignments. *PLoS ONE* 5:e9490. doi: 10.1371/journal.pone.0009490

Quast, C., Pruesse, E., Yilmaz, P., Gerken, J., Schweer, T., Yarza, P., et al. (2013). The SILVA ribosomal RNA gene database project: improved data processing and web-based tools. *Nucl. Acids Res.* 41:D590. doi: 10.1093/nar/gks1219

Quin, L. D. (2000). *A Guide to Organophosphorus*. New York, NY: Wiley-Interscience.

Radax, R., Hoffmann, F., Rapp, H. T., Leininger, S., and Schleper, C. (2012). Ammonia-oxidizing archaea as main drivers of nitrification in cold-water sponges. *Environ. Microbiol.* 14, 909–923. doi: 10.1111/j.1462-2920.2011.02661.x

Ribes, M., Dziallas, C., Coma, R., and Riemann, L. (2015). Microbial diversity and putative diazotrophy in high- and low- microbial-abundance mediterranean sponges. *Appl. Environ. Microbiol.* 81, 5683–5693. doi: 10.1128/AEM.01320-15

Ribes, M., Jiménez, E., Yahel, G., López-Sendino, P., Diez, B., Massana, R., et al. (2012). Functional convergence of microbes associated with temperate marine sponges. *Environ. Microbiol.* 14, 1224–1239. doi: 10.1111/j.1462-2920.2012.02701.x

Rix, L., Ribes, M., Coma, R., Martin, J.ahn, T., and De Goeij, J. M., Dick Van Oevelen, et al. (2020). Heterotrophy in the earliest gut: a single-cell view of heterotrophic carbon and nitrogen assimilation in sponge-microbe symbioses. *ISME J.* 14, 2554–2567. doi: 10.1038/s41396-020-0706-3

Rooks, C., Kar-Hei Fang, J., Mørkved, P. T., Zhao, R., Tore Rapp, H., Xavier, J. J., et al. (2020). Deep-sea sponge grounds as nutrient sinks: denitrification is common in boreo-Arctic sponges. *Biogeosciences* 17, 1231–1245. doi: 10.5194/bg-17-1231-2020

Sangrador-Vegas, A., Mitchell, A. L., Chang, H. Y., Yong, S. Y., and Finn, R. D. (2016). GO annotation in InterPro: why stability does not indicate accuracy in a sea of changing annotations. *Database* 2016:baw027. doi: 10.1093/database/baw027

Scheffers, S. R., Nieuwland, G., Bak, R. P. M., and Van Duyl, F. C. (2004). Removal of bacteria and nutrient dynamics within the coral reef framework of Curacao (Netherlands Antilles). *Coral Reefs* 23, 413–422. doi: 10.1007/s00338-004-0400-3

Schläppy, M.-L., Schöttner, S. I., Lavik, G., Kuypers, M. M. M., de Beer, D., and Hoffmann, F. (2010). Evidence of nitrification and denitrification in high and low microbial abundance sponges. *Mar. Biol.* 157, 593–602. doi: 10.1007/s00227-009-1344-5

Schmidt, O. (1870). *Grundzüge einer Spongien-Fauna des Atlantischen Gebietes*. Leipzing: Wilhelm Engelmann, 1–88.

Segata, N., Izard, J., Waldron, L., Gevers, D., Miropolsky, L., Garrett, W. S., et al. (2011). Metagenomic biomarker discovery and explanation. *Genome Biol.* 12:R60. doi: 10.1186/gb-2011-12-6-r60

Smith, S. V. (1984). Phosphorus versus nitrogen limitation in the marine environment. *Limnol. Oceanogr.* 29, 1149–1160. doi: 10.4319/lo.1984.29.6.1149

Southwell, M. W., Popp, B. N., and Martens, C. S. (2008a). Nitrification controls on fluxes and isotopic composition of nitrate from Florida Keys sponges. *Mar. Chem.* 108, 96–108. doi: 10.1016/j.marchem.2007.10.005

Southwell, M. W., Weisz, J. B., Martens, C. S., and Lindquist, N. (2008b). *In situ* fluxes of dissolved inorganic nitrogen from the sponge community on Conch Reef, Key Largo, Florida. *Limnol. Oceanogr. Methods* 53, 986–996. doi: 10.4319/lo.2008.53.3.0986

Steinert, G., Busch, K., Bayer, K., Kodami, S., Arbizu, P. M., Kelly, M., et al. (2020). Compositional and quantitative insights into bacterial and archaeal communities of South Pacific Deep-Sea Sponges (Demospongiae and Hexactinellida). *Front. Microbiol.* 11:716. doi: 10.3389/fmicb.2020.00716

Strickland, J. D. H., and Parsons, T. R. (1972). *A practical handbook of seawater analysis, 2nd Edn*. Ottawa, ON: Fisheries Research Board of Canada.

Subina, N. S., Thorat, B. R., and Gonsalves, M.-J. (2018). Nitrification in intertidal sponge *Cinachyrella cavernosa*. *Aquat. Ecol.* 52, 155–164. doi: 10.1007/s10452-018-9651-x

Tabachnick, K. R. (1994). "Distribution of recent Hexactinellida," in *Sponges in Time and Space*, eds. R. M. W. van Soest, T. M. G. van Kempen, and J. C. Braekman (Rotterdam: A.A. Balkema), 225–232.

Ternan, N. G., Mc Grath, J. W., Mc Mullan, G., and Quinn, J. P. (1998). Review: organophosphonates: occurrence, synthesis and biodegradation by microorganisms. *World J. Microbiol. Biotechnol.* 14, 635–647. doi: 10.1023/A:1008848401799

Thomas, T., Moitinho-Silva, L., Lurgi, M., Björk, J. R., Easson, C., Astudillo-García, C., et al. (2016). Diversity, structure and convergent evolution of the global sponge microbiome. *Nat. Commun.* 7:11870. doi: 10.1038/ncomms11870

Tian, R. M., Sun, J., Cai, L., Zhang, W. P., Zhou, G. W., Qiu, J. W., et al. (2016). The deep-sea glass sponge Lophophysema eversa harbours potential symbionts responsible for the nutrient conversions of carbon, nitrogen and sulfur. *Environ. Microbiol.* 18, 2481–2494. doi: 10.1111/1462-2920.13161

Uritskiy, G. V., Diruggiero, J., and Taylor, J. (2018). MetaWRAP - A flexible pipeline for genome-resolved metagenomic data analysis 08 Information and Computing Sciences 0803 Computer Software 08 Information and Computing Sciences 0806 Information Systems. *Microbiome* 6:158. doi: 10.1186/s40168-018-0541-1

Vacelet, J., Boury-Esnault, N., and Harmelin, J. G. (1994). Hexactinellid Cave, a unique deep-sea habitat in the scuba zone. *Deep. Res. I* 41, 965–973. doi: 10.1016/0967-0637(94)90013-2

Van Duyl, F. C., Hegeman, J., Hoogstraten, A., and Maier, C. (2008). Dissolved carbon fixation by sponge–microbe consortia of deep water coral mounds in the northeastern Atlantic Ocean. *Mar. Ecol. Prog. Ser.* 358, 137–150. doi: 10.3354/meps07370

Villarreal-Chiu, J. F., Quinn, J. P., and McGrath, J. W. (2012). The genes and enzymes of phosphonate metabolism by bacteria, and their distribution in the marine environment. *Front. Microbiol.* 3. doi: 10.3389/fmicb.2012.00019

White, A. K., and Metcalf, W. W. (2007). Microbial metabolism of reduced phosphorus compounds. *Annu. Rev. Microbiol.* 61, 379–400. doi: 10.1146/annurev.micro.61.080706.093357

Wilkinson, C. R., and Fay, P. (1979). Nitrogen fixation in coral reef sponges with symbiotic cyanobacteria. *Nature* 279, 527–529. doi: 10.1038/279527a0

Wilkinson, C. R., Summons, R. E., and Evans, E. (1999). Nitrogen fixation in symbiotic marine sponges: ecological significance and difficulties in detection. *Mem. Queensl. Museum* 44, 667–673.

Wuchter, C., Abbas, B., Coolen, M. J. L., Herfort, L., van Bleijswijk, J., Timmers, P., et al. (2006). Archaeal nitrification in the ocean. *Proc. Natl. Acad. Sci. U. S. A.* 103, 12317–12322. doi: 10.1073/pnas.0600756103

Yahel, G., Whitney, F., Reiswig, H. M., Eerkes-Medrano, D. I., and Leys, S. P. (2007). *In situ* feeding and metabolism of glass sponges (Hexactinellida, Porifera) studied in a deep temperate fjord with a remotely operated submersible. *Limnol. Oceanogr.* 52, 428–440. doi: 10.4319/lo.2007.52.1.0428

Zakem, E. J., Al-Haj, A., Church, M. J., Van Dijken, G. L., Dutkiewicz, S., Foster, S. Q., et al. (2018). Ecological control of nitrite in the upper ocean. *Nat. Commun.* 9, 1–13. doi: 10.1038/s41467-018-03553-w

Zhang, F., Jonas, L., Lin, H., and Hill, R. T. (2019). Microbially mediated nutrient cycles in marine sponges. *FEMS Microbiol. Ecol.* 95. doi: 10.1093/femsec/fiz155

Conflict of Interest: The authors declare that the research was conducted in the absence of any commercial or financial relationships that could be construed as a potential conflict of interest.

Copyright © 2021 Maldonado, López-Acosta, Busch, Slaby, Bayer, Beazley, Hentschel, Kenchington and Rapp. This is an open-access article distributed under the terms of the Creative Commons Attribution License (CC BY). The use, distribution or reproduction in other forums is permitted, provided the original author(s) and the copyright owner(s) are credited and that the original publication in this journal is cited, in accordance with accepted academic practice. No use, distribution or reproduction is permitted which does not comply with these terms.

frontiers in Marine Science

ORIGINAL RESEARCH
published: 19 March 2021
doi: 10.3389/fmars.2021.604879

A Deep-Sea Sponge Loop? Sponges Transfer Dissolved and Particulate Organic Carbon and Nitrogen to Associated Fauna

*Martijn C. Bart[1], Meggie Hudspith[1], Hans Tore Rapp[2†], Piet F. M. Verdonschot[1,3] and Jasper M. de Goeij[1]**

[1] Department of Freshwater and Marine Ecology, Institute for Biodiversity and Ecosystem Dynamics (IBED), University of Amsterdam, Amsterdam, Netherlands, [2] Department of Biological Sciences, University of Bergen, Bergen, Norway, [3] Wageningen Environmental Research, Wageningen University and Research, Wageningen, Netherlands

Cold-water coral reefs and sponge grounds are deep-sea biological hotspots, equivalent to shallow-water tropical coral reefs. In tropical ecosystems, biodiversity and productivity are maintained through efficient recycling pathways, such as the sponge loop. In this pathway, encrusting sponges recycle dissolved organic matter (DOM) into particulate detritus. Subsequently, the sponge-produced detritus serves as a food source for other organisms on the reef. Alternatively, the DOM stored in massive sponges was recently hypothesized to be transferred to higher trophic levels through predation of these sponges, instead of detritus production. However, for deep-sea sponges, the existence of all prerequisite, consecutive steps of the sponge loop have not yet been established. Here, we tested whether cold-water deep-sea sponges, similar to their tropical shallow-water counterparts, take up DOM and transfer assimilated DOM to associated fauna via either detritus production or predation. We traced the fate of ^{13}carbon (C)- and ^{15}nitrogen (N)-enriched DOM and particulate organic matter (POM) in time using a pulse-chase approach. During the 24-h pulse, the uptake of ^{13}C/^{15}N-enriched DOM and POM by two deep-sea sponge species, the massive species *Geodia barretti* and the encrusting species *Hymedesmia* sp., was assessed. During the subsequent 9-day chase in label-free seawater, we investigated the transfer of the consumed food by sponges into brittle stars via two possible scenarios: (1) the production and subsequent consumption of detrital waste or (2) direct feeding on sponge tissue. We found that particulate detritus released by both sponge species contained C from the previously consumed tracer DOM and POM, and, after 9-day exposure to the labeled sponges and detritus, enrichment of ^{13}C and ^{15}N was also detected in the tissue of the brittle stars. These results therefore provide the first evidence of all consecutive steps of a sponge loop pathway via deep-sea sponges. We cannot distinguish at present whether the deep-sea sponge loop is acting through a detrital or predatory pathway, but conclude that both scenarios are feasible. We conclude that sponges could play an important role in the recycling of DOM in the many deep-sea ecosystems where they are abundant, although *in situ* measurements are needed to confirm this hypothesis.

Keywords: deep-sea sponge loop, brittle star, carbon, nitrogen, transfer, detritus, predation, DOM

OPEN ACCESS

Edited by:
Joana R. Xavier, University of Porto, Portugal

Reviewed by:
Gitai Yahel, Ruppin Academic Center, Israel
Eduardo Carlos Meduna Hajdu, Federal University of Rio de Janeiro, Brazil

****Correspondence:***
Jasper M. de Goeij
j.m.degoeij@uva.nl

† Deceased

Specialty section:
This article was submitted to Deep-Sea Environments and Ecology, a section of the journal Frontiers in Marine Science

Received: *10 September 2020*
Accepted: *22 February 2021*
Published: *19 March 2021*

Citation:
Bart MC, Hudspith M, Rapp HT, Verdonschot PFM and de Goeij JM (2021) A Deep-Sea Sponge Loop? Sponges Transfer Dissolved and Particulate Organic Carbon and Nitrogen to Associated Fauna. Front. Mar. Sci. 8:604879. doi: 10.3389/fmars.2021.604879

INTRODUCTION

In the deep-sea, sponges and cold-water corals (CWC) form complex reef structures, which support rich communities of suspension-feeding fauna and play crucial roles as habitat and feeding grounds for motile taxa, including commercial fish species (Miller et al., 2012). These ecosystems are amongst the most productive deep-sea habitats and they are responsible for significant carbon (C) and nitrogen (N) cycling (van Oevelen et al., 2009; Radax et al., 2012; Kutti et al., 2013; Cathalot et al., 2015). In fact, CWC reefs and sponge grounds have been identified as benthic biodiversity hotspots, even comparable to tropical coral reefs in terms of grams organic C m^{-2} and kg dry weight km^{-2} (Polovina, 1984; van Oevelen et al., 2009; Grebmeier et al., 2015; Maldonado et al., 2017).

Paramount to the productivity of benthic ecosystems in oligotrophic waters is their capacity to efficiently retain and recycle resources. The largest organic resource in the oceans is dissolved organic matter (DOM) (Benner et al., 1992), but this complex mixture of polysaccharides, proteins, and lipids is deemed biologically unavailable to most heterotrophic organisms (Carlson, 2002). However, DOM is known to be processed by bacterioplankton and then returned to the classic food chain through planktonic grazing, a pathway termed the microbial loop (Azam et al., 1983). Essentially, by consuming DOM, bacteria remineralize nutrients that would otherwise be lost to the environment (Fenchel, 2008).

Within shallow-water tropical coral reefs, an additional DOM recycling pathway has been established: the sponge loop (de Goeij et al., 2013). In this pathway, encrusting sponges that dominate the surface of cryptic habitats (e.g., crevices, cavities), but also occupy exposed reef surfaces, assimilate DOM and produce significant amounts of particulate detritus (de Goeij et al., 2013; Alexander et al., 2014; Rix et al., 2016, 2017; Lesser et al., 2020). This detritus subsequently feeds the detrital food chain (de Goeij et al., 2013; Rix et al., 2018). Carbon fluxes through these ubiquitous, but largely hidden and thus usually "overlooked" sponges can amount to daily gross primary production rates of the entire reef (de Goeij et al., 2013, 2017). However, no detritus production was found for several sponges with a non-encrusting, but massive, emergent growth form, that generally occur on the exposed reef (McMurray et al., 2018; Wooster et al., 2019). Therefore, a complementary sponge-loop pathway was hypothesized, in which sponge-assimilated DOM is transferred to higher trophic levels via direct predation on sponge tissue (McMurray et al., 2018; Pawlik and McMurray, 2020). To date, this predatory sponge loop has not yet been confirmed. Whether via detritus production or predation, the sponge loop, together with the microbial loop, helps to explain how tropical shallow-water coral reefs maintain a high productivity and biodiversity in otherwise oligotrophic marine environments (de Goeij et al., 2013; Rix et al., 2016; Pawlik and McMurray, 2020).

The (re)cycling and transfer of DOM could be of particular importance for benthic deep-sea ecosystems as, for large parts of the year, particulate phytodetritus transported from the ocean surface cannot fulfill the carbon demands of these systems (Gooday, 2002; Duineveld et al., 2004, 2007; van Oevelen et al., 2009; Kahn et al., 2018). Recently, first evidence was found that the sponge-loop pathway may not just operate on tropical shallow-water coral reefs, but also in the deep-sea (Rix et al., 2016; Bart et al., 2020a,b; Maier et al., 2020). The capacity to take up DOM represents the first step of the sponge loop (de Goeij et al., 2013), and both encrusting and massive deep-sea sponges have been shown to utilize DOM as a food source (Rix et al., 2016; Bart et al., 2020a,b; Maier et al., 2020). The second step of the sponge loop is the assimilation of DOM into particulate organic matter (POM), leading to either the release of detritus (including pseudo faeces) or an increase in sponge biomass. Using stable isotope tracers, multiple studies have shown that deep-sea sponges are capable of assimilating DOM into biomass (Rix et al., 2016; Kazanidis et al., 2018; Bart et al., 2020a; Maier et al., 2020). Additionally, the encrusting deep-sea sponge *Hymedesmia coriacea* was found to convert 39% of the organic C derived from coral mucus into detritus (Rix et al., 2016), and two massive deep-sea sponge species, *Geodia barretti* and *Mycale lingua*, were found to take up DOM and produce POM, although at much lower rates (0.03 and 3%, respectively) as percentage of their biomass (Maier et al., 2020). However, the third—ecologically critical, but most difficult to experimentally identify—step of the sponge loop has not been established in the deep-sea to date: the transfer of assimilated DOM by sponges to higher trophic levels. Note also that all the aforementioned studies on DOM cycling by deep-sea sponges are based on *ex situ* measurements in controlled laboratory settings. The existence and ecological relevance of a deep-sea sponge loop has therefore not been established to date.

Dissolved organic carbon (DOC) may represent more than 90% of the daily carbon intake of sponges (de Goeij et al., 2017), including deep-sea species (Bart et al., 2020b), but DOM is clearly not the only food source of sponges. In fact, they are established as very efficient filter-feeders of organic particles, such as bacterio-, and phytoplankton (e.g., Reiswig, 1971; Pile et al., 1996; Leys et al., 2018). Food bacteria, as part of their POM diet, were found to be assimilated more efficiently into sponge tissue compared to DOM (Kazanidis et al., 2018; Bart et al., 2020a), implying that bacteria are a high quality and therefore crucial food source to sponges. Currently, it is unknown how the processing of DOM and POM by encrusting and massive sponges affects the subsequent steps of the sponge loop.

The present study aims to test the hypothesis that, similar to their tropical counterparts, deep-sea sponges transfer assimilated DOM and POM to associated fauna, following the prerequisite, consecutive steps of the sponge loop. Therefore, we qualitatively investigated the potential retention and subsequent transfer of C and N derived from DOM and POM (i.e., bacterioplankton) via two species of deep-sea sponges, the massive species *Geodia barretti* and the encrusting species *Hymedesmia* sp., to sponge-associated fauna (i.e., brittle stars). Brittle stars (Echinodermata: Ophiuroidea) are a predominant member of deep-sea ecosystems (Stöhr et al., 2012) and sponge infauna (Clark, 1933; Duarte and Nalesso, 1996). They are known to feed on (pseudo-)fecal droppings of bivalves (Maier et al., 2020), and, in tropical shallow-water ecosystems, on sponge detritus (Rix et al., 2018). Brittle stars may also directly feed on sponge tissue

(Morison, 1979; McClintock, 1994). We traced the fate of ^{13}C- and ^{15}N-enriched DOM and POM in time using an *ex situ* pulse-chase experiment. The assimilation of ^{13}C/^{15}N-enriched DOM and POM into the two sponge species was assessed during the 24-h pulse. The transfer of assimilated DOM and POM by the two sponges (via either detritus or direct predation) into brittle stars was investigated during the subsequent 9-day chase, after transfer of the pulse-labeled sponges to label-free running seawater aquaria containing brittle stars.

MATERIALS AND METHODS

Study Areas, Sponge Collection, and Maintenance

This study investigated the nutritional relationship between two North-Atlantic deep-sea sponge species, the massive species *Geodia barretti* and the encrusting species *Hymedesmia* sp., and one deep-sea brittle star species, *Ophiura* sp. (**Figure 1A** and **Supplementary Table 1**).

Whole, intact *Geodia barretti* individuals were carefully collected by ROV (Remotely Operated Vehicle), during the G.O. Sars cruise 2018108 (August 2018) at a sponge ground on the Tromsøflaket, a sea bank in the western Barents Sea (70°47′13.9″N 18°03′23.8″E). The Barents Sea is a shelf sea with an average depth of 230 m (Sundfjord et al., 2007). The benthic community at the Tromsøflaket is primarily dominated by scattered large specimens of *G. barretti*, which account for approximately 90% of the benthic biomass (Buhl-Mortensen et al., 2009; Jørgensen et al., 2015). In addition, Actinaria, Bryozoa, Crustacea, Echinodermata, Echiura, and Hydrozoa are part of the benthic community (Kędra et al., 2017). *Hymedesmia* sp. and *Ophiura* sp. were carefully collected attached to their rocky substrate by ROV at Stjernsund reef (70°30′N, 22°30′E), a 30 km long, 3.5 km wide, > 400 m deep glacial sound in northern Norway that connects the Altafjord to North-Atlantic waters (Rüggeberg et al., 2011; Rovelli et al., 2015). This cold-water coral reef is characterized by the presence of the reef framework-forming scleractinian coral *Lophelia pertusa* and reef-associated fauna such as sponges, crustaceans, and other corals (Rovelli et al., 2015).

Sponges and brittle stars were kept on board the research vessel in the dark in 20-L flow-through tanks in a climate room at 6°C. North-Atlantic seawater was pumped in from 6 m water depth at 30 L h^{-1}. All individuals were transported without air-exposure to the laboratory facilities at the University of Bergen, Norway, where the experiments took place. In Bergen, sponges and brittle stars were kept in a dark climate room (8°C) in multiple 20-L flow-through aquaria systems. Each holding tank contained a maximum of five sponge individuals and five brittle stars. Flow originated from unfiltered water, pumped from 200 m depth from the outer fjord near Bergen at ∼ 50 L h^{-1} with a temperature ranging from 6 to 8°C. All sponges were acclimatized for a minimum of 1 week prior to the incubation experiments and all sponges and their attached rocky substrates were cleared from epibionts prior to incubations.

Preparation of ^{13}C/^{15}N-Labeled DOM and POM

Isotopically enriched DOM was prepared by axenically culturing the marine diatom *Phaeodactylum tricornutum* in multiple 2 L Fernbach flasks on F/2 medium amended with ^{15}N (80%)-$NaNO_3$ (*Eurisotop*, CLM-157) and ^{13}C (99%)-$NaHCO_3$ (*Eurisotop*, CLM-441) (de Goeij et al., 2008; Bart et al., 2020a). Non-labeled axenic *P. tricornutum* pre-cultures were added (60 mL) to 1 L of sterile labeled F/2 medium in a flow cabinet. The diatoms were grown at 20°C on a 12:12 day:night cycle. After 10 day, diatoms were concentrated on a 0.45 μm filter (147 mm ø) and carefully flushed from the filter with sterile artificial seawater. Subsequently, the collected diatoms were centrifuged for 10 min at 750 × *g*, the supernatant was removed and the pellet was frozen at -20°C. To lyse the cells and release ^{13}C/^{15}N-labeled DOM, the frozen diatoms were lyophilized in a FD5515 *Ilchin Biobase* freeze-drier, after which MilliQ water was added and the solution was placed in an ultrasonic bath for 10 min. Lastly, the DOM solution was filtered over a 0.7 μm GF/F filter and subsequently over a 0.2 μm polycarbonate filter. The filtrate was collected, lyophilized, and analyzed for C and N content and isotopic composition. Before adding DOM to the incubations, aliquots of 5 mL were made by dissolving the lyophilized DOM in MilliQ to a final concentration of 80 μmol L^{-1} DOC or 15 μmol L^{-1} DON added to each incubation.

Isotopically-enriched POM was prepared by labeling ambient seawater bacterioplankton (de Goeij et al., 2008; Bart et al., 2020a). Briefly, seawater bacteria were concentrated by prefiltering natural seawater over a 0.7 μm GF/F filter and subsequent ultrafiltration (0.2 μm; Vivaflow). The inoculum was added to M63 medium (Miller, 1972), amended with thiamine (0.00001%) and $MgSO_4$ (67 μmol L^{-1}). Labeled bacterial cultures were amended with ^{13}C (99%)-glucose (1 g L^{-1}, glucose D U-13C6, *Euriso-Top*, CLM-1396) and ^{15}N (99%)-NH_4Cl (1.2 g L^{-1}, *Euriso-Top*, NLM-467-5). The culture was grown for 48 h in the dark at 25°C and labeled bacteria were isolated by centrifuging (5 min, 10,000 × *g*), rinsing the pellet in 0.2 μm filtered seawater, centrifuging again, and resuspending the pellet in 0.2 μm filtered seawater before dividing in aliquots to a final concentration of 0.5 × 10^6 bacteria mL^{-1} (approximately 12 μmol L^{-1} bacterial carbon (BC) and 1 μmol L^{-1} bacterial nitrogen (BN) added to each incubation) and storing at 4°C.

Experimental Set-Up

A schematic of the pulse-chase experimental set-up is shown in **Figure 1B** and comprised three phases: a pulse, a washing, and a chase phase. From here on, for simplicity and to distinguish between the two sponge loop pathways scenarios—i.e., the hypothesis that massive sponges are predominantly cycling resources through the predatory pathway and encrusting sponges predominantly through the detrital pathway—we will refer to *G. barretti* as "massive," *Hymedesmia.* sp. as "encrusting" and *Ophiura* sp. as "brittle star."

Phase 1: pulse—During the pulse, we continuously administered two tracer ^{13}C/^{15}N-labeled food sources (DOM and POM) to individuals of both species using air-tight 3-L

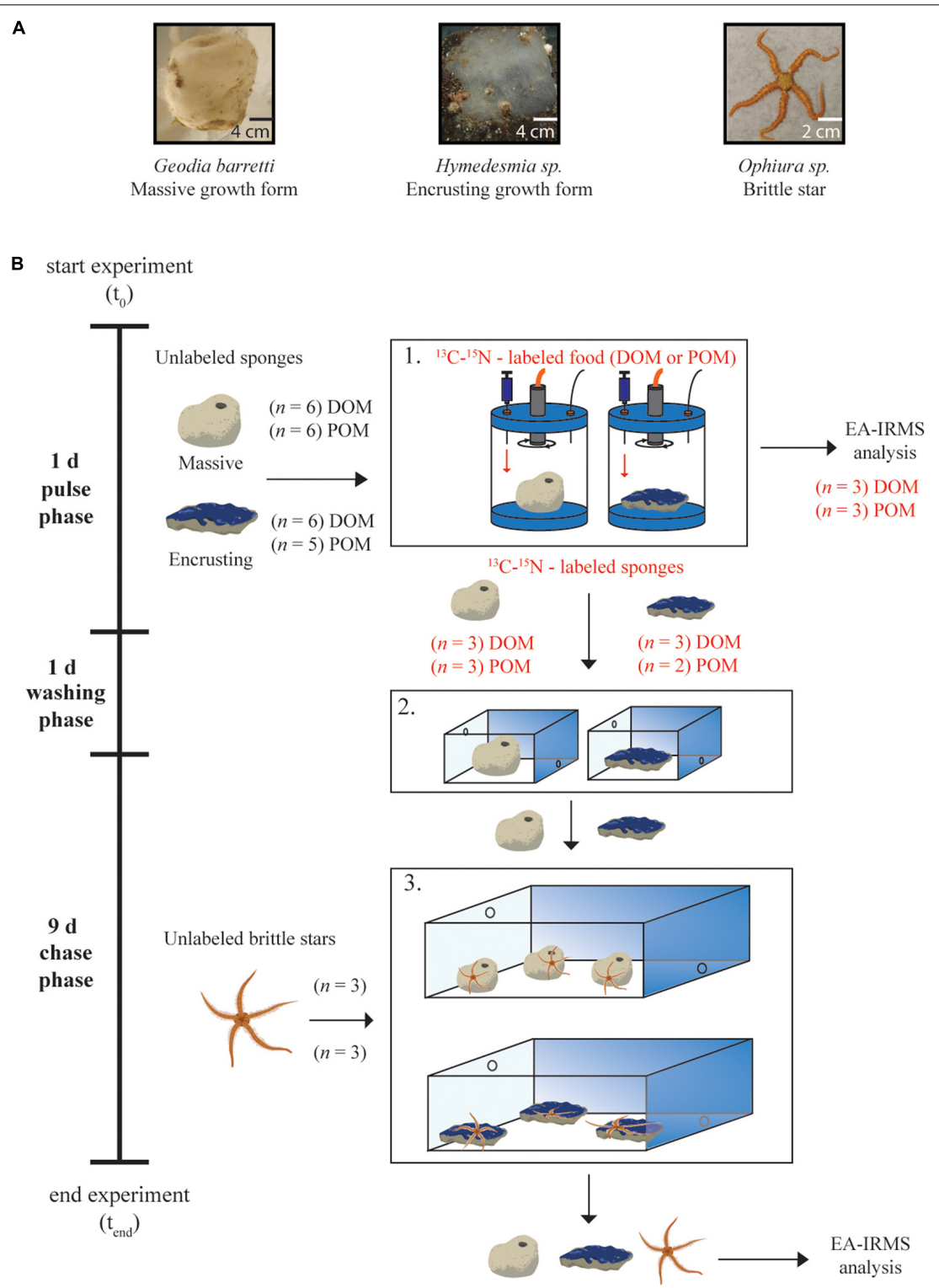

FIGURE 1 | Experimental set up. **(A)** Organisms used in this study. **(B)** Two tracer $^{13}C/^{15}N$-labeled food sources [dissolved or particulate organic matter (DOM or POM, respectively)] were fed to a total of 23 sponge individuals of the massive sponge *Geodia barretti* and the encrusting sponge *Hymedesmia* sp. for a total of 24 h in individual *ex situ* chambers (pulse phase). Three individuals of each species per food source were sacrificed for EA-IRMS-analysis after 24. The remaining three sponge individuals (or 2 for encrusting POM) were then transferred to individual 10-L running seawater flow-through aquaria for 24 h (washing phase). Lastly, the individuals were pooled per species and food source and transferred to 20-L running seawater flow-through aquaria with 3 brittle stars (*Ophiura* sp.) per tank for a further 9-day (chase). At the end of the experiment, tissue samples of all organisms were taken and analyzed for enrichment of ^{13}C – ^{15}N by EA-IRMS.

FIGURE 2 | *Geodia barretti* and *Ophiura* sp. After placing them at random position in the aquaria, brittle stars settled themselves on the surface of the sponges.

incubation flow chambers (Bart et al., 2020a,b). Six individuals of both species were fed DOM, six individuals of the massive sponge were fed POM and five individuals of the encrusting sponge were fed POM. Prior to the incubations, chambers were acid washed (0.4 mol L^{-1} HCl) overnight. During the experiment, the chambers were kept in a water bath to maintain a constant seawater temperature (ranging from 6 to 8°C depending on the incubation). Incubation water was replenished every 8 h (24 h total incubation time) to ensure that sponge individuals were regularly receiving fresh seawater after which new, labeled substrate was added. At the end of the incubation, sponges were removed from the chamber and rinsed in 0.2 μm filtered unlabeled seawater. This experiment was part of a larger isotope-tracer study conducted simultaneously and the uptake rates of DOM and POM by massive and encrusting sponges (n = 3 per species, per food source) were taken from already published data (**Figure 3**, gray marked area) (Bart et al., 2020a). To test the direct uptake rates of DOM and POM by brittle stars, separate incubations (n = 3 per food source) were performed according to the aforementioned protocol. After the 24-h incubation period, brittle stars were directly sacrificed and placed in a drying oven for 48 h at 60°C. After drying, tissue was homogenized with mortar and pestle and stored in a desiccator until further analysis by EA-IRMS.

Phase 2: washing—Post-labeling, sponge individuals were transferred to individual 10-L label-free running seawater flow through aquaria for 24 h to ensure no residual ^{13}C- and ^{15}N-labeled substrate remained on the (inner and outer) surface of the sponges.

Phase 3: chase—Post-washing, DOM-fed and POM-fed massive and encrusting sponges were placed in four 20-L label-free running seawater flow-through aquaria together with 3 unlabeled brittle stars per tank: one tank with three DOM-fed massive sponges plus brittle stars, one with three DOM-fed encrusting sponges plus brittle stars, one with three POM-fed massive sponge plus brittle stars, and one with two POM-fed encrusting sponges plus brittle stars. After placing the brittle stars at random positions in each aquarium, they settled themselves on the surface of the sponges (**Figure 2**). Detritus was collected every 3-day during the chase from each tank with a sterile plastic pipette, pooled per timepoint and frozen at -80°C for later isotopic analysis (Rix et al., 2018). After 9-day, all sponges and brittle stars were rinsed in 0.2 μm filtered, unlabeled seawater, shortly dipped in ultrapure water to remove salts, and carefully removed from their rocky substrate using a sterile scalpel blade (i.e., sponges) and oven-dried (48 h at 60°C). Then, tissue was homogenized with mortar and pestle and stored in a desiccator until further analysis for C and N content and stable isotope enrichment (^{13}C and ^{15}N) by EA-IRMS (see below sections for details on flux calculations). Background detritus samples and tissue samples from each species were collected prior to the pulse-chase experiment and served as non-labeled controls.

DOM and POM Tracer Incorporation Rate Calculations

DOM and POM substrates, labeled and non-labeled sponge tissue, brittle star, and detritus samples were analyzed for organic C and total N content on an elemental analyzer [Elementar Isotope cube (*Elementar GmbH*, Langenselbold, Germany)] coupled to a BioVision isotope ratio mass spectrometer *(Elementar ltd*, Manchester, United Kingdom) for simultaneous measurement of organic carbon and nitrogen content and ^{13}C:^{12}C and ^{15}N:^{14}N ratios. Before analysis, samples were lyophilized for 24 h in a FD5515 *Ilchin Biobase* freeze drier. After freeze-drying, approximately 10 mg per sample was weighed out into separate tin capsules and acidified. The peak area (from the elemental analyzer) to content ratio was calculated with respect

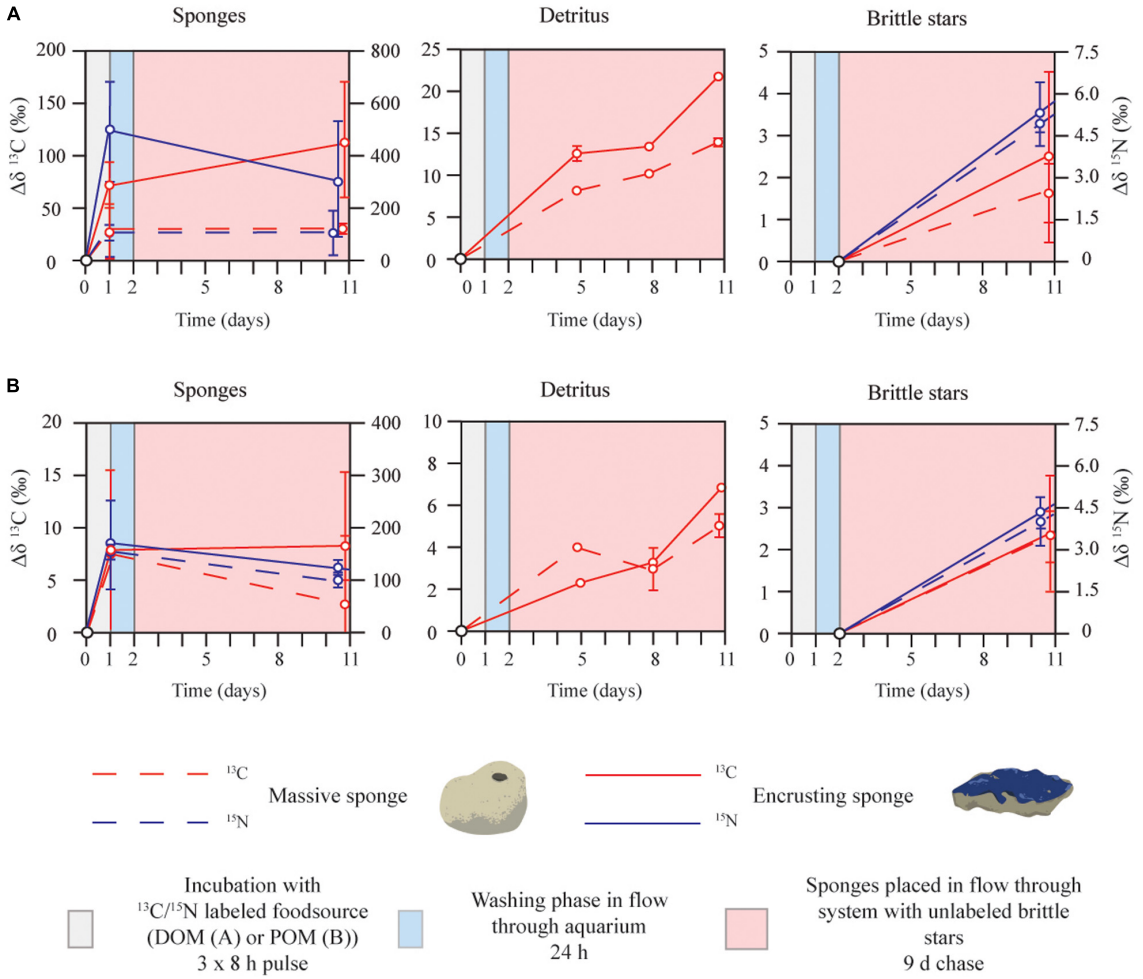

FIGURE 3 | Sponge-driven transfer of dissolved organic matter (DOM) **(A)** and particulate organic matter (POM) **(B)**, to sponge associated fauna in an *ex situ* aquarium set-up. The dashed and solid lines represent the fate of ^{13}C (red line) and ^{15}N (blue line) incorporated by massive sponges and encrusting sponges, respectively. After an initial 24-h pulse (gray shading; data obtained from Bart et al., 2020a) and a subsequent 24-h washing phase (blue shading), unlabeled brittle stars were introduced to the aquaria for a 9-day chase. Data are shown as mean ± SD above-background isotope tracer incorporation ($\Delta\delta^{13}C‰$ and $\Delta\delta^{15}N‰$) of each aquarium [**(A)** one aquarium with DOM-fed encrusting sponges and one with DOM-fed massive sponges and, **(B)** one aquarium with POM-fed encrusting sponges, and one with POM-fed massive sponges] for sponges, detritus, and detritivores. Unfortunately, ^{15}N-detritus data were not analyzed. Note the difference in scale on the *Y*-axis between panels. Data is also shown in **Supplementary Table 3**.

to several replicates of a standard (acetanilide) of known C and N content. To calculate the ^{13}C:^{12}C and ^{15}N:^{14}N ratios, C and N stable isotope ratios are expressed in standard delta notation as:

$$\delta^{13}C \text{ or } \delta^{15}N \ (\%) = \left(\frac{R_{sample}}{R_{ref} - 1} \right) \times 1000$$

where R is the ratio of ^{13}C:^{12}C or ^{15}N:^{14}N in the sample (R_{sample}; e.g., sponge tissue, detritus) or reference material: Vienna Pee Dee Belemnite for C (R_{ref} = 0.01118) and atmospheric nitrogen for N (R_{ref} = 0.00368). The above background enrichment of ^{13}C or ^{15}N in the samples was calculated as the excess fractional abundance of ^{13}C or ^{15}N in the samples compared with the background (i.e., non-enriched) values of non-labeled control samples (n = 3 for massive sponges, n = 4 for encrusting sponges, n = 2 for detritus). Unfortunately, the ^{15}N-detritus background measurements could not be analyzed and therefore no ^{15}N-enrichment of detritus samples was calculated.

$$E_{sample} = F_{sample} - F_{background}$$

where F is the fractional abundance of heavy isotope (^{13}C or ^{15}N) in the sample calculated as:

$$F_{sample \text{ or } background} = \frac{\delta^{13}C}{\delta^{13}C + \delta^{12}C} \text{ or } \frac{\delta^{15}N}{\delta^{15}N + \delta^{14}N}$$

and

$$F_{sample \text{ or } background} = \left(\frac{\delta^{13}C \text{ or } \delta^{15}N}{1000 + 1} \right) \times R_{ref}$$

Total tracer incorporation was calculated by multiplying the excess fractional abundance (E_{sample}) by the total C_{org} or N

content (μmol) of the tissue, divided by the labeling efficiency (as atom%) of the food source. Rates were then normalized to time and tissue C or N content of the sponges or detritivores.

Both detritus (detrital pathway) and the sponge tissue itself (predatory pathway) are considered stable-isotope-enriched food sources to brittle stars during the label-free chase. We calculated brittle star tracer uptake rates for two hypothetical scenarios: in scenario 1 with detritus as food source (using the labeling efficiency of detritus), and in scenario 2 with sponge tissue as food source (using the labeling efficiency of the sponge tissue).

The C:N ratios of DOM- and POM-derived transfer to brittle stars were calculated by dividing the organic C tracer incorporation rate by the total N tracer incorporation rate.

Statistics

Statistical analysis was performed in Primer V7 (Clarke and Gorley, 2015) with the add-on PERMANOVA+ (Anderson et al., 2008). Permutational multivariate analysis of variance (PERMANOVA) with Monte Carlo tests were used as this method is robust for low sample replication and non-normally distributed data. PERMANOVAs were run using Type III sum of squares and unrestricted permutation of raw data (9999 permutations); resemblance matrices were conducted using Euclidean distances. Individual one-way PERMANOVAs were conducted to test (1) the effect of treatment timepoint (24 h vs. 11-day) on stable isotope enrichment ($\delta^{13}C$ and $\delta^{15}N$) of sponge tissue after incubation with isotopically labeled DOM or POM, and (2) differences between brittle star tracer incorporation rates when sponges were fed DOM or POM. These incorporation rates were calculated assuming transfer from sponge to brittle star via detritus or via direct predation. Adjustments for multiple tests were made using the Bonferroni procedure. Full statistical output is available in **Supplementary Table 2**.

RESULTS

Incorporation of Tracer-Isotope Food Sources

The massive and encrusting sponge species assimilated DOM- and POM-derived ^{13}C and ^{15}N during the 24-h pulse (data obtained from Bart et al., 2020a). Stable isotope enrichment of sponge tissue did not significantly change between the end of the pulse and end of the chase phase (**Figures 3A,B**, left panels; **Supplementary Tables 2**, **3**) for both sponge species, except for POM-fed massive sponges, where tissue isotopic enrichment decreased significantly during the chase for ^{13}C.

Released detritus showed a continuous increase in above-background ^{13}C-enrichment (no ^{15}N data available) during the chase (**Figures 3A,B**, middle panels), demonstrating turnover of DOM and POM by sponges. After 9-day exposure to the labeled sponges and detritus, above-background enrichment of ^{13}C and ^{15}N was also detected in the tissue of the brittle stars (**Figures 3A,B**, right panels). This demonstrates transfer of sponge-assimilated DOM and POM to brittle stars.

Detrital or Predatory Transfer of DOM and POM to Brittle Stars

Both detritus and the sponge tissue itself are possible sources of enrichment found in brittle stars after the label-free chase phase. Thus, transfer of DOM and POM via sponges to brittle stars is possible via detritus feeding (scenario 1) and/or by predation on sponge tissue (scenario 2).

In scenario 1 (**Figure 4A** and **Supplementary Table 4**), brittle star uptake rates of detrital-C from POM-fed massive and encrusting sponges were higher compared to DOM-fed sponges, however, these differences were not significant (**Supplementary Table 2**).

In scenario 2 (**Figure 4B** and **Supplementary Table 4**), brittle star uptake rates of sponge tissue-C from POM-fed massive sponges were significantly higher than for DOM-fed massive sponges, while a similar, but non-significant trend was found between C_{DOM} and C_{POM} transfer for encrusting sponges (**Supplementary Table 2**).

For the transfer of tissue-N via predation, no significant differences were found in brittle star uptake rates between DOM- and POM-fed sponges, for both massive and encrusting sponges (**Supplementary Tables 2**, **4**).

The C:N ratios of uptake by brittle stars under scenario 2 (direct tissue predation) were lower for DOM-fed sponges (1.3 for massive and encrusting) than for POM-fed sponges (15 and 8 for massive and encrusting, respectively).

Direct uptake of DOM and POM by brittle stars (**Figure 4C**) was one to three orders of magnitude lower than transfer through scenario 1 or 2 (**Supplementary Table 4**).

DISCUSSION

This study provides the first evidence of all three consecutive steps of the sponge loop in deep-sea sponges. The two investigated deep-sea sponge species take up and assimilate DOM and POM, subsequently turn sponge-assimilated DOM and POM into detritus, and transfer carbon and nitrogen derived from both food sources to associated fauna. Transfer of assimilated food to associated fauna by sponges is possible via two scenarios: (1) via the production of detrital waste or (2) via direct predation on sponge tissue. The plausibility of both scenarios, and their potential ecological relevance for deep-sea ecosystems, are discussed below.

Transfer of DOM via Detrital and/or Predatory Pathway?

At present, DOM cycling by various types of sponges and its relevance for marine ecosystems, is a heavily debated topic (e.g., de Goeij et al., 2017; Leys et al., 2018; Pawlik and McMurray, 2020; Rix et al., 2020). The original sponge-loop hypothesis proposed that coral reef sponges recycle DOM by converting it into particulate detritus, which is then used by various detritivorous organisms and thereby re-enters the classical food chain (de Goeij et al., 2013). This pathway was tested on sponge species with mm-thin sheet to cm-thick

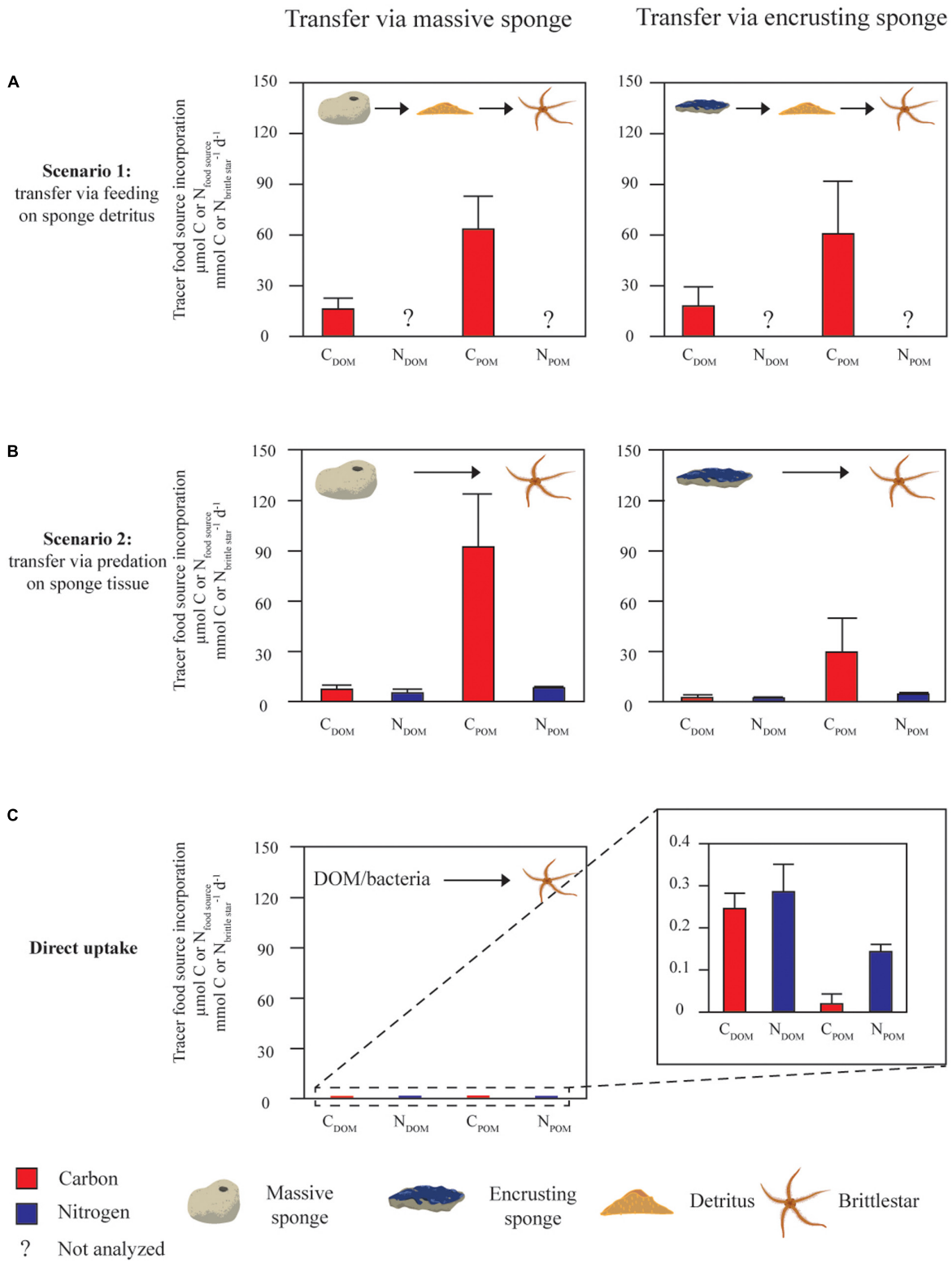

FIGURE 4 | Uptake of carbon (C) and nitrogen (N) by brittle stars via feeding on sponge detritus **(A)** or predation on sponge tissue **(B)** after sponges were fed isotopically labeled DOM or POM, versus direct uptake of DOM or POM by brittle stars **(C)** (values are expressed as µmol tracer C or N per mmol brittle star C or N per day, mean ± SD). In scenario 1 **(A)** brittle star tracer uptake rates were quantified with enriched detritus as food source, in scenario 2 **(B)**, uptake rates were calculated with the enriched sponge tissue as food source. The bottom panel **(C)** shows direct incorporation of tracer C and N by brittle stars after a 24 h pulse of isotopically labeled DOM and POM. Data are also shown in **Supplementary Table 4**.

(e.g., conulose, lobate, ficiform) encrusting growth forms—i.e. following the contours of the surface rather than growing upward—typically inhabiting crevices of the reef framework, but also appearing on the open reef. Based on encrusting sponges alone, sponge-loop carbon cycling is estimated to amount to the gross primary production rates of an entire coral reef ecosystem (de Goeij et al., 2013). Interestingly, massive upright growing sponges, living on the exposed parts of the reef, were not found to produce significant quantities of detritus (McMurray et al., 2018; Wooster et al., 2019). Massive sponges may allocate the majority of assimilated C in three-dimensional (upward) tissue growth, while (mm to cm-thin) encrusting species are restricted to space-limited, two-dimensional growth. Consequently, encrusting sponges may invest relatively more carbon in cell turnover, shedding and detritus production compared to massive species. This hypothesis was strengthened by recent work of Maier et al. (2020), who showed that deep-sea sponge detritus production rates of the lobate encrusting species *Mycale lingua,* exceeded detritus production rates of the globular massive species *G. barretti* by two orders of magnitude. McMurray et al. (2018) therefore proposed an alternative, predatory sponge-loop pathway for massive, non-space limited sponge species. Based on the limited number of replicates used in our study due to the difficulties obtaining and experimenting with live deep-sea organisms, we cannot rule out one of these scenarios, and will discuss both.

Deep-sea detrital sponge loop—Multiple studies have shown that sponge species from various deep-sea ecosystems produce particulate waste material in the form of detritus or fecal pellets (Witte and Graf, 1996; Rix et al., 2016; Kahn et al., 2018; Maier et al., 2020). Only few studies have quantified the release of detritus. The encrusting sponge *Hymedesmia coriacea* was found to convert 39% of ingested coral-derived DOM (i.e. coral mucus) into detritus (Rix et al., 2016), and five species of tropical shallow-water encrusting sponges released on average 12% of their biomass daily (Alexander et al., 2014). In comparison, the massive sponge *G. barretti* released very small amounts of detritus (0.03% of their biomass daily) (Maier et al., 2020). Yet, from an ecological perspective, detritus production by massive sponges can still have a significant effect on C turnover in marine ecosystems. The average total organic C content (C_{org}) of the massive *G. barretti* species in our experiments outweighed the organic C content of our encrusting sponges by three orders of magnitude (on average 6.5 g C_{org} (*G. barretti*) versus 0.008 g C_{org} (*Hymedesmia* sp.) per individual). Consequently, even when the relatively small *G. barretti* individuals used in our study release only 0.03% of its C_{org} as particulate detritus, detritus release rates would amount to 2 mg C d^{-1} per sponge individual. In contrast, a 12–39% C_{org} release by the much smaller encrusting sponges would mean a release of 1–3 mg C d^{-1} per sponge individual, which is similar to the absolute amount of detritus production by the massive sponge. Although little is known about the relative contribution of encrusting versus massive sponges in deep-sea ecosystems, the carbon standing stock of *G. barretti* in deep-sea ecosystems, such as the Western Barents Sea, can add up to 200 g C m^{-2} (Klitgaard and Tendal, 2004, converted to g C via Bart et al., 2020b). *Geodia barretti* can thus potentially produce 66 mg detritus per m^{-2} d^{-1}, which amounts to an abundant supply of particulate organic carbon to the local deep-sea benthos. For example, Piepenburg and Schmid (1996) estimated a mineralization rate of 21.9 mg C m^{-2} d^{-1} for benthic brittle stars on the North-East Greenland shelf even though this area is extremely rich in epifauna (30–340 individuals m^{-2}), and strongly dominated (80–98% of the total amount of organisms) by brittle stars.

Deep-sea predatory sponge loop—Spongivory is a strategy performed by various animals, including echinoderms (Randall and Hartman, 1968; Pawlik, 2011), and sponge spicules have been found in the stomachs of various brittle star species (Pearson and Gage, 1984). A study on 1165 deep-sea ophiuroid individuals of six different species by Pearson and Gage (1984) showed that deep-sea brittle stars are trophic generalists lacking dietary specialization. Feeding strategies ranged from detritivory to scavenging and even suspension feeding. Indeed, we found brittle stars to be capable of directly feeding on small amounts of our tracer DOM and POM during incubations (**Figure 4C**). Yet, rates of direct tracer incorporation were up to three orders of magnitude lower compared to the incorporation of sponge-derived C and N. Some massive sponge species are known to produce metabolites that deter predation (Chanas et al., 1997; Lindel et al., 2000) and thus spongivory is mostly seen on species that lack chemical defenses and have faster growth and reproduction rates (Pawlik, 2011). In contrast, chemically defended individuals that grow relatively slowly may be long lived, and therefore important for the sequestration and storage of C as biomass (McMurray et al., 2018). The massive HMA sponge used in our study, *G. barretti*, is known to produce various metabolites that inhibit biofouling (Sjögren et al., 2004; Hedner et al., 2008), but their effect on possible predators is unknown. Furthermore, it is difficult to make a genuine comparison with spongivory in shallow-water tropical systems, as deep-sea sponge metabolism is much slower due to lower ambient temperatures (Bart et al., 2020b), and deep-sea sponges are generally known for their longevity and C sequestration (Fallon et al., 2010; Kahn et al., 2015).

Ecological Relevance of DOM and POM Cycling Through a Sponge Loop

A comparison of potential deep-sea sponge-loop scenarios and comparing dissolved and particulate food sources reveals two interesting trends: when sponges feed on POM, relatively more C is transferred to associated fauna, compared to DOM. Secondly, relatively more DOM-derived C appears to be transferred via detritus compared to predation. This implies that POM (i.e. microbial plankton) is rather stored in sponge biomass, whereas DOM is mostly respired. This corresponds with the observations made by Kazanidis et al. (2018) and Bart et al. (2020a) that sponges use DOM for maintenance metabolism and turnover, while bacteria serve as an important food source for anabolic processes and are preferably incorporated into tissue. This is further reflected in the C:N ratios of uptake under the predatory sponge loop by brittle stars after sponge-feeding on DOM or

POM. The drastically decreased C:N after DOM-feeding (1.3) compared to POM-feeding (8–15) does not reflect that brittle stars obtain more N from DOM, but rather that the sponges *lost* more C from the isotopically enriched source, likely through respiration. Deep-sea sponges are indeed found to assimilate POM at very high assimilation efficiencies (up to 97%) compared to DOM (32–77%) (Bart et al., 2020a). This strengthens our hypothesis that DOM and POM are both essential parts of deep-sea sponge diet, as source of maintenance and as building blocks, respectively. This could also have ecological consequences for the wider associated ecosystem and food web, since both C and N may transfer at different rates according to the diet of sponges and the chosen feeding strategy of associated fauna.

It is important to note that both the detrital and predatory scenario are plausible for both types of sponges (i.e. massive and encrusting) and for both food sources (i.e. DOM and POM), and we cannot distinguish between the two scenarios under the current experimental approach. Moreover, our limited replication, in both sponge species and species of associated fauna, and the effect of concentration and lability of ambient DOM in time and space available to sponges living in different deep-sea ecosystems, make it very difficult to extrapolate our data to deep-sea benthic ecosystem-wide processes. The main aim of our study was to establish whether (common) deep-sea sponges possess all the consecutive steps of a sponge loop, rather than to show its potential ecological importance. To assess the full importance of sponge-loop pathways in the deep-sea, both qualitatively and quantitatively—many questions remain to be answered. For example, the relative importance of a deep-sea sponge loop may vary with the abundance and feeding activity of other benthic suspension feeders in deep-sea benthic ecosystems, such as CWC reefs and sponge grounds, that could participate in the cycling of DOM and POM. A recent extensive isotope tracer study by Maier et al. (2020) showed a four time higher production of detritus after DOM- and POM-feeding by the bivalve *Acesta excavate* compared to the sponge *G. barretti*. This detritus was further incorporated by brittle stars, suggesting that bivalves may be the main recyclers of organic matter within the CWC reefs under study, and the sponge loop in the deep-sea may in fact be better qualified as a "suspension feeder" loop. Interestingly, this was not found for shallow water tropical coral reefs, where other suspension feeders did not take part in a DOM-metazoan-detritus-detritivore pathway, but was restricted to sponges (de Goeij et al., 2013). Note, however, that Maier et al. (2020) did not test the recycling of sponge-produced detritus to associated fauna and that sponge *M. lingua* was the highest producer of detritus, i.e., 25 times higher production of detritus compared to the bivalve *A. excavata*. To estimate each organisms' role in the recycling of DOM and POM in deep-sea benthic ecosystems, resource fluxes need to be extrapolated to respective biomass estimates within these ecosystems. Furthermore, there is a lack of *in situ* studies to verify *ex situ* rates presented to date. *In situ* studies to determine uptake rates of ambient DOM and the use of stable-isotope tracer food sources on deep-sea benthic communities, including multiple sponge- and other suspension-feeding species and associated fauna, will shed light on how sponges drive food webs in the dark deep-sea.

DATA AVAILABILITY STATEMENT

The original contributions presented in the study are included in the article/**Supplementary Material**, further inquiries can be directed to the corresponding author/s.

AUTHOR CONTRIBUTIONS

JG and HR acquired the funding. MB and JG designed the experiments. JG, HR, and MB collected the animals. MB conducted the incubations experiments. MB, JG, and MH performed the data analyses and designed the tables and figures. MB, JG, MH, and PV wrote the manuscript. All co-authors approved the manuscript. All authors contributed to the article and approved the submitted version.

FUNDING

This project has received funding from the European Research Council under the European Union's Horizon 2020 Research and Innovation Programme (SponGES grant agreement no. 679849 and ERC starting grant agreement no. 715513 to JG). This document only reflects the authors' views and the Executive Agency for Small and Medium-sized Enterprises (EASME) is not responsible for any use that may be made of the information it contains.

ACKNOWLEDGMENTS

We dedicate this work to our EU Horizon 2020 SponGES coordinator, colleague, and friend HR who sadly passed away, too soon, on March 7 2020 before he could witness the outcomes of his project. We thank all our collaborators at the SponGES project, and all colleagues at the Department of Biological Sciences at the University of Bergen, Norway, for the use of facilities and equipment. Many thanks to the ROV crew of the ÆGIR 6000 for their careful collection of the sponges. Thanks to Erik Wurz for his help maintaining the onboard aquaria. We also thank Jorien Schoorl for her technical assistance at the University of Amsterdam. Many thanks also to Sara Campana, Titus Rombouts, and Clea van de Ven for their help with the algal batch cultures, and Angela Marulanda Gomez for her help in the field. Lastly, we thank Gina Fields for her help with the design and development of the figures.

SUPPLEMENTARY MATERIAL

The Supplementary Material for this article can be found online at: https://www.frontiersin.org/articles/10.3389/fmars.2021.604879/full#supplementary-material

REFERENCES

Alexander, B. E., Liebrand, K., Osinga, R., van der Geest, H. G., Admiraal, W., Cleutjens, J. P., et al. (2014). Cell turnover and detritus production in marine sponges from tropical and temperate benthic ecosystems. *PLoS One.* 9:e109486. doi: 10.1371/journal.pone.010948

Anderson, M. J., Clarke, K. R., and Gorley, R. N. (2008). *PERMANOVA+ for PRIMER: guide to software and statistical methods*. Plymouth: PRIMER-E.

Azam, F., Fenchel, T., Field, J. G., Gray, J. S., Meyer-Reil, L. A., and Thingstad, F. (1983). The ecological role of water-column microbes in the sea. *Mar. Ecol. Prog. Ser.* 10, 257–263. doi: 10.3354/meps010257

Bart, M. C., de Kluijver, A., Hoetjes, S., Absalah, S., Mueller, B., Kenchington, E. L., et al. (2020a). Differential processing of dissolved and particulate organic matter by deep-sea sponges and their microbial symbionts. *Sci. Rep.* 10:17515.

Bart, M. C., Mueller, B., Rombouts, T., van de Ven, C., Tompkins, G., Osinga, R., et al. (2020b). Dissolved organic carbon (DOC) is essential to balance the metabolic demands of North-Atlantic deep-sea sponges. *Limnol. Oceanogr.* doi: 10.1002/lno.11652

Benner, R., Pakulski, J. D., McCarthy, M., Hedges, J. I., and Hatcher, P. G. (1992). Bulk chemical characteristics of dissolved organic matter in the ocean. *Science* 255, 1561–1564. doi: 10.1126/science.255.5051.1561

Buhl-Mortensen, P., Dolan, M., and Buhl-Mortensen, L. (2009). Prediction of benthic biotopes on a Norwegian offshore bank using a combination of multivariate analysis and GIS classification. *ICES J. Mar. Sci.* 66, 2026–2032. doi: 10.1093/icesjms/fsp200

Carlson, C. A. (2002). "Production and removal processes," in *Biogeochemistry of Marine Dissolved Organic Matter*, eds D. A. Hansell and C. A. Carlson (San Diego, CA: Academic Press), 91–151. doi: 10.1016/b978-012323841-2/50006-3

Cathalot, C., Van Oevelen, D., Cox, T. J., Kutti, T., Lavaleye, M., Duineveld, G., et al. (2015). Cold-water coral reefs and adjacent sponge grounds: hotspots of benthic respiration and organic carbon cycling in the deep sea. *Front. Mar. Sci.* 2:37. doi: 10.3389/fmars.2015.00037

Chanas, B., Pawlik, J. R., Lindel, T., and Fenical, W. (1997). Chemical defense of the Caribbean sponge *Agelas clathrodes* (Schmidt). *J. Exp. Mar. Biol. Ecol.* 208, 185–196. doi: 10.1016/s0022-0981(96)02653-6

Clark, H. L. (1933). *A Handbook of the Littoral Echinoderms of Puerto Rico and the Other West Indian Islands. Scientific Survey of Porto Rico and the Virgin Islands*, Vol. 16. New York, NY: Academy of Sciences.

Clarke, K. R., and Gorley, R. N. (2015). *Getting Started With PRIMER v7*. Plymouth: PRIMER-E.

de Goeij, J. M., Lesser, M. P., and Pawlik, J. R. (2017). "Nutrient fluxes and ecological functions of coral reef sponges in a changing ocean," in *Climate Change, Ocean Acidification and Sponges*, eds J. Carballo, and J. Bell (Switzerland, AG: Springer, Cham), 373–410. doi: 10.1007/978-3-319-59008-0_8

de Goeij, J. M., Moodley, L., Houtekamer, M., Carballeira, N. M., and Van Duyl, F. C. (2008). Tracing ^{13}C-enriched dissolved and particulate organic carbon in the bacteria-containing coral reef sponge *Halisarca caerulea*: evidence for DOM-feeding. *Limnol. Oceanogr.* 53, 1376–1386. doi: 10.4319/lo.2008.53.4.1376

de Goeij, J. M., Van Oevelen, D., Vermeij, M. J., Osinga, R., Middelburg, J. J., De Goeij, A. F., et al. (2013). Surviving in a marine desert: the sponge loop retains resources within coral reefs. *Science* 342, 108–110. doi: 10.1126/science.1241981

Duarte, L. F. L., and Nalesso, R. (1996). The sponge *Zygomycale parishii* (Bowerbank) and its endobiotic fauna. *Estuar. Coast. Mar. Sci.* 42, 139–151. doi: 10.1006/ecss.1996.0011

Duineveld, G. C., Lavaleye, M. S., Bergman, M. J., De Stigter, H., and Mienis, F. (2007). Trophic structure of a cold-water coral mound community (Rockall Bank, NE Atlantic) in relation to the near-bottom particle supply and current regime. bull. *Mar. Sci.* 81, 449–467.

Duineveld, G. C. A., Lavaleye, M. S. S., and Berghuis, E. M. (2004). Particle flux and food supply to a seamount cold-water coral community (Galicia Bank. NW Spain). *Mar. Ecol. Prog. Ser.* 277, 13–23. doi: 10.3354/meps277013

Fallon, S. J., James, K., Norman, R., Kelly, M., and Ellwood, M. J. (2010). A simple radiocarbon dating method for determining the age and growth rate of deep-sea sponges. *Nucl. Instrum. Methods Phys. Res., B.* 268, 1241–1243. doi: 10.1016/j.nimb.2009.10.143

Fenchel, T. (2008). The microbial loop–25 years later. *J. Exp. Mar. Biol. Ecol.* 366, 99–103. doi: 10.1016/j.jembe.2008.07.013

Gooday, A. J. (2002). Biological responses to seasonally varying fluxes of organic matter to the ocean floor: a review. *J. Oceanogr.* 58, 305–332.

Grebmeier, J. M., Bluhm, B. A., Cooper, L. W., Danielson, S. L., Arrigo, K. R., Blanchard, A. L., et al. (2015). Ecosystem characteristics and processes facilitating persistent macrobenthic biomass hotspots and associated benthivory in the pacific arctic. *Progr. Oceanogr.* 136, 92–114. doi: 10.1016/j.pocean.2015.05.006

Hedner, E., Sjögren, M., Hodzic, S., Andersson, R., Göransson, U., Jonsson, P. R., et al. (2008). Antifouling activity of a dibrominated cyclopeptide from the marine sponge *Geodia barretti*. *J. Nat. Prod.* 71, 330–333. doi: 10.1021/np0705209

Jørgensen, L. L., Ljubin, P., Skjoldal, H. R., Ingvaldsen, R. B., Anisimova, N., and Manushin, I. (2015). Distribution of benthic megafauna in the Barents Sea: baseline for an ecosystem approach to management. *ICES J. Mar. Sci.* 72, 595–613. doi: 10.1093/icesjms/fsu106

Kahn, A. S., Chu, J. W., and Leys, S. P. (2018). Trophic ecology of glass sponge reefs in the strait of Georgia. *Br. Columbia. Sci. Rep.* 8:756.

Kahn, A. S., Yahel, G., Chu, J. W., Tunnicliffe, V., and Leys, S. P. (2015). Benthic grazing and carbon sequestration by deep-water glass sponge reefs. *Limnol. Oceanogr.* 60, 78–88. doi: 10.1002/lno.10002

Kazanidis, G., van Oevelen, D., Veuger, B., and Witte, U. F. (2018). Unravelling the versatile feeding and metabolic strategies of the cold-water ecosystem engineer *Spongosorites coralliophaga* (Stephens, 1915). *Deep Sea Res. Part I Oceanogr. Res. Pap.* 141, 71–82. doi: 10.1016/j.dsr.2018.07.009

Kędra, M., Renaud, P. E., and Andrade, H. (2017). Epibenthic diversity and productivity on a heavily trawled Barents Sea bank (Tromsøflaket). *Oceanologia* 59, 93–101. doi: 10.1016/j.oceano.2016.12.001

Klitgaard, A. B., and Tendal, O. S. (2004). Distribution and species composition of mass occurrences of large-sized sponges in the northeast Atlantic. *Progr. Oceanogr.* 61, 57–98. doi: 10.1016/j.pocean.2004.06.002

Kutti, T., Bannister, R. J., and Fosså, J. H. (2013). Community structure and ecological function of deep-water sponge grounds in the traenadypet MPA—Northern Norwegian continental shelf. *Cont. Shelf Res.* 69, 21–30. doi: 10.1016/j.csr.2013.09.011

Lesser, M. P., Mueller, B., Pankey, M. S., Macartney, K. J., Slattery, M., and de Goeij, J. M. (2020). Depth-dependent detritus production in the sponge. *Halisarca caerulea*. Limnol. Oceanogr. 65, 1200–1216. doi: 10.1002/lno.11384

Leys, S. P., Kahn, A. S., Fang, J. K. H., Kutti, T., and Bannister, R. J. (2018). Phagocytosis of microbial symbionts balances the carbon and nitrogen budget for the deep-water boreal sponge *Geodia barretti*. *Limnol. Oceanogr.* 63, 187–202. doi: 10.1002/lno.10623

Lindel, T., Hoffmann, H., Hochgürtel, M., and Pawlik, J. R. (2000). Structure–activity relationship of inhibition of fish feeding by sponge-derived and synthetic pyrrole–imidazole alkaloids. *J. Chem. Ecol.* 26, 1477–1496.

Maier, S. R., Kutti, T., Bannister, R. J., Fang, J. K. H., van Breugel, P., van Rijswijk, P., et al. (2020). Recycling pathways in cold-water coral reefs: use of dissolved organic matter and bacteria by key suspension feeding taxa. *Sci. Rep.* 10: 9942.

Maldonado, M., Aguilar, R., Bannister, R. J., Bell, J. J., Conway, K. W., Dayton, P. K., et al. (2017). "Sponge grounds as key marine habitats: a synthetic review of types, structure, functional roles and conservation concerns," in *Marine Animal Forests: the Ecology of Benthic Biodiversity Hotspots*, eds S. Rossi, L. Bramanti, A. Gori, and C. Orejas Saco del Valle (Switzerland: Springer International Publishing).

McClintock, J. B. (1994). Trophic biology of Antarctic shallow-water echinoderms. *Mar. Ecol. Prog. Ser.* 111, 191–202. doi: 10.3354/meps111191

McMurray, S. E., Stubler, A. D., Erwin, P. M., Finelli, C. M., and Pawlik, J. R. (2018). A test of the sponge-loop hypothesis for emergent Caribbean reef sponges. *Mar. Ecol. Prog. Ser.* 588, 1–14. doi: 10.3354/meps12466

Miller, J. H. (1972). *Experiments in Molecular Genetics*. New York, NY: Cold Spring Harbor Laboratory, Cold Spring Harbor.

Miller, R. J., Hocevar, J., Stone, R. P., and Fedorov, D. V. (2012). Structure-forming corals and sponges and their use as fish habitat in Bering Sea submarine canyons. *PLoS One.* 7:e33885. doi: 10.1371/journal.pone.0033885

Morison, G. W. (1979). *Studies on the Ecology of the Sub-Antarctic ophiuroid Ophionotus Hexactis*. [M. Phil. Thesis].[London (UK)]: University of London.

Pawlik, J. R. (2011). The chemical ecology of sponges on Caribbean reefs: natural products shape natural systems. *Bioscience* 61, 888–898. doi: 10.1525/bio.2011.61.11.8

Pawlik, J. R., and McMurray, S. E. (2020). The emerging ecological and biogeochemical importance of sponges on coral reefs. *Ann. Rev. Mar. Sci.* 12, 315–337. doi: 10.1146/annurev-marine-010419-010807

Pearson, M., and Gage, J. D. (1984). Diets of some deep-sea brittle stars in the Rockall Trough. *Mar. Biol.* 82, 247–258. doi: 10.1007/bf00392406

Piepenburg, D., and Schmid, M. K. (1996). Distribution, abundance, biomass, and mineralization potential of the epibenthic megafauna of the Northeast Greenland shelf. *Mari. Biol.* 125, 321–332. doi: 10.1007/bf00346313

Pile, A. J., Patterson, M. R., and Witman, J. D. (1996). In situ grazing on plankton < 10 μm by the boreal sponge *Mycale lingua*. *Mar. Ecol. Prog. Ser.* 141, 95–102. doi: 10.3354/meps141095

Polovina, J. J. (1984). Model of a coral reef ecosystem. *Coral reefs* 3, 1–11. doi: 10.1007/bf00306135

Radax, R., Hoffmann, F., Rapp, H. T., Leininger, S., and Schleper, C. (2012). Ammonia-oxidizing archaea as main drivers of nitrification in cold-water sponges. *Environ. Microbiol.* 14, 909–923. doi: 10.1111/j.1462-2920.2011.02661.x

Randall, J. E., and Hartman, W. D. (1968). Sponge-feeding fishes of the West Indies. *Mar. Biol.* 1, 216–225. doi: 10.1007/bf00347115

Reiswig, H. M. (1971). Particle feeding in natural populations of three marine demosponges. *Biol. Bull.* 141, 568–591. doi: 10.2307/1540270

Rix, L., de Goeij, J. M., Mueller, C. E., Struck, U., Middelburg, J. J., Van Duyl, F. C., et al. (2016). Coral mucus fuels the sponge loop in warm-and cold-water coral reef ecosystems. *Sci. Rep.* 6:18715.

Rix, L., de Goeij, J. M., van Oevelen, D., Struck, U., Al-Horani, F. A., Wild, C., et al. (2018). Reef sponges facilitate the transfer of coral-derived organic matter to their associated fauna via the sponge loop. *Mari. Ecol. Prog. Ser.* 589, 85–96. doi: 10.3354/meps12443

Rix, L., de Goeij, J. M., van Oevelen, D., Struck, U., Al-Horani, F. A., Wild, C., et al. (2017). Differential recycling of coral and algal dissolved organic matter via the sponge loop. *Funct. Ecol.* 31, 778–789. doi: 10.1111/1365-2435.12758

Rix, L., Ribes, M., Coma, R., Jahn, M. T., de Goeij, J. M., van Oevelen, D., et al. (2020). Heterotrophy in the earliest gut: a single-cell view of heterotrophic carbon and nitrogen assimilation in sponge-microbe symbioses. *ISME J.* 14, 2554–2567. doi: 10.1038/s41396-020-0706-3

Rovelli, L., Attard, K. M., Bryant, L. D., Flögel, S., Stahl, H., Roberts, J. M., et al. (2015). Benthic O_2 uptake of two cold-water coral communities estimated with the non-invasive eddy correlation technique. *Mar. Ecol. Prog. Ser.* 525, 97–104. doi: 10.3354/meps11211

Rüggeberg, A., Flögel, S., Dullo, W. C., Hissmann, K., and Freiwald, A. (2011). Water mass characteristics and sill dynamics in a subpolar cold-water coral reef setting at Stjernsund, northern Norway. *Mar. Geol.* 282, 5–12. doi: 10.1016/j.margeo.2010.05.009

Sjögren, M., Göransson, U., Johnson, A. L., Dahlström, M., Andersson, R., Bergman, J., et al. (2004). Antifouling activity of brominated cyclopeptides from the marine sponge *Geodia barretti*. *J. Nat. Prod.* 67, 368–372. doi: 10.1021/np0302403

Stöhr, S., O'Hara, T. D., and Thuy, B. (2012). Global diversity of brittle stars (Echinodermata: Ophiuroidea). *PLoS One.* 7:e31940. doi: 10.1371/journal.pone.0031940

Sundfjord, A., Fer, I., Kasajima, Y., and Svendsen, H. (2007). Observations of turbulent mixing and hydrography in the marginal ice zone of the Barents Sea. *J. Geophys. Res. Oceans.* 112:C05008.

van Oevelen, D., Duineveld, G., Lavaleye, M., Mienis, F., Soetaert, K., and Heip, C. H. (2009). The cold-water coral community as hotspot of carbon cycling on continental margins: a food-web analysis from Rockall Bank (Northeast Atlantic). *Limnol. Oceanogr.* 54, 1829–1844. doi: 10.4319/lo.2009.54.6.1829

Witte, U., and Graf, G. (1996). Metabolism of deep-sea sponges in the greenland-Norwegian Sea. *J. Exp. Mar. Biol. Ecol.* 198, 223–235. doi: 10.1016/0022-0981(96)00006-8

Wooster, M. K., McMurray, S. E., Pawlik, J. R., Morán, X. A., and Berumen, M. L. (2019). Feeding and respiration by giant barrel sponges across a gradient of food abundance in the Red Sea. *Limnol. Oceanogr.* 64, 1790–1801. doi: 10.1002/lno.11151

Conflict of Interest: The authors declare that the research was conducted in the absence of any commercial or financial relationships that could be construed as a potential conflict of interest.

Copyright © 2021 Bart, Hudspith, Rapp, Verdonschot and de Goeij. This is an open-access article distributed under the terms of the Creative Commons Attribution License (CC BY). The use, distribution or reproduction in other forums is permitted, provided the original author(s) and the copyright owner(s) are credited and that the original publication in this journal is cited, in accordance with accepted academic practice. No use, distribution or reproduction is permitted which does not comply with these terms.

frontiers in Marine Science

ORIGINAL RESEARCH
published: 24 March 2021
doi: 10.3389/fmars.2021.611539

The Hexactinellid Deep-Water Sponge *Vazella pourtalesii* (Schmidt, 1870) (Rossellidae) Copes With Temporarily Elevated Concentrations of Suspended Natural Sediment

Erik Wurz[1], Lindsay Beazley[2], Barry MacDonald[2], Ellen Kenchington[2], Hans Tore Rapp[3] and Ronald Osinga[1]*

[1] Department of Marine Animal Ecology, Wageningen University & Research, Wageningen, Netherlands, [2] Department of Fisheries and Oceans, Bedford Institute of Oceanography, Dartmouth, NS, Canada, [3] Centre for Geobiology, Department of Biology, University of Bergen, Bergen, Norway

OPEN ACCESS

Edited by:
Cristina Gambi, Marche Polytechnic University, Italy

Reviewed by:
Andreu Santin Muriel, Institute of Marine Sciences (ICM-CSIC), Spain
Tina Molodtsova, P.P. Shirshov Institute of Oceanology (RAS), Russia

***Correspondence:**
Erik Wurz
erik.wurz@wur.nl

Specialty section:
This article was submitted to Deep-Sea Environments and Ecology, a section of the journal Frontiers in Marine Science

Received: *29 September 2020*
Accepted: *02 March 2021*
Published: *24 March 2021*

Citation:
Wurz E, Beazley L, MacDonald B, Kenchington E, Rapp HT and Osinga R (2021) The Hexactinellid Deep-Water Sponge Vazella pourtalesii (Schmidt, 1870) (Rossellidae) Copes With Temporarily Elevated Concentrations of Suspended Natural Sediment. Front. Mar. Sci. 8:611539. doi: 10.3389/fmars.2021.611539

Plumes of re-suspended sediment potentially smother and clog the aquiferous system of filter-feeding sponges with unknown implications for their health. For the first time, we examined the physiological responses of repeated exposure to natural sediment in the glass sponge *Vazella pourtalesii*, which forms dense sponge grounds in Emerald Basin off Nova Scotia, Canada. *Ex situ* chamber-based measurements of bacterial clearance and oxygen consumption (respiration) rates indicated that individuals subjected to elevated concentrations of suspended sediment expressed normal clearance and respiration rates over 7 days of sediment exposure, indicating an ability to cope with elevated concentrations of indigestible sediment particles. However, clearance rates significantly declined after 14 days of sediment exposure, suggesting an inability to cope with long-term exposure to increased sediment load. Therefore, long-term exposure to elevated concentrations of suspended sediment should be avoided in order to minimize adverse effects on the abundant *Vazella* sponge grounds.

Keywords: sponge grounds, *Vazella pourtalesii*, re-suspended sediment, bottom-trawling, marine conservation area

INTRODUCTION

Sponges (Porifera) play a pivotal role within the marine ecosystems they inhabit from tropical shallow waters to abyssal depths. Providing three-dimensional structures and secondary substrates through a diversity of growth forms, they function as microhabitats themselves, increasing local faunal biodiversity (Beazley et al., 2013, 2015; Hawkes et al., 2019). Sponges are also key players in benthic-pelagic energy transfer and biochemical processing by filtering large volumes of seawater (Maldonado et al., 2012, 2017; De Goeij et al., 2013; Pham et al., 2019). The use of advanced technologies such as remotely operated vehicles (ROVs) has provided evidence of the vast diversity and abundance of sponges in the majority of deep-sea ecosystems (Maldonado et al., 2017). In specific oceanographic settings, they can represent up to 94% of the benthic biomass

(Murillo et al., 2012). Over the past decade, such sponge-dominated deep-sea habitats have been characterized as sponge grounds (Hogg et al., 2010).

With the increasing discovery of these important sponge communities in the deep-sea also comes evidence of their destruction, caused mainly by the use of bottom-tending fishing gears (Hogg et al., 2010). Bottom trawling has direct and indirect effects on sessile, filter-feeding sponges. In addition to direct removal, damage, or burying, fishing gear re-suspends bottom sediments (Hogg et al., 2010). Depending on the gear used, seabed structure, and distance from the impact site, particle concentrations of up to 500 mg L^{-1} can be reached behind the path of a trawl (Durrieu de Madron et al., 2005). In a disturbance experiment in the Mediterranean Sea, the average concentration behind a trawl was measured at 50 mg L^{-1}, with the predominant proportion of re-suspended particles made up of silty clay (grain size 1–63 μm) (Durrieu de Madron et al., 2005). Plumes of particles within the micron scale may stay suspended for days and be transported by oceanic currents over vast distances (Puig et al., 2012). Thus, generated plumes have the potential to indirectly impact habitats kilometers away from the impact site over an extended period of time (Hogg et al., 2010; Mengual et al., 2016; Grant et al., 2019).

Previous studies have found that sponges are negatively impacted by low concentrations of suspended particles. Exposure to suspended particle concentrations between 10 and 95 mg L^{-1} has resulted in decreased pumping efficiency and filtering capacity in some species (Bell et al., 2015; Grant et al., 2018). Strehlow et al. (2017) showed that the demosponge *Ianthella basta* (Pallas, 1766) (Ianthellidae) incorporated suspended sediment particles as small as 4.2 μm from the surrounding sea water into its mesohyl. The authors postulated that this particle size is well within the range of bacterioplankton that filter-feeding sponges predominantly utilize as a food source. Its uptake therefore could cause serious deleterious effects on sponge health. At the same time, some sponge species have developed mechanisms to exclude or excrete ingested sediment. These mechanisms include mucus production, exclusion of particles by incurrent pores, closure of oscula and pumping cessation, expulsion of particles from the aquiferous system, and structural component regression to reduce the volume of the aquiferous system and limit pumping and clearance capacity (Strehlow et al., 2017). These active mechanisms require additional energetic expenditures, and it is unknown if sponges can sustain those over long time periods (Bell et al., 2015; Schönberg, 2016a,b; Strehlow et al., 2016).

While the effects of sediment exposure on glass sponges are less understood compared to demosponges, Tompkins-Macdonald and Leys (2008) demonstrated that *Rhabdocalyptus dawsoni* (Lambe, 1893) (Rossellidae) arrests pumping when subjected to suspended particle concentrations of 36 mg L^{-1}, confirming a response of hexactinellids to suspended particles. An *in situ* study (Grant et al., 2018) on the reef-forming glass sponge *Aphrocallistes vastus* Schulze, 1886 (Aphrocallistidae) from the northeast Pacific showed that suspended particles in concentrations as low as 4.4 mg L^{-1} caused sponges to arrest their pumping with prolonged phases of "coughing" patterns in pumping activities. The arrests and "coughing" patterns are thought to protect the sponge's aquiferous system from clogging and help remove ingested particles. At the same time, reduced pumping and thus filtering activity limit feeding and waste product excretion and can result in adverse effects on overall metabolism and health of individual sponges and consequently the biogenic habitats they form (Grant et al., 2018).

The hexactinellid sponge *V. pourtalesii* (Schmidt, 1870) (Rossellidae) is distributed along the continental margin of eastern North America, from the Florida Keys in the southeastern United States to the Scotian Shelf off Nova Scotia, Canada, where it forms extensive sponge grounds between 160 and 200 m depth (**Figure 1**; Beazley et al., 2018). The densest known aggregations of *V. pourtalesii* occur in Emerald Basin, a deep-water basin on the central Scotian Shelf, where this species reaches heights (up to 40 cm) and densities (up to 4 individuals per m^2) (Maldonado et al., 2020) not observed elsewhere across its distribution range. The presence of *V. pourtalesii* sponge grounds in Emerald Basin was first noted by fishermen when fishing for pollock and redfish using otter trawl gear (Fuller, 2011; Beazley et al., 2018).

The highest biomass/densities of *Vazella pourtalesii* from commercial bycatch (where catch biomass up to 5900 kg in a single tow has been reported), research vessel trawl catch data, and *in situ* camera surveys (described in Beazley et al., 2018) are reported to occur in two localized areas of Emerald Basin: the eastern flank of Sambro Bank, and on a shallower saddle between Emerald Basin's Main and Northern Basins, to the west of the area known to fisherman as "The Patch" (see **Figure 2**; Fuller, 2011; Beazley et al., 2018). Conservation of sponge grounds has gained international attention since they were listed as species vulnerable to bottom contact fishing gears by the Food and Agriculture Organization of the United Nations (FAO, 2009) in the international guidelines written in response to the United Nations General Assembly resolutions aimed at protecting vulnerable marine ecosystems. Deep-sea sponge aggregations are included in the OSPAR List of threatened and/or declining species and habitats (OSPAR agreement 2008-6), and regional fisheries management organizations such as the North Atlantic Fisheries Organization have introduced management measures to protect sponge habitats (NAFO, 2021). In Canada, sponge grounds may qualify as sensitive benthic areas, the Canadian equivalent of vulnerable marine ecosystems (DFO, 2017a). In order to protect these dense aggregations from adverse impacts of bottom trawling, in 2013, Fisheries and Oceans Canada (DFO) implemented two sponge conservation areas (the Sambro Bank and Emerald Basin Sponge Conservation Areas, referred to herein as SCAs) prohibiting the use of bottom-tending gears. However, groundfish fishing activities continue to occur almost immediately adjacent to the borders of these two conservation areas (DFO, 2017b), potentially affecting the sponge grounds and abundant megafaunal communities within the SCAs (Hawkes et al., 2019) via re-suspension of sediment.

Here, in a laboratory setting, we report for the first time the physiological response of *V. pourtalesii* to long-term exposure of an ecologically relevant concentration (50 mg L^{-1}) (Tjensvoll et al., 2013; Kutti et al., 2015) of suspended natural bottom sediment, thereby evaluating an indirect effect of bottom trawling

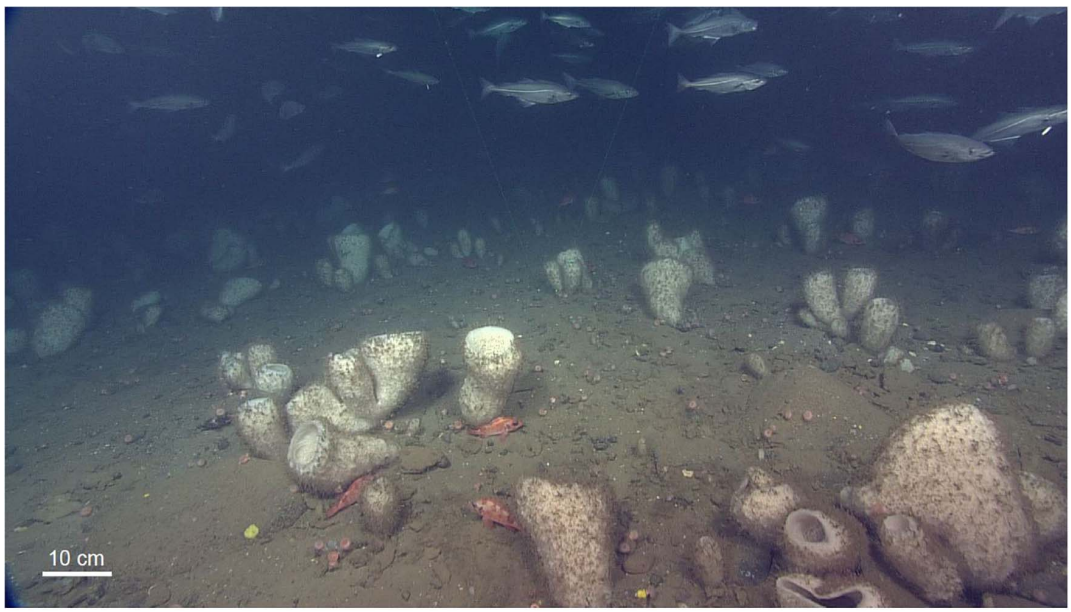

FIGURE 1 | Sponge grounds formed by *Vazella pourtalesii* in the Sambro Bank Sponge Conservation Area, Emerald Basin, Nova Scotia, Canada. Image is a frame grab from video collected using the ROV ROPOS in 2017. Depth is 155 m, and location is 43°53.6513 N, −63°4.6513 W.

activity. Animal performance was quantified by assessing oxygen removal rates and clearance rates for bacterioplankton, thus providing the first insight into the physiological responses of this species to sediment exposure. Subsequent recovery after sediment exposure was evaluated using scanning electron microscopy (SEM) techniques and qualitative observations. Knowledge on the responses of *V. pourtalesii* to repeated sediment exposure may help provide insight into the biological considerations needed for effective closure area design and management of glass sponge grounds in the northwest Atlantic.

MATERIALS AND METHODS

Collection of Animals

During an oceanographic mission to the *Vazella* sponge grounds of Emerald Basin in 2017 (**Figure 2**; see Beazley et al., 2017 for mission details) in support of the EU-funded Horizon 2020 project SponGES, the ROV ROPOS[1], a 40 hp Science/Work Class ROV owned and operated by the non-profit Canadian Scientific Submersible Facility (CSSF), was deployed from the Canadian Coast Guard Ship *Martha L. Black* to collect specimens of *V. pourtalesii* for *ex situ* experimentation. A total of 23 sponges were collected over four separate deployments of ROPOS, three of which occurred in the center of the Sambro Bank SCA at approximately 160 m depth (Collection Location 1 in **Figure 2**), and one that spanned across the southern border of the closure at approximately 217 m depth (Collection Location 2, **Figure 2**). During collection, the manipulator arm of ROPOS was carefully used to collect sponges by their substrate attachment point (pebbles and cobbles) and placed them in the ROPOS "biobox" where they remained submerged upon recovery. Once onboard, the sponges were transferred in a submerged state to an insulated 500 L polyethylene holding tank inside a refrigerated shipping container. The sponges were placed in individual compartments (10 cm by 10 cm) of a grid at the bottom of the holding tank to help keep them stationary. Subsurface water (<5 m) was pumped into a tank on deck using a portable pump, which was then distributed to a tank inside the refrigerated container, chilled to 9 °C, and then slowly pumped via a peristaltic pump (1.2 L min^{-1}) to the holding tank containing the sponge specimens. The chilled water tank was refilled twice a day, resulting in four water exchanges per day.

Sampling deep-water fauna for experimentation is a logistical and technological challenge. Sampling via the ROV's manipulator arm required delicate and precise handling of sponges within the target size range. Due to this time-consuming process, along with impediments to sampling from inclement weather, only a limited number of individuals could be collected. At the same time, *V. pourtalesii* has been recognized as a vulnerable species (Beazley et al., 2018) and as a result, removal of animals for experimentation should be kept to a minimum. Due to these limitations and challenges, the study was performed with a minimum number of individuals to account for independent replication.

Acclimatization to *ex situ* Experimental Conditions

The sponges were transferred to facilities at the Bedford Institute of Oceanography (BIO), Nova Scotia, Canada, where they were maintained in a 500 L holding tank supplied with coarsely

[1]https://www.ropos.com/

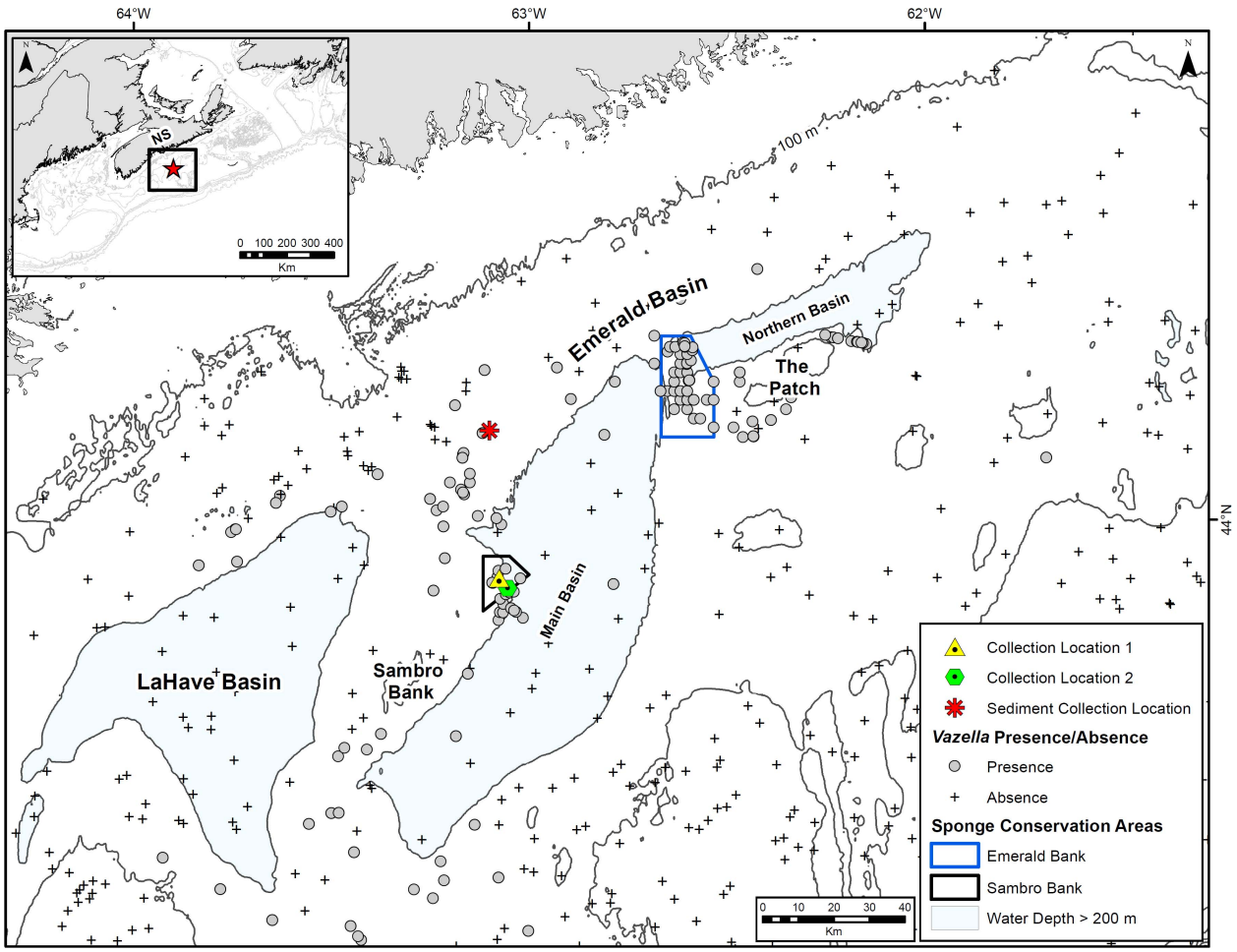

FIGURE 2 | Location of collection sites for *ex situ* experiments in the Sambro Bank Sponge Conservation Area, Emerald Basin, Nova Scotia. Also shown is the location of sediment collection north of Emerald Basin, and the presence–absence of *Vazella pourtalesii* from commercial bycatch records, and DFO optical (camera) and multispecies research vessel trawl surveys.

filtered saltwater from the adjacent Bedford Basin, the intake of which is 200 m from shore and at a depth of 17 m at low tide (∼3 m off bottom). Salinity was 30.5 ± 0.2 PSU over the course of 10 months. To ensure full recovery from sampling and transportation, sponges were acclimatized under the above conditions for 7 months. A non-axenic phytoplankton culture was routinely added to the sponge holding system to stimulate bacterial growth in the header tank during this time period. Two to three times per week, 3–7 L of cultured phytoplankton at 1–5 × 10^6 cells mL^{-1} was added to the header tank that supplied the sponge holding tank.

Collection of Sediments

In order to emulate the natural sediment regime of the *Vazella* sponge grounds, sediment for use in the exposure trials was collected 22 nautical miles north of the sponge collection locations in Emerald Basin (**Figure 2**). There, a Van Veen grab sampler was deployed at 170 m depth until 100 L of sediment was collected. The surficial sediments here are described as LaHave Clay, a loosely compacted silty clay that is mainly confined to the basins and depressions of the Scotian Shelf (King, 1970). LaHave Clay overlays Emerald Silt and Scotian Shelf Drift (i.e., glacial till), the latter of which the densest aggregations of *V. pourtalesii* are most associated with (Beazley et al., 2018). This location was chosen due to its proximity to several presence records of *V. pourtalesii*. Prior to exposure to the sponges, the collected sediment was sieved to a fraction < 63 μm in the laboratory and kept cool (4°C).

Suspended Sediment Exposure

Of the 23 sponges collected, three perished during the 7-month acclimatization period, leaving 20 specimens for experimentation. Numbers from 1 to 20 were assigned to the sponges for identification throughout the experiment. After acclimatization, 10 40 L tanks with a flow-through sea water supply were set up as experimental units for replication between two treatment groups. Sea water (9°C) was supplied to each individual tank with a flow rate of ∼0.5 L min^{-1}. Water

temperature in the experimental tanks was stable over the course of the experiment (mean = 8.96 ± 0.05 °C). Equally-sized sponges were distributed randomly between two treatments, with each of the control and treatment (i.e., sediment-exposed) groups consisting of 10 individuals each, with two individuals per tank (**Figure 3**).

Prior to the start of the experiment, sponges in the control were unintentionally exposed to air bubbles that potentially formed due to temperature-induced off gassing of oxygen-saturated seawater (temperature difference of 0.5 °C from the header tank to the experimental unit). Upon notice of microbubbles, sponges were returned to the 500 L maintenance tank until the experimental setup had been improved. Sponges assigned to the sediment-exposed group remained in the 500 L holding tank at all times during this time period. Once the experimental setup was operational, sponges were placed back in their respective tanks the experiment commenced. No deleterious effects of microbubble exposure were evident in the control sponges upon the start of the experiment. We subsequently acquired control data on the respiration and clearance rate from colleagues working on this same species in the same aquaria facilities at another time (Bart et al., 2020) in order to compare these rates with our potentially compromised control sponges.

The sediment-exposed group received a concentration of suspended natural bottom sediments of 50 mg L^{-1} for 12 h per day for 21 days, while the control group remained untouched. The 12 h exposure cycle was chosen to emulate the natural tidal oscillation experienced off Nova Scotia. Each of the five sediment treatment tanks received pulses of high concentration sediment stock solution (**Figure 3**). Pulses of stock solution were delivered by five membrane pumps (EW-F31VC-20EPF5, IWAKI). Average frequency was one pulse of 1-min length per 5 min, resulting in 25 mL stock solution being added per pulse to each of the tanks in the exposed group. Aquarium pumps (CompactON 300, Eheim) kept dosed sediment volumes in suspension. The end concentrations of suspended sediment and particle size distribution in each of the five tanks were monitored with a particle analyzer (LISST-100X, Sequoia) at days 0, 7, 14, and 21. Settled sediment was removed from the bottom of each tank by careful siphoning after each exposure cycle of 12 h.

Physiological Measurements

The physiological performance (respiration rate and bacterial clearance rate) of *V. pourtalesii* assigned to the control and sediment-exposed groups was assessed with chamber-based incubations after 7, 14, and 21 days. Before each incubation, sediment-exposed sponges were given a 3 h recovery period after the last pulse of sediment. During this period, the tank volume was turned over by fresh seawater approximately four times, so that sponges were exposed to clear water prior to the start of each incubation. The bottom plate of the incubation chamber was put in its respective tank, and a sponge was placed on the plate. Sponges were left to recover for 1 h before an acrylic chamber that sealed to the bottom plate was placed over each sponge. The lid of the chamber was equipped with a stirrer for circulation and a dissolved oxygen sensor (HQ30D equipped with LDO sensors, Hach) calibrated to 100% saturation according to the manufacturer. Dissolved oxygen concentrations were measured every minute over 4 h, and

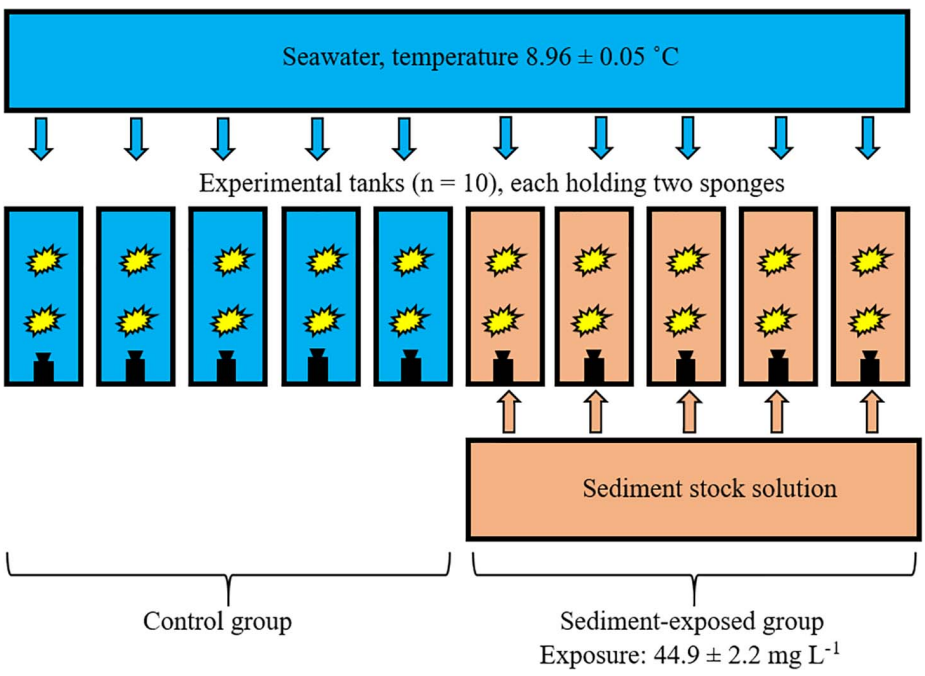

FIGURE 3 | Experimental design used in this study. Ten individual tanks, each holding two sponges (yellow shapes), were supplied with sea water. Each tank was equipped with a pump (black shapes). Five tanks received dosages of a sediment stock solution for 12 h per day.

respiration rates (R) in μmol O_2 h^{-1} gDM^{-1} were calculated as outlined by Tjensvoll et al. (2013) using the following equation:

$$R\left[\mu mol\ O_2 h^{-1}\ gDM^{-1}\right] = ((c_2 - c_1)\ t^{-1} * V_{net})\ gDM^{-1},$$

where c_1 and c_2 are the concentration of dissolved oxygen at start and end of the incubation in μmol O_2 L^{-1}, t is the time of the incubation in hours, V_{net} is the volume of the incubation chamber after subtracting the volume of the respective sponge in mL, and gDM is the total dry mass of the incubated animal in grams. Wet mass was measured on a scale after taking the sponge out of the water and allowing the water to drain for 10 s. Volume of individual sponges was measured by water replacement in a graded beaker prior to sampling for microscopy approaches (see section "Recovery Potential and Electron Microscopy"). To make the rates assessed in this study comparable to published datasets, we used the conversion factor (mL:gDM = 5.2) from Bart et al. (2020) to calculate dry mass from sponge volume.

Water samples were drawn from the chamber at the beginning and the end of the 4 h incubations via tubes inserted through the lid. Samples for bacterioplankton quantification were fixed with glutaraldehyde (end-concentration 0.5%) for 10 min before flash freezing in liquid nitrogen and −80 °C storage. Bacterial concentration in the water samples was assessed by flow cytometry (Brussaard et al., 2010) and clearance rates for bacterioplankton in mL water cleared per mL sponge volume per minute (mL mL^{-1} min^{-1}) were calculated as outlined by Robertson et al. (2017) using the following equation:

$$\text{Clearance rate}\ \left[mL\ mL^{-1}\ min^{-1}\right] = V_{net}\ t^{-1}\ \ln\left(n_{start}\ n_{end}^{-1}\right)\ V_{sponge}{}^{-1},$$

where V_{net} is the volume of the incubation chamber after subtracting the volume of the respective sponge in mL, t is the time of the incubation in min, n_{start} and n_{end} are the concentrations of bacterioplankton at start and end of the incubation in counts mL^{-1}, and V_{sponge} is the total volume of the incubated animal in milliliters. Empty chamber incubations (n = 2 per treatment group) without a sponge were performed twice throughout the experiment to account for background respiration and non-sponge related dynamics in bacterioplankton. The average of the four empty chamber incubations was subtracted from the sponge incubations of the respective treatment.

Data Analysis

Statistical tests were performed with GraphPad Prism 8 Version 8.2.1(441), August 20, 2019 using a general linear model analysis of variance (Sediment; two levels nominal 0 or 50 mg L^{-1}, n = 5) with multiple comparisons. For analysis, measurements of individual sponges were averaged per tank resulting in five independent replicates per treatment. We tested for tank effects prior to the analysis (Kutti et al., 2015), and influence of tank was identified as low (Control group: clearance rate: p = 0.12; respiration rate: p = 0.14; Sediment-exposed group: clearance rate: p = 0.78; respiration rate: p = 0.20). Values are given in mean ± standard deviation (SD) if not stated otherwise.

Recovery Potential and Electron Microscopy

After 3 weeks of exposure to suspended sediment, we followed the potential recovery of exposed individuals of *V. pourtalesii* for up to 38 days after the last exposure, with unexposed sponges as the control group. In order to determine the level of clogging by sediment in the aquiferous system, structural components from sediment-exposed sponges were collected for examination using SEM techniques. Due to financial limitations, analysis of structural components of all sponges was unfeasible and only a minimum number of replicates were analyzed to account for individual differences between sponges. Three hours after the last exposure to sediment (considered day 0 of the recovery phase), one sediment-exposed sponge was removed from its tank and subsampled by extracting a ∼1 cm^3 sample through the body wall of the lower and upper halves of the sponge (specimens were halved at their mid-point based on total height). Two control sponges were sampled after 3 and 12 days of the recovery phase. On the final day of the recovery phase (day 38), two sediment-exposed sponges (Sponges 14 and 19) and one control (Sponge 8) were subsampled for examination using SEM to determine if sediment was still present in their body.

Subsamples were preserved in a 1:4:5 ratio of 25% glutaraldehyde, 0.34 M sodium chloride (NaCl), and 0.4 M phosphate-buffered saline (PBS) (i.e., "Fixative 1"). The Fixative 1 solution was changed after 0.5 h, and the samples were stored in 4°C for ∼2 months. The final step for SEM fixation involved rinsing the samples of Fixative 1 using a 1:1 ratio of 0.4 M PBS and 0.6 M NaCl and fixing the samples in a 1:1 ratio of 4% osmium tetroxide and 0.6 M PBS (i.e., "Fixative 2") for approximately 2 h. Samples were then rinsed of Fixative 2 three times in distilled water for 10 min each and dehydrated through a series of ascending alcohol concentrations diluted from 100% anhydrous ethyl alcohol: 50 and 70% alcohol (10 min each), 80, 90, 95, and 100% alcohol (3 × 10 min each). In order to create even surfaces from which the intact aquiferous system could be observed, the 1 cm^3 subsamples were freeze fractured in liquid nitrogen. Fractured pieces were then dried using liquid carbon dioxide in a Leica EM CPD300 (Critical Point Dryer) at the Scientific Imaging Suite at Dalhousie University, Halifax, Nova Scotia.

After critical point drying, samples were mounted on SEM stubs using a carbon-based paste, and sputter coated using a Leica EM ACE200 vacuum coater at a speed of 30 mA for 325 s, which equated to a 25 nm-thick coating of gold/palladium. To determine the degree of clogging, the coated samples were initially viewed and imaged using a Zeiss 1455VP scanning electron microscope operating with an acceleration voltage of 20 kV, and SmartSEM V05.05 SEM operating software.

Initial SEM examination of the sediment-exposed sponge sampled on recovery day 1 (Sponge 16) revealed poor results from freeze fracturing, likely due to the high density of spicules. Instead of freeze fracturing with liquid nitrogen, the 1 cm^3 subsamples collected on all subsequent days were sectioned into

smaller pieces using a sharp razor to create both cross sections across the atrial surface, and longitudinal sections through the body wall from the pinacoderm to atrial surfaces. Both the longitudinal and cross sections were fixed for SEM according to the techniques described above.

To identify the potential presence of accumulated particles in sediment-exposed sponge structural components, the elemental composition was examined using SEM/energy dispersive X-ray spectroscopy (EDS) techniques. Samples were examined and imaged using a Hitachi S-4700 Cold-Field Emission SEM operating at 10 kV (also at Dalhousie University). The atomic weight as a percentage of total weight was calculated for each of four or five randomly chosen point locations over the unknown matter. Samples of the matter were taken using an attached 80 mm^2 X-Max EDS detector (Oxford Instruments, Concord, MA, United States) and associated Inca software. All elements were analyzed (normalized). Given that the mounted structural components of *V. pourtalesii* were not flat, polished, or homogeneous, which are requirements for standardized quantitative analysis using EDS, we chose to convert the atomic weight information into elemental presence/absence. Due to the use of carbon-based mounting media, the presence of carbon in the samples must be discounted, as well as the presence of osmium, which is likely a remnant of the fixation process. The elemental composition of the sediment used in the experiment was also examined using SEM/EDS techniques to serve as a comparison to the matter found in the sponge's structural components. Sediment (unfixed) was mounted on an SEM stub using carbon-coated double-sided tape, and gold/palladium coated to a thickness of 15 nm.

RESULTS

Survival

All 10 sponges in the treatment group survived repeated exposure to suspended sediment over the course of the 21-day experiment (indicated by observations of active pumping and by respiration and clearance rate assessments) and no structure necrosis or other signs of decreased health status were observed in the treatment group over the course of the experiment. Initially, sediments accumulated only on the long spicules of the exposed individuals, but with repeated exposure, the atrial surfaces eventually became covered in sediment particles and turned brown in color (**Figure 4**). In the control group, three sponges showed signs of necrosis (gray/black colored structural components) after 10 days in the experimental tanks and eventually perished (**Supplementary Figure 1**). These sponges deteriorated relatively quickly (within 3 days after the initial signs of discoloration), and no signs of necrosis were evident in the remaining sponges throughout the 21-day experiment. It cannot be ruled out that the mortality in the control group was induced by a short exposure to micro-bubbles at the beginning of the experiment. Thus, all sponges from the control group may

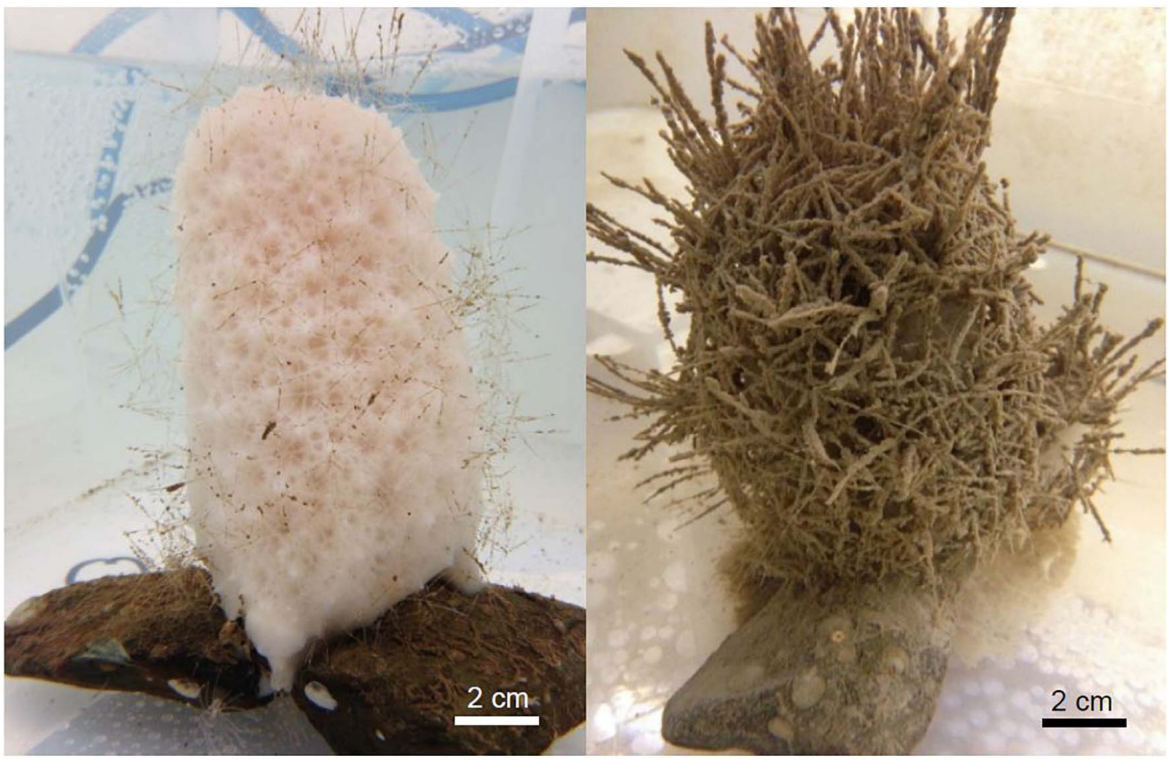

FIGURE 4 | Individuals of *Vazella pourtalesii* from the control (left) and the exposure (right) group after 7 days in the experiment. The long spicules and atrial surface of the exposed sponges eventually became densely covered with sediment particles.

have been compromised in their physiological performance. For this reason, data from the control group evaluated in this study were augmented by a published dataset (Bart et al., 2020) on the physiological rates of *V. pourtalesii*. Respiration and clearance rates of *V. pourtalesii* described by Bart et al. (2020) ($n = 7$) were assessed in a similar manner as in this study (chamber-based incubations) and were performed in the same aquaria facilities.

Suspended Sediment Exposure

The average suspended particle concentration in the treatment tanks during the 12 h exposure phase over the course of the 21-day experiment was 44.9 ± 2.2 mg L^{-1}. Particle concentrations at the beginning of the experiment (33.6 ± 2.5 mg L^{-1}) were below the targeted threshold of 50 mg L^{-1}, but steadily increased up to 56.9 ± 2.1 mg L^{-1} at day 21 (**Figure 5**). The control treatment had an average suspended particle concentration of 1.9 ± 0.8 mg L^{-1}. Particles < 6 μm were prevalent in the suspended sediment representing a fraction of 73% of the total concentration (mg L^{-1}). A fraction of 10% was represented by particles as large as ∼184 μm (**Figure 6**).

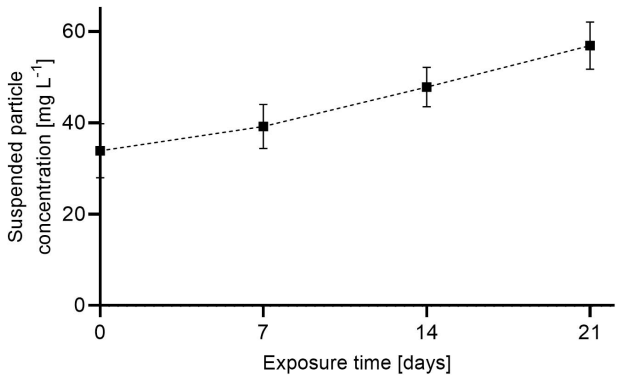

FIGURE 5 | Average of end concentrations ± SD of suspended sediment in exposure ($n = 5$) and control tanks ($n = 5$) throughout the experiment. Overall average exposure level was 44.9 ± 2.2 mg L^{-1}. Suspended sediment concentration in the control tanks was assessed once in the beginning of the experiment (1.9 ± 0.8 mg L^{-1}).

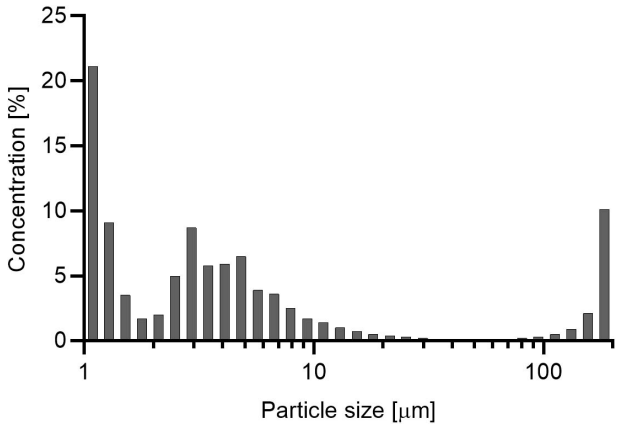

FIGURE 6 | Percentage of concentration per size class of the suspended sediment in end-concentration. 73% of suspended particles are represented in the size class from 1 to 6 μm.

Physiological Performance

The respiration and clearance rates of *V. pourtalesii* in the two treatment groups measured during the chamber incubations on days 7, 14, and 21 are summarized in **Table 1**. Decrease in oxygen concentration in the closed chambers was linear over time. Respiration rates of individuals from the literature control and sediment-exposed groups were comparable at each of the three measured time points (days 7, 14, and 21; **Figure 7**). However, respiration rates increased slightly in the sediment exposed group over the 21-day experiment, with rates ranging from 1.89 ± 0.15 μmol O_2 h^{-1} gDM^{-1} at day 7 to 2.66 ± 0.51 μmol O_2 h^{-1} gDM^{-1} at day 21. No effect of sediment treatment or time of exposure was detected [$F_{(3,18)} = 1.96$, $p = 0.156$]. Clearance rates (**Figure 8**) significantly differed between the sediment-exposed and the control group from Bart et al. (2020) on days 14 and 21 ($p = 0.028$ and $p = 0.006$, respectively; see **Table 1**). Clearance rates in the sediment-exposed group declined over time with rates ranging from 0.97 ± 0.17 mL mL^{-1} min^{-1} at day 7 to 0.53 ± 0.15 mL mL^{-1} min^{-1} at day 21. After 14 days of sediment exposure, clearance rates differed significantly from the control group and continued to decrease until the last assessment after 21 days [day 14: $F_{(3,18)} = 6.40$, $p = 0.028$: day 21: $F_{(3,18)} = 6.40$, $p = 0.006$].

Observations of Accumulated Material After Sediment Exposure

After each 12 h cycle of sediment exposure, settled sediment was removed from the bottom of each tank. Within 30 min after sediment removal, flocculate matter, possibly representing sloughed mucous-coated sediment, was observed accumulating next to the sponges (**Figure 9**). Particles had a flocculated appearance; small pellets of sediment clumped together by a translucent material and settled on the bottom of the aquaria. This matter was not present at the bottom of the tanks of the control group. Video observations of outflow of sediment-exposed individuals showed that the large accumulated particles were expelled with high velocity from the osculum (see **Supplementary Video 1**).

Recovery Potential and Scanning Electron Microscopy Examination

The atrial surfaces of most individuals in the sediment-exposed group returned to their pre exposure state approximately 14 days after last exposure. Of the three sponges left to recover to day 38, all appeared to have cleared their pinacoderm of sediment completely. Two sediment-exposed sponges appeared to be in the process of dying, with dark sections of structural components indicating necrosis. Another sediment-exposed sponge (**Figure 10**), while appearing to nearly recover, self-dislodged from its basal attachment and floated to the top of the tank on day 38 and was dissected. Some structure necrosis was also evident in this individual.

TABLE 1 | Overview of the assessed physiological parameters in *Vazella pourtalesii* under elevated concentrations of suspended particles (Sediment, $n = 5$) and the literature control group ($n = 7$) (Bart et al., 2020).

Parameter	Treatment		Day 7	Day 14	Day 21
Respiration rate	Sediment, this study		1.89 ± 0.15	2.28 ± 0.53	2.66 ± 0.51
($\mu molO_2\ gDM^{-1}\ h^{-1}$)	Bart et al. (2020)	3.39 ± 1.76	–	–	–
Clearance rate	Sediment, this study		0.97 ± 0.17	0.83 ± 0.20[b]	0.53 ± 0.15[b]
($mL\ mL^{-1}\ min^{-1}$)	Bart et al. (2020)	2.22 ± 1.26[a]	–	–	–

Mean values ± SD. Significant differences are indicated by corresponding letter pairs. A graphical representation of these values can be found in ***Figures 7, 8****.*

Scanning electron microscopy/EDS analysis (**Supplementary Table 1**) revealed that the sediment used in the exposure experiment consisted of a wide variety of grains and elemental composition, with textural differences between grains observed. The presence of aluminum, silicate, potassium, iron, magnesium, and chloride was evident in the grains. The presence of both calcium and silicate suggests that the sediment grains are both calcareous and siliceous in origin. These grains were largely absent from the three control sponges sampled, where the observed matter was comprised mostly of carbon (although note contamination from mounting media) and oxygen.

Due to the poor results of freeze fracturing and manual razor sectioning of the structural components, observations of the exact location of sediments within the aquiferous system of the sponges were not possible. Nonetheless, observations on the composition/origin of matter observed among the spicules of the mesohyl were made to assess recovery. The elemental composition of the matter observed within the mesohyl of a sediment-exposed sponge (sampled on day 1 of the recovery phase) was most similar to that of the two analyzed sediment samples. Here, iron, aluminum, magnesium, and potassium were all constituents of the sample, suggesting the presence of sediments inside the sponge. Examination of the sediment-exposed sponges (Sponges 14 and 19) sampled on day 38 revealed an elemental composition more similar to control Sponge 8 (sampled on day 38) than sediment-exposed Sponge 16 and the two controls. For sediment-exposed Sponge 19, the observed matter was comprised of carbon, nitrogen, oxygen, sodium,

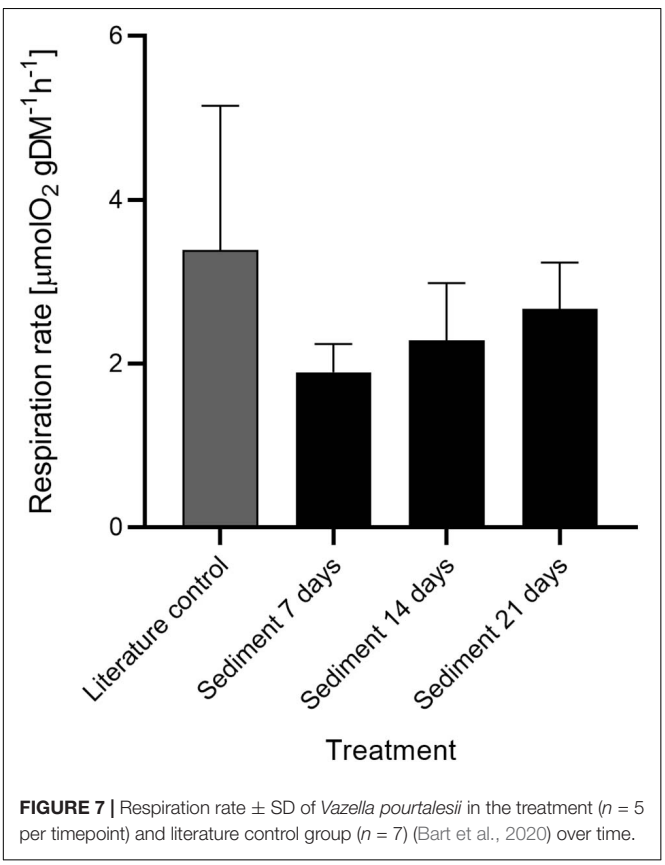

FIGURE 7 | Respiration rate ± SD of *Vazella pourtalesii* in the treatment ($n = 5$ per timepoint) and literature control group ($n = 7$) (Bart et al., 2020) over time.

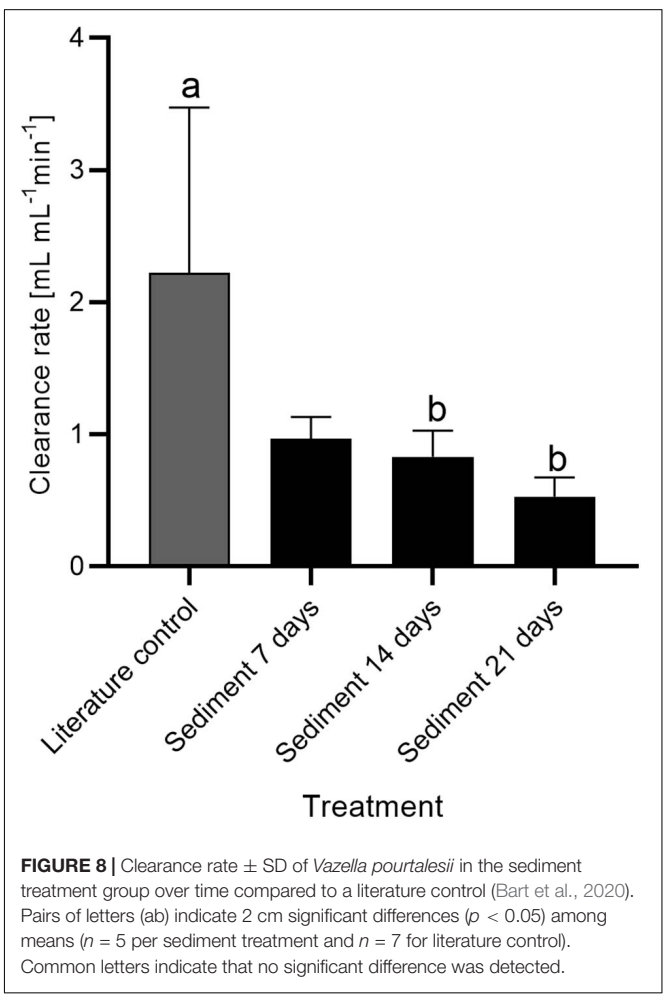

FIGURE 8 | Clearance rate ± SD of *Vazella pourtalesii* in the sediment treatment group over time compared to a literature control (Bart et al., 2020). Pairs of letters (ab) indicate 2 cm significant differences ($p < 0.05$) among means ($n = 5$ per sediment treatment and $n = 7$ for literature control). Common letters indicate that no significant difference was detected.

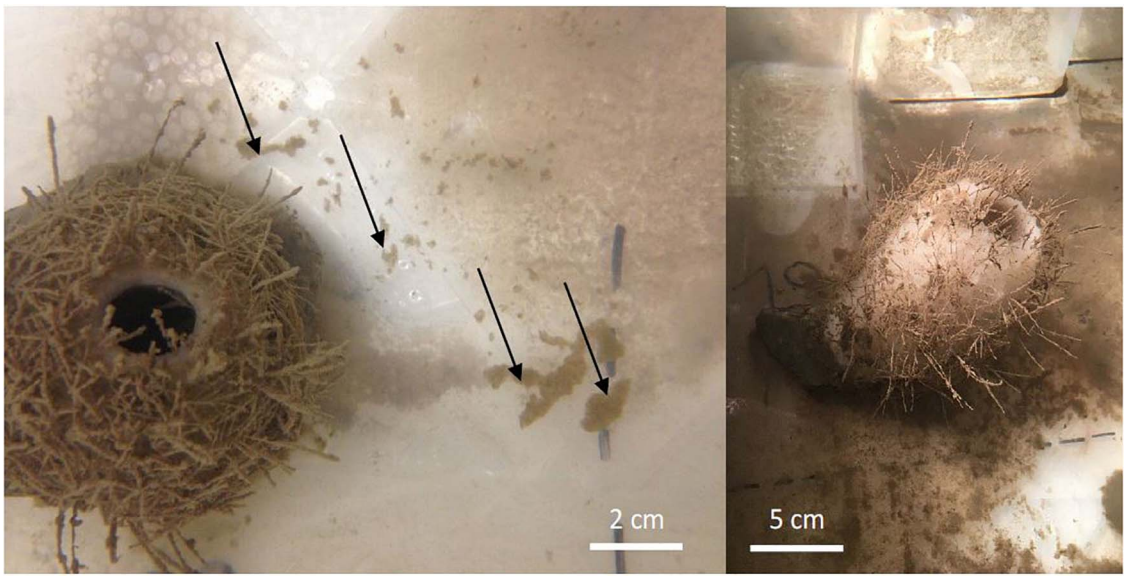

FIGURE 9 | Left: *Vazella pourtalesii* in top view with flocculated matter (black arrows) accumulated in the tank after initial removal of settled sediment particles Right: *V. pourtalesii* in experimental tank with accumulated sediment particles on the tank bottom after 12 h of exposure.

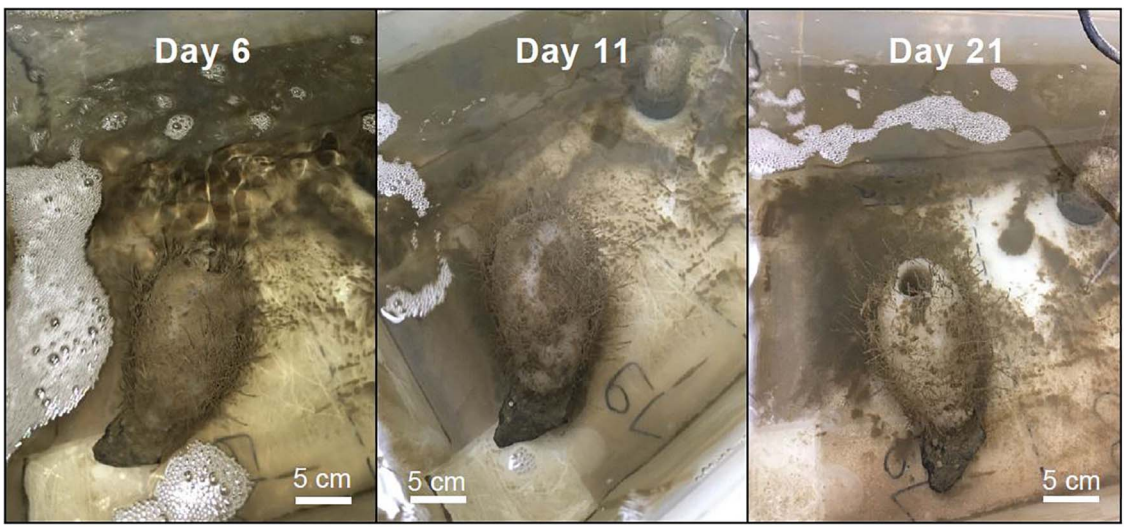

FIGURE 10 | Succession of recovery of a sediment-exposed sponge at 6, 11, and 21 days after sediment exposure stopped. This sponge was sampled for SEM/EDS analysis 38 days after sediment exposure.

biogenic silica, aluminum, and sulfur. The sulfur was possibly related to the decaying state of the sponge prior to sampling.

The similar elemental composition found in the sediment-exposed and the control sponges (longitudinal sections), and the lack of iron, potassium, aluminum, and calcium, which were indicative of the sediments, indicate that sediment-exposed individuals had mostly cleared the sediment from their structural components over the course of the 38-day recovery period. However, observations of the cross-section sample from sediment-exposed Sponge 14 revealed the presence of matter with a similar elemental composition to that of the sediment, suggesting high variability in the location of sediment within the body of the same individual.

DISCUSSION

Physiological Response of *Vazella pourtalesii* to Natural Suspended Sediment

Under the laboratory conditions of this study, *V. pourtalesii* survived repeated exposure to seawater with particle

concentrations up to 57 mg L^{-1} over the course of 21 days. There was no difference in respiration rates between the sediment-exposed and literature control group throughout the experiment. These findings are in line with experimental work on deep-water demosponges exposed to a similar sediment concentration as used in this study. For example, Kutti et al. (2015) found that oxygen consumption rates in *Geodia barretti* Bowerbank, 1858 (Geodiidae) remained stable over time when exposed to natural suspended sediment (50 mg L^{-1}) for up to 50 days, indicating that this species is adapted to cope with periods of higher natural water turbidity.

However, in this study, *V. pourtalesii* individuals exposed to sediment expressed reduced bacterial clearance rates after 14 days of exposure. *In situ* and *ex situ* studies showed that some species of glass sponges arrest pumping when exposed to different concentrations of natural sediment, whereas others do not. For instance, the glass sponge *A. vastus* maintained pumping during exposure to sediment concentrations up to 36 mg L^{-1} in an aquaria-based study (Tompkins-Macdonald and Leys, 2008), while Grant et al. (2019) found that concentrations as low as 2.8–6.4 mg L^{-1} caused arrests in the glass sponge *R. dawsoni* from the Hecate Strait reef complex, but no arrests were observed in *Farrea occa* Bowerbank, 1862 (Farreidae) when exposed to similar concentrations as reached in our study (57 mg L^{-1}). Grant et al. (2018) reported short-term arrests of pumping activities in glass sponges as a response to elevated particle concentrations. These reported arrests never exceeded intervals of ∼80 min, likely to avoid oxygen depletion in the sponge's structural components. While we have not directly measured or observed whether short-term cessation in pumping occurred in our experiment, the increasing brown coloration of the sponges over the course of the experiment, as well as the presence of sediments in the structural components of exposed *V. pourtalesii* individuals as indicated by SEM, suggests that the animals were actively pumping during the 12 h exposure cycles.

Sponges respond to sediment stress via closure of incurrent pores (the ostia) and osculae and the reduction of the aquiferous system via structure regression. These morphological responses result in the cessation of pumping (Tompkins-Macdonald and Leys, 2008). In addition, expulsion of particles from the aquiferous system, and mucus production (Strehlow et al., 2017) have been observed after sediment exposure. Particles up to 1 mm in diameter were observed in the excurrent flow of the sponges after sediment exposure (**Supplementary Video 1**, osculum diameter ∼2 cm). Particles had a flocculated appearance, and small pellets of sediment clumped together by a translucent material and settled on the bottom of the aquaria. No accumulation of such particles was observed at any time throughout the experiment in the control sponges. Excretion of pellets of indigestible particulate matter is linked to an increase in mucus production, a known stress response exhibited by both demosponges (Strehlow et al., 2017; Grant et al., 2019) and hexactinellids (Kahn et al., 2018). However, mucus production is an energy-demanding process (McGrath et al., 2017), and prolonged exposure to suspended natural sediment likely has an adverse effect on a sponge's ability to maintain this coping mechanism. A decrease in bacterial clearance rates with sediment exposure, as observed in our study, is indicative for sediment induced cessation of pumping. If the sponges reduce their pumping activity, energy input will decrease and hence, continued coping with sediment will start to consume energy at the expense of other processes. Thus, processes such as growth, structural component maintenance (Shore, 1971; De Goeij et al., 2009), reproduction, and cell renewal (Bell, 2002; Alexander et al., 2014) might be compromised under prolonged events of elevated suspended particle concentrations. This could result in an energy deficiency and adverse effects on overall sponge health (Grant et al., 2019).

Recently, *V. pourtalesii* has been shown to predominantly utilize dissolved organic carbon to fuel its metabolic requirements (Bart et al., 2020). It remains to be investigated whether this species can increase the uptake of dissolved organic matter to counteract the reduced uptake of bacterioplankton resulting from repeated sediment exposure. Also unknown is to what extent pathways for dissolved organic matter uptake in *V. pourtalesii* are dependent on pumping and as such affected by the presence of elevated levels of natural suspended sediment. Additionally, a decrease in pumping could result in a reduced capacity to evacuate indigestible sediment particles and accumulation within the sponge's structural components.

Recovery After Sediment Exposure

Individuals left to recover for up to 38 days after last sediment exposure appeared to clear their pinacoderm of sediment and were similar in appearance to sponges in the control group. However, SEM/EDS techniques indicated that after 38 days, sediment particles were still present in certain structural component sections of one individual, suggesting high variability in the location of sediment within the structural components and possibly high variability between individuals in the ability to expel accumulated, indigestible particles. Visual observations made during the experiment indicated that sediments tended to accumulate inside and at the base of the atrium of this barrel-shaped species. It is likely that structural components closer to the base will take longer to clear indigestible particles. In our study, all samples for SEM were extracted from the bottom portion of the sponge (based on total height) suggesting that structural components located further away from the base of the sponge might have been cleaned more efficiently from accumulated sediment particles than the sampled regions of sponge structural components. Despite the visual recovery of some individuals, a number of *V. pourtalesii* perished over the course of the 38-day recovery phase. As some individuals in the control group also showed signs of structure necrosis and perished, the cause of death cannot evidently be linked solely to exposure to suspended particles. To assess the physiological recovery potential of *V. pourtalesii* after long-term sediment exposure, parameters such as oxygen uptake and bacterial clearance rates should also be monitored throughout the recovery period in future studies.

Potential Adaptations to a Dynamic Environment

It is hypothesized that glass sponges in deep-sea environments may utilize sediment-borne bacteria as an additional food source. Stable carbon and nitrogen isotope examinations of glass sponges collected off the Pacific coast of Canada showed ingestion of sediment-borne bacteria re-suspended by tidal oscillations (Kahn et al., 2018). Sediments in deep-sea environments have been found to be 100–1000 times more rich in heterotrophic bacteria than the overlying water column (Kuwae and Hosokawa, 1999). Furthermore, Grant et al. (1987) showed that the fine silty sediments on the Scotian Shelf and particularly in Emerald Basin contain a high proportion of easily re-suspended organic particles and postulated that lateral transport of organic material makes the Scotian Shelf a sink for organic carbon. The potential trophic interaction of *V. pourtalesii* and sediment borne re-suspended organic matter has not been investigated up to date. However, our incubation-based assessments of physiological parameters suggest that *V. pourtalesii* tolerates re-suspended particles, rather than utilizing and benefiting from the potentially bacteria-and particle-enriched water layers. The assessed respiration rates suggest that there is no metabolic benefit of the presence of suspended sediment enriched seawater for these sponges.

Emerald Basin is subjected to higher tidal variability and mixing compared to other areas of the Scotian Shelf (Petrie and Smith, 1977). Tidal oscillations and storm events have the potential to re-suspend small grain particles that may remain suspended in the water column for several days (Bogucki et al., 1997; Boegman and Stastna, 2019). In addition to seasonal short-term resuspension events, persistent nepheloid (sediment enriched) layers with particle concentrations of up to 8 mg L^{-1} have been described to occur on the Scotian Shelf (Spinrad et al., 1983; Pilskaln et al., 1998). Similar resuspension events with a duration of several days were observed during a 10-month deployment of an autonomous benthic lander in the Sambro Bank Sponge Conservation Area (Hanz et al., 2021; see Beazley et al., 2017 for deployment details). Dynamic oceanographic characteristics and sponge occurrences are often linked in the North Atlantic. For instance, the distribution of the glass sponge *Pheronema carpenteri* (Thomson, 1869) (Pheronematidae) at the Porcupine Seabight (northeast Atlantic) is thought to be linked to areas where bottom currents are intensified due to internal waves (Rice et al., 1990). The causal link was suggested to be an increase in the supply of food related to the occurrence of the internal waves. The same oceanographic settings might be a possible explanation for the occurrence of dense demosponge grounds in the Faroe-Shetland basin (Davison et al., 2019). Our findings suggest that *V. pourtalesii* might be adapted to tolerate natural suspended sediment up to a certain concentration and exposure time. This is corroborated by the proliferation of this species in this highly dynamic environment subjected to periodic re-suspension events. However, the observed reduction in clearance efficiency with sediment exposure over time indicates that potential coping mechanisms and adaptations are compromised when sediment exposure occurs over a longer time scale.

Implications for Conservation Management

While the results of this study indicate no adverse physiological effects (respiration and clearance rates) of short-term sediment exposure (7 days), prolonged (14–21 days) exposure to re-suspended sediment from bottom trawling may impair physiological rates in *V. pourtalesii* as a response mechanism. Over time, this may result in an energy deficit and reduction in overall sponge health. With a concentration well below the described re-suspension potential of a trawl (up to 500 mg L^{-1}, see section "Introduction"), these likely negative impacts on the physiology of *V. pourtalesii* could be amplified in its natural setting if exposed to re-suspended sediments from trawling. Future studies should include different concentrations of suspended sediment in combination with longer exposure times to detect potential thresholds for adverse effects of suspended sediments on *V. pourtalesii*.

The Sambro Bank and Emerald Basin Sponge Conservation Areas were designed to protect two of the more significant concentrations of *V. pourtalesii* on the Scotian Shelf identified from biomass/density observations from commercial bycatch records, research vessel trawl catch data, and *in situ* camera observations. However, kernel density analyses applied to research vessel trawl survey catch data to identify hotspots in sponge biomass (all Porifera, including *V. pourtalesii*; Kenchington et al., 2016), indicated that less than 2% of the significant concentrations formed primarily by *V. pourtalesii* in the area known as the Scotian Gulf, which includes Emerald Basin, are encompassed by the closed areas. Similar results were found when examining the proportion of protected suitable habitat of *V. pourtalesii* generated from random forest species distribution modeling (see Beazley et al., 2018). The percentage overlap between the significant concentrations of all Porifera, including *V. pourtalesii*, and groundfish fishing effort using mobile-gears revealed that 29.4% of the area occupied by these significant concentrations was subjected to some level of fishing (DFO, 2017b; Koen-Alonso, 2018), with most effort occurring in the lowest percentile (low effort). Nonetheless, this lower effort does not imply that significant adverse impacts of fishing to *V. pourtalesii* are absent in these sensitive benthic areas (Koen-Alonso, 2018). Depending on the type of gear and composition of the benthic community, few interactions can cause serious irreversible damage (NAFO, 2011), and the greatest impacts to these ecosystems, such as irreversible damage or complete removal, are often caused by the first fishing events (DFO, 2006; Pham et al., 2019).

Grant et al. (2018) modeled the indirect footprint of a trawl adjacent to an existing bottom fishing closure and estimated that the re-suspended sediment plumes spread as far as 6 km from the initial trawling site. They concluded that fishing effort along the boundaries of sponge conservation area rendered the dense sponge grounds inside it vulnerable to suspended sediments. Although the trajectory and retention rates of sediment plumes from bottom fishing in Emerald Basin were not measured in this study, the close proximity of existing bottom fishing to the SCAs on the Scotian Shelf (Koen-Alonso, 2018) may have the

potential to impact the dense *Vazella* grounds that reside within them. Here, buffer zones of a sufficient dimension could be established around the SCAs to minimize the indirect impact of downstream sediment re-suspension by bottom gear to the sponge ground community inside the closed areas. Although there was no adverse effect evident the first 7 days of sediment exposure, an additional mitigation measure could be a temporal staggering of fishing activities within the same area to allow the sponges to recover following trawling events. In this area, the groundfish fishery operates year-round, from April 1 to March 31 but has a 3-month period of high fishing activity from July to September with individual trips occurring on the scale of 5 days and with multiple sets spread out over multiple areas (D. Fenton, Fisheries and Oceans Canada, pers. comm.). Thus, the 21-day period chosen for this experiment likely represents a worst-case scenario of sustained fishing activity from different vessels in the vicinity of the sponge grounds within the peak fishing period. The Scotian Shelf is subjected to ongoing structural developments such as offshore oil and gas extraction (Breeze and Horsman, 2005). The impacts of sediments contaminated with drilling muds or potential spills of crude oil on glass sponges are at present poorly understood. The present study on the physiological response of *V. pourtalesii* to a concentration of natural suspended sediment may act as a blueprint for the design of these elaborate experiments.

CONCLUSION

In this aquaria-based *ex situ* study, *V. pourtalesii* was found to cope with increased levels of natural suspended sediment for a period of 7 days. As this glass sponge species thrives in a dynamic shelf environment, *V. pourtalesii* is likely adapted to periodic, current-induced re-suspension events. However, our observations of decreasing clearance rates over time could indicate impaired filtration capacities cumulating in negative impacts on biological functions such as growth, structural components repair mechanisms and reproduction, and a metabolic deficit with adverse implications for overall animal health. Following the precautionary approach, the application of buffer zones to the current management measures for this species on the Scotian Shelf, and temporal coordination of sediment re-suspending activities may help mitigate the potentially adverse long-term effects on the unique ecosystem the *Vazella* grounds represent on the Scotian Shelf.

DATA AVAILABILITY STATEMENT

The original contributions presented in the study are included in the article/**Supplementary Material**, further inquiries can be directed to the corresponding author/s.

AUTHOR CONTRIBUTIONS

EW: conceptualization, methodology, formal analysis, data curation, writing—original draft, review and editing, and visualization. LB: investigation, resources, data curation, writing—original draft, writing—review and editing, visualization, and funding acquisition. BM: investigation, resources, and writing—review and editing. EK: conceptualization, resources, writing—review and editing, supervision, project administration, and funding acquisition. RO: conceptualization, methodology, resources, writing—original draft, writing—review and editing, supervision, project administration, and funding acquisition. All authors contributed to the article and approved the submitted version.

FUNDING

This work was funded through the SponGES—Deep-sea Sponge Grounds Ecosystems of the North Atlantic: An Integrated Approach Towards Their Preservation And Sustainable Exploitation, under H2020—the EU Framework Programme for Research and Innovation (Grant Agreement No. 679849) with Canadian contribution from Fisheries and Oceans Canada Strategic Program for Ecosystem-Based Research and Advice (SPERA) and International Governance Strategy (IGS).

ACKNOWLEDGMENTS

We thank the captain, crew, and scientific participants of the cruise on the Canadian Coast Guard vessel *Martha L. Black* for successful operations and maintenance of sampled sponges onboard. Thanks to the ROPOS team for efficient and delicate sampling of sponges by remotely operated vehicle (ROV). We thank Ping Li and Patricia Scallion from Dalhousie University's Scientific Imaging Suite and SEM-FIB Facilities, respectively, for their training and assistance in SEM/EDS analyses, and Marieve Bouchard-Marmen, Emily Baker (both DFO), and Gabrielle Tompkins (Dalhousie University) for their assistance in preparing samples for SEM/EDS analysis. We also thank Diede Maas and Tim Wijgerde (Wageningen University and Research, WUR) for their invaluable assistance with the data analysis. We thank Anna Noordeloos (Royal Netherlands Institute for Sea Research, NIOZ), Jasper de Goeij (University of Amsterdam, UvA), and Martijn Bart (UvA) for their assistance in establishing the flow cytometry analysis and frequent content meetings. We thank Furu Mienis (NIOZ) and Ulrike Hanz (NIOZ) for support with analyzing the sediment characteristics and sharing insights into the particle dynamics on the Scotian shelf. We thank the Institute for Marine Research, Bergen and namely Raymond Bannister, for the supplies of experimental equipment. Finally, we thank Detmer Sipkema (WUR) and Rob Joosten (WUR) for generously sharing the flow cytometer and help with analyzing samples.

SUPPLEMENTARY MATERIAL

The Supplementary Material for this article can be found online at: https://www.frontiersin.org/articles/10.3389/fmars.2021.611539/full#supplementary-material

REFERENCES

Alexander, B. E., Liebrand, K., Osinga, R., van der Geest, H. G., Admiraal, W., Cleutjens, J. P. M., et al. (2014). Cell turnover and detritus production in marine sponges from tropical and temperate benthic ecosystems. *PLoS One* 9:e109486. doi: 10.1371/journal.pone.0109486

Bart, M. C., Mueller, B., Rombouts, T., Ven, C., Tompkins, G., Osinga, R., et al. (2020). Dissolved organic carbon (DOC) is essential to balance the metabolic demands of four dominant North-Atlantic deep-sea sponges. *Limnol. Oceanogr.* 9999, 1–14. doi: 10.1002/lno.11652

Beazley, L., Kenchington, E. L., Murillo, F. J., and Sacau, M. D. M. (2013). Deep-sea sponge grounds enhance diversity and abundance of epibenthic megafauna in the Northwest Atlantic. *ICES J. Mar. Sci.* 70, 1471–1490. doi: 10.1093/icesjms/fst124

Beazley, L., Kenchington, E., Yashayaev, I., and Murillo, F. J. (2015). Drivers of epibenthic megafaunal composition in the sponge grounds of the Sackville Spur, northwest Atlantic. *Deep Sea Res. Part I Oceanogr. Res. Pap.* 98, 102–114. doi: 10.1016/j.dsr.2014.11.016

Beazley, L., Pham, C., Murillo, J., and Kenchington, E. (2017). *Cruise Report for the DFO/SponGES CCGS Martha L. Black Oceanographic Mission (MLB2017001), August 31 to September 7, 2017.* Canadian Technical Report of Fisheries and Aquatic Sciences 3242. Dartmouth, NS: Bedford Institute of Oceanography.

Beazley, L., Wang, Z., Kenchington, E., Yashayaev, I., Rapp, H. T., Xavier, J. R., et al. (2018). Predicted distribution of the glass sponge *Vazella pourtalesi* on the Scotian Shelf and its persistence in the face of climatic variability. *PLoS One* 13:e0205505. doi: 10.1371/journal.pone.0205505

Bell, J. J. (2002). Regeneration rates of a sublittoral demosponge. *J. Mar. Biol. Assoc. UK* 82, 169–170. doi: 10.1017/S0025315402005295

Bell, J. J., McGrath, E., Biggerstaff, A., Bates, T., Bennett, H., Marlow, J., et al. (2015). Sediment impacts on marine sponges. *Mar. Pollut. Bull.* 94, 5–13. doi: 10.1016/j.marpolbul.2015.03.030

Boegman, L., and Stastna, M. (2019). Sediment resuspension and transport by internal solitary waves. *Annu. Rev. Fluid Mech.* 51, 129–154. doi: 10.1146/annurev-fluid-122316-045049

Bogucki, D., Dickey, T., and Redekopp, L. G. (1997). Sediment resuspension and mixing by resonantly generated internal solitary waves. *J. Phys. Oceanogr.* 27, 1181–1196. doi: 10.1175/1520-04851997027<1181:SRAMBR<2.0.CO;2

Breeze, H., and Horsman, T. (2005). *The Scotian Shelf: An Atlas of Human Activities*. Dartmouth, NS: Fisheries and Oceans Canada.

Brussaard, C. P. D., Payet, J. P., Winter, C., and Weinbauer, M. G. (2010). Quantification of aquatic viruses by flow cytometry. *Man. Aquat. Viral Ecol.* 11, 102–107. doi: 10.4319/mave.2010.978-0-9845591-0-7.102

Davison, J. J., van Haren, H., Hosegood, P., Piechaud, N., and Howell, K. L. (2019). The distribution of deep-sea sponge aggregations (Porifera) in relation to oceanographic processes in the Faroe-Shetland Channel. *Deep Sea Res. Part I Oceanogr. Res. Pap.* 146, 55–61. doi: 10.1016/j.dsr.2019.03.005

De Goeij, J. M., de Kluijver, A., van Duyl, F. C., Vacelet, J., Wijffels, R. H., de Goeij, A. F. R. M., et al. (2009). Cell kinetics of the marine sponge *Halisarca caerulea* reveal rapid cell turnover and shedding. *J. Exp. Biol.* 212, 3892–3900. doi: 10.1242/jeb.034561

De Goeij, J. M., van Oevelen, D., Vermeij, M. J. A., Osinga, R., Middelburg, J. J., de Goeij, A. F. P. M., et al. (2013). Surviving in a marine desert: the sponge loop retains resources within coral reefs. *Science* 342, 108–110. doi: 10.1126/science.1241981

DFO (2006). *Impacts of Trawl Gears and Scallop Dredges on Benthic Habitats, Populations and Communities.* DFO Canadian Science Advisory Secretariat Science Advisory Report 2006/025. Dartmouth: DFO.

DFO (2017a). *Delineation of Significant Areas of Coldwater Corals and Sponge-Dominated Communities in Canada's Atlantic and Eastern Arctic Marine Waters and their Overlap with Fishing Activity.* DFO Canadian Science Advisory Secretariat Science Advisory Report 2017/007. Dartmouth: DFO.

DFO (2017b). *Guidance on the Level of Protection of Significant Areas of Coldwater Corals and Sponge-Dominated Communities in Newfoundland and Labrador Waters.* DFO Canadian Science Advisory Secretariat Science Advisory Report 2017/030. Dartmouth: DFO.

Durrieu de Madron, X., Ferré, B., Le Corre, G., Grenz, C., Conan, P., Pujo-Pay, M., et al. (2005). Trawling-induced resuspension and dispersal of muddy sediments and dissolved elements in the Gulf of Lion (NW Mediterranean). *Cont. Shelf Res.* 25, 2387–2409. doi: 10.1016/j.csr.2005.08.002

FAO (2009). *International Guidelines for the Management of Deep-Sea Fisheries in the High Seas*. Rome: FAO, 73.

Fuller, S. (2011). *Diversity of Marine Sponges in the Northwest Atlantic*. Ph.D. thesis, Dalhousie University, Halifax, NS.

Grant, J., Volckaert, F., and Roberts-Regan, D. L. (1987). Resuspendable organic matter in nova scotian shelf and slope sediments. *Cont. Shelf Res.* 7, 1123–1138. doi: 10.1016/0278-4343(87)90102-6

Grant, N., Matveev, E., Kahn, A. S., and Leys, S. P. (2018). Suspended sediment causes feeding current arrests *in situ* in the glass sponge *Aphrocallistes vastus*. *Mar. Environ. Res.* 137, 111–120. doi: 10.1016/j.marenvres.2018.02.020

Grant, N., Matveev, E., Kahn, A. S., Archer, S. K., Dunham, A., Bannister, R. J., et al. (2019). Effect of suspended sediments on the pumping rates of three species of glass sponge *in situ*. *Mar. Ecol. Prog. Ser.* 615, 79–100. doi: 10.3354/meps12939

Hanz, U., Beazley, L., Kenchington, E., Duineveld, G., Rapp, H. T., and Mienis, F. (2021). Seasonal variability in near-bed environmental conditions in the *Vazella pourtalesii* glass sponge grounds of the Scotian Shelf. *Front. Mar. Sci.* 7:1179. doi: 10.3389/fmars.2020.597682

Hawkes, N., Korabik, M., Beazley, L., Rapp, H. T., Xavier, J. R., and Kenchington, E. (2019). Glass sponge grounds on the Scotian Shelf and their associated biodiversity. *Mar. Ecol. Prog. Ser.* 614, 91–109. doi: 10.3354/meps12903

Hogg, M. M., Tendal, O. S., Conway, K. W., Pomponi, S. A., van Soest, R. W. M., Gutt, J., et al. (2010). *Deep Sea Sponge Grounds: Reservoirs of Biodiversity.* UNEP-WCMC Biodiversity Series No: 32. Cambridge: UNEP-WCMC, 27–31. doi: 10.1016/S0378-777X(80)80057-6

Kahn, A. S., Chu, J. W. F., and Leys, S. P. (2018). Trophic ecology of glass sponge reefs in the Strait of Georgia, British Columbia. *Sci. Rep.* 8:756. doi: 10.1038/s41598-017-19107-x

Kenchington, E., Beazley, L., Lirette, C., Murillo, F., Guijarro, J., Wareham, V., et al. (2016). *Delineation of Coral and Sponge Significant Benthic Areas in Eastern Canada Using Kernel Density Analyses and Species Distribution Models.* Canadian Science Advisory Secretariat Research Document 2016/093. Dartmouth, NS: Fisheries and Oceans Canada, 178.

King, L. (1970). *Surficial Geology of the Halifax-Sable Island Map Area*. Ottawa, ON: Marine Science Branch, Canada Department of Energy, Mines and Resources, 16.

Koen-Alonso, M. (2018). *Analysis of the Overlap between Fishing Effort and Significant Benthic Areas in Canada's Atlantic and Eastern Arctic Marine Waters.* Canadian Science Advisory Secretariat (CSAS). Research Document 2018/015. Dartmouth, NS: Fisheries and Oceans Canada.

Kutti, T., Bannister, R. J., Fosså, J. H., Krogness, C. M., Tjensvoll, I., and Søvik, G. (2015). Metabolic responses of the deep-water sponge *Geodia barretti* to suspended bottom sediment, simulated mine tailings and drill cuttings. *J. Exp. Mar. Biol. Ecol.* 473, 64–72. doi: 10.1016/j.jembe.2015.07.017

Kuwae, T., and Hosokawa, Y. (1999). Determination of abundance and biovolume of bacteria in sediments by dual staining with 4′,6-diamidino-2-phenylindole and acridine orange: relationship to dispersion treatment and sediment characteristics. *Appl. Environ. Microbiol.* 65, 3407–3412.

Maldonado, M., Aguilar, R., Bannister, R. J., Bell, J. J., Conway, K. W., Dayton, P. K., et al. (2017). "Sponge grounds as key marine habitats: a synthetic review of types, structure, functional roles, and conservation concerns," in *Marine Animal Forests: The Ecology of Benthic Biodiversity Hotspots*, eds S. Rossi, L. Bramanti, A. Gori, and C. Orejas (Cham: Springer International Publishing AG), 14–25. doi: 10.1007/978-3-319-21012-4_24

Maldonado, M., Beazley, L., López-Acosta, M., Kenchington, E., Casault, B., Hanz, U., et al. (2020). Massive silicon utilization facilitated by a benthic-pelagic coupled feedback sustains deep-sea sponge aggregations. *Limnol. Oceanogr.* 66, 366–391. doi: 10.1002/lno.11610

Maldonado, M., Ribes, M., and van Duyl, F. C. (2012). Nutrient fluxes through sponges. biology, budgets, and ecological implications. *Adv. Mar. Biol.* 62, 113–182. doi: 10.1016/B978-0-12-394283-8.00003-5

McGrath, E. C., Smith, D. J., Jompa, J., and Bell, J. J. (2017). Adaptive mechanisms and physiological effects of suspended and settled sediment on barrel sponges. *J. Exp. Mar. Biol. Ecol.* 496, 74–83. doi: 10.1016/j.jembe.2017.07.013

Mengual, B., Cayocca, F., Le Hir, P., Draye, R., Laffargue, P., Vincent, B., et al. (2016). Influence of bottom trawling on sediment resuspension in the

'Grande-Vasière' area (Bay of Biscay, France). *Ocean Dyn.* 66, 1181–1207. doi: 10.1007/s10236-016-0974-7

Murillo, F. J., Muñoz, P. D., Cristobo, J., Ríos, P., González, C., Kenchington, E., et al. (2012). Deep-sea sponge grounds of the Flemish Cap, Flemish Pass and the Grand Banks of Newfoundland (Northwest Atlantic Ocean): distribution and species composition. *Mar. Biol. Res.* 8, 842–854. doi: 10.1080/17451000.2012.682583

NAFO (2011). *Report of the 4th Meeting of the NAFO Scientific Council Working Group on Ecosystem Approach to Fisheries Management (WGEAFM).* 30 November to 10 December 2011, Dartmouth, Canada. NAFO SCS Document 11/22. Serial No. N6006. Dartmouth, NS: NAFO.

NAFO (2021). *Conservation and Enforcement Measures.* NAFO/COM Doc. 21-10. Serial No. N7153. Dartmouth, NS: NAFO.

Petrie, B., and Smith, P. C. (1977). Low-frequency motions on the Scotian shelf and slope. *Atmosphere* 15, 117–140. doi: 10.1080/00046973.1977.9648435

Pham, C. K., Murillo, F. J., Lirette, C., Maldonado, M., Colaço, A., Ottaviani, D., et al. (2019). Removal of deep-sea sponges by bottom trawling in the Flemish Cap area: conservation, ecology and economic assessment. *Sci. Rep.* 9:15843. doi: 10.1038/s41598-019-52250-1

Pilskaln, C. H., Churchill, J. H., and Mayer, L. M. (1998). Resuspension of sediment by bottom trawling in the Gulf of Maine and potential geochemical consequences. *Conserv. Biol.* 12, 1223–1229. doi: 10.1046/j.1523-1739.1998.0120061223.x

Puig, P., Canals, M., Company, J. B., Martín, J., Amblas, D., Lastras, G., et al. (2012). Ploughing the deep sea floor. *Nature* 489, 286–289. doi: 10.1038/nature11410

Rice, A. L., Thurston, M. H., and New, A. L. (1990). Dense aggregations of a hexactinellid sponge, *Pheronema carpenteri*, in the Porcupine Seabight (northeast Atlantic Ocean), and possible causes. *Prog. Oceanogr.* 24, 179–196. doi: 10.1016/0079-6611(90)90029-2

Robertson, L. M., Hamel, J. F., and Mercier, A. (2017). Feeding in deep-sea demosponges: influence of abiotic and biotic factors. *Deep Sea Res. Part I Oceanogr. Res. Pap.* 127, 49–56. doi: 10.1016/j.dsr.2017.07.006

Schönberg, C. H. L. (2016a). *Effects of Dredging on Benthic Filter Feeder Communities, with a Focus on Sponges.* Report of Theme 6-Project 6.1.1 Prepared for the Dredging Science Node. Perth: Western Australian Marine Science Institution, 139.

Schönberg, C. H. L. (2016b). Happy relationships between marine sponges and sediments-a review and some observations from Australia. *J. Mar. Biol. Assoc. UK* 96, 493–514. doi: 10.1017/S0025315415001411

Shore, R. E. (1971). Growth and renewal studies of the choanocyte population in *Hymeniacidon sinapium* (Porifera: Demospongiae) using colcemid and 3-H thymidine. *J. Exp. Zool.* 177, 359–363. doi: 10.1002/jez.1401770310

Spinrad, R. W., Zaneveld, J. R. V., and Kitchen, J. C. (1983). A study of the optical characteristics of the suspended particles in the benthic nepheloid layer of the Scotian Rise (North Atlantic). *J. Geophys. Res.* 88, 7641–7645. doi: 10.1029/JC088iC12p07641

Strehlow, B. W., Jorgensen, D., Webster, N. S., Pineda, M. C., and Duckworth, A. (2016). Using a thermistor flowmeter with attached video camera for monitoring sponge excurrent speed and oscular behaviour. *PeerJ* 4:e2761. doi: 10.7717/peerj.2761

Strehlow, B. W., Pineda, M. C., Duckworth, A., Kendrick, G. A., Renton, M., Wahab, M. A. A., et al. (2017). Sediment tolerance mechanisms identified in sponges using advanced imaging techniques. *PeerJ* 5:e3904. doi: 10.7717/peerj.3904

Tjensvoll, I., Kutti, T., Fosså, J. H., and Bannister, R. J. (2013). Rapid respiratory responses of the deep-water sponge *Geodia barretti* exposed to suspended sediments. *Aquat. Biol.* 19, 65–73. doi: 10.3354/ab00522

Tompkins-Macdonald, G. J., and Leys, S. P. (2008). Glass sponges arrest pumping in response to sediment: implications for the physiology of the hexactinellid conduction system. *Mar. Biol.* 154, 973–984. doi: 10.1007/s00227-008-0987-y

Conflict of Interest: The authors declare that the research was conducted in the absence of any commercial or financial relationships that could be construed as a potential conflict of interest.

Copyright © 2021 Wurz, Beazley, MacDonald, Kenchington, Rapp and Osinga. This is an open-access article distributed under the terms of the Creative Commons Attribution License (CC BY). The use, distribution or reproduction in other forums is permitted, provided the original author(s) and the copyright owner(s) are credited and that the original publication in this journal is cited, in accordance with accepted academic practice. No use, distribution or reproduction is permitted which does not comply with these terms.

frontiers in Marine Science

ORIGINAL RESEARCH
published: 17 May 2021
doi: 10.3389/fmars.2021.637810

Bioactivity of Biosilica Obtained From North Atlantic Deep-Sea Sponges

Olesia Dudik[1,2], Sara Amorim[1,2], Joana R. Xavier[3,4], Hans Tore Rapp[4], Tiago H. Silva[1,2], Ricardo A. Pires[1,2]* and Rui L. Reis[1,2]*

[1] 3B's Research Group, I3Bs – Research Institute on Biomaterials, Biodegradables and Biomimetics, University of Minho, Headquarters of the European Institute of Excellence on Tissue Engineering and Regenerative Medicine, Guimarães, Portugal, [2] ICVS/3B's - PT Government Associate Laboratory, Guimarães, Portugal, [3] CIIMAR – Interdisciplinary Centre of Marine and Environmental Research, Terminal de Cruzeiros de Leixões, Matosinhos, Portugal, [4] Department of Biology and K.G. Jebsen Centre for Deep-sea Research, University of Bergen, Bergen, Norway

Demosponges are a well-known source of a plethora of bioactive compounds. In particular, they are able to form a skeleton by direct deposition of silica in a process catalyzed by silicatein. Herein, we isolated biosilicas from five different Atlantic deep-sea sponges *Geodia atlantica* (GA), *Geodia barretti* (GB), *Stelletta normani* (SN), *Axinella infundibuliformis* (AI), and *Phakellia ventilabrum* (PV) to explore the bioactivity and osteogenic capacity of its silica-based materials. We chemically characterized the isolated biosilicas and evaluated them for their bioactivity to deposit Ca and P on their surface (by immersion in simulated body fluid, SBF). GB-, SN-, AI-, and PV-based biosilicas did not generate a stable calcium phosphate (CaP) layer over time in the presence of SBF, however, the GA-derived one was able to form a CaP surface layer (at a Ca/P ratio of ∼1.7, similar to the one observed for hydroxyapatite), that was stable during the 28 days of testing. In addition, no cytotoxicity toward L929 and SaOs2 cells was observed for the GA-based biosilica up to a concentration of 10 mg/mL. Overall, the GA-based biosilica presents the characteristics to be used in the development of biomaterials for bone tissue engineering (BTE).

Keywords: bioactivity, biosilica, bioceramics, tissue engineering, deep-sea sponges

OPEN ACCESS

Edited by:
Ellen Kenchington, Bedford Institute of Oceanography (BIO), Canada

Reviewed by:
Matthias Wiens, Johannes Gutenberg University Mainz, Germany
Shirley A. Pomponi, Florida Atlantic University, United States

***Correspondence:**
Tiago H. Silva
tiago.silva@i3bs.uminho.pt
Ricardo A. Pires
rpires@i3bs.uminho.pt

Specialty section:
This article was submitted to Deep-Sea Environments and Ecology, a section of the journal Frontiers in Marine Science

Received: *04 December 2020*
Accepted: *23 April 2021*
Published: *17 May 2021*

Citation:
Dudik O, Amorim S, Xavier JR, Rapp HT, Silva TH, Pires RA and Reis RL (2021) Bioactivity of Biosilica Obtained From North Atlantic Deep-Sea Sponges. Front. Mar. Sci. 8:637810. doi: 10.3389/fmars.2021.637810

INTRODUCTION

The marine environment is a source of a wide range of compounds, which have been subject of intense research due to their potential biomedical application. It has been reported the extracted and purified marine-origin chemicals present antibiotic, anticancer, anti-inflammatory and antiviral activities, among many others (Marris, 2006). In addition, silica-based chemical structures, as the ones found in marine sponges (Thakur and Müller, 2004; Venkatesan et al., 2016), have the potential to be used as bioactive and osteogenic biomaterials relevant for bone tissue engineering (BTE) applications.

The most common way used by marine sponges to produce their biosilica-based skeleton is through deposition/assembly catalyzed by silicatein (i.e., α, β, and γ isoforms). During this process, siliceous spicules are formed through the direct deposition of silica along the axial direction of the silicatein filaments (Cha et al., 1999; Müller et al., 2008; Ehrlich et al., 2010a).

Biosilica represents the main component of the matrix of these spicules (Ehrlich et al., 2010b; Kulakovskaya et al., 2012; Wang et al., 2012); however, collagen, being the predominant protein in the organic matrix of marine sponges, is also present. In this sense, sponge spicules are regarded as a composite material (Schröder et al., 2008). In addition, several reports demonstrated that biogenic polyphosphates (linear inorganic polymers) are also involved in the formation of biosilica (Kulaev et al., 2005).

The hierarchical organization of sponge skeletons and spicules containing amorphous silica (classes Demospongiae, Hexactinellida, and Homoscleromorpha) or calcium carbonate (class Calcarea) inspired researchers to use them in the development of biomaterials for BTE (Silva et al., 2012; Barros et al., 2014; Odatsu et al., 2015; Lewandowska-Łańcucka et al., 2015; Antoniac et al., 2016; Wysokowski et al., 2018). The use of this biosilica has been considered as a promising biomimetic approach to recapitulate the inorganic part of the bone extracellular matrix (ECM) (Dudik et al., 2018).

It has been shown that biosilica promotes osteoblast proliferation and function (Wang et al., 2013). In fact, Schröder et al. reported that the silica-containing bioactive surfaces generated through silicatein-mediated catalysis induce the formation of hydroxyapatite (HA) crystals under SaOs2 cell culture (Schröder et al., 2005). Wiens et al. (2010a,b) also revealed the osteogenic potential of biosilica in their studies, showing that it is able to promote the formation of HA crystals and increase the gene expression of SaOs2 cells. More recently, Barros et al. demonstrated that ceramic structures obtained upon calcination of marine sponges (i.e., *Petrosia ficiformis*, *Agelas oroides*, and *Chondrosia reniformis*) are non-cytotoxic and have the potential to be used as substitutes of synthetic Bioglass (Barros et al., 2016).

A wide range of bioceramic-based strategies, typically using calcium phosphates (CaP) and/or bioactive glasses, or polymers (e.g., naturally derived collagen type I), as well as hybrid materials, created by the mixture of bioceramics and polymeric structures, have been developed targeting BTE (Rezwan et al., 2006; Fu et al., 2011; Amorim et al., 2014; Fernandes et al., 2016). In the case of bioactive silica-based glasses, they are able to bind and integrate into the bone tissue through the formation of a silica gel layer. It is reported that this layer attracts and stimulates osteoprogenitor cells to proliferate and to differentiate into osteoblasts, which, in turn, start the synthesis and deposition of ECM and its mineralization (Blunt et al., 2005; Blunt et al., 2010). Fabrication of glass and glass-ceramic scaffolds with architectures mimicking the 3D interconnected porosity of natural bone has been explored (Rezwan et al., 2006; Rahaman et al., 2011; Kaur et al., 2014). In general, adequate mechanical strength and controlled degradation rates are two of the most relevant properties for application to a BTE strategy.

Within the use of composites as biomaterials for BTE, marine building blocks are establishing a representative role (Silva et al., 2012), namely following the studies reporting the use of: collagen combined with calcium phosphates (Elango et al., 2016; Diogo et al., 2018, 2020); biosilica from sponges (Müller et al., 2004), but also from diatoms (Le et al., 2018); polyphosphates inspired in the materials found in sponges (Wang et al., 2018); among many others. Interest in marine biomaterials for BTS has been associated with the sustainable production methodologies, namely benefiting from strategies proposed for the valorization of marine by-products, such as fish bones and skins, but also due to the absence of ethical or health constraints, which are usually associated with the use of mammal-derived components.

Herein, we focus on the evaluation of the biomedical potential of biosilica derived from five North Atlantic deep-sea sponge species of the class Demospongiae, namely *Geodia atlantica* (GA), *Geodia barretti* (GB), *Stelletta normani* (SN) (order Tetractinellida), and *Axinella infundibuliformis* (AI), *Phakellia ventilabrum* (PV) (order Axinellida). We report on their physicochemical characterization, bioactivity (herein referred as the ability to promote the formation of CaP layer on the surface of the biosilicas) and cytotoxicity under *in vitro* conditions, as a screening methodology to develop marine-based biosilica structures with potential to be used in BTE.

MATERIALS AND METHODS

Materials

Sponge Samples

Sponge samples of the species *Geodia atlantica* (GA), *Geodia barretti* (GB), *Stelletta normani* (SN), *Axinella infundibuliformis* (AI), and *Phakellia ventilabrum* (PV) were collected in Korsfjord, Norway, using a triangular dredge, at depths between 332 and 97 m for GA, GB, PV and between 292 and 226 m for SN and AI. Upon collection, samples were fragmented and preserved in 99% ethanol. Taxonomic identifications were made from the analyses of external and internal morphological characteristics. Representative fragments, i.e., comprising both the sponge ectosome (external part) and choanosome (inner part), were selected for further materials processing and characterization.

Chemicals

Sodium chloride (PanReac AppliChem, Spain), sodium hydrogen carbonate (Merck, Germany), potassium chloride (VWR International, Portugal), di-potassium hydrogen phosphate trihydrate (Merck, United Kingdom), Tris(hydroxymethyl)-aminomethane, magnesium chloride hexahydrate and calcium chloride (Sigma-Aldrich, Portugal), sodium sulfate (Sigma-Aldrich, Australia), hydrochloric acid (Fisher Scientific, United Kingdom) were used for preparation of simulated body fluid (SBF). All the reagents were ACS reagent grade. 1,000 mg/L Ca ICP standard solution (Alfa Aesar, Germany) and 1,000 mg/L P ICP standard solution (Merck, Germany) were used for preparation of calibration standards. Ultrapure water was used throughout the study.

Extraction of Bioceramics From Deep-Sea Sponges

The marine sponges were calcinated in a furnace (FornoCeramica, Portugal) at 800°C for 6 h in order to remove the whole organic components thereby extracting the inorganic part. Prior to the calcination process, the samples were cut into pieces and washed repeatedly with ultrapure water.

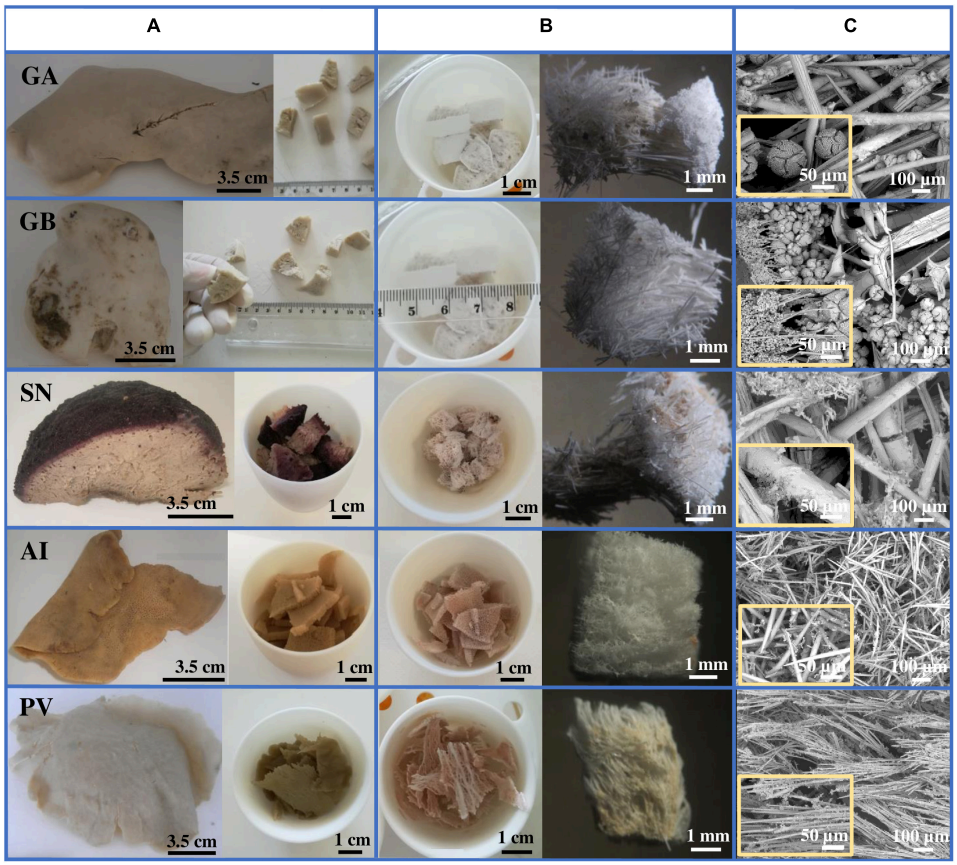

FIGURE 1 | (A) GA, GB, SN, AI, and PV marine sponge specimens and corresponding sponge pieces before calcination. **(B)** Corresponding sponge-derived biosilicas obtained upon calcination and close-up of each calcined sponge piece. **(C)** SEM images showing silica-based spicules obtained upon calcination.

TABLE 1 | Quantification of the chemical elements present in the biosilicas obtained from the different marine sponges.

Sponge species	Composition (Wt%)								
	O	Si	Ca	Na	P	Mg	K	S	Al
GA—*Geodia atlantica*	54.0	37.5	1.9	2.5	1.6	0.9	1.3	0.4	–
GB—*Geodia barretti*	53.3	38.4	1.2	3.2	0.7	0.8	0.8	0.2	1.3
SN—*Stelletta normani*	53.7	36.6	2.7	1.9	1.1	1.0	0.8	0.8	1.4
AI—*Axinella infundibuliformis*	54.8	35.1	2.7	2.0	1.5	1.7	0.8	1.1	0.3
PV—*Phakellia ventilabrum*	53.3	39.2	1.9	1.2	0.7	0.7	0.9	0.6	1.5

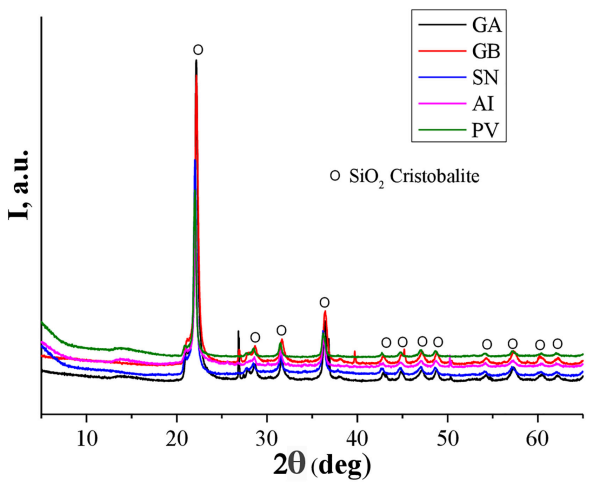

FIGURE 2 | XRD powder patterns of the biosilicas obtained from the tested marine sponges.

Bioactivity Assessment

The biosilicas obtained from the different marine sponges were immersed in SBF. The SBF was prepared according to the procedure described by Kokubo and Takadama (2006). The initial concentrations of calcium and phosphorus ions in SBF were 2.5 and 1 mmol/L, respectively. The samples were immersed in SBF using plastic tubes, under a powder-to-liquid ratio of 1.5 mg: 1 mL (Jones et al., 2001; Yu et al., 2012; Greasley et al., 2016), using aliquots of 15 mg of each biosilica per 10 mL of SBF. Samples were placed in a thermostatic water bath at 37°C, for 6 h,

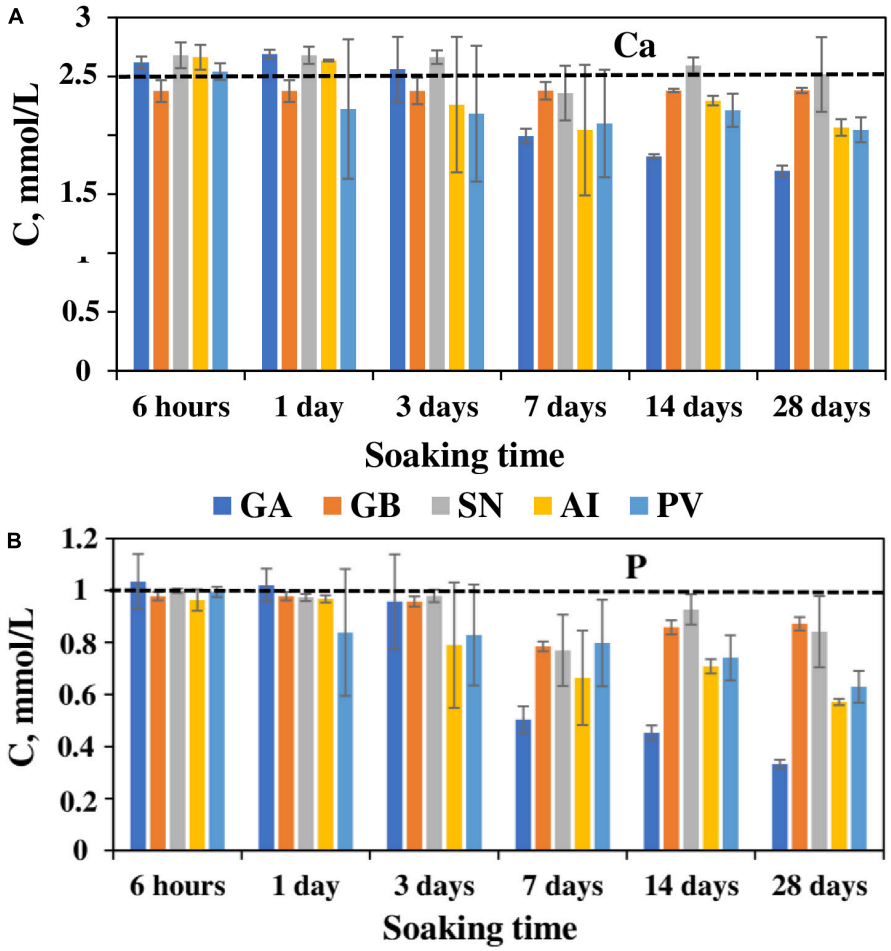

FIGURE 3 | Changes in Ca **(A)** and P **(B)** concentrations in the SBF solutions after immersion of the different biosilicas during 28 days.

1, 3, 7, 14, and 28 days under constant agitation (i.e., 60 rpm). Three samples of each biosilica were used per test, with average values reported. At each time point the SBF was separated from the solid and used to determine the Ca and P concentrations. The solid was washed with distilled water, dried at 37°C and assessed microscopically.

Characterization of the Biosilica Surface

Scanning Electron Microscopy and Energy Dispersive X-Ray Spectroscopy

Scanning electron microscopy (SEM) was carried out on a JSM-6010 LV microscope (JEOL, Japan) equipped with an energy dispersive (EDS) x-ray spectroscope (Oxford Instruments, United Kingdom) under a working distance of 10–12 mm and a beam energy of 10.0 kV. The low vacuum mode allowed non-conductive biosilicas (samples before grinding) to be observed and analyzed without conductive coating. Powders of biosilicas before and after immersion in SBF were platinum coated (apx. 2 nm) prior to the analysis. EDS analysis was performed at four points using a beam energy of 15.0 kV and a magnification of 500×. EDS spectra were analyzed using the Aztec software from Oxford Instruments) and presented as a semi-quantitative evaluation.

Fourier Transform Infrared Spectroscopy

Fourier transform infrared spectroscopy (FTIR) spectra were collected on an IR Prestige-21 spectrometer (Shimadzu, Japan) as an average of 32 scans, a wavenumber range between 4,000 and 400 cm^{-1} and a resolution of 4 cm^{-1}. A press (Pike, United States) was used to prepare transparent pellets containing biosilica powders mixed with potassium bromide.

X-Ray Diffraction

X-ray diffraction (XRD) analysis was executed on a XRD diffractometer (Bruker D8 Advance, Germany), operating using a Cu-Kα radiation in θ/2θ mode, in the range between 6° and 70°, using a step increment of 0.04° and an acquisition time of 1 s per step.

Thermogravimetric Analysis

Thermogravimetric analysis of the sponge samples was carried out on Simultaneous Thermogravimetric Analyzer STA7000 (Hitachi, Japan) under a temperature range from 23 to 800°C

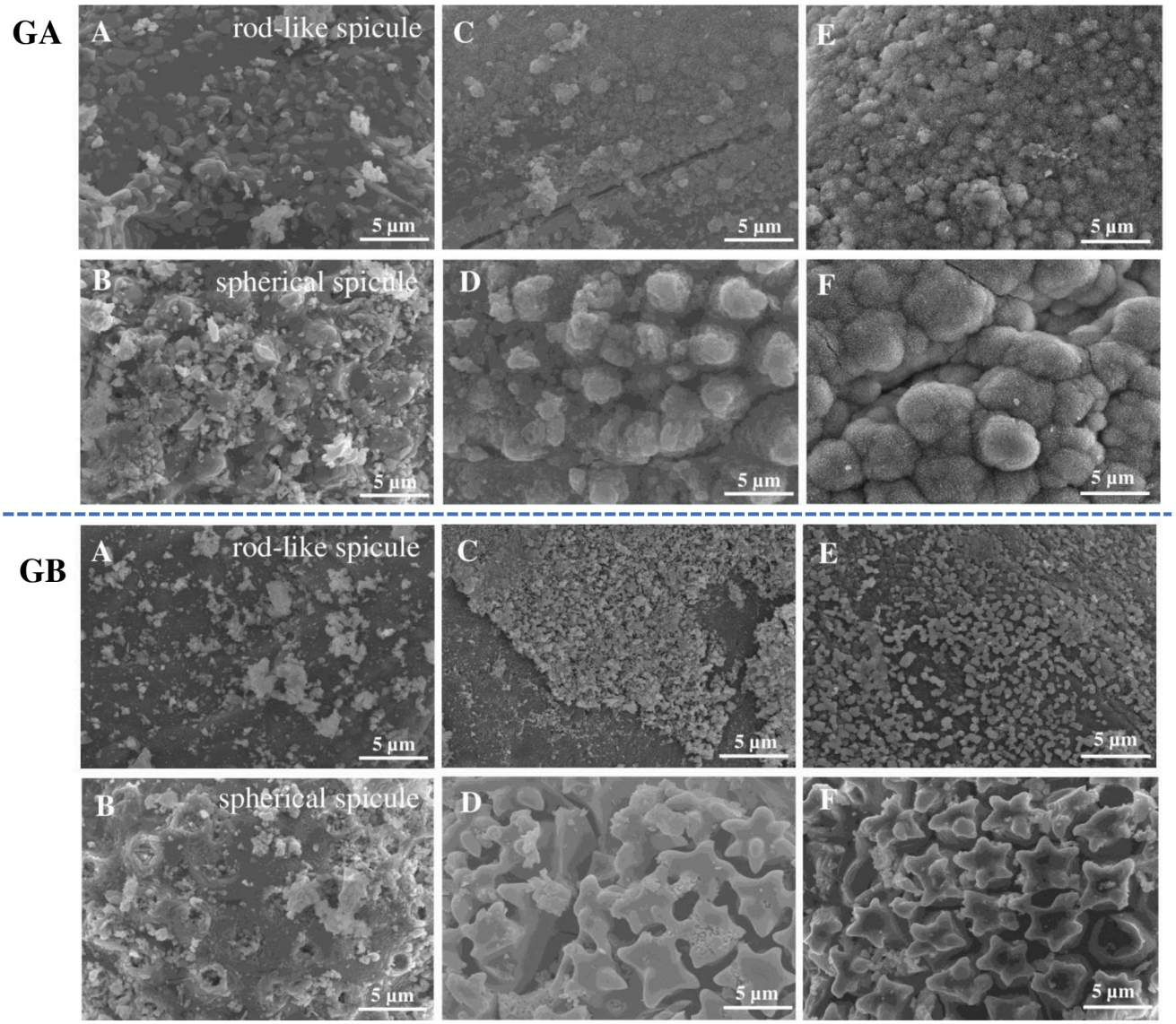

FIGURE 4 | SEM micrographs of the biosilicas obtained from GA and GB before immersion in SBF **(A,B)**, after 7 days of immersion in SBF **(C,D)**, and after 28 days of immersion in SBF **(E,F)**. Scale bar: 5 µm.

and a heating rate of 10°/min in an oxygen atmosphere. For each biosilica, it was used a sample weight of 8–10 mg.

Inductively Coupled Plasma Optical Emission Spectrometry

Inductively coupled plasma—optical emission spectrometry (ICP-OES) was used to determine the Ca and P concentrations present in the SBF before and after the immersion of the biosilicas. The ICP-OES analysis was performed on a ICP spectrometer (HORIBA JY 2000-2, United States), using the absorption wavelengths of λ = 317.93 nm and λ = 214.91 nm for Ca and P, respectively. Concentrations of Ca and P were calculated from standard calibration curves prepared using standard solutions from 0 to 10 ppm.

Cytotoxicity Studies

The cytotoxicity of the biosilicas was evaluated following an established protocol based on ISO/EN 10 993 standard (ISO 10993-5, 2009) guidelines, using an immortalized mouse lung fibroblast cell line (L929) and Sarcoma cell line (SaOs2) purchased from the European Collection of Cell Cultures. In brief, biosilicas (100, 50, and 10 mg/mL; 3 samples from the biosilica obtained from the same sponge were used throughout the analysis) were incubated in DMEM culture medium (Dulbecco's Modified Eagle's Medium—low glucose) with 10% heat-inactivated fetal bovine serum (FBS; Biochrom AG, Germany) and 1% antibiotic/antimycotic solution (containing a final concentration of penicillin 100 units/mL and streptomycin 100 mg/mL; Gibco, United Kingdom), for

TABLE 2 | Chemical composition of the surface of the biosilicas after 28 days of immersion in simulated body fluid (SBF).

Sponge species	Composition (Wt%)								
	O	Si	Ca	Na	P	Mg	K	S	Al
GA—*Geodia atlantica*	54.3	15.4	18.6	0.4	10.6	0.7	–	–	–
GB—*Geodia barretti*	55.0	37.9	2.2	1.1	1.9	0.5	0.3	–	0.9
SN—*Stelletta normani*	56.6	39.4	0.7	0.7	0.3	0.5	0.4	–	1.4
AI—*Axinella infundibuliformis*	54.8	40.3	1.2	0.8	0.9	1.2	0.5	–	0.2
PV—*Phakellia ventilabrum*	56.0	42.0	0.8	0.3	0.4	0.2	0.3	–	–

24 h in a water bath at 37°C and 60 rpm. The leachables of each sample were collected and filtered using a 0.22 μm syringe filter. L929 and SaOs2 cells (11,000 cells.cm^{-2}) were cultured in a 96-well plate in DMEM and after 24 h, the media were replaced by the collected biosilica extracts. Cell viability was evaluated by AlamarBlue assay after 24 and 72 h. The percentage of reduced AlamarBlue was calculated according to the manufacturer instructions (Bio-Rad). The results presented were normalized to the absorbance obtained for control cells cultured in DMEM (positive control) and correspond to the average of three measurements (±standard deviation).

Statistical Analysis

The data obtained from the ICP analysis and cytotoxicity tests were expressed as mean ± standard deviation (SD). The statistical analysis of the cytotoxicity study was performed by using the Shapiro-Wilk test ($p < 0.05$) to check if the data presented a normal distribution. The data did not follow a normal distribution and, as a consequence, were analyzed using the Mann-Whitney test. The statistically significant differences are represented with * for $p < 0.05$ and ** for $p < 0.01$.

RESULTS AND DISCUSSION

Characterization of the Biosilica Samples

Biosilica structures were obtained after calcination of the sponges (**Figures 1A,B**, before and after treatment) as described in the methods section. In all the cases, the biosilicas were fragile 3D structures composed of siliceous spicules with different sizes and shapes (**Figure 1B**). The elimination of the organic matrix resulted in an amount of loose spicules, indicating that the spicules were embedded into the organic matrix which, upon calcination, lost its solid support. Moreover, SEM analysis confirmed that all the spicules were cracked after the calcination step, probably due to the degradation of the organic components, such as proteins (e.g., silicateins and collagen) that occurs during the heating process (**Figure 1C**). The microscopic observation of the biosilicas obtained from GA and GB revealed the presence of different types of spicules, such as sterrasters (microscleres, spherical) and dichotriaenes (megascleres), which have been previously reported and reviewed (Cárdenas et al., 2013).

Thermogravimetric analysis showed that the organic portion of the marine sponges were removed upon calcination at 800°C during 6 h, with the silica content of these sponges accounting to about 50–60% of their dry mass (**Supplementary Figure 1**, example of TG and DTG curves obtained for GB). The weight loss observed in the lower temperature region (i.e., $T_{max} \sim 100$°C, weight loss ∼ 8%) is attributed to water desorption. Further weight loss in the temperature region between 200 and 544°C with a total mass loss of about 40% corresponds to the thermal decomposition of the sponge's organic components.

EDS, XRD, and FTIR analysis showed that the inorganic part of the marine sponges is mainly composed of silicates, compatible with biosilica spicules. However, EDS data revealed that they also contained traces of other elements, such as Ca, Na, P, Mg, K, and S. Moreover, Al was also found, but only in the biosilicas obtained from GB, SN, AI, and PV (**Table 1**). The elemental composition of the biosilicas demonstrates their inherent ability to bind to other essential cations, such as Ca^{2+}, Mg^{2+}, K^{+}, Na^{+}, and Al^{3+}. In their FTIR spectra (**Supplementary Figure 2**), the shoulder at apx. 1,650 cm^{-1} can be attributed to adsorbed water. The bands at 1,099 and 790 cm^{-1} are assigned to the O-Si-O asymmetrical and symmetrical stretching vibrations, respectively, from the Si-O-Si network. The broad band at ∼3,425 cm^{-1} corresponds to the stretching vibrations of −OH from the Si-OH moieties (Khan et al., 2017).

The XRD powder patterns (**Figure 2**) of the biosilicas obtained upon calcination revealed the presence of the most intense peak at 22° 2θ and less intense peaks between 28 and 65° 2θ, which correspond to Cristobalite crystalline phase (COD 9015087) (Xue et al., 2015), confirming that the main structural inorganic component of the sponges are silicates.

Assessment of Bioactivity

To assess the bioactivity of the generated biosilicas (herein referred as the ability of the biosilicas to promote the deposition of CaP layer on their surface), samples were immersed in SBF for different timeframes. At each timepoint, the solution was filtered and analyzed by ICP to determine the Ca and P concentrations. After separation of the biosilica materials from the SBF solution, their surface morphology was analyzed by SEM, while EDS was used to quantify the Ca and P concentrations present in the inorganic structures formed on the surface of the biosilicas.

ICP analysis of the SBF solutions, at the different timepoints of the evaluation of the bioactivity (**Figure 3**), demonstrated that the concentration of Ca and P in the SBF solution increased for several samples up to day 1 (increase of Ca concentration for the biosilicas generated from GA, SN, AI, and increase of P concentration for GA-based biosilica). This could be explained by the diffusion of Ca and P ions present in the biosilica samples into the SBF. Afterwards, for the GB-, SN-, AI-, and PV-derived biosilicas, a decrease of Ca and P concentration was observed between day 1 and day 7, followed by a stabilization up to day 28, showing that these ions were responsible for the formation of a CaP layer on their surfaces. The GA-based biosilicas had an overall higher consumption of Ca and P from SBF leading to its

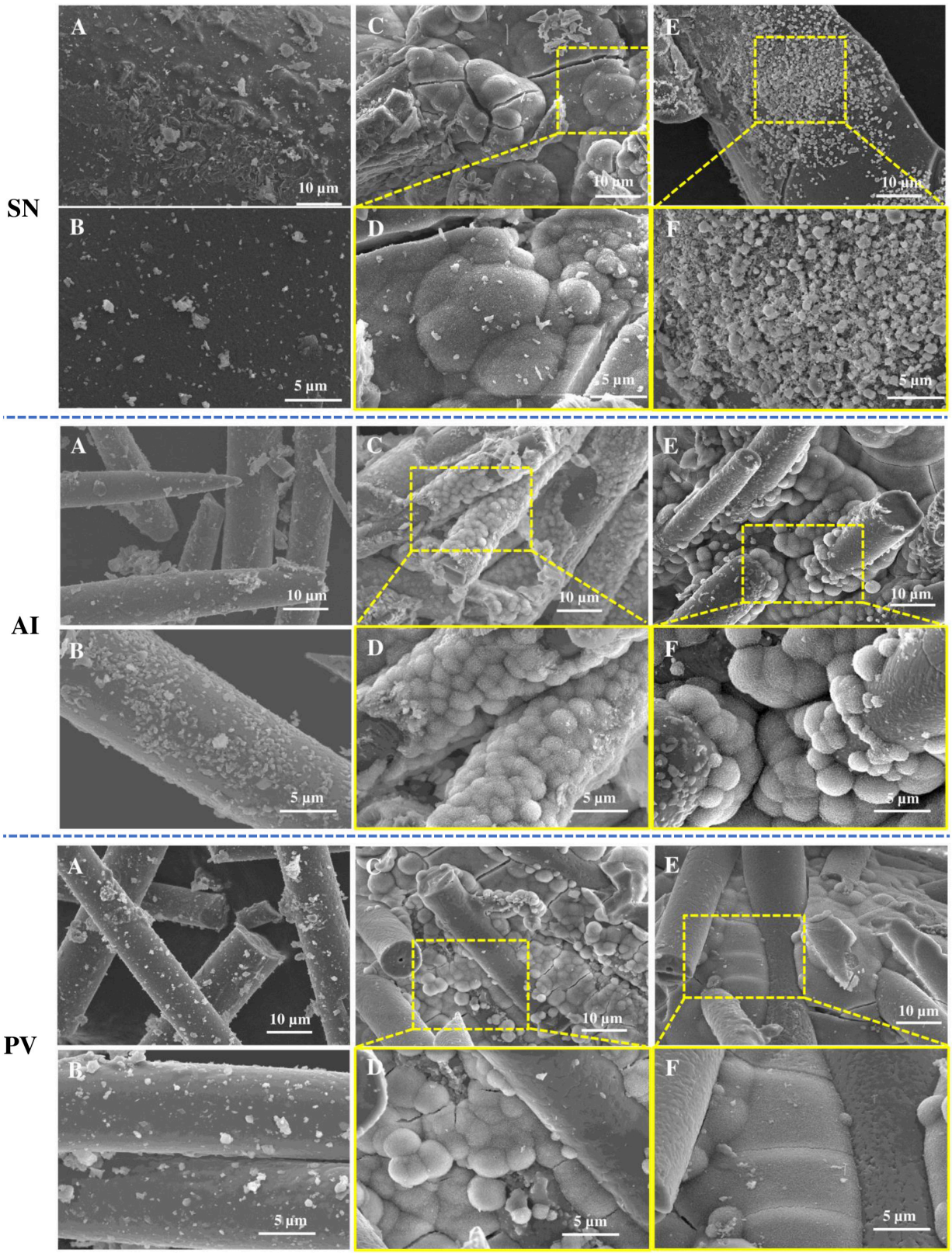

FIGURE 5 | SEM micrographs of the biosilicas obtained from SN, AI, and PV before immersion in SBF **(A,B)**, after 7 days of immersion in SBF **(C,D)**, and after 28 days of immersion in SBF **(E,F)**. Scale bars: 5 and 10 µm.

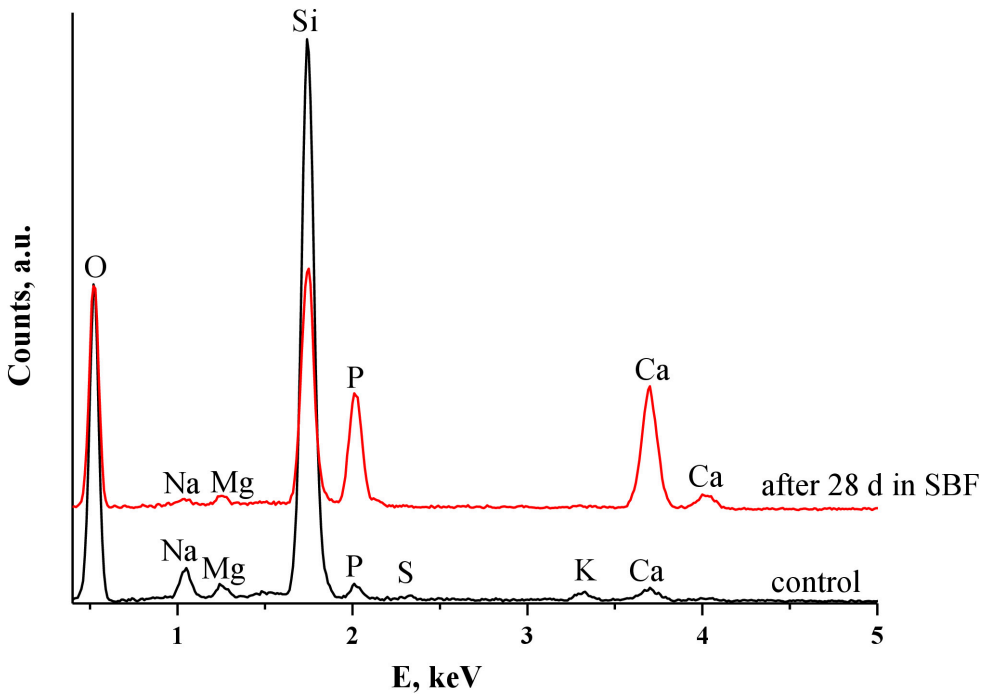

FIGURE 6 | EDS spectra of GA-derived biosilica before and after immersion in SBF (for 28 days).

deposition on the biosilica surface between day 3 and day 28 (as shown in the SEM analysis, **Figure 4**).

The formation of the CaP layer on the biosilica surface was monitored by SEM and EDS. SEM observation showed that, after immersion in SBF for 28 days, GA-based biosilicas presented the formation of cauliflower structures typical of hydroxyapatite (HA) on the surface of both types of spicules (**Figure 4**). Moreover, the EDS analysis (**Table 2**) showed that the detected CaP structures present a Ca/P ratio of ∼1.7, which is similar to the one expected to be present in HA, confirming its presence in the biosilica surface (Bailey et al., 2009). In contrast to these results, GB-based biosilicas, after immersion in SBF for 7 days, presented dispersed CaP structures only on the rod-like spicules, that noticeably decrease through the 28 days of the evaluation of bioactivity (**Figure 4**).

In the case of the spicules obtained from the SN, PV-, and AI-based biosilicas the formation of dispersed CaP deposits was observed on their surface throughout the whole 28 days of testing. However, especially in the case of the SN-derived biosilica, an additional reduction of CaP deposits was detected after 28 days of immersion (**Figure 5**), confirming that the generated CaP structures are not stable over longer timeframes.

In general, the SEM/EDS data are consistent with the results obtained by ICP, revealing a significant and stable increase in Ca and P content only on the surface of GA-based biosilica after immersion in SBF for 28 days (**Figure 6** and **Table 2**). In fact, it has been previously reported that the bioactivity of biosilicas is correlated with their chemical composition (Barros et al., 2016), where the presence of Ca, Mg, and P promotes the nucleation and growth of HA on their surface, while biosilicas that do not contain Ca, Mg, nor P, did not show any inherent bioactivity. We did not confirm this trend in the biosilicas obtained from the species herein studied, as all of them presented similar values of Ca/Mg/P concentrations, however, it is relevant to point out that the GA-based biosilica (the one with higher bioactivity) is, in fact, the one that had the higher concentration of P in its initial composition (**Table 1**). Our results give a strong evidence that the GA-based biosilica should be able to promote the regeneration of bone tissue and, consequently, it is highly relevant for the development of BTE strategies. However, this evaluation was executed using chemical methodologies that do not guarantee *per si* the cytocompatibility of the tested biosilica formulations.

Evaluation of Cytotoxicity

To guarantee that the proposed formulations can indeed be used under the biological environment, we tested the cytotoxicity of the developed sponge-based biosilicas. L929 and SaOS2 cells were cultured in the presence of extracts from the biosilicas generated from the sponges GA, GB, SN, AI, and PV. In the cases of GB, SN, AI, and PV, a cellular metabolic activity was detected between 65 and 100%, demonstrating the non-cytotoxic behavior of the biosilica originating from these sponges (**Figure 7**). The GA-based biosilica was non-cytotoxic only at a concentration of 10 mg/mL, being toxic for the highest concentrations, i.e., 50 and 100 mg/mL. The non-cytotoxic behavior of the herein tested biosilicas (which is concentration dependent in the case of GA) suggest their potential use in the BTE. Of note, the metabolic activity of the SaOs2, when in contact with GB− (10 mg/mL) and SN-based (100 mg/mL) biosilicas after 72 h, is higher than the control experiment.

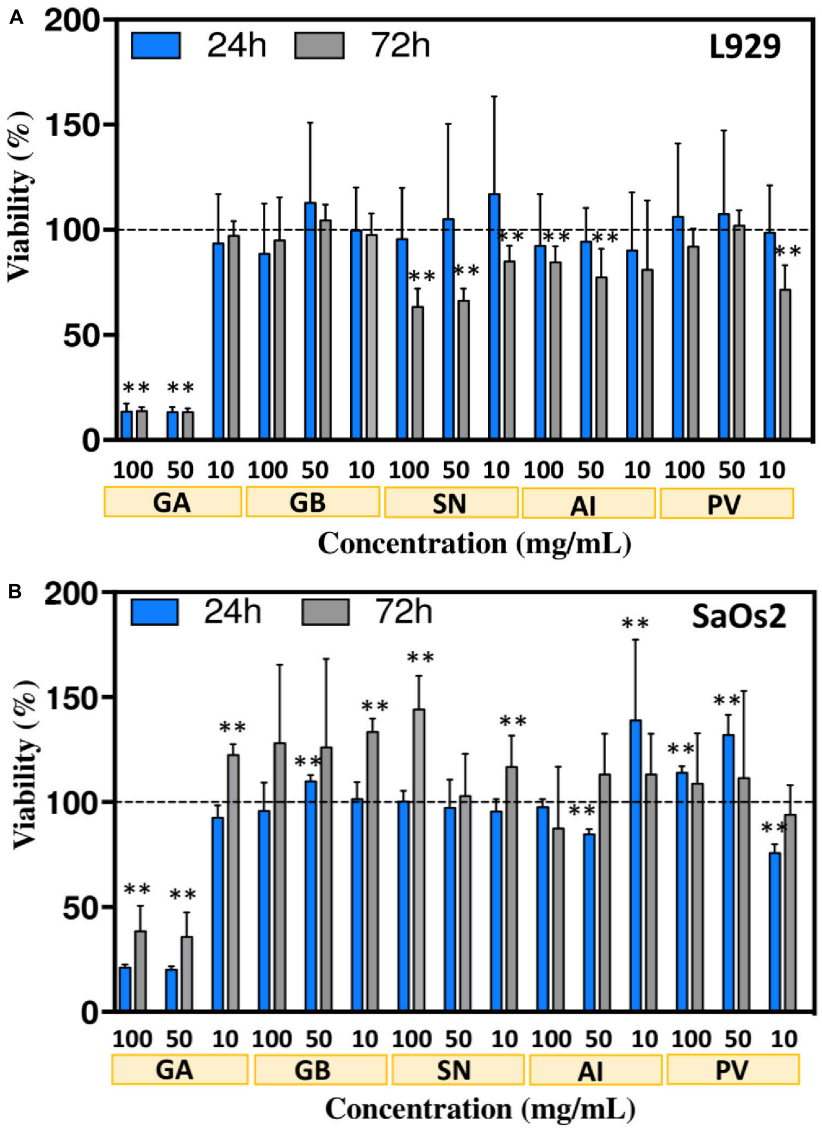

FIGURE 7 | Viability of L929 **(A)** and SaOs2 **(B)** cells, measured using the AlamarBlue assay, when cultured in contact with different concentrations of the extracts from the sponge-based biosilicas, i.e., 10, 50, and 100 mg/mL. Metabolic activity was evaluated after 24 and 72 h of cell culture. The data are presented as mean ± SD and the statistical differences are represented with * for $p < 0.05$ and ** for $p < 0.01$.

Barros et al. (2016) previously evaluated the suitability of different biosilicas as substitutes of synthetic Bioglass, by assessing the metabolic activity of L929 cells in the presence of extracts from biosilicas of the species *Petrosia ficiformis*, *Agelas oroides*, and *Chondrosia reniformis*. In all the cases the cell metabolic activity was between 80 and 100% confirming their non-cytotoxic character. In addition, Gabbai-Armelin et al. (2019) showed that extracts from biosilica obtained from *Tedania ignis* and *Dragmacidon reticulatum* marine sponges, at a concentration of 50 mg/mL, promoted the increment of cell viability. Our results showed that the presence of biosilica from the GB, SN, AI, and PV sponges is non-cytotoxic. The only biosilica with limited cell compatibility (i.e., the GA-derived biosilica) demonstrates a higher concentration of CaP structures on their surface after immersion in SBF. A possible explanation for the observed toxicity is the increment of pH generated from the release of cations from the biosilica structure, as has been observed for Bioglass (Brückner et al., 2016). In fact, we observed an increase in the pH of the medium after 3 days of incubation in the presence of biosilica particles, showing the highest value for GA-based biosilica (**Supplementary Table 1**). This result is consistent with the higher susceptibility of the cells to the extracts obtained from this type of biosilica, especially at higher concentrations, i.e., 100 and 50 mg/mL. In fact, this type of observation has been also reported by Wanandi et al. (2017) showing that the release of cations leads to the alkalinization of the culture medium, which, in turn, causes

cell death. Importantly, when reducing the concentration of the biosilica to 10 mg/mL, the cell viability is not affected. Moreover, the concentration of cations in the medium after 3 days of incubation (**Supplementary Table 2**), shows a significant reduction of P and Ca content in the medium (due to the deposition of CaP) while significantly increasing the Si content (a known promoter of osteogenesis) (Götz et al., 2019). These differences in the composition of the medium is consistent with the higher bioactivity of GA-derived biosilica and its ability to promote new bone formation. Overall, our results indicate that the GA-derived biosilica are suitable to be further tested in the context of BTE and regeneration.

CONCLUSION

In this study, biosilicas were obtained by calcination of five North Atlantic deep-sea sponges, i.e., *Geodia atlantica* (GA), *Geodia barretti* (GB), *Stelletta normani* (SN), *Axinella infundibuliformis* (AI), and *Phakellia ventilabrum* (PV), and their bioactivity was evaluated by incubation in SBF. Our results showed that the GB-based biosilica has a reduced capacity to promote the deposition of stable CaP structures. In addition, the SN-, AI-, and PV-based biosilicas demonstrated the capacity to generate some CaP domains in their surface, however, they are not stable over longer periods of time (i.e., 28 days). Overall, the biosilica obtained from GA presented the highest bioactivity, and it is not cytotoxic at a concentration of 10 mg/mL. Based on our findings we conclude that the GA-based biosilica (at a concentration up to 10 mg/mL) has potential to be used in BTE applications.

DATA AVAILABILITY STATEMENT

The original contributions presented in the study are included in the article/**Supplementary Material**, further inquiries can be directed to the corresponding author/s.

AUTHOR CONTRIBUTIONS

OD: research design, experimental work, data aquisition and treatment, discussion, and manuscript draft preparation. SA: experimental work, data aquisition and treatment, discussion, and contribution to manuscript writing. JRX: collecting, identification and characterization of the sponge species used in the work, and contribution to the discussion of the results. HTR: collecting, identification and characterization of the sponge species used in the work, and contribution to the discussion of the results. THS: research conceptualization and design, supervision, discussion, manuscript revision, funding acquisition, and project management. RAP: research conceptualization and design, supervision, discussion, manuscript writing and revision, funding acquisition, and project management. RLR: supervision, manuscript revision, funding acquisition, and project management.

FUNDING

This research has been performed with funding from the European Union's Horizon 2020 research and innovation programme under Grant Agreements No. 679849 (SponGES) and No. 668983 (FORECAST). Funding from the European Regional Development Fund, through Atlantic Area Program, under the scope of BlueHuman project (EAPA_151/2016) is also acknowledged. JRX research was also supported by National Funds through FCT, the Portuguese Foundation for Science and Technology within the scope of UIDB/04423/2020, UIDP/04423/2020, and CEECIND/00577/2018.

SUPPLEMENTARY MATERIAL

The Supplementary Material for this article can be found online at: https://www.frontiersin.org/articles/10.3389/fmars.2021.637810/full#supplementary-material

REFERENCES

Amorim, S., Martins, A., Neves, N. M., Reis, R. L., and Pires, R. A. (2014). Hyaluronic acid/poly-l-lysine bilayered silica nanoparticles enhance the osteogenic differentiation of human mesenchymal stem cells. *J. Mater. Chem. B* 2, 6939–6946. doi: 10.1039/c4tb01071j

Antoniac, I., Lesci, I. G., Blajan, A. I., Vitioanu, G., and Antoniac, A. (2016). Bioceramics and biocomposites from marine sources. *Key Eng. Mater.* 672, 276–292.

Bailey, M. J., Coe, S., Grant, D. M., Grime, G. W., and Jeynes, C. (2009). Accurate determination of the Ca: P ratio in rough hydroxyapatite samples by SEM-EDS, PIXE and RBS – a comparative study. *X Ray Spectr.* 38, 343–347. doi: 10.1002/xrs.1171

Barros, A. A., Aroso, I. M., Silva, T. H., Mano, J. F., Duarte, A. R. C., and Reis, R. L. (2014). Surface modification of silica-based marine sponge bioceramics induce hydroxyapatite formation. *Cryst. Growth Des.* 14, 4545–4552. doi: 10.1021/cg500654u

Barros, A. A., Aroso, I. M., Silva, T. H., Mano, J. F., Duarte, A. R. C., and Reis, R. L. (2016). In vitro bioactivity studies of ceramic structures isolated from marine sponges. *Biomed. Mater.* 11:045004. doi: 10.1088/1748-6041/11/4/045004

Blunt, J. W., Copp, B. R., Munro, M. H. G., Northcote, P. T., and Prinsep, M. R. (2005). Marine natural products. *Nat. Prod. Rep.* 22, 15–61. doi: 10.1039/b415080p

Blunt, J. W., Copp, B. R., Munro, M. H. G., Northcote, P. T., and Prinsep, M. R. (2010). Marine natural products. *Nat. Prod. Rep.* 27, 165–237. doi: 10.1039/b906091j

Brückner, R., Tylkowski, M., Hupa, L., and Brauer, D. S. (2016). Controlling the ion release from mixed alkali bioactive glasses by varying modifier ionic radii and molar volume. *J. Mater. Chem. B* 4, 3121–3134. doi: 10.1039/C5TB02426A

Cárdenas, P., Rapp, H. T., Klitgaard, A. B., Best, M., Thollesson, M., and Tendal, O. S. (2013). Taxonomy, biogeography and DNA barcodes of Geodia species (Porifera, Demospongiae, Tetractinellida) in the Atlantic boreo-arctic region. *Zool. J. Linnean Soc.* 169, 251–311. doi: 10.1111/ZOJ.12056

Cha, J. N., Shimizu, K., Zhou, Y., Christiansen, S. C., Chmelka, B. F., Stucky, G. D., et al. (1999). Silicatein filaments and subunits from a marine sponge direct the polymerization of silica and silicones in vitro. *Proc. Natl. Acad. Sci.U.S.A.* 96, 361–365. doi: 10.1073/pnas.96.2.361

Diogo, G. S., Marques, C. F., Sotelo, C. G., Pérez-Marin, R. I., Pirraco, R. P., Reis, R. L., et al. (2020). Cell-laden biomimetially mineralized shark-skin-collagen-based 3d printed hydrogels for the engineering of hard tissues. *ACS Biomater. Sci. Eng.* 6, 3664–3672. doi: 10.1021/acsbiomaterials.0c00436

Diogo, G. S., Senra, E. L., Pirraco, R. P., Canadas, R. F., Fernandes, E. M., Serra, J., et al. (2018). Marine collagen/apatite composite scaffolds envisaging hard tissue applications. *Mar. Drugs.* 16:269. doi: 10.3390/md16080269

Dudik, O., Leonor, I., Xavier, J. R., Rapp, H. T., Pires, R. A., Silva, T. H., et al. (2018). Sponge-derived silica for tissue regeneration. *Mater. Today* 21, 577–578. doi: 10.1016/j.mattod.2018.03.025

Ehrlich, H., Demadis, K. D., Pokrovsky, O. S., and Koutsoukos, P. G. (2010a). Modern views on desilicification: biosilica and abiotic silica dissolution in natural and artificial environments. *Chem. Rev.* 110, 4656–4689. doi: 10.1021/cr900334y

Ehrlich, H., Deutzmann, R., Brunner, E., Cappellini, E., Koon, H., Solazzo, C., et al. (2010b). Mineralization of the metre-long biosilica structures of glass sponges is templated on hydroxylated collagen. *Nat Chem.* 2, 1084–1088. doi: 10.1038/nchem.899

Elango, J., Zhang, J., Bao, B., Palaniyandi, K., Wang, S., Wu, W., et al. (2016). Rheological, biocompatibility and osteogenesis assessment of fish collagen scaffold for bone tissue engineering. *Int. J. Biol. Macromol.* 91, 51–59. doi: 10.1016/j.ijbiomac.2016.05.067

Fernandes, J. S., Martins, M., Neves, N. M., Fernandes, M. H. V., Reis, R. L., and Pires, R. A. (2016). Intrinsic antibacterial borosilicate glasses for bone tissue engineering applications. *ACS Biomater. Sci. Eng.* 2, 1143–1150. doi: 10.1021/acsbiomaterials.6b00162

Fu, Q., Saiz, E., Rahaman, M. N., and Tomsia, A. P. (2011). Bioactive glass scaffolds for bone tissue engineering: state of the art and future perspectives. *Mater. Sci. Eng. C Mater. Biol. Appl.* 31, 1245–1256. doi: 10.1016/j.msec.2011.04.022

Gabbai-Armelin, P. R., Kido, H. W., Cruz, M. A., Prado, J. P. S., Ivanzi, I. R., Custódio, M. R., et al. (2019). Characterization and cytotoxicity evaluation of a marine sponge biosilica. *Mar. Biotechnol.* 21, 65–75. doi: 10.1007/s10126-018-9858-9

Götz, W., Tobiasch, E., Witzleben, S., and Schulze, M. (2019). Effects of silicon compounds on biomineralization, osteogenesis, and hard tissue formation. *Pharmaceutics* 11:117. doi: 10.3390/pharmaceutics11030117

Greasley, S. L., Page, S. J., Chen, S., Martin, R. A., Riveiro, A., Hanna, J. V., et al. (2016). Controlling particle size in the Stöber process and incorporation of calcium. *J. Colloid Interface Sci.* 469, 213–223. doi: 10.1016/j.jcis.2016.01.065

ISO 10993-5 (2009). *Biological Evaluation of Medical Devices – Part 5: Tests for in Vitro Cytotoxicity*. Available online at: http://nhiso.com/wp-content/uploads/2018/05/ISO-10993-5-2009.pdf

Jones, J. R., Sepulveda, P., and Hench, L. L. (2001). Dose-dependent behavior of bioactive glass dissolution. *J. Biomed. Mater. Res.* 58, 720–726. doi: 10.1002/jbm.10053

Kaur, G., Pandey, O. P., Singh, K., Homa, D., Scott, B., and Pickrell, G. (2014). A review of bioactive glasses: their structure, properties, fabrication and apatite formation. *J. Biomed. Mater. Res. A* 102, 254–274. doi: 10.1002/jbm.a.34690

Khan, A. S., Khalid, H., Sarfraz, Z., Khan, M., Iqbal, J., Muhammad, N., et al. (2017). Vibrational spectroscopy of selective dental restorative materials. *Appl. Spectrosc. Rev.* 52, 507–540. doi: 10.1080/05704928.2016.1244069

Kokubo, T., and Takadama, H. (2006). How useful is SBF in predicting in vivo bone bioactivity? *Biomaterials* 27, 2907–2915. doi: 10.1016/j.biomaterials.2006.01.017

Kulaev, I. S., Vagabov, V. M., and Kulakovskaya, T. V. (2005). *The Biochemistry of Inorganic Polyphosphates*, 2nd Edn. New York,NY: John Wiley & Sons.

Kulakovskaya, T. V., Vagabov, V. M., and Kulaev, I. S. (2012). Inorganic polyphosphate in industry, agriculture and medicine: modern state and outlook. *Process Biochem.* 74, 1–10. doi: 10.1016/j.procbio.2011.10.028

Le, T. D. H., Liaudanskaya, V., Bonani, W., Migliaresi, C., and Motta, A. (2018). Enhancing bioactive properties of silk fibroin with diatom particles for bone tissue engineering applications. *J. Tissue Eng. Regen. Med.* 12, 89–97. doi: 10.1002/term.2373

Lewandowska-Łańcucka, J., Fiejdasz, S., Rodzik, Ł., Koziel, M., and Nowakowska, M. (2015). Bioactive hydrogel-nanosilica hybrid materials: a potential injectable scaffold for bone tissue engineering. *Biomed. Mater.* 10:015020. doi: 10.1088/1748-6041/10/1/015020

Marris, E. (2006). Marine natural products: drugs from the deep. *Nature* 443, 904–905. doi: 10.1038/443904a

Müller, W. E. G., Schröder, H. C., Wiens, M., Peroviæ-Ottstadt, S., Batel, R., and Müller, I. M. (2004). Traditional and modern biomedical prospecting: part II-the benefits: approaches for a sustainable exploitation of biodiversity (secondary metabolites and biomaterials from sponges). *Evid. Based. Complement. Alternat. Med.* 1, 133–144. doi: 10.1093/ecam/neh030

Müller, W. E. G., Wang, X., Kropf, K., Boreiko, A., Schlossmacher, U., Brandt, D., et al. (2008). Silicatein expression in the hexactinellid *Crateromorpha meyeri*: the lead marker gene restricted to siliceous sponges. *Cell Tissue Res.* 333, 339–351. doi: 10.1007/s00441-008-0624-6

Odatsu, T., Azimaie, T., Velten, M. F., Vu, M., Lyles, M. B., Kim, H. K., et al. (2015). Human periosteum cell osteogenic differentiation enhanced by ionic silicon release from porous amorphous silica fibrous scaffolds. *J. Biomed. Mater. Res. Part A.* 103, 2797–2806. doi: 10.1002/jbm.a.35412

Rahaman, M. N., Day, D. E., Bal, B. S., Fu, Q., Jung, S. B., Bonewald, L. F., et al. (2011). Bioactive glass in tissue engineering. *Acta Biomater.* 7, 2355–2373. doi: 10.1016/j.actbio.2011.03.016

Rezwan, K., Chen, Q. Z., Blaker, J. J., and Boccaccini, A. R. (2006). Biodegradable and bioactive porous polymer/inorganic composite scaffolds for bone tissue engineering. *Biomaterials* 27, 3413–3431. doi: 10.1016/j.biomaterials.2006.01.039

Schröder, H. C., Boreiko, O., Krasko, A., Reiber, A., Schwertner, H., and Müller, W. E. G. (2005). Mineralization of SaOS-2 cells on enzymatically (silicatein) modified bioactive osteoblast-stimulating surfaces. *J. Biomed. Mater. Res. Part B Appl. Biomater.* 75, 387–392. doi: 10.1002/jbm.b.30322

Schröder, H. C., Wang, X., Tremel, W., Ushijima, H., and Müller, W. E. G. (2008). Biofabrication of biosilica-glass by living organisms. *Nat. Prod. Rep.* 25, 455–474. doi: 10.1039/b612515h

Silva, T. H., Alves, A., Ferreira, B. M., Oliveira, J. M., Reys, L. L., Ferreira, R. J. F., et al. (2012). Materials of marine origin: a review on polymers and ceramics of biomedical interest. *Int. Mater. Rev.* 57, 276–306. doi: 10.1179/1743280412Y.0000000002

Thakur, N. L., and Müller, W. E. G. (2004). Biotechnological potential of marine sponges. *Curr. Sci.* 86, 1506–1512.

Venkatesan, J., Anil, S., Chalisserry, E. P., and Kim, S. K. (2016). "Marine sponges as future biomedical models," in *Marine Sponges: Chemicobiological and Biomedical Applications*, eds P. Ramjee and E. Hermann (New Delhi: Springer India), 349–357. doi: 10.1007/978-81-322-2794-6_18

Wanandi, S. I., Yustisia, I., Neolaka, G. M. G., and Jusman, S. W. A. (2017). Impact of extracellular alkalinization on the survival of CD24-/CD44+human breast cancer stem cells associated with cellular metabolic shifts. *Braz. J. Med. Biol. Res.* 50, e6538. doi: 10.1590/1414-431X20176538

Wang, X., Schröder, H. C., Feng, Q., Draenert, F., and Müller, W. E. G. (2013). The deep-sea natural products, biogenic polyphosphate (bio-polyp) and biogenic silica (bio-silica), as biomimetic scaffolds for bone tissue engineering: fabrication of a morphogenetically-active polymer. *Mar. Drugs* 11, 718–746. doi: 10.3390/md11030718

Wang, X., Schröder, H. C., and Müller, W. E. G. (2018). Amorphous polyphosphate, a smart bioinspired nano-/bio-material for bone and cartilage regeneration: towards a new paradigm in tissue engineering. *J. Mater. Chem. B* 6, 2385–2412. doi: 10.1039/C8TB00241J

Wang, X., Schröder, H. C., Wiens, M., Ushijima, H., and Müller, W. E. G. (2012). Bio-silica and bio-polyphosphate: applications in biomedicine (bone

formation). *Curr. Opin. Biotechnol.* 23, 570–578. doi: 10.1016/j.copbio.2012.01.018

Wiens, M., Wang, X., Schloßmacher, U., Lieberwirth, I., Glasser, G., Ushijima, H., et al. (2010a). Osteogenic potential of biosilica on human osteoblast-like (SaOS-2) cells. *Calcif. Tissue Int.* 87, 513–524. doi: 10.1007/s00223-010-9408-6

Wiens, M., Wang, X., Schröder, H. C., Kolb, U., Schlossmacher, U., Ushijima, H., et al. (2010b). The role of biosilica in the osteoprotegerin/RANKL ratio in human osteoblast-like cells. *Biomaterials* 31, 7716–7725. doi: 10.1016/j.biomaterials.2010.07.002

Wysokowski, M., Jesionowski, T., and Ehrlich, H. (2018). Biosilica as a source for inspiration in biological materials science. *Am. Mineral.* 103, 665–691. doi: 10.2138/am-2018-6429

Xue, S.-H., Xie, H., Ping, H., Li, Q.-C., Su, B.-L., and Fu, Z.-Y. (2015). Induced transformation of amorphous silica to cristobalite on bacterial surfaces. *RSC Adv.* 5, 71844–71848. doi: 10.1039/c5ra13619a

Yu, B., Turdean-Ionescu, C. A., Martin, R. A., Newport, R. J., Hanna, J. V., Smith, M. E., et al. (2012). Effect of calcium source on structure and properties of sol-gel derived bioactive glasses. *Langmuir* 28, 17465–17476. doi: 10.1021/la303768b

Disclaimer: This document reflects only the authors' views and the Executive Agency for Small and Medium-sized Enterprises (EASME) is not responsible for any use that may be made of the information it contains.

Conflict of Interest: The authors declare that the research was conducted in the absence of any commercial or financial relationships that could be construed as a potential conflict of interest.

Copyright © 2021 Dudik, Amorim, Xavier, Rapp, Silva, Pires and Reis. This is an open-access article distributed under the terms of the Creative Commons Attribution License (CC BY). The use, distribution or reproduction in other forums is permitted, provided the original author(s) and the copyright owner(s) are credited and that the original publication in this journal is cited, in accordance with accepted academic practice. No use, distribution or reproduction is permitted which does not comply with these terms.

frontiers in Marine Science

ORIGINAL RESEARCH
published: 28 May 2021
doi: 10.3389/fmars.2021.600087

Diversity, Distribution and Phylogenetic Relationships of Deep-Sea Lithistids (Porifera, Heteroscleromorpha) of the Azores Archipelago

Joana R. Xavier[1,2], David J. Rees[2], Raquel Pereira[3], Ana Colaço[4,5], Christopher K. Pham[4,5] and Francisca C. Carvalho[2,6]*

[1] CIIMAR – Interdisciplinary Centre of Marine and Environmental Research, University of Porto, Matosinhos, Portugal, [2] Department of Biological Sciences, University of Bergen, Bergen, Norway, [3] Systematic Biology, Department of Organismal Biology, Evolutionary Biology Centre, Uppsala University, Uppsala, Sweden, [4] Okeanos – Instituto de Investigação em Ciências do Mar, Universidade dos Açores, Horta, Portugal, [5] IMAR – Instituto do Mar, Horta, Portugal, [6] Section of Taxonomy and Evolution, Department of Natural History, University Museum of Bergen, University of Bergen, Bergen, Norway

OPEN ACCESS

Edited by:
Jose Angel Alvarez Perez, Universidade do Vale do Itajaí, Brazil

Reviewed by:
Cristiana Castello-Branco, Smithsonian National Museum of Natural History (SI), United States
Tina Molodtsova, P. P. Shirshov Institute of Oceanology (RAS), Russia

***Correspondence:**
Joana R. Xavier
jxavier@ciimar.up.pt

Specialty section:
This article was submitted to Deep-Sea Environments and Ecology, a section of the journal Frontiers in Marine Science

Received: *28 August 2020*
Accepted: *12 April 2021*
Published: *28 May 2021*

Citation:
Xavier JR, Rees DJ, Pereira R, Colaço A, Pham CK and Carvalho FC (2021) Diversity, Distribution and Phylogenetic Relationships of Deep-Sea Lithistids (Porifera, Heteroscleromorpha) of the Azores Archipelago. Front. Mar. Sci. 8:600087. doi: 10.3389/fmars.2021.600087

Lithistid sponges are globally distributed in temperate and sub-tropical areas, constituting an important component of deep-sea benthic communities where they form structurally complex and vulnerable marine ecosystems (VMEs). In this study, we assess the diversity and investigate the spatial and bathymetric distribution of the lithistid sponges of the Azores archipelago (North Atlantic) based on historical records and examination of samples accidentally collected during deep-sea longline fishing operations in the region. Eleven lithistid species are recognized to occur in the Azores, including *Leiodermatium tuba*, recently described from material collected in several Northeast Atlantic seamounts that is hereby reported for the first time to the archipelago. We provide molecular barcodes (mtDNA COI and rRNA 28S) for seven of these species, including *Discodermia ramifera*, *Macandrewia azorica*, and *Exsuperantia archipelagus*, for which the Azores constitutes the type locality. We further discuss the phylogenetic and biogeographic affinities of the Azorean lithistids in the context of the Porifera classification, and the wider Northeast Atlantic upper bathyal fauna. Our study also warrants the addition of some lithistid species to the list of VME indicators for the Northeast Atlantic in support of the sustainable management and conservation of these species and habitats, as well as the ecological functions they deliver.

Keywords: bathyal, rock sponges, oceanic islands, seamounts, biodiversity, biogeography, vulnerable marine ecosystems, conservation

INTRODUCTION

Lithistids are a polyphyletic group of demosponges, distributed across three orders and 13 families, which share the presence of a hypersilicified skeleton formed by an intricately articulated spicule type called desmas (Pisera and Lévi, 2002). They are found distributed globally in temperate and sub-tropical areas largely in the upper bathyal zone, and seem to be particularly prevalent in oceanic

(island and seamount) environments (e.g., Schlacher-Hoenlinger et al., 2005; Carvalho et al., 2015, 2020; Schuster et al., 2018). Knowledge of the diversity, ecology and phylogenetic affinities of these sponges has greatly increased in recent years, with new species and habitats described for understudied areas (Carvalho et al., 2015, 2020; Maldonado et al., 2015; Schuster et al., 2018; Ríos et al., 2020), (phylo)diversity and distribution patterns assessed (Pomponi et al., 2001; Kelly et al., 2007; Schuster et al., 2021), and considerable changes proposed regarding their placement within the poriferan classification system proposed (Cárdenas et al., 2011; Morrow and Cárdenas, 2015; Schuster et al., 2015).

Recently, lithistid sponges were found forming structural habitats, aggregations and reef-like formations, in the upper bathyal in the western Mediterranean (Maldonado et al., 2015) and the northeast Atlantic (Ríos et al., 2020), possibly analogous to reef habitats which developed and thrived during the Mesozoic in shallower waters (Kauffman et al., 2000). While the ecological role of lithistid aggregations is yet to be investigated, sponge habitats dominated by other groups (e.g., such as geodiids and hexactinellids) were shown to serve as habitat for numerous invertebrate and fish species (e.g., Hawkes et al., 2019), also performing numerous functions in bentho-pelagic coupling and nutrient recycling (Cathalot et al., 2015; Maldonado et al., 2020; Rooks et al., 2020).

Sponge habitats meet several of the vulnerability criteria, viz. uniqueness or rarity, functional significance, fragility, low recovery potential, and structural complexity, defined for vulnerable marine ecosystems (VMEs) by the Food and Agriculture Organization within the scope of the International Guidelines for the Management of Deep-Sea Fisheries in the High Seas (FAO, 2009, ICES, 2020). Therefore, uncovering their distribution patterns is critical to inform the development of appropriate conservation measures to ensure long-term sustainability and minimize the impacts of the various anthropogenic activities operating over the deep seafloor.

In the Northeast Atlantic, the Azores archipelago constitutes the region for which the lithistid fauna has been most comprehensively investigated. Since the description of the first lithistid for the area (*Macandrewia azorica* Gray, 1859), nine species were reported to the archipelago largely thanks to the studies by the French sponge taxonomist Émile Topsent, resulting from the historical expeditions of Prince Albert I of Monaco between 1885 and 1915 onboard the vessels Princesse Alice I and II and Hirondelle I and II (Topsent, 1892, 1898, 1904, 1928; see also Porteiro, 2009). However, it was not until recent that new data and samples became available as a result of an increase of the exploration efforts toward the deeper environments of this archipelago. These, alongside recent studies describing the lithistids of the Macaronesian archipelagos of Madeira and Selvagens (Carvalho et al., 2015) and seamounts off the Iberian margin and South of the Azores (Carvalho et al., 2020), allow for the first time a comparison of the lithistid assemblages of the Lusitanian and Mediterranean marine provinces.

Thus, the main aims of this study were to: (i) investigate the patterns of spatial and bathymetric distribution of the lithistid sponges throughout the Azores archipelago from the integration of historical records and newly obtained data and samples; (ii) assess their diversity and phylogenetic relationships; and (iii) explore the biogeographic affinities of the species occurring on the Azores in the context of the wider Northeast Atlantic and Mediterranean bathyal fauna.

MATERIALS AND METHODS

Study Area

The Azores is an oceanic volcanic archipelago that lies above the Mid-Atlantic Ridge in the North Atlantic Ocean. The seafloor is mostly deep, but a large number of seamounts, a fraction of the Mid-Atlantic Ridge, and the slopes of the islands compose the shallowest parts (Perán et al., 2016). Underwater it is characterized by the presence of numerous seamounts, isolated or associated with the Mid-Atlantic ridge (Morato et al., 2008), that host a wide variety of open-ocean and deep-sea organisms. The region is considered a biodiversity hotspot for several groups of organisms, from cetaceans and other megafauna (Silva et al., 2014; Afonso et al., 2020) to benthic corals (Braga-Henriques et al., 2013; Sampaio et al., 2019). A convergence of oceanographic processes manifests in the Azores Archipelago, designated as a confluence zone between the west and the east North Atlantic. Different dominant oceanographic processes affect the west and the east groups not only by the water mass composition but also in their nutrient (climatological) profiles (Caldeira and Reis, 2017). Various water masses, e.g., the Eastern North Atlantic Central Water (ENACW), the Mediterranean Outflow Water (MOW), and the North Atlantic Deep Water (NADW) are found in the region at different depths (Bashmachnikov et al., 2015 and references therein). The Azores region is located in oligotrophic waters where primary production and carbon flux to the seafloor are lower than other Atlantic areas (Abell et al., 2013). Seafloor environmental conditions show high spatial and temporal (seasonal/inter-annual) variability (Amorim et al., 2017).

Literature and Database Review

An extensive review of the sponge taxonomic literature (e.g., Gray, 1859; Topsent, 1892, 1898, 1904, 1928; Lévi and Vacelet, 1958) as well as biodiversity data portals (e.g., OBIS, GBIF) was performed and all records of lithistid sponges contained within the Azores EEZ were compiled in an excel spreadsheet following Darwin Core (DwC) data standards (Wieczorek et al., 2012). Five specimens, collected outside the EEZ, on the Irving and Plato seamounts located southern of the archipelago were also included for completeness. For each record, information on expedition (vessel, year), location (station no., coordinates and depth), sampling gear (e.g., trawl, longline), and taxonomic identification (as reported and currently accepted) was assembled (see **Supplementary Material 1**). Collection data of the specimens examined here and occurrences, both historical and recent, are publicly available in the PANGAEA data repository[1], and in the

[1]https://doi.pangaea.de/10.1594/PANGAEA.921772

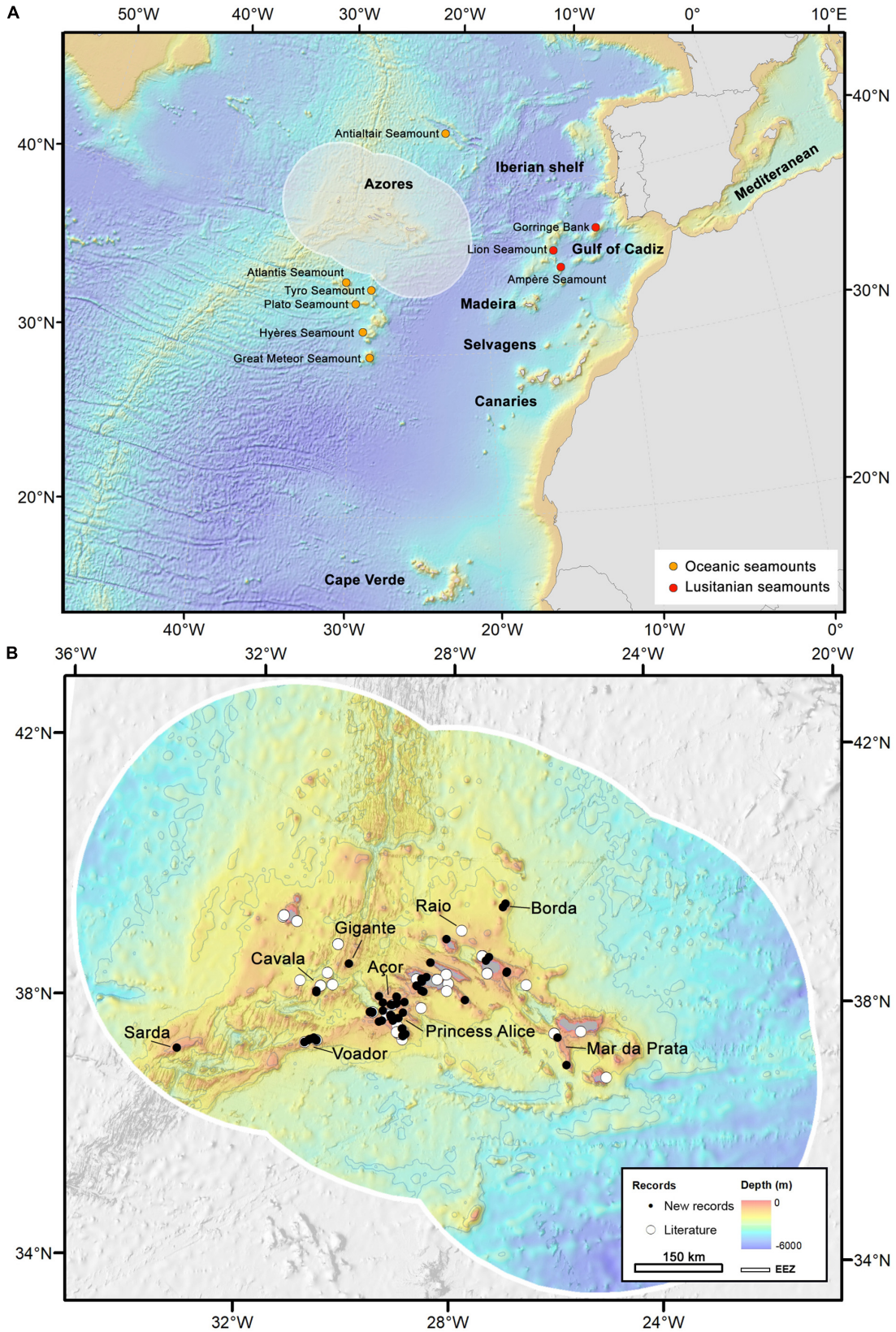

FIGURE 1 | Map of the study area. **(A)** Overall geographical setting, Northeast Atlantic and Mediterranean Sea, with archipelagos and main seamounts indicated. **(B)** The Azores EEZ with some geomorphological features indicated, and distribution of occurrence records: white circles represent records from the literature whereas black dots represent specimens analyzed in this study.

SponGIS data portal[2] developed in scope of the H2020 SponGES project[3].

Sampling and Identification

New material and information were collected during several scientific expeditions (2006–2008; 2010–2011; 2017), experimental fishing surveys and bycatch monitoring through fisheries observers in the course of various projects and programs, both past and ongoing in the region, such as SponGES, MERCES, Discardless, CoralFish (see also section "Acknowledgments"). Sampling was performed according to national Portuguese laws and approved by the Azorean Directorate of Sea Affairs of the Azores Autonomous region through the CCPI 03/2017/DRCT for the samples collected during the SponGES project.

Specimens were identified from analyses of external and/or internal morphological characteristics such as habitus, texture, consistency, surface ornamentation and oscula distribution, skeletal arrangement and spicular composition, following standard methods (Boury-Esnault and Rützler, 1997). Detailed morphological descriptions are not provided in this study as taxonomic studies of neighboring areas (Madeira and Selvagens archipelagos, Northeast Atlantic seamounts), including many of the species herein reported, were recently presented (Carvalho et al., 2015, 2020; Carvalho and Pisera, 2019).

DNA Extraction and Sequencing

Genomic DNA was extracted from small pieces of choanosomal tissue using a DNeasy Blood and Tissue kit (QIAGEN), following the instructions of the manufacturer. The Folmer region of the mitochondrial cytochrome *c* oxidase subunit I (COI), and the C1–D2 region of the nuclear ribosomal 28S gene were amplified and sequenced. The COI and 28S fragments were amplified using the primer pairs LCO1490 and HCO2198 (Folmer et al., 1994) or dgLCO1490 and dgHCO2198 (Meyer et al., 2005), and C1'ASTR and D2 (Lê et al., 1993; Cárdenas et al., 2010), respectively. The polymerase chain reaction conditions used follow the protocols as in Schuster et al. (2015). Obtained amplicons were purified with a solution of Exonuclease 1 (EXO, 10 U μL-1) and shrimp alkaline phosphatase (SAP, 10 U μL-1 USB®), and Sanger sequenced in both directions with Big Dye® Terminator v3.1, on a capillary-based Applied Biosystem 3730XL Analyzer. The molecular work was carried out at Biodiversity Laboratories (BDL, DNA Section) at the Department of Biological Sciences (University of Bergen). Generated sequences were deposited in GenBank under accession nos. MW006490– MW006541 for rRNA 28S (C1–D2) and MW000672– MW000696 for mtDNA COI (see **Supplementary Material 2**).

Phylogenetic Reconstructions

Obtained sequences were verified using the Basic Local Alignment Search Tool (BLAST) available at http://www.ncbi.nlm.nih.gov/BLAST/. Sequence quality checks, assembly and editing were performed in Geneious v.10.0.9[4] (Kearse et al., 2012) and aligned using Muscle (Edgar, 2004). Several sequences of the orders Tetractinellida Marshall, 1876 and Sphaerocladina Schrammen, 1924 were downloaded from GenBank and used in these alignments (see **Supplementary Material 2**, also deposited in PANGAEA[5]) according to the new classification of Demospongiae Sollas, 1885 (Morrow and Cárdenas, 2015). Sequences belonging to the order Sphaerocladina were used as outgroups. The final datasets comprise 192 sequences for mtDNA COI and 212 sequences for rRNA 28S, of which 25 and 48, respectively, are new. Phylogenetic reconstructions were performed for the individual markers under Bayesian Inference, as implemented in MrBayes v3.2 (Ronquist et al., 2012) and Maximum Likelihood as implemented in RaxML v.8 (Stamatakis, 2014) via the CIPRES Science Gateway V.3.3[6]. Reconstructions under Bayesian Inference were obtained under two runs and four Metropolis-coupled Markov chains (MCMC) over 100 million generations, sampled every hundredth generation and with a burnin of 0.25, and the best-fitting model for both genes (GTR + G + I) as estimated by jModelTest v.2.1.7 (Darriba et al., 2012) calculated under the Akaike Information Criterion (AIC). For the Maximum Likelihood analysis, the GTRGAMMAI model was used and 1000 rapid bootstrapping replicates performed. The obtained phylogenetic trees were visualized in FigTree v.1.4.4[7] and edited in Adobe® Illustrator® (2019).

Biogeographic Affinities

To examine the biogeographic affinities of the lithistid fauna in the context of the wider Northeast Atlantic and Mediterranean we built a presence/absence data matrix based on literature records and our own data for five oceanic archipelagos (Azores, Madeira, Selvagens, Canaries, and Cape Verde), two seamount groups (the oceanic seamounts located south of the Azores, and the Lusitanian seamounts off the Southwestern European shelf), as well as for the continental slopes of the Iberian margin, the Gulf of Cadiz and the Mediterranean Sea. This species × area matrix was then used to build a pairwise similarity matrix using the Bray-Curtis coefficient as implemented in PRIMER 7 (Clarke and Gorley, 2015).

RESULTS

A total of 47 individual records, representing 10 species, seven genera, distributed across seven families and two orders (Tetractinellida and Bubarida Morrow and Cárdenas, 2015), were compiled from the literature for the region. Detailed information on such records, including nomenclatural changes as verified in the World Porifera Database (Van Soest et al., 2021), can be found in **Supplementary Material 1**. In addition, 82 specimens collected as bycatch from bottom longline fishing operations were examined and assigned to seven species. Combined, the two datasets, elevate to 11 the total number of lithistid species reported from the Azores archipelago (see systematic

[2]www.spongis.org

[3]www.deepseasponges.org

[4]http://www.geneious.com

[5]https://doi.pangaea.de/10.1594/PANGAEA.929934

[6]http://www.phylo.org/index.php/

[7]http://tree.bio.ed.ac.uk/software/figtree/

list below, and following sections) (**Figures 1**, **2**). Of these, *Neophrissospongia nolitangere* (Schmidt, 1870) and *Macandrewia azorica* Gray, 1859 were the most commonly captured, with 22 and 20 individuals collected, followed by *Leiodermatium* spp. ($N = 25$, collectively) and *Exsuperantia archipelagus* Carvalho and Pisera (2019) ($N = 12$) (**Supplementary Material 1**). Specimens within the genus *Leiodermatium* Schmidt, 1870 could not be assigned with full confidence to the two species previously reported for the Azores archipelago, i.e., *Leiodermatium lynceus* Schmidt (1870) and *Leiodermatium pfeifferae* (Carter, 1873), either because we did not find consistency in the characters traditionally used to distinguish the two species, i.e., location of the inhalant and exhalant openings (ostia and oscula), the thickness of the plate and the hispidity of its margin; or, in some instances, because we only had access to small fragments which prevented such analyses. These were therefore retained as *L.* cf. *lynceus* and *L.* cf. *pfeifferae* when they seemed more similar to one of the species, and as *Leiodermatium* sp. *indet.*, following the open nomenclature standards proposed by Sigovini et al. (2016) and Horton et al. (2021), when they appeared somewhat intermediate or only small fragments were available.

Systematic List

Phylum PORIFERA Grant, 1836
Class DEMOSPONGIAE Sollas, 1885
Subclass HETEROSCLEROMORPHA Cárdenas et al., 2012
Order TETRACTINELLIDA Marshall, 1876
Suborder ASTROPHORINA Sollas, 1877
Family CORALLISTIDAE Sollas, 1888
Genus *Neophrissospongia* Pisera and Lévi, 2002
Species ***Neophrissospongia nolitangere*** (Schmidt, 1870)
Family THEONELLIDAE Lendenfeld, 1903
Genus *Discodermia* du Bocage, 1869
Species ***Discodermia ramifera*** Topsent, 1892*
Family MACANDREWIIDAE Schrammen, 1924
Genus *Macandrewia* Gray, 1859
Species ***Macandrewia azorica*** Gray, 1859*
Species *Macandrewia ramosa* Topsent, 1904*
Species *Macandrewia robusta* Topsent, 1904*
Family PHYMARAPHINIIDAE Schrammen, 1924
Genus Exsuperantia Özdikmen, 2009
Species ***Exsuperantia archipelagus*** Carvalho and Pisera, 2019*
Suborder SPIROPHORINA Bergquist and Hogg, 1969
Family AZORICIDAE Sollas, 1888
Genus *Leiodermatium* Schmidt, 1870
Species ***Leiodermatium* (cf.) *lynceus*** Schmidt, 1870
Species ***Leiodermatium* (cf.) *pfeifferae*** (Carter, 1873)
Species ***Leiodermatium tuba*** Carvalho and Xavier, 2020
Family SIPHONIDIIDAE Lendenfeld, 1903
Genus *Siphonidium* Schmidt, 1879
Species *Siphonidium ramosum* (Schmidt, 1870)
Order BUBARIDA Morrow and Cárdenas, 2015
Family DESMANTHIDAE Topsent, 1893
Genus *Petromica* Topsent, 1898
Subgenus *Petromica* (*Petromica*) Topsent, 1898
Species *Petromica* (*Petromica*) *grimaldii* Topsent, 1898*

Highlighted in bold font are species found in the present study; * denote species for which the type-locality is in the Azores archipelago.

Diversity and Distribution

Of the seven species identified from the material collected as bycatch from longline fisheries in the Azores, one (*Leiodermatium tuba*) constitutes a new record for the archipelago. Similarly, the specimens DOP 5850 and DOP 5853 collected at 461–501 m depth in the Plato seamount constitute the first record of *Neophrissospongia nolitangere* in this group of oceanic seamounts, thereby extending the known distribution of the species.

Overall, both historical and recent records are widely distributed across the archipelago, on island slopes and offshore seamounts, but are mostly concentrated in the central island group, south of the islands of Faial and Pico (**Figures 1**, **3**). Except for the five specimens collected from the Plato and Irving seamounts, all specimens were collected on the Azores plateau and within the EEZ. The genus *Macandrewia* (family Macandrewiidae) is the most widely distributed, with the species *Macandrewia azorica* being found on all islands' groups. In the Eastern island group, no records were found for *N. nolitangere*, *Discodermia ramifera*, *Siphonidium ramosum,* and *Petromica* (*Petromica*) *grimaldii*. On the other hand, in the Western island group only *P.* (*P.*) *grimaldii*, *M. azorica, M. ramosa,* and *Exsuperantia archipelagus* have been recorded. Several species of *Leiodermatium* spp., *M. azorica*, *E. archipelagus*, *D. ramifera,* and *S. ramosum* are also recorded in the topographic highs of the Mid-Atlantic Ridge between the Western and Central island groups (**Figure 3**).

With regards to bathymetric distribution, the majority of the records ($N = 82$) and species ($S = 9$) were found in the upper bathyal between 200–800 m depth, peaking at 300–400 m depth. Comparatively, the number of records and species for the circalittoral zone above 200 m or for the lower bathyal zone below 800 m depth were much lower, with 14 records ($S = 6$) for the former, and 13 records ($S = 5$) for the latter. The shallowest record is that of *D. ramifera* recorded at 98 m depth east of the Açor bank, and the deepest of *M. azorica* found at 1495 m depth in the deep slope east of Santa Maria Island. The species *N. nolitangere*, *D. ramifera*, *M. azorica,* and *L.* (cf.) *lynceus* were found to be restricted to depths above 800 m, whereas *E. archipelagus*, *L.* (cf.) *pfeifferae,* and *P. grimaldii* further extend to deeper areas (down to 1250 m, depending on the species). *Macandrewia ramosa* and *M. robusta* (family Macandrewiidae) are the only two lithistid species exclusively found in the deeper zones (>1100 m depth), whereas *L. tuba* and *S. ramosum* were only found in the upper bathyal, between 622–723 m and 349–793 m depth, respectively (**Figure 4** and **Supplementary Material 1**).

Phylogenetic Relationships

In total, we obtained 25 mtDNA COI and 48 partial rRNA 28S sequences representing four and seven species, respectively (**Supplementary Material 2**). Phylogenetic trees obtained separately for the mtDNA COI and the 28S rRNA regions

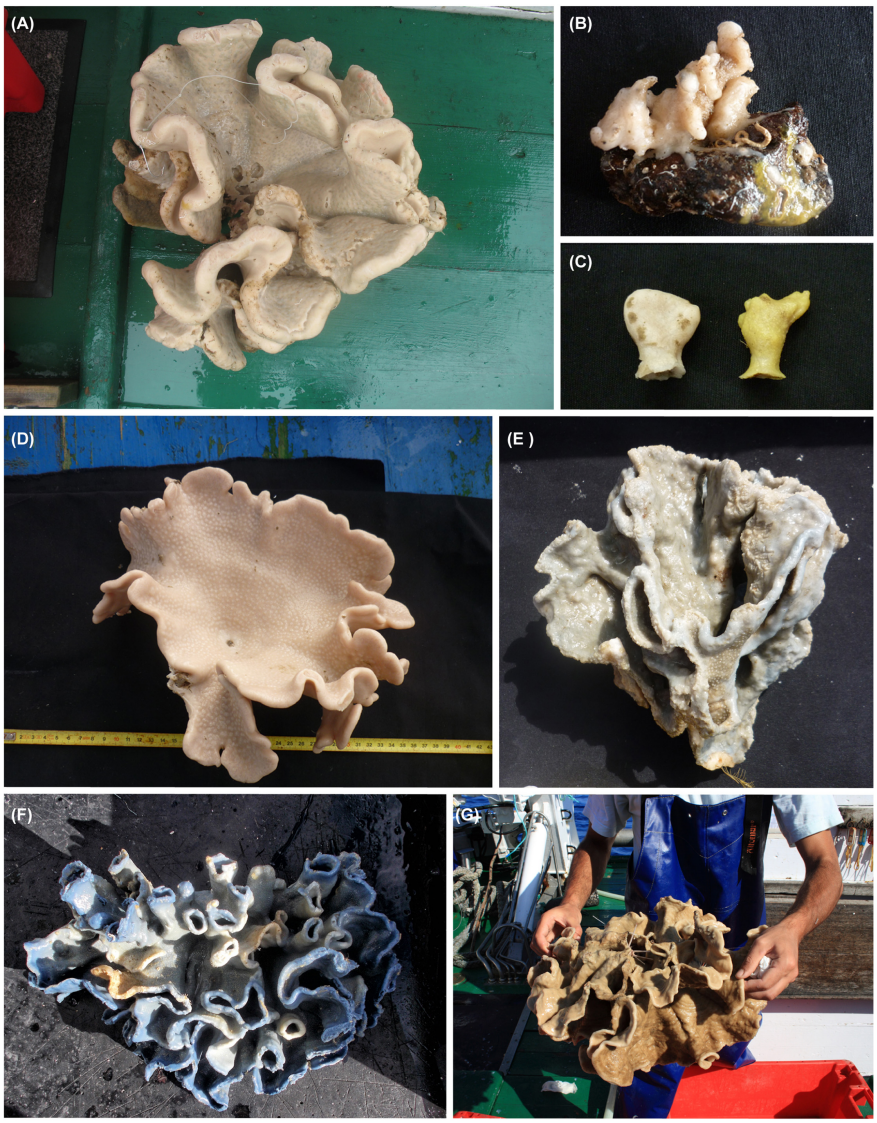

FIGURE 2 | Example of lithistid sponges of the Azores, collected and analyzed in the present study. **(A)** *Neophrissospongia nolitangere* (DOP 5323), **(B)** *Discodermia ramifera* (DOP 6477), **(C)** *Exsuperantia archipelagus* (DOP 6212), **(D)** *Macandrewia azorica* (DOP 6601), **(E)** *Leiodermatium* cf. *lynceus* (DOP 6429), **(F)** *Leiodermatium* cf. *pfeifferae* (DOP 11102), **(G)** *Leiodermatium tuba* (DOP 2975).

were largely congruent, both in overall topology as well as with high support at species and genus levels with a decrease in support toward deeper (family level) nodes (**Figures 5**, **6** and **Supplementary Material 3**).

Within the family Macandrewiidae, all specimens assigned to *Macandrewia azorica* formed a clade with maximum support with a single rRNA 28S sequence of *M. rigida* Lévi and Lévi (1989), from the Solomon Islands, available on GenBank (PP_{28S} = 1; BS_{28S} = 100) (**Figure 6**). In the COI tree, the clade comprising all of the Azorean specimens was retrieved with only moderate support (PP_{COI} = 0.77; BS_{COI} = 62), sister to a clade formed by two sequences of unidentified *Macandrewia* spp. from South Africa, within a highly supported *Macandrewia* sp. clade (PP_{COI} = 1; BS_{COI} = 79). Within the Azorean *Macandrewia* clade, two sequences (DOP 2866 and DOP 6249) formed a separate but only moderately supported sub-clade (PP_{COI} = 0.80, BS_{COI} = 64) (**Figure 5**).

Sequences obtained for *Discodermia ramifera* were retrieved in a highly supported clade (PP_{28S} = 1; BS_{28S} = 93; PP_{COI} = 1, BS_{COI} = 98) with the Mediterranean species *D. polymorpha* Pisera and Vacelet (2011) in an equally monophyletic *Discodermia* spp. clade (PP_{28S} = 1, BS_{28S} = 93; PP_{COI} = 1; BS_{COI} = 98), sister to *Theonella* spp. Similarly, all sequences of *Exsuperantia archipelagus* were grouped into a clade with maximum support (PP_{28S} = 1; BS_{28S} = 100; PP_{COI} = 1; BS_{COI} = 100) together with sequences (available in GenBank) previously obtained for this archipelago and the seamounts located south of the Azores. In the COI tree, some sub-structuring was observed

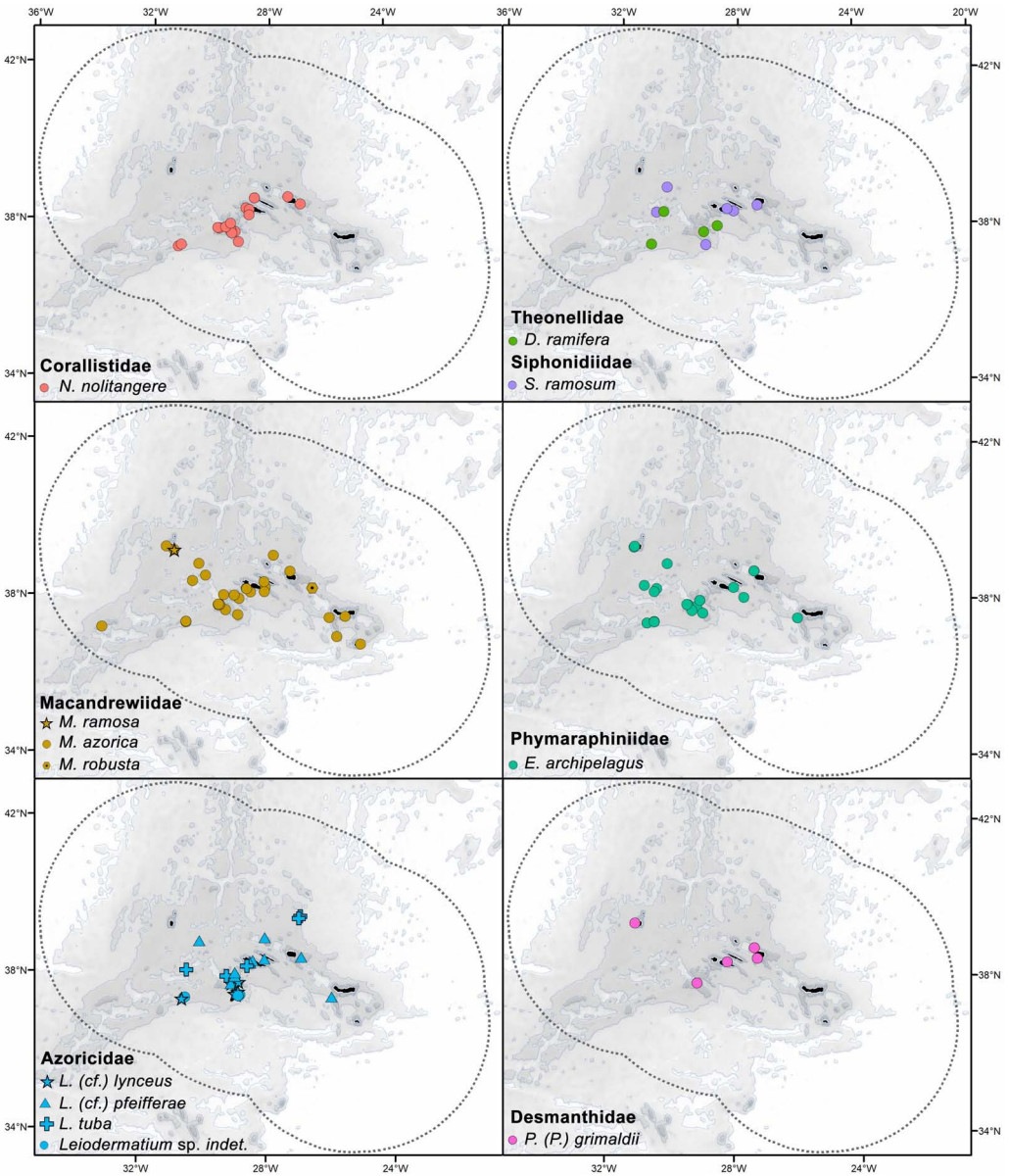

FIGURE 3 | Distribution of lithistid species within the Azores EEZ based on literature records and analyzed specimens.

with two sequences, presenting 1 bp difference to the remaining ones, forming a sub-clade strongly supported in the Bayesian analysis (PP_{COI} = 0.97) and moderately supported by maximum likelihood (BS_{COI} = 64) (**Figures 5**, **6**).

In the COI tree, all specimens of *Neophrissospongia nolitangere* collected in the Azores archipelago formed a highly supported clade (PP_{COI} = 0.98, BS_{COI} = 99) sister to *N. galapagoensis* Schuster, 2018 from the Galapagos islands (**Figure 5**). However, in the 28S tree and with the addition of two sequences of *Neophrissospongia* spp. from Western Australia, the Azorean clade is not supported (PP_{28S} = 0.53, BS_{28S} = 78) (**Figure 6**). This *Neophrissospongia* spp. clade is retrieved as sister to a larger clade comprising the genera *Herengeria* Lévi and Lévi (1988), *Corallistes* Schmidt (1870), *Neoschrammeniella* Pisera and Lévi (2002), and *Isabella* Schlacher-Hoenlinger et al. (2005) within family Corallistidae.

For the Spirophorina suborder we were only able to obtain 28S sequences and all attempts at amplifying the mtDNA COI marker failed. Within this suborder, our reconstructions show all our sequences of *Leiodermatium* spp. in a highly supported clade (PP_{28S} = 1; BS_{28S} = 97), within which two groups are found: one clade grouping specimens identified as *L.* cf. *pfeifferae*, *L.* cf. *lynceus* and *Leiodermatium* sp. (PP_{28S} = 0.98, BS_{28S} = 85) and one group with specimens identified as *L. tuba* (DOP 4862, DOP 11254, DOP 11445) only strongly supported in the maximum likelihood analysis (PP_{28S} = 0.55,

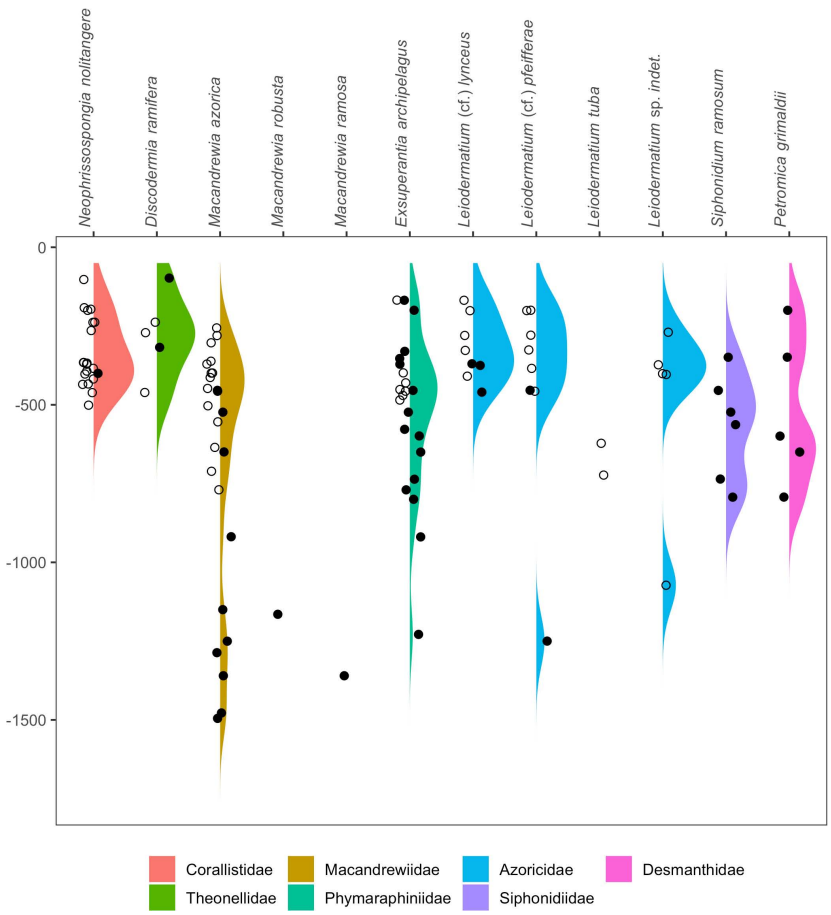

FIGURE 4 | Ridge plots of bathymetric distribution records for each individual species based on georeferenced literature records (closed circles) and analyzed specimens (open circles). Colors correspond to each individual family.

BS_{28S} = 84). *Leiodermatium* spp. is found as sister to *Aciculites* spp., but only with moderate to low support (PP_{28S} = 0.83, BS_{28S} = 59). A monophyletic clade comprising representatives of the genera *Leiodermatium* (family Azoricidae) and *Aciculites* Schmidt, 1879 + *Scleritoderma* Sollas, 1888 + *Microscleroderma* Kirkpatrick (1903) (family Scleritodermidae Sollas, 1888) is retrieved with maximum support in our Bayesian analysis (PP_{28S} = 1) but only moderately supported in the maximum likelihood analysis (BS_{28S} = 69) (**Figure 6**). Unfortunately, no specimens, and therefore no sequences were obtained for *Macandrewia robusta* and *M. ramosa* (family Macandrewiidae), *Siphonidium ramosum* (family Siphonidiidae) or *Petromica* (*Petromica*) *grimaldii* (family Desmanthidae), all known to occur in the archipelago.

Biogeographic Affinities

Examining the faunal similarities across the Northeast Atlantic and the Mediterranean Sea, we found the Azores lithistid assemblage to be most similar (51.9%) to the one occurring in the oceanic seamounts located to the south of the archipelago with seven species shared. This was followed by the Canaries and Madeira archipelagos, with 45.5 and 44.4% (five and four species shared), respectively. The lowest levels of similarity were found between the Azores and Iberian slope (no species shared) and the Cape Verde archipelago with which it only shares *Leiodermatium pfeifferae* (**Figure 7**, **Table 1**, and see also **Supplementary Material 4**). Of the 38 lithistid species occurring in the Northeast Atlantic and Mediterranean Sea, only one (*Macandrewia ramosa* Topsent, 1904) has been exclusively reported in the Azores (**Table 1**).

DISCUSSION

Diversity

From the integration of historical records and newly obtained data and samples we expanded considerably our knowledge of the diversity and spatial distribution of an important and vulnerable group of deep-sea sponges (lithistid demosponges) in the Azores archipelago. *Leiodermatium tuba*, recently described from material collected on various oceanic seamounts located South of the Azores as well as on the Gorringe Bank and the Canaries (Carvalho et al., 2020), is reported here for the

first time raising to 11 the number of lithistids in the Azores archipelago. When compared with other areas of the Atlanto-Mediterranean region this diversity is the third highest, only lower than that found in the oceanic seamounts (16 species) and the Mediterranean Sea (14 species) and similar to the richness found in the Canaries. Together, the Azores and the oceanic seamounts harbor 20 species, i.e., 54% of all lithistid species of this region, and may therefore be considered a lithistid diversity hotspot of the central North Atlantic. However, such diversity is still modest when compared with the tropical Western Atlantic, a region where latest estimates suggest the occurrence of at least 88 lithistid species (Schuster et al., 2021) and that is also recognized by its high Poriferan richness overall (Van Soest et al., 2012). Considering that the Azores harbor an additional 270+ (non-lithistid) deep-sea sponge species (Topsent, 1904, Xavier et al. unpublished data), as well as a rich cold-water coral fauna (Braga-Henriques et al., 2013; Sampaio et al., 2019) further emphasizes the value of this region as a reservoir of deep-sea biodiversity.

In the Azores, the spatial patterns of distribution, with a considerably higher number of records southwest of Faial and Pico islands (central island group) reflect collection efforts. This area has a complex topography and comprises several seamounts (e.g., Açor and Princesse Alice banks) which were

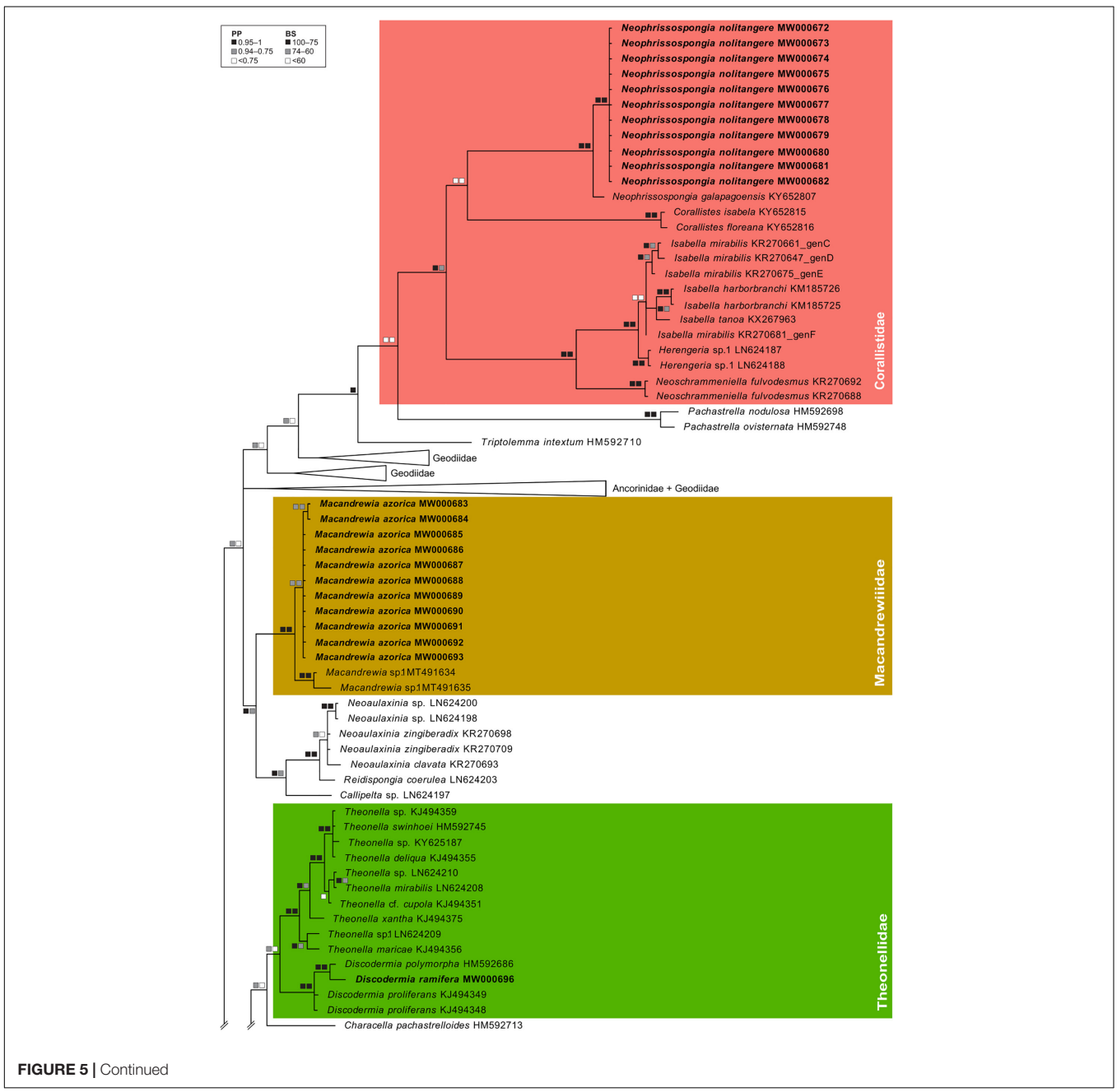

FIGURE 5 | Continued

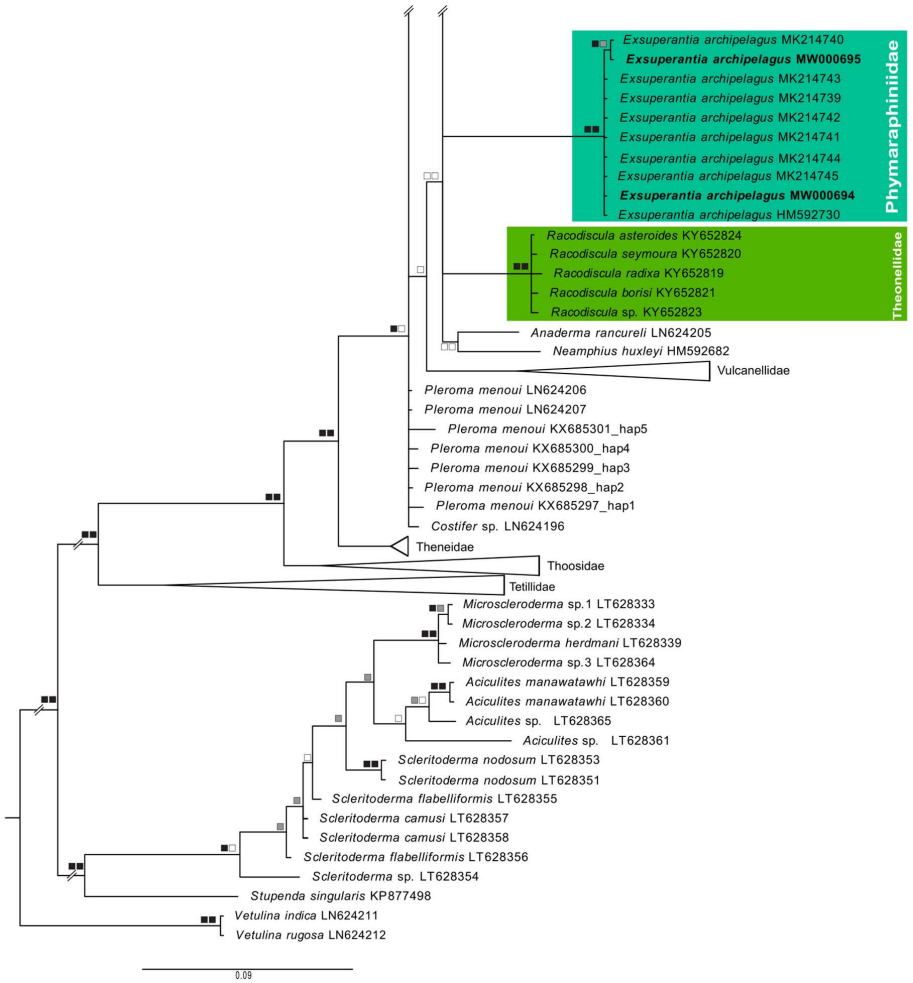

FIGURE 5 | Phylogenetic reconstruction of the mtDNA COI gene for lithistids recorded in the Azores archipelago. Bayesian posterior probabilities (PP, left square) and maximum likelihood bootstrap support (BS, right square) values are provided on the branches. If only one square is shown, it means the clade was not retrieved in the Maximum Likelihood analysis. Sequences generated in this study are in bold. Families encompassing lithistid species found in the present study are highlighted in color.

surveyed during historical expeditions and are traditionally used as fishing grounds of the small-scale longline fisheries fleet in the region.

Bathymetric Distribution

The Azorean lithistid fauna is composed of a mix of steno- and eurybathic species, mostly overlapping in upper bathyal depths between 200 and 600 m. In general, distribution ranges observed for the various species in the Azores are similar to those reported for other northeast Atlantic archipelagos and seamounts (e.g., Carvalho et al., 2015, 2020, see also **Table 1**). However, it is important to note the uneven number of records for some species (e.g., only two records for *Macandrewia ramosa* and *M. robusta* below 1100 m in the literature), as well as some uncertainty regarding the taxonomic identification of some specimens both examined in this and previous studies (e.g., *Leiodermatium* spp. and *M. azorica*), which may be confounding observed spatial and bathymetric ranges.

The highest species diversity and number of records found in the upper bathyal (200–800 m) suggests that oceanographic conditions may be optimal at this depth range for lithistids. The pattern here observed for lithistids agrees well with previous findings of highest diversity of cold-water corals between 300 and 900 m in the archipelago (Braga-Henriques et al., 2013). However, this pattern may also partly result from considerably higher collection efforts in this depth range targeted by the fisheries from which the specimens of both studies have been obtained.

While we lack high-resolution data to investigate which environmental factors drive the distribution of the various species or the assemblage as a whole, it is accepted that availability and diversity of geomorphological features with steep slopes and limited sedimentation (island slopes, near shore banks and offshore seamounts) play an important role in providing the hard substrate needed for lithistid settlement and growth (Pomponi et al., 2001; Kelly et al., 2007). Investigating the

role of other factors such as depth, temperature, salinity, and nutrients shown to be important predictors for the distribution of deep-sea sponge species and communities (e.g., Knudby et al., 2013; Howell et al., 2016; Alvarez et al., 2017; Murillo et al., 2018) will be critical to better understand the ecology of this important group.

Phylogenetic Relationships

Phylogenetic reconstructions based on two molecular markers traditionally used in the group, i.e., the mitochondrial COI and the ribosomal 28S, confirmed our morphology-based assignments, corroborated previous findings regarding the classification and phyletic status of some groups (e.g.,

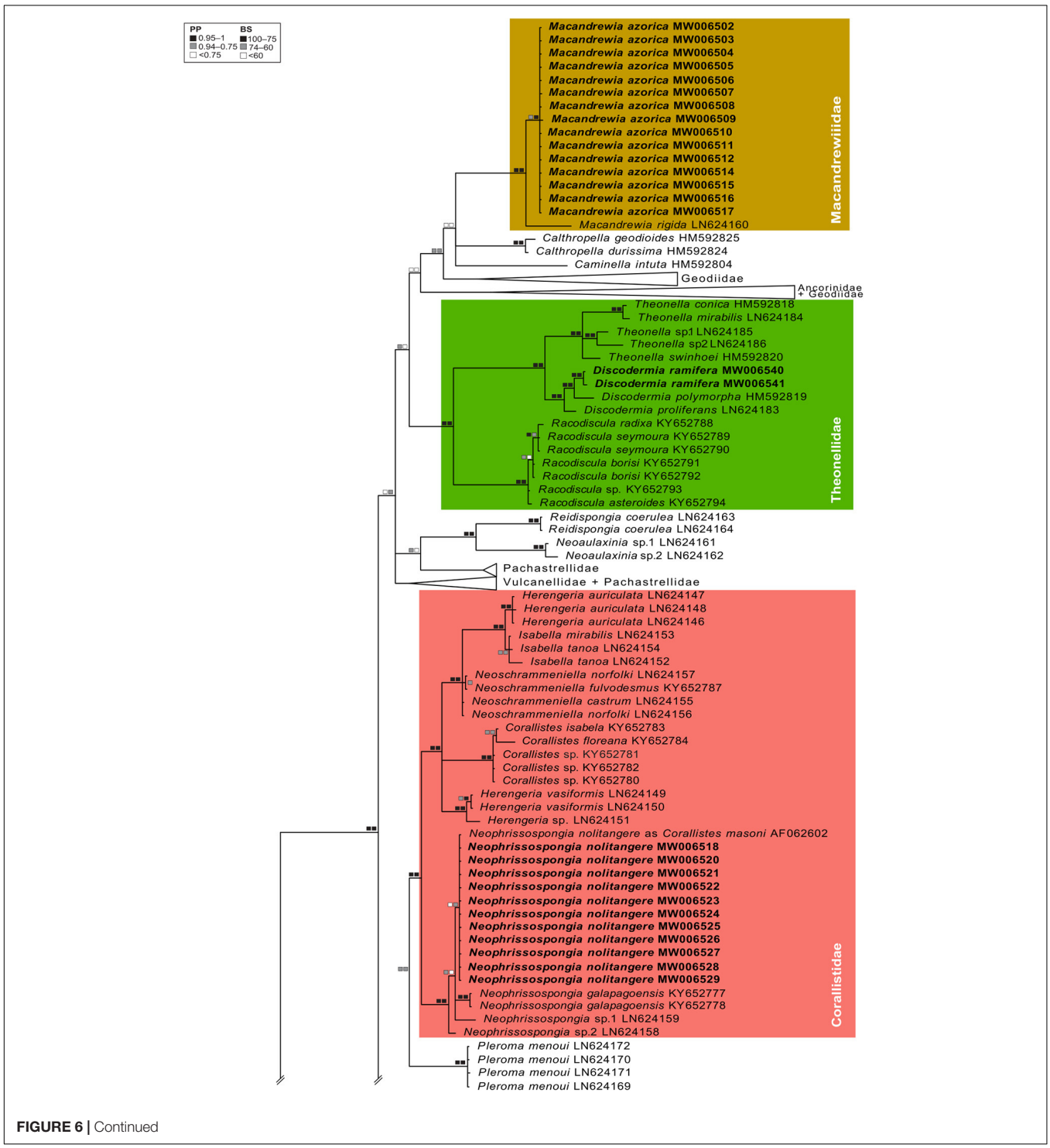

FIGURE 6 | Continued

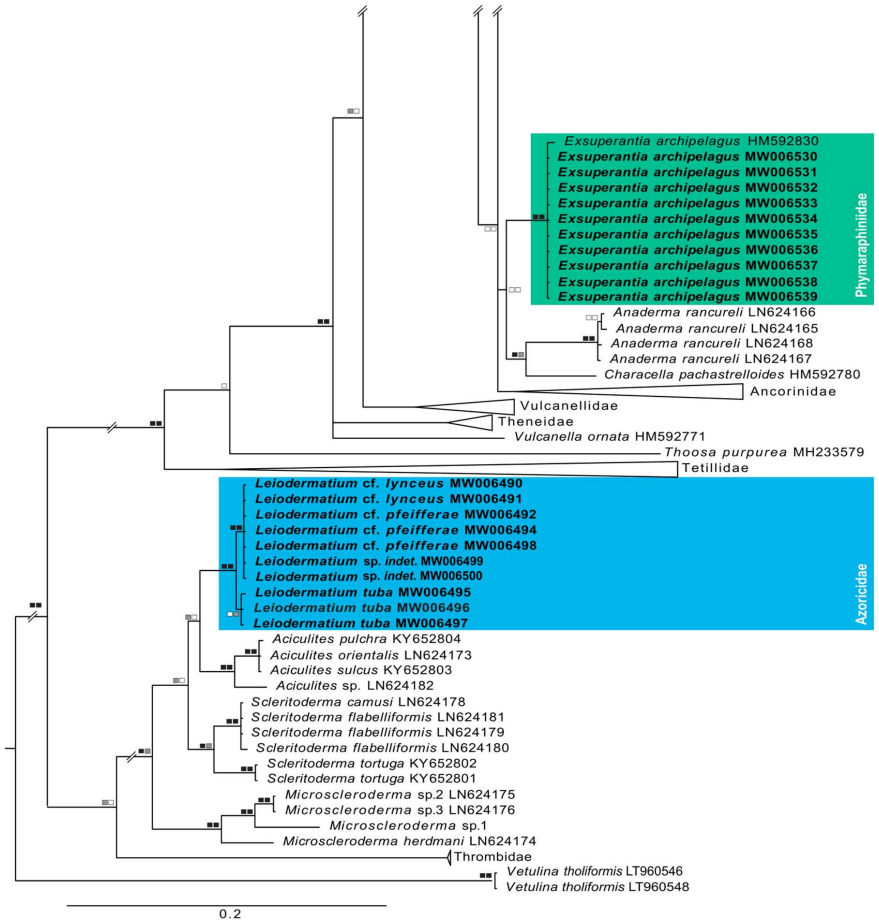

FIGURE 6 | Phylogenetic reconstruction of the 28S rRNA C1–D2 region for lithistids recorded in the Azores archipelago. Bayesian posterior probabilities (PP, left square) and maximum likelihood bootstrap support (BS, right square) values are given on the branches. If only one square is shown, it means the clade was not retrieved in the Maximum Likelihood analysis. Sequences generated in this study are in bold. Families encompassing lithistid species found in the present study are highlighted in color.

Carvalho and Pisera, 2019; Schuster et al., 2021) and further shed light into some long-standing species-level taxonomic problems. In the majority of cases, specimens assigned to a given species formed species-level monophyletic clades or clustered with GenBank sequences of other congeneric species. This was the case for *Neophrissospongia nolitangere*, *Macandrewia azorica*, *Discodermia ramifera*, and *Exsuperantia archipelagus*.

In *N. nolitangere*, all specimens had identical (COI) or near-identical (28S) sequences and formed a robust clade with the Pacific *N. galapagoensis*. In the future it is important to compare the Azores specimens with the two new, as yet undescribed, species found in the Caribbean (Schuster et al., 2021) as these may prove much more closely related. Similarly, all our *M. azorica* specimens form a clade consistent with a species level relationship, although the phylogenetic support was only moderate in the COI tree. The 1 bp difference found in COI for two specimens (DOP 2866 and DOP 6249) is likely to reflect some intraspecific genetic variability associated with the depth at which the specimens were found (635 and 711 m), considerably deeper than most other specimens. The 1 bp difference found in COI for one specimen of *E. archipelagus* confirms the variability previously reported for this species by Carvalho and Pisera (2019). In this case, no distinctive patterns were found in relation to spatial or bathymetric distribution. Such small levels of intraspecific genetic variability, while not commonly reported, have been previously found in other tetractinellid sponges, such as *Geodia barretti* Bowerbank, 1858 (Cárdenas et al., 2013). Comparatively higher levels of variation in COI were also found in the genus *Isabella* from the Norfolk Ridge (off New Caledonia), warranting the description of a new species (*Isabella tanoa* Ekins et al., 2016) and the recognition of a morphologically cryptic species complex for *Isabella mirabilis* Schlacher-Hoenlinger et al. (2005; Ekins et al., 2016).

A close relationship of *Discodermia ramifera* with the Mediterranean *D. polymorpha* was strongly supported, in comparison to another congener from the southwest Pacific (*D. proliferans* Lévi and Lévi, 1983). Unfortunately, no sequences were available of other *Discodermia* spp. from the Northeast Atlantic [*D. arbor* Carvalho and Xavier, 2020, *D. kellyae* Carvalho and Xavier 2020, *D. polydiscus* (Bowerbank, 1869)

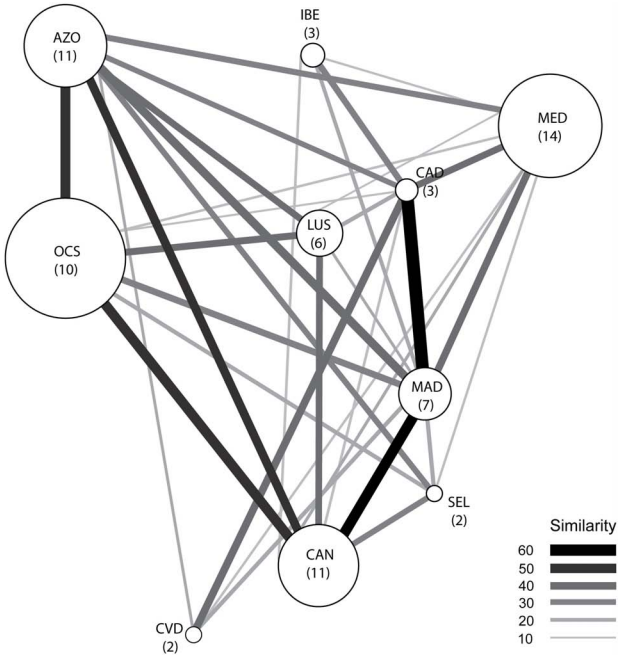

FIGURE 7 | Network of the lithistid faunal similarities across the Northeast Atlantic and Mediterranean Sea. Size of the nodes (areas) is proportional to the number of species in that area (indicated between brackets), whereas thickness and color of the lines between nodes represents Bray–Curtis similarity (%). Areas codes: AZO, Azores; MAD, Madeira; SEL, Selvagens; CAN, Canaries; CVD, Cape Verde; OCS, oceanic seamounts; LUS, Lusitanian seamounts; IBE, Iberian Atlantic margin; CAD, Gulf of Cadiz; MED, Mediterranean Sea.

and *D. verrucosa* Topsent, 1928] which would allow to better understand their phylogenetic and biogeographic relationships.

An important finding of our study was the fact that neither through morphological examination nor molecular data we were able to confidently assign our *Leiodermatium* specimens to the two species – *Leiodermatium lynceus* and *Leiodermatium pfeifferae* (see section "Results") – long reported to occur in the region (Topsent, 1892, 1904; Lévi and Vacelet, 1958) and throughout the Northeast Atlantic and Mediterranean Sea. In fact, all specimens which morphologically seemed most similar to *L. pfeifferae* or *L. lynceus*, and those which we could not assign to either species (*Leiodermatium* sp. *indet.*), grouped in a strongly supported clade in our 28S tree. Similar to previous studies, we failed to obtain COI sequences for any of our *Leiodermatium* specimens, further corroborating the hypothesis that a type I intron, similar to those found in other genera of the family Scleritodermidae (Schuster et al., 2017) may also be present in this genus as also suggested by Schuster et al. (2021).

Our results suggest that the Azorean *Leiodermatium* sp. *indet.* specimens, and possibly other records previously assigned in the literature to *L. pfeifferae* and *L. lynceus*, may represent either (i) a single species of *Leiodermatium* with some morphological variability; (ii) a complex of species where reduced genetic differentiation and morphological plasticity hamper unequivocal species-level discrimination, or (iii) a case of hybridization or incomplete lineage sorting between closely related species. If the former hypothesis is confirmed, *L. pfeifferae* would become a junior synonym of *L. lynceus*, type-species of the genus, following the priority principle (Article 23) of the International Code of Zoological Nomenclature (ICZN, 1999). However, a detailed taxonomic revision including examination of additional specimens collected from both species' type-localities (Portugal mainland slope for *L. lynceus* and Madeira island for *L. pfeifferae*), and other Northeast Atlantic localities, as well as an improved molecular dataset including other mitochondrial and nuclear markers, would be needed to support this or other nomenclatural act(s). A future comparison, both morphological and molecular, with the eight *Leiodermatium* species recently proposed by Schuster et al. (2021) for the tropical western Atlantic would further allow a complete review of the systematics and biogeography of this genus in the Atlantic.

Biogeographic Affinities

The Azores lithistid fauna is largely composed of species with a broader northeast Atlantic or Atlanto-Mediterranean distribution, and very low endemism (one single species). This is in accordance with previous findings both for sponges (Xavier and Van Soest, 2012) and other taxonomic groups in shallow waters (Freitas et al., 2019), as well as for cold-water corals in which a putative endemism of 14–15% was observed in the region (Braga-Henriques et al., 2013; Sampaio et al., 2019). Comparably low endemism levels have also been reported for the New Zealand lithistid assemblages at similar spatial scales (Kelly et al., 2007).

The highest similarity found between the Azores and the oceanic seamounts lithistid assemblages was expected given the geographical proximity and similar environmental conditions (temperature, salinity, oxygen and major nutrients) observed at the seafloor (Amorim et al., 2017). The occurrence of *Leiodermatium tuba* in the Azores and of *Neophrissospongia nolitangere* on these oceanic seamounts, herein reported for the first time, further suggests that as surveys and taxonomic efforts increase, more species will be found to be shared between these two regions, and possibly other, as previously posited by Carvalho et al. (2020).

The upper bathyal (200–1000 m depth) of the area comprising the Azores archipelago and the oceanic seamounts, where the vast majority of the lithistid records are found, is dominated by the North Atlantic Central Water, which presents a salinity of 35.2 – 36.7 PSU, temperatures between 8.5°–19°C and high median concentration of oxygen (94%) (Palma et al., 2012; Bashmachnikov et al., 2015). Below this depth there is only a limited influence of Subarctic Intermediate Water and Mediterranean Outflow Water below this depth (Bashmachnikov et al., 2015).

The major North Atlantic water masses and current pathways have been shown to structure the diversity and distribution of deep-sea sponges and corals, as well as the habitats they form (Puerta et al., 2020; Roberts et al., 2021). The large-scale circulation of the temperate northeast Atlantic is dominated

TABLE 1 | Spatial and bathymetric distribution of lithistid sponges (Porifera, Demospongiae, Heteroscleromorpha) across the Northeast Atlantic and Mediterranean Sea.

Family/Species	Oceanic archipelagos					Seamounts		Continental slope		
	AZO	MAD	SEL	CAN	CVD	OCS	LUS	IBE	CAD	MED
CORALLISTIDAE Sollas, 1888										
Corallistes elegantior Schmidt, 1870								data n.a.		
Corallistes masoni (Bowerbank, 1869)		480–610		415–417						
Corallistes microtuberculatus Schmidt, 1870					data n.a.					
Isabella harborbranchi Carvalho et al., 2015				133–366						
Neophrissospongia endoumensis Pisera and Vacelet, 2011										5[c]
Neophrissospongia nana Manconi and Serusi, 2008										6[c]
Neophrissospongia nolitangere (Schmidt, 1870)	102–501	317	358	10–20[c]; 295–450		461–501				313-352 20–22[c]
Neophrissospongia radjae Pisera and Vacelet, 2011										data n.a.[c]
Neoschrammeniella bowerbankii (Johnson, 1863)		113–669						486–672[aff.]	530–912	12–30[c]; 400–640
Neoschrammeniella inaequalis Carvalho and Xavier, 2020							460–675			
Neoschrammeniella piserai Carvalho and Xavier, 2020						695				
Neoschrammeniella pomponiae Carvalho and Xavier, 2020						480				
Neoschrammeniella sp.						580–610				
THEONELLIDAE Lendenfeld, 1903										
Discodermia arbor Carvalho and Xavier, 2020						330				
Discodermia kellyae Carvalho and Xavier, 2020						580				
Discodermia polydiscus (Bowerbank, 1869)				10–20[c]				data n.a.		
Discodermia polymorpha Pisera and Vacelet, 2011										3–30[c]; 60–360
Discodermia ramifera Topsent, 1892	98–318					300–461 338–520[cf.]				
Discodermia verrucosa Topsent, 1928		476–497		303–400		338–520				
Discodermia sp.						304				
Theonella annulata				146						
MACANDREWIIDAE Schrammen, 1924										

(Continued)

TABLE 1 | Continued

Family/Species	Oceanic archipelagos					Seamounts		Continental slope		
	AZO	MAD	SEL	CAN	CVD	OCS	LUS	IBE	CAD	MED
Macandrewia azorica Gray, 1859	256–1495		361	480[cf.] 1340–1530		420–1000[cf.]				
Macandrewia minima Carvalho and Xavier, 2020						615				
Macandrewia ramosa Topsent, 1904	1360									
Macandrewia robusta Topsent, 1904	1165					705				
Macandrewia schusterae Carvalho and Xavier, 2020						520–805	605–675			
Macandrewia sp.						225–280	900			
PHYMARAPHINIIDAE Schrammen, 1924										
Exsuperantia archipelagus Carvalho and Pisera, 2019	168–1229	563		408–1530		280–1000				
Exsuperantia levii Carvalho and Xavier, 2020						480				
AZORICIDAE Sollas, 1888										
Leiodermatium lynceus Schmidt, 1870	370–460 201–594 [cf.]	402–741		281–1530		480	305–320		948	207–700 430–469[cf.]
Leiodermatium pfeifferae (Carter, 1873)	454–1250 200–457[cf.]	data n.a.			183–234				704–734	615–890
Leiodermatium tuba Carvalho and Xavier, 2020	622–723			660		330–710	805–1035			
Leiodermatium sp. *indet*.	270–1073									
SCLERITODERMIDAE Sollas, 1888										
Aciculites mediterranea Manconi et al., 2006										8[c]
Microscleroderma lamina Pérez et al., 2004										2[c]
Microscleroderma spirophora Lévi, 1960					18–107					
SIPHONIDIIDAE Lendenfeld, 1903										
Gastrophanella phoeniciensis Pérez et al., 2004										2[c]
Siphonidium elongatus Carvalho and Xavier, 2020				470		480–545	460–675			
Siphonidium ramosum (Schmidt, 1870)	349–793[?]									20–1000[?]
DESMANTHIDAE Topsent, 1893										
Desmanthus incrustans (Topsent, 1889)										2-40
Petromica (Petromica) grimaldii Topsent, 1898	200–914						255–265			

(Continued)

TABLE 1 | Continued

Family/Species	Oceanic archipelagos					Seamounts		Continental slope		
	AZO	MAD	SEL	CAN	CVD	OCS	LUS	IBE	CAD	MED
Sulcastrella tenens (Vacelet, 1969)										210–240
Total no. of species in each region (no. of species shared with the Azores)	11	7 (4)	2 (2)	11 (5)	3 (1)	16 (7)	6 (3)	3 (0)	3 (2)	14 (4)
No. of potential endemic species (% in relation to all northeast Atlantic and Mediterranean species)	1 (2.6)	0 (0)	0 (0)	2 (5.3)	3 (7.9)	6 (15.7)	0 (0)	1 (2.6)	0 (0)	9 (23.7)

Bathymetric ranges presented in meters. Oceanic archipelagos: AZO, Azores; MAD, Madeira; SEL, Selvagens; CAN, Canaries (including the Saharan upwelling ecoregion); CVD, Cape Verde (including the Sahelian upwelling ecoregion); Seamounts: OCS, oceanic seamounts, include the Antialtair, Atlantis, Tyro, Plato, Hyères, and the Great Meteor seamounts; LUS, Lusitanian seamounts, include Lion, Gorringe, and Àmpere seamounts. Continental slope: IBE, Iberian Atlantic margin; CAD, Gulf of Cadiz; MED, Mediterranean Sea. Data n.a., depth data not available.

[c] Indicates species occurring in submerged caves, [cf.] and [aff.] correspond to records with some degree of species-level uncertainty, and [?] correspond to records of doubtful validity for the area (see discussion).

Sources of records: this study, Carvalho et al. (2015, 2020) (and references therein), Maldonado et al. (2015); Carvalho and Pisera (2019), Sitjà et al. (2019); Ríos et al. (2020), and Pisera and Gerovasileiou (2021).

by the Azores Current (AzC) that flows eastwards toward the Iberian margin (Carracedo et al., 2014). Importantly, the AzC southward and eastward branches have been identified as an important transport pathway between the Azores archipelago and the oceanic seamounts of the Great Meteor complex and the Lusitanian seamounts, respectively (Lima et al., 2020). The AzC therefore provides the physical connectivity needed for the dispersal of sponge larvae between these regions. However, the considerably largest distances between the Azores, the Lusitanian seamounts and Iberian shelf, over abyssal areas is likely to limit successful dispersal of the generally short-lived and lecitotrophic larvae typical of sponges, resulting in a much lower similarity between these regional assemblages.

Our results suggest that the complex and dynamic oceanographic circulation patterns of the northeast Atlantic, as well as a rich topography with numerous seamounts provide the conditions for these typically bathyal species to disperse and maintain regional-scale distributions and low endemism. This has in fact been observed in other tetractinellid groups (Cárdenas et al., 2013; Cárdenas and Rapp, 2015) and cladorhizids (Hestetun et al., 2015, 2017) with similar depth distributions.

Conservation

In our study, the vast majority (87%) of the lithistid records obtained as a result of bycatch of longline fisheries corresponded to large and potentially habitat-building species (*Neophrissospongia nolitangere*, *Macandrewia azorica*, and *Leiodermatium* spp.). This finding suggests that sponge species attaining large sizes, with a more complex morphology and with a dense hypersilicified skeleton may be more vulnerable to this activity than smaller species (*Discodermia ramifera*), or those with looser or softer skeletal structure [*Petromica* (*Petromica*) *grimaldii*]. These results concur with previous studies which showed that although bottom longline fishing has a reduced impact on deep-sea corals (another VME-indicator taxon) when compared to bottom trawling, the removal rates were significantly higher in corals with more complex morphology (Sampaio et al., 2012; Pham et al., 2014).

Notably, deep-sea sponges are presumed to exhibit slow growth rates and high longevity (Leys and Lauzon, 1998; Fallon et al., 2010; Kahn et al., 2016), which renders them particularly vulnerable to both environmental and anthropogenic disturbances. An age between 135 and 160 years was established for a specimen of *Corallistes undulatus* Lévi and Lévi (1983) (family Corallistidae), roughly 30 cm in diameter, collected on the Norfolk Ridge (Ellwood et al., 2007). Accidental longline capture of specimens of similar and larger sizes, thus possibly centennial in age, in the Azores is not uncommon. So, while the impact of bottom longline fisheries may be negligible in terms of the number of individuals removed from the seafloor, over time its selectivity for larger/older individuals may cause shifts in community composition and population structure and consequently alter or compromise the function(s) of the ecosystem at local scales.

Taking such considerations into account, our results further support the recent addition of lithistid tetractinellids, particularly those in the genera *Leiodermatium*, *Neophrissospongia*, *Neoschrammeniella,* and *Macandrewia* to the list of VME indicators for the Northeast Atlantic (ICES, 2020), and their proposed inclusion in Annex III of the EU deep-sea access regulations (EU Reg. 2016/2336) toward preventing significant adverse impacts on these VMEs (EU, 2016).

Whether these lithistid species form dense habitats as those found dominated by *Leiodermatium pfeifferae* on seamounts in the Western Mediterranean (Maldonado et al., 2015), and suspected for *M. azorica* on the Hyères seamount (Carvalho et al., 2020) requires verification using *in situ* observation systems such as remotely operated or autonomous underwater vehicles (ROVs/AUVs), and cameras.

Larger scale investigations, currently underway, of the patterns of diversity and distribution of lithistids across the entire North Atlantic, as well as their underpinning ecological and evolutionary drivers will allow to coordinate efforts toward conservation of these species, habitats and the ecological functions they deliver.

DATA AVAILABILITY STATEMENT

The datasets generated and analyzed in this study can be found in the PANGAEA data repository (https://doi.pangaea.de/10.1594/PANGAEA.921772 and https://doi.pangaea.de/10.1594/PANGAEA.929934), and in the SponGIS data portal (www.spongis.org). Sequences are deposited in GenBank under accession nos. MW006490–MW006541 for rRNA 28S (C1–D2) and MW000672–MW000696 for mtDNA COI gene fragments.

AUTHOR CONTRIBUTIONS

JX and FC designed the study. JX, RP, and FC identified the samples. DR and FC generated the sequence data. JX, RP, CP, and FC analyzed the data. AC and CP contributed the samples and data. JX wrote the draft of the manuscript. JX, RP, CP, and FC prepared the figures and tables. All the authors contributed the text and reviewed the manuscript.

FUNDING

This research has been performed in the scope of the SponGES project, which received funding from the European Union's Horizon 2020 Research and Innovation Programme under grant agreement No. 679849. This document reflects only the authors' views and the Executive Agency for Small and Medium-sized Enterprises (EASME) is not responsible for any use that may be made of the information it contains. JX research is further supported by national funds through FCT Foundation for Science and Technology within the scope of UIDB/04423/2020, UIDP/04423/2020, and CEECIND/00577/2018. RP research is supported by the Swedish Taxonomic Species Initiative (Svenska artprojektet) dha 159/09 1.4 grant. AC is supported by Foundation for Science and Technology (FCT) investigator contract IF/00029/2014/CP1230/CT0002. AC and CP are supported through the strategic project UIDB/05634/2020 and UIDP/05634/2020, and through the project FunAzores-ACORES 01-0145-FEDER-000123.

ACKNOWLEDGMENTS

We thank all fishers, fisheries observers, students, and technicians involved in the collection and curation of the specimens, and particularly to Cristina Gutiérrez-Zárate and Íris Sampaio for their support with the specimens and data from the COLETA. Filipe Mora Porteiro (IMAR/Okeanos, University of the Azores) is also acknowledged for his support in the early stages of this study. We further thank our colleague Astrid Schuster (CIIMAR and University of Southern Denmark) for support with the translation from German of some original descriptions. We acknowledge the two reviewers for their thoughtful suggestions that improved the manuscript. This study is dedicated to our dear colleague and friend Hans Tore Rapp, sponge scientist and deep-sea explorer, whom we deeply miss.

SUPPLEMENTARY MATERIAL

The Supplementary Material for this article can be found online at: https://www.frontiersin.org/articles/10.3389/fmars.2021.600087/full#supplementary-material

REFERENCES

Abell, R. E., Brand, T., Dale, A. C., Tilstone, G. H., and Beveridge, C. (2013). Variability of particulate flux over the Mid-Atlantic ridge. *Deep Sea Res. Part II Top. Stud. Oceanogr.* 98, 257–268. doi: 10.1016/j.dsr2.2013.10.005

Afonso, P., Fontes, J., Giacomello, E., Magalhães, M. C., Martins, H. R., Morato, T., et al. (2020). The Azores: a mid-Atlantic hotspot for marine megafauna research and conservation. *Front. Mari. Sci.* 6:826. doi: 10.3389/fmars.2019.00826

Alvarez, B., Frings, P. J., Clymans, W., Fontorbe, G., and Conley, D. J. (2017). Assessing the Potential of Sponges (Porifera) as indicators of ocean dissolved si concentrations. *Front. Mar. Sci.* 4:373. doi: 10.3389/fmars.2017.00373

Amorim, P., Perán, A. D., Pham, C. K., Juliano, M., Cardigos, F., Tempera, F., et al. (2017). Overview of the ocean climatology and its variability in the Azores region of the North Atlantic including environmental characteristics at the seabed. *Front. Mar. Sci.* 4:56. doi: 10.3389/fmars.2017.00056

Bashmachnikov, I., Nascimento, Ä., Neves, F., Menezes, T., and Koldunov, N. V. (2015). Distribution of intermediate water masses in the subtropical northeast Atlantic. *Ocean Sci.* 11, 803–827. doi: 10.5194/os-11-803-2015

Bergquist, P. R., and Hogg, J. J. (1969). Free amino acid patterns in Demospongiae: a biochemical approach to sponge classification. *Cahiers de Biologie Marine* 10, 205–220.

Boury-Esnault, N., and Rützler, K. (1997). *Thesaurus of Sponge Morphology: Smithsonian Contributions to Zoology*. Washington, DC: Smithsonian Institution Press.

Bowerbank, J. S. (1869). A Monograph of the Siliceo-fibrous Sponges. Part I. *Proc. Zool. Soc. London* 1, 66–100. doi: 10.1111/j.1469-7998.1869.tb07296.x

Braga-Henriques, A., Porteiro, F. M., Ribeiro, P. A., de Matos, V., Sampaio, Í, Ocana, O., et al. (2013). Diversity, distribution and spatial structure of the cold-water coral fauna of the Azores (NE Atlantic). *Biogeosciences* 10, 529–590. doi: 10.5194/bgd-10-529-2013

Caldeira, R. M. A., and Reis, J. C. (2017). The azores confluence zone. *Front. Mar. Sci.* 4:37. doi: 10.3389/fmars.2017.00037

Cárdenas, P., Pérez. T., and Boury-Esnault, N. (2012). "Sponge systematics facing new challenges," in *Advances in Sponge Science: Phylogeny, Systematics, Ecology*, eds M. A. Becerro, M. J. Uriz, M. Maldonado, and X. Turon (Amsterdam: Elsevier), 79–209. doi: 10.1016/B978-0-12-387787-1.00010-6

Cárdenas, P., and Rapp, H. T. (2015). Demosponges from the northern Mid-Atlantic Ridge shed more light on the diversity and biogeography of North Atlantic deep-sea sponges. *J. Mar. Biol. Assoc. U.K.* 95, 1475–1516. doi: 10.1017/S0025315415000983P

Cárdenas, P., Rapp, H. T., Klitgaard, A. B., Best, M., Thollesson, M., and Tendal, O. S. (2013). Taxonomy, biogeography and DNA barcodes of *Geodia* species (Porifera, Demospongiae, Tetractinellida) in the Atlantic

boreo-arctic region. *Zool. J. Linnean Soc.* 169, 251–311. doi: 10.1111/zoj.12056

Cárdenas, P., Rapp, H. T., Schander, C., and Tendal, O. S. (2010). Molecular taxonomy and phylogeny of the Geodiidae (Porifera, Demospongiae, Astrophorida) - combining phylogenetic and Linnaean classification. *Zool. Scripta* 39, 89–106. doi: 10.1111/j.1463-6409.2009.00402.x

Cárdenas, P., Xavier, J. R., Reveillaud, J., Schander, C., and Rapp, H. T. (2011). Molecular phylogeny of the Astrophorida (Porifera, Demospongiae^{P}) reveals an unexpected high level of spicule homoplasy. *PLoS One* 6:e18318. doi: 10.1371/journal.pone.0018318

Carracedo, L. I., Gilcoto, M., Mercier, H., and Pérez, F. F. (2014). Seasonal dynamics in the Azores-Gibraltar Strait region: a climatologically-based study. *Prog. Oceanogr.* 122, 116–130. doi: 10.1016/j.pocean.2013.12.005

Carter, H. J. (1873). On the Hexactinellidae and Lithistidae generally, and particularly on the Aphrocallistidae, *Aulodictyon*, and *Farreae*, together with facts elicited from their deciduous structures and descriptions respectively of three new species. *Ann. Magaz. Nat. Hist.* 12, 349–373. doi: 10.1080/00222937308680782

Carvalho, F. C., Cárdenas, P., Ríos, P., Cristobo, J., Rapp, H. T., and Xavier, J. R. (2020). Rock sponges (lithistid demosponges) of the Northeast Atlantic seamounts, with the description of 10 new species. *PeerJ* 8:e8703. doi: 10.7717/peerj.8703

Carvalho, F. C., and Pisera, A. (2019). Revision of the genus *Exsuperantia* Özdikmen, 2009 (Tetractinellida: Phymaraphiniidae) with description of a new species from the Atlantic Ocean. *Zootaxa* 4613, 135–151. doi: 10.11646/zootaxa.4613.1.7

Carvalho, F. C., Pomponi, S. A., and Xavier, J. R. (2015). Lithistid sponges of the upper bathyal of Madeira, Selvagens and Canary Islands, with description of a new species of *Isabella*. *J. Mar. Biol. Assoc. U.K.* 95, 1287–1296. doi: 10.1017/s0025315414001179

Cathalot, C., Van Oevelen, D., Cox, T. J. S., Kutti, T., Lavaleye, M., Duineveld, G., et al. (2015). Cold-water coral reefs and adjacent sponge grounds: hotspots of benthic respiration and organic carbon cycling in the deep sea. *Front. Mar. Sci.* 2:37. doi: 10.3389/fmars.2015.00037

Clarke, K. R., and Gorley, R. N. (2015). *PRIMER v7: User Manual/Tutorial*. Plymouth: PRIMER-E.

Darriba, D., Taboada, G. L., Doallo, R., and Posada, D. (2012). jModelTest 2: more models, new heuristics and parallel computing. *Nat. Methods* 9, 772–772. doi: 10.1038/nmeth.2109

Edgar, R. C. (2004). MUSCLE: multiple sequence alignment with high accuracy and high throughput. *Nucleic Acids Res.* 32, 1792–1797. doi: 10.1093/nar/gkh340

Ekins, M., Erpenbeck, D., Wörheide, G., and Hooper, J. N. A. (2016). A new species of lithistid sponge hiding within the *Isabella mirabilis* species complex (Porifera: Demospongiae: Tetractinellida) from seamounts of the Norfolk Ridge. *Zootaxa* 4136, 433–460. doi: 10.11646/zootaxa.4136.3.2

Ellwood, M. J., Kelly, M., and Richer de Forges, B. (2007). Silica banding in the deep-sea lithistid sponge *Corallistes undulatus*: investigating the potential influence of diet and environment on growth. *Limnol. Oceanogr.* 52, 1865–1873. doi: 10.4319/lo.2007.52.5.1865

EU (2016). *Regulation (EU) 2016/2336 of the European Parliament and of the council of 14 December 2016 Establishing Specific Conditions for Fishing for Deep-Sea Stocks in the North-East Atlantic and Provisions for Fishing in International Waters of the North-East Atlantic and Repealing Council Regulation (EC) No 2347/2002*. Brussels: European Union.

Fallon, S. J., James, K., Norman, R., Kelly, M., and Ellwood, M. J. (2010). A simple radiocarbon dating method for determining the age and growth rate of deep-sea sponges. *Nuclear Instrum. Methods Phys. Res. Sect. B* 268, 1241–1243. doi: 10.1016/j.nimb.2009.10.143

FAO (2009). *International Guidelines for the Management of Deep-sea Fisheries in the High Seas. Directives Internationales sur la Gestion de la pêche Profonde en haute mer. Directrices Internacionales para la Ordenación de las Pesquerías de Aguas Profundas en Alta Mar. 73 pp*. Rome: Food and Agriculture Organization of the United Nations.

Folmer, O., Black, M., Hoeh, W., Lutz, R., and Vrijenhoek, R. (1994). DNA primers for amplification of mitochondrial cytochrome c oxidase subunit I from diverse metazoan invertebrates. *Mol. Mar. Biol. Biotechnol.* 3, 294–299.

Freitas, R., Romeiras, M., Silva, L., Cordeiro, R., Madeira, P., González, J. A., et al. (2019). Restructuring of the 'Macaronesia' biogeographic unit: a marine multi-taxon approach. *Sci. Rep.* 9:15792. doi: 10.1038/s41598-019-51786-6

Gray, J. E. (1859). Description of *MacAndrewia* and *Myliusia*, two new forms of Sponges. *Proc. Zool. Soc. Lond.* 27, 437–440.

Hawkes, N., Korabik, M., Beazley, L., Rapp, H. T., Xavier, J. R., and Kenchington, E. (2019). Glass sponge grounds on the Scotian Shelf and their associated biodiversity. *Mar. Ecol. Prog. Ser.* 614, 91–109. doi: 10.3354/meps12903

Hestetun, J. T., Fourt, M., Vacelet, J., Boury-Esnault, N., and Rapp, H. T. (2015). Cladorhizidae (Porifera, Demospongiae, Poecilosclerida) of the deep Atlantic collected during Ifremer cruises, with a biogeographic overview of the Atlantic species. *J. Mar. Biol. Assoc. U. K.* 95, 1311–1342. doi: 10.1017/s0025315413001100

Hestetun, J. T., Tompkins-MacDonald, G., and Rapp, H. T. (2017). A review of carnivorous sponges (Porifera: Cladorhizidae) from the Boreal North Atlantic and Arctic. *Zool. J. Linnean Soc.* 181, 1–69. doi: 10.1093/zoolinnean/zlw022

Horton, T., Marsh, L., Bett, B. J., Gates, A. R., Jones, D. O. B., Benoist, N. M. A., et al. (2021). Recommendations for the standardisation of Open taxonomic nomenclature for image-based identifications. *Front. Mar. Sci.* 8:620702. doi: 10.3389/fmars.2021.620702

Howell, K. L., Piechaud, N., Downie, A. L., and Kenny, A. (2016). The distribution of deep-sea sponge aggregations in the North Atlantic and implications for their effective spatial management. *Deep Sea Res. Part I Oceanogr. Res. Pap.* 115, 309–320. doi: 10.1016/j.dsr.2016.07.005

ICES (2020). ICES/NAFO Joint Working Group on Deep-water Ecology (WGDEC). *ICES Sc. Rep.* 2:171. doi: 10.17895/ices.pub.6095

ICZN (1999). *International Code of Zoological Nomenclature*, 4th Edn, London: The International Trust for Zoological Nomenclature.

Johnson, J. Y. (1863). Description of a new siliceous sponge from the coast of Madeira. *Proc. Zool. Soc. London*, 257–259.

Kahn, A. S., Vehring, L. J., Brown, R. R., and Leys, S. P. (2016). Dynamic change, recruitment and resilience in reef-forming glass sponges. *J. Mar. Biol. Assoc. U. K.* 96, 429–436. doi: 10.1017/s0025315415000466

Kauffman, E. G., Herm, D., Johnson, C. C., Harries, P., and Höfling, R. (2000). The ecology of Cenomanian lithistid sponge frameworks, Regensburg area, Germany. *Lethaia* 33, 214–235. doi: 10.1080/00241160025100071

Kearse, M., Moir, R., Wilson, A., Stones-Havas, S., Cheung, M., Sturrock, S., et al. (2012). Geneious Basic: an integrated and extendable desktop software platform for the organization and analysis of sequence data. *Bioinformatics* 28, 1647–1649. doi: 10.1093/bioinformatics/bts199

Kelly, M., Ellwood, M., Tubbs, L., and Buckeridge, J. (2007). "The lithistid Demospongiae in New Zealand waters: species composition and distribution," in *Porifera Research. Biodiversity, Innovation and Sustainability. Livros de Museu Nacional 28*, eds M. R. Custódio, G. Lôbo-Hajdu, E. Hajdu, and G. Muricy (Rio de Janeiro: Routledge), 393–404.

Kirkpatrick, R. (1903). Descriptions of South African Sponges. Part II. *Marine Investigations in South Africa* 2, 171–180, pl. IV.

Knudby, A., Kenchington, E., and Murillo, F. J. (2013). Modeling the distribution of *Geodia* Sponges and Sponge grounds in the Northwest Atlantic. *PLoS One* 8:e82306. doi: 10.1371/journal.pone.0082306

Lê, H. L. V., Lecointre, G., and Perasso, R. (1993). A 28S rRNA-based phylogeny of the gnathostomes: first steps in the analysis of conflict and congruence with morphologically based cladograms. *Mol. Phylogenet. Evol.* 2, 31–51. doi: 10.1006/mpev.1993.1005

Lévi, C. (1960). Spongiaires des côtes occidentales africaines. *Bulletin de l'Institut français d'Afrique noire. A. Sciences naturelles* 22, 743–769.

Lévi, C., and Lévi, P. (1983). Eponges Tétractinellides et Lithistides bathyales de Nouvelle-Calédonie. *Bull. du Muséum national d'Histoire naturelle (4)* 5, 101–168.

Lévi, C., and Lévi, P. (1988). Nouveaux Spongiaires Lithistides bathyaux à affinités crétacées de la Nouvelle-Calédonie. *Bulletin du Muséum national d'Histoire naturelle* 10, 241–263.

Lévi, C., and Lévi, P. (1989). "Spongiaires (MUSORSTOM 1 & 2)," in *Résultats des Campagnes MUSORSTOM 4. Mémoires du Muséum national d'Histoire naturelle*, Vol. 143, ed. J. Forest (Série A: Zoologie), 25–103.

Lévi, C., and Vacelet, J. (1958). Éponges récoltées dans l'Atlantique oriental par le 'Président Théodore-Tissier' (1955-1956). *Revue Travaux l'Institut Pêches Marit.* 22, 225–246.

Leys, S. P., and Lauzon, N. R. J. (1998). Hexactinellid sponge ecology: growth rates and seasonality in deep water sponges. *J. Exper. Mar. Biol. Ecol.* 230, 111–129. doi: 10.1016/s0022-0981(98)00088-4

Lima, M. J., Sala, I., and Caldeira, R. M. A. (2020). Physical connectivity between the NE Atlantic seamounts. *Front. Mar. Sci.* 7:238. doi: 10.3389/fmars.2020.00238

Maldonado, M., Aguilar, R., Blanco, J., García, S., Serrano, A., and Punzón, A. (2015). Aggregated clumps of lithistid sponges: a singular, reef-like bathyal habitat with relevant paleontological connections. *PLoS One* 10:e0125378. doi: 10.1371/journal.pone.0125378

Maldonado, M., López-Acosta, M., Sitjà, C., García-Puig, M., Galobart, C., Ercilla, G., et al. (2020). Sponge skeletons as an important sink of silicon in the global oceans. *Nat. Geosci.* 19, 815–822. doi: 10.1038/s41561-019-0430-7

Manconi, R., and Serusi, A. (2008). Rare sponges from marine caves: discovery of *Neophrissospongia nana* nov. sp. (Demospongiae, Corallistidae) from Sardinia with an annotated checklist of Mediterranean lithistids. *ZooKeys* 4, 71–87. doi: 10.3897/zookeys.4.39

Manconi, R., Serusi, A., and Pisera, A. (2006). A new Mediterranean 'lithistid' sponge, *Aciculites mediterranea* sp. nov. (Porifera: Demospongiae) from a dark marine cave in Sardinia. *J. Mar. Biolog. Assoc. U.K.* 86, 691–698. doi: 10.1017/S0025315406013580

Meyer, C. P., Geller, J. B., and Paulay, G. (2005). Fine scale endemism on coral reefs: archipelagic differentiation in turbinid gastropods. *Evolution* 59, 113–125. doi: 10.1554/04-194

Morato, T., Machete, M., Kitchingman, A., Tempera, F., Lai, S., Menezes, G., et al. (2008). Abundance and distribution of seamounts in the Azores. *Mar. Ecol. Prog. Ser.* 357, 17–21. doi: 10.3354/meps07268

Morrow, C., and Cárdenas, P. (2015). Proposal for a revised classification of the Demospongiae (Porifera). *Front. Zool.* 12:7. doi: 10.1186/s12983-015-0099-8

Murillo, F. J., Kenchington, E., Tompkins, G., Beazley, L., Baker, E., Knudby, A., et al. (2018). Sponge assemblages and predicted archetypes in the eastern Canadian Arctic. *Mar. Ecol. Prog. Ser.* 597, 115–135. doi: 10.3354/meps12589

Özdikmen, H. (2009). Substitute names for eight sponge genus group names (Porifera). *Munis Entomology & Zoology* 4, 212–218.

Palma, C., Lillebø, A. I., Borges, C., Souto, M., Pereira, E., Duarte, A. C., et al. (2012). Water column characterisation on the Azores platform and the sea mounts south of the archipelago. *Mar. Pollut. Bull.* 64, 1884–1894. doi: 10.1016/j.marpolbul.2012.06.015

Perán, A. D., Pham, C. K., Amorim, P., Cardigos, F., Tempera, F., and Morato, T. (2016). Seafloor characteristics in the Azores region (North Atlantic). *Front. Mar. Sci.* 3:204. doi: 10.3389/fmars.2016.00204

Pérez, T., Vacelet, J., Bitar, G., and Zibrowius, H. (2004). Two new lithistids (Porifera: Demospongiae) from a shallow eastern Mediterranean cave (Lebanon). *J. Mar. Biolog. Assoc. U.K.* 84, 15–24. doi: 10.1017/S0025315404008859h

Pham, C., Diogo, H., Menezes, G., Porteiro, F., Braga-Henriques, A., Vandeperre, F., et al. (2014). Deep-water longline fishing has reduced impact on vulnerable marine ecosystems. *Sci. Rep.* 4:4837. doi: 10.1038/srep04837

Pisera, A., and Gerovasileiou, V. (2021). Lithistid demosponges of deep-water origin in marine caves of the north-eastern Mediterranean Sea. *Front. Mar. Sci.* 8:630900. doi: 10.3389/fmars.2021.630900

Pisera, A., and Lévi, C. (2002). "'Lithistid' Demospongiae," in *Systema Porifera. A Guide to the Classification of Sponges 1*, eds J. N. A. Hooper and R. W. M. Van Soest (New York, NY: Kluwer Academic Plenum), 299–301. doi: 10.1007/978-1-4615-0747-5_33

Pisera, A., and Vacelet, J. (2011). Lithistid sponges from submarine caves in the Mediterranean: taxonomy and affinities. *Scientia Marina* 75, 17–40. doi: 10.3989/scsimar.2011.75n1017

Pomponi, S. A., Kelly, M., Reed, J. A., and Wright, E. A. (2001). Diversity and bathymetric distribution of lithistid sponges in the tropical western Atlantic region. *Bull. Biol. Soc. Washington* 10, 344–353.

Porteiro, F. M. (2009). The importance of Prince's Albert I of monaco campaigns to the knowledge of the Azores Seas. *Boletim Nuìcleo Cult. Horta* 18, 189–219.

Puerta, P., Johnson, C., Carreiro-Silva, M., Henry, L.-A., Kenchington, E., Morato, T., et al. (2020). Influence of Water masses on the biodiversity and biogeography of deep-sea benthic ecosystems in the North Atlantic. *Front. Mar. Sci.* 7:239. doi: 10.3389/fmars.2020.00239

Ríos, P., Prado, E., Carvalho, F. C., Sánchez, F., Rodríguez-Basalo, A., Xavier, J. R., et al. (2020). Community composition and habitat characterization of a rock sponge aggregation (Porifera, Corallistidae) in the Cantabrian Sea. *Front. Mar. Sci.* 7:578. doi: 10.3389/fmars.2020.00578

Roberts, E. M., Bowers, D. G., Meyer, H. K., Samuelsen, A., Rapp, H. T., and Cárdenas, P. (2021). Water masses constrain the distribution of deep-sea sponges in the North Atlantic Ocean and Nordic Seas. *Mar. Ecol. Prog. Ser.* 659, 75–96. doi: 10.3354/meps13570

Ronquist, F., Teslenko, M., van der Mark, P., Ayres, D. L., Darling, A., Höhna, S., et al. (2012). MrBayes 3.2: efficient bayesian phylogenetic inference and model choice across a large model space. *Syst. Biol.* 61, 539–542. doi: 10.1093/sysbio/sys029

Rooks, C., Fang, J. K.-H., Mørkved, P. T., Zhao, R., Rapp, H. T., Xavier, L., et al. (2020). Deep-sea sponge grounds as nutrient sinks: denitrification is common in boreo-Arctic sponges. *Biogeosciences* 17, 1231–1245. doi: 10.5194/bg-17-1231-2020

Sampaio, Í, Braga-Henriques, A., Pham, C., Ocaña, O., de Matos, V., Morato, T., et al. (2012). Cold-water corals landed by bottom longline fishery in the Azores. *J. Mar. Biol. Assoc. U. K.* 92, 1547–1555. doi: 10.1017/s0025315412000045

Sampaio, Í, Freiwald, A., Porteiro, F. M., Menezes, G., and Carreiro-Silva, M. (2019). Census of Octocorallia (Cnidaria: Anthozoa) of the Azores (NE Atlantic) with a nomenclature update. *Zootaxa* 4550, 451–498. doi: 10.11646/zootaxa.4550.4.1

Schlacher-Hoenlinger, M. A., Pisera, A., and Hooper, J. N. A. (2005). Deep-sea "lithistid" assemblages from the Norfolk Ridge (New Caledonia), with description of seven new species and a new genus (Porifera, Demospongiae). *Zoosystema* 27, 649–698.

Schmidt, O. (1870). *Grundzüge einer Spongien-Fauna des Atlantischen Gebietes*. Leipzig: Wilhelm Engelmann.

Schuster, A., Cárdenas, P., Pisera, A., Pomponi, S. A., Kelly, M., Wörheide, G., et al. (2018). Seven new deep-water Tetractinellida (Porifera: Demospongiae) from the Galápagos Islands - morphological descriptions and DNA barcodes. *Zool. J. Linnean Soc.* 184, 273–303. doi: 10.1093/zoolinnean/zlx110

Schuster, A., Erpenbeck, D., Pisera, A., Hooper, J. N. A., Bryce, M., Fromont, J., et al. (2015). Deceptive desmas: molecular phylogenetics suggests a new classification and uncovers convergent evolution of lithistid demosponges. *PLoS One* 10:e116038. doi: 10.1371/journal.pone.0116038

Schuster, A., Lopez, J. V., Becking, L. E., Kelly, M., Pomponi, S. A., Wörheide, G., et al. (2017). Evolution of group I introns in Porifera: new evidence for intron mobility and implications for DNA barcoding. *BMC Evol. Biol.* 17:82. doi: 10.1186/s12862-017-0928-9

Schuster, A., Pomponi, S., Pisera, A., Cárdernas, P., Kelly, M., Wörheide, G., et al. (2021). Systematics of 'lithistid' tetractinellid demosponges from the Tropical Western Atlantic - implications for phylodiversity and bathymetric distribution. *PeerJ* 9:e10775.

Sigovini, M., Keppel, E., and Tagliapietra, D. (2016). Open nomenclature in the biodiversity era. *Methods Ecol. Evol.* 7, 1217–1225.

Silva, M. A., Prieto, R., Cascão, I., Seabra, M. I., Machete, M., Baumgartner, M. F., et al. (2014). Spatial and temporal distribution of cetaceans in the mid-Atlantic waters around the Azores. *Mar. Biol. Res.* 10, 123–137. doi: 10.1080/17451000.2013.793814

Sitjà, C., Maldonado, M., Farias, C., and Rueda, J. L. (2019). Deep-water sponge fauna from the mud volcanoes of the Gulf of Cadiz (North Atlantic, Spain). *J. Mar. Biol. Assoc. U. K.* 99, 807–831. doi: 10.1017/S0025315418000589

Stamatakis, A. (2014). RAxML version 8: a tool for phylogenetic analysis and post-analysis of large phylogenies. *Bioinformatics* 30, 1312–1313. doi: 10.1093/bioinformatics/btu033

Topsent, E. (1889). Quelques spongiaires du Banc de Campêche et de la Pointe-à-Pître. *Mémoires de la Société zoologique de France* 2, 30–52.

Topsent, E. (1892). Contribution aì l'eìtude des Spongiaires de l'Atlantique Nord (Golfe de Gascogne, Terre-Neuve, Acçores). *Reìsult. Campag. Sci. Accompl. Prince Albert I Monaco* 2, 1–165.

Topsent, E. (1893). Nouvelle série de diagnoses d'éponges de Roscoff et de Banyuls. *Archives de Zoologie expérimentale et générale. 3) 1 (Notes et Revue 10)*, xxxiii–xliii.

Topsent, E. (1898). Éponges nouvelles des Açores. *Mémoir. Soc. Zool. France* 11, 225–255.

Topsent, E. (1904). Spongiaires des Acçores. *Reìsult. Campag. Sci. Accompl. Prince Albert I Monaco* 25, 1–280.

Topsent, E. (1928). Spongiaires de l'Atlantique et de la Meìditerraneìe provenant des croisieÌres du Prince Albert ler de Monaco. *Reìsult. Campag. Sci. Accompl. Prince Albert I Monaco* 74, 1–376.

Vacelet, J. (1969). Eponges de la Roche du Large et de l'étage bathyal de Méditerranée (Récoltes de la soucoupe plongeante Cousteau et dragages). *Mémoires du Muséum national d'Histoire naturelle. A, Zoologie* 59, 145–219.

Van Soest, R. W. M., Boury-Esnault, N., Hooper, J. N. A., Rützler, K., de Voogd, N. J., Alvarez, B., et al. (2021). *World Porifera Database*. Available online at: http://www.marinespecies.org/porifera (accessed January 03, 2021).

Van Soest, R. W. M., Boury-Esnault, N., Vacelet, J., Dohrmann, M., Erpenbeck, D., de Voogd, N. J., et al. (2012). Global diversity of Sponges (Porifera). *PLoS One* 7:e35105. doi: 10.1371/journal.pone.0035105

Wieczorek, J., Bloom, D., Guralnick, R., Blum, S., Döring, M., Giovanni, R., et al. (2012). Darwin Core: an evolving community-developed biodiversity data standard. *PLoS One* 7:e29715. doi: 10.1371/journal.pone.0029715

Xavier, J. R., and Van Soest, R. W. M. (2012). Diversity patterns and zoogeography of the Northeast Atlantic and Mediterranean shallow-water sponge fauna. *Hydrobiologia* 687, 107–125. doi: 10.1007/978-94-007-4688-6_11

Conflict of Interest: The authors declare that the research was conducted in the absence of any commercial or financial relationships that could be construed as a potential conflict of interest.

Copyright © 2021 Xavier, Rees, Pereira, Colaço, Pham and Carvalho. This is an open-access article distributed under the terms of the Creative Commons Attribution License (CC BY). The use, distribution or reproduction in other forums is permitted, provided the original author(s) and the copyright owner(s) are credited and that the original publication in this journal is cited, in accordance with accepted academic practice. No use, distribution or reproduction is permitted which does not comply with these terms.

frontiers in Marine Science

ORIGINAL RESEARCH
published: 15 June 2021
doi: 10.3389/fmars.2021.662899

Mediterranean Coral Provinces as a Sponge Diversity Reservoir: Is There a Mediterranean Cold-Water Coral Sponge Fauna?

Andreu Santín[1], Jordi Grinyó[1,2], Maria Jesús Uriz[3], Claudio Lo Iacono[1], Josep Maria Gili[1] and Pere Puig[1]*

[1] Institut de Ciències del Mar (ICM-CSIC), Barcelona, Spain, [2] Department of Ocean Systems Sciences, NIOZ Royal Netherlands Institute for Sea Research and Utrecht University, Den Burg, Netherlands, [3] Centre d'Estudis Avançats de Blanes (CEAB-CSIC), Blanes, Spain

Cold-water coral reefs (CWC) are known to be biodiversity hotspots, however, the sponge assemblages found to dwell within these habitats haven not been studied in depth to date in the Mediterranean Sea. The present article provides the first insight on the associated sponge fauna of the recently discovered CWC communities on the Catalan Margin and, to a lesser extent, the Cabliers Coral Mound Province, while also reviewing the current knowledge of the sponge fauna dwelling in all the Mediterranean CWC provinces. In regards to the studied areas, some rare species are cited for the first time in the Mediterranean or redescribed, while two of them, *Hamacantha (Hamacantha) hortae* sp. nov. and *Spongosorites cabliersi* sp. nov. are new to science. At a basin scale, Mediterranean CWC appear as poriferan biodiversity hotspots, yet current diversity values on each site rather represent a small fraction of its actual fauna. Additionally, the existence of an endemic sponge fauna exclusively dwelling on CWC is refuted. Nonetheless, the sponge fauna thriving in Mediterranean CWC appears to be unique, and different from that of other Atlantic regions. Finally, with the current knowledge, the sponge fauna from the Mediterranean CWC is grouped in three distinguishable clusters (Alboran Sea, Western and Eastern Mediterranean), which appears to be determined by the basins water circulation, specially the Levantine Intermediate Water and the Atlantic Water following a western-eastern pattern from the Strait of Gibraltar to the Adriatic Sea. Overall, sponge living in Mediterranean CWC are still poorly explored in most areas, yet they appear to be good candidates for biogeographical studies.

Zoobank Registration: LSID urn:lsid:zoobank.org:pub:E58A3DFF-EDC5-44FC-A274-1C9508BF8D15.

Keywords: sponges (Porifera), cold water coral (CWC), new species, biogeography, remotely operated vehicles (ROV), Mediterranean Sea

OPEN ACCESS

Edited by:
Shirley A. Pomponi, Florida Atlantic University, United States

Reviewed by:
Sergi Taboada, Autonomous University of Madrid, Spain
Giorgio Bavestrello, University of Genoa, Italy

****Correspondence:***
Andreu Santín
santin@icm.csic.es

Specialty section:
This article was submitted to Deep-Sea Environments and Ecology, a section of the journal Frontiers in Marine Science

Received: *01 February 2021*
Accepted: *12 May 2021*
Published: *15 June 2021*

Citation:
Santín A, Grinyó J, Uriz MJ, Lo Iacono C, Gili JM and Puig P (2021) Mediterranean Coral Provinces as a Sponge Diversity Reservoir: Is There a Mediterranean Cold-Water Coral Sponge Fauna? Front. Mar. Sci. 8:662899. doi: 10.3389/fmars.2021.662899

INTRODUCTION

Coral dominated ecosystems are amongst the most exceptional and endangered benthic habitats all over the world (Hughes et al., 2002; Roberts et al., 2002). From a functional point of view, they play a major role in benthic-pelagic coupling processes and biogeochemical cycles (Wild et al., 2008) by creating a flow between water-column productivity and the benthic realm (Lesser, 2006). From a structural point of view, reef-building corals act as ecosystem engineers (*sensu* Jones et al., 1994), forming complex biogenic frameworks and providing niches, nursery grounds or shelter for a wide variety of organisms (Jensen and Frederiksen, 1992; Plaisance et al., 2009; Messmer et al., 2011). As so, they result in a heterogeneity increase in the abundance and functional diversity of the associated fauna (Buhl-Mortensen et al., 2010; Linley et al., 2017), giving them the status of biodiversity hotspots (Hughes et al., 2002; Roberts et al., 2002).

The cold-water corals (CWC) *Desmophyllum pertusum* (Linnaeus 1758) (hereon referred as *Lophelia pertusa*) and *Madrepora oculata* Linnaeus 1758 are slow growing, reef-forming species, with an almost worldwide distribution (Roberts et al., 2009b). Both species can build reefs several hundreds of meters tall and, due to their three-dimensional structure, they alter the water flux and sedimentation rates across their bodies, creating a myriad of different microhabitats within the reef (Roberts et al., 2009b; Buhl-Mortensen et al., 2016 and references within both). Like their shallow waters counterparts, their complex configuration provides suitable habitat and nursery ground for other species (Rogers, 1999; Henry and Roberts, 2007; Henry et al., 2013), even commercial fish (Baillon et al., 2012; Corbera et al., 2019), which has led to the consideration of CWC as deep-sea biodiversity hotspots (Roberts et al., 2009b; Henry and Roberts, 2016), as they greatly enhance the biodiversity of the areas where they occur (Jensen and Frederiksen, 1992). This, paired with their long lifespan (Buhl-Mortensen et al., 2010) and susceptibility to anthropogenic impacts (Rogers, 1999; Orejas et al., 2009), has prompted their inclusion as Vulnerable Marine Ecosystems (VMEs) by United Nations General Assembly (2007) (UNGA Resolution 61/105), the Food and Agriculture Organization (FAO, 2008; General Fisheries Commission for the Mediterranean (GFCM S.A.C.), 2008) and the OSPAR commission (OSPAR, 2009, 2010). Nevertheless, and despite the rapid increase of information regarding the associated CWC reef biodiversity over the last two decades, considerable knowledge gaps still exist, specially outside of the North Atlantic area (Henry and Roberts, 2016). In this regard, studies focusing on the fauna associated with CWC habitats consistently note the high proportion of suspension and filter feeders such as sponges, cnidarians, bryozoans, crinoids, ophiuroids or ascidians, which are suspected to benefit from shelter and elevated feeding positions (Henry and Roberts, 2007; Roberts et al., 2009b; Buhl-Mortensen et al., 2016; Corbera et al., 2019). In this sense, studies and projects focusing on North-Atlantic CWC habitats have reported more than 1.300 associated species (Roberts et al., 2006), representing a 30% increase from less than a decade ago (Rogers, 1999), yet it is expected that this number will continue growing as further work to characterize the high faunal diversity of NE Atlantic cold-water coral reefs is ongoing (Roberts et al., 2006). In this regard, CWC-associated sponges in the North Atlantic might be amongst the globe's most well-characterized, with studies focusing partially or fully on their biodiversity, distribution and spatial and trophic ecology having been undertaken during the past decades (e.g., Henry and Roberts, 2007; van Soest et al., 2007; Roberts et al., 2009a; van Soest and Beglinger, 2009; Kazanidis and Witte, 2016; Kazanidis et al., 2016). Amongst others, these studies have highlighted the vast diversity of CWC-associated Porifera (van Soest and De Voogd, 2015), which is often underrepresented (Henry and Roberts, 2016), and started unveiling their ecological importance for the reefs, with sponges enhancing the reef's biodiversity (Kazanidis et al., 2016), and being key actors in the biogeochemical cycles (Rix et al., 2016, 2017; Bart et al., 2021) and eroding processes (Beuck and Freiwald, 2005; Beuck et al., 2007, 2010) within CWC reefs.

On the contrary, despite a surging interest and research focus on CWC ecosystems in the Mediterranean Sea (Evans et al., 2019), less than 500 species have been recorded so far associated with CWC reefs (Rueda et al., 2019). Currently, from all their known accompanying fauna, Porifera stands out as one of the most diverse groups associated with Mediterranean CWC, with ca. 90 species recorded so far (Rueda et al., 2019), yet it is still far beyond Atlantic records for the same phyla (van Soest and Lavaleye, 2005; van Soest et al., 2007; van Soest and De Voogd, 2015). Additionally, while CWC ecosystems are known to occur across the whole Mediterranean basin, almost all data regarding Mediterranean CWC associated sponges comes from the Italian margin (Bertolino et al., 2019) and the Gulf of Lions (Vacelet, 1969), with information for the rest of the basin being almost anecdotal and limited to just a few species (e.g., Aguilar et al., 2011; Boury-Esnault et al., 2015; Fabri et al., 2017; Santín et al., 2020b). As so, Mediterranean CWC might be considered as suitable environments for the discovery of new or rare species (Cardone et al., 2019; Santín et al., 2020b). Furthermore, while CWC support diverse associated fauna, most of it seems to be rather facultative than endemic to CWC, yet this is still to be assessed (Rueda et al., 2019). Finally, prior works on Atlantic CWC have suggested that geographical distance between CWC and water currents might be amongst the most important factors shaping the diversity and composition of CWC sponge associated fauna (van Soest et al., 2007; van Soest and De Voogd, 2015). Regarding the later, invertebrates' larvae might act as passive particles in a given water mass, thus being their transport tied to their said water mass movements (Shanks et al., 2002). The Mediterranean Sea, being a semi-enclosed basin (Robinson et al., 2001), with a single connection to the Atlantic through the Strait of Gibraltar, poses a perfect setting to test such hypotheses. In this regard, the Mediterranean is a concentration basin (evaporation exceeds precipitation and runoff), which circulation is mainly marked by two water masses: the inflowing Atlantic Water (AW) and the Levantine Intermediate Water (LIW) (Menna and Poulain, 2010). In this sense, the LIW is formed at the eastern Mediterranean by cooling and evaporation of the surface mixed layer, yet the exact process of the LIW formation and the exact locality where it occurs is still subject of debate

(Hayes et al., 2019). After its formation, the LIW flows westwards at a depth of 200 – 600 m toward the Adriatic Sea and the Sicily Channel, from which it enters the western Mediterranean Sea, eventually exiting the basin through the Strait of Gibraltar as the Western Intermediate Water (WIW) (Robinson et al., 2001; Menna and Poulain, 2010). Flowing on opposing direction is the Atlantic Water (AW), which enters the Mediterranean Sea through the Strait of Gibraltar, down to 200 m depth, to compensate for the water's evaporation net loss across the basin. It flows throughout the western part of the basin subjected to cyclonic anticyclonically mesoscale phenomena, gradually becoming the Modified Atlantic Water (MAW), which flows into the eastern part of the basin through the Strait of Sicily, where it transforms into the Levantine Surface Water (LSW), ultimately taking part in the formation of the LIW (Robinson et al., 2001). Currently, Mediterranean CWC' distribution is believed to be marked by the Levantine Intermediate Water (LIW) (Chimienti et al., 2019), thus it would also be expected to have a major influence in the growth and distribution of CWC associated fauna.

During the ABIDES (Assessment of Bottom-trawling Impacts in Deep-sea Sediments, September, 2017) project, CWCs ecosystems were discovered at several locations within the Blanes Canyon (north-western Mediterranean Sea), always associated with the presence of exposed rocky outcrops. While the presence of CWC in the area was known from incidental Agassiz trawl data (Zabala et al., 1993; Rosell and Uriz, 2002; Aymà et al., 2019), the occurrence of living CWCs reefs in this canyon had not been documented before, and represented an unexpected finding, especially considering that they occur in a heavily trawled area (De Leo et al., 2019; Puig et al., 2019). During the ABIDES-ROV oceanographic cruise, it was possible to recollect a few pieces of *M. oculata* from a canyon wall, which proved to be rich in sponges (Santín et al., 2018a). Additionally, during the MELCOR (MELilla CORals, June 2012) Cruise, the Cabliers Coral Mound in the Alboran Sea, the largest coral mound found alive in the Mediterranean Sea up to date (Corbera et al., 2019), was characterized and sampled for the first time. Again, a diverse associated sponge fauna was detected in CWC fragments (Costa et al., 2018), yet it still needs to be studied in depth.

In this context, this paper aims to (i) provide the first insight into the associated poriferan fauna of the recently discovered CWCs in the Blanes Canyon and in the Cabliers Coral Mound, (ii) testing whether or not a Mediterranean CWC endemic sponge fauna exists, (iii) gaining insight on the diversity and possible relationships between the associated sponge fauna of CWC provinces within the Mediterranean (iv) exploring the possible role of the Mediterranean water masses circulation in the distribution of CWC sponge fauna across the Mediterranean basin.

MATERIALS AND METHODS

Definition of the Mediterranean Cold-Water Coral Provinces

Cold-water coral reefs provinces are typically defined as areas with large coral growth and colony density (Taviani et al., 2011), yet the term is not without controversy (Chimienti et al., 2019; Orejas and Jiménez, 2019). Originally termed for CWCs occurring in the Atlantic (Taviani et al., 2011), currently there are eight CWC provinces recognized in the Mediterranean basin so far (Taviani et al., 2017; Chimienti et al., 2019; Angeletti et al., 2020), being: the "Eastern Alboran CWC province (eA)," the "Gulf of Lions CWC province (GoL)," the "South Sardinia CWC province (sS)," the "South Malta CWC province (M)," the "Santa Maria di Leuca CWC province (SMdL)," the "Bari Canyon CWC province (BC)," all as defined in Chimienti et al. (2019), and the recently discovered "Corsica Channel CWC province (CC)," as defined by Angeletti et al. (2020). For the purpose of the present paper, three additional sites are considered for analysis despite not being defined as CWC provinces: the "Catalan Margin (CM)" the "Strait of Gibraltar-western Alboran (SoG-wA)" and the "Albanian subfossil reefs (AL)."

Catalan Margin Area (CM)

Spanning from the Ligurian Sea to the northern area of the Catalan margin, the Gulf of Lions' continental margin displays one of the highest canyon densities of the world (Würtz, 2012), with the Cap de Creus and Lacaze-Duthiers canyons being its westernmost representatives. South to the aforementioned canyons, we found the Palamós (also known as La Fonera) and the Blanes canyons, which are classified alongside the Gulf of Lions as an Ecologically or Biologically Significant Area (EBSA) by the Regional Activity Center for Specially Protected Areas (Gabrie et al., 2012). While until recently all known CWC communities in the Catalan coast were restricted to the Cap de Creus Canyon (Orejas et al., 2009), recent explorations in the Palamós and the Blanes canyons have started reporting the occurrence of living CWC communities in both areas (Lastras et al., 2016; Puig and Gili, 2019; Santín et al., 2020a,b). In its most recent revision, Chimienti et al. (2019) excluded La Fonera canyon from the Gulf of Lions CWC province, yet it acknowledged the presence of CWC reefs communities in the area. As so, both the Palamós and the Blanes canyons are here treated as a separate entity from the Gulf of Lions CWC province, yet further discussion regarding whether they should be considered a new CWC province, or part of the Gulf of Lions' one, falls of the scope of the present paper.

Gibraltar-Western Alboran Area (SoG-wA)

The existence of dead CWC communities in the Western Alboran Sea has been long documented (Margreth et al., 2011; Palomino et al., 2011), yet the actual presence of living reefs is restricted to La Línea and Guadiaro canyons (Vázquez et al., 2015), with additional sporadic observations of isolated colonies (Palomino et al., 2011), and also being suspected to occur in the deep-sea area around Ceuta (Pardo et al., 2011). Regarding the Strait of Gibraltar, it was not until recent years that the presence of living CWC banks was reported in the area (Álvarez-Pérez et al., 2005). In this sense, the Strait of Gibraltar and its surrounding areas subjected to a series of particular oceanographic conditions with an outflow of Mediterranean Water (40 – 900 m depth) toward the Atlantic and the inflow of superficial Atlantic water on its

inner area, which could justify its consideration as a distinct extra-Mediterranean CWC province (Chimienti et al., 2019). Additionally, while still scarce, a few articles have reported the presence of sponges attached to coral rubble in the Gibraltar Straits and the Ceuta area (Topsent, 1928; Boury-Esnault et al., 1994). As so, while information is scant, the uniqueness of the area justifies its inclusion as the easternmost CWC site considered for the study.

The Albanian Subfossil Reefs (AL)

The presence of subfossil CWC reefs in Albanian waters had long been known by fishermen, yet it was not until recent years that their presence was properly documented (Nasto et al., 2018), quickly followed by the discovery of isolated, yet alive, *M. oculata* and *L. pertusa* colonies (Angeletti et al., 2014). While all data regarding its sponge fauna comes from a single sampling of the subfossil reefs (Nasto et al., 2018), the Albanian waters represent a unique CWC site, as it is one of the only known south-eastern Adriatic CWC communities, and it has been suggested that it might play a major role on the connectivity of two of the Adriatic and Ionian Sea CWC communities (Chimienti et al., 2019), which, objectively, makes it worthy of inclusion. Finally, the area is also part of the Ionian Sea EBSA area (Gabrie et al., 2012), established in part due to the exceptional presence of CWC in the area.

The Blanes Canyon

The ABIDES-ROV cruise took place from the 9th to 19th of September 2017, on board of the R/V 'Sarmiento de Gamboa,' using the Remotely Operated Vehicle (ROV) '*Liropus 2000.*' The main goal of this cruise was to evaluate the impacts of bottom trawling activities on submarine canyon flanks of the Catalan continental margin (north-western Mediterranean Sea). During the exploration of the Blanes submarine canyon (**Figure 1A**) a vertical wall expanding from 670 to 860 m depth was surveyed (**Supplementary Material 1**). The wall was densely covered by colonies of the reef building scleractinians *L. pertusa* (**Figure 2A**), *M. oculata* (**Figures 2B–F**), the solitary coral *Desmophyllum dianthus* (Esper, 1794) (**Figure 2F**), found along with scattered colonies of the antipatharians *Parantipathes larix* (Esper, 1788) and the gorgonian *Muriceides lepida* Carpine and Grasshoff, 1975.

The Cabliers Coral Mound Province

The "MELCOR" cruise took place from the 25th May to 1st of June 2012, on board the R/V 'Garcia del Cid' (Lo Iacono, 2012). During the cruise, the Cabliers Coral Mound was entirely mapped for the first time through the acquisition of multibeam swath bathymetry (**Figure 1B**). The Cabliers Coral Mound Province develops on a volcanic substrate within a depth of 290 – 700 m, and consists of a system of linear ridge-like Cold-Water Coral mounds, up to 140 m tall, aligned for up to 20 km along an NNE-SSW direction (Lo Iacono et al., 2014). The top of the mound is characterized by thriving cold-water coral reefs, mainly composed by the framework building scleractinian *M. oculata* and *L. pertusa*, whose colonies reach larger dimensions compared to similar reefs of the Mediterranean (Corbera et al., 2019). The reefs are accompanied by several species including the glass sponge *Asconema setubalense* Kent, 1870, the scleractinian *Dendrophyllia cornigera* (Lamarck, 1816), the black corals *Phanopathes* cf. *rigida* (Pourtalès, 1880) and *P. larix* (Corbera et al., 2019). Martin-Rauschert dredges were collected on the

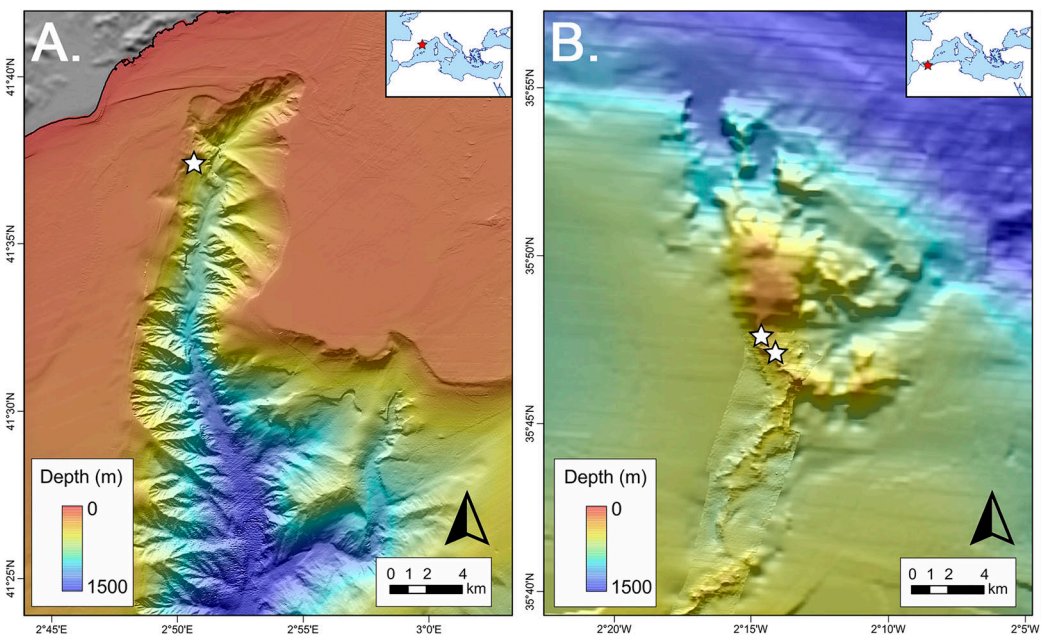

FIGURE 1 | (A) Location of the collection site (white star) in the Blanes Canyon, north-western Mediterranean Sea). **(B)** Location of the collection site (white stars) in the Cabliers Coral Mound, in the Alboran Sea. Projected view [UTM Zone 31N (WGS84)] with geographic (WGS84) coordinates indicated for reference.

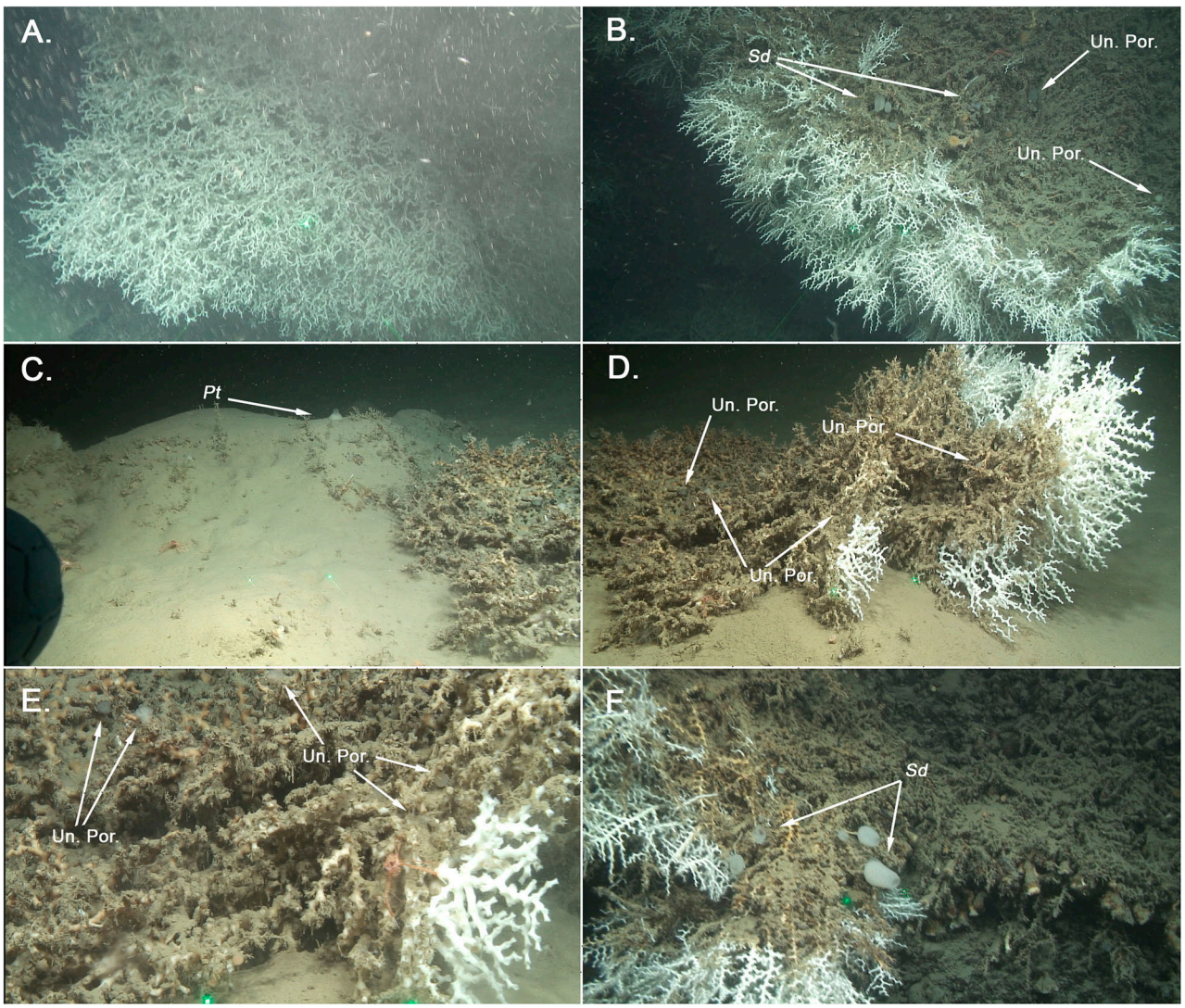

FIGURE 2 | (A) Colony of *Lophelia pertusa* growing on a vertical wall on the Blanes Canyon at ca. 840 m depth (41°34′872″N 02°50′986″E). **(B)** Partially death colony of *Madrepora oculata*, growing on a vertical wall at ca. 600 m depth (41°37′642″N 02°51′4265′E). *Sd* signals de presence of the Sponge *Sympagella delauzei*, whereas Un. Por. correspond to unidentified sponges. **(C)** Partially buried colony of *M. oculata* (rear). *Pt* signals an individual of *Polymastia tissieri* growing amidst the sand/rubble matrix at ca. 680 m depth at the eastern flank of the canyon (41°30′338″N 02°56′04″E). **(D)** Partially buried colony of *M. oculata* (front). Un. Por. correspond to unidentified sponges. **(E)** Close up of the partially buried colony, where a *Munida* sp. (reddish crab) can be seen alongside unidentified sponges (Un. Por.). **(F)** *Sympagella delauzei* (*Sd*) individuals growing onto the dead skeleton of a *M. oculata* colony at ca. 600 m depth (41°37′642″N 02°51′4265′E).

dead coral frameworks and coral rubble deposits surrounding the above described living reefs (**Supplementary Material 1**).

Sample Collection

During the ABIDES-ROV cruise, a few pieces of *L. pertusa* and *M. oculata* were retrieved from the Blanes Canyon, north-western Mediterranean Sea (41°37′642″N 02°51′426′E), at ca. 600 m depth, by means of the articulated arm of the ROV. The coral rubble samples consisted of three small, broken colony fragments and a single medium-sized piece of *M. oculata*, (ca. 23 – 23 cm wide) which had been originally collected to estimate the age of the reef. Thus, the sample was not preserved neither in formaldehyde nor in alcohol, but was let to dry instead. A few additional sponge specimens were found attached to a living piece of *M. oculata*, being preserved in absolute ethanol (see **Supplementary Material 2**).

During the "MELCOR" cruise, several fragments of coral rubble composed by both *L. pertusa* and *M. oculata* were sampled by means of a Martin Rauscher epibenthic sledge, at a depth range between 340 and 350 m depth (**Figure 1B**, being fixed in 4% formaldehyde and posteriorly transferred at 70% ethanol). Part of this samples were sent to the Università degli Studi di Genova (UNIGE) for further study (Costa et al., 2018), while a single piece of *Madrepora* and a few isolated sponge individuals remained at the Institut de Ciències del Mar (ICM-CSIC), having those been used for the present study (see **Supplementary Material 2**).

Sample Identification

Once back in the laboratory, the largest sponge samples (>1 cm^2) were detached from the coral rubble and individualized in Eppendorf containers, whereas smaller ones (<1 cm^2). Provisional identifications were made by examination of teased preparations of fragments, made permanent by mounting in Canada balsam. To obtain spicule preparations for both optical and scanning electron microscopy (SEM) fragments of the sponges were dissolved with nitric acid (HNO_3) following the procedures described in Cristobo et al. (1993) and Uriz et al. (2017). The SEM observation was conducted through a HITACHI TM3000 TableTop scanning electron microscope from the Centre d'Estudis Avançats de Blanes (CEAB) and a HITACHI S-3500 N scanning electron microscope from the Institut de Ciències del Mar (ICM-CSIC), both at 5 Kv. Spicule dimensions are given as maximum and minimum length and width for each spicule category with the average values being given in between in italics followed by ±the Standard Deviation (i.e., MIN. – MEAN ± SD – MAX.). Unless stated, all spicule measurements were based on 40 spicules.

All the material examined has been labeled and deposited in the Museu de Ciències Naturals de Barcelona (MZB), following the reference number specified in the species' examined material (**Supplementary Material 2**). Species classification has followed the current proposed classification for sponges in the World Porifera Database (van Soest et al., 2021).

Diversity Estimates and Statistical Analyses

In order to be able to compare between the selected CWC sites (as defined in section "Definition of the Mediterranean Cold-Water Coral Provinces"), a careful examination of the current bibliography dealing with CWC in the Mediterranean was conducted, in search for any relevant data regarding the occurrence of sponges in the aforementioned CWC coral sites. To such aim, a systematic literature search was conducted using the biographic database Web of Science (WoS) in September 2020. Specifically, an advanced search was confined by the combination of the terms "sponge" or "Porifera," "Mediterranean" and a third term, "cold-water coral," "*Lophelia*" or "*Madrepora.*" Published articles until September 2020, including scientific papers, book chapters and workshop and congress proceeding, were screened and included in the analysis if they contained information regarding the presence of sponge species growing onto CWC in the Mediterranean Sea. Additionally, 'historical papers' susceptible of containing relevant information were checked regardless of whether or not they were retrieved by the search engine, as WoS is known to offer an incomplete coverage of old literature (Marx, 2012). Finally, the reference lists of all articles were checked for any additional relevant studies. Due to the widely varying procedence and quality of the information, which included presence/absence, semiquantitative and quantitative data, incidence data was selected as the most appropriate approach to establish comparisons between areas, thus simplifying information available into a presence/absence matrix. Basic diversity estimates were then calculated, including number of species per area, shared species between areas, and percentage of exclusive Mediterranean endemism and percentage of North Atlantic sponge fauna on each area. Additionally, graphics were produced regarding (i) the total number of sponge species identified vs. total publications involving sponges' in Mediterranean CWC through time, both at a basin scale and for each area individually, (ii) the total number of species identified based on collected material and/or ROV per area and (iii) a randomized species accumulation curve to estimate the total number of species at a basin scale. Finally, a Jaccard dissimilarity matrix was generated for the 10 evaluated CWC sites defined in section "Definition of the Mediterranean Cold-Water Coral Provinces," which was later represented as dendrogram (average linkage) and a non-metric multidimensional scaling (nMDS) for visual exploration by means of the package *vegan* (Oksanen et al., 2019), available for the R software platform (R Core Team, 2019). After an initial visual assessment of the plots, a 25% similarity threshold was applied for cluster delimitation. Later on, a one-way PERMANOVA (Anderson, 2001) was applied to test for differences in species composition between the clusters using the *adonis* function (999 permutations) of the *vegan* package (Oksanen et al., 2019). Posteriorly, additional tests were applied to elucidate whether or not clusters might be influenced by the geographical distance between CWC sites. To such aim, the geographic distances between all 10 sites were calculated and transformed into Euclidean distance matrix, which was then confronted with the Jaccard dissimilarity matrix by means of a Mantel tests (999 permutations) using the *mantel* function of the *vegan* package (Oksanen et al., 2019). Finally, a Person correlation was applied between the geographical linear distance between sites and the Jaccard dissimilarity matrix using the *cor.test* function, available on the *stats* package, and graphically represented using the *tidyverse* (Wickham et al., 2019) and *ggpubr* (Kassambara, 2020) packages, all available for the R software platform (R Core Team, 2019).

RESULTS

Systematic Description

A total of 184 sponge specimens could be detected within the analyzed material, accounting for a total of 46 species that could be identified at least to genus level, with 39 corresponding to the Blanes Canyon and 7 to the Cabliers Coral Mound (**Table 1**, **Figure 3**, and **Supplementary Material 2**). In both areas, three out of the four Porifera classes (Calcarea, Demospongiae, Hexactinella) were present in the samples, only lacking Homoscleromorpha representatives. Calcarea and Hexactinellida were represented by three species and four species respectively, while all the others corresponded to Demospongiae, with Poecilosclerida being the most diverse order present. From those, *Poecillastra taviani* (Tetractinellida; **Figure 3D**) and *Acanthancora schmidti* (Poecilosclerida) were the most abundant, with 72 and 21 individuals, respectively.

Below, a morphological description is provided for those species deemed rare, faunistically relevant or new to science,

TABLE 1 | Comparative table including all known sponge species that have been recorded within CWC provinces in the Mediterranean Sea.

Species	SoG -wA	eA	CM	GoL	CC	sS	M	SMdL	AL	BC
CALCAREA										
CLATHRINIDA										
Ascandra corallicola (Rapp, 2006)[C]			39							
LEUCOSOLENIDA										
Aphroceras cf. *ensata* (Bowerbank, 1858)			39							
Leucosolenia aff. *variabilis* Haeckel, 1870		39								
Sycon sp.			39							
HOMOSCLEROMORPHA										
HOMOSCLEROPHORIDA										
Plakina cf. *monolopha* Schulze, 1880								13		
Plakortis cf. *simplex* Schulze, 1880								10; 13		20
DEMOSPONGIAE										
AGELASIDA										
Hymerhabdia sp.		28								
Hymerhabdia oxytrunca Topsent, 1904		28	39	3						20
Hymerhabdia typica Topsent, 1892									30	20
Prosuberites longispinus Topsent, 1893										20
AXINELLIDA										
Acantheurypon pilosella (Topsent, 1904)	1; 7	28				27; 31				
Axinella sp.						29				
Axinella cannabina (Esper, 1794)*								10; 13		
cf. *Axinella damicornis* (Esper, 1794)			22							
Axinella infundibuliformis (Linnaeus, 1759)		34								
Axinella minuta Lévi, 1957										20
Euryopn spp.			39							
Eurypon cinctum Sarà, 1960										20
Eurypon clavatum (Bowerbank, 1866)				3				10	30	
Eurypon denisae Vacelet, 1969[C]				3						
Eurypon hispidulum (Topsent, 1904)	1			3						
Eurypon mixtum (Topsent, 1928)	1	39								
Eurypon obtusum Vacelet, 1969*,[C]				3						
Eurypon pulitzeri Cavalcanti, Santos and Pinheiro, 2018*										20
cf. *Eurypon viride* (Topsent, 1889)				3						
Janulum spinispiculum (Carter, 1876)	7	7		3		31	17			
Phakellia robusta Bowerbank, 1866				3	36		17		30	20
Rhabdeurypon spinosum Vacelet, 1969*				3						
BIEMNIDA										
Biemna partenopea Pulitzer-Finali, 1978*										20
Biemna tenuisigma Pulitzer-Finali, 1978*										20
Biemna variantia (Bowerbank, 1858)				3						
Rhabderemia profunda Boury-Esnault et al., 1994						31				
BUBARIDA										
Bubaris sp. 1								10; 13		
Bubaris sp. 2										20
Bubaris sp. *sensu* Vacelet, 1969*,[C]				3						20
Bubaris carcisis Vacelet, 1969*				3		31				
Bubaris subtyla Pulitzer-Finali, 1983										20
Bubaris vermiculata (Bowerbank, 1866)									30	20
cf. *Cerbaris curvispiculifer* (Carter, 1880)				3						20
Dictyonella obtusa (Schmidt, 1862)*				3						
Monocrepidium vermiculatum Topsent, 1898		28		3						
Sulcastrella tenens (Vacelet, 1969)*,[C]				3						
CLIONAIDA										
Cliona sp.								13		
Diplastrella bistellata (Schmidt, 1862)				3						
Spiroxya heteroclita Topsent, 1896*								10; 13		
Spiroxya levispira (Topsent, 1898)				8		27; 29		10; 12; 13		
Spiroxya pruvoti (Topsent, 1900)						31				
DESMACELLIDA										
Desmacella annexa Schmidt, 1870				3				10; 13		
Desmacella infundibuliformis (Vosmaer, 1885)		28								
Desmacella inornata (Bowerbank, 1866)	7	7	39	3	4	27; 31	17	10; 13	30	20
Dragmatella aberrans (Topsent, 1890)				3						
DENDROCERATIDA										
Chelonaplysilla psammophila (Topsent, 1928)				3						
Spongionella pulchella (Sowerby, 1804)				3						
HAPLOSCLERIDA										
Calyx nicaeensis (Risso, 1826)*				3						
Haliclona spp.		39				29; 31				
Haliclona (*Reniera*) spp.		39	22			27				
Haliclona (*Flagellia*) *hiberniae* van Soest, 2017			39	3		31		10; 13	30	20

(Continued)

TABLE 1 | Continued

Species	SoG -wA	eA	CM	GoL	CC	sS	M	SMdL	AL	BC
Haliclona (*Gellius*) *arnesenae* (Arndt, 1927)				3						
Haliclona (*Gellius*) *bioxeata* (Boury-Esnault et al., 1994)* C	7	28								
Haliclona (*Gellius*) *lacazei* (Topsent, 1893)		28								
Haliclona (*Halichoclona*) *magna* (Vacelet, 1969)*				3; 24; 35						
Haliclona (*Reniera*) *cratera* (Schmidt, 1862)		28								
Siphonodictyon infestum (Johnson, 1889)	9		39			31		12		20
MERLIIDA										
Hamacantha spp.									30	
Hamacantha (*Hamacantha*) *hortae* sp. nov. *,C			39							
Hamacantha (*Hamacantha*) *azorica* Topsent, 1904			39				17			
Hamacantha (*Hamacantha*) *johnsoni* (Bowerbank, 1864)	1; 7		39	3		27; 31		10; 13	30	20
Hamacantha (*Hamacantha*) *lundbecki* Topsent, 1904				3		31				
Hamacantha (*Vomerula*) *falcula* (Bowerbank, 1874)			22	3; 19; 30	4; 36	27; 31	17			
Hamacantha (*Vomerula*) *papillata* Vosmaer, 1885				3				10	30	20
POECILOSCLERIDA										
Acanthancora schmidti (Topsent, 1898)			39							
Anisocrella hymedesmina Topsent, 1927	7	28		3						
Antho spp.								10		
Antho (Acarnia) signata (Topsent, 1904)								10; 13	30	
Antho (Antho) involvens (Schmidt, 1864)										20
Cladorhiza cf. *abyssicola* Sars, 1872		7	39	26						
Clathria (*Microciona*) sp. 1			39							
Clathria (*Microciona*) sp. 2			39							
Clathria (*Microciona*) sp. 3		39								
Clathria (*Microciona*) *armata* (Bowerbank, 1862)						31				
Clathria (*Microciona*) *atrasanguinea* (Bowerbank, 1862)						31				
Clathria (*Microciona*) *frogeti* (Vacelet, 1969)*,C			39	3						
Clathria (*Microciona*) *gradalis* Topsent, 1925			39							20
Clathria (*Paresperia*) *anchorata* (Carter, 1874)	7			3		27; 31				
Crella sp.			22							
Crella (*Pytheas*) *alba* (Vacelet, 1969)*,C		28	39	3						
Crella (*Yvesia*) *pyrula* (Carter, 1876)	7									
Crellastrina alecto (Topsent, 1898)								10; 13		
Damiria curvata (Vacelet, 1969)*,C		28		3						
Discorhabdella hindei Boury-Esnault et al., 1992*	6; 7	28; 39								
Esperiopsis strongylophora Vacelet, 1969*,C				3						
Forcepia (*Leptolabis*) *megachela* (Maldonado, 1992)*						31				
Hamigera bibiloni Santín et al., 2020b*,C			38; 39							
Hymedesmia spp.			28; 39							
Hymedesmia (*Hymedesmia*) *depressa* Topsent, 1928	7									
Hymedesmia (*Hymedesmia*) *gracilisigma* Topsent, 1928		28		3						
Hymedesmia (*Hymedesmia*) *jeanvaceleti* van Soest and Hooper, 2020*,C				3						
Hymedesmia (*Hymedesmia*) *mutabilis* (Topsent, 1904)			39	3		27; 31		10; 13	30	
Hymedesmia (*Hymedesmia*) *paupertas* (Bowerbank, 1866)		15								
Hymedesmia (*Hymedesmia*) *peachii* Bowerbank, 1882			5							
Hymedesmia (*Hymedesmia*) *pennata* Brøndsted, 1932	7									
Hymedesmia (*Hymedesmia*) *plicata* Topsent, 1928			39	3						
Hymedesmia (*Hymedesmia*) *pugio* Lundbeck, 1910	7						17			
Hymedesmia (*Hymedesmia*) *quadridentata* Cardone et al., 2019*,C			39			31; 32				
Hymedesmia (*Hymedesmia*) *serrulata* Vacelet, 1969*,C				3						
Hymedesmia (*Hymedesmia*) *zetlandica* Bowerbank, 1864		28								
Latrunculia rugosa (Vacelet, 1969)*,C				3						
Latrunculia (*Biannulata*) *citharistae* Vacelet, 1969		28				31				
Lissodendoryx sp. 1			39							
Lissodendoryx sp. 2			39							
Lissodendoryx (*Lissodendoryx*) cf. *polymorpha* (Topsent, 1890)			39							
Lycopodina hypogea (Vacelet and Boury-Esnault, 1996)		14	39				14; 17			
Melonanchora emphysema (Schmidt, 1875)			39	3						
Mycale (Mycale) cf. *massa* (Schmidt, 1862)			39	3						
Phorbas fictitius (Bowerbank, 1866)			5			31				
Plocamionida ambigua (Bowerbank, 1866)	7	7; 28	5	3				13		
Plocamionida tylotata Brøndsted, 1932						31				20
Podospongia lovenii Barboza du Bocage, 1869		28		3						
Sceptrella insignis (Topsent, 1890)	1			3		27		10; 13	30	20
POLYMASTIIDA										
Atergia corticata Stephens, 1915	7									
Polymastia spp.			39						30	
Polymastia penicillus (Montagu, 1814)				3						
Polymastia polytylota Vacelet, 1969C		7		3						
Polymastia tissieri (Vacelet, 1961)			39				17			
Pseudotrachya hystrix (Topsent, 1890)	7			3		31				

(Continued)

TABLE 1 | Continued

Species	SoG -wA	eA	CM	GoL	CC	sS	M	SMdL	AL	BC
SUBERITIDA										
Protosuberites rugosus (Topsent, 1893)	7			3						
Pseudosuberites hyalinus (Ridley and Dendy, 1877)			39	3						
Spongosorites spp.								13		
Spongosorites cabliersi sp. nov. *,C		39								
Stylocordyla pellita (Topsent, 1904)				3			11			
Suberites sp. 1						27				
Suberites sp. 2								13		
Suberites sp. 3								13		
Topsentia pachastrelloides (Topsent, 1892)	1									
TETHYIDA										
Timea sp.									30	
Timea chondrilloides (Topsent, 1904)				3				10; 13		
TETRACTINELLIDA										
Alectona millari Carter, 1879						27				
Annulastrella schmidti Maldonado, 2002	1									
Annulastrella verrucolosa (Pulitzer-Finali, 1983)*				3		31				
Calthropella (*Calthropella*) *pathologica* (Schmidt, 1868)				3				10; 13		
Characella pachastrelloides (Carter, 1876)							17			
Dercitus (Stoeba) plicatus (Schmidt, 1868)								13		
Discodermia polydiscus (Bowerbank, 1869)				3						
Erylus papulifer Pulitzer-Finali, 1983*								10; 13		
Geodia sp.		33								
Geodia anceps (Vosmaer, 1894)								10; 13		
Geodia conchilega Schmidt, 1862						31				
Geodia nodastrella Carter, 1876								10; 13	30	
Jaspis incrustans (Topsent, 1890)							17	10; 13	30	20
Jaspis johnstonii (Schmidt, 1862)	1			3						
Leiodermatium cf. *lynceus* Schmidt, 1870								10; 13	30	
Pachastrella spp.									30	
Pachastrella monilifera Schmidt, 1868	7	33			4; 36	27; 29	17	10; 13	18; 30	16; 18; 20; 23
Poecillastra spp.						27; 29				
Poecillastra compressa (Bowerbank, 1866)			22	3; 19; 24; 35		27; 29	17	10; 13	18; 30	16; 18; 20; 23
Poecillastra tavianii Cardone et al., 2019*,C			39			31; 32				
Siphonidium ramosum (Schmidt, 1870)				3		31	11	10; 13	30	
Stelleta sp.					36					
Thrombus abyssi (Carter, 1873)							17	10; 13		
Vulcanella gracilis (Sollas, 1888)	7	28		3	4; 36	27; 31	11; 17	10; 13	30	
Vulcanella horrida (Schmidt, 1870)					4					
TRACHICLADIDA										
Trachycladus minax (Topsent, 1888)				3						
VERONGIIDA										
Hexadella cf. *dedritifera* Topsent, 1913		28	39			29		10; 13	30	18
Hexadella cf. *cripta* Reveillaud et al., 2012				24; 25; 35						
Hexadella pruvoti Topsent, 1896*										20
Hexadella racovitzai Topsent, 1896			22							
HEXACTINELLIDAE										
LYSSACINOSIDA										
Rossellidae ind.			39							
Asconema setubalense Kent, 1870		15; 21; 33; 37; 39								
Oopsacas minuta Topsent, 1927*	1		39	24; 25; 35		31				
Sympagella delauzei Boury-Esnault et al., 2015		7; 21	39	25	36					
SCEPTRULOPHORA										
Farrea bowerbanki Boury-Esnault et al., 2017				25						
Tretodictyum reiswigi Boury-Esnault et al., 2017	7	28; 34	39	3; 24; 25			17	10; 13		
Total	27	37	47	69	8	38	17	38	23	29

**Species endemic to the Mediterranean Sea, according to the World Porifera Database (van Soest et al., 2021).*

Species marked with C, indicate species that, by the time being, have only been recorded from CWC environments. Each number indicates the reporting article for any given species on each CWC site, as in: Sog-wA, Strait of Gibraltar-western Alboran; eA, eastern Alboran; CM, Catalan Margin; GoL, Gulf of Lions; CC, Corsica Channel; sS, south of Sardinia; M, Maltese waters; SMdL, Santa Maria di Leuca; AL, Albanian subfossil reefs; BC, Bari Canyon.

The complete list of references are listed at table footnote. Accession numbers for the material from the eA and CM used for this study can be accessed in the ***Supplementary Material 2****.*

(1) Topsent (1928); (2) Sarà (1958); (3) Vacelet (1969); (4) Pulitzer-Finali (1983); (5) Uriz and Rosell (1990); (6) Boury-Esnault et al. (1992); (7) Boury-Esnault et al. (1994); (8) Rosell and Uriz (2002); (9) Álvarez-Pérez et al. (2005); (10) Longo et al. (2005); (11) Zibrowius and Taviani (2005); (12) Beuck et al. (2010); (13) Mastrototaro et al. (2010); (14) Aguilar et al. (2011); (15) Pardo et al. (2011); (16) Bo et al. (2012); (17) Calcinai et al. (2013); (18) Angeletti et al. (2014); (19) Fabri et al. (2014); (20) D'Onghia et al. (2015); (21) Boury-Esnault et al. (2015); (22) Lastras et al. (2016); (23) Taviani et al., (2016); (24) Fabri et al. (2017); (25) Fabri et al. (2017) combined with Boury-Esnault et al. (2017). Fabri et al. (2017) mentioned Farrea sp. associated with CWC in the Cassidaigne Canyon. Later on Boury-Esnault et al. (2017) described F. bowerbanki from the same location, yet without any specific mention to its occurrence in CWC habitats. For the time being, this is the only accepted Mediterranean Farrea, so it is here assumed both records referred to the same species.; (26) Fourt et al. (2017); (27) Taviani et al. (2017); (28) Costa et al. (2018); (29) Moccia et al. (2018); (30) Nasto et al. (2018); (31) Bertolino et al. (2019); (32) Cardone et al. (2019); (33) Corbera et al. (2019); (34) This paper, based on unpublished data from Corbera et al. (2019); (35) Fabri et al. (2019); (36) Angeletti et al. (2020); (37) de la Torriente et al. (2020); (38) Santín et al. (2020b); (39) This work.

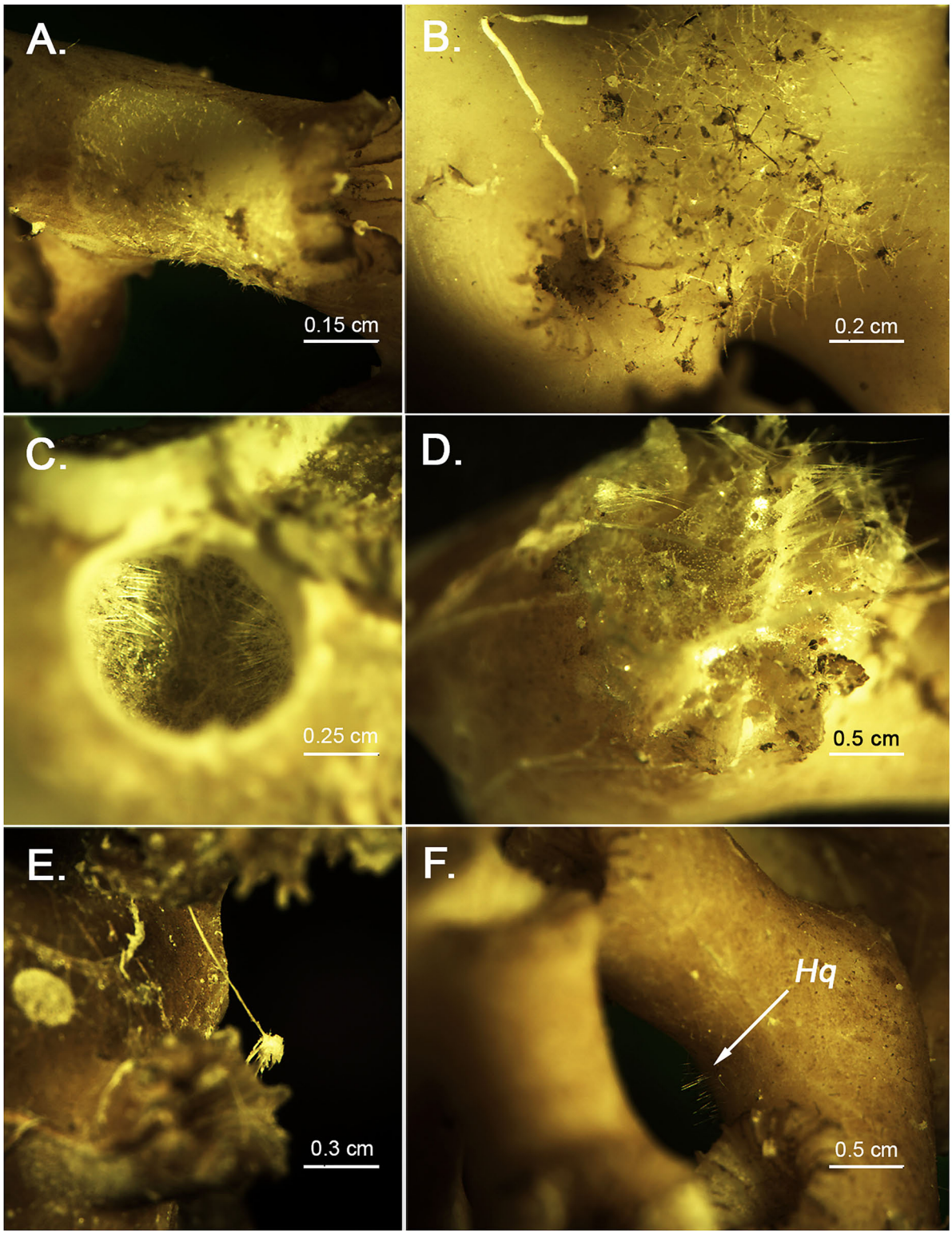

FIGURE 3 | Close up of several sponge species growing onto the *Madrepora* rubble **(A)** holotype of *Hamacantha* (*Hamacantha*) *hortae* sp. nov. **(B)** Individual of *Tetrodictyum reiswigi*. **(C)** Sphincter caused by the boring sponge *Siphonodictyon infestum*, known to erode the calcareous skeleton of several CWC species. **(D)** *Poecillastra taviani* individual growing inside a dead polyp. Interestingly enough, and despite the huge number of individuals encountered (over 70), practically all individuals dwelled exclusively inside the polyps, which might be interpreted as a niche preference for cavities and other burrows. **(E)** Individual of the carnivorous sponge *Lycopodina hypogea*, which had been previously recorded in the area associated with marine debris (Santín et al., 2020a). **(F)** Encrusting individual of *Hymedesmia* (*Hymedesmia*) *quadridentata,* with a clear hispidation visible to the naked eye.

and from which enough material was collected to allow for their proper identification and description. Several other potential new or rare species were collected, yet the scarcity of the material did not allow for a proper taxonomical characterization of the samples. Acronyms used for the examined material correspond with those on the **Supplementary Material 1**, were additional information is provided for each specimen.

Class DEMOSPONGIAE Sollas, 1885
SubClass Heteroscleromorpha Cárdenas et al., 2012
Order HAPLOSCLERIDA Topsent, 1928
Family CHALINIDAE Gray, 1867
Genus *Haliclona* Gray, 1841

Haliclona (*Flagellia*) *hiberniae* van Soest, 2017

Material examined: *H.* (*F.*) *hiberniae*: Hh_1; Hh_2; Hh_3; Hh_4; Hh_5; Hh_ 6. *Haliclona* (*Reniera*) sp.: HRsp_1. *Haliclona* sp. Hsp_1.

Additional comparative material: *Haliclona* (*Flagellia*) sp., Cap de Creus, north-western Mediterranean Sea (42°20′37.5″N 3°19′50.8″E), ca. 120 m depth, collected by dredging by local fishermen attached to a rock, Summer 2019.

Diagnosis:

Small, beige, cushion-shaped sponges, growing attached to coral rubble. They usually present a roundish body (ca. 10 mm × 5 mm) with a clear osculum more or less located at the center of the sponge, which might be absent or inconspicuous in smaller individuals. The sponge is rather lax, with a clearly visible reticulation of interconnected fibers and a hairy appearance due to projecting spicules.

Skeleton: Rather confused ascending paucispiculate tracks of megascleres connected by single spicules (**Figure 4**), with sponging being only visible at the nodes. Microscleres are numerous, arranged without any discernible pattern, yet mostly concentrating toward the spicular tracts.

Spicules: Oxeas: mostly straight or slightly curved, with acerate ends (330 – *384* ± 30.7 – 434.4 × 6 – *11.1* ± 1.3 – 14 μm). Flagellosigma I (**Figure 4**, F1): Clearly asymmetrical, with one side being larger than the other, yet the degree of it is subjected to individual variability. Additionally, the larger shaft tends to be more straight compared to the shortest side, which describes a more pronounced curvature. The tips are both recurved, with the shortest end's tip being gently curved compared with the larger tip ending, which is more abruptly recurved, as if it were a hook (86 – *95.8* ± 4.9 – 105.2 μm). Flagellosigma II (**Figure 4**, F2): similar to flagellosigma I, the main difference being their size (27.5 – *53* ± 8.4 – 76.2 μm). Sigma I: symmetrical, describing a gentle curvature (51 – *59.1* ± 2.7 – 64.4 μm). Sigma II: smaller than sigma I, and describing a deeper curve when compared (20.6 – *32.9* ± 6.9 – 41 μm).

Remarks:

The subgenus *Flagellia* van Soest, 2017 was recently erected to encompass all *Haliclona* species which shared the possession

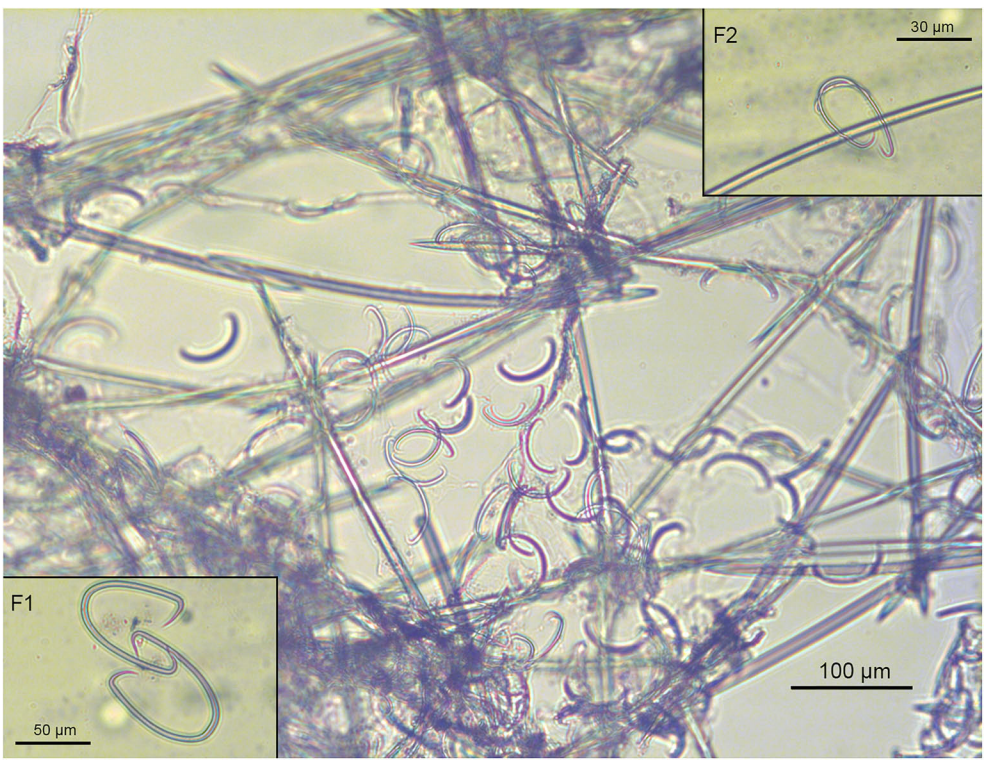

FIGURE 4 | *Haliclona* (*Flagellia*) *hiberniae* spicular set and skeletal arrangement as seen with an optical microscope. The skeleton is formed by paucispiculated tracts of oxeas, with abundant sigmas and flagelosigmas (F1 and F2), both in two categories. Scale bars: General, 100 μm; F1, 30 μm and F2, 50 μm.

of flagellosigmas, a unique sigma-like spicule with asymmetrical ends and a more or less ovoid shape (van Soest, 2017). From all their current accepted species, only three are present in the North Atlantic area (**Table 2**). From those, *H.* (*F.*) *xenomorpha* has two categories of oxeas and stout flagellosigmas (Dinn, 2020), whereas *H.* (*F.*) *porosa* possess a single flagellosigma and sigma categories as opposed to *H.* (*F.*) *hiberniae* (van Soest, 2017), which possess two of each (**Table 2**). As so, while *H.* (*F.*) *xenomorpha* is easily told apart from its North Atlantic counterparts and the current material (Dinn, 2020), both *H.* (*F.*) *porosa* and *H.* (*F.*) *hiberniae* have been described from CWC environments, and the size range of *H.* (*F.*) *porosa* flagellosigmas' encompasses both flagellosigma categories in *H.* (*F.*) *hiberniae*, being told apart from subtle differences in overall shape and tip curvature (van Soest, 2017). Nevertheless, in *H.* (*F.*) *porosa* sigmas appear in a single category and are consistently rare (van Soest, 2017), whereas in the examined specimens they are abundant and clearly divisible in two categories (**Figure 4**), for which the examined specimens are here assigned to *H.* (*F.*) *hiberniae*.

While recently described, *H.* (*F.*) *hiberniae* had long been recorded from the Atlanto-Mediterranean region under the name of '*Gellius flagilifer*' and '*Gellius vagabundus*' (Babiç, 1922; Vacelet, 1969), and it is plausible that several Mediterranean records for said species correspond in fact to *H.* (*F.*) *hiberniae* (van Soest, 2017). While the current specimens represent the first confirmed records for the Spanish Mediterranean waters, '*Gellius flagilifer*' had been previously recorded from the Alboran Sea (Sitjà and Maldonado, 2014), the Catalan coast (Bibiloni, 1981), and the Balearic Archipelago (Bibiloni, 1990), with the Alboran Sea records already being suspected to correspond to *H.* (*F.*) *hiberniae* (van Soest, 2017). Regarding the Catalan and Balearic records, both seem to fit well within *H. (F.) hiberniae*, with two clear sigma and flagellosigma categories, all within size range (Bibiloni, 1981, 1990). Nevertheless, an additional *Haliclona* (*Flagellia*) sp. sample examined from the Catalan continental shelf, while also possessing two categories of sigma and flagelosigmas, presented differences with the *H.* (*F.*) *hiberniae* samples from the CWC environments, mainly in shape (heavily encrusting and spinny, vs. cushion shaped bodies) and stouter, larger oxeas (ca. 500 × 15 μm). As so, older records for *G. flagilifer* and *G. vagabundus* from shallow Mediterranean areas might correspond to a yet undescribed *Haliclona* (*Flagellia*) species, close to *H.* (*F.*) *hiberniae,* for which their assignment to the later should be taken with caution until further data can be obtained.

Finally, in the Atlantic the species has been mostly reported from CWC communities, were it seems to be fairly abundant (van Soest, 2017). Nevertheless, the species seems to be less abundant in the Mediterranean CWC communities, with only four other records, three as *G. flagilifer* (Vacelet, 1969; Longo et al., 2005; D'Onghia et al., 2015) and one as *H.* (*F.*) cf. *hiberniae* (Bertolino et al., 2019) reported. Nevertheless, it is possible that more records will surface in other CWC communities across the Mediterranean once their accompanying fauna is properly inventoried.

Order MERLIIDA Vacelet, 1979
Family HAMACANTHIDAE Gray, 1872
Genus *Hamacantha* Gray, 1867

Hamacantha (*Hamacantha*) *hortae* Santín, Grinyó, Uriz, and Gili sp. nov.

Material examined: *H.* (*H.*) *hortae* sp. nov.: *Holotype* – MZB 2020-0967 – Blanes Canyon, north-western Mediterranean Sea (41°37′642′′N 02°51′426′E), 'ABIDES' survey, ca. 600 m depth, 2018; MZB 2020-0927 – slide of the holotype. *Paratypes* – MZB 2020-0968 – 1 individual; MZB 2020-0927 – microscopic slide of MZB 2020-0968; MZB 2020-0977 – 2 individuals; all attached to *Madrepora* rubble, same location as the holotype. *Hamacantha* (*Hamacantha*) *azorica* Topsent, 1904: Ha_1; Ha_2; Ha_3. *Hamacantha* (*Hamacantha*) *johnsoni* (Bowerbank, 1864): Hj_1; Hj_2; Hj_3; Hj_4.

Diagnosis:

Small encrusting sponge (**Figure 3A**; all examined species less than ca. 1 cm^2), with a smooth, sparsely lumpy surface. No

TABLE 2 | Comparative table between the North Atlantic *Haliclona (Flagellia)* species, including the locality (Loc.) and depth of the sample, as well as the measurement of their spicular complement.

Species	Loc./Depth	Oxea	Flagelosigma	Sigma
Haliclona (Flagellia) hiberniae van Soest, 2017	Rockall Bank, Ireland[1]: */ 560 m	288 – *367* – 419 × 6 – *11.1* – 14 μm	**(I)** 64 – *104* – 159 μm **(II)** 13 – *29.5* – 55 μm	**(I)** 53 – *76* – 92 μm **(II)** 28 – *33.5* – 39 μm
	Blanes Canyon, Spain[2]/ ca. 700 m	330 – *384* ± 30.7 – 434.4 × 6 – *11.1* – 14 μm	**(I)** 86 – *95.8* ± 4.9 – 105.2 μm **(II)** 27.5 – *53* ± 8.4 – 76.2 μm	**(I)** 51 – *59.1* ± 2.7 – 64.4 μm **(II)** 20.6 – 32.9 ± 6.9 – 41 μm
Haliclona (Flagellia) porosa (Fristedt, 1887)	Barents Sea[1]/ca. 250 m	243 – *271* – 297 × 8 – *9.7* – 12 μm	48– *82* – 108 μm	45 – 48 μm
	Mauritania[1]/114 m	267 – *307* – 333 × 8.5 – 11.2 – 13 μm	57 – *109* – 156 μm	40 – *51* – 61 μm
	Northern Baffin[3] Bay/333 m	250 – *282* – 314 × 11 – *14* – 16 μm	38 – *58* – 70 μm	60 – 63 μm
Haliclona (Flagellia) xenomorpha Dinn, 2020	Gulf of St. Lawrence[3]: */69 m	**(I)** 250 – *272* – 298 × 12 – *13* – 17 μm **(II)** 183 – *219* – 245 × 3.7 – *6.1* – 9 μm	**(I)** 56 – *68* – 108 μm **(II)** 32 – *51* – 95 μm	39 – *58* – 82 μm

*Numbers after Locality indicate the reference for each sample; * indicates this is the holotype of the species.*
(1) van Soest (2017); (2) Present study; (3) Dinn (2020).

oscula could be observed. The ectosome is translucent, which allows to easily distinguish the megascleres at naked eye. Color bright white when dry.

Skeleton: The ectosome is frail, translucent and easily detachable, consisting on a loose tangential reticulation of oxeas, with the occasional presence of diancistras. On the contrary, megascleres on the choanosome are arranged in tracts, which occur both parallel and perpendicular to the ectosome, occasionally traversing it. Tylostyles are present in the form of exotyles on the perpendicular tracts. Diancistras occur along the choanosomal tracts without any discernible patter. All samples had low spicular density, with huge spaces between tracts.

Spicules: Tylostyles (**Figures 5**, **6A**): Robust, straight with cleat marked tyles and an acerate end, their width slightly decreases while approaching the acerate tip. They occur in low numbers and exclusively in the choanosomal tracks, mostly perpendicular to the sponge's surface, with the tyle point toward it, becoming exotyles (369.7 – *452* ± 60 – 573.4 × 4.9 – *5.7* ± 0.9 – 7.3 μm). Oxea I (**Figures 5**, **6B**): Robust, with acerate ends, on very rare occasions, telescoped. They are usually slightly bent at two thirds of its length (348.2 – *410.3* ± 55 – 567.2 × 4.9 – *6.3* ± 0.8 – 8.7 μm). Oxea II (**Figures 5**, **6C**): Smaller and slender than oxea I, with a somewhat more prominent bending that the later. The least abundant of the two oxea categories, could only be found in the holotype and two out of three of the paratypes (91.9 – *188.2* ± 49.9 – 235.2 × 2.9 – *3.7* ± 0.6 – 4.4 μm). Diancistra I (**Figures 5**, **6D,E,G**): Typical of the genus, with and stout, straight shaft, with recurved hook-like endings. One of the endings presents a gentler curvature, with a clear rounded notch and a slightly bigger hook-like end, whereas the other presents a more acute angle, with a smaller, elongated notch, and a slightly slimmer hook-like end. The inner side of the shaft presents a subtle depression on the middle, with fimbriae on both sides, with the fimbriae closer to the rounded-notch end usually resembling a blade. There is a certain degree of variation on said pattern, as diancistras with both ends "rounded-notched" occasionally occur. Finally, both ends are not on the same plane as the shaft, but usually bent (ca. 45° in opposing directions; **Figure 6G**) in regards to it (123 – *139* ± 11.1 – 159.2 μm). Diancistra II (**Figures 5**, **6F**): With a strongly bent shaft (boomerang-like), with asymmetrical, recurved acerate ends. One of them is "sigma-like," with a gentle curvature and a long, acerate tip, while the other one is considerably smaller, describing a markedly narrow curvature. They are considerably scarce, with no more than 20 observed per specimen (33.8 – *35.8* ± 1.9 – 37.5 μm).

Etymology:

The name *hortae* is chosen in honor of the neighborhood of Horta (Catalonia, Spain). Known at least since the early X century, it was an independent village until 1904, when it got annexed to Barcelona. Yet, it still retains nowadays the aura of

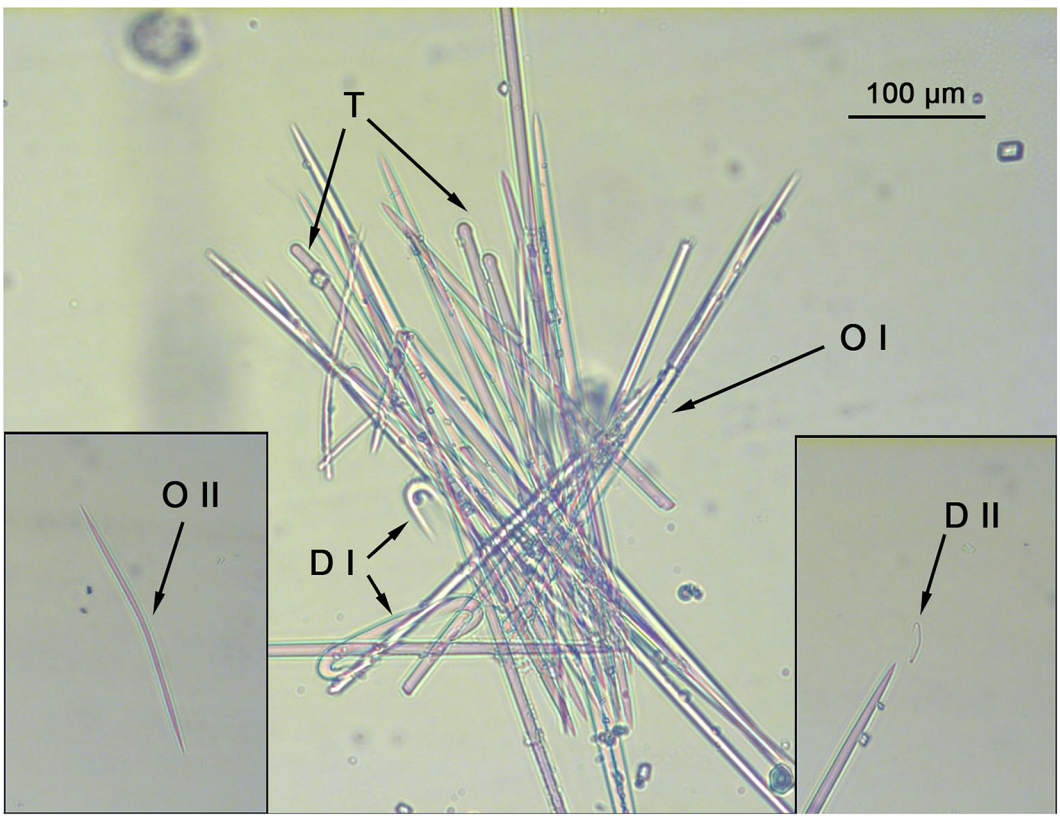

FIGURE 5 | *Hamacantha* (*Hamacantha*) *hortae* sp. nov. spicular set. The skeleton is formed by loose tracts of tylostyles (T) and oxeas in two size categories (O I and O II), with diancistras in two size categories (D I and D II) scattered around. Scale bar, 100 μm.

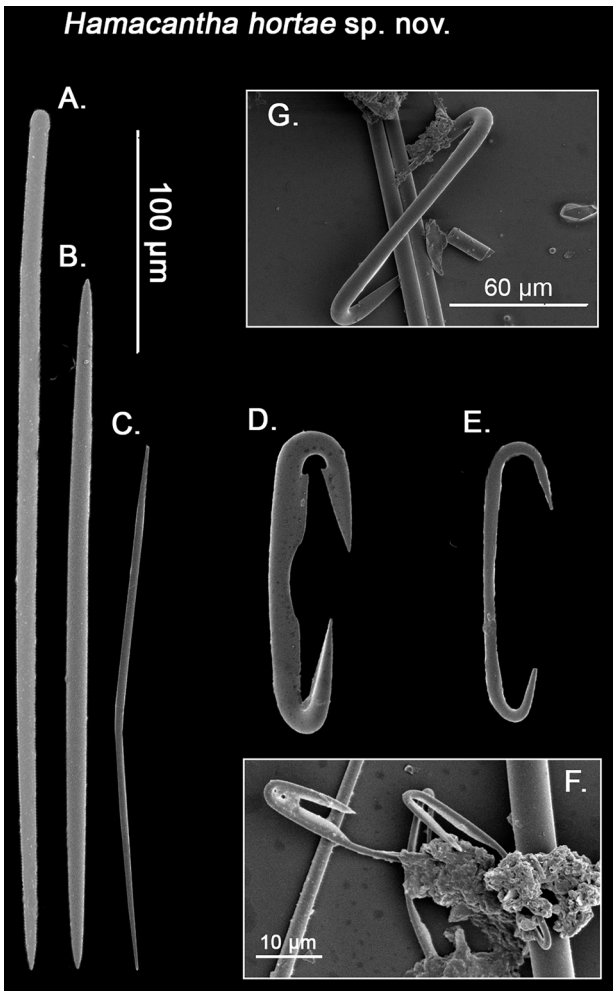

FIGURE 6 | SEM imagining of *Hamacantha* (*Hamacantha*) *hortae* sp. nov. spicular set. **(A)** Tylostyle; **(B)** Oxea I; **(C)** Oxea II; **(D)** Diancistra I; **(E)** developmental form of diancistra I, still lacking the hook-like expansions; **(F)** Diancistra II and **(G)** Lateral view of Diancistra I. Scale bar for **(A–E)** 100 μm; scale bar for **(F)** 20 μm; and scale bar for **(G)** 60 μm.

being a village within a city, exemplified by one of its popular mottos "*Horta no és ni serà mai Barcelona*" (Horta is not and will never be Barcelona).

Remarks:

Characterized by the possession of diancistras, the genus *Hamacantha* is easily identifiable and relatively common within deep-sea and other dark habitats around the world (Hajdu and Castello-Branco, 2014; Hajdu et al., 2015; Ise et al., 2019). Currently, the genus is classified in three subgenera, *Hamacantha* (*Hamacantha*), *Hamacantha* (*Vomerula*), and *Hamacantha* (*Zygherpe*), which are told apart by their main megascleres (Oxea vs. Style vs. Tylostyle). In this sense, *H.* (*H.*) *hortae* sp. nov. would fit within the *Hamacantha* subgenus, where it is easily distinguishable from all other known species of *Hamacantha (Hamacantha)* due to its lack of sigmas and the possession of two categories of oxeas, and the additional presence of tylostyles as megascleres (**Table 3**). While *H.* (*H.*) *hortae* sp. nov. has been here assigned to *Hamacantha* (*Hamacantha*) as oxeas are its most abundant megasclere category, the species represents a crack on the current *Hamacantha* subgeneric classification (Hajdu, 2002), as the presence of tylostyles is the diagnostic feature for the subgenus *Zygherpe* (Hajdu et al., 2015). In this sense, tylostyle bearing *Hamacantha* species are considerably rare, with only two species known so far, both occurring in the Pacific (Laubenfels, 1932; Hajdu et al., 2015). Yet, their tylostyles resemble those of *H.* (*H.*) *hortae* sp. nov., which might suggest a certain degree of relationship between species. Nevertheless, *Hamacantha* subgenus was erected based on classification convenience and do not necessarily represent a monophyletic clade (Hajdu, 2002; Hajdu et al., 2015). While currently there are no molecular data for any *Hamacantha* species, *H.* (*H.*) *hortae* sp. nov. seems to reinforce such view and, additionally, would support a closer relationship between *Hamacantha* (*Zygherpe*) and *Hamacantha* (*Hamacantha*) species than with *Hamacantha* (*Vomerula*), despite the later possessing styles as main megascleres.

Order POECILOSCLERIDA Topsent, 1928
Family CLADORHIZIDAE Dendy, 1922
Genus *Cladorhiza* Sars, 1872
Cladorhiza cf. *abyssicola* Sars, 1872

Material examined: *C.* cf. *abyssicola*: Ca_1

Diagnosis:

Stipitate sponge with branching lateral processes. Color in spirit is translucent yellow.

Skeleton: The sponges' body and branches are formed by a dense axis of mycalostyles, whereas anchorate anisochelae and sigmas are found scattered across the whole body of the sponge, with sigmas being less abundant that chelae.

Spicules: Mycalostyles (**Figure 7A**): Almost straight, usually in the form of styles with a blunt end. (290.1 – *329.3* ± 32.1 – 390 × 8.9 – *10.2* ± 2.1 – 15.3 μm). Anisochelae (**Figure 7B**): chelae with clear unequal ends, the bigger one with well-formed acerate alae and visible fimbriae attached to the shaft, whereas the other end consists of five spaced underdeveloped alae, in the form of claw-like appendages. (12.5 – *21.4* ± 1.5 – 23.9 μm). Sigmas (**Figure 7C**): Large sigmas, with a C-like contour and acerate tips (72.3 – *85.3* ± 7.7 – 95.4 μm).

Remarks:

While currently there are ca. 200 carnivorous sponge species accepted worldwide (van Soest et al., 2021), only two have been recorded in the Mediterranean so far; *Lycopodina hypogea* (Vacelet and Boury-Esnault, 1996) and the North Atlantic *C. abyssicola,* easily told apart from each other based on their external appearance and spicular set. *Cladorhiza abyssicola* is far less abundant than *L. hypogea*, having only been found five times in the Mediterranean prior to this study (Babiç, 1922; Vacelet, 1969; Boury-Esnault et al., 1994; Fourt et al., 2017; Hestetun et al., 2017), being this its first report for the Catalan coast. Nevertheless, other North Atlantic *Cladorhiza* are very close to or practically indistinguishable from *C. abyssicola*

TABLE 3 | Comparative table between the North Atlantic *Hamacantha (Hamacantha)* species, including the locality (Loc.) and depth of the sample, as well as the measurement of their spicular complement.

Species	Loc./Depth	Oxea	Tylostyle	Dianciaster	Sigmas (S)/Toxas (T)
Hamacantha (Hamcantha) boomerang Hajdu and Castello-Branco, 2014	Campos Basin, Brazil[1]: */607 m	271 – *462.3* – 630 × 7 – *12.1* – 18 μm	–	**(I)** 125 – *141.4* – 155 μm **(II)** 45 – *57.9* – 69 μm **(III)** 20 – *23.3* – 29 μm	**(T)** 58 – *68.6* – 82 μm
Hamacantha (Hamacantha) johnsoni (Bowerbank, 1864)	Cassidaigne Canyon, France[2]/170 – 300 m	340 – 530 × 7.5 – 10 μm	–	**(I)** 100 – 140 μm **(II)** 22 – 23 μm	**(S)** 20 – 30 μm
	English Channel[3]/ca. – 450 – 1300 m	450 – *500* – 600 μm	–	**(I)** 145 – 160 μm **(II)** 30 – 35 μm	**(S)** 20 – 25 μm
	Blanes[4]/ca. 700 m	391 – *619* – *727* × 5.1 – *7.9* – 10.2 μm	–	**(I)** 158 – *181.3* – 199.2 μm **(II)** 37.3 – *41.5* – 44.8 μm	**(S)** 20.5 – *30.3* – 38.9 μm
Hamacantha (Hamacantha) lundbecki Topsent, 1904	Cassidaigne Canyon, France[2]/210 – 310 m	150 – 245 × 5 – 10 μm	–	**(I)** 130 – 170 μm **(II)** 10 – 27 μm	**(S)** 20 – 35 μm
Hamacantha (Hamacantha) schmidtii (Carter, 1882)	Bermuda[1]: */227 m	390 – *416.3* – 495 × 9.4 – *10.8* – 12.8 μm	–	**(I)** 109 – *118.1* –124 μm **(II)** 44 – *50* – 54 μm **(III)** 26 – *36.5* – 41 μm	–
Hamacantha (Hamacantha) hortae sp. nov.	Blanes[4]/ca. 700 m	**(I)** 348.2 – *410.3* ± 55 – 567.2 × 4.9 ± 1.1 – *6.3* – 8.7 μm **(II)** 91.9 – *188.2* ± 49.9 – 235.2 × 2.9 – *3.7* ± 0.6 – 4.4 μm	369.7 – *452* ± 60 – 573.4 × 4.9 – *5.7* – 7.3 μm	**(I)** 123 – *139* ± 11.1 – 159.2 μm **(II)** 33.8 – *35.8* ± 1.9 – 37.5 μm	–

*Upper numbers after each locality indicate the reference from where the data is taken from; * indicates this is the holotype of the species.*
(1) Hajdu and Castello-Branco (2014); (2) Vacelet (1969); (3) Stephens (1921); (4) Present study.

(Göcke et al., 2016; Hestetun et al., 2017), with the possibility of 'cryptic *Cladorhiza*' within Mediterranean records having already been noted (Fourt et al., 2017). Overall, a 'rare' species record for the Mediterranean basin, which suggests further investigation including molecular techniques.

Family HYMEDESMIIDAE Topsent, 1928
Genus *Acanthancora* Gray, 1867

Acanthancora schmidti (Topsent, 1898)

Material examined: *A. schmidti*: As_1; As_2; As_3; As_4; As_5; As_6; As_7; As_8; As_9; As_10; As_11; As_12; As_13; As_14; As_15; As_16; As_17; As_18; As_19; As_20; As_21.

Diagnosis:

Small smooth encrusting sponge (ca. 1 cm^2), without apparent oscula or any other distinguishing external characteristics. Color dull white, "bone-like" when dry.

Skeleton: The ectosome consists of a tangential layer of strongyles, without a clear distinguishable organization, alongside a relatively dense layer of chelae. The choanosome consists of erect acanthostyles in a single category attached to a basal layer of spongin.

Spicules: Strongyles (**Figure 8A**): Tornotes modified into strongyles, with a thin, straight shaft with polytylote processes and rounded ends. Styloid modifications are rare, but present in some individuals (167.2 – *203.2* ± 10.1 – 240 × 2.5 – *2.9* ± 0.8 – 4.2 μm). Acanthostyles (**Figure 8B**): Small, stout acanthostyles, with spines all over the shaft and head, and an acerate end. The head's spines are robust and round-ended, whereas the shaft's ones have a hook-like appearance, with the hook always pointing toward the head. Two categories could eventually be distinguished, yet there are no morphological distinctive traits between bigger and smaller acanthostyles (105 – *125.5* ± 23.6 – 253 × 12.2 – *14.3* ± 1.7 – 15.1 μm). Chelae (**Figure 8C**): Peculiar, strongly acanthose chelae, with spines terminating in rounded to acerate ends, with a prevalence for the former. They possess four teeth, with the central two possessing two considerably developed rounded alae each, whereas the two lateral teeth are reduced to curved expansions with a thinner shaft and short, small rounded alae in comparison. The chelae's shaft is robust and heavily spinned on its external side, with spine morphology varying from smaller, rounded wart-like ones to wide, stout spines with almost acerate ends. Very regular in size (31 – *35.1* ± 0.5 – 35.9 μm). Chiastosigmas (**Figure 8D**): small sigma derivative, with 4 – 6 rays, typically 5, protruding from a central disk. The shafts are curved as in forming a sphere, giving the chiastosigmas the appearance of an empty ball when looked from the side. In 4-rayed morphs, the shafts are symmetrical with each other, whereas in 5- and 6- rayed morphs, this symmetry is lost. The central disk varies from a flat, ovoid plate to a subtle sphere. Finally, the shafts inner face is almost entirely serrulated except for its basal area, while also ending with heavily recurved tips, as in a claw (5 – *6.3* ± 0.7 – 7.4 μm).

Remarks:

The genus *Acanthancora* is easily recognizable due to their peculiar acanthose chelae, a characteristic only shared with the ill-known *Pseudohalichondria*. Nevertheless, the latter refers to massive specimens with plumose skeleton and lacking acanthostyles, whereas *Acanthancora* possess a hymedesmid skeletal organization and acanthostyles, easily telling them apart (van Soest, 2002).

In his original and subsequent descriptions, Topsent noted the presence of chiastosigmas as a diagnostic character for

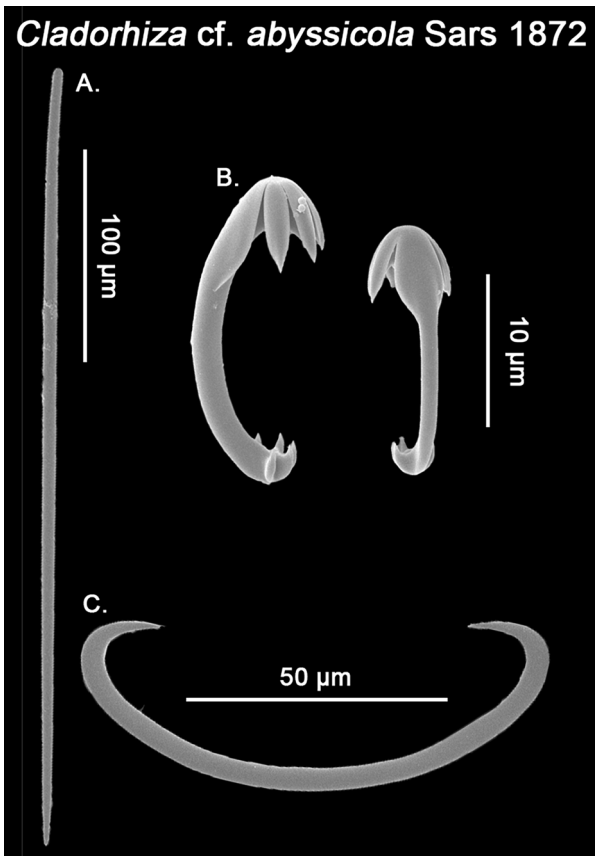

FIGURE 7 | SEM imagining of *Cladorhiza cf. abyssicola* spicular set. **(A)** Mycalostyes; **(B)** Anchorate anisochelae; **(C)** Sigma. Scale bar for **(A)** 100 µm; scale bar for **(B)** 10 µm; and scale bar for **(C)** 50 µm.

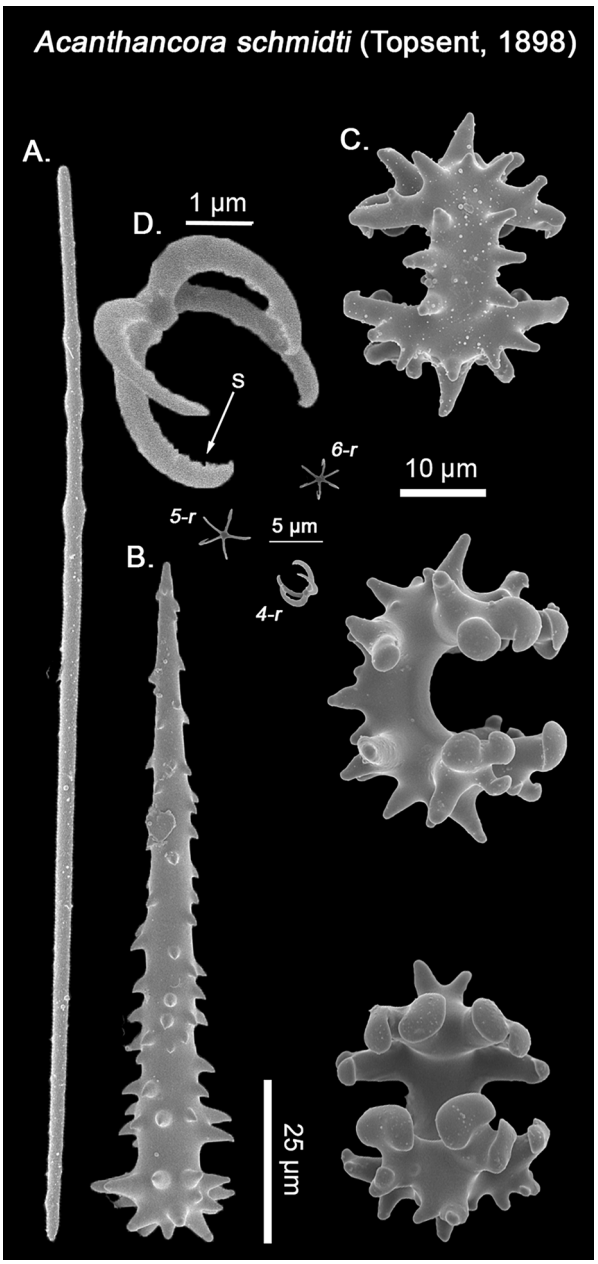

FIGURE 8 | SEM imagining of *Acanthancora schmidti* spicular set. **(A)** Strongyle with polytylote processes; **(B)** Acanthostyle. **(C)** Rear, lateral and frontal view of the acanthose chelae; **(D)**. Four-rayed (*4-r*), five-rayed (*5-r*), and six-rayed (*6-r*) chiastosigmas, with a close up of a four-rayed chiastosigma, with visible serrulated shafts (S). Scale bar for **(A–C)** 25 µm; Scale bar for **(D)**, close up chiastosigmas 1 µm, and scale bar for **(D)**, general view of the chiastosigmas types, 5 µm.

Acanthancora (Topsent, 1904, 1928), yet in the rexamination of *Acanthancora* type material no chiastosigmas could be found (van Soest, 2002). After careful examination of the current material, no chiastosigmas could be observed with an optic microscope but become apparent with SEM imaging, being almost as abundant as the chelae. Thus, chiastosigmas do appear to be proper for the species, yet a re-examination of the type material of all other known *Acanthancora* would be necessary to determine if it is a shared trait for the genus, or just species-specific. While this represents the first record for *Acanthancora* in the Mediterranean, two other species are known to occur in North Atlantic waters. From those, *A. schmidti* is distinguished from *Acanthancora aenigma* (Lundbeck, 1910) due to the bigger size of the ectosomal tornotes and lack of chiastosigmas in the later, yet the species remains insufficiently described (Lundbeck, 1910) and its synonymy with *A. schmidti* cannot be ruled out in the future. Concerning *A. schmidti* and *Acanthancora clavatancora* Topsent, 1927, Topsent (1928) mainly distinguished *A. clavatancora* as possessing polytylote styles and chelae with rounded spines, whereas, in contrast, *A. schmidti* possessed ectosomal polytylote strongyles and chelae with acerate spines, with otherwise all spicules in a similar size-range category (**Table 4**). Nevertheless, the analyzed material possessed both ectosomal polytylote strongyles, rarely styloids, and chelae with rounded spines, blurring the separation between both species. In light of these findings, it seems there is no longer any clear difference that would justify

TABLE 4 | Comparative table between the North Atlantic *Acanthancora*, including the locality (Loc.) and depth of the sample, as well as the measurement of their spicular complement.

Species	Loc./Depth	Tornote	Acanthostyle	Chelae	Other
Acanthancora aenigma (Lundbeck, 1910)	Denmark Strait[1]: */566 m	320 – 430 × 6 – 7 μm	130 – 340 × 14 – 21 μm	28 – 35 μm	–
Acanthancora clavatancora Topsent, 1927	Azores[2]/1331 m	**(Sty)** 205 – 260 × 4 – 5 μm	130 – 210 μm	35 μm	**(Ch)** present
Acanthancora schmidti (Topsent, 1898)	Azores[3]/349 – 599 m	**(Str)** 200 – 220 × 3 μm	112 – 260 × 7 – 15 μm	Present [1"]	**(Ch)** 7 – 8 μm
	Blanes Canyon, Spain[3]/ ca. 700 m	**(Str)** 167.2 – *203.2* ± 10.1 – 240 × 2.5 – *2.9* ± 0.8 – 4.2 μm	105 – *125.5* ± 23.6 – 253 × 12.2 – *14.3* ± 1.7 – 15.1 μm	31 – *35.1* ± 0.5 – 35.9 μm	**(Ch)** 5 – *6.3* ± 0.7 – 7.4 μm

*Superscript numbers after each locality indicate the reference from where the data is taken from; * indicates this is the holotype of the species. Styles (Sty), Storngyles (Str), Chiastosigmas (Ch). Superscript numbers followed by two apostrophes indicate footnotes.*
(1) Lundbeck (1910); (2) Topsent (1928); (3) Topsent (1904); (4) Present study.
***(1")** Topsent (1904) gave the internal aperture (12–14 μm) and the shaft's width from a frontal (5 μm) and lateral (7 μm) views, but did not mention the total length of the chelae. Said measurement have also been recorded for the analyzed material, and are in accordance with Topsent's records.*

both being considered separate species, as already suggested by van Soest (2002).

Genus *Hymedesmia* Gray, 1858

Hymedesmia (Hymedesmia) quadridentata Cardone et al., 2019.

Material examined: *H.* (*H.*) *quadridentata*: Hq_1; Hq_2; Hq_3; Hq_4. *Hymedesmia* sp.: Hsp_1; Hsp_2; Hsp_3; Hsp_4. *Hymedesmia* (*Hymedesmia*) cf. *mutabilis* (Topsent, 1904): Hm_1; Hm_2; *Hymedesmia* (*Hymedesmia*) cf. *plicata* Topsent, 1928: Hp_1.

Diagnosis:

Heavily encrusting sponge, extremely hispid due to projecting acanthostyles protruding the sponge (**Figure 3F**). Color gray-white when dry. Smaller individuals might appear as translucent-gray stains, slightly hispid/velvety at the binocular microscope, which can be easily overlocked as discolorations of the skeletal framework if it were not by the apparent hispidation.

Skeleton: Typical from the genus (**Figure 9**), with acanthostyles single erect on the substrate, with tylostyles as ectosomal spicules, arranged parallel to the sponge surface. Chelae and sigmas concentrate toward the base of the sponge.

Spicules: Tylostyles: Slightly curved, with asymmetrical inflated ends. They appear to be scarce, as less than 10 could be measured (188 – *195.2* ± 17.6 – 215 × 2.4 – *3.9* ± 1.7 – 6.7 μm). Acanthostyles I (**Figure 9**): mostly straight, with an acerate end. They possess round, spinose heads, with most spines appearing blunt or with roundish terminations. Contrary to the head, the shaft and acerate tip are almost devoid of spines (368.5 – *600.5* ± 95.2 – 799.2 × 11.6 – *17.2* ± 2.4 – 19.4 μm). Acanthostyles II (**Figure 9**): smaller in size than the acanthostyles I and, contrary to these, spines are common from the head to the middle of the shaft (124.3 – *185.7* ± 42.9 – 319.2 × 8.7 – *11.2* ± 2.9 – 17.5 μm). Acanthostyles III (**Figure 9**): the smallest and most abundant acanthostyle category, identical in shape to the other two, but contrary to these they are completely spinned (55 – *74.3* ± 22.1 – 151.5 × 6.3 – *8* ± 1.2 – 10.7 μm). Chelae I (**Figure 9**): typical arcuate isochelae, with a curved shaft and three free alae (22.2 – *25.2* ± 1.7 – 28 μm). Chelae II (**Figure 9**): "C" shaped unguliferate chelae, with a curved shaft and four small unguliferous teeth on each end (21.8 – *25.1* ± 2.4 – 30.8 μm). Sigmas I (**Figure 9**): "C" shaped sigmas, rarely "S" shaped, with recurved ends. They are slightly asymmetrical, giving the impression that they don't bent on the middle of the shaft, but at 2/3 of its length (50 – *59.5* ± 5.6 – 75.5 μm). Sigma II (**Figure 9**): pretty much identical to Sigmas I, but smaller (7.3 – *12.5* ± 3.8 – 22.8 μm).

Remarks:

The genus *Hymedesmia* is amongst the most diverse within Porifera, and it is also recognized as one of the most abundant taxa in CWC environments (Goodwin et al., 2011). Nevertheless, from all known *Hymedesmia*, the presence of unguliferous chelae is a rare feature, shared by just a few species worldwide (Cardone et al., 2019). In the North Atlantic only three species, *H. (H.) mucronata*, *H. (H.) zetlandica,* and *H. (H.) quadridentata*, possess unguliferous chelae. From these, *H. (H.) mucronata* is only known from its type locality in the Azores, and widely differs from the present material in terms of spicular size while, at the same time, it only possesses a single category of sigmas (Topsent, 1904). On the other hand, both *H. (H.) zetlandica* and *H. (H.) quadridentata* are present in the Mediterranean CWC communities (Bertolino et al., 2019), yet *H. (H.) zetlandica* possesses a single category of sigmas and considerably smaller acanthostyles (van Soest, 2002), which clearly tells it apart from *H. (H.) quadridentata*. Contrary to *H. (H.) quadridentata*'s original description (Cardone et al., 2019) three acanthostyles categories could be differentiated in the present material, yet they would fit in range of the original two acanthostyles categories described, and wouldn't justify erecting a new species. Interestingly enough, *H. (H.) zetlandica*, possessing unguliferous chelae, is the type species of the genus *Hymedesmia*, yet barely no more than half-a-dozen other species share such characteristic. Additionally, the unguliferous chelae morphology widely varies between those *Hymedesmia* possessing such, with teeth ranging from two to four, and, in the case of *H. zetlandica*,

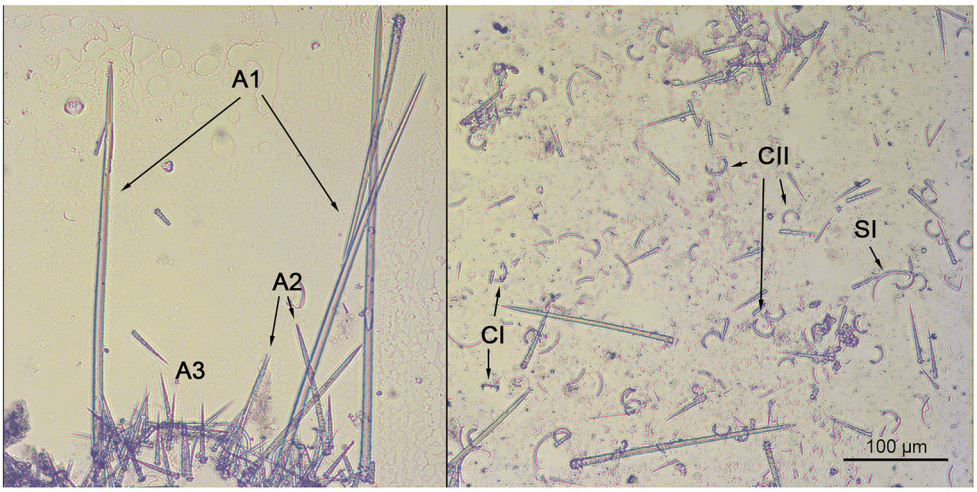

FIGURE 9 | *Hymedesmia* (*Hymedesmia*) *quadridentata* skeletal arrangement and spicular set. **Left:** Hymedesmoid skeleton, typical of the genus, with three acanthostyle categories (A1, A2, A3) erect on the substrate. **Right:** General view of *H.* (*H.*) *quadridentata* microscleres, including two categories of sigmas (SI and SII) and two categories of chelae (CI and CII), one of them with four unguliferous alae (CII). Scale bar 100 μm.

TABLE 5 | Comparative table between the North Atlantic *Hymedesmia (Hymedesmia)* species with unguliferous chelae, including the locality (Loc.) and depth of the sample, as well as the measurement of their spicular complement.

Species	Loc./Depth	Tylostles	Acanthostyles	Isochelae	Sigmas
Hymedesmia (Hymedesmia) quadridentata Cardone et al., 2019	north-east Sardinia[1]: */ca. 260 m	170 – *194* – 235 × 2.5 μm	**(I)** 265 – *390* – 550 × 10 – *15.3* – 20 μm **(II)** 55 – *124.2* – 215 × 7.5 – *9.2* – 12.5 μm	**(A)** 20 – *22* – 25 μm (**U[4]**) 17.5 – *22.3* – 25 μm	**(I)** 35 – *55.5* – 82.5 μm **(II)** 12.5 – *14.8* – 17.5 μm
	Blanes[2]/ca. 700 m	188 – *195.2* ± 17.6 – 215 × 2.4 – *3.9* ± 1.7 – 6.7 μm	**(I)** 368.5 – *600.5* ± 95.2 – 799.2 × 11.6 – *17.2* ± 2.4 – 19.4 μm **(II)** 124.3 – *185.7* ± 42.9 – 319.2 × 8.7 – *11.2* ± 2.9 – 17.5 μm **(III)** 55 – *74.3* ± 22.1 – 151.5 × 6.3 – *8* ± 1.2 – 10.7 μm	**(A)** 22.2 – *25.2* ± 1.7 – 28 μm (**U[4]**) 21.8 – *25.1* ± 2.4 – 30.8 μm	**(I)** 50 – *59.5* ± 5.6 – 75.5 μm **(II)** 7.3 – *12.5* ± 3.8 – 22.8 μm
Hymedesmia (Hymedesmia) mucronata (Topsent, 1904)	Azores[3]: */880 m	360 – 375 × 4 μm	**(I)** 300 – 500 × 4 μm **(II)** 120 μm	**(A)** 26 μm (**U[3]**) 26 μm	25 – 35 μm
Hymedesmia (Hymedesmia) zetlandica Bowerbank, 1864	Shetland[4]: *, United Kingdom	225 – 255 × 5 – 8 μm	80 – 145 × 10 –20 μm	**(A)** 20 – 30 μm (**U[2]**) 10 – 15 μm	40 – 70 μm

*Arcuate and unguliferous chelae are indicated as (A) and (U) respectively, while the upper number in the later indicates the number of teeth (U^3 or U^4). Upper numbers after each locality indicate the reference from where the data is taken from; * indicates this is the holotype of the species.*
(1) Cardone et al. (2019); (2) Present study; (3) Topsent (1904); (4) van Soest (2002).

being additionally spinned (**Table 5**). Currently, the genus *Hymedesmia* is mainly built around the shared possession of an "hymedesmiid skeleton," yet such character is believed to be linked with the encrusting habitus of most *Hymedesmia* rather than a real synapomorphy for the genus, which is already known to be polyphyletic (Redmond et al., 2013; Ríos et al., 2020). As so, the new discovery or rediscovery of more of these "deviant" *Hymedesmia*, specially once molecular data of such can be obtained, might eventually led to a complete reorganization of the genus.

Order SUBERITIDA Chombard and Boury-Esnault, 1999
Family HALICHONDRIIDAE Gray, 1867
Genus *Spongosorites* Topsent, 1896

Spongosorites cabliersi Santín, Grinyó and Lo Iacono sp. nov.

Material examined: *S. cabliersi* sp. nov.: *Holotype* – MZB 2020-0936 – Cabliers Coral Mound, western Alboran Sea (35°47′58″N 2°15′17″ W), 'MELCOR' survey, 340 m depth, 2012. *Paratype* – MZB 2020-0937 – Cabliers Coral Mound, western Alboran Sea (35°47′58″N 2°15′17″ W), 'MELCOR' survey, 340 m depth, 2012.

Diagnosis:

Both the holotype and paratype consist of fragments of a massive, lumpy sponge, with a smooth appearance. The sponge possesses a thin, translucid ectosome, firmly attached to the choanosome, and can only be peeled off as flakes. The choanosome is cavernous, with several openings of varying size. The sponge is hardly compressible. Color in spirit, orange to brown.

Skeleton: The ectosome is made of loose reticulation of strongyloxeas, parallel to the sponge's surface and without a clear organization. The choanosome on the other hand is of an 'halichlonoid' nature, densely packed with strongyleoxeas which occur in a rather confused manner, without a clear direction.

Spicules: Strongyleoxeas (**Figure 10**): Robust oxeas with blunt terminations (**Figure 10A**), which gives them appearance of strongyleoxeas, with a 'cigar-shaped' appearance. They are mostly straight, with a slight or subtle central bending, sometimes showing a subtle double bending toward the tips instead. They possess the same width across the spicule except for its terminations, which end in a characteristic short tapering, with either a blunt or a mucronate tip, typically with 1 to 2 tapering points (**Figure 10B**). Albeit very rare, true style or strongyle modifications might occur (194 – *349.2* ± 52.2 – 388 × 9.8 – *15.2* ± 4.2 – 19.4 μm). It is to be noted however, that while smaller spicules can be found, most of them fall between 320 – 360 μm size range.

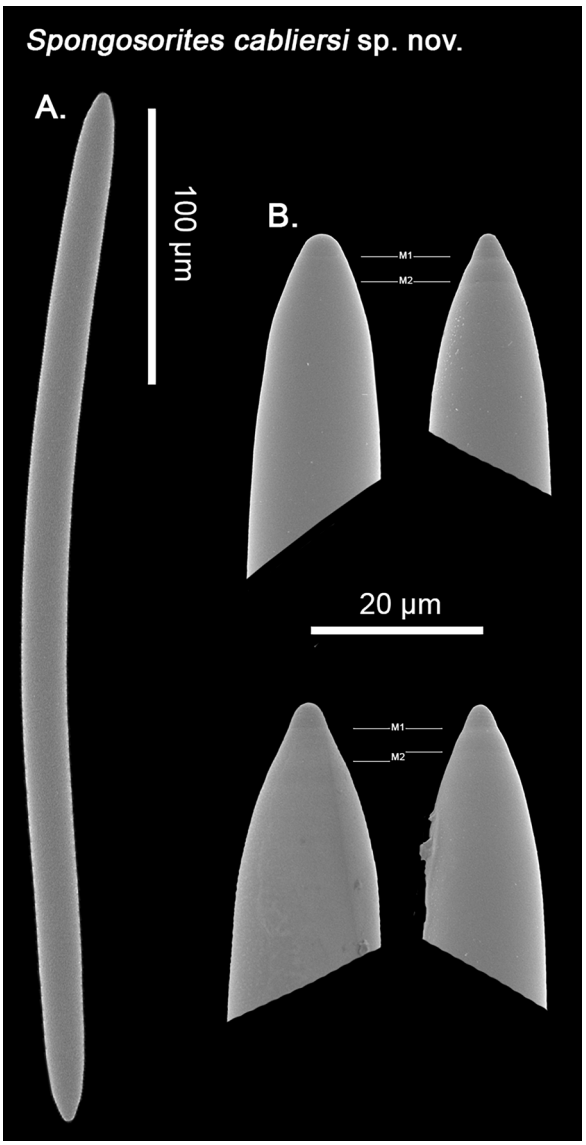

FIGURE 10 | SEM imagining of *Spongosorites cabliersi* sp. nov. spicular set. **(A)** General view of the strongyleoxeas. **(B)** Close up of the strongyleoxea's heads, with a more or less mucronated end, preceded by more two tapering points (M1 and M2), which might be more or less marked between individual spicules. Scale bar for **(A)** 100 μm; scale bar for **(B)** 20 μm.

Etymology:

The name *cabliersi* refers to the area in which the sample was collected, the Cabliers Coral Mound. This CWC reef is of special ecological relevance because of the large extension (at least 5.2 km) of coral communities found in exceptional thriving conditions and for their pristine state of conservation (Corbera et al., 2019).

Remarks:

The genus *Spongosorites* is closely aligned with *Topsentia*, with which it shares several diagnostic characters (Bertolino et al., 2015). In this sense, the current material has been assigned to *Spognosorites* due to the possession of bent oxeas and a smooth surface, with its only oxea category being smaller than 600 μm. Nevertheless, species differentiation with *Spongosorites* is hazardous, as it mostly relies on subtle differences in the spicules (Picton and Goodwin, 2007). In this sense, from all the described *Spongosorites* in the North Atlantic (**Table 6**), *Spongosorites cabliersi* sp. nov. differs from most of them in the possession of a relatively small single oxea category, with only another four species possessing a single oxea category in the same size range. From those, *Spongosorites calcicola* and *Spongosorites flavens* would be the closest to the current material, with *Spongosorites difficilis* and *Spongosorites coralliophaga* being told apart due to their possession of oxeas with long, accerate tampering ends (Lundbeck, 1902; Stephens, 1915). *Spongosorites calcicola* is so far only known to occur in shallow Irish muddy bottoms, and possesses oxeas with closely resemble those of *S. cablersi* sp. nov. being mostly straight or slightly bent, with blunt or mucronate endings (Picton and Goodwin, 2007). Nevertheless, they are described as possessing a proportional width to length ratio, whereas in *S. cabliersi* sp. nov. this is not the case, being of the same width regardless of the length of the spicules with, additionally, *S. cabliersi* sp. nov. strongyloxeas doubling in width those of *S. calcicola*. Finally, *S. calcicola* is said to possess numerous large oscula and a bright lemon color not lost when after preservation, none of which appears to be shared with *S. cabliersi* sp. nov. On the other hand, *S. flavens* is an ill-known species, being mostly known from Italian and Adriatic coasts (Pulitzer-Finali, 1983) and the Alboran Sea (Maldonado, 1992, 1993), thus co-occurring with *S. cabliersi* sp. nov. in the later. Nevertheless, its oxeas are defined as slightly fusiform, with frequent tetratological modifications (Pulitzer-Finali, 1983; Maldonado, 1993) not observed in *S. cabliersi* sp. nov. while, at the same time, they are also considerably thinner (**Table 6**). As so, *S. cabliersi* sp. nov. is characterized by a single straight to slightly bent strongyloxea size category with a constant, robust width, and blunt to mucronate, short-tapering endings, which tells it apart from all other North Atlantic *Spongosorites* described so far.

TABLE 6 | Comparative table between the Eastern North Atlantic *Spongosorites* species, including the locality (Loc.) and depth of the sample, as well as the measurement of their spicular complement.

Species	Loc./Depth	Oxeas
Spongosorites annandalei (Ferrer Hernández, 1923)	Santander[1]; */Unknown	**(I)** 400 – 800 × 12 μm **(II)** 320 – 400 × 5 μm **(S)** in the same size range as the oxeas
Spongosorites calcicola Picton and Goodwin, 2007	Rathlin Island, Ireland[2]; */ 560 m	50 – 410 × 4 – 10 μm
Spongosorites coralliophaga (Stephens, 1915)	West of Ireland[3]; */1146 – 1300 m	80 – 550 × 2.5 – 11 μm
Spongosorites cavernicola Bibiloni, 1993	Mallorca[4]; */5 m (cave)	**(I)** 150 – 350 × 4 – 15 μm **(II)** 150 – 200 × 4 – 6 μm
Spongosorites cabliersi sp. nov.	Cabliers, Alboran Sea[5]/ ca. 700 m	194 – *349.2* ± 52.2 – 388 × 9.8 – *15.2* ± 4.2 – 19.4 μm
Spongosorites dendyi (Topsent, 1927)	Cape Verde[6]; */91 m	**(I)** (300) 500 × (5) 16 – 21 μm **(II)** 45 – 145 × 7 μm
Spongosorites difficilis (Lundbeck, 1902)	South of Iceland[7]; */ca. 1450 m	60 – 370 × 4 – 8 (10) μm
Spongosorites flavens Pulitzer-Finali, 1983	Tremiti Islands[8]; */6 m (cave)	60 – 380 (480) × 2 – 9 μm
Spongosorites intrincatus (Topsent, 1982)	Bari[8]/30 m	60 – 750 × 1 – 12 μm
Spongosorites maximus Uriz, 1983	Catalan Coast[9]; */150 – 250 m	**(I)** 1500 – 2500 × 48 – 78 μm **(II)** 380 – 450 × 11 – 17 μm **(III)** 130 – 200 × 2– 5 μm **(IV)** 30 – 50 × 2– 3 μm
Spongosorites placenta (Topsent, 1896)	Azores[6]/550m	**(I)** 300 – 330 (470) × 5 – 6 μm **(II)** 70 –120 μm

*Size range outliers are marked between brackets (). Numbers after Locality indicate the reference for each sample; * indicates this is the holotype of the species; (S) styles.*
(1) Ferrer Hernández (1923); (2) Picton and Goodwin (2007); (3) Stephens (1915); (4) Bibiloni (1993); (5) Present study; (6) Topsent (1928); (7) Lundbeck (1902); (8) Pulitzer-Finali (1983); (9) Uriz (1983).

Diversity Estimates Amongst CWC Provinces

The bibliographical search reported 37 papers or conference presentations which included data regarding the presence of sponge species associated with Mediterranean CWC frameworks, with approximately 2 – 4 papers per CWC site (**Figure 11** and **Tables 1**, **7**). While the oldest paper dates back almost a century (Topsent, 1928), it was not until 2010–2015 that the Mediterranean CWC sponge fauna began to be properly inventoried (**Figure 11A**). While, overall, a clear increment in number of publications and recorded species has been occurring yearly since then at a basin scale (**Figure 11A**), this is not the case for all the evaluated CWC sites (**Figure 11B**). As an example, the Gulf of Lions, which corresponds to the best studied area so far (**Tables 1**, **7** and **Supplementary Materials 3, 4**), has barely increased in the total number of recorded species since the early 70s (Vacelet, 1969) despite the continuous exploration of the CWC communities in the area (Fabri et al., 2014, 2017, 2019; Fourt et al., 2017). In this sense, most sites follow a similar trend, with a single publication each representing a sharp increase in the total number of sponge species recorded (**Figure 11B**), while most other publications barely contribute to expand the total pool of identified species. Additionally, ROV based publications account for a relatively low number of the total species identified on each area (ca. 3 – 5 per area), with a maximum of just 8 species identified for the GoL (**Figure 11C**).

The total number of sponge species associated with CWC was 172, with 143 (83%) having been identified to species level (**Tables 1**, **7**). Most sites had between 25 and 35 species per area except for the Gulf of Lions, the Maltese waters and the Corsica Channel, which reported 69, 17, and 8 species, respectively (**Tables 1**, **7**). Due to the low number of reported species in the Corsica Channel, records from nearby coral rubble in the Gulf of Liguria (four species; Sarà, 1958; Pulitzer-Finali, 1983) were included as part of this area given their proximity. The percentage of local endemism for each site was considerably low (**Table 7**), with only two out of 10 areas having endemic species and representing, in both cases, less than a 10% of the total sponge species on each area. Nevertheless, and despite that most of the encountered species corresponded to North Atlantic fauna, Mediterranean endemic sponges consistently represented 10–20% of the total sponge fauna on most sites (**Table 7**), except for the Corsica Channel, the Maltese waters and Albanian waters, where no Mediterranean endemics were present. However, those three areas are amongst the least explored of all Mediterranean CWC sites, and the presence of Mediterranean endemic sponges should be expected in all of them once sampling effort increases. Regarding their distribution, only one species sponges, only, *Desmacella inornata* (Bowerbank, 1866), is currently present at all the evaluated sites (**Table 1**), but it is likely that other common species, such as *Poecillastra compressa* (Bowerbank, 1866), *Pachastrella monilifera* Schmidt, 1868 or *Hamacantha (Hamacantha) johnsoni* (Bowerbank, 1864) might be present at all or most of the CWC sites, but haven't yet been recorded everywhere due to a lack of sampling effort. In this sense, several species that appear to be limited to the western Mediterranean, such as *Oopsacas minuta* Topsent, 1927, are in fact known from other deep-sea environments on the eastern Mediterranean (Bakran-Petricioli et al., 2007), thus their absence might also be a results of the currently insufficient sampling effort rather than ecological requirements.

The beta diversity revealed a low number of shared species between CWC sites, rarely exceeded more than 20% (**Supplementary Material 3**). Similarly, when paired together, none of the investigated areas accounted for more than a 40% of the total diversity of sponge in the basin (**Supplementary Material 4**). This is in concurrence with the randomized species accumulation curve (**Supplementary Material 5**), which is far from reaching an asymptote, and shows high standard deviation values of across the curve, implying that the current knowledge on the Mediterranean poriferan diversity is still far from its peak.

Finally, the relationship between the different evaluated CWC sites was represented by means of a dendrogram and nMDS (**Figure 12**). With a threshold of 25% similarity four groups could be clearly distinguished, which were also significantly different amongst each other (PERMOANOVA, *F* 1.4741, *p-value* 0.042*).

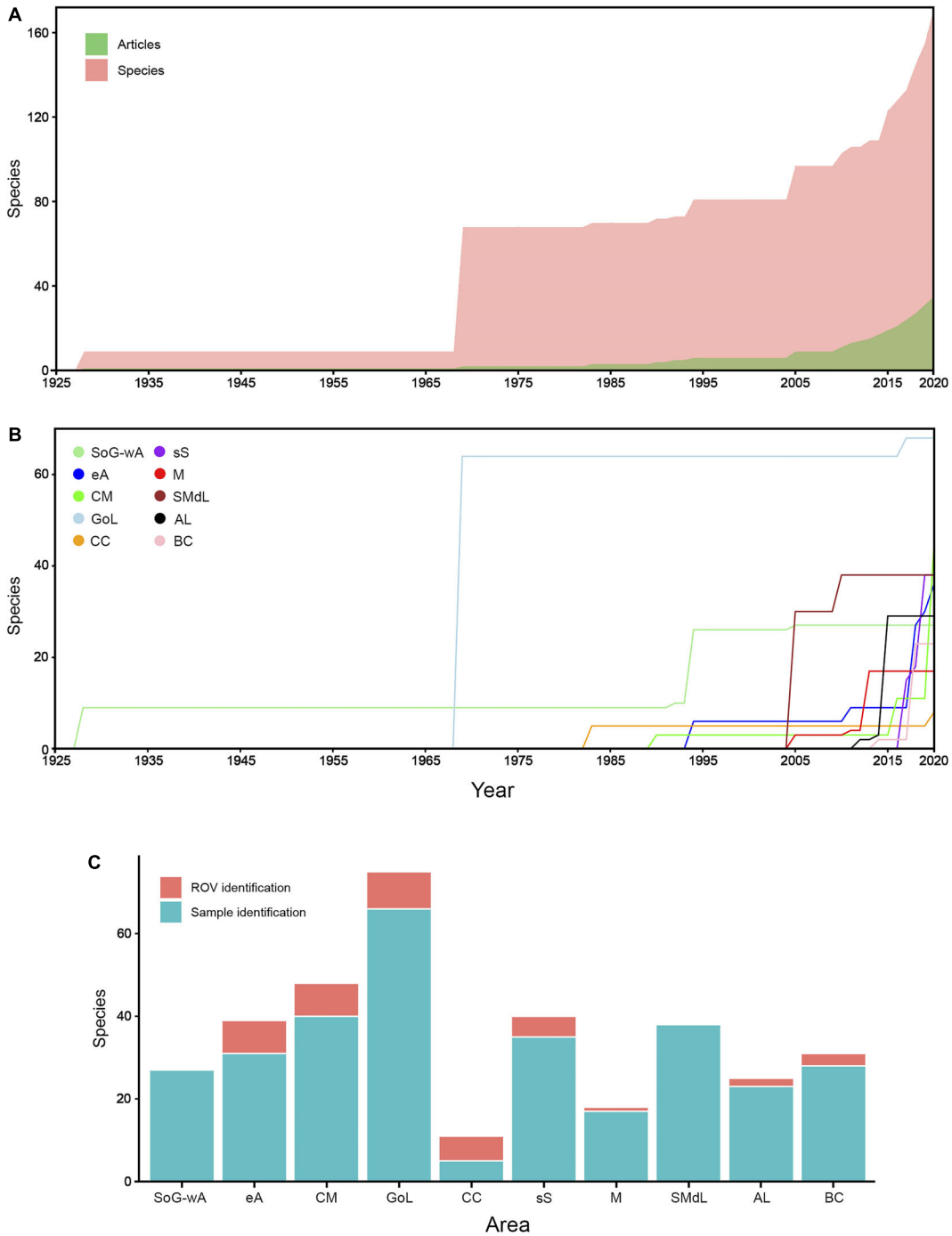

FIGURE 11 | (A) Cumulative timeline of the total number of species (light red) and total number of publications (light green) including data regarding sponge living within Mediterranean CWC. **(B)** Cumulative timeline of the total number of sponge species associated with CWC on each one of the evaluated areas: SoG-wA (light green); eA (navy blue); CM (bright green); GoL (sky blue); CC (orange); sS (purple); M (red); SMdL (carmine); AL (black); BC (pink). **(C)** Stacked barplots showing the total number of sponge species identified on each area based on sample identification (duck blue) and/or ROV based identification (red). Note that the sum of both might be higher than the total amount of identified species per area, as the same species might have been identified by both sample and ROV.

In this sense, clusters appeared to partially reflect geographic regions within the Mediterranean Sea, with both Alboran sites grouped together, as well as all western (Catalan Margin, Gulf of Lions and the south of Sardinia) and eastern (Santa Maria di Leuca, Bari Canyon and the Albanian coasts) Mediterranean sites (**Figures 12**, **13**). The fourth cluster did not follow any geographical pattern, including the Corsica Channel (western Mediterranean) and the Maltese waters (eastern Mediterranean).

TABLE 7 | Comparative table between all the analyzed CWC provinces.

	SoG-wA	eA	CM	GoL	sS	CC	M	SMdL	AL	BC
Species per area	27 [27] (15.3%)	37 [32] (19.8%)	48 [36] (26.2%)	69 [68] (39%)	38 [33] (22.1%)	8 [7] (4.7%)	17 [17] (9.9%)	38 [33] (22.7%)	23 [19] (13.4%)	28 [26] (26.3%)
Total species	172 (143 to species level)									
Exclusive to each site	0 (0%)	0 (0%)	2 (4.5%)	5 (7.5%)	0 (0%)	0 (0%)	0 (0%)	0 (0%)	0 (0%)	0 (0%)
Mediterranean endemics per area	3 (11.1%)	4 (12.5%)	6 (16.7%)	16 (23.5%)	6 (18.2%)	0 (0%)	0 (0%)	3 (9.1%)	0 (0%)	5 (19.2%)
Total Med. Endemics	33 (23.1%)									
North Atlantic species per area	24 (88.9%)	28 (87.5%)	30 (83.3%)	52 (76.5%)	27 (81.8%)	8 (100%)	17 (100%)	30 (90.9%)	19 (100%)	21 (80.8%)
Total N. A. species	110 (76.9%)									
Papers per area	4	9	5	8	4	3	3	3	2	4
Total papers	37									

Including: total number of species per area in regards to total sponge fauna associated with CWC in the basin (172 spp.); total number of sponge species identified from Mediterranean CWC down to genus and species (between brackets) level; total number of sponge species exclusive to each CWC site (i.e., not recorded outside CWC formations in said area); total number of Mediterranean endemic sponges and total number of North Atlantic sponges associated with each CWC province in regards to total sponge fauna on each site; total number of Mediterranean sponge endemics and total number of North Atlantic in regards to the total CWC sponge fauna for the basin down to species level (143 spp.); number of papers dealing with sponge fauna on each site; total number of papers dealing, or mentioning in part, sponge associated with CWC in the Mediterranean Sea.

Sog-wA, Strait of Gibraltar-western Alboran; eA, eastern Alboran; CM, Catalan Margin; GoL, Gulf of Lions; CC, Corisca Channel; sS, south of Sardinia; M, Maltese waters; SMdL, Santa Maria di Leuca; AL, Albanian subfossil reefs; BC, Bari Canyon.

Yet this final cluster is most likely an artifact due to the low number of species recorded in both sites (**Tables 1**, **7**), which are insufficiently characterized when compared to all other the other Mediterranean CWC provinces. As so, we excluded both the CC and M sites from the PERMANOVA analysis, and ran it again (F 2.4428, *p-value* 0.005**), resulting in a stronger differentiation between clusters. Regarding the possible influence of geographical distance between CWC sites and its associated sponge fauna composition, the Mantel test proved statistically significant (rM 0.4474, *p-value* 0.006**), thus indicating that geographical distance was at least partially responsible for the CWC sponge communities' composition. In this sense, the Person correlation also proved statistically significant (n = 45 pairwise comparisons, R 0.48, t 3.4861 *p-value* 0.001***), with closer sites being more similar than distant sites (**Supplementary Material 6**), supporting the nMDS and dendrogram clustering.

DISCUSSION

In general terms, the sponge fauna associated with CWC Mediterranean communities did not differ much from their Atlantic counterparts, both being dominated by Demospongiae from the orders Poecilosclerida and Tetractinellida, as it has already been described by van Soest and De Voogd (2015). Hexactinellida, while not as numerous, are still common in most of the basin, specifically its western side as stated in previous studies (Boury-Esnault et al., 2015, 2017) whereas, on the contrary, Calcarea and Homoscleromorpha have been seldomly recorded, and their presence is currently testimonial.

Diversity Estimates, Sampling Effort and Identification Bias

Currently, over 172 potential poriferan species have been found to occur within Mediterranean CWC provinces (**Table 1**), well behind data published for CWC in the North Atlantic (ca. 260 potential species; van Soest and De Voogd, 2015), yet almost doubling those from the last review on Mediterranean CWC sponge fauna (ca. 90 species; Rueda et al., 2019). On the other hand, when considered individually, almost none of the CWC sites accounted for more than ca. 20% of the total sponge diversity observed for the basin (**Table 7**). Moreover, the species accumulation curve for the basin is far from asymptotic (**Supplementary Material 5**), altogether suggesting that the poriferan fauna associated with CWC in the Mediterranean is still underrepresented both, at a local (CWC sites) and global (whole Mediterranean basin) scale, despite the increasing effort to map it.

In this sense, sampling effort and taxonomic resolution seems like the most likely explanation for the current diversity values observed. Regarding sampling effort, CWC are known to be highly heterogeneous substrates (Buhl-Mortensen et al., 2010), thus sponge diversity and abundance widely varies between areas of the reef, with higher sponge abundance and diversity on dead coral frameworks or mixed substrates than living CWC (van Soest et al., 2007), which in turn means sampling effort heavily constraints the pool of species to be encountered. As an example, van Soest et al. (2007) identified over 150 sponge species from over 126 boxcores within three different CWC mount off the coast of Ireland, with sponges' diversity per core ranging between 0 and 57 species. Yet, even so, total poriferan diversity was estimated to be underrepresented in the area (van Soest and Lavaleye, 2005; van Soest et al., 2007). Currently, while CWC sponge research in the Mediterranean has considerably increased during the past decade (Rueda et al., 2019), this still mostly comes from sparse, fragmentary CWC material, usually no more than a few pieces of coral per study (Longo et al., 2005; Calcinai et al., 2013; Bertolino et al., 2019; present study). Considering this in more detail, the East Alboran CWC province contains, amongst other CWC sites, the Cabliers Coral Mound, which extends for over 25 km, and has an average high between 70 and 140 m (Corbera et al., 2019). In contrast, our knowledge of its associated

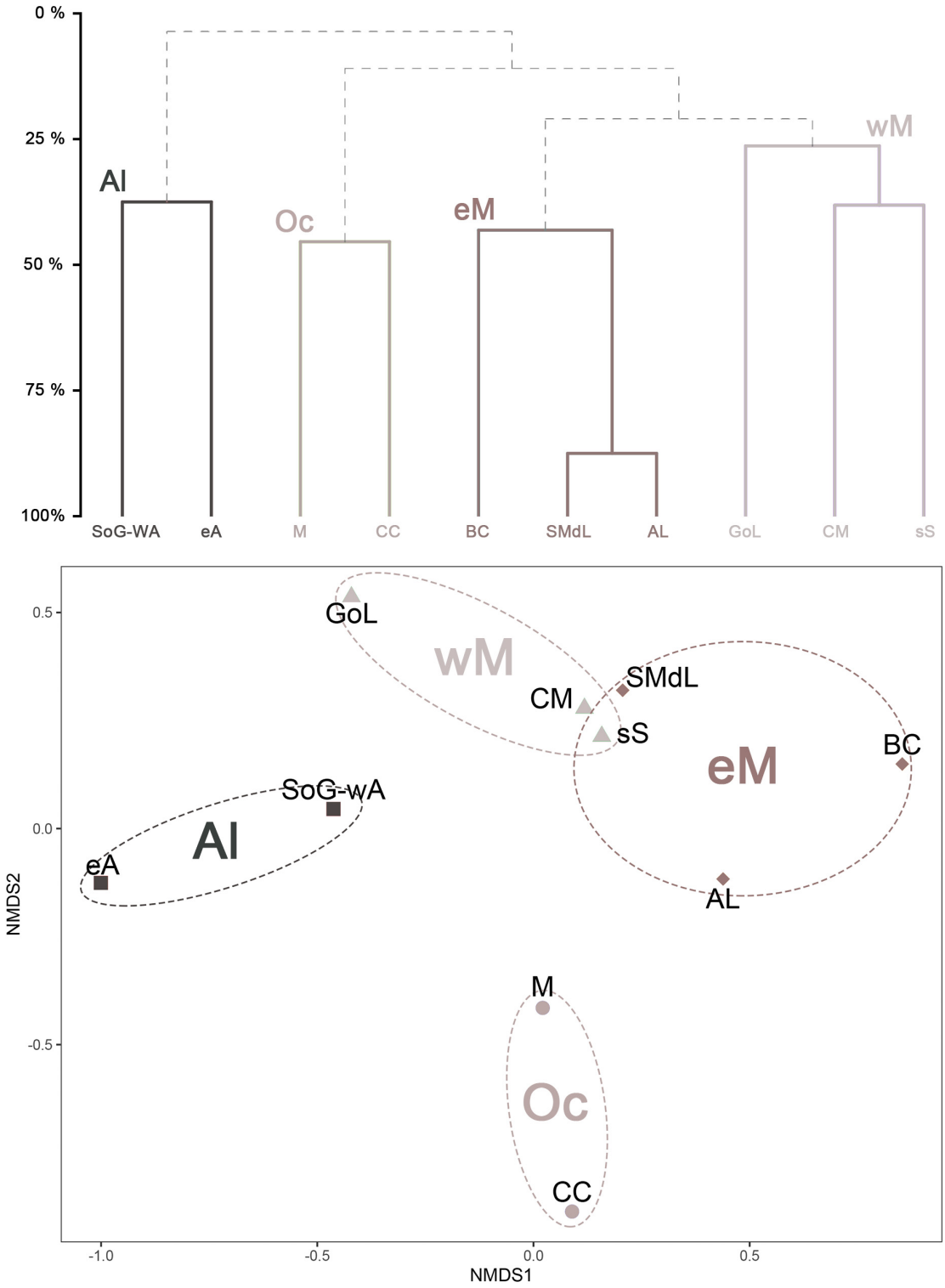

FIGURE 12 | Top: dendrogram representing the sample clustering based on a Bray–Curtis dissimilarity matrix. A 25% similarity threshold was used for clustering. Clusters are differently shaded on a gray-scale to ease visual group identification. **Bottom:** non-metric multidimensional scaling (nMDS) ordination plot. CWC provinces are represented based on a presence/absence matrix of their associated sponge assemblages. A stress estimate of 0.048 was obtained, indicating a good fit. Clusters are differently shaded on a gray-scale to ease visual group identification, as in the dendrogram. Strait of Gibraltar and western Alboran (SoG-wA); eastern Alboran (eA); Catalan Margin (CM); Gulf of Lions (GoL); South of Sardinia (sS); Corsica Channel (CC); Maltese waters (M); Santa Maria di Leuca (SMdL); Albanian coasts (AL); Bari Canyon (BC); Alboran cluster (Al); western Mediterranean cluster (wM); eastern Mediterranean cluster (eM); Outlier cluster (Oc).

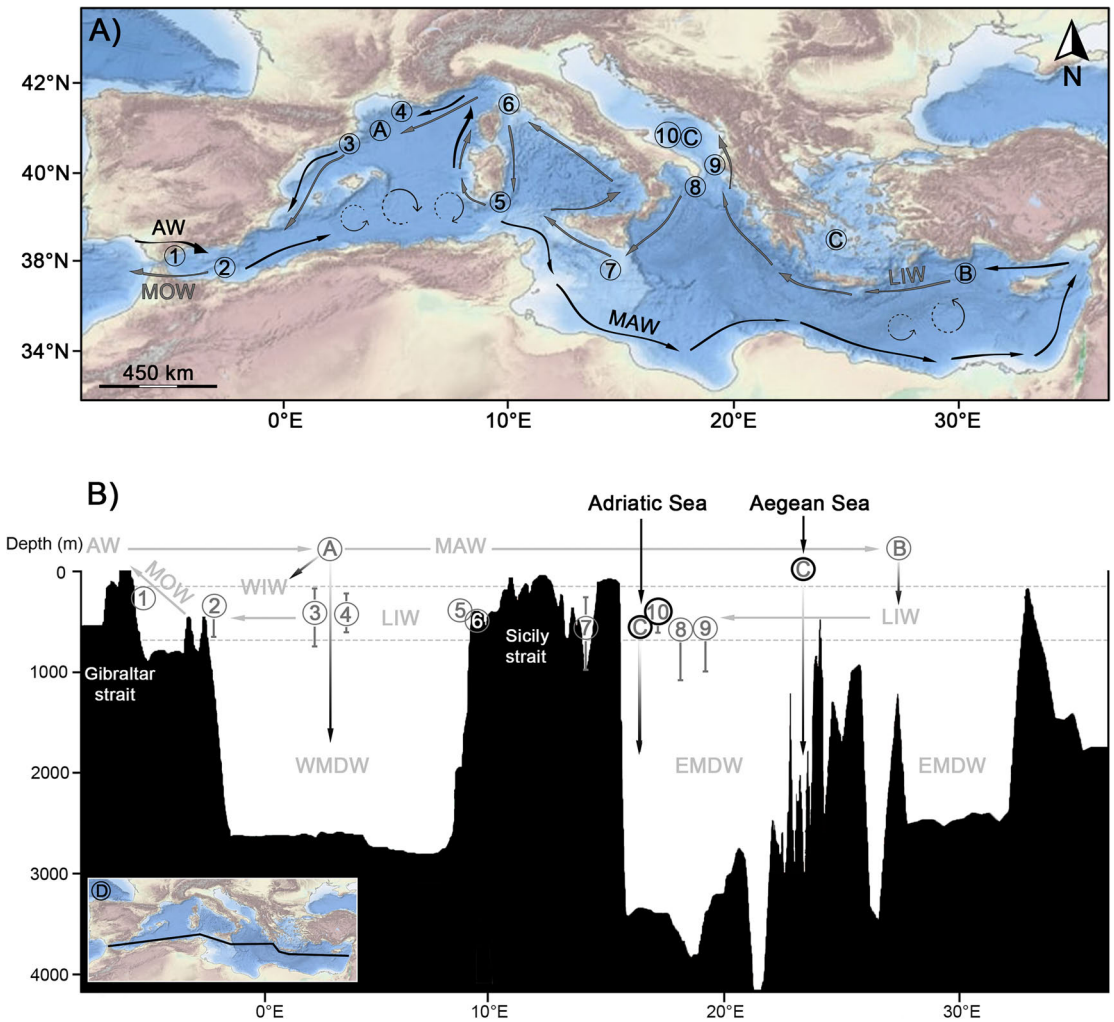

FIGURE 13 | (A) Bathymetric map of the Mediterranean Sea, with all CWC provinces (numbers) evaluated represented alongside a simplified schematic representation of its water masses circulation and formation (Letters). **(B)** Vertical profile of the Mediterranean Sea with all CWC provinces depth ranges represented alongside a simplified schematic representation of its water masses circulation (arrows) and formation (letters). The whiskers on each number represent the depth range of occurrence for each CWC province according to Chimienti et al. (2019) with additional data for the Corsica Channel from Angeletti et al. (2020) and for the Catalan Margin from the De Leo et al. (2019) and Puig et al. (2019). 1: Strait of Gibraltar and western Alboran (SoG-wA); 2: eastern Alboran (eA); 3: Catalan Margin (CM); 4: Gulf of Lions (GoL); 5: South of Sardinia (sS); 6: Corsica Channel (CC); 7: Maltese waters (M); 8: Santa Maria di Leuca (SMdL); 9: Albanian coasts (AL); 10: Bari Canyon (BC). Water masses are abbreviated as follows: AW, Atlantic Water; MAW, Modified Atlantic Water; LIW, Levantine Intermediate Water; WIW, Winter Intermediate Water; WDMW, Western Mediterranean Deep Water; EMDW, Eastern Mediterranean Deep Water; MOW, Mediterranean Outflow Water. A, area of formation of the WIW and WDMW; B, suspected area of formation of the LIW based on Hayes et al. (2019); C, areas of formation of the EMDW; D, Approximate geographical representation of the area represented on the vertical profile. The bathymetric metadata and Digital Terrain Model data products have been obtained and modified from the EMODnet Bathymetry portal – http://www.emodnet-bathymetry.eu.

sponge fauna comes from just a few pieces of dead coral, less than 0.04 m^2 (Costa et al., 2018; present study) and 5 megafaunal species observed by ROV (Boury-Esnault et al., 2015; Corbera et al., 2019), a trend that is extensive to all other CWC provinces of the Mediterranean.

Finally, while CWC research in the Mediterranean dates back to 1970s (**Figure 11A**), it is not until the first decade of the 21th century that biological and ecological studies flourish, thanks to the development and advances in deep-sea robotics and other deep-sea imaging techniques (Orejas and Jiménez, 2019). Nevertheless, while video footage has boosted our knowledge on deep-sea environments (Aguilar et al., 2011; Bo et al., 2012; D'Onghia et al., 2015; Taviani et al., 2017; Chimienti et al., 2019; Fabri et al., 2019), the taxonomic resolution of these techniques widely varies between phyla (Fabri et al., 2014, 2019). As an example, Bertolino et al. (2019) in their study of the sponges associated with CWC in the South of Sardinia CWC province, they could only identify three species by ROV [*Poecillastra compressa* (Bowerbank, 1866), *Pachastrella monilifera* Schmidt, 1868, *Phakellia robusta* (Bowerbank, 1866)], whereas a total of 28 could be identified from the collected CWC rubble studied. Yet, the analysis of collected material is not extent of taxonomic

resolution hazards. Porifera is generally considered a rather difficult to identify phylum (Reveillaud et al., 2011; van Soest et al., 2012), whose proper identification usually requires of qualified experts (van Soest et al., 2012) and the combined used of morphological and molecular tools (Reveillaud et al., 2010, 2011) and, even so, sometimes species identification cannot be reached (van Soest, 2009). This is exacerbated with deep-sea samples, as the encrusting nature of most species, alongside the paucity of the material might compromise species identification. Furthermore, the cryptic nature of several encrusting sponges living in coral reefs ecosystems (van Soest, 2009), as well as poriferan groups with few distinctive morphological traits (e.g., Halichondrida or Haplosclerida; van Soest, 2009; van Soest, 2017), has led researchers to assign specimens to the closest available names, creating 'complex species,' which ultimately leads to the underestimation of their diversity until those are properly resolved (Reveillaud et al., 2010, 2011).

Sponge Diversity on Mediterranean CWC Provinces

As already mentioned, the current knowledge on the Mediterranean CWC sponge fauna is still fragmentary and underrepresented (**Figure 11** and **Table 7**), but potentially as diverse as in the Atlantic region. Currently, estimates for sponge diversity in Atlantic CWC would be in range of that of other ecosystems on the same region (van Soest and De Voogd, 2015). Contrarily, while at a basin scale Mediterranean CWC appear to be hotspots of sponge diversity (**Tables 1**, **7** and **Supplementary Materials 3, 4**), at a local scale (CWC province), diversity values trail behind other deep and shallow Mediterranean habitats. In this sense, sponge grounds along the Mediterranean continental shelves and upper slopes (Sitjà and Maldonado, 2014; Bertolino et al., 2015; Santín et al., 2018b, 2019) or even shallow circalittoral environments (Pulitzer-Finali, 1983; Bibiloni, 1990; Maldonado, 1993; Bertolino et al., 2013) or caves (Gerovasileiou and Voultsiadou, 2012) show diversity values (50 – 100 species per article) exceeding those of the evaluated CWC provinces individually, yet this is likely to be a result of the higher sampling effort in shallower environments.

While at a basin scale CWC appear as sponge hotspots, there are still knowledge gaps regarding the main drivers for CWC sponges' diversity (van Soest and De Voogd, 2015) as well as their ecology (Kazanidis and Witte, 2016; Rix et al., 2016; Kazanidis et al., 2018) and their role as biological structures (Buhl-Mortensen et al., 2010; Kazanidis et al., 2016). In this sense, it is known that depth is strongly linked with changes in the composition of sponge assemblages (Santín et al., 2018b, 2019), including CWC associated sponges (Longo et al., 2005; van Soest and De Voogd, 2015), yet it is suspected it might just be a proxy of other abiotic factors in play, such as temperature or food availability (van Soest and De Voogd, 2015). In fact, this concurs with previous observations of vertical sponge diversity, which showed low correlation with temperature and salinity values over a 500 m depth range (Maldonado and Young, 1996). Contrary to other areas of the world, the Mediterranean deep-sea benthic fauna, including sponges, is known to be mostly eurybathic (Bouchet and Taviani, 1992), with some species even occurring from the shallow littoral areas to over 1000 m depth (Santín et al., 2020b). In this sense, the Mediterranean Sea, contrary to the Atlantic, is known to be homothermic (ca. 13°C) below 200 m, where all CWC provinces occur, whereas in the Atlantic, water temperature decreases gradually until 3000 m (Bouchet and Taviani, 1992). As so, while temperature might play a major role in shaping sponge diversity in the Atlantic, this would not seem to be the case for Mediterranean CWC. On the contrary, other factors such as substrate availability (Maldonado and Young, 1996; Sitjà and Maldonado, 2014; Santín et al., 2018b), food supply (van Soest and De Voogd, 2015; Robertson et al., 2017), the presence of predators (Robertson et al., 2017) or historical factors and large-scale phenomena (Gage, 2004) might be or have been theorized to play a major role in shaping Mediterranean deep-sea sponge communities, including those in CWC.

Is There a Mediterranean Endemic CWC Fauna?

Cold-water coral reefs in the Mediterranean are typically known to occur in submarine canyons (Puig and Gili, 2019), where the topography of the area creates localized circulation patterns which might induce larvae retention within the reef, limit species' dispersal, and potentially enhance rates of speciation within the reef (Roberts et al., 2006). Nevertheless, levels of endemism in CWC sponge fauna seems to be really low, with only 10% of all known species having been recorded exclusively from CWC ecosystems across their distribution (**Tables 1**, **7**). In this sense, Porifera is a highly plastic phylum (van Soest et al., 2012), which might allow them to adapt to a wide myriad of environments, helping them expand their vertical distribution (Bertolino et al., 2019). Most sponge species found in Mediterranean CWC are also known to occur in other hard-substrate ecosystems (Bertolino et al., 2019), a trend that also occurs in the North Atlantic (van Soest and Lavaleye, 2005; van Soest et al., 2007). As so, Mediterranean CWC sponge fauna seems to support the view that sponges living on CWC are mostly facultative, and not settling preferentially on CWC over other hard substrates.

Yet, present results might suggest the existence, to a certain level, of a Mediterranean CWC sponge fauna, different from that on the Atlantic. In this sense, the Mediterranean Sea is characterized by low endemism and diversity values when compared to the fauna of the Northeast Atlantic, a fact mostly linked to the Messinian Salinity Crisis (Bouchet and Taviani, 1992; Emig and Geistdoerfer, 2004). During this crisis, it is thought that the Mediterranean was almost completely desiccated, leaving to a massive extinction of the basin's fauna (Hsü et al., 1973). Nevertheless, the view of a completely desiccated Mediterranean has recently been challenged (Krijgsman et al., 2018), since there are evidences supporting that the connection with the Atlantic was not lost completely during the crisis (Gili et al., 1998; Krijgsman et al., 2018), as there is speculation on the existence of areas with almost normal salinity values during this period (Por, 1989). This seems to be supported by the existence of Mediterranean Tethyan relicts, which refers to species whose current distribution dates back to the closing of the Indo-Pacific-Mediterranean

connection (Hou and Li, 2018). In this sense, several deep-sea Porifera have been proposed as possible Tethyan relicts (Boury-Esnault et al., 1992, 1994; Maldonado and Uriz, 1995; Pisera et al., 2018; Santín et al., 2020b), supporting the view that the component of Tethyan relicts on the deep-sea fauna of the Mediterranean Sea and neighboring Atlantic areas might be higher than originally thought. Thus, the current Mediterranean deep-sea fauna would be a mix between the survivors of the Messinian Salinity Crisis and the restocking fauna from the Atlantic (Emig and Geistdoerfer, 2004). This would concur with the current observed trend, with the larger fraction of sponges found in all sites also being present in the Atlantic (**Table 7**), yet with a consistent ca. 20% of sponge species in all sites being Mediterranean endemics (**Table 7**). As so, while endemic CWC Porifera appear to be very rare, it could be concluded that Mediterranean CWC sponge fauna is unique, and differing from that of other Atlantic regions.

Biogeography Amongst Mediterranean CWC Sponge Communities

As seen, the Mediterranean CWC provinces are a hotspot of sponge diversity, which composition is the result of a myriad of intertwined biotic and abiotic factors. Sponges have long been proven to be an excellent tool for a biogeography approach, as they are a major component of most benthic ecosystems (Maldonado and Uriz, 1995; Carballo et al., 1997; Xavier and Van Soest, 2012) with overall low dispersal capabilities (Mariani et al., 2006), which in turn translates into clear geographical diversity patters (Xavier and Van Soest, 2012; Roberts et al., 2021). Nevertheless, so far only shallow species had been considered for such type of approach, with deep-sea sponges rarely ever being considered until recently (Sitjà, 2020; Sitjà et al., 2020; Roberts et al., 2021).

Clustering of the evaluated sites supports the presence of at least three different CWC sponge clusters in the Mediterranean Sea (**Figure 12**), with a 4th one mostly likely being an artifact due to insufficient data (see Section "Diversity Estimates Amongst CWC Provinces"). In this sense, while there is a current sampling bias for all the considered areas (see Section "Diversity estimates, sampling effort and identification bias"), previous studies in CWC communities have highlighted that the sponge fauna dwelling on these reefs tends to be represented by a few, very abundant species, whilst all other occur in relatively low numbers (van Soest and Lavaleye, 2005; van Soest et al., 2007; van Soest and De Voogd, 2015), allowing for an exploratory comparison between sites, assuming that the most common sponges on each site have already been sampled.

From a biogeographical point of view, two main water masses might be suspected to be the drivers behind any possible pattern of sponge diversity within Mediterranean CWC: The Atlantic Water (AW) and the Levantine Intermediate Water (LIW) with, additionally, the Strait of Gibraltar and the Strait of Sicily being the most likely geographical barrier for dispersal (Sitjà, 2020). Assuming that sponge assemblage's composition is dependent on larval supply (Reveillaud et al., 2010), and considering the main currents occurring in the Mediterranean Sea (**Figures 13A,B**), several explanations can be proposed to explain the current pattern observed in the basin.

First of all, it is known that the Strait of Gibraltar is both the door and the biggest barrier for benthic species dispersal between the Atlantic and Mediterranean populations, including sponges (Maldonado and Uriz, 1995; Carballo et al., 1997). Yet, the Strait is not a clear-cut barrier, but a rather complex buffer zone including the Gulf of Cadiz and the Alboran Sea (Carballo et al., 1997; Sitjà et al., 2020). As so, species with Mediterranean affinities can exist outside the basin in the Gulf of Cadiz waters under the Mediterranean Outflow Water (MOW) influence (Sitjà et al., 2020), whereas Atlantic species might find their limit of distribution at the Alboran Sea (Carballo et al., 1997). This could explain the grouping of both Alboran CWC sites, which would include the presence of Atlantic species which does not occur in the Mediterranean Sea far beyond the area of major influence of the AW, even if the exact limiting factors are not well-understood (e.g., *Asconema setubalense* Kent, 1870; Pardo et al., 2011; Sitjà and Maldonado, 2014; Boury-Esnault et al., 2015). The two remaining groups reflect a western-eastern pattern, separated by the Strait of Sicily (**Figures 12**, **13**). Regarding the western Mediterranean cluster, the CM and the GoL are located at the area of influence of the Northern Current, which flows southwards from the Gulf of Liguria to the Catalan coast (Robinson et al., 2001). This surface current is influenced by the MAW, which in the Gulf of Lions is known to be subjected to up and downwelling processes, as well as being a major component of the deep-water formation (Millot, 1990; Palanques and Puig, 2018). As so, the sinking of the Northern Current might bring larvae down to the CWC occurring in the Gulf of Lions and nearby areas (**Figure 13B**), much like upwelling events have been hypothesized to maintain the connectivity and larval flux between deep-sea and cave environments in the zone (Vacelet et al., 1994). Finally, the sS site is located in the LIW flow toward the GoL and CM areas (**Figures 13A,B**), so a passive transport of larvae from one to the others seems feasible. This would be supported by the present finding of high abundances of *H.* (*H.*) *quadridentata* and *P. tavianii* in the CM area, which were recently described from the sS CWC province (Cardone et al., 2019) and haven't been found anywhere else so far.

The third group would include all CWC sites east of the Strait of Sicily (SMdL, AL, and BC) except for the Maltese waters, which clusters with the Corsica Channel area due to a major lack of data in both compared to all other CWC sites. Santa Maria di Leuca is located on the near the entrance of the Adriatic Sea (**Figure 13A**), were the LIW enters the Adriatic to form the Eastern Mediterranean Deep Water (EMDW). In this sense, the Strait of Sicily (**Figure 13B**) would pose as a second geographical barrier for any Atlantic migrant (Pansini, 1987), further reducing the pool of species that might make it to the eastern section of the Mediterranean when compared to its western counterpart (Bouchet and Taviani, 1992). As so, it could be hypothesized that the sponge fauna from the AL and BC might come from the pool of species found at the SMdL, rather than directly from the Atlantic or any other CWC province in the Mediterranean (Taviani et al., 2011; Angeletti et al., 2014; Chimienti et al., 2019). In this sense, while genetic studies are

still scarce, there are evidences than gene flow between *Lopehlia* and *Madrepora* reefs at both sides of the Strait of Gibraltar is currently relatively low (Boavida et al., 2019), which would also seem to be the case for its associated fauna (e.g., the polychaete *Eunice norvegica*; Boavida et al., 2019), and it would not be unreasonable to expect a similar pattern for species leaving at both sides of the strait of Sicily. Finally, this western-eastern pattern would be supported by the correlation between dissimilarity in species composition vs. geographical distance between sites (**Supplementary Material 6**), which suggests that the closer to CWC sites area, the more their sponge fauna is shared, thus supporting the view that closer CWC provinces are to have a higher connectivity and shared number of species than distant ones.

Thus, the connectivity between CWC Mediterranean sponge populations could be explained by passive larval dispersal enhanced by LIW and AW currents and limited by the existence of geographical barriers (Gary et al., 2020) and which would be facilitated by the existence of intermediate or stepping-stones populations, as theorized for other sponge species (Padua et al., 2018). In this sense, it is also worth noticing the importance of stochasticity and asexual reproduction might have for the configuration of CWC sponge assemblages. It is well documented that stochastic settlement of larvae plays a major role in the composition of benthic communities, both in term of abundance and diversity (Edwards and Stachowicz, 2011), most likely including those living in association with CWC. Given the aforementioned limitations for larval dispersal between CWC, it should be expected that, if reproductive, self-recruitment and asexual reproduction would be more important than external larval supply in sustaining the Mediterranean CWC sponges' populations, especially considering that (i) water circulation around CWC favors a semi-enclosed dynamic (Roberts et al., 2006) and (ii) the generally poor-swimming capabilities of sponge larvae (Mariani et al., 2006) and (iv) the frequent occurrence of asexual reproduction in sponges populations (e.g., Teixidó et al., 2006). In this sense, *P. taviani* and *A. schmidti* [the first recently described by Cardone et al. (2019), the latter by Topsent (1904, 1928) a century ago, and just recently reencountered in the Cantabrian Sea, Heres et al. (2014)], were the most abundant species within the Catalan Margin CWC (**Supplementary Material 1**) whilst, prior to this finding, they were both considered rare species. While it could be argued that their abundance might indicate a higher degree of adaptation to their environmental setting than other sponges, it is hard to believe that they might be much better adapted than any of the other small encrusting sponges encountered, their abundance most likely being the result of stochastic reproductive events rather than favourability.

As so, much as their shallow counterparts (Jones et al., 2009 and references within), CWC could be theorized to be semi-enclosed ecosystems for sponges, with limited external larval input and mostly sustained by self-recruiting and asexual reproduction of its existing fauna, fueled by the larval retention caused by local hydrodynamics around the reefs (Roberts et al., 2006) and, thus, critically affected by stochastic events (e.g., first arrival, settlement success, mortality events) that have occurred during the reef's history. Nevertheless, this remains speculative, as currently, no studies have evaluated the genetic connectivity between and within CWC reef sponges while, the same time, our current knowledge on the behavior, ecology and physiology of sponge remains scant (Mariani et al., 2006; Bo et al., 2012; Robertson et al., 2017; Santín et al., 2019), even more for those occurring in deep-sea ecosystems (Maldonado et al., 2020).

CONCLUSION

The present article provided the first insight on the associated sponge fauna of the recently discovered CWC communities on the Catalan Margin and, to a lesser extent, the Cabliers Coral Mound Province, with the description of several new or rare species. From a global point of view, the present article highlights, despite an overall lack of knowledge, the role of CWC in general, and of Mediterranean CWC in particular, as biodiversity hotspots for sponges, the major bullet points being:

- The observed poriferan diversity values on Mediterranean CWC currently represent a small fraction of its actual fauna rather than reflecting the real diversity on each area, which is suspected to be highly underrepresented.
- The existence of an endemic CWC sponge fauna is refuted, yet the Mediterranean CWC sponge fauna appears to be unique and different from that of other Atlantic regions, having being shaped by the basin's geological and hydrological history, and consisting of a mixture of Atlantic migrants and pre-Messinian relict fauna.
- The sponge assemblage at a specific CWC province cannot be explained by a single or reduced group of factors, but it might be the result of a complex interaction between species' evolutionary history, their life traits and both abiotic and biotic factors as well as the reef's own long-term history.
- The current composition of the Mediterranean CWC sponge assemblages seems to be determined by the basin's water circulation, specially the Levantine Intermediate Water and the Atlantic Water, with a western-eastern pattern from the Strait of Gibraltar to the Adriatic Sea.
- Cold-water corals might act as semi-enclosed ecosystems for sponges, which might be rather sustained by asexual reproduction and self-recruitment than external larval supply.
- Overall, sponge living in CWC appear as good candidates for biogeographical studies, and might help understand the connectivity between CWC sites, yet there is still a current major lack of knowledge on the topic.

DATA AVAILABILITY STATEMENT

The datasets presented in this study can be found in online repositories. The names of the repository/repositories and accession number(s) can be found below: ZooBank (urn:lsid:zoobank.org:pub:E58A3DFF-EDC5-44FC-A274-1C9508BF8D15).

AUTHOR CONTRIBUTIONS

AS, JG, JMG, and MU conceived of the presented idea. PP and CL devised the framework projects from which the samples came from. JG, PP, and CL attended the oceanographic surveys and collected the samples. AS and MU performed the SEM imaging and other analyses. AS wrote the manuscript with inputs from all other authors, whom provided critical feedback and helped shape the research, analysis and manuscript. All the authors contributed to the article and approved the submitted version.

FUNDING

Samples from the Blanes Canyon were collected during the ABIDES project (Ref. CTM2015-65142-R) and analyzed during the ABRIC project (Ref. RTI2018-096434-B-I00), both funded by the Spanish Ministry of Science and Innovation and granted to PP. Samples from the Cabliers Coral Mound were collected during the MELCOR Cruise in the frame of the FP7 EU Marie Curie ProjectGeo-Habit (GA29874) granted to CL and the SHAKE Project (Ref. CGL2011-30005-C02-02) funded by the Spanish Ministry of Science and Innovation. Finally, AS was the recipient of the 2019 Young Scientist Best Paper Award of the Department of Marine Biology and Oceanography at the Institute of Marine Sciences, which provided funding for the SEM imaging. With the institutional support of the 'Severo Ochoa Centre of Excellence' accreditation (CEX2019-000928-S).

ACKNOWLEDGMENTS

We thank the crew of the R/V *Sarmiento de Gamboa* and the crew of the ROV '*Liropus2000*' pilots. We also thank the entire crew of the R/V *Garcia del Cid*, in particular the captain Eduardo Otal, and the UTM-CSIC technicians Marcos Pastor, Cristina Alvarez, and Joel Sanz for their help during the MELCOR oceanographic survey; Ruth Durán for her help creating the maps; Carlota Ruiz for listening to endless conjecturations and her aid with bibliography; José Manuel Fortuño (ICM-CSIC) for his technical assistance during SEM image acquisition and finally, Francesc Uribe, curator of the MZB, for his technical assistance.

SUPPLEMENTARY MATERIAL

The Supplementary Material for this article can be found online at: https://www.frontiersin.org/articles/10.3389/fmars.2021.662899/full#supplementary-material

REFERENCES

Aguilar, R., López Correa, M., Calcinai, B., Pastor, X., De La Torriente, A., and Garcia, S. (2011). First records of *Asbestopluma hypogea* Vacelet and Boury-Esnault, 1996 (Porifera, Demospongiae Cladorhizidae) on seamounts and in bathyal settings of the Mediterranean Sea. *Zootaxa* 2925, 33–40. doi: 10.11646/zootaxa.2925.1.3

Álvarez-Pérez, G., Busquets, P., De Mol, B., Sandoval, N. G., Canals, M., and Casamor, J. L. (2005). "Deep-water coral occurrences in the Strait of Gibraltar," in *Cold-water corals and ecosystems*, eds A. Freiwald and J. M. Roberts (Berlin: Springer), 207–221. doi: 10.1007/3-540-27673-4_10

Anderson, M. J. (2001). A new method for non-parametric multivariate analysis of variance. *Austral. Ecol.* 26, 32–46. doi: 10.1111/j.1442-9993.2001.01070.pp.x

Angeletti, L., Castellan, G., Montagna, P., Remia, A., and Taviani, M. (2020). The "Corsica Channel Cold-Water Coral Province"(Mediterranean Sea). *Front. Mar. Sci.* 7:661. doi: 10.3389/fmars.2020.00661

Angeletti, L., Taviani, M., Canese, S., Foglini, F., Mastrototaro, F., Argnani, A., et al. (2014). New deep-water cnidarian sites in the southern Adriatic Sea. *Med. Mar. Sci.* 15, 263–273. doi: 10.12681/mms.558

Aymà, A., Aguzzi, J., Canals, M., Company, J. B., Lastras, G., Mecho, A., et al. (2019). "Occurrence of living Cold-Water Corals at large depths within submarine canyons of the northwestern Mediterranean Sea", in Mediterranean Cold-Water Corals: Past, Present and Future, eds C. Orejas and C. Jiménez (Springer International Publishing AG, part of Springer Nature). *Coral Reefs World Ser.* 9, 271–284. doi: 10.1007/978-3-319-91608-8_26

Babiç, K. (1922). Monactinellida und Tetractinellida des Adriatischen Meeres. *Zool. Jahrb. Abt. Syst. Geog. Biol. Tiere* 46, 217–302.

Baillon, S., Hamel, J. F., Wareham, V. E., and Mercier, A. (2012). Deep cold-water corals as nurseries for fish larvae. *Front. Ecol. Environ.* 10, 351–356. doi: 10.1890/120022

Bakran-Petricioli, T., Vacelet, J., Zibrowius, H., Petricioli, D., Chevaldonné, P., and Raa, T. (2007). New data on the distribution of the 'deep-sea' sponges *Asbestopluma hypogea* and *Oopsacas minuta* in the Mediterranean Sea. *Mar. Ecol.* 28(Suppl. 1), 10–23. doi: 10.1111/j.1439-0485.2007.00179.x

Bart, M. C., Hudspith, M., Rapp, H. T., Verdonschot, P. F., and De Goeij, J. M. (2021). A deep-sea sponge loop? sponges transfer dissolved and particulate organic carbon and nitrogen to associated fauna. *Front. Mar. Sci.* 8:229. doi: 10.3389/fmars.2021.604879

Bertolino, M., Bo, M., Canese, S., Bavestrello, G., and Pansini, M. (2015). Deep sponge communities of the Gulf of St Eufemia (Calabria, southern Tyrrhenian Sea), with description of two new species. *J. Mar. Biolog. Assoc. U K.* 95, 1371–1387. doi: 10.1017/s0025315413001380

Bertolino, M., Cerrano, C., Bavestrello, G., Carella, M., Pansini, M., and Calcinai, B. (2013). Diversity of Porifera in the Mediterranean coralligenous accretions, with description of a new species. *ZooKeys* 336, 1–37.

Bertolino, M., Ricci, S., Canese, S., Cau, A., Bavestrello, G., Pansini, M., et al. (2019). Diversity of the sponge fauna associated with white coral banks from two Sardinian canyons (Mediterranean Sea). *J. Mar. Biolog. Assoc. U K.* 99, 1735–1751. doi: 10.1017/s0025315419000948

Beuck, L., and Freiwald, A. (2005). "Bioerosion patterns in a deep-water *Lophelia pertusa* (Scleractinia) thicket (Propeller Mound, northern Porcupine Seabight," in *Cold-water Corals and Ecosystems*, eds A. Freiwald and J. M. Roberts (Berlin: Springer-Verlag), 915–936. doi: 10.1007/3-540-27673-4_47

Beuck, L., Freiwald, A., and Taviani, M. (2010). Spatiotemporal bioerosion patterns in deep-water scleractinians from off Santa Maria di Leuca (Apulia, Ionian Sea). *Deep Sea Res. Part II Top. Stud. Oceanogr.* 57, 458–470. doi: 10.1016/j.dsr2.2009.08.019

Beuck, L., Vertino, A., Stepina, E., Karolczak, M., and Pfannkuche, O. (2007). Skeletal response of *Lophelia pertusa* (Scleractinia) to bioeroding sponge infestation visualised with micro-computed tomography. *Facies* 53, 157–176. doi: 10.1007/s10347-006-0094-9

Bibiloni, M. A. (1981). Estudio sistemático de orden Poecilosclerida (Demospongia) de la Costa Brava (Gerona). *Bol. Inst. Esp. Océano.* 6, 103–154.

Bibiloni, M. A. (1990). *Fauna de esponjas de las islas Baleares: Variación cualitativa y cuantitativa de la población de esponjas en un gradiente batimétrico: comparación Baleares-costa catalana*. Ph. D. Thesis. Barcelona: Universitat de Barcelona, 483.

Bibiloni, M. A. (1993). Some new or poorly known sponges of the Balearic Islands (western Mediterranean). *Scien. Mar.* 57, 307–318.

Bo, M., Bertolino, M., Bavestrello, G., Canese, S., Giusti, M., Angiolillo, M., et al. (2012). Role of deep sponge grounds in the Mediterranean Sea: a case

study in southern Italy. *Hydrobiologia* 687, 163–177. doi: 10.1007/978-94-007-4688-6_14

Boavida, J., Becheler, R., Addamo, A. M., Sylvestre, F., and Arnaud-Haond, S. (2019). "Past, Present and Future Connectivity of Mediterranean Cold-Water Corals: Patterns, Drivers and Fate in a Technically and Environmentally Changing World". in Mediterranean Cold-Water Corals: Past, Present and Future, eds C. Orejas and C. Jiménez (Springer International Publishing AG, part of Springer Nature). *Coral Reefs World Ser.* 9, 357–372. doi: 10.1007/978-3-319-91608-8_31

Bouchet, P., and Taviani, M. (1992). The Mediterranean deep-sea fauna: pseudopopulations of Atlantic species? *Deep Sea Res. Pt. A Oceanogr. Res. Pap.* 39, 169–184.

Boury-Esnault, N., Pansini, M., and Uriz, M. J. (1992). — *Discorhabdella hindei* n.sp. (Porifera, Demospongiae), a new Tethyan relict of pre-Messinian biota? *J. Nat. History* 26, 1–7. doi: 10.1080/00222939200770011

Boury-Esnault, N., Pansini, M., and Uriz, M. J. (1994). Spongiaires bathyaux de la mer d'Alboran et du golfe ibéro-marocain. *Mém. Mus. Natl. Hist. Nat.* 160, 1–174.

Boury-Esnault, N., Vacelet, J., Dubois, M., Goujard, A., Fourt, M., Perez, T., et al. (2017). New hexactinellid sponges from deep Mediterranean canyons. *Zootaxa* 4236, 118–134. doi: 10.11646/zootaxa.4236.1.6

Boury-Esnault, N., Vacelet, J., Reiswig, H. M., Fourt, M., Aguilar, R., and Chevaldonné, P. (2015). Mediterranean hexactinellid sponges, with the description of a new *Sympagella* species (Porifera, Hexactinellida). *J. Mar. Biolog. Assoc. U K.* 95, 1353–1364. doi: 10.1017/s0025315414001891

Buhl-Mortensen, L., Vanreusel, A., Gooday, A. J., Levin, L. A., Priede, I. G., Buhl-Mortensen, P., et al. (2010). Biological structures as a source of habitat heterogeneity and biodiversity on the deep ocean margins. *Mar. Ecol.* 31, 21–50. doi: 10.1111/j.1439-0485.2010.00359.x

Buhl-Mortensen, P., Buhl-Mortensen, L., and Purser, A. (2016). ""Trophic Ecology and Habitat Provision in Cold-Water Coral Ecosystems"," in *Marine Animal Forests, The Ecology of Benthic Biodiversity Hotspots*, eds S. Rossi, L. Bramanti, A. Gori, and C. Orejas (Switzerland: Springer), 919–944. doi: 10.1007/978-3-319-21012-4_20

Calcinai, B., Moratti, V., Martinelli, M., Bavestrello, G., and Taviani, M. (2013). Uncommon sponges associated with deep coral bank and maërl habitats in the Strait of Sicily (Mediterranean Sea). *Ita. J. Zool.* 80, 412–423. doi: 10.1080/11250003.2013.786763

Carballo, J. L., Naranjo, S., and Garcia-Gómez, J. C. (1997). Where does the Mediterranean Sea begin? Zoogeographical affinities of the littoral sponges of the Straits of Gibraltar. *J. Biogeogr.* 24, 223–232. doi: 10.1046/j.1365-2699.1997.00082.x

Cárdenas, P., Pérez, T., and Boury-Esnault, N. (2012). Sponge systematics facing new challenges. *Adv. Mar. Biol.* 61, 79–209.

Cardone, F., Pansini, M., Corriero, G., and Bertolino, M. (2019). Two new species of deep-sea sponges (Porifera, Demospongiae) from submarine canyons of the Sardinian continental margin (western Mediterranean Sea). *Zootaxa* 4688, 407–419. doi: 10.11646/zootaxa.4688.3.7

Chimienti, G., Bo, M., Taviani, M., and Mastrototaro, F. (2019). "Occurrence and Biogeography of Mediterranean Cold-Water Corals," in *Mediterranean Cold-Water Corals: Past, Present and Future*, eds C. Orejas and C. Jiménez (Berlin: Springer International Publishing AG).

Chombard, C., and Boury-Esnault, N. (1999). "Good congruence between morphology and molecular phylogeny of Hadromerida, or how to bother sponge taxonomists," in *Proceedings of the 5th International Sponge Symposium 1998*, Vol. 44, ed. J. N. A. Hooper (Brisbane, OLD: Memoirs of the Queensland Museum), 100.

Corbera, G., Lo Iacono, C., Gràcia, E., Grinyó, J., Pierdomenico, M., Huvenne, V. A., et al. (2019). Ecological characterisation of a Mediterranean cold-water coral reef: Cabliers Coral Mound Province (Alboran Sea, western Mediterranean). *Prog. Oceanog.* 175, 245–262. doi: 10.1016/j.pocean.2019.04.010

Costa, G., Bo, M., Grinyó, J., Lo Iacono, C., Pansini, M., and Bertolino, M. (2018). "A first preliminary study of the sponge fauna associated to white coral banks from the Alboran Sea," in *4th International Workshop on Taxonomy of Atlanto-Mediterranean Deep-Sea and Cave Sponges 2018*, eds C. T. Pérez, N. Boury-Esnault, P. Cárdenas, P. Chevaldonné, A. Ereskovsky, C. Ruiz, et al. (IWTAM: Marseille), 32.

Cristobo, F. J., Urgorri, V., Solórzano, M. R., and Ríos, P. (1993). "Métodos de recogida, estudio y conservación de las colecciones de poríferos," in *Simposio Internacional sobre Preservación y Conservación de Colecciones de Historia Natural (Comunicaciones Sobre la Situación, Preservación y Conservación de Colecciones de Historia Natural)*, Vol. 2, eds B. Thomas, F. Palacios, and M. C. Martínez-López, 277–287.

de la Torriente, A., Aguilar, R., González-Irusta, J. M., Blanco, M., and Serrano, A. (2020). Habitat forming species explain taxonomic and functional diversities in a Mediterranean seamount. *Ecol. Indic.* 118:106747. doi: 10.1016/j.ecolind.2020.106747

De Leo, F., Puig, P., Lo Iacono, C., Durán, R., Grinyó, J., Ambroso, S., et al. (2019). "First observations of Living Cold Water Corals surrounded by fishing grounds in Blanes Canyon (NW Mediterranean)," in *7th Internation Symposium on Deep-Sea Corals, July 29 – August 2, 2019, Cartagena, Colombia* (Colombia: ISDSC).

Dendy, A. (1922). "Report on the sigmatotetraxonida collected by H.M.S.'Sealark' in the Indian Ocean," in *Reports of the Percy Sladen Trust Expedition to the Indian Ocean in 1905*, Vol. 7, (London: Transactions of the Linnean Society of London), 1–18.

Dinn, C. (2020). A new species of Haliclona (Flagellia) Van Soest, 2017 (Porifera, Demospongiae, Heteroscleromorpha) from the Gulf of St. Lawrence, Canada. *Zootaxa* 4778, 3910–3395.

D'Onghia, G., Capezzuto, F., Cardone, F., Carlucci, R., Carluccio, A., Chimienti, et al. (2015). Macro- and megafauna recorded in the submarine Bari Canyon (southern Adriatic, Mediterranean Sea) using different tools. *Med. Mar. Sci.* 16, 180–196. doi: 10.12681/mms.1082

Edwards, K. F., and Stachowicz, J. J. (2011). Spatially stochastic settlement and the coexistence of benthic marine animals. *Ecology* 92, 1094–1103. doi: 10.1890/10-1332.1

Emig, C. C., and Geistdoerfer, P. (2004). The Mediterranean deep-sea fauna: historical evolution, bathymetric variations and geographical changes. *Carnets Géol.* 2004:3230.

Evans, J., Knittweis, L., Borg, J. A., and Schembri, P. J. (2019). "Cold-Water Corals in the Mediterranean: A History of Discovery," in *Mediterranean Cold-Water Corals: Past, Present and Future*, eds C. Orejas and C. Jiménez (Berlin: Springer International Publishing AG).

Fabri, M. C., Bargain, A., Pairaud, I., Pedel, L., and Taupier-Letage, I. (2017). Cold-water coral ecosystems in Cassidaigne Canyon: an assessment of their environmental living conditions. *Deep Sea Res. Part II Top. Stud. Oceanogr.* 137, 436–453. doi: 10.1016/j.dsr2.2016.06.006

Fabri, M. C., Pedel, L., Beuck, L., Galgani, F., Hebbeln, D., and Freiwald, A. (2014). Megafauna of vulnerable marine ecosystems in French Mediterranean submarine canyons: Spatial distribution and anthropogenic impacts. *Deep Sea Res. Part II Top. Stud. Oceanogr.* 104, 184–207. doi: 10.1016/j.dsr2.2013.06.016

Fabri, M. C., Vinha, B., Allais, A. G., Bouhier, M. E., Dugornay, O., Gaillot, A., et al. (2019). Evaluating the ecological status of cold-water coral habitats using non-invasive methods: An example from Cassidaigne canyon, northwestern Mediterranean Sea. *Prog. Oceanog.* 178:102172. doi: 10.1016/j.pocean.2019.102172

FAO (2008). *Report of the Technical Consultation on International Guidelines for the Management of Deep-sea Fisheries in the High Seas. Rome, 4–8 February and 25–29 August 2008. FAO Fisheries and Aquaculture Report, No. 881*. Rome: FAO, 1–42.

Ferrer Hernández, F. (1923). Más datos para el conocimiento de las esponjas de las costas españolas. *Boletín Pescas* 7, 247–272.

Fourt, M., Goujard, A., Pérez, T., and Chevaldonné, P. (2017). Guide de la faune profonde de la mer Méditerranée. Explorations des roches et des canyons sous-marins des côtes françaises. Patrimoines naturels. *Publicat. Sci. Museum Natl. d'Histoire Nat. Paris* 75, 1–184.

Gabrie, C., Lagabrielle, E., Crochelet, E., Meola, B., Webster, C., Claudet, J., et al. (2012). *The status of marine protected areas in the Mediterranean Sea. MedPAN and RAC/ SPA*. Gland: *IUCN*, 256.

Gage, J. D. (2004). Diversity in deep-sea benthic macrofauna: the importance of local ecology, the larger scale, history and the Antarctic. *Deep Sea Res. Part II Top. Stud. Oceanogr.* 51, 1689–1708. doi: 10.1016/j.dsr2.2004.07.013

Gary, S. F., Fox, A. D., Biastoch, A., Roberts, J. M., and Cunningham, S. A. (2020). Larval behaviour, dispersal and population connectivity in the deep sea. *Scient. Rep.* 10, 1–12.

General Fisheries Commission for the Mediterranean (GFCM, S.A.C.) (2008). *Criteria for the identification of sensitive habitats of relevance for the management of priority species, General Fisheries Commission for the Mediterranean- Scientific Advisory Committee –Sub –Committee on Marine Environment and Ecosystems (SCMEE), Eleventh Season, Marrakech, Morocco, 1–5 December 2008*. Rome: General Fisheries Commission for the Mediterranean.

Gerovasileiou, V., and Voultsiadou, E. (2012). Marine Caves of the Mediterranean Sea: A Sponge Biodiversity Reservoir within a Biodiversity Hotspot. *PLoS One* 7:e39873. doi: 10.1371/journal.pone.0039873

Gili, J. M., Bouillon, J., Pagès, F., Palanques, A., Puig, P., and Heussner, S. (1998). Origin and biogeography of the deep-water Mediterranean Hydromedusae including the description of two new species collected in submarine canyons of Northwestern Mediterranean. *Sci. Mar.* 62, 113–134.

Göcke, C., Hestetun, J. T., Uhlir, C., Freiwald, A., Beuck, L., et al. (2016). Cladorhiza corallophila sp. nov., a new carnivorous sponge (Cladorhizidae, Demospongiae) living in close association with Lophelia pertusa and Madrepora oculata (Scleractinia). *Zootaxa* 4168, 512–524. doi: 10.11646/zootaxa.4168.3.4

Goodwin, C. E., Picton, B. E., and van Soest, R. W. M. (2011). *Hymedesmia (Porifera: Demospongiae: Poecilosclerida) from Irish and Scottish cold-water coral reefs, with a description of five new species* J. *Mar. Biolog. Assoc. U K.* 91, 979–997. doi: 10.1017/s0025315411000014

Hajdu, E. (2002). "Family Hamacanthidae Gray, 1872," in *Systema Porifera. A guide to the classification of sponges*, Vol. 1, eds J. N. A. Hooper and R. W. M. van Soest (New York, NY: Kluwer Academic), 665–668. doi: 10.1007/978-1-4615-0747-5_72

Hajdu, E., and Castello-Branco, C. (2014). Hamacantha (Hamacantha) boomerang sp. nov. from deep-sea coral mounds at Campos Basin, SW Atlantic, and redescription of H. (H.) schmidtii (Carter, 1882) (Hamacanthidae, Poecilosclerida, Demospongiae). *Zootaxa* 3753, 384–390. doi: 10.11646/zootaxa.3753.4.7

Hajdu, E., Hooker, Y., and Willenz, P. (2015). New Hamacantha from Peru and resurrection of Zygherpe as subgenus (Demospongiae, Poecilosclerida, Hamacanthidae). *Zootaxa* 3926, 87–99. doi: 10.11646/zootaxa.3926.1.3

Hayes, D. R., Schroeder, K., Poulain, P.-M., Testor, P., Mortier, L., Bosse, A., et al. (2019). "Review of the Circulation and Characteristics of Intermediate Water Masses of the Mediterranean: Implications for Cold-Water Coral Habitats," in *Mediterranean Cold-Water Corals: Past, Present and Future*, eds C. Orejas and C. Jiménez (Berlin: Springer International Publishing AG).

Henry, L. A., and Roberts, J. M. (2016). "Global biodiversity in cold-water coral reef ecosystems," in *Marine Animal Forests, The Ecology of Benthic Biodiversity Hotspots*, eds S. Rossi, L. Bramanti, A. Gori, and C. Orejas (Berlin: Springer), 235–256. doi: 10.1007/978-3-319-21012-4_6

Henry, L. A., Navas, J. M., Hennige, S. J., Wicks, L. C., Vad, J., and Roberts, J. M. (2013). Cold-water coral reef habitats benefit recreationally valuable sharks. *Biol. Cons.* 161, 67–70. doi: 10.1016/j.biocon.2013.03.002

Henry, L.-A., and Roberts, J. M. (2007). Biodiversity and ecological composition of macrobenthos on cold-water coral mounds and adjacent off-mound habitat in the bathyal Porcupine Seabight, NE Atlantic. *Deep Sea Res. Part I Oceanogr. Res. Pap.* 54, 654–672. doi: 10.1016/j.dsr.2007.01.005

Heres, P., Cristobo, J., and Ríos, P. (2014). "*Acanthancora schmidti* (Topsent, 1898) (Porifera, Poecilosclerida), new record in the Cantabrian Sea," in *XVIII Simposio Ibérico de Estudios de Biología Marina*, eds P. Ríos, L. A. Suárez, and J. Cristobo (Gijón: Centro Oceanográfico de Gijón).

Hestetun, J. T., Tompkins-Macdonald, G., and Rapp, H. T. (2017). A review of carnivorous sponges (Porifera: Cladorhizidae) from the Boreal North Atlantic and Arctic. *Zool. J. Linn. Soc.* 181, 1–69. doi: 10.1093/zoolinnean/zlw022

Hou, Z., and Li, S. (2018). Tethyan changes shaped aquatic diversification. *Biol. Rev*. 93, 874–896.

Hsü, K. J., Ryan, W. B. F., and Cita, M. B. (1973). Late Miocene desiccation of the Mediterranean. *Nature* 242, 240–244. doi: 10.1038/242240a0

Hughes, T. P., Bellwood, D. R., and Connolly, S. R. (2002). Biodiversity hotspots, centres of endemicity, and the conservation of coral reefs. *Ecol. Lett.* 5, 775–784. doi: 10.1046/j.1461-0248.2002.00383.x

Ise, Y., Woo, S. P., Tan, S. H., and Fujita, T. (2019). First record of *Hamacantha* (Porifera, Demospongiae, Merliida, Hamacanthidae) from Japan, with description of two new species. *Zootaxa* 4657, 474–482. doi: 10.11646/zootaxa.4657.3.3

Jensen, A., and Frederiksen, R. (1992). The fauna associated with the bank-forming deepwater coral *Lophelia pertusa* (Scleractinaria) on the Faroe shelf. *Sarsia* 77, 53–69. doi: 10.1080/00364827.1992.10413492

Jones, C. G., Lawton, J. H., and Shachak, M. (1994). "Organisms as ecosystem engineers," in *Ecosystem management*, eds F. B. Samson and F. L. Knopf (New York, NY: Springer), 130–147. doi: 10.1007/978-1-4612-4018-1_14

Jones, G. P., Almany, G. R., Russ, G. R., Sale, P. F., Steneck, R. S., Van Oppen, M. J. H., et al. (2009). Larval retention and connectivity among populations of corals and reef fishes: history, advances and challenges. *Coral Reefs* 28, 307–325. doi: 10.1007/s00338-009-0469-9

Kassambara, A. (2020). *ggpubr: 'ggplot2' Based Publication Ready Plots. R package version 0.4.0*. Berlin: R Core Team.

Kazanidis, G., and Witte, U. F. (2016). The trophic structure of *Spongosorites coralliophaga*-coral rubble communities at two northeast Atlantic cold water coral reefs. *Mar. Biol. Res.* 12, 932–947. doi: 10.1080/17451000.2016.1216569

Kazanidis, G., Henry, L. A., Roberts, J. M., and Witte, U. F. (2016). Biodiversity of *Spongosorites coralliophaga* (Stephens, 1915) on coral rubble at two contrasting cold-water coral reef settings. *Coral Reefs* 35, 193–208. doi: 10.1007/s00338-015-1355-2

Kazanidis, G., van Oevelen, D., Veuger, B., and Witte, U. F. (2018). Unravelling the versatile feeding and metabolic strategies of the cold-water ecosystem engineer *Spongosorites coralliophaga* (Stephens, 1915). *Deep Sea Res. Part I Oceanogr. Res. Pap.* 141, 71–82. doi: 10.1016/j.dsr.2018.07.009

Krijgsman, W., Capella, W., Simon, D., Hilgen, F. J., Kouwenhoven, T. J., Meijer, P. T., et al. (2018). The Gibraltar corridor: Watergate of the Messinian salinity crisis. *Mar. Geol.* 403, 238–246. doi: 10.1016/j.margeo.2018.06.008

Lastras, G., Canals, M., Ballesteros, E., Gili, J. M., and Sanchez-Vidal, A. (2016). Cold-water corals and anthropogenic impacts in La Fonera submarine canyon head, Northwestern Mediterranean Sea. *PLoS One* 11:e0155729. doi: 10.1371/journal.pone.0155729

Laubenfels, M. W. (1932). The marine and fresh-water sponges of California. *Proc. U S. Natl. Mus.* 81, 1–140. doi: 10.5479/si.00963801.81-2927.1

Lesser, M. P. (2006). Benthic–pelagic coupling on coral reefs: feeding and growth of Caribbean sponges. *J. Exp. Mar. Biol. Ecol.* 328, 277–288. doi: 10.1016/j.jembe.2005.07.010

Linley, T. D., Lavaleye, M., Maiorano, P., Bergman, M., Capezzuto, F., Cousins, N. J., et al. (2017). Effects of cold-water corals on fish diversity and density (European continental margin: Arctic, NE Atlantic and Mediterranean Sea): Data from three baited lander systems. *Deep Sea Res. Part II Top. Stud. Oceanogr.* 145, 8–21. doi: 10.1016/j.dsr2.2015.12.003

Lo Iacono, C. (2012). *MELCOR (MELillaCORals). Geomorphologic, Ecologic and Environmental Study of CWC Mounds in the Mediterranean Moroccan Margin. Cruise Report*. United Kingdom: National Oceanography Centre.

Lo Iacono, C., Gràcia, E., Ranero, C. R., Emelianov, M., Huvenne, V. A., Bartolomé, R., et al. (2014). The West Melilla cold water coral mounds, Eastern Alboran Sea: Morphological characterization and environmental context. *Deep Sea Res. Part II Top. Stud. Oceanogr.* 99, 316–326. doi: 10.1016/j.dsr2.2013.07.006

Longo, C., Mastrototaro, F., and Corriero, G. (2005). Sponge fauna associated with a Mediterranean deep-sea coral bank. *J. Mar. Biolog. Assoc. U K.* 85, 1341–1352. doi: 10.1017/s0025315405012518

Lundbeck, W. (1902). Porifera. (Part I.) Homorrhaphidae and Heterorrhaphidae. *Danish Ingolf-Expedit.* 6, 1–108.

Lundbeck, W. (1910). Porifera. (Part III.) Desmacidonidae. *Danish Ingolf Expedit.* 6, 1–124.

Maldonado, M. (1992). Demosponges of the red coral bottoms from the Alboran Sea. *J. Nat. Hist.* 26, 1131–1161. doi: 10.1080/00222939200770661

Maldonado, M. (1993). *Demosponjas litorales de Alborán: faunística y biogeografía*. Ph. D Thesis. Barcelona: Universitat de Barcelona, 496.

Maldonado, M., and Uriz, M. J. (1995). Biotic affinities in a transitional zone between the Atlantic and the Mediterranean: a biogeographical approach based on sponges. *J. Biogeog.* 22, 89–110. doi: 10.2307/2846075

Maldonado, M., and Young, C. M. (1996). Bathymetric patterns of sponge distribution on the Bahamian slope. *Deep Sea Res. Part I Oceanogr. Res. Pap.* 43, 897–915. doi: 10.1016/0967-0637(96)00042-8

Maldonado, M., López-Acosta, M., Beazley, L., Kenchington, E., Koutsouveli, V., and Riesgo, A. (2020). Cooperation between passive and active silicon transporters clarifies the ecophysiology and evolution of biosilicification in sponges. *Sci. Adv.* 6:eaba9322. doi: 10.1126/sciadv.aba9322

Margreth, S., Gennari, G., Rüggeberg, A., Comas, M. C., Pinheiro, L. M., and Spezzaferri, S. (2011). Growth and demise of cold-water coral ecosystems on mud volcanoes in the West Alboran Sea: The messages from the planktonic and benthic foraminifera. *Mar. Geol.* 282, 26–39. doi: 10.1016/j.margeo.2011.02.006

Mariani, S., Uriz, M. J., Turon, X., and Alcoverro, T. (2006). Dispersal strategies in sponge larvae: integrating the life history of larvae and the hydrologic component. *Oecologia* 149, 174–184. doi: 10.1007/s00442-006-0429-9

Marx, W. (2012). Tracking historical papers and their citations. *Eur. Sci. Ed.* 38, 35–37.

Mastrototaro, F., d'Onghia, G., Corriero, G., Matarrese, A., Maiorano, P., Panetta, P., et al. (2010). Biodiversity of the white coral bank off Cape Santa Maria di Leuca (Mediterranean Sea): An update. *Deep Sea Res. Part II Top. Stud. Oceanogr.* 57, 412–430. doi: 10.1016/j.dsr2.2009.08.021

Menna, M., and Poulain, P. M. (2010). Mediterranean intermediate circulation estimated from Argo data in 2003–2010. *Ocean Sci.* 6, 331–343. doi: 10.5194/os-6-331-2010

Messmer, V., Jones, G. P., Munday, P. L., Holbrook, S. J., Schmitt, R. J., and Brooks, A. J. (2011). Habitat biodiversity as a determinant of fish community structure on coral reefs. *Ecology* 92, 2285–2298. doi: 10.1890/11-0037.1

Millot, C. (1990). The gulf of Lions' hydrodynamics. *Cont. Shelf Res.* 10, 885–894. doi: 10.1016/0278-4343(90)90065-t

Moccia, D., Cau, A., Alvito, A., Canese, S., Cannas, R., Bo, M., et al. (2018). New sites expanding the "Sardinian cold-water coral province" extension: A new potential cold-water coral network? *Aquat. Conserv.* 29, 153–160. doi: 10.1002/aqc.2975

Nasto, I., Cardone, F., Mastrototaro, F., Panetta, P., Rosso, A., Sanfilippo, R., et al. (2018). Benthic invertebrates associated with subfossil cold-water coral frames and hardgrounds in the Albanian deep waters (Adriatic Sea). *Turk. Zool. Derg.* 42, 360–371. doi: 10.3906/zoo-1708-44

Oksanen, J., Blanchet, F. G., Friendly, M., Kindt, R., Legendre, P., McGlinn, D., et al. (2019). *vegan: Community Ecology Package. R package version 2.5-6*. Vienna: R Core Team.

Orejas, C., and Jiménez, C. (2019). "An Introduction to the Research on Mediterranean Cold-Water Corals," in *Mediterranean Cold-Water Corals: Past, Present and Future*, eds C. Orejas and C. Jiménez (Berlin: Springer International Publishing AG).

Orejas, C., Gori, A., Iacono, C. L., Puig, P., Gili, J. M., and Dale, M. R. (2009). Cold-water corals in the Cap de Creus canyon, northwestern Mediterranean: spatial distribution, density and anthropogenic impact. *Mar. Ecol. Prog. Ser.* 397, 37–51. doi: 10.3354/meps08314

OSPAR (2009). *Background Document for Lophelia pertusa* reefs. Luxembourg: OSPAR commission Publication.

OSPAR (2010). *Background Document for Coral gardens*. Luxembourg: OSPAR commission Publication.

Padua, A., Cunha, H. A., and Klautau, M. (2018). Gene flow and differentiation in a native calcareous sponge (Porifera) with unknown dispersal phase. *Mar. Biod.* 48, 2125–2135. doi: 10.1007/s12526-017-0742-z

Palanques, A., and Puig, P. (2018). Particle fluxes induced by benthic storms during the 2012 dense shelf water cascading and open sea convection period in the northwestern Mediterranean basin. *Mar. Geol.* 406, 119–131.

Palomino, D., Vázquez, J. T., Ercilla, G., Alonso, B., López-González, N., and Díaz-del-Río, V. (2011). Interaction between seabed morphology and water masses around the seamounts on the Motril Marginal Plateau (Alboran Sea, Western Mediterranean). *Geo-Mar. Lett.* 31, 465–479. doi: 10.1007/s00367-011-0246-y

Pansini, M. (1987). "Littoral demosponges from the banks of the Strait of Sicily and the Alboran Sea.", in Taxonomy of Porifera from the N.E. Atlantic and Mediterranean Sea eds J. Vacelet and N. Boury-Esnault (Springer-Verlag: Berlin, Heidelberg). *NATO ASI Ser. G* 13, 149–185. doi: 10.1007/978-3-642-70892-3_8

Pardo, E., Rubio, R. A., García, S., and Ubero, J. (2011). Documentación de arrecifes de corales de agua fría en el Mediterráneo occidental (Mar de Alborán). *Chronica Nat.* 2011, 20–34.

Picton, B. E., and Goodwin, C. E. (2007). Sponge biodiversity of Rathlin Island, Northern Ireland. *J. Mar. Biolog. Assoc. U K.* 87, 1441–1458. doi: 10.1017/s0025315407058122

Pisera, A., Łukowiak, M., Fromont, J., and Schuster, A. (2018). First record of the genus *Vetulina* Schmidt, 1879 (Porifera: Demospongiae: Sphaerocladina) from the Indian Ocean with the description of two new species: biogeographic and evolutionary significance. *Mar. Biod.* 48, 1529–1539. doi: 10.1007/s12526-017-0658-7

Plaisance, L., Knowlton, N., Paulay, G., and Meyer, C. (2009). Reef-associated crustacean fauna: biodiversity estimates using semi-quantitative sampling and DNA barcoding. *Coral Reefs* 28, 977–986. doi: 10.1007/s00338-009-0543-3

Por, F. D. (1989). "Postface: The Legacy of Tethys—Or the Guise of a Conclusion," in *The Legacy of Tethys*, ed. F. D. Por (Dordrecht: Springer), 165–168. doi: 10.1007/978-94-009-0937-3_7

Puig, P., and Gili, J. M. (2019). "Submarine Canyons in the Mediterranean: A Shelter for Cold-Water Corals," in *Mediterranean Cold-Water Corals: Past, Present and Future*, eds C. Orejas and C. Jiménez (Berlin: Springer).

Puig, P., Lo Iacono, C., Durán, R., Grinyó, J., Ambroso, S., De Leo, et al. (2019). "Living Cold Water Corals surrounded by fishing grounds in Blanes Canyon (NW Mediterranean)," in *GeoHab 2019 Annual Conference* (St. Petersburg: GeoHab).

Pulitzer-Finali, G. (1983). A collection of Mediterranean Demospongiae (Porifera) with, in appendix, a list of the Demospongiae hitherto recorded from the Mediterranean Sea. *Ann. Mus. Civ. Stor. Nat. Giacomo Doria* 84, 445–621.

R Core Team (2019). *R: A Language and Environment for Statistical Computing*. Vienna: R Core Team.

Redmond, N. E., Morrow, C. C., Thacker, R. W., Diaz, M. C., Boury-Esnault, N., Cárdenas, P., et al. (2013). Phylogeny and systematics of Demospongiae in light of new small-subunit ribosomal DNA (18S) sequences. *Integr. Comp. Biol.* 53, 388–415. doi: 10.1093/icb/ict078

Reveillaud, J., Remerie, T., van Soest, R., Erpenbeck, D., Cárdenas, P., Derycke, S., et al. (2010). Species boundaries and phylogenetic relationships between Atlanto-Mediterranean shallow-water and deep-sea coral associated *Hexadella* species (Porifera, Ianthellidae). *Mol. Phylogenet. Evol.* 56, 104–114. doi: 10.1016/j.ympev.2010.03.034

Reveillaud, J., van Soest, R., Derycke, S., Picton, B., Rigaux, A., and Vanreusel, A. (2011). Phylogenetic relationships among NE Atlantic *Plocamionida* Topsent (1927) (Porifera, Poecilosclerida): under-estimated diversity in reef ecosystems. *PLoS One* 6:e16533. doi: 10.1371/journal.pone.0016533

Ríos, P., Riesgo, A., Taboada, S., and Cristobo, J. (2020). A new species of *Isodictya* (Porifera: Poecilosclerida) from the Southern Ocean. *Polar Biol.* 43, 523–533. doi: 10.1007/s00300-020-02654-x

Rix, L., De Goeij, J. M., Mueller, C. E., Struck, U., Middelburg, J. J., Van Duyl, F. C., et al. (2016). Coral mucus fuels the sponge loop in warm-and cold-water coral reef ecosystems. *Sci. Rep.* 6, 1–11. doi: 10.1007/978-3-319-17001-5_6-1

Rix, L., de Goeij, J. M., van Oevelen, D., Struck, U., Al-Horani, F. A., Wild, C., et al. (2017). Differential recycling of coral and algal dissolved organic matter via the sponge loop. *Funct. Ecol.* 31, 778–789. doi: 10.1111/1365-2435.12758

Roberts, C. M., McClean, C. J., Veron, J. E., Hawkins, J. P., Allen, G. R., McAllister, D. E., et al. (2002). Marine biodiversity hotspots and conservation priorities for tropical reefs. *Science* 295, 1280–1284. doi: 10.1126/science.1067728

Roberts, E. M., Bowers, D. G., Meyer, H. K., Samuelsen, A., Rapp, H. T., and Cárdenas, P. (2021). Water masses constrain the distribution of deep-sea sponges in the North Atlantic Ocean and Nordic Seas. *Mar. Ecol. Prog. Ser.* 659, 75–96. doi: 10.3354/meps13570

Roberts, J. M., Davies, A. J., Henry, L. A., Dodds, L. A., Duineveld, G. C. A., Lavaleye, M. S. S., et al. (2009b). Mingulay reef complex: an interdisciplinary study of cold-water coral habitat, hydrography and biodiversity. *Mar. Ecol. Prog. Ser.* 397, 139–151. doi: 10.3354/meps08112

Roberts, J. M., Wheeler, A. J., and Freiwald, A. (2006). Reefs of the deep: the biology and geology of cold-water coral ecosystems. *Science* 312, 543–547. doi: 10.1126/science.1119861

Roberts, J., Wheeler, A. J., Freiwald, A., and Cairns, S. (2009a). *Cold-Water Corals. The Biology and Geology of Deep-Sea Coral Habitats*. Cambridge: Cambridge University Press.

Robertson, L. M., Hamel, J. F., and Mercier, A. (2017). Feeding in deep-sea demosponges: Influence of abiotic and biotic factors. *Deep Sea Res. Part I Oceanogr. Res. Pap.* 127, 49–56. doi: 10.1016/j.dsr.2017.07.006

Robinson, A. R., Leslie, W. G., Theocharis, A., and Lascaratos, A. (2001). "Mediterranean sea circulation," in *1st edition of the Encyclopedia of Ocean Sciences*, eds J. H. Steele, S. A. Thorpe, and K. K. Turekian (Amsterdam: Elsevier Ltd).

Rogers, A. D. (1999). The Biology of *Lophelia pertusa* (Linnaeus 1758) and Other Deep-Water Reef-Forming Corals and Impacts from Human Activities. *Int. Rev. Hydrobiol.* 84, 315–406. doi: 10.1002/iroh.199900032

Rosell, D., and Uriz, M. J. (2002). Excavating and endolithic sponge species (Porifera) from the Mediterranean: species descriptions and identification key. *Organisms Divers. Evolut.* 2, 55–86. doi: 10.1078/1439-6092-00033

Rueda, J. L., Urra, J., Aguilar, R., Angeletti, L., Bo, M., García-Ruiz, C., et al. (2019). "Cold-Water Coral Associated Fauna in the Mediterranean Sea and Adjacent Areas," in *Mediterranean Cold-Water Corals: Past, Present and Future*, eds C. Orejas and C. Jiménez (Berlin: Springer).

Santín, A., Grinyó, J., Ambroso, S., Uriz, M. J., Dominguez-Carrió, C., et al. (2019). Distribution patterns and demographic trends of demosponges at the Menorca Channel (Northwestern Mediterranean Sea). *Prog. Oceanog.* 173, 9–25. doi: 10.1016/j.pocean.2019.02.002

Santín, A., Grinyó, J., Ambroso, S., Uriz, M. J., Gori, A., Dominguez-Carrió, C., et al. (2018a). Sponge assemblages on the deep Mediterranean continental shelf and slope (Menorca Channel, Western Mediterranean Sea). *Deep Sea Res. Part I Oceanogr. Res. Pap.* 131, 75–86. doi: 10.1016/j.dsr.2017.11.003

Santín, A., Grinyó, J., Bilan, M., Ambroso, S., and Puig, P. (2020a). First report of the carnivorous sponge *Lycopodina hypogea* (Cladorhizidae) associated with marine debris, and its possible implications on deep-sea connectivity. *Mar. Poll. Bull.* 159:111501. doi: 10.1016/j.marpolbul.2020.111501

Santín, A., Grinyó, J., Uriz, M. J., Gili, J. M., and Puig, P. (2020b). First deep-sea *Hamigera* (Demospongiae: Porifera) species associated with Cold-Water Corals (CWC) on antipodal latitudes of the world. *Deep Sea Res. Part I Oceanogr. Res. Pap.* 164:103325. doi: 10.1016/j.dsr.2020.103325

Santín, A., Uriz, M. J., and Puig, P. (2018b). "Cryptic and rare sponges associated with Cold-Water Corals of the Blanes Canyon (northwestern Mediterranean Sea)," in *4th International Workshop on Taxonomy of Atlanto-Mediterranean Deep-Sea and Cave Sponges 2018*, eds C. T. Pérez, N. Boury-Esnault, P. Cárdenas, P. Chevaldonné, A. Ereskovsky, C. Ruiz, et al. (Marseille: MBE).

Sarà, M. (1958). Contributo all consoscenza dei Poriferi del Mar Ligure. *Ann. Mus. Civ. Stor. Nat. Giacomo Doria* 70, 207–244.

Shanks, A. L., Largier, J., Brink, L., Brubaker, J., and Hooff, R. (2002). Observations on the distribution of meroplankton during a downwelling event and associated intrusion of the Chesapeake Bay estuarine plume. *J. Plankton Res.* 24, 391–416. doi: 10.1093/plankt/24.4.391

Sitjà, C. (2020). *The bathyal connections between the Mediterranean Sea and the Northeastern Atlantic Ocean: an assessment using deep-water sponges as a case study*. Ph. D. thesis. Barcelona: Universitat de Barcelona, 360.

Sitjà, C., and Maldonado, M. (2014). New and rare sponges from the deep shelf of the Alboran Island (Alboran Sea, Western Mediterranean). *Zootaxa* 3760, 141–179. doi: 10.11646/zootaxa.3760.2.2

Sitjà, C., Maldonado, M., Farias, C., and Rueda, J. L. (2020). Export of bathyal benthos to the Atlantic through the Mediterranean outflow: Sponges from the mud volcanoes of the Gulf of Cadiz as a case study. *Deep Sea Res. Part I Oceanogr. Res. Pap.* 163:103326. doi: 10.1016/j.dsr.2020.103326

Stephens, J. (1915). Sponges of the Coasts of Ireland. I.- The Triaxonia and part of the Tetraxonida. *Fisher. Ireland Sci. Investigat.* 1914, 1–43.

Stephens, J. (1921). Sponges of the Coasts of Ireland. II. The Tetraxonida (concluded). Scientific Investigations of the Fisheries Branch. *Depart. Agricult. Ireland* 1920, 1–75.

Sollas, W. J. (1885). A classification of the sponges. *Ann. Magaz Nat. Hist.* 16:395.

Taviani, M., Angeletti, L., Antolini, B., Ceregato, A., Froglia, C., Lopez Correa, M., et al. (2011). "Geo-biology of Mediterranean deep-water coral ecosystems," in *Marine research at CNR. Dipartamento Terra e Ambiente*, eds E. Brugnoli, G. Cavaretta, S. Mazzola, F. Trincardi, M. Ravaioli, and R. Santoleri (Roma: Consiglio Nazionale delle Ricerche), 705–720.

Taviani, M., Angeletti, L., Canese, S., Cannas, R., Cardone, F., Cau, A., et al. (2017). The "Sardinian cold-water coral province" in the context of the Mediterranean coral ecosystems. *Deep Sea Res. Part II Top. Stud. Oceanogr.* 145, 61–78. doi: 10.1016/j.dsr2.2015.12.008

Teixidó, N., Gili, J. M., Uriz, M. J., Gutt, J., and Arntz, W. E. (2006). Observations of asexual reproductive strategies in Antarctic hexactinellid sponges from ROV video records. *Deep Sea Res. Pt. II Top. Stud. Oceanogr.* 53, 972–984.

Topsent, E. (1904). Spongiaires des Açores. Résultats des campagnes scientifiques accomplies par le Prince Albert I. *Monaco* 25, 1–280.

Topsent, E. (1928). Spongiaires de l'Atlantique et de la Méditerranée provenant des croisières du Prince Albert ler de Monaco. Résultats des campagnes scientifiques accomplies par le Prince Albert I. *Monaco* 74, 1–376.

United Nations General Assembly (2007). *Resolution 61/105, Sustainable fisheries, including through the 1995 Agreement for the Implementation of the Provisions of the United Nations Convention on the Law of the Sea of 10 December 1982 relating to the Conservation and Management of Straddling Fish Stocks and Highly Migratory Fish Stocks, and related instruments, A/RES/61/105*. New York, NY: United Nations General Assembly.

Uriz, M. J. (1983). Monografía I. Contribución a la fauna de esponjas (Demospongia) de Cataluña. *Anal. Sección Ciencias Colegio Univers. Gerona* 7, 1–220.

Uriz, M. J., Garate, L., and Agell, G. (2017). Molecular phylogenies confirm the presence of two cryptic Hemimycale species in the Mediterranean and reveal the polyphyly of the genera Crella and Hemimycale (Demospongiae: Poecilosclerida). *PeerJ* 5:e2958.

Uriz, M. J., and Rosell, D. (1990). Sponges from bathyal depths (1000–1750 m) in the Western Mediterranean Sea. *J. Nat. Hist.* 24, 373–391. doi: 10.1080/00222939000770281

Vacelet, J. (1969). Eponges de la Roche du Large et de l'étage bathyal de Méditerranée (Récoltes de la soucoupe plongeante Cousteau et dragages). *Mém. Mus. Natl. Hist. Nat. A Zool.* 59, 145–219.

Vacelet, J. (1979). "Descriptions et affinités d'une éponge sphinctozoaire actuelle," in *Biologie des Spongiaires. Sponge Biology*, Vol. 291, eds C. Lévi and N. Boury-Esnault (Paris: Colloques Internationaux du Centre National de la Recherché Scientifique), 483–493.

Vacelet, J., Boury-Esnault, N., and Harmelin, J. G. (1994). Hexactinellid cave, a unique deep-sea habitat in the scuba zone. *Deep Sea Res. Part I Oceanogr. Res. Pap.* 41, 965–973. doi: 10.1016/0967-0637(94)90013-2

van Soest, R. W. (2009). New sciophilous sponges from the Caribbean (Porifera: Demospongiae). *Zootaxa* 2107, 1–40. doi: 10.11646/zootaxa.2107.1.1

van Soest, R. W. M. (2002). "Family Hymedesmiidae," in *Systema Porifera. A guide to the classification of sponges*, eds J. N. A. Hooper and R. W. M. van Soest (New York, NY: Kluwer Academic).

van Soest, R. W. M. (2017). *Flagellia*, a new subgenus of *Haliclona* (Porifera, Haplosclerida). *Eur. J. Taxon.* 351, 1–48. doi: 10.1007/978-3-319-23534-9_1

van Soest, R. W. M., and Beglinger, E. J. (2009). New bioeroding sponges from Mingulay coldwater reefs, north-west Scotland. *J. Mar. Biolog. Assoc. U K.* 89, 329–335. doi: 10.1017/s0025315408002725

van Soest, R. W. M., and De Voogd, N. J. (2015). Sponge species composition of north-east Atlantic cold-water coral reefs compared in a bathyal to inshore gradient. *J. Mar. Biolog. Assoc. U K.* 95, 1461–1471. doi: 10.1017/s0025315413001410

van Soest, R. W. M., and Lavaleye, M. S. S. (2005). Diversity and abundance of sponges in bathyal coral reefs of Rockall Bank, NE Atalantic, from boxcore samples. *Mar. Biol. Res.* 1, 338–349. doi: 10.1080/17451000500380322

van Soest, R. W. M., Boury-Esnault, N., Hooper, J. N. A., Rützler, K., de Voogd, N. J., Alvarez, B., et al. (2021). *World Porifera Database*. Ostend: World Register of Marine Species.

van Soest, R. W. M., Boury-Esnault, N., Vacelet, J., Dohrmann, M., Erpenbeck, D., De Voogd, N. J., et al. (2012). Global diversity of sponges (Porifera). *PLoS One* 7:e35105. doi: 10.1371/journal.pone.0035105

van Soest, R. W. M., Cleary, D. F. R., de Kluijver, M. J., Lavaleye, M. S. S., Maier, C., and van Duyl, F. C. (2007). Sponge diversity and community composition in Irish bathyal coral reefs. *Contrib. Zool.* 76, 121–142. doi: 10.1163/18759866-07602005

Vázquez, J. T., Ercilla, G., Alonso, B., Juan, C., Rueda, J. L., Palomino, D., et al. (2015). "Submarine Canyons and related features in the Alboran Sea: continental margins and major isolated reliefs," in *Submarine canyon dynamics in the Mediterranean and tributary seas: An integrated geological, oceanographic and biological perspective*, ed. F. Briand (Monaco: CIESM Publisher).

Wickham, H., Averick, M., Bryan, J., Chang, W., McGowan, L. D. A., François, R., et al. (2019). Welcome to the Tidyverse. *J. Open Source Softw.* 4:1686. doi: 10.21105/joss.01686

Wild, C., Jantzen, C., Struck, U., Hoegh-Guldberg, O., and Huettel, M. (2008). Biogeochemical responses following coral mass spawning on the Great Barrier Reef: pelagic–benthic coupling. *Coral Reefs* 27, 123–132. doi: 10.1007/s00338-007-0298-7

Würtz, M. (2012). "Submarine canyons and their role in the Mediterranean ecosystem," in *Mediterranean Submarine Canyons: Ecology and Governance*, ed. M. Würtz (Switzerland: IUCN), 11–26.

Xavier, J. R., and Van Soest, R. W. (2012). Diversity patterns and zoogeography of the Northeast Atlantic and Mediterranean shallow-water sponge fauna. *Hydrobiologia* 687, 107–125.

Zabala, M., Maluquer, P., and Hermelin, J. G. (1993). Epibiotic bryozoans on deep-water seleractinian corals from the Catalonia slope (western Mediterranean, Spain, France). *Sci. Mar.* 57, 65–78.

Zibrowius, H., and Taviani, M. (2005). "Remarkable sessile fauna associated with deep coral and other calcareous substrates in the Strait of Sicily, Mediterranean Sea," in *Cold-water Corals and Ecosystems*, eds A. Freiwald and J. M. Roberts (Berlin: Springer-Verlag), 807–819. doi: 10.1007/3-540-27673-4_42

Conflict of Interest: The authors declare that the research was conducted in the absence of any commercial or financial relationships that could be construed as a potential conflict of interest.

Copyright © 2021 Santín, Grinyó, Uriz, Lo Iacono, Gili and Puig. This is an open-access article distributed under the terms of the Creative Commons Attribution License (CC BY). The use, distribution or reproduction in other forums is permitted, provided the original author(s) and the copyright owner(s) are credited and that the original publication in this journal is cited, in accordance with accepted academic practice. No use, distribution or reproduction is permitted which does not comply with these terms.

frontiers in Marine Science

ORIGINAL RESEARCH
published: 04 October 2021
doi: 10.3389/fmars.2021.701218

Life in the Fast Lane: Modeling the Fate of Glass Sponge Larvae in the Gulf Stream

Shuangqiang Wang[1], Ellen Kenchington[1], Zeliang Wang[1] and Andrew J. Davies[2]*

[1] Bedford Institute of Oceanography, Fisheries and Oceans Canada, Dartmouth, NS, Canada, [2] Department of Biological Sciences, University of Rhode Island, Kingston, RI, United States

Effective conservation management of deep-sea sponges, including design of appropriate marine protected areas, requires an understanding of the connectivity between populations throughout a species' distribution. We provide the first consideration of larval connectivity among deep-sea sponge populations along the southeastern coast of North America, illustrate the influence of the Gulf Stream on dispersal, and complement published distribution models by evaluating colonization potential. Connectivity among known populations of the hexactinellid sponge *Vazella pourtalesii* was simulated using a 3-D biophysical dispersal model throughout its distribution from Florida, United States to Nova Scotia, Canada. We found no exchange with an estimated pelagic larval duration of 2 weeks between populations north and south of Cape Hatteras, North Carolina at surface, mid-water and seabed release depths, irrespective of month of release or application of a horizontal diffusion constant specific to cross-Gulf Stream diffusivity. The population north of Cape Hatteras and south of Cape Cod was isolated. There was some evidence that Gulf Stream eddies formed near Cape Hatteras could travel to the northwest, connecting the populations in the two sub-regions, however that would require a much longer pelagic duration than what is currently known. More likely almost all larval settlement will be in the immediate area of the adults. At sub-regional scales, connectivity was found from the Strait of Florida through to the Blake Plateau, southeastern United States, with the latter area showing potential for recruitment from more than one source population. The influence of the Charleston Bump, a shallow feature rising from the Blake Plateau, was substantial. Particles seeded just north of the Bump were transported greater distances than those seeded to the south, some of which were caught in an associated gyre, promoting retention at the seabed. To the north on the Scotian Shelf, despite weaker currents and greater distances between known occurrences, unidirectional transport was detected from Emerald Basin to the Northeast Channel between Georges and Browns Banks. These major conclusions remained consistent through simulations run with different averaging periods for the currents (decades to daily) and using two ocean model products (BNAM and GLORYS12V1).

Keywords: connectivity, *Vazella pourtalesii*, deep-sea sponge, Charleston Bump, Gulf Stream, particle tracking models

OPEN ACCESS

Edited by:
Clara F. Rodrigues, University of Aveiro, Portugal

Reviewed by:
Matthieu Le Hénaff, University of Miami, United States
Johan Van Der Molen, Royal Netherlands Institute for Sea Research (NIOZ), Netherlands
Chris Rooper, National Marine Fisheries Service (NOAA), United States

****Correspondence:***
Ellen Kenchington
Ellen.Kenchington@dfo-mpo.gc.ca

Specialty section:
This article was submitted to Deep-Sea Environments and Ecology, a section of the journal Frontiers in Marine Science

Received: *27 April 2021*
Accepted: *01 September 2021*
Published: *04 October 2021*

Citation:
Wang S, Kenchington E, Wang Z and Davies AJ (2021) Life in the Fast Lane: Modeling the Fate of Glass Sponge Larvae in the Gulf Stream. Front. Mar. Sci. 8:701218. doi: 10.3389/fmars.2021.701218

INTRODUCTION

Sponges fill a wide variety of functional roles in many marine ecosystems, having significant influence on local substrates, bentho-pelagic coupling and associations with other organisms (Bell, 2008; Maldonado et al., 2017). While sponges are often widely distributed as isolated specimens, their ecological importance is greater where they form dense aggregations, known as "sponge grounds" (Hogg et al., 2010). Those aggregations have drawn substantial attention in recent years, particularly from ecological and conservation perspectives. However, they remain understudied compared to other structure-forming biogenic habitats such as coral reefs (Bell, 2008).

Globally, destructive anthropogenic activities, such as bottom contact fishing and deep-sea mining, and climatic variability have increased concern for the protection of deep-sea sponges (Hogg et al., 2010) and the ecosystem services they provide. The large vase-shaped glass sponge *Vazella pourtalesii*, endemic to the western North Atlantic, is a long-lived ecologically significant species that has been the focus of recent research and conservation efforts. The dense sponge grounds formed by this species have local ecological importance, as species richness and abundances are three to four times higher in the presence of *V. pourtalesii* (Hawkes et al., 2019) and these sponges significantly influence biogeochemical cycling of silicon (Maldonado et al., 2020) and other nutrients (Bart et al., 2020). Consequently *V. pourtalesii* is considered to be an ecosystem engineer. Beazley et al. (2021) predicted that its distribution under future (2046–2065) climate change could increase up to four times its present-day size and shift into deeper waters and higher latitudes, particularly in its northern range.

Effective conservation management of *V. pourtalesii* and other deep-sea sponges, including design of appropriate marine protected areas, can be supported by predictive species distribution models (Knudby et al., 2013; Beazley et al., 2018, 2021; Murillo et al., 2018). However, that approach can only provide some of the required information and often does not consider the ability of a species to disperse into isolated areas of predicted suitable habitat. More generally, an understanding of connectivity within and between spatially separated populations is important for habitat management in order to design effective protection networks and enable restoration of damaged habitats (Kool et al., 2013), and thus attracts broad interest from both scientists and managers (Simons et al., 2013; Kenchington et al., 2019; Ross et al., 2020; Wang et al., 2020). Knowledge of connectivity can enhance our comprehension of species distributions and is an important supplement to species distribution modeling, particularly if species responses under future climate projections are to be interpreted reliably (Holloway et al., 2016). Beazley et al. (2021) did not model colonization potential for their habitat predictions for *V. pourtalesii* and so whether the species will be a "climate change winner" capable of colonizing the large expanse of seabed identified in their models, remains an open question.

A primary tool for assessing the connectivity of benthic marine species are larval dispersal models that couple numerical hydrodynamic data with a tracking algorithm that follows released "particles," representing larvae, as they move along flow fields (e.g., Bartsch and Knust, 1994; Marinone et al., 2008; Ashford et al., 2010; Paris et al., 2013; Lange and Van Sebille, 2017; Delandmeter and Van Sebille, 2019). If known, larval characteristics and behavior, including such processes as swimming, mortality, buoyancy and response to extrinsic variables, can be incorporated into the tracking algorithm (e.g., Bartsch and Knust, 1994; Wolanski et al., 1997; Metaxas and Saunders, 2009; Gary et al., 2020).

In this study, we developed passive 3-D Lagrangian particle tracking models to investigate the physical connectivity of *V. pourtalesii* in the western North Atlantic. We aimed to further develop our understanding of the published predicted distribution of this species under present and future conditions (Beazley et al., 2021) and determine how different populations may be connected, isolated and/or retain larvae. We do so by identifying physical connections among currently occupied areas, estimating the maximal extent of larval transport, and determining the influences of location and depth on potential dispersal patterns.

V. pourtalesii was first described (as *Holtenia pourtalesii*) from samples taken from the Florida Keys, United States, between 282 and 593 m water depth (Schmidt, 1870; Reiswig, 1996). However, its range extends from there to the Emerald Basin on the Scotian Shelf, off Nova Scotia, Canada (**Figures 1**, **2**), where the species reaches its highest densities and forms extensive sponge grounds which have been protected from bottom contact fishing (Beazley et al., 2018). Further south it is generally only found in low numbers for reasons that are not well understood (Beazley et al., 2021). This species' distribution falls within the Temperate North Atlantic realm and both the Cold Temperate and Warm Temperate Northwest Atlantic biogeographic provinces of Spalding et al. (2007), a distribution shared with at least 1664 other sponge species (Van Soest et al., 2012) such as *Tetilla laminaris symmetrica* and *Clathria* (*Clathria*) *prolifera*. A single observation from the Azores (Tabachnick, 1994) has been discounted in recent studies on this species, after discussion with local scientists and failure to locate the voucher specimen (Beazley et al., 2021). In Emerald Basin, *V. pourtalesii* has been linked to areas of low topographic relief and warm, saline waters ($>5°C$, $>34‰$), relatively low oxygen (≈ 2.6–$3\ ml\ l^{-1}$) and high nutrient concentrations (Beazley et al., 2018). That area is subject to strong inter-annual variability in average bottom temperature and salinity (Beazley et al., 2018), ranging from 4 to 12°C and 34 to 35.2, respectively, between 1950 and 2015, leading to a conclusion that this species may be resilient to changing climatic conditions (Beazley et al., 2021).

The physical oceanography of this region is very well studied, which allows for a detailed understanding of the conditions governing dispersal and distributions and enhanced interpretation of connectivity models. Two major current and water mass systems dominate the area occupied by *V. pourtalesii*: the fast moving Gulf Stream with its associated Warm Slope Water, and the continental-shelf waters from the Gulf of St. Lawrence to Cape Hatteras (**Figure 2**). The Gulf Stream exits from the Gulf of Mexico, transporting very warm, saline water and flows very swiftly along the shelf break, northwards

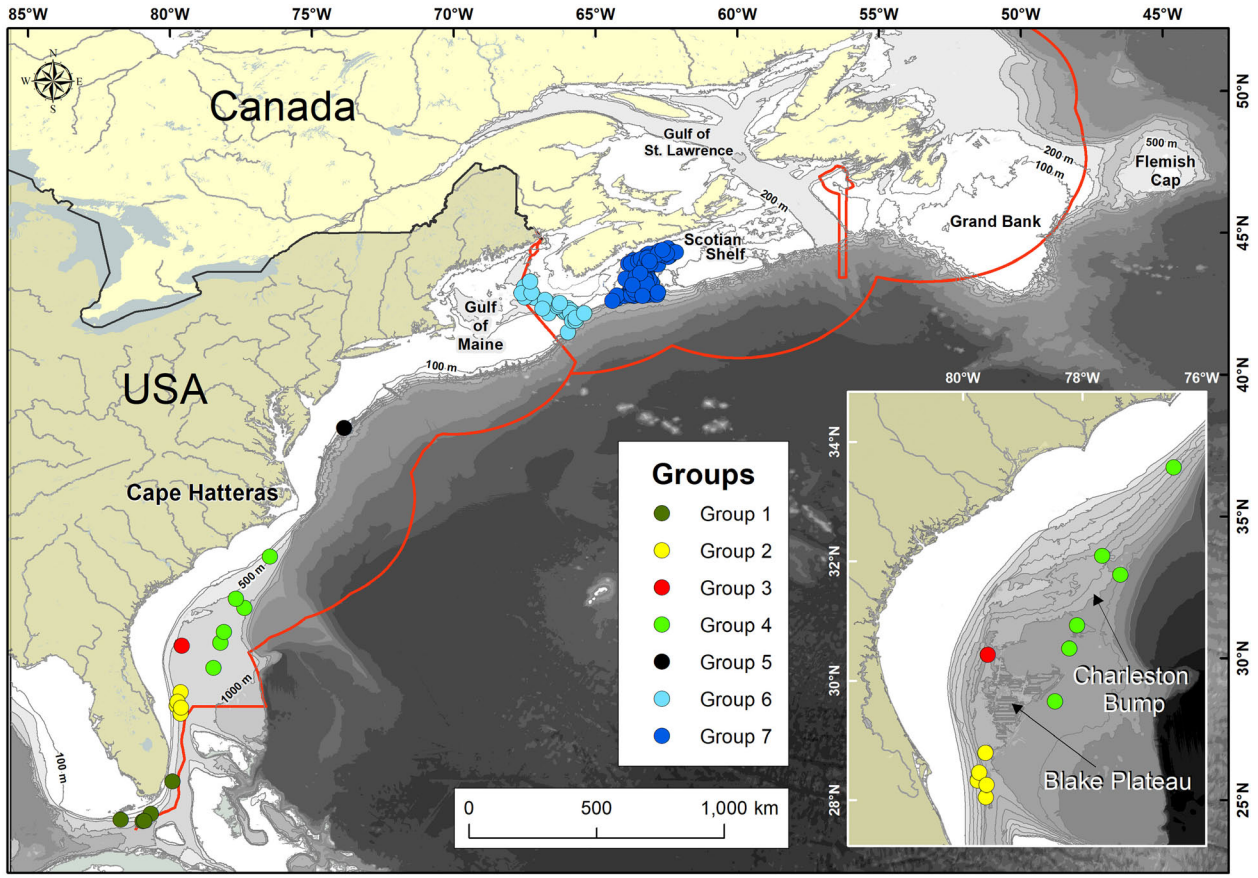

FIGURE 1 | Place names and locations of confirmed occurrences of *V. pourtalesii* along the eastern coast of North America. Occurrences are colour-coded by their assigned Group (1–7). The inset shows the area of the Blake Plateau with the location of the Charleston Bump. Red line indicates the exclusive economic zones of the United States, Canada, and France (with respect to Saint Pierre and Miquelon). Additional place names, general position of major currents and water masses, topography, and undersea features in the study area are provided in **Figure 2**.

to Cape Hatteras, North Carolina, where it breaks away from the continent, thereafter heading northeast and east to pass south of Grand Bank (Rossby et al., 1985). Before reaching Cape Hatteras, the Gulf Stream flows over the Blake Plateau, which projects from the continental slope at depths of approximately 700 m. At the northern end of the Blake Plateau, the Charleston Bump rises to about 375 m depth, deflecting the Gulf Stream, intensifying bottom currents and causing downstream eddy formation, mixing and upwelling (Popenoe and Manheim, 2001). The resulting Charleston Gyre becomes more prominent when the Gulf Stream is strong and transports Gulf Stream water inshore (McClain and Atkinson, 1985). Beazley et al. (2021) predicted some increase in suitable habitat for *V. pourtalesii* in this region in their climate projection models.

After passing Cape Hatteras, the Gulf Stream takes the form of a complex of meanders and eddies which entrain continental shelf waters, forming a new water mass, the Warm Slope Water (WSW), between the shelf break and the Gulf Stream's northern "Cold Wall." The WSW circulates in a gyre over the continental slope between Cape Hatteras and Cape Cod (Csanady and Hamilton, 1988; Fratantoni and Pickart, 2007; Kang and Curchitser, 2013) but a portion escapes the gyre, passes the flank of Georges Bank and thence heads east to round Grand Bank between the shelf break and the north wall of the Gulf Stream (**Figure 2**). South of Nova Scotia, the shelf/slope boundary, which delimits the WSW at the surface, usually lies south of the shelf break but some of that water mass extends beneath the shelf waters and, subsurface, reaches to the continental slope. It intermittently floods over a saddle between two offshore banks, Emerald and LaHave, filling the depths of Emerald Basin (**Figure 2**). There it provides the warm, saline layer within which the *V. pourtalesii* aggregations are found (Drinkwater et al., 2003; Hanz et al., 2021).

The waters of the continental shelf from Nova Scotia to Cape Hatteras have their principal origin in the Gulf of St. Lawrence, where a three-layer system forms in summer (two-layered in winter: Koutitonsky and Bugden, 1991). Only the very cold, low-salinity Cold Intermediate Layer (CIL) and, in summer, the warm surface layer, can cross the shallow banks of the eastern Scotian Shelf (Han and Loder, 2003), whence they flow southwestwards, with the Nova Scotia Current following the coast (**Figure 2**). Clockwise gyres circle the various banks; some

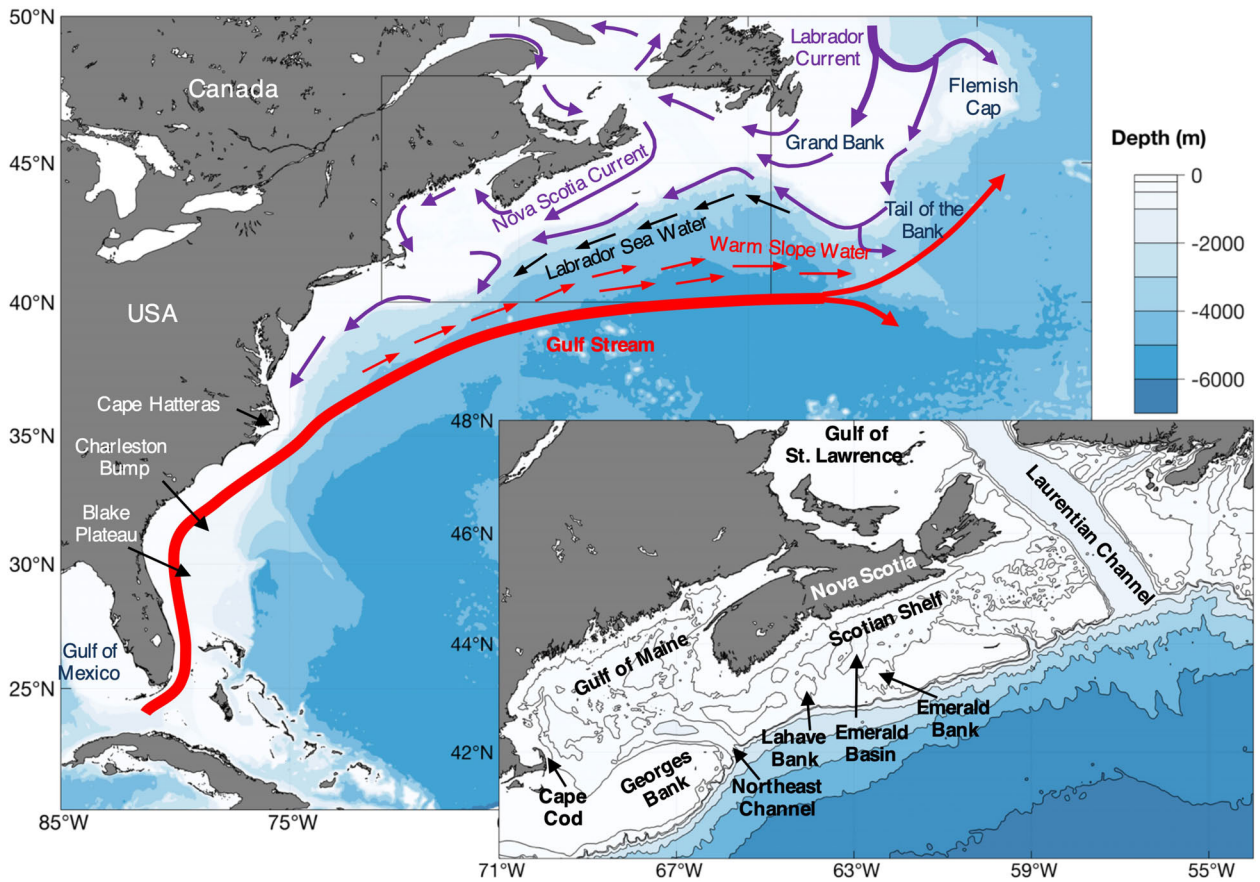

FIGURE 2 | Geographic place names, general position of major currents and water masses, topography, and undersea features in the study area. The inset area is outlined in gray on the large map. See also **Figure 1** and **Supplementary Figure 1**.

moving anticlockwise in Emerald Basin over the *V. pourtalesii*. These water masses form the surface waters over the sponge grounds in Emerald Basin. All three layers in the Gulf of St. Lawrence outflow merge with cold, low salinity water from the north and are carried around Grand Bank by the Labrador Current. Together, they continue southwestwards along the edge of the Scotian Shelf as a shelf-break current, contributing water to the gyres around the outer banks (Loder et al., 1997, 1998; Han et al., 1999). The CIL and summer surface layers from the Scotian Shelf flow into the Gulf of Maine, which also receives a deep inflow of WSW through the Northeast Channel (Townsend et al., 2015), covering the sponge grounds there. Beazley et al. (2021) predicted range expansion into the Gulf of St. Lawrence in their future scenarios, accounting for much of the predicted increase in suitable habitat for *V. pourtalesii*.

An alternative water mass, Labrador Sea Water (LSW), traverses the upper continental slope off Nova Scotia (**Figure 2**). LSW, which forms much of the deep water of the North Atlantic, circulates within the Labrador Sea and the Subpolar Gyre. Although some moves southward, contributing to the Atlantic Meridional Overturning Circulation (AMOC), it does not follow the continental margin. Rather, it breaks away at Flemish Cap, flows east to the Mid-Atlantic Ridge and does not return westwards until far to the south (Biló and Johns, 2019). Only a minor amount of LSW rounds the Tail of Grand Bank where, at upper-slope depths, it lies between the WSW and the continental slope. That tongue of LSW sometimes extends only to the western flank of Grand Bank but can penetrate much further, historically far beyond Cape Cod (**Figure 2**). Along that extent of the continental margin, the WSW and colder, less saline LSW form what has been described as a "coupled slope-water system," with the front between the two water masses moving along the continental slope in response to basin-scale atmospheric forcing (Petrie and Drinkwater, 1993; Marsh et al., 1999; MERCINA Working Group, 2001; Greene and Pershing, 2003). In 1997–1998, there was a major intrusion of LSW onto the shelf, which extended to beyond Georges Bank. It flushed the depths of Emerald Basin, lowering temperatures there by more than 4°C, and penetrated into the Gulf of Maine through the Northeast Channel (Drinkwater et al., 2003), flooding the *V. pourtalesii* grounds in both areas before being replaced by WSW once more after a few months. These events explain the strong inter-annual variability in temperature and salinity (Beazley et al., 2018) experienced by the sponge grounds in these areas, as noted above.

The waters in the Gulf of Maine are modified by local freshwater inputs and by tidal mixing but they generally circulate

anticlockwise around the Gulf and then clockwise around Georges Bank (Loder et al., 1998; Townsend et al., 2015). The Gulf of Maine was another key area predicted to see large increases in suitable habitat of *V. pourtalesii* under 2046–2065 climate conditions (Beazley et al., 2021).

By way of a flow around Cape Cod and another off the southern flank of Georges Bank, the shelf waters pass Cape Cod and continue southwards toward Cape Hatteras, where they contribute to the formation of the WSW. While velocities there are generally low, there is a well-developed current over the upper continental slope south of 39°N (Levin et al., 2018). Beazley et al. (2021) identified a very narrow and fragmented margin of this upper slope area, between Cape Cod and Cape Hatteras, as suitable habitat that did not show large changes in their habitat projections for the future.

Collectively these currents, associated eddies and water masses control to varying degrees the distribution of benthic invertebrate species in this region which rely on physical dispersal of gametes and larvae. For sponges, which are believed to have very short larval dispersal durations of hours to days (Kenchington et al., 2019; see section "Biological Traits of *V. pourtalesii* for Particle Tracking Modeling"), particle tracking models initiated from sites of known occurrence (**Figure 1**) can greatly assist in interpreting species distributions models of predicted occurrence by identifying dispersal kernels. Areas of high predicted probability of occurrence that also lie within dispersal ranges of known occurrences are more likely to be populated as both favorable environmental conditions and recruitment trajectories align. Conversely, areas of predicted habitat that cannot be occupied through passive dispersal from known occurrences are less likely to be colonized. Further, particle tracking models can help to identify "source" and "sink" populations which is important information for the construction of protected area networks (Crowder et al., 2000).

MATERIALS AND METHODS

Distribution of *V. pourtalesii*

The known distribution of *V. pourtalesii* was mapped on a 1 km^2 grid, from presence only records (**Figure 1**). Occurrence data for waters off Canada were drawn from catches of Fisheries and Oceans, Canada (DFO) research-vessel trawl surveys (2007–2019), DFO and Natural Resources Canada optical benthic surveys (1989–2018) and fishery observer records of commercial fishery bycatches (1997–2007 and 2010–2015). For areas off the United States, occurrence data were obtained from Reiswig (1996), the NOAA Deep-Sea Coral Data Portal (2009–2011) and NOAA *Okeanos Explorer* research cruises EX1806 and EX1903 (2018–2019). In total, there were known occurrences found in 136, 1 km^2 grid cells. As those were highly clustered, the occurrences were further classified into one of seven regional groups, numbered sequentially from their southern to northern locations (**Figure 1** and **Table 1**).

Biological Traits of *V. pourtalesii* for Particle Tracking Modeling

Empirical data on the distribution of early life-history stages of benthic marine organisms, and sponges in particular (Leys and Ereskovsky, 2006), is extremely limited, and only a few sponge species have been studied to date (Leys and Ereskovsky, 2006). Therefore, particle tracking models are often the only tool available for assessing larval connectivity (Ospina-Alvarez et al., 2020). Modeling connectivity through larval drift using particle tracking requires input of at least the spawning season and the duration of the planktonic phase (pelagic larval duration; PLD). The timing of *V. pourtalesii* spawning is not currently known and all Hexactinellida are currently thought to be viviparous (Leys and Ereskovsky, 2006). Preliminary histological evidence suggests larval release in summer (July and/or August; Dr. A. Riesgo, Museo Nacional de Ciencias Naturales, Madrid, Spain, personal communication). Consistent with this initial

TABLE 1 | Number of *Vazella pourtalesii* occurrence records, average seabed depth of occurrences, and number of particles released in each simulation model for each of seven Groups, and the six occurrence sites in Group 4.

Group	Number of *Vazella pourtalesii* occurrence records	Average depth of occurrence records (m)	Number of particles released in each group
1	5	363	5,727
2	5	640	7,280
3	1	821	2,601
4	6	757	10,404
5	1	563	580
6	28	238	45,382
7	90	182	75,463
Group 4 #1	1	819	2,601
Group 4 #2	1	876	2,601
Group 4 #3	1	885	2,601
Group 4 #4	1	859	2,601
Group 4 #5	1	663	2,601
Group 4 #6	1	443	2,601

observation, a sediment trap deployed from September to June within the sponge grounds on the Scotian Shelf contained no *V. pourtalesii* larvae (Hanz et al., 2021), as has been documented for other invertebrate larvae (Hanna, 1984) which are thought to passively sink through the water column, and the benthic lander supporting the traps was not colonized. We therefore modeled releases during each calendar month but, for some questions, focused solely on July and/or August, the most likely reproductive season.

The PLD of *V. pourtalesii* is also unknown, but all sponge larvae observed to date from the limited number of observations made, have been observed to be lecithotrophic and thus their planktonic phases are thought to be very short, generally from a few minutes to about 2 weeks (Leys and Ereskovsky, 2006; Maldonado, 2006; Kenchington et al., 2019). To delimit the maximum connectivity for *V. pourtalesii*, we therefore assumed a PLD of 2 weeks.

Most sponge larvae are ciliated (Maldonado, 2006) and some may be capable of a mean swimming velocity of 5.78 ± 2.25 mm s^{-1} (Montgomery et al., 2019, 2020). However, those results have been challenged (Lanna and Riesgo, 2020) and even if valid, there remains a lack of information on the directionality of sponge larval swimming behavior needed to make use of the information in particle tracking models. Vertical distribution has important consequences for larval transport and dispersal trajectories (Edwards et al., 2007; Gary et al., 2020; Wang et al., 2020). However, the vertical movements of *V. pourtalesii* larvae, like those of many sponge species, remain unknown (Kenchington et al., 2019), although settlement of *V. pourtalesii* has been observed on artificial substrates about 5 m off the bottom (Busch et al., 2020). In the absence of better information, larval release was modeled at three depths: the average seabed depth of recorded occurrences of *V. pourtalesii* in the relevant regional group (**Table 1**), mid-water from the seabed to the surface, and the surface, to capture three vertical strata that might be reached through active swimming behavior (Vaz et al., 2016).

Lagrangian Particle Tracking

Three-dimensional (3-D) passive particle tracking was performed using the Parcels framework version 2.1 (Lange and Van Sebille, 2017; Delandmeter and Van Sebille, 2019) in a spatial domain bounded by the 20°–50°N parallels, the 40° and 85°W meridians and the coastline. Climatological mean and monthly–mean vertical and horizontal currents, averaged over 1990–2015 and for selected years, were obtained from the Bedford Institute of Oceanography North Atlantic Model (BNAM) (Brickman et al., 2016, 2018; Wang et al., 2016, 2018, 2019). BNAM is an eddy-resolving model of the North Atlantic Ocean, based on Nucleus for European Modeling of the Ocean (NEMO) 2.3, with a nominal resolution of 1/12°. BNAM can resolve eddies with a diameter greater than ∼80 km in the Gulf Stream region. For eddies smaller than 80 km and greater than 50 km (meso-scale eddies), BNAM will permit this type of eddy to exist, but cannot resolve them, while eddies smaller than 50 km (small-scale eddies) cannot be resolved. BNAM models the entire water column in 50 levels, their thicknesses increasing from 1 m at the surface to 200 m at a depth of 1,250 and 460 m at the bottom of the deepest basins (Wang et al., 2018). Partial cells were introduced in BNAM for the bottom layer, improving representation of the seabed; bottom depths being taken from the 2019 General Bathymetric Chart of the Oceans (GEBCO) global bathymetric grid.[1] BNAM results have been independently validated using a variety of observational data (Wang et al., 2018).

Ocean Model Data

Our particle tracking model experiments used different extractions from BNAM. The first was long-term data (1990–2015) averaged over the full time series, referred to hereafter as "long-term averaged currents." Beazley et al. (2018, 2021) used BNAM long-term averaged current velocities, along with other similarly extracted oceanographic variables, as environmental predictors in their species distribution modeling of *V. pourtalesii*, and use of long-term averages as environmental predictors are widely used in species distribution models (e.g., Morato et al., 2020; Downie et al., 2021). Similar to the long-term averaged currents we also extracted data averaged over individual months across the full time series, referred to hereafter as "long-term averaged monthly currents." These were needed to examine seasonal differences in connectivity. In that data set all data from a given month, e.g., July, was extracted and averaged. Our use of long-term averaged currents extracted from BNAM (Wang et al., 2018) provides important information on overall mean dispersal patterns (Edwards et al., 2007) and enhances broad-scale understanding of species distributions (Beazley et al., 2018, 2021). However we recognize that anomalous events and eddies may also play a role in dispersal and delimiting distributions, and that averaging over the long-term masks some of this variation. To investigate the roles of inter-annual variability and narrower averaging windows on connectivity, we additionally selected six individual years within the 1990–2015 time period to examine the effects on dispersal during periods of Gulf Stream variability (see section "Selection of Years for Examination of Inter-Annual Variability"). Climatological monthly averaged currents were extracted from BNAM for each of those years individually, and used to compare the dispersal trajectories with models using the long-term averaged currents and long-term averaged monthly currents. For context, Kang and Curchitser (2013) reported that the average duration of all anticyclonic eddies in this region is 31 days, with maximum durations of 165 days. We refer to these data as "monthly averaged currents within selected years" hereafter to distinguish from the long-term averaged monthly currents. Using the monthly averaged currents within selected years data greatly enhanced the eddy fields in the study area over the long-term averaged currents (**Supplementary Figure 1**). For the selected year 2010 only (see section "Selection of Years for Examination of Inter-Annual Variability"), 5-day averaged current products were available from BNAM. We additionally extracted those data for July 2010 in order to further examine the effect of using averaged data on the connectivity matrices.

[1] https://www.gebco.net/data_and_products/gridded_bathymetry_data/gebco_2019/gebco_2019_info.html; accessed 4/12/2021.

Selection of Years for Examination of Inter-Annual Variability

The Gulf Stream is the essential component of the upper limb of the Atlantic Meridional Overturning Circulation (AMOC), transporting heat from low to high latitudes, and modulating climate at both local and global scales. Change in the strength of the Gulf Stream can be a good indicator for the changes in the AMOC. Wind and heat flux are the two dominant driving factors for ocean circulation patterns, and wind is believed to drive the western boundary currents, such as the Gulf Stream. Winter convection in the Labrador Sea resulting from heat flux has been found to be important in driving the Labrador Current, which interacts with the Gulf Stream at the tip of the Grand Banks, potentially impacting the Gulf Stream. Numerous studies have identified the significance of the North Atlantic Oscillation (NAO) variability on the AMOC. Wang et al. (2019) demonstrated that the NAO's role on AMOC variability is through the wind-driven Ekman transport component of the AMOC, and its impact is shown on changes of the AMOC at high frequency. Winter convection is an essential mechanism for the AMOC variability at low frequency (Wang et al., 2019). Wang et al. (2019) reported that the AMOC was high before the early 2000s, and became weaker afterward.

In this study we chose the years 1993, 1996, 2001, 2008, 2010, and 2015, to investigate single year connectivity and inter-annual variability in connectivity patterns. Each year was selected for the expression of particular features in the BNAM model: 1993 was a year in the high winter NAO years during the early 1990s with a strong AMOC; 1996 saw a large drop in the winter NAO index, however, there was a strong AMOC; 2001 was the year that Wang et al. (2016) reported a shift of the Labrador Current, and in which year the winter NAO action centers shifted westward; Hakkinen and Rhines (2009) reported a shift of the surface current in the North Atlantic Ocean starting from the early 2000s as well; 2008 was the year when the winter deep convection event in the Labrador Sea returned after years of absence (Yashayaev and Loder, 2009); 2010 was a year with a low winter NAO index, and Häkkinen et al. (2013) reported that the principal component (PC1) of the sea surface height in the North Atlantic Ocean had an abrupt change that year; and 2015 was a recent year with a high winter NAO index. The years 2001, 2008, 2010, and 2015 all had weak AMOC compared to the selected years from the 1990s.

Inter-Model Comparisons

A source of uncertainty in our analyses is the choice of hydrodynamic ocean model used in the particle tracking experiments. Differences among model outputs are to be expected (Delhez et al., 2004; Callies et al., 2011; Hufnagl et al., 2017) but in areas where strong currents influence distribution, it is anticipated that results will be similar (see Kenchington et al., 2019 vs. Wang et al., 2020). We conducted an inter-model comparison to examine the robustness of our conclusion of no exchange of *V. pourtalesii* larvae from known occurrences between areas north and south of Cape Hatteras, with an estimated pelagic larval duration of 2 weeks. The two ocean models compared were BNAM and GLORYS.[2] The GLORYS12VI model is a global ocean eddy-resolving product defined on a standard regular grid with 1/12° horizontal resolution, and 50 vertical levels (interpolated from an Arakawa C native grid). Products are available as daily mean, monthly mean, and pluri-annual-climatology-mean values from 1993 to 2019 (Fernandez and Lellouche, 2021). Here we used daily mean GLORYS data and the monthly mean BNAM data from July in each of the 6 years for particle released from the surface when $k_h = 0$ m^2 s^{-1}, to conduct the inter-model comparisons. Surface releases are expected to show the largest potential for connectivity because of the greater spatial coverage shown in their particle releases compared to those of mid-depth and seabed releases (**Supplementary Figures 11–22**, **24**). The use of the daily mean values from GLORYS, unavailable in BNAM, further allows exploration of the impact of averaging over different time periods on the connectivity matrices.

Both BNAM and GLORYS12V1 are eddy-resolving models and have the ability to nowcast deep ocean mesoscale variability such as eddies and movement of currents and fronts (Hurlburt et al., 2009). However, the two ocean models differ in a number of key aspects: (1) BNAM is a basin-scale North Atlantic Model which requires global ocean model data as open boundary conditions. In BNAM the open boundary data are from the GLORYS reanalysis product (Global Ocean Reanalyses and Simulations, version1; Ferry et al., 2010). GLORYS12V1 is a global model and so no boundary conditions are required; (2) BNAM is a prognostic model, with outputs obtained from governing equations directly, which accords with the physical processes. In contrast, GLORYS12V1 is a data-assimilative model, created by assimilating model output from the NEMO 3.1 ocean model and the LIM2 EVP sea ice model with observational data (Reijnders, 2020); (3) The surface forcing of BNAM is taken from a combination of CORE (Coordinated Ocean-ice Reference Experiments) and NCEP/NCAR reanalysis forcing. Model forcing variables include air temperature, wind velocities and humidity; daily short- and long-wave radiation, and total precipitation (rain plus snow) (Wang et al., 2019). In GLORYS12V1, atmospheric forcings are provided with 3- and 24-hourly frequencies by the ERA-interim dataset, including precipitation and radiative fluxes (shortwave and longwave) corrections (Fernandez and Lellouche, 2021). Many parameter settings are also different between the two models, so discrepancies between trajectories can arise from many aspects.

Lagrangian Transport Modeling

Particle tracking results are sensitive to the resolution of the spatial grid of the underlying model (Putman and He, 2013) and BNAM is limited to scales of 5–10 km. Such a coarse grid is necessary to cover a large spatial domain (McVeigh et al., 2017) such as that covering *V. pourtalesii* distribution. Oceanographic models with a finer grid could be employed to better understand particle movements but they require extensive ground-truthing, which BNAM has been given (Brickman et al.,

[2]https://resources.marine.copernicus.eu/?option=com_csw&view=details&product_id=GLOBAL_REANALYSIS_PHY_001_030

2018; Wang et al., 2018). Further, higher resolution models over this spatial extent would require computer resources that are not currently available to most researchers; a situation that will likely improve as access to high-speed computers increases.

Horizontal diffusivity was alternatively modeled as zero or k_h = 250 m^2 s^{-1}, the latter value being appropriate for mixing across the Gulf Stream (Bower et al., 1985; Anderson et al., 2000). Use of a non-zero value for k_h is expected to have a greater effect on maximum, than on mean, transport distances and end positions (Edwards et al., 2007), partially simulates small-scale larval swimming behavior through the introduction of a random walk (Codling et al., 2004), and mimics some of the variance in the currents which was mostly removed in the averaging process.

Simulated larvae were advected within the Parcels model using the fourth-order Runge-Kutta method as the integration scheme, with a time step of 10 min. The latter ensures that particles cannot cross a model grid cell in a single step, allowing for more accurate estimates of particle retention. To determine the initial locations for larval release, occurrence records of *V. pourtalesii* were superimposed on a 0.1° spatial grid. Particles were seeded uniformly over each occupied cell, at 0.002° intervals, resulting in 2,601 particles for each fully populated grid cell (**Table 1**). Particles overlying the average depth of the occurrence records (**Table 1**) were retained and used for the simulations. Any particles occurring over deeper or shallower water, such as in regions with high bathymetric variability, were removed prior to modeling in order to relate the model scenarios as closely as possible to known occurrences. The same numbers of particles were used for each model release depth, to facilitate comparisons. The number of particles released in each regional group are provided in **Table 1** and ranged from 580 (Group 5) to 75,463 (Group 7), reflecting the number of occurrences in each of the release areas and the slope of the seabed in the 0.1° grid cells. The same procedure was used for particle releases in experiment four (**Table 2**, section "Model Simulations") using each of the six occurrence records in that region, each filtered for their specific seabed depth (**Table 1**).

The results of simulated larval dispersal experiments were evaluated using connectivity matrices, showing the percentage of particles from each source occurrence cell within a Group that either passed over or terminated in another receiving occurrence cell within a Group. Transit time distributions (TTD; McGuire and McDonnell, 2006) were calculated for particle movements from source occurrence cells within Groups to receiving occurrence cells within Groups. Individual-based dispersal was displayed as histograms of the flow distances traveled from each release point (Kool et al., 2013). Those distances were calculated from individual particle trajectories as the sum across the 2-week PLD of straight-line distances between the start and end positions of each 10-min time step. The median, 95th percentile and maxima of the distances were determined. Dispersal kernels were mapped using individual trajectories and/or averaged end positions.

Model Simulations

Particle tracking models are capable of generating many potential outputs. To clarify their interpretation, this study undertook four discrete experiments (**Table 2**) all using the long-term averaged currents and/or long-term averaged monthly currents. The first experiment aimed to explore both dispersal (connectivity and maximum flow distances) during each calendar month, and the effect of introducing horizontal mixing by setting k_h at either zero or 250 m^2 s^{-1}. The effect of horizontal mixing was pronounced and maintained for all further steps. Although Parcels is a 3-D tracking model, in this region the horizontal velocities created by the Gulf Stream greatly exceed any vertical movement (upwelling or downwelling) and the vertical velocities are generally very small ($\sim 10e^{-4}$ m s^{-1}). As larval vertical migration and swimming ability is unknown for *V. pourtalesii* as for most other sponges (section "Biological Traits of *V. pourtalesii* for Particle Tracking Modeling"), we have created three vertical strata for particle releases in all of our experiments (seabed, mid-water and surface) to allow for swimming-mediated vertical migration, although the seabed scenarios are at this time considered to be the most representative of larval behavior. Results of the first experiment showed little seasonal variation. Therefore, the second experiment assessed the connectivity between occurrence cells among Groups only during the suspected spawning months of July and August using the long-term averaged monthly currents, which were compared to the connectivity simulated using long-term averaged currents (averaged over all months from 1990 to 2015). The connectivity matrices generated in that experiment showed consistent connections in both July and August. Therefore, the remaining steps only considered particle releases in July. In the third experiment, data exported from the second experiment were used to generate frequency histograms of flow distances, for July only. The median, 95th percentile and maximum flow distances were determined. In the fourth and final experiment, larval dispersal from Group 4 was studied in detail as that area is strongly impacted by the Gulf Stream and particles may disperse in various directions (Edwards et al., 2007). Three release sites were located north of the Charleston Bump, and three more to the south, based on the six occurrence records from that area (**Table 1**). Additional release depths (surface, 100, 200, 400, 600, and 800 m) were used, to better capture variations in swimming-mediated vertical larval transport through the water column. At two release points, bottom depth was insufficient for the deepest releases. Those locations were not used in compiling statistics for the depths concerned.

For the six individual years selected for more detailed study of annual variability in the time series, connectivity between Groups was assessed for releases in July and in January using the respective monthly–averaged currents for each year evaluated (1993, 1996, 2001, 2008, 2010, and 2015) and setting k_h at either zero or 250 m^2 s^{-1}. These simulations were also performed for the 5-day averaged currents for July, 2010. Median, 95th percentile and maximum flow distances were calculated for July of each year under both diffusivity settings using the monthly–averaged currents. July simulations reflect the suspected spawning time of *V. pourtalesii* and allow for comparisons with results obtained from the use of the long-term averaged currents for July. At this season anticyclonic eddies are both large and intense (Kang and Curchitser, 2013).

TABLE 2 | Summary of sequential particle tracking simulation experiments utilizing long-term averaged and long-term monthly averaged BNAM ocean data, averaged from 1990 to 2015.

Experiment	Objective	Particle release depths	Calendar months	Diffusivity (m^2 s^{-1})
1	Dispersal during each calendar month	Surface, mid-water, and seabed	January–December	0, 250
2	Connectivity between Groups	Surface, mid-water, and seabed	July, August, and long-term average	0, 250
3	Flow distances	Surface, mid-water, and seabed	July only	0, 250
4	Dispersal for Group 4	Surface, 100, 200, 400, 600, and 800 m	July only	0, 250

Experiments 2 and 3 were applied to the monthly averaged currents within selected years and Experiment 2 was applied to the 5-day averaged currents for July, 2010, as described in section "Model Simulations."

January was chosen as a contrasting month when anticyclonic eddies are fewer in number and on average smaller than in July (Kang and Curchitser, 2013).

RESULTS

Dispersal Characteristics Throughout the Year

The median, 95th percentile and maximum flow distances of released particles (**Table 3**) and their mean end positions (**Figure 3** and **Supplementary Figure 2**) for each month show that seasonal differences in median flow distances were small for surface releases and negligible for those at the seabed. The 95th percentile and maximum flow distances were an order of magnitude greater than the median in all release depth simulations (**Table 3**). Adding horizontal mixing (k_h = 250 m^2 s^{-1}) greatly increased flow distances (**Table 3**) but had only a small effect on direction (**Figure 3** and **Supplementary Figure 2**). Depth of release had a small influence on mean end position for Groups 4–7 (**Figures 3D–F** and **Supplementary Figures 2D–F**). For Groups 1–3 the influence was larger; particles released at the seabed moved much less than those released at the surface or mid-water (**Figures 3A–C** and **Supplementary Figures 2A–C**). This pattern held under both horizontal mixing scenarios of k_h at either zero or 250 m^2 s^{-1}.

Connectivity Between Groups

Connectivity Based on Long-Term Averaged Currents

The connectivity matrices calculated from tracking particles released in July (**Figures 4A,B**) were similar to those for August releases, and those produced using annual averages (**Supplementary Figures 3**, **4**). Incorporation of horizontal mixing in the model increased the number of connections (**Figures 4A,B**) and the area of the dispersal kernels more than their maximum extent (**Figures 5**, **6** and **Supplementary Figures 5**, **6**).

Releases in July identified connections among the southerly Groups 1, 2, 3, and 4 but only limited retention within any of them, when modeled with a 2-week PLD (**Figure 5** and **Supplementary Figure 5**). In contrast, retention was identified within each of the northerly Groups 5, 6, and 7 but there was only little connection between the Groups. Group 7, however, was linked unidirectionally to Group 6 (**Figure 6** and **Supplementary Figure 6**). Our simulations showed no exchanges between the four Groups south of Cape Hatteras and the three northern Groups, regardless of release depth or horizontal diffusivity values used. Fewer connections and more retentions were observed with releases at the seabed than with those at the surface, while mid-water releases returned intermediate results (**Figures 4A,B**). The choice of 2-week PLD was to delimit the maximum possible connectivity in one spawning event. Lesser flow distances are not so much possible as almost certain. If *V. pourtalesii* larvae settle after a day or so, there would be close to 100% retention within each Group.

Particles released from Group 1 were carried by the Gulf Stream, with the surface releases reaching beyond Cape Hatteras, while the addition of horizontal diffusivity broadened the dispersion of particles, with less effect on flow distance (**Figures 5A,E,I** and **Supplementary Figures 5A,E,I**). Particles released from Groups 2 and 3 showed similar end points to those released from Group 1, despite their more northerly start positions (**Figure 5** and **Supplementary Figure 5**). Group 4 releases revealed two different flow modes, some particles being retained in the area, while others moved northward along the continental slope (**Figures 5D,H,L** and **Supplementary Figures 5D**,**H**,**L**) and is further examined in section "Dispersal from Group 4 on the Blake Plateau using Long-Term Averaged Currents." Because of the swift transport of particles in the southern portion of the Gulf Stream and the slower movement further north, combined with its own large size, Group 4 received particles from each of Groups 1, 2, and 3, in addition to local retention, when horizontal diffusivity was included in the model. No other Group had equivalent redundancy of larval sources (**Figure 4B**), potentially conferring increased resilience to Group 4.

Particle releases from Group 5 showed the greatest effect of including horizontal diffusivity in the model. Without it, in seabed releases, 85% of particles remained in the area, whereas addition of horizontal mixing resulted in 94% of particles leaving the Group.

Transit time distribution analysis (**Figure 7**) for those groups showing connections (**Figures 4A,B**), suggests that particles released from Group 3 showed strong peaks in the time taken to establish connections. Peaks in connections (with Group 4) were made in 2.5 days in surface models, 5 days in mid-water models and 12 days in models with particles released from the seabed (**Figure 7**). Similar peaks were seen in the

TABLE 3 | Median, 95th percentile and maximum flow distances (km) of particles released at each of three depths, by calendar month and alternative values of diffusivity using long-term averaged monthly currents (1990–2015).

			k_h = 0			
Release depth	**January**	**February**	**March**	**April**	**May**	**June**
Surface	160/1012/1437	190/1010/1473	203/992/1518	156/1011/1555	119/1104/1577	127/1078/1593
Mid-water	59/845/1165	59/875/1166	61/901/1201	34/924/1232	31/905/1206	60/926/1194
Seabed	30/341/593	29/349/581	15/359/599	16/360/626	15/370/592	29/389/576
Release depth	**July**	**August**	**September**	**October**	**November**	**December**
Surface	88/1017/1623	91/1134/1616	118/1243/1554	116/1068/1420	138/997/1375	153/990/1408
Mid-water	63/935/1246	32/903/1245	60/887/1183	58/841/1160	58/852/1135	87/862/1149
Seabed	15/377/602	16/341/620	13/328/524	31/320/610	28/291/554	43/318/577
			k_h = 250 m^2 s^{-1}			
Release depth	**January**	**February**	**March**	**April**	**May**	**June**
Surface	1450/1720/1989	1459/1711/1995	1457/1729/2031	1437/1731/2062	1451/1756/2061	1462/1764/2096
Mid-water	1436/1599/1843	1451/1611/1852	1423/1631/1881	1435/1597/1880	1423/1628/1873	1451/1632/1885
Seabed	1389/1469/1627	1387/1466/1624	1366/1466/1645	1358/1476/1634	1352/1470/1628	1367/1447/1647
Release depth	**July**	**August**	**September**	**October**	**November**	**December**
Surface	1466/1775/2135	1459/1805/2120	1441/1797/2056	1455/1722/1962	1456/1699/1942	1462/1698/1959
Mid-water	1461/1623/1907	1444/1611/1904	1448/1599/1864	1462/1588/1841	1458/1605/1827	1445/1587/1837
Seabed	1381/1462/1664	1368/1447/1645	1386/1465/1622	1395/1474/1631	1382/1460/1618	1354/1471/1628

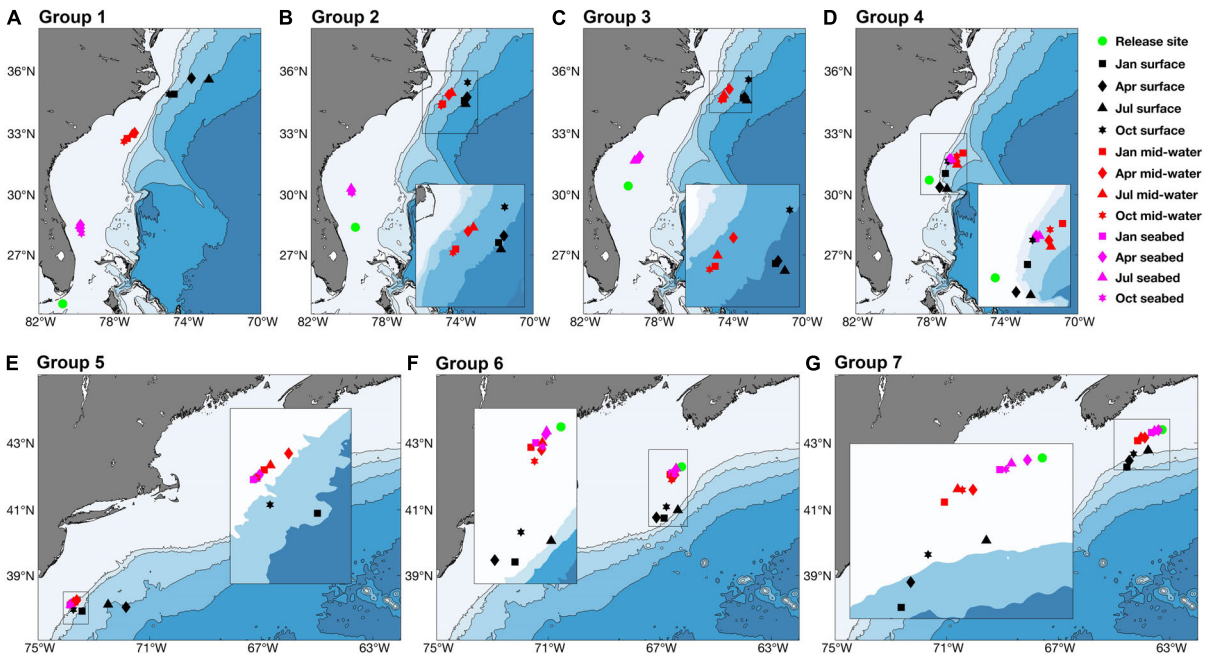

FIGURE 3 | Mean ending positions of particles released at each of three depths in January, April, July, or October using long-term averaged currents in release sites from **(A)** Group 1, **(B)** Group 2, **(C)** Group 3, **(D)** Group 4, **(E)** Group 5, **(F)** Group 6, and **(G)** Group 7, modeled with k_h = 0. (For results from modeling with k_h = 250 m^2 s^{-1}, see **Supplementary Figure 2**.) Filled green circles denote mean release position of particles in the Group.

connection times for particles released from Groups 1 and 2 at mid-water and the surface. Group 7 has more protracted and longer transit times compared to the other groups regardless of release position (**Figure 7**), with no clear peaks forming in the transit time distributions (**Figure 7**). This is because of the large distance needed to connect to Group 6 (**Figure 1**) in addition to the speed and direction of the prevailing currents (**Figure 2**).

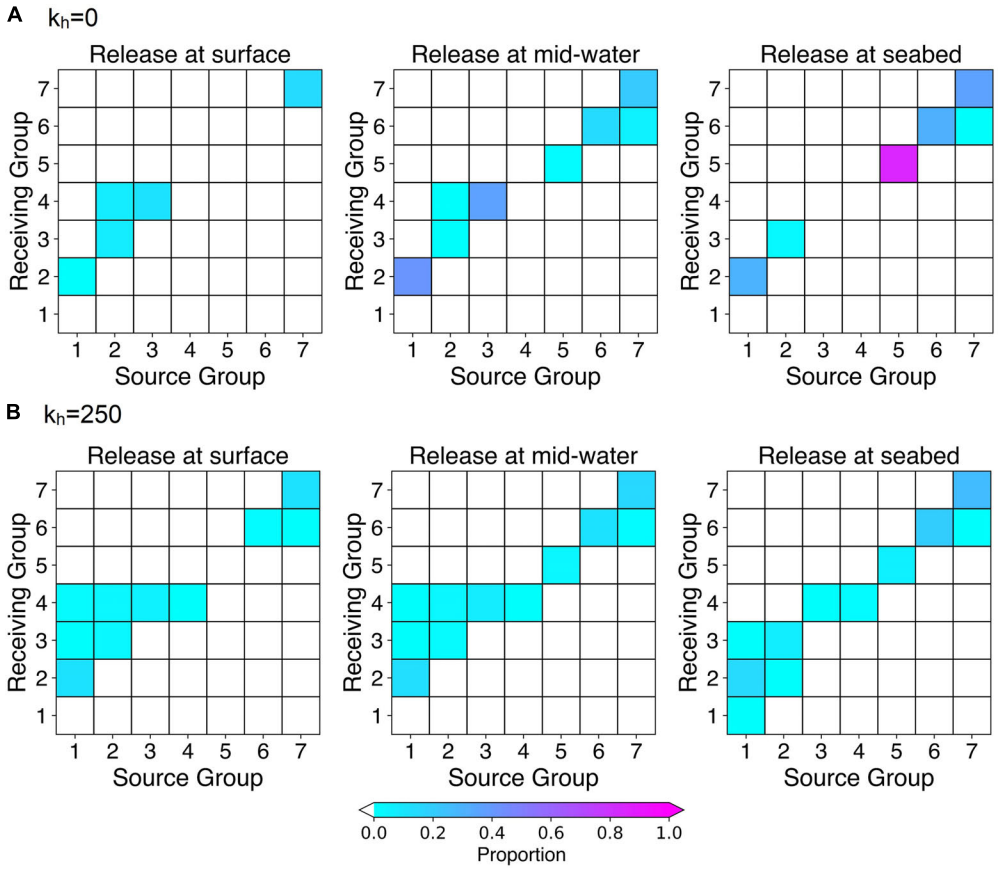

FIGURE 4 | Results of particle tracking simulations using long-term averaged ocean currents from July after a 2-week drift duration for releases from the surface, mid-water depths and the seabed. Connectivity matrices showing the proportion of modeled particles released from each of the occupied grid cells in each of the seven Groups (Source) passing over or terminating in another occupied grid cell in another Group (Receiving Area). Diagonal cells indicate particle retention within the occupied cells within each Group. **(A)** when k_h = 0 and **(B)** when k_h = 250 m^2 s^{-1}.

Connectivity Based on Currents Within Selected Years

As observed for the connectivity assessment of inter-month variation in release times utilizing long-term averaged monthly currents from 1990 to 2015 (section "Connectivity Based on Long-Term Averaged Currents"), there was little difference between the July and January connectivity matrices in each of the 6 years that were modeled using monthly mean currents extracted for each year individually. In both July and January models with diffusivity k_h = 250 m^2 s^{-1}, 191 connections were made, of which only 13 differed between the month/years, mostly between Groups 7 and 6 in the northern portion of the range (**Supplementary Figures 7**, **8**). When diffusivity was set to k_h = 0 m^2 s^{-1} in the July models, 100 connections were made (**Supplementary Figure 9**), while in January 102 connections were identified (**Supplementary Figure 10**)—both less than achieved when using k_h = 250 m^2 s^{-1}. There were 24 differences in connections between these months, with the only identical patterns showing at the seabed in 2001 and 2008. The greatest difference between months occurred in 2010 at mid-water release depths where 6 differences in connections were observed with more connections in July than in January.

Comparing the number of connections made between the models utilizing July long-term averaged currents (**Figure 4**) with those made in July of each of the six individual years, with diffusivity k_h = 250 m^2 s^{-1} (**Supplementary Figure 7**), there was also very little difference (**Table 4**). At the surface, only one connection did not appear in one of the years (2008; **Table 4**). Mid-depth releases showed few differences in connectivity (**Table 4**) with lost connections from Group 7 to Group 6 occurring in 1993 and 2001 but otherwise with the same connectivity patterns. At the seabed, connections were lost between Group 7 and Group 6 on the Scotian Shelf in 1993 and 2001, while in 2008 and 2010 connections were added between Groups 1 and 2 with 4 (**Table 4**). Of all of these differences, every loss of a connection in 1 year was maintained in another year (**Table 4**) resulting in no net loss of connections between the models run using data from individual years and those runs using the long-term averaged data. However, the models with data from the individual years identified two new connections at the seabed not seen in the long-term averaged results: between Group 2 and

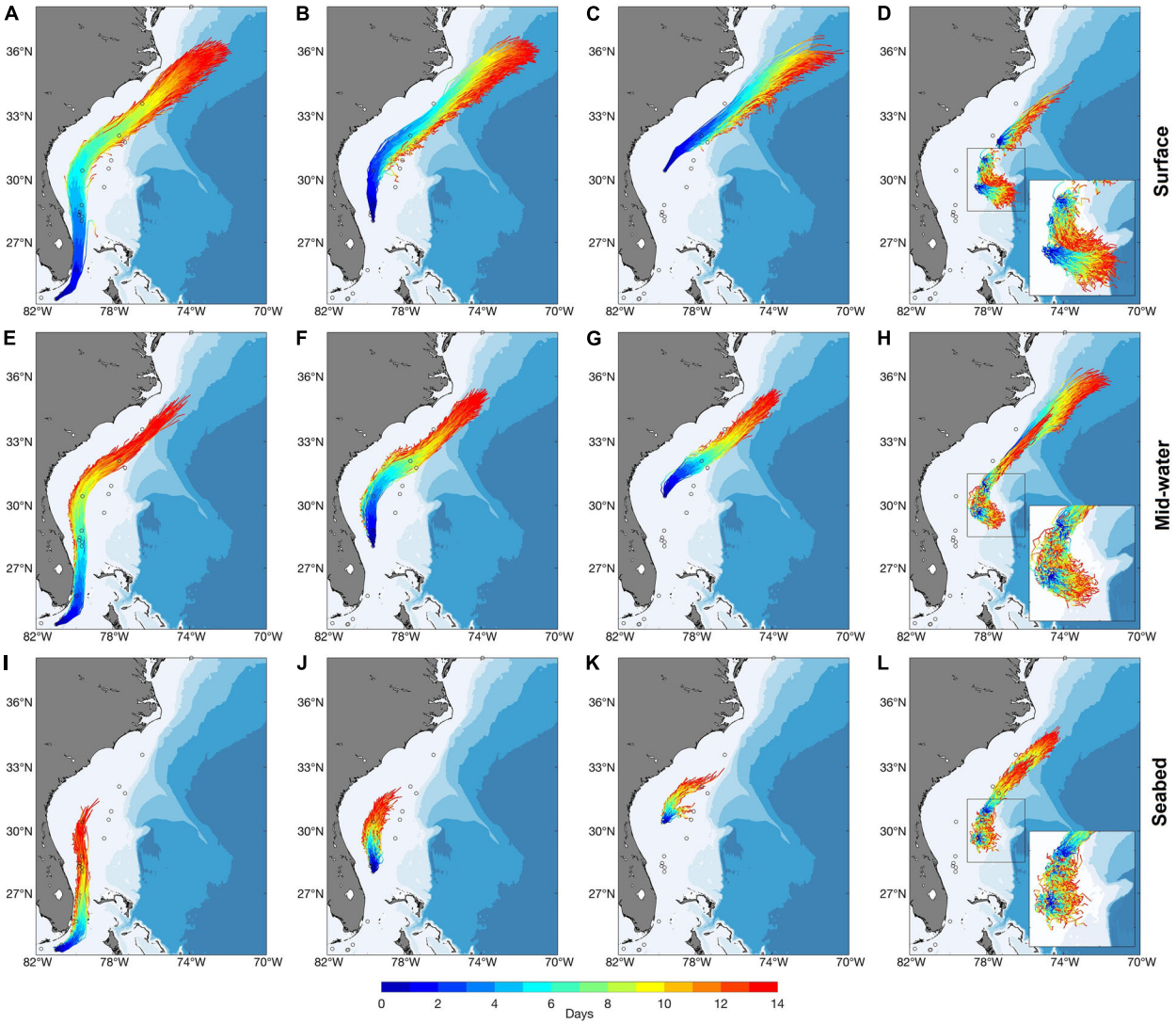

FIGURE 5 | Trajectories of particles released from occupied grid cells in Groups 1, 2, 3, and 4 [Groups 1 **(A,E,I)**, 2 **(B,F,J)**, 3 **(C,G,K)**, and 4 **(D,H,L)**] at the surface **(A–D)**, mid-water **(E–H)** and the seabed **(I–L)** in July using long-term averaged currents, modeled with k_h = 250 m^2 s^{-1}. (Inset shows a close up of trajectories from Group 4 occurrences. Open circles indicate the locations of occurrence records. For results from modeling with k_h = 0, see **Supplementary Figure 5**).

Group 4 (in 2008 and 2010) and Group 1 and Group 4 (in 2010) (**Table 4**). When k_h was set to 0 m^2 s^{-1} (**Table 4**) more differences were identified than with k_h = 250 m^2 s^{-1}, however most of those were lost connections in individual years; all but one of which was found in another of the years examined. There was only one novel connection added and that was between Group 1 and Group 4 at the surface in 2015.

Together these results show that the loss of variability created by using the long-term monthly averaged currents did not strongly affect the connectivity linkages although with diffusivity k_h = 250 m^2 s^{-1}, two new seabed connections were identified, and with diffusivity k_h = 0 m^2 s^{-1}, one new surface connection was identified, all in the southern part of the range. Novel particle retentions were seen with k_h = 0 m^2 s^{-1} in Groups 1, 5, and 4 not seen in the long-term monthly averaged current simulations. None of the new connections showed connectivity with Group 5, the relatively isolated population between Cape Hatteras and Cape Cod that was thought to be linked to the southern sub-region through Gulf Stream eddies breaking off north of Cape Hatteras.

Examination of the dispersal kernels for these models run with the July or January averaged currents for each of the 6 years with diffusivity k_h = 250 m^2 s^{-1} (**Supplementary Figures 11–16**, respectively), compared with those produced from the July long-term averaged currents (**Figure 8**), show enhanced gyre formation at all three release depths in the Blake Plateau area which is most pronounced in 2015. The surface releases show strong offshore dispersal in July and also to a lesser extent in January in many of the individual years, not seen in models using the July long-term averaged currents (**Supplementary Figure 1**),

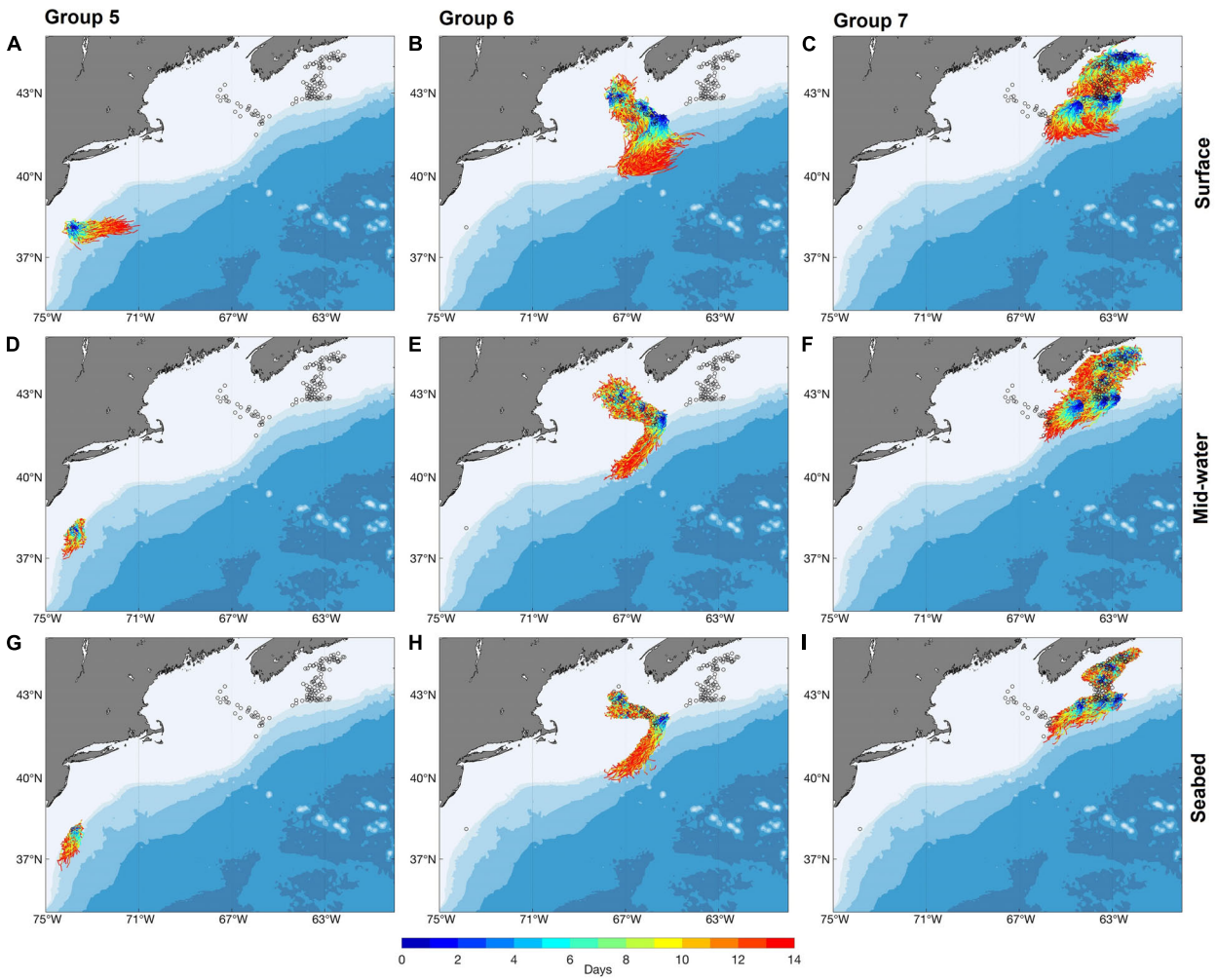

FIGURE 6 | Trajectories of particles released from occupied grid cells in Groups 5, 6, and 7 [Groups 5 **(A,D,G)**, 6 **(B,E,H)**, and 7 **(C,F,I)**] at the surface **(A–C)**, mid-water **(D–F)**, and the seabed **(G–I)** in July using long-term averaged currents, modeled with k_h = 250 m^2 s^{-1}. (Open circles indicate the locations of occurrence records. For results from modeling with k_h = 0, see **Supplementary Figure 6**).

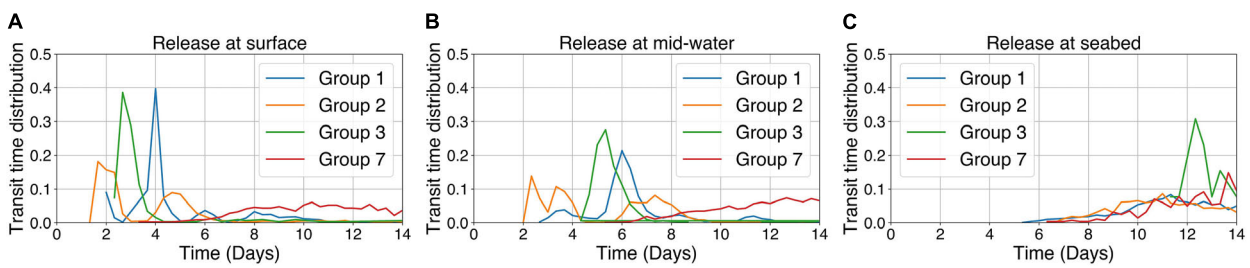

FIGURE 7 | Transit time distribution for connections between the occupied grid cells in each of the Groups passing over or terminating in another occupied grid cell in another Group for particles released from the four Groups (1, 2, 3, and 7) using long-term averaged currents showing connectivity (**Figures 4A,B**) with k_h = 250 m^2 s^{-1}. **(A)** Particles released from the surface; **(B)** Particles released from mid-water depths; and **(C)** Particles released from the seabed.

indicating that loss of larvae to the system through entrainment into the Gulf Stream is likely to be greater than indicated from the models run with long-term averaged currents. None of the scenarios show connectivity from any of the release sites to Group 5, however in January 1996 the models for mid-depth releases show particles from Group 4 reaching a gyre of Group 5 particles (**Supplementary Figure 15B**). If spawning occurred at that time of the year, this could provide a means of

TABLE 4 | Comparison of connectivity patterns from three release depths between results utilizing July long-term averaged currents, with those found in the same month in each of six individual years, that is monthly averaged currents within selected years (differences documented relative to the former; differences in retention not shown).

Year	Description	Surface	Mid-Depth	Seabed
		k_h = 250 m^2 s^{-1}		
1993	High winter NAO; strong AMOC	No differences	Connection lost from Group 7 to Group 6	Connection lost from Group 7 to Group 6 and from Group 3 to Group 4
1996	Large drop in winter NAO; strong AMOC	No differences	No differences	No differences
2001	Shift in Labrador Current and NAO action centers; weak AMOC	No differences	Connection lost from Group 7 to Group 6	Connection lost from Group 7 to Group 6
2008	Winter deep convection returns in Labrador Sea; weak AMOC	Connection lost from Group 7 to Group 6	No differences	Connection added from Group 2 to Group 4
2010	Low winter NAO; change in sea surface height; weak AMOC	No differences	No differences	Connections added from Groups 1 and 2 to Group 4
2015	High winter NAO; weak AMOC	No differences	No differences	No differences
		k_h = 0 m^2 s^{-1}		
1993	High winter NAO; strong AMOC	Connection lost from Group 1 to Group 2	Connection lost from Group 7 to Group 6 and from Group 2 to Group 4	Connection lost from Group 7 to Group 6
1996	Large drop in winter NAO; strong AMOC	Connection lost from Group 3 to Group 4	Connection lost from Group 3 to Group 4	No differences
2001	Shift in Labrador Current and NAO action centres; weak AMOC	Connection lost from Group 1 to Group 2	Connection lost from Group 2 to Group 3, Group 3 to Group 4, Group 7 to Group 6	Connection lost from Group 7 to Group 6
2008	Winter deep convection returns in Labrador Sea; weak AMOC	No differences	Connection lost from Group 2 to Group 3, Group 7 to Group 6	Connection lost from Group 7 to Group 6
2010	Low winter NAO; change in sea surface height; weak AMOC	Connection lost from Group 1 to Group 2	Connection lost from Group 3 to Group 4	No differences
2015	High winter NAO; weak AMOC	Connection lost from Groups 2 and Group 3 to Group 4; Added Connection from Group 1 to Group 4	Connections lost from Group 2 to Group 3 and Group 4, Group 7 to Group 6	Connection lost from Group 7 to Group 6

All drift durations were of 2 weeks with diffusivity k_h = 250 m^2 s^{-1} and k_h = 0 m^2 s^{-1}.

connection to Group 5, assuming that the larval duration was also greater than 14 days. Similarly, in 1993 in the surface models for January (**Supplementary Figure 14A**), larvae from Group 3 track close to Group 5. Further, these potential connections are only seen when the diffusivity constant is applied, and without it (k_h = 0 m^2 s^{-1}) there are no connections at all with Group 5 which remains very isolated with generally high retention in both July and January in each of the years and for all release depths (**Supplementary Figures 17–22**). July surface releases in 2015 show offshore movement from Group 5 (**Supplementary Figure 17F**).

Simulations run using the 5-day average BNAM data for July, 2010 with and without the diffusivity constant (**Supplementary Figures 23**, **24**) showed retention in Group 5 at the seabed as seen with the July monthly averaged data for that year, and no connections to Group 5 from or to any of the other Groups. The dispersal kernels produced from the 5-day averaged data covered a greater area than that of the July monthly averaged data and eddies and meanders were more pronounced in the former, particularly with k_h = 0 m^2 s^{-1}. There was also less impact of using the diffusivity constant as expected with the smaller averaging window, and the July monthly averaged results with k_h = 250 m^2 s^{-1} are more similar to those produced with the 5-day averages with and without diffusivity factored in. The greatest difference between the trajectories in the dispersal kernels produced using the 5-day average simulations are seen at the surface (**Supplementary Figures 11**, **17**, **24**) with the dispersal kernels becoming more similar at mid-depth (**Supplementary Figures 12**, **18**, **24**) and the seabed (**Supplementary Figures 13**, **19**, **24**). At the surface, with k_h = 0 m^2 s^{-1}, well-developed meanders show in the dispersal kernels as the particles track in the Gulf Stream. The Group 4

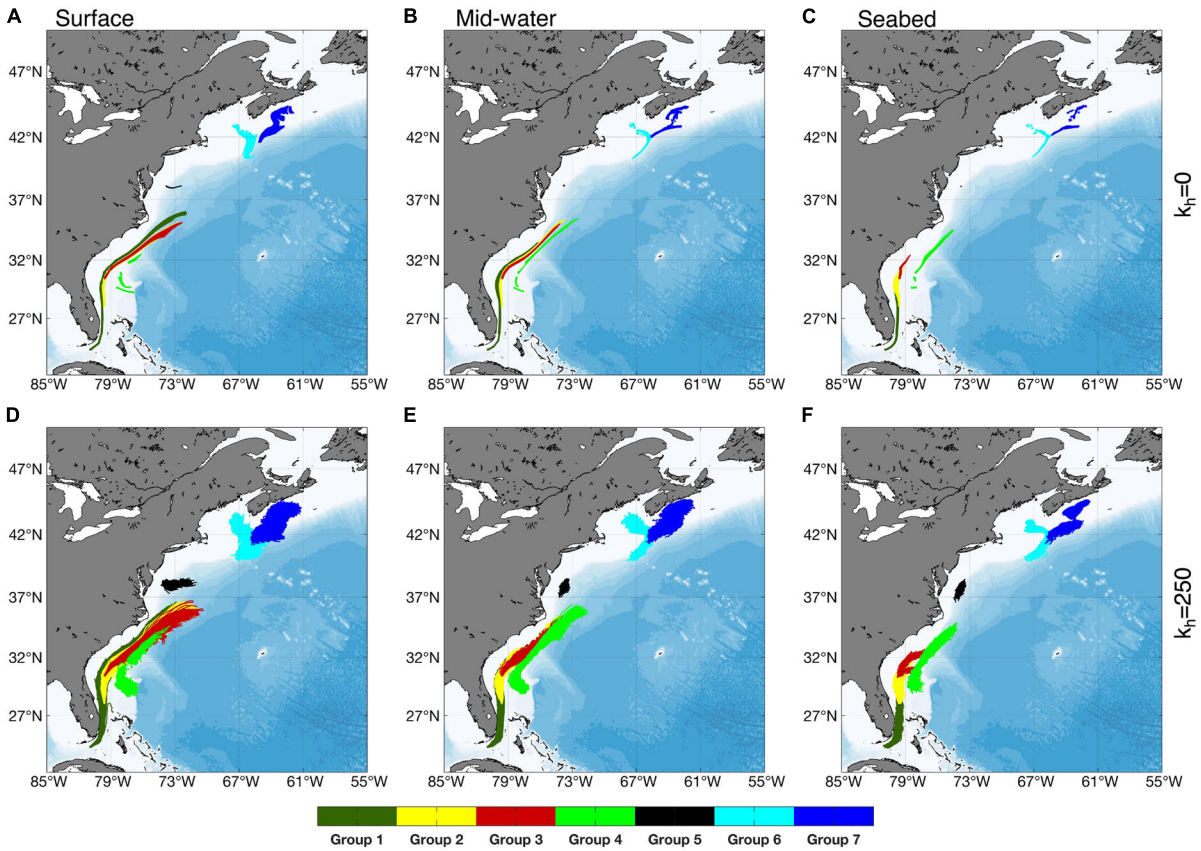

FIGURE 8 | Dispersal kernels from particle releases in July using long-term averaged currents from each of the occupied grid cells in each of the seven Groups (**Table 1**) at three release depths (surface, **(A,D)**; mid-water, **(B,E)**; seabed, **(C,F)** when k_h = 0 **(A–C)**, and when k_h = 250 m^2 s^{-1} **(D–F)**.

particles are much more dispersed over the Blake Plateau and some move directly offshore there.

Flow Distances

For any release depth, the greatest distances traveled were by particles introduced into the Gulf Stream where it is strongest in the south, and were progressively less for those released into it further north. Those released in the three Groups north of Cape Hatteras had flow distances ranked in accord with the strengths of their local currents (**Supplementary Table 1** and **Figure 9**). Except for those originating in Group 4, flow distances were greatest for particles released at the surface and least for those released at the seabed when horizontal diffusivity was incorporated in the model but especially when it was not. For Group 4, flow distances of mid-water releases were generally greatest and, with k_h = 0, the maximum movement amongst particles released at the seabed exceeded that of surface releases. Moreover, the distance interval between 50 and 95% of particle connectivity is 487 km at mid-water and 286 km at the seabed, both of which are the largest spread among all groups (**Figure 9**). This large distance interval disappears when the diffusivity constant is applied, with the distance interval between 50 and 95% of larval connectivity dropping to 95 km in mid-water particle releases and 54 km in seabed releases (**Supplementary Table 1** and **Figure 9**). The same patterns were seen in individual years (**Supplementary Table 2**) and flow distances were high similar to those produced using the long-term average data. Group 4 shows a strong bimodality in particle distribution at all three depths (**Figure 9**), reflective of the physical oceanography of the area of the Blake Plateau.

Throughout, the addition of horizontal diffusivity greatly increased the flow distances. Group 5 releases were particularly affected (**Supplementary Tables 1**, **2**). Despite the great increases in flow distance produced when a diffusivity constant is applied, the lack of connectivity between areas north and south of Cape Hatteras, North Carolina at surface, mid-water and seabed release depths is maintained (**Figure 8**).

Dispersal From Group 4 on the Blake Plateau Using Long-Term Averaged Currents

Within Group 4, the depth and especially the location of particle release has a strong influence on mean end positions (**Figure 10**). The mean end positions and directions were almost unaffected by introduction of horizontal diffusivity. Particles released south of the Charleston Bump (Group 4 #1, #2) moved only short distances to the south or southeast, regardless of release depth.

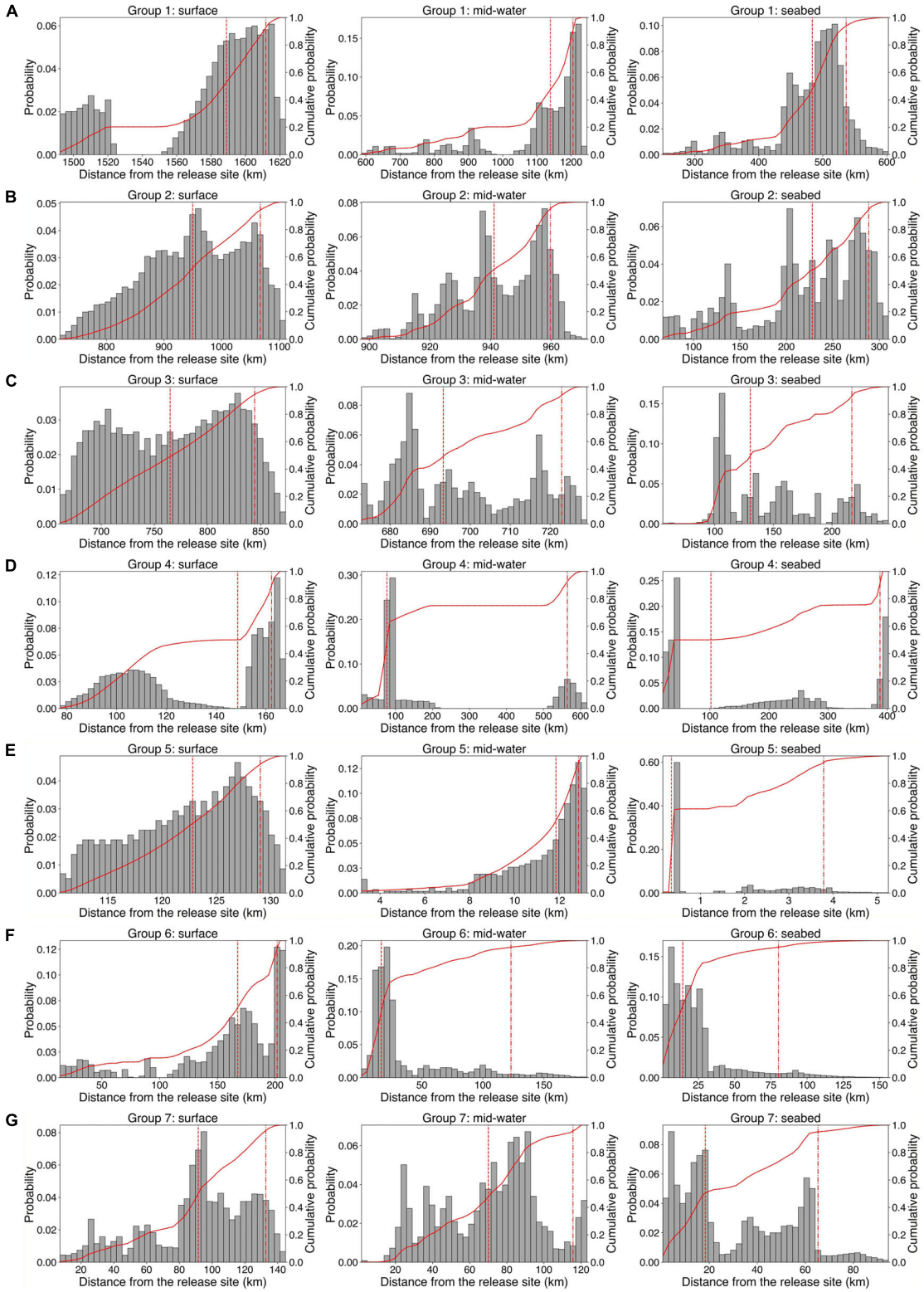

FIGURE 9 | Frequency distributions of maximum flow distances of particles released in July using long-term averaged currents from occupied grid cells in each Group at each release depth, modeled with $k_h = 0$. **(A)** Group 1, **(B)** Group 2, **(C)** Group 3, **(D)** Group 4, **(E)** Group 5, **(F)** Group 6, and **(G)** Group 7. Bars show the dispersal probability values over the specified distance interval from the release sites, and red solid lines show the cumulative probability. The red dashed and dotted lines indicate the median and 95th percentile of the distances.

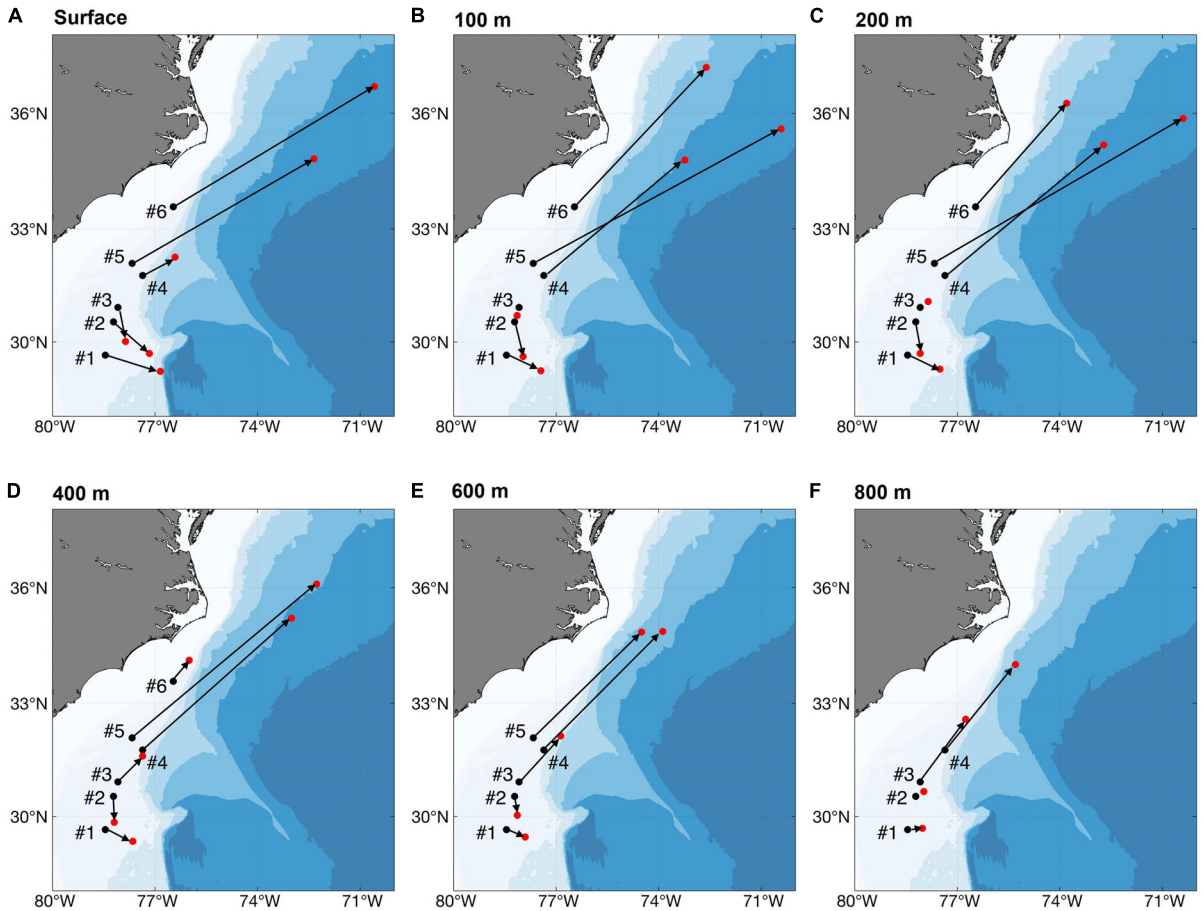

FIGURE 10 | Release positions (black dots), mean ending points (red dots) and net displacements of particles released within Group 4, north and south of Charleston Bump, at various release depths, using long-term averaged currents modeled with k_h = 0. **(A)** Surface, **(B)** 100 m, **(C)** 200 m, **(D)** 400 m, **(E)** 600 m, and **(F)** 800 m. "#" denotes the individual occurrence record in Group 4.

Releases north of the Bump (Group 4 #4, #5, #6) were transported greater distances to the northeast. Surface releases from Group 4 #3 moved like the particles from Group 4 #1 and #2, but those released at 400 m or deeper moved to the northeast.

Inter-Model Comparison

Results using both ocean model products support the main conclusion from our analyses, i.e., that documented populations of *V. pourtalesii* are not physically connected between areas north and south of Cape Hatteras (Groups 1–4), nor between the Scotian Shelf populations (Groups 6 and 7) and those north of Cape Hatteras (Group 5) (**Figure 1**). The connectivity matrices produced from the daily averaged GLORYS12VI surface products (**Supplementary Figure 25**) show no connections between Group 5 and any other Group, with no particle retention. Connections were made between the Groups in the southern sub-region ranging from two Groups connecting in 2008 to four Groups connecting in 1996, with Group 4 showing the only retention and that in 2010 only. However, our results showed differences between the particle trajectories run using the surface July monthly averaged BNAM and daily averaged GLORYS12VI for each of the six selected years, as was expected (compare **Supplementary Figures 11**, **26**, respectively where k_h = 250 m^2 s^{-1} in the former and k_h = 0 m^2 s^{-1} in the later, allowing for the greatest opportunity for connections). Gulf Stream transport shows differences in the shape of the dispersal kernels in particular. **Figure 11** compares the dispersal kernels and connectivity matrices from particle releases from each of the occupied grid cells in each of the seven Groups (**Table 1**) from the surface in July, 2010, using BNAM monthly averaged currents (k_h = 250 m^2 s^{-1}), BNAM 5-day averaged currents (k_h = 0 m^2 s^{-1} and k_h = 250 m^2 s^{-1}), and GLORYS12VI daily averaged currents (k_h = 0 m^2 s^{-1}). The BNAM models with k_h = 250 m^2 s^{-1} but differing in the number of days used to average the products shows a much more diffusive pattern in the dispersal kernels with the smaller averaging period, as would be expected. However there are more connections and retentions in the southern sub-region using the monthly averaged results compared with the 5-day averaged currents. Therefore, while the latter disperses particles over a larger area, they are not tracking over the locations of the known occurrences. Common results across all four models are retention in Groups 7 and 6 in the

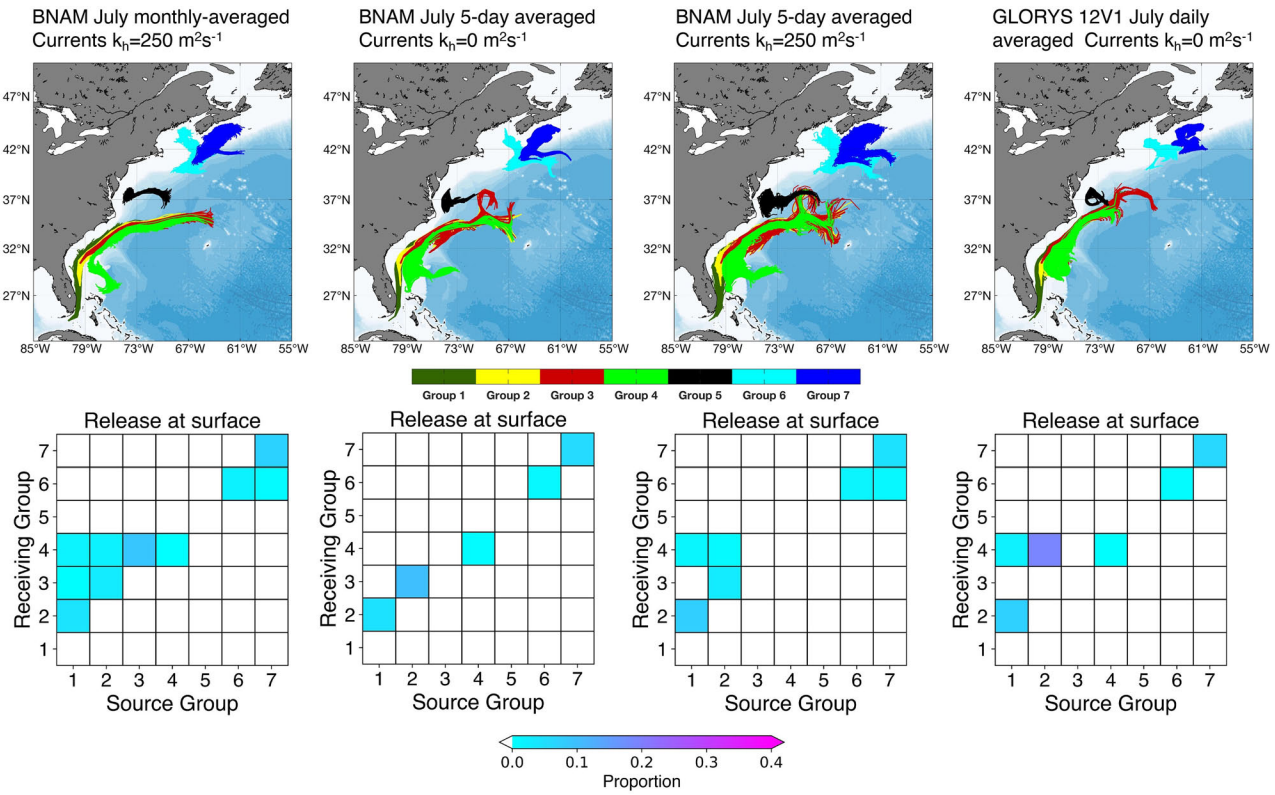

FIGURE 11 | Dispersal kernels and connectivity matrices from particle releases from each of the occupied grid cells in each of the seven Groups (**Table 1**) from the surface in July 2010, using BNAM monthly averaged currents (k_h = 250 m^2 s^{-1}), BNAM 5-day averaged currents (k_h = 0 m^2 s^{-1} and k_h = 250 m^2 s^{-1}) and GLORYS12VI daily averaged currents (k_h = 0 m^2 s^{-1}) in the particle tracking models.

northern region, and connection between Groups 1 and 2 in the southern sub-region (**Figure 11**).

DISCUSSION

Regional-Scale Connectivity

Particle tracking has shown that connectivity among *V. pourtalesii* populations may be very different in the south and the north of its range. South of Cape Hatteras, larvae of this deep-living species are released into the swift-flowing Gulf Stream, which will carry them far enough to provide strong, though unidirectional, connections between the Straits of Florida and the continental slope south of Cape Hatteras, including our Groups 1–4. These connections vary based on the degree to which larvae rise in the water column and their persistence there (**Figure 5**). Similar rapid dispersal over long distances by the Gulf Stream has been seen in studies of other deep-sea species in this region (Young et al., 2012). In contrast, the tracking of particles released in Group 4 demonstrated the complexity that can arise from the interaction of a major current with seabed topography, specifically the Charleston Bump and its associated gyre (McClain and Atkinson, 1985; Popenoe and Manheim, 2001). That gyre may retain *V. pourtalesii* larvae south of the Bump, including those from Groups 1, 2 and 3, creating redundancy in recruitment in that region. Redundancy in connectivity networks occurs when there is more than one connectivity path leading to a population. This is a positive feature as it helps to mitigate against the risk of recruitment failure by providing alternate connectivity routes. An outcome of such redundancy may be enhanced genetic diversity conferring greater resilience to climate change to the population (cf. Ramos et al., 2018).

Given the weaker currents of the continental shelf and the absence of the Gulf Stream, particles released from *V. pourtalesii* areas north of Cape Hatteras had lower dispersal distances (**Supplementary Table 2**) and greater retention within their source areas than those to the south (**Figure 4** and **Supplementary Figure 7**), especially for those released near the seabed or at mid-water depths. However, unidirectional larval transport from Emerald Basin (Group 7) to the Northeast Channel (Group 6) is possible, if the species PLD is as long as 2 weeks (**Figure 6**). While that connection may be valuable in maintaining the downstream *V. pourtalesii* populations over the long term and enhancing its genetic diversity, most larvae dispersed away from their parental areas are likely doomed, whereas those retained confer local resilience through high levels of larval supply in suitable habitats. Retention is a particularly important process for reef-forming

organisms (Swearer et al., 1999; Jones et al., 2009), leading to enhanced recruitment and establishment of populations that dominate the community, as with the formation of sponge ground habitats in Groups 6 and 7. One of the outcomes from our assessment of inter-annual variation in connectivity was increased retention over that detected using the long-term averaged current data in our models. Groups 1, 3, and 4 in the southern part of the range showed retention in individual years at all depths, while Group 5 between Cape Hatteras and Cape Cod, showed retention in surface releases not found in the models using the long-term averages. These results reinforce the role of retention in maintaining these populations and the need to protect local populations as a first priority.

No connections were found between the *V. pourtalesii* in Group 5 occurring on the continental slope between Cape Hatteras and Cape Cod, and those elsewhere in any of the models run (using long-term averaged currents, monthly averaged currents in individual years, 5-day averaged currents in July, 2010 and GLORYS12V1 daily averaged currents in July, 2010). However, warm-core eddies are shed from the Gulf Stream after it passes Cape Hatteras south of the Group 5 occurrence (Kang and Curchitser, 2013). While no connections with Group 5 were found in our models of monthly averaged data in individual years, there was some suggestion that larvae from the south (Groups 3 and 4) could connect with a dispersal gyre in the vicinity of Group 5 in some years in January and with the GLORYS12V1 daily averaged currents in July, 2010. Therefore, there is potential for larvae from southern release sites to reach Group 5, particularly at the surface and mid-water depths with diffusivity included, although the 2-week PLD limits the likelihood that such larvae would be viable both in this area and in eddies cut off the Gulf Stream further north. Connectivity from the Northeast Channel (Group 6) to Group 5 is less likely (**Figures 9**, **8**). In individual years particles that reached the continental slope from Group 6 were entrained in currents that brought them further eastward, rather that westward toward Group 5 (e.g., **Supplementary Figures 11**, **12F**, **13F**). Further study is needed to investigate the roles of eddies, particularly smaller and short-lived eddies, for the connectivity in this region as they remain the most likely means of explaining the establishment of the Group 5 population. Beazley et al. (2021) found that suitable habitat for this species is very limited in the bight between Cape Hatteras and Cape Cod. Nevertheless, there may be unknown upstream populations that link to Group 5 providing larval sources, and/or creating links between known occurrences which could also explain the establishment of that population. Its persistence is likely maintained through retention (**Figure 4**).

This summary of regional-scale connectivity appears little influenced by any seasonal cycle and is consistent in the face of uncertainty over the timing of larval release in *V. pourtalesii*. It is also largely independent of the effects of horizontal mixing. Introduction of a non-zero value of the horizontal diffusion constant (k_h), a controversial alternative in particle tracking studies (Hunter et al., 1993; Kelly et al., 2020), did have a large effect on the modeled transport trajectories but had little impact on the connectivity matrices presented here, only extending the connections among the southern Groups and adding some retention pathways for those groups. It also had little effect on the mean ending positions, with most of the increased flow distance therefore attributed to the random walks at each of the 2,016 time steps in an individual particle trajectory. Therefore including the diffusivity constant increased the area of the dispersal kernel more than the distance from the source (**Figure 8**), and comparisons with its effect using different averaging periods demonstrated that it did successfully replace some of the variability lost in using the averaged data.

The effects of inter-annual variation on connectivity in July currents were not as profound as expected. This is likely because the eddy fields were largely offshore from the sponge populations. The most significant difference observed was that the surface currents showed strong offshore dispersal in many of the individual years that was not seen in models using the long-term averaged currents, indicating that loss of larvae to the system through entrainment into the Gulf Stream may be even greater than indicated from the models run with long-term averaged currents. As noted, a few novel connections and retentions were revealed in the models using shorter averaging periods, however, those did not change the general pattern of connectivity in the sub-regional populations north and south of the Gulf Stream and in the area between Cape Hatteras and Cape Cod.

Our results showed differences between the dispersal kernels produced with BNAM and GLORYS12VI, as was expected, however, both models support the main conclusion from our analyses, that documented populations of *V. pourtalesii* are not connected between areas south of Cape Hatteras (Groups 1–4), and to its north [between the Scotian Shelf populations (Groups 6 and 7) and those on the continental slope north of Cape Hatteras (Group 5)]. This result was produced despite the use of different averaging periods and ocean models, and is likely due to the overwhelming influence of the Gulf Stream, allowing for little opportunity for particles to escape from its offshore trajectory, once entrained. Opportunities for entrainment increased with shorter averaging periods used in the models and with the application of the diffusivity constant. Thus while the sub-regional connectivity and retention patterns varied, the main conclusions regarding the connectivity between northern and southern populations, the downstream connectivity of populations within those regions, and the importance of larval retention appear robust.

Effects of Larval Vertical Distribution and Pelagic Duration

The depth of particle release had substantial effects on modeled movements, particularly when horizontal diffusion was incorporated. Releases at the surface and mid-depths (other than those in Group 4) were transported further and faster, whilst particles released at the seabed were more likely to be retained within their source Groups. Similar results have been obtained in other particle-tracking studies and show that the extent of upward movement from the seafloor is a key determinant in dispersal of larvae of benthic species away from their source

sites (Edwards et al., 2007; Young et al., 2012; Kool et al., 2015; McVeigh et al., 2017). Most recently, Gary et al. (2020) investigated the influence of vertical swimming behaviors on the dispersal of deep-sea larvae and found that vertical distribution, especially residence time near the surface, had a large impact on theoretical dispersal.

With only limited available information on larval growth and movement in *V. pourtalesii*, we did not attempt to further integrate their swimming behavior into the 3-D models, nor to examine the effect of vertical position on the advective pathways directly. Thus, potential effects of larval swimming behavior can only be estimated through comparison of the movements of particles released at various depths. There were clear differences amongst those, notably with releases in the southern portion of Group 4, but the connectivity matrices show a concordance in broad patterns across depths, especially with non-zero horizontal diffusivity included in the model. Thus, the conclusion that there is some retention of larvae, along with unidirectional connections in the south (Groups 1–4) and from Group 7 to Group 6 (**Figure 4**), may be robust to assumptions about larval vertical distribution.

The more-critical unknown is the PLD. If that of *V. pourtalesii* is short by the standards of other sponges, perhaps no more than a few minutes (Maldonado, 2006; Kenchington et al., 2019), then almost all larval settlement will be in the immediate area of the adults. Longer PLDs would mean greater connectivity, up to the 2-week planktonic drifts modeled here.

Predicted Distributions and Potential for Larval Supply

Beazley et al. (2021) modeled the distribution of *V. pourtalesii*, based on the predicted occurrence probability from random forest and generalized additive models, under present and future climate conditions, using Representative Concentration Pathway intermediate (RCP 4.5) and worst-case (RCP 8.5) CO_2 concentration scenarios for the period 2046–2065. Their present-day species distribution models showed a discontinuous distribution of *V. pourtalesii* with two centers of high probability of occurrence, respectively, the Scotian Shelf and Northeast Channel, and the Blake Plateau in the south, with a low probability of occurrence in between. In random forest models both surface and bottom currents were influential in determining the predicted distributions in the south (Beazley et al., 2021). The present study has shown that there is no direct connection between those centers through larval transport, supporting the species distribution model conclusions.

Our particle tracking suggests that the center of occurrence on the Blake Plateau noted by Beazley et al. (2021) may be supported by recruitment of larvae released into the Gulf Stream further south, from sites as far away as the Straits of Florida (either directly or through settlement at intermediate locations), and aided by retention in the gyre south of the Charleston Bump. *V. pourtalesii* is not found to the west of the known faunal boundary between the Gulf of Mexico and the Atlantic, which is marked by genetic discontinuities even in species with trans-boundary distributions, indicating contemporary obstructions to gene flow (Avise, 1992). With the powerful flow of the Gulf Stream and limited suitable habitat to the westward, it is unlikely that *V. pourtalesii* could extend its distribution beyond the reef-edge off the Florida Keys. Our particle tracking modeling found that retentive settlement there, in Group 1, only occurred with particles released at the seabed and only if the model included horizontal diffusivity representing, in this case, the presence of local eddies. Cyclonic eddies have been shown to be very important to recruitment of larval damselfish on mesophotic coral reef ecosystems in the Florida Keys area where Group 1 is located (Vaz et al., 2016) and could also influence sponge dispersal at this southern range boundary.

In the north, the situation is very different. During the Pleistocene, the Scotian Shelf was covered in ice until 20 ka BP. By 12 ka BP, an extensive coastal plain with large islands and shallow seas had formed (Pielou, 1991; Shaw et al., 2002, 2006; Paul and Schäfer-Neth, 2003; Schäfer-Neth and Paul, 2003). Present conditions have developed gradually through the millennia since, presumably allowing *V. pourtalesii* to colonize the Northeast Channel and Emerald Basin through post-Pleistocene range expansion as hypothesized for other species (Kenchington et al., 2009).

Beazley et al. (2021) predicted that the area of suitable habitat for the species will enlarge in the future in both the south and north under the RCP scenarios tested, with the greatest increases in the deeper parts of the Gulf of Maine and Gulf of St. Lawrence. However, the latter is unlikely to be colonized quickly as it lies upstream of contemporary occurrences of *V. pourtalesii* and projected climate change is not expected to alter the current directionality in this sub-region (Brickman et al., 2018), leaving distributional expansion dependent on fortuitous flow reversals during extreme events. Conversely, our study suggests that the sponge populations in Emerald Basin and the Northeast Channel may already benefit from a moderate degree of larval retention (enhanced in the models with shorter averaging periods), possibly supplemented by a unidirectional connection from the Basin to the Channel. From the latter, future suitable habitat in the Gulf of Maine should be colonized readily, provided that the existing sponge grounds can be protected from anthropogenic harm.

CONCLUSION

This study used 3-D biophysical particle dispersal models to simulate hydrodynamic connectivity among known concentrations of the deep-sea hexactinellid sponge *Vazella pourtalesii* throughout its distribution on the east coast of North America. We have shown that intense ocean currents, primarily the Gulf Stream, shape the contemporary distribution of this species, creating two sub-regions roughly separated at Cape Hatteras, United States, and concurs with present day and future predicted distribution models for this species. The addition of connectivity modeling to complement published distribution models informs both modeling approaches for this species. We found no exchange with a 2-week time period (estimated maximum pelagic larval duration for *V. pourtalesii*) between areas north and south of Cape Hatteras, at surface, mid-water

and seabed release depths, irrespective of month of release, application of a horizontal diffusion constant specific to cross-Gulf Stream diffusivity, or use of different averaging periods for ocean currents. This coincides with a gap in suitable habitat in the area north of Cape Hatteras and south of Cape Cod in both present and future predicted distributions (Beazley et al., 2021). Monthly averaged models for selected years suggest that it may be possible that eddy transport of larvae from the Gulf Stream could supply *V. pourtalesii* larvae from the south to the area northwest of Cape Hatteras (Group 5), connecting the two sub-regions. Such eddies are not fully resolved in our models and smaller eddies could be the means of larval transport from the south to Group 5. However, the viability of such larvae would require a longer PLD than 2 weeks, which is already thought to be a maximum duration from what is known of sponge larval biology. Furthermore, our models do not include larval mortality which would act to also limit connectivity. At sub-regional scales, the influence of the Charleston Bump, a topographic high rising from the Blake Plateau, southeastern United States, was profound. Particles seeded north of the Bump were transported greater distances than those seeded to the south, which were caught in an associated gyre, promoting retention in seabed releases. Connectivity among populations in the southern sub-region was shown to be highly probable, with the Blake Plateau south of the Bump an area with considerable redundancy from downstream populations, potentially conferring increased resilience through genetic mixing from multiple source populations. This area is also likely a sink, with larvae either being retained or transported by the Gulf Stream into deep waters. Despite weaker currents in the northern sub-region, with higher particle retention, our dynamic models show downstream connectivity between the Emerald Basin and Northeast Channel areas. Population genetic studies, focusing on the two sub-regions, could help to establish whether these patterns also represent genetic subdivisions. Our connectivity modeling could be used in combination with the species distribution models (Beazley et al., 2021) to construct explicit spatial hypotheses for population genetic studies of *V. pourtalesii* following a seascape genetic framework (Kenchington et al., 2006, 2015; Zeng et al., 2020). Long-term conservation of this ecologically important species should focus on the protection of local populations, given that retention appears to be a prominent factor in our dispersal models.

DATA AVAILABILITY STATEMENT

The 3-D Lagrangian particle simulator (Parcels) is freely available at https://www.oceanparcels.org. Monthly mean currents from the Bedford Institute of Oceanography North Atlantic Model (BNAM) results averaged over the 1990–2015 period for the Northwest Atlantic Ocean are available online on the Federal Government of Canada Open Data Portal (https://open.canada.ca/data/en/dataset/dd5ef0d6-d588-4f4f-99e5-27c4bdfddf6a). The GLORYS12V1 ocean products with daily means for the surface are publically available from the Copernicus Marine Service data portal (see text footnote 2).

AUTHOR CONTRIBUTIONS

EK and AD acquired the funding. SW performed the data analyses and produced the tables and figures. All authors contributed to the writing of the manuscript, take responsibility for the content, approved the submitted version, and designed the experiments.

FUNDING

This research was funded through the Fisheries and Oceans Canada (DFO) Strategic Program for Ecosystem-Based Research and Advice (SPERA) project "Evaluation of the Effectiveness of Two Sponge Conservation Areas in the Maritimes Region: Identifying Patterns of Dispersal, Connectivity, and Recovery Potential of the Russian Hat Sponge *Vazella pourtalesii*," DFO's International Governance Strategy Science Program through project "Marine Biological Diversity Beyond Areas of National Jurisdiction (BBNJ): 3-Tiers of Diversity (Genes-Species-Communities)," and the H2020 EU Framework Programme for Research and Innovation Project SponGES (Deep-sea Sponge Grounds Ecosystems of the North Atlantic: an integrated approach toward their preservation and sustainable exploitation) (Grant Agreement no. 679849). This document reflects only the authors' views, and the Executive Agency for Small and Medium-sized Enterprises (EASME) is not responsible for any use that may be made of the information it contains.

ACKNOWLEDGMENTS

We thank Lindsay Beazley and Cam Lirette (DFO) for their support in the early stages of this work. Drs. T. J. Kenchington and F. J. Murillo provided thoughtful reviews as part of the DFO internal review process, which helped to improve the manuscript.

SUPPLEMENTARY MATERIAL

The Supplementary Material for this article can be found online at: https://www.frontiersin.org/articles/10.3389/fmars.2021.701218/full#supplementary-material

REFERENCES

Anderson, L. A., Robinson, A. R., and Lozano, C. J. (2000). Physical and biological modeling in the Gulf Stream region: I. Data assimilation methodology. *Deep Sea Res. Part I Oceanogr. Res. Pap.* 47, 1787–1827. doi: 10.1016/S0967-0637(00)00019-4

Ashford, J., La Mesa, M., Fach, B. A., Jones, C., and Everson, I. (2010). Testing early life connectivity using otolith chemistry and particle-tracking simulations. *Can. J. Fish. Aquat. Sci.* 67, 1303–1315. doi: 10.1139/F10-065

Avise, J. C. (1992). Molecular population structure and the biogeographical history of a regional fauna: a case history with lessons for conservation biology. *Oikos* 63, 62–76. doi: 10.2307/3545516

Bart, M. C., De Kluijver, A., Hoetjes, S., Absalah, S., Mueller, B., Kenchington, E., et al. (2020). Differential processing of dissolved and particulate organic matter by deep-sea sponges and their microbial symbionts. *Sci. Rep.* 10:17515. doi: 10.1038/s41598-020-74670-0

Bartsch, J., and Knust, R. (1994). Simulating the dispersion of vertically migrating sprat larvae (*Sprattus sprattus* (L.)) in the German Bight with a circulation and transport model system. *Fish. Oceanogr.* 3, 92–105. doi: 10.1111/j.1365-2419.1994.tb00052.x

Beazley, L., Kenchington, E., Murillo, F. J., Brickman, D., Wang, Z., Davies, A. J., et al. (2021). Climate change winner in the deep sea? Predicting the impacts of climate change on the distribution of the glass sponge *Vazella pourtalesii*. *Mar. Ecol. Prog. Ser.* 657, 1–23. doi: 10.3354/meps13566

Beazley, L., Wang, Z., Kenchington, E., Yashayaev, I., Rapp, H. T., Xavier, J. R., et al. (2018). Predicted distribution of the glass sponge *Vazella pourtalesi* on the Scotian Shelf and its persistence in the face of climatic variability. *PLoS One* 13:e0205505. doi: 10.1371/journal.pone.0205505

Bell, J. J. (2008). The functional roles of marine sponges. *Estuar. Coast. Shelf Sci.* 79, 341–353. doi: 10.1016/j.ecss.2008.05.002

Biló, T. C., and Johns, W. E. (2019). Interior pathways of Labrador Sea Water in the North Atlantic from the Argo perspective. *Geophys. Res. Lett.* 46, 3340–3348. doi: 10.1029/2018GL081439

Bower, A. S., Rossby, H. T., and Lillibridge, J. L. (1985). The Gulf stream—barrier or blender? *J. Phys. Oceanogr.* 15, 24–32. doi: 10.1175/1520-0485(1985)015<0024:TGSOB>2.0.CO;2

Brickman, D., Hebert, D., and Wang, Z. (2018). Mechanism for the recent ocean warming events on the Scotian Shelf of eastern Canada. *Cont. Shelf Res.* 156, 11–22. doi: 10.1016/j.csr.2018.01.001

Brickman, D., Wang, Z., and Detracey, B. (2016). Variability of current streams in Atlantic Canadian waters: a model study. *Atmos. Ocean* 54, 218–229. doi: 10.1080/07055900.2015.1094026

Busch, K., Beazley, L., Kenchington, E., Whoriskey, F., Slaby, B. M., and Hentschel, U. (2020). Microbial diversity of the glass sponge Vazella pourtalesii in response to anthropogenic activities. *Conserv. Genet.* 21, 1001–1010. doi: 10.1007/s10592-020-01305-2

Callies, U., Plüß, A., Kappenberg, J., and Kapitza, H. (2011). Particle tracking in the vicinity of Helgoland, North Sea: a model comparison. *Ocean Dyn.* 61, 2121–2139. doi: 10.1007/s10236-011-0474-8

Codling, E. A., Hill, N. A., Pitchford, J. W., and Simpson, S. D. (2004). Random walk models for the movement and recruitment of reef fish larvae. *Mar. Ecol. Prog. Ser.* 279, 215–224. doi: 10.3354/meps279215

Crowder, L. B., Lyman, S. J., Figueira, W. F., and Priddy, J. (2000). Source-sink population dynamics and the problem of siting marine reserves. *Bull. Mar. Sci.* 66, 799–820.

Csanady, G. T., and Hamilton, P. (1988). Circulation of slopewater. *Cont. Shelf Res.* 8, 565–624. doi: 10.1016/0278-4343(88)90068-4

Delandmeter, P., and Van Sebille, E. (2019). The Parcels v2.0 Lagrangian framework: new field interpolation schemes. *Geosci. Model Dev.* 12, 3571–3584. doi: 10.5194/gmd-12-3571-2019

Delhez, E., Damm, J. M. P., de Goede, E., de Kok, J. M., Dumas, F., Jones, J. E., et al. (2004). What can we expect from shelf seas models: the NOMADS2 Project. *J. Mar. Syst.* 45, 39–53. doi: 10.1016/j.jmarsys.2003.09.003

Downie, A.-L., Piechaud, N., Howell, K., Barrio Froján, C., Sacau, M., and Kenny, A. (2021). Reconstructing baselines: use of habitat suitability modelling to predict pre-fishing condition of a vulnerable marine ecosystem. *ICES J. Mar. Sci.* 0, 1–13. doi: 10.1093/icesjms/fsab154

Drinkwater, K., Petrie, B., and Smith, P. (2003). Climate variability on the Scotian Shelf during the 1990s. *ICES Mar. Sci. Symp.* 219, 40–49.

Edwards, K., Hare, J., Werner, F., and Seim, H. (2007). Using 2-dimensional dispersal kernels to identify the dominant influences on larval dispersal on continental shelves. *Mar. Ecol. Prog. Ser.* 352, 77–87. doi: 10.3354/meps07169

Fernandez, E., and Lellouche, J. M. (2021). *Product User Manual For the Global Ocean Physical Reanalysis product GLOBAL_REANALYSIS_ PHY_001_030. Issue 1.2. EU Copernicus Marine Service – Public Ref: CMEMS-GLO-PUM-001-030*.

Ferry, N., Parent, L., Garric, G., Barnier, B., and Jourdain, N. C. (2010). Mercator global eddy permitting ocean reanalysis GLORYS1V1: description and results. *Merc. Ocean Q. Newslett0* 36, 15–27.

Fratantoni, P. S., and Pickart, R. S. (2007). The western North Atlantic shelfbreak current system in summer. *J. Phys. Oceanogr.* 37, 2509–2533. doi: 10.1175/JPO3123.1

Gary, S. F., Fox, A. D., Biastoch, A., Roberts, J. M., and Cunningham, S. A. (2020). Larval behaviour, dispersal and population connectivity in the deep sea. *Sci. Rep.* 10:10675. doi: 10.1038/s41598-020-67503-7

Greene, C. H., and Pershing, A. J. (2003). The flip-side of the North Atlantic Oscillation and modal shifts in slope-water circulation patterns. *Limnol. Oceanogr.* 48, 39–322. doi: 10.4319/lo.2003.48.1.0319

Hakkinen, S., and Rhines, P. B. (2009). Shifting surface currents of the northern North Atlantic Ocean. *J. Geophys. Res. Oceans* 114:C04005. doi: 10.1029/2008JC004883

Häkkinen, S., Rhines, P. B., and Worthen, D. L. (2013). Northern North Atlantic sea surface height and ocean heat content variability. *J. Geophys. Res. Oceans* 118, 3670–3678. doi: 10.1002/jgrc.20268

Han, G., and Loder, J. W. (2003). Three-dimensional seasonal-mean circulation and hydrography on the eastern Scotian Shelf. *J. Geophys. Res* 108:3136. doi: 10.1029/2002JC001463

Han, G., Loder, J. W., and Smith, P. C. (1999). Seasonal-mean hydrography and circulation in the Gulf of St. Lawrence and on the eastern Scotian and southern Newfoundland shelves. *J. Phys. Ocean.* 29, 1279–1301. doi: 10.1175/1520-0485(1999)029<1279:SMHACI>2.0.CO;2

Hanna, C. A. (1984). *Initial Settlement of Marine Invertebrate Larvae : The Role of Passive Sinking in a Near-Bottom Turbulent Flow Environment*. Doctoral thesis. Dartmouth MA: Massachusetts Institute of Technology. doi: 10.1575/1912/2210

Hanz, U., Beazley, L., Kenchington, E., Duineveld, G., Rapp, H. T., and Mienis, F. (2021). Seasonal variability in near-bed environmental conditions in the Vazella pourtalesii glass sponge grounds of the Scotian Shelf. *Front. Mar. Sci.* 08:2021. doi: 10.3389/fmars.2020.597682

Hawkes, N., Korabik, M., Beazley, L., Rapp, H., Xavier, J., and Kenchington, E. (2019). Glass sponge grounds on the Scotian Shelf and their associated biodiversity. *Mar. Ecol. Prog. Ser.* 614, 91–109. doi: 10.3354/meps12903

Hogg, M., Tendal, O., Conway, K., Pomponi, S., van Soest, R., Gutt, J., et al. (2010). *Deep-sea Sponge Grounds: Reservoirs of Biodiversity. UNEP-WCMC Biodiversity Series 32*. Cambridge: UNEP-WCMC.

Holloway, P., Miller, J. A., and Gillings, S. (2016). Incorporating movement in species distribution models: how do simulations of dispersal affect the accuracy and uncertainty of projections? *Int. J. Geogr. Inf. Sci.* 30, 2050–2074. doi: 10.1080/13658816.2016.1158823

Hufnagl, M., Payne, M., Lacroix, G., Bolle, L. J., Daewel, U., Dickey-Collas, M., et al. (2017). Variation that can be expected when using particle tracking models in connectivity studies. *J. Sea Res.* 127, 133–149. doi: 10.1016/j.seares.2017.04.009

Hunter, J. R., Craig, P. D., and Phillips, H. E. (1993). On the use of random walk models with spatially variable diffusivity. *J. Comput. Phys.* 106, 366–376. doi: 10.1016/S0021-9991(83)71114-9

Hurlburt, H. E., Brassington, G. B., Drillet, Y., Kamachi, M., Benkiran, M., Bourdallé-Badie, R., et al. (2009). High-resolution global and basin-scale ocean analyses and forecasts. *Oceanography* 22, 110–127. doi: 10.5670/oceanog.2009.70

Jones, G. P., Almany, G. R., Russ, G. R., Sale, P. F., Steneck, R. S., Van Oppen, M. J. H., et al. (2009). Larval retention and connectivity among populations of corals and reef fishes: history, advances and challenges. *Coral Reefs* 28, 307–325. doi: 10.1007/s00338-009-0469-9

Kang, D., and Curchitser, E. N. (2013). Gulf Stream eddy characteristics in a high-resolution ocean model. *J. Geophys. Res. Oceans* 118, 4474–4487. doi: 10.1002/jgrc.20318

Kelly, S. J., Popova, E., Aksenov, Y., Marsh, R., and Yool, A. (2020). They came from the Pacific: how changing Arctic currents could contribute to an ecological regime shift in the Atlantic Ocean. *Earths Future* 8:e2019EF001394. doi: 10.1029/2019EF001394

Kenchington, E. L., Nakashima, B. S., Taggart, C. T., and Hamilton, L. C. (2015). Genetic structure of capelin (*Mallotus villosus*) in the northwest Atlantic Ocean. *PLoS One* 10:e0122315. doi: 10.1371/journal.pone.0122315

Kenchington, E., Harding, G., Jones, M. W., and Prodöhl, P. A. (2009). Pleistocene glaciation events shape genetic structure across the range of the American

lobster, *Homarus americanus*. *Mol. Ecol.* 18, 1654–1667. doi: 10.1111/j.1365-294X.2009.04118.x

Kenchington, E., Patwary, M. U., Zouros, E., and Bird, C. J. (2006). Genetic differentiation in relation to marine landscape in a broadcast-spawning bivalve mollusc (*Placopecten magellanicus*). *Mol. Ecol.* 15, 1781–1796. doi: 10.1111/j.1365-294X.2006.02915.x

Kenchington, E., Wang, Z., Lirette, C., Murillo, F. J., Guijarro, J., Yashayaev, I., et al. (2019). Connectivity modelling of areas closed to protect vulnerable marine ecosystems in the northwest Atlantic. *Deep Sea Res. Part I Oceanogr. Res. Pap.* 143, 85–103. doi: 10.1016/j.dsr.2018.11.007

Knudby, A., Kenchington, E., and Murillo, F. J. (2013). Modeling the distribution of *Geodia* sponges and sponge grounds in the northwest Atlantic. *PLoS One* 8:e82306. doi: 10.1371/journal.pone.0082306

Kool, J. T., Huang, Z., and Nichol, S. L. (2015). Simulated larval connectivity among Australia's southwest submarine canyons. *Mar. Ecol. Progr. Ser.* 539, 77–91. doi: 10.3354/meps11477

Kool, J. T., Moilanen, A., and Treml, E. A. (2013). Population connectivity: recent advances and new perspectives. *Landsc. Ecol.* 28, 165–185. doi: 10.1007/s10980-012-9819-z

Koutitonsky, V. G., and Bugden, G. L. (1991). The physical oceanography of the Gulf of St. Lawrence: a review with emphasis on the synoptic variability of the motion. *Can. Spec. Publ. Fish. Aquat. Sci.* 113, 57–90.

Lange, M., and Van Sebille, E. (2017). Parcels v0.9: prototyping a Lagrangian ocean analysis framework for the petascale age. *Geosci. Model Dev.* 10, 4175–4186. doi: 10.5194/gmd-10-4175-2017

Lanna, E., and Riesgo, A. (2020). Sponge larvae do not swim that fast: a reply to Montgomery et al. (2019). *J. Mar. Biol. Assoc. U.K.* 100, 181–183. doi: 10.1017/S0025315419000870

Levin, J., Wilkin, J., Fleming, N., and Zavala-Garay, J. (2018). Mean circulation of the Mid-Atlantic Bight from a climatological data assimilative model. *Ocean Model.* 128, 1–14. doi: 10.1016/j.ocemod.2018.05.003

Leys, S. P., and Ereskovsky, A. V. (2006). Embryogenesis and larval differentiation in sponges. *Can. J. Zool.* 84, 262–287. doi: 10.1139/z05-170

Loder, J. W., Han, G., Hannah, C. G., Greenberg, D. A., and Smith, P. C. (1997). Hydrography and baroclinic circulation in the Scotian shelf region: winter versus summer. *Can. J. Fish. Aquat. Sci.* 54(Suppl. 1), 40–56. doi: 10.1139/f96-153

Loder, J. W., Petrie, B., and Gawarkiewicz, G. G. (1998). "The coastal ocean off northeastern North America: a large-scale view," in *The Sea, Volume 11: The Global Coastal Ocean - Regional Studies and Syntheses*, eds A. R. Robinson and K. Brink (New York, NY: John Wiley & Sons), 105–133.

Maldonado, M. (2006). The ecology of the sponge larva. *Can. J. Zool.* 84, 175–194. doi: 10.1139/z05-177

Maldonado, M., Aguilar, R., Bannister, R. J., Bell, J. J., Conway, K. W., Dayton, P. K., et al. (2017). "Sponge grounds as key marine habitats: a synthetic review of types, structure, functional roles, and conservation concerns," in *Marine Animal Forests*, eds S. Rossi, L. Bramanti, A. Gori, and C. Orejas (Cham: Springer International Publishing), 1–39. doi: 10.1007/978-3-319-21012-4_24

Maldonado, M., Beazley, L., Lopez-Acosta, M., Kenchington, E., Casault, B., Hanz, U., et al. (2020). Massive silicate utilization facilitated by a benthic-pelagic coupled feedback sustains deep-sea sponge aggregations. *Limnol. Oceanogr.* 66, 366–391. doi: 10.1002/lno.11610

Marinone, S. G., Ullo, M. J., Parés-Sierra, A., Lavín, M. F., and Cudney-Bueno, R. (2008). Connectivity in the northern Gulf of California from particle tracking in a three-dimensional numerical model. *J. Mar. Syst.* 71, 149–158. doi: 10.1016/j.jmarsys.2007.06.005

Marsh, R., Petrie, B., Weidman, C. R., Dickson, R. R., Loder, J. W., Hannah, C. G., et al. (1999). The 1882 tilefish kill – a cold event in shelf waters off the north-eastern United States? *Fish. Oceanog.* 8, 39–49. doi: 10.1046/j.1365-2419.1999.00092.x

McClain, C. R., and Atkinson, L. P. (1985). A note on the Charleston Gyre. *J. Geophys. Res.* 90, 11857–11861. doi: 10.1029/JC090iC06p11857

McGuire, K. J., and McDonnell, J. J. (2006). A review and evaluation of catchment transit time modeling. *J. Hydrol.* 330, 543–563. doi: 10.1016/j.jhydrol.2006.04.020

McVeigh, D. M., Eggleston, D. B., Todd, A. C., Young, C. M., and He, R. (2017). The influence of larval migration and dispersal depth on potential larval trajectories of a deep-sea bivalve. *Deep Sea Res. Part I Oceanogr. Res. Pap.* 127, 57–64. doi: 10.1016/j.dsr.2017.08.002

MERCINA Working Group. (2001). Oceanographic responses to climate in the northwest Atlantic. *Oceanography* 14, 76–82. doi: 10.5670/oceanog.2001.25

Metaxas, A., and Saunders, M. (2009). Quantifying the "bio-" components in biophysical models of larval transport in marine benthic invertebrates: advances and pitfalls. *Biol. Bull.* 216, 257–272. doi: 10.1086/BBLv216n3p257

Montgomery, E. M., Hamel, J. F., and Mercier, A. (2019). Larval nutritional mode and swimming behaviour in ciliated marine larvae. *J. Mar. Biol. Assoc. U.K.* 99, 1027–1032. doi: 10.1017/S0025315418001091

Montgomery, E. M., Hamel, J. F., and Mercier, A. (2020). Larval nutritional mode and swimming behaviour in ciliated marine larvae – CORRIGENDUM. *J. Mar. Biol. Assoc. U.K.* 100, 189–191. doi: 10.1017/S0025315419001176

Morato, T., González-Irusta, J.-M., Dominguez-Carrió, C., Wei, C.-L., Davies, A., Sweetman, A. K., et al. (2020). Climate-induced changes in the suitable habitat of cold-water corals and commercially important deep-sea fishes in the North Atlantic. *Glob. Change Biol.* 26, 2181–2202. doi: 10.1111/gcb.14996

Murillo, F. J., Kenchington, E., Tompkins, G., Beazley, L., Baker, E., Knudby, A., et al. (2018). Sponge assemblages and predicted archetypes in the eastern Canadian Arctic. *Mar. Ecol. Prog. Ser.* 597, 115–135. doi: 10.3354/meps12589

Ospina-Alvarez, A., de Juan Mohan, S., Alós, J., Basterretxea, G., Alonso-Fernández, A., Follana-Berná, G., et al. (2020). MPA network design based on graph theory and emergent properties of larval dispersal. *Mar. Ecol. Prog. Ser.* 650, 309–326. doi: 10.3354/meps13399

Paris, C. B., Helgers, J., van Sebille, E., and Srinivasan, A. (2013). Connectivity modeling system: A probabilistic modeling tool for the multi-scale tracking of biotic and abiotic variability in the ocean. *Environ. Modell. Softw.* 42, 47–54. doi: 10.1016/j.envsoft.2012.12.006

Paul, A., and Schäfer-Neth, C. (2003). Modeling the water masses of the Atlantic Ocean at the last glacial maximum. *Paleoceanogr* 18, 1058–1084. doi: 10.1029/2002PA000783

Petrie, B., and Drinkwater, K. (1993). Temperature and salinity variability on the Scotian Shelf and in the Gulf of Maine 1945–1990. *J. Geophys. Res* 98, 20079–20089. doi: 10.1029/93JC02191

Pielou, E. C. (1991). *After the Ice Age: The Return of Life to Glaciated North America*. Chicago, IL: The University of Chicago Press. doi: 10.7208/chicago/9780226668093.001.0001

Popenoe, P., and Manheim, F. T. (2001). Origin and history of the Charleston Bump – Geological formations, currents, bottom conditions, and their relationship to wreckfish habitats on the Blake Plateau. *Am. Fish. Soc. Symp.* 25, 43–94.

Putman, N. F., and He, R. (2013). Tracking the long-distance dispersal of marine organisms: sensitivity to ocean model resolution. *J. R. Soc. Interface* 10:20120979. doi: 10.1098/rsif.2012.0979

Ramos, J. E., Pecl, G. T., Moltschaniwskyj, N. A., Semmens, J. M., Souza, C. A., and Strugnell, J. M. (2018). Population genetic signatures of a climate change driven marine range extension. *Sci. Rep.* 8:9558. doi: 10.1038/s41598-018-27351-y

Reijnders, B. J. H. R. (2020). *Assessing Ocean Surface Connectivity in the Arctic: Capabilities and Caveats of Community Detection in Lagrangian Flow Networks.* Master thesis. Utrecht: Utrecht University. doi: 10.5194/egusphere-egu21-201

Reiswig, H. M. (1996). Redescription and placement of the rossellid genus *Vazella* Gray (Hexactinellida : Lyssacinosida). *Bull. Instr. Sci. Nat. Belg.* 66, 135–141.

Ross, R. E., Nimmo-Smith, W. A. M., Torres, R., and Howell, K. L. (2020). Comparing deep-sea larval dispersal models: A cautionary tale for ecology and conservation. *Front. Mar. Sci.* 12:2020. doi: 10.3389/fmars.2020.00431

Rossby, T., Bower, A. S., and Shaw, P. T. (1985). Particle pathways in the gulf stream. *Bull. Am. Meteorol. Soc.* 66, 1106–1110. doi: 10.1175/1520-0477(1985)066<1106:PPITGS>2.0.CO;2

Schäfer-Neth, C., and Paul, A. (2003). "The Atlantic ocean at the last glacial maximum: 1. objective mapping of the GLAMAP sea-surface conditions," in *The South Atlantic in the Late Quatenary: Reconstruction of Material Budgets and Current Systems*, eds G. Wefer, S. Mulitza, and V. Ratmeyer (Berlin: Springer-Verlag), 531–548. doi: 10.1007/978-3-642-18917-3_23

Schmidt, O. (1870). *Grundzüge einer Spongien-Fauna des Atlantischen Gebietes*. Leipzig: Wilhelm Engelmann.

Shaw, J., Gareau, P., and Courtney, R. C. (2002). Palaeogeography of Atlantic Canada 13–0 kyr. *Q. Sci. Rev.* 21, 1861–1878. doi: 10.1016/S0277-3791(02)00004-5

Shaw, J., Piper, D. J. W., Fader, G. B. J., King, E. L., Todd, B. J., Bell, T., et al. (2006). A conceptual model ofthe deglaciation of Atlantic Canada. *Q. Sci. Rev.* 25, 2059–2081. doi: 10.1016/j.quascirev.2006.03.002

Simons, R. D., Siegel, D. A., and Brown, K. S. (2013). Model sensitivity and robustness in the estimation of larval transport: a study of particle tracking parameters. *J. Marine Syst.* 119-120, 19–29. doi: 10.1016/j.jmarsys.2013.03.004

Spalding, M. D., Fox, H. E., Allen, G. R., Davidson, N., Ferdaña, Z. A., Finlayson, M., et al. (2007). Marine ecoregions of the world: a bioregionalization of coastal and shelf areas. *BioScience* 57, 573–583. doi: 10.1641/B570707

Swearer, S. E., Caselle, J. E., Lea, D. W., and Warner, R. R. (1999). Larval retention and recruitment in an island population of a coral-reef fish. *Nature* 402, 799–802. doi: 10.1038/45533

Tabachnick, K. (1994). "Distribution of recent hexactinellida," in *Sponges in Time and Space: Biology, Chemistry, Paleontology*, eds R. V. K. Van Soest, T. M. G. van Kempen, and J.-C. Braekamn (Rotterdam: Balkema), 225–232.

Townsend, D. W., Pettigrew, N. R., Thomas, M. A., Neary, M. G., McGillicuddy, D. J. Jr., and O'Connell, J. (2015). Water masses and nutrient sources to the Gulf of Maine. *J. Mar. Res.* 73, 93–122. doi: 10.1357/002224015815848811

Van Soest, R. W. M., Boury-Esnault, N., Vacelet, J., Dohrmann, M., Erpenbeck, D., De Voogd, N. J., et al. (2012). Global diversity of sponges (Porifera). *PLoS One* 7:e35105. doi: 10.1371/journal.pone.0035105

Vaz, A. C., Paris, C. B., Olascoaga, M. J., Kourafalou, V. H., Kang, H., and Reed, J. K. (2016). The perfect storm: match-mismatch of bio-physical events drives larval reef fish connectivity between Pulley Ridge mesophotic reef and the Florida Keys. *Cont. Shelf Res.* 125, 136–146. doi: 10.1016/j.csr.2016.06.012

Wang, S., Kenchington, E. L., Wang, Z., Yashayaev, I., and Davies, A. J. (2020). 3-D Ocean particle tracking modeling reveals extensive vertical movement and downstream interdependence of closed areas in the northwest Atlantic. *Sci. Rep.* 10:21421. doi: 10.1038/s41598-020-76617-x

Wang, Z., Brickman, D., and Greenan, B. J. W. (2019). Characteristic evolution of the Atlantic Meridional Overturning circulation from 1990 to 2015: An eddy-resolving ocean model study. *Deep Sea Res. Part I Oceanogr. Res. Pap.* 149:103056. doi: 10.1016/j.dsr.2019.06.002

Wang, Z., Brickman, D., Greenan, B. J. W., and Yashayaev, I. (2016). An abrupt shift in the Labrador current system in relation to winter NAO events. *J. Geophys. Res. Oceans* 121, 5338–5349. doi: 10.1002/2016JC011721

Wang, Z., Lu, Y., Greenan, B., Brickman, D., and DeTracey, B. (2018). BNAM: an eddy-resolving North Atlantic ocean model to support ocean monitoring. *Can. Tech. Rep. Hydrogr. Ocean. Sci.* 327, vii+18.

Wolanski, E., Doherty, P., and Carleton, J. (1997). Directional swimming of fish larvae determines connectivity of fish populations on the Great Barrier Reef. *Nat. Sci.* 84, 262–268. doi: 10.1007/s001140050394

Yashayaev, I., and Loder, J. W. (2009). Enhanced production of Labrador Sea Water in 2008. *Geophys. Res. Lett.* 36:L01606. doi: 10.1029/2008GL036162

Young, C. M., He, R., Emlet, R. B., Li, Y., Qian, H., Arellano, S. M., et al. (2012). Dispersal of deep-sea larvae from the Intra-American Seas: simulations of trajectories using ocean models. *Integr. Comp. Biol.* 52, 483–496. doi: 10.1093/icb/ics090

Zeng, C., Rowden, A. A., Clark, M. R., and Gardner, P. A. (2020). Species-specific genetic variation in response to deep-sea environmental variation amongst vulnerable marine ecosystem indicator taxa. *Sci. Rep.* 10:2844. doi: 10.1038/s41598-020-59210-0

Conflict of Interest: The authors declare that the research was conducted in the absence of any commercial or financial relationships that could be construed as a potential conflict of interest.

Publisher's Note: All claims expressed in this article are solely those of the authors and do not necessarily represent those of their affiliated organizations, or those of the publisher, the editors and the reviewers. Any product that may be evaluated in this article, or claim that may be made by its manufacturer, is not guaranteed or endorsed by the publisher.

Copyright © 2021 Wang, Kenchington, Wang and Davies. This is an open-access article distributed under the terms of the Creative Commons Attribution License (CC BY). The use, distribution or reproduction in other forums is permitted, provided the original author(s) and the copyright owner(s) are credited and that the original publication in this journal is cited, in accordance with accepted academic practice. No use, distribution or reproduction is permitted which does not comply with these terms.

frontiers in Marine Science

ORIGINAL RESEARCH
published: 28 October 2021
doi: 10.3389/fmars.2021.703297

Can Environmental Conditions at North Atlantic Deep-Sea Habitats Be Predicted Several Years Ahead? ——Taking Sponge Habitats as an Example

Feifei Liu[1], Ute Daewel[1], Annette Samuelsen[2], Sebastian Brune[3], Ulrike Hanz[4,5], Holger Pohlmann[6], Johanna Baehr[3] and Corinna Schrum[1,3]*

[1] Institute of Coastal Systems-Analysis and Modeling, Helmholtz-Zentrum Hereon, Geesthacht, Germany, [2] Nansen Environmental and Remote Sensing Center, and Bjerknes Centre for Climate Research, Bergen, Norway, [3] Institute of Oceanography, Center for Earth System Research and Sustainability (CEN), Universität Hamburg, Hamburg, Germany, [4] Alfred Wegener Institute, Bremerhaven, Germany, [5] Royal Netherlands Institute for Sea Research (NIOZ), Texel, Netherlands, [6] Max Planck Institute for Meteorology, Hamburg, Germany

OPEN ACCESS

Edited by:
Ellen Kenchington, Bedford Institute of Oceanography (BIO), Canada

Reviewed by:
Patricia Puerta, Oceanographic Center of the Balearic Islands, Spanish Institute of Oceanography (IEO), Spain
Furu Mienis, Royal Netherlands Institute for Sea Research (NIOZ), Netherlands

***Correspondence:**
Feifei Liu
feifei.liu@hereon.de

Specialty section:
This article was submitted to Deep-Sea Environments and Ecology, a section of the journal Frontiers in Marine Science

Received: *30 April 2021*
Accepted: *29 September 2021*
Published: *28 October 2021*

Citation:
Liu F, Daewel U, Samuelsen A, Brune S, Hanz U, Pohlmann H, Baehr J and Schrum C (2021) Can Environmental Conditions at North Atlantic Deep-Sea Habitats Be Predicted Several Years Ahead? ——Taking Sponge Habitats as an Example. Front. Mar. Sci. 8:703297. doi: 10.3389/fmars.2021.703297

Predicting the ambient environmental conditions in the coming several years to one decade is of key relevance for elucidating how deep-sea habitats, like for example sponge habitats, in the North Atlantic will evolve under near-future climate change. However, it is still not well known to what extent the deep-sea environmental properties can be predicted in advance. A regional downscaling prediction system is developed to assess the potential predictability of the North Atlantic deep-sea environmental factors. The large-scale climate variability predicted with the coupled Max Planck Institute Earth System Model with low-resolution configuration (MPI-ESM-LR) is dynamically downscaled to the North Atlantic by providing surface and lateral boundary conditions to the regional coupled physical-ecosystem model HYCOM-ECOSMO. Model results of two physical fields (temperature and salinity) and two biogeochemical fields (concentrations of silicate and oxygen) over 21 sponge habitats are taken as an example to assess the ability of the downscaling system to predict the interannual to decadal variations of the environmental properties based on ensembles of retrospective predictions over the period from 1985 to 2014. The ensemble simulations reveal skillful predictions of the environmental conditions several years in advance with distinct regional differences. In areas closely tied to large-scale climate variability and ice dynamics, both the physical and biogeochemical fields can be skillfully predicted more than 4 years ahead, while in areas under strong influence of upper oceans or open boundaries, the predictive skill for both fields is limited to a maximum of 2 years. The simulations suggest higher predictability for the biogeochemical fields than for the physical fields, which can be partly attributed to the longer persistence of the former fields. Predictability is improved by initialization in areas away from the influence of Mediterranean outflow and areas with weak coupling between the upper and deep oceans. Our study highlights the ability of the downscaling regional system to predict

the environmental variations at deep-sea benthic habitats on time scales of management relevance. The downscaling system therefore will be an important part of an integrated approach towards the preservation and sustainable exploitation of the North Atlantic benthic habitats.

Keywords: sponge habitat, deep-sea, predictability, regional downscaling prediction, interannual to decadal variability, environmental conditions

INTRODUCTION

The deep sea, which encompasses depths below around 200 m, was initially considered to be a "marine desert" with low density and biomass of benthic species (Sanders and Hessler, 1969). Today we know that it can host a variety of unique ecosystems like for example cold-water coral (CWC) reefs and sponge grounds (Roberts et al., 2006; Hogg et al., 2010; Cathalot et al., 2015). In the deep North Atlantic Ocean, numerous benthic habitats widely spread across a broad spectrum of geomorphological features such as shelves, slopes, seamounts, mid-ocean ridges, canyons and fjords (Cárdenas and Rapp, 2015; Roberts et al., 2018; Kazanidis et al., 2019a,b,c; Meyer et al., 2020a,b), which are associated with a wide range of depths through the mesopelagic and bathyal zones and even at abyssal and hadal depths (Vacelet and Custódio, 2007; Hestetun et al., 2019). These deep-sea habitats have gained increasing attention in recent years from both ecological and conservation perspectives, as they are found to be vital for the well-being of the entire ocean and biosphere (e.g., Sweetman et al., 2017; Levin et al., 2019). Sponge habitats and CWCs, for example, provide ecosystem goods and services like the provision of habitats and food sources for associated benthic and pelagic species (Bett and Rice, 1992; Maldonado et al., 2017; Hawkes et al., 2019) and thereby sustain hotspots of biodiversity in the deep sea (Klitgaard and Tendal, 2004; Buhl-Mortensen et al., 2010; Beazley et al., 2013, 2015; Maldonado et al., 2017; Meyer et al., 2019). Further they are of fundamental importance for the benthic–pelagic coupling and marine biogeochemical cycling (Pile and Young, 2006; Oevelen et al., 2009; Smith et al., 2009; Maldonado et al., 2019).

The deep-sea environmental conditions, including but not limited to the physical (e.g., temperature, salinity, current velocity, and bottom shear) and biogeochemical properties (e.g., nutrients and oxygen concentrations), are crucial constrains of the biodiversity, distribution, and connectivity patterns of the deep-sea habitats (e.g., Levin, 2003; Woulds et al., 2007; Yasuhara and Danovaro, 2016; Puerta et al., 2020). For instance, temperature influences metabolic rates and enzyme activities in organisms, resulting in different temperature envelopes for their species thriving (Hochachka and Somero, 1968; Yasuhara and Danovaro, 2016). Salinity, together with temperature, defines the water density — a key parameter with which the occurrence of some important habitats, for example CWCs in the northeastern Atlantic, is found to be correlated (Dullo et al., 2008). In addition, temperature and salinity are often used as proxies of water masses that are associated with circulation patterns, which is a key physical process in influencing the distribution and density of the benthic habitats through transporting food or larvae (Puerta et al., 2020; Roberts et al., 2021). Inorganic nutrients are crucial components for the construction of organisms, with silicate as an example being an essential element for building the skeleton of most deep-sea sponges (Howell et al., 2016; Maldonado et al., 2020, 2021). Oxygen is an important electron acceptor for biogeochemical processes and therefore fundamental for aerobic life. If oxygen decreases below a certain threshold, organisms experience a variety of stressors, limiting their distributions like for example in oxygen minimum zones (Vaquer-Sunyer and Duarte, 2008; Keeling et al., 2010). Those environmental conditions vary among different benthic habitats. As a result, the deep-sea species have their own preferred ranges of environmental properties, connected to their optimal growth and feeding conditions and the spreading or retention of larvae (e.g., Klitgaard and Tendal, 2004; Roberts et al., 2021). For instance, the reef-forming CWCs *Lophelia pertusa* (as well as the non-reef-forming CWC species *Desmophyllum dianthus* which is significantly similar to *Lophelia* molecularly and morphologically, Addamo et al., 2016) and *Madrepora oculata* are mainly found at a temperature range of 4–12°C (Naumann et al., 2014), while octocorals survive at a narrower and lower temperature range of 1.6–6.1°C (Buhl-Mortensen et al., 2015). The boreal sponge grounds with *Geodia barretti*, *Stryphnus ponderosus*, and *Stelletta normani* are only rarely occurring at temperatures lower than 3°C, whereas cold-water sponge grounds with *Geodia parva*, *Geodia hentscheli*, *Geodia phlegraei*, *Stelletta rhaphidiophora*, and *Schaudinnia rosea* can live in waters below zero degrees (Hogg et al., 2010; Roberts et al., 2021).

Emerging evidences show that changes in environmental conditions will affect habitat integrity and representativeness, and thus will alter species distributions and interactions (Meyer et al., 2015; Pecl et al., 2017; Puerta et al., 2020). For instance, Blacker (1957, 1965) mapped changes in the distribution of sponges off West Spitzbergen and he ascribed the changes to a stronger inflow of Atlantic water, which was reflected in a change of water mass properties. Erekovsky (1995) found a nearly seven-fold decrease of sponges in the Barents Sea between 1920–1950 and 1960–1980 which was presumed to be related to a shift in the polar front (Klitgaard and Tendal, 2004). Even though the response of deep-sea habitats to environmental changes varies among species and locations (e.g., Buhl-Mortensen et al., 2015; Hanz et al., 2020, 2021; Puerta et al., 2020), it is suggested that many of the habitats are often living in a fragile equilibrium. They are likely not able to adapt to abrupt changes in the environment because of their slow growth rates and long life spans (Yasuhara et al., 2008, 2014; Roark et al., 2009; Morrison et al., 2020).

Climate change and anthropogenic activities are bringing significant changes in the environmental properties of the deep ocean, which are likely to move beyond the limits of past natural variability by the end of 21st century (Purkey and Johnson, 2010; Levin and Le Bris, 2015; Sweetman et al., 2017; Perez et al., 2018). Such unprecedented environmental changes could further provoke a cascade of deleterious ecological consequences like sponge demise (Sweetman et al., 2017). In fact, footprints of climate change on deep-sea environmental conditions have already been reported in recent decades (Purkey and Johnson, 2010; Stramma et al., 2010; Morato et al., 2020), which in turn have raised substantial pressures on the deep-sea habitats (e.g., Yasuhara et al., 2016; Strand et al., 2017). In 2006 and 2008, mass mortalities events of the deep-water sponge *Geodia barretti* at the Tisler Reef on the sill of the Kosterfjord along the Norwegian shelf were observed to coincide with a series of uncharacteristically large and rapid increases in bottom water temperature, which exceeded the typical short-term physiological limits of the host reef, principally *Lophelia pertusa* (Guihen et al., 2012). It was inferred that the unexpected temperature increase was associated with climate change and that future temperature shock events at this site might have a swift and negative impact on the local CWC reef ecosystems. Johnson et al. (2018) predicted that in a 20–50 year timeframe most of the deep-sea Area-Based Management Tools (ABMTs) in the North Atlantic would be affected by climate change, implying that significant changes of the deep-sea ecosystem might take place in the near future. Because of the high vulnerability of these deep-sea habitats to the effects of anthropogenic disturbance and climate change, the benthic invertebrates, e.g., CWC reefs and sponge habitats, are classified as 'vulnerable marine ecosystems (VMEs)' by the Food and Agriculture Organization of the United Nations (FAO, 2009), which are in need of enhanced conservation and protection on account of their longevity and expected long recovery times after disturbance (Levin et al., 2019).

In face of ongoing environmental changes, addressing the increasing pressures placed on the deep-sea habitats is an urgent task requiring thorough evaluation of cumulative impacts (Johnson et al., 2018). To date, numbers of studies, including modeling prediction endeavors, have been conducted to investigate the possible impacts of future climate change on deep-sea benthic ecosystems (Knudby et al., 2013; Sweetman et al., 2017; Beazley et al., 2018, 2021; Bell et al., 2018; Johnson et al., 2018; Morato et al., 2020; Pearman et al., 2020; Puerta et al., 2020). However, most of the studies were based on environmental conditions that were projected into the end of the 21st century with a broad range of assumptions on future greenhouse gas emissions, world population growth and technology development (Riahi et al., 2011; Van Vuuren et al., 2011). Those climate projections explain well the long-term trends while there is low confidence in the interannual to decadal variability at a given point in time (Befort et al., 2020; Lee et al., 2021). Therefore, the estimated deep-sea ecosystem status is scenario dependent and potentially presents a high degree of uncertainty at short timescales (Payne et al., 2016; Beazley et al., 2021). By far, few studies regarding the impacts of near-term environmental changes (i.e., over the next years to one decade in the future) on the benthic habitats have been reported, mostly because that reliable predictions of the environment variations in the near-term future are lacking (Johnson et al., 2017). One exception is Johnson et al. (2018), who drew the information of environmental changes over the next 30 years from a compilation of climate projection (IPCC 5th Assessment Report) covering the North Atlantic and other published works with varying sub-regional focuses (Johnson et al., 2017). In spite of the compilation work, they pointed out that more precise and detailed oceanographic data are needed.

In view of a practical protection and sustainable management of the deep-sea habitats, effective and reliable predictions of the natural and anthropogenic-derived variations of the deep-sea environmental factors in the coming years to one decade is required to inform management decisions (Tommasi et al., 2017). Decadal oceanic predictions, encompassing predictions on annual, multi-annual to decadal timescales, are proven to be a suitable approach for this goal (Borchert et al., 2019). A major advantage of decadal predictions compared to centennial climate projections is that the former can integrate the known knowledge from the past into the future—the predictability can be assessed by performing retrospective forecasts of the historical period and comparing them against subsequent observations (Smith et al., 2019). The system is credible for forecasting the future once it shows skillful predictions in the past (Brune et al., 2018; Borchert et al., 2019; Smith et al., 2019). However, to our knowledge, it is still poorly known how many years in advance the environmental conditions at the North Atlantic deep-sea habitats can be predicted, owing to the fact that there is no operational decadal predictions dedicated to the deep sea. To close this knowledge gap, we make a first trial to assess the predictability of the deep-sea environmental factors with a novel downscaling regional decadal prediction system with the main focus on the deep North Atlantic Ocean.

We choose the coupled regional physical-ecosystem model (HYCOM-ECOSMO) for the regional downscaling, with particular considerations of the deep-sea dynamics. For instance, in the physical model, HYCOM (Bleck, 2002), isopycnal levels facilitate good conservation of water-mass and tracer properties in the deep ocean, representing an advantage for simulations focusing on deep-sea habitats at depth (Winther and Evensen, 2006). The ecosystem model, ECOSMO (Daewel and Schrum, 2013), includes a single layer of sediments with parameterizations for processes of settling, resuspension and burial (when sediment can no longer be resuspended) happening at the bottom ocean (Samuelsen et al. submitted to this issue, under review). The model has been shown the capability of reproducing the observed states of the environmental properties at the deep North Atlantic Ocean over the historical period of 1948–2014 (Samuelsen et al., 2019; Samuelsen et al. submitted to this issue, under review). We therefore use the same model configuration with Samuelsen et al. (2019) in our study to perform the decadal predictions.

Specifically, in this study we aim at (1) setting up a downscaling prediction system with retrospective predictions of the marine environmental factors over the period of 1985–2014; (2) assessing the predictability of selected environmental factors at the deep-sea habitats. For assessing the predictability, we

choose sponge habitats as examples, which are key components of benthic marine ecosystems in the deep North Atlantic from intertidal to abyssal depths (e.g., Rice et al., 1990; Klitgaard and Tendal, 2004; Beazley et al., 2013). In this study, 21 sponge habitats are selected, covering almost all of the biggest known sponge habitats through the North Atlantic (**Figure 1** and **Tables 1, 2**). In addition, we choose four parameters (temperature, salinity, concentrations of silicate and oxygen) for detailed analysis since they are the most important predictor variables in species distribution models (e.g., Knudby et al., 2013; Beazley et al., 2018; Morato et al., 2020; Rodríguez-Basalo et al., 2021) and have shown to influence the benthic habitats at present as mentioned earlier in this section. Therefore, they are used to represent the physical and biogeochemical fields.

This paper is organized as follows. First, we introduce the downscaling strategy and the methods used to assess the predictability. Subsequently, the potential predictability of the four environmental factors is evaluated over the 21 sponge habitats. Then the possible factors influencing the predictability, the limitations and potentials of the prediction, as well as the applicability of the prediction in the deep-sea habitat management are discussed, which are followed by a final conclusion.

MODEL AND METHODS

Model Description

The downscaling prediction is performed based on a regional coupled physical-ecosystem model, covering part of the southern Atlantic and the whole domain of the North Atlantic and the Arctic Ocean (**Figure 2**). The regional model is forced at the ocean surface and lateral boundaries by output from decadal climate predictions, which are based on fully coupled global earth system models (ESMs), so that large-scale variability of the climate is dynamically downscaled to the regional model domain.

The regional model, HYCOM-ECOSMO, consists of the physical ocean model Hybrid Coordinate Ocean Model (HYCOM; Bleck, 2002), including a sea ice component, and the ECOSystem Model (ECOSMO) which is a medium-complexity biogeochemical model (Daewel and Schrum, 2013). HYCOM uses a curvilinear grid with a horizontal resolution of approximately 20–70 km. Similar with Sakov et al. (2012) and Samuelsen et al. (2015), the model uses hybrid coordinates in vertical, with z-levels in the upper ocean and mixed layer and isopycnal levels in the deep ocean. Consequently, the vertical layers will be re-distributed along with changes in the deep ocean density fields. The upper five layers are fixed as z-coordinates, ensuring that the vertical resolution of the upper ocean is maintained, which is particularly important for resolving the gradient of light in the upper ocean when computing primary production. At the open boundaries, which are placed between the equator and 30°S in the south, at the Strait of Gibraltar in the east and at the Bering Strait in the north, we mimic the treatments used in Hansen and Samuelsen (2009) and Samuelsen et al. (2015) to set a relaxation zone of 20 model grids, over which the modeled physical fields (temperature, salinity and density) and biogeochemical fields (alkalinity, DIC, nitrate, phosphate, silicate and oxygen) are relaxed toward prescribed fields. The relaxation is strongest at the outer grid cell and is linearly decreased toward the interior of the model, with a relaxation time-scale on the outer grid cell of 20 days.

ECOSMO resolves four nutrients (nitrate, phosphate, silicate, and ammonium), two types of phytoplankton functional groups (diatoms and flagellates) as well as two classes of zooplankton functional groups (herbi- and omnivorous). In addition, particulate and dissolved organic material, and oxygen are included. In the model, constant element ratios consistent with the classical Redfield stoichiometry is applied (Tett et al., 1985). The three nutrients (nitrate, phosphate, and silicate) are tracked in the bottom sediments using simplified 0d bulk parametrizations for sedimentation, resuspension, and remineralization in the sediment layer. ECOSMO is online coupled with HYCOM, sharing the same model grids. A detailed description of the model can be found in Samuelsen et al. (submitted to this issue, under review).

The global decadal climate prediction used in this study is based on the coupled Max Planck Institute Earth System Model with low-resolution configuration (MPI-ESM-LR baseline-1, Pohlmann et al., 2013). The ocean component of MPI-ESM-LR uses bipolar configuration, with one pole over Greenland and another over Antarctica, leading to the spatial resolution ranging from 15 km around Greenland to 185 km in the tropical area (Jungclaus et al., 2013). The capability of this ESM to predict the variability in the upper ocean of the North Atlantic several years in advance has been identified both for the physical states (e.g., Müller et al., 2014; Polkova et al., 2019) and for the biogeochemistry (e.g., Li et al., 2016).

Simulations

Three sets of simulations are involved in the downscaling prediction system: the reconstruction simulation, the ensemble of initialized simulations and the ensemble of uninitialized simulations. A schematic diagram showing the regional simulations as well as the relevant global simulations are illustrated in **Figure 3**.

Based on the availability of the forcing data, the simulation period differs among the three sets of regional simulations. Results over a common period of 1985–2014 are used for analysis of the predictability. The three sets of simulations are described as follows:

(i) A 67-year (1948–2014) simulation (referred to "reconstruction simulation" hereafter) is used to provide a long, consistent time series of the environmental conditions at deep-sea sponge habitats in the North Atlantic. In this simulation, a global high-resolution atmospheric reanalysis product based on the atmospheric model ECHAM6 (Schubert-Frisius and Feser, 2015) is used to provide forcing to the regional model at the ocean surface. The modeled temperature, salinity and density at the open boundaries are relaxed toward climatological monthly fields from the Generalized Digital Environment Model (GDEM; Carnes, 2009), while the modeled nutrients (nitrate, phosphate, and silicate) and oxygen are relaxed toward World Ocean Atlas (WOA2013) monthly climatology

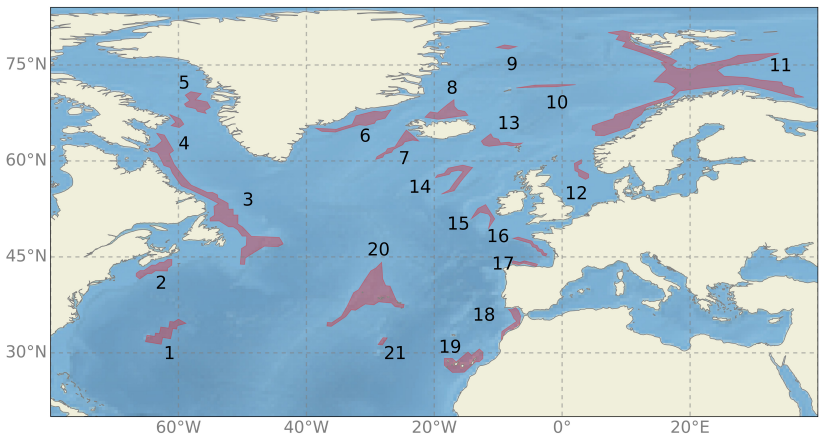

FIGURE 1 | Map of the North Atlantic Ocean including part of the Arctic Ocean showing the locations of the 21 sponge habitats studied in this paper. The habitats are ordered from 1 to 21, with the corresponding number marked on the map.

(Garcia et al., 2013a,b). The simulation has been well validated by being compared with observations at the same location and on the same date (Samuelsen et al., 2019), providing us confidence that this simulation is able to reproduce the interannual to decadal variations of the environmental properties in the simulation period.

(ii) An ensemble of five initialized prediction simulations (referred to "initialized simulations" hereafter), is started from the reconstruction simulation on 1 January in each year over the period 1978–2014. Each simulation has a length of 8 years. Six-hourly atmospheric forcing is obtained from five out of ten randomly selected members of the initialized simulations of MPI-ESM-LR. In this implementation, the five regional simulations have identical initial conditions. Perturbations, represented by the differences of the atmospheric forcing among the five global members, quickly transfer to the regional ocean through the air-sea interactions. In order to include the effect of large-scale variability, which may propagate through the open boundaries into the regional model domain, the modeled temperature, salinity and density at the relaxation zones are relaxed toward the corresponding MPI-ESM-LR monthly fields of the initialized simulations. To avoid possible climatic shock between the reconstruction and the initialized simulations, we apply a bias-correction method to include both the observed climatology and the variability from the global prediction system mimicking the methods described in Pozo Buil et al. (2021) as follows:

$$OBC^{i,t} = OBC^{t}_{clim} + OBC^{i,t}_{anom.},$$

where OBC stands for the open boundary conditions toward which the modeled fields are relaxed, OBC_{clim} stands for the GDEM climatologically monthly fields, $OBC_{anom.}$ is the monthly anomaly of the MPI-ESM-LR initialized simulations, which is obtained by subtracting the climatologically monthly mean of the MPI-ESM-LR assimilation (**Figure 3**), i is the ensemble member from 1 to 5 and t is the month from 1 to 12. Boundaries of biogeochemical variables are relaxed toward the WOA2013 monthly climatology.

(iii) An ensemble of five uninitialized prediction simulations (referred to "uninitialized simulations" hereafter) is performed for the period 1952–2014, which is started from the reconstruction simulation on 1 January 1952 and forced with 6-hourly atmospheric data from five out of ten randomly selected members of the uninitialized simulations of MPI-ESM-LR. As our analysis focuses on the period of 1985–2014, we assume that the model has lost the memory of the initial conditions after more than 30 years of integration. The treatment of the open boundaries is the same as in the initialized simulations but with the calculation of the monthly anomalies based on the climatology of the MPI-ESM-LR uninitialized simulations.

The above three sets of regional simulations are used to assess the skill of retrospective predictions of the four variables. The results will provide confidence for a further attempt to forecast the future evolution of environmental conditions in the forthcoming years to one decade.

Study Sites

In this work, we focus on 21 sponge habitats in the North Atlantic (**Figure 1**). Those habitats represent good geographical coverage of the North Atlantic and a diversity of species (**Table 1**). The locations of those habitats are obtained from the EU Project "SponGES[1]". They are first digitalized and then mapped on our model grids. Detailed information about the individual habitat, including the name, the dominant sponge species, the depth ranges, the sponge density, the topographical feature and the corresponding references is listed in **Table 1**. The main water masses that each sponge habitat is associated with are listed in **Table 2**.

Despite the fact that some areas are shallower than 200 m and may not represent the deep sea, they are still considered in the analysis because of their importance in hosting sponge habitats that are of great interest to the sponge communities. For instance, the Scotian Shelf off Nova Scotia (Habitat 2), with

[1]http://www.deepseasponges.org/?page_id=45

TABLE 1 | The habitat number given in our study and the corresponding name, sponge grounds/main sponge species, depths of highest sponge occurrence, sponge density, topographical feature, and related references.

Habitat no.	Region name	Sponge grounds/main sponge species	Depth of highest sponge occurrence (*range of depth in model*) (m)	Sponge density	Topographical feature	References
1	New England Seamounts and Corner Rise Seamounts	*Rossellidae sponges Euplectella* sp.	1000–2500 *(855–4853)*	No data	Seamount	Lapointe et al., 2020
2	Vazella Ground/Scotian Shelf	*Vazella pourtalesi*	∼75–935 *(26.3–1613)*	Up to 16 ind/m^2	Continental shelf	Beazley et al., 2013, Hawkes et al., 2019
3	Flemish Cap and Great Banks	Astrophorid grounds *Geodia* spp. *Asconema* sp.	128–1700 *(44–1400)*	0.0017 kg/m^2	Continental margin	Murillo et al., 2012, Knudby et al., 2013, Pham et al., 2019
4	Labrador and Newfoundland shelves	Boreal grounds	500–2000 *(278–754)*	Up to 500 kg "sponge catch"	Continental shelf	Knudby et al., 2013, Guijarro et al., 2016, Culwick et al., 2020
5	Davis Strait Toqqusaq Bank	Boreal grounds and cold-water grounds	200–900 *(99–467)*	Up to 6 ind/m^2	Strait	Buhl-Mortensen et al., 2019, Roberts et al., 2021
6	Denmark Strait	Boreal grounds and cold-water grounds *Geodia* spp.	200–1000 *(186–1079)*	<2000 kg in a trawl	Continental margin/fjords/upper slope/slope of the banks	Klitgaard and Tendal, 2004, Roberts et al., 2021
7	South of Iceland Reykjanes Ridge	Boreal grounds *Geodia* spp. *Pheronema* sp.	<1400 *(143–1529)*	>20.000 kg in a trawl	Ridge	Copley et al., 1996, Klitgaard and Tendal, 2004
8	Northern Iceland Kolbeinsey Ridge/North of Iceland	cold-water grounds *Geodia* spp. *Chondrocladia gigantea, Cladorhiza* sp. *Tetilla cranium Schaudinnia* sp.	<840 *(106–1332)*	20–24 ind/m^2	Continental margin	Witte and Graf, 1996, Klitgaard and Tendal, 2004, Cárdenas et al., 2013
9	East Greenland Shelf	Arctic, cold-water grounds *tetractinellids G. hentscheli, G. parva, S. rhaphidiophora* and *Thenea valdiviae*	<800 *(180–254)*	Up to 200 ind/m^2	Shelf	Klitgaard and Tendal, 2004
10	Schulz Bank	*Schaudinnia* sp. *Stelleta* sp. *Geodia* spp.	500–800 *(1017–2570)*	>10 ind/m^2	Seamount (Mid-Atlantic Ridge)	Meyer et al., 2019
11	Northern Norway to Spitzbergen/Western Barents Sea	Astrophorid grounds *Geodia* sp.	150–350 *(34–1022)*	5–6 kg/m^2	Continental shelf sea	Klitgaard and Tendal, 2004
12	Norway Shelf	Boreal grounds Geodia spp. *Caulophacus arcticus, Stryphnus* sp., *Aplysilla* sp.	100–400 *(61–136)*	Up to 6 ind/m^2 1.8–45 kg/m^2	Continental margin/fjords	Klitgaard and Tendal, 2004, Kutti et al., 2013, Maldonado et al., 2017, Buhl-Mortensen et al., 2019
13	Northeast Iceland Shelf	Boreal grounds *Geodia* spp.	200–500 *(66–968)*	No data	Shelf plateau close to the shelf break	Roberts et al., 2021
14	Rockall Bank and Hatton Bank	*Nodastrella asconemaoida*	524–857 *(430–1262)*	0.7–7 ind/m^2	Plateau	van Soest et al., 2007
15	Porcupine Seabight Goban Spur Malin Slope	*"Holtenia ground" Pheronema carpenteri, Rosella nodastrella*	650–3000 *(143–952)*	1.5–5 ind/m^2	Continental slope/canyon	Rice et al., 1990, Hughes and Gage, 2004
16	La Danois Bank	*Asconema setubalense Pheronema carpenter Neoschrammeniella sp.*	400–1200 *(105–545)*	0.2 ind/m^2	Elongated shelf-adjacent seamount	Tabachnick and Menshenina, 2007, Ríos et al., 2020
17	Bay of Biscay Aviles canyon	Lithistid grounds (multispecific) *Asconema* sp. Pheronema sp.	140–2000 *(10–4864)*	0.09–0.27 ind/m^2	Continental margin/canyon	Xavier and van Soest, 2007, Rodríguez-Basalo et al., 2021
18	African continental margin off Morocco Gorringe Bank Gulf of Cadiz	*Pheronema* sp.	740–1350 *(20–2090)*	Up to 6 ind/m^2 Up to 1.1 kg/m^2	Continental slope	Rice et al., 1990, Barthel et al., 1996, Xavier and van Soest, 2007, Maldonado et al., 2017

(Continued)

TABLE 1 | (Continued)

Habitat no.	Region name	Sponge grounds/main sponge species	Depth of highest sponge occurrence (*range of depth in model*) (m)	Sponge density	Topographical feature	References
19	Canary Islands Tropic Seamount	*Asconema setubalense*	800–3000 *(48–4165)*	Up to 5 ind/m^2	Seamount	Ramiro-Sánchez et al., 2019
20	Azores Condor Seamount Saldanha Mound Chaucer Seamount	*Pheronema* sp. *Poliopogon amadou*	400–4022 *(68–3163)*	No data	Seamount	Rice et al., 1990, Tempera et al., 2012
21	Great Meteor Seamount	*Poliopogon amadou*	2600–2700 *(1002–2483)*	Up to 5 ind/m^2	Seamount	Xavier et al., 2015

In the fourth column, the values in brackets show the range of depth in the regional model HYCOM-ECOSMO.

a range of depth from 75 m to 935 m (**Table 1**), is home to a globally unique arrogation of the glass sponge *Vazella pourtalesii*. Management measures to protect sponge habitats (and CWCs as well) have been implemented in this area such as bottom-fishery closures implemented by Fisheries and Oceans Canada (Breeze and Fenton, 2007; Beazley et al., 2021). Thus, assessments of the predictability of the environmental variables are meaningful. Sponge habitats in part of the Arctic Ocean are also considered. Note that the model depths at each habitat are not always in the same range with the observations (**Table 1**) because of the inconsistent locations between observations and the model, as well as that the model resolution is not sufficient to resolve the fine structures of the topography.

Analysis Methods

Our analysis is based on the annual mean values at the bottom layer of the water column over the sponge habitats. The bottom layer is represented by the last isopycnal layer of the model.

For the initialized simulations, we first construct time series from the 8-year long individual simulation as a function of lead time. For instance, the time series of lead year 1 is obtained by concatenating the first lead year of every 8-year long initialized simulation and thus covers a period of 1978–2014. This method applies to lead year 1 to 8, resulting in eight time series over 1978–2014, 1979–2015, …, 1985–2021, respectively. The time series of the anomalies in the common period 1985–2014 are used for the following statistical analysis. Anomalies of the three types of simulations are calculated by subtracting their respective climatological means. For the uninitialized simulations, the climatology is calculated from their ensemble mean, while for the initialized simulations with additionally respect to the lead time. The time series are all linearly detrended with the long-term trend being removed to emphasize the predictability in interannual to decadal variability.

Owing to the lack of adequate observational data to represent the interannual to decadal variability, the predictions are verified against the reconstruction simulation to quantify the potential predictive skills. In this way, we assume the modeled fields in the reconstruction simulation are proxies of the historical variability. Therefore, we present in this paper the potential predictability, an upper limit of the predictability, which is obtained by considering a perfect reconstruction of the reality (Boer et al., 2013). The comparison between the initialized and uninitialized simulations is used to assess the improvement of the prediction due to initialization.

We quantify the predictive skill with the anomaly correlation coefficient (ACC) and the normalized mean absolute error (NMAE). The ACC has an emphasis on evaluating the phasing of the predictions against the reconstruction and is calculated between the ensemble means of the prediction simulations (both for uninitialized and initialized simulations) and the reconstruction (Brady et al., 2020):

$$ACC\left(x,y\right) = \frac{\sum_{i=1}^{N} x_i^{'} \cdot y_i^{'}}{\sqrt{\sum_{i=1}^{N} \left(x_i^{'}\right)^2} \cdot \sqrt{\sum_{i=1}^{N} \left(y_i^{'}\right)^2}},$$

where $x^{'}$ is the anomaly of the prediction ensemble mean, $y^{'}$ is the anomaly of the reconstruction, and N is the number of years (30 years from 1985 to 2014). The ACC is a function of lead time in the initialized simulations. A nonparametric bootstrapping approach with 500 bootstrap samples following Goddard et al. (2013) is used to quantify the significance of the correlation skill with the null hypothesis that the two time series are uncorrelated.

The NMAE is used to assess the divergence between mean trajectories of the prediction simulations and reconstruction and is a measure of the accuracy in predicting anomaly magnitudes (Brady et al., 2020). It is the mean absolute error (MAE) of the ensemble mean relative to the reconstruction, then normalized by the interannual standard deviation of the reconstruction. MAE is used here instead of bias metrics such as the root mean square error (RMSE), as it is more accurate in assessing average model bias (Willmott and Matsuura, 2005).

$$NMAE(x,y) = \frac{\frac{1}{N}\sum_{i=1}^{N} |x_i^{'} - y_i^{'}|}{\sigma_{y^{'}}},$$

where $\sigma^{'}y$ is the standard deviation of the reconstruction over the assessing period. NMAE increases as the prediction error grows. When NMAE < 1, the prediction error falls within the variability of the reconstruction and we determine that the prediction is accurate.

Based on the ACC and NMAE, we further define potential predictability horizon (referred to 'predictability horizon' hereafter) as the time at which skillful prediction is lost (Séférian et al., 2014). In this study, it is identified as the maximum lead year of the initialized simulations for which the ACC is significantly positive at 95% and the NMAE is

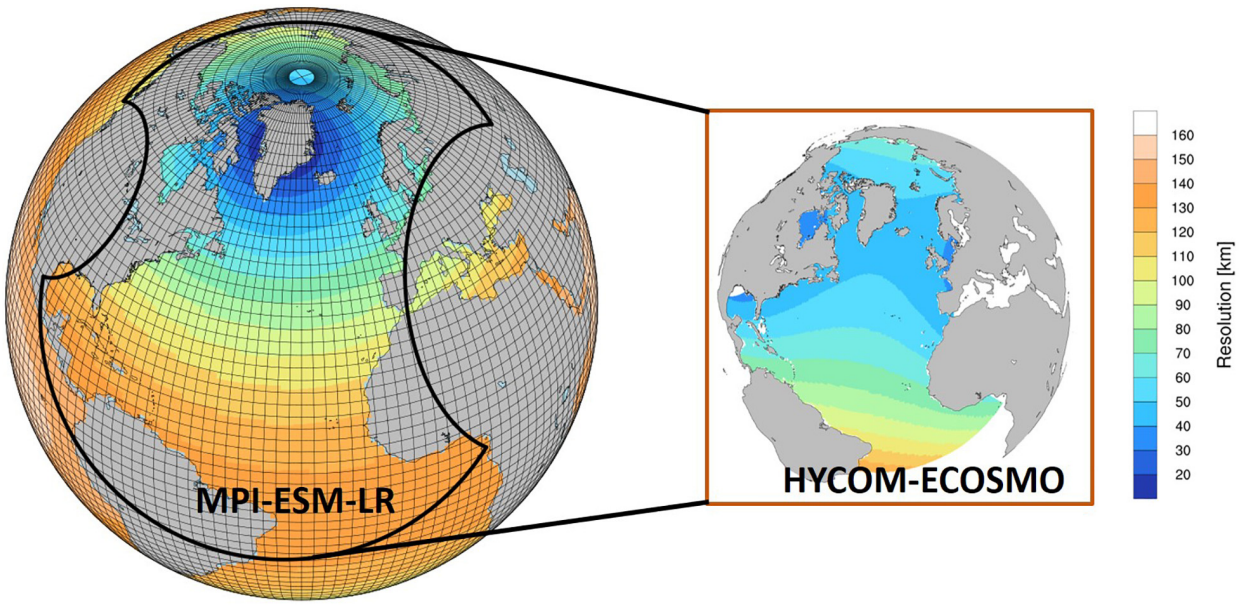

FIGURE 2 | Sketch of the downscaling prediction system. Decadal predictions with the coupled Max Planck Institute Earth System Model with low-resolution configuration (MPI-ESM-LR) provide surface and lateral boundary conditions to the regional coupled physical-ecosystem model HYCOM-ECOSMO. Colors illustrate the horizontal resolution of the ocean models. Grid lines over the global model show the grid of the atmospheric model. Note not all grid-lines are shown.

significantly smaller than 1. Note that when determining the predictability horizon, we don't stick to the comparison between the initialized and uninitialized simulations. The comparison of the two prediction simulations is used to assess the benefit of initialization.

Finally, we classify the sponge habitats into five categories based on the predictability horizon in the physical fields (temperature and salinity) and biogeochemical fields (concentrations silicate and oxygen). The five categories are:

1) High predictability in both physical (Phy.) and biogeochemical (BGC) fields (referred to "High Phy.&BGC") – the predictability horizon is longer than (including) 4 years for at least one variable in each of the two fields (physical and biogeochemical);
2) High predictability only in biogeochemical fields (referred to "High BGC") – the predictability horizon is longer than (including) 4 years for at least one variable in the biogeochemical fields but no such long predictability in the physical fields;
3) High predictability only in physical fields (referred to "High Phy.") – the predictability horizon is longer than (including) 4 years for at least one variable in the physical fields but no such long predictability in the biogeochemical fields;
4) Moderate predictability in physical and biogeochemical fields (referred to "Moderate Phy.&BGC") – predictability horizon in both two fields is less than 4 years, there are at least one variable in the two fields having predictability of longer than 2 years.
5) Low predictability in both physical and biogeochemical fields (referred to "Low Phy.&BGC") – no variable has predictability of longer than 2 years.

RESULTS

Potential Predictive Skill at the Lead Time of 2 Years

The potential predictability (referred to 'predictability' hereafter for simplicity) is first assessed with the predictive skill at a lead time of 2 years (**Figures 4–6**). The initialized simulations produce skillful predictions of bottom temperature, salinity, concentrations of silicate and oxygen at a large portion of sponge habitats, as illustrated by the maps of the ACCs (**Figures 4A–D**). The ACCs of the four variables share similar spatial patterns, with high (>0.8) ACCs in the subtropical area (Habitats 1, 19–21), the subpolar gyre (SPG, 60°W–10°W, 50°N–65°N) area (Habitats 6–8, 13–14) and along the North American and Greenland margin (Habitats 2–5). In those areas, the correlations with the initialized simulations are significantly higher than those with the uninitialized simulations, implying improved predictability due to initialization (**Figure 4** and **Supplementary Figure S1**). In contrast, there are no significant correlation skills at sponge habitats along the European margin (Habitats 12, 15–18), as well as the Habitat 10 in the Nordic Sea in the initialized simulations, indicating no predictability at those areas. In the uninitialized simulations, the correlations over most of the sponge habitats are low and seldom significantly different from zero (**Figures 4E–H**). Exceptions are found in the SPG

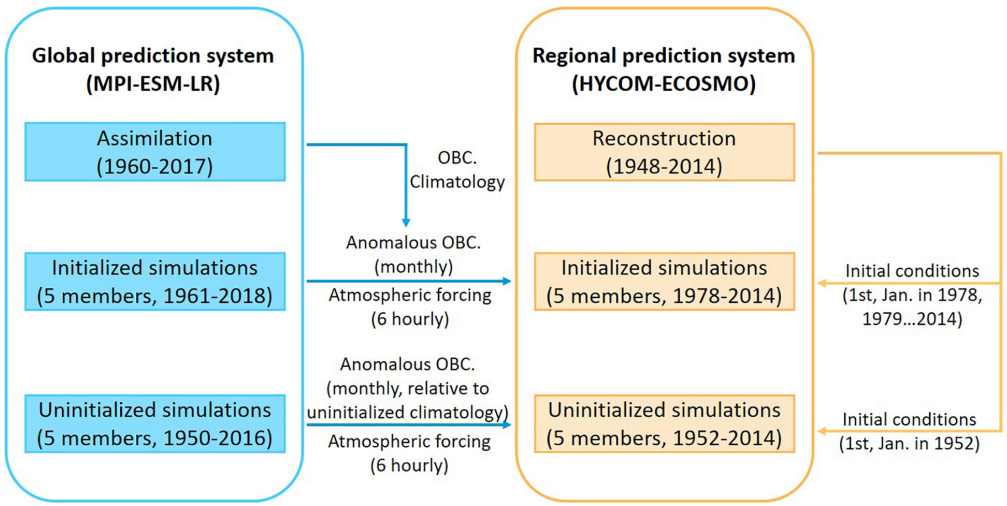

FIGURE 3 | Schematic diagram describing how the three sets of simulations with the regional prediction system are built. Blue box: Ensembles of initialized and uninitialized simulations from the global prediction system (MPI-ESM-LR) provide 6-hourly atmospheric forcing and monthly anomalous open boundary conditions (OBC) to the corresponding ensembles of initialized and uninitialized simulations with the regional prediction system (HYCOM-ECOSMO). The anomaly fields of the initialized simulations from MPI-ESM-LR are based on the assimilation run, while the anomaly fields of the uninitialized simulations from MPI-ESM-LR are based on their own climatology. Orange box: Reconstruction with HYCOM-ECOSMO provides initial conditions for the initialized and uninitialized simulations within the same regional prediction system.

area and the Newfoundland and Labrador margin (Habitats 3–7, 14) for silicate and oxygen, as relatively high correlations emerge even without initializations (**Figures 4G,H**). The high correlations in the uninitialized simulations indicate that certain predictability in those two variables rises from external forcing or internal variations, and imply that the predictability in those two variables will be maintained to longer periods than temperature and salinity, which is corroborated later by the potential predictability horizon.

The spatial distribution of the MAEs of the predictions against the reconstruction indicated by the NMAEs coincides with the ACCs, as high NMAEs are corresponding with low ACCs (**Figures 4**, **5**). At sponge habitats along the North American margin and open waters of the Atlantic as well as along the African margin (Habitats 1–10, 13–14, 19–21) in the initialized simulations, the NMAEs are significantly smaller than 1 (**Figures 5A–D**), indicating that the mean error of the prediction primarily falls within the magnitude of the interannual variability. At those habitats, the prediction errors are smaller in the initialized simulations than in the uninitialized simulations, providing additional evidence for the improved predictive skill due to initialization (**Figure 5** and **Supplementary Figure S1**). In contrast, the NMAEs at the sponge habitats along the European margin (Habitats 11–12, 15–18) are close to or even higher than 1 in both the initialized and uninitialized simulations, showing no significant benefit from initialization.

The improved predictive skills of the interannual to decadal variations due to initialization is directly reflected by the detrended time series of the four variables (**Figure 6**). Here we show the time series at Habitat 11 and 14 (see **Figure 1**), dominated by interannual and decadal variability, respectively. We use the time series with a lead time of 2 years with the initialized simulations to analyze the source of the improved predictive skill. At Habitat 11, the temperature and oxygen are dominated by interannual variations (**Figures 6A,D**) as illustrated by the reconstruction. Such variations are well captured by the initialized simulations in terms of both the phasing and amplitude. In contrast, the uninitialized simulations fail to predict such variations but only show a smoother temporal evolution. For silicate, the simulated increase in the uninitialized simulations is delayed by about 10 years as compared with the reconstruction (**Figure 6C**). The weak or even absence of predictive skill in the uninitialized simulations indicates that the uninitialized simulations mostly capture only the long-term trend in response to the external forcing such as climate evolution caused by rising carbon emissions, and that the initialized simulations, in addition to tracking the long-term trend, are capable of maintaining the interannual to decadal variations for some years. The reconstructed variability of salinity is rather weak, varying within a limited range of ∼0.03. Neither the initialized nor the uninitialized simulations capture the variability well (**Figure 6B**). At Habitat 14, the time series of the variables demonstrate significant decadal variability (**Figures 6E–H**). Predictions with the initialized simulations agree well with those reconstructed decadal variations. The uninitialized simulations show chronological increasing/decreasing trends with maxima/minima at around the year 2000, leading to a biased phasing of the variations in particular before 2000.

Potential Predictability Horizon

The predictability of the four variables degrades along with lead times, as is evidenced by the comparison of time series at lead times of 2 years (**Figure 6**) and of 4 years (**Figure 7**). After 2 years, the initialized simulations, on the

TABLE 2 | The habitat number given in our study, the corresponding name, the associated water masses and related references.

Habitat no.	Region name	Water masses	References
1	New England Seamounts and Corner Rise Seamounts	North Atlantic deep western boundary current water	Pickart, 1992
2	Vazella Ground/Scotian Shelf	Warm Slope Water originating from the Gulf Stream, North Atlantic Central Water, Labrador Sea Water, Labrador Current Water, Mixed Water	Petrie and Drinkwater, 1993
3	Flemish Cap and Great Banks	Gibbs Fracture Zone Water, Denmark Strait Overflow Water	Roberts et al., 2021
4	Labrador and Newfoundland shelves	Gibbs Fracture Zone Water, Denmark Strait Overflow Water	Roberts et al., 2021
5	Davis Strait Toqqusaq Bank	(West Greenland) Irminger Atlantic Water, Baffin Bay Deep Water, (Canadian) Arctic Water	Roberts et al., 2021
6	Denmark Strait	(Irminger Current) Irminger Atlantic Water, Re-circulating Atlantic Water, Polar Water, (Nordic Seas) Arctic Water	Roberts et al., 2021
7	South of Iceland Reykjanes Ridge	Subpolar Mode Water, Labrador Sea Water, Iceland-Scotland Overflow Water	Roberts et al., 2021
8	Northern Iceland Kolbeinsey Ridge/North of Iceland	Norwegian Sea Arctic Intermediate Water, Norwegian Sea Deep Water, Arctic Ocean Deep Water	Roberts et al., 2021
9	East Greenland Shelf	Polar Water, Re-circulating Atlantic Water, Upper Polar Deep Water, Arctic Ocean Deep Water	Roberts et al., 2021
10	Schulz Bank	Norwegian Sea Deep Water, Norwegian Sea Arctic Intermediate Water	Roberts et al., 2021
11	Northern Norway to Spitzbergen/Western Barents	Norwegian Sea Arctic Intermediate Water, Norwegian Sea Atlantic Water, Norwegian Sea Deep Water	Roberts et al., 2021
12	Norway Shelf	Atlantic Inflow Norwegian Trench Inflow	Turrell, 1992
13	Northeast Iceland Shelf	Arctic Intermediate Water, Norwegian Sea Deep Water	Roberts et al., 2021
14	Rockall Bank and Hatton Bank	Lower Deep Water (Antarctic Bottom Water), Northeast Atlantic Deep Water, Labrador Sea Water, East North Atlantic Central Water	Roberts et al., 2021
15	Porcupine Seabight Goban Spur Malin Slope	Northeast Atlantic Deep Water, East North Atlantic Central Water, Labrador Sea Water, Lower Deep Water (Antarctic Bottom Water)	Roberts et al., 2021
16	La Danois Bank	Mediterranean Water, Eastern North Atlantic Central Water, Labrador Sea Water	Puerta et al., 2020, Roberts et al., 2021
17	Bay of Biscay Aviles Canyon	Mediterranean Water, Eastern North Atlantic Central Water, Labrador Sea Water	Puerta et al., 2020, Roberts et al., 2021
18	African continental margin off Morocco Gorringe Bank Gulf of Cadiz	Northeast Atlantic Deep Water, Mediterranean Water, East North Atlantic Central Water	Roberts et al., 2021
19	Canary Islands Tropic Seamount	North Atlantic Central Water, South Atlantic Central Water, Antarctic Intermediate Water, Upper North Atlantic Deep Water, Mediterranean Water	Ramiro-Sánchez et al., 2019
20	Azores Condor Seamount Saldanha Mound Chaucer Seamount	Northeast Atlantic Deep Water, Mediterranean Water, East North Atlantic Central Water	Roberts et al., 2021
21	Great Meteor Seamount	North Atlantic Deep Water, Mediterranean Water, Canary Current Water, Antarctic Bottom Water	Brenke, 2002, Heinz et al., 2004

one hand, lose their ability to capture the variations in the reconstruction (e.g., temperature and oxygen at Habitat 11 at lead year 4, **Figures 7A,D**) and, on the other hand, generate artificial variations that do not exist in the reconstruction (e.g., salinity at Habitat 14 at lead year 4, **Figure 7F**). The predictability of the low-frequency (decadal to multi-decadal) variations is retained longer than the high-frequency (interannual to multi-year) variations. The degradation of the predictability is also evidenced in the decreasing of the ACCs and the increasing of the NMAEs along with the lead times (**Figures 8**, **9**).

The predictability horizon of the four variables from the initialized simulations varies among sponge habitats and variables (**Figures 8**, **9**). In this study, the predictability horizon is more constrained by the NMAEs. For instance, high ACCs with 95% significance last until the lead time of 4 years for salinity at Habitats 14, but the predictability horizon is only 1 year because of the rapid increase of NMAE (**Figures 8**, **9**). We find robust high/low predictability of the environmental properties at certain sponge habitats, e.g., at Habitat 14, three out of the four variables can be predicted up to 4 years in advance while at Habitat 17, the predictive skills for all the four variables are lost within 2 years. In addition, we find that in a large part of the sponge habitats (e.g., Habitats 1–3, 5–7, 11, 14–15, 19–21), the predictability last longer in the biogeochemical fields than in the physical fields.

The map of the categories illustrates a distinct regional difference in the predictability (**Figure 10**). High predictability, defined as predictability horizon of more than 4 years, exists in both physical and biogeochemical fields at two habitats inside the North Atlantic SPG (Habitats 13, 14) and one on the East Greenland Shelf (Habitat 9). High predictability of the biogeochemical fields is also found at numbers of habitats either spreading along the western margins (Habitats 3, 5–7) or in the open ocean (Habitats 1, 20) with additional one

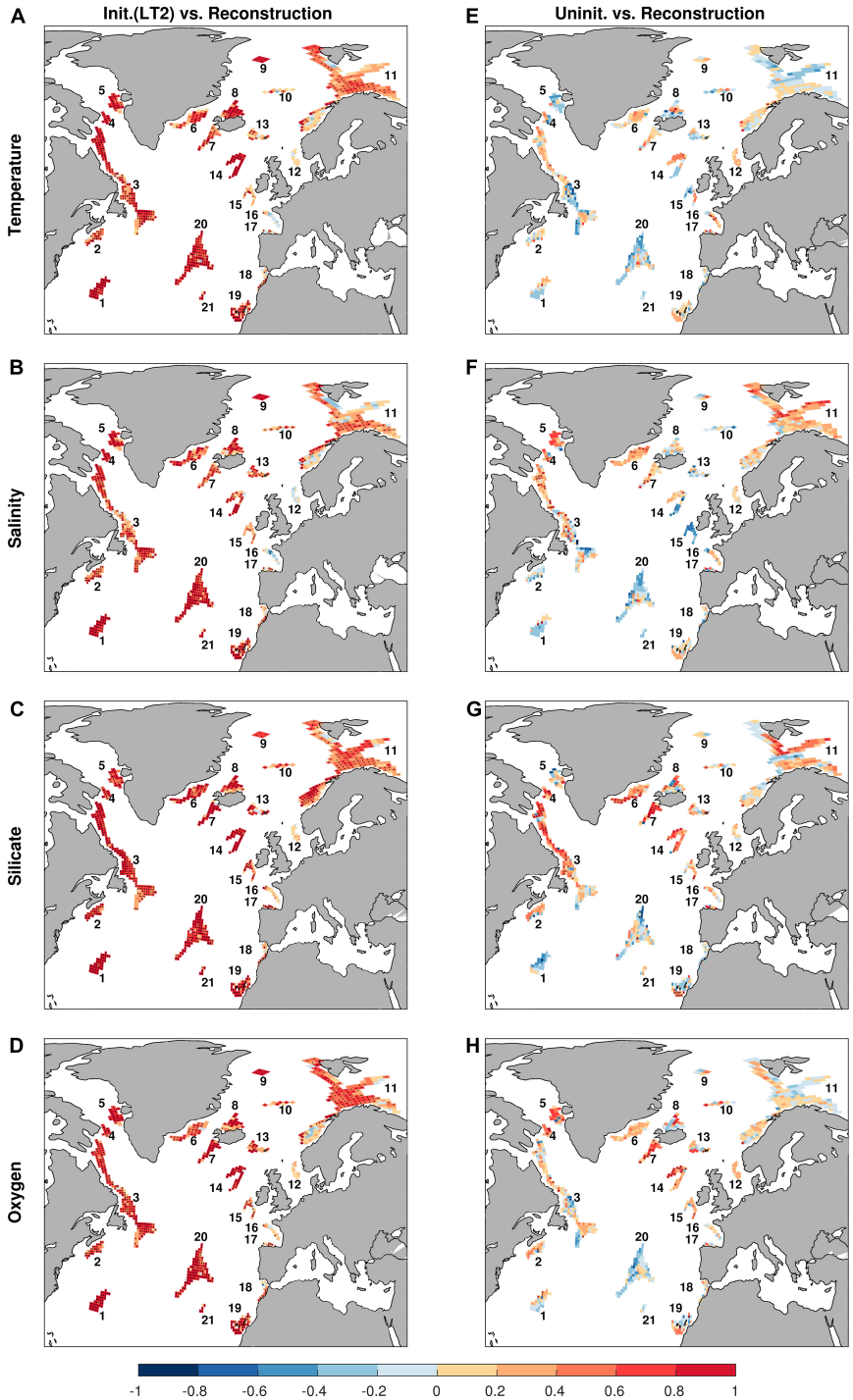

FIGURE 4 | Anomaly correlation coefficients (ACCs) for temperature **(A,E)**, salinity **(B,F)**, silicate **(C,G)**, and oxygen **(D,H)**. Left column **(A–D)**: correlations between the initialized simulations at a lead time of 2 years and the reconstruction. Right column **(E–H)**: correlations between the uninitialized simulations and the reconstruction. Stippling denotes statistically significant correlations at the 95% level based on a bootstrap approach with 500 bootstrapped resamples.

along the African margin (Habitat 19). For those habitats, the predictability of the physical fields is less than 4 years. In contrast, at Habitat 8, north of the Iceland, the physical fields can be predicted more than 4 years ahead while the biogeochemical fields are less predictable. Some habitats (Habitats 2, 4, 11) located in the marginal seas are characterized by moderate predictability, as at least one field can be predicted more than 2 years in advance but none of the variables are skillfully

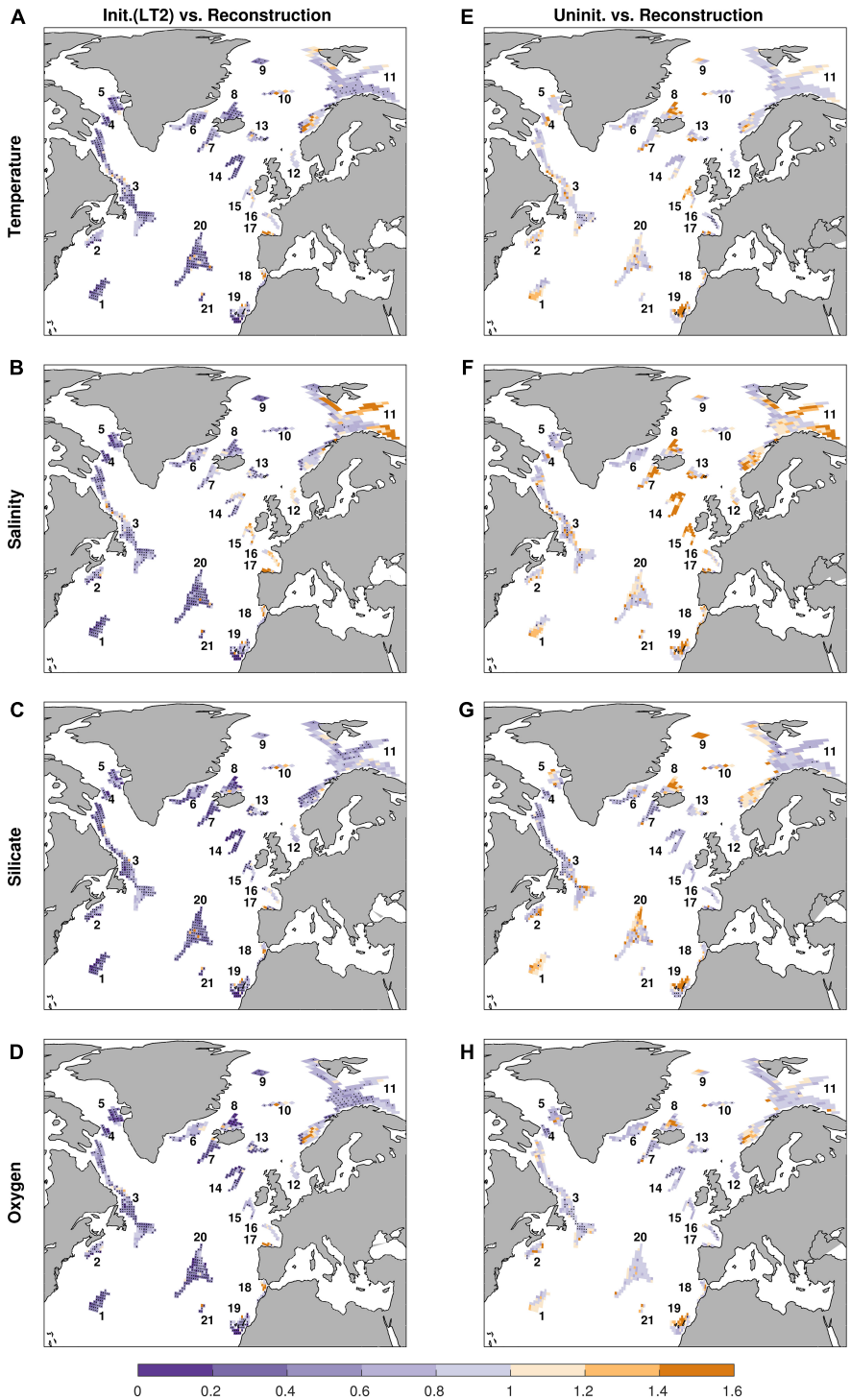

FIGURE 5 | Normalized mean absolute errors (NMAEs) for temperature **(A,E)**, salinity **(B,F)**, silicate **(C,G)**, and oxygen **(D,H)**. Left column **(A–D)**: NMAEs of initialized simulations at a lead time of 2 years. Right column **(E–H)**: NMAEs of uninitialized simulations. Stippling denotes NMAEs less than 1 at the 95% significance level based on a bootstrap approach with 500 bootstrapped resamples.

predictable for more than 4 years. There are six habitats, with five located in the European margin (Habitats 12, 15–18) and one located in the open Nordic Sea (Habitat 10), subject to low predictable environmental conditions, as both the physical and biogeochemical fields lose their predictive skill quickly within 2 years.

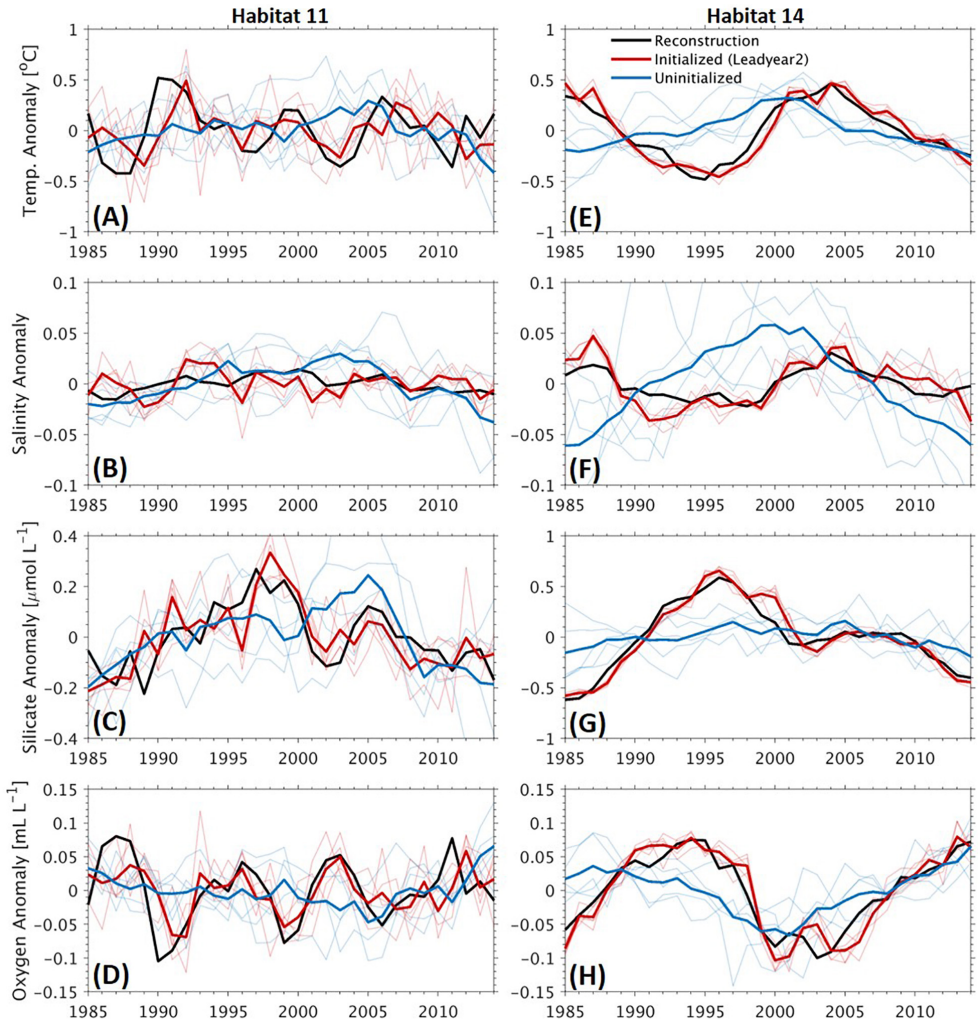

FIGURE 6 | Time series of detrended anomalies of annual mean temperature **(A,E)**, salinity **(B,F)**, concentrations of silicate **(C,G)**, and oxygen **(D,H)** at sponge habitats 11 **(A–D)** and 14 **(E–H)**. Bold black lines: reconstruction, bold red/blue lines: ensemble means of the initialized/uninitialized simulations at a lead time of 2 years, thin red/blue lines: individual members of the initialized/uninitialized simulations. The locations of the two habitats can be seen in **Figure 1**.

DISCUSSION

Mechanisms Underlying the Spatial Patterns of the Predictability

The sponge habitats involved in this study are subject to a diversity of geographical and geomorphological features and depths (**Table 1**), which are associated with substantial spatial variability in their hydrographic settings like water masses, local circulation patterns, interactions with upper oceans. Those differences suggest different underlying mechanisms describing/limiting the predictability.

High predictability for both the physical and the biogeochemical fields is found at sponge habitats in the SPG area (Habitats 13 and 14). A close coherence between the winter North Atlantic Oscillation (NAO) index and decadal changes in the deep-water temperature and salinity in the SPG area was identified during 1950–2000, which was attributed to the NAO-induced regulation of the relative contribution of cold fresh subpolar water and warm saline subtropical water to the deep-water formation (Sarafanov, 2009). The dominating water masses (e.g., Northeast Atlantic Deep Water) in these areas (**Table 2**) are integral to the Atlantic meridional overturning circulation (AMOC) (Rhein et al., 2011). This implies that the high predictive skills of the deep-sea environmental properties are largely prompted by NAO-AMOC related climate variability. In addition, we notice that Habitat 9, which is shallow with a mean depth of 200 m, free from the AMOC influence and covered by sea ice most of the year (Rudels, 1995), is characterized by high predictability for both the physical and biogeochemical fields. This skillful predictability arises probably from sea ice processes, as suggested by Jacox et al. (2020) that persistence of sea ice can cascade into predictability of the marine ecosystems.

Low predictability is found in the Gulf of Cadiz (Habitat 18), a region under the influence of the Mediterranean outflow.

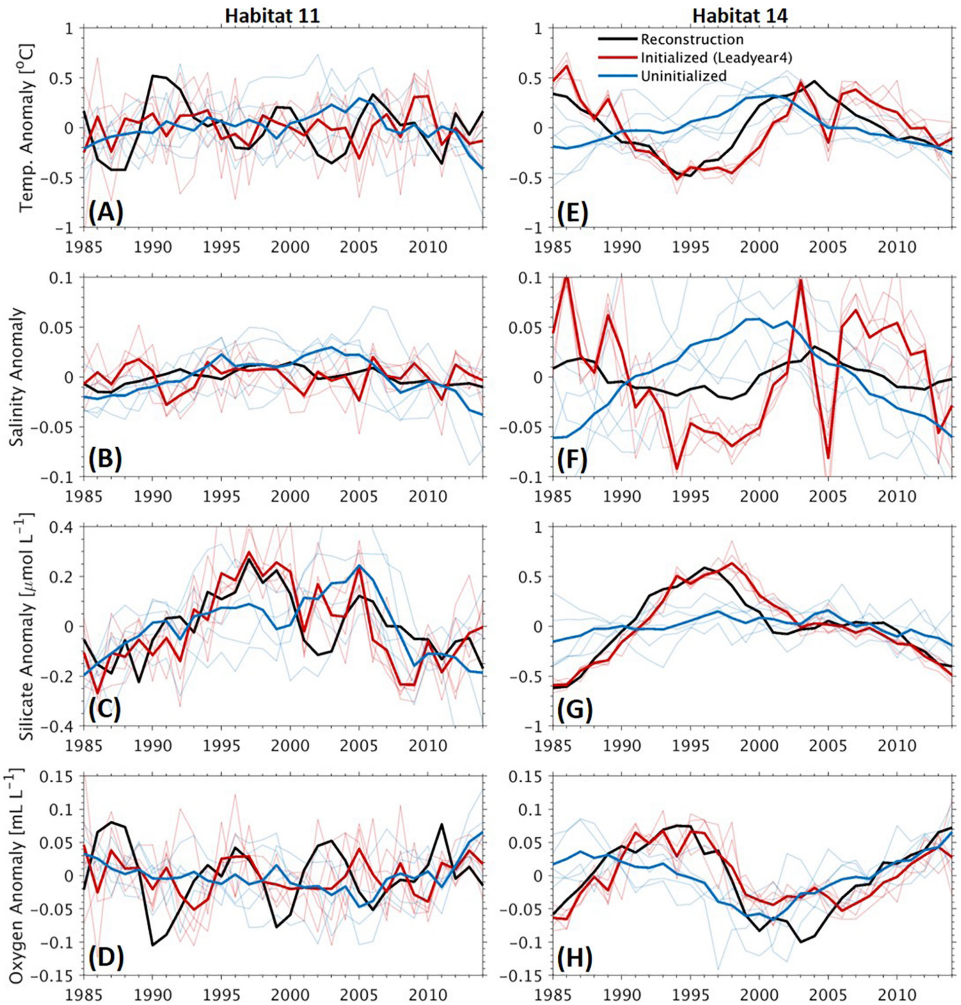

FIGURE 7 | Time series of detrended anomalies of annual mean temperature **(A,E)**, salinity **(B,F)**, concentrations of silicate **(C,G)**, and oxygen **(D,H)** at sponge habitats 11 **(A–D)** and 14 **(E–H)**. Bold black lines: reconstruction, bold red/blue lines: ensemble means of the initialized/uninitialized simulations at a lead time of 4 years, thin red/blue lines: individual members of the initialized/uninitialized simulations. The locations of the two habitats can be seen in **Figure 1**.

In the regional model, the simulated Mediterranean outflow is constrained by the restoring fields provided by the global predictions, as the eastern open boundary is placed near the Strait of Gibraltar (**Figure 2**). However, the water masses of the Mediterranean outflow are not well described by the global model because of its low resolution in the Mediterranean Sea (Marsland et al., 2003; Jungclaus et al., 2013; Malanotte-Rizzoli et al., 2014). The bias carried by the global model further propagates into the North Atlantic along the pathway of the Mediterranean outflow from the Strait of Gibraltar (Habitat 18) into the Bay of Biscay (Habitats 16, 17) and further reaches the southwest of Porcupine bank (Habitat 15) through a combination of narrow slope currents and mixing processes with the North Atlantic Current (Iorga and Lozier, 1999a,b; Bower et al., 2002), which in turn leads to low predictability of the environmental properties in those areas (Habitats 15–17). An opposite case is the Habitat 19, which receives less influence from the Mediterranean outflow (Iorga and Lozier, 1999a,b; Pastor et al., 2012). As a result, both the physical and biogeochemical fields at this site show high correlations between the initialized simulations with the reconstruction, albeit that the predictability of temperature and salinity is more constrained by high NMAEs.

In the lower layers of the ocean, a vigorous coupling with the upper ocean will likely degrade the predictability of the variations of the bottom environment, since the unpredictable signal of the atmosphere will cascade into the lower layers via the vertical exchange (e.g., Boer, 2004; Fransner et al., 2020). Thus, the low predictability at Habitat 12, the shallowest area among the 21 habitats, is attributed to the mean depth of 93 m, which suggests a profound impact of the atmospheric forcing through strong mixing between the ocean surface and bottom (Mathis et al., 2015). Although this habitat is influenced by the Atlantic inflow, which is found significantly correlated with large-scale atmosphere circulation NAO (Hjøllo et al., 2009), predictability is not sustained long in this area.

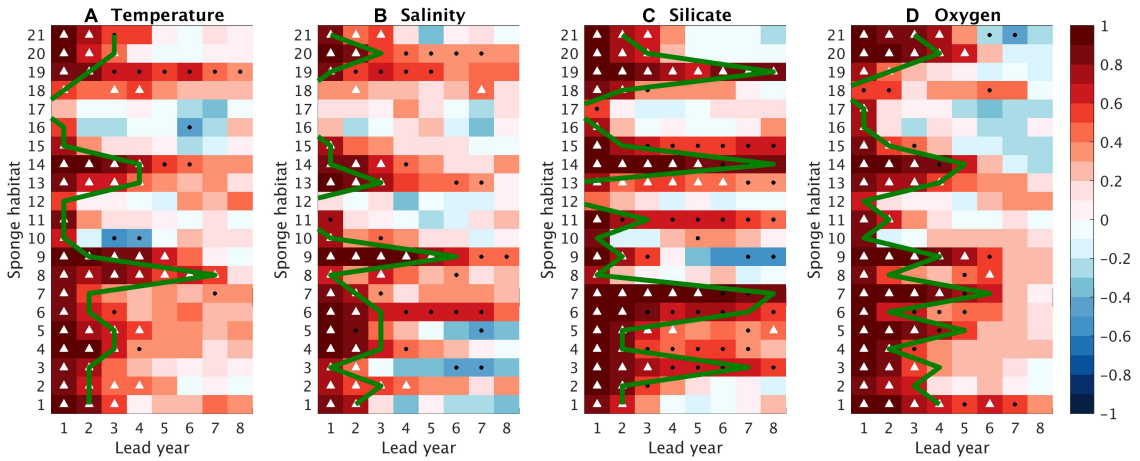

FIGURE 8 | Anomaly correlation coefficients (ACCs, in colors) as a function of lead time (*x* axis) and sponge habitat (*y* axis) for **(A)** Temperature, **(B)** Salinity, **(C)** Silicate, and **(D)** Oxygen. White triangles indicate that the ACCs are significant and significantly exceed the ACCs with the uninitialized simulations; black dots denote that the ACCs are significant but not significantly larger than the uninitialized simulations. Green lines indicate the predictability horizon, which is defined as the last lead year when ACCs are significant and the NMAEs are significantly smaller than 1. Significance is tested based on a bootstrap approach with 500 bootstrapped resamples.

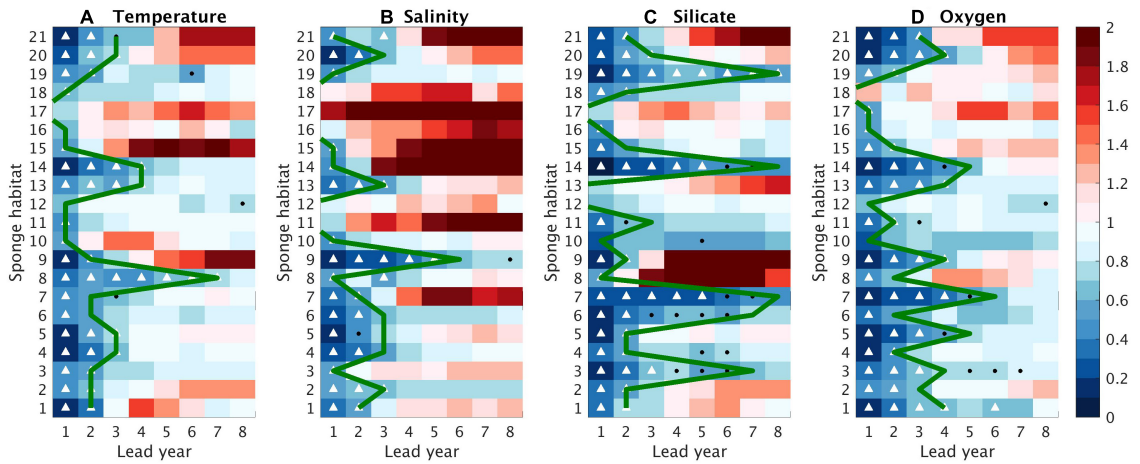

FIGURE 9 | Normalized mean absolute errors (NMAEs) as a function of lead time (*x* axis) and sponge habitat (*y* axis) for **(A)** Temperature, **(B)** Salinity, **(C)** Silicate, and **(D)** Oxygen. White triangles indicate that the NMAEs are significantly smaller than 1 and significantly smaller than the NMAEs with the uninitialized simulations; black dots denote that the NMAEs are significantly smaller than 1but not significantly smaller than the uninitialized simulations. NMAE > 1 is considered as no predictability. Green lines, identical with the green lines in **Figure 8**, indicate the predictability horizon, which is defined as the last lead year when ACCs are significant and the NMAEs are significantly smaller than 1. Significance is tested based on a bootstrap approach with 500 bootstrapped resamples.

In Habitat 10 (near the Schulz Bank), the bottom ocean is occupied by the Norwegian Sea Deep Water (Roberts et al., 2021). This water mass, a mixture of relatively cold and fresh Greenland Sea Deep Water with warmer, saltier Eurasian Basin Deep Water from the Arctic Ocean, can be traced only for a short distance (Swift and Koltermann, 1988). In addition, the mixture is highly variable, as the formation of the Greenland Sea Deep Water is depending on the convective processes that are highly associated with fluctuating atmospheric conditions (Blindheim and Rey, 2004). As a result, the water properties are less predictable and show low predictability.

Over a large fraction of the habitats, the predictive skills for the biogeochemical fields are higher than for the physical fields. Similar findings in the upper ocean have been reported by several studies (e.g., Séférian et al., 2014; Li et al., 2016). The reasons for this finding are under investigation. Enhanced persistence likely plays a role. In this study, the persistence of silicate, estimated to 3 years, is longer than that of temperature and salinity maintaining only to 1 year, suggesting a longer memory of silicate variations than the physical fields in the deep ocean (**Supplementary Figure S2**).

It is suggested that the deep ocean is expected to be more predictable than the surface layer, supported by the explanation

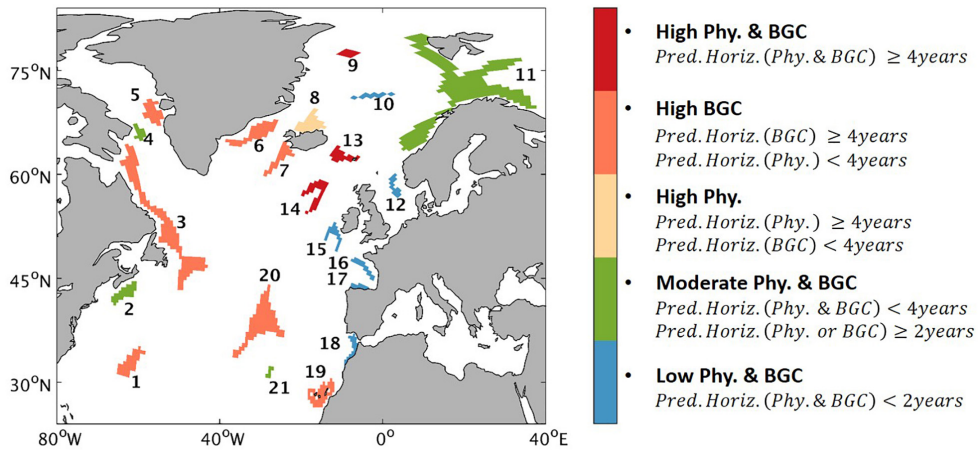

FIGURE 10 | Map of the sponge habitats showing the five categories of predictability. (1) High predictability in both physical (Phy.) and biogeochemical (BGC) fields (referred to "High Phy.&BGC") – the predictability horizon is longer than (including) 4 years for at least one variable in each of the two fields (physical and biogeochemical). (2) High predictability only in biogeochemical fields (referred to "High BGC") – the predictability horizon is longer than (including) 4 years for at least one variable in the biogeochemical fields but no such long predictability in the physical fields. (3) High predictability only in physical fields (referred to "High Phy.") – the predictability horizon is longer than (including) 4 years for at least one variable in the physical fields but no such long predictability in the biogeochemical fields. (4) Moderate predictability in physical and biogeochemical fields (referred to "Moderate Phy.&BGC") – predictability horizon in both two fields is less than 4 years, there are at least one variable in the two fields having predictability of longer than 2 years. (5) Low predictability in both physical and biogeochemical fields (referred to "Low Phy.&BGC") – no variable has predictability of longer than 2 years.

that the deep ocean is not directly coupled to the high-frequency atmosphere, the variability of which is relatively unpredictable (Frölicher et al., 2020). The increasing of the predictability with depth is evidenced on global or basin scales within a perfect modeling framework (Frölicher et al., 2020). However, this does not guarantee high predictability of the deep sea on smaller spatial scales such as at sponge habitats in this study. The spatial patterns of the predictability (**Figures 8–10**) reveal that different regional processes operating on a range of spatio-temporal scales are playing important roles in controlling/limiting the predictability. A good understanding of the local processes such as circulation patterns, mass transport and interactions with atmosphere/sediment helps to explain the predictability and thus to provide insights into the possible improvement of the current prediction systems. For instance, it is widely realized that the global coupled models don't capture the spatial scales required to correctly represent the Mediterranean ocean climate (Somot et al., 2008; Sasaki et al., 2020), since this climate is strongly driven by regional-scale topography and local winds, which are not resolved until the spatial resolution reaches certain values (Li, 2006). Therefore, an extension of the regional model domain to cover the whole Mediterranean Sea with an increased horizontal resolution is a promising way to better describe the water properties of the Mediterranean outflow and thus will probably improve the ability to predict the environmental factors at Habitats 15–18.

Prediction Into the Future

In this study, our analysis is based on a retrospective prediction (hindcast) in the past 30 years. We gain confidence from the analysis that our regional prediction system can be used to predict deep-sea environmental conditions in the near future, which is important for evaluating whether the environmental conditions are moving beyond the levels of 'typical' or natural variability that the sponges may have adapted to tolerate (Roberts et al., 2021). Currently the extension of the historical prediction into the future is limited by the length of the atmospheric forcing used to drive the reconstruction, which ends in the early 2015. It is promising to apply the prediction system into the future once the continued production of the atmospheric forcing with the related model is ready (Frauke Feser, personal communication).

Benchmark of Observation-Based Assessment

In assessing predictive skills, we are challenged by the lack of observations. The potential predictability, as deduced by comparing the prediction simulations against the reconstruction, is the upper limit of the predictability horizon with a given prediction system (e.g., Séférian et al., 2014). Such predictability horizons are hardly obtained in a real forecast, since it would require a perfect initialization and nudging of all fields in the model (Boer et al., 2013). Alternatively, the effective predictability horizon, requiring observationally based products to verify the prediction skill (Penny et al., 2019), provides a more restrictive and unbiased estimate of the predictability (Séférian et al., 2014).

However, the amount of observations in the deep sea, especially in specific benthic habitat, is constrained due to the high cost and limited technological capabilities (Levin et al., 2019). While there are short-term monitoring time-series at some habitats (e.g., Hanz et al., 2021), long-term monitoring

time series are missing at most sponge habitats. The existing collective database, such as World Ocean Database (WOD, Boyer et al., 2018) and GLODAPv2 (Olsen et al., 2016) are possible sources of long-term time series. However, caution should be taken when interpreting those data since available observations are usually not equally or even normally distributed in space nor in time (Schrum et al., 2006). For instance, the variability displayed by the time series of the bottom temperature at Habitat 14 extracted from WOD, is mainly associated with the depths and dates of the observations, as high temperatures are coincided with shallow depths (**Supplementary Figure S3**). The variability shown by this time series is therefore not representative of the interannual variability, which can not be simply compared with the modeled annual mean. In the model validation section of Samuelsen et al. (2019), the station observations were compared directly to the model result from the same date and location to avoid the issue discussed above. It is also demonstrated by IPCC 6th Assessment Report that the estimated predictive skill can be degraded by errors in observational dataset used for verification, suggesting that skill may tend to be underestimated, particularly for variables whose observational uncertainties are relatively large (Lee et al., 2021). In this sense, we don't show the comparison of the prediction against observations.

Implications of the Prediction System in Deep-Sea Benthic Habitats Preservation and Management

The assessment in this study provides a synoptic view of the spatial patterns of the predictability of deep-sea environmental factors over the widespread sponge habitats in the North Atlantic, providing the sponge community an indication to what extent the prediction of the environmental conditions can be used. For instance, reconstructed decadal variations of the four variables at the Rockall Bank (Habitat 14) demonstrate a tendency of the sponge habitat toward a status of being exposed to multiple stressors (simultaneous warming and decreasing silicate and oxygen concentrations) during 1995–2005. Although no negative impact of such change on the sponge habitat was documented in the past, we deduce that similar changes might occur in the future and are likely to be intensified by anthropogenic-induced climate change. Those changes in the near future might lead to a possibility that the environmental conditions move beyond the historical natural variability and become severe threats to the sponges. The high predictability of 4 years allows an effective prediction of such possible changes. Once the phase of change is predicted as continuously increasing/decreasing in temperature and salinity/silicate and oxygen in the coming 4 years, alert can be provided to the related management. This is of particular importance also for other benthic habitats living there, for instance the CWC reefs, the distribution of which are closely linked with environmental variations such as large-scale circulation patterns that can be traced by oceanographical variables (Schulz et al., 2020). In recent years, marine heat waves have been reported more frequently under climate change (Frölicher et al., 2018). The marine heat waves might affect deep-sea ecosystems, particularly for the CWCs and sponges inhabiting shallower waters in the northern areas of the North Atlantic such as the Norwegian area (Habitat 12) (Guihen et al., 2012). Despite the low predictability of temperature (1 year) in that region (**Figures 8–10**), it is still meaningful to predict the bottom temperature 1 year ahead to identify the possible occurrence of marine heat waves and mass mortality events, thus allowing reactions to mitigate damage.

Species distribution models, predicting the possible degree of habitats loss or gain under future climate change, offer a powerful tool in the deep sea for the effective management and conservation (Pearman et al., 2020). Those predictive models, based upon species-environment relationships, require accurately predicted environmental factors as important predictor variables (Guisan and Zimmermann, 2000). However, many knowledge gaps remaining in the biological processes and oceanographic dynamics hamper the models' credibility (Puerta et al., 2020). In particular, the use of present-day database (e.g., World Ocean Atlas) or the long-term climate projection to provide oceanographic parameters to the species distribution models are likely to raise additional sources of uncertainty (Burgos et al., 2020). Several studies have emphasized the importance of incorporating oceanographic data to improve the predictive capability of benthic species distribution models (e.g., Pearman et al., 2020). Environmental variables required by the habitats prediction vary among species, locations and models (e.g., Knudby et al., 2013; Beazley et al., 2018; Morato et al., 2020; Pearman et al., 2020). In addition, it is suggested that the deep-sea ecosystems are likely to be impacted by multiple stressors (Büscher et al., 2017). Our downscaling prediction system describes more environmental variables than we analyzed here, e.g. currents, other nutrients (nitrate, phosphate), primary production, pH, particulate organic carbon flux and so on. Therefore, the system has potentials to offer predictions for more variables and locations, and thus facilitate the prediction of a wider range of deep-sea benthic species like CWC reefs which are also prevailing in the North Atlantic for example on the Rockall Bank (Habitat 14). In that sense, our prediction will finally help to set up management strategies like how to improve the current deep-sea management tools, e.g., ABMTs (Johnson et al., 2018) and how to adapt the sustainable development to climate changes (Armstrong et al., 2019).

CONCLUSION

We have made an attempt for the first time to assess the potential predictability of the interannual to decadal variations of the deep-sea environmental conditions in the North Atlantic under the ongoing climate change. The assessments are based on a novel operational downscaling regional decadal prediction system dedicated to the deep-sea dynamics. Model results of four environmental parameters (temperature, salinity, concentrations of silicate and oxygen) over 21 sponge habitats are used as an example to assess the predictability. Our results demonstrate the potential of the regional model to predict the

environmental conditions multiple years in advance in the deep North Atlantic Ocean.

Based on our analysis, we draw the following conclusions:

1. Variations of both physical (temperature and salinity) and biogeochemical (concentrations of silicate and oxygen) conditions are potentially predictable several years in advance.
2. The predictability of the four variables is subject to distinct regional differences, with the potential predictability horizon varying from less than 2 years for all variables at sponge habitats along the European margin to more than 4 years in the SPG area and the Arctic Ocean.
3. In areas with high predictability, the variations of the environmental conditions are associated with ocean overturning structures (e.g., AMOC) that are regulated by large-scale climate variability such as the NAO or with the persistence of sea ice, while in areas with low predictability, the deep-sea environmental variations are under remarkable influence of the atmosphere or the local circulations such as the Mediterranean outflow.
4. The biogeochemical fields are more predictable than the physical fields at a large portion of the sponge habitats, partly due to the longer persistence of biogeochemical fields than the physical counterparts.
5. Predictability is significantly improved by initialization in areas with weak air-sea coupling and areas free from the influence of the Mediterranean outflow.

Overall, our analysis demonstrates the capacity of the downscaling regional system for skillfully predicting the variations of the environmental conditions at deep-sea sponge habitats in the near future. The assessment of the predictability can be applied to other ocean parameters (e.g., pH and other nutrients) and at other benthic habitats (e.g., CWC reefs). The downscaling prediction system can therefore help to improve management in the deep-sea ecosystems on interannual to decadal timescales.

DATA AVAILABILITY STATEMENT

The raw data supporting the conclusions of this article will be made available by the authors, without undue reservation.

AUTHOR CONTRIBUTIONS

CS, UD, and FL designed this study. FL, CS, UD, SB, and JB developed the downscaling prediction system and designed the simulations. FL conducted the numerical simulations supported by AS and UD. The analysis was performed by FL supported by SB and CS. The result interpretation and discussion were conducted by FL and UH. Inputs for the regional model from MPI-ESM-LR simulations were provided by HP. FL led the writing of the manuscript with inputs from all co-authors, who discussed the results and commented on the manuscript at every stage. All authors contributed to the article and approved the submitted version.

FUNDING

FL and AS are supported by project SponGES (Grant Agreement No. 679849). JB and CS are supported by project CLICCS (Grant Agreement No. 390683824). JB and SB are supported by Copernicus (contract C3S-330). The MPI-ESM-LR simulations were performed within the German Federal Ministry for Education and Research (BMBF) project MiKlip under Grant Number FKZ 01LP1519A.

ACKNOWLEDGMENTS

This research has been performed in the scope of the SponGES project, which received funding from the European Union's Horizon 2020 Research and Innovation Program under Grant Agreement No. 679849. The study is a contribution to the Deutsche Forschungsgemeinschaft (DFG, German Research Foundation) under Germany's Excellence Strategy—EXC 2037 "Climate, Climatic Change, and Society" (CLICCS)—Project: 390683824, and a contribution to the Center for Earth System Research and Sustainability (CEN) of Universität Hamburg. JB and SB are supported by Copernicus Climate Change Service, funded by the EU, under contract C3S-330. The MPI-ESM-LR simulations were performed within the German Federal Ministry for Education and Research (BMBF) project MiKlip under Grant Number FKZ 01LP1519A. Computational resources were made available by the German Climate Computing Center (DKRZ). We thank Dr. Hongmei Li and Dr. Vimal Koul for their big help in analyzing the model results. We thank the two reviewers for their constructive and helpful comments for improving the manuscript.

SUPPLEMENTARY MATERIAL

The Supplementary Material for this article can be found online at: https://www.frontiersin.org/articles/10.3389/fmars.2021.703297/full#supplementary-material

REFERENCES

Addamo, A. M., Vertino, A., Stolarski, J., García-Jiménez, R., Taviani, M., and Machordom, A. (2016). Merging scleractinian genera: the overwhelming genetic similarity between solitary *Desmophyllum* and colonial *Lophelia*. *BMC Evol. Biol.* 16:108. doi: 10.1186/s12862-016-0654-8

Armstrong, C. W., Vondolia, G. K., Foley, N. S., Henry, L. A., Needham, K., and Ressurreição, A. (2019). Expert assessment of risks posed by climate change and anthropogenic activities to ecosystem services in the deep North Atlantic. *Front. Mar. Sci.* 6:158. doi: 10.3389/fmars.2019.00158

Barthel, D., Tendal, O. S., and Thiel, H. (1996). A wandering population of the hexactineliid sponge pheronema carpenteri on the continental slope off

morocco, Northwest Africa. *Mar. Ecol.* 17, 603–616. doi: 10.1111/j.1439-0485.1996.tb00420.x

Beazley, L. I., Kenchington, E. L., Murillo, F. J., and Sacau, M. D. M. (2013). Deep-sea sponge grounds enhance diversity and abundance of epibenthic megafauna in the Northwest Atlantic. *ICES J. Mar. Sci.* 70, 1471–1490. doi: 10.1093/icesjms/fst124

Beazley, L., Kenchington, E., Yashayaev, I., and Murillo, F. J. (2015). Drivers of epibenthic megafaunal composition in the sponge grounds of the Sackville Spur, northwest Atlantic. *Deep Sea Res. 1 Oceanogr. Res. Pap.* 98, 102–114. doi: 10.1016/j.dsr.2014.11.016

Beazley, L., Wang, Z., Kenchington, E., Yashayaev, I., Rapp, H. T., Xavier, J. R., et al. (2018). Predicted distribution of the glass sponge vazella pourtalesi on the scotian shelf and its persistence in the face of climatic variability. *PLoS One* 13:e0205505. doi: 10.1371/journal.pone.0205505

Beazley, L., Kenchington, E., Murillo, F. J., Brickman, D., Wang, Z., Davies, A. J., et al. (2021). Climate change winner in the deep sea? Predicting the impacts of climate change on the distribution of the glass sponge *Vazella pourtalesii*. *Mar. Ecol. Prog. Ser.* 657, 1–23. doi: 10.3354/meps13566

Bell, J. J., Bennett, H. M., Rovellini, A., and Webster, N. S. (2018). Sponges to be winners under near-future climate scenarios. *Bioscience* 68, 955–968. doi: 10.1093/biosci/biy142

Befort, D. J., O'Reilly, C. H., and Weisheimer, A. (2020). Constraining projections using decadal predictions. *Geophys. Research Lett.* 47:e2020GL087900.

Bett, B. J., and Rice, A. L. (1992). The influenceof hexactinellid sponge (*Pheronema carpenteri*) spicules on the patchy distribution of macrobenthos in the porcupine seabight (*bathyal ne atlantic*). *Ophelia* 36, 217–226. doi: 10.1080/00785326.1992.10430372

Blacker, R. W. (1957). Benthic animals as indicators of hydrographic conditions and climatic change in Svalbard waters. *Fish. Investig.* 20, 1–49.

Blacker, R. W. (1965). *Recent Changes in the Benthos of the West Spitzbergen Fishing Grounds*. Vancouver, BC: International Commission for the Northwest Atlantic Fisheries special Publication.

Bleck, R. (2002). An oceanic general circulation model framed in hybrid isopycnic-Cartesian coordinates. *Ocean Model.* 4, 55–88.

Blindheim, J., and Rey, F. (2004). Water-mass formation and distribution in the Nordic Seas during the 1990s. *ICES J. Mar. Sci.* 61, 846–863. doi: 10.1016/j.icesjms.2004.05.003

Boer, G. J. (2004). Long time-scale potential predictability in an ensemble of coupled climate models. *Clim. Dyn.* 23, 29–44. doi: 10.1007/s00382-004-0419-8

Boer, G. J., Kharin, V. V., and Merryfield, W. J. (2013). Decadal predictability and forecast skill. *Clim. Dyn.* 41, 1817–1833. doi: 10.1007/s00382-013-1705-0

Borchert, L. F., Düsterhus, A., Brune, S., Müller, W. A., and Baehr, J. (2019). Forecast-oriented assessment of decadal hindcast skill for North Atlantic SST. *Geophys. Res. Lett.* 46, 11444–11454. doi: 10.1029/2019gl084758

Bower, A. S., Le Cann, B., Rossby, T., Zenk, W., Gould, J., Speer, K., et al. (2002). Directly measured mid-depth circulation in the northeastern North Atlantic Ocean. *Nature* 419, 603–607. doi: 10.1038/nature01078

Boyer, T. P., Baranova, O.K. Coleman, C., Garcia, H. E., Grodsky, A., Locarnini, R. A., et al. (2018). "World ocean database 2018," in *NOAA Atlas NESDIS 87. and GLODAPv2*, ed. A. V. Mishonov (Silver Spring, MD: National Centers for Environmental Information Ocean Climate Laboratory).

Brady, R. X., Lovenduski, N. S., Yeager, S. G., Long, M. C., and Lindsay, K. (2020). Skillful multiyear predictions of ocean acidification in the California current system. *Nat. Commun.* 11:2166.

Breeze, H., and Fenton, D. G. (2007). Designing management measures to protect cold-water corals off Nova Scotia, Canada. *Bull. Mar. Sci.* 81, 123–133.

Brenke, N. (2002). "The benthic community of the Great Meteor Bank," in *Proceedings of the ICES Annual Science Conference and ICES Centenary*, (Copenhagen).

Brune, S., Düsterhus, A., Pohlmann, H., Müller, W. A., and Baehr, J. (2018). Time dependency of the prediction skill for the North Atlantic subpolar gyre in initialized decadal hindcasts. *Clim. Dyn.* 51, 1947–1970. doi: 10.1007/s00382-017-3991-4

Buhl-Mortensen, L., Vanreusel, A., Gooday, A. J., Levin, L. A., Priede, I. G., Buhl-Mortensen, P., et al. (2010). Biological structures as a source of habitat heterogeneity and biodiversity on the deep ocean margins. *Mar. Ecol.* 31, 21–50. doi: 10.1111/j.1439-0485.2010.00359.x

Buhl-Mortensen, L., Olafsdottir, S. H., Buhl-Mortensen, P., Burgos, J. M., and Ragnarsson, S. A. (2015). Distribution of nine cold-water coral species (*Scleractinia and Gorgonacea*) in the cold temperate North Atlantic: effects of bathymetry and hydrography. *Hydrobiologia* 759, 39–61. doi: 10.1007/s10750-014-2116-x

Buhl-Mortensen, L., Burgos, J. M., Steingrund, P., Buhl-Mortensen, P., Ólafsdóttir, S. H., and Ragnarsson, S. Á (2019). *Vulnerable Marine Ecosystems (VMEs): Coral and Sponge VMEs in Arctic and Sub-Arctic Waters–Distribution and Threats*. Copenhagen: Nordic Council of Ministers.

Burgos, J. M., Buhl-Mortensen, L., Buhl-Mortensen, P., Ólafsdóttir, S. H., Steingrund, P., Ragnarsson, S. Á, et al. (2020). Predicting the distribution of indicator taxa of vulnerable marine ecosystems in the Arctic and Sub-arctic Waters of the Nordic Seas. *Front. Mar. Sci.* 7:131. doi: 10.3389/fmars.2020.00131

Büscher, J. V., Form, A. U., and Riebesell, U. (2017). Interactive effects of ocean acidification and warming on growth, fitness and survival of the cold-water coral Lophelia pertusa under different food availabilities. *Front. Mar. Sci.* 4:101. doi: 10.3389/fmars.2017.00101

Carnes, M. R. (2009). *Description and Evaluation of GDEM-V 3.0*. Mississippi, MS: Naval Research Lab Stennis Space Center Ms Oceanography Divdtic.

Cathalot, C., Van Oevelen, D., Cox, T. J., Kutti, T., Lavaleye, M., Duineveld, G., et al. (2015). Cold-water coral reefs and adjacent sponge grounds: hotspots of benthic respiration and organic carbon cycling in the deep sea. *Front. Mar. Sci.* 2:37. doi: 10.3389/fmars.2015.00037

Cárdenas, P., Rapp, H. T., Klitgaard, A. B., Best, M., Thollesson, M., and Tendal, O. S. (2013). Taxonomy, biogeography and DNA barcodes of Geodia species (*Porifera, Demospongiae, Tetractinellida*) in the Atlantic boreo-arctic region. *Zool. J. Linn. Soc.* 169, 251–311. doi: 10.1111/zoj.12056

Cárdenas, P., and Rapp, H. T. (2015). Demosponges from the Northern Mid-Atlantic Ridge shed more light on the diversity and biogeography of North Atlantic deep-sea sponges. *J. Mar. Biol. Assoc. U.K.* 95, 1475–1516. doi: 10.1017/s0025315415000983

Copley, J. T. P., Tyler, P. A., Sheader, M., Murton, B. J., and German, C. R. (1996). Megafauna from sublittoral to abyssal depths along the Mid-Atlantic Ridge south of Iceland. *Oceanol. Acta* 19, 549–559.

Culwick, T., Phillips, J., Goodwin, C., Rayfield, E. J., and Hendry, K. R. (2020). Sponge density and distribution constrained by fluid forcing in the deep sea. *Front. Mar. Sci.* 7:395. doi: 10.3389/fmars.2020.00395

Daewel, U., and Schrum, C. (2013). Simulating long-term dynamics of the coupled North Sea and Baltic Sea ecosystem with ECOSMO II: model description and validation. *J. Mar. Syst.* 119, 30–49. doi: 10.1016/j.jmarsys.2013.03.008

Dullo, W. C., Flögel, S., and Rüggeberg, A. (2008). Cold-water coral growth in relation to the hydrography of the Celtic and Nordic European continental margin. *Mar. Ecol. Prog. Ser.* 371, 165–176. doi: 10.3354/meps07623

Erekovsky, A. V. (1995). Materials to the faunistic study of the White and Barents seas sponges. 5. quantitative distribution. *Berl. Geowissenschaftliche Abh.* 16, 709–714.

FAO (2009). *International Guidelines for the Management of Deep-sea Fisheries in the High Seas*. Rome: Food and Agriculture Organization.

Fransner, F., Counillon, F., Bethke, I., Tjiputra, J., Samuelsen, A., Nummelin, A., et al. (2020). Ocean biogeochemical predictions—initialization and limits of predictability. *Front. Mar. Sci.* 7:386. doi: 10.3389/fmars.2020.00386

Frölicher, T. L., Fischer, E. M., and Gruber, N. (2018). Marine heatwaves under global warming. *Nature* 560, 360–364. doi: 10.1038/s41586-018-0383-9

Frölicher, T. L., Ramseyer, L., Raible, C. C., Rodgers, K. B., and Dunne, J. (2020). Potential predictability of marine ecosystem drivers. *Biogeosciences* 17, 2061–2083. doi: 10.5194/bg-17-2061-2020

Garcia, H. E., Boyer, T. P., Locarnini, R. A., Antonov, J. I., Mishonov, A. V., Baranova, O. K., et al. (2013a). *World Ocean Atlas 2013. Volume 3, Dissolved Oxygen, Apparent Oxygen Utilization, and Oxygen Saturation*. Silver Spring, MD: National Oceanographic Data Center.

Garcia, H. E., Locarnini, R. A., Boyer, T. P., Antonov, J. I., Baranova, O. K., Zweng, M. M., et al. (2013b). *World Ocean Atlas 2013. Volume 4, Dissolved Inorganic Nutrients (Phosphate, Nitrate, Silicate)*. Silver Spring, MD: National Oceanographic Data Center.

Goddard, L., Kumar, A., Solomon, A., Smith, D., Boer, G., Gonzalez, P., et al. (2013). A verification framework for interannual-to-decadal

predictions experiments. *Clim. Dyn.* 40, 245–272. doi: 10.1007/s00382-012-1481-2

Guihen, D., White, M., and Lundälv, T. (2012). Temperature shocks and ecological implications at a cold-water coral reef. *Mar. Biodivers. Rec.* 5:e68.

Guijarro, J., Beazley, L., Lirette, C., Kenchington, E., Wareham, V., Gilkinson, K., et al. (2016). *Species Distribution Modelling of Corals and Sponges from Research Vessel Survey Data in the Newfoundland and Labrador Region for use in the Identification of Significant Benthic Areas*. Ottawa, OTT: Fisheries and Oceans Canada.

Guisan, A., and Zimmermann, N. E. (2000). Predictive habitat distribution models in ecology. *Ecol. Model.* 135, 147–186. doi: 10.1016/s0304-3800(00)00354-9

Hansen, C., and Samuelsen, A. (2009). Influence of horizontal model grid resolution on the simulated primary production in an embedded primary production model in the Norwegian Sea. *J. Mar. Syst.* 75, 236–244. doi: 10.1016/j.jmarsys.2008.10.004

Hanz, U., Beazley, L., Kenchington, E., Duineveld, G., Rapp, H. T., and Mienis, F. (2020). Seasonal variability in near-bed environmental conditions in the Vazella pourtalesii glass sponge grounds of the Scotian Shelf. *Front. Mar. Sci.* 7:1179. doi: 10.3389/fmars.2021.696777

Hanz, U., Roberts, E. M., Duineveld, G., Davies, A., van Haren, H., Rapp, H. T., et al. (2021). Long-term observations reveal environmental conditions and food supply mechanisms at an Arctic deep-sea sponge ground. *J. Geophys. Res.* 126, e2020JC016776.

Hawkes, N., Korabik, M., Beazley, L., Rapp, H. T., Xavier, J. R., and Kenchington, E. (2019). Glass sponge grounds on the Scotian Shelf and their associated biodiversity. *Mar. Ecol. Prog. Ser.* 614, 91–109. doi: 10.3354/meps12903

Heinz, P., Ruepp, D., and Hemleben, C. (2004). Benthic foraminifera assemblages at great meteor seamount. *Mar. Biol.* 144, 985–998. doi: 10.1007/s00227-003-1257-7

Hestetun, J. T., Rapp, H. T., and Pomponi, S. (2019). Deep-sea carnivorous sponges from the Mariana Islands. *Front. Mar. Sci.* 6:371. doi: 10.3389/fmars.2019.00371

Hjøllo, S. S., Skogen, M. D., and Svendsen, E. (2009). Exploring currents and heat within the North Sea using a numerical model. *J. Mar. Syst.* 78, 180–192. doi: 10.1016/j.jmarsys.2009.06.001

Hochachka, P. W., and Somero, G. N. (1968). The adaptation of enzymes to temperature. *Comp. Biochem. Phys.* 27, 659–668. doi: 10.1016/0010-406x(68)90605-1

Hogg, M. M., Tendal, O. S., Conway, K. W., Pomponi, S. A., Gutt, J., Krautter, M., et al. (2010). *Deep-Sea Sponge Grounds: Reservoirs of Biodiversity*. Cambridge: World Conservation Monitoring Centre.

Howell, K. L., Piechaud, N., Downie, A. L., and Kenny, A. (2016). The distribution of deep-sea sponge aggregations in the North Atlantic and implications for their effective spatial management. *Deep Sea Res. 1 Oceanogr. Res. Pap.* 115, 309–320. doi: 10.1016/j.dsr.2016.07.005

Hughes, D. J., and Gage, J. D. (2004). Benthic metazoan biomass, community structure and bioturbation at three contrasting deep-water sites on the northwest European continental margin. *Prog. Oceanogr.* 63, 29–55. doi: 10.1016/j.pocean.2004.09.002

Iorga, M. C., and Lozier, M. S. (1999a). Signatures of the Mediterranean outflow from a North Atlantic climatology: 1. Salinity and density fields. *J. Geophys. Res. Oceans* 104, 25985–26009. doi: 10.1029/1999jc900115

Iorga, M. C., and Lozier, M. S. (1999b). Signatures of the Mediterranean outflow from a North Atlantic climatology: 2. Diagnostic velocity fields. *J. Geophys. Res. Oceans* 104, 26011–26029. doi: 10.1029/1999jc900204

Jacox, M. G., Alexander, M. A., Siedlecki, S., Chen, K., Kwon, Y. O., Brodie, S., et al. (2020). Seasonal-to-interannual prediction of North American coastal marine ecosystems: Forecast methods, mechanisms of predictability, and priority developments. *Prog. Oceanogr.* 183:102307. doi: 10.1016/j.pocean.2020.102307

Johnson, D., Ferreira, M. A., and Kenchington, E. (2017). *Report on Priorities for an Expert Assessment of North Atlantic MPAs, EBSAs, and VMEs in ABNJ. Contribution to the EU H2020 Atlas Project, Project Deliverable 7 2*. Victoria, VIC: ATLAS.

Johnson, D., Ferreira, M. A., and Kenchington, E. (2018). Climate change is likely to severely limit the effectiveness of deep-sea ABMTs in the North Atlantic. *Mar. Policy* 87, 111–122. doi: 10.1016/j.marpol.2017.09.034

Jungclaus, J. H., Fischer, N., Haak, H., Lohmann, K., Marotzke, J., Matei, D., et al. (2013). Characteristics of the ocean simulations in the max planck institute ocean model (MPIOM) the ocean component of the MPI-Earth system model. *J. Adv. Model. Earth Syst.* 5, 422–446. doi: 10.1002/jame.20023

Kazanidis, G., Vad, J., Henry, L. A., Neat, F., Berx, B., Georgoulas, K., et al. (2019a). Distribution of deep-sea sponge aggregations in an area of multisectoral activities and changing oceanic conditions. *Front. Mar. Sci.* 6:163. doi: 10.3389/fmars.2019.00163

Kazanidis, G., Vad, J., Henry, L.-A., Neat, F., Berx, B., Georgoulas, K., et al. (2019b). Environmental and biological data from deep-sea sponge aggregations in the Faroe-Shetland Channel Nature Conservation Marine Protected Area. *PANGAEA* doi: 10.1594/PANGAEA.897592

Kazanidis, G., Vad, J., Henry, L.-A., Neat, F., Berx, B., Georgoulas, K., et al. (2019c). Seabed images and corresponding environmental data from deep-sea sponge aggregations in the Faroe-Shetland Channel Nature Conservation Marine Protected Area. *PANGAEA* doi: 10.1594/PANGAEA.897604

Keeling, R. F., Körtzinger, A., and Gruber, N. (2010). Ocean deoxygenation in a warming world. *Annu. Rev. Mar. Sci.* 2, 199–229. doi: 10.1146/annurev.marine.010908.163855

Klitgaard, A. B., and Tendal, O. S. (2004). Distribution and species composition of mass occurrences of large-sized sponges in the northeast Atlantic. *Prog. Oceanogr.* 61, 57–98. doi: 10.1016/j.pocean.2004.06.002

Knudby, A., Kenchington, E., and Murillo, F. J. (2013). Modeling the distribution of Geodia sponges and sponge grounds in the Northwest Atlantic. *PLoS One* 8:e82306. doi: 10.1371/journal.pone.0082306

Kutti, T., Bannister, R. J., and Fosså, J. H. (2013). Community structure and ecological function of deep-water sponge grounds in the traenadypet MPA—Northern Norwegian continental shelf. *Cont. Shelf Res.* 69, 21–30.

Lapointe, A., Watling, L., and Gontz, A. M. (2020). "Deep-sea benthic megafaunal communities on the New England and corner rise seamounts, Northwest Atlantic Ocean," in *Seafloor Geomorphology as Benthic Habitat*, eds P. Harris and E. Baker (Amsterdam: Elsevier), 917–932.

Lee, J. Y., Marotzke, J., Bala, G., Cao, L., Corti, S., Dunne, J. P., et al. (2021). "Future global climate: scenario-based projections and near-term information," in *Climate Change 2021: The Physical Science Basis. Contribution of Working Group I to the Sixth Assessment Report of the Intergovernmental Panel on Climate Change*, eds V. Masson-Delmotte, P. Zhai, A. Pirani, S. L. Connors, C. Péan, S. Berger, et al. (Cambridge: Cambridge University Press).

Levin, L. A. (2003). Oxygen minimum zone benthos: adaptation and community response to hypoxia. *Oceanogr. Mar. Biol. Annu. Rev.* 41, 1–45.

Levin, L. A., and Le Bris, N. (2015). The deep ocean under climate change. *Science* 350, 766–768. doi: 10.1126/science.aad0126

Levin, L. A., Bett, B. J., Gates, A. R., Heimbach, P., Howe, B. M., Janssen, F., et al. (2019). Global observing needs in the deep ocean. *Front. Mar. Sci.* 6:241. doi: 10.3389/fmars.2019.00241

Li, H., Ilyina, T., Müller, W. A., and Sienz, F. (2016). Decadal predictions of the North Atlantic CO 2 uptake. *Nat. Commun.* 7:11076.

Li, L. Z. (2006). Atmospheric GCM response to an idealized anomaly of the Mediterranean sea surface temperature. *Clim. Dyn.* 27, 543–552. doi: 10.1007/s00382-006-0152-6

Malanotte-Rizzoli, P., Artale, V., Borzelli-Eusebi, G. L., Brenner, S., Crise, A., Gacic, M., et al. (2014). Physical forcing and physical/biochemical variability of the Mediterranean Sea: a review of unresolved issues and directions for future research. *Ocean Sci.* 10, 281–322. doi: 10.5194/os-10-281-2014

Maldonado, M., Aguilar, R., Bannister, R. J., Bell, J. J., Conway, K. W., Dayton, P. K., et al. (2017). *Sponge Grounds as Key Marine Habitats: a Synthetic Review of Types, Structure, Functional Roles, and Conservation Concerns*. Cham: Springer International Publishing.

Maldonado, M., López-Acosta, M., Sitjà, C., García-Puig, M., Galobart, C., Ercilla, G., et al. (2019). Sponge skeletons as an important sink of silicon in the global oceans. *Nat. Geosci.* 12, 815–822. doi: 10.1038/s41561-019-0430-7

Maldonado, M., López-Acosta, M., Beazley, L., Kenchington, E., Koutsouveli, V., and Riesgo, A. (2020). Cooperation between passive and active silicon transporters clarifies the ecophysiology and evolution of biosilicification in sponges. *Sci. Adv.* 6:eaba9322. doi: 10.1126/sciadv.aba9322

Maldonado, M., Beazley, L., López-Acosta, M., Kenchington, E., Casault, B., Hanz, U., et al. (2021). Massive silicon utilization facilitated by a benthic-pelagic coupled feedback sustains deep-sea sponge aggregations. *Limnol. Oceanogr.* 66, 366–391. doi: 10.1002/lno.11610

Marsland, S. J., Haak, H., Jungclaus, J. H., Latif, M., and Röske, F. (2003). The max-planck-institute global ocean/sea ice model with orthogonal curvilinear coordinates. *Ocean Model.* 5, 91–127. doi: 10.1016/S1463-5003(02)00015-X

Mathis, M., Elizalde, A., Mikolajewicz, U., and Pohlmann, T. (2015). Variability patterns of the general circulation and sea water temperature in the North Sea. *Prog. Oceanogr.* 135, 91–112. doi: 10.1016/j.pocean.2015.04.009

Meyer, H. K., Roberts, E. M., Mienis, F., and Rapp, H. T. (2020a). *Megafauna Abundances Observed During a Sponges Cruise With RV G.O. Sars and ROV Ægir 6000 in Sognefjord, Norway*. Brussels: Data Publisher for Earth & Environmental Science.

Meyer, H. K., Roberts, E. M., Mienis, F., and Rapp, H. T. (2020b). *Megafauna Abundances With Corresponding Environmental and Nutrient Variables From a Sponges Cruise With RV G.O. Sars and ROV Ægir 6000 From Two ROV Dives in Sognefjord, Norway*. Brussels: Data Publisher for Earth & Environmental Science.

Meyer, H. K., Roberts, E. M., Rapp, H. T., and Davies, A. J. (2019). Spatial patterns of arctic sponge ground fauna and demersal fish are detectable in autonomous underwater vehicle (AUV) imagery. *Deep Sea Res. 1 Oceanogr. Res. Pap.* 153:103137.

Meyer, K. S., Sweetman, A. K., Young, C. M., and Renaud, P. E. (2015). Environmental factors structuring Arctic megabenthos—a case study from a shelf and two fjords. *Front. Mar. Sci.* 2:22. doi: 10.3389/fmars.2015.00022

Morato, T., González-Irusta, J. M., Dominguez-Carrió, C., Wei, C. L., Davies, A., Sweetman, A. K., et al. (2020). Climate-induced changes in the suitable habitat of cold-water corals and commercially important deep-sea fishes in the North Atlantic. *Glob. change Biol.* 26, 2181–2202.

Morrison, K. M., Meyer, H. K., Roberts, E. M., Rapp, H. T., Colaço, A., and Pham, C. K. (2020). The first cut is the deepest: trawl effects on a deep-sea sponge ground are pronounced four years on. *Front. Mar. Sci.* 7:1059. doi: 10.3389/fmars.2020.605281

Müller, W. A., Pohlmann, H., Sienz, F., and Smith, D. (2014). Decadal climate predictions for the period 1901–2010 with a coupled climate model. *Geophys. Res. Lett.* 41, 2100–2107. doi: 10.1002/2014GL059259

Murillo, F. J., Muñoz, P. D., Cristobo, J., Ríos, P., González, C., Kenchington, E., et al. (2012). Deep-sea sponge grounds of the flemish cap, flemish pass and the grand banks of newfoundland (Northwest Atlantic Ocean): distribution and species composition. *Mar. Biol. Res.* 8, 842–854. doi: 10.1080/17451000.2012.682583

Naumann, M. S., Orejas, C., and Ferrier-Pagès, C. (2014). Species-specific physiological response by the cold-water corals *Lophelia pertusa* and *Madrepora oculata* to variations within their natural temperature range. *Deep Sea Res. 2 Top. Stud. Oceanogr.* 99, 36–41. doi: 10.1016/j.dsr2.2013.05.025

Oevelen, D. V., Duineveld, G., Lavaleye, M., Mienis, F., Soetaert, K., and Heip, C. H. (2009). The cold-water coral community as hotspot of carbon cycling on continental margins: a food-web analysis from Rockall Bank (northeast Atlantic). *Limnol. Oceanogr.* 54, 1829–1844. doi: 10.4319/lo.2009.54.6.1829

Olsen, A., Key, R. M., van Heuven, S., Lauvset, S. K., Velo, A., Lin, X., et al. (2016). The global ocean data analysis project version 2 (GLODAPv2) – an internally consistent data product for the world ocean. *Earth Syst. Sci. Data* 8, 297–323. doi: 10.5194/essd-8-297-2016

Pastor, M. V., Peña-Izquierdo, J., Pelegrí, J. L., and Marrero-Díaz, Á (2012). Meridional changes in water mass distributions off NW Africa during November 2007/2008. *Cienc. Mar.* 38, 223–244. doi: 10.7773/cm.v38i1b.1831

Payne, M. R., Barange, M., Cheung, W. W., MacKenzie, B. R., Batchelder, H. P., Cormon, X., et al. (2016). Uncertainties in projecting climate-change impacts in marine ecosystems. *ICES J. Mar. Sci.* 73, 1272–1282.

Pearman, T. R. R., Robert, K., Callaway, A., Hall, R., Iacono, C. L., and Huvenne, V. A. (2020). Improving the predictive capability of benthic species distribution models by incorporating oceanographic data–Towards holistic ecological modelling of a submarine canyon. *Prog. Oceanogr.* 184:102338.

Pecl, G. T., Araújo, M. B., Bell, J. D., Blanchard, J., Bonebrake, T. C., Chen, I. C., et al. (2017). Biodiversity redistribution under climate change: impacts on ecosystems and human well-being. *Science* 355:eaai9214.

Penny, S. G., Akella, S., Balmaseda, M. A., Browne, P., Carton, J. A., Chevallier, M., et al. (2019). Observational needs for improving ocean and coupled reanalysis, S2S prediction, and decadal prediction. *Front. Mar. Sci.* 6:391. doi: 10.3389/fmars.2019.00391

Perez, F. F., Fontela, M., García-Ibáñez, M. I., Mercier, H., Velo, A., Lherminier, P., et al. (2018). Meridional overturning circulation conveys fast acidification to the deep Atlantic Ocean. *Nature* 554, 515–518. doi: 10.1038/nature25493

Petrie, B., and Drinkwater, K. (1993). Temperature and salinity variability on the Scotian Shelf and in the Gulf of Maine 1945–1990. *J. Geophys. Res. Oceans* 98, 20079–20089. doi: 10.1029/93jc02191

Pham, C. K., Murillo, F. J., Lirette, C., Maldonado, M., Colaço, A., Ottaviani, D., et al. (2019). Removal of deep-sea sponges by bottom trawling in the Flemish Cap area: conservation, ecology and economic assessment. *Sci. Rep.* 9:15843.

Pickart, R. S. (1992). Water mass components of the North Atlantic deep western boundary current. *Deep Sea Res. A. Oceanogr. Res. Pap.* 39, 1553–1572. doi: 10.1016/0198-0149(92)90047-w

Pile, A. J., and Young, C. M. (2006). The natural diet of a hexactinellid sponge: benthic–pelagic coupling in a deep-sea microbial food web. *Deep Sea Res. 1 Oceanogr. Res. Pap.* 53, 1148–1156. doi: 10.1016/j.dsr.2006.03.008

Pohlmann, H., Mueller, W. A., Kulkarni, K., Kameswarrao, M., Matei, D., Vamborg, F. S. E., et al. (2013). Improved forecast skill in the tropics in the new MiKlip decadal climate predictions. *Geophys. Res. Lett.* 40, 5798–5802.

Polkova, I., Brune, S., Kadow, C., Romanova, V., Gollan, G., Baehr, J., et al. (2019). Initialization and ensemble generation for decadal climate predictions: a comparison of different methods. *J. Adv. Model. Earth Sys.* 11, 149–172. doi: 10.1029/2018MS001439

Pozo Buil, M., Jacox, M. G., Fiechter, J., Alexander, M. A., Bograd, S. J., Curchitser, E. N., et al. (2021). A dynamically downscaled ensemble of future projections for the California current system. *Front. Mar. Sci.* 8:324. doi: 10.3389/fmars.2021.612874

Puerta, P., Johnson, C., Carreiro-Silva, M., Henry, L. A., Kenchington, E., Morato, T., et al. (2020). Influence of water masses on the biodiversity and biogeography of deep-sea benthic ecosystems in the North Atlantic. *Front. Mar. Sci.* 7:239. doi: 10.3389/fmars.2020.00239

Purkey, S. G., and Johnson, G. C. (2010). Warming of global abyssal and deep Southern Ocean waters between the 1990s and 2000s: Contributions to global heat and sea level rise budgets. *Journal of Climate* 23, 6336–6351. doi: 10.1175/2010jcli3682.1

Rhein, M., Kieke, D., Hüttl-Kabus, S., Roessler, A., Mertens, C., Meissner, R., et al. (2011). Deep water formation, the subpolar gyre, and the meridional overturning circulation in the subpolar North Atlantic. *Deep Sea Res. 2 Top. Stud. Oceanogr.* 58, 1819–1832. doi: 10.1016/j.dsr2.2010.10.061

Ramiro-Sánchez, B., González-Irusta, J. M., Henry, L. A., Cleland, J., Yeo, I., Xavier, J. R., et al. (2019). Characterization and mapping of a deep-sea sponge ground on the tropic seamount (Northeast Tropical Atlantic): implications for spatial management in the high seas. *Front. Mar. Sci.* 6:278. doi: 10.3389/fmars.2019.00278

Riahi, K., Rao, S., Krey, V., Cho, C., Chirkov, V., Fischer, G., et al. (2011). RCP 8.5—A scenario of comparatively high greenhouse gas emissions. *Clim. Change* 109, 33–57. doi: 10.1007/s10584-011-0149-y

Rice, A. L., Thurston, M. H., and New, A. L. (1990). Dense aggregations of a hexactinellid sponge, Pheronema carpenteri, in the porcupine seabight (northeast Atlantic Ocean), and possible causes. *Prog. Oceanogr.* 24, 179–196. doi: 10.1016/0079-6611(90)90029-2

Ríos, P., Prado, E., Carvalho, F. C., Sánchez, F., Rodríguez-Basalo, A., Xavier, J. R., et al. (2020). Community composition and habitat characterization of a rock sponge aggregation (*Porifera, Corallistidae*) in the Cantabrian Sea. *Front. Mar. Sci.* 7:578. doi: 10.3389/fmars.2020.00578

Roark, E. B., Guilderson, T. P., Dunbar, R. B., Fallon, S. J., and Mucciarone, D. A. (2009). Extreme longevity in proteinaceous deep-sea corals. *Proc. Natl. Acad. Sci. U.S.A.* 106, 5204–5208. doi: 10.1073/pnas.0810875106

Roberts, E. M., Mienis, F., Rapp, H. T., Hanz, U., Meyer, H. K., and Davies, A. J. (2018). Oceanographic setting and short-timescale environmental variability at an Arctic seamount sponge ground. *Deep Sea Res. 1 Oceanogr. Res. Pap.* 138, 98–113. doi: 10.1016/j.dsr.2018.06.007

Roberts, E. M., Bowers, D. G., Meyer, H. K., Samuelsen, A., Rapp, H. T., and Cárdenas, P. (2021). Water masses constrain the distribution of deep-sea sponges in the North Atlantic Ocean and Nordic Seas. *Mar. Ecol. Prog. Ser.* 659, 75–96. doi: 10.3354/meps13570

Roberts, J. M., Wheeler, A. J., and Freiwald, A. (2006). Reefs of the deep: the biology and geology of cold-water coral ecosystems. *Science* 312, 543–547. doi: 10.1126/science.1119861

Rodríguez-Basalo, A., Prado, E., Sánchez, F., Ríos, P., Gómez-Ballesteros, M., and Cristobo, J. (2021). High resolution spatial distribution for the hexactinellid sponges *Asconema setubalense* and *Pheronema carpenteri* in the Central Cantabrian Sea. *Front. Mar. Sci.* 8:129. doi: 10.3389/fmars.2021.612761

Rudels, B. (1995). The thermohaline circulation of the Arctic Ocean and the Greenland Sea. *Philos. Trans. R. Soc. Lond. A* 352, 287–299. doi: 10.1098/rsta.1995.0071

Sakov, P., Counillon, F., Bertino, L., Lisæter, K. A., Oke, P. R., and Korablev, A. (2012). TOPAZ4: an ocean-sea ice data assimilation system for the North Atlantic and Arctic. *Ocean Sci.* 8, 633–656. doi: 10.5194/os-8-633-2012

Samuelsen, A., Hansen, C., and Wehde, H. (2015). Tuning and assessment of the HYCOM-NORWECOM V2. 1 biogeochemical modeling system for the North Atlantic and Arctic oceans. *Geosci. Model Dev.* 8, 2187–2202.

Samuelsen, A., Schrum, C., Daewel, U., Castano-Primo, R., and Yumruktepe, V. Ç (2019). *SponGES Deliverable 7.6 - Report on Historic Climate and Ecosystem Data*. Berkeley, CA: National Energy Research Scientific Computing Center.

Sanders, H. L., and Hessler, R. R. (1969). Ecology of the deep-sea benthos. *Science* 163, 1419–1424.

Sarafanov, A. (2009). On the effect of the North Atlantic Oscillation on temperature and salinity of the subpolar North Atlantic intermediate and deep waters. *ICES J. Mar. Sci.* 66, 1448–1454. doi: 10.1093/icesjms/fsp094

Sasaki, H., Kida, S., Furue, R., Aiki, H., Komori, N., Masumoto, Y., et al. (2020). A global eddying hindcast ocean simulation with OFES2. *Geosci. Model Dev.* 13, 3319–3336. doi: 10.5194/gmd-13-3319-2020

Schubert-Frisius, M., and Feser, F. (2015). *Global High Resolution Climate Reconstruction with ECHAM6 using the spectral nudging technique, run by Helmholtz-Zentrum Geesthacht*. Hamburg: World Data Center for Climate.

Schulz, K., Soetaert, K., Mohn, C., Korte, L., Mienis, F., Duineveld, G., et al. (2020). Linking large-scale circulation patterns to the distribution of cold water corals along the eastern Rockall Bank (northeast Atlantic). *J. Mar. Syst.* 212:103456.

Schrum, C., Alekseeva, I., and John, M. S. (2006). Development of a coupled physical–biological ecosystem model ECOSMO: part I: model description and validation for the North Sea. *J. Mar. Syst.* 61, 79–99.

Séférian, R., Bopp, L., Gehlen, M., Swingedouw, D., Mignot, J., Guilyardi, E., et al. (2014). Multiyear predictability of tropical marine productivity. *Proc. Natl. Acad. Sci. U.S.A.* 111, 11646–11651. doi: 10.1073/pnas.1315855111

Smith, D. M., Eade, R., Scaife, A. A., Caron, L. P., Danabasoglu, G., DelSole, T. M., et al. (2019). Robust skill of decadal climate predictions. *NPJ Clim. Atmos. Sci.* 2:13.

Smith, K. L., Ruhl, H. A., Bett, B. J., Billett, D. S. M., Lampitt, R. S., and Kaufmann, R. S. (2009). Climate, carbon cycling, and deep-ocean ecosystems. *Proc. Natl. Acad. Sci. U.S.A.* 106, 19211–19218. doi: 10.1073/pnas.0908322106

Somot, S., Sevault, F., Déqué, M., and Crépon, M. (2008). 21st century climate change scenario for the Mediterranean using a coupled atmosphere–ocean regional climate model. *Glob. Planet. Change* 63, 112–126. doi: 10.1016/j.gloplacha.2007.10.003

Stramma, L., Schmidtko, S., Levin, L. A., and Johnson, G. C. (2010). Ocean oxygen minima expansions and their biological impacts. *Deep Sea Res. 1 Oceanogr. Res. Pap.* 57, 587–595. doi: 10.1016/j.dsr.2010.01.005

Strand, R., Whalan, S., Webster, N. S., Kutti, T., Fang, J. K. H., Luter, H. M., et al. (2017). The response of a boreal deep-sea sponge holobiont to acute thermal stress. *Sci. Rep.* 7:1660.

Sweetman, A. K., Thurber, A. R., Smith, C. R., Levin, L. A., Mora, C., Wei, C. L., et al. (2017). Major impacts of climate change on deep-sea benthic ecosystems. *Elementa* 4:5.

Swift, J. H., and Koltermann, K. P. (1988). The origin of Norwegian Sea deep water. *J. Geophys. Res. Oceans* 93, 3563–3569. doi: 10.1029/jc093ic04p03563

Tabachnick, K. R., and Menshenina, L. L. (2007). Revision of the genus Asconema (*Porifera*: *Hexactinellida: Rossellidae*). *J. Mar. Biol. Assoc. U.K.* 87, 1403–1429. doi: 10.1017/s0025315407058158

Tempera, F., Giacomello, E., Mitchell, N. C., Campos, A. S., Henriques, A. B., Bashmachnikov, I., et al. (2012). "Mapping condor seamount seafloor environment and associated biological assemblages (Azores, Ne Atlantic)," in *Proceedings of the Seafloor Geomorphology as Benthic Habitat*, (Amsterdam: Elsevier), 807–818. doi: 10.1016/b978-0-12-385140-6.00059-1

Tett, P., Droop, M. R., and Heaney, S. I. (1985). The Redfield ratio and phytoplankton growth rate. *J. Mar. Biol. Assoc. U.K.* 65, 487–504. doi: 10.1017/s0025315400050566

Tommasi, D., Stock, C. A., Hobday, A. J., Methot, R., Kaplan, I. C., Eveson, J. P., et al. (2017). Managing living marine resources in a dynamic environment: the role of seasonal to decadal climate forecasts. *Prog. Oceanogr.* 152, 15–49.

Turrell, W. R. (1992). New hypotheses concerning the circulation of the northern North Sea and its relation to North Sea fish stock recruitment. *ICES J. Mar. Sci.* 49, 107–123. doi: 10.1093/icesjms/49.1.107

Vacelet, J., and Custódio, M. R. (2007). Diversity and evolution of deep-sea carnivorous sponges. Porifera research: biodiversity, innovation and sustainability. *Série Livros* 28, 107–115.

van Soest, R. W., Cleary, D. F., de Kluijver, M. J., Lavaleye, M. S., Maier, C., and van Duyl, F. C. (2007). Sponge diversity and community composition in Irish bathyal coral reefs. *Contrib. Zool.* 76, 121–142. doi: 10.1163/18759866-07602005

Van Vuuren, D. P., Edmonds, J., Kainuma, M., Riahi, K., Thomson, A., Hibbard, K., et al. (2011). The representative concentration pathways: an overview. *Clim. Change* 109, 5–31. doi: 10.1007/s10584-011-0148-z

Vaquer-Sunyer, R., and Duarte, C. M. (2008). Thresholds of hypoxia for marine biodiversity. *Proc. Natl. Acad. Sci. U.S.A.* 105, 15452–15457. doi: 10.1073/pnas.0803833105

Willmott, C. J., and Matsuura, K. (2005). Advantages of the mean absolute error (MAE) over the root mean square error (RMSE) in assessing average model performance. *Clim. Res.* 30, 79–82. doi: 10.3354/cr030079

Winther, N. G., and Evensen, G. (2006). A hybrid coordinate ocean model for shelf sea simulation. *Ocean Model.* 13, 221–237. doi: 10.1016/j.ocemod.2006.01.004

Witte, U., and Graf, G. (1996). Metabolism of deep-sea sponges in the Greenland-Norwegian Sea. *J. Exp. Mar. Biol. Ecol.* 198, 223–235. doi: 10.1016/0022-0981(96)00006-8

Woulds, C., Cowie, G. L., Levin, L. A., Andersson, J. H., Middelburg, J. J., Vandewiele, S., et al. (2007). Oxygen as a control on sea floor biological communities and their roles in sedimentary carbon cycling. *Limnol. Oceanogr.* 52, 1698–1709.

Xavier, J., and van Soest, R. (2007). Demosponge fauna of Ormonde and Gettysburg Seamounts (Gorringe Bank, north-east Atlantic): diversity and zoogeographical affinities. *J. Mar. Biol. Assoc. U.K.* 87, 1643–1653. doi: 10.1017/s0025315407058584

Xavier, J. R., Tojeira, I., and Van Soest, R. W. (2015). On a hexactinellid sponge aggregation at the Great Meteor seamount (North-east Atlantic). *J. Mar. Biol. Assoc. U.K.* 95, 1389–1394.

Yasuhara, M., Cronin, T. M., Demenocal, P. B., Okahashi, H., and Linsley, B. K. (2008). Abrupt climate change and collapse of deep-sea ecosystems. *Proc. Natl. Acad. Sci. U.S.A.* 105, 1556–1560. doi: 10.1073/pnas.0705486105

Yasuhara, M., Okahashi, H., Cronin, T. M., Rasmussen, T. L., and Hunt, G. (2014). Response of deep-sea biodiversity to abrupt deglacial and H olocene climate changes in the N orth A tlantic O cean. *Glob. Ecol. Biogeogr.* 23, 957–967. doi: 10.1111/geb.12178

Yasuhara, M., and Danovaro, R. (2016). Temperature impacts on deep-sea biodiversity. *Biol. Rev.* 91, 275–287.

Yasuhara, M., Doi, H., Wei, C. L., Danovaro, R., and Myhre, S. E. (2016). Biodiversity–ecosystem functioning relationships in long-term time series and palaeoecological records: deep sea as a test bed. *Philos. Trans. R. Soc. B Biol. Sci.* 371:20150282.

Conflict of Interest: The authors declare that the research was conducted in the absence of any commercial or financial relationships that could be construed as a potential conflict of interest.

Publisher's Note: All claims expressed in this article are solely those of the authors and do not necessarily represent those of their affiliated organizations, or those of the publisher, the editors and the reviewers. Any product that may be evaluated in this article, or claim that may be made by its manufacturer, is not guaranteed or endorsed by the publisher.

Copyright © 2021 Liu, Daewel, Samuelsen, Brune, Hanz, Pohlmann, Baehr and Schrum. This is an open-access article distributed under the terms of the Creative Commons Attribution License (CC BY). The use, distribution or reproduction in other forums is permitted, provided the original author(s) and the copyright owner(s) are credited and that the original publication in this journal is cited, in accordance with accepted academic practice. No use, distribution or reproduction is permitted which does not comply with these terms.

frontiers in Marine Science

ORIGINAL RESEARCH
published: 24 March 2022
doi: 10.3389/fmars.2022.737164

Environmental Change at Deep-Sea Sponge Habitats Over the Last Half Century: A Model Hindcast Study for the Age of Anthropogenic Climate Change

Annette Samuelsen[1], Corinna Schrum[2,3], Veli Çağlar Yumruktepe[1], Ute Daewel[2] and Emyr Martyn Roberts[4†]*

[1] Nansen Environmental and Remote Sensing Centre, Bjerknes Centre for Climate Research, Bergen, Norway, [2] Institute of Coastal Systems Analysis and Modelling, Helmholtz-Zentrum Hereon, Geesthacht, Germany, [3] Institute of Oceanography, CEN, Universität Hamburg, Hamburg, Germany, [4] Department of Biological Sciences, University of Bergen, Bergen, Norway

OPEN ACCESS

Edited by:
Jose Angel Alvarez Perez, Universidade do Vale do Itajaí, Brazil

Reviewed by:
Dorte Janussen, Senckenberg Museum, Germany
Julian Mariano Burgos, Marine and Freshwater Research Institute, Iceland

***Correspondence:**
Annette Samuelsen
annette.samuelsen@nersc.no

†Present address:
Emyr Martyn Roberts, School of Ocean Sciences, Bangor University, Menai Bridge, United Kingdom

Specialty section:
This article was submitted to Deep-Sea Environments and Ecology, a section of the journal Frontiers in Marine Science

Received: *06 July 2021*
Accepted: *21 February 2022*
Published: *24 March 2022*

Citation:
Samuelsen A, Schrum C, Yumruktepe VÇ, Daewel U and Roberts EM (2022) Environmental Change at Deep-Sea Sponge Habitats Over the Last Half Century: A Model Hindcast Study for the Age of Anthropogenic Climate Change. Front. Mar. Sci. 9:737164. doi: 10.3389/fmars.2022.737164

Deep-sea sponges inhabit multiple areas of the deep North Atlantic at depths below 250 m. Living in the deep ocean, where environmental properties below the permanent thermocline generally change slowly, they may not easily acclimatize to abrupt changes in the environment. Until now consistent monitoring timeseries of the environment at deep sea sponge habitats are missing. Therefore, long-term simulation with coupled bio-physical models can shed light on the changes in environmental conditions sponges are exposed to. To investigate the variability of North Atlantic sponge habitats for the past half century, the deep-sea conditions have been simulated with a 67-year model hindcast from 1948 to 2014. The hindcast was generated using the ocean general circulation model HYCOM, coupled to the biogeochemical model ECOSMO. The model was validated at known sponge habitats with available observations of hydrography and nutrients from the deep ocean to evaluate the biases, errors, and drift in the model. Knowing the biases and uncertainties we proceed to study the longer-term (monthly to multi-decadal) environmental variability at selected sponge habitats in the North Atlantic and Arctic Ocean. On these timescales, these deep sponge habitats generally exhibit small variability in the water-mass properties. Three of the sponge habitats, the Flemish Cap, East Greenland Shelf and North Norwegian Shelf, had fluctuations of temperature and salinity in 4–6 year periods that indicate the dominance of different water masses during these periods. The fourth sponge habitat, the Reykjanes Ridge, showed a gradual warming of about 0.4°C over the simulation period. The flux of organic matter to the sea floor had a large interannual variability, that, compared to the 67-year mean, was larger than the variability of primary production in the surface waters. Lateral circulation is therefore likely an important control mechanism for the influx of organic material to the sponge habitats. Simulated oxygen varies interannually by less than 1.5 ml/l and none of the sponge habitats studied had oxygen concentrations below hypoxic

levels. The present study establishes a baseline for the recent past deep conditions that future changes in deep sea conditions from observations and climate models can be evaluated against.

Keywords: water masses, biogeochemistry, hydrography, ocean modeling, North Atlantic, decadal variability, deep-sea sponges

INTRODUCTION

Deep-sea sponges are found globally in a range of settings, such as fjords, continental shelf edges/slopes, mid-ocean ridges, and seamounts (Cárdenas and Rapp, 2015; Roberts et al., 2018; Kazanidis et al., 2019; Meyer et al., 2020). They also occur across a wide depth range, through the mesopelagic and bathyal zones and even at abyssal and hadal depths (Vacelet, 2007; Hestetun et al., 2019). The numerous known sponge-dominated communities spread throughout the North Atlantic Ocean include boreo-Arctic astrophorid grounds (Klitgaard and Tendal, 2004; Murillo et al., 2012; Cárdenas et al., 2013; Knudby et al., 2013; Roberts et al., 2018): multispecific assemblages of large astrophorid species and/or glass sponges (Hexactinellida), which are often further classified as either boreal (e.g., off the Faroe Islands, Norway, South of Iceland, the Labrador and Newfoundland shelves, and parts of Davis Strait) or cold-water grounds (e.g., north of Iceland, the Denmark Strait, off East Greenland, and north of Svalbard). There are also monospecific aggregations of glass sponges (Rice et al., 1990; Dohrmann et al., 2012; Beazley et al., 2021; Rodríguez-Basalo et al., 2021), such as *Pheronema carpenteri* (e.g., along the European and northwest African continental shelves and slopes, and off the Azores archipelago), *Nodastrella asconemaoida* (Rockall Bank, west of Ireland), *Asconema setubalense* (Le Danois Bank, Cantabrian Sea), and *Vazella pourtalesi* (Scotian Shelf, Canada). Beyond these ground types, there are also sponge-dominated communities of variable species diversity, composition, density and patchiness, which do not fall neatly into the above categories (e.g., sponge gardens found in the Aviles Canyon of the Cantabrian Sea, on the seamounts of the Azores archipelago, and on the New England seamounts).

Deep-sea sponges are presently the subject of much scientific interest, owing to the realization that sponges and sponge-dominated ecosystems provide a multitude of important goods and services (Hogg et al., 2010). They are known to play a key role in habitat provision (Bett and Rice, 1992; Hawkes et al., 2019), acting as ecosystem engineers and sustaining hotspots of biomass and biodiversity (Klitgaard, 1995; Beazley et al., 2013). They are also a significant biotechnological and biomedical resource: their secondary metabolites are a promising source of bioactive compounds and their structures have inspired biomimetic research (Belarbi, 2003; Sundar et al., 2003; Leal et al., 2012; Dudik et al., 2018). Sponges, and particularly dense ground aggregations, are also likely to be of fundamental importance to biogeochemical cycling, benthic-pelagic coupling, and carbon and silicon sequestration in the deep sea (Pile and Young, 2006; Bell, 2008; Bart et al., 2021).

Deep-sea sponges are known to be vulnerable to the direct and indirect effects of physical disturbance, for example from bottom trawling (Morrison et al., 2020; Wurz et al., 2021), and deep-sea sponge grounds have been classified as a "habitat under immediate threat and/or decline" by the OSPAR Commission (OSPAR Commission, 2008) and a "vulnerable marine ecosystem (VME)" by the Food and Agriculture Organization of the United Nations (FAO, 2009). Since certain deep-sea sponge species can be very slow-growing (Pusceddu et al., 2014), reproduce infrequently (Klitgaard and Tendal, 2004), and take millennia to form grounds (Murillo et al., 2016), it is often inferred that sponges may also be vulnerable to other environmental change (Hogg et al., 2010). There is concern in the deep-sea research community around changes occurring because of anthropogenic activities and potentially moving beyond the limits of past natural variability. Relatively little is known still about deep-sea sponge sensitivities to environmental fluctuations and more persistent trends under climate change (Maldonado, 2006; Bell, 2008).

Recent studies have been able to characterize present-day environmental conditions and short timescale (sub-hourly to seasonal) variability inside sponge grounds from *in situ* measurements (e.g., Roberts et al., 2018; Davison et al., 2019; Hanz et al., 2021a,b). Two studies, focused on different sponge grounds in the Northwest Atlantic, have demonstrated that some sponge populations may have persisted in the face of considerable past environmental variability over longer timescales (centuries to millennia) (Murillo et al., 2016; Beazley et al., 2018). Looking forward in time, Beazley et al. (2021) used a species distribution modeling approach, together with predicted environmental conditions from a North Atlantic Ocean model, to project changes in sponge (*Vazella pourtalesi*) suitable habitat into the future (2046–2065), with potential positive and negative impacts of climate change being identified.

Despite such progress, very few long timeseries of the physical and biogeochemical conditions, to which deep-sea sponges have been exposed, exist. In particular, environmental trends and variability over the past 60–70 years of climate change (Hansen et al., 2011) have not been adequately quantified across a broad range of oceanographic regions in areas of relevance to deep-sea sponges. Characterizing this period at key sites is necessary to (1) understand how present day observations relate to conditions and change experienced by sponges in the recent past, and (2) adequately parameterize studies of sponge sensitivity to the future environmental change likely under sustained climate change (Bindoff et al., 2019).

To shed light on the deep-sea environmental variability of recent decades and provide a longer-term (1948–2014) dataset of physical and biogeochemical variables at various deep-sea

sponge habitats in the North Atlantic/Arctic Ocean, a coupled physical-biological model, HYCOM-ECOSMO, has been used. The 67-year model simulation was interrogated to identify long-term changes or large interannual variability in physical and biogeochemical variables at four mid- to high latitude areas known to host dense sponge habitats: Flemish Cap (FLC), Reykjanes Ridge (RYR), North Norwegian Shelf (NNS) and the East Greenland Shelf (EGS). Statistical analyses of the extracted, site-specific environmental timeseries are presented and discussed considering whether present conditions have changed beyond the historical range of variability.

MATERIALS AND METHODS

The coupled physical-biological model, HYCOM-ECOSMO, was used to simulate environmental variability at various deep-sea sponge habitats in the North Atlantic/Arctic Ocean over the period 1948–2014. The hybrid coordinates of the physical model, HYCOM (Bleck, 2002), allow for good vertical resolution in the upper layer for adequately representing the surface mixed layer as well as resolving the vertical structure of light-dependent biogeochemical processes in the photic zone, and density-following coordinates provide good water mass conservation in the deep sea (Ross et al., 2016). The biogeochemical model, ECOSMO (Daewel and Schrum, 2013; Yumruktepe et al., 2021), includes the main phytoplankton functional types for the North Atlantic Ocean, nutrients, and a single layer of sediments with parameterizations for settling, resuspension and burial (when sediment can no longer be resuspended). The coupled model therefore lends itself to investigating interactions between physical and biogeochemical variables and to simulating the deep-sea environment, and it can be applied in studies of relevance to deep-sea organisms, including sponges (as in the present work). Using three different *in situ* datasets the model was evaluated with respect to deep-sea water masses above sponge habitats, where observations were available. The evaluation of the model fields is presented in a separate report (Samuelsen et al., 2019), but relevant results are also included in this paper.

ECOSMO is coupled online, such that the transport (mixing and advection) of the biogeochemical model compartments is done as a part of the HYCOM tracer-transport routines and the time stepping of the two models is aligned. The physical fields influence the results of the biogeochemical model through currents, temperature, and salinity, but there is no feedback from the ECOSMO to HYCOM.

Physical Model

HYCOM (Bleck, 2002) is an ocean model with hybrid vertical coordinates, which means it has the option to use a combination of depth-level coordinates (z-level), topography-following coordinates and density-following (isopycnal) coordinates. In the present setup (Samuelsen et al., 2015), we use a combination of z-levels in the upper ocean and mixed layer and isopycnal levels in the deep, stratified ocean. Consequently, changes in the deep ocean density fields, results in a changed distribution of vertical layers. Isopycnal levels facilitate good conservation of water-mass and tracer properties in the deep ocean, which can be considered an advantage for a simulation focusing on sponge habitat at depth. The upper 5 layers are fixed as z-level coordinates, this ensures that the vertical resolution of the upper ocean is maintained, which is important for simulating the gradient of sunlight in the upper ocean when computing primary production. The model system also includes a sea ice model (Drange and Simonsen, 1996). It is based on the elastic-viscous-plastic rheology (EVP: Hunke and Dukowicz, 1997) and is well tested for our study area (e.g., Xie et al., 2016).

Biogeochemical Model

ECOSMO, is a medium complexity biogeochemical model (**Figure 1**). The version used here, ECOSMO II(CHL) (Yumruktepe et al., 2021), resolves four nutrients (nitrate, phosphate, silicate and ammonium), two types of phytoplankton functional groups (diatoms and flagellates) as well as two classes of zooplankton functional groups (herbi- and omnivorous). In addition, state variables for both particulate and dissolved organic material, and oxygen are included. The model uses constant element ratios consistent with the classical Redfield stoichiometry. The three nutrients nitrate, phosphate, and silicate are also tracked in the bottom sediments using simplified 0d bulk parametrizations for sedimentation, resuspension, and remineralization in the sediment layer. Due to their different reactions inside the sediment, the nutrients are separated into three separate sediment pools. The biogeochemical model has been described in detail in Daewel and Schrum (2013), hereafter referred to as DS2013. In the present study, the model is coupled to a different physical model and additional modification of the model configuration and parameterization are applied to make the model suitable for the area and the research question (Yumruktepe et al., 2021). The changes are further explained in the following.

Among other changes, chlorophyll has been added as a prognostic model compartment. The formulation followed Bagniewski et al. (2011) and the equations for the prognostic state variable for chlorophyll within each phytoplankton type is as follows:

$$\frac{\partial \mathrm{Chl_P}}{\partial \mathrm{t}} = \rho_P \mu_\mathrm{P} \mathrm{P} - \sum_{\mathrm{i}=1}^{2} \mathrm{g_i} \left(\mathrm{Chl_P}\right) \mathrm{Z_i} - \mathrm{m_P Chl_P}$$

Here Chl_P is the chlorophyll content of the phytoplankton functional type, where subscript P either represents flagellates or diatoms. The local growth rate of the phytoplankton type is represented by μ_P and P is phytoplankton concentration, either flagellates or diatoms. In the summation symbol i = 1,2 specifies the two zooplankton types (Z_i) and g_i is the zooplankton grazing rate. In the last term m_P is the phytoplankton mortality rate. The phytoplankton-specific photo-acclimation factor, ρ_P, is formulated as follows:

$$\rho_P = \frac{\theta_\mathrm{P}^{\max} \mu_\mathrm{P} \mathrm{P}}{\alpha_\mathrm{P} \mathrm{PAR}\ \mathrm{Chl}_P}$$

where θ_P^{max} is the maximum chlorophyll-to-carbon ratio, α_P is the initial slope of the photosynthesis-irradiance curve, and

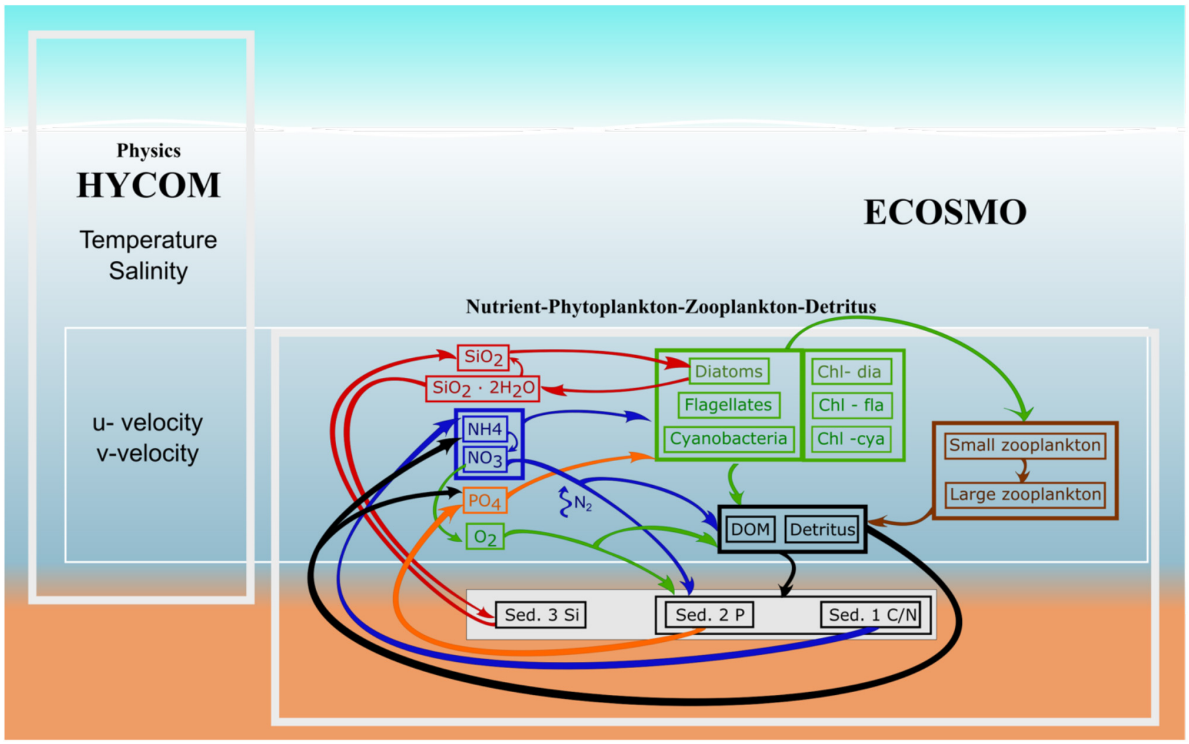

FIGURE 1 | ECOSMO flow chart, showing the model variables and their interactions with each other. The three sediments are Sed. 1, particulate organic sediment, Sed. 2, Iron bound phosphorous, and Sed. 3, the silicate sediment pool.

PAR is the photosynthetically active radiation. The local ratio is then computed at each time-step taking into account the local irradiance and the predefined range of chlorophyll-to-carbon ratios (given in **Table 1**). The model then integrates this into the phytoplankton growth and loss terms. With these equations, the model chlorophyll is decoupled from the carbon concentrations, and the chlorophyll-to-carbon ratio can vary with depth, regionally, and seasonally. For example, the model chlorophyll adapts to higher light exposure in summer periods by decreasing the chlorophyll-to-carbon ratio. All parameter values are the same as in Bagniewski et al. (2011), who optimized the model parameters for a site in the North Atlantic. They use a nitrogen-based model, therefore the parameters adopted for chlorophyll_a equations are converted to carbon-units following the classical Redfield stoichiometry.

The physical model typically has a large influence on the results of biogeochemical models (Skogen and Moll, 2005) and these models often require retuning to produce comparable results after being coupled to a new physical model when used in a different model setup or, more importantly, run for a different region. Therefore, some parameters needed adjustment as part of a tuning that occurred after coupling ECOSMO to HYCOM and changing the modeled region from the North Sea and Baltic Sea to open ocean North Atlantic (**Table 2**). Some additional changes were implemented in the model after evaluating the

TABLE 1 | Parameters used in the flexible Chl/C-ratio formulation.

Parameter name	Value	Unit
Maximum chlorophyll-to-carbon ratio for diatoms	0.037	mg Chl/mg C
Minimum chlorophyll-to-carbon ratio for diatoms	0.0063	mg Chl/mg C
Maximum chlorophyll-to-carbon ratio for flagellates	0.048	mg Chl/mg C
Minimum chlorophyll-to-carbon ratio for flagellates	0.0063	mg Chl/mg C

TABLE 2 | The ECOSMO model parameters that have been tuned for HYCOM-ECOSMO compared to those in Daewel and Schrum (2013).

Parameter description	Value	DS2013 value	Unit
Maximum growth rate for diatoms	1.95	1.3	1/day
Maximum growth rate for flagellates	1.65	1.1	1/day
Phytopl. self-shading*	0.041	0.03	m^2/mg Chl (m^2/mmolN)
Grazing rate mesozoopl. on diatoms	1.2	0.8	1/day
Grazing rate microzoopl. on flagellates	1.5	1.0	1/day
Grazing rate mesozoopl. on microzoopl.	0.75	0.5	1/day
Mesozoopl. mortality rate	0.2	0.1	1/day
Microzoopl. mortality rate	0.4	0.2	1/day
Detritus sedimentation rate	5.0	3.5	m/day
Opal sinking rate	10.0	5.0	m/day

**The phytoplankton self-shading was originally a function of phytoplankton biomass, but in the present model it is a function of chlorophyll.*

result in the lower layers and the sediments. The denitrification rate for sediments was modeled with an exponential temperature dependence in DS2013, where the function worked well because the original model only covered the North Sea and Baltic Sea with only moderate temperature variations among the regions. However, when the model encompasses both the equator and the Arctic, the modeled difference in denitrification rates between the coldest and the warmest region is up to two orders of magnitude (**Figure 2**). To reduce the difference in denitrification between warm and cold regions, the denitrification rate is now also a function of latitude and temperature, such that the temperature at which this process works at medium efficiency decreases with latitude, while the direct temperature dependency is weaker than in the original model formulation.

The original formulation for temperature-dependence is as follows:

$$Temperature_dependence_{DS2013} = \exp(0.15 \cdot T)$$

The modified equation is as follows:

$$Temperature_dependence = 1 + 20\frac{T^2}{(0.25 * lat + 25)^2 + T^2}$$

A comparison of the two formulations is illustrated in **Figure 2**.

The model did in some cases accumulate large amounts of sediments on the bottom. DS2013 employs a constant burial rate; we have changed this to a burial rate that is dependent on the amount of sediment, that is when there is more sediment present, the burial rate is higher. Sediments are resuspended when the bottom stress is above a certain threshold of 0.007 N/m^2. The resuspended material is distributed over one or more of the deepest model layers, the criteria being that the layer depths must add up to at least 5 m. This is necessary since the isopycnal layer depths are variable and can range from centimeters to hundreds of meters.

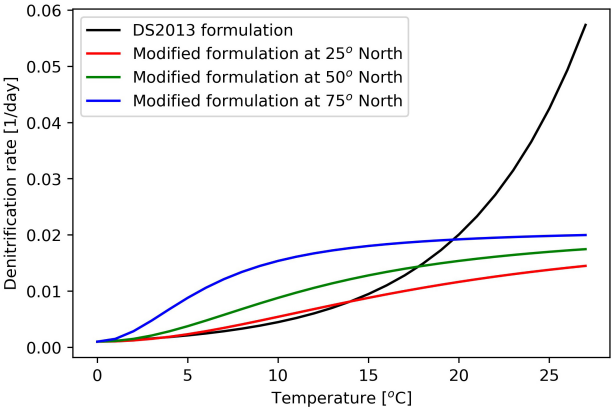

FIGURE 2 | Comparison of original and new formulation for denitrification.

Model Simulation Configuration: Region and Forcing

The simulation was done on a relatively coarse grid that varies between 30 and 70 km and has the highest resolution in mid-latitude in the North Atlantic. Although higher resolution has been shown previously to give better results with respect to nutrients (Samuelsen et al., 2015), the coarse resolution was chosen to make the long-term run feasible computationally and to allow for testing the model with different biogeochemical parameters.

In order to have consistent atmospheric forcing at a reasonable resolution a global high-resolution climate reconstruction based on the atmospheric model ECHAM6 was chosen (Schubert-Frisius and Feser, 2015). This dataset is publicly available and can be downloaded (after registration). The temporal resolution is 1 h, but this was reduced to a 6-h resolution for the dataset that was used to force this model. The dataset has a resolution of about 50 km and surface winds, air temperature, dew-point temperature as well as cloud coverage and precipitation were used to force the physical model. The biogeochemical model also requires input of the part of the short-wave radiation that enters the water column.

River runoff is modeled using a hydrological model, TRIP (Oki and Sud, 1998). The resulting river forcing is a monthly climatology. Hence, this simulation does not include any interannual variability in the river runoff. The river runoff affects the sea water salinity, the river temperature is not included as a forcing in this model. River nutrient loads are derived from the model dataset GlobalNEWS (Mayorga et al., 2010; Seitzinger et al., 2010). Annual discharges of nitrate, phosphate and silicate from different river basins, were used to construct the nutrient river load to force the model. The nutrient loads were scaled by the volume flux of runoff from TRIP, constructing a monthly climatology of nutrient loads.

The model was initialized from climatology, the physical model was spun up from rest and with density fields initialized from climatological values from the Generalized Digital Environment Model (GDEM: Carnes, 2009) fields for temperature and salinity. Initially the physical model was forced with climatological atmospheric forcing for 5 years, and then the model was run for another 4 years with the real-time data from 1948 to the end of 1951, this was repeated 4 times adding up to a total of 21 year spin up for the physical model. The biogeochemical model was initialized from climatology, World Ocean Atlas 2013 for nitrate, phosphate, silicate (Garcia et al., 2013a) and oxygen (Garcia et al., 2013b), while the other biogeochemical variables were initialized from constant low levels. ECOSMO was initialized in the second round of running the model from 1948 to 1951 and in total ECOSMO was spun up for 12 years before initializing the run that is analyzed here.

The sea surface temperature of the model was relaxed toward climatological temperature with a relaxation time scale of 200 days. Furthermore, the boundaries of the model domain that are located between zero and 30 degrees south of the equator, the entrance of the Mediterranean and the Bering Strait were relaxed toward the climatology of temperature, salinity, nitrate, phosphate, silicate and oxygen. Relaxation is strongest at the outer grid cell and is gradually decreased toward the interior of the model over 20 grid cells and the relaxation time scale on

the outermost grid cell is 20 days. The climatological datasets used for relaxation are the same as those used for initialization. All the deep-sea variables of the dataset were extracted 1 m above the sea floor.

Validation Dataset

Three datasets were used to evaluate the quality of the model simulation. The first dataset was collected by the Norwegian Institute of Marine Research and contains nutrients, oxygen and pigments from the areas surrounding Norway (Institute of Marine Research, 2018). The dataset can be accessed via the Norwegian Marine Data Centre (NMDC)[1] and include observations from 1980 to 2017. The second dataset was downloaded from the World Ocean Database.[2] This dataset contains numerous observations of salinity and temperature from both CTDs and XBTs, and in addition this dataset contains some oxygen observations. Finally, the dataset GLODAPv2 Bottle data (Olsen et al., 2016) was used, this dataset contains nutrients, hydrography and variables related to carbon chemistry. The three datasets are hereafter referred to as NMDC, WOD, and GLODAP. Very few observations are obtained immediately above the bottom, to only evaluate the deepest water masses, only observations collocating with the deepest layer of the model was included in the validation.

Study Site

In this work, we have focused on regions known to host suitable habitat for sponges of the family Geodiidae, which are often a key constituent of boreo-Arctic-type sponge grounds (Klitgaard and Tendal, 2004; Cárdenas et al., 2013) and which are emerging as being amongst the more studied deep-sea sponges with better known distributions. We have selected areas corresponding to four of the study sites identified in Roberts et al. (2021a) and focused our investigation of interannual variability on these known sponge habitats. The regions are the Flemish Cap (FLC) off the east coast of North America, the Reykjanes Ridge (RYR) to the south of Iceland, the North Norwegian Shelf (NNS) off the coast of Norway and the East Greenland Shelf (EGS) off the northeast coast of Greenland (**Figure 3**). These sponge habitats were selected because they represent good geographical coverage of the North Atlantic and a diversity of hydrographic settings. They are also far enough away from the lateral boundaries of the model domain to not be directly influenced by the relaxation to climatology, and in three cases (FLC, RYR, and NNS) hydrographic observations were available with which to evaluate model performance.

The Flemish Cap is a shallow bank off the continental shelf of eastern Canada. It is about 200 km across and at the shallowest it is about 150 m. The deep-sea sponge community composition in the area is typically of boreal type, being dominated by astrophorids (*Geodia* spp., including *Geodia atlantica*, *Geodia barretti*, *Geodia macandrewii*, *Geodia phlegraei*) and *Asconema* sp., although some colder-water species are found at greater depths. The largest concentrations of sponges are found along the slopes of the bank (Murillo et al., 2012). The water masses at FLC consist of Labrador Current Slope Water (LCSW) with temperature of 3–4°C and salinities of 34–35 and Atlantic Water coming from the south from the North Atlantic Current, typically warmer than 4°C and with salinities greater than 34.8 (Colbourne and Foote, 2000).

The Reykjanes Ridge is located to the south of Iceland and is a part of the mid-Atlantic ridge. The landscape is rocky ground (although soft substrata also occur) and the depth ranges from about 500 to 2,000 m. The water masses at intermediate depth at RYR include Subpolar Mode Water which is about 6°C in the RYR area, and is characterized by high oxygen levels because of its recent contact with the atmosphere (Petit, 2018). There is also Labrador Sea Water with temperature around 3°C and salinities around 34.8 (Fröb et al., 2018) and in deeper layers dense (> 27.8 kg m^{-3}) and saline (> 34.98) Iceland-Scotland Overflow Water (ISOW) originally formed by deep convection (Petit, 2018) and a mix of ISOW and the overlying Atlantic water known as Icelandic Slope Water (Yashayaev et al., 2007). Sponge communities at RYR are characterized by demosponges of the genera *Geodia* and *Phakellia*, together with *Poecillastra compressa*, and by hexactinellids such as *Aphrocallistes beatrix* and *Asconema* spp. (Copley et al., 1996; Kuznetsov and Detinova, 2001; Cárdenas and Rapp, 2015). Whilst the sponge communities at RYR are also largely boreal in type, being dominated by, for example, *G. atlantica*, *G. barretti*, *G. macandrewii*, *G. phlegraei*, the occurrence of strict Arctic species (*Geodia hentscheli*, *Stelletta rhaphidiophora*) is reported, likely because of the influence of Iceland-Scotland Overflow Water along the flanks of the ridge (Cárdenas and Rapp, 2015).

In the offshore area of the North Norwegian Shelf upper water masses are North Atlantic Water and Norwegian Coastal Water, typically separated by being above and below salinity of 35.0. The water on the continental shelf edge (200–300 m) is primarily North Atlantic Water, typically in the range 6–8°C with the warmest temperatures in the fall (Skarðhamar et al., 2005). In the deeper layers there are Norwegian Sea Arctic Intermediate Water of 0.5 to –0.5°C and Norwegian Sea Deep Water ($<$ –0.5°C) (Buhl-Mortensen et al., 2012). The depth in this region ranges from 100 to 3,000 m. Sponge grounds in this area are of boreal type and are dominated by assemblages of astrophorids (genera *Geodia*, *Stryphnus*, and *Stelletta*) (Buhl-Mortensen et al., 2009; Hogg et al., 2010).

The East Greenland Shelf is the shallowest of the regions we are investigating, located mostly on the shelf off northeast Greenland, with a maximum depth of about 800 m. The region is covered by sea ice most of the year and therefore has low primary production. The water masses are Polar Surface Water exiting the Arctic, about –1°C, and salinity as low as 30 on the surface and increasing to 34.5 toward the bottom (de Steur et al., 2009). The area can also be influenced by recirculating Atlantic water from the Fram Strait (Rudels et al., 2002). Sponge assemblages in this region are of Arctic, or cold-water, type, and are composed of the tetractinellids *G. hentscheli*, *G. parva*, *S. rhapidiophora* and *Thenea valdiviae*, together with the hexactinellids *Schaudinnia rosea*, *Trichasterina borealis*, *Scyphidium septentrionale*, and *Asconema foliatum* (Klitgaard and Tendal, 2004).

[1] http://prod1.nmdc.no/UserInterface/#/

[2] https://www.nodc.noaa.gov/OC5/WOD/pr_wod.html

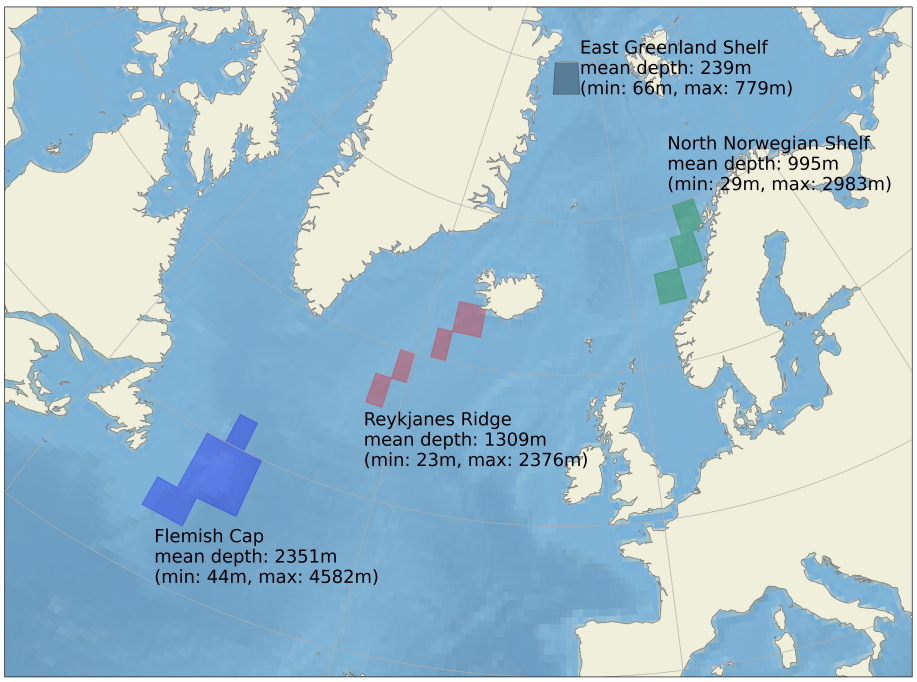

FIGURE 3 | The four areas of sponge habitat that are the focus of this paper. The minimum, maximum and mean depth for each study site based on the model bathymetry, are shown together with the geographical extent.

Time Series Extraction

From the original dataset of 0.1° resolution we constructed a monthly time series from each region by spatially averaging over each region (**Figure 1**), distinguishing between regions with bottom depth 200–700 m and areas deeper than 700 m. There was an increasing trend of both silicate and nitrate at all the sponge grounds investigated that have no corresponding trend in the observational datasets used (see model evaluation section below). Therefore we present the nitrate and silicate time series with the linear trend removed, retaining only the annual cycle and the interannual variability. Because of the relatively coarse grid used in the simulation, the depth given in **Figure 3**, which is extracted from the model bathymetry is not always consistent with the depths given in the literature for these sponge habitats.

RESULTS

Model Evaluation at the Selected Sponge Habitats

The region used for validating FLC is larger than the area used in this paper and stretches further north along the coast of Canada. There were more than 1,000 hydrographic observations from WOD which showed that the model had a warm bias of about 1°C and a salinity bias of 0.15. There was a limited number of observations from GLODAP that resulted in a similar temperature bias, but a smaller salinity bias of 0.05. A potential cause of this warm bias in this region is the late separation of the Gulf Stream which is a common problem in numerical ocean models (Ezer, 2016). In this region, the modeled oxygen ranged from 4.5 to 8 ml/l, but the observed oxygen was more stable, ranging between 5.5 and 6.5 ml/l. Silicate had a positive bias of about 3 mmol/m^3, phosphate a small negative bias and the simulated nitrate was overall very good. There were only about 50 nutrient observations available for the whole time period. At the RYR there were only about 50 hydrographical observations that yielded a cold bias of about 0.6°C and a salinity bias of only 0.03. The North Norwegian Shelf had the largest number of observations (> 2,500) of the three regions. The analysis yielded a fresh bias of 0.18 and a cold bias of 1.18°C. At the NNS the model produces a positive trend of all three nutrients that is not present in any of the datasets that we compare to. In the EGS we found no observations for model comparisons and thus cannot provide an evaluation of the model performance in this region. The error statistics FLC, RYR and NNS are summarized in **Supplementary Tables 1–3**, and an evaluation of the model applied to sponge habitats throughout the North Atlantic can be found in Samuelsen et al. (2019).

Mean Conditions and Annual Cycle

In the following we report on the areas, differentiating between areas where the bathymetry is between 200 and 700 m and deeper than 700 m. Areas with bathymetry above 200 m have not been analyzed. Where nothing else is stated, the main value given is from the upper region and the number in parentheses is from the deeper region. These deeper areas are characterized by relatively stable conditions year-round. However, clear annual cycles still emerge (**Supplementary Figures 1–4**). The three mid-latitude

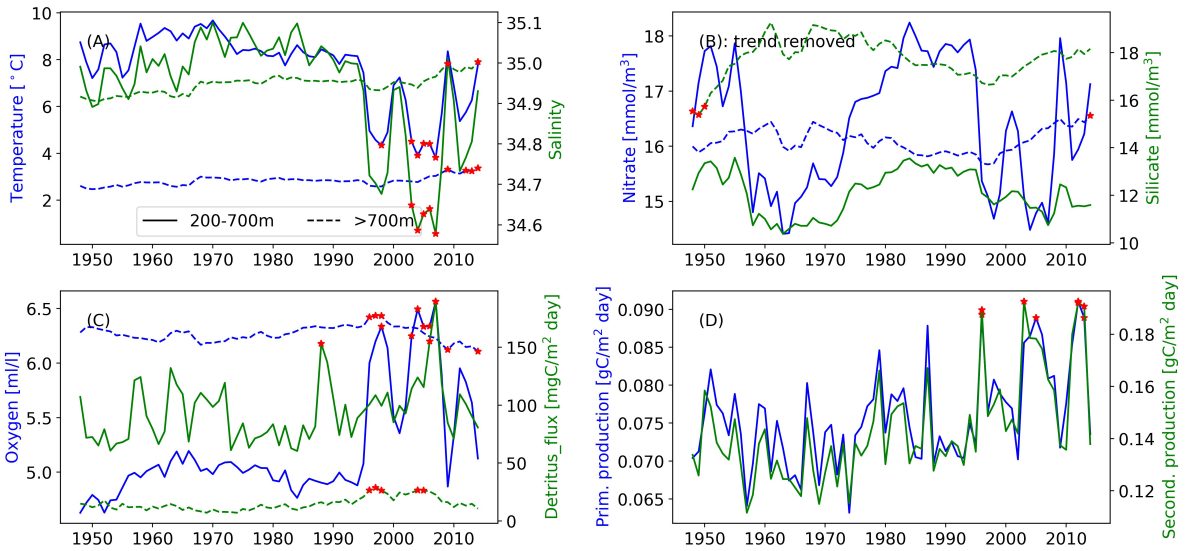

FIGURE 4 | Timeseries of the annual mean of different variables illustrating the interannual variability at the Flemish Cap for **(A)** temperature (blue) and salinity (green), **(B)** nitrate (blue) and silicate (green), and **(C)** oxygen (blue) and detritus (green). Solid lines are areas with bottom depth between 200 and 700 m, dashed lines are areas deeper than 700 m. **(D)** Depth-integrated primary production (blue) and secondary production (green) from the full area. Red stars indicate years when values are outside two standard deviations of the temporal mean.

sponge habitats (FLC, RYR, NNS), are colder and fresher during spring and warmer and saltier during the autumn. At the Flemish Cap, the mean temperature is 7.7°C (2.8°C) with a range of 0.8°C (0.04°C) and salinity varies from 34.88 to 34.98 and a range of 0.003 in the deeper layers. The temperature range at the RYR and NNS are 0.7°C (0.07°C) and 0.2°C (0.08°C), respectively, but on average the RYR is warmer with 6.0°C (4.9°C) compared to 4.8°C (0.03°C) at NNS. The salinity variations are only 0.02 at RYR and 0.04 at NNS over the annual cycle. In the EGS, the temperature variation is about 0.03°C, while the range of salinity is 0.01, with the most saline water in the autumn, potentially the retraction of sea ice from the area allows for the intrusion of more saline waters from the Fram Strait.

Similarly, nutrients and oxygen have small annual variations. Nutrients are higher in the autumn than in the spring at all the sponge habitats, but the variations are likely too small to influence the sponges. All sponge areas are quite well oxygenated with oxygen levels of 6 ml/l or above, except above 700 m at FLC where the mean is 5.2 ml/l. RYR has the largest annual cycle of oxygen of only 0.26 ml/l, with minimum in the autumn. Variations in the oxygen levels at these selected sponge habitats are quite closely the inverse to variations in temperature, therefore oxygen at the sponge grounds can potentially be predicted quite well by the change in temperature. Such close relationships between temperature and oxygen are common in deeper water masses as cold water can dissolve more oxygen, though the dissolved oxygen declines due to remineralization with time away from the surface. In the model mean state distribution of bottom oxygen (not shown) there are areas of low oxygen ∼2 ml/l at the bottom of the Baffin Bay and in the Gulf of St. Lawrence, but these low-oxygen waters do not intrude into other regions. The nitrate-to-silicate ratio decreases as the presence of Arctic water of Pacific origin becomes more prevalent, is above 1 at the NNS, about 1 at RYR and below 1 at FLC and in the EGS, but it should be kept in mind that where we have observations the model overestimates the silicate concentration.

At the FLC the flux of detritus to the sea floor is at a minimum in February and peaks in August, 2 months after the maximum secondary production. The detritus flux stays relatively high until October. At the other 3 sponge habitats the minimum occurs between April and June, with the maximum in September/October. The factors playing a role here are the depth of the sponge habitats and the progression of the phytoplankton bloom and corresponding zooplankton growth from south to north over the season. Because of the low productivity in the EGS the downward flux of detritus is only around 5. mgC/m^{2}day, only about 2–10% of the influx of particulate organic matter at the other sponge habitats. Below 700 m, the detritus flux is low and even.

Long Term Trends and Interannual Variability

Looking at annual means of the model variables over the simulation period at the sponge habitats (**Figures 4**–**7**), the three southernmost sponge regions have temperature ranges of about 5.9°C (0.9°C) at FLC, 1.1°C (0.7°C) at RYR, 1.1°C (0.5°C) at NNS, and 0.5°C (0.4°C) at EGS. The salinity range was 0.5 at FLC, less than 0.1 at NNS and RYR, but 0.2 in the EGS. The strongest temperature trend is a cooling trend of –0.53°C per decade at

the Flemish Cap above 700 m (**Table 3**) accompanied by a very small freshening (**Table 4**). A closer inspection of the timeseries of temperature and salinity (**Figure 4A**) shows that there are three large intrusions of cold, fresh waters, most likely of polar origin in the mid-1990s, 2000s, and 2010s. The intruding water is about 4°C colder and 0.2 fresher than normal. At RYR (**Figure 5**) and NNS (**Figure 6**) there are positive temperature trends of 0.06°C above 700 m and 0.08°C below 700 m, respectively (**Tables 3**, **5**). This is accompanied by a small increase in salinity at RYR, but a very small freshening trend in the NNS. At RYR there is a relatively stable increase in temperature and salinity over the whole simulation period, while at NNS there is cooling in the 1970s and 80s and warming in the 90s. Unlike at the other sponge habitats, the salinity and temperature at NNS have periods in the 1960s and late 1990s when the change is out of phase, i.e., there is a fresh and warm water mass. At both these sponge habitats the simulated temperature has a similar warming trend to the observations. At EGS the temperature trend is very small, but there are fluctuations with warmer and more saline waters in the 70s, 80s and 2000s that last for about 5 years each (**Figure 7**). Anomalous conditions, defined as values more than two standard deviations away from the mean (red stars in **Figures 4**–**7**), occur primarily at the beginning or end of the timeseries, except for NNS that has a fresh period in the 1980s.

Nitrate and silicate are increasing over the model period at all four sponge habitats over the simulation period, however, from the comparison to observations, we believe these trends are a model artifact, thus the timeseries shown in **Figures 4**–**7** have been detrended and no trends are presented for these variables. When the trend is removed, all four sponge habitats show an interannual variability of both nutrients of O(1 mmol/m^3). From the monthly timeseries the largest occur above 700 m at the FLC with > 4 mmol/m^3 nitrate and >4 mmol/m^3 silicate over a 10-year period (**Supplementary Tables 4**, **6**). At FLC and EGS there are variabilities in nitrate on a timescale from 3 to 10 years, at RYR and NNS the variability is multi-decadal. The variability of silicate is more multidecadal in nature at all four locations and has a similar long-term variability to nitrate at FLC and NNS (**Figures 4**, **6**). Anomalous conditions occur in both depth ranges, lower nutrients in the deeper part of the water masses occur at NNS and coincide with a freshening, in the last 5 years of the simulation.

The oxygen at FLC shows an increasing trend of 0.17 ml/l/decade (**Supplementary Table 8**) above 700 m while the remaining habitats have low oxygen trends. At FLC and NNS the detritus flux increases by 3.9 and 2.4 mgC/m^2 day/decade, respectively (**Supplementary Table 10**). Detritus fluxes at the sponge grounds exhibit year-to-year variations, while oxygen exhibit slower, multi-decadal variations. Above 700 m, on longer time-scales the higher flux of detritus is associated with higher oxygen concentration in the waters at FLC, RYR and NNS (**Figures 4**–**6**), while at the EGS oxygen and detritus flux have an inverse relationship (**Figure 7**). At EGS the deeper detritus flux exceeds the shallower region. Anomalous high values occur most often in the deep regions in the 1990s and 2000s at FLC and EGS and in the 1970s and 2000s at RYR.

For primary and secondary production, we did not distinguish between depths as this made very little difference for these variables. Primary and secondary production (**Figure 4**–**7D**) vary in a seemingly unrelated way to the changes in the deep sea. The interannual variability of primary and secondary production follow each other very closely. At FLC and NNS there is a slight [O(2.0×10^{-3}) gC/m^{2}day/decade] positive trend of primary production over the simulation period. This is potentially related to increasing nutrient concentrations, but warming could also play a role as growth is more efficient at higher temperatures. Anomalous years occur toward the end of the period at FLC and NNS, and intermittently throughout at the two other sponge habitats.

On interannual timescales there are co-variabilities between the water-masses and the biogeochemical properties at FLC and EGS. Nitrate co-varies with large fluctuations in the water masses in the EGS where the relationship is strongest with temperature ($r = 0.9$), and FLC where the relationship is strongest with salinity below 700 m ($r = 0.79$). Additionally, oxygen has a strong inverse relationship ($r < -0.9$) with temperature below 700 m at these sponge habitats. The detritus flux is also connected to water masses where higher-temperature water is associated with more detritus flux ($r = 0.67$) at EGS and colder water is associated with more detritus flux ($r = -0.8$) at FLC below 700 m. At FLC the two intrusions of colder fresher water mass are accompanied by an increase in oxygen and detritus flux beyond what is simulated by the model in the period before (**Figure 4**). This oxygen-rich water mass is LCSW originating from the north on the shelf off Canada.

TABLE 3 | Summary of temperature properties at the four sponge habitats in waters with bottom depth 200–700 m: Period mean, decadal trend, the maximum change in the monthly mean over a period of 12, 36 months, and 10 years, and the temporal mean of the spatial standard deviation.

	Flemish Cap	Reykjanes Ridge	North Norwegian Shelf	East Greenland Shelf
Period mean [°C]	7.672	5.982	4.809	–1.035
Decadal trend [°C/decade]	–0.527	0.060	–0.060	0.001
Max annual change [°C]	4.192	1.122	0.679	0.316
Max 3-year change [°C]	5.242	1.485	1.002	0.459
Max 10-year change [°C]	5.304	1.728	1.275	0.558
Spatial standard deviation [°C]	1.610	0.264	1.059	0.166

TABLE 4 | Summary of salinity properties at the four sponge habitats in waters with bottom depth 200–700 m: period mean, decadal trend, the maximum change in the monthly mean over a period of 12, 36 months, and 10 years, and the temporal mean of the spatial standard deviation.

	Flemish Cap	Reykjanes Ridge	North Norwegian Shelf	East Greenland Shelf
Period mean	34.940	35.075	34.951	34.532
Decadal trend [1/decade]	–0.037	0.008	–0.002	0.022
Max annual change	0.424	0.094	0.089	0.122
Max 3-year change	0.506	0.111	0.112	0.191
Max 10-year change	0.543	0.111	0.121	0.255
Spatial standard deviation	0.272	0.031	0.085	0.099

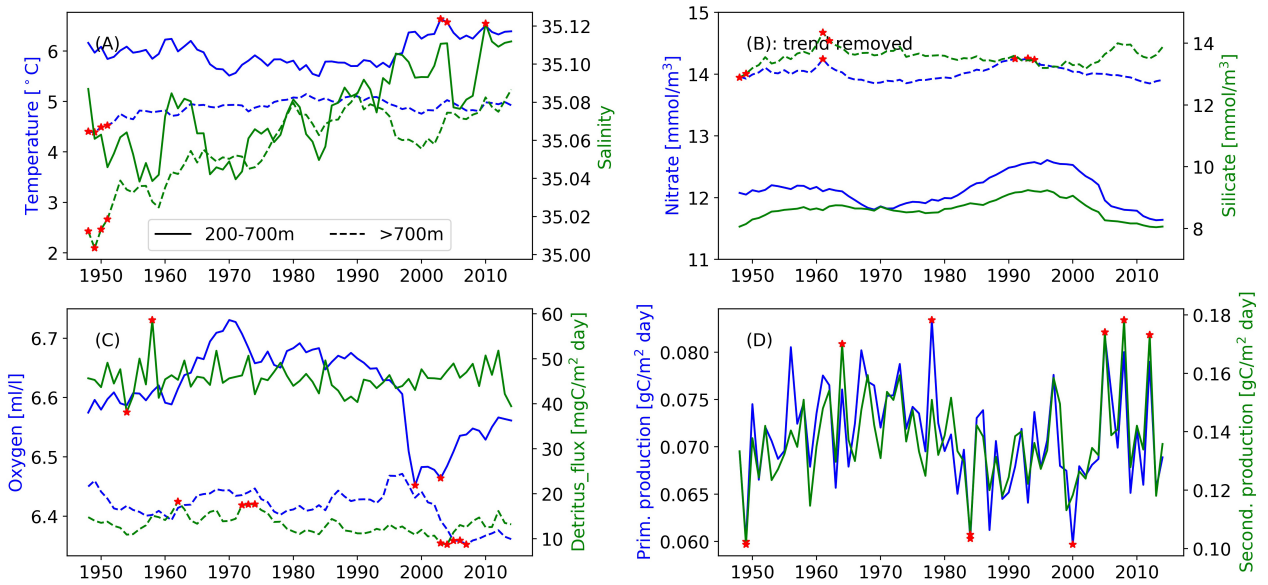

FIGURE 5 | Timeseries of the annual mean of different variables illustrating the interannual variability at the Reykjanes Ridge for **(A)** temperature (blue) and salinity (green), **(B)** nitrate (blue) and silicate (green), and **(C)** oxygen (blue) and detritus (green). Solid lines are areas with bottom depth between 200 and 700 m, dashed lines are areas deeper than 700 m. **(D)** Depth-integrated primary production (blue) and secondary production (green) from the full area. Red stars indicate years when values are outside two standard deviations of the temporal mean.

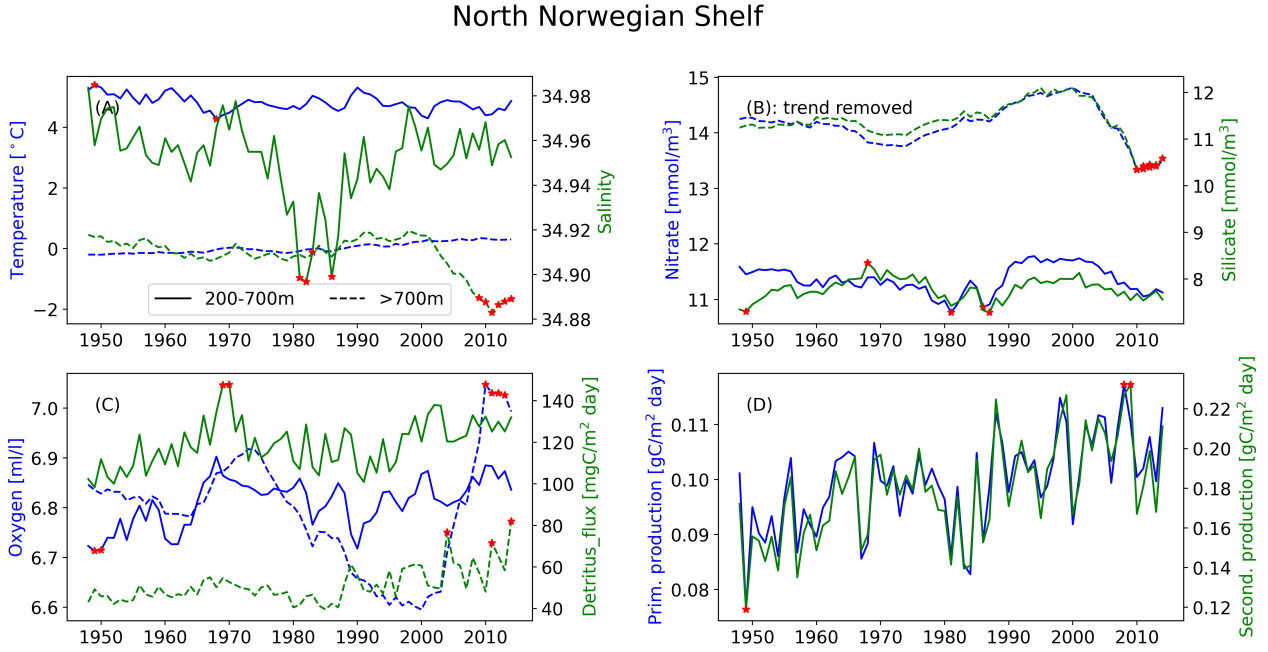

FIGURE 6 | Timeseries of the annual mean of different variables illustrating the interannual variability at the North Norwegian Shelf for **(A)** temperature (blue) and salinity (green), **(B)** nitrate (blue) and silicate (green), and **(C)** oxygen (blue) and detritus (green). Solid lines are areas with bottom depth between 200 and 700 m, dashed lines are areas deeper than 700 m. **(D)** Depth-integrated primary production (blue) and secondary production (green) from the full area. Red stars indicate years when values are outside two standard deviations of the temporal mean.

TABLE 5 | Summary of temperature properties at the four sponge habitats areas with bottom deeper than 700 m: Period mean, decadal trend, the maximum change in the monthly mean over a period of 12, 36 months, and 10 years, and the temporal mean of the spatial standard deviation.

	Flemish Cap	Reykjanes Ridge	North Norwegian Shelf	East Greenland Shelf
Period mean [°C]	2.829	4.886	0.028	–0.863
Decadal trend [°C/decade]	0.069	0.044	0.081	–0.004
Max annual change [°C]	0.359	0.299	0.278	0.226
Max 3-year change [°C]	0.471	0.399	0.278	0.316
Max 10-year change [°C]	0.674	0.595	0.392	0.336
Spatial standard deviation [°C]	1.506	1.017	0.894	0.053

Visual inspection of animations of the model results showed that the southward extension of this water mass is an annual event on the areas inshore of the Flemish Cap, but only in the later years does it extend west onto the Flemish Cap. The three warm peaks in the EGS are accompanied by increased detritus flux, but no corresponding increase in the local biological production is seen. Simultaneously there are temporary decreases in oxygen. The above indicates that these may be a result of advection of water masses from further east in the Fram Strait which are warmer, saltier and with a higher concentration of detritus. The absolute variability of temperature is 0.3°C while the detritus flux to the sea floor increases sixfold during the "warm" periods, although the absolute value is also very low. Oxygen and nitrate have a strong negative relationship of ($r < -0.8$) at both these sponge habitats.

At NNS and RYR water masses and the biogeochemical variables are not so tightly connected. Also here oxygen is negatively correlated to temperature, by $r = -0.87$ at RYR and $r = -0.92$ at NNS, above 700 m. Below 700 m, no correlation could be found. The strongest relationship is found between oxygen and nutrients ($r > -0.97$) at NNS below 700 m.

DISCUSSION

There are numerous deep-sea sponge habitats across the North Atlantic Ocean. At selected sponge habitats there are short-term monitoring timeseries (e.g.,Hanz et al., 2021b), at others physical ocean reanalysis products have been used to study the conditions (Beazley et al., 2018). However, at most sponge habitats long-term monitoring time series are missing. Here, we present a coupled physical-biogeochemical model hindcast of the North Atlantic covering the period from 1948 to 2014. To our knowledge, this is the first time such a model hindcast has been produced specifically with the aim of representing environmental conditions at deep-sea sponge habitats.

The purpose of this study is to use the model hindcast to investigate the mean conditions and long-term variability at sponge habitats over the last half century. Whilst outputs from ocean models can be used in species distribution modeling (SDM) approaches to predict distributional shifts and answer biogeographical questions (e.g., Beazley et al., 2021), and the dataset generated here has similar utility, in this work we extract timeseries data across a suite of environmental variables at known sponge habitats with a view to informing a baseline understanding of conditions experienced by extant populations in the recent past. It is generally thought that the deep sea, below the permanent thermocline, provides a relatively stable environment for the organisms living there and therefore it is possible that these organisms may not be able to acclimatize to abrupt changes in their environment. However, the sensitivity of sponges to changes in the environment is poorly known. One experiment (Strand et al., 2017) suggested that deep-sea boreal sponges were quite resilient to temperature increase alone, but may be sensitive to multiple stressors such as a simultaneous warming and decreasing oxygen concentrations. However, *G. Barretti* in the Skagerrak suffered mass mortality after being subjected to abrupt advection of warmer water (Guihen et al., 2014). Bell et al. (2018) found that sponges appear to be less sensitive to warming than other benthic taxa and may therefore emerge as a winner under climate change, although the work had a focus on shallow-water sponges in various settings (rather than North Atlantic/Arctic deep-sea sponges, as considered here). For shallow sponges, it was found that they were more tolerant to warming than corals, but a large warming, such as that in the RCP8.5 climate change scenario, would harm the sponge population (Bennett et al., 2017). Another study found that one species of coral and one species of sponge coming from a Norwegian fjord reacted negatively to heating and suspended sediment, but the coral was more sensitive (Scanes et al., 2018). Work from the Northwest Atlantic has shown that deep-sea sponge grounds may have persisted in the face of considerable environmental variability over 100s–1000s of years (Murillo et al., 2016; Beazley et al., 2018).

From the timeseries analyzed we identified that abrupt changes to the water masses could occur. At FLC above 700 m the temperature changes by more than 4° over just 1 year and at EGS the change was 0.31°C which is large compared to the mean annual range of 0.03°C. These abrupt changes were accompanied by changes in salinity, oxygen and detritus flux to the seabed as well. This is new information for 3 of the 4 sites selected (RYR, NNS, EGS). Whilst the magnitude of the fluctuations is relatively small, these results can help inform future studies of sponge sensitivity to environmental change. We assume that because any large/mature specimens collected in these areas in recent times (Roberts et al., 2021b) likely represent individuals of many decades to centuries in age (Prado et al., 2021), they appear to have persisted despite this level of variability.

The distribution of certain species of sponges is connected to specific water masses (Klitgaard and Tendal, 2004; Roberts et al., 2021a) and they likely have preferred ranges of environmental variables, connected to optimal growth conditions, feeding and the spreading or retention of larvae. Sponges are mainly slow-growing, and where they have been physically removed, for example by bottom trawling, it may take several decades to re-establish the population (Morrison et al., 2020). Any loss of sponge habitat to environmental change could potentially have large consequences for deep-sea ecosystems, in terms of the loss of hotspots of biodiversity, stepping stones of

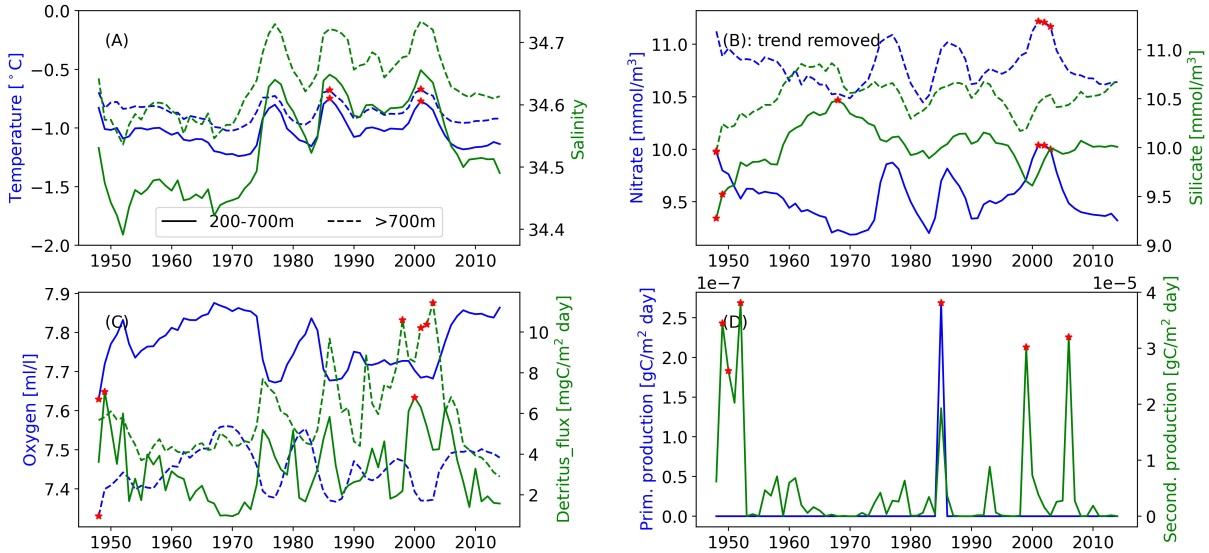

FIGURE 7 | Timeseries of the annual mean of different variables illustrating the interannual variability at the East Greenland Shelf for **(A)** temperature (blue) and salinity (green), **(B)** nitrate (blue) and silicate (green), and **(C)** oxygen (blue) and detritus (green). Solid lines are areas with bottom depth between 200 and 700 m, dashed lines are areas deeper than 700 m. **(D)** Depth-integrated primary production (blue) and secondary production (green) from the full area. Red stars indicate years when values are outside two standard deviations of the temporal mean.

connectivity, and nutrient cycling (Hogg et al., 2010), and if the environment changes permanently this would likely inhibit recovery. Therefore, one of the main contributions of this study is to establish the mean conditions and range of variability seen by deep-sea sponges in the past, so that as new data on sponge sensitivity to environmental change becomes available, we can evaluate whether conditions are moving beyond species' ecophysiological tolerances.

We observe both trends and interannual variations in the environmental conditions at the deep-sea sponge habitats investigated here. The magnitude of the fluctuations are generally small and that is reflected both in the annual cycle at each of the sponge habitats (see **Supplementary Figures 1–4**) and the interannual timeseries (**Figures 4–7**). The seasonal cycle at the sponge habitats investigated fluctuates with less than 1°C over the season and in the East Greenland Shelf the seasonal fluctuation is < 0.1°C. Seasonal fluctuations in salinity are similarly small. Nitrate and silicate vary by < 1 mmol/m^3 and though there are clear seasonal cycles in oxygen, the range of the annual cycle is < 0.3 ml/l. The interannual variability present in the model will either be caused by variability present in the atmospheric forcing used or internal dynamics within the ocean-biogeochemical system. Given that the sponge habitats are present at several hundred meters depth, the impact from the forcing will not be immediate and can take several years to reach these depths, depending on the area. At the RYR there is a gradual warming of the water masses and there are warming trends at both NNS and EGS. This is most likely the result of the warming present in the atmospheric reanalysis forcing. There is also a positive trend of surface primary production at the FLC and the NNS. This can be either due to increased growth at increased temperature or increased availability of nutrients. The timeseries constructed here have been averaged over a large range of depths which would smooth the variability and it is therefore likely that the local variations are larger than the averaged ones reported here. The mean spatial standard deviation is a measure of the spatial variability in the region (**Tables 3–6** and **Supplementary Tables 4–11**). Typically, the temporal fluctuation, on a monthly timescale, is larger than the spatial variability above 700 m and smaller than the spatial variability below 700 m.

When water masses exist in close vicinity of each other and shift in space, it can manifest locally as a large environmental change happening over a short time. Such variations from shifts in water masses are most likely the cause of the fluctuations with duration of 4–6 years of about 4°C at FLC (**Figure 4**) and 0.3°C

TABLE 6 | Summary of salinity properties at the four sponge habitats in areas with bottom deeper than 700 m: Period mean, decadal trend, the maximum change in the monthly mean over a period of 12, 36 months, and 10 years, and the temporal mean of the spatial standard deviation.

	Flemish Cap	Reykjanes Ridge	North Norwegian Shelf	East Greenland Shelf
Period mean	34.947	35.058	34.909	34.634
Decadal trend [1/decade]	0.009	0.008	–0.002	0.015
Max annual change	0.044	0.030	0.028	0.116
Max 3-year change	0.051	0.041	0.037	0.139
Max 10-year change	0.077	0.055	0.051	0.198
Spatial standard deviation	0.089	0.056	0.029	0.031

at EGS (**Figure 7**). At FLC, the water mass variability in the last two decades is visibly different from the variability of the first four decades (**Figure 4**), and is characterized as anomalous in several years during the 2000s. This area is influenced by North Atlantic waters, but also LCSW. The intrusion of colder, fresher water is similar to that reported on in Colbourne and Foote (2000) who analyze observations from 1960 to 1996, but the cooling periods they report on do not coincide temporally with the model. The two earliest periods occurring in the 1970s and 1980s, were attributed to anomalously low heat flux, while the period in the 1990s, was attributed to advection. From the model result it seems that changes in the Arctic may facilitate more frequent occurrences of colder, more productive water masses on the Flemish Cap. The accompanying increase in detritus flux from this water mass will increase the food availability to the sponges. The East Greenland Shelf area is relatively shallow, but being covered by sea ice for most of the year it has been protected from the direct forcing of the atmosphere. However, the second half of the hindcast period showed more variability. It is therefore likely that the simulated changes in the later period at both these sponge habitats can be connected to loss of sea ice thickness and extent in the Arctic Ocean (Stroeve et al., 2012; Ivanova et al., 2014; Onarheim and Årthun, 2017) that exposes the ocean to more direct atmospheric forcing and eventually influencing the regions downstream of the Arctic.

Changes in the biogeochemistry occur by a more direct route than changes in physical variables, that is via the sinking of organic material which propagates faster vertically in the ocean than physical properties. The hindcast shows that there can be very large variability in the flux of organic carbon to the sea floor. This can affect the growth of sponges, though bacteria and dissolved organic matter can also be important food-sources for the sponges (Bart et al., 2021; Hanz et al., 2021b). Too much sedimentation can in fact be a problem for sponges, as it can clog their filtration system (Klitgaard and Tendal, 2004). Fluctuations in detritus flux are at some places, such as the Norwegian Sea, connected to fluctuations in primary production, and at others, such as Flemish Cap, connected to fluctuations in water masses. Since the model also permits resuspension of detritus from the sea floor, periods of large detrital flux downwards can also be a result of resettling of suspended detritus. Presently, we have no way of distinguishing the two in the model, though the distinction is important as the freshly formed detritus has a better nutritional value (Van Engeland et al., 2019; Hanz et al., 2021b).

Many of the uncertainties in this study are connected to the relatively coarse resolution of the model used for the hindcast. Sponges are frequently found in areas of steep bathymetry, though it does not exclude them from being found in areas of flat bathymetry as well (Maldonado et al., 2017). Massive topographic structures such as the continental shelf break and the mid-Atlantic ridge will be present, but individual seamounts will be missing in the current model of 20–70 km resolution. There is always a trade-off between high and low resolution in numerical models: High-resolution will give good representation of bathymetry and currents on a fine scale, while at the same time increasing computational requirements and limiting the duration of sensitivity simulations. The flux of detritus to the sea floor in the EGS is likely higher than estimated here, as we are missing the flux of sinking sea ice algae in this model. Given the long time-scale and large area of the here presented simulation we settled for a coarser model resolution. This allowed us to test several parameter configurations for the biogeochemical model during the development of the hindcast before settling on the ones presented here. Still, the parameterization of sediment processes in ECOSMO is implemented using a simplified approach, which does not represent the vertical variation of biogeochemical processes within the sediment. The increasing trend of nutrients, and especially silicate, that we believe to be a model artifact represent some imbalance of the sources and sinks of nutrients. In fact, the deep-sea sponges themselves account for a missing process in the model as they can be a significant sink for silicate in the ocean and because of their high volume are an important player in the marine silicate cycle (Maldonado et al., 2019).

The flux of organic material to the sea floor can also be of terrigenous origin. This has, for example, been observed in the Fram Strait (Bauerfeind et al., 2009). During the melting season, runoff from glaciers can also transport materials from land into the ocean. A good dataset that provides the interannual variability of river loads of nutrient and organic material is to our knowledge not available and would be of great benefit for both local and basin-scale biogeochemical modeling.

Small-scale variability, such as internal waves/tides and inertial motions are considered to be of importance for deep-sea sponges (Hanz et al., 2021a). For example, internal waves have also been observed to cause large variability of biogeochemical properties in the deep sea in the vicinity of seamounts (Findlay et al., 2014). Tidal fluctuations, mixing by internal waves and, in shallower regions, storms can contribute to periodic resuspension of sediments. In fact, the sinking of organic material from surface productivity alone is understood to not always be a sufficient energy source for deep-sea sponges (Hanz et al., 2021b). Additionally, tides and internal motions play an important role in the dispersal of larvae in the vicinity of bathymetric features (Lavelle and Mohn, 2010). Monthly averaged model fields, such as the ones used here, will not resolve these kinds of motion; they must be modeled by high-resolution simulations (e.g., Mohn et al., 2014). Because of the focus on long-term and large-scale variability, we did not include tidal forcing in this model simulation. However, the long-term dataset is provided as monthly mean fields that low-pass filter tide-induced processes in the ocean. Even though tides in the model would increase the overall primary production, as a result of increased mixing and higher detritus flux, especially in the shallower regions (Zhao et al., 2019), we do not expect the interannual variability, the main focus of this paper, to be influenced by tides.

A key question in this paper was whether environmental conditions are moving beyond the variability seen in the recent past. One obstacle to answer this question is that the whole simulation period is subject to global warming, so even in this long simulation, we do not have true baseline values to compare it to. To establish whether there were values that were outside the "normal" range of variability, we identified values outside

two standard deviations of the temporal mean of the annual timeseries. If one variable in either of the depth ranges at one study site was more than two standard deviations away from its mean, we counted this as one anomalous occurrence. These anomalous conditions occur more frequently toward the beginning and end of the simulation period. In the first 4 years of the simulation, it happened on average 7.5 times per year that one variable in one of the depth ranges had anomalous values, while in the period 1952–2000, this frequency was about once per year. In the period from 2000 to 2014 the frequency was about 6 times per year. The results from this model therefore show that the environment is changing over time which results in anomalies outside the "normal" at the beginning and end of the timeseries.

The dataset can potentially also be used for analyzing the deep-sea environment and variability relevant to other organisms, such as deep-sea corals and fishes, for example as part of SDM or as a support when analyzing observations of deep-sea habitats. With climate change ongoing, there is a question as to whether environmental conditions that have prevailed for 100s of years are about to disappear. What this would mean for deep-sea sponges and other ecosystem engineers remains poorly understood. Better computational capacity and faster machines also open the possibility for higher-resolution, long-term simulations in the future. In addition, a nesting modeling strategy can be applied that allows very high model resolution at selected locations for a closer study of individual sponge habitats. This would be useful for studies of larval dispersal, where small-scale processes are thought to be important or to characterize the range of local, small-scale variability at specific locations.

Based on the above results and discussion we conclude that:

* This study analyses the variability at four locations in the North Atlantic known to host dense sponge aggregations. It demonstrates that the model can be used to learn about how the deep-sea conditions fluctuate and change over time on monthly to multi-decadal time-scales.

* Both at intermediate (200–700 m) and deeper (greater than 700 m) depths the long-term mean conditions change relatively slowly. The most abrupt changes are associated with advection of different water masses and occur over timescales less than a year and can persist for several years.

* A gradual warming of the water masses was detected in the central Atlantic at the Reykjanes ridge.

* The biogeochemical properties are tightly connected to water mass properties, as demonstrated by correlations between physical quantities and biogeochemical quantities.

* Anomalous values, defined as values more than 2 standard deviations away from the long-term means, are more frequent toward the beginning and end of the timeseries indicating that the "normal" range of variability fluctuates with time. This occurs both at mid depth and in the deepest layers.

AUTHOR'S NOTE

This document reflects only the authors' views and the Executive Agency for Small and Medium-sized Enterprises (EASME) is not responsible for any use that may be made of the information it contains.

DATA AVAILABILITY STATEMENT

The datasets presented in this study can be found in online repositories. The names of the repository/repositories and accession number(s) can be found below: https://doi.pangaea.de/10.1594/PANGAEA.889396.

AUTHOR CONTRIBUTIONS

AS performed the model simulations and analyzed the model results and wrote the manuscript with input from all co-authors. CS was involved with the configuration of the model experiments and obtaining the model forcing. ER contributed by relating results to sponge habitats and ecology. UD and VY worked on the coupled model configuration and validation. All authors contributed to the article and approved the submitted version.

FUNDING

AS, VY, and ER were supported by the European Union's Horizon 2020 SponGES Project (Grant no. 679849). VY and UD were supported by the CMEMS R&D project ZOOMBI. The computations were performed on the Norwegian Sigma2 infrastructure under the projects NN9481K and NS9481K. This research has been performed in the scope of the SponGES project, which received funding from the European Union's Horizon 2020 Research and Innovation Programme under grant agreement no. 679849.

ACKNOWLEDGMENTS

We thank to Rocio Castano Primo who obtained the *in situ* observations and wrote routines for model validation. Paco Cárdenas is thanked for useful discussions on the benthic fauna at Reykjanes Ridge.

SUPPLEMENTARY MATERIAL

The Supplementary Material for this article can be found online at: https://www.frontiersin.org/articles/10.3389/fmars.2022.737164/full#supplementary-material

REFERENCES

Bagniewski, W., Fennel, K., Perry, M. J., and D'Asaro, E. A. (2011). Optimizing models of the North Atlantic spring bloom using physical, chemical and bio-optical observations from a Lagrangian float. *Biogeosciences* 8, 1291–1307. doi: 10.5194/bg-8-1291-2011

Bart, M. C., Hudspith, M., Rapp, H. T., Verdonschot, P. F. M., and de Goeij, J. M. (2021). A Deep-Sea Sponge Loop? Sponges Transfer Dissolved and Particulate Organic Carbon and Nitrogen to Associated Fauna. *Front. Mar. Sci.* 8:1–12. doi: 10.3389/fmars.2021.604879

Bauerfeind, E., Nöthig, E.-M., Beszczynska, A., Fahl, K., Kaleschke, L., Kreker, K., et al. (2009). Particle sedimentation patterns in the eastern Fram Strait during 2000–2005: Results from the Arctic long-term observatory HAUSGARTEN. *Deep Sea Res. Part I Oceanogr. Res. Pap.* 56, 1471–1487. doi: 10.1016/j.dsr.2009.04.011

Beazley, L. I., Kenchington, E. L., Murillo, F. J., Sacau, M., and del, M. (2013). Deep-sea sponge grounds enhance diversity and abundance of epibenthic megafauna in the Northwest Atlantic. *ICES J. Mar. Sci.* 70, 1471–1490. doi: 10.1093/icesjms/fst124

Beazley, L., Kenchington, E., Murillo, F. J., Brickman, D., Wang, Z., Davies, A. J., et al. (2021). Climate change winner in the deep sea? predicting the impacts of climate change on the distribution of the glass sponge *Vazella pourtalesii*. *Mar. Ecol. Prog. Ser.* 657, 1–23. doi: 10.3354/meps13566

Beazley, L., Wang, Z., Kenchington, E., Yashayaev, I., Rapp, H. T., Xavier, J. R., et al. (2018). Predicted distribution of the glass sponge *Vazella pourtalesi* on the Scotian Shelf and its persistence in the face of climatic variability. *PLoS One* 13:e0205505. doi: 10.1371/journal.pone.0205505

Belarbi, E. (2003). Producing drugs from marine sponges. *Biotechnol. Adv.* 21, 585–598. doi: 10.1016/S0734-9750(03)00100-9

Bell, J. J. (2008). The functional roles of marine sponges. *Estuar. Coast. Shelf Sci.* 79, 341–353. doi: 10.1016/j.ecss.2008.05.002

Bell, J. J., Bennett, H. M., Rovellini, A., and Webster, N. S. (2018). Sponges to be winners under near-future climate scenarios. *Bioscience* 68, 955–968. doi: 10.1093/biosci/biy142

Bennett, H. M., Altenrath, C., Woods, L., Davy, S. K., Webster, N. S., and Bell, J. J. (2017). Interactive effects of temperature and *p*CO2 on sponges: from the cradle to the grave. *Glob. Chang. Biol.* 23, 2031–2046. doi: 10.1111/gcb.13474

Bett, B. J., and Rice, A. L. (1992). The influenceof hexactinellid sponge (*Pheronema carpenteri*) spicules on the patchy distribution of macrobenthos in the porcupine seabight (bathyal ne atlantic). *Ophelia* 36, 217–226. doi: 10.1080/00785326.1992.10430372

Bindoff, N. L., Cheung, W. W. L., Kairo, J. G., Arístegui, J., Guinder, V. A., Hilmi, N., et al. (2019). "Changing Ocean, Marine Ecosystems, and Dependent Communities SE - 477," in *Intergovernmental Panel on Climate Change*, eds H.-O. Pörtner, D. C. Roberts, V. Masson-Delmotte, P. Zha, E. Poloczansk, K. Mintenbeck, et al. (Geneva: IPCC).

Bleck, R. (2002). An oceanic general circulation model framed in hybrid isopycnic-Cartesian coordinates. *Ocean Model.* 4, 55–88. doi: 10.1016/s1463-5003(01)00012-9

Buhl-Mortensen, L., Bøe, R., Dolan, M. F. J., Buhl-Mortensen, P., Thorsnes, T., Elvenes, S., et al. (2012). "Banks, Troughs, and Canyons on the Continental Margin off Lofoten, Vesterålen, and Troms, Norway," in *Seafloor Geomorphology as Benthic Habitat*, eds P. T. Harris and E. K. Baker (Amsterdam: Elsevier), 703–715. doi: 10.1016/B978-0-12-385140-6.00051-7

Buhl-Mortensen, P., Dolan, M., and Buhl-Mortensen, L. (2009). Prediction of benthic biotopes on a Norwegian offshore bank using a combination of multivariate analysis and GIS classification. *ICES J. Mar. Sci.* 66, 2026–2032. doi: 10.1093/icesjms/fsp200

Cárdenas, P., and Rapp, H. T. (2015). Demosponges from the Northern Mid-Atlantic Ridge shed more light on the diversity and biogeography of North Atlantic deep-sea sponges. *J. Mar. Biol. Assoc. U K.* 95, 1475–1516. doi: 10.1017/S0025315415000983

Cárdenas, P., Rapp, H. T., Klitgaard, A. B., Best, M., Thollesson, M., and Tendal, O. S. (2013). Taxonomy, biogeography and DNA barcodes of *Geodia* species (Porifera, Demospongiae, Tetractinellida) in the Atlantic boreo-arctic region. *Zool. J. Linn. Soc.* 169, 251–311. doi: 10.1111/zoj.12056

Carnes, M. R. (2009). *Description and Evaluation of GDEM-V 3.0*. Washington, D.C: Naval Research Laboratory.

Colbourne, E. B., and Foote, K. D. (2000). Variability of the stratification and circulation on the flemish cap during the decades of the 1950s-1990s. *J. Northwest Atl. Fish. Sci.* 26, 103–122. doi: 10.2960/J.v26.a5

Copley, J. T. P., Tyler, P. A., Sheader, M., Murton, B. J., and German, C. R. (1996). Megafauna from sublittoral to abyssal depths along the Mid-Atlantic ridge south of Iceland. *Oceanol. Acta* 19, 549–559.

Daewel, U., and Schrum, C. (2013). Simulating long-term dynamics of the coupled North Sea and Baltic Sea ecosystem with ECOSMO II: Model description and validation. *J. Mar. Syst.* 119–120, 30–49. doi: 10.1016/j.jmarsys.2013.03.008

Davison, J. J., van Haren, H., Hosegood, P., Piechaud, N., and Howell, K. L. (2019). The distribution of deep-sea sponge aggregations (Porifera) in relation to oceanographic processes in the Faroe-Shetland Channel. *Deep Sea Res. Part I Oceanogr. Res. Pap.* 146, 55–61. doi: 10.1016/j.dsr.2019.03.005

de Steur, L., Hansen, E., Gerdes, R., Karcher, M., Fahrbach, E., and Holfort, J. (2009). Freshwater fluxes in the East Greenland Current: A decade of observations. *Geophys. Res. Lett.* 36:L23611. doi: 10.1029/2009GL041278

Dohrmann, M., Göcke, C., Reed, J., and Janussen, D. (2012). Integrative taxonomy justifies a new genus, *Nodastrella* gen. nov., for North Atlantic "*Rossella*" species (Porifera: Hexactinellida: Rossellidae). *Zootaxa* 3383:1. doi: 10.11646/zootaxa.3383.1.1

Drange, H., and Simonsen, K. (1996). *Formulation of air-sea fluxes in the ESOP2 version of MICOM*. Bergen: Nansen Environmental and Remote Sensing Center.

Dudik, O., Leonor, I., Xavier, J. R., Rapp, H. T., Pires, R. A., Silva, T. H., et al. (2018). Sponge-derived silica for tissue regeneration. *Mater. Today* 21, 577–578. doi: 10.1016/j.mattod.2018.03.025

Ezer, T. (2016). Revisiting the problem of the Gulf Stream separation: On the representation of topography in ocean models with different types of vertical grids. *Ocean Model.* 104, 15–27. doi: 10.1016/j.ocemod.2016.05.008

FAO (2009). *International Guidelines for the Management of Deep-sea Fisheries in the High Seas*. Rome: FAO.

Findlay, H. S., Hennige, S. J., Wicks, L. C., Navas, J. M., Woodward, E. M. S., and Roberts, J. M. (2014). Fine-scale nutrient and carbonate system dynamics around cold-water coral reefs in the northeast Atlantic. *Sci. Rep.* 4, 1–10. doi: 10.1038/srep03671

Fröb, F., Olsen, A., Pérez, F. F., Garciá-Ibáñez, M. I., Jeansson, E., Omar, A., et al. (2018). Inorganic carbon and water masses in the Irminger Sea since 1991. *Biogeosciences* 15, 51–72. doi: 10.5194/bg-15-51-2018

Garcia, H. E., Locarnini, R. A., Boyer, T. P., Antonov, J. I., Baranova, O. K., Zweng, M. M., et al. (2013a). *WORLD OCEAN ATLAS 2013 Volume 4: Dissolved Inorganic Nutrients (phosphate, nitrate, silicate)*. Washington, D.C: NOAA, doi: 10.1182/blood-2011-06-357442

Garcia, H. E., Locarnini, R. A., Boyer, T. P., Antonov, J. I., Mishonov, A. V., Baranova, O. K., et al. (2013b). *World Ocean Atlas 2013. Vol. 3: Dissolved Oxygen, Apparent Oxygen Utilization, and Oxygen Saturation*. Washington, D.C: NOAA.

Guihen, D., White, M., and Lundälv, T. (2014). Temperature shocks and ecological implications at a cold-water coral reef. *ANZIAM J.* 5, 1–10. doi: 10.1017/S1755267212000413

Hansen, J., Sato, M., Kharecha, P., and Von Schuckmann, K. (2011). Earth's energy imbalance and implications. *Atmos. Chem. Phys.* 11, 13421–13449. doi: 10.5194/acp-11-13421-2011

Hanz, U., Beazley, L., Kenchington, E., Duineveld, G., Rapp, H. T., and Mienis, F. (2021a). Seasonal Variability in Near-bed Environmental Conditions in the *Vazella pourtalesii* Glass Sponge Grounds of the Scotian Shelf. *Front. Mar. Sci.* 7:597682. doi: 10.3389/fmars.2020.597682

Hanz, U., Roberts, E. M., Duineveld, G., Davies, A., van Haren, H., Rapp, H. T., et al. (2021b). Long-term Observations Reveal Environmental Conditions and Food Supply Mechanisms at an Arctic Deep-Sea Sponge Ground. *J. Geophys. Res. Ocean* 126:2020JC016776. doi: 10.1029/2020JC016776

Hawkes, N., Korabik, M., Beazley, L., Rapp, H., Xavier, J., and Kenchington, E. (2019). Glass sponge grounds on the Scotian Shelf and their associated biodiversity. *Mar. Ecol. Prog. Ser.* 614, 91–109. doi: 10.3354/meps12903

Hestetun, J. T., Rapp, H. T., and Pomponi, S. (2019). Deep-sea carnivorous sponges from the Mariana Islands. *Front. Mar. Sci.* 6:1–22. doi: 10.3389/fmars.2019.00371

Hogg, M. M., Tendal, O. S., Conway, K. W., Pomponi, S. A., Van Soest, R. W. M., Gutt, J., et al. (2010). *Deep-sea sponge grounds: Reservoirs of biodiversity*. Cambridge: World Conservation Monitoring Centre.

Hunke, E. C., and Dukowicz, J. K. (1997). An elastic-viscous-plastic model for sea ice dynamics. *J. Phys. Oceanogr.* 27, 1849–1867. doi: 10.1175/1520-0485(1997)027<1849:aevpmf>2.0.co;2

Institute of Marine Research (2018). *Næ ringssalt-, oksygen- og klorofylldata i norske havområder fra 1980-2017*. Bergen: Institute of Marine Research.

Ivanova, N., Johannessen, O. M., Pedersen, L. T., and Tonboe, R. T. (2014). Retrieval of arctic sea ice parameters by satellite passive microwave sensors: A comparison of eleven sea ice concentration algorithms. *IEEE Trans. Geosci. Remote Sens.* 52, 7233–7246. doi: 10.1109/TGRS.2014.2310136

Kazanidis, G., Vad, J., Henry, L.-A., Neat, F., Berx, B., Georgoulas, K., et al. (2019). Environmental and biological data from deep-sea sponge aggregations in the Faroe-Shetland Channel Nature Conservation Marine Protected Area. *PANGAEA* 2019:897592. doi: 10.1594/PANGAEA.897592

Klitgaard, A. B. (1995). The fauna associated with outer shelf and upper slope sponges (Porifera, Demospongiae) at the Faroe Islands, northeastern Atlantic. *Sarsia* 80, 1–22. doi: 10.1080/00364827.1995.10413574

Klitgaard, A. B., and Tendal, O. S. (2004). Distribution and species composition of mass occurrences of large-sized sponges in the northeast Atlantic. *Prog. Oceanogr.* 61, 57–98. doi: 10.1016/j.pocean.2004.06.002

Knudby, A., Kenchington, E., and Murillo, F. J. (2013). Modeling the Distribution of *Geodia* Sponges and Sponge Grounds in the Northwest Atlantic. *PLoS One* 8:e82306. doi: 10.1371/journal.pone.0082306

Kuznetsov, A. P., and Detinova, N. N. (2001). "Bottom fauna of the Reykjanes Ridge area," in *Composition and structure of themarine bottom biota*, eds A. P. Kuznetsov and O. Zezina (Moscow: VNIRO Publishing House), 6–18.

Lavelle, J. W., and Mohn, C. (2010). Motion, Commotion, and Biophysical Connections at Deep Ocean Seamounts. *Oceanography* 23, 90–103. doi: 10.5670/oceanog.2010.64

Leal, M. C., Puga, J., Serôdio, J., Gomes, N. C. M., and Calado, R. (2012). Trends in the Discovery of New Marine Natural Products from Invertebrates over the Last Two Decades – Where and What Are We Bioprospecting? *PLoS One* 7:e30580. doi: 10.1371/journal.pone.0030580

Maldonado, M. (2006). The ecology of the sponge larva. *Can. J. Zool.* 84, 175–194. doi: 10.1139/z05-177

Maldonado, M., Aguilar, R., Bannister, R. J., James, J., Conway, K. W., Dayton, P. K., et al. (2017). *Marine Animal Forests*. Berlin: Springer, doi: 10.1007/978-3-319-17001-5

Maldonado, M., López-Acosta, M., Sitjà, C., García-Puig, M., Galobart, C., Ercilla, G., et al. (2019). Sponge skeletons as an important sink of silicon in the global oceans. *Nat. Geosci.* 12, 815–822. doi: 10.1038/s41561-019-0430-7

Mayorga, E., Seitzinger, S. P., Harrison, J. A., Dumont, E., Beusen, A. H. W., Bouwman, A. F., et al. (2010). Global Nutrient Export from WaterSheds 2 (NEWS 2): Model development and implementation. *Environ. Model. Softw.* 25, 837–853.

Meyer, H. K., Roberts, E. M., Mienis, F., and Rapp, H. T. (2020). Megafauna abundances observed during a SponGES cruise with RV G.O. Sars and ROV Ægir 6000 in Sognefjord, Norway. *PANGAEA* 2020:914801. doi: 10.1594/PANGAEA.914799

Mohn, C., Rengstorf, A., White, M., Duineveld, G., Mienis, F., Soetaert, K., et al. (2014). Linking benthic hydrodynamics and cold-water coral occurrences: A high-resolution model study at three cold-water coral provinces in the NE Atlantic. *Prog. Oceanogr.* 122, 92–104. doi: 10.1016/j.pocean.2013.12.003

Morrison, K. M., Meyer, H. K., Roberts, E. M., Rapp, H. T., Colaço, A., and Pham, C. K. (2020). The First Cut Is the Deepest: Trawl Effects on a Deep-Sea Sponge Ground Are Pronounced Four Years on. *Front. Mar. Sci.* 7:1–13. doi: 10.3389/fmars.2020.605281

Murillo, F. J., Kenchington, E., Lawson, J. M., Li, G., and Piper, D. J. W. (2016). Ancient deep-sea sponge grounds on the Flemish Cap and Grand Bank, northwest Atlantic. *Mar. Biol.* 163, 1–11. doi: 10.1007/s00227-016-2839-5

Murillo, F. J., Muñoz, P. D., Cristobo, J., Ríos, P., González, C., Kenchington, E., et al. (2012). Deep-sea sponge grounds of the Flemish Cap, Flemish Pass and the Grand Banks of Newfoundland (Northwest Atlantic Ocean): Distribution and species composition. *Mar. Biol. Res.* 8, 842–854. doi: 10.1080/17451000.2012.682583

Oki, T., and Sud, Y. C. (1998). Design of Total Runoff Integrating Pathways (TRIP) – A global river channel network. *Earth Interact.* 2, 1–37.

Olsen, A., Key, R. M., van Heuven, S., Lauvset, S. K., Velo, A., Lin, X., et al. (2016). The Global Ocean Data Analysis Project version 2 (GLODAPv2) – an internally consistent data product for the world ocean. *Earth Syst. Sci. Data* 8, 297–323. doi: 10.5194/essd-8-297-2016

Onarheim, I. H., and Årthun, M. (2017). Toward an ice-free Barents Sea. *Geophys. Res. Lett.* 44, 8387–8395. doi: 10.1002/2017GL074304

OSPAR Commission (2008). *Case Reports for the OSPAR List of Threatened and/or Declining Species and Habitats*. London: OSPAR Commission.

Petit, T. (2018). *Characterization of the circulation around, above and across (through fracture zones) the Reykjanes Ridge*. Reading: University of Reading, 1–201.

Pile, A. J., and Young, C. M. (2006). The natural diet of a hexactinellid sponge: Benthic–pelagic coupling in a deep-sea microbial food web. *Deep Sea Res. Part I Oceanogr. Res. Pap.* 53, 1148–1156. doi: 10.1016/j.dsr.2006.03.008

Prado, E., Cristobo, J., Rodríguez-Basalo, A., Ríos, P., Rodríguez-Cabello, C., and Sánchez, F. (2021). *In situ* Growth Rate Assessment of the Hexactinellid Sponge *Asconema setubalense* Using 3D Photogrammetric Reconstruction. *Front. Mar. Sci.* 8:1–16. doi: 10.3389/fmars.2021.612613

Pusceddu, A., Bianchelli, S., Martin, J., Puig, P., Palanques, A., Masque, P., et al. (2014). Chronic and intensive bottom trawling impairs deep-sea biodiversity and ecosystem functioning. *Proc. Natl. Acad. Sci.* 111, 8861–8866. doi: 10.1073/pnas.1405454111

Rice, A., Thurston, M., and New, A. (1990). Dense aggregations of a hexactinellid sponge, *Pheronema carpenteri*, in the Porcupine Seabight (northeast Atlantic Ocean), and possible causes. *Prog. Oceanogr.* 24, 179–196. doi: 10.1016/0079-6611(90)90029-2

Roberts, E. M., Bowers, D. G., Meyer, H. K., Samuelsen, A., Rapp, H. T., and Cárdenas, P. (2021a). Water masses constrain the distribution of deep-sea sponges in the North Atlantic Ocean and Nordic Seas. *Mar. Ecol. Prog. Ser.* 659, 75–96. doi: 10.3354/meps13570

Roberts, E. M., Bowers, D. G., Meyer, H. K., Samuelsen, A., Rapp, H. T., and Cárdenas, P. (2021b). Occurrence records of *Geodia* species (Porifera, Demospongiae, Tetractinellida) from the North Atlantic and Arctic Oceans. *PANGAEA* 2021:924531. doi: 10.1594/PANGAEA.924531

Roberts, E. M., Mienis, F., Rapp, H. T., Hanz, U., Meyer, H. K., and Davies, A. J. (2018). Oceanographic setting and short-timescale environmental variability at an Arctic seamount sponge ground. *Deep. Res. Part I Oceanogr. Res. Pap.* 138, 98–113. doi: 10.1016/j.dsr.2018.06.007

Rodríguez-Basalo, A., Prado, E., Sánchez, F., Ríos, P., Gómez-Ballesteros, M., and Cristobo, J. (2021). High Resolution Spatial Distribution for the Hexactinellid Sponges *Asconema setubalense* and *Pheronema carpenteri* in the Central Cantabrian Sea. *Front. Mar. Sci.* 8:612761. doi: 10.3389/fmars.2021.612761

Ross, R. E., Nimmo-Smith, W. A. M., and Howell, K. L. (2016). Increasing the depth of current understanding: Sensitivity testing of deep-sea larval dispersal models for ecologists. *PLoS One* 11:1–25. doi: 10.1371/journal.pone.0161220

Rudels, B., Fahrbach, E., Meincke, J., Budéus, G., and Eriksson, P. (2002). The East Greenland Current and its contribution to the Denmark Strait overflow. *ICES J. Mar. Sci.* 59, 1133–1154. doi: 10.1006/jmsc.2002.1284

Samuelsen, A., Hansen, C., and Wehde, H. (2015). Tuning and assessment of the HYCOM-NORWECOM V2.1 biogeochemical modeling system for the North Atlantic and Arctic oceans. *Geosci. Model Dev.* 8, 2187–2202. doi: 10.5194/gmd-8-2187-2015

Samuelsen, A., Schrum, C., Daewel, U., Castano-Primo, R., and Yumruktepe, V. Ç (2019). *SponGES Deliverable 7.6 - Report on historic climate and ecosystem data*. Berkeley, CA: National Energy Research Scientific Computing Center.

Scanes, E., Kutti, T., Fang, J. K. H., Johnston, E. L., Ross, P. M., and Bannister, R. J. (2018). Mine Waste and Acute Warming Induce Energetic Stress in the Deep-Sea Sponge *Geodia atlantica* and Coral *Primnoa resedeaformis*; Results From a Mesocosm Study. *Front. Mar. Sci.* 5:129. doi: 10.3389/fmars.2018.00129

Schubert-Frisius, M., and Feser, F. (2015). *Global High Resolution Climate Reconstruction with ECHAM6 using the spectral nudging technique, run by Helmholtz-Zentrum Geesthacht*. Hamburg: University of Hamburg, doi: 10.1594/WDCC/CLISAP_MPI-ESM-XR_t255l95

Seitzinger, S. P., Mayorga, E., Bouwman, A. F., Kroeze, C., Beusen, A. H. W., Billen, G., et al. (2010). Global river nutrient export: A scenario analysis of past and future trends. *Global Biogeochem. Cycles* 24:3587.

Skarðhamar, J., Svendsen, H., and Skardhamar, J. (2005). Circulation and shelf-ocean interaction off North Norway. *Cont. Shelf Res.* 25, 1541–1560. doi: 10.1016/j.csr.2005.04.007

Skogen, M. D., and Moll, A. (2005). Importance of ocean circulation in ecological modeling: An example from the North Sea. *J. Mar. Syst.* 57, 289–300. doi: 10.1016/j.jmarsys.2005.06.002

Strand, R., Whalan, S., Webster, N. S., Kutti, T., Fang, J. K. H., Luter, H. M., et al. (2017). The response of a boreal deep-sea sponge holobiont to acute thermal stress. *Sci. Rep.* 7:1660. doi: 10.1038/s41598-017-01091-x

Stroeve, J. C., Serreze, M. C., Holland, M. M., Kay, J. E., Malanik, J., and Barrett, A. P. (2012). The Arctic's rapidly shrinking sea ice cover: a research synthesis. *Clim. Change* 110, 1005–1027. doi: 10.1007/s10584-011-0101-1

Sundar, V. C., Yablon, A. D., Grazul, J. L., Ilan, M., and Aizenberg, J. (2003). Fibre-optical features of a glass sponge. *Nature* 424, 899–900. doi: 10.1038/424899a

Vacelet, J. (2007). "Diversity and evolution of deep-sea carnivorous sponges," in *Porifera research : biodiversity, innovation and sustainability*, ed. M. R. Custódio (Rio de Janeiro: Museu Nacional), 107–115.

Van Engeland, T., Godø, O. R., Johnsen, E., Duineveld, G. C. A., and van Oevelen, D. (2019). Cabled ocean observatory data reveal food supply mechanisms to a cold-water coral reef. *Prog. Oceanogr.* 172, 51–64. doi: 10.1016/j.pocean.2019.01.007

Wurz, E., Beazley, L., MacDonald, B., Kenchington, E., Rapp, H. T., and Osinga, R. (2021). The Hexactinellid Deep-Water Sponge *Vazella pourtalesii* (Schmidt, 1870) (Rossellidae) Copes With Temporarily Elevated Concentrations of Suspended Natural Sediment. *Front. Mar. Sci.* 8:1–15. doi: 10.3389/fmars.2021.611539

Xie, J., Counillon, F., Bertino, L., Tian-Kunze, X., and Kaleschke, L. (2016). Benefits of assimilating thin sea ice thickness from SMOS into the TOPAZ system. *Cryosphere* 10, 2745–2761. doi: 10.5194/tc-10-2745-2016

Yashayaev, I., Bersch, M., and van Aken, H. M. (2007). Spreading of the Labrador Sea Water to the Irminger and Iceland basins. *Geophys. Res. Lett.* 34, 1–8. doi: 10.1029/2006GL028999

Yumruktepe, V. Ç, Samuelsen, A., and Daewel, U. (2021). ECOSMO II(CHL): a marine biogeochemical model for the North Atlantic and the Arctic. *Geosci. Model Dev. Discuss.* 2021:279. doi: 10.5194/gmd-2021-279

Zhao, C., Daewel, U., and Schrum, C. (2019). Tidal impacts on primary production in the North Sea. *Earth Syst. Dyn.* 10, 287–317. doi: 10.5194/esd-10-287-2019

Conflict of Interest: The authors declare that the research was conducted in the absence of any commercial or financial relationships that could be construed as a potential conflict of interest.

Publisher's Note: All claims expressed in this article are solely those of the authors and do not necessarily represent those of their affiliated organizations, or those of the publisher, the editors and the reviewers. Any product that may be evaluated in this article, or claim that may be made by its manufacturer, is not guaranteed or endorsed by the publisher.

Copyright © 2022 Samuelsen, Schrum, Yumruktepe, Daewel and Roberts. This is an open-access article distributed under the terms of the Creative Commons Attribution License (CC BY). The use, distribution or reproduction in other forums is permitted, provided the original author(s) and the copyright owner(s) are credited and that the original publication in this journal is cited, in accordance with accepted academic practice. No use, distribution or reproduction is permitted which does not comply with these terms.

Advantages of publishing in Frontiers

OPEN ACCESS
Articles are free to read for greatest visibility and readership

FAST PUBLICATION
Around 90 days from submission to decision

HIGH QUALITY PEER-REVIEW
Rigorous, collaborative, and constructive peer-review

TRANSPARENT PEER-REVIEW
Editors and reviewers acknowledged by name on published articles

Frontiers
Avenue du Tribunal-Fédéral 34
1005 Lausanne | Switzerland

Visit us: www.frontiersin.org
Contact us: frontiersin.org/about/contact

REPRODUCIBILITY OF RESEARCH
Support open data and methods to enhance research reproducibility

DIGITAL PUBLISHING
Articles designed for optimal readership across devices

FOLLOW US
@frontiersin

IMPACT METRICS
Advanced article metrics track visibility across digital media

EXTENSIVE PROMOTION
Marketing and promotion of impactful research

LOOP RESEARCH NETWORK
Our network increases your article's readership